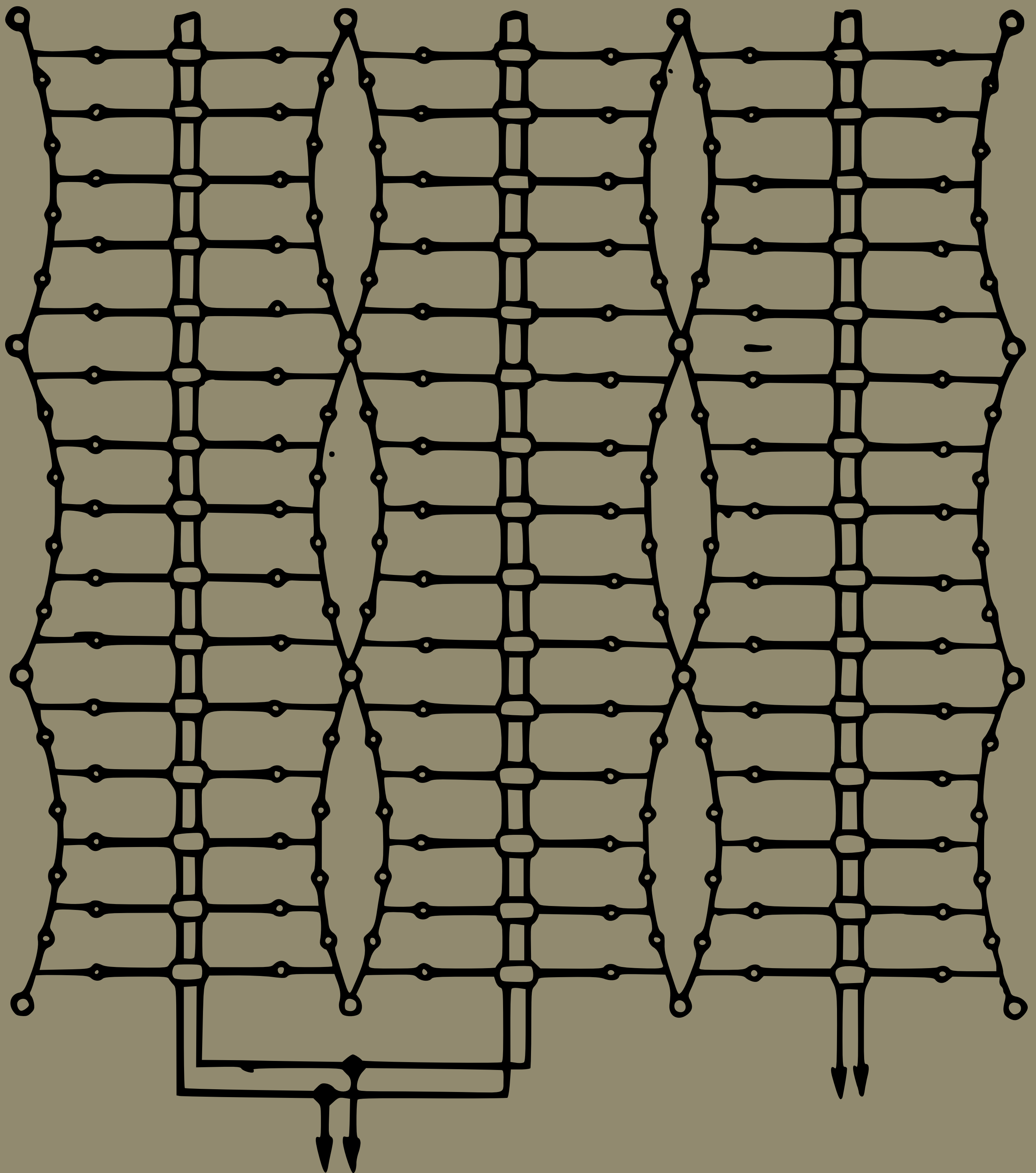


G.T. Markov

ANTENNAS



Progress Publishers Moscow

Antennas



Progress Publishers

First published 1958

CONTENTS

Introduction	9
1-1. Purpose	9
1-2. Maxwell's Equations	10

Part One

GENERAL THEORY OF RADIO WAVE RADIATION AND RECEPTION

<i>Chapter One. Radiation from Elementary Sources</i>	15
1-1. Radiation of an Electric Dipole	15
1-2. Radiation of a Magnetic Dipole	18
1-3. Radiation of an Elementary Electric Loop	19
1-4. Radiation of an Elementary Magnetic Loop	22
1-5. Effects of a Perfectly Conducting Infinite Plane on the Radiation from Elementary Sources	23
1-6. Unidirectional Radiation	27
1-7. Radiation of a Rotating Field	29
<i>Chapter Two. Radiation of Dipoles of Finite Length</i>	31
2-1. The Electric Dipole	31
2-2. The Integral Equation Method	32
2-3. Current Distribution in a Symmetrical Dipole in the First Approximation	34
2-4. Field Intensity of the Dipole in the Radiation Zone	38
2-5. Calculating Power Radiated by an Antenna by the Poynting Vector Method	41
2-6. Field Intensity in the Vicinity of the Antenna	44
2-7. Calculating the Power Radiated by an Antenna by the Induced EMF Method. Input Resistance of a Symmetrical Antenna	48
2-8. Calculating the Input Resistance of an Antenna by Reducing It to a Homogeneous Long Line with Losses	53
2-9. Radiation of a Symmetrical Magnetic Antenna. Sym- metrical Slot in Screen	57

2-10. Additional Remarks Concerning the Current Distribution in an Antenna	62
2-11. The Eigenfunctions Method	68
Chapter Three. Radiation of Two Coupled Antennas	77
3-1. Directional Diagrams of Antennas	77
3-2. Mutual and Total Impedances of Antennas	83
3-3. Active Reflector	86
3-4. Passive Antenna	87
3-5. Calculating Mutual Resistance of Antennas	89
Chapter Four. Radiator Systems and Antenna Parameters	93
4-1. General	93
4-2. Radiation of a Linear Co-Phased Dipole Array	93
4-3. Radiation of a Linear Dipole Array with a Variable Phase	99
4-4. Radiation Resistance of a Dipole System	102
4-5. Radiation of Continuous System of Sources with a Travelling Wave	103
4-6. Application of the Equivalent Surface Currents Theorem to the Calculation of the Radiation Characteristics of Antennas	108
4-7. Radiation of an Ideal Plane Antenna	112
4-8. Effect of Changes of Field Amplitude and Phase in a Plane Antenna on the Directional Diagram	116
4-9. Antenna Parameters	122
4-10. Definition of the Current Distribution in an Antenna in Accordance with a Prescribed Directional Diagram	130
Chapter Five. The Influence of the Earth and Metal Bodies on Antenna Radiation	157
5-1. Radiation of a Symmetrical Dipole Located over Plane Earth	157
5-2. Radiation of an Asymmetrical Dipole Disposed on the Surface of Plane Earth	162
5-3. The Influence of the Earth on the Radiation of Multiple Antennas	164
5-4. The Influence of an Infinite Circular Cylinder on the Radiation of an Electric Dipole	166
5-5. The Influence of an Infinite Circular Cylinder on the Radiation of a Longitudinal Slot	171
Chapter Six. Receiving Antenna Theory	177
6-1. A Symmetrical Dipole in the Field of a Plane Electromagnetic Wave	177
6-2. Power Dissipated in the Load of a Receiving Symmetrical Dipole.	180

6-3. Current Distribution in a Receiving Dipole	182
6-4. Application of the Principle of Reciprocity to the Study of the Properties of Receiving Antennas	183
6-5. Effective Area of an Antenna	187
6-6. Mutual Resistance of Receiving and Transmitting Antennas	188

Part Two

TRANSMISSION LINES OF RADIO WAVES

<i>Chapter Seven. Transmission Line Theory</i>	190
7-1. General	190
7-2. Rectangular Waveguide Theory	192
7-3. Circular Waveguide Theory	207
7-4. Brief Information Regarding Coaxial Lines	219
7-5. Single-Wire Line Theory	221
7-6. Other Transmission Lines	228
<i>Chapter Eight. Methods for Matching the Line to the Load</i> . .	234
8-1. Twin-Wire Line Equivalent to a Waveguide	234
8-2. Transmission Lines of Finite Length	235
8-3. Narrow-Band Matching of the Line to the Load . . .	239
8-4. Broad-Band Matching of the Line to the Load . . .	244
8-5. Matching the Line to the Load in a Broad Frequency Range	250
<i>Chapter Nine. Parameters and Elements of Transmission Lines</i>	254
9-1. Two-Wire and Four-Wire Lines	254
9-2. Coaxial Lines	260
9-3. Waveguide Lines	264
9-4. Switching Devices and Duplexers	280
9-5. Devices Employing Ferrites	288

Part Three

TYPES OF ANTENNA DEVICES

<i>Chapter Ten. Ultrashort-Wave Antennas</i>	306
10-1. Antenna Types	306
10-2. Simple Antennas of the Wire Type	306
10-3. Simple Antennas of the Slot Type	313
10-4. Construction of Simple Wideband Antennas . . .	320

10-5. Multi-Unit Antennas	334
10-6. Slot Waveguide Antennas	340
10-7. Director Antennas	349
10-8. Helical Antennas	355
10-9. Dielectric Rod Antennas	361
10-10. Horn Antennas	368
10-11. Slow Phase Velocity Impedance Antennas	377
10-12. Lens Antennas	384
10-13. Parabolic Antennas	402
10-14. Other Reflector Antennas	416
<i>Chapter Eleven. Short-Wave Antennas</i>	<i>422</i>
11-1. Classification of Antennas	422
11-2. Simple Dipoles of the Tuned Type	423
11-3. Simple Dipoles of the Multiple-Tuned Type	424
11-4. Corner Antenna	426
11-5. Multiple Short-Wave Antennas of the Tuned Type .	427
11-6. Multiple Short-Wave Antennas of the Multiple-Tuned Type	431
11-7. Rhombic Antenna	433
11-8. Travelling-Wave Antenna	441
11-9. Diversity Radio Reception	450
<i>Chapter Twelve. Medium- and Long-Wave Antennas</i>	<i>451</i>
12-1. Classification of Antennas	451
12-2. T- and L-Antennas	451
12-3. U-Antennas and Antennas with Multiple Downleads	462
12-4. Mast Antennas	464
12-5. Slot Antennas on Low Supports	472
12-6. Wave Antennas	474
12-7. Frame Antennas	478
12-8. Radiogoniometers	481
Appendixes	484
Bibliography	509

SYMBOLS INDEX

- A —vector potential.
 a —radius, transverse dimension of waveguide.
 B —reactive conductivity, magnetic induction.
 b —transverse dimension of waveguide.
 C —electric capacitance.
 v_1 —velocity of light in vacuum.
 D —directive gain, electric induction, distance between wires, dimension of antenna (output) opening.
 d —diameter, distance between antennas, distance between dipoles.
 E —electric field intensity.
 \mathcal{E} —electromotive force.
 e —electric field intensity, electric.
 F —focus, frequency.
 f —frequency, focal distance, reflection coefficient.
 G —active conductance.
 H —magnetic field intensity, height.
 h —height, propagation constant, magnetic field intensity, effective length.
 I —linear current.
 i —imaginary unit.
 J —current surface density.
 j —current volumetric density.
 K —travelling-wave ratio.
 k —wave number (phase coefficient) for free space.
 k_1 —surface capacity factor.
 L —length, inductance.
 l —length of dipole arm, length of line segment, light.
 M —mutual inductance, magnetisation.
 \mathcal{M} —magnetomotive force.
 m —ratio of current moduli, number of dipoles in array row, magnetic moment.
 n —number of rows in array, number of windings, coefficient of refraction.
 P —power, polarisation of medium.
 p —reflection coefficient, electric moment of dipole.
 Q —linear charge, quality.
 q —surface density of electric charge.
 R —active resistance, distance, radius.
 r —distance, radius.
 S —Poynting vector.
 s —area.
 T —period.
 t —time.
 U —voltage.
 V —volume.
 v —phase velocity.
 W —wave impedance.
 X —reactance.
 Y —total (complex) conductance.
 Z —(complex) impedance.
 α —coefficient of phase, angle, electric (magnetic) polarisability of field.

β —attenuation constant, angle.
 γ —propagation constant, angle.
 Δ —angle.
 δ —angle of losses.
 ϵ —permittivity of medium,
antenna amplification
coefficient.
 η —efficiency factor.
 ρ —volumetric density of charge,
resistivity.
 σ —specific conductance.

θ —angle between wire axis
and direction towards point
of observation.
 ϑ —angle.
 λ —wave-length.
 μ —permeability of medium.
 ξ —velocity of light to phase
velocity ratio.
 φ —angle.
 ψ —phase shift angle.
 ω —angular frequency.

Introduction

I-1 Purpose

Antennas are essential components of transmitting and receiving systems. They are coupled with the transmitter or the receiver through feeders or waveguides. Sometimes this coupling is direct, requiring no feeder devices.

The high-frequency electromagnetic oscillations excited by the transmitter are conveyed along the feeder system as plane waves and on reaching the antenna they are transformed by the latter into free-space spherical waves. The plane waves associated with the feeder line transfer electromagnetic energy from the transmitter to the antenna. The free spherical waves generated by the antenna carry electromagnetic energy from the antenna into the infinity, i.e., their waveguide is free space. The transmitting antenna is said to radiate electromagnetic energy.

The electromagnetic waves travelling in space excite in the receiving antenna oscillations of high-frequency currents. Plane waves are excited in the feeder system coupling the antenna with the receiver and are conveyed to the receiver. These waves carry high-frequency energy exciting the receiving set. The receiving antenna is said to receive electromagnetic energy. Note that only part of the power reaching the receiving antenna is transmitted to the receiver. The rest of the energy is radiated back into surrounding space.

The main purpose of a transmitting antenna-feeder system is to transmit electromagnetic energy from the transmitter to the antenna and then into surrounding space with maxi-

imum efficiency and without noticeable distortions of the modulating signal. The other purpose is to distribute the radiated energy in space in a definite pattern. In one case, the energy is to be radiated uniformly in all directions; in another case, it is to be radiated in a sufficiently narrow beam. The receiving antenna and the feeder line coupling it with the receiver should also operate at a maximum efficiency and possess a sufficiently wide pass-band. The response of the antenna to the waves arriving from various directions should follow a prescribed law, i.e., it will just like a transmitting antenna, possess a definite directivity.

I-2. Maxwell's Equations

Modern antenna theory is based entirely on the basic equations of electromagnetic theory, viz., Maxwell's equations. These equations are the generalisation of data gained by experience and their validity has been confirmed by practice.

Throughout this course we shall always be concerned with such electromagnetic processes as are harmonic in time, or vary in time as $\sin \omega t$; or as $e^{i\omega t}$ in complex form. Furthermore, we shall write the vector of the instantaneous value of the electric field intensity as $\mathbf{e} = \text{Im} (\dot{\mathbf{E}} e^{i\omega t})$, where $\dot{\mathbf{E}}$ is the field complex amplitude; for simplicity, complex amplitudes will be written further on without dots above the letters. Complex electromagnetic waves may be regarded as sums of harmonic oscillations, i.e., they may be expressed in the form of a Fourier expansion.

We shall keep to the rationalised practical metre-kilogram-second-coulomb system of units. We shall consider a homogeneous and isotropic medium assuming the existence of a given distribution of the exciting (external) electric and magnetic currents for some of the regions.

Under these conditions Maxwell's equations may be written in differential form as:

$$\begin{aligned} \text{rot } \mathbf{H} &= i\omega\epsilon' \mathbf{E} + \mathbf{j}^e; \\ \text{rot } \mathbf{E} &= -i\omega\mu \mathbf{H} - \mathbf{j}^M, \end{aligned} \quad (\text{I-1})$$

where \mathbf{E} is the complex amplitude of the electrical field intensity, in volts per metre;

\mathbf{H} , the complex amplitude of the magnetic field intensity, in amperes per metre;

$\epsilon' = \epsilon \left(1 - i \frac{\sigma}{\omega \epsilon} \right)$, the complex dielectric constant of the medium;

ϵ , the dielectric constant of the medium, in farads per metre; in vacuum:

$$\epsilon_0 = \frac{10^{-9}}{36\pi} \text{ f/m};$$

μ , the permeability of the medium, in henries per metre; in vacuum $\mu_0 = 4\pi \cdot 10^{-7} \text{ h/m}$;

σ , the conductivity of the medium, in mhos per metre;

\mathbf{j}^e , the complex amplitude of the external electric current density in amperes per square metre;

\mathbf{j}^M , the complex amplitude of the external magnetic current density, in volts per square metre.

The external magnetic current is a fictitious quantity, since magnetic charges are non-existent in nature. However, the introduction of this concept makes for a relatively simple analysis of the radiation of slots in conducting screens.

The relations (I-1) are usually supplemented with the following equations:

$$\begin{aligned} \operatorname{div} \mathbf{E} &= \frac{\rho}{\epsilon'}, \\ \operatorname{div} \mathbf{H} &= \frac{m}{\mu}, \end{aligned} \quad (\text{I-2})$$

where ρ and m are space densities of the electric and of the magnetic charge respectively.

The equations (I-2) are derived from the equations (I-1), for the continuity equations are always valid

$$\begin{aligned} \operatorname{div} \mathbf{j}^e + i\omega\rho &= 0, \\ \operatorname{div} \mathbf{j}^M + i\omega m &= 0. \end{aligned} \quad (\text{I-3})$$

Note that for free space, the quantity

$$v_1 = \frac{1}{\sqrt{\epsilon_0 \mu_0}} = 3 \times 10^8$$

is expressed in metres per second representing the velocity of light in vacuum; and then the quantity

$$W_0 = \sqrt{\frac{\mu_0}{\epsilon_0}} = 120 \pi \approx 376.6$$

is expressed in ohms representing the wave impedance of free space. Note also that

$$k_0 = \omega \sqrt{\epsilon_0 \mu_0} = \frac{\omega}{v_1} = \frac{2\pi}{\lambda_0}$$

is the wave number (phase coefficient) and λ_0 is the wavelength (in metres) of the waves travelling in free space.

Incidentally, it follows from the equations (I-3) that in defining fields one may proceed from the current distribution alone, since charges can be readily defined provided the distribution of the currents in the radiator system has been given. This is precisely the way we shall proceed from now on.

Two auxiliary vectors are usually introduced to solve Maxwell's equations (I-1): the vector potential of the electric currents A^e and the vector potential of the magnetic currents A^M . Furthermore, the electromagnetic field vectors, E and H , are determined by means of the auxiliary vectors through these equations:

$$\begin{aligned} E &= -i\omega\mu A^e + \frac{1}{i\omega\epsilon'} \text{grad div } A^e - \text{rot } A^M; \\ H &= -i\omega\epsilon' A^M + \frac{1}{i\omega\mu} \text{grad div } A^M + \text{rot } A^e. \end{aligned} \quad (I-4)$$

Substituting (I-4) into (I-1), we obtain the following vector heterogeneous wave equations for the auxiliary potentials

$$\begin{aligned} \Delta A^e + k^2 A^e &= -j^e; \\ \Delta A^M + k^2 A^M &= -j^M, \end{aligned} \quad (I-5)$$

where

$$\begin{aligned} \Delta A &= \text{grad div } A - \text{rot rot } A; \\ k &= \omega \sqrt{\epsilon' \mu}. \end{aligned}$$

In defining the radiations from antenna systems, the integration of Maxwell's equations may thus be reduced to the

integration of the vector heterogeneous wave equations (1-5).

It will be reminded that the solutions of Maxwell's equations are unique, when:

a) they satisfy the boundary conditions on the surface of discontinuity;

b) they satisfy the infinite boundary conditions; in other words, they follow the law of radiation at infinity;

c) they are finite throughout, provided they refer to either a space or a surface distribution of exciting currents. If the electromagnetic field is excited by a linear distribution of currents, the solutions of Maxwell's equations will possess a dipole singularity, i.e., the field must tend towards infinity as the point of observation is brought nearer to a linear radiating current.

The boundary conditions on the surface of discontinuity of two media are expressed as the continuity of the tangential components of the intensity of the electric and magnetic fields between medium 1 and medium 2

$$E_{t1} = E_{t2}, \quad H_{t1} = H_{t2}. \quad (1-6)$$

On a perfectly conducting surface the boundary conditions assume different form. On the surface of an ideal conductor the tangential component of the electric field intensity vanishes altogether while the normal component is equal to the ratio of the electric charge surface density to the dielectric constant of the medium surrounding the conductor:

$$E_t = 0, \quad E_n = \frac{q}{\epsilon}. \quad (1-7)$$

As for the magnetic field intensity in the same case, its normal component vanishes while the tangential component is equal to the surface density of the electric current:

$$H_n = 0, \quad H_t = J^e \text{ when } \mathbf{H} \perp \mathbf{J}^e. \quad (1-8)$$

The boundary conditions at infinity amount to this: the electromagnetic perturbation will move away from the exciting sources into infinity as travelling waves. There can be no waves travelling from infinity to the exciting sources.

Let us mention also the complex form of Poynting's theorem:

$$\begin{aligned} \frac{1}{2} \int_s [\mathbf{E}\mathbf{H}^*]_n ds + i\omega \int_V \left(\frac{\mu |\mathbf{H}|^2}{2} - \frac{\epsilon |\mathbf{E}|^2}{2} \right) dV + \\ + \int_V \frac{\sigma |\mathbf{E}|^2}{2} dV = \frac{1}{2} \int_V (-j^M \mathbf{H}^* - j^e \mathbf{E}) dV, \end{aligned} \quad (1-9)$$

where n is the external normal to the surface s enclosing the volume V which contains the exciting sources.

The right-hand side of this equation defines the complex power output which is taken from the generators. The first term in the left-hand side defines the complex power as leaving the volume V , the second term defines the reactive power stored in the volume V and the third term defines the power dissipated as heat in the volume V . The power leaving the volume V is described by the complex Poynting vector

$$\mathbf{S} = \frac{1}{2} [\mathbf{E}, \mathbf{H}^*]. \quad (1-10)$$

PART ONE

General Theory of Radio Wave Radiation and Reception

CHAPTER ONE

Radiation from Elementary Sources

1-1. Radiation of an Electric Dipole

We shall begin this course of "Antenna Theory" by investigating the radiation from elementary sources, i.e., sources whose geometrical dimensions are small in comparison with the wave-length of the oscillations which they excite. Furthermore, we shall assume that the reader is familiar with the Hertz dipole theory.

Let us assume that we have a boundless homogeneous space. Let the vector distribution of the density of the exciting electric or magnetic current $\mathbf{j}(x', y', z')$, be given for a certain limited volume V of this space. The vector potential of these currents at a certain spatial point $P(x, y, z)$ is known as:

$$\mathbf{A}(x, y, z) = \frac{1}{4\pi} \int_V \mathbf{j}(x', y', z') \frac{e^{-ikr}}{r} dV, \quad (1-1)$$

where

$$r = \sqrt{(x-x')^2 + (y-y')^2 + (z-z')^2}.$$

The expression (1-1) is the solution of the vector wave heterogeneous equations (1-5). The solution is unique since it satisfies the boundary condition at infinity and has a finite value throughout.

By substituting this expression into the equations (1-4), we can define the vector of the electric field intensity \mathbf{E} and the vector of the magnetic field intensity \mathbf{H} for any point of the space.

Let the exciting current be electric and directed along the z -axis of Cartesian coordinates. Let us suppose that the current occupies an infinitesimal volume of space at the origin of the coordinates, i.e., let there be an electric Hertz dipole with a momentum $I^e l$, where I^e is the current of the dipole in amperes and l is its length in metres (Fig. 1-1). In this case the vector potential will have only the z -axis component and we shall write the relation (1-1) as:

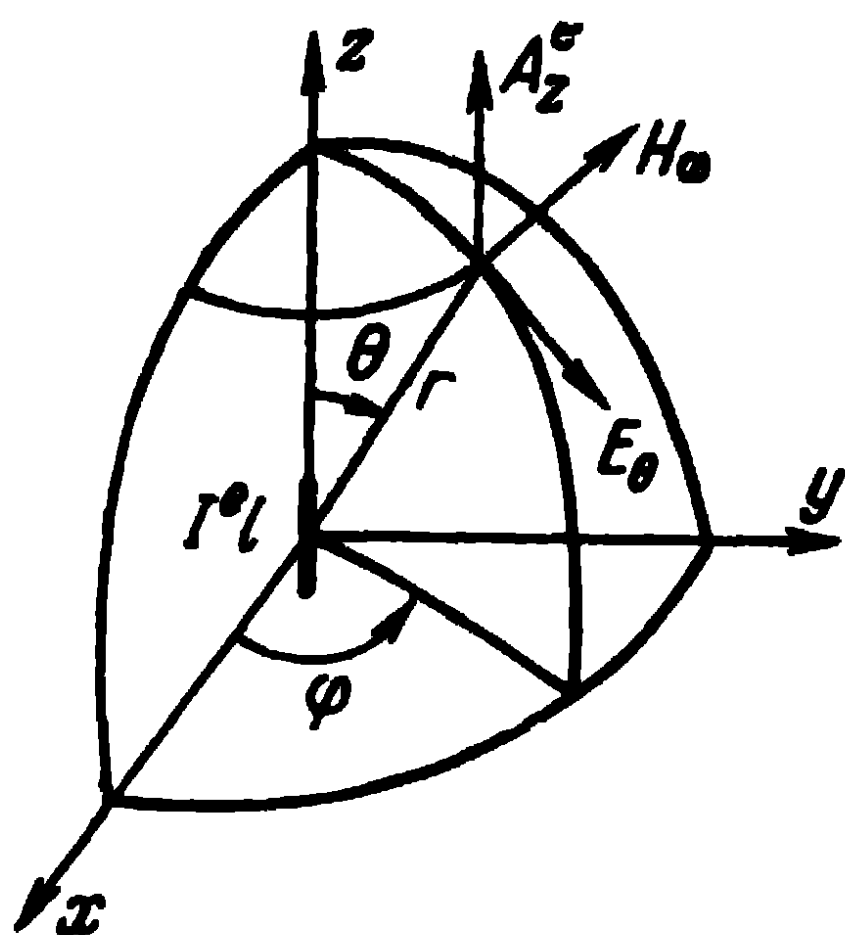


Fig. 1-1. An electric dipole.

where

$$A_z^e = \frac{I^e l}{4\pi} \frac{e^{-ikr}}{r}, \quad (1-2)$$

$$r = \sqrt{x^2 + y^2 + z^2}.$$

We shall now turn our attention to the field of the dipole in the zone of radiation ($r \gg \lambda$) and, by substituting (1-2) into (1-4), we shall describe the zone of radiation in the spherical coordinates r, θ, φ .

$$\begin{aligned} H_\varphi &= i \frac{I^e l k}{4\pi} \sin \theta \frac{e^{-ikr}}{r}; \\ E_\theta &= i \frac{I^e l k^2}{4\pi \omega \epsilon} \sin \theta \frac{e^{-ikr}}{r}, \end{aligned} \quad (1-3)$$

where θ is the angle between the axis of the dipole and the direction to the point of observation of the field.

It follows from (1-3) that a) the Hertz dipole radiates travelling waves moving away into infinity at the velocity of light in the given medium; b) the surfaces of equal phases of these waves are spheres with their centres coinciding with the position of the dipole; c) the amplitudes of electric and magnetic fields intensities vary inversely proportional to the distance between the point of observation and the dipole; d) the vectors of the electric and magnetic fields are mutually perpendicular, being perpendicular to the direction of propagation of the wave and oscillating in phase; e) the vector \mathbf{E} lies in a plane passing through the dipole (in a meridian plane), the vector \mathbf{H} lying in an azimuth plane; furthermore, the ratio of their magnitudes is equal

to the wave impedance of the space

$$\frac{E_\theta}{H_\phi} = \frac{k}{\omega \epsilon} = \sqrt{\frac{\mu}{\epsilon}} \text{ ohms.}$$

In contradistinction to the vector potential, the magnitudes of the electric and magnetic fields intensities depend on the angle of observation θ . Because of axial symmetry, the field does not depend on the angle of observation ϕ . The graphs showing the field intensity magnitude plotted as a function of the angle of observation are known as directional

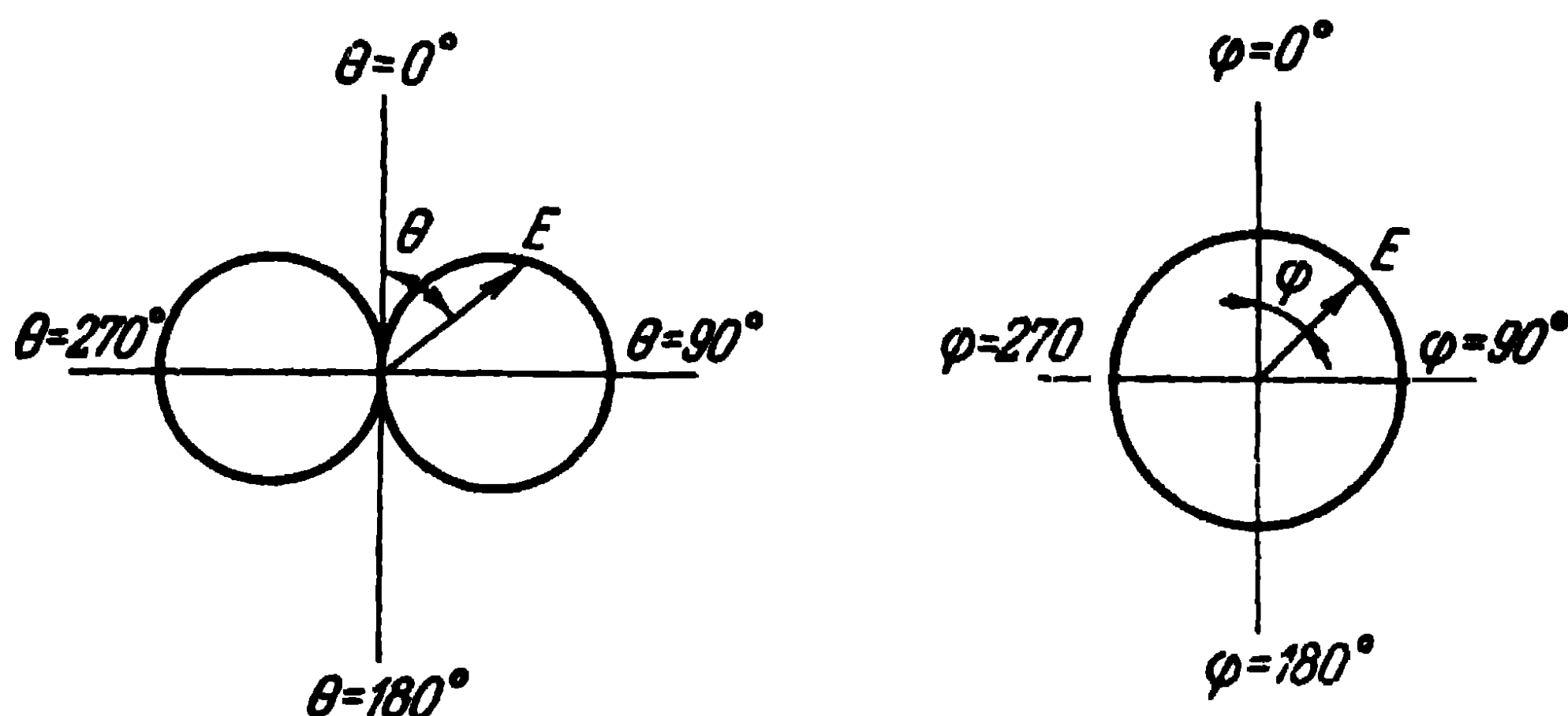


Fig. 1-2. Directional diagrams of the dipole.

diagrams (characteristics). We see that in the meridian plane (in the plane of the vector E), the dipole directional diagram is a sinusoid plotted in polar coordinates. This curve may conventionally be termed a "figure of eight". In the azimuth plane (in the plane of the vector H), the directional diagram of the dipole represents a circle (Fig. 1-2). Thus, the Hertz dipole radiates the maximum energy in a direction perpendicular to its axis, radiating none along the axis.

The power radiated by the Hertz dipole can be defined using the Poynting vector procedure as follows

$$P_\Sigma = \frac{1}{2} I^2 R_{\Sigma d}, \quad (1-4)$$

where $R_{\Sigma d}$ is the dipole radiation resistance, expressed for a lossless medium as:

$$R_{\Sigma d} = \frac{2\pi}{3} \sqrt{\frac{\mu}{\epsilon}} \left(\frac{l}{\lambda} \right)^2, \quad (1-5)$$

where λ is the wave-length for a given medium.

In the case of vacuum, the expression becomes:

$$R_{\Sigma d} = 20 (k_0 l)^2 = 80\pi^2 \left(\frac{l}{\lambda_0} \right)^2, \quad (1-6)$$

where λ_0 is the wave-length for vacuum.

1-2. Radiation of a Magnetic Dipole

Now, let the exciting current be a magnetic dipole with a moment $I^M l$, lying at the origin of the coordinates and directed along the z -axis (Fig. 1-3). The vector potential of the dipole is given by:

$$A_z^M = \frac{I^M l}{4\pi} \frac{e^{-ikr}}{r}. \quad (1-7)$$

In accordance with the expressions (1-4), the components of electric and magnetic fields in the radiation zone are

$$\begin{aligned} E_\varphi &= -i \frac{I^M l k}{4\pi} \sin \theta \frac{e^{-ikr}}{r} \\ H_\theta &= i \frac{I^M l k^2}{4\pi\omega\mu} \sin \theta \frac{e^{-ikr}}{r} \end{aligned} \quad (1-8)$$

We see that a magnetic dipole, just like an electric one, radiates spherical waves which move away into infinity with the velocity of light.

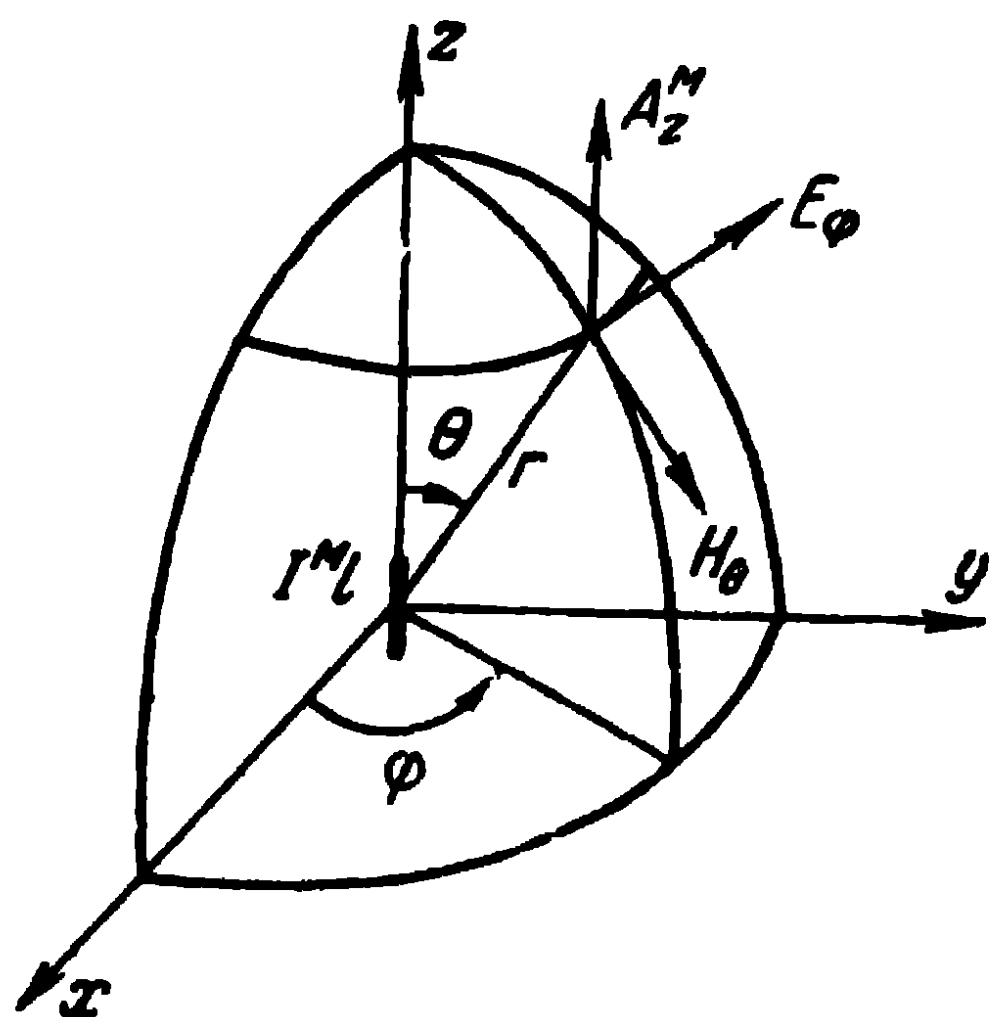


Fig. 1-3. A magnetic dipole.

The directional diagrams of a magnetic dipole coincide with those of an electric one, i.e., its radiation is maximal in the equatorial plane and zero along the axis. We see that in the meridian plane there are electric lines of force in the case of an electric dipole, and there are magnetic lines of force in the case of a magnetic dipole.

Comparing the radiations of the electric dipole with those of the magnetic one we can easily bring out the following rule: if the moment of the electric dipole current is equal to that of the magnetic dipole current, the magnetic field of the electric dipole is equal to the electric field of the magnetic

dipole and of reverse sign. Furthermore, the electric field of the electric dipole differs from the magnetic field of the magnetic dipole by $W^2 = \frac{\mu}{\epsilon}$ times and of the same sign. This constitutes the interchangeability of fields produced by elementary dipoles of electric and of magnetic types.

The power radiated by the magnetic dipole, calculated after Poynting is evidently expressed as:

$$P_{\Sigma} = \frac{1}{2} I^2 G_{\Sigma d}, \quad (1-9)$$

where $G_{\Sigma d}$ is the radiation conductivity of the magnetic dipole expressed as

$$G_{\Sigma d} = \frac{2\pi}{3} \sqrt{\frac{\epsilon}{\mu}} \left(\frac{l}{\lambda} \right)^2. \quad (1-10)$$

By comparing (1-5) and (1-10) we shall find that

$$G_{\Sigma d} = \frac{R_{\Sigma d}}{W^2}, \quad (1-11)$$

where $W = \sqrt{\frac{\mu}{\epsilon}}$ is the wave impedance of the medium.

The expression (1-11) enables us to define the radiation conductivity of a magnetic dipole provided the radiation resistance of an electric dipole of the same length is known.

1-3. Radiation of an Elementary Electric Loop

Let there be in an unbounded space a circular electric loop of radius a with a uniformly distributed current I_0 . Let the centre of the loop coincide with the origin of the coordinates and the axis of the loop be directed along the z -axis. In spherical coordinates, the loop current will then only have the ϕ -component. Let us calculate the field of the loop in the zone of radiation. Referring to Fig.1-4, let us choose on the loop two elements of current $I_0 a d\phi$ symmetrically relative to the x -axis and, considering these current elements as electric dipoles, let us write the expression of the vector potential caused by them at point M of the xz -plane. Furthermore, it should be noted that the potential caused at point M by the x -components of these current elements is zero, as the difference in distance between the elements and point of observation is zero, with the current element

components being of opposite signs. The radiation may be due only to the y -axis components of the current elements; their vector potential will be doubled and have the component

$$dA_{\varphi}^e = \frac{2I_1^e \cos \varphi a d\varphi e^{-ikr}}{4\pi r}. \quad (1-12)$$

It should be noted here that, since the point of observation of the field is at infinity the beams from all the loop elements

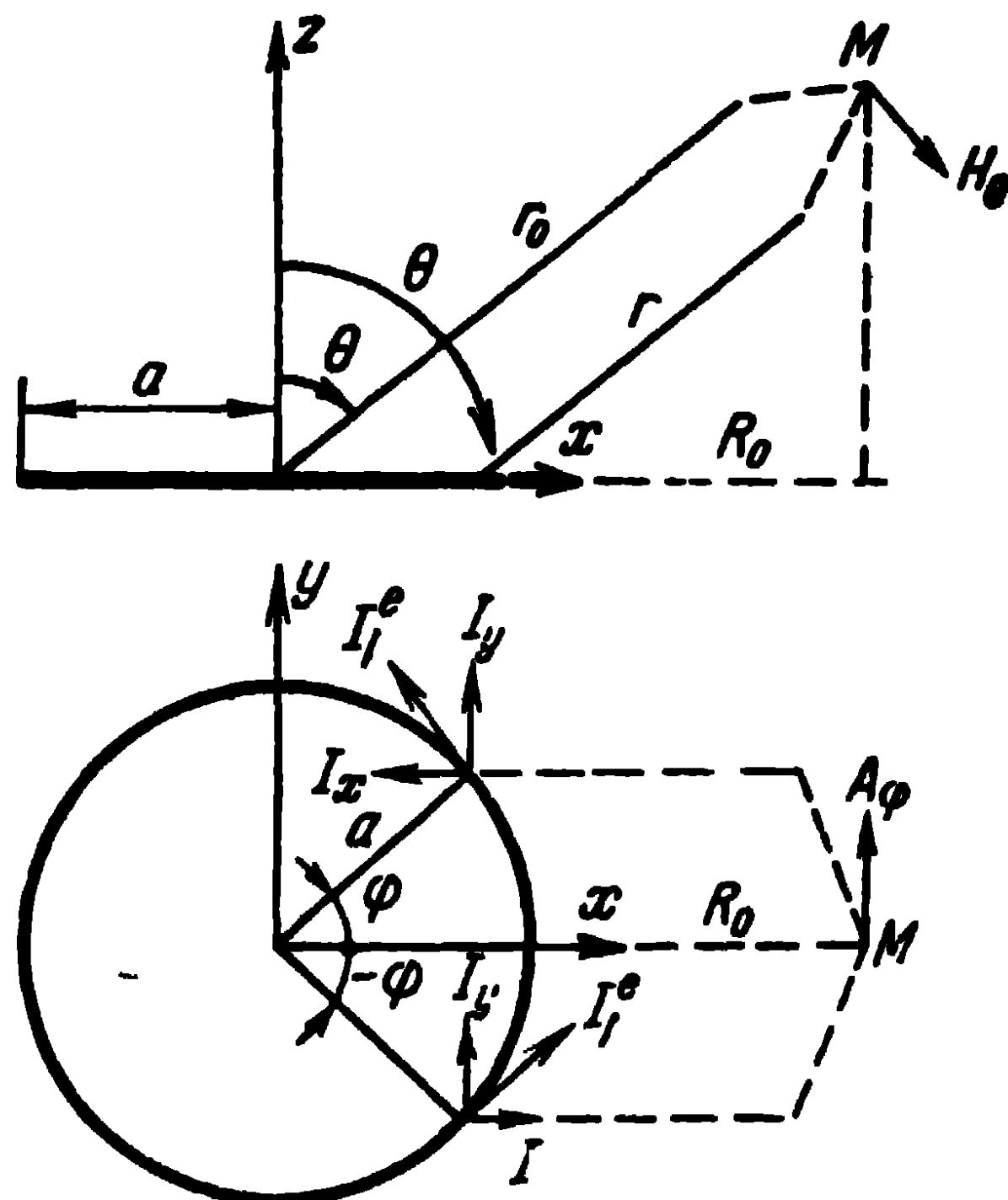


Fig. 1-4. Explaining the calculation of the field of an electric loop.

can be considered parallel and the field phase will be calculated from the loop centre as the basis. We may then assume with a high degree of accuracy that in the expression (1-12)

$$\frac{1}{r} \approx \frac{1}{r_0};$$

$$r \approx r_0 - a \cos \varphi \sin \theta.$$

Substituting these expressions into (1-12) and summing up the radiations of all the loop elements, we shall find that

$$A_{\varphi}^e = \frac{2I_1^e a}{4\pi} \frac{e^{-ikr_0}}{r_0} \int_{\varphi=0}^{\pi} e^{ika \cos \varphi \sin \theta} \cos \varphi d\varphi. \quad (1-13)$$

Now, let us assume the loop radius to be small in comparison with the wave-length $ka \ll 1$. Then we may state that in (1-13)

$$e^{ika \cos \varphi \sin \theta} \approx 1 + ika \cos \varphi \sin \theta.$$

Integrating (1-13) under those conditions we shall find that

$$A_{\varphi}^e \approx i \frac{I_1^e ka^2}{4} \sin \theta \frac{e^{-ikr_0}}{r_0}.$$

Further, taking into account that from (1-4) $\text{div } \mathbf{A}^e = 0$ we have

$$E_{\varphi} = \frac{I_1^e \omega \mu ka^2}{4} \sin \theta \frac{e^{-ikr_0}}{r_0}. \quad (1-14)$$

The magnetic field intensity is then expressed as

$$H_{\theta} = - \frac{E_{\varphi}}{\sqrt{\frac{\mu}{\epsilon}}}. \quad (1-15)$$

We see that the radiation of an electric loop is similar to that of a magnetic dipole. On comparing (1-14) and (1-8), we obtain:

$$I^M l = i \omega \mu I_1^e s, \quad (1-16)$$

where $s = \pi a^2$ is the area of the loop.

An electric loop of small radius may thus be regarded as a magnetic dipole whose axis coincides with that of the loop and whose moment is defined by (1-16).

The loop gives rise to maximal radiation in its plane and radiates no electromagnetic energy along its axis, besides the field produced by this loop has the same polarisation as the magnetic dipole field.

The radiation resistance of the electric loop is defined as the ratio of the radiated power to the square of the effective value of the current in the loop

$$R_{\Sigma l} = \frac{2P_{\Sigma}}{|I_1^e|^2}.$$

But according to (1-16) $|I_1^e| = \frac{I^M l}{\omega \mu s}$. From (1-9), we shall write that

$$R_{\Sigma l} = \frac{2P_{\Sigma}}{I^M{}^2} \frac{\omega^2 \mu^2 s^2}{l^2} = G_{\Sigma d} \frac{\omega^2 \mu^2 s^2}{l^2} \quad (1-17)$$

or, substituting here the expression (1-10), we obtain

$$R_{\Sigma 1} = \frac{8}{3} \sqrt{\frac{\mu}{\epsilon}} \frac{\pi^2 s^2}{\lambda^4}. \quad (1-18)$$

For vacuum, this formula becomes

$$R_{\Sigma 1} = \frac{320\pi^4 s^2}{\lambda_0^4}. \quad (1-19)$$

The expression above is usually applied to the calculation of the radiation resistance of loop antennas. It should be pointed out that whereas the electric dipole radiation resistance is inversely proportional to the square of the wave-length, the radiation resistance of an electric loop of small radius is inversely proportional to the fourth power of the wave-length.

1-4. Radiation of an Elementary Magnetic Loop

Now, let us consider an elementary magnetic loop with a uniformly distributed current I_1^M . Let the centre of the loop coincide with the origin of the coordinates and let us direct the loop-axis along the z-axis. By analogy with the electric loop, we may immediately write the expression for the magnetic loop field intensity in the zone of radiation

$$H_{\varphi} = \frac{I_1^M \omega \epsilon k a^2}{4} \sin \theta \frac{e^{-ikr_0}}{r_0};$$

$$E_{\theta} = \sqrt{\frac{\mu}{\epsilon}} H_{\varphi}. \quad (1-20)$$

Comparing (1-20) with (1-3), we obtain

$$I^e l = -i\omega \epsilon I_1^M s. \quad (1-21)$$

In this case the elementary magnetic loop may be regarded as an electric dipole with the current moment defined by (1-21). The loop radiates a field which has the same polarization as the field of an electric dipole and its directional diagram coincides with that of a dipole.

We may introduce the concept of radiation conductivity of the loop, which is defined as the ratio of its radiated power to the square of the effective magnetic current. From

(1-21) we can write that the conductivity of the loop

$$G_{\Sigma l} = \frac{2P_{\Sigma}}{|I^e|^2} \frac{\omega^2 \epsilon^2 s^2}{l^2} = R_{\Sigma d} \frac{\omega^2 \epsilon^2 s^2}{l^2}. \quad (1-22)$$

Substituting here expression (1-5), we obtain

$$G_{\Sigma l} = \frac{8}{3} \sqrt{\frac{\epsilon}{\mu}} \frac{\pi^2 s^2}{\lambda^4}. \quad (1-23)$$

Comparing (1-23) with (1-18), we may write

$$G_{\Sigma l} = \frac{R_{\Sigma l}}{W^2}, \quad (1-24)$$

where $R_{\Sigma l}$ is the radiation resistance of an electric loop of the same radius.

We see that the radiation conductivity of a magnetic loop, is related to the radiation resistance of an electric loop in the same way as the radiation conductivity of a magnetic dipole is related to the radiation resistance of an electric dipole.

1-5. Effects of a Perfectly Conducting Infinite Plane on the Radiation from Elementary Sources

We have been so far considering the radiation of dipoles and loops in an unbounded space.

Let these antenna dipoles and loops now lie at a certain height above a perfectly conducting infinite plane h (Fig.1-5). Due to the electromagnetic field of the antenna dipoles and loops surface electric currents are induced on the plane. Let us consider the direction of these induced currents. In the case of a horizontal electric antenna the surface currents flow parallel to the current in the antenna dipoles. In the case of a vertical electric antenna and a horizontal magnetic loop, they flow in radial directions. In the case of a horizontal magnetic antenna dipoles, the induced currents have components parallel to the antenna axis as well as those perpendicular to it. Finally, in the case of a vertical magnetic dipoles and a horizontal electric loop, the induced surface currents have azimuth components.

In the upper and lower half-spaces of the plane the induced surface currents give rise to secondary fields which (once the plane is considered infinitely thin) are symmetrical in relation to this plane. Since the plane is a perfect conductor

and infinite, it screens the lower half-space, and the induced currents will be so distributed that the secondary field at any point of the lower half-space will be equal in magnitude to the primary field produced by the dipoles and loops in that half-space and of opposite sign.

This leads us to what is known as a mirror method, in which the upper half-space secondary field will be assumed to remain the same if we remove the conducting plane and place in a mirror point a source of such current as is equal in magnitude to that of the real source and is so directed that the tangential component of the total electric field vanishes on the surface of the plane under consideration.

In the case of a horizontal electric dipole, a horizontal electric loop and a vertical magnetic dipole, the current of the mirror image, as shown in Fig. 1-5, *a*, *b* and *c*, flows in a direction opposite to that of the current of the real source. In the case of a vertical electric dipole, a horizontal magnetic loop and a horizontal magnetic dipole, as shown in

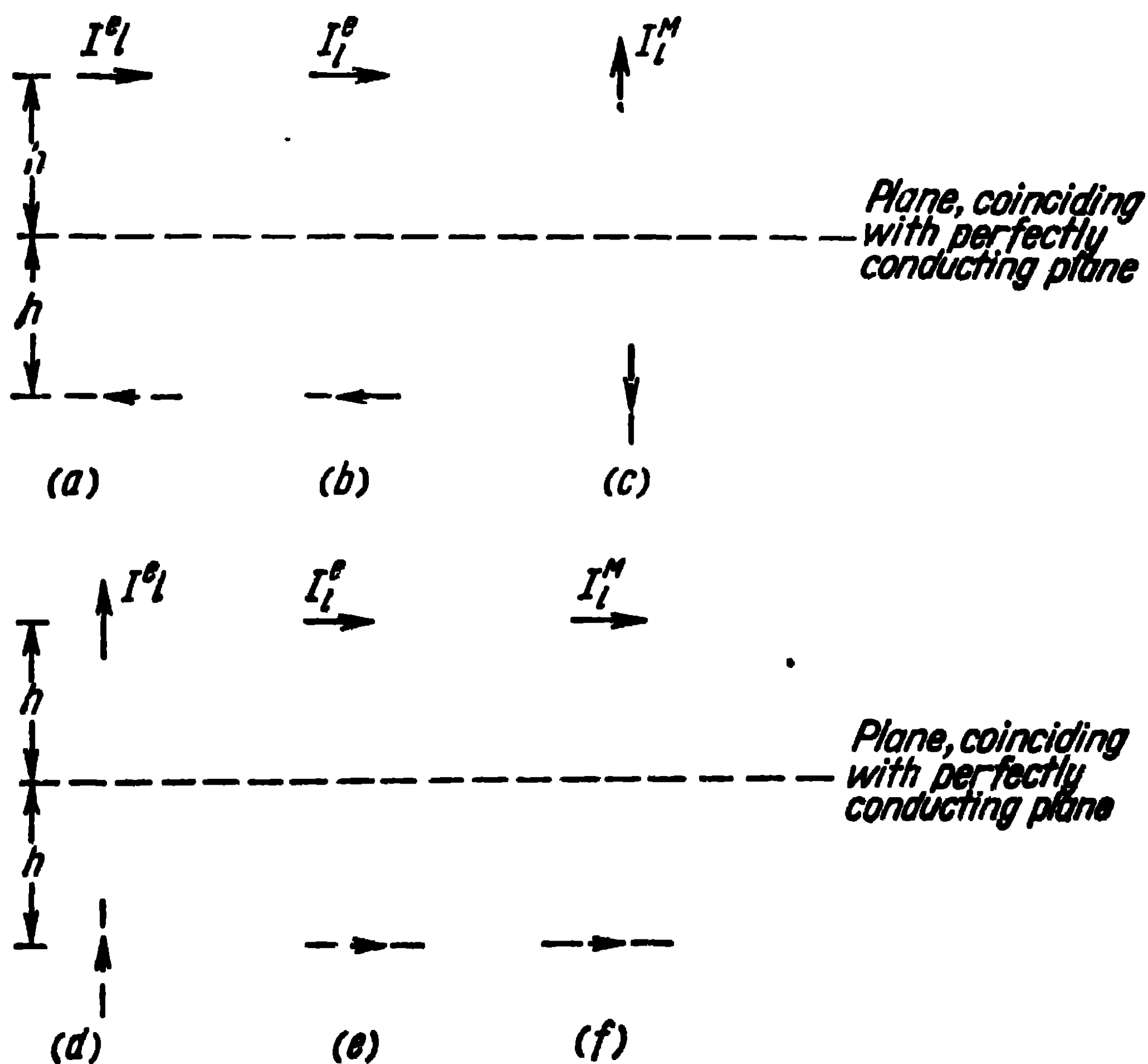


Fig. 1-5. Direction of current in mirror image.

Fig. 1-5, *d*, *e* and *f*, the current in the mirror image flows in the same direction as that of the real source.

When the source is just above the plane, in the case of a horizontal electric dipole, a horizontal electric loop and a vertical magnetic dipole, the primary and secondary fields are of equal magnitude and of opposite signs, the total field is equal to zero and the radiation vanishes. And inversely, in the case of a vertical electric dipole, a horizontal magnetic loop and a horizontal magnetic dipole, the primary and secondary fields are equal in magnitude and sign and the total field is double that of the same source in free space.

As for the resistance and conductivity of the radiation of the sources, they are equal to zero in the first case and doubled in the second case. The doubling of the radiation resistance and conductivity is connected with the fact that, in that case, the density of the radiated energy at every point of the space is quadrupled, whereas the power is radiated only in the upper half-space.

Thus, the radiation resistance of a vertical electric dipole of length l lying on the surface of a perfectly conducting plane is expressed as:

$$R_{\Sigma d} = \frac{4\pi}{3} \sqrt{\frac{\mu}{\epsilon}} \left(\frac{l}{\lambda} \right)^2. \quad (1-25)$$

The radiation conductivity of a horizontal magnetic loop lying on the plane is expressed as:

$$G_{\Sigma l} = \frac{16}{3} \sqrt{\frac{\epsilon}{\mu}} \frac{\pi^2 s^2}{\lambda^4} \quad (1-26)$$

and that of a horizontal magnetic dipole lying on the plane as:

$$G_{\Sigma d} = \frac{4\pi}{3} \sqrt{\frac{\epsilon}{\mu}} \left(\frac{l}{\lambda} \right)^2. \quad (1-27)$$

The directional diagrams in a vertical plane of a vertical electric dipole, a horizontal magnetic loop and a horizontal magnetic dipole lying on the surface of the plane under consideration ($h=0$) are shown in Fig. 1-6. As can be seen, the vertical electric dipole and the horizontal magnetic loop radiate maximum energy along the surface of the plane and give no radiation in a direction perpendicular to the plane. The horizontal magnetic dipole has an undirected radiation in its equatorial plane and a radiation in the form of half a figure of eight in the meridian plane.

The horizontal magnetic loop and horizontal magnetic dipole lying on the surface of an infinite perfectly conducting

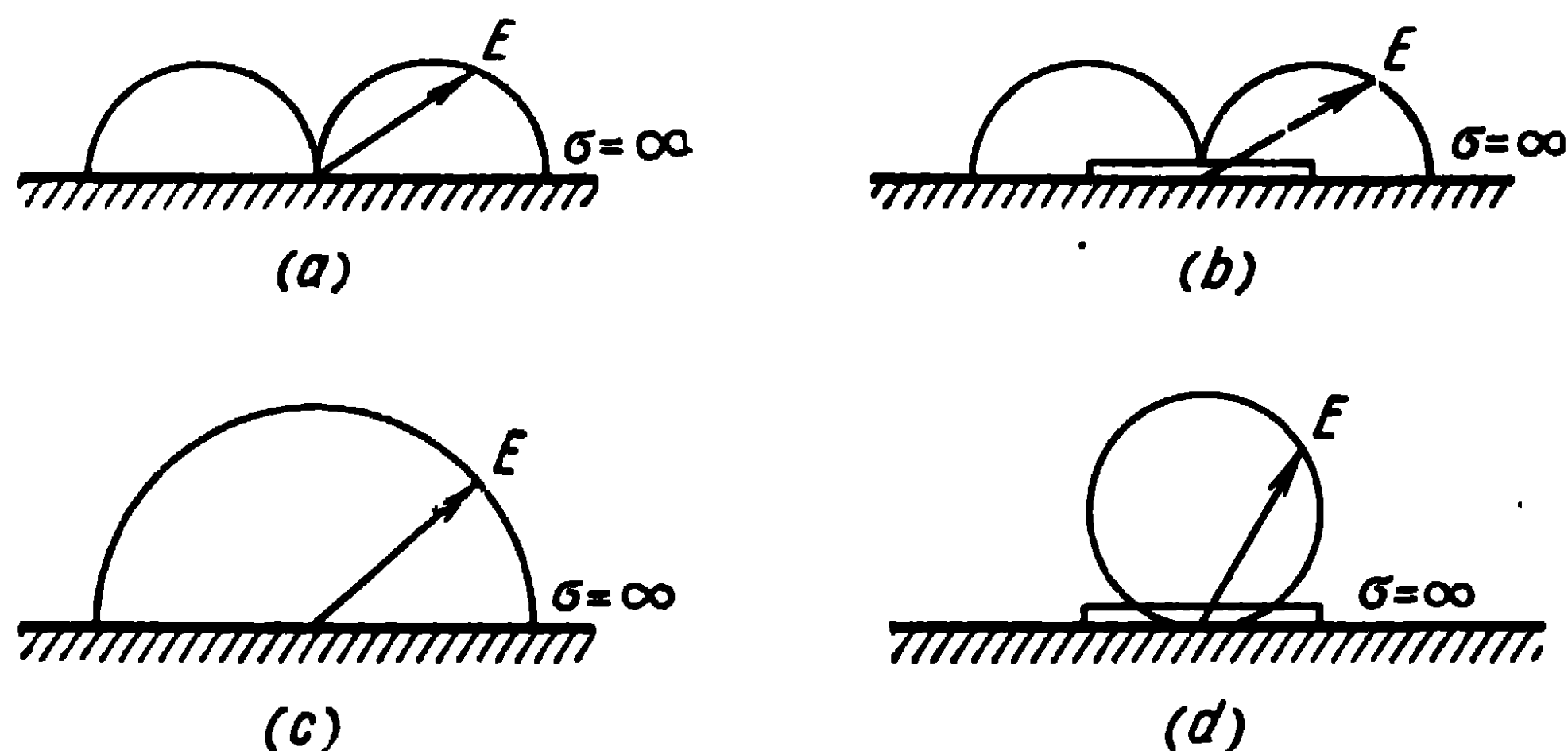


Fig. 1-6. Directional diagrams in vertical plane:

a) of a vertical electric dipole; b) of a horizontal magnetic loop; c) of a horizontal magnetic dipole in the equatorial plane of the dipole; d) of a horizontal magnetic dipole in its meridian plane.

plane examined above represent, in fact, radiating slots cut in a conducting screen. In practical work these slots may be excited through a coaxial line and a rectangular waveguide, as shown in Figs. 1-7 and 1-8.

The magnetic current of these antennas is but the difference of potential (voltage) between the edges of the slot.

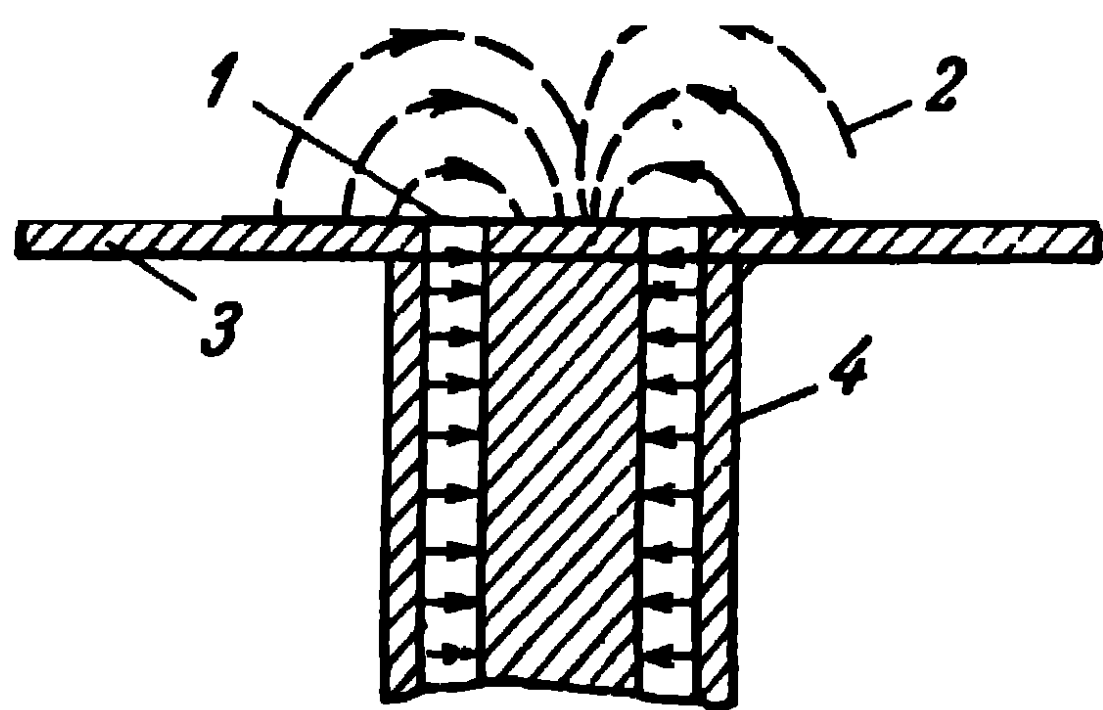


Fig. 1-7. Excitation of an annular slot by a coaxial line:

1—slot in the screen; 2—electric lines of force; 3—conducting screen; 4—coaxial line.

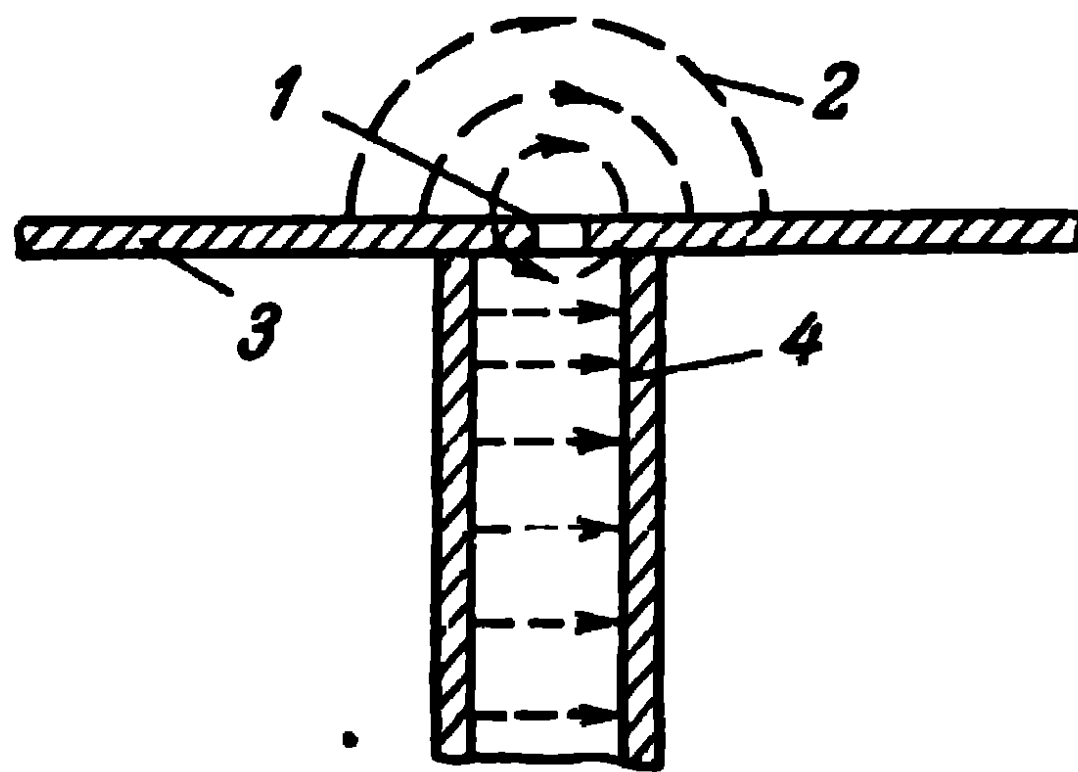


Fig. 1-8. Excitation of a slot by a waveguide:

1—slot in the screen; 2—electric lines of force; 3—conducting screen; 4—rectangular waveguide.

The ratio of the power radiated through the slot to the square of the effective value of the voltage of the slot determines the radiation conductivity of a slot antenna. Thus, the radiation conductivity of an elementary annular slot antenna

may be determined from (1-26) and the radiation conductivity of an elementary linear slot antenna from (1-27).

The slots cut in a conducting screen may also be excited by a twin feeder (Fig. 1-9). Slot antennas of this kind radiate

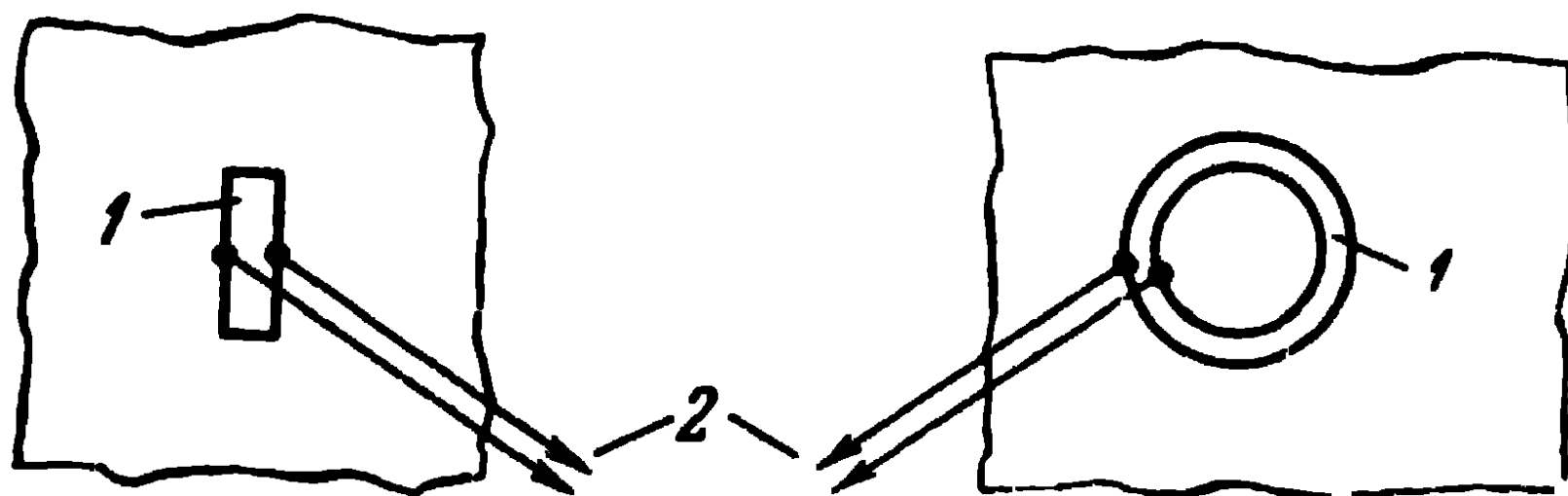


Fig. 1-9. Excitation of bilateral slots:
1—slot in the screen, 2—twin feeder.

in both half-spaces and are called bilateral slot antennas, whereas the slot antennas shown in Figs. 1-7 and 1-8 radiate

in one half-space only and are known as unilateral. Evidently, the radiation conductivity of bilateral slot antennas is double that of their unilateral counterparts.

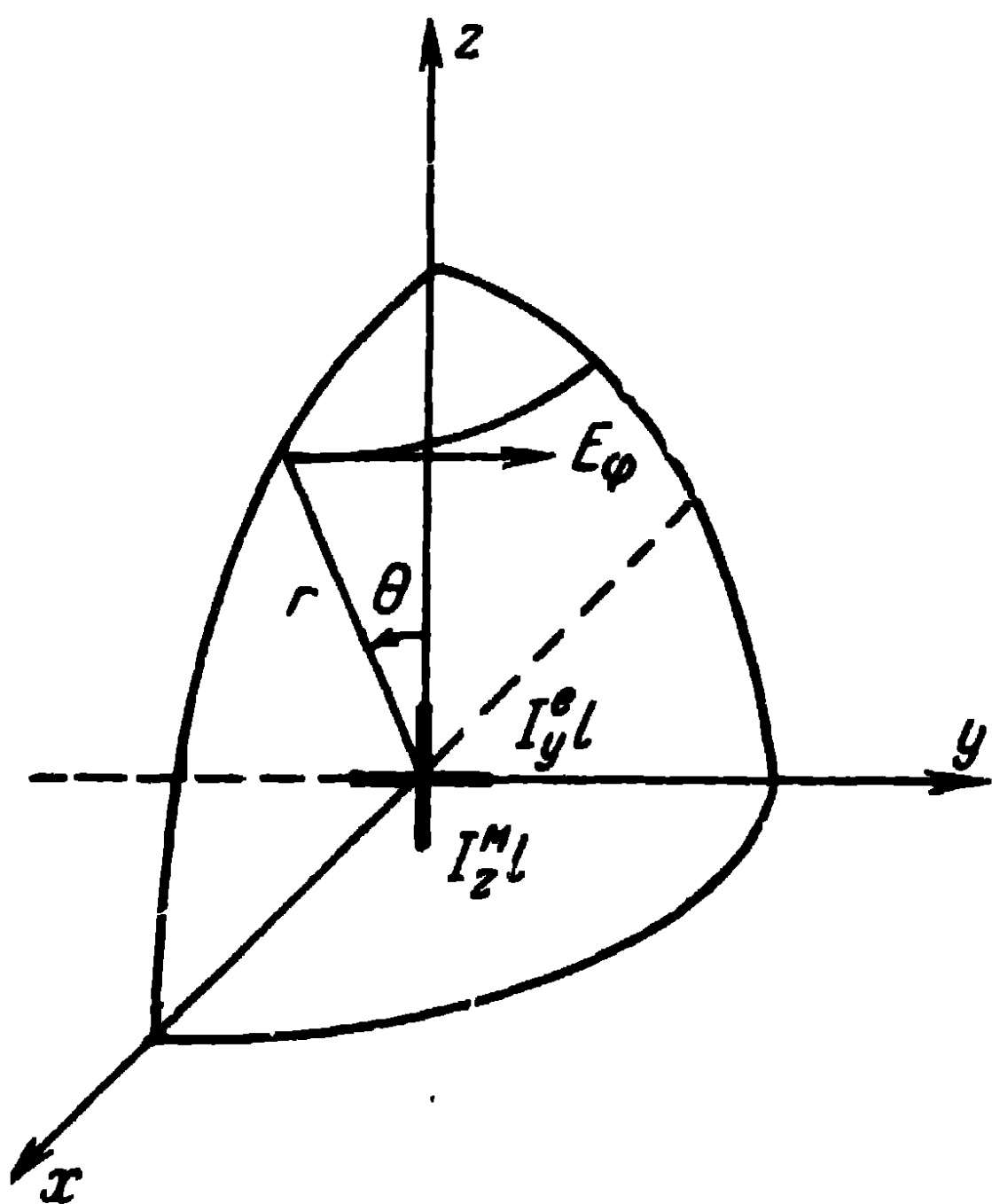


Fig. 1-10. Explaining the calculation of a unidirectional radiation.

It should be noted that the simple expressions given above for calculating directional diagrams as well as the radiation resistance and conductivity of elementary wire and slot antennas are valid only in the case of a perfectly conducting plane screen of infinite extension. The mirror method can be used and simple expres-

sions for the radiated field can be obtained only in that case. In all other cases, the influence of conducting screens on the radiation of antennas is more complex.

1-6. Unidirectional Radiation

Let us consider the radiation in free space of electric and magnetic elementary dipoles in superposition. Let the electric dipole be directed along the y -axis and the magnetic

dipole along the z -axis (Fig. 1-10). Let the currents in the dipoles oscillate with the same frequency ω . Let us consider the radiation fields of the dipoles in the xz -plane. This plane is the equatorial plane of the electric dipole and therefore from (1-3), its field is given by

$$E_{\varphi}^e = i \frac{I_y^e l k^2}{4\pi\omega\epsilon} \frac{e^{-ikr}}{r}.$$

In accordance with (1-8), the field intensity of the magnetic dipole at the same point of observation is:

$$E_{\varphi}^M = -i \frac{I_z^M l k}{4\pi} \sin \theta \frac{e^{-ikr}}{r}.$$

Since the directions of the field vectors of the electric and magnetic dipoles coincide, the magnitude of the total field at the point of observation is given by the arithmetic sum of the magnitudes of the field vectors

$$E_{\varphi} = i \frac{I_y^e l k^2}{4\pi\omega\epsilon} \frac{e^{-ikr}}{r} \left(1 - \frac{I_z^M}{I_y^e} \frac{\omega\epsilon}{k} \sin \theta \right). \quad (1-28)$$

Let the excitation intensity of the dipoles be such that the amplitude ratio of their currents is defined by the ratio

$$\frac{I_z^M}{I_y^e} = -\frac{k}{\omega\epsilon} = -\sqrt{\frac{\mu}{\epsilon}},$$

i.e., it is equal to the wave impedance of the surrounding medium.

Then, the radiation of superposed elementary dipoles, electric and magnetic, for the xz -plane is given by

$$E_{\varphi} = i \frac{I_y^e l k^2}{4\pi\omega\epsilon} \frac{e^{-ikr}}{r} (1 + \sin \theta). \quad (1-29)$$

We have obtained an expression to define the unilateral radiation of such a system. In fact, in the positive x -direction, when $\theta=90^\circ$, the radiation of the dipoles is double that of one of the dipoles in that direction. In the negative x -direction, when $\theta=-90^\circ$, the radiation of the dipoles equals zero.

The directional diagram of so superposed electric and magnetic elementary dipoles is shown in Fig. 1-11, has the form of a cardioid. In the xy -plane, the directional diagram

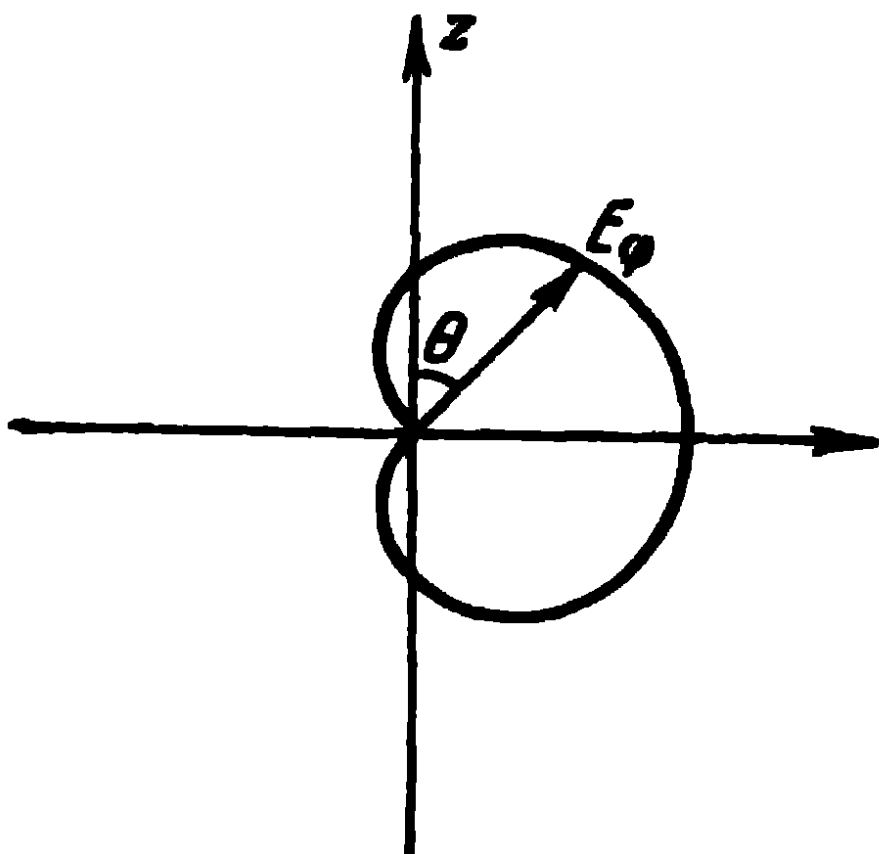


Fig. 1-11. Directional diagram of an electric dipole and a magnetic dipole in superposition.

of the dipoles will likewise have the form of a cardioid.

A practical example of such a system may be

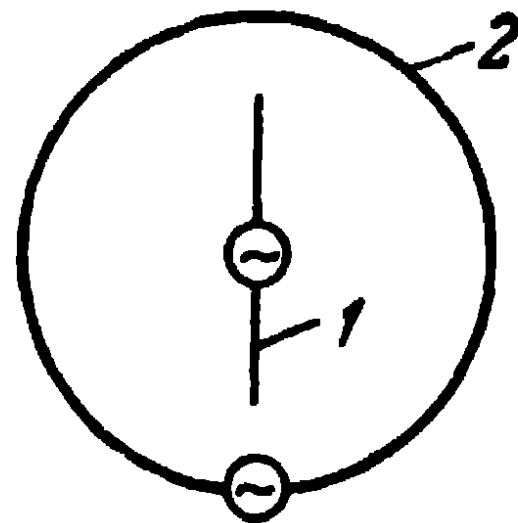


Fig. 1-12. Cardioid antenna:
1—dipole; 2—loop

afforded by an antenna arrangement consisting of an electric dipole and an electric loop superposed as shown in Fig. 1-12. Antennas of this kind, known as cardioid antennas, are utilised in direction finding.

1-7. Radiation of a Rotating Field

Let us consider the radiation of two electric (or magnetic) dipoles lying in space at right angles to each other and excited with their currents 90° out of phase. Furthermore, the amplitudes of the currents in the dipoles are assumed equal.

To begin with, let us consider the radiation field in the plane of the dipoles in the yz -plane (Fig. 1-13). In that plane, the field vectors of both electric dipoles coincide in direction and in accordance with (1-3) they are expressed as:

$$E'_\theta = i \frac{I_y^e l k^2}{4\pi\omega\epsilon} \cos \theta \frac{e^{-ikr}}{r};$$

$$E''_\theta = i \frac{I_z^e l k^2}{4\pi\omega\epsilon} \sin \theta \frac{e^{-ikr}}{r}.$$

But $I_z^e = I_y^e e^{-i90^\circ}$, hence the total field will be

$$E_\theta = i \frac{I_y^e l k^2}{4\pi\omega\epsilon} \frac{e^{-ikr}}{r} e^{-i\theta}. \quad (1-30)$$

Thus, in the yz -plane, the amplitude of the field does not depend on the angle θ (the directional diagram is a circle) and the phase variation of the field in that plane follows the travelling-wave law, which is indicated by the factor $e^{-i\theta}$.

In the x -direction, the field vectors of both dipoles are at right angles to each other and have a 90° phase difference. Consequently, the end of the vector of the total field rotates

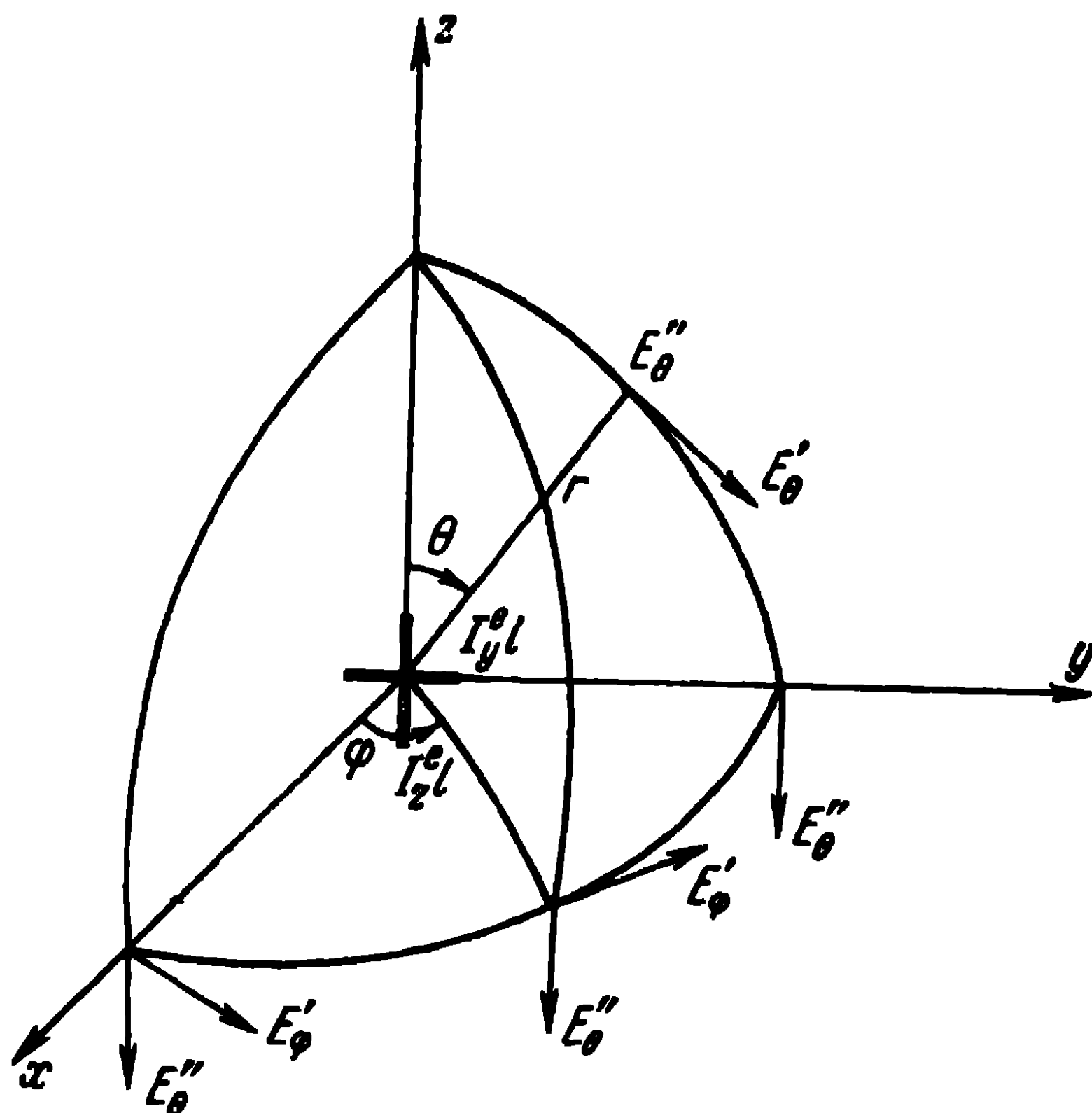


Fig. 1-13. Illustrating the calculation of the radiation of a rotating field.

in a plane perpendicular to the direction of wave propagation, i.e., a rotating field with a circular polarisation is radiated in the x -direction.

In all other cases, the crosslike arrangement under consideration radiates a rotating field with an elliptical polarisation; in particular, in the xy -plane, the radiation with a circular polarisation in the x -direction turns into a radiation with an elliptical polarisation in a direction forming a certain angle $\varphi < 90^\circ$ with the x -axis and then, into a radiation with a linear polarisation in the y -direction.

We have therefore an elementary arrangement radiating continuously in all directions; there is no direction in which the radiation would equal zero.

CHAPTER TWO

Radiation of Dipoles of Finite Length

2-1. The Electric Dipole

Let us consider the radiation of what is known as a symmetrical electric dipole, which is the simplest antenna and very often an essential element of various complex antenna systems.

A symmetrical dipole is a rectilinear cylindrical conductor of length $2l$ and radius a , fed in the centre by a high-frequency oscillator (Fig. 2-1). The high-frequency oscillator may be connected into the antenna by means of, for example, a twin feeder.

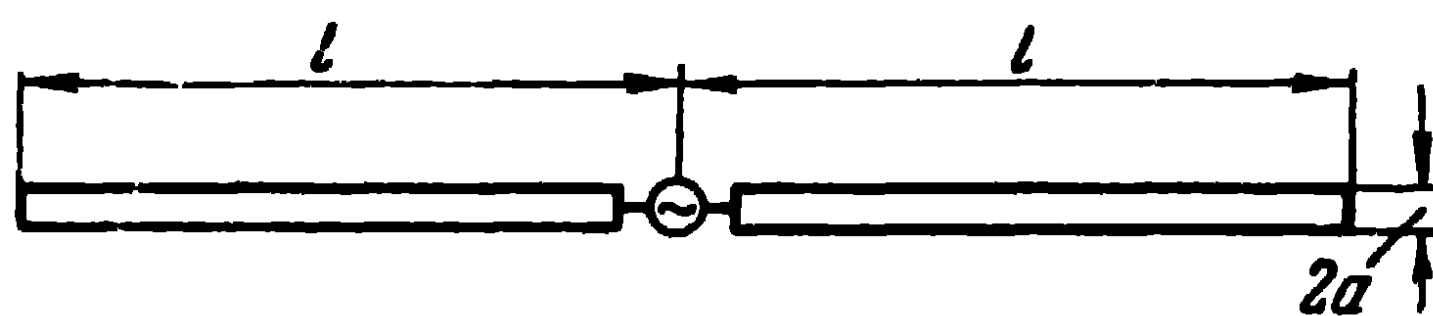


Fig. 2-1. A symmetrical dipole.

The oscillator emf will then induce in the dipole electric currents distributing them so that the electromagnetic field set up in the surrounding space may satisfy both Maxwell's equations and the boundary conditions. If, as we shall henceforward assume, the dipole is a perfect conductor (conductivity $\sigma = \infty$), the boundary conditions on the dipole surface are such that the tangential component of the electric field intensity is equal to zero everywhere but in the region of the external emf. In the region of the external emf,

i.e., where the high-frequency oscillator exerts its effect, the sum of the tangential components of the external emf and of electric field intensity is zero.

The problem of defining the electromagnetic radiation consists, first of all, in relating the current in the dipole with the electromagnetic field set up by this current. If the distribution of the current in the antenna is given, the electromagnetic field can be readily defined from the equations (1-1) and (1-4). However, the distribution of the current along the dipole is not known beforehand, and therefore the problem of defining the field in space becomes considerably more complex.

From a strict electrodynamic approach, there are two methods for solving the problem of the dipole excitation, viz., the integral equation method and the eigenfunctions method. We shall give a brief description of the former.

2-2. The Integral Equation Method

Let there be, in free space, an infinitely thin magnetic loop in the form of a ring of radius a and width b . In accordance with (1-1), the vector potential of this loop is defined as:

$$\mathbf{A}^M = \frac{1}{4\pi} \int_s \mathbf{J}^M \frac{e^{-ikR}}{R} ds, \quad (2-1)$$

where the integration is done over the loop surface and \mathbf{J}^M is the vector of the surface magnetic current density.

In the problem under consideration, the magnetic current in the cylindrical coordinates r, φ, z has only an azimuth component $J^M = J_\varphi^M$. Calculating the x - and y -components of vector \mathbf{A}^M from (2-1) and taking into account that $J_x^M = -J_\varphi^M \sin \varphi'$ and $J_y^M = J_\varphi^M \cos \varphi'$, and then that $A_\varphi^M = -A_x^M \sin \varphi + A_y^M \cos \varphi$, we obtain the following expression for the azimuth component of the vector potential of the magnetic loop:

$$A_\varphi^M(r, \varphi, z) = \frac{1}{4\pi} \int_{z' = -\frac{b}{2}}^{+\frac{b}{2}} \int_{\varphi' = 0}^{2\pi} J_\varphi^M(a, \varphi, z') \cos(\varphi' - \varphi) \times \\ \times \frac{e^{-ikR}}{R} a dz' d\varphi', \quad (2-2)$$

where

$$R = \sqrt{(z - z')^2 + r^2 + a^2 - 2ra \cos(\varphi' - \varphi)}$$

is the distance between the point of observation (r, φ, z) and the point of the sources (a, φ', z') .

Since the magnetic current J_φ^M does not depend on the angle φ , the vector potential has only an azimuth component, which, likewise, does not depend on the angle φ .

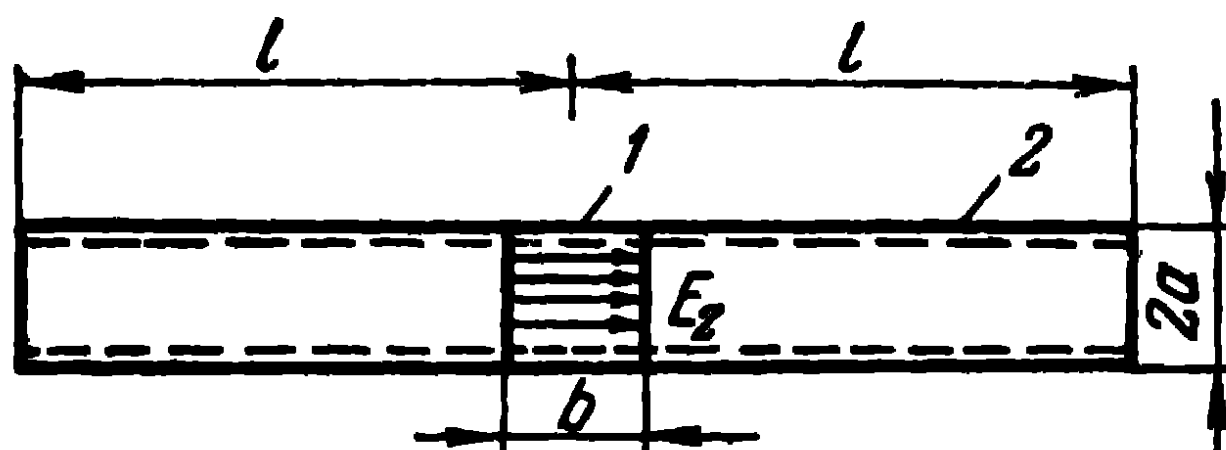


Fig. 2-2. Illustrating the integral equation method:

1—magnetic loop; 2—conducting tube

The intensity of the loop electric field is found from the expression $E^M = -\text{rot } A^M$ having both a radial component and a longitudinal component.

$$\begin{aligned} E_r^M &= \frac{\partial A_\varphi^M}{\partial z}; \\ E_z^M &= -\frac{1}{r} \frac{\partial}{\partial r} (r A_\varphi^M); \\ E_\varphi^M &= 0. \end{aligned} \quad (2-3)$$

Let us place a perfectly conducting cylinder of radius a and length $2l$ symmetrically in the magnetic loop field. Under the effect of the magnetic loop field there will be induced in the conductor such surface electric currents as will have longitudinal components J_z^e on the cylindrical conductor surface and radial components J_r^e on the conductor end plates.

To simplify the calculations and avoid taking account of the existence of electric currents on the end plates, we may regard the conductor as a tube with infinitely thin walls (Fig. 2-2). The induced currents will have then only longitudinal components, flowing along the outer as well as the inner surface of the tube. The vector potential of the induced currents has only a longitudinal component and is

expressed as:

$$A_z^e(r, \varphi, z) = \frac{1}{4\pi} \int_{z'=-l}^{+l} \int_{\varphi'=0}^{2\pi} \frac{I_z^e(z')}{2\pi a} \frac{e^{-ikR}}{R} a dz' d\varphi', \quad (2-4)$$

where I_z^e is the total current in the z -section of the conductor, equal to zero at its ends, $I_z^e(\pm l) = 0$.

The intensity of the electric field caused by the induced currents is expressed as $E^e = \frac{1}{i\omega\epsilon} (k^2 A^e + \text{grad div } A^e)$ having both a radial component and a longitudinal component

$$\begin{aligned} E_r^e &= \frac{1}{i\omega\epsilon} \frac{\partial^2 A_z^e}{\partial r \partial z}; \\ E_z^e &= \frac{1}{i\omega\epsilon} \left(k^2 A_z^e + \frac{\partial^2 A_z^e}{\partial z^2} \right); \\ E_\varphi^e &= 0. \end{aligned} \quad (2-5)$$

The electric current induced in the dipole is so distributed that the longitudinal component of the total electric field, i.e., the field of the current of the loop and that of the induced currents, is equal in magnitude and opposed in sign to the external emf on the conductor surface. We obtain then the following equations:

$$\left| \frac{\partial^2 A_z^e}{\partial z^2} + k^2 A_z^e \right|_{r=a} = i\omega\epsilon \left| \frac{1}{r} \frac{\partial}{\partial r} (r A_\varphi^M) \right|_{r=a+0} - i\omega\epsilon E_z^{\text{ext}}. \quad (2-6)$$

Here, the external emf E_z^{ext} is, in fact, the magnetic current (with the reverse sign) of the exciting loop J_φ^M . The vector potentials A_φ^M and A_z^e are expressed by (2-2) and (2-4).

Since the unknown function, i.e., the electric current I_z^e is the integrand in the expression (2-4), the equation (2-6) will be, to put it precisely, an integro-differential equation. We shall examine below the solution of the equation (2-6) in the first approximation.

2-3. Current Distribution in a Symmetrical Dipole in the First Approximation

In many practical cases, thin dipoles are utilised, i.e., dipoles of such thickness as is small in comparison with their length and that of the transmitting wave. We shall

therefore assume the radius of the dipole to be infinitely small: $\frac{a}{l} \ll 1$ and $\frac{a}{\lambda} \ll 1$. The magnitude of the vector potential A_z^e at point $z' = z$ on the surface of the conductor will therefore be determined in essence by electric currents flowing in the vicinity of point $z' = z$, and for $\frac{a}{\lambda} \rightarrow 0$, the influence of the currents flowing on the remaining portions of the dipole, can be disregarded, unless at point $z' = z$ the current is zero. We may approximate the expression (2-4), for $r = a$, as follows:

$$A_z^e = \frac{1}{4\pi} \int_{z' = z - \Delta}^{z + \Delta} I_z^e(z') \frac{e^{-ikR_1}}{R_1} dz', \quad (2-7)$$

where

$$R_1 = \sqrt{(z - z')^2 + a^2},$$

Δ is a constant, small in comparison with the wave-length. But since for $z - \Delta < z' < z + \Delta$, we may assume that $e^{-ikR_1} \approx 1$ and that the current within this interval is constant and equal to that at point $z' = z$, instead of (2-7) we have:

$$A_z^e \approx I_z^e \Omega, \quad (2-8)$$

where

$$\Omega = \frac{1}{4\pi} \int_{z' = z - \Delta}^{z + \Delta} \frac{dz'}{\sqrt{(z - z')^2 + a^2}} = \frac{1}{4\pi} \ln \frac{\sqrt{a^2 + \Delta^2} + \Delta}{\sqrt{a^2 + \Delta^2} - \Delta}.$$

Assuming that $a \ll \Delta$, we obtain:

$$\Omega = \frac{1}{2\pi} \ln \frac{2\Delta}{a}. \quad (2-9)$$

It follows from (2-9) that with vanishing a the quantity Ω will tend towards infinity, the expression (2-8) becoming more and more accurate as the remaining part of the (2-4) integral becomes finite.

We shall further suppose that the external emf is applied to an infinitely small section of wire in the centre of the dipole. And since the radius of the wire a is small in comparison with the wave-length, the effect of the magnetic loop may be replaced by that of an equivalent electric dipole, assuming the dipole moment, in accordance with (1-21), to

be equal to $I_z^e l = -i\omega \epsilon J_\varphi^M b\pi a^2$. The vector potential of this dipole has a finite magnitude small in comparison with that defined by (2-8) at all points of the wire, except those in the region of the external emf.

Thus, for all points of the antenna, except those at which an external emf is applied and where the current may equal zero, the integro-differential equation (2-6) may be approximated to the following differential equation:

$$\frac{d^2 I_z^e}{dz^2} + k^2 I_z^e = 0. \quad (2-10)$$

This is a so-called telegraph equation, valid for a long lossless line. Taking into account that the current at the ends of the antenna equals zero and designating the current at the feed points of the antenna by I_0 , the solution of the equation (2-10) may be expressed as:

$$I_z^e = I_0 \frac{\sin k(l - |z|)}{\sin kl}. \quad (2-11)$$

We may also obtain with the same approximation the distribution of the electric charge in the antenna. Making use of the continuity equation (1-3), which, for the linear current, is written as:

$$\frac{dI_z^e}{dz} + i\omega Q = 0,$$

where Q is the charge per unit length of dipole, we obtain:

$$Q_{z>0} = \frac{k}{i\omega} I_0 \frac{\cos k(l-z)}{\sin kl}, \quad Q_{z<0} = -\frac{k}{i\omega} I_0 \frac{\cos k(l+z)}{\sin kl}. \quad (2-12)$$

Thus, in a thin antenna, the current and charge are approximately distributed in accordance with the sine law. As follows, however, from the very analysis which led to the expression (2-11), with the radius of the wire tending towards zero the current distribution only nears a sinusoidal distribution, without ever actually becoming sinusoidal. The expression (2-11), in particular, is not valid for current nodes, in which the current neither obeys the sine law, nor is equal to zero.

In the majority of cases met with in antenna theory, the current in a symmetrical dipole is assumed distributed in

accordance with (2-11). This assumption considerably simplifies all the calculations and in most cases the results obtained are close to those real.

It follows from (2-11) and (2-12) that:

a) current nodes (zeros) and charge antinodes are set up at the ends of the antenna;

b) current antinodes and charge nodes (zeros) are set up at the distance of a quarter of a wave-length from the dipole ends. Then, yet another quarter of a wave-length farther, current nodes and charge antinodes are set up in the same way, etc.;

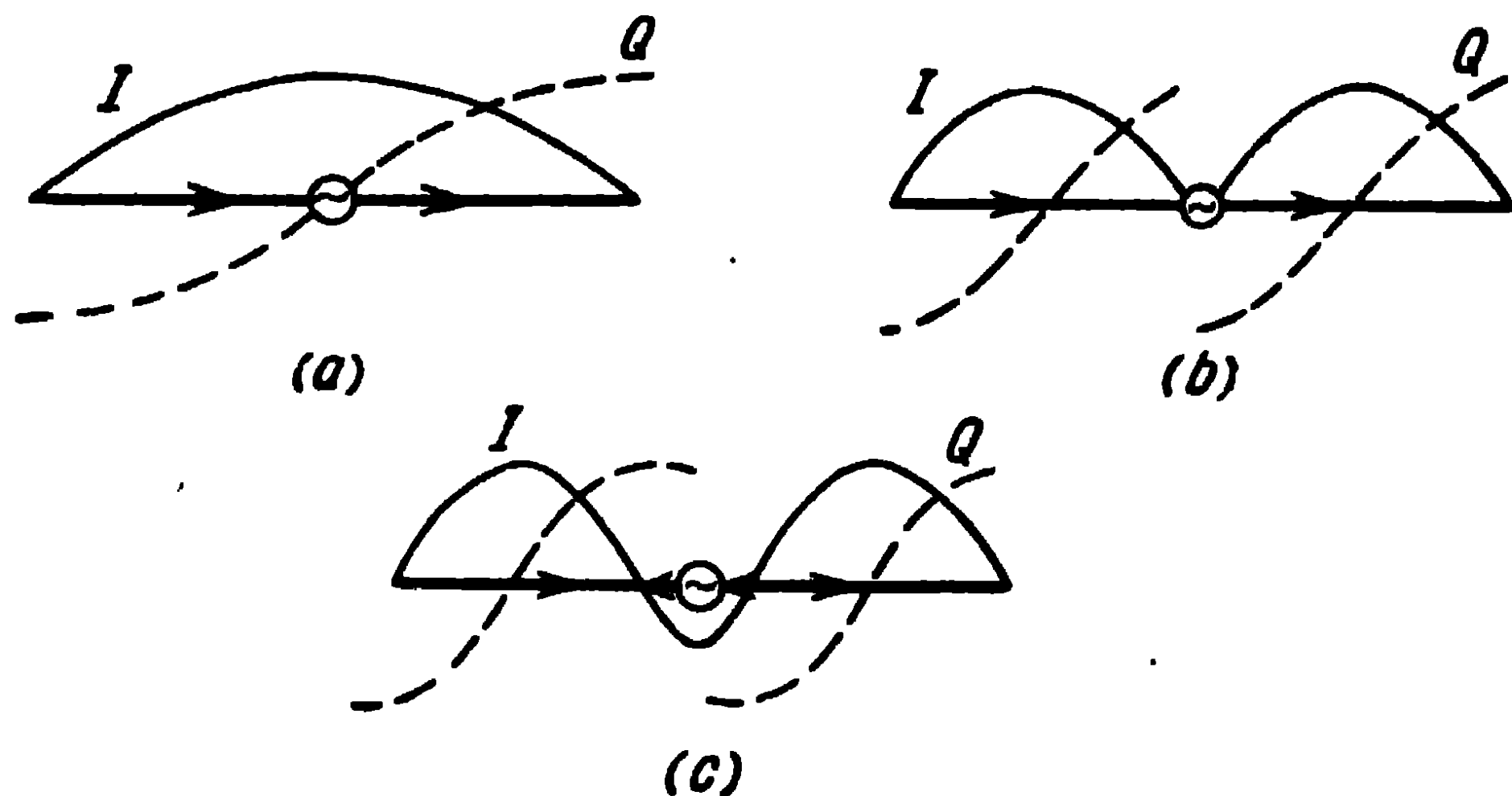


Fig. 2-3. Current and charge distribution in a symmetrical dipole:

$$a-l = \frac{\lambda}{4}; \quad b-l = \frac{\lambda}{2}; \quad c-l = \frac{5\lambda}{8}$$

c) the current and charge at every point of the dipole are 90° out of phase;

d) a current antinode, node or some intermediate value, is set up at the feed points of the dipole, depending on the relation of the dipole length to the wave-length;

e) along the dipole the phases of current and charge change by 180° when passing through zero.

A number of characteristic current and charge distributions along a dipole is given in Fig. 2-3. It should be noted that a symmetrical dipole with an overall length of $2l$ equal to half a wave-length is known as a half-wave dipole. A dipole of $2l$ length equal to a full wave-length is known as a wave dipole.

Throughout this course we shall assume that the current unless otherwise specified is distributed in accordance with the sine law.

2-4. Field Intensity of the Dipole in the Radiation Zone

Let the current distribution in the dipole be given. We can then determine the field of the antenna at any point of space, including very distant ones, i.e., in the radiation zone. Furthermore, since the antenna is thin, we shall neglect the radiation of the magnetic current caused by the discontinuity in the centre of the antenna.

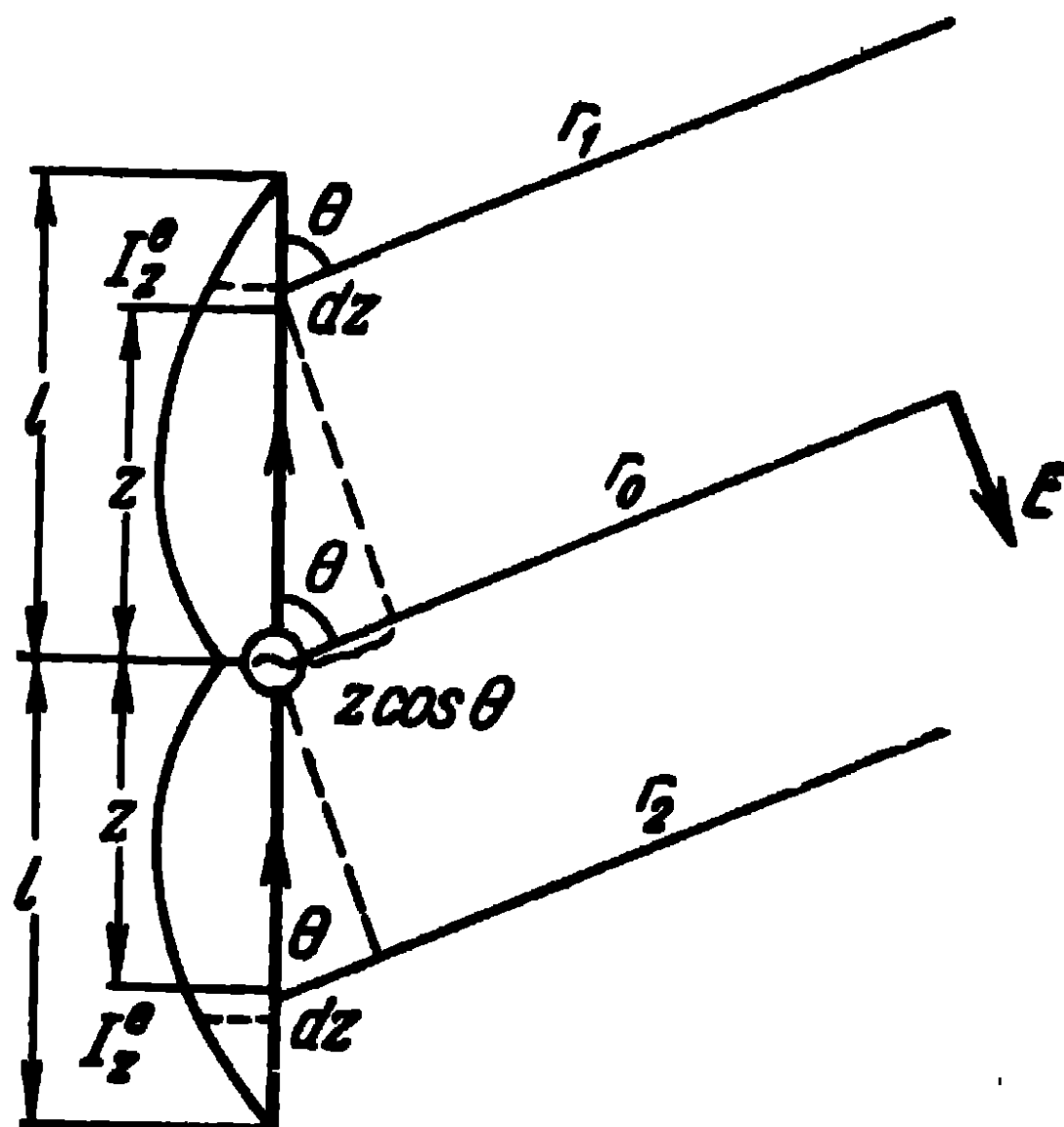


Fig. 2-4. Explaining the calculation of the field intensity of a symmetrical antenna.

Turning to Fig. 2-4, let us mark out at the point z of the wire an element of length dz . In accordance with (1-3), the intensity of the electric field caused by the element dz of the antenna in the zone of radiation equals:

$$dE_1 = i \frac{I_z^e dz k^2}{4\pi\omega\epsilon r_1} \sin \theta e^{-ikr_1}. \quad (2-13)$$

The field intensity caused by another element dz lying symmetrically to the first one relatively to the centre of the antenna, at the same point in space equals:

$$dE_2 = i \frac{I_z^e dz k^2}{4\pi\omega\epsilon r_2} \sin \theta e^{-ikr_2}. \quad (2-14)$$

We assume directions r_1 and r_2 to be parallel, since the point of observation is infinitely distant and at any rate lies at a distance considerably greater than the length of the antenna.

Substituting the expression of the current at the point $z = l - z = l_0 \frac{\sin k(l-z)}{\sin kl}$ into the expressions (2-13) and (2-14) and adding up these expressions, we obtain:

$$dE = dE_1 + dE_2 = i \frac{l_0 dz k^2}{4\pi\omega\epsilon} \sin\theta \frac{\sin k(l-z)}{\sin kl} \left[\frac{e^{-ikr_1}}{r_1} + \frac{e^{-ikr_2}}{r_2} \right].$$

Taking further into account that

$$\begin{aligned} \frac{1}{r_1} &\approx \frac{1}{r_2} \approx \frac{1}{r_0}; \\ r_1 &= r_0 - z \cos\theta, \\ r_2 &= r_0 + z \cos\theta \end{aligned}$$

and that

$$\sin k(l-z) = \frac{1}{2i} [e^{ik(l-z)} - e^{-ik(l-z)}],$$

we obtain

$$\begin{aligned} dE &= \frac{l_0 dz k^2 \sin\theta}{8\pi\omega\epsilon \sin kl r_0} e^{-ikr_0} [e^{ik(l-z)} - e^{-ik(l-z)}] \times \\ &\quad \times [e^{ikz \cos\theta} + e^{-ikz \cos\theta}]. \end{aligned}$$

Integrating this expression along the length of the antenna from $z=0$ to $z=l$, we have:

$$E = i \frac{60 l_0}{r_0 \sin kl} e^{-ikr_0} \frac{\cos(kl \cos\theta) - \cos kl}{\sin\theta}, \quad (2-15)$$

where we have substituted for vacuum $\frac{k}{2\pi\omega\epsilon} = 60$.

The expression (2-15) defines the electric field intensity of a symmetrical antenna in the radiation zone. In particular, for a half-wave antenna $(l = \frac{\lambda}{2})$, this expression becomes:

$$E = i \frac{60 l_0}{r_0} e^{-ikr_0} \frac{\cos\left(\frac{\pi}{2} \cos\theta\right)}{\sin\theta}. \quad (2-16)$$

The curves described by (2-15) and giving the dependence of the values of the intensity of field E on the angle of observation θ , are known as the directional diagrams (characteristics) of the antenna in its meridional plane. Directional diagrams are usually erected in polar coordinates (sometimes in Cartesian ones).

It should be pointed out that, owing to axial symmetry, the radiation in the equatorial plane of the antenna is uniform and therefore, the directional diagram of the antenna in that plane represents a circle, in polar coordinates.

It should be further pointed out that the field intensity phase does not depend on the angle of observation θ and to an observer in the zone of radiation, the waves seem to

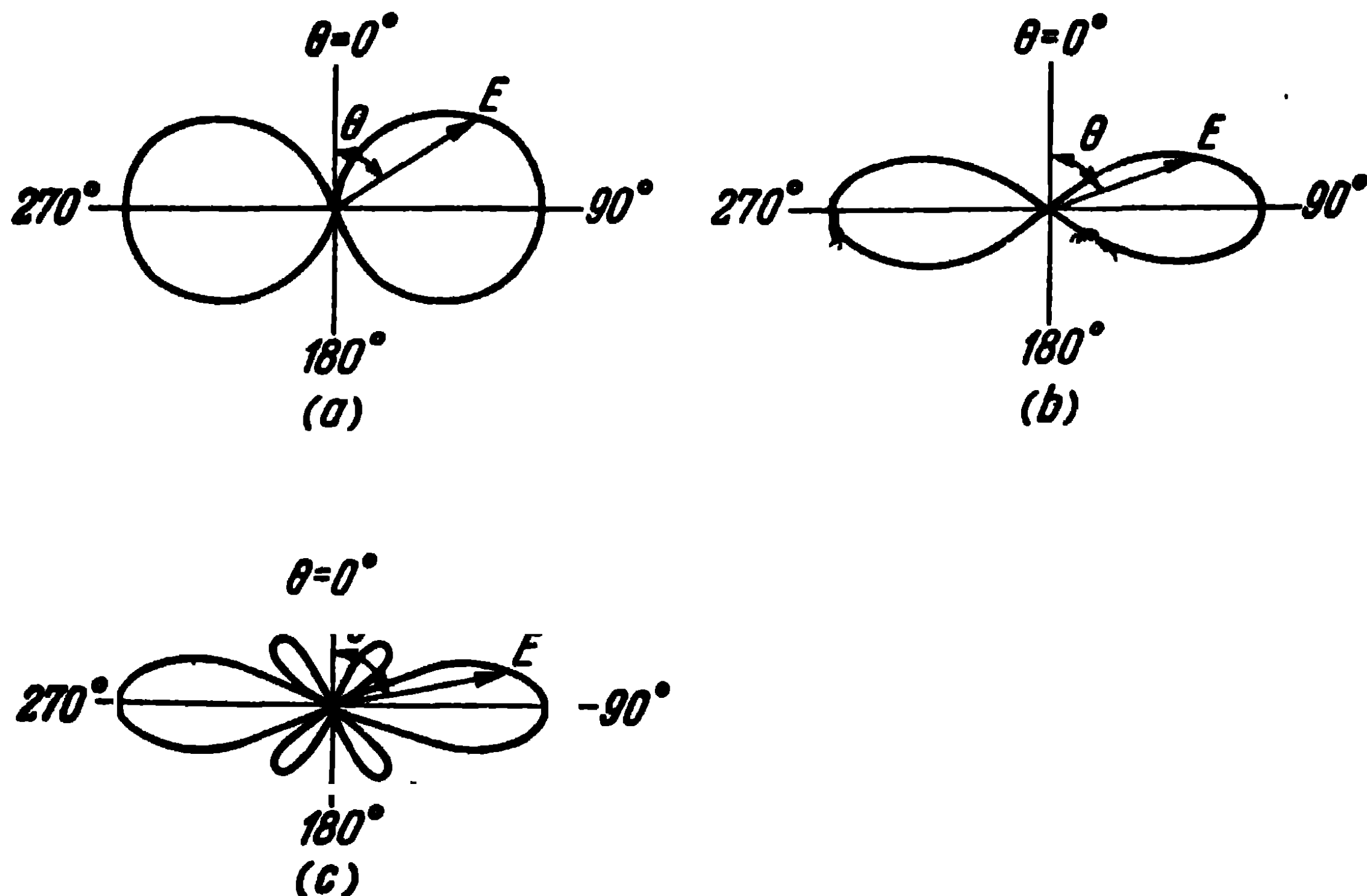


Fig. 2-5. Directional diagrams of a symmetrical antenna:

- $a-l = \frac{\lambda}{4}$; angle of aperture of 80° ;
- $b-l = \frac{\lambda}{2}$, angle of aperture of 44° ;
- $c-l = \frac{5}{8} \lambda$, angle of aperture of 31° .

originate from a point coinciding with the centre of the antenna. This point is usually referred to as the antenna phase centre.

Fig. 2-5 gives the directional diagrams of the antenna in its meridional plane for three particular cases: $l = \frac{\lambda}{4}$, $l = \frac{\lambda}{2}$ and $l = \frac{5}{8} \lambda$. The same figure gives the values of the angles of aperture of the directional diagrams, i.e., of the angles within the limits of which the field intensity does not fall by more than $\sqrt{2}$ times below the field intensity in the direction of the maximum radiation. This aperture angle is

often referred to as the half-power width of the directional diagram.

An analysis of the expression (2-15) and of the curves in Fig. 2-5 shows that, when $2l < \lambda < 4l$, the directional diagram has only one lobe, with its maximum in the direction which forms with the axis of the antenna an angle $\theta = 90^\circ$. As the wave-length diminishes, this lobe becomes narrower (the angle of aperture of the directional diagram becomes smaller). When $l > \frac{\lambda}{2}$, the major (main) lobe of the directional diagram becomes still narrower and there appear, in addition, minor (side) lobes. With a further decrease of the wave-length, the major lobe begins to decrease, whereas the additional minor lobes increase. Thus, when, for example, $l = \lambda$, the radiation vanishes in the direction $\theta = 90^\circ$.

It should be noted that in the direction of the antenna axis, just as in the direction of the dipole axis, the radiation is always zero.

2-5. Calculating Power Radiated by an Antenna by the Poynting Vector Method

Let us consider the power radiated by a symmetrical antenna. Using the Poynting vector method, let us calculate the power radiated through a sphere whose centre coincides with that of the antenna. Furthermore, the sphere radius is taken such as to ensure that the surface of the sphere is in the zone of radiation.

The average power flow conveyed through a unit area perpendicular to the direction of the power motion is expressed by the Poynting vector

$$\mathbf{S} = \frac{1}{2} [\mathbf{E}, \mathbf{H}^*]. \quad (1-10)$$

Since in the zone of radiation, the vector \mathbf{E} is in phase with the vector \mathbf{H} (in the case of a lossless medium) and their relation is equal to the intrinsic resistance of space, we have

$$|\mathbf{S}| = \frac{EE^*}{240\pi}, \quad (2-17)$$

furthermore, the only component of vector \mathbf{S} is perpendicular to the surface of the sphere.

The power radiated by the antenna is expressed as:

$$P_{\Sigma} = \frac{1}{240\pi} \int E E^* ds, \quad (2-18)$$

where ds is defined in spherical coordinates by the expression $ds = r_0^2 \sin \theta d\theta d\varphi$ (Fig. 2-6).

Substituting into (2-18) the expression for E from (2-15), we obtain:

$$P_{\Sigma} = \frac{30I_0^2}{\sin^2 kl} \int_0^{\pi} \frac{[\cos(kl \cos \theta) - \cos kl]^2}{\sin \theta} d\theta. \quad (2-19)$$

If we relate the radiated power to the square of the current at the antinode of the antenna $I_a = \frac{I_0}{\sin kl}$ (here and further on we have in mind the current amplitude values), we obtain a quantity expressed in ohms and known as the radiation resistance of the antenna:

$$R_{\Sigma a} = \frac{2P_{\Sigma}}{I_a^2}. \quad (2-20)$$

The integration of the expression (2-19) leads to the following expression for the radiation resistance of the antenna (related to the current antinode), first obtained by Ballantyne in 1924 [1]:

$$R_{\Sigma a} = 30 \{ 2[C + \ln 2kl - \text{Ci } 2kl] + \cos 2kl [C + \ln kl + \text{Ci } 4kl - 2\text{Ci } 2kl] + \sin 2kl [\text{Si } 4kl - 2\text{Si } 2kl] \}, \quad (2-21)$$

where $C = 0.5772$ is the Euler's constant;

$$\text{Si } x = \int_0^x \frac{\sin u}{u} du, \text{ the integral sine;}$$

$$\text{Ci } x = - \int_x^{\infty} \frac{\cos u}{u} du, \text{ the integral cosine.}$$

The integral sines and cosines can be expressed by the following series [2]:

$$\begin{aligned} \text{Si } x &= x - \frac{1}{3} \frac{x^3}{3!} + \frac{1}{5} \frac{x^5}{5!} - \dots, \\ \text{Ci } x &= C + \ln x - \frac{1}{2} \frac{x^2}{2!} + \frac{1}{4} \frac{x^4}{4!} - \dots \end{aligned}$$

As can be seen from (2-21), the radiation resistance of a symmetrical antenna depends on the ratio of the length of the antenna to the wave-length. Thus, for example, the

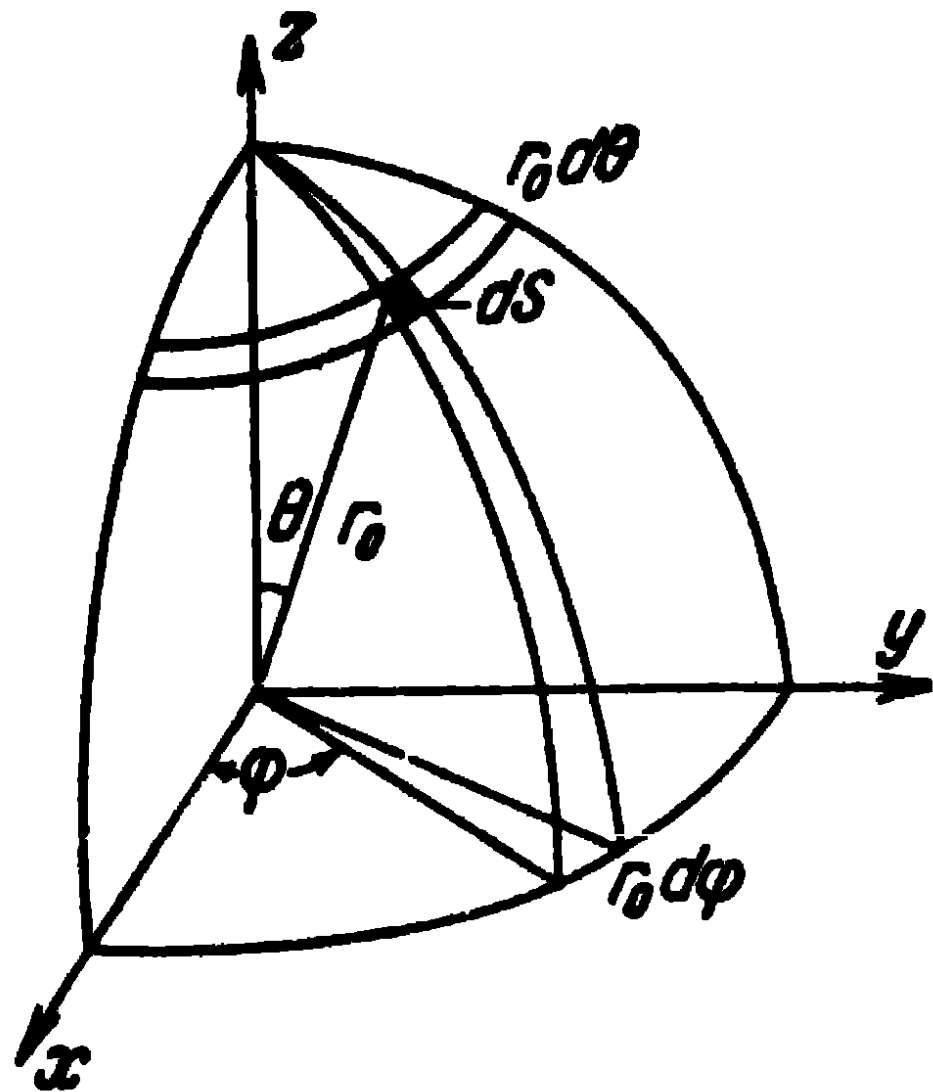


Fig 2 6 Explaining the calculation of the radiated power

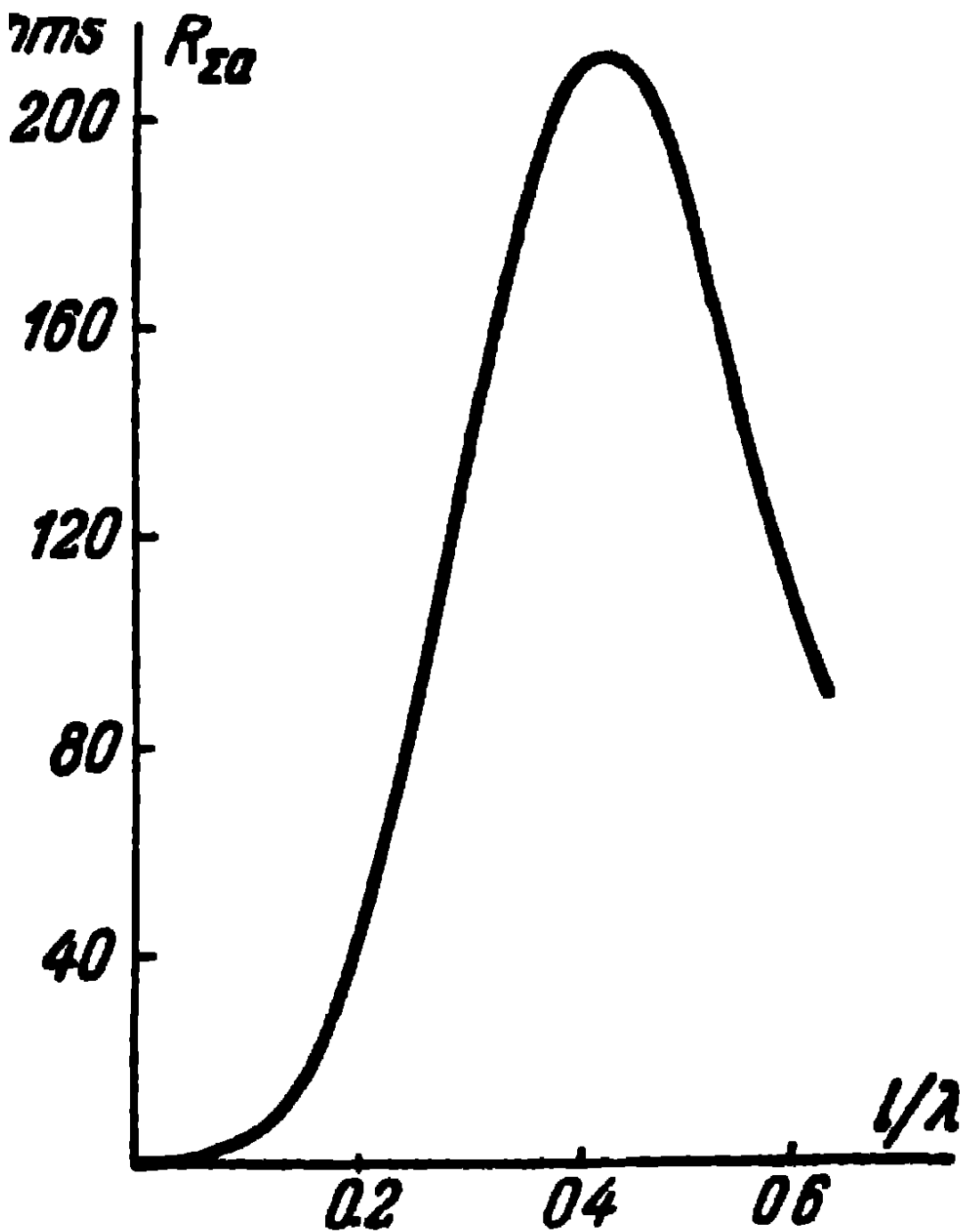


Fig 2 7 Radiation resistance of symmetrical antenna

radiation resistance of a half-wave antenna ($\frac{l}{\lambda}=0.25$) is 73.1 ohms and the radiation resistance of a wave antenna ($\frac{l}{\lambda}=0.5$) is 199 ohms

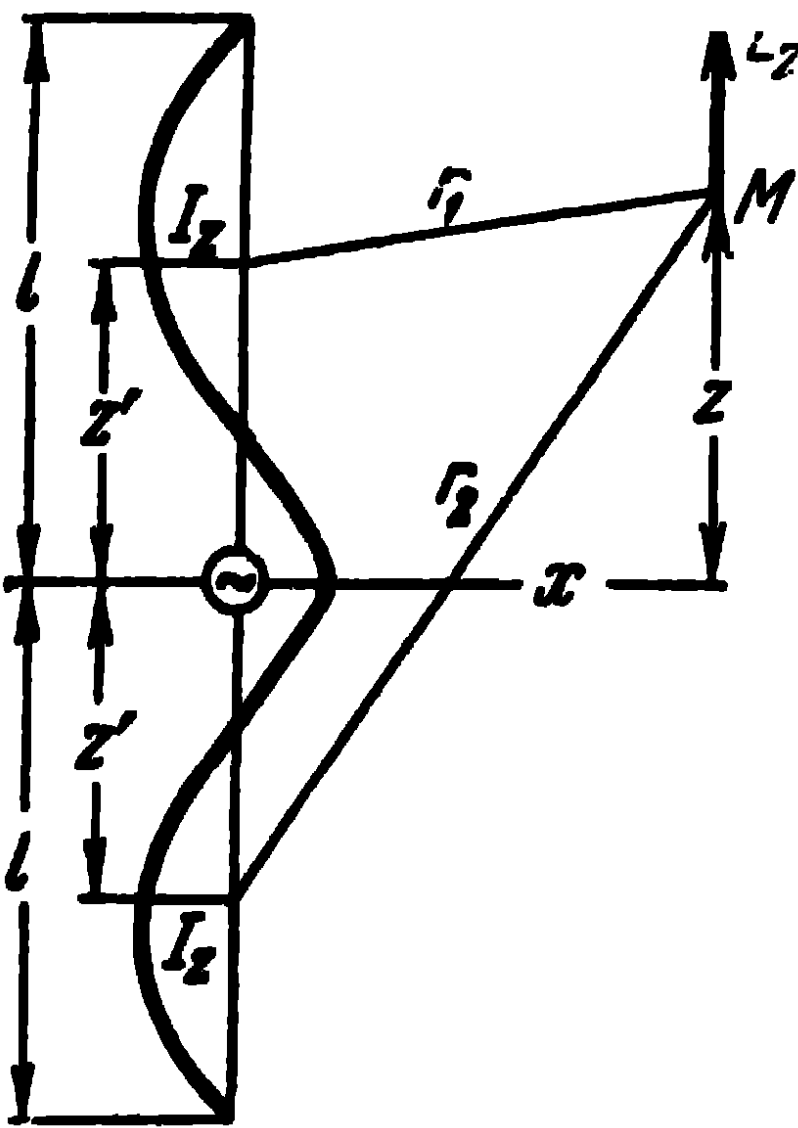
Table 2-1

l/λ	$R_{\Sigma a}$ ohms	l/λ	$R_{\Sigma a}$ ohms	l/λ	$R_{\Sigma a}$ ohms	l/λ	$R_{\Sigma a}$ ohms	l/λ	$R_{\Sigma a}$ ohms	l/λ	$R_{\Sigma a}$ ohms
0 125	6 4	0 225	54	0 325	144	0 425	209	0 525	185	0 625	105
0 150	13	0 250	73 1	0 350	168	0 450	212	0 550	166	0 650	93
0 175	23	0 275	96	0 375	187	0 475	210	0 575	145	0 675	87
0 200	36	0 300	120	0 400	200	0 500	199	0 600	127	0 700	85

The values of the radiation resistances of a symmetrical antenna situated in free space, related to the current anti-node, for a number of values of $\frac{l}{\lambda}$ are given in Table 2-1 and Fig. 2-7.

2-6. Field Intensity in the Vicinity of the Antenna

We have been considering the field intensity of the antenna in the zone of radiation. Knowing this field has enabled us to define the radiation intensity of a symmetrical antenna in various directions, as well as the power radiated by this antenna. Now, let us investigate the field intensity in the vicinity of the symmetrical antenna. Here again, since the



antenna has a small radius, we shall neglect the radiation of the magnetic field in the gap of the antenna.

Let us, to begin with, find the component of the electric field intensity parallel to the axis of the antenna. In accordance with (1-4), this component is expressed as:

$$E_z = \frac{1}{i\omega\epsilon} \left(k^2 A_z^e + \frac{d^2 A_z^e}{dz^2} \right). \quad (2-22)$$

The vector potential at point M (Fig. 2-8) equals:

Fig. 2-8. Explaining the calculation of the field in the vicinity of the antenna.

$$A^e = \frac{1}{4\pi} \int_{z'=0}^l I_z \left(\frac{e^{-ikr_1}}{r_1} + \frac{e^{-ikr_2}}{r_2} \right) dz'. \quad (2-23)$$

The integration in (2-23) extends from $z' = 0$ to $z' = l$, since we have taken account of the currents symmetrically distant from the centre of the antenna and situated at distances $r_1 = \sqrt{x^2 + (z - z')^2}$ and $r_2 = \sqrt{x^2 + (z + z')^2}$ from the point of observation M. Substituting (2-23) into (2-22) and taking into account that

$$\frac{\partial^2 r_1}{\partial z^2} = \frac{\partial^2 r_1}{\partial z'^2}, \quad \frac{\partial^2 r_2}{\partial z^2} = \frac{\partial^2 r_2}{\partial z'^2},$$

we obtain:

$$E_z = \frac{1}{i\omega\epsilon 4\pi} \int_{z'=0}^l \left\{ I_z \frac{\partial^2}{\partial z'^2} \left(\frac{e^{-ikr_1}}{r_1} + \frac{e^{-ikr_2}}{r_2} \right) + k^2 I_z \left(\frac{e^{-ikr_1}}{r_1} + \frac{e^{-ikr_2}}{r_2} \right) \right\} dz'.$$

Twice integrating this last expression by parts, we find:

$$E_z = \frac{1}{i\omega\epsilon 4\pi} \left[I_z \frac{\partial}{\partial z'} \left(\frac{e^{-lkr_1}}{r_1} + \frac{e^{-lkr_2}}{r_2} \right) \right]_{z'=0}^l -$$

$$- \frac{1}{i\omega\epsilon 4\pi} \left[\frac{\partial I_z}{\partial z'} \left(\frac{e^{-lkr_1}}{r_1} + \frac{e^{-lkr_2}}{r_2} \right) \right]_{z'=0}^l +$$

$$+ \frac{1}{i\omega\epsilon 4\pi} \int_{z'=0}^l \left(\frac{d^2 I_z}{dz'^2} + k^2 I_z \right) \left(\frac{e^{-lkr_1}}{r_1} + \frac{e^{-lkr_2}}{r_2} \right) dz'.$$

Taking into account that the current at the ends of the antenna equals zero and that, on the other hand,

$$\frac{\partial}{\partial z'} \left(\frac{e^{-lkr_1}}{r_1} + \frac{e^{-lkr_2}}{r_2} \right)$$

when $z'=0$, also equals zero we have:

$$E_z = - \frac{1}{i\omega\epsilon 4\pi} \left[\frac{dI_z}{dz} \right]_{z=l} \left(\frac{e^{-lkr_1}}{R_1} + \frac{e^{-lkr_2}}{R_2} \right) +$$

$$+ \frac{2}{i\omega\epsilon 4\pi} \left[\frac{dI_z}{dz} \right]_{z=0} \frac{e^{-lkr_0}}{R_0} +$$

$$+ \frac{1}{i\omega\epsilon 4\pi} \int_{z'=0}^l \left(\frac{d^2 I_z}{dz'^2} + k^2 I_z \right) \left(\frac{e^{-lkr_1}}{r_1} + \frac{e^{-lkr_2}}{r_2} \right) dz', \quad (2-24)$$

where $R_1 = \sqrt{x^2 + (z-l)^2}$ is the distance from the upper end of the antenna to the point of observation M ;
 $R_2 = \sqrt{x^2 + (z+l)^2}$, the distance from the lower end of the antenna to the point of observation M ;
 $R_0 = \sqrt{x^2 + z^2}$, the distance from the centre of the antenna to the same point M .

Assuming the sine distribution of the current along the antenna

$$I_z = I_0 \frac{\sin k(l-z)}{\sin kl},$$

we obtain:

$$\left[\frac{dI_z}{dz} \right]_{z=l} = - \frac{kI_0}{\sin kl}, \quad \left[\frac{dI_z}{dz} \right]_{z=0} = -kI_0 \frac{\cos kl}{\sin kl}.$$

Thus, in the vicinity of a thin antenna, the longitudinal component of the electric field intensity, i.e., the component parallel to the axis of the wire, may be represented

as follows:

$$E_z = -i \frac{30I_0}{\sin kl} \left\{ \frac{e^{-ikR_1}}{R_1} + \frac{e^{-ikR_2}}{R_2} - 2 \cos kl \frac{e^{-ikR_0}}{R_0} \right\}, \quad (2-25)$$

where account is taken of the fact that for vacuum, $\frac{k}{\omega \epsilon 4\pi} = 30$.

It follows from the expression (2-25) that the intensity of the electric field E_z on the surface of the antenna (when $x=a$) does not equal zero. As an example, Fig. 2-9 shows the distribution of $E_z(a)$ along a half-wave antenna ($l = \frac{\lambda}{4}$).

We see that the resistive component, i.e., the component of the electric field intensity, which is in phase with the current, remains almost constant along the whole length of the antenna, whereas the reactive component, i.e., the component of the electric field intensity which is in phase with the current, tends towards infinity at the ends of the antenna when $a \rightarrow 0$. Actually, however, the tangential component of the electric field intensity $E_z(a)$ must be equal to zero on the surface of the antenna. But we

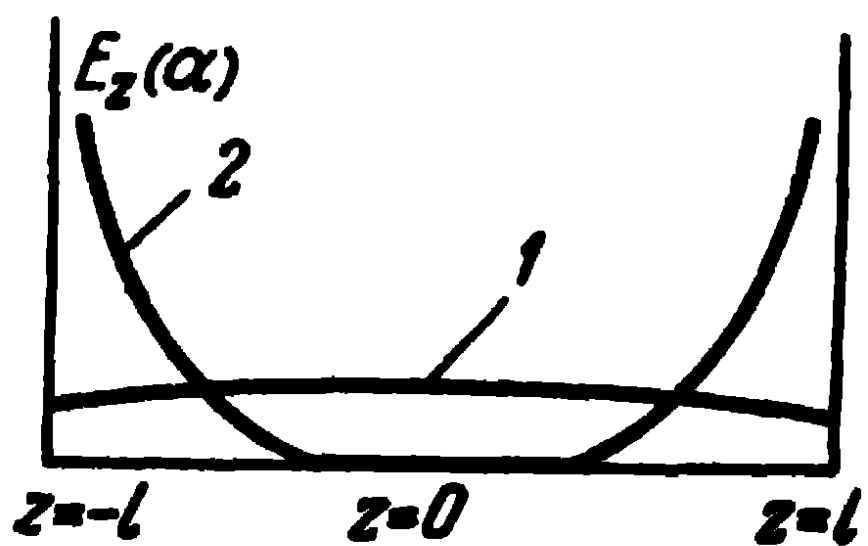


Fig. 2-9. Distribution of resistive and reactive components of field intensity along antenna; 1—resistive component, 2—reactive component

assumed a sinusoidal, i.e., an approximate distribution of the current along the antenna and we have, furthermore, neglected the magnetic field current in the gap of the antenna; that is why the component $E_z(a)$ should not vanish on the surface of the antenna even though the latter is assumed to be an ideal conductor.

Let us now find (in the cylindrical coordinates x, φ, z) the other components of the electromagnetic field intensity, viz., E_x , i.e., the normal component of the electric field intensity and H_φ , the azimuth component of the magnetic field intensity.

It follows from the first Maxwell's equation in cylindrical coordinates that

$$\begin{aligned} i\omega \epsilon E_z &= \frac{1}{x} \frac{\partial}{\partial x} (x H_\varphi), \\ i\omega \epsilon E_x &= -\frac{\partial H_\varphi}{\partial z}. \end{aligned} \quad (2-26)$$

Writing (2-25) as:

$$E_z = \frac{30I_0}{k \sin kl} \frac{1}{x} \frac{\partial}{\partial x} \left\{ e^{-ikR_1} + e^{-ikR_2} - 2 \cos kl e^{-ikR_0} \right\}$$

and comparing with (2-26), we obtain:

$$H_{\varphi} = i \frac{I_0}{4\pi x \sin kl} \{ e^{-ikR_1} + e^{-ikR_2} - 2 \cos k l e^{-ikR_0} \}, \quad (2-27)$$

where an equivalent quantity $\frac{1}{120\pi}$ has been substituted for the factor $\frac{\omega\epsilon}{k}$.

Substituting now (2-27) into the expression for E_x (2-26), we have:

$$E_x = i \frac{30I_0}{x \sin kl} \left\{ \frac{e^{-ikR_1}}{R_1} (z-l) + \frac{e^{-ikR_2}}{R_2} (z+l) - 2 \cos kl \frac{e^{-ikR_0}}{R_0} z \right\}. \quad (2-28)$$

Equations (2-27) and (2-28) express the magnetic field intensity and the normal component of the electric field intensity in the vicinity of a symmetrical antenna.

It should be noted that in the case of an antenna whose radius tends towards zero, the normal component of the electric field intensity on the surface of the antenna, expressed by (2-28), tends towards infinity, whereas the tangential component of the electric field intensity, expressed by (2-25), remains finite everywhere except at the ends of the antenna. Thus the vector of the electric field intensity is almost perpendicular to the axis of the antenna. This enables to assert that the approximate sinusoidal current distribution along the antenna provides a distribution of the electromagnetic field in the space surrounding the antenna (including the wave zone) close to reality.

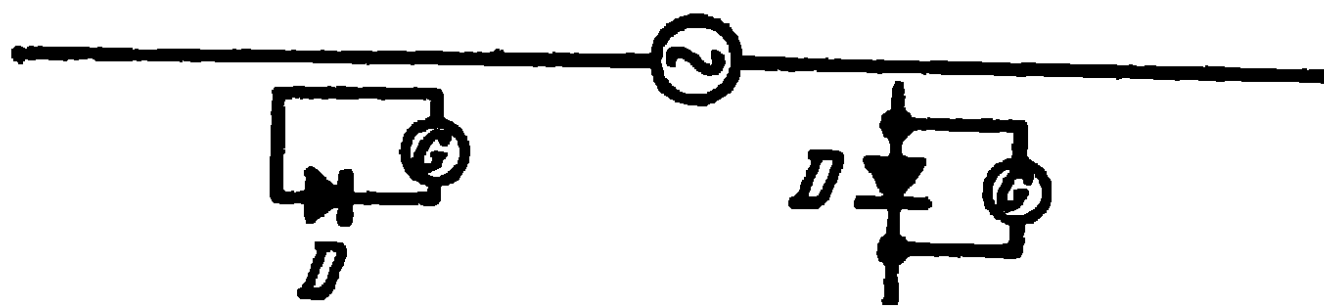


Fig 2 10 Methods of measuring current and charge in an antenna

It should be noted that the magnetic field intensity on the antenna surface determines the current in the antenna while the normal component of the electric field determines its charge. This results from the following equations:

$$\begin{aligned} I_s &= 2\pi a H_{\varphi}(a), \\ Q_s &= 2\pi a \epsilon E_x(a), \end{aligned} \quad (2-29)$$

where $H_\varphi(a)$ and $E_x(a)$ are the intensities of the magnetic and electric fields on the surface of the antenna at the point of observation.

The expressions (2-29) enable the experimental definition of the current and charge distribution along the antenna. A loop may be used to measure the current and a dipole to measure the distribution of the charge; their position is shown in Fig. 2-10. The dimensions of the loop and dipole should be small in comparison with the length of the antenna and the wave-length, otherwise the field will be distorted and the measurement inaccurate.

Incidentally, the expressions (2-29) show that for a given magnitude of the current (and consequently also of the charge), the magnetic field intensity and the normal component of the electric field intensity on the surface of the antenna increase as the radius of the antenna decreases.

2-7. Calculating the Power Radiated by an Antenna by the Induced EMF Method. Input Resistance of a Symmetrical Antenna

In the Poynting vector method, the integration was performed over a spherical surface of an infinitely large radius. However, since the space surrounding the antenna is free, we may perform the integration over any surface enclosing the antenna in order to calculate the power radiated by the antenna.

The surface is a cylinder with height $2L$ and radius x ; a symmetrical antenna is placed in the centre of the cylinder along its axis (Fig. 2-11). Let us examine the Poynting vector on the surface of this cylinder. The normal components of the Poynting vector in cylindrical coordinates are expressed as:

$$\begin{aligned} S_x &= -\frac{1}{2}E_z H_\varphi^*; \\ S_z &= \frac{1}{2}E_x H_\varphi^*. \end{aligned} \tag{2-30}$$

Evidently, the integral of the normal component of the Poynting vector over the surface of the cylinder defines the power fed to the antenna and radiated by it. Moreover, since E and H are no longer in phase, as was the case in the radiation zone [see equations (2-25), (2-27) and (2-28)], the

power is expressed in complex form, i.e., it has an active component (radiated power) as well as a reactive one (power oscillating in the vicinity of the antenna).

Let the cylindrical surface under consideration coincide with the antenna surface, i.e., let us assume that $x=a$, $L=l$. Then, when the radius of the antenna a tends towards zero, the integrals over the upper and lower bases of the cylinder (antenna) will tend towards zero and the power is defined by integrating only over the lateral surface of the cylinder (antenna):

$$P = 2 \int_{z=0}^l \int_{\varphi=0}^{2\pi} S_x a dz d\varphi. \quad (2-31)$$

Substituting into (2-31) the expression S_x from (2-30) and taking account of the fact that the field does not depend on the coordinate φ , we obtain:

$$P = - \int_{z=0}^l E_z(a) 2\pi a H_\varphi^* dz. \quad (2-32)$$

Taking further into account that $2\pi a H_\varphi^* = I_z^*$, instead of (2-32) we have

$$P = - \int_{z=0}^l E_z(a) I_z^* dz. \quad (2-33)$$

Thus, in order to define the power radiated by the antenna, we must take the product of the current by the tangential component of the electric field intensity on the surface of the antenna and integrate this product along the antenna. Since the electric field intensity on the surface of the antenna $E_z(a)$ is, in fact, the emf per unit length of the antenna induced by the current in the antenna, this method of computing the power is known as the induced emf method. The induced emf method was proposed simultaneously by D. A. Rozhansky [3] and L. Brillouin [4], and later applied to antennas by I. G. Klyatskin [5].

It should be noted that, actually, on the surface of the antenna, the tangential component of the electric field

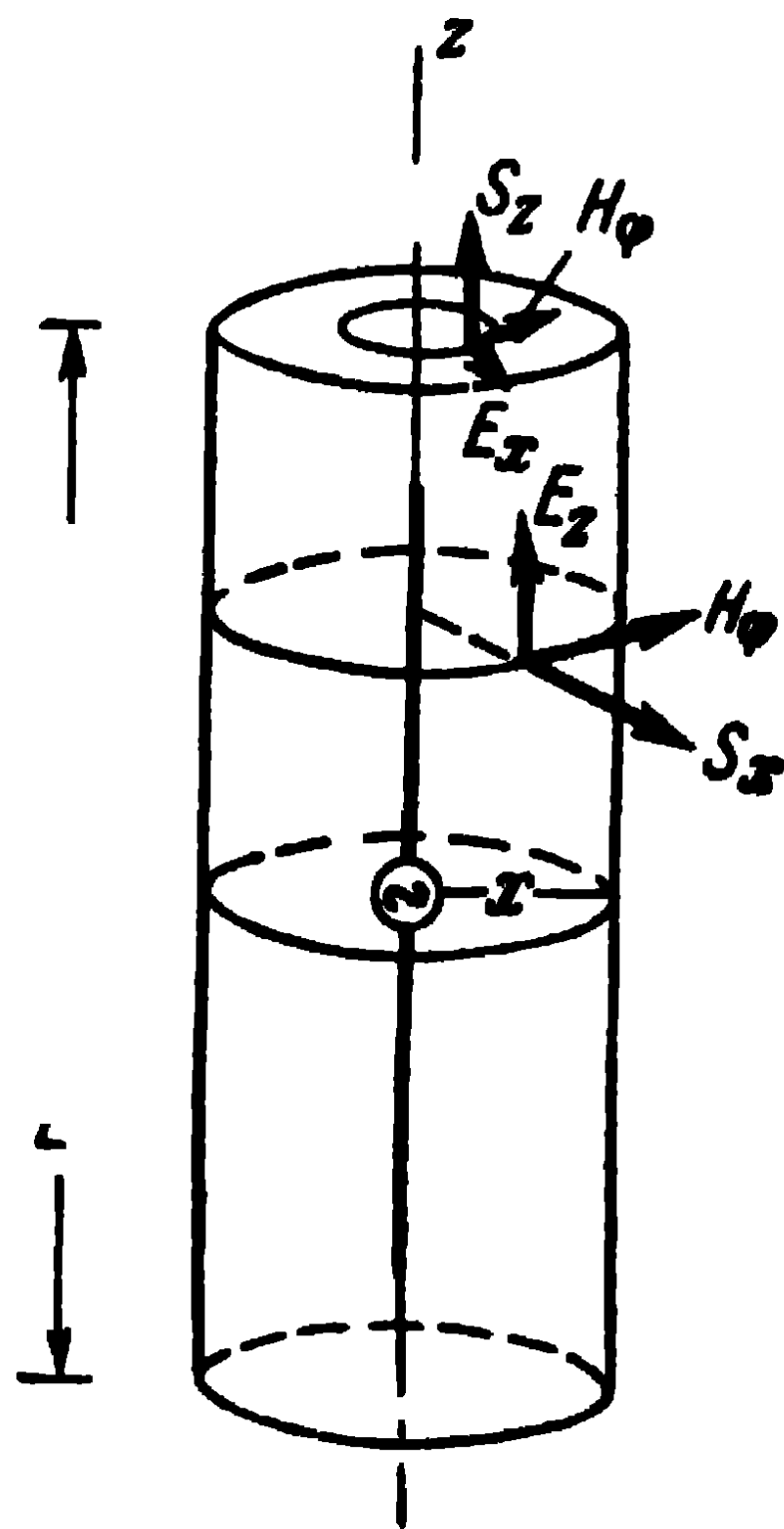


Fig. 2-11. Explaining the calculation of the radiated power.

intensity is, as was mentioned above, equal to zero everywhere except in the region of the external emf's. For this reason, the integration (2-33) should, in fact, be reduced to an integration within the region of the external emf's. We are considering the external emf (the generator's emf) impressed in the centre of the antenna on a small section of its length $2\Delta l$, where the current may be regarded as constant and equal to the current at the feed points of the antenna I_0^* . For this reason, the expression (2-33) is found to equal

$$P = \frac{I_0^* U}{2} \quad (2-34)$$

where
$$U_0 = -2 \int_{z=0}^{\Delta l} E_z(a) dz = 2 \int_{z=0}^{\Delta l} E_z^{\text{ext}} dz$$

is the voltage applied by the oscillator to the antenna.

But let us go back to the expression (2-33) relating the power to the square of the current in the antinode as was done above. We may write:

$$P = \frac{I_a I_a^* Z_{\Sigma a}}{2}, \quad (2-35)$$

where

$$Z_{\Sigma a} = -\frac{2}{I_a I_a^*} \int_{z=0}^l E_z(a) I_z^* dz \quad (2-36)$$

represents the complex resistance of the antenna in relation to the current in the antinode. The active component of this resistance represents the radiation resistance; as for the reactive component, it represents the reactance of the antenna in relation to the current at the antinode.

Let us calculate the complex resistance of a symmetrical antenna of arbitrary length and vanishingly small radius. Substituting into (2-36) the expression for $E_z(a)$ from (2-25) and $I_z = I_a \sin k(l-z)$, we obtain:

$$Z_{\Sigma a} = 30 \int_{z=0}^l \left\{ \frac{e^{-ik(R_1-l+z)}}{R_1} - \frac{e^{-ik(R_1+l-z)}}{R_1} + \frac{e^{-ik(R_2-l+z)}}{R_2} - \frac{e^{-ik(R_2+l-z)}}{R_2} - 2 \cos kl \frac{e^{-ik(R_0-l+z)}}{R_0} + 2 \cos kl \frac{e^{-ik(R_0+l-z)}}{R_0} \right\} dz.$$

As a result of the integration of this expression, we obtain for the limit case $\frac{a}{\lambda} \rightarrow 0$, $\frac{a}{l} \rightarrow 0$:

$$Z_{\Sigma a} = R_{\Sigma a} + iX_{\Sigma a},$$

where

$$R_{\Sigma a} = 30 \{ 2 [C + \ln 2kl - \text{Ci} 2kl] + \cos 2kl [C + \ln kl + \text{Ci} 4kl - 2\text{Ci} 2kl] + \sin 2kl [\text{Si} 4kl - 2\text{Si} 2kl] \}, \quad (2-38)$$

$$X_{\Sigma a} = 30 \left\{ \sin 2kl \left[C - \ln \frac{l}{ka} + \text{Ci} 4kl - 2\text{Ci} 2kl \right] - \cos 2kl [\text{Si} 4kl - 2\text{Si} 2kl] + 2\text{Si} 2kl \right\}. \quad (2-39)$$

The active component of the antenna resistance thus obtained is the same as when calculated by the Poynting vector method (2-21). This is fully justified since in both cases, we integrated the Poynting vector over closed surfaces enclosing a symmetrical antenna with a sinusoidal current distribution. The shape and dimensions of the surface of integration do not matter in this case since we are considering an antenna in a lossless space and the whole of its radiated power is lost into infinity. As for the reactive component of the antenna resistance, it determines the power oscillating in the vicinity of the antenna. Consequently, the magnitude of the reactance of the antenna depends on the surface of integration of the Poynting vector. When the radius of the wire a tends towards zero, in accordance with (2-39), the reactance of the antenna tends towards infinity, with the exception of the half-wave antenna, in which case it is found to equal 42.5 ohms.¹

If we relate the complex resistance of the antenna to the current at the feed points (in the centre of the antenna), we must take account of the fact that $I_a = \frac{I_0}{\sin kl}$.

Then

$$\begin{aligned} R_{\Sigma 0} &= \frac{R_{\Sigma a}}{\sin^2 kl}; \\ X_{\Sigma 0} &= \frac{X_{\Sigma a}}{\sin^2 kl}. \end{aligned} \quad (2-40)$$

¹ Thus, for resonant tuning, half-wave antennas should be somewhat shortened.

The resistances $R_{\Sigma 0}$ and $X_{\Sigma 0}$ are called the antenna radiation and reactance, related to the current at the feed points. These resistances are also called the resistive (active) and reactive components of the input resistance of the antenna (in the absence of losses in the antenna), since they represent the resistance between the input terminals of the antenna, to which the oscillator is connected.

When an antenna is short ($l/\lambda \ll 1$), the trigonometrical and integral sines and cosines may be expanded in series

$$\sin kl = kl - \frac{(kl)^3}{3!} + \dots;$$

$$\cos kl = 1 - \frac{(kl)^2}{2!} + \dots;$$

$$\operatorname{Si} kl = kl - \frac{(kl)^3}{3 \cdot 3!} + \dots,$$

$$\operatorname{Ci} kl = C + \ln kl - \frac{(kl)^2}{2 \cdot 2!} + \dots$$

Substituting these expansions into (2-38) and (2-39) and taking into consideration only the main terms of the expansion, we obtain the following rather simple formulas for the antenna input resistance:

$$R_{\Sigma 0} = 20 (kl)^2; \quad (2-41)$$

$$X_{\Sigma 0} = -W_w \cot kl \quad (2-42)$$

where

$$W_w = 120 \left(\ln \frac{l}{a} - 1 \right) \quad (2-43)$$

represents the antenna wave impedance.

Thus, it appears that the active resistance of a short antenna may be calculated from the same expression as for a dipole antenna [see (1-6)], and the reactance, from the expression for the long lossless line disconnected at the end.

The expressions (2-41) and (2-42) are used for antennas of a length smaller than a quarter of a wave-length.

When the antenna is fed in the potential antinode ($\frac{l}{\lambda} = 0.5, 1.0, \text{ etc.}$), the calculation of the magnitude of the input resistance of the antennas by means of (2-40) gives infinitely large values. This is understandable because, according to the assumptions we made regarding the current distribution along the antenna, the current at the feed points is found to equal zero. Actually, in this case, the current at

the potential antinodes is never equal to zero and even though the input resistance does become large, it nevertheless remains finite.

For this reason, the expressions (2-40) are not valid when the antennas are fed in the vicinity of the potential antinode. They still give satisfactory results for comparatively thin antennas, whose length is smaller than $l/\lambda=0.4$.

2-8. Calculating the Input Resistance of an Antenna by Reducing It to a Homogeneous Long Line with Losses

As we saw above, the expressions for calculating the input resistance of a symmetrical antenna as obtained by the induced emf method fail to give accurate results when the antennas are fed in the vicinity of current nodes.

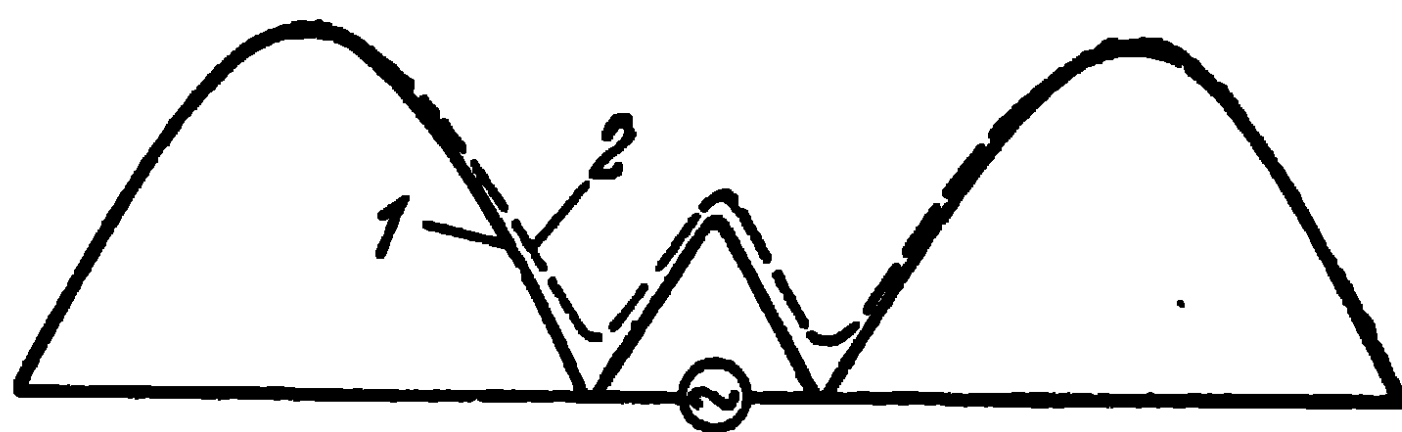


Fig. 2-12. Distribution of current amplitude along a symmetrical antenna:
1—circular sine law; 2—hyperbolic sine law.

To avoid the arising difficulties, in technical calculations, the current is assumed to be distributed along the antenna in accordance with the hyperbolic sine law (Fig. 2-12), i.e., it is assumed that, as a result of the radiation, each element of the antenna possesses a certain active resistance.

The actual distribution of the radiated power is complicated and from the standpoint of physics, the assumption mentioned just now is unjustified. However, in engineering practice, it is quite in order to suppose the radiation resistance to be distributed uniformly along the antenna.

The method examined below for calculating the antenna input resistance consists of three distinct stages. To begin with, using the induced emf method, we determine the antenna radiation resistance in relation to the current antinode, the current distribution being assumed sinusoidal. Then, taking into account the conservation of the radiated power condition, the resistance is distributed uniformly

along the entire antenna. After that, applying to such a homogeneous line with losses the equation for long lines, the input resistance of the antenna is found.

In accordance with the conservation of the radiated power condition, the integral along the whole length of the antenna of the product of the square of the current by the active resistance of the antenna infinitely small element is equal to the product of the square of the current in the antinode by the radiation resistance in relation to the current antinode computed under the assumption that the current distribution is sinusoidal,

$$\frac{I_a^2 R_{\Sigma a}}{2} = 2 \int_{z=0}^l \frac{I_z^2 R_1}{2} dz. \quad (2-44)$$

Substituting here $I_z = I_a \sin k(l-z)$, we obtain:

$$R_{\Sigma a} = 2R_1 \int_{z=0}^l \sin^2 k(l-z) dz.$$

But once $\sin^2 k(l-z) = \frac{1}{2} [1 - \cos 2k(l-z)]$, the integration yields

$$R_1 = \frac{R_{\Sigma a}}{l \left(1 - \frac{\sin 2kl}{2kl} \right)}. \quad (2-45)$$

Equation (2-45) defines the distributed radiation resistance of a symmetrical antenna per unit of length.

Now, we may consider the antenna as a long line whose propagation constant is:

$$\gamma = \beta + ik, \quad (2-46)$$

where

$k = \frac{2\pi}{\lambda}$ is the wave number;

$\beta = \frac{R_1}{W_w}$, the attenuation constant.

It should be noted that the distributed resistance causes a slight change in the wave impedance of the antenna. This should be written as:

$$W_{w1} = \sqrt{\frac{2R_1 + i\omega L_1}{i\omega C_1}} = \sqrt{\frac{L_1}{C_1}} \sqrt{1 - i\frac{2R_1}{\omega L_1}} \approx W_w \left(1 - i\frac{R_1}{\omega L_1} \right)$$

or, since

$$\frac{R_1}{\omega L_1} = \frac{\beta W_w}{\omega L_1} = \frac{\beta}{\omega \sqrt{L_1 C_1}} = \frac{\beta}{k},$$

we have:

$$W_{w1} \approx W_w \left(1 - i \frac{\beta}{k}\right). \quad (2-47)$$

Consequently, the antenna wave impedance should be regarded as a complex value.

Using the expressions for a long line with losses, the expression for the input impedance of a symmetrical antenna may be written as:

$$Z_{\Sigma 0} = W_w \left(1 - i \frac{\beta}{k}\right) \text{cth}(\beta l + i k l). \quad (2-48)$$

Transforming (2-48) in accordance with the expression

$$\text{cth}(\beta l + i k l) = \frac{\text{sh } 2\beta l - i \sin 2kl}{\text{ch } 2\beta l - \cos 2kl}$$

we obtain:

$$Z_{\Sigma 0} = R_{\Sigma 0} + iX_{\Sigma 0} = W_w \frac{\text{sh } 2\beta l - \frac{\beta}{k} \sin 2kl}{\text{ch } 2\beta l \cos 2kl} - iW_w \frac{\sin 2kl + \frac{\beta}{k} \text{sh } 2\beta l}{\text{ch } 2\beta l - \cos 2kl}. \quad (2-49)$$

Here, the wave impedance is usually defined in accordance with (2-43). The expression (2-49) together with (2-43) and (2-45) are used in many technical calculations of real antennas.

To simplify the calculations, Table 2-2 supplies the values of the distributed radiation impedance $R_1 l$ of a symmetrical antenna, depending on the ratio of the length of the antenna to the wave-length.

Table 2-2

l/λ	$R_1 l$, ohms	l/λ	$R_1 l$, ohms	l/λ	$R_1 l$, ohms	l/λ	$R_1 l$, ohms	l/λ	$R_1 l$, ohms
0.125	17.6	0.250	73.0	0.375	155.0	0.500	199.0	0.625	121.0
0.150	26.3	0.275	88.0	0.400	168.0	0.525	194.0	0.650	105.0
0.175	36.5	0.300	104.0	0.425	181.0	0.550	181.0	0.675	93.0
0.200	47.0	0.325	120.0	0.450	192.0	0.575	163.0	0.700	91.0
0.225	60.5	0.350	138.0	0.475	199.0	0.600	151.0		

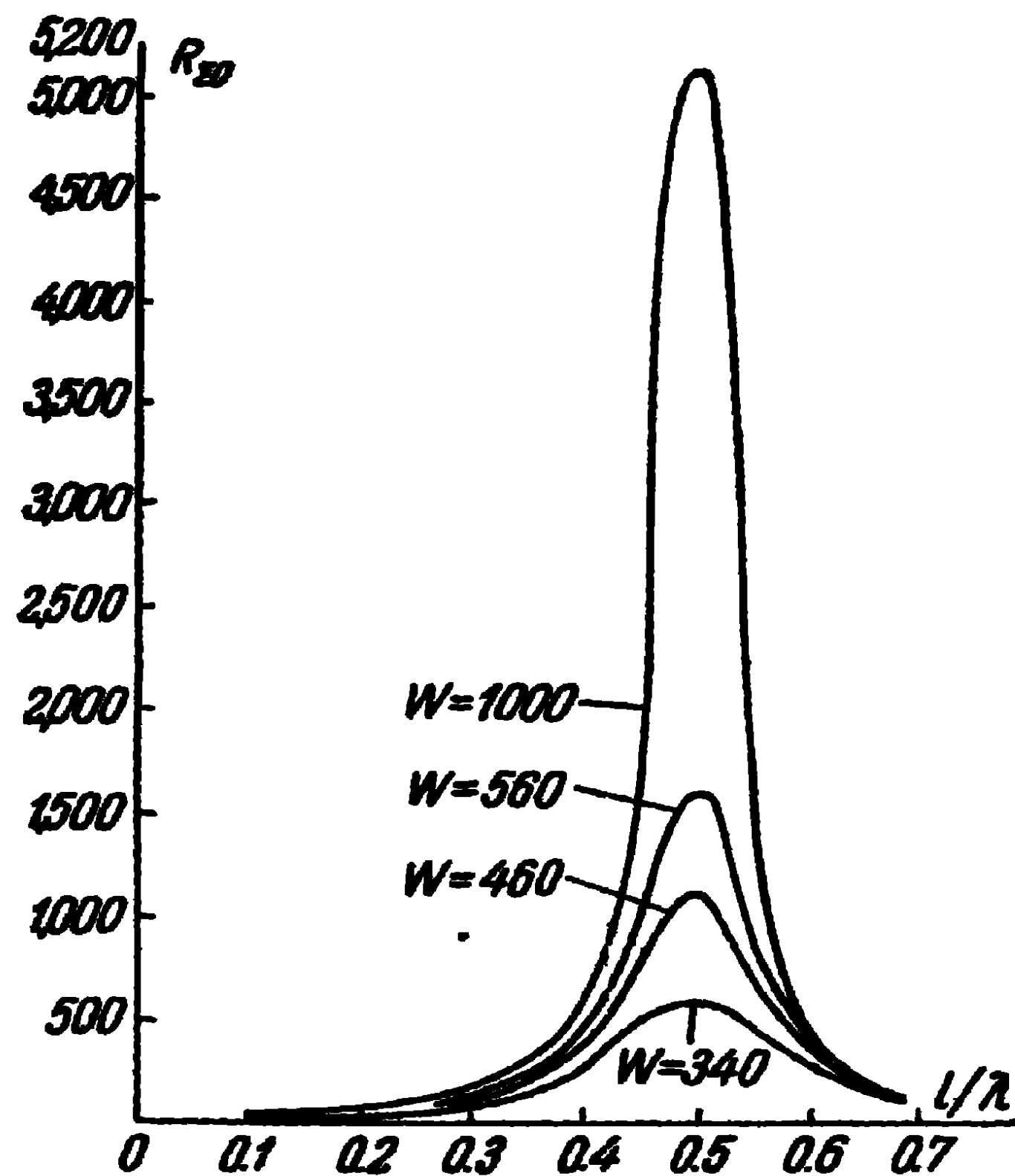


Fig. 2-13. Input resistance of a symmetrical antenna (resistive component).

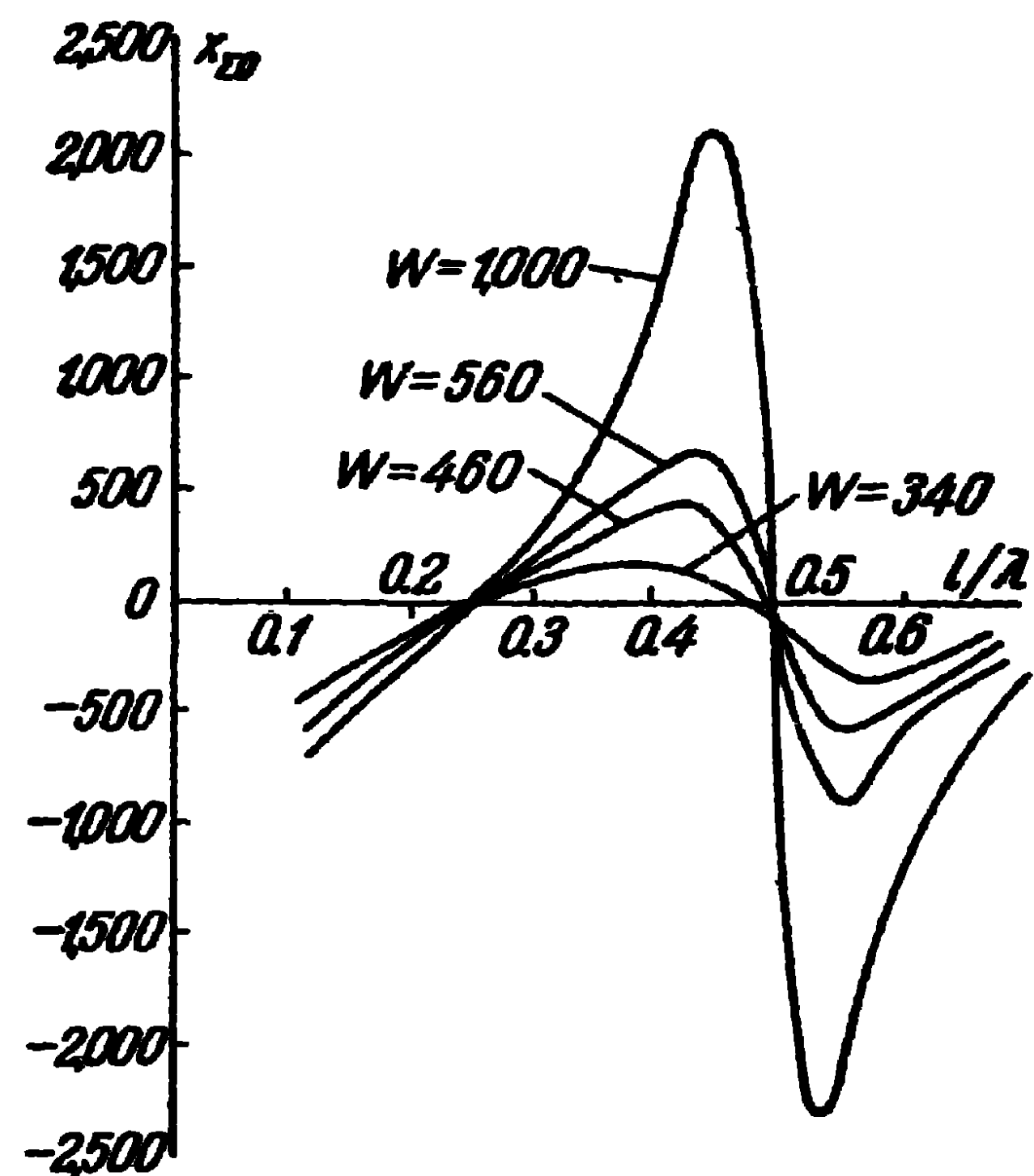


Fig. 2-14. Input resistance of a symmetrical antenna (reactive component).

In Figs. 2-13 and 2-14, the resistive R_{Σ_0} and reactive X_{Σ_0} components of the input resistance of a symmetrical antenna are plotted against the ratio of the length of the antenna to the wave-length l/λ , for a series of values of wave impedances of the antenna W_w . An examination of the curves shows that:

1) the active part of the antenna input resistance has its maximum value in the presence of an antiresonance ($l/\lambda \approx 0.5$). This maximum value depends on the antenna wave impedance: the larger the radius of the antenna, i.e., the smaller its wave impedance, the smaller the maximum;

2) the maximum of the reactive part of the input resistance is about half the maximum of the active part ($X_{\Sigma_{0\max}} \approx \frac{R_{\Sigma_{0\max}}}{2}$). This maximum value of the reactive part of the resistance depends also on the antenna wave impedance and is all the smaller as the wave impedance is smaller;

3) for small values of the length of the antenna ($l/\lambda < 0.25$) the reactive part of the input resistance has a negative sign. When $0.25 < l/\lambda < 0.5$, the reactive part of the input resistance has a positive sign, then negative again and so on. It should be noted that the input resistance of the antenna in the presence of an antiresonance ($l/\lambda \approx 0.5$) may be approximately defined from the simplified expression

$$R_{\Sigma_0} = \frac{W_w^2}{R_{\Sigma_a}}, \quad (2-50)$$

which is derived from (2-49).

If the antenna is short, i.e., $l/\lambda < 0.2$, the input resistance of the antenna may be expressed as

$$R_{\Sigma_0} = \frac{R_{\Sigma_a}}{\sin^2 kl}; \quad (2-40)$$

$$X_{\Sigma_0} = -W_w \cot kl. \quad (2-42)$$

2-9. Radiation of a Symmetrical Magnetic Antenna. Symmetrical Slot in Screen

Although magnetic currents do not exist in nature, we may examine the radiation of a magnetic antenna in free space by analogy with an electric antenna.

Let us imagine an ideally conducting cylindrical magnetic antenna of length $2l$ and radius a symmetrically excited in the centre by an external mmf (Fig. 2-15). There will

arise in the conductor a magnetic current which will be so distributed that the tangential component of the magnetic field intensity will be equal to zero everywhere except in the region of the external mmf. In the region of the external mmf, the sum of the tangential component of the magnetic field intensity and the external mmf equals zero.

Since the vector potential of magnetic currents obeys the same equation as the vector potential of electric currents and the boundary conditions with respect to the magnetic field in the case of a magnetic antenna coincide with

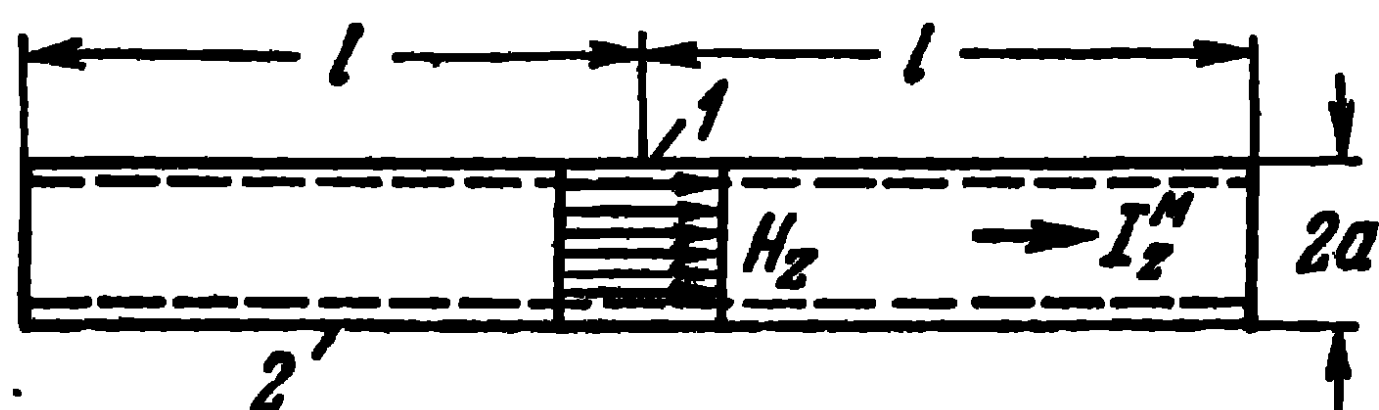


Fig. 2-15. A symmetrical magnetic antenna:
1—electric loop; 2—magnetic conductor tube.

the boundary conditions with respect to the electric field in the case of an electric antenna, the distribution of the magnetic current in a magnetic antenna coincides with the distribution of the electric current in an electric antenna.

Thus, in a vanishingly thin symmetrical magnetic antenna, the current in the first approximation is distributed in accordance with the sine law

$$I_z^M = I_0^M \frac{\sin k(l - |z|)}{\sin kl}, \quad (2-51)$$

where I_0^M is the magnetic current at the feed points of the antenna.

Now, we may use the principle of the interchangeability of the fields of the electric and magnetic antennas formulated in Chapter One and write the expressions for the electromagnetic field set up by the magnetic antenna corresponding to those of the field for the electric antenna (2-15), (2-25), (2-27) and (2-28).

In the radiation zone, the electromagnetic field of the magnetic antenna is defined as

$$\left. \begin{aligned} H_\theta &= i \frac{k}{2\pi\omega\mu} \frac{I_0^M}{r_0 \sin kl} e^{-ikr_0} \frac{\cos(kl \cos \theta) - \cos kl}{\sin \theta}; \\ E_\varphi &= -H_\theta \sqrt{\frac{\mu}{\epsilon}}. \end{aligned} \right\} \quad (2-52)$$

In the vicinity of a symmetrical magnetic antenna, the electromagnetic field is

$$\left. \begin{aligned} H_z &= -i \frac{k}{4\pi\omega\mu} \frac{I_0^M}{\sin kl} \left\{ \frac{e^{-ikR_1}}{R_1} + \frac{e^{-ikR_2}}{R_2} - \right. \\ &\quad \left. - 2 \cos kl \frac{e^{-ikR_0}}{R_0} \right\}, \\ H_x &= i \frac{k}{4\pi\omega\mu} \frac{I_0^M}{x \sin kl} \left\{ \frac{e^{-ikR_1}}{R_1} (z-l) + \right. \\ &\quad \left. + \frac{e^{-ikR_2}}{R_2} (z+l) - 2 \cos kl \frac{e^{-ikR_0}}{R_0} z \right\}; \\ E_\varphi &= -i \frac{I_0^M}{4\pi x \sin kl} \{ e^{-ikR_1} + e^{-ikR_2} - 2 \cos kl e^{-ikR_0} \}. \end{aligned} \right\} \quad (2-53)$$

To define the radiation conductivity of a symmetrical magnetic antenna, we may use the expression (1-11) and write:

$$G_{\Sigma a} = \frac{R_{\Sigma a}}{W^2}, \quad (2-54)$$

where $R_{\Sigma a}$ is the radiation resistance of the symmetrical electric antenna,

$W = \sqrt{\frac{\mu}{\epsilon}}$, the wave impedance of space,

$G_{\Sigma a}$, the radiation conductivity of a symmetrical magnetic antenna of the same length as the electric antenna

Thus, for example, for a half-wave electric antenna $R_{\Sigma a} = 73.1$ ohms. In accordance with (2-54), for a half-wave magnetic antenna, we obtain:

$$G_{\Sigma a} = \frac{73.1}{(377.6)^2} = 0.000514 \text{ ohm}^{-1};$$

for a wave electric antenna $R_{\Sigma a} = 199$ ohms. In accordance with (2-54), for a wave magnetic antenna, we obtain:

$$G_{\Sigma a} = \frac{199}{(377.6)^2} = 0.0014 \text{ ohm}^{-1}.$$

Generalising (2-54), we may obviously write:

$$Y_{\Sigma 0} = \frac{Z_{\Sigma 0}}{W^2}, \quad (2-55)$$

where $Z_{\Sigma 0}$ is the complex input resistance of the electric antenna;

$Y_{\Sigma 0}$, the complex input conductivity of the magnetic antenna with the same geometrical dimensions as the electric antenna.

Let the magnetic antenna have a rectangular cross section of length b and width τ , b being $\gg \tau$. When this antenna is placed on an ideally conducting infinite plane, a unilateral slot is formed in a screen of length $2l$ and width b , excited in the centre (Fig. 2-16). The distribution of the magnetic

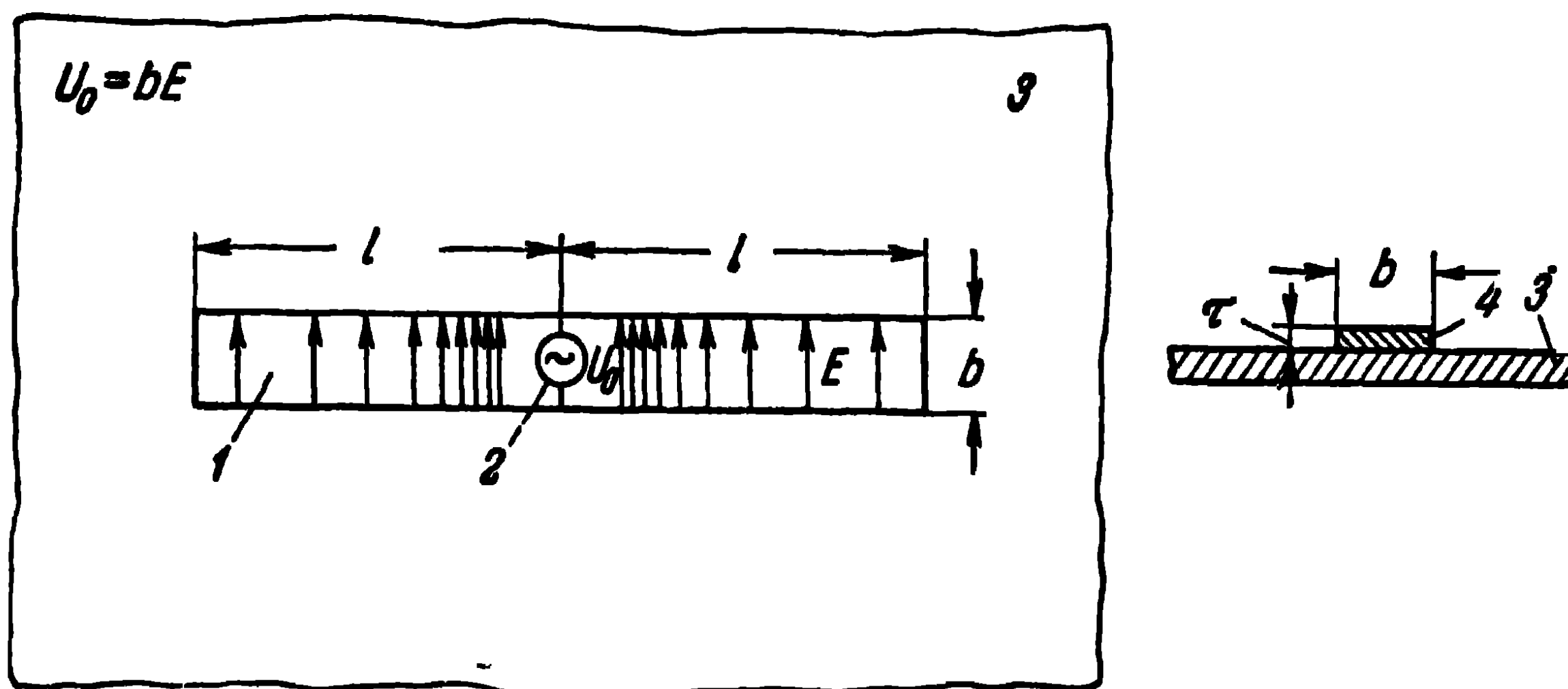


Fig. 2-16. Symmetrical slot:

1—slot in screen; 2—electric generator; 3—screen; 4—magnetic antenna.

current (of the electric field intensity) in the slot is, evidently, defined by (2-51). Using the mirror method, we find that the electromagnetic field of the slot in the half-space is doubled in comparison with the field of the magnetic antenna in free space. On the shadow side of the screen, the field equals zero everywhere.

As for the radiation conductivity and the input conductivity of the slot, they are also doubled and expressed as:

$$G_{\Sigma a} = \frac{2R_{\Sigma a}}{W^2}; \quad (2-54a)$$

$$Y_{\Sigma 0} = \frac{2Z_{\Sigma 0}}{W^2}, \quad (2-55a)$$

where $R_{\Sigma a}$ and $Z_{\Sigma 0}$ are the radiation resistance and the input resistance of the electric antenna of cross-section dimensions $b \times \tau$ in the case of free space¹;

$G_{\Sigma a}$ and $Y_{\Sigma 0}$, the radiation conductivity and the input conductivity of a slot in a screen, whose dimensions correspond to those of an electric antenna.

If the same slot is made bilateral (Fig. 2-17), the radiation conductivity and the input conductivity will again be doubled and will be expressed as:

$$G_{\Sigma a} = \frac{4R_{\Sigma a}}{W^2}; \quad (2-54b)$$

$$Y_{\Sigma 0} = \frac{4Z_{\Sigma 0}}{W^2}. \quad (2-55b)$$

In accordance with these expressions, the radiation conductivity of, for example, a bilateral half-wave slot equals $G_{\Sigma a} = 0.002052 \text{ ohm}^{-1}$.

Above, we have, by introducing the concept of the magnetic antenna, calculated the radiation of a slot in a plane screen of infinite extension, using the expressions for the radiation of the corresponding electric antenna in free space.

The direct connection between the radiation of a slot in a screen and that of the corresponding electric antenna in free space was established by A. A. Pistolokors [6,7] who formulated the so-called duality

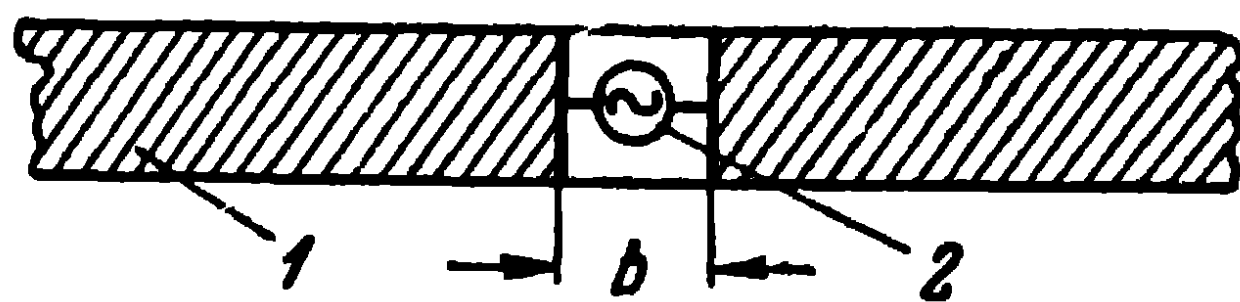


Fig. 2-17. Bilateral slot in conducting screen:

1—screen; 2—oscillator.

principle, which states that the problem regarding the radiation of a slot in a screen corresponds to that regarding the radiation of a metal strip of the same length and width located at the place of the slot. In the plane in which the slot was cut, the empty regions and those filled with an ideal conductor change places. Accordingly, E and H change places in the boundary conditions in that plane. Moreover, they do so in the whole of the external space. A. A. Pistolokors has established that from the point of view of setting up of the field intensity, 1A of electric current in a metal antenna is equivalent to $60\pi = 188.4 \text{ V}$ in a slot

¹ According to M. A. Leontovich (*JETP*, 1946, No. 6), a strip of width b may be regarded as equivalent to a cylinder of radius $a = b/4$.

radiator. As can be seen from (2-55b), the input conductivity of a slot in a screen differs from the input resistance of an electric antenna likewise by $(60\pi)^2$ times.

The duality principle is fairly simple to generalise for the case of a source-free space. Let this space be bounded by a surface s and let us suppose that an electric field E_0 is prescribed on one part of the surface and a magnetic field H_0 on the other one.

In accordance with the uniqueness theorem, the boundary conditions on the surface s under consideration completely determine the field inside the bounded region. Let us introduce into Maxwell's equations

$$\begin{aligned}\text{rot } \mathbf{H} &= i\omega\epsilon\mathbf{E}; \\ \text{rot } \mathbf{E} &= -i\omega\mu\mathbf{H}\end{aligned}$$

the new variables

$$\mathbf{E}_s = \sqrt{i\omega\epsilon} \mathbf{E} \text{ and } \mathbf{H}_s = \sqrt{-i\omega\mu} \mathbf{H}.$$

They are related as follows:

$$\begin{aligned}\text{rot } \mathbf{H}_s &= k\mathbf{E}_s; \\ \text{rot } \mathbf{E}_s &= k\mathbf{H}_s.\end{aligned}$$

This means that the solution for \mathbf{E}_s in the existence of boundary conditions on the surface

$$E_{s0} = f_1(x, y, z), \quad H_{s0} = f_2(x, y, z),$$

will also be valid for \mathbf{H}_s , if we interchange the boundary conditions, i.e., if we assume:

$$H_{s0} = f_1(x, y, z), \quad E_{s0} = f_2(x, y, z).$$

Thus, the duality principle can be stated as follows: "The solution of Maxwell's equations for a magnetic field for the given boundary conditions is also the solution of the same equations for an electric field in the boundary conditions, where the \mathbf{E} and \mathbf{H} fields are interchanged. Moreover, to the same boundary values of \mathbf{H} , in the first case, and \mathbf{E} , in the second one, will correspond the same values of these fields at the point of observation in both cases."

2-10. Additional Remarks Concerning the Current Distribution in an Antenna

We have shown above that the current in a symmetrical electric antenna and the intensity in a symmetrical bilateral slot in an infinite screen are, in the first approximation,

distributed according to the sinusoidal law. This result was derived from the approximate solution of the equation (2-6).

Let us now examine a more strict solution of this equation. To this end, let us return to the expression of the vector potential of the electric currents (2-4) and, conforming to the work of M. Leontovich and M. Levin [8], let us consider the integral

$$T = \int_{z'=-l}^l I_z^e(z') \frac{e^{-ikR}}{R} dz', \quad (2-56)$$

where

$$R = \sqrt{(z-z')^2 + \varrho^2}; \quad \varrho^2 = r^2 + a^2 - 2ar \cos(\varphi' - \varphi).$$

If we take into account that when $z' < z$,

$$z' = z - \sqrt{R^2 - \varrho^2}, \quad dz' = -\frac{R dR}{\sqrt{R^2 - \varrho^2}}$$

and when $z' > z$,

$$z' = z + \sqrt{R^2 - \varrho^2}, \quad dz' = +\frac{R dR}{\sqrt{R^2 - \varrho^2}},$$

the expression (2-56) may be written thus:

$$T = - \int_{z'=-l}^z I_z^e(z') \frac{e^{-ikR}}{\sqrt{R^2 - \varrho^2}} dR + \int_{z'=z}^l I_z^e(z') \frac{e^{-ikR}}{\sqrt{R^2 - \varrho^2}} dR.$$

Let us further take into consideration that

$$\frac{dR}{\sqrt{R^2 - \varrho^2}} = d \ln \frac{R + \sqrt{R^2 - \varrho^2}}{2\Delta},$$

where Δ is constant and assumed small in comparison with the length of the antenna and that of the wave.

Integrating by parts in the expression T and taking into account that $I_z^e(\pm l) = 0$, we obtain:

$$\begin{aligned} T = & -2I_z^e(z) e^{-ik\varrho} \ln \frac{\varrho}{2\Delta} + \\ & + \int_{z'=-l}^z \ln \frac{R + \sqrt{R^2 - \varrho^2}}{2\Delta} \left[I_z^e(z') - ikI_z^e(z') \times \frac{z'-z}{R} \right] \times \\ & \times e^{-ikR} dz' - \int_{z'=z}^l \ln \frac{R + \sqrt{R^2 - \varrho^2}}{2\Delta} \times \\ & \times \left[I_z^e(z') - ikI_z^e(z') \frac{z'-z}{R} \right] e^{-ikR} dz'. \end{aligned}$$

In the vicinity of the antenna surface, when $ka \ll 1$, we may approximately assume:

$$R \simeq |z' - z|, \quad R + \sqrt{R^2 - a^2} \approx 2|z' - z|, \quad e^{-ikR} \simeq 1$$

and noting that, when $r > a$

$$\int_{\varphi'=\varphi}^{2\pi+\varphi} \ln \frac{R}{2\Delta} d\varphi' = 2 \ln \frac{r}{2\Delta},$$

we obtain the following expression for the vector potential on the surface of the wire:

$$A_z^e = -\frac{1}{2\pi} I_z^e(z) \ln \frac{a}{2\Delta} + \frac{1}{4\pi} V[I_z^e, z], \quad (2-57)$$

where

$$\begin{aligned} V[I_z^e, z] &= \int_{z'=-l}^z \ln \frac{2(z-z')}{2\Delta} [I_z^e(z') + ik I_z^e(z')] e^{-ik(z-z')} dz' - \\ &- \int_{z'=z}^l \ln \frac{2(z'-z)}{2\Delta} [I_z^e(z') - ik I_z^e(z')] e^{-ik(z'-z)} dz' = \\ &= \int_{z'=-l}^l \ln \frac{2|z-z'|}{2\Delta} [ik I_z^e(z') + \frac{z-z'}{|z-z'|} I_z^e(z')] e^{-ik|z-z'|} dz'. \end{aligned}$$

In (2-57), the first term coincides with the expression (2-8) obtained at the beginning of the present chapter, and the second term is the additional one, which we had earlier discarded.

Substituting now the expression (2-57) into the equation (2-6), we arrive at the following integro-differential equation, investigated by Hallen [9] and later, by Leontovich and Levin [8],

$$\frac{d^2 I_z^e}{dz^2} + k^2 I_z^e = i\omega\epsilon 4\pi \times \{K + G[I_z^e, z]\} \quad (2-58)$$

where

$$\begin{aligned} \chi &= \frac{1}{2 \ln \frac{a}{2\Delta}}; \quad i\omega\epsilon 4\pi G = \frac{d^2 V}{dz^2} + k^2 V; \\ K &= E_z^{\text{ext}} - \left[\frac{1}{r} \frac{\partial}{\partial r} (r A_\varphi^M) \right]_{r=a+0}. \end{aligned}$$

Note that the second term in the expression K is usually neglected, which is permissible in the case of thin antennas [10].

Since χ is a small quantity ($a \ll \Delta$), let the solution of the expression (2-58) be represented in the form of a series:

$$I_z = I_{0z} + \chi I_{1z} + \chi^2 I_{2z} + \dots$$

By substituting this series into the equation (2-58) and the boundary condition for the current and considering the coefficients of the terms of the same power as equal, we obtain the following system of differential equations:

$$\begin{aligned} I_{0z}'' + k^2 I_{0z} &= 0, & I_{0z}(\pm l) &= 0; \\ I_{1z}'' + k^2 I_{1z} &= i\omega\epsilon 4\pi \{K + G[I_{0z}, z]\}, & I_{1z}(\pm l) &= 0; \\ I_{2z}'' + k^2 I_{2z} &= i\omega\epsilon 4\pi G[I_{1z}, z], & I_{2z}(\pm l) &= 0; \\ \dots & & & \end{aligned} \quad (2-59)$$

The equations thus obtained are solved by the method of successive approximations.

Let us first examine a half-wave antenna. From the first equation and the first boundary condition of (2-59), we see that, irrespective of the distribution of the external emf in the antenna, the current in it has a sinusoidal distribution

$$I_{0z} = I_0 \frac{\sin k(l - |z|)}{\sin kl} = I_0 \cos kz. \quad (2-60)$$

Multiplying the second equation of (2-59) by I_{0z} and integrating in the interval from $-l$ to $+l$ we obtain:

$$i\omega\epsilon 4\pi \int_{-l}^l \{K + G[I_{0z}, z]\} I_{0z} dz = 0.$$

Substituting here (2-60) and noting that

$$G[I_{0z}, z] = I_0 G[\cos kz, z],$$

we find:

$$I_0 = - \frac{\int_{-l}^l K \cos kz dz}{\int_{-l}^l G[\cos kz, z] \cos kz dz}.$$

If we neglect the second item in K and consider that the external emf is applied in the centre of the antenna on an infinitely small area, so that $E_z^{\text{ext}} = U\delta(z-0)$, where U is the voltage at the gap of the antenna and $\delta(z-0)$, the delta-function which is equal to zero everywhere with the exception of the point $z=0$, where it is equal to infinity, and in addition

$$\int_{-\infty}^{\infty} \delta(z-0) dz = 1,$$

then

$$\int_{-l}^l K \cos kz dz = \int_{-l}^l U \cos kz \delta(z-0) dz = U.$$

Consequently

$$I_0 = \frac{U}{Z_{\text{in}}},$$

where

$$Z_{\text{in}} = \int_{-l}^l G[\cos kz, z] \cos kz dz,$$

evidently represents the input resistance of a half-wave symmetrical antenna. The calculation of this integral leads to the quantity

$$Z_{\text{in}} = 73.1 + i42.5 \text{ ohms.}$$

Thus, the input resistance of a half-wave antenna is found to be complex and its reactive component is of an inductive nature. For resonant tuning the antenna has to be shortened. A more detailed investigation of the solutions of the system (2-59) shows that the amount by which a half-wave antenna should be shortened to reach the resonant length may be defined as:

$$\frac{\Delta l}{l} = - \frac{0.225}{\ln \frac{l}{a}}.$$

Now let us examine an antenna of length other than half a wave. From the equations (2-59), we see that when the length of the antenna is not divisible by half the wavelength, the first equation has only a zero solution, so that $I_{0z}=0$ and $G[I_{0z}, z]=0$.

In the case of an arbitrary distribution of the external emf, the solution of the second equation (2-59) may be written as:

$$I_{1z} = -\frac{i\omega\epsilon 4\pi}{k \sin 2kl} \left\{ \sin k(l-z) \int_{z'=-l}^z K(z') \sin k(l+z') dz' + \right. \\ \left. + \sin k(l+z) \int_{z'=z}^l K(z') \sin k(l-z') dz' \right\}.$$

Let a lumped emf be applied in the centre of the antenna, so that $K \approx E_z^{\text{ext}} = U\delta(z'-0)$. Then, the distribution of the current in the antenna will, in the first approximation, be expressed as:

$$I_z = \chi I_{1z} = -\frac{i\omega\epsilon 2\pi U \chi}{k \cos kl} \sin k(l-|z|). \quad (2-61)$$

The ratio between the voltage and the current at the gap of the antenna represents the antenna input resistance and, in this approximation, it is found to be purely reactive

$$X_{\text{in}} = \frac{U}{I_z(0)} = i \frac{60}{\chi} \cot kl.$$

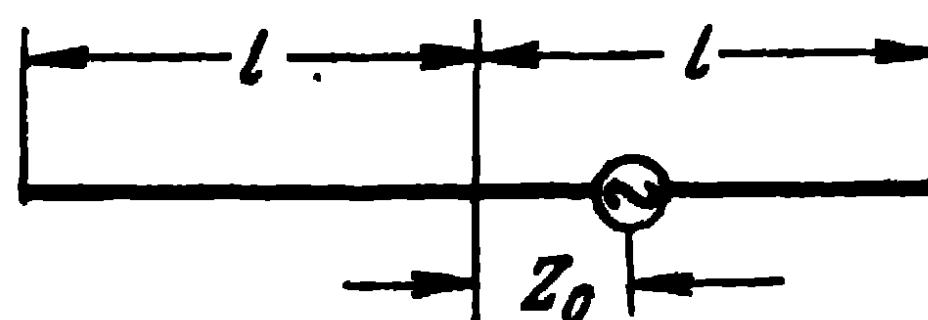


Fig. 2-18. An asymmetrically excited antenna.

To calculate the inphase component of the input resistance, the next approximation for the current should be calculated. However, this will not be done here.

Let now the emf be lumped not in the centre of the antenna but at a certain point z_0 (Fig. 2-18). Then $K \approx E_z^{\text{ext}} = U\delta(z'-z_0)$ and the distribution of the current in the antenna is, in the first approximation, expressed:

$$I_z = \chi I_{1z} = -\frac{i\omega\epsilon 4\pi U \chi}{k \sin 2kl} \sin k(l+z) \sin k(l-z_0);$$

when $z > z_0$

$$I_z = \chi I_{1z} = -\frac{i\omega\epsilon 4\pi U \chi}{k \sin 2kl} \sin k(l-z) \sin k(l+z_0). \quad (2-62)$$

Thus, in that case, the distribution of the current in the antenna, which remains sinusoidal to the left and right of the point where the generator is connected to the antenna depends on the location of this point. It can be seen from

(2-62) that the currents amplitudes in the arms of the antenna are unequal and depend on the ratio $\sin k(l+z_0)/\sin k(l-z_0)$. Fig. 2-19 shows a number of current distribution curves which differ substantially from those in Fig. 2-3. Thus, when $l_2=l+z_0=0.25\lambda$ and $l_1=l-z_0=0.5\lambda$, the current in the left arm of the antenna is vanishingly small relatively to the current in the right arm of the antenna. When $l_2=l+z_0=0.25\lambda$ and $l_1=l-z_0=0.75\lambda$, the direction of the current in the antenna is different from that in a wave antenna in the case of a symmetrical excitation. It is only in the

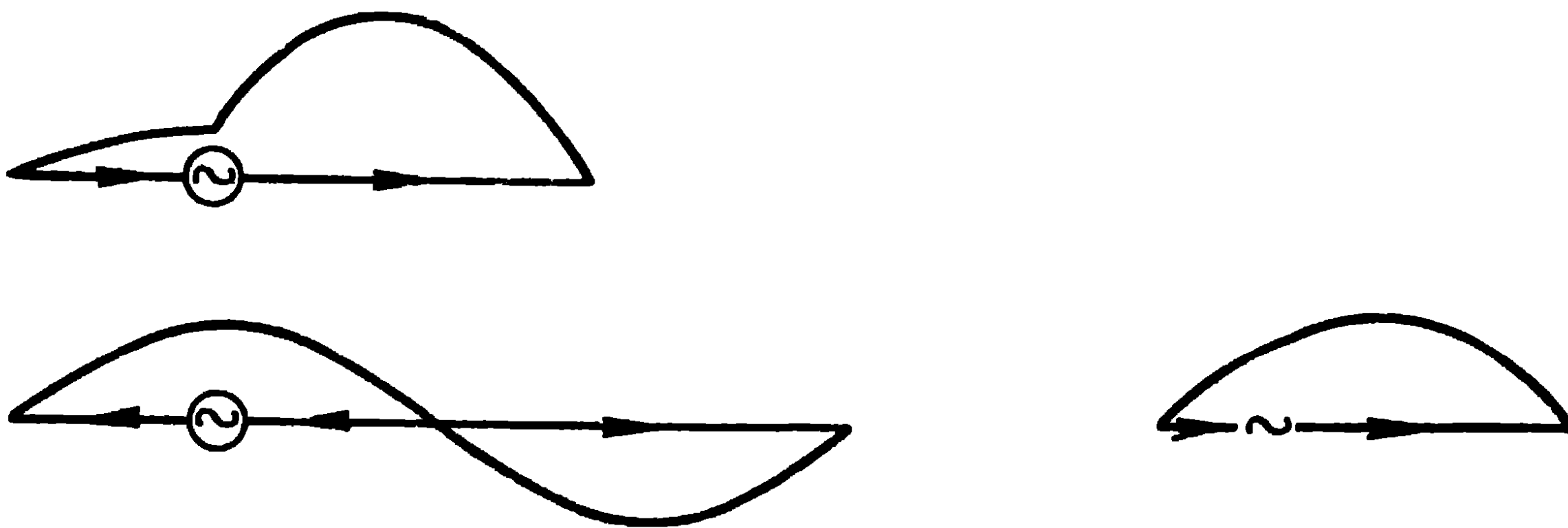


Fig. 2-19. Current distribution in an asymmetrical antenna.

case of a half-wave (resonant) antenna that the distribution of the current does not depend on the feeding point of the antenna.

The same kind of electric field distribution as in Fig. 2-19 takes also place in a bilateral slot, if it is excited asymmetrically, i.e., when the slot is fed as shown in Fig. 2-16, but not in its centre.

Next, we shall turn to the calculation of the current distribution in the antenna by another method, viz., the eigenfunctions method.

2-11. The Eigenfunctions Method

In the eigenfunctions method, the symmetrical antenna is considered as an ideally conducting prolate spheroid excited by a circular magnetic loop lying directly on the surface of the spheroid (Fig. 2-20).

Let us introduce the coordinates of the prolate spheroid obtained by the rotation of the ellipses around the major axis. We get a system of spheroids the orthogonal surfaces of which are a system of two-sheets hyperboloids. Let us

direct the z -axis of a rectangular system of coordinates along the major axis of the ellipse and let d be the focal distance (Fig. 2-21) and φ the azimuth angle, the azimuth of the x -axis being zero. The sign of φ should be determined by the

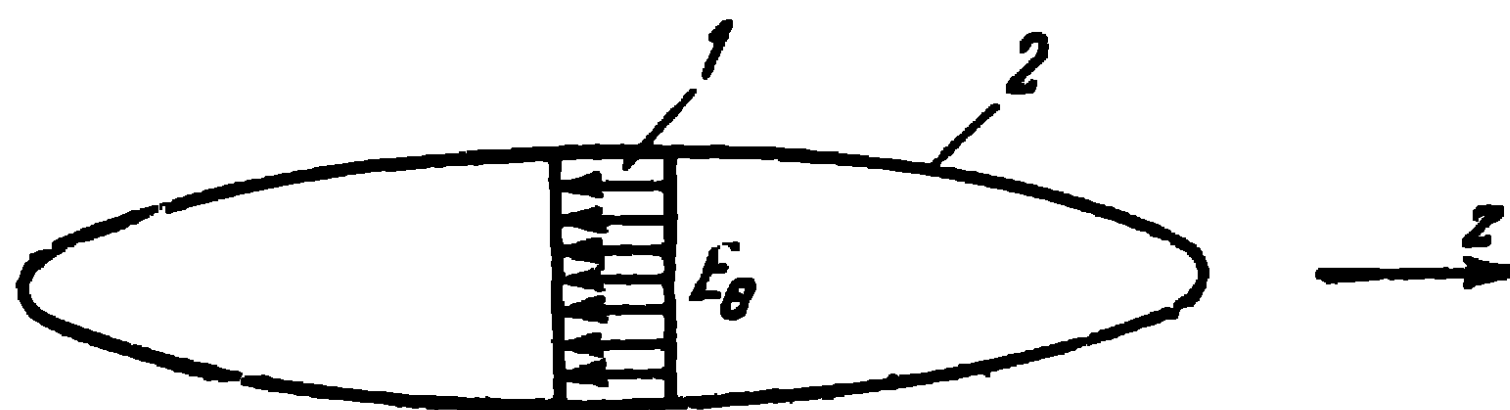


Fig. 2-20. Explaining the eigenfunctions method:
1—magnetic loop, 2—conducting spheroid.

right-hand screw rule. The coordinate surfaces of the spheroid are defined by the equations

$$\operatorname{ch} \psi = \frac{r_1 + r_2}{d}, \quad \cos \theta = \frac{r_1 - r_2}{d}$$

and the connection between the rectangular coordinates and

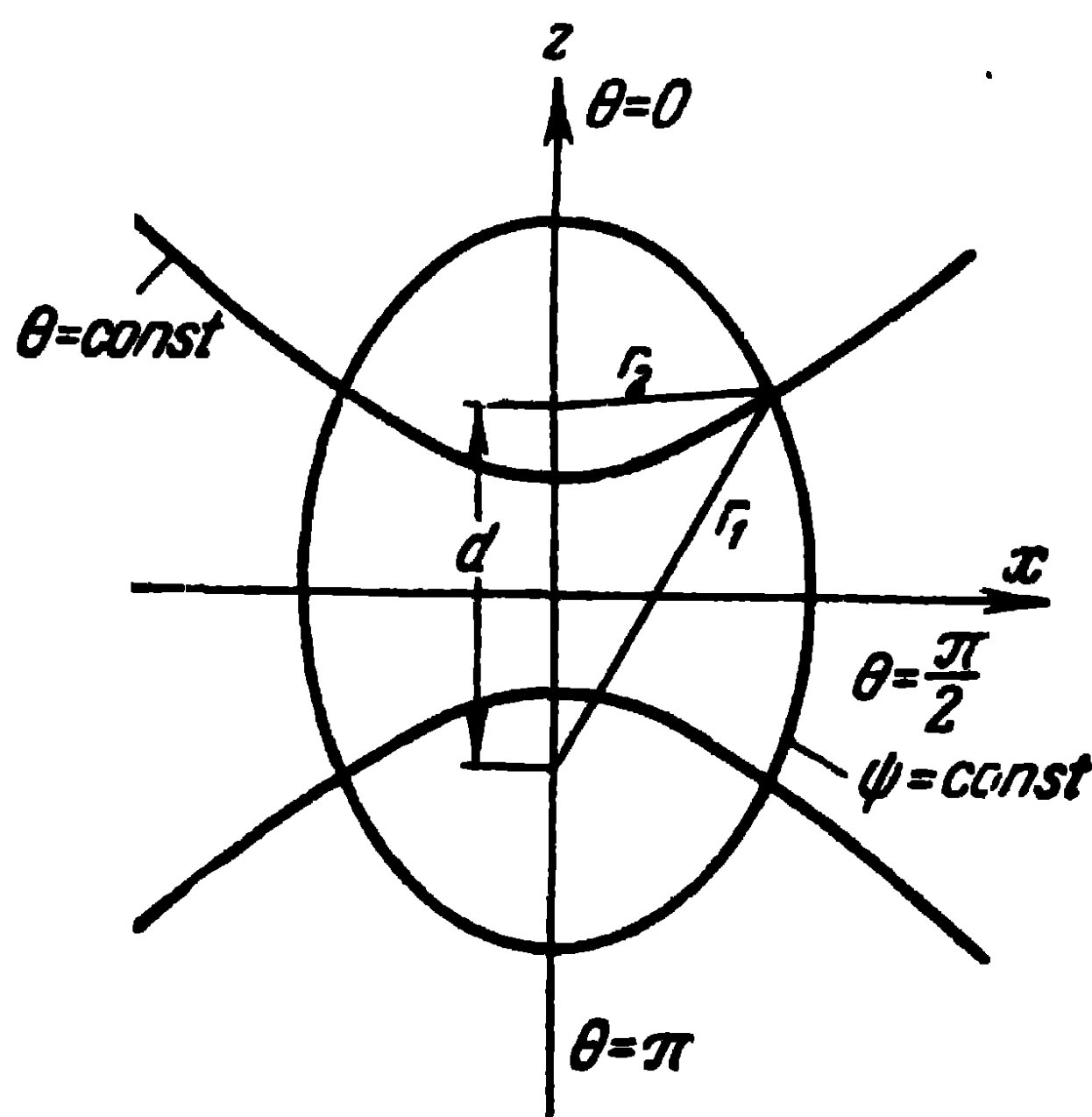


Fig. 2-21. Spheroid coordinates.

the spheroidal ones is found from the equations

$$x = \frac{d}{2} \operatorname{sh} \psi \sin \theta \cos \varphi;$$

$$y = \frac{d}{2} \operatorname{sh} \psi \sin \theta \sin \varphi;$$

$$z = \frac{d}{2} \operatorname{ch} \psi \cos \theta.$$

If we take ψ , θ , φ as the spheroidal coordinates, the relation between the spheroidal and rectangular components of a certain vector F is expressed as:

$$\begin{aligned} F_\psi &= F_x \frac{1}{h_1} \frac{d}{2} \operatorname{ch} \psi \sin \theta \cos \varphi + F_y \frac{1}{h_1} \frac{d}{2} \operatorname{ch} \psi \sin \theta \sin \varphi + \\ &\quad + F_z \frac{1}{h_1} \frac{d}{2} \operatorname{sh} \psi \cos \theta; \\ F_\theta &= F_x \frac{1}{h_1} \frac{d}{2} \operatorname{sh} \psi \cos \theta \cos \varphi + F_y \frac{1}{h_1} \frac{d}{2} \operatorname{sh} \psi \cos \theta \sin \varphi - \\ &\quad - F_z \frac{1}{h_1} \frac{d}{2} \operatorname{ch} \psi \sin \theta; \\ F_\varphi &= -F_x \sin \varphi + F_y \cos \varphi, \end{aligned} \quad (2-63)$$

where $h_1 = h_2 = \frac{d}{2} \sqrt{\operatorname{ch}^2 \psi - \cos^2 \theta}$ are the scale factors.

Let an infinitely thin magnetic loop of elliptical form lie in an infinite space. The vector potential of this loop is expressed by (2-1). In the problem under consideration, the magnetic current has only an azimuth component $J^M = J_\varphi^M$, so that when the ratios (2-63) are applied to the expression (2-1) for the azimuth component of the vector potential we get the expression

$$A_\varphi^M(\psi, \theta, \varphi) = \frac{1}{4\pi} \int_s J_\varphi^M(\psi', \theta', \varphi') \cos(\varphi' - \varphi) \frac{e^{-ikR}}{R} ds, \quad (2-64)$$

where

$$\begin{aligned} \int_s \dots ds &= \int_{\theta'=\theta_1}^{\theta_2} \int_{\varphi'=0}^{2\pi} \dots h'_1 h'_3 d\theta' d\varphi'; \\ h'_1 &= \frac{d}{2} \sqrt{\operatorname{ch}^2 \psi' - \cos^2 \theta'}; \\ h'_3 &= \frac{d}{2} \operatorname{sh} \psi' \sin \theta'. \end{aligned}$$

To solve the problem by the eigenfunctions method, the function $G = \frac{1}{4\pi} \frac{e^{-ikR}}{R}$ is represented in the form of a spheroidal functions expansion, i.e., in the form of an infinite double sum of space harmonics:

$$\begin{aligned} G &= \frac{1}{4\pi} \frac{e^{-ikR}}{R} = \frac{k}{2\pi i} \sum_{n=0}^{\infty} \sum_{m=0}^{\infty} \frac{\varepsilon_m}{N_{mn}} \cos m(\varphi' - \varphi) \times \\ &\quad \times S_{mn}^{(1)}(c, \cos \theta') S_{mn}^{(1)}(c, \cos \theta) \times \\ &\quad \times \begin{cases} R_{mn}^{(1)}(c, \operatorname{ch} \psi') R_{mn}^{(4)}(c, \operatorname{ch} \psi) & \text{for } \psi > \psi'; \\ R_{mn}^{(4)}(c, \operatorname{ch} \psi') R_{mn}^{(1)}(c, \operatorname{ch} \psi) & \text{for } \psi < \psi', \end{cases} \end{aligned} \quad (2-65)$$

where

$$\varepsilon_m = 1 \text{ when } m=0, \varepsilon_m = 2 \text{ when } m=1, 2, 3 \dots, k= \\ = \frac{2\pi}{\lambda}, \quad c = k \frac{d}{2};$$

$S_{mn}^{(1)}$, the angular spheroidal function of the first kind similar to the associated Legendre functions;

$R_{mn}^{(1)}$, the radial spheroidal function of the first kind similar to the Bessel function of the half-entire order;

$R_{mn}^{(4)}$, the radial spheroidal function of the fourth kind similar to the Hankel function of the second kind of the half-entire order,

$$N_{mn} = 2 \sum_{k=0}^{\infty} \frac{(\cdot d_k^n)^2 (k+2m)!}{k! (2k+2m+1)}.$$

In the last expression, a dash after the symbol of the sum indicates that the summing up occurs for even values of k if n is even, and for odd values of k if n is odd.

The expression (2-65) is the solution of the wave equation for the G function in spheroidal coordinates.

Note that because of axial symmetry, the magnetic current of the loop does not depend on the angle φ . Hence, substituting (2-65) into (2-64) and taking into account that

$$\int_{\varphi'=0}^{2\pi} \cos(\varphi' - \varphi) \cos m(\varphi' - \varphi) d\varphi' = \begin{cases} 0 & \text{when } m \neq 1; \\ \frac{2\pi}{\varepsilon_m} & \text{when } m = 1, \end{cases}$$

we obtain:

$$A_{\varphi}^M(\psi, \theta) = - \int_{\psi'=\psi_1}^{\psi_2} J_{\varphi}^M(\psi', \theta') h_1 h_3 d\theta' ik \times \\ \times \sum_{n=0}^{\infty} \frac{1}{N_{1n}} S_{1n}^{(1)}(c, \cos \theta') S_{1n}^{(1)}(c, \cos \theta) \times \\ \times \begin{cases} R_{1n}^{(1)}(c, \text{ch } \psi') R_{1n}^{(4)}(c, \text{ch } \psi) & \text{for } \psi > \psi'; \\ R_{1n}^{(4)}(c, \text{ch } \psi') R_{1n}^{(1)}(c, \text{ch } \psi) & \text{for } \psi < \psi'. \end{cases} \quad (2-66)$$

Thus, the azimuth component of the vector potential does not depend on the angle φ . As for the radial A_{ψ}^M and meridional A_{θ}^M components of the vector potential, due to axial symmetry, they equal zero.

If an ideally conducting spheroid, the radial coordinate of the surface of which will be designated by $\psi_0 < \psi'$, is now introduced symmetrically into the field of the magnetic loop under consideration, electric currents will be induced on the surface of the spheroid, the currents which have only a longitudinal component $J_e = J_\theta$. Under the influence of the surface electric currents, a secondary field is formed of such a value that the total field, i.e., the field of the currents of the magnetic loop plus the field of the currents of the spheroid, has no tangential component of the electric field intensity on the surface of the spheroid. The secondary field may be regarded as the field of the primary wave, reflected by the spheroid and moving away towards infinity, i.e., it may be represented in the form of the expression (2-66) with unknown reflection coefficients of the space harmonics

$$A_\varphi^{\text{M. refl}}(\psi, \theta) = - \int_{\theta'=\theta_1}^{\theta_2} J_\varphi^{\text{M}}(\psi', \theta') h_1 h_3 d\theta' ik \times \\ \times \sum_{n=0}^{\infty} \frac{a_n}{N_{1n}} S_{1n}^{(1)}(c, \cos \theta') S_{1n}^{(1)}(c, \cos \theta) R_{1n}^{(1)}(c, \text{ch } \psi') \times \\ \times R_{1n}^{(4)}(c, \text{ch } \psi), \quad (2-67)$$

where a_n are the reflection coefficients of the space harmonics, determined from the boundary conditions on the surface of the spheroid. In accordance with (1-4), the vector of the electric field intensity is expressed as:

$$\mathbf{E} = \text{rot } \mathbf{A}^{\text{M}}$$

and since $A^{\text{M}} = A_\varphi^{\text{M}}$, the components of the \mathbf{E} vector in prolate spheroid coordinates are:

$$E_\psi = - \frac{1}{h_1 h_3} \frac{\partial}{\partial \theta} (h_3 A_\varphi^{\text{M}}); \\ E_\theta = \frac{1}{h_1 h_3} \frac{\partial}{\partial \psi} (h_3 A_\varphi^{\text{M}}); \\ E_\varphi = 0. \quad (2-68)$$

Thus, the boundary condition on the surface of the spheroid for the total vector potential may be written in the following form:

$$\left| \frac{\partial}{\partial \psi} (h_3 A_\varphi^{\text{M. tot}}) \right|_{\psi=\psi_0} = 0. \quad (2-69)$$

Adding up (2-67) and (2-66) when $\psi < \psi'$ and substituting into (2-69), we obtain for the coefficients of expansion a_n :

$$a_n = - \frac{\frac{\partial}{\partial \psi_0} \left[\frac{d}{2} \operatorname{sh} \psi_0 R_{1n}^{(1)}(c, \operatorname{ch} \psi_0) \right]}{\frac{\partial}{\partial \psi_0} \left[\frac{d}{2} \operatorname{sh} \psi_0 R_{1n}^{(4)}(c, \operatorname{ch} \psi_0) \right]} \frac{R_{1n}^{(4)}(c, \operatorname{ch} \psi')}{R_{1n}^{(1)}(c, \operatorname{ch} \psi')} \quad (2-70)$$

The solution thus obtained satisfies Maxwell's equations, the boundary conditions on the surface of the ellipsoid and at infinity and is therefore the unique solution. Now substitute (2-70) into (2-67) and add it to (2-66). Then, placing the magnetic loop on the surface of the spheroid, i.e., assuming $\psi' = \psi_0$ and taking account, furthermore, that

$$R_{1n}^{(1)}(c, \operatorname{ch} \psi_0) \frac{\partial R_{1n}^{(4)}(c, \operatorname{ch} \psi_0)}{\partial \psi_0} - R_{1n}^{(4)}(c, \operatorname{ch} \psi_0) \frac{\partial R_{1n}^{(1)}(c, \operatorname{ch} \psi_0)}{\partial \psi_0} = \frac{1}{ik \frac{d}{2} \operatorname{sh} \psi_0},$$

we obtain

$$A_{\varphi}^{\text{M. tot}}(\psi, \theta) = - \int_{\theta'=\psi_0}^{\psi_2} J_{\varphi}^{\text{M}} h_{10} h'_{30} d\theta' \sum_{n=0}^{\infty} \frac{1}{N_{1n}} \times \\ \times S_{1n}^{(1)}(c, \cos \theta') S_{1n}^{(1)}(c, \cos \theta) \times \\ \times \frac{R_{1n}^{(4)}(c, \operatorname{ch} \psi)}{\frac{\partial}{\partial \psi_0} \left[\frac{d}{2} \operatorname{sh} \psi_0 R_{1n}^{(4)}(c, \operatorname{ch} \psi_0) \right]} \quad (2-71)$$

where

$$h_{10} = \frac{d}{2} \sqrt{\operatorname{ch}^2 \psi_0 - \cos^2 \theta'}; \quad h'_{30} = \frac{d}{2} \operatorname{sh} \psi_0 \sin \theta'.$$

Thus, the expression (2-71) provides the solution of the problem of the excitation of an ideally conducting spheroid of a circular magnetic loop with a uniform azimuth distribution of the magnetic current J_{φ}^{M} . The magnetic loop located on the surface of an ideally conducting spheroid forms a circular slot on the spheroid and the magnetic current J_{φ}^{M} is equal in magnitude and opposite in sign to the electric field intensity E_{θ} in the slot.

The electric field intensity in the space surrounding the spheroid is determined by substituting (2-71) into (2-68).

It should be further noted that since $A_\psi^M = A_\theta^M = 0$ and A_φ^M does not depend on the angle φ , $\text{div} A^M = 0$. Hence, in accordance with (1-4), the magnetic field intensity will be expressed as:

$$H_\varphi = -i\omega\epsilon A_\varphi^{M, \text{tot}}.$$

We may now also write the expression for the electric current induced on the spheroid. The surface density of the electric current is expressed as:

$$J_\theta^e = -H_\varphi|_{\psi=\psi_0} = -i\omega\epsilon \sum_{n=0}^{\infty} \frac{1}{N_{1n}} S_{1n}^{(1)}(c, \cos \theta) \times \\ \times \frac{R_{1n}^{(4)}(c, \text{ch } \psi_0)}{\frac{\partial}{\partial \psi_0} \left[\frac{d}{2} \text{sh } \psi_0 R_{1n}^{(4)}(c, \text{ch } \psi_0) \right]} \int_{\theta'=0}^{\theta_2} J_\varphi^M S_{1n}^{(1)}(c, \cos \theta') \times h'_{10} h'_{30} d\theta'. \quad (2-72)$$

Thus, the eigenfunctions method, which is the strict classical method for solving the problem under consideration, enables to determine the exact value of the electromagnetic field in the space surrounding the antenna and the exact value of the electric current distribution in the antenna.

The difficulty in calculating the field according to the expressions obtained consists in that the terms in the series do not always decrease sufficiently fast. However, the angular and radial spheroidal functions are partly tabulated [11] and this makes the calculations easier.

The strict solution of the problem regarding the excitation of a spheroid by an infinitely narrow slot located in the centre of the antenna, was first given by Chu and Stratton [12]. Designating the voltage at the slot in the centre of the antenna as U , we obtain in that case in (2-72):

$$\int_{\theta'=0}^{\theta_2} J_\varphi^M S_{1n}^{(1)}(c, \cos \theta') h'_{10} h'_{30} d\theta' = U S_{1n}^{(1)}(c, 0) \frac{d}{2} \text{sh } \psi_0.$$

Further, if we take account of the fact that the full current flowing through the cross section of the spheroid is expressed as:

$$I_\theta^e = \int_{\varphi=0}^{2\pi} J_\theta^e h_{30} d\varphi,$$

we obtain the following expression for the current at the feed points of the antenna I_0^e

$$I_0^e = \frac{-i\omega k}{60} U \left(\frac{d}{2} \operatorname{sh} \psi_0 \right)^2 \times \\ \times \sum_{n=0}^{\infty} \frac{R_{1n}^{(4)}(c, \operatorname{ch} \psi_0) [S_{1n}^{(1)}(c, 0)]^2}{N_{1n} \frac{\partial}{\partial \psi_0} \left[\frac{d}{2} \operatorname{ch} \psi_0 R_{1n}^{(4)}(c, \operatorname{ch} \psi_0) \right]} . \quad (2-73)$$

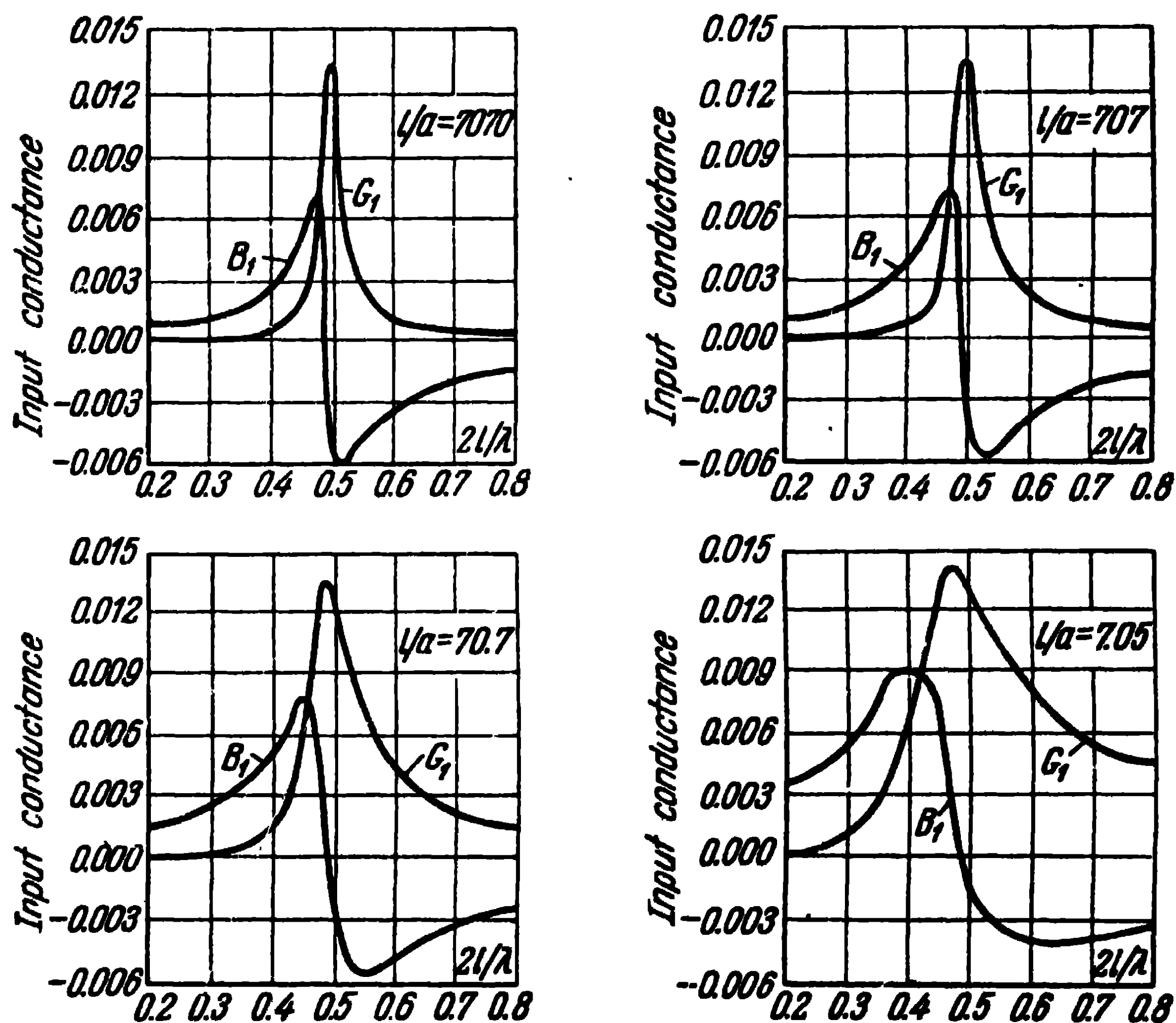


Fig. 2-22. Curves of the input conductance of an antenna.

Evidently, the ratio of the current to the voltage represents the input conductance of the antenna

$$Y_{\Sigma 0} = \sum_{n=0}^{\infty} (G_n + iB_n), \quad (2-74)$$

where

$$G_n + iB_n = \frac{-i\omega k}{60} \left(\frac{d}{2} \operatorname{sh} \psi_0 \right)^2 \times \\ \times \frac{[S_{1n}^{(1)}(c, 0)]^2 R_{1n}^{(4)}(c, \operatorname{ch} \psi_0)}{N_{1n} \frac{\partial}{\partial \psi_0} \left[\frac{d}{2} \operatorname{sh} \psi_0 R_{1n}^{(4)}(c, \operatorname{ch} \psi_0) \right]}.$$

In Fig. 2-22 the active G_1 and reactive B_1 parts of the input conductance are plotted as a function of the ratio of the length of the antenna to the wave-length $2l/\lambda$ for a series of ratios of the length of the antenna to its largest diameter $2l/2a$. The values of the conductance when $n=3.5...$ for the given dimensions of the antenna are relatively small and are not given here. It is seen from the curves that the maximums of the active part of the conductance G_1 occur in the vicinity of $2l/\lambda=0.5$. The reactive parts of the conductance pass through zero when $2l/\lambda$ is somewhat smaller than 0.5. Thus, the resonant length of the antenna is found to be somewhat smaller than half a wave-length; moreover it is the smaller the thicker the antenna is. When the diameter of the antenna changes, the active part of the conductance in the vicinity of the half-wave length remains practically unchanged, whereas the reactive part of the conductance increases when the diameter diminishes. If we pass from the conductance to the resistances, we obtain the following resistance values for the half-wave length:

$$\begin{aligned} Z_{\Sigma_0} &= 73 + i 30 \text{ ohms when } l/a = 7,070; \\ Z_{\Sigma_0} &= 73 + i 24 \text{ ohms when } l/a = 707; \\ Z_{\Sigma_0} &= 73 + i 12 \text{ ohms when } l/a = 70,7. \end{aligned}$$

Calculations show that the current distribution curves along the antenna are close to the sinusoid.

CHAPTER THREE

Radiation of Two Coupled Antennas

3-1. Directional Diagrams of Antennas

We have discussed the radiation of a single symmetrical antenna in detail. Let us now examine the radiation of two symmetrical antennas in free space.

Two parallel antennas of the same length lie at a distance d from each other (Fig. 3-1). Voltage U_1 (of frequency ω) is applied to the first antenna and voltage U_2 (of the same frequency) to the second antenna. Electric currents will arise in the antennas the complex amplitudes of which will be designated

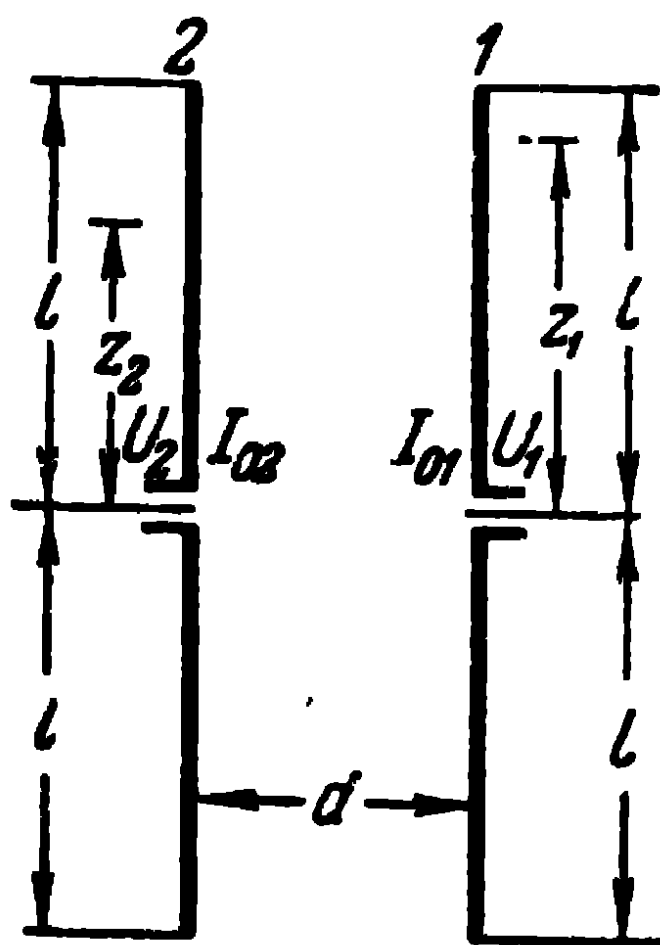


Fig. 3-1. Coupled antennas.

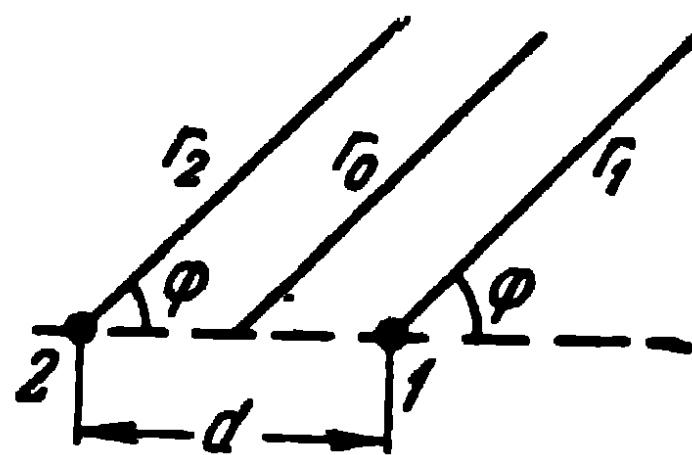


Fig. 3-2. Explaining the calculation of radiation characteristics.

by I_{01} at the feed points of the first antenna and by I_{02} at the feed points of the second antenna. Their ratio will be as follows:

$$\frac{I_{02}}{I_{01}} = me^{j\psi}, \quad (3-1)$$

where m is the ratio of currents amplitudes;
 ψ —phase shift between currents.

The points of interest, in the first place, are the fields which are set up by this pair of antennas in the radiation zone. Let us first examine the equatorial plane of the antennas (Fig. 3-2). In that plane, the radiation of each of the antennas is non-directional. However, due to mutual radiation, their fields interfere with each other: in some directions they are added up, in others deducted one from the other.

If we assume their current distribution to be sinusoidal, the field of each of the antennas is defined by (2-15). In the equatorial plane, we have for the first antenna

$$E_1 = i \frac{60 I_{01}}{r_1 \sin kl} (1 - \cos kl) e^{-ikr_1} \quad (3-2)$$

and for the second one

$$E_2 = i \frac{60 I_{02}}{r_2 \sin kl} (1 - \cos kl) e^{-ikr_2}. \quad (3-3)$$

The field vectors at the point of observation are parallel, so that (3-2) and (3-3) can be added up arithmetically. It should be noted in addition that the point of observation of the field is at infinity, so that, in adding up, we may, with a high degree of accuracy, assume:

$$\frac{1}{r_1} \approx \frac{1}{r_2} \approx \frac{1}{r_0}, \quad r_2 - r_0 = \frac{d}{2} \cos \varphi, \quad r_1 - r_0 = -\frac{d}{2} \cos \varphi,$$

where φ is the angle between the direction towards the point of observation and the line joining the centres of the antennas;

r_0 is the distance from the centre of the plane formed by the antennas to the point of observation.

Thus, we obtain for the total field:

$$E = i \frac{60 I_{01}}{r_0 \sin kl} (1 - \cos kl) e^{-ikr_0} \left[e^{i \frac{kd}{2} \cos \varphi} + m e^{i\psi} e^{-i \frac{kd}{2} \cos \varphi} \right]. \quad (3-4)$$

As is seen from (3-4), the amplitude and phase of the total field depend on the angle of observation φ and on the ratio of the currents. Let us examine some cases of excitation when the antennas are excited in co-phase, i.e., let $m=1$ and $\psi=0$. Then the expression (3-4) will be reduced to the following one:

$$E = i \frac{120 I_{01}}{r_0 \sin kl} (1 - \cos kl) e^{-ikr_0} \cos \left(\frac{kd}{2} \cos \varphi \right). \quad (3-5)$$

It can be seen from (3-5) that the shape of the directional diagram of co-phased antennas depends on the ratio between the distance of the antennas and the wave-length. There are directions in which, by comparison with the field intensity of one single antenna, the field intensity of the antennas is doubled. These directions are determined from the condition

$$\cos \left(\frac{kd}{2} \cos \varphi_{\max} \right) = \pm 1,$$

or

$$\cos \varphi_{\max} = \frac{n\lambda}{d}, \quad n = 0, 1, 2 \dots \quad (3-6)$$

Thus, the first radiation maximum occurs for any values of $\frac{d}{\lambda}$ and coincides with the direction $\varphi_{\max} = \pm \frac{\pi}{2}$. This is understandable since in that direction, the difference of the ray paths equals zero. The second radiation maximum occurs when $\frac{d}{\lambda} = 1$ and coincides with the direction $\varphi_{\max} = 0^\circ, 180^\circ$.

At the same time, there are directions in which the radiation of the antennas equals zero. These directions are determined from the condition

$$\cos \left(\frac{kd}{2} \cos \varphi_0 \right) = 0,$$

or

$$\cos \varphi_0 = \frac{n\lambda}{2d}, \quad n = 1, 3 \dots \quad (3-7)$$

Thus, when $\frac{d}{\lambda} < 0.5$, there are no directions in which the radiation equals zero. The first zero of radiation occurs when $\frac{d}{\lambda} = 0.5$ and coincides with the directions $\varphi_0 = 0^\circ, 180^\circ$.

Fig. 3-3 shows the amplitude directional characteristics of co-phased antennas for a series of values of $\frac{d}{\lambda}$, as calculated from equation (3-5).

As regards the phase directional characteristic, it can be seen from (3-5) that for a value of $\frac{d}{\lambda} < 0.5$, it represents a circle, i.e., when the angle φ changes, the phase of the field remains unchanged. For values of $\frac{d}{\lambda} \geq 0.5$,

the phase of the field changes by 180° when passing through the zero of radiation.

Now, let the antennas be in antiphase, i.e., let $m=1$ and $\psi=180^\circ$. The expression (3-4) will then be reduced to the following one:

$$E = -\frac{120 I_{01}}{r_0 \sin kl} (1 - \cos kl) e^{-ikr_0} \sin \left(\frac{kd}{2} \cos \varphi \right). \quad (3-8)$$

In that case, when $\varphi=90^\circ$ and $\varphi=270^\circ$, the radiation is always equal to zero, irrespective of the ratio $\frac{d}{\lambda}$. The directions in which the field is doubled are determined from the condition

$$\cos \varphi_{\max} = \frac{n\lambda}{2d}, \quad n=1, 3 \dots \quad (3-9)$$

It can be seen that when $\frac{d}{\lambda} < 0.5$, there is no direction with a double value of the field intensity. When $\frac{d}{\lambda} = 0.5$, the field is doubled in the direction $\varphi_{\max}=0^\circ, 180^\circ$. The zeros of radiation are determined from the condition

$$\cos \varphi_0 = \frac{n\lambda}{d}, \quad n=0, 1, 2 \dots \quad (3-10)$$

and as noted above, the first zero of radiation occurs for any values of $\frac{d}{\lambda}$ in the direction $\varphi_0=90^\circ, 270^\circ$. The second zero of radiation occurs when $\frac{d}{\lambda}=1$ and coincides with the directions $\varphi_0=0^\circ, 180^\circ$.

Fig. 3-3 shows the amplitude directional characteristics of antiphase antennas for a series of values of $\frac{d}{\lambda}$. It should be noted that for any values of $\frac{d}{\lambda}$, the phase characteristics of antiphase antennas change by 180° when passing through the zero of radiation.

The excitation of antennas in quadrature, i.e., when $m=1$ and $\psi=90^\circ$, is also of interest. In that case (3-4) is written as:

$$E = i \frac{120 I_{01}}{r_0 \sin kl} (1 - \cos kl) e^{-ikr_0 + i 45^\circ} \cos \left(45^\circ - \frac{kd}{2} \cos \varphi \right). \quad (3-11)$$

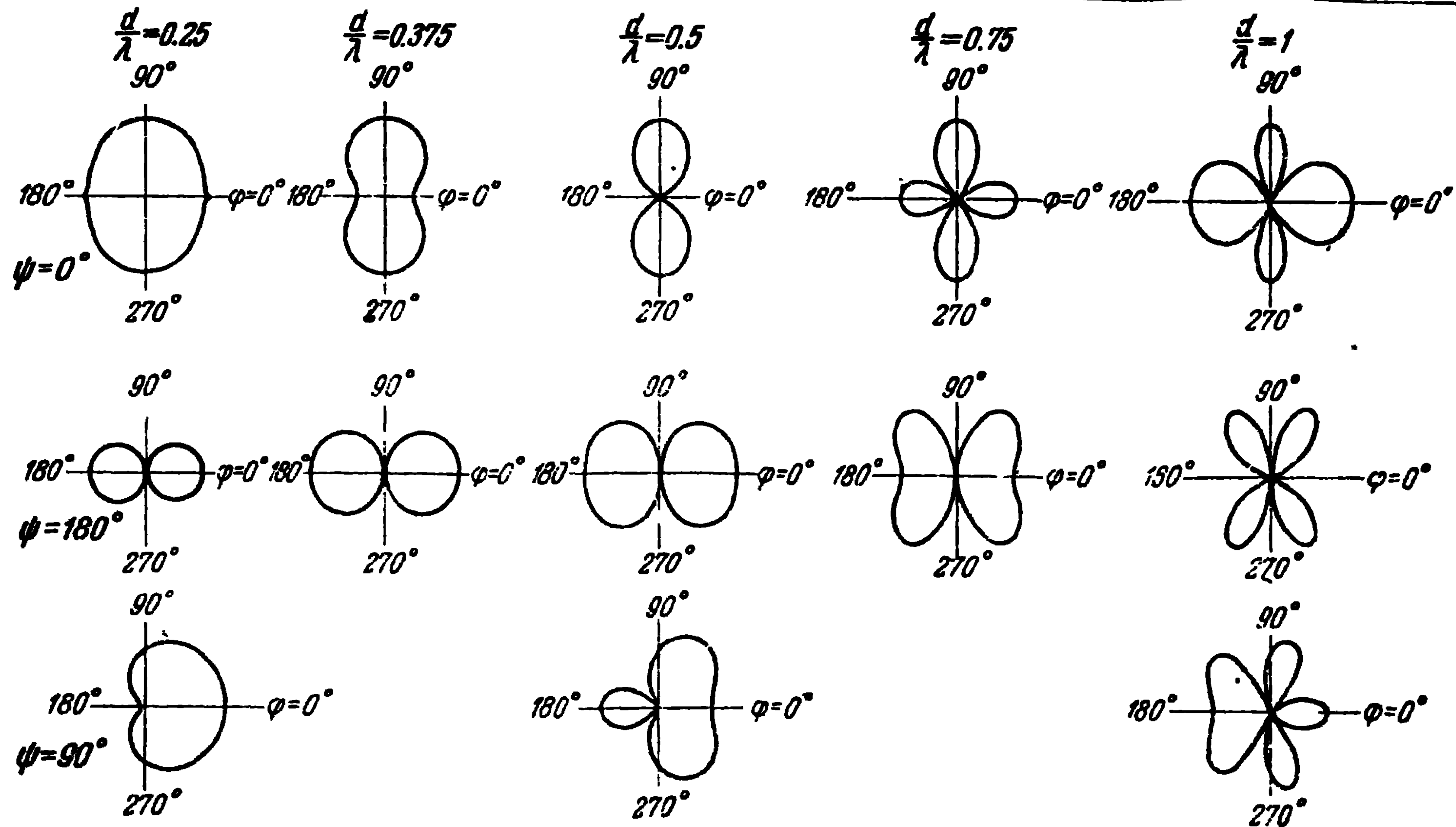


Fig. 3-3. Directional characteristics of two coupled antennas for various distances between them (d) and various phase shifts (ψ).

When the distance between the antennas is equal to a quarter of a wave-length ($\frac{kd}{2} = 45^\circ$) the radiation in the direction $\varphi = 180^\circ$ equals zero and, in the direction $\varphi = 0$, it is doubled in comparison with the radiation of a single antenna with the same current. The amplitude directional characteristic has the shape of a cardioid and the second antenna, which reflects energy towards the first antenna is known as a reflector. The same figure shows the amplitude directional characteristics for a number of values of $\frac{d}{\lambda}$ when the antennas are excited in quadrature.

It is easy to define also the expression for the field intensity in the radiation zone, in the plane of the axes of the antennas. In that plane, the field of each of the antennas is defined by (2-15). Designating once again by r_1 the distance from the centre of antenna 1 to the point of observation and by r_2 , the distance from the centre of antenna 2 to the same point and adding up the fields, we obtain the following expression for the total field:

$$E = i \frac{60 I_{01}}{r_0 \sin kl} e^{-ikr_0} \frac{\cos(kl \cos \theta) - \cos kl}{\sin \theta} \times \\ \times \left[e^{i \frac{kd}{2} \sin \theta} + me^{i\psi} e^{-i \frac{kd}{2} \sin \theta} \right], \quad (3-12)$$

where θ is the angle between the direction towards the point of observation and the antenna axis.

An examination of (3-12) shows that the directional characteristic of two symmetrical antennas in their common meridional plane represents the product of two factors. The first factor, which is defined by the expression $\frac{\cos(kl \cos \theta) - \cos kl}{\sin \theta}$ represents the directional characteristic of a single antenna; the second factor, which is defined by the expression $\left[e^{i \frac{kd}{2} \sin \theta} + me^{i\psi} e^{-i \frac{kd}{2} \sin \theta} \right]$, represents the factor of the combined radiation of the two antennas.

3-2. Mutual and Total Impedances of Antennas

Let us consider the interaction between the antennas. The longitudinal component of the electric field intensity set up by each of the antennas in the system under consideration (Fig. 3-1), is expressed by (2-25). The component E_{z_1} set up on the surface of antenna 1 will consist of two items

$$E_{z_1} = E_{z_{11}} + E_{z_{12}},$$

where $E_{z_{11}}$ is the component of the electric field intensity induced by the currents of antenna 1;

$E_{z_{12}}$, the component of the electric field intensity, induced by the currents of antenna 2.

In just the same way, the component of the electric field intensity E_{z_2} set up on the surface of antenna 2 will consist of two items

$$E_{z_2} = E_{z_{22}} + E_{z_{21}}$$

where $E_{z_{22}}$ is the component of the electric field intensity induced by the currents of antenna 2;

$E_{z_{21}}$, the component of the electric field intensity, induced by the currents of antenna 1.

Using the induced emf method, in conformity with (2-33), the power fed from the generator to antenna 1 is:

$$P_1 = - \int_{z_1=0}^{z_1=l} E_{z_{11}} I_{z_1}^* dz_1 - \int_{z_1=0}^{z_1=l} E_{z_{12}} I_{z_1}^* dz_1, \quad (3-13)$$

and the power fed from the generator to antenna 2,

$$P_2 = - \int_{z_2=0}^{z_2=l} E_{z_{22}} I_{z_2}^* dz_2 - \int_{z_2=0}^{z_2=l} E_{z_{21}} I_{z_2}^* dz_2, \quad (3-14)$$

where I_{z_1} is the current at the point z_1 of antenna 1;

I_{z_2} is the current at the point z_2 of antenna 2.

On the other hand, the power fed to the antennas may be expressed as:

$$\begin{aligned} P_1 &= \frac{I_{01}^* U_1}{2}; \\ P_2 &= \frac{I_{02}^* U_2}{2}. \end{aligned} \quad (3-15)$$

On comparing (3-15) with (3-13) and (3-14), for two coupled antennas, we obtain equations similar to Kirchhoff's equations for coupled contours with lumped constants,

$$\left. \begin{aligned} U_1 &= I_{01}Z_{11} + I_{02}Z_{12}, \\ U_2 &= I_{02}Z_{22} + I_{01}Z_{21}, \end{aligned} \right\} \quad (3-16)$$

where

$$Z_{11} = -\frac{2}{I_{01}I_{01}^*} \int_{z_1=0}^l E_{z11} I_{z1}^* dz_1; \quad (3-17)$$

$$Z_{22} = -\frac{2}{I_{02}I_{02}^*} \int_{z_2=0}^l E_{z22} I_{z2}^* dz_2; \quad (3-18)$$

$$Z_{12} = -\frac{2}{I_{01}^*I_{02}} \int_{z_1=0}^l E_{z12} I_{z1}^* dz_1; \quad (3-19)$$

$$Z_{21} = -\frac{2}{I_{02}^*I_{01}} \int_{z_2=0}^l E_{z21} I_{z2}^* dz_2. \quad (3-20)$$

Here, Z_{11} and Z_{22} represent the separate resistances of antennas 1 and 2, i.e., the resistance of each of the antennas in the absence of the

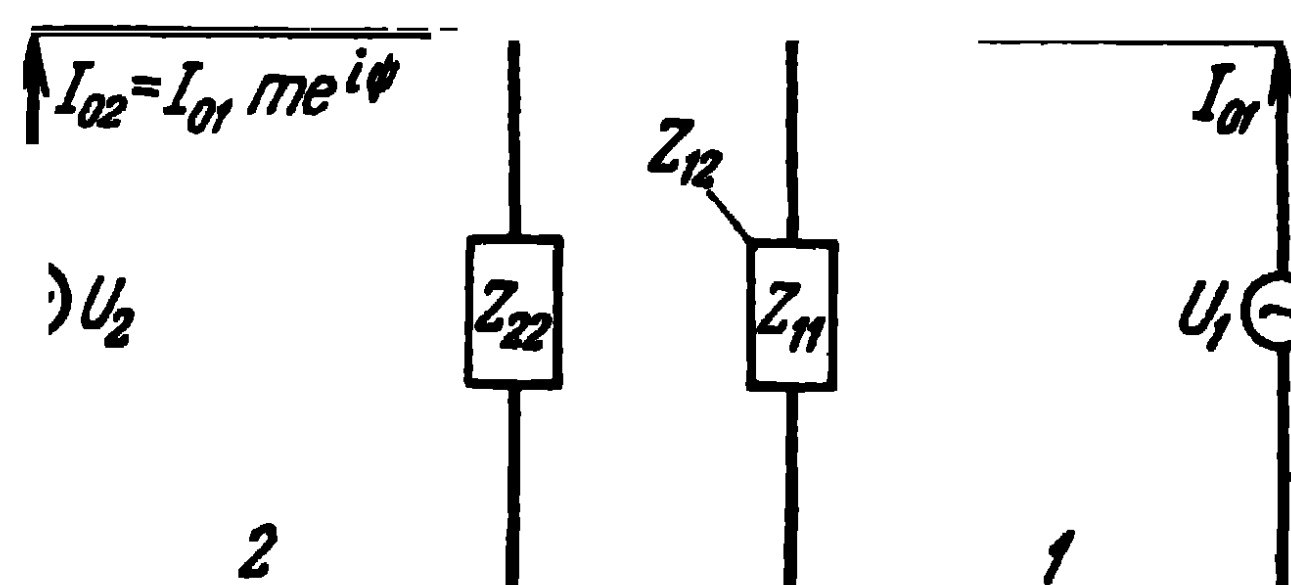


Fig. 3-4 Equivalent circuit of two coupled antennas.

other, and Z_{12} and Z_{21} , these-called mutual or coupling resistances. Moreover, they are all related to the currents at the feed points of the antennas.

It is seen from (3-19) and (3-20) that the mutual resistances are equal $Z_{12} = Z_{21}$. A more detailed analysis shows that this equality is likewise maintained even when the antennas are of different lengths. From now on, we shall therefore speak of the mutual resistance as of a quantity which is defined according either to (3-19) or (3-20). The mutual resistances of the antennas are complex quantities.

On the basis of (3-16), we may reduce two coupled antennas to the equivalent circuit shown in Fig. 3-4.

Dividing the first equation (3-16) by I_{01} and the second one by I_{02} , we obtain the expressions for the full input impedances of antennas 1 and 2:

$$\left. \begin{aligned} Z_{01} &= \frac{U_1}{I_{01}} = Z_{11} + me^{i\psi} Z_{12}; \\ Z_{02} &= \frac{U_2}{I_{02}} = Z_{22} + \frac{1}{m} e^{-i\psi} Z_{12} \end{aligned} \right\} \quad (3-21)$$

In these equations, the second terms in the right-hand side represent the resistances introduced by the second antenna into the first one and by the first antenna into the second one.

In the case of arbitrary current amplitudes and phases, the introduced resistances are not of equal magnitude and depend on the ratio of the currents in the antennas as well as on the geometrical dimensions of the radiating system, which is seen from the expressions given in Paragraph 3-5. It is only in the case of co-phasal oscillations with equal amplitudes ($me^{i\psi} = 1$) that the introduced resistances become equal to each other and to the mutual resistance. Incidentally, this explains why mutual resistances are sometimes taken as the resistances introduced in the presence of co-phased oscillations.

If we assume that $Z_{11} = R_{11} + iX_{11}$, $Z_{22} = R_{22} + iX_{22}$ and $Z_{12} = R_{12} + iX_{12}$ the equations (3-21) may be given the following form convenient for calculation purposes:

$$\begin{aligned} Z_{01} &= R_{11} + m(R_{12} \cos \psi - X_{12} \sin \psi) + i[X_{11} + m(R_{12} \sin \psi + \\ &\quad + X_{12} \cos \psi)]; \\ Z_{02} &= R_{22} + \frac{1}{m}(R_{12} \cos \psi + X_{12} \sin \psi) + i\left[X_{22} - \frac{1}{m}(R_{12} \sin \psi - \right. \\ &\quad \left. - X_{12} \cos \psi)\right]. \end{aligned} \quad (3-22)$$

The equations enable to calculate the full input impedances of the two coupled antennas if the ratios of the currents, i.e., m and ψ are known beforehand.

When reactances are connected at the antenna input with the object of tuning them up, the quantities $X_{11} + X_{1t}$ and $X_{22} + X_{2t}$, where X_{1t} and X_{2t} are reactances inserted into the antennas at their feed points and not associated with the radiation process, should be introduced into all the above given expressions, instead of the separate reactances X_{11} and X_{22} .

Let us now define the power fed to the system and radiated by each of the antennas.

The power supplied from the generator to antenna 1 and radiated by the system is:

$$P_{\Sigma 1} = \frac{I_{01} I_{01}^*}{2} [R_{11} + m(R_{12} \cos \psi - X_{12} \sin \psi)], \quad (3-23)$$

and the power supplied to antenna 2 and radiated by the system is:

$$P_{\Sigma 2} = \frac{I_{02} I_{02}^*}{2} \left[R_{22} + \frac{1}{m} (R_{12} \cos \psi + X_{12} \sin \psi) \right]. \quad (3-24)$$

The total power radiated by the system is equal to the sum of (3-23) and (3-24):

$$P_{\Sigma} = \frac{I_{01} I_{01}^*}{2} [R_{11} + m^2 R_{22} + 2m R_{12} \cos \psi]. \quad (3-25)$$

Whence we determine the radiation resistance of the whole system with respect to the current at the feed points of antenna 1:

$$R_{\Sigma 0} = R_{11} + m^2 R_{22} + 2m R_{12} \cos \psi. \quad (3-26)$$

3-3. Active Reflector

As we saw in Paragraph 3-1, if $m=1$, $\psi=90^\circ$ and $\frac{d}{\lambda} = \frac{1}{4}$, antenna 2 reflects energy towards antenna 1. In that case, the field in the direction of antenna 1 in the radiation zone is doubled in comparison with the field of one antenna. To obtain the stated ratio of the currents ($m=1$, $\psi=90^\circ$), both antennas should be fed at a definite relation between the feeding voltages U_1 and U_2 . In that case, antenna 2 is referred to as the active reflector.

Therefore, in accordance with the expressions (3-22), the full input impedances of the antennas are:

$$\begin{aligned} Z_{01} &= R_{11} - X_{12} + i(X_{11} + R_{12}), \\ Z_{02} &= R_{22} + X_{12} + i(X_{22} - R_{12}). \end{aligned} \quad (3-27)$$

It follows from this equation as well as from (3-26) that the radiation resistance of an antenna with an active reflector is:

$$R_{\Sigma 0} = R_{11} + R_{22}. \quad (3-28)$$

3-4. Passive Antenna

Let antenna 2 be passive, i.e., such that it is not fed from the generator ($U_2=0$) and is excited by the field of antenna 1.

Let a reactance X_{2t} be connected to antenna 2 with the object of tuning it up (Fig. 3-5). The equivalent circuit of such a system is similar to that represented in Fig. 3-4 and differs from it only in that, instead of the generator of voltage U_2 , the reactance X_{2t} is connected to contour 2.

For this circuit, Kirchhoff's equations are written as:

$$\begin{aligned} U_1 &= I_{01}Z_{11} + I_{02}Z_{12}; \\ 0 &= I_{02}(Z_{22} + iX_{2t}) + I_{01}Z_{12}. \end{aligned} \quad (3-29)$$

The left-hand side of the second equation is zero because $U_2=0$. Incidentally, it follows that $Z_{02} = \frac{U_2}{I_{02}} = 0$, i.e., since it is passive, the full impedance of antenna 2 equals zero. The second equation (3-29) enables to determine the current induced in the passive antenna,

$$\frac{I_{02}}{I_{01}} = - \frac{Z_{12}}{Z_{22} + iX_{2t}}. \quad (3-30)$$

Substituting (3-30) into the first equation (3-29), we obtain the expression for the impedance of the active antenna, i.e., of antenna 1,

$$Z_{01} = Z_{11} - \frac{Z_{12}^2}{Z_{22} + iX_{2t}}. \quad (3-31)$$

On comparing (3-30) with (3-1), we obtain the following expressions convenient for calculation purposes

$$m = \sqrt{\frac{R_{12}^2 + X_{12}^2}{R_{22}^2 + (X_{22} + X_{2t})^2}}; \quad (3-32)$$

$$\psi = \pi + \arctan \frac{X_{12}}{R_{12}} - \arctan \frac{X_{22} + X_{2t}}{R_{22}}. \quad (3-33)$$

The expressions (3-32) and (3-33) are generally used for calculating the current amplitudes and phases in a passive antenna.

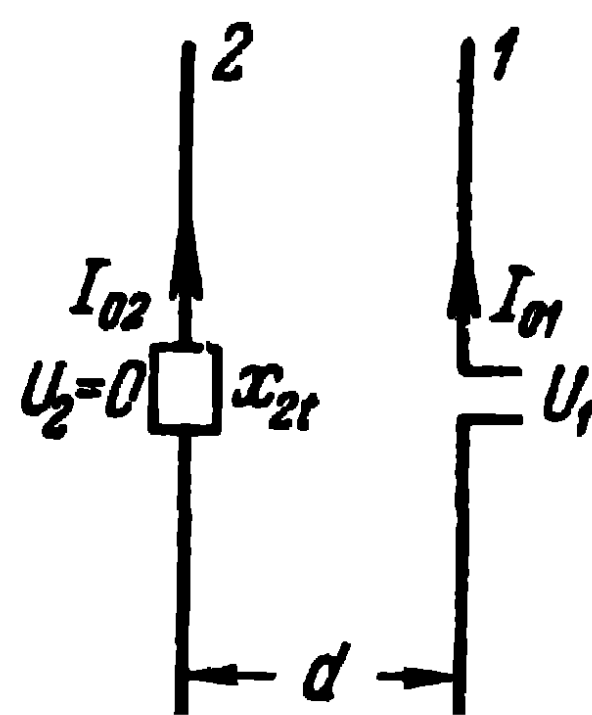


Fig. 3-5. System consisting of one active and one passive antennas.

Since $Z_{02}=0$, the radiation resistance of a system consisting of an active and a passive antennas is expressed as:

$$R_{\Sigma 0} = R_{11} + m(R_{12} \cos \psi - X_{12} \sin \psi). \quad (3-34)$$

When $X_{21}=0$, the current in the passive antenna is always smaller than that in the active antenna ($m < 1$), and diminishes continuously as the distance between the antennas increases, owing to the fact that the magnitude of the coupling resistance is always smaller than that of the resistance of the passive antenna.

When the distance between the antenna is very small, owing to the fact that $Z_{12} \rightarrow Z_{22}$, we have: $m \approx 1$, $\psi \approx \pi$ and $R_{\Sigma 0} \approx 0$. In that case, the two antennas system ceases to radiate, because the energy supplied to the system by the oscillator does not take up the entire space between the antennas.

When the passive antenna is tuned in resonance and $X_{22} + X_{21} = 0$, the current in it reaches its maximum value at all distances; at small ones, d may become larger than the current in the active antenna. In the case of resonance, (3-32) and (3-33) take the following form:

$$m = \sqrt{\frac{R_{12}^2 + X_{12}^2}{R_{22}}}; \quad (3-32a)$$

$$\psi = \pi + \arctan \frac{X_{12}}{R_{12}}. \quad (3-33a)$$

When the value and phase (depending on distance d and tuning X_{21}) of the current excited in the passive antenna are such that the maximum field is set up in the direction of the active antenna and the minimum field, in the direction of the passive antenna, the latter is referred to as a passive reflector. However, the passive antenna may be tuned up in such a way that the maximum energy will be radiated in the direction of the passive antenna and the minimum energy, in the direction of the active antenna. In that case, the passive antenna directs energy in its own direction and is consequently referred to as a director.

In the case of a passive reflector, the optimum distance between the antennas lies between $d=0.2\lambda$ and $d=0.25\lambda$. Hence the difference between the directional diagram and that of the antenna with an active reflector (Fig. 3-3) is

that in the passive reflector, there is always a lobe in the direction of the reflector, whereas no such lobe is observed in the case of the active reflector. This is due to the fact that it is impossible in the passive antenna to fulfil simultaneously the conditions $m=1$ and $\psi=90^\circ$ when $\frac{d}{\lambda}=0.25$, since the operator can only change the magnitude and sign of the resistance X_{2t} .

3-5. Calculating Mutual Resistance of Antennas

To calculate the mutual resistance of antennas, the general expression (3-19) obtained by the induced emf method is used. This method was first applied to the calculation of the mutual resistances of antennas forming part of antenna systems by A. A. Pistolokors in 1928. Applying the expression (3-19) to the calculation of the coupling of two parallel antennas of equal length, as shown in Fig. 3-1, one needs to substitute into it the corresponding values of E_{z12} and I_{z1} . If we assume the distribution of the current to be sinusoidal, $I_{z1} = \frac{I_{01}}{\sin kl} \sin k(l-z)$, the expression for E_{z12} will be obtained in the form of (2-25). The calculation proceeds in just the same way as shown in Paragraph 2-7. As a result, we obtain the following expression:

$$\begin{aligned} Z_{12} = & \frac{30}{\sin^2 kl} \{ [1 + 2e^{-ikl} \cos kl] [\text{Ci } kd - \\ & - \text{Ci } k(\sqrt{d^2 + l^2} - l) - i \text{Si } kd + i \text{Si } k(\sqrt{d^2 + l^2} - l)] + \\ & + [1 + 2e^{ikl} \cos kl] [\text{Ci } kd - \text{Ci } k(\sqrt{d^2 + l^2} + l) - \\ & - i \text{Si } kd + i \text{Si } k(\sqrt{d^2 + l^2} + l)] + e^{i2kl} [\text{Ci } k(\sqrt{d^2 + 4l^2} + 2l) - \\ & - \text{Ci } k(\sqrt{d^2 + l^2} + l) - i \text{Si } k(\sqrt{d^2 + 4l^2} + 2l) + \\ & + i \text{Si } k(\sqrt{d^2 + l^2} + l)] + e^{-i2kl} [\text{Ci } k(\sqrt{d^2 + 4l^2} - 2l) - \\ & - \text{Ci } k(\sqrt{d^2 + l^2} - l) - i \text{Si } k(\sqrt{d^2 + 4l^2} - 2l) + \\ & + i \text{Si } k(\sqrt{d^2 + l^2} - l)] \}. \end{aligned} \quad (3-35)$$

In the limit case, when the antennas 1 and 2 coincide ($d=0$), this expression defines also the natural resistance of the symmetrical antenna $Z_{11}=Z_{22}$.

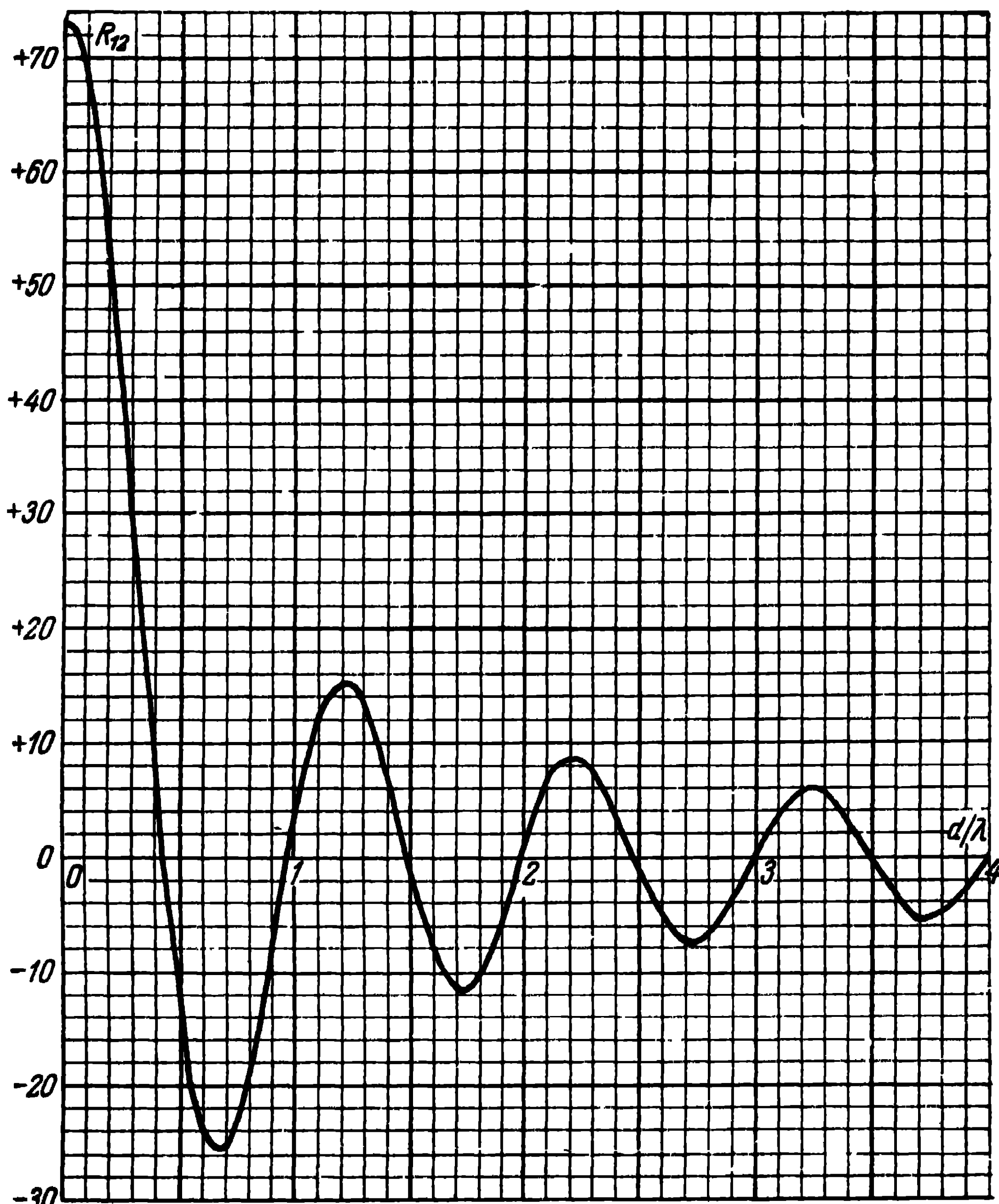


Fig. 3-6. Curve of the resistive component of the mutual resistance of half-wave antennas.

Figs. 3-6 and 3-7 give the curves of the resistive R_{12} and reactive X_{12} components of the mutual resistance of half-wave antennas, calculated by means of (3-35). As can be seen from these curves, in the limit case $d=0$, for infinitely thin antennas, the mutual resistance passes into the natural resistance of the half-wave antenna and ac-

quires the values $R_{12}=R_{11}=73.1$ ohms and $X_{12}=X_{11}=42.5$ ohms.

Appendix I contains a table of the values of R_{12} , as calculated by A. A. Pistolokors and first published by him in 1928 [13]. Appendix II contains the tables of the values of R_{12} and X_{12} , as composed by V. V. Tatarinov and published by him in 1936 [2]. The tables concern half-wave antennas spaced at a distance d apart and displaced along the axis by a distance h in wave-lengths.

To illustrate the performance of two coupled antennas, one of which is passive, Fig. 3-8 shows the curves of $R_{\Sigma 0}$, ψ , I_{02} , I_0 , $E_{z=0}$ and E_m as a function of the mag-

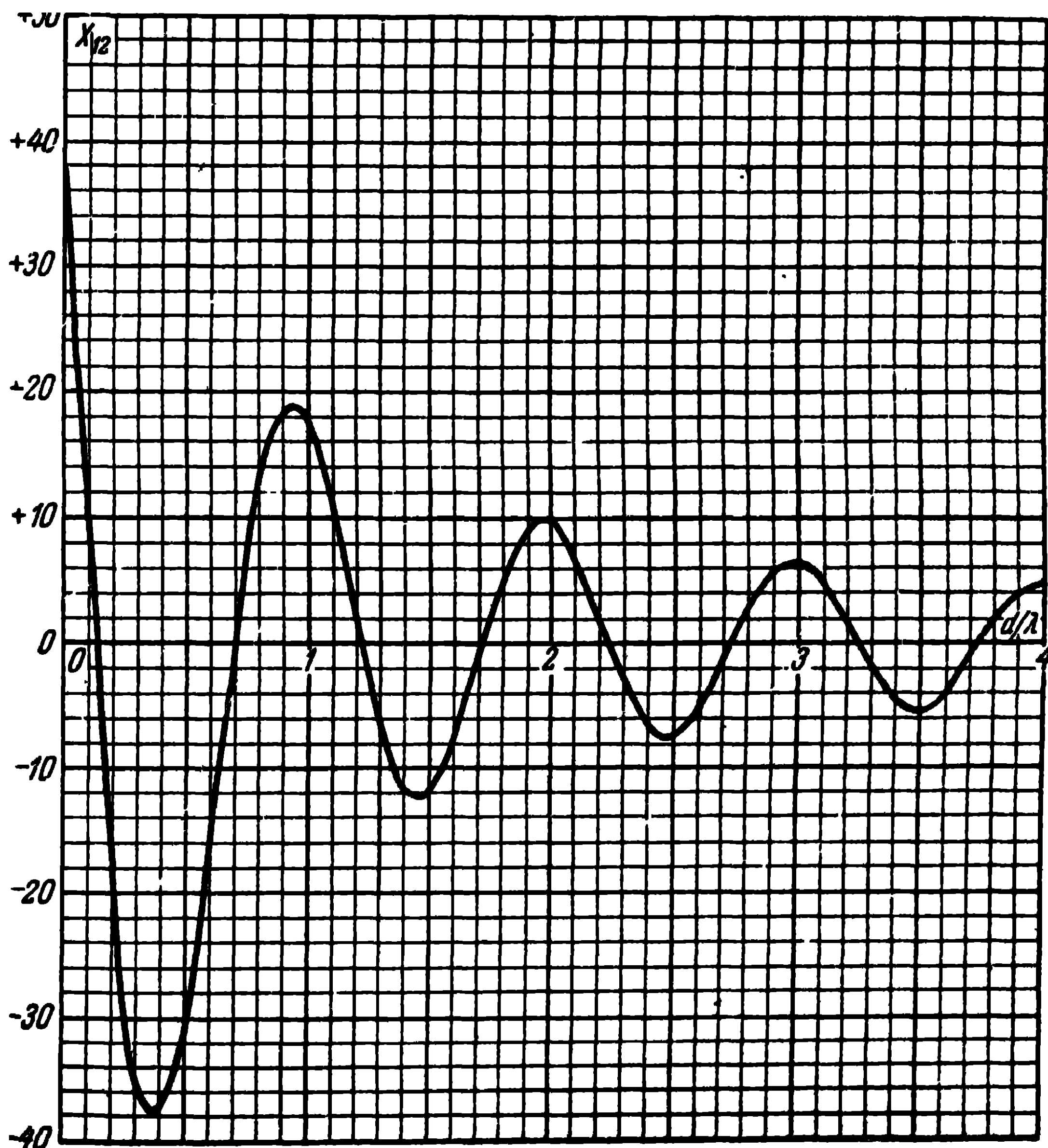


Fig. 3-7. Curve of the reactive component of the mutual resistance of half-wave antennas.

nitude of the passive antenna reactive impedance $X_{22} + X_{2t}$. In the same figure, the currents I_{02} and I_{01} and the field

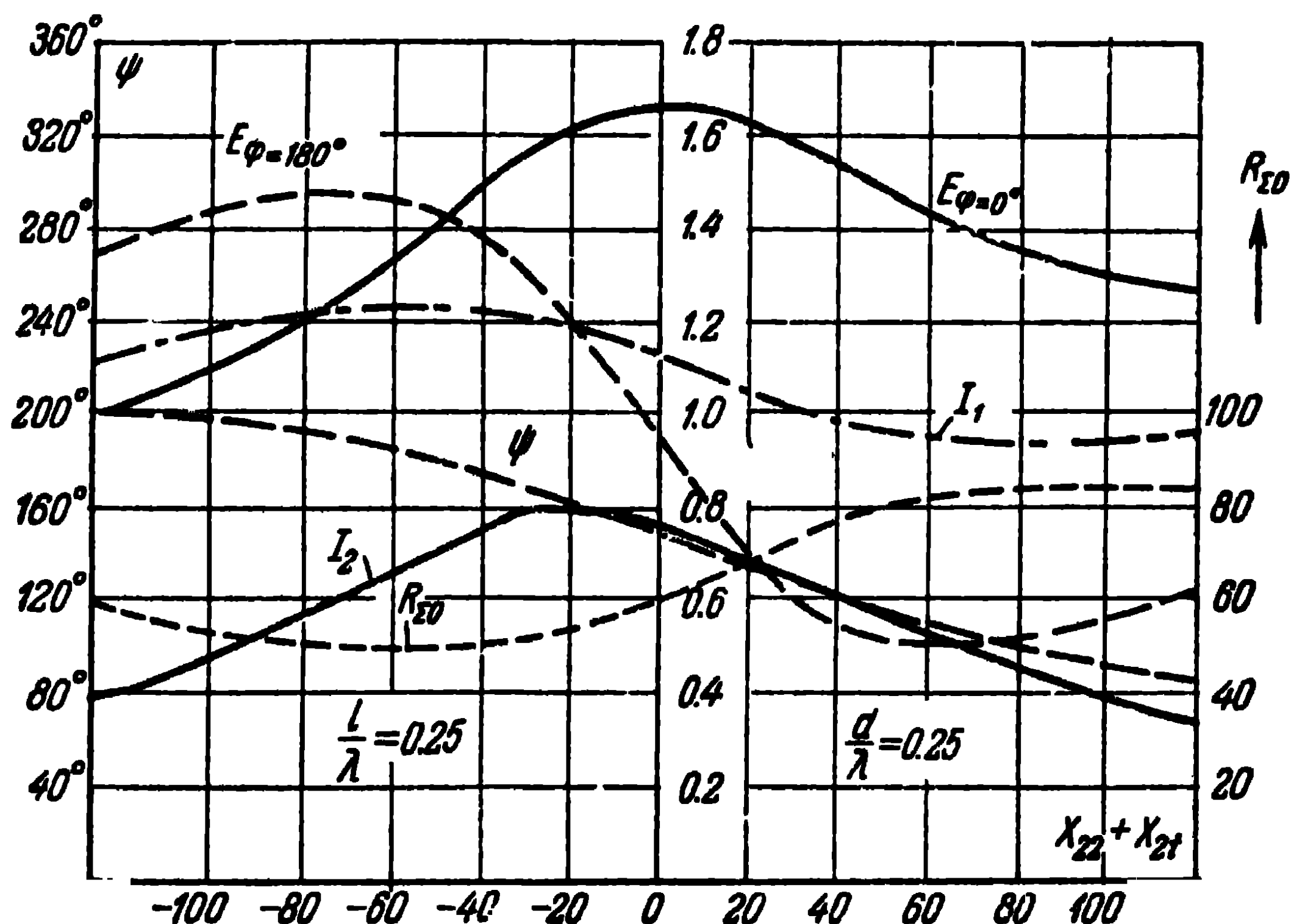


Fig. 3-8. Type of operation of a system consisting of an active and a passive antennas plotted as a function of the tuning of the passive antenna.

intensity in the direction of the active antenna $E_{\varphi=0}$ and in the direction of the passive antenna $E_{\varphi=180^\circ}$ are given in relation to the current and field intensity of one single antenna on condition that the radiated power remains the same in both cases. As is seen from this figure, the passive antenna plays the role of a reflector when its reactive impedance $X_{22} + X_t$ is positive, i.e., is of an inductive nature; this same antenna plays the role of a director when $X_{22} + X_t$ is negative, i.e., has a capacitive nature.

CHAPTER FOUR

Radiator Systems and Antenna Parameters

4-1. General

In the preceding chapters, we saw how, by combining dipoles or antennas (electric as well as magnetic), one could obtain various directional characteristics.

In the present chapter, we shall discuss methods of obtaining highly directional characteristics or radiation characteristics by means of systems consisting of a large number of relatively simple radiators discretely or continuously distributed in space. Methods of obtaining highly directional characteristics deserve special attention due to the practical importance of devices with characteristics of this particular kind.

The systems of radiators are made up of wire, slot, dielectric or other types of radiators. In all cases, use is made of the radio wave interference phenomenon according to which, the radiation of all the radiators are added up in some directions and subtracted in others, due to differences in path length of the rays from separate elements of the system and differences in the phases of the currents in these elements.

We shall examine separate systems of radiators with different current amplitude and phase distributions, without going into details as to how these distributions can be obtained.

4-2. Radiation of a Linear Co-Phased Dipole Array

Many antenna systems utilised in practice are made up of half-wave dipoles suitably disposed in space and excited at definite ratios of current amplitudes and phases. We shall

Investigate the radiation of a system of dipoles lying on one plane and excited in co-phase.

Let nm half-wave dipoles, forming a linear array as shown in Fig. 4-1, lie at a distance d_1 apart between the centres

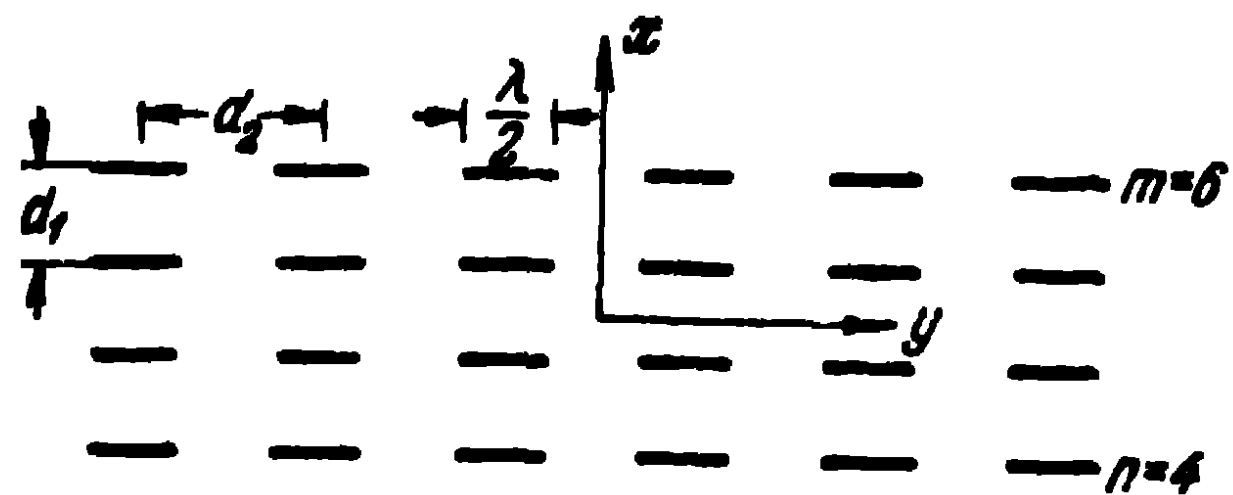


Fig. 4-1. Array of half-wave dipoles.

of neighbouring dipoles in different rows, and at a distance d_2 between the centres of neighbouring dipoles in one row (n being the number of rows of dipoles and m , the number of dipoles in one row).

In accordance with (2-16), the field intensity of each of the dipoles in the radiation zone is:

$$E = E_0 \frac{\cos\left(\frac{\pi}{2} \cos \theta\right)}{\sin \theta}, \quad (4-1)$$

where θ is the angle between the direction towards the point of observation and the axis of the dipole;

$E_0 = i \frac{60 I_a}{r_0} e^{-ikr_0}$, the field intensity of the dipole in its equatorial plane at the distance r_0 .

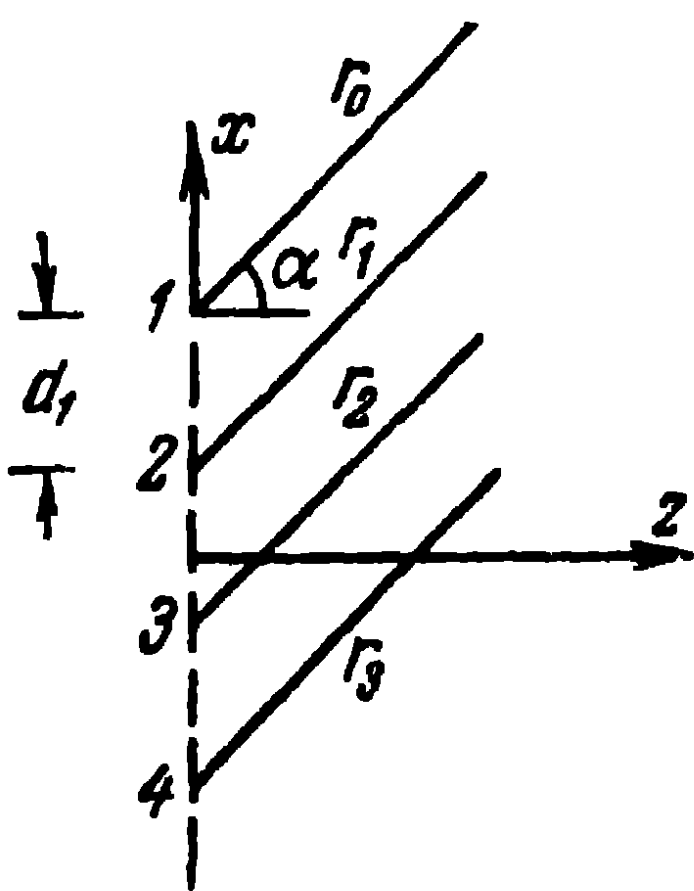


Fig. 4-2. Explaining the calculation of the radiation of a dipole array in the magnetic vector plane.

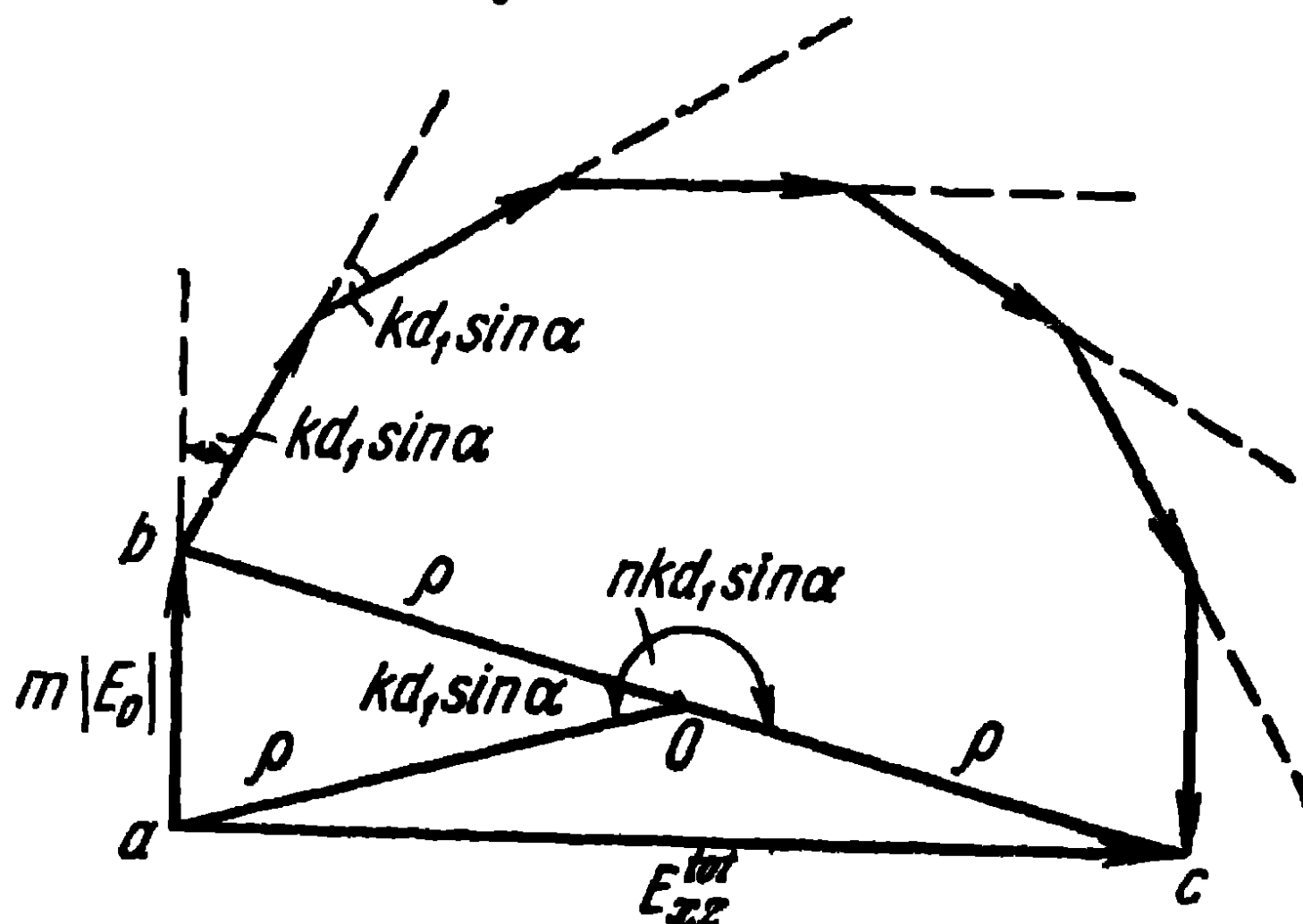


Fig. 4-3. Vector diagram of the composition of the fields of a system of dipoles.

To begin with, let us investigate the field in the xz -plane, i.e., in the equatorial plane of the dipoles or in the

magnetic vector plane (Fig. 4-2). Since at the point of observation, the directions of the field vectors from the separate dipoles coincide, the resultant field intensity of the system in that plane is defined as

$$E_{xz}^{\text{tot}} = mE_0 [1 + e^{-ikd_1 \sin \alpha} + e^{-i2kd_1 \sin \alpha} + \dots + e^{-i(n-1)kd_1 \sin \alpha}].$$

We have taken into account that, because $\frac{1}{r_0} \approx \frac{1}{r_1} \approx \dots \approx \frac{1}{r_{n-1}}$ the amplitudes of the field E_0 of all the dipoles are the same and the difference in path length of the rays from neighbouring rows equals $r_r - r_{r-1} = d_1 \sin \alpha$, where α is the angle between the direction towards the point of observation and the z -axis.

This expression corresponds to the vector diagram shown in Fig. 4-3. Let ρ be the radius of the circumference described near the polygon formed by the vectors $m|E_0|e^{-ikd_1 \sin \alpha}$. Then, from the triangle abo , we find

$$m|E_0| = 2\rho \sin\left(\frac{kd_1}{2} \sin \alpha\right),$$

and from the triangle aco , we find

$$|E_{xz}^{\text{tot}}| = 2\rho \sin\left(\frac{nk d_1}{2} \sin \alpha\right).$$

Hence

$$|E_{xz}^{\text{tot}}| = m|E_0| \frac{\sin\left(\frac{nk d_1}{2} \sin \alpha\right)}{\sin\left(\frac{kd_1}{2} \sin \alpha\right)}. \quad (4-2)$$

We have used the factor m because from the point of view of the formation of the directional diagram in the equatorial plane, all the dipoles of one row behave as one dipole with current $I = mI_1$, where I_1 is the current amplitude in one dipole.

Let us analyse the expression (4-2). When $\alpha = 0$ $E_{xz}^{\text{tot}} = nm|E_0|$, i.e., in a direction perpendicular to the plane of the array, the field intensity is equal to that of one dipole in the system, multiplied by the total number of dipoles. The radiation zero occurs in the direction defined from the condition

$$\frac{nk d_1}{2} \sin \alpha_0 = N\pi, \quad N = 1, 2, 3$$

from which we derive

$$\sin \alpha_0 = \frac{N\lambda}{nd_1} \quad (4-3)$$

Thus, for example, when $n=8$ and $d_1 = \frac{\lambda}{2}$ $\sin \alpha_0 = \frac{N}{4}$ and there is no radiation in the direction of the angles $\alpha_0 = 14.5^\circ$, $\alpha_0 = 30^\circ$ and $\alpha_0 = 48.6^\circ$.

Fig. 4-4 gives the directional diagram for that case, calculated from (4-2).

As can be seen, the directional diagram has a major lobe and a number of minor side ones. The number of minor lobes is the larger, the larger the number of rows of dipoles. In the example under consideration, the width of the major lobe at the zeros of radiation equals 29° . In the general case, when there is a large number of dipoles and they are spaced sufficiently wide apart, the width

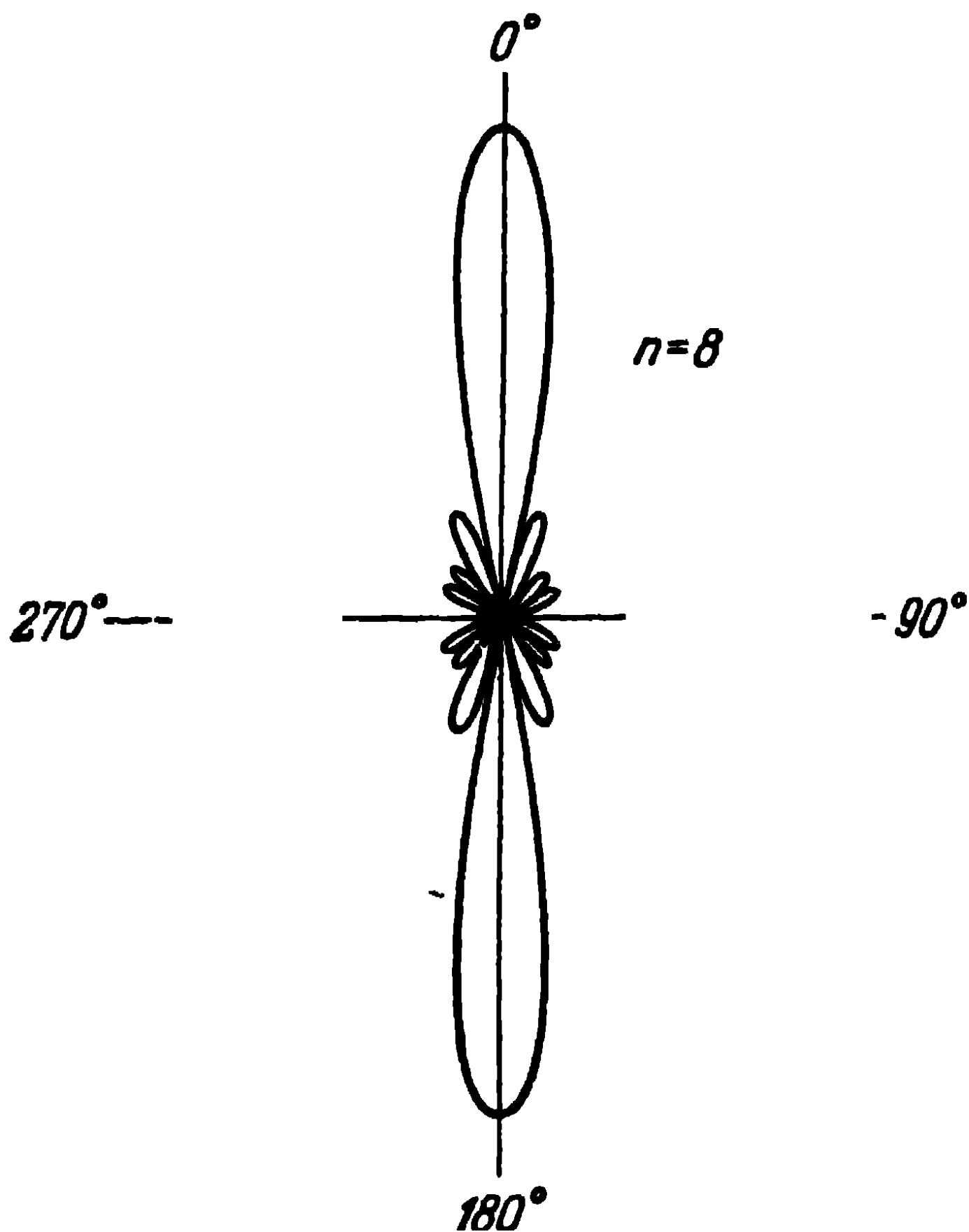


Fig. 4-4. Directional diagram of a co-phased dipole array.

of the major lobe at the zeros may be defined by the following simplified expression derived from (4-3)

$$2\alpha_n = 2 \frac{\lambda}{L} [\text{rad}]. \quad (4-4)$$

where $L \approx nd_1$.

Thus, the directivity of the co-phased array is all the larger as the width (or length) of the system L is larger relative to the wave-length λ .

Let us now define the minor radiation maximums. For small values of d_1 in comparison with the wave-length, the variation of denominator in (4-2) can be neglected in the region of the minor maximums, so that the position of the

minor maximums can be found from the condition

$$\sin \left(\frac{nk d_1}{2} \sin \alpha_{\max} \right) = \pm 1.$$

Hence

$$\sin \alpha_{\max} = \frac{2N+1}{2} \frac{\lambda}{n d_1}, \quad N = 1, 2, 3 \dots \quad (4-5)$$

Substituting this value into (4-2), we obtain:

$$|E_{xz}^{\text{tot}}(\alpha_{\max})| = m |E_0| \frac{1}{\sin \left(\frac{2N+1}{n} \frac{\pi}{2} \right)}. \quad (4-6)$$

We see that the magnitudes of the maximums of the minor lobes of the directional diagram of a co-phased array cannot be smaller than $\frac{1}{n}$ of the magnitude of the maximum of the major lobe, because in (4-6) the denominator is always smaller than unity.

It can be further seen from (4-6) that for a large value of n , the magnitude of the maximum of the first minor lobe equals approximately

$$|E_{xz}^{\text{tot}}(\alpha_{\max})| = nm |E_0| \frac{2}{3\pi},$$

i. e., constitutes approximately $\frac{1}{5}$ of the magnitude of the maximum of the major lobe.

Let us also note that it follows from (4-2) that the number of dipoles in a row of the co-phased array does not influence the form of the directional diagram in the magnetic vector plane and determines only the absolute value of the field intensity.

Let us now examine the directional diagram of the array in the yz -plane, i.e., in the electric vector plane. Let β be the angle between the direction towards the point of observation and the z -axis in that plane (Fig. 4-5). Then, similarly to the above, we obtain for the total field in the radiation zone the expression

$$E_{yz}^{\text{tot}} = n E_0 \frac{\cos \left(\frac{\pi}{2} \sin \beta \right)}{\cos \beta} [1 + e^{-i k d_2 \sin \beta} + e^{-i 2 k d_2 \sin \beta} + \dots + e^{-i (m-1) k d_2 \sin \beta}],$$

or

$$|E_{yz}^{\text{tot}}| = n |E_0| \frac{\cos\left(\frac{\pi}{2} \sin \beta\right)}{\cos \beta} \frac{\sin\left(\frac{mkd_2}{2} \sin \beta\right)}{\sin\left(\frac{kd_2}{2} \sin \beta\right)}. \quad (4-7)$$

Here, the first factor on the right-hand side of (4-7) (disregarding the factors n and $|E_0|$ which do not depend on the direction) represents the directional characteristic of a

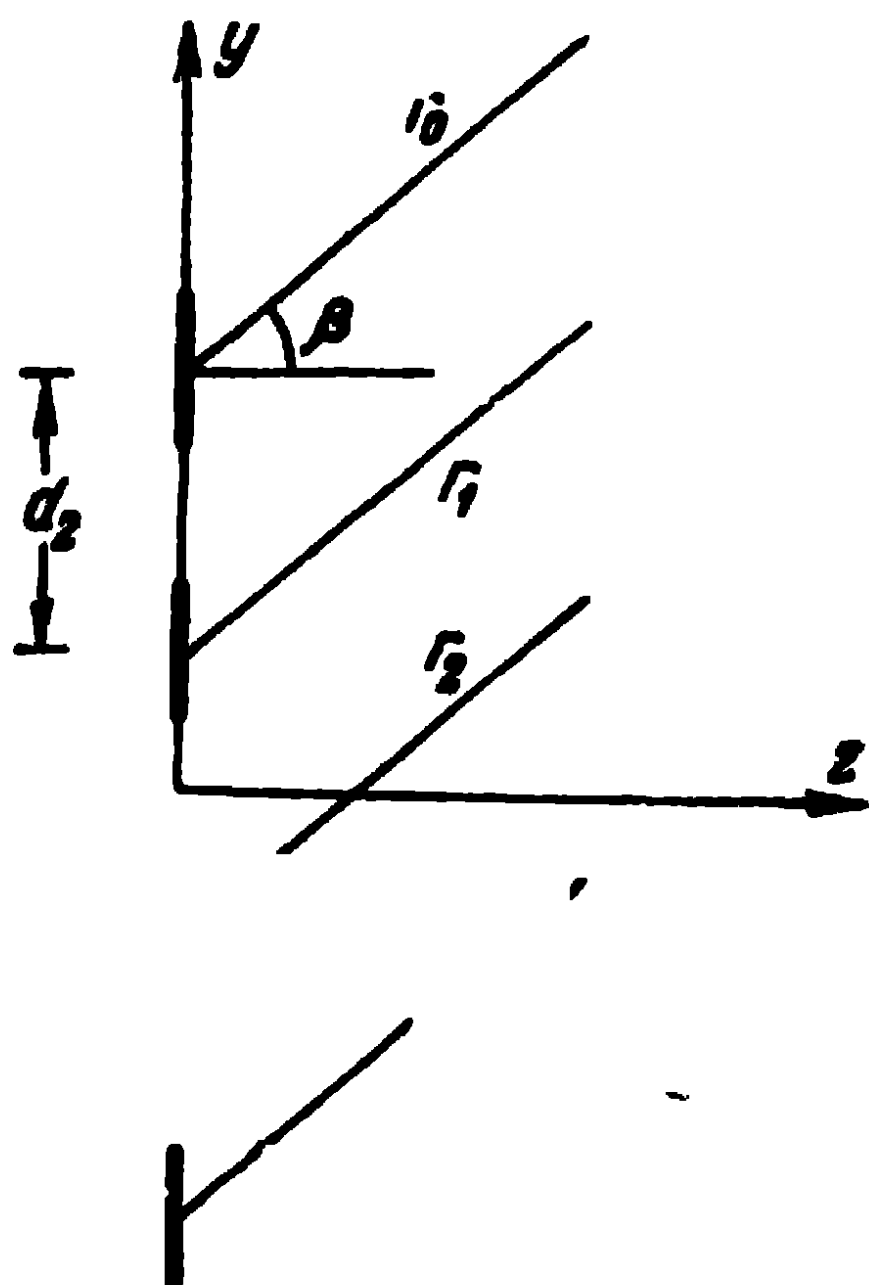


Fig. 4-5. Explaining the calculation of the radiation of a dipole array in the electric vector plane.

half-wave dipole and the second factor is that of the combination of the radiation of the non-directional radiators. All the deductions which were drawn with regard to (4-2) apply also to this second factor in (4-7). It is clear that the form of the directional diagram in the electric vector plane depends on the number of dipoles in one row m and does not depend on the number of rows n . Only the radiation intensity depends on the number of rows in that plane.

It should be further noted that when the array is square, i. e., when $n=m$ and $d_1=d_2$, the directivity of the radiation in the plane of the electric vector of the array is somewhat larger than the radiation

directivity in the plane of the magnetic vector, due to the presence of the first factor in (4-7), i. e., due to the directivity of the radiation of the dipole in its meridional plane.

The expressions (4-2) and (4-7) define the directional diagrams of the co-phased array in the two principal planes. One could also determine the radiation in the other planes, but the picture of the radiation in these two planes is found to be perfectly adequate for technical purposes.

In antenna theory, one often meets the concept of normalised radiation characteristics, by which one understands the ratio of the magnitude of the field intensity in the radiation zone in a given direction to the magnitude of the field intensity in the radiation zone in the direction of the maxi-

mum radiation. Thus, for the magnetic vector plane, the normalised radiation characteristic of a co-phased array is expressed as

$$F(\alpha) = \frac{|E_{xz}^{\text{tot}}|}{nm|E_0|} = \frac{1}{n} \frac{\sin\left(\frac{nk d_1}{2} \sin \alpha\right)}{\sin\left(\frac{k d_1}{2} \sin \alpha\right)}, \quad (4-8)$$

and for the electric vector plane, the normalised radiation characteristic of the array is given as the product of two normalised radiation characteristics

$$F(\beta) = F_1(\beta) F_2(\beta), \quad (4-9)$$

where

$$F_1(\beta) = \frac{\cos\left(\frac{\pi}{2} \sin \beta\right)}{\cos \beta} \quad (4-10)$$

is the normalised characteristic of a half-wave dipole, and

$$F_2(\beta) = \frac{1}{m} \frac{\sin\left(\frac{m k d_2}{2} \sin \beta\right)}{\sin\left(\frac{k d_2}{2} \sin \beta\right)} \quad (4-11)$$

the normalised characteristic of m non-directional radiators.

4-3. Radiation of a Linear Dipole Array with Variable Phase

Let us examine an array consisting of one row of half-wave dipoles (Fig. 4-6) excited by currents of equal amplitude but with a phase shift ψ between the currents of neighbouring dipoles, so that

$$I_r = I_1 e^{+i(r-1)\psi},$$

where $r=1, 2, 3, \dots, n$.

Designating by φ the angle between the direction towards the point of observation and the x -axis in

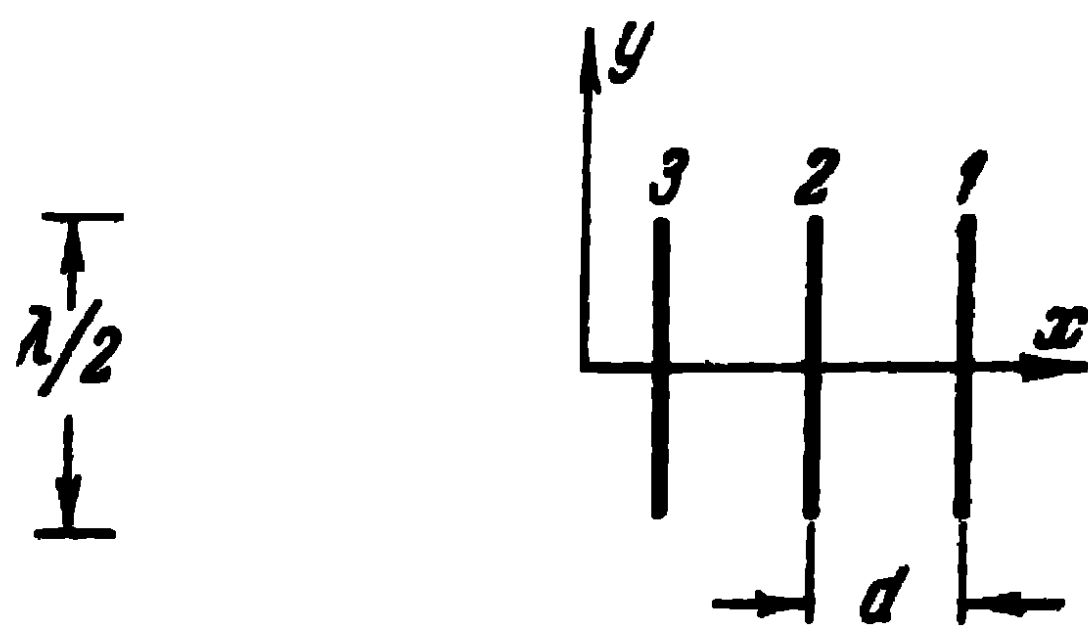


Fig. 4-6. Dipole array with variable current phase.

the magnetic vector plane (Fig. 4-7), we obtain for the total field in the radiation zone:

$$E_{xz}^{\text{tot}} = E_0 [1 + e^{+i(\psi - kd \cos \varphi)} + \dots + e^{+i(n-1)(\psi - kd \cos \varphi)}],$$

where

$$E_0 = i \frac{60 I_a}{r_0} e^{-ikr_0}.$$

Hence the directional diagram of the array is expressed as

$$|E_{xz}^{\text{tot}}| = |E_0| \frac{\sin \left[\frac{n}{2} (\psi - kd \cos \varphi) \right]}{\sin \left[\frac{1}{2} (\psi - kd \cos \varphi) \right]}. \quad (4-12)$$

Let us examine particular cases of excitation of the array. When $\psi = 0$, we get the case of the co-phased dipoles discussed earlier. Assuming that in (4-12) $\psi = 180^\circ$, we obtain the expression for the antiphase dipole array:

$$|E_{xz}^{\text{tot}}| = |E_0| \frac{\sin \left[\frac{n}{2} (180^\circ - kd \cos \varphi) \right]}{\sin \left[\frac{1}{2} (180^\circ - kd \cos \varphi) \right]}. \quad (4-13)$$

It follows from this expression that in the direction $\varphi = \pm 90^\circ$, when n is even, the radiation vanishes. If we assume that $d/\lambda = 0.5$, then, in the direction of the axis of the array ($\varphi = 0^\circ$ and $\varphi = 180^\circ$), the radiation will be at its maximum and equal to $n|E_0|$.

Assuming that in (4-12) $\psi = kd$, we obtain the expression for the dipole array with a phase varying in accordance with the travelling-wave law:

$$|E_{xz}^{\text{tot}}| = |E_0| \frac{\sin \left[\frac{nk d}{2} (1 - \cos \varphi) \right]}{\sin \left[\frac{k d}{2} (1 - \cos \varphi) \right]}. \quad (4-14)$$

We see that in the direction $\varphi = 0$, such a system always gives a maximum of radiation equal to $n|E_0|$, irrespective of the value of d/λ . When $d/\lambda = 0.25$ and n is an odd number,

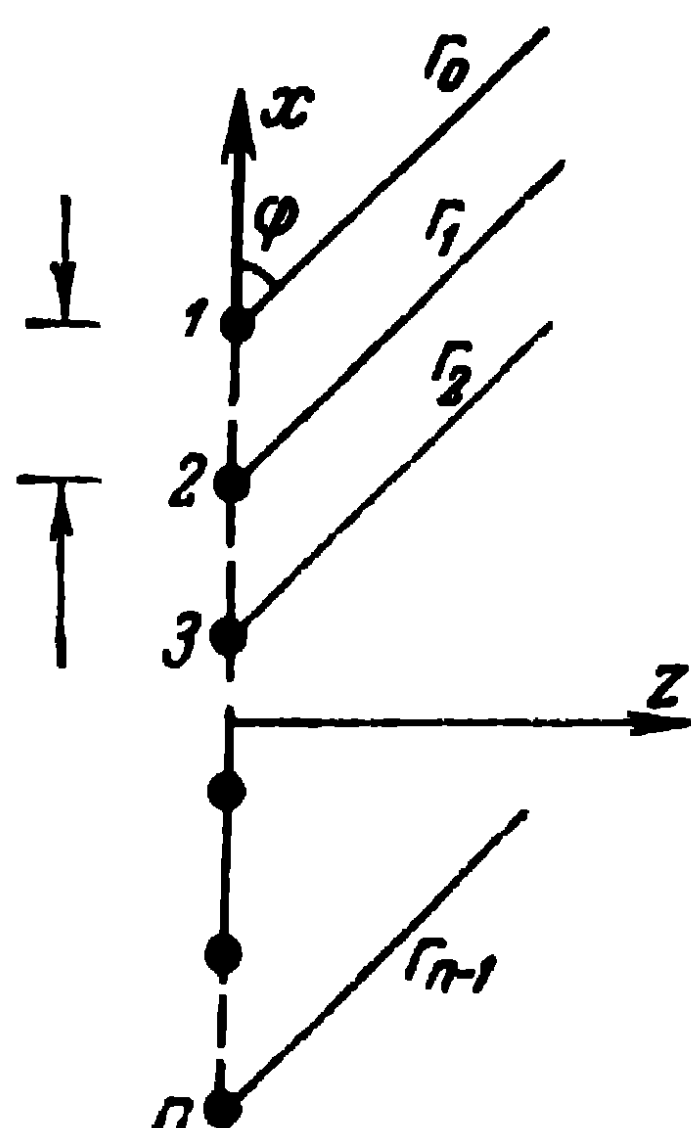


Fig. 4-7. Explaining the calculation of the radiation of a dipole array with variable phase.

we get a zero of radiation in the direction $\varphi=180^\circ$. Thus, in this last case, the radiation is found to be unidirectional: the energy is radiated in the direction of the motion of the wave in the array, none being radiated in the reverse direction. Fig. 4-8 shows the directional diagram of an array of eight dipoles spaced at a distance $\lambda/4$ apart and oscillating with a phase shift $\psi=90^\circ$.

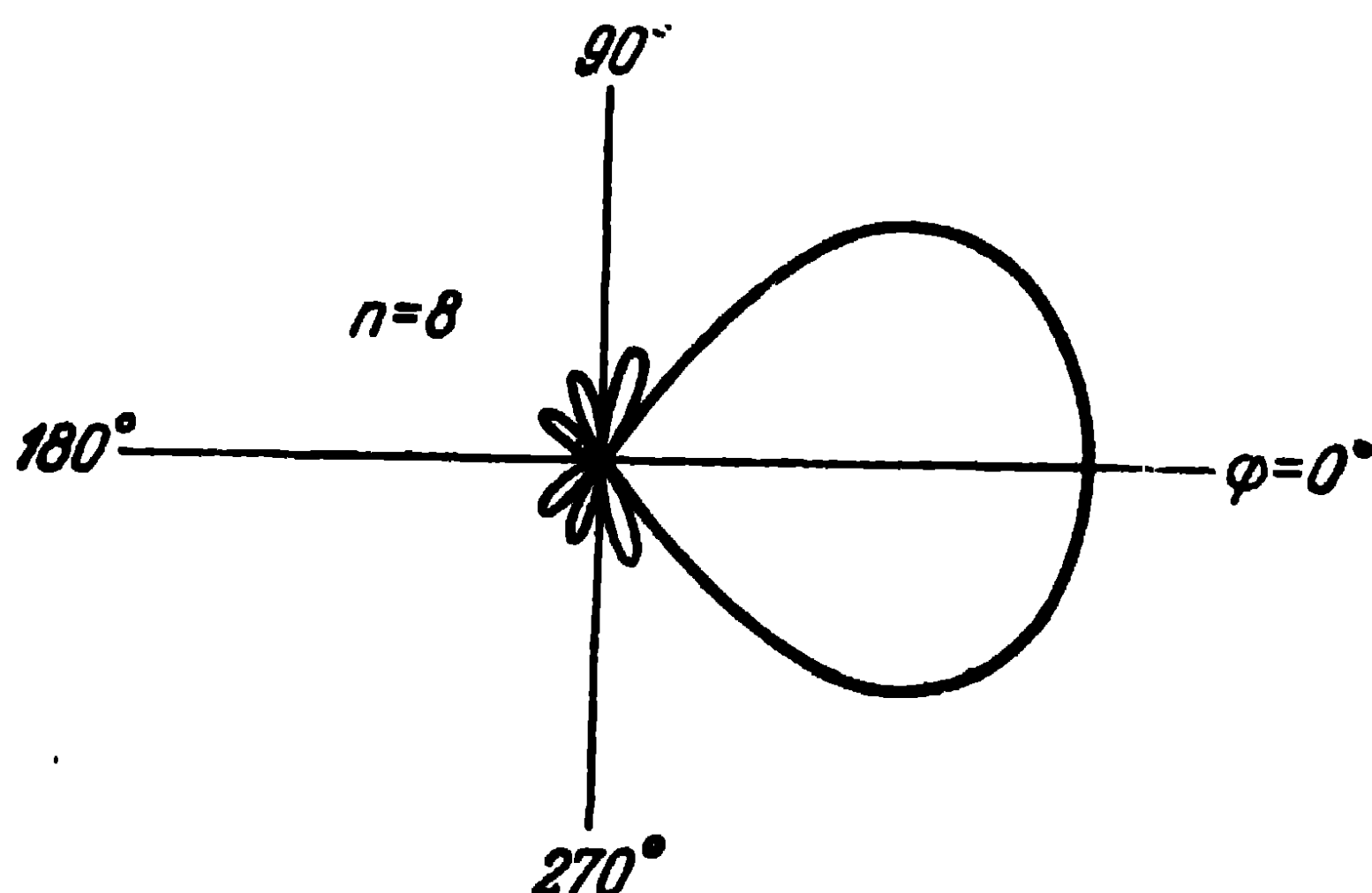


Fig 4-8. Directional diagram of an array with a travelling wave.

If the antennas are arranged in one line at a distance d apart (in accordance with Fig. 4-5, but taking into account that the angle θ is complementary relative to the angle β in that figure) and excited with a phase shift of the currents ψ , the directional diagram is expressed as

$$|E_{xz}^{\text{tot}}| = |E_0| \frac{\cos\left(\frac{\pi}{2} \cos \theta\right)}{\sin \theta} \frac{\sin\left[\frac{n}{2} (\psi - kd \cos \theta)\right]}{\sin\left[\frac{1}{2} (\psi - kd \cos \theta)\right]} . \quad (4-15)$$

It is also of interest to note that from (4-12) as well as from (4-15), it follows that the principal maximum of radiation in the general case lies in the direction which is determined from the condition

$$\cos \theta_{\text{max}} = \frac{\psi}{kd} . \quad (4-16)$$

Thus, for example, when $d/\lambda=0.5$ and $\psi=10^\circ$, we have $\theta_{\text{max}} = \pm 86.8^\circ$.

4-4. Radiation Resistance of a Dipole System

In the two preceding paragraphs of the present chapter we have examined characteristic examples of the formation of highly directional radiation characteristics by means of a linear array of half-wave dipoles. To obtain a definite distribution of the amplitudes and phases of the currents in the dipoles, we have to know the resistance at the terminals of the dipoles of the given system.

Extending to the dipole system the relations for two coupled dipoles discussed in Chapter Three, let us write for an array of n dipoles, the following system of Kirchhoff's equations:

$$\begin{aligned} U_1 &= I_1 Z_{11} + I_2 Z_{12} + \dots + I_n Z_{1n}; \\ U_2 &= I_1 Z_{21} + I_2 Z_{22} + \dots + I_n Z_{2n}; \\ &\vdots \\ U_n &= I_1 Z_{n1} + I_2 Z_{n2} + \dots + I_n Z_{nn}, \end{aligned} \quad (4-17)$$

where U_k and I_k are the voltage and current at the terminals of the k -th dipole;

Z_{pk} , the mutual resistance between the p -th and k -th dipoles;

Z_{kk} , the resistance of the k -th dipole proper.

Dividing U_k by I_k , we obtain the resistance of the k -th antenna, with due account to the effect of all the other dipoles in the system

$$Z_k = \frac{I_1}{I_k} Z_{k1} + \frac{I_2}{I_k} Z_{k2} + \dots + Z_{kk} + \dots + \frac{I_n}{I_k} Z_{kn}. \quad (4-18)$$

Thus, to determine the impedance of a dipole we have to know the resistance of the dipole, the mutual resistance between that dipole and all the other ones, as well as the magnitudes and phases of the currents in all the dipoles relatively to the current amplitude and phase in that dipole.

To give an example, let us calculate the active part of the impedance of one dipole in the co-phased array of half-wave dipoles shown in Fig. 4-1, when $m=2$, $n=2$, $d_1=\frac{\lambda}{2}$ and $d_2=\frac{\lambda}{2}$. Note that in this example, the impedance of all the separate dipoles are equal due to their symmetrical arrangement. Since $\frac{I_k}{I_1}=1$, in accordance with (4-18), the active part of the impedance of the first dipole will be:

$$R_1 = R_{11} + R_{12} + R_{13} + R_{14}.$$

From A. Pistolokors's table (see Appendix I) we find: $R_{11}=73.1$ ohms, $R_{12}=-12.36$ ohms, $R_{13}=26.4$ ohms, $R_{14}=-11.8$ ohms. Consequently, the impedance of each of the four dipoles will be $R_1=R_2=R_3=R_4=75.34$ ohms.

The computation of the active as well as the reactive part of the impedance of the antenna in any other system is performed as in the example quoted.

4-5. Radiation of Continuous Systems of Sources with a Travelling Wave

Let us investigate the radiation of a thin rectilinear conductor of length L , through which there flows an electric current varying along the conductor in accordance with the travelling-wave law:

$$I_x = I_0 e^{-ikx} \quad (4-19)$$

where I_0 is the current at the origin of the conductor.

Let us choose on the conductor an element of current $I_x dx$ (Fig. 4-9). In accordance with (1-3), the field of this element in the radiation zone is:

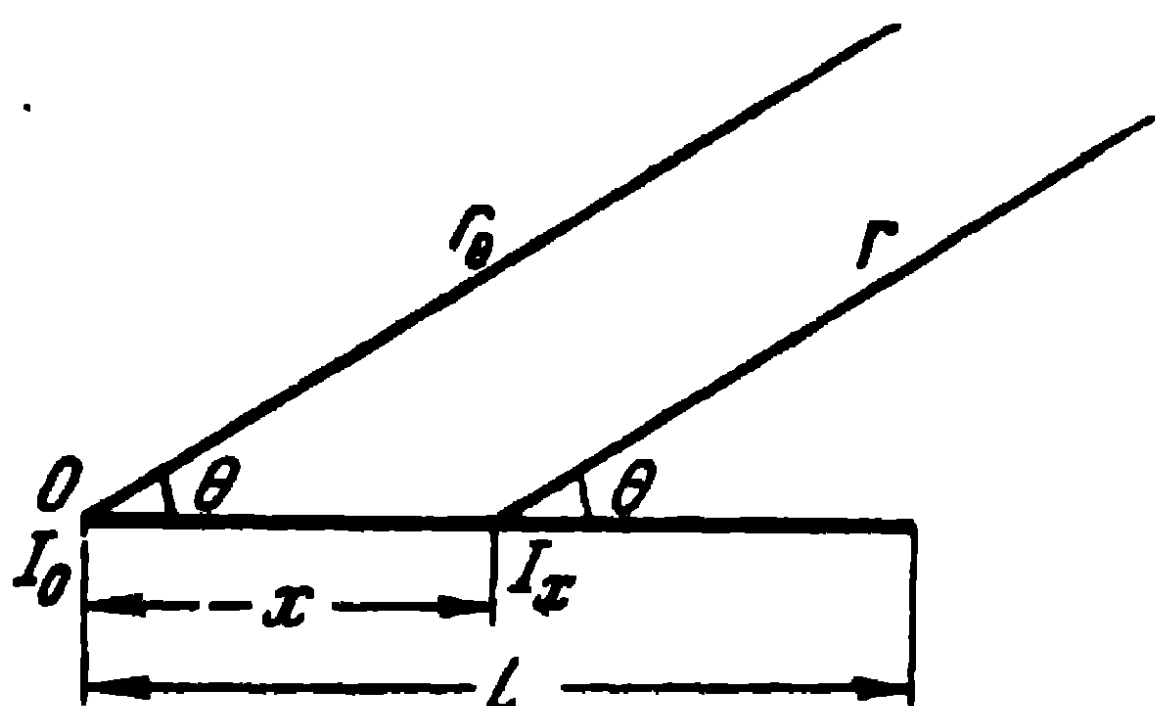


Fig. 4-9. Explaining the calculation of the radiation of a conductor with a travelling wave of the current.

$$dE = i \frac{I_x dx k^2}{4\pi\omega\epsilon} \sin \theta \frac{e^{-ikr}}{r}.$$

Substituting here the expression (4-19) and taking into account that for the radiation zone, $\frac{1}{r_0} \approx \frac{1}{r}$ and $r = r_0 - x \cos \theta$, we have for the total field:

$$E = i \frac{I_0 k^2}{4\pi\omega\epsilon} \sin \theta \frac{e^{-ikr_0}}{r_0} \int_{x=0}^L e^{-ikx(1-\cos \theta)} dx.$$

The stated integration yields

$$E = i \frac{I_0 k^2 L}{4\pi\omega\epsilon} \sin \theta \frac{e^{-ikr_0}}{r_0} e^{-i\Phi} \frac{\sin \Phi}{\Phi}, \quad (4-20)$$

where

$$\Phi = \frac{kL}{2} (1 - \cos \theta).$$

To begin with, note that in the direction of the conductor axis, the radiation equals zero, because when $\theta=0$, $\sin \theta=0$. The main maximum of radiation is at an angle to the axis of the conductor that satisfies the condition $0 < \theta_{\max} < 90^\circ$,

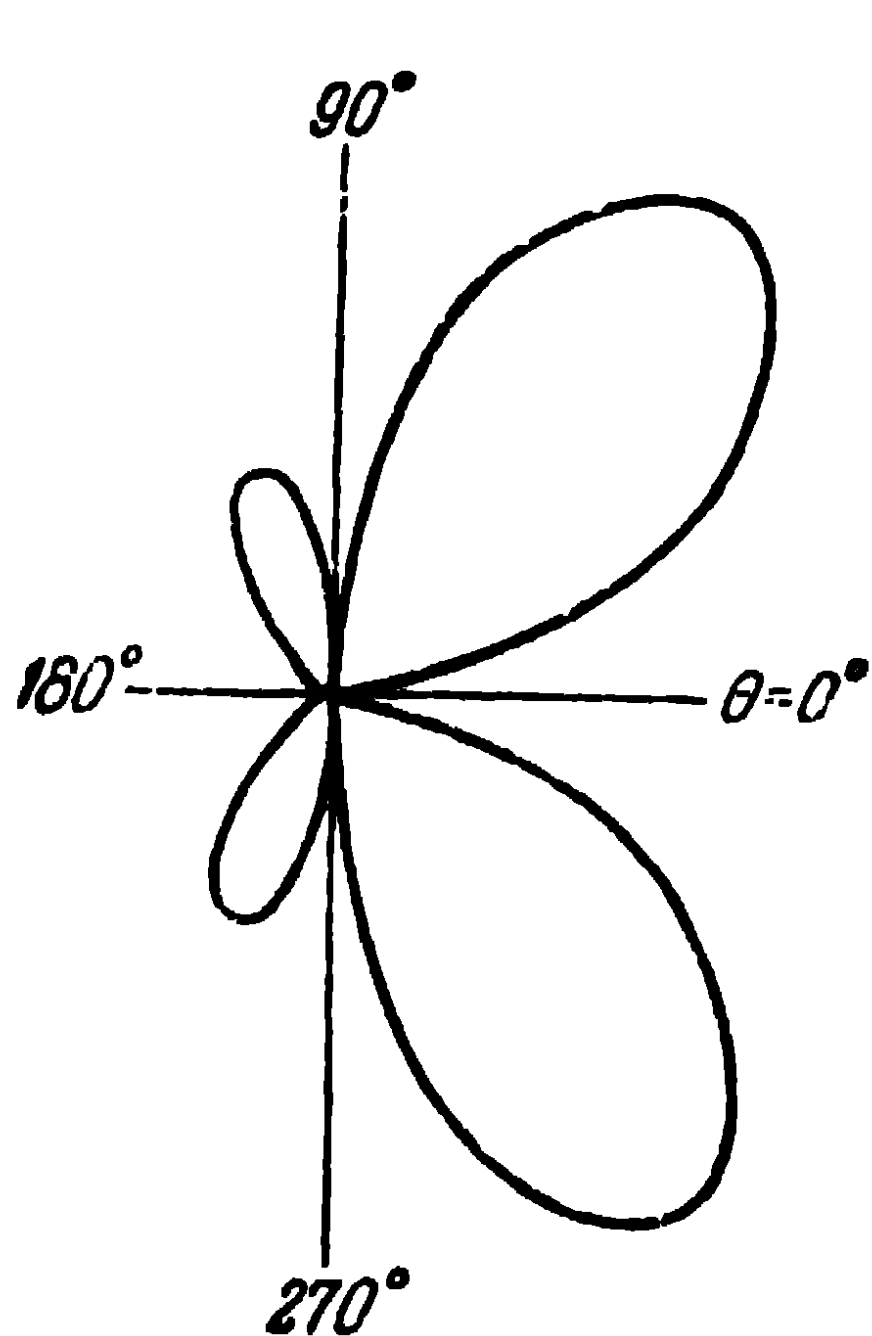


Fig. 4-10. Directional diagram of a conductor with a travelling wave of the current $L/\lambda=1.0$.

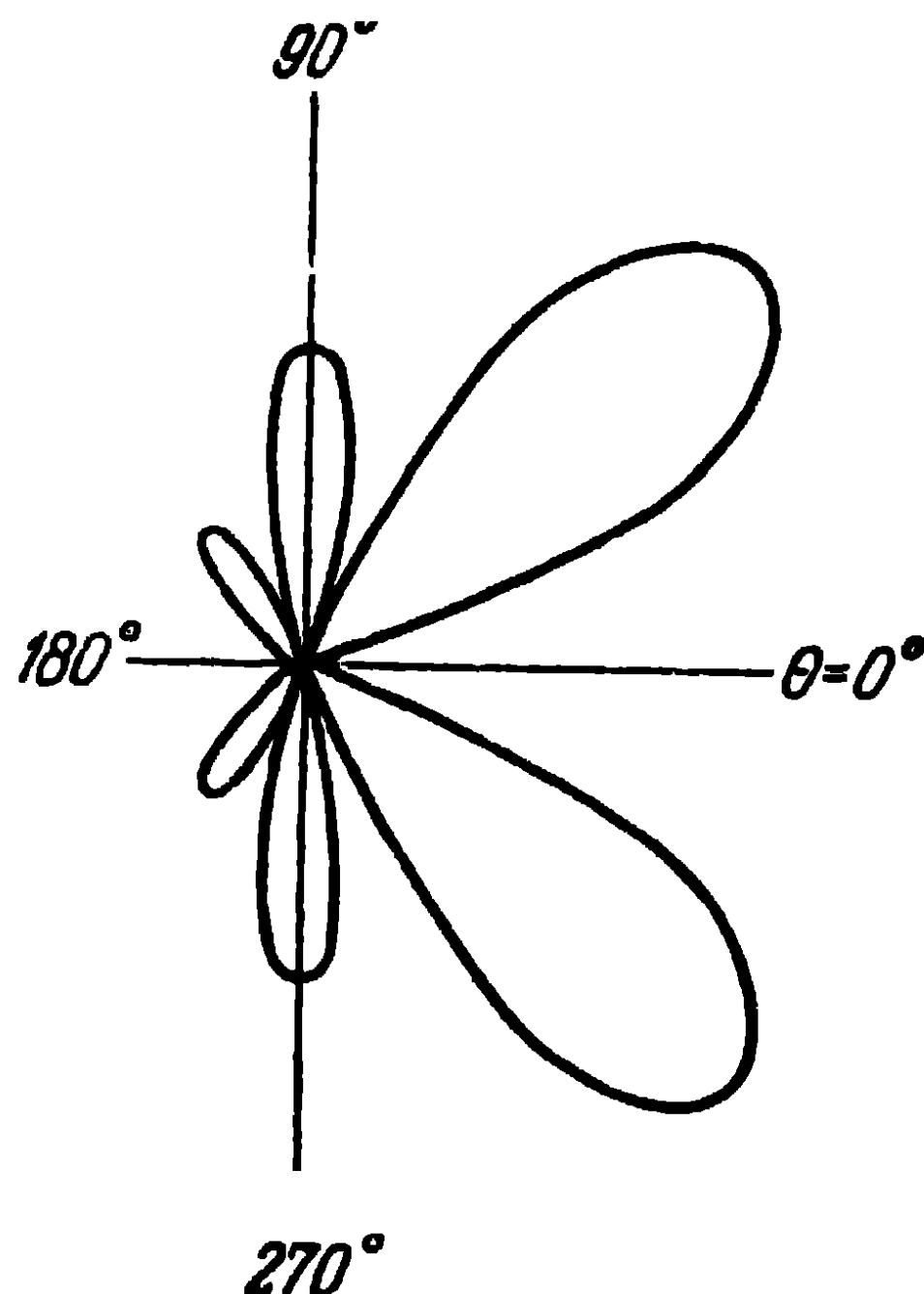


Fig. 4-11. Directional diagram of a conductor with a travelling wave of the current $L/\lambda=1.5$.

i.e., the radiation of a conductor with a travelling wave of the current is directed at a certain angle to the conductor in the direction of travel of the wave. Furthermore, the

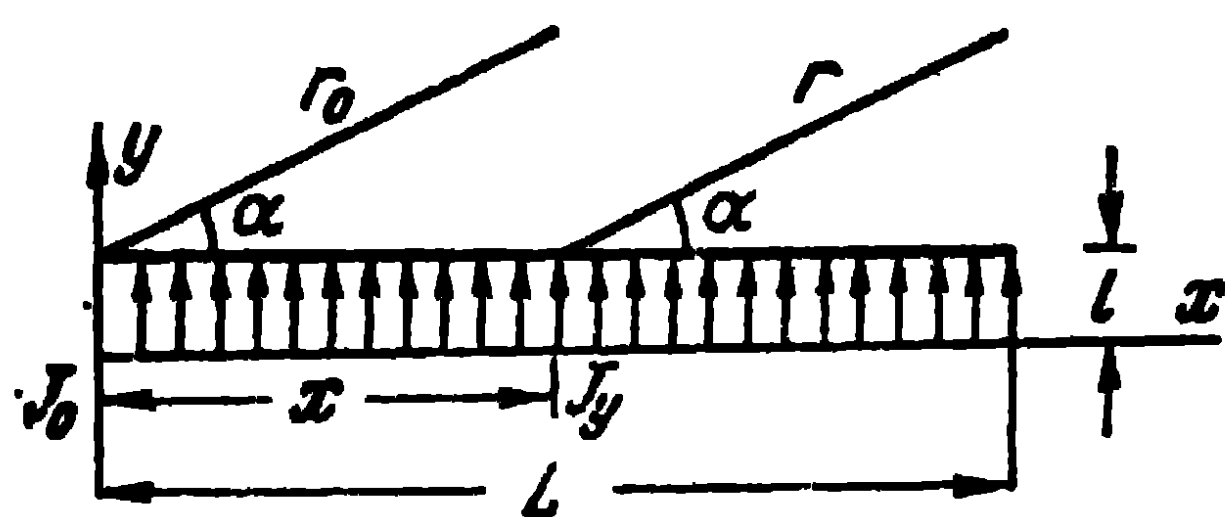


Fig. 4-12. Layer of transverse electric currents.

longer the conductor relatively to the wave-length, the closer is the main maximum of radiation against the conductor axis and the larger the number of minor lobes. This is illustrated in Figs. 4-10 and 4-11 showing the directional diagram of the conductor for $L/\lambda=1.0$ and $L/\lambda=1.5$, calculated according to formula (4-20).

We have examined the radiation of a conductor with a travelling wave of the longitudinal current. In practice one meets travelling-wave antennas in which the electric currents have components perpendicular to the axis of the

antenna. Let us therefore examine the radiation of a thin layer of transverse electric currents propagated along the layer in accordance with the travelling-wave law (Fig. 4-12). Let J_0 be the density of the surface current at the beginning of the layer. Then, the density of the current at the point x of the system will be:

$$J_y = J_0 e^{-ik\xi x}, \quad (4-21)$$

where $\xi = \frac{v_l}{v}$ is the ratio of the velocity of light to the phase velocity of the current wave in the layer.

Let us select at the point x of the layer, an element of current $J_y ldx$. The intensity of the field set up by this element in the radiation zone in the xy -plane will be:

$$dE = i \frac{J_y ldx k^2}{4\pi\omega\epsilon} \cos \alpha \frac{e^{-ikr}}{r},$$

where α is the angle between the antenna axis and the direction towards the point of observation.

Integrating this expression along the whole length of the layer, we obtain:

$$E_{(xy)} = i \frac{J_0 l k^2}{4\pi\omega\epsilon} \cos \alpha \frac{e^{-ikr_0}}{r_0} e^{-i\psi} \frac{\sin \Psi}{\Psi}, \quad (4-22)$$

where

$$\Psi = \frac{kL}{2} (\xi - \cos \alpha).$$

If we eliminate the factor $\cos \alpha$ from (4-22), we obtain an expression which defines the field in the xz -plane of the antenna.

Note that the main radiation maximum occurs in the direction which is determined from the condition $\Psi = 0$ or

$$\cos \alpha_{\max} = \xi.$$

This condition is fulfilled when $\xi \leq 1$, i.e., when the phase velocity of the wave in the layer is equal to or higher than that of light. When $\xi = 0$, the velocity of the wave in the layer equals infinity (co-phased oscillation of currents) and the angle of the radiation maximum α_{\max} is found to equal 90° . When $\xi \rightarrow 1$, the velocity of the wave approaches that of light and the direction of the radiation maximum approaches the axis of the layer ($\alpha_{\max} \rightarrow 0$).

Let us determine the width of the directional diagram when $\xi=1$, i.e., when the radiation maximum coincides with the axis of the layer ($\alpha_{\max}=0$). Assuming that in (4-22) $\Psi=\pi$, the following expression is obtained for the determination of the width of the directional diagram at the zeros of radiation:

$$\cos \alpha_0 = 1 - \frac{\lambda}{L}.$$

When $\frac{L}{\lambda} \gg 1$, the angle α is sufficiently small and for the width of the directional diagram at the zeros of radiation, we obtain the approximate expression:

$$2\alpha_0 = 2 \sqrt{2 \frac{\lambda}{L}}. \quad (4-23)$$

For the determination of the width of the directional diagram at half power, we assume that in (4-22)

$$\sin \left[\frac{kL}{2} (1 - \cos \alpha_{1/2}) \right] = 0.707 \left[\frac{kL}{2} (1 - \cos \alpha_{1/2}) \right],$$

from which we obtain the approximate relation

$$2\alpha_{1/2} = 2 \sqrt{0.886 \frac{\lambda}{L}}. \quad (4-24)$$

When $\xi > 1$, the wave phase velocity in the layer is inferior to that of light. In that case, in accordance with (4-22), the maximum of the major lobe of the directional diagram coincides with the layer axis. At the same time, the size of this lobe relatively to that of the minor lobes or the radiation intensity in the principal direction depends in a complex way on the value of L/λ , whereas when $\xi=1$ the radiation in the principal direction is the larger the larger is L/λ .

As we shall see below, to each value of the relative velocity of the wave in the layer ($\frac{v}{v_1} < 1$) there corresponds a definite electric length of the layer (L/λ) for which the maximum radiation of energy occurs in the main direction. This relation is found from the condition $\Psi = \frac{\pi}{2}$ and is defined by the ratio

$$\frac{L}{\lambda} = \frac{1}{2(\xi - 1)}. \quad (4-25)$$

Antennas with a low phase velocity, the dimensions of which satisfy the condition (4-25) are usually referred to as antennas of axial radiation of optimum length.

The width of the major lobe of the directional diagram at the zeros of radiation is determined from the expression

$$\cos \alpha_0 = \xi - \frac{\lambda}{L},$$

and if we substitute in it the value of ξ taken from the condition (4-25), the width of the major lobe at the zeros is determined from the expression

$$\cos \alpha_0 = 1 - \frac{\lambda}{2L}.$$

For a highly directional radiation we may assume that

$$\cos \alpha_0 \approx 1 - \frac{\alpha_0^2}{2}. \text{ Then}$$

$$2\alpha_0 = 2 \sqrt{\frac{\lambda}{L}}. \quad (4-26)$$

As for the width of the directional diagram of an antenna of optimum length at half power, it is obtained from the expression

$$\sin \left[\frac{kL}{2} (\xi - \cos \alpha_{1/2}) \right] = 0.707 \frac{2}{\pi} \left[\frac{kL}{2} (\xi - \cos \alpha_{1/2}) \right]$$

and for $\frac{L}{\lambda} \gg 1$, it is approximately defined as

$$2\alpha_{1/2} = 2 \sqrt{0.28 \frac{\lambda}{L}}. \quad (4-27)$$

Comparing (4-23) and (4-24) with (4-26) and (4-27), we note that an antenna with a low phase velocity of optimum length has a narrower directional diagram than an antenna the phase velocity of which is equal to the velocity of light.

A comparison of (4-23) and (4-26) with (4-4) shows that antennas of axial radiation possess a considerably lower directivity than antennas of the same length consisting of a series of linear dipoles with a co-phased excitation. This is due to the fact that antennas with an axial radiation concentrate energy in a narrow bunch of waves in two planes whereas co-phased linear antennas concentrate energy in a narrow bunch of waves in one plane only.

As for the minor lobes of the directional diagram, it is clear that for an antenna of optimum length with an axial radiation, the magnitude of the maximum of the first minor lobe amounts to $1/3$ of the magnitude of the maximum of the major lobe.

Note in addition that if the length of the antenna is doubled in comparison with the optimum one, i.e., the length determined from the condition (4-25), then in the principal direction ($\alpha=0$), the radiation is found to equal zero.

Let us consider the example of an optimum antenna of axial radiation. Let $\xi=1.1$; then $L/\lambda=5$ and the width of the directional diagram at the zeros is $2\alpha_0=51.5^\circ$ and at half power, $2\alpha_{0.5}=27.2^\circ$.

4-6. Application of the Equivalent Surface Currents Theorem to the Calculation of the Radiation Characteristics of Antennas

Before we continue to discuss the radiation of other possible systems, let us dwell on the equivalent surface electric and magnetic currents theorem, known to the reader from the course on electromagnetic field theory [14 and 15].

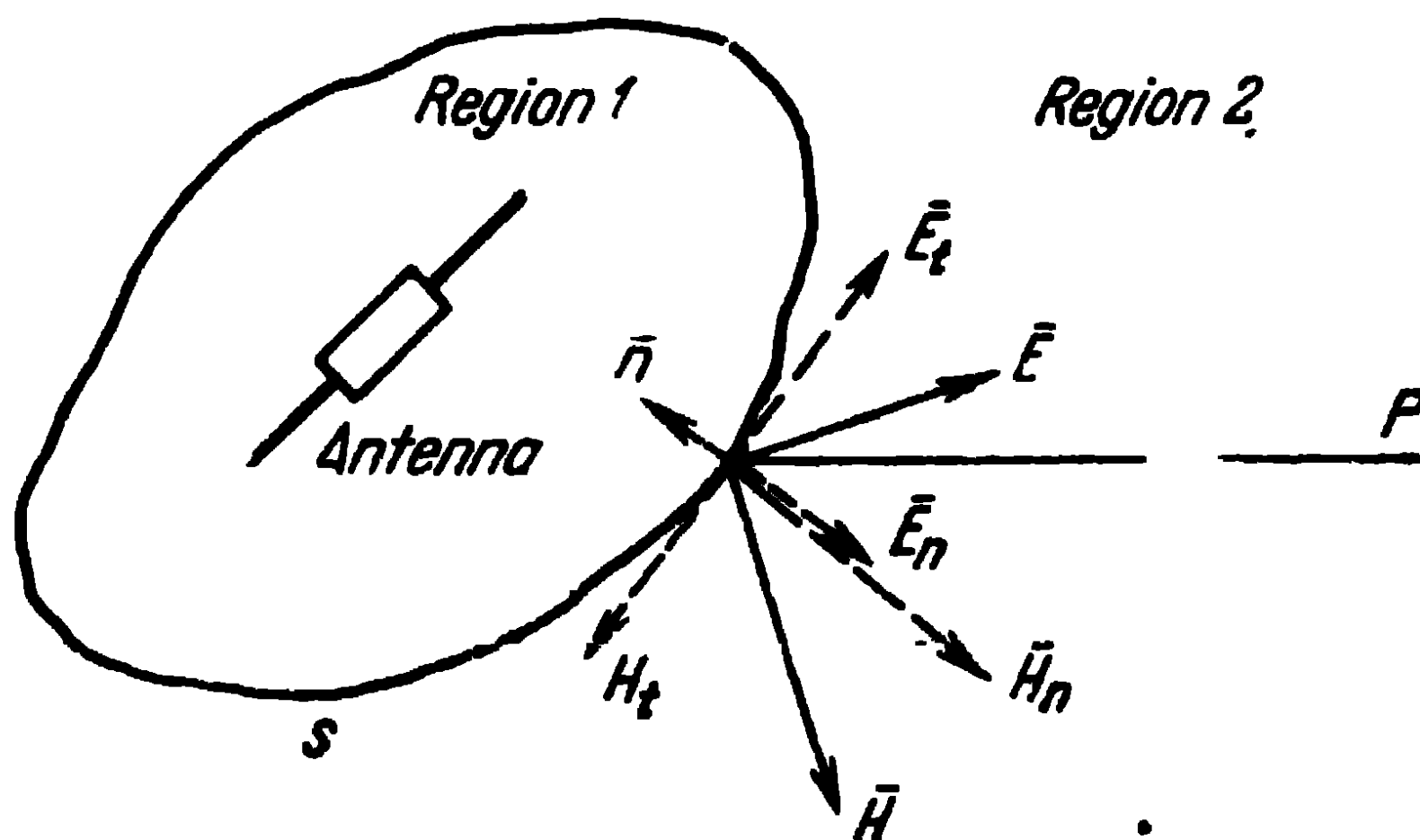


Fig. 4-13. Explaining the equivalent surface currents theorem.

Here is a brief explanation of this theorem. Let us examine the radiation of an antenna lying in a free space. Let \mathbf{E} and \mathbf{H} be the vectors of the electromagnetic field set up by the antenna. Let us divide the whole of the space with the arbitrary closed surface s enveloping the antenna into two regions: 1 and 2 (Fig. 4-13).

Let us expand the \mathbf{E} and \mathbf{H} vectors on the surface s in two component vectors, one tangential and the other normal to the surface:

$$\begin{aligned}\mathbf{E} &= \mathbf{E}_t + \mathbf{E}_n; \\ \mathbf{H} &= \mathbf{H}_t + \mathbf{H}_n.\end{aligned}$$

Using the linearity of Maxwell's equations, let us mentally examine two pairs of vectors separately:

1) the pair of vectors \mathbf{H}_t and \mathbf{E}_n , assuming that $\mathbf{E}_t=0$ and $\mathbf{H}_n=0$;

2) the pair of vectors \mathbf{E}_t and \mathbf{H}_n assuming that $\mathbf{H}_t=0$ and $\mathbf{E}_n=0$.

In the first case, the surface s behaves as an ideal electric conductor, since the magnetic field vector on it has only a tangential component and the electric field vector, only a normal component. That is why, in that case, a surface electric current appears to flow on the surface s , the density of which is expressed as

$$\mathbf{J}^e = [\mathbf{H}_t, \mathbf{n}] = [\mathbf{H}, \mathbf{n}], \quad (4-28)$$

where \mathbf{n} is the external normal to the surface under consideration (region 2).

The vector potential of this fictitious surface electric current at a certain point P of the region 2 may be determined from the expression

$$\mathbf{A}^e = \frac{1}{4\pi} \int_s \mathbf{J}^e \frac{e^{-ikr}}{r} ds, \quad (4-29)$$

and the intensity of the electric and magnetic fields at the same point P , from the expressions

$$\begin{aligned}\mathbf{H}^e &= \text{rot } \mathbf{A}^e; \\ \mathbf{E}^e &= -i\omega\mu\mathbf{A}^e + \frac{1}{i\omega\epsilon} \text{grad div } \mathbf{A}^e.\end{aligned} \quad (4-30)$$

In the second case, the surface s behaves as an ideal magnetic conductor, since the electric field vector on it has only a tangential component and the magnetic field vector, only a normal component. That is why, in that second case, a surface magnetic current appears to flow on the surface s , its density being equal to the tangential component of the electric field intensity and determined from the expression

$$\mathbf{J}^m = [\mathbf{n}, \mathbf{E}_t] = [\mathbf{n}, \mathbf{E}]. \quad (4-31)$$

The vector potential of the fictitious surface magnetic current at the point P is determined from the expression

$$\mathbf{A}^M = \frac{1}{4\pi} \int_s \mathbf{J}^M \frac{e^{-ikr}}{r} ds, \quad (4-32)$$

and the electric and magnetic fields at the point P are determined from the expressions

$$\begin{aligned} \mathbf{E}^M &= -\text{rot } \mathbf{A}^M, \\ \mathbf{H}^M &= -i\omega\epsilon' \mathbf{A}^M + \frac{1}{i\omega\mu} \text{grad div } \mathbf{A}^M. \end{aligned} \quad (4-33)$$

The total field at the point of observation P is thus defined by the sum

$$\begin{aligned} \mathbf{E} &= \mathbf{E}^e + \mathbf{E}^M, \\ \mathbf{H} &= \mathbf{H}^e + \mathbf{H}^M. \end{aligned} \quad (4-34)$$

Thus, the field in the region 2, which is free from sources and bounded by the surface s , may be set up by the electric and magnetic currents distributed on that surface and, in that sense, the real sources in the region 1 may be replaced by the "equivalent" surface electric and magnetic currents.

The choice of the surface s enveloping the true sources of the field is absolutely arbitrary. In the case of, for example, a symmetrical dipole, the surface s can be coincided with the surface of an ideal conductor in the centre of which there is a gap for connecting a high-frequency oscillator. In this case, the fictitious surface electric currents are identical to the real surface electric currents flowing on the surface of the conductor. As for the gap in the conductor, within this gap, the surface electric current as well as the surface magnetic current are fictitious and provide an equivalent substitute for the real electric currents flowing in the internal region of the gap in the conductor.

It is frequently found more convenient to calculate the radiation characteristics of antennas by performing the integration not over the volume which contains the real sources of the field but over a certain closed surface enclosing the real sources. This is the way to calculate, for example, the directional characteristics of horn-type antennas, covering the horn with the surface s and integrating the radiation of the fictitious sources lying at the output opening of the horn (neglecting the radiation of the sources disposed on the remaining part of the surface s).

Now that we have given the necessary explanations regarding the equivalence theorem, let us select on the surface s under consideration an elementary area ds and define the field created by this area at the point P . It is evident that we must regard this area as a Huygens element. Let us coincide the area with the xy -plane of a Cartesian system of coordinates and let the origin of this system lie in this area (Fig. 4-14).

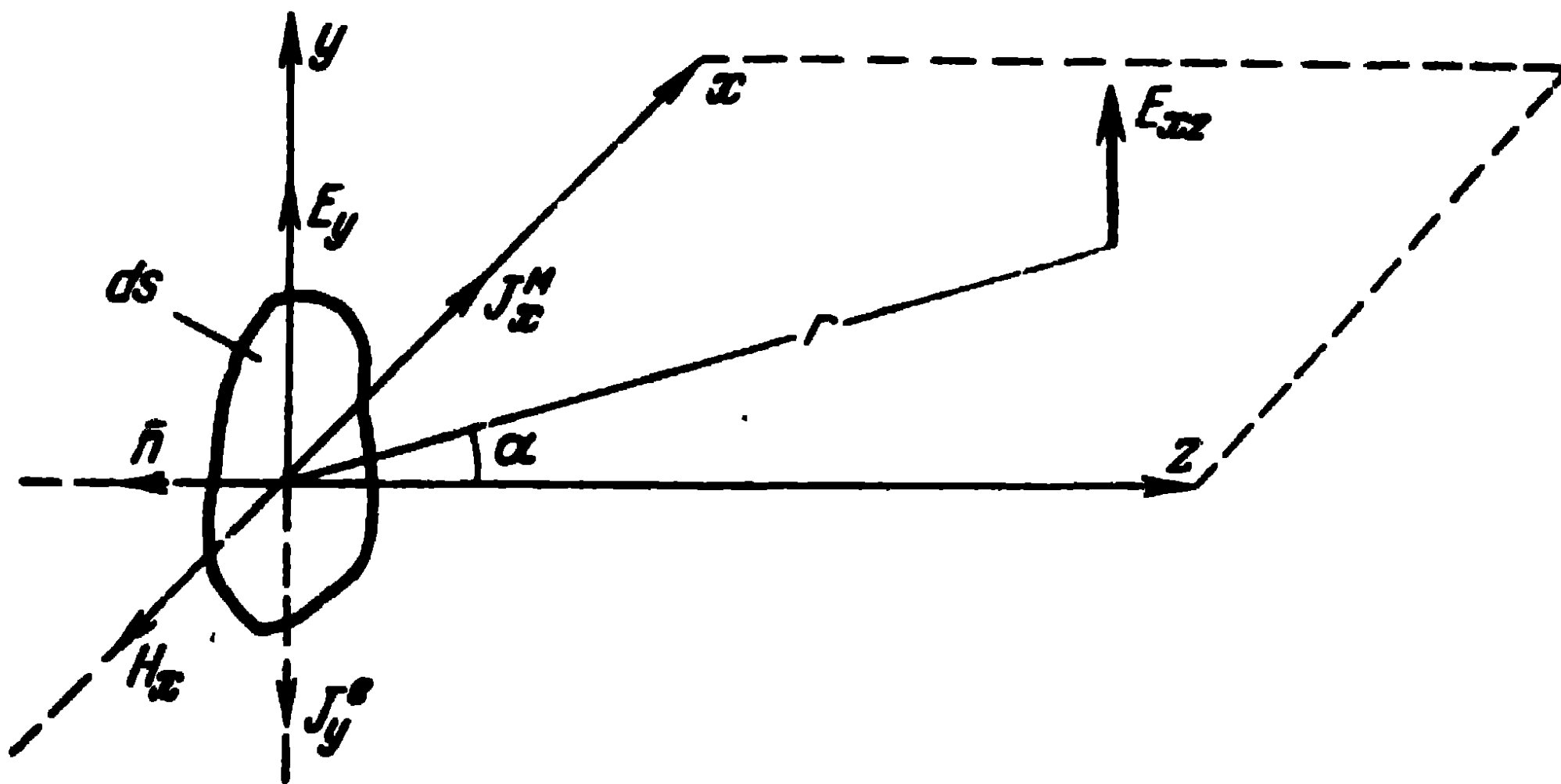


Fig. 4-14. Explaining the radiation of a Huygens element.

Let the vector of the electric field intensity coincide with the y -axis, the vector of the magnetic field intensity with the negative direction of the x -axis, and the normal to the area, with the negative direction of the z -axis. Then, in accordance with (4-28) and (4-31), the densities of the surface electric and magnetic currents will be:

$$J_y^e = H_x, \quad J_x^m = E_y. \quad (4-35)$$

Let us investigate the field in the radiation zone in the xz -plane.

Since the electric moment of the elementary area equals $J_y^e ds$ and the magnetic moment equals $J_x^m ds$, in accordance with (1-3), the electric field intensity caused by the electric dipole at the point P will be:

$$dE_{(xz)}^e = i \frac{J_y^e ds k^2}{4\pi\omega\epsilon} \frac{e^{-lkr}}{r},$$

and, in accordance with (1-8), the electric field intensity set up by the magnetic dipole will be:

$$dE_{(xz)}^m = -i \frac{J_x^m ds k}{4\pi} \cos \alpha \frac{e^{-lkr}}{r^2}$$

The total field will be found to equal:

$$dE_{(xz)} = i \frac{J_y^e ds k^2}{4\pi\omega\epsilon} \frac{e^{-ikr}}{r} \left(1 - \frac{J_x^M}{J_y^e} \frac{\omega\epsilon}{k} \cos \alpha \right). \quad (4-36)$$

When the surface s is in the radiation zone (relatively to the real sources),

$$\frac{J_x^M}{J_y^e} = \frac{E_y}{H_x} = -\frac{k}{\omega\epsilon} \quad \text{and} \quad J_y^e = -\frac{\omega\epsilon}{k} E_y.$$

Hence (4-36) becomes:

$$dE_{(xz)} = -i \frac{E_y ds}{2\lambda r} (1 + \cos \alpha) e^{-ikr}. \quad (4-37)$$

For the radiation in the yz -plane, we obtain in a similar way:

$$dE_{(yz)} = -i \frac{E_y ds}{2\lambda r} (1 + \cos \beta) e^{-ikr}, \quad (4-38)$$

where β is the angle between the z -axis and the direction towards the point of observation in the yz -plane.

Thus, the expressions (4-37) and (4-38) define the radiation of the Huygens element. The radiation of such a system has already been investigated in Chapter One. The directional diagram of a Huygens element has the form of a cardioid; it is shown in Fig. 1-11.

4-7. Radiation of an Ideal Plane Antenna

Let us discuss the radiation of an ideal plane antenna of dimensions a and b . Let the plane of the antenna coincide with the xy -plane (Fig. 4-15) and let the field of the antenna be prescribed as:

$$\frac{E_y}{(-H_x)} = \frac{k}{\omega\epsilon}.$$

The phases and amplitudes are the same at any point of the antenna.

Let us investigate the field at the point P in the xz -plane. Let us select on the antenna an elementary area of dimensions $b dx$.

In accordance with (4-37), the field intensity of this area at the point P is:

$$dE_{(xz)} = -i \frac{E_y b dx}{2\lambda r_0} (1 + \cos \alpha) e^{-ikr_0 + ikx \sin \alpha},$$

where, r_0 is the distance from the centre of the antenna to the point of observation. The total field of the whole of the antenna at the point P is determined as the integral of the

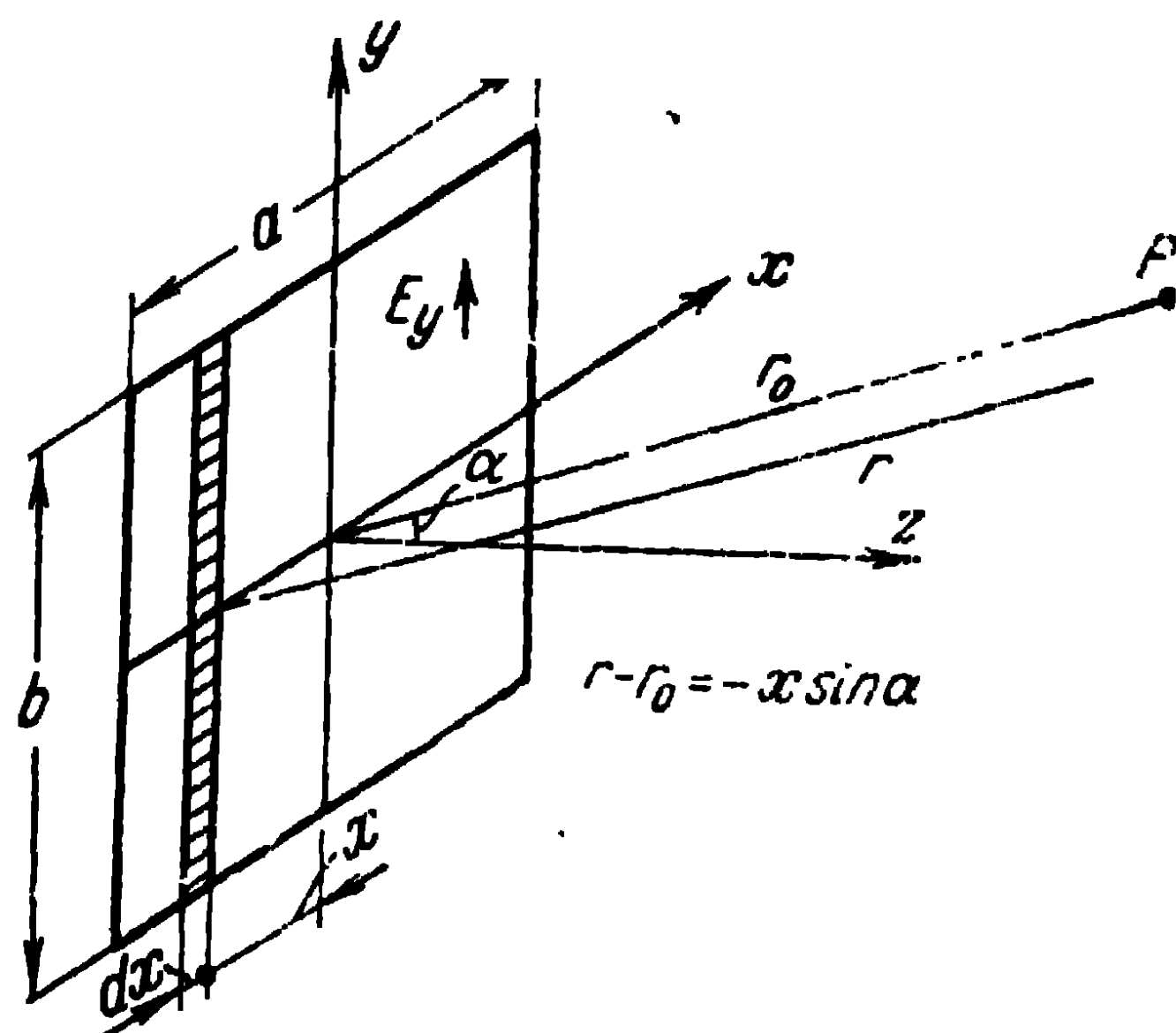


Fig. 4-15. An ideal plane antenna.

preceding expression taken along the x -axis from

$$x = -\frac{a}{2} \text{ to } x = +\frac{a}{2} :$$

$$E_{(xz)} = -i \frac{E_y b}{2\lambda r_0} (1 + \cos \alpha) e^{-ikr_0} \int_{x=-a/2}^{a/2} e^{ikx \sin \alpha} dx.$$

After performing the stated integration and reducing the similar terms, we obtain:

$$E_{(xz)} = -i \frac{E_y ab}{2\lambda r_0} (1 + \cos \alpha) \frac{\sin \Psi}{\Psi} e^{-ikr_0}, \quad (4-39)$$

where

$$\Psi = \frac{ka}{2} \sin \alpha.$$

Similarly, for the yz -plane, we obtain the expression

$$E_{(yz)} = -i \frac{E_y ab}{2\lambda r_0} (1 + \cos \beta) \frac{\sin \Phi}{\Phi} e^{-ikr_0}, \quad (4-40)$$

where

$$\Phi = \frac{kb}{2} \sin \beta.$$

Let us now draw the necessary conclusions from (4-39) and (4-40). First of all, note that the maximum value of the

field intensity occurs in a direction perpendicular to the plane of the antenna ($\alpha=0$) and is equal to:

$$|E| = \frac{E_{yab}}{\lambda r_0}, \quad (4-41)$$

i.e., it is equal to the field intensity in the antenna multiplied by the area of the antenna and divided by the product of the wave-length by the distance from the antenna to the point of observation.

The zero radiation directions in the xz -plane are determined from the condition $\sin \Psi_0 = 0$ or $\frac{ka}{2} \sin \alpha_0 = \pi N$, where $N = 1, 2, 3, \dots$

Hence

$$\sin \alpha_0 = \frac{N\lambda}{a}. \quad (4-42)$$

From this expression we see that in the xz -plane, the number of directions in which the radiation vanishes will be all the larger as the ratio a/λ is larger. In just the same way, the zero radiation directions in the yz -plane are determined from the condition

$$\sin \beta_0 = \frac{N\lambda}{b}, \quad N = 1, 2, 3 \dots \quad (4-43)$$

and the number of the zero radiation directions in that plane will be all the larger as the ratio b/λ is larger.

When the dimensions of the antenna are large in comparison with the wave-length, the width of the major lobe of the directional diagram at the zeros of radiation is determined from the expressions

$$2\alpha_0 \approx 115^\circ \frac{\lambda}{a} \text{ and } 2\beta_0 \approx 115^\circ \frac{\lambda}{b}. \quad (4-44)$$

Obviously, as can be inferred from (4-42) and (4-43), there will be no radiation zeros if $\lambda > a$ and $\lambda > b$.

Let us also stress that in the xz -plane, the directional diagram of the antenna does not depend on the dimension b of the antenna, and in the yz -plane, it does not depend on the dimension a of the antenna.

Fig. 4-16 shows the directional diagram of an ideal plane antenna where the value of the function $\frac{\sin \Psi}{\Psi}$ is plotted

on the y -axis and the argument $\Psi = \pi a \sin \alpha$ on the x -axis.

We see that the magnitude of the maximum of the first minor lobe amounts to approximately $1/5$ of the major lobe. Let it be reminded that in a linear co-phased array of half-wave dipoles, the first minor lobe has the same relative intensity.

The same diagram shows the width of the major lobe at half power $2\alpha_{1/2}$, i.e., the size of the angle α , within which

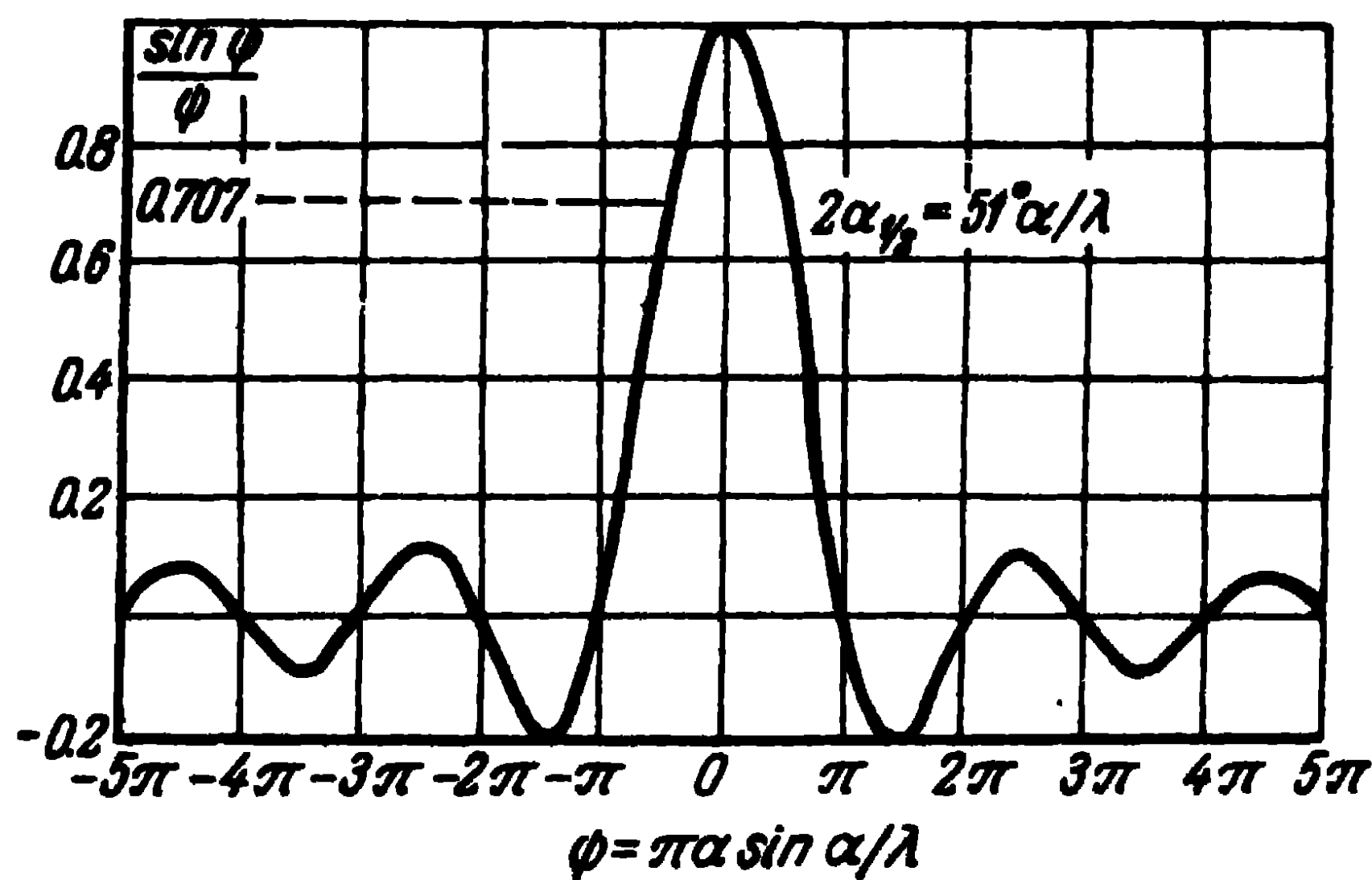


Fig. 4-16. Directional diagram of an ideal plane antenna.

the field intensity does not fall below 0.707 of the magnitude of the field intensity in the main direction. We see that the width of the major lobe at half power of an ideal plane antenna is expressed as:

$$2\alpha_{1/2} = 51^\circ \frac{\lambda}{a} \text{ or } 2\beta_{1/2} = 51^\circ \frac{\lambda}{b}. \quad (4-45)$$

The power radiated by an ideal plane antenna is fairly simple to calculate. Indeed, the power radiated by 1 m^2 of the antenna equals $S = \frac{|E|^2}{240\pi}$ and, consequently, the power radiated by the whole of the antenna equals

$$P_{\Sigma} = \frac{|E|^2 ab}{240\pi} \quad (4-46)$$

Here, E represents the amplitude value of the electric field intensity on the surface of an ideal plane antenna.

4-8. Effect of Changes of Field Amplitude and Phase in a Plane Antenna on the Directional Diagram

In the preceding paragraph, we examined the radiation of an ideal plane antenna with a uniform distribution of its field amplitudes and phases. Let us now consider a plane antenna of the same dimensions a and b in which the field phase will be assumed constant in the whole of the antenna, the field amplitude being assumed constant only in the direction of the y -axis and changing along the x -axis as

$$C_1 + C_2 \cos\left(\frac{\pi x}{a}\right), \text{ i.e.,} \\ E_y = E_0 \left[C_1 + C_2 \cos\left(\frac{\pi x}{a}\right) \right]. \quad (4-47)$$

Since the distribution of the field amplitude and phase along the y -axis has not changed, the form of the directional diagram in the yz -plane remains the same as for the co-phased plane antenna. For this reason, the radiation will be considered only in the xz -plane of the antenna.

Referring to Fig. 4-15 and substituting into (4-37) the expression (4-47), the integration along the x -axis yields:

$$E_{(xz)} = -i \frac{E_0 b}{2\lambda r_0} (1 + \cos \alpha) \times \\ \times e^{-ikr_0} \int_{x=-\frac{a}{2}}^{\frac{a}{2}} \left[C_1 + C_2 \cos\left(\frac{\pi x}{a}\right) \right] e^{ikx \sin \alpha} dx.$$

Performing the stated integration and reducing the similar terms, we arrive at the following expression:

$$E_{(xz)} = -i \frac{E_0 ab}{2\lambda r_0} (1 + \cos \alpha) e^{-ikr_0} \times \\ \times \left[C_1 \frac{\sin \Psi}{\Psi} + C_2 \frac{2}{\pi} \frac{\cos \Psi}{1 - \left(\frac{2}{\pi} \Psi\right)^2} \right], \quad (4-48)$$

where

$$\Psi = \frac{ka}{2} \sin \alpha.$$

Let us now consider special cases of the distribution of the field amplitude in the antenna. Let $C_1 = 1$ and $C_2 = 0$.

This gives us the case of the co-phasal surface already considered in Paragraph 4-7.

Let $C_1=0$ and $C_2=1$. This is the case of a co-sinusoidal distribution of the field amplitude in the direction of the x -axis, when the field at the edges of the antenna falls down to zero. We have:

$$E_{(xz)} = -i \frac{E_0 ab}{2\lambda r_0} (1 + \cos \alpha) \frac{2}{\pi} \frac{\cos \Psi}{1 - \left(\frac{2}{\pi} \Psi\right)^2} e^{-ikr_0}. \quad (4-49)$$

The directions in which the radiation vanishes are determined from the condition

$$\cos \Psi_0 = 0 \text{ or } \frac{ka}{2} \sin \alpha_0 = \frac{\pi}{2} N, \quad N=3,5,\dots$$

Hence

$$\sin \alpha_0 = \frac{N\lambda}{2a}, \quad N=3,5,\dots \quad (4-50)$$

In the case of a high directivity, the width of the major lobe between the zeros of radiation is approximately expressed as

$$2\alpha_0 \approx 172^\circ \frac{\lambda}{a}. \quad (4-51)$$

i.e., the major lobe of the directional diagram between the zeros of radiation will, in that case, be 1.5 times wider than the major lobe of an ideal co-phased antenna provided the size of the antenna is the same. The half-power width of the major lobe of the directional diagram is, in that case, determined from the expression

$$2\alpha_{1/2} = 67^\circ \frac{\lambda}{a}. \quad (4-52)$$

At the same time, the relative magnitude of the minor lobes decreases and the maximum of the first lobe constitutes now only $1/11$ of the magnitude of the maximum of the major lobe.

Now let $C_1=1/2$ and $C_2=1/2$. Here, although we do get a maximum of the field amplitude in the middle of the antenna, the field decreases towards the edges down to only $1/2$ of the maximum value. In that case, for a highly directional antenna, the width of the major lobe between the zeros may be defined from the expression

$$2\alpha_0 \approx 143^\circ \frac{\lambda}{a}. \quad (4-53)$$

The half-power width of the directional diagram may be defined from the expression

$$2\alpha_{1/2} = 57.3^\circ \frac{\lambda}{a}. \quad (4-54)$$

The value of the maximum of the first minor lobe constitutes 0.095 of the value of the maximum of the major lobe.

Thus, the faster the amplitude of the field in the antenna decreases towards its edges, the wider the major lobe and the smaller the relative amplitudes of the minor lobes of the directional diagram.

Now, let us consider the influence on the directional diagrams of a linear change of the field phase in the antenna. Let the field intensity in the antenna change as

$$E_y = E_0 e^{-ik_1 x}. \quad (4-55)$$

In accordance with (4-37), at the point of observation in the xz -plane, the field intensity caused by the element on the antenna surface is:

$$dE_{(xz)} = -i \frac{E_0 b dx}{2\lambda r_0} (1 + \cos \alpha) e^{-ikr_0 + i(k \sin \alpha - k_1) x}.$$

Integrating this expression over the antenna surface, we obtain:

$$E_{(xz)} = -i \frac{E_0 ab}{2\lambda r_0} (1 + \cos \alpha) \frac{\sin \Psi'}{\Psi'} e^{-ikr_0}, \quad (4-56)$$

where $\Psi' = \frac{ka}{2} \sin \alpha - \frac{k_1 a}{2}$.

Note that $\frac{k_1 a}{2} = \psi_1$ represents the difference of phase between the field in the centre and at the antenna edges.

It can be seen from (4-56) that the maximum radiation occurs for the condition $\Psi' = 0$ and its direction is determined from the expression

$$\sin \alpha_{\max} = \frac{\psi_1 \lambda}{\pi a}. \quad (4-57)$$

As for the zero radiation directions, they are determined from the condition $\Psi' = \pm N\pi$ and may be calculated from the expression

$$\sin \alpha_0 = \pm N \frac{\lambda}{a} + \frac{\psi_1 \lambda}{\pi a}, \quad N = 1, 2, 3, \dots \quad (4-58)$$

Thus, we see that in the case of a linear change of phase in the antenna, the form of the directional diagram remains

identical to that of the directional diagram of a co-phased antenna, i.e., is described by the function $\frac{\sin \Psi}{\Psi}$, but the direction of the maximum radiation differs from the normal to the plane of the antenna by an angle determined in accordance with (4-57).

Such a linear change of phase at the output opening of antennas is utilised for diagram scanning (hunting) in radar antennas. A detailed analysis of (4-56) shows that when $k_1 \ll k$ the form of the directional diagram of the antenna undergoes but an insignificant distortion in the course of the hunting process.

Let us consider the directional properties of an antenna the field phase of which changes as $k_2 x^2$. Such a phase distribution occurs, for example, in the case of horn-type antennas.

In the present case, the field intensity in the antenna is expressed as

$$E_y = E_0 e^{-ik_2 x^2}. \quad (4-59)$$

In accordance with (4-37), the field intensity at the point of observation lying in the xz -plane of the element of the radiating surface equals:

$$dE_{(xz)} = -i \frac{E_0 b dx}{2\lambda r_0} (1 + \cos \alpha) e^{-ikr_0 + i(k \sin \alpha - k_2 x) x}.$$

To determine the intensity of the field set up by the whole antenna at any point of the xz -plane, this expression should be integrated over the radiating surface. As a result, we obtain a rather complex expression containing Fresnel's integrals (see [16] for example).

Fig. 4-17 shows the directional diagram of a plane antenna, calculated in accordance with the expression just mentioned. In this figure, $\psi_2 = k_2 \left(\frac{a}{2}\right)^2$ is the phase shift between the fields at the edges and in the centre of the radiating surface. As shown in the figure, in the case of a quadratic change of phase, the maximum of radiation corresponds to the direction $\alpha = 0$. The major lobe of the directional diagram widens and, in the case of sufficiently large phase shifts, it is divided into two. The level of the minor lobes increases; furthermore, the zero radiation directions vanish. For large values of ψ_2 , the minor lobes are entirely absorbed by the widening major lobe.

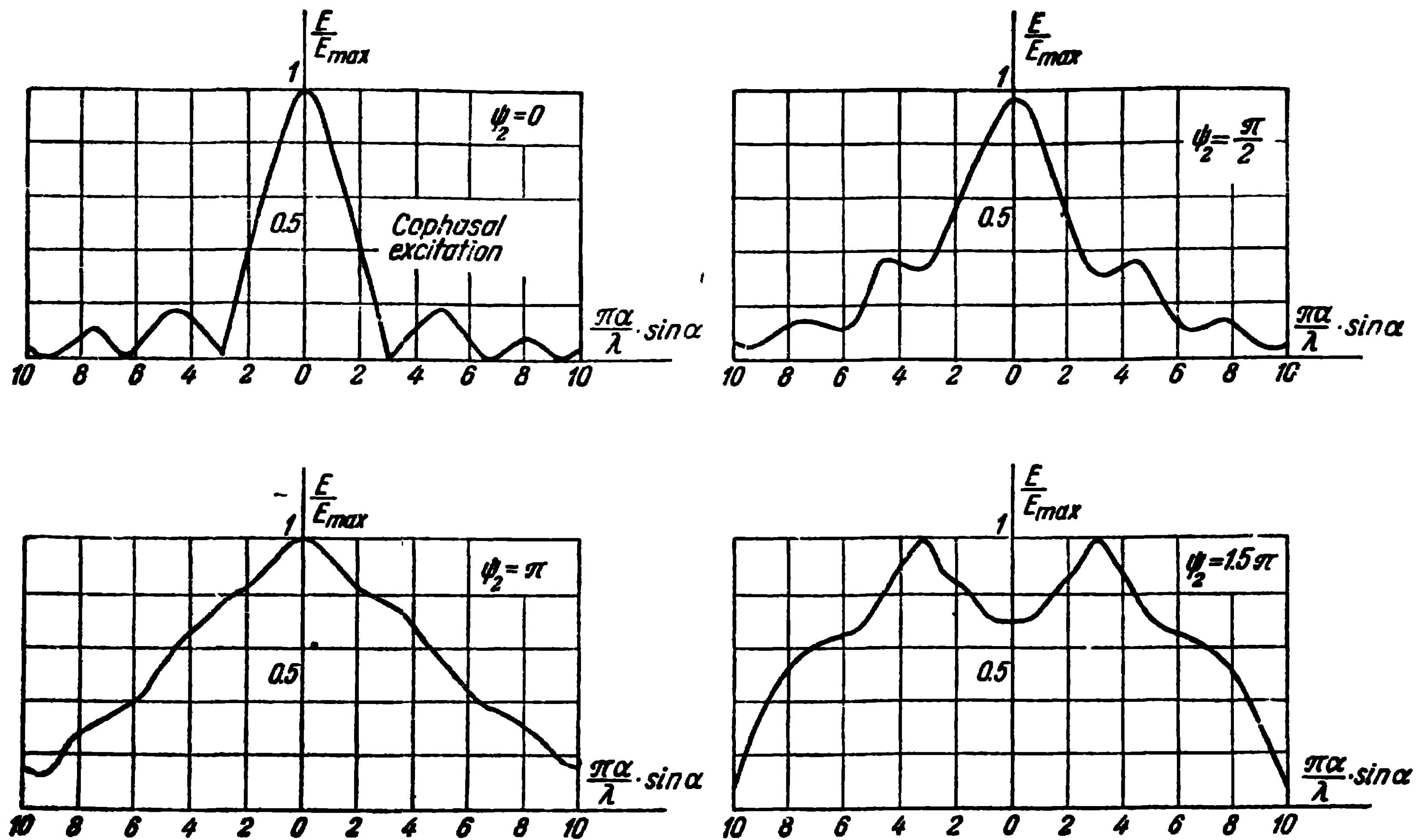


Fig. 4-17. Influence of a quadratic change of phase on the directional diagram of a plane antenna.

It is also of interest to consider the directional diagram of a plane antenna in case the phase of the field changes as $k_3 x^3$. In practice, this change of phase occurs in lens and parabolic antennas when the radiator is taken out of the focus.

Let the field intensity on the radiating surface change as

$$E_y = E_0 e^{-ik_3 x^3} \quad (4-60)$$

The field intensity at the point of observation in the xz -plane caused by the antenna element is:

$$dE_{(xz)} = -i \frac{E_0 b dx}{2\lambda r_0} (1 + \cos \alpha) e^{-ikr_0 + i(k \sin \alpha - k_3 x^2) x}.$$

The integration of this expression over the radiating surface is rather complicated. Usually, the directional diagrams are calculated by means of approximate expressions [16], which are also fairly complicated and are not given here. On the whole, the properties of the directional diagram of a plane antenna with the cubic change of phase under consideration can be summarised as follows.

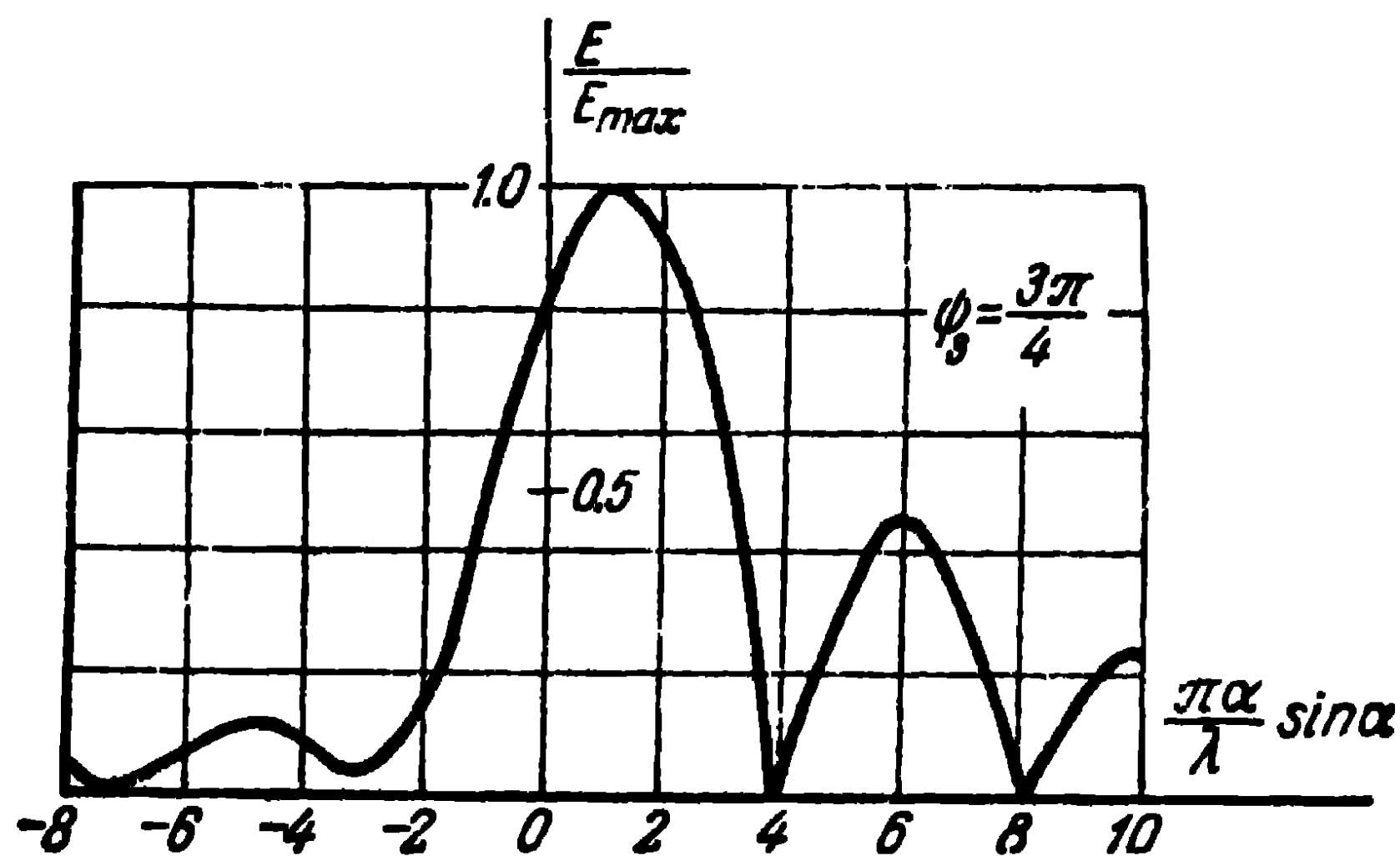


Fig. 4-18. Influence of a cubic change of phase on the directional diagram of a plane antenna.

Just as in the case of a linear change of phase, the direction of the maximum of radiation deviates from the normal to the plane of the antenna, but this deviation is attended by a distortion of the directional diagram (Fig. 4-18). When a phase changes but little at the edge of the surface

(ψ_3) , the direction of the maximum radiation may be determined from the expression

$$\sin \alpha_{\max} = \frac{0.6\psi_3\lambda}{\pi a}. \quad (4-61)$$

When $\psi_3 \leq \lambda$, the error in the determination of the direction of the radiation maximum does not exceed a few per cent. A comparison of (4-61) and (4-57) shows that the deviation of the radiation maximum direction is small in the case of the cubic change of phase than in that of the linear one (by approximately 1.7 times).

The distortion of the form of the directional diagram consists in that the major lobe widens and becomes asymmetrical; the level of the minor lobes increases on one side of the major lobe and decreases on the other one; furthermore, the decrease in the level of the minor lobes occurs on the opposite side to the direction of deviation of the major lobe.

If, with the field phase changes on the radiating surface, the field amplitude drops towards the edges, the influence of a change of phase on the directional diagram decreases.

4-9. Antenna Parameters

Antenna systems may be characterised by a number of parameters which enable us to appraise and compare the antennas. In particular, the width of the directional diagram between the zeros $2\alpha_0$ and $2\alpha_{1/2}$ at half power can be considered as belonging to parameters of this kind.

In the present paragraph, we shall consider other useful parameters. The field intensity in the radiation zone of any antenna can be represented in the following form:

$$E = i \frac{30kh_{\text{eff}}I}{r} e^{-ikr} F(\theta, \varphi) e^{i\psi}, \quad (4-62)$$

where $F(\theta, \varphi)$ is the amplitude normalised directional characteristic of the antenna;

ψ , the phase directional characteristic of the antenna;

I , the current at the point of the antenna to which the phase directional characteristic applies;

h_{eff} , the so-called effective length of the antenna.

The concept of the amplitude normalised directional characteristic of antennas has already been given in Paragraph 4-2. The phase characteristics of antennas were also mentioned earlier. The effective length is mentioned here for the first time. To make things clear, let us examine the application of (4-62) to some radiating systems. For an electric dipole lying in free space, the electric field intensity is expressed as

$$E_{\theta} = i \frac{30klI^e}{r} \sin \theta e^{-ikr}.$$

On comparing this expression with (4-62), we obtain:

$$F(\theta) = \sin \theta, \quad \psi = 0, \quad h_{\text{eff}} = l, \quad (4-63)$$

i.e., the amplitude normalised directional characteristic of the dipole represents a sinusoid ("figure of eight") in a polar system of coordinates; the phase characteristic does not depend on the angle of observation θ and represents a sphere in space and a circle on a plane; the effective length of the dipole is equal to its geometrical length and measured in metres.

For a symmetrical electric dipole in free space, the electric field intensity is expressed as

$$E = i \frac{60I_0}{r_0} e^{-ikr_0} \frac{\cos(kl \cos \theta) - \cos kl}{\sin kl \sin \theta}.$$

The amplitude normalised directional characteristic of a symmetrical electric dipole is expressed as

$$F(\theta) = \frac{\cos(kl \cos \theta) - \cos kl}{\sin \theta (1 - \cos kl)}.$$

Then, on comparing this expressions with (4-62), we obtain:

$$\psi = 0, \quad h_{\text{eff}} = \frac{\lambda}{\pi} \frac{1 - \cos kl}{\sin kl}. \quad (4-64)$$

As we see, the effective length of a symmetrical dipole is not equal to its actual length and is a function of the length of the dipole as well as of the wave-length. The effective length of a half-wave dipole $\left(l/\lambda = \frac{1}{2}\right)$ for example, equals

$h_{\text{eff}} = \frac{\lambda}{\pi} = \frac{2}{\pi} l$, i.e., constitutes 0.635 of the overall length of the dipole.

The effective length of a symmetrical dipole may be determined by integrating the function of the current along the whole length of the dipole and relating this integral to the current at the feed points of the dipole:

$$h_{\text{eff}} = \frac{2}{I_0} \int_{z=0}^l I_0 \frac{\sin k(l-z)}{\sin kl} dz = \frac{\lambda}{\pi} \frac{1 - \cos kl}{\sin kl}$$

Hence, the term effective length of an antenna may be understood as the length of a dipole with a uniform current distribution, which sets up the same magnitude of field intensity in the direction of the maximum radiation as the antenna under discussion with the same current at the feed points.

As for the phase directional characteristic, in the case of a symmetrical dipole, it does not depend on the angle of observation θ either and, in polar coordinates, represents a circle. Note that the calculation of the field phase in the above expression is performed relatively to the radius-vector applied to the centre of the dipole. If the radius-vector is related to another point of the antenna, the phase directional characteristic relatively to this point will no longer be spherical.

In the case of a co-phased array of nm half-wave dipoles, the electric field intensity in the magnetic vector plane is expressed as

$$E = i \frac{60 I_a m}{r_0} e^{-ikr_0} \frac{\sin \left(\frac{nk d_1}{2} \sin \alpha \right)}{\sin \left(\frac{k d_1}{2} \sin \alpha \right)},$$

where r_0 is the distance from the centre of the array to the point of observation of the field.

The amplitude normalised directional characteristic is defined by the expression

$$F(\alpha) = \frac{1}{n} \frac{\sin \left(\frac{nk d_1}{2} \sin \alpha \right)}{\sin \left(\frac{k d_1}{2} \sin \alpha \right)}.$$

The phase directional characteristic is spherical ($\psi=0$) and, consequently, the effective length of the antenna is expressed as:

$$h_{\text{eff}} = \frac{\lambda}{\pi} nm. \quad (4-65)$$

Note that, in practice, the concept of the effective length of an antenna is applied only when discussing the radiation of simple wire antennas. That is why the expression of h_{eff} will not be applied to other radiating systems, although this could be done, if desired.

The concept of the directive gain, first put forward by A. Pistolokors in 1929 [17], is current today in antenna theory and practice. By directive gain one understands the ratio of the square of the magnitude of the intensity of the field set up by the antenna in a given direction to the mean (along all directions) value of the square of the field intensity

$$D = \frac{|E|^2}{E_{\text{mean}}^2}. \quad (4-66)$$

Let us express the mean value of the square of the field intensity through the power radiated by the antenna. The power may be expressed as the product of the surface of a sphere of radius r_0 by the mean value of the Poynting vector on the surface of the sphere:

$$P_{\Sigma} = 4\pi r_0^2 S_{\text{mean}}.$$

But the mean value of the Poynting vector is

$$S_{\text{mean}} = \frac{E_{\text{mean}}^2}{240\pi},$$

hence

$$E_{\text{mean}}^2 = \frac{60P_{\Sigma}}{r_0^2}. \quad (4-67)$$

Substituting (4-67) into (4-66), we obtain:

$$D = \frac{|E|^2 r_0^2}{60P_{\Sigma}}. \quad (4-68)$$

It was in this form that the expression for the directive gain was put forward by M. S. Neuman.

Let us examine the application of this expression to a number of antennas. For a Hertzian dipole, the magnitude of the field intensity in the direction of the maximum radiation is $|E| = \frac{30klI}{r_0}$, and the power it radiates, $P_{\Sigma} = \frac{I^2}{2} 20(kl)^2$. Consequently, the directive gain is $D = 1.5$.

In the case of a symmetrical dipole in free space, the magnitude of the field intensity in the direction perpendicular to the dipole axis and the power radiated by the dipole are:

$$E = \frac{60 I_0}{r_0} \frac{1 - \cos kl}{\sin kl},$$

$$P_{\Sigma} = \frac{I_0^2}{2 \sin^2 kl} R_{\Sigma a}.$$

Consequently, for a symmetrical dipole, the directive gain is expressed as:

$$D = \frac{120}{R_{\Sigma a}} (1 - \cos kl)^2. \quad (4-69)$$

For a half-wave dipole, for example, $kl = 90^\circ$ and $R_{\Sigma a} = 73.1$ ohms and, therefore, $D = 1.64$ and for a wave dipole, $kl = 180^\circ$ and $R_{\Sigma a} = 199$ ohms and, therefore, $D = 2.41$.

As we saw earlier, for a co-phased array of half-wave dipoles, the magnitude of the field intensity in the direction of the maximum radiation is:

$$|E| = \frac{60 I_a}{r_0} nm$$

and the power radiated by that dipole array is:

$$P_{\Sigma} = \frac{I_a^2}{2} R_{\Sigma a} nm,$$

where $R_{\Sigma a}$ is the mean magnitude of the radiation resistance of a dipole in the system.

Consequently, the directive gain is expressed as

$$D = \frac{120}{R_{\Sigma a}} nm. \quad (4-70)$$

Thus, for example, for an array consisting of four dipoles ($n=2$, $m=2$), the radiation resistance of a dipole in the system is $R_{\Sigma a} = 75.34$ ohms and the directive gain is therefore $D = 6.37$.

In the case of an ideal plane antenna, the magnitude of the field intensity in the direction of the maximum radiation equals:

$$|E| = \frac{E_{ys}}{\lambda_0},$$

and the power radiated by the antenna is:

$$P_{\Sigma} = \frac{E_y^2 s}{240\pi},$$

consequently, the directive gain is expressed as

$$D = \frac{4\pi s}{\lambda^2}, \quad (4-71)$$

where $s=ab$ is the area of the antenna.

Let, for example, the area of an ideal plane antenna equal 1 m^2 and let this antenna be excited by a wave $\lambda=10 \text{ cm}$. The directive gain of the antenna is then $D=1,256$. If we excite the same antenna by a wave $\lambda=3 \text{ cm}$, the directive gain will be $D=13,956$. In the case of a cosinusoidal distribution of the field amplitude along one of the sides of an ideal plane antenna, the field intensity in the principal direction is $|E| = \frac{E_y s}{\lambda r_0} \frac{2}{\pi}$, and the radiated power,

$$P_{\Sigma} = \frac{E_y^2 s}{240\pi} \frac{1}{2}.$$

Hence, the directive gain is determined from the expression

$$D = 0.81 \frac{4\pi s}{\lambda^2}.$$

Let us quote one more expression for the directive gain, which is often found useful. In accordance with (4-62), the magnitude of the square of the antenna field intensity in a given direction is:

$$|E|^2 = \frac{30^2 k h_{\text{eff}}^2 / r_0^2}{r_0^2} F^2(\theta, \varphi).$$

The mean value of the square of the field intensity of the antenna along all directions is expressed as

$$E_{\text{mean}}^2 = \frac{1}{4\pi r_0^2} \int_0^\pi \int_0^{2\pi} |E|^2 r_0^2 \sin \theta d\theta d\varphi.$$

Substituting these expressions into the initial expression (4-66), we obtain:

$$D = \frac{4\pi F^2(\theta, \varphi)}{\int_0^\pi \int_0^{2\pi} F^2(\theta, \varphi) \sin \theta d\theta d\varphi}; \quad (4-72)$$

where $F(\theta, \varphi)$ is the amplitude normalised directional characteristic of the antenna.

The expression (4-72) enables us, in particular, to calculate the directive gain by means of the graphic integration of a known space directional characteristic and to obtain an approximate estimation of the magnitude of the directive gain. Indeed, assuming that within the limits of a certain solid angle $\Delta\omega = \Delta\theta\Delta\varphi$ $F(\theta, \varphi) = 1$, and that outside its limits $F(\theta, \varphi) = 0$, we obtain the following approximate expression

$$D \approx \frac{4\pi}{\Delta\theta\Delta\varphi}. \quad (4-73)$$

Thus, in the case of an ideal plane antenna, for example, the width of the directional diagram at half power equals $0.89 \frac{\lambda}{a}$ and $0.89 \frac{\lambda}{b}$ in the two principal planes. Substituting these values into (4-73), we obtain:

$$D = 1.27 \frac{4\pi s}{\lambda^2},$$

although a more accurate definition of the directive gain of an ideal plane antenna is given by (4-71).

In the case of an axial radiation antenna with a phase velocity equal to the velocity of light, the width of the directional diagram at half power is defined by (4-24). If we consider the directional diagram to be symmetrical relatively to the antenna axis, the substitution of (4-24) into (4-73) yields the following expression for the directive gain:

$$D = 3.55 \frac{L}{\lambda},$$

whereas the use of (4-72) leads to the more accurate expression:

$$D = 4 \frac{L}{\lambda}. \quad (4-74)$$

According to this expression, the directive gain is the larger the larger is L/λ .

In a slow-wave axial radiation antenna, the directive gain depends on the ratio between the electric length L/λ and the relative phase velocity ξ . Taking (4-22) and (4-72) into account, the maximum directive gain is obtained when $\psi = \frac{\pi}{2}$, i.e., when the fields in the main direction from the

first and the last elements of the antenna are in antiphase. The substitution of (4-27) into (4-73) yields a somewhat higher value of $D = 11.2 \frac{L}{\lambda}$ whereas the use of (4-72) yields the more accurate expression:

$$D = 7.2 \frac{L}{\lambda}. \quad (4-75)$$

Apart from the directive gain, the concept of the antenna power gain is also used. By antenna power gain ϵ , one understands the ratio of the square of the intensity of the field set up by the antenna under discussion in a given direction to the square of the intensity of the field set up by a half-wave dipole in its equatorial plane. It is furthermore assumed that the power fed to the antenna and dipole under investigation is the same and that the half-wave dipole lies in free space. Since the directive gain of a half-wave dipole equals 1.64, the expressions quoted yield

$$\epsilon = \frac{D\eta}{1.64}, \quad (4-76)$$

where η is the efficiency of the given antenna.

Note that, sometimes, the power gain of the antenna is defined not in relation to a half-wave dipole but in relation to a hypothetical (omnidirectional) radiator. In that case, the coefficient 1.64 in (4-76) is omitted.

The antenna efficiency is defined as the ratio of the power radiated by the antenna to the power fed to the antenna, consisting of the radiation power and the power of the losses in the antenna,

$$\eta = \frac{P_{\Sigma 0}}{P_{\Sigma 0} + P_{\text{losses}}}. \quad (4-77)$$

If we relate the radiation power and the power of the losses to the square of the current at the feed points of the antenna, the expression for the efficiency will be:

$$\eta = \frac{R_{\Sigma 0}}{R_{\Sigma 0} + R_{\text{losses}}}, \quad (4-78)$$

where R_{losses} is the resistance of the losses of the antennas related to the current at the antenna feed points.

Apart from the parameters h_{eff} , D , ϵ , η , the concept of the effective area of the antenna s_{eff} is also used in antenna

theory and practice. This concept will be dealt with later during our study of the receiving antenna theory.

The parameters of some types of antennas will be discussed in the course of our study of the corresponding types of antennas.

4-10. Definition of the Current Distribution in an Antenna in Accordance with a Prescribed Directional Diagram

a) Stating the Problem

Until now we have been defining the directional diagrams of antennas knowing their current distribution. Thus, we discussed two ways of achieving highly directional antennas: by way of the uniform distribution on a plane of the current in amplitude and co-phase, and by way of the travelling-wave current distribution along a certain straight line in space. The question arises as to whether these are the unique ways of obtaining directional antennas. Is it not possible to establish other distributions of the current in an antenna, such as would ensure still narrower directional diagrams than in the cases stated above while permitting the use of antennas of reduced size? Apparently these and similar problems may arise when designing antennas with any form of directional diagram and not only highly directional ones.

The answers to these questions can be obtained by solving the problem in the following manner: having prescribed the form of the directional diagram, we look for the distribution of the current on a certain straight line or on a plane in space that will ensure the prescribed directional diagram. Stated in this manner, the problem will not have just one unique solution. In other words, we shall obtain several possible current distributions, each of which will ensure the given form of the directional diagram. This is confirmed, for example, by the results obtained during the investigation of the co-phasal distribution and of the current distribution in accordance with the travelling-wave law. As we saw earlier, the directional diagrams obtained in both cases have an identical shape. A comparison of the current distributions obtained in this way gives a unique answer to the question as to which of them is the optimum

one from the point of view of, say, the minimum size of the antenna or of the simplicity of its design.

The problems of antenna technique where the form of the directional diagram is considered prescribed as well as where the current distribution corresponding to that directional diagram is being sought, are referred to as the reverse problems of electrodynamics. The importance of stating and solving these problems is not limited to the purpose of finding out the optimum current distributions for frequently utilised forms of directional diagrams for which the design principles of the corresponding antenna systems are known, as in the example examined above. When the necessary directional diagrams are of complex form, the determination of the current distributions which will ensure these diagrams, i.e., the synthesis of antenna systems with directional diagrams of special form may have an independent and, frequently, prime importance for technical purposes. Sometimes, the object of the reverse problems of electrodynamics is not to find the current distribution in the antenna but a certain parameter, directly connected with the geometry of the antenna and determining its diagram. Such a parameter may be the distance between the elementary radiators of which the antenna is made up, for example, the depth of the grooves of a ridged antenna, or the length of the dipoles in an array of equally spaced dipoles, etc. We shall be concerned with the problems of the first type where the object is to find the function of the current distribution on the antenna. The problems of the second type may be reduced to those of the first type, since, eventually, the above-mentioned parameters of these problems define the current distribution in the antenna.

Let us examine the various mathematical methods which will enable to establish the connection between the directional diagram and the function of the current distribution. To begin with, we shall investigate the Fourier integral method, which enables to establish many general principles and to arrive at estimates which have to be taken into account for solving the reverse problems of electrodynamics.

b) The Fourier Integral Method

Let us examine the reverse electrodynamic problem stated as follows: radiating elements (elementary electric currents, for example) are distributed along the x -axis, within the

interval $-\infty \leq x \leq +\infty$ (Fig. 4-19), in accordance with the expression

$$I(x) = u(x) e^{i\psi(x)}$$

where $u(x)$ is the amplitude distribution of the currents of the radiating elements;

$\psi(x)$, the phase distribution of the currents of the radiating elements along the x -axis.

The field of each of the radiating elements in the far zone ($r \rightarrow \infty$) may be written as:

$$dE = AI(x) dx \frac{e^{-ikr}}{r}$$

where r is the distance from the radiating element to the point of observation P ;

A is a certain constant number (the radiating elements are considered as non-directional).

Let the function of the directional diagram of the linear system under consideration $F(\theta)$, which, in the general case, is complex, be prescribed. We have to define the distribution of the amplitude and phase of the currents of the radiating elements on the x -axis that will ensure this directional diagram of the linear antenna under consideration.

The total field set up by all the elements lying on the x -axis is expressed as:

$$E(P) = A \frac{e^{-ikr_0}}{r_0} \int_{-\infty}^{\infty} I(x) e^{ikx \cos \theta} dx.$$

In this expression, the directional diagram is described by the function

$$f(\theta) = \int_{-\infty}^{\infty} I(x) e^{ikx \cos \theta} dx. \quad (4-79)$$

In accordance with the conditions of the problem, we need to find the distribution of the sources for which the directional diagram described by (4-79) should approach the prescribed function $F(\theta)$ with the required accuracy, i.e.,

$$F(\theta) = \int_{-\infty}^{\infty} I(x) e^{ikx \cos \theta} dx. \quad (4-80)$$

Let us introduce a new variable determined from the expression

$$\xi = k \cos \theta. \quad (4-81)$$

When θ changes in the whole range of the values under consideration from 0 to π , ξ changes within the interval $-k \leq \xi \leq k$. Taking account of (4-81), the expression (4-80) may be written as

$$F(\xi) = \int_{-\infty}^{\infty} I(x) e^{i\xi x} dx. \quad (4-82)$$

But on the right-hand side of this expression, we have the Fourier transformation of the function $I(x)$. This means that the function $I(x)$ can be found from the expression

$$I(x) = \frac{1}{2\pi} \int_{-\infty}^{\infty} F(\xi) e^{-i\xi x} d\xi. \quad (4-83)$$

Thus, the expression (4-83) yields the current distribution along the x -axis needed to obtain the prescribed directional diagram $F(\theta)$. Note that, in accordance with (4-81), the function $F(\xi)$ coincides with the directional diagram of the linear system under consideration only in the interval $-k \leq \xi \leq k$. This means that, while leaving the function $F(\xi)$ unchanged in the interval $-k \leq \xi \leq k$, its value may be arbitrarily prescribed outside of the interval. Furthermore, it may happen that various distributions of the radiating elements $I(x)$ along the x -axis will correspond to the same form of the directional diagram of the antenna which is described by the function $F(\xi)$ when $-k \leq \xi \leq k$ because, in accordance with (4-83), $I(x)$ is defined by the function $F(\xi)$ on the whole of the axis $-\infty \leq \xi \leq \infty$. Taking account of the above, the current corresponding to the prescribed function of the directional diagram

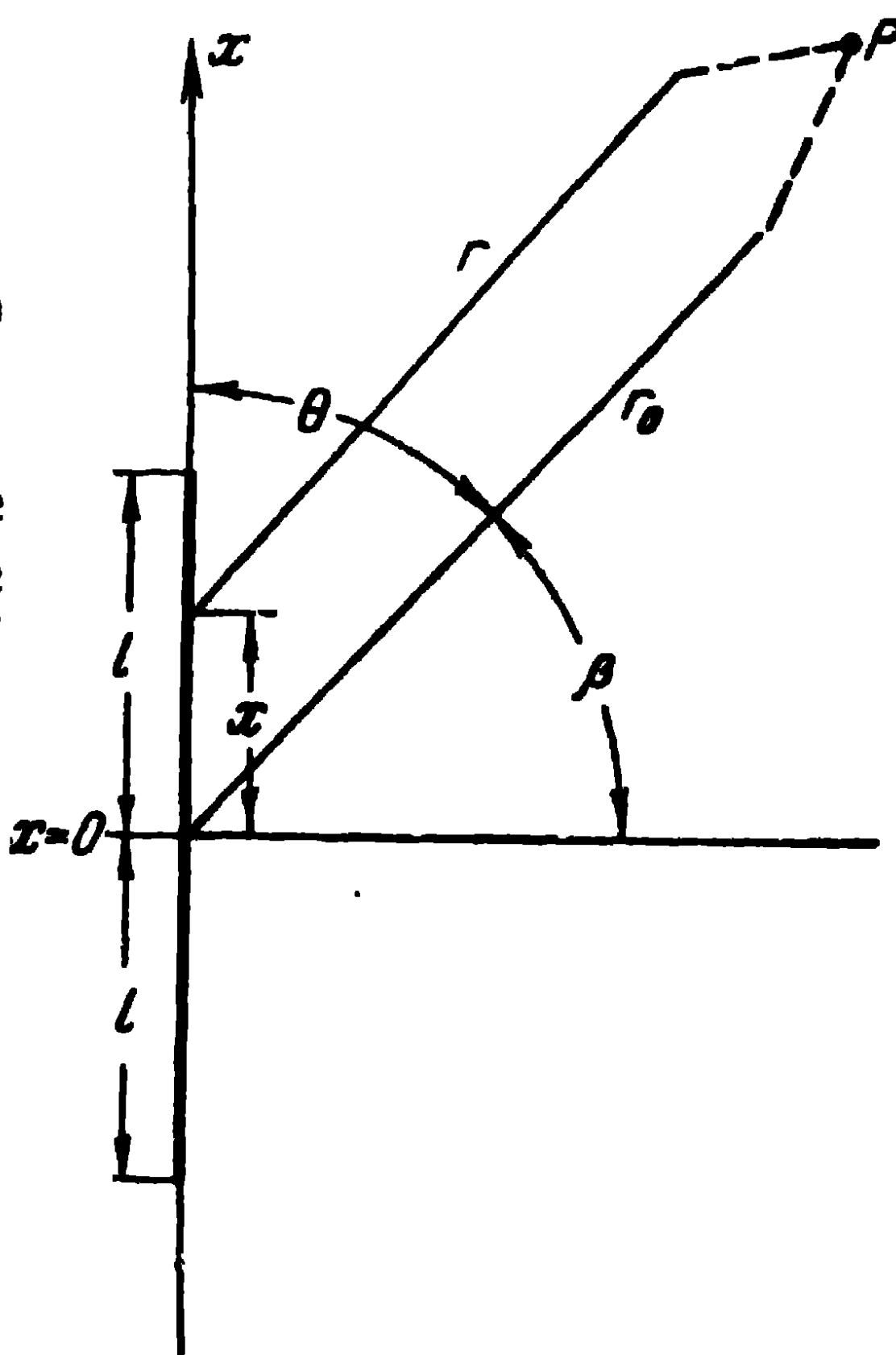


Fig. 4-19. System of coordinates utilised.

$F(\theta) = F\left(\arccos \frac{\xi}{k}\right)$ can be written in the form of two items

$$I(x) = \frac{1}{2\pi} \int_{-k}^k F(\xi) e^{-i\xi x} d\xi + \frac{1}{2\pi} \left[\int_{-\infty}^{-k} F(\xi) e^{-i\xi x} d\xi + \int_k^{\infty} F(\xi) e^{-i\xi x} d\xi \right] = I_1(x) + I_2(x). \quad (4-84)$$

Consequently, the whole straight line $-\infty \leq \xi \leq \infty$ serves as the line of integration for the item $I_2(x)$, with the exception of the section $-k \leq \xi \leq k$. The definition of the current in accordance with the prescribed directional diagram $F(\xi)$ is arbitrary because the item of the current $I_2(x)$ may be prescribed arbitrarily. Let us investigate the physical meaning of each of the items in (4-84).

Since the directional diagram of the antenna [i.e., the values of the function $F(\xi)$ on the section $-k \leq \xi \leq k$], corresponds to the field in the far zone, and the field in the far zone itself defines the power radiated by the antenna, the first item $I_1(x)$ completely defines the power radiated by the antenna and is therefore referred to as the active or radiating current.

Thus, the addition of the item $I_2(x)$ changes only the near field of the antenna and, consequently, changes only the oscillating reactive power accumulated near the antenna. Hence, the item $I_2(x)$ is referred to as the reactive current of the antenna.

It may be shown that, if we define the quality of the antenna system Q as the ratio of the reactive power accumulated near the antenna (coupled with the electric as well as the magnetic field) to the radiated power, we may obtain for it the expression

$$Q = \frac{\int_{-\infty}^{-k} |F(\xi)|^2 d\xi + \int_k^{\infty} |F(\xi)|^2 d\xi}{\int_{-k}^k |F(\xi)|^2 d\xi}. \quad (4-85)$$

The structure of this expression is easy to explain on the basis of the preceding arguments. The exact proof is asso-

ciated with complicated mathematical calculations and is not given here [18].

As will be shown in the following section, the width of the directional diagram which may be obtained from a linear antenna of finite length $2l$, is defined by the quantity Q . Let us pass on to the estimations which enable to establish such a connection.

c) Antennas with Fast and Slow Change of Current Phase

In accordance with the above, the velocity with which the current phase changes in an antenna is determined by the magnitude of the derivative of the function $\psi(x)$. Let us agree that the name "antennas with a slow change of phase" [19] will be used to designate antennas for which the following inequalities are satisfied

$$\begin{aligned} \max |\psi'(x)| &< k \quad \text{when} \quad -l \leq x \leq l, \\ \max |\psi''(x)| &< k^2 \quad \text{when} \quad -l \leq x \leq l, \end{aligned} \quad (4-86)$$

where $k = \frac{2\pi}{\lambda}$ is the wave number. These inequalities mean that the current phase in the antenna changes more slowly than the phase of a plane wave propagated in vacuum. Antennas for which the current phase changes faster will be designated as ultradirectional. The meaning of this term will be explained later.

Let us estimate the width of the directional diagram between the zeros for antennas with a slow change of current phase. In accordance with (4-79), the normalised directional diagram of a linear antenna of dimension $2l$ (Fig. 4-19) may be written as:

$$f_1(\theta) = \frac{\int_{-l}^l u(x) e^{i[kx \cos \theta + \psi(x)]} dx}{\max \left| \int_{-l}^l u(x) e^{i[kx \cos \theta + \psi(x)]} dx \right|}. \quad (4-87)$$

Let us note that, for antennas with a slow change of the current phase, it may be approximately assumed that in the direction of the maximum of the directional diagram, the fields of the antenna separate elements are added up in

co-phase, i. e.,

$$\max \left| \int_{-l}^l u(x) e^{i[kx \cos \theta + \psi(x)]} dx \right| \approx \int_{-l}^l u(x) dx. \quad (4-88)$$

The correctness of such an assumption is easily verified for the case $\psi'(x) = k_1$, where k_1 is a constant magnitude satisfying the inequality $0 \leq k_1 \leq k$.

In this particular case, one may always find such an angle θ_{\max} for which $k \cos \theta_{\max} = k_1$ and the fields of all the elements at the point P disposed at such an angle are added up in co-phase. Naturally, this angle θ_{\max} corresponds to the direction of the maximum radiation of the given linear antenna. In the general case, since the velocity with which the current phase changes on the antenna is limited, one may always find a direction of θ for which the fields of all the radiating elements distributed along the x -axis are added up almost in co-phase, i.e., the phase displacements due to the difference in path length of the rays arriving at the point P almost entirely compensate the phase displacements between the fields of the separate elements due to the function $\psi(x)$.

Taking account of (4-88), we may rewrite (4-87) as:

$$f_1(\theta) = \frac{\int_{-l}^l u(x) e^{i[kx \cos \theta + \psi(x)]} dx}{\int_{-l}^l u(x) dx}. \quad (4-89)$$

Let us estimate in modulus the magnitude of the derivative of the function $f_1(\theta)$, defined by (4-89),

$$\left| \frac{\partial f_1(\theta)}{\partial \theta} \right| \leq \frac{k l |\sin \theta| \int_{-l}^l \frac{|x|}{l} u(x) dx}{\int_{-l}^l u(x) dx}.$$

Let us designate

$$p_u = \frac{\int_{-l}^l \frac{|x|}{l} u(x) dx}{\int_{-l}^l u(x) dx}$$

then we shall obtain

$$\left| \frac{\partial f_1(\theta)}{\partial \theta} \right| \leq kl p_u. \quad (4-90)$$

Let us note that the coefficient p_u is not larger than unity; furthermore, it reaches this maximum value if the current in the antenna is concentrated at the points $x = \pm l$ (i.e., in that case, the value of the reducing item $\frac{|x|}{l}$ which influences the magnitude of the integral in the numerator of the expression for p_u is at its maximum).

In the other cases, the factor $\frac{|x|}{l}$ reduces the magnitude of the integral in the numerator of the expression for p_u relatively to the magnitude of the integral in the denominator, since at all points except $x = \pm l$, $\frac{|x|}{l} < 1$.

Substituting for p_u into (4-90) the maximum value of this coefficient, which is equal to unity, we find:

$$\left| \frac{\partial f_1(\theta)}{\partial \theta} \right| \leq kl.$$

Thus, the velocity of change of the modulus of the normalised directional diagram of a linear antenna cannot exceed the electric length of the antenna in the case of a slow change of current phase in the antenna. But the velocity of change of a normalised directional diagram determines the width of the antenna directional diagram.

Indeed, if the velocity of change of the normalised directional diagram for a change of the angle θ does not exceed a certain magnitude $f'_{\max}(\theta)$, the angle $\Delta\theta$ within the limits of which the directional diagram changes from its maximum magnitude, equal to unity, to the magnitude $a < 1$, cannot be smaller than the quantity $\frac{1-a}{f'_{\max}(\theta)}$ if we assume that at all values of θ within $\Delta\theta$, the velocity of

change is maximum and equals $|f'_{\max}(\theta)|$. On the strength of this, we may write the evident inequality for the width of the directional diagram between the zeros

$$2\theta_0 \leq \frac{2}{f'_{\max}(\theta)} = \frac{2}{klp_u} = \frac{\lambda}{\pi lp_u}. \quad (4-91)$$

For a co-phased and uniform distribution of the radiating sources along a linear antenna, we have established in Paragraph 4-2 that the width of the directional diagram between the zeros equals:

$$2\theta_0 = \frac{\lambda}{l} [\text{rad}].$$

Consequently, for antennas with a slow change of current phase, the width of the directional diagram may be obtained πp_u times smaller than in the case of a co-phasal current distribution, through the corresponding choice of the current distribution $I(x)$. However, one should take into account that if we are to obtain a sufficiently small level for the minor lobes of the directional diagram, the quantity p_u should be smaller than 0.5 ($p_u = 0.5$ for a uniform distribution of the amplitude). Consequently, the co-phasal and uniform distribution of the radiating sources is near enough to the optimum from the point of view of obtaining the minimum width of the directional diagram (for prescribed dimensions of the antenna) if we limit ourselves to the investigation of antennas with a slow change of current phase.

In the case of antennas with a rapid change of current phase, the inequality (4-88) is not valid. Hence, instead of (4-90), on the strength of (4-89), one should write

$$\left| \frac{df_1(\theta)}{d\theta} \right| \leq p_\psi p_u kl, \quad (4-92)$$

where

$$p_\psi = \frac{\int_{-l}^l u(x) dx}{\max \left| \int_{-l}^l u(x) e^{i[kx \cos \theta + \psi(x)]} dx \right|}. \quad (4-93)$$

The coefficient p_ψ shows the number by which the amplitudes of the currents in an antenna with a rapid change of

phase need to be multiplied so as to obtain the same value of the field in the direction of the maximum of the directional diagram as for a co-phased antenna in which the distribution of the current amplitude corresponds to that in the antenna with a rapid change of current phase under investigation. Since the coefficient p_ψ may be as large as desired, the width of the directional diagram between the zeros for antennas with a rapid change of current phase for the prescribed dimension of the antenna $2l$ may be obtained as small as desired. That is why antennas with a rapid change of phase are often called ultradirectional antennas.

The following conclusions may be drawn from the above.

For the prescribed dimension $2l$ of an antenna, we may obtain a directional diagram of any form. However, an increase in the velocity of change of the directional diagram with a change of the angle, at the prescribed dimension of the antenna, requires an increase of the velocity of change of current phase in the antenna, and this, in accordance with (4-93) requires, for the prescribed value of the field in the far zone of the antenna, an increase of the current amplitude in the antenna.

From the point of view of the practical design of the antenna, an increase of the velocity of change of the phase of its current will render it more complex, since a larger number of discrete sources will be needed for approximating with sufficient accuracy the continuous current distribution theoretically obtained. Furthermore, an increase of the amplitude of the currents in the antenna leads, for the same radiated power (for the same field in the far zone), to a decrease of the efficiency of the antenna, if the surface along which the currents flow, possesses a finite conductivity.

It should be noted that, in practice, it is nevertheless found possible to achieve ultradirectional antennas with even higher velocities of change of current phase than $\psi'(x)=k$, so that, from the point of view of the practical design of antennas for the current distribution obtained, the boundary between antennas with a slow change of current phase and ultradirectional antennas is somewhat relative.

This applies to antennas in which the ultradirectivity effect is achieved through a slow phase velocity.

In the general case, a slow phase velocity is not necessarily associated with obtaining ultradirectional diagrams. For this reason, all the estimations quoted do not

apply to just any antenna with a slow phase velocity but only to antennas in which the distribution of the amplitude and phase of currents is prescribed specifically with the object of obtaining the ultradirectional effect. In particular, all that was said above does not apply to travelling-wave antennas with a slow phase velocity, for which the width of the directional diagram is even larger than in the case of a co-phased antenna of the same length.

Let us also note that if we do not alter the form of the directional diagram but make the antenna each time with a decreasing dimension of l , then beginning from a certain dimension of l , we shall eventually arrive at ultradirectional antennas. At the same time, a decrease of l will raise the quality factor of the antenna Q , since when l decreases, the active current remains unchanged (conventionally, the directional diagram does not change in the case of a change of l) and an increase of the current amplitude in the antenna can only be connected with an increase of the reactive currents and, therefore, with an increase of the reactive fields in the vicinity of the antenna. Thus, an increase of the degree of ultradirectivity of the antenna leads to an improvement of its quality factor and this leads to the narrowing of the pass-band of the antenna from the point of view of its input resistance, since the input resistance of antennas of high quality factor are very closely dependent on the frequency.

The direct connection between the velocity with which the current phase changes in an antenna and its quality factor enables to classify antennas into ordinary and ultradirectional antennas, not only from the point of view of the velocity of the change of the current phase in the antenna but also from the point of view of the so-called ultradirectivity coefficient, which equals

$$\gamma = 1 + Q,$$

where Q is the quality factor of the antenna, determined in accordance with (4-85).

As can be seen from the preceding arguments, the ultradirectivity coefficient reflects the ratio of the sum of the radiated and reactive powers accumulated near the antenna to the radiated power. The boundary between ordinary and ultradirectional antennas is, in that case, a certain, also relative, quantity for which the practical design of an

antenna system is still possible. This boundary value γ is usually considered to be of the order of several tens.

As follows from the definition of γ , this parameter is closely connected with the phase velocity of the currents in the antenna and it is possible to establish a simple correspondence between the magnitude of the parameter γ and that of the phase velocity of the currents in the antenna determining the boundary between ordinary and ultradirectional antennas.

In conclusion, note that the Fourier integral method is seldom applied to the practical calculation of antennas in accordance with a prescribed diagram, because by substituting into (4-83) an arbitrary function of the directional diagram, we obtain, in the general case, a current which differs from zero along the whole of the axis $-\infty \leq x \leq \infty$. In practice, the dimension of the antenna or the range within which this dimension may be varied is usually specified in advance, so that other methods are used for practical calculations, in particular the partial directional diagrams method.

True, such mathematical restrictions may be imposed on the function $F(\xi)$ that, in calculating the current distribution in accordance with (4-83), the value of the current will differ from zero only within a certain finite interval on the x -axis (see, for example, [18]). However, for practical calculations, this method is too complicated.

d) The Partial Directional Diagrams Method

Let the function of the elementary radiators distribution $I(x)$ in the interval $-l \leq x \leq l$ be prescribed as a sum m of functions

$$I(x) = \sum_{n=0}^m A_n I_n(x). \quad (4-94)$$

Then, the function of the directional diagram $f(\theta)$ will be represented as a sum of partial diagrams $f_n(\theta)$ to each of which corresponds, in the interval $-l \leq x \leq l$, its own function of current distribution $I_n(x)$.

Indeed,

$$f(\theta) = \int_{-l}^l I(x) e^{ikx \cos \theta} dx = \int_{-l}^l \sum_{n=0}^m A_n I_n(x) e^{ikx \cos \theta} dx.$$

Changing the order of the integration and summation and introducing the designations

$$f_n(\theta) = \int_{-l}^l I_n(x) e^{ikx \cos \theta} dx,$$

we find

$$f(\theta) = \sum_{n=0}^m A_n f_n(\theta).$$

Then, the solution of the reverse electrodynamic problem is reduced to the expansion of the prescribed directional diagram $F(\theta)$ in accordance with the system of functions $f_n(\theta)$. The coefficients A_n of this expansion enable, in accordance with (4-94), to construct in the interval $-l \leq x \leq l$ the current distribution which corresponds to the prescribed diagram $F(\theta)$. Note that the current distribution thus obtained will be different from zero in the prescribed interval $-l \leq x \leq l$ inasmuch as the current $I_n(x)$ corresponding to each partial diagram $f_n(\theta)$ differs from zero only on that section. Furthermore, from the mathematical point of view, the system of functions $I_n(x)$ can always be prescribed in such a way that the velocity of the phase change will, for each of them, be less than k . Then, an ultradirectional antenna will not be obtained by just any combination of the currents $I_n(x)$. However, in all these cases, in order to obtain a sufficiently accurate approximation of the prescribed diagram by a system of functions $f_n(\theta)$, the dimension chosen for the antenna should satisfy the condition (4-91) and the system of functions of the partial directional diagrams should be sufficiently complete.

The partial directional diagrams method enables the quantitative estimation of the influence of the degree of ultradirectivity of the antenna on its current amplitude. The graph of Fig. 4-20 shows how the ratio of the amplitude (maximum) of the current U_{\max} in an ultradirectional antenna of length $2l$ to the current amplitude in a co-phased antenna U_0 of length $2l$ varies with the quantity $2l/\gamma$, the directional diagram of which is represented as:

$$f_0(\theta) = \frac{\sin[kl \cos \theta]}{kl \cos \theta}.$$

The calculation was effected by the partial diagrams method; moreover, for the ultradirectional antenna, the directional diagram was prescribed as:

$$\tilde{f}(\theta) = \frac{\sin [\alpha kl \cos \theta]}{\alpha kl \cos \theta},$$

where α is the coefficient, larger than unity, characterising the degree of ultradirectivity.

The functions taken as the functions $I_n(x)$ were:

$$I_{2n}(x) = \frac{1}{k\pi \sqrt{l^2 - x^2}} \times T_{2n} \left[\sqrt{1 - \left(\frac{x}{l}\right)^2} \right];$$

$$I_{2n+1}(x) = \frac{(-1)^{n-1} l}{k\pi \sqrt{l^2 - x^2}} \times T_{2n+1} \left[\frac{x}{l} \right],$$

where T_{2n} and T_{2n+1} are the even and odd Chebyshev polynomials of the corresponding arguments.

Then, the corresponding partial diagrams are represented as:

$$f_n(\theta) = J_n(kl \cos \theta),$$

where J_n is the Bessel function of n order.

The expansion of $f(\theta)$ in a $f_n(\theta)$ series is easy to perform owing to the completeness of the Bessel functions system.

The calculations have also shown that the current phase in the antenna changes from point to point.

An examination of the graph in Fig. 4-20 enables us to conclude that the practical effect of the ultradirectivity can be utilised to raise the directivity of antennas of small length, where the needed increase of current amplitude is not high.

An attempt to utilise the ultradirectivity effect for antennas of great length ($\frac{2l}{\lambda} > 1$) will cause the power gain to fall as α increases due to the sharp increase of the

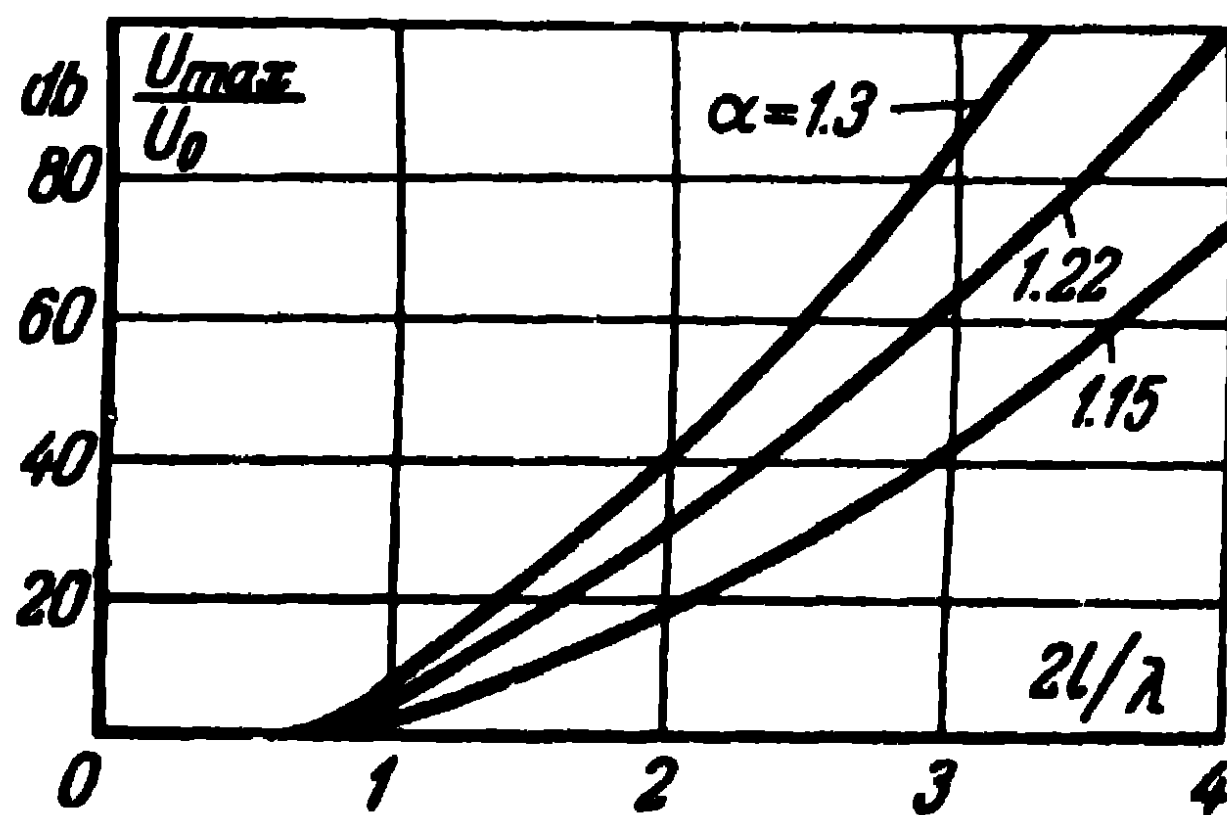


Fig. 4-20. Graph illustrating the amplitude of the currents in an ultradirectional antenna.

amplitudes of the currents and the attending sharp decrease of the antenna efficiency caused by an increase of its losses.

Thus, the present investigation of the methods for solving the reverse problems of electrodynamics, which do not, of course, cover the whole variety of methods of this kind used in antenna technique, shows that the solution of the reverse problem regarding the calculation of the current distribution in an antenna in accordance with a prescribed function of the directional diagram does not present any difficulties of principle. Furthermore, it follows from the expressions (4-83) and (4-84) cited above, that prescribing the modulus of the directional diagram, which is usually adequate for practical purposes, does not yet provide a unique definition of the current distribution along a linear conductor, due to the fact that, in accordance with (4-84), when prescribing the modulus of the directional diagram, the determination of even the active current of the antenna $I_1(x)$ is not unique (with an accuracy of up to the arbitrary phase characteristic of the antenna). This means that when the directional diagram is prescribed in this way, with the phase of the function $F(\xi)$ varying in the interval $-k \leq \xi \leq k$ and the function $F(\xi)$ assuming different forms for $\xi > k$, the current distribution may vary within a wide range. In the absence of a unique solution to the reverse electrodynamic problem, there arises the possibility of imposing on the prescribed function of the directional diagram a whole series of conditions ensuring current distributions which, apart from the prescribed directional diagram, would also confer to the antenna a series of desirable characteristics, such as efficiency, a wide pass-band, simplicity of construction, etc. The mathematical expression of these conditions may usually be found only in the case we know a concrete way of obtaining the current distribution. So far, the general approach to the problem regarding the obtention of optimum current distributions from the point of view of efficiency, wide pass-band, etc., has not been worked out in antenna technique.

e) The Chebyshev Polynomials

Apart from the possibilities indicated above for obtaining optimum current distributions, the form of the directional diagram is itself often prescribed non-unique. Indeed,

the technical characteristics usually required of a directional diagram by the radio-technical system to which the given antenna is connected, are limited to the width of the directional diagram (at the zeros or at half power) and to the level of the minor lobes. Moreover, from the point of view of the characteristics of the radio-technical system as a whole, the form of the minor lobes and their distribution in the non-operating sector of space are more or less indifferent. However, due to constructional considerations (dimensions and simplicity of the antenna system) this question is by no means indifferent inasmuch as the current distribution depends on the values of the function of the directional diagram $F(\xi)$ in the whole range of angles.

We are thus confronted with the problem of finding the optimum forms for the directional diagrams of highly directional antennas which, for prescribed width of the directional diagram and level of the minor lobes, would reduce the dimensions of the antennas down to a minimum.

The problem may be formulated in two ways:

1. The dimensions of the antenna system and the level of the minor lobes being prescribed, determine the current distribution in the antenna that will ensure the minimum width of the major lobe.

2. The width of the directional diagram being prescribed, determine the current distribution in the antenna that will ensure the minimum level of the minor lobes for the dimensions chosen for the antenna system.

Stated in this way, the reverse problems of electrodynamics are solved with the help of the Chebyshev polynomials; we shall give a brief outline of their properties. A more systematic account of the theory and properties of these polynomials may be found in the literature (see, for example, [21]).

The Chebyshev polynomials have the following form:

$$T_m(x) = \cos(m \arccos x). \quad (4-95)$$

It is easy to prove that the function cited here is the polynomial of power m with respect to the variable x . Let us make the substitution $x = \cos \delta$ and utilise the expression for the expansion of $\cos m\delta$ in a $\cos \delta$ power series:

$$\begin{aligned} \cos m\delta = & \cos^m \delta - \binom{m}{2} \cos^{m-2} \delta \sin^2 \delta + \\ & + \binom{m}{4} \cos^{m-4} \delta \sin^4 \delta + \dots, \end{aligned} \quad (4-96)$$

where

$$\binom{m}{k} = \frac{m!}{k! (m-k)!}.$$

If we replace $\sin^2 \delta = 1 - \cos^2 \delta$ and, in turn, $\cos \delta = x$ we obtain the following expressions for the first seven Chebyshev polynomials:

$$\begin{aligned} T_0(x) &= 1; \\ T_1(x) &= x; \\ T_2(x) &= 2x^2 - 1; \\ T_3(x) &= 4x^3 - 3x; \\ T_4(x) &= 8x^4 - 8x^2 + 1; \\ T_5(x) &= 16x^5 - 20x^3 + 5x; \\ T_6(x) &= 32x^6 - 48x^4 + 18x^2 - 1; \\ T_7(x) &= 64x^7 - 112x^5 + 56x^3 - 7x. \end{aligned} \tag{4-97}$$

Fig. 4-21 shows the graph of the function $T_7(x)$ for $0 \leq x \leq 1.3$. In the interval $-1.3 \leq x \leq 0$, the form of the graph of the function $T_7(x)$ is similar to the one shown.

As can be seen from the graph, all the maximums of the Chebyshev polynomial on the segment $-1 \leq x \leq 1$ are equivalent and equal to unity and the number of the zeros of the function on that segment is equal to the power of the polynomial. Outside the segment $-1 \leq x \leq 1$, when $|x| > 1$ T_7 , on the modulus grows steadily without restrictions. According to the polynomials theory used here, the functions T_n constructed within the segment $-1 \leq x \leq 1$ in agreement with the above-mentioned rule, are the polynomials of least deviation from zero. This means that the deviation of the modulus of these polynomials from zero at the points of the maximum values of the polynomials on the segment $-1 \leq x \leq 1$ is at a minimum in comparison with any other polynomial of the same power with real coefficients and with a highest-term coefficient equal to unity.

Let us now consider the same Chebyshev polynomial $T_7(x)$ on the segment $-1 \leq x \leq 1$ but with a changed scale $T_7(\alpha_0 x)$ where $\alpha_0 > 1$. In that case, the graph of the function $T_7(\alpha_0 x)$ on the segment $-1 \leq x \leq 1$ (Fig. 4-22) acquires the characteristic form of a multilobe directional diagram, the maximum of which occurs for $x = \pm 1$. The level of the minor lobes of this multilobe diagram is determined by the

ratio $\frac{1}{T_7(\alpha_0)}$, because, in accordance with the graph in Fig. 4-22, the amplitude of the major lobe equals $T_7(\alpha_0)$ and the amplitude of the minor lobe equals unity. In accordance with (4-95), the distance along the x -axis between the point with the maximum value and the first zero of the function (Δx in Fig. 4-22), is written as:

$$\Delta x = 1 - \frac{1}{\alpha_0} \cos \frac{\pi}{2m}, \quad (4-98)$$

where m is the power of the polynomial.

For $m=7$, this yields:

$$\Delta x = \left(1 - \frac{1}{\alpha_0} \cos \frac{\pi}{14} \right).$$

The position of the zeros x_0 and the maximums x_m of the function on the x -axis is determined by the relations

$$\alpha_0 x_0 = \cos \frac{(2p+1)\pi}{2m};$$

$$\alpha_0 x_m = \cos \frac{p\pi}{m}, \quad (4-99)$$

where p is the ordinal number of the zero or maximum and m is the power of the polynomial. For the graph shown in Fig. 4-22, it should be assumed that $m=7$. Similar expressions will apply to the polynomials $T_m(x)$ of any order m .

Now assume that for an antenna of a certain definite design, the directional diagram may be represented in the form of a polynomial of power m at the variable x , proportional to the cosine or sine of the angle of observation and that, in addition, the coefficients of this polynomial may be given any value through varying the elements of the antenna.

If we consider that the power of the polynomial is prescribed, the coefficients of the polynomials should be chosen

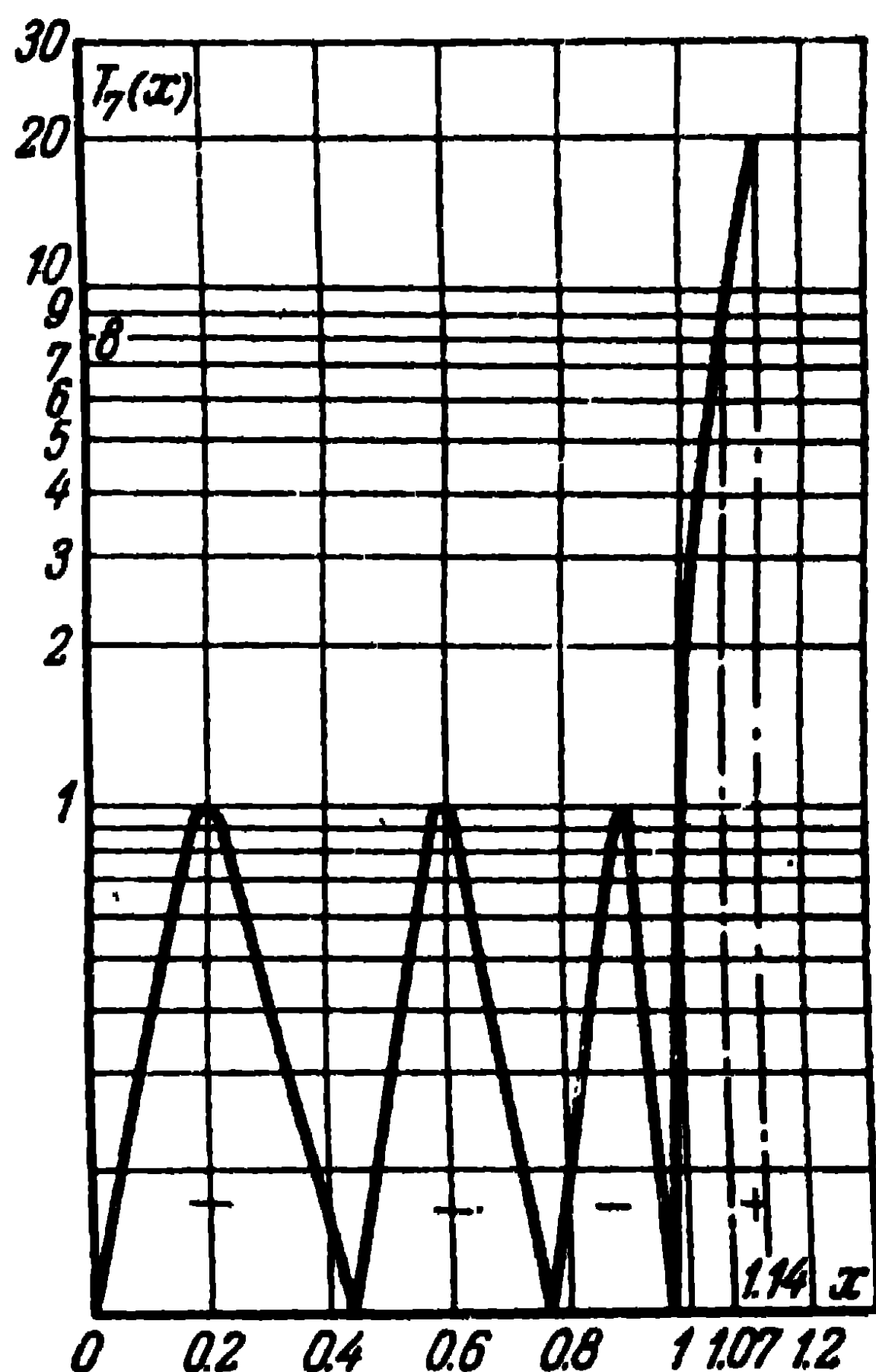


Fig. 4-21. Graph of the Chebyshev polynomial $T_7(x)$.

so as to correspond to the coefficients of the Chebyshev polynomial $T_m(\alpha_0 x)$ of the same order m . Then, for the prescribed level of the minor lobes $\frac{1}{T_m(\alpha_0)}$, the width of the directional diagram at the scale of the variable x will be at its minimum and, conversely, for a prescribed distance on the x -axis between the maximum of the diagram and

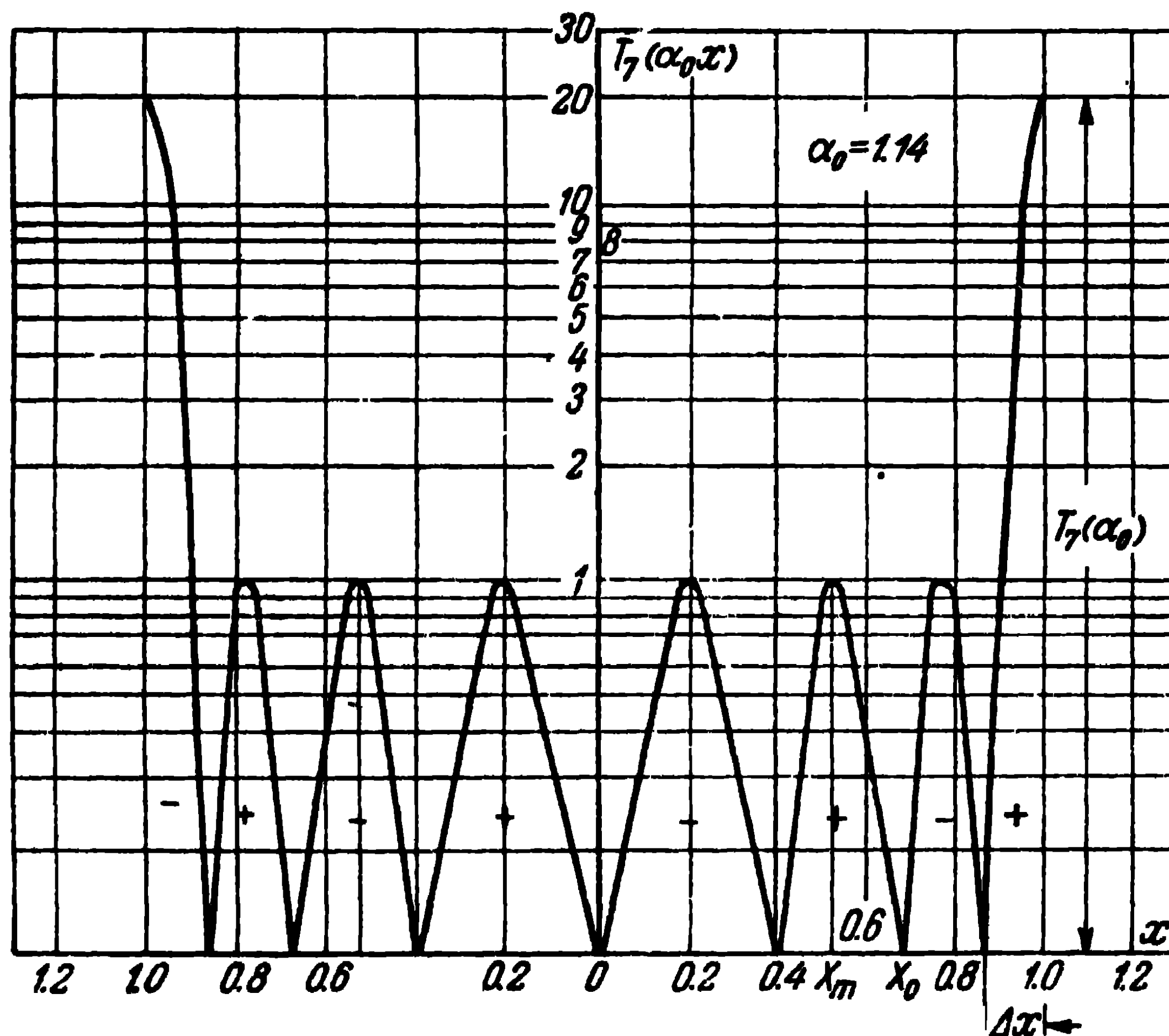


Fig. 4-22. Graph of the Chebyshev polynomial $T_7(\alpha_0 x)$.

the zero (Δx), the level of the minor lobes will be at its minimum. The last assertion is directly derived from the properties of the Chebyshev polynomial inasmuch as, among all the polynomials of the same power, the maximums of the minor lobes (on the segment $-1 \leq x \leq 1$) of this polynomial differ the least from zero. The first statement is easily proved if we take into account that outside the segment $-1 \leq x \leq 1$, among all the polynomials with real coefficients of the same power, the Chebyshev polynomial possesses the highest velocity of increase when $|x|$ becomes larger than unity.

Taking advantage of the above favourable properties of the Chebyshev polynomials, we can construct antennas with a directional diagram of optimum form. Let us illustrate this on the example of a co-phased multi-unit linear antenna.

*f) Designing an Antenna with
a Directional Diagram of Optimum Form*

Let us examine a concrete antenna system which may be optimised by the Chebyshev polynomials. Suppose an antenna system is prescribed as an array of radiators equally

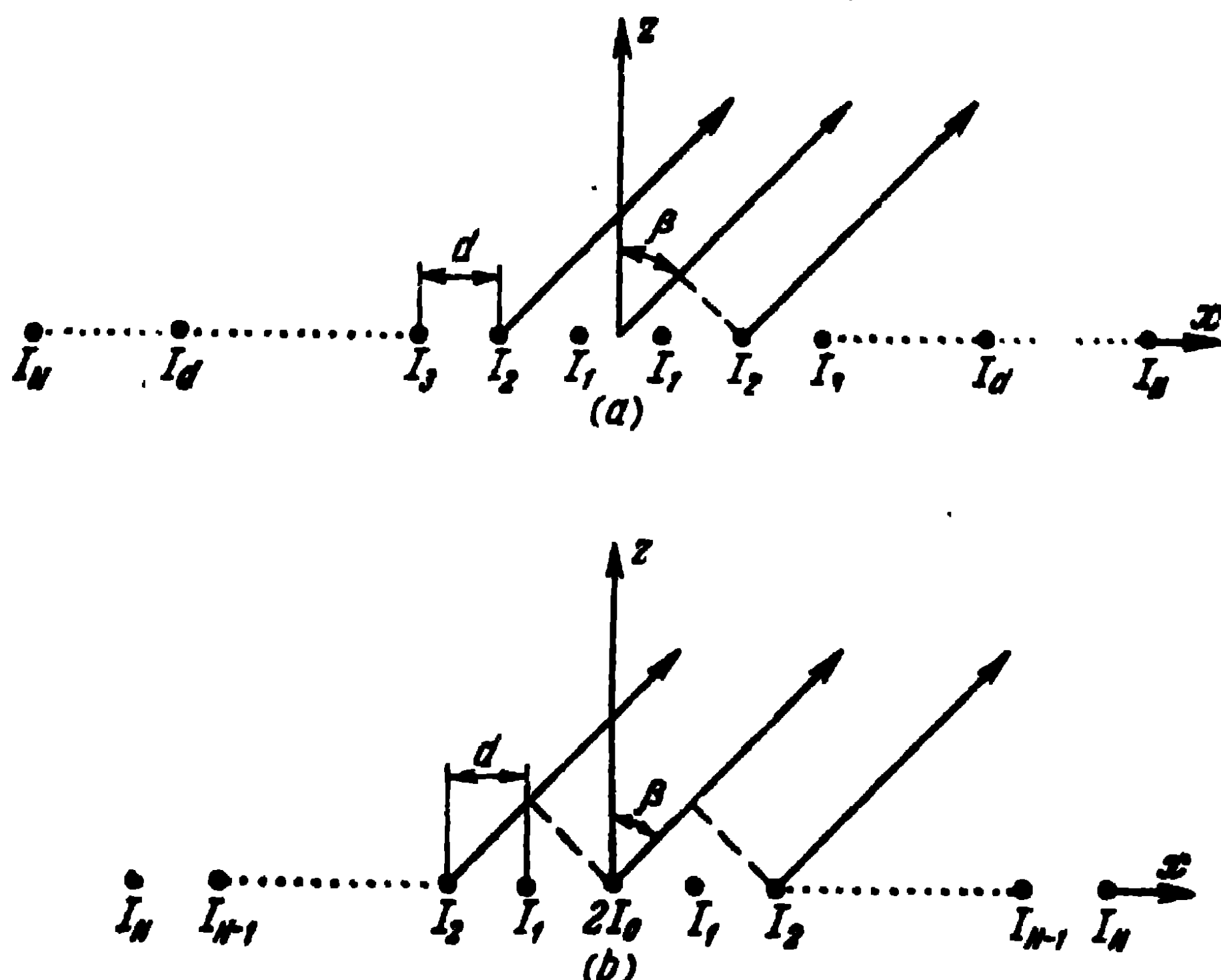


Fig. 4-23. Distribution of the dipoles along a linear antenna:
a—even number of dipoles; b—odd number of dipoles

spaced at a distance d apart along the x -axis (Fig. 4-23). All the radiators have a co-phased feed and the directional diagram of each radiator in free space represents a circle in the xz -plane, i.e., we are examining only the combination factor and taking no account of the directional properties of each radiator.

The field of such a system of sources in the far zone in the case of an even number of radiating elements in line is (without taking account of the phase factor):

$$|E_{\Sigma N}(\beta)| = \left| \sum_{k=1}^N I_d \cos \left\{ \frac{2k-1}{2} \left(\frac{2\pi}{\lambda} d \right) \sin \beta \right\} \right| \quad (4-100)$$

and, correspondingly, for an odd number of sources:

$$|E_{2N+1}(\beta)| = \left| \sum_{k=0}^N I_d \cos \left\{ k \left(\frac{2\pi d}{\lambda} \sin \beta \right) \right\} \right|. \quad (4-101)$$

If we introduce the new variable u equal to:

$$u = \frac{\pi d}{\lambda} \sin \beta, \quad (4-102)$$

we obtain:

$$\begin{aligned} |E_{2N}(\theta)| &= \left| \sum_{k=1}^N I_d \cos (2k-1)u \right|; \\ |E_{2N+1}(\theta)| &= \left| \sum_{k=0}^N I_d \cos 2ku \right|. \end{aligned} \quad (4-103)$$

On substituting $x = \cos u$, each of these expressions can be reduced to the expression of the polynomial of $2N-1$ and $2N$ powers respectively. To this end, we make use of (4-96) and replace $\sin^2 u$ by $(1 - \cos^2 u)$. Following a number of transformations, we obtain instead of (4-103):

$$\begin{aligned} |E_{2N}(\theta)| &= \sum_{q=1}^N \left[\sum_{k=q}^N I_d A_{2q-1}^{2k-1} \right] x^{2q-1}; \\ |E_{2N+1}(\theta)| &= \sum_{q=0}^N \left[\sum_{k=q}^N I_d A_{2q}^{2k} \right] x^{2q} \end{aligned} \quad (4-104)$$

where

$$\begin{aligned} A_{2q-1}^{2k-1} &= (-1)^{k-q} \sum_{p=k-q}^{k-1} \binom{p}{p-k+q} \binom{2k-1}{2p}; \\ A_{2q}^{2k} &= (-1)^{k-q} \sum_{p=k-q}^k \binom{p}{p-k+q} \binom{2k}{2p}. \end{aligned}$$

Thus, the directional diagram of an array of co-phased dipoles is expressed by a polynomial of $2N-1$ power or $2N$ of the variable x , changing from -1 to $+1$. The power of the polynomial is determined by the number of dipoles in the

array (it is one less than the overall number of dipoles), i.e., for the prescribed distance between the dipoles, the power of the polynomial is closely connected with the dimensions of the linear antenna. The coefficients of the polynomials (4-104) are expressed in the form of polynomials of various powers of the currents in the dipoles and they may be given any value through the adequate choice of these currents.

Thus, we have obtained a practicable antenna system which enables us to make use of the properties of the Chebyshev polynomials and construct an antenna with a directional diagram of optimum form if the currents in the dipoles I_d are chosen in such a way that the coefficients of the polynomials in (4-104) would correspond to the coefficients of the Chebyshev polynomials of the same orders. The condition of the equality of the coefficients may be written as:

$$\begin{aligned} \left[\sum_{k=q}^N I_d A_{2q-1}^{2k-1} \right] &= a_{2q-1}^{2N-1} (\alpha_0)^{2q-1}; \\ \left[\sum_{k=q}^N I_d A_{2q}^{2k} \right] &= a_{2q}^{2N} (\alpha_0)^{2q}; \end{aligned} \quad (4-105)$$

where a_{2q-1}^{2N-1} is the coefficient in the $2N-1$ order Chebyshev polynomial of x^{2q-1} in (4-97);

a_{2q}^{2N} , the coefficient in the $2N$ order Chebyshev polynomial of x^{2q} in (4-97).

The order of re-evaluation of the parameters of the directional diagram represented by the Chebyshev polynomial, from the variable x into real parameters (level of the minor lobes and width of the directional diagram) of the antenna under consideration (i.e., the re-evaluation from the variable x to the variable β) will be given in the following section.

Let us now consider how we should choose the distance d between the dipoles in order to obtain a directional diagram of optimum form. To this end, let us analyse the expression which connects the variable x in the expressions (4-104) to the variable β corresponding to the angle of the point of observation with respect to the linear antenna under consideration, and the nature of the changes of the graphs

of the same functions of the directional diagrams but constructed once in the $x, F(x)$ coordinates and then in the $\beta, F(\beta)$ coordinates for various values of d .

In accordance with the above,

$$x = \cos u = \cos \left[\frac{\pi d}{\lambda} \sin \beta \right].$$

As can be seen from this expression, the range of change of the variable is limited to the segment $-1 \leq x \leq 1$ for any range of change of the variable u . Let us investigate how the range of change of the variable u influences the character of the directional diagrams. Since the range of change of u is determined by the magnitude of d , let us take several particular values of d .

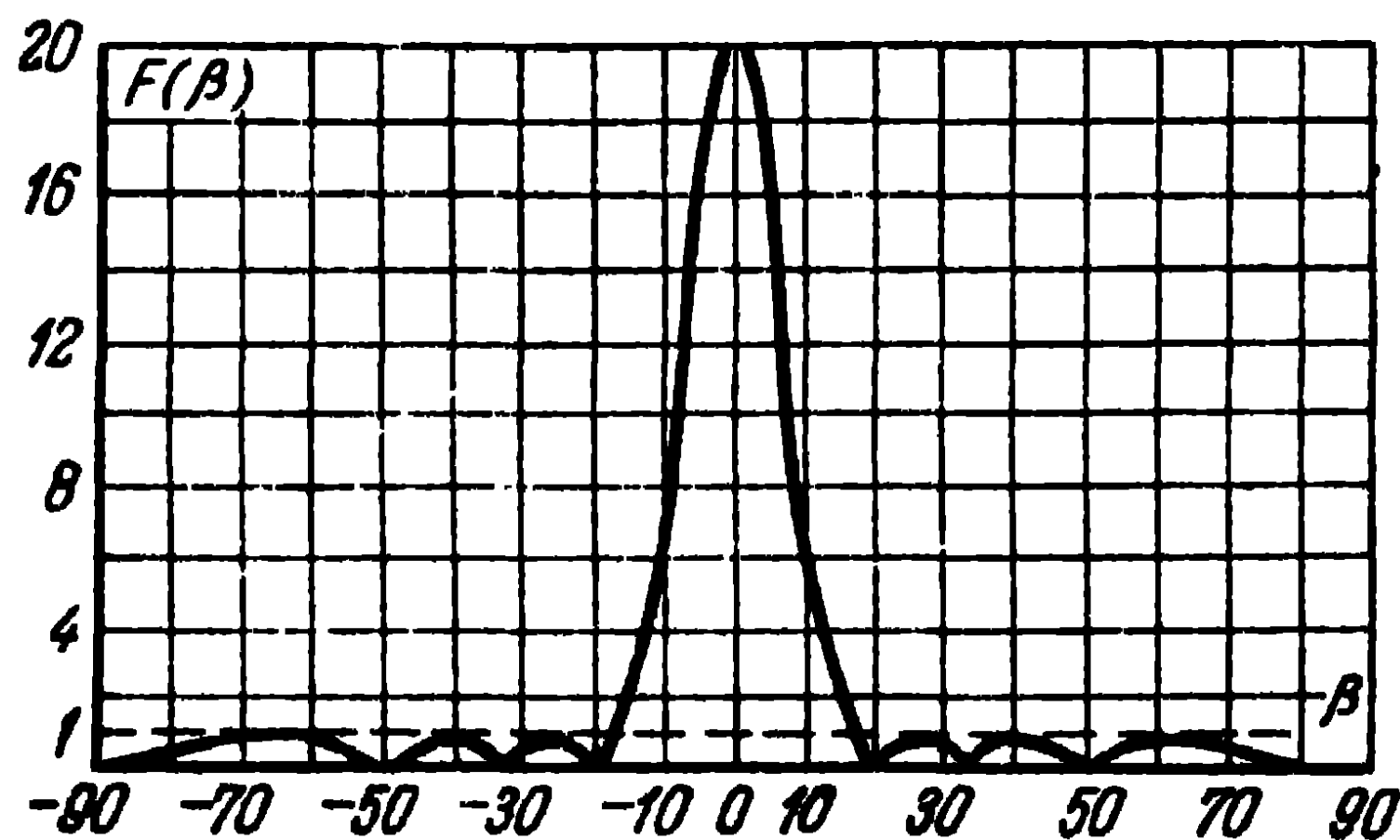


Fig. 4-24 Optimum directional diagram for $2N=8$.

1. Let $d = \frac{\lambda}{2}$, then $u = \frac{\pi}{2} \sin \beta$ and when the angle β changes from $-\frac{\pi}{2}$ to $+\frac{\pi}{2}$, the variable u changes in the interval from $-\frac{\pi}{2}$ to $\frac{\pi}{2}$. At the same time, the graphs of one and the same function $F(x)$ (let us take, for example, the function represented in Fig. 4-22) and $F(\beta)$ have the same character (the function $F(\beta)$ is represented in Fig. 4-24).

2. If $d = \lambda$, the graph for $F(x)$ remains the same (Fig. 4-22), and the graph for $F(\beta)$ acquires quite a different form (Fig. 4-25), since, when $d = \lambda$, $u = \pi \sin \beta$ and when

β changes from $-\frac{\pi}{2}$ to $\frac{\pi}{2}$, u changes from $-\pi$ to π , which corresponds to the change of x from -1 to 1 through 0 and back to -1 .

3. When $\frac{d}{\lambda} < \frac{1}{2}$ on the graphs $F(\beta)$ constructed for one and the same function $F(x)$, as the ratio $\frac{d}{\lambda}$ decreases, so does the number of lobes in the directional diagram of a linear antenna.

Having investigated all these particular cases we can draw the following conclusions.

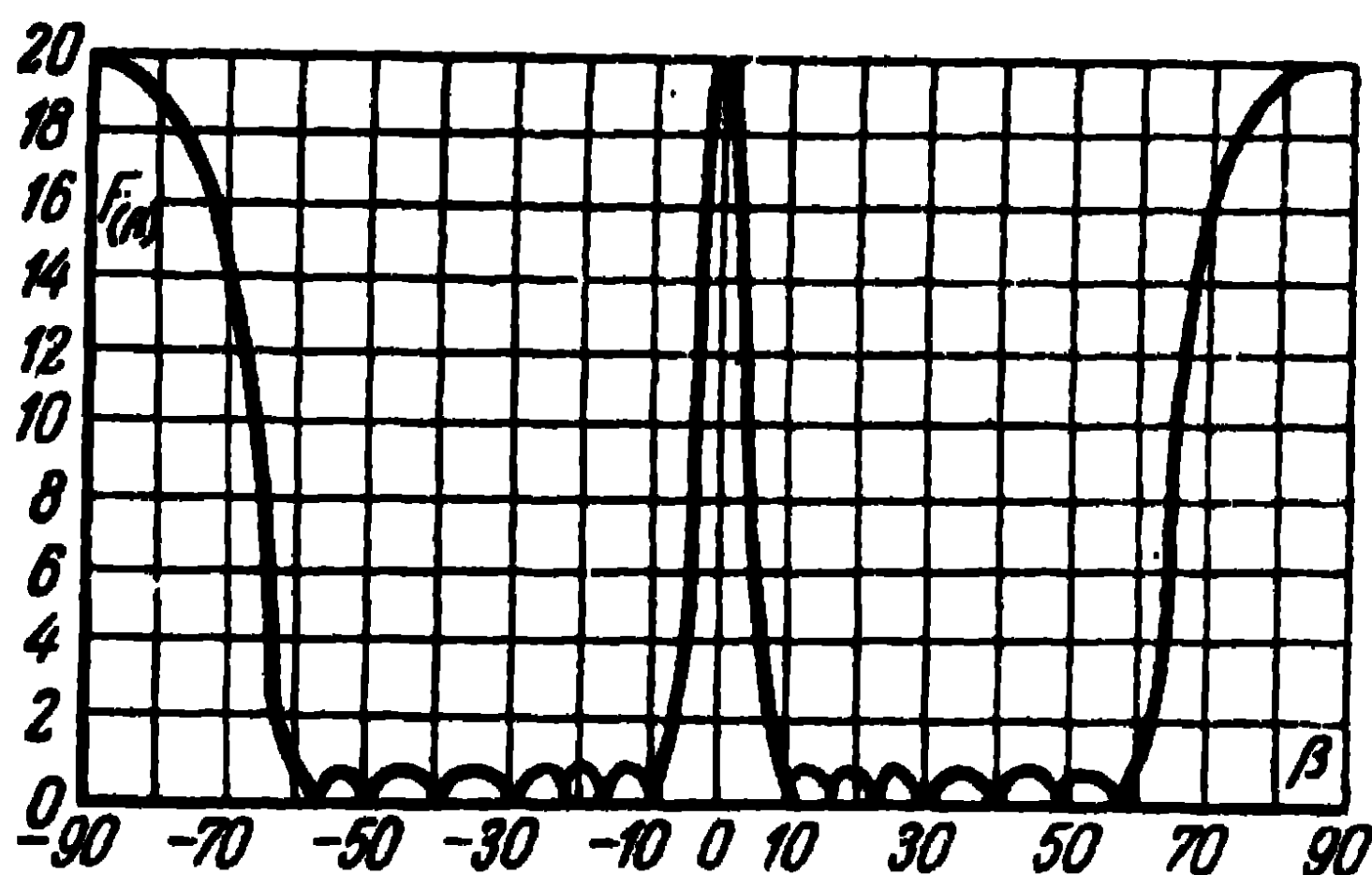


Fig 4-25. Directional diagram for $d=\lambda$.

When $d=\frac{\lambda}{2}$, the directional diagram of a linear antenna is described by the graph of the Chebyshev polynomial provided the condition (4-105) is fulfilled when its argument changes from 0 to 1 .

When $d < \frac{\lambda}{2}$, the directional diagram is described by only part of this graph and when $d > \frac{\lambda}{2}$, there occurs a larger or lesser repetition of this graph at the angle β .

When $d=\lambda$, an additional maximum is obtained along the linear antenna ($\beta=\frac{\pi}{2}$) equal to the principal maximum when $\beta=0$, and in the case of the utilisation of non-directional elements in an array, placing the radiator at such a distance gives rise to a directional diagram of unsatisfactory form.

If we leave aside the values of d close to λ , then, for any $d < \lambda$, we obtain the same form of directional diagram, in which a change of d only leads to a change of the number of minor lobes. Thus, it is possible to obtain a directional diagram with the same level of the minor lobes and the same width of the major lobe between the zeros from systems with any distance between the dipoles smaller than λ but with the same number of elements. But, as follows from the above, ultradirectional antennas can be obtained in the case of small $\frac{d}{\lambda}$; this will manifest itself in that the currents in the elements of the linear antenna will sharply change from element to element. From this point of view, it is preferable to choose d within the range of from $\frac{\lambda}{2}$ to $\lambda - \Delta$ without reaching the values of d for which a second major lobe begins to appear when $\beta = \frac{\pi}{2}$.

*g) Computation of a Linear Antenna with
a Directional Diagram of Optimum Form*

1. Given are the width of the directional diagram between the zeros $2\beta_0$ and the distance d between the dipoles. In accordance with (4-99), the location of the zeros of the directional diagram represented by the Chebyshev polynomial of the m order on the x -axis is defined as:

$$\alpha_0 x_0 = \cos \frac{(2p+1)\pi}{2m};$$

the first zero of the diagram, which determines the width of the major lobe, corresponds to the case $p=0$.

Then

$$x_0 = \cos \left(\frac{\pi d}{\lambda} \sin \beta_0 \right) = \cos \frac{\pi}{2m} \frac{1}{\alpha_0}. \quad (4-106)$$

We select m and α_0 in such a way that the condition (4-106) should be fulfilled; whereupon one should take into account that the larger the value chosen for m , the smaller the level of the minor lobes of the dipole array.

The values found for α_0 and m as well as that of $\frac{d}{\lambda}$ which

we know from the conditions of the problem, are substituted into the expressions (4-105) which establish the relation between the coefficients of the Chebyshev polynomial of the m order and the coefficients of the polynomials of the $2N$ or $2N-1$ order expressing the directional diagram of a system consisting of $2N+1$ and $2N$ dipoles (expression 4-104). At the same time, one should take into account that $m=2N-1$ for a system consisting of $2N$ dipoles and $m=2N$ for a system consisting of $2N+1$ dipoles. We obtain a system of equations for defining the currents in the dipoles I_d .

Example 1. The given width of the directional diagram is $2\beta_0=35^\circ$. The distance chosen between the dipoles is $d=\frac{\lambda}{2}$. We prescribe $m=7$ (the number of the dipoles $2N=8$) and determine the parameter α_0 :

$$\alpha_0 = \frac{\cos \frac{\pi}{2m}}{\cos \left(\frac{\pi}{2} \sin \beta_0 \right)} = 1.095.$$

Hence, in accordance with (4-97)

$$T_7(1.095) = 9.1.$$

Consequently, the level of the minor lobes is:

$$R = 20 \log \left(\frac{1}{9.1} \right) = -19.2 \text{ db.}$$

In accordance with (4-105), the system of equations for defining the currents will become:

$$\begin{aligned} 64I_4 &= 64(\alpha_0)^7 \rightarrow I_4 = 1.89; \\ 16I_3 - 112I_4 &= -112(\alpha_0)^5 \rightarrow I_3 = 2.21; \\ 4I_2 - 20I_3 + 56I_4 &= 56(\alpha_0)^3 \rightarrow I_2 = 2.88; \\ I_1 - 3I_2 + 5I_3 - 7I_4 &= 7(\alpha_0) \rightarrow I_1 = 3.17. \end{aligned}$$

Example 2. The given level of the minor lobes is 30 db. The number of dipoles in the antenna is $2N=8$, the distance between them is $d=\frac{\lambda}{2}$.

We find $20 \log T_r(a_0) = -30 \text{ db}$. Hence $a_0 = 1.18$. According to (4-105), the system of equations for defining the currents becomes:

$$\begin{aligned} 64I_4 &= 64(1.18)^7 \rightarrow I_4 = 3.18; \\ 16I_3 - 112I_4 &= -112(1.18)^6 \rightarrow I_3 = 6.3; \\ 4I_2 - 20I_3 + 56I_4 &= 56(1.18)^5 \rightarrow I_2 = 12; \\ I_1 - 3I_2 + 5I_3 - 7I_4 &= 7 \cdot 1.18 \rightarrow I_1 = 12.15. \end{aligned}$$

At the same time, the width of the directional diagram $2\beta_0$ is:

$$\begin{aligned} \cos\left(\frac{\pi}{2} \sin \beta_0\right) &= \frac{\cos\left(\frac{\pi}{2m}\right)}{a_0} = 0.826; \\ \sin \beta_0 &= 0.382, \quad 2\beta_0 = 45^\circ. \end{aligned}$$

CHAPTER FIVE

The Influence of the Earth and Metal Bodies on Antenna Radiation

5-1. Radiation of a Symmetrical Dipole Located over Plane Earth

So far, we have been considering antenna systems located in free space. Under actual conditions, antennas are installed near the surface of the earth or near various metal bodies. In many cases, due to its high conductivity, the earth is regarded as an infinite ideally conducting plane surface. Hence the estimation of the influence of the earth on the radiation of antennas can be considerably simplified and the mirror method applied.

As for the estimation of the influence of metal bodies on the radiation of antennas, here too we are forced to idealise the conditions of the problem and consider bodies of the simplest form. To begin with, let us discuss the problem of the radiation of a symmetrical dipole situated above the earth.

To simplify the problem, let us assume that the earth is an ideal conductor and plane. Let us place a symmetrical dipole (Fig. 5-1) at a distance h above the earth and let us construct its mirror image relatively to the earth. Then, in the case of a vertical dipole, the current in the mirror image will have the same direction as the current in the dipole itself, and in the case of a horizontal dipole, the current in the mirror image will have the opposite direction.

Let us calculate the intensity of the field set up by the dipole in the radiation zone in the presence of the earth, assuming

that Δ is the angle between the horizon and the direction towards the point of observation in the vertical plane (Fig. 5-2). Let r_1 be the distance from the dipole to the point of observation, r_2 , the distance from the mirror image of the dipole and r_0 , the distance from the intersection with the plane of the line joining the dipole to its mirror image.

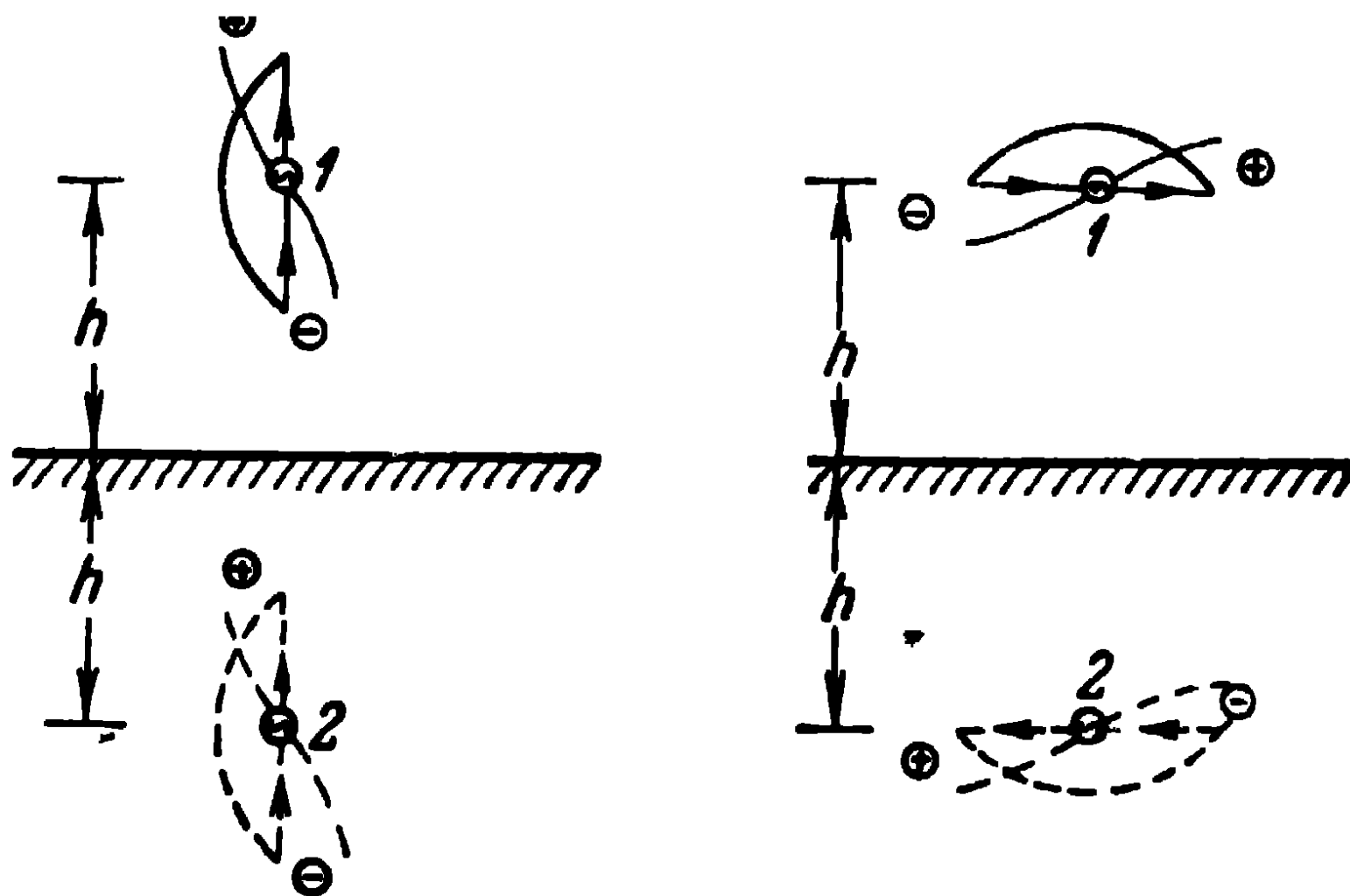


Fig. 5-1. Constructing the mirror images of dipoles:
1—dipole; 2—mirror image of the dipole.

Since $r_1 = r_0 - h \sin \Delta$, $r_2 = r_0 + h \sin \Delta$, the total field of the dipole and of its mirror image is expressed as:

$$E = i \frac{120 I_a}{r_0} e^{-ikr_0} \frac{\cos(kl \sin \Delta) - \cos kl}{\cos \Delta} \cos(kh \sin \Delta) \quad (5-1)$$

in the case of a vertical dipole (in its meridional plane) and

$$E = - \frac{120 I_a}{r_0} e^{-ikr_0} (1 - \cos kl) \sin(kh \sin \Delta) \quad (5-2)$$

in the case of a horizontal dipole (in its equatorial plane).

An examination of the expressions (5-1) and (5-2) reveals that in the direction of the horizon (on the surface of the earth), the vertical dipole sets up the maximum field intensity, whereas the horizontal dipole does not radiate at all in that direction.

Fig. 5-3 shows a number of directional diagrams of a dipole installed horizontally. It can be seen that when the dipole is low ($h < \lambda/4$), the maximum of radiation is directed upwards at an angle $\Delta = 90^\circ$. Raising the dipole leads to a decrease of the radiation upwards and when $h = \lambda/2$,

the maximum of radiation is at an angle $\Delta = 30^\circ$. A further increase of h leads to the appearance of additional lobes in the directional diagrams, their number increasing as h increases, and the maximum of the first lobe from the horizon pressing itself closer and closer to the horizon.

If we take into account the finite conductivity of the earth, the mirror method becomes invalid and the problem of the radiation of the dipole becomes considerably more complicated.

Even though the exact solution of the problem concerning the influence of the earth of finite conductivity on the radiation of antennas is possible, it leads to very complicated results. That is why we shall not dwell on the methods of the exact solution of the problem and shall give the approximate method applied in practice.

For the field in the radiation zone, the influence of the earth may be estimated by means of the reflection coefficients. Here again, we assume the surface of

the earth to be plane and construct the mirror image of the antenna relatively to this surface, as was done in Fig. 5-2. The current amplitude and phase in the mirror image are supposed to depend on the angle of observation of the field. The ratio of the complex amplitude of the current in the mirror image to the complex amplitude of the current in the antenna will be considered as equal to the reflection coefficient. Thus, two rays will reach the reception point: one coming directly from the antenna and the other, reflected from the surface of the earth in accordance with optical laws.

Disregarding the influence of the earth, let the field intensity of a symmetrical dipole be:

$$E_1 = E_{\max} F(\Delta), \quad (5-3)$$

where E_{\max} is the field intensity of the dipole in the direction of the maximum radiation.

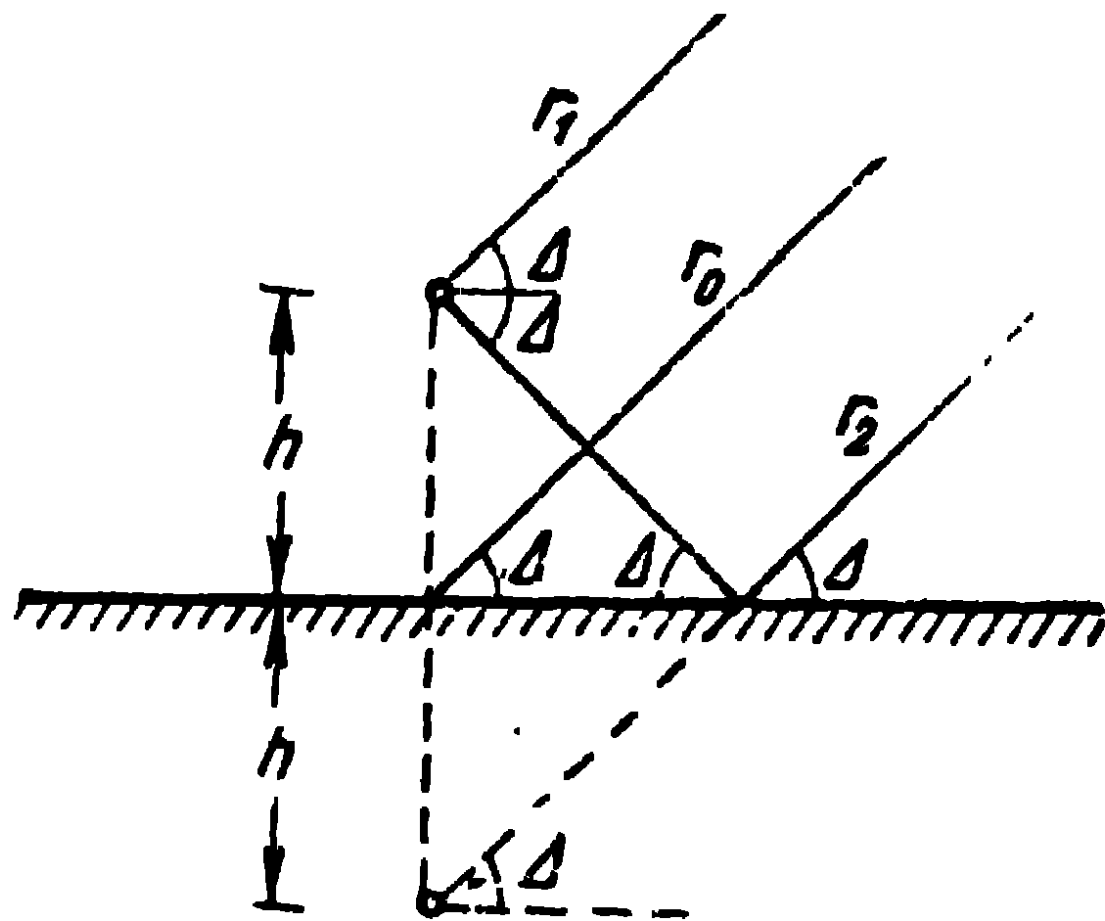


Fig. 5-2 Calculating the directivity diagram of the dipole.

$F(\Delta)$ is the normalised directional characteristic of the dipole.

In that case, the field intensity of the wave reflected from the earth at the same point of observation is:

$$E_z = E_{\max} F(\Delta) |f| e^{-\alpha k h \sin \Delta + i\Phi}. \quad (5-4)$$

Consequently, the total field intensity is defined by the

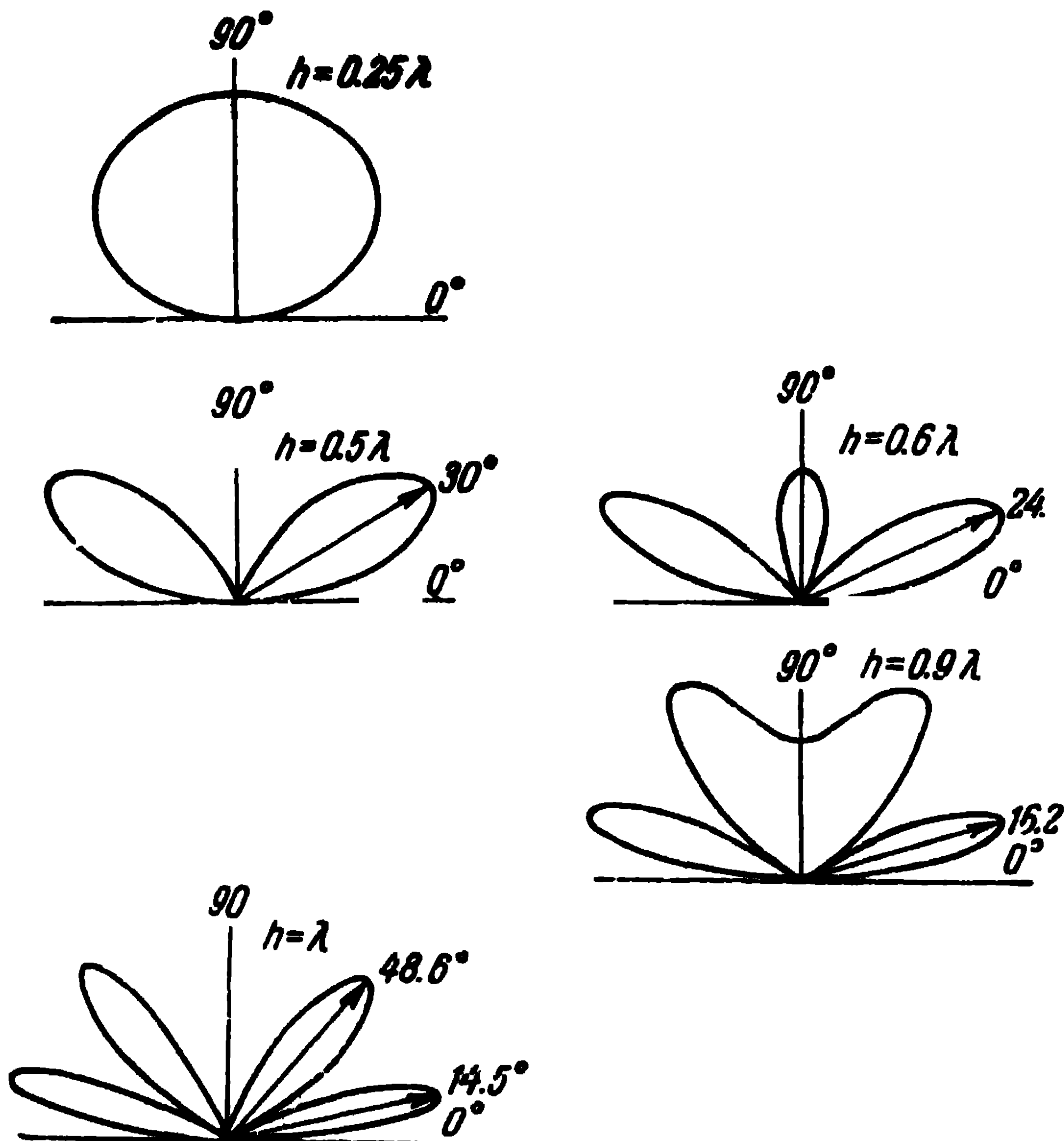


Fig. 5-3 Directional diagrams of a horizontal dipole in the vertical plane.

expression

$$E = E_1 + E_z = E_{\max} F(\Delta) [1 + |f| e^{-\alpha k h \sin \Delta + i\Phi}], \quad (5-5)$$

where the reflection coefficient for a vertical dipole is defined as:

$$f_v = |f_v| e^{i\Phi_v} = \frac{\epsilon'_r \sin \Delta - \sqrt{\epsilon'_r - \cos^2 \Delta}}{\epsilon'_r \sin \Delta + \sqrt{\epsilon'_r - \cos^2 \Delta}}, \quad (5-6)$$

and for a horizontal dipole, by the expression

$$f_h = |f_h| e^{+i\phi_h} = \frac{\sin \Delta - \sqrt{\epsilon_r' - \cos^2 \Delta}}{\sin \Delta + \sqrt{\epsilon_r' - \cos^2 \Delta}}. \quad (5-7)$$

In (5-6) and (5-7), ϵ_r' is the complex relative permittivity

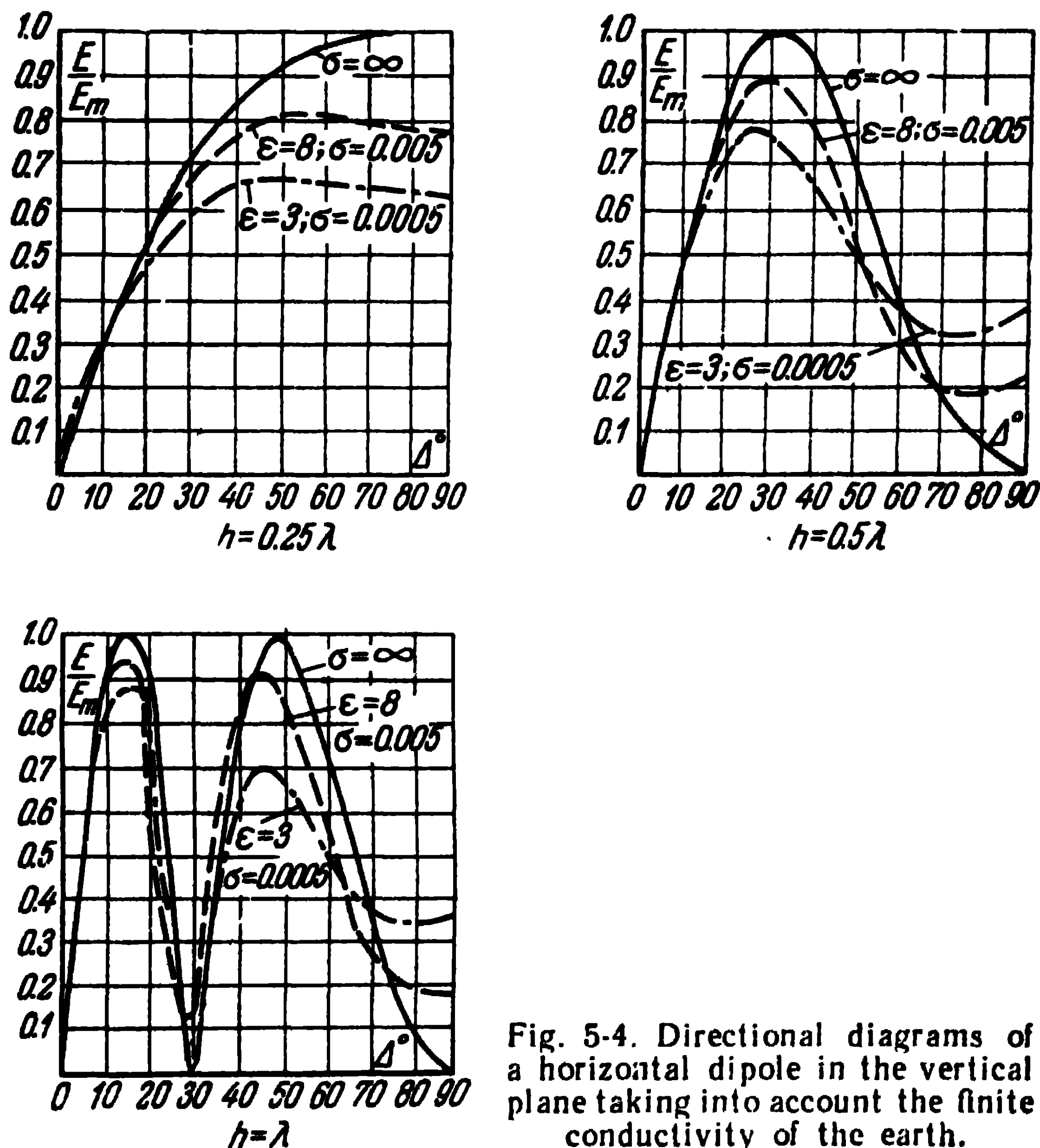


Fig. 5-4. Directional diagrams of a horizontal dipole in the vertical plane taking into account the finite conductivity of the earth.

of the earth, equal to:

$$\epsilon_r' = \frac{\epsilon}{\epsilon_0} \left(1 - i \frac{\sigma}{\omega \epsilon} \right). \quad (5-8)$$

Fig. 5-4 shows the directional diagrams of a horizontal dipole plotted in Cartesian coordinates in accordance with the above-mentioned expressions [22] when $\lambda = 30\text{m}$ for

ideally conducting earth ($\sigma = \infty$), wet earth ($\epsilon_r = 8$, $\sigma = 0.005^{-1} \text{ m}$) and dry earth ($\epsilon_r = 3$, $\sigma = 0.0005^{-1} \text{ m}$). As can be seen from this figure, the influence of the earth on the directional diagram amounts, on the whole, to a certain widening of the diagram and the replacement of the zero radiation directions by minimum radiation directions.

As for the influence of the earth on the radiation resistance and the input resistance of a symmetrical dipole, in order to simplify the problem, the earth is considered as an ideal conductor, in which case, the radiation resistance is defined as the sum of the natural resistance of the dipole and the resistance introduced into the dipole by its mirror image. At the same time, the input resistance of the dipole is determined from the engineering expressions (2-49).

5-2. Radiation of an Asymmetrical Dipole Disposed on the Surface of Plane Earth

Let us investigate once again the electromagnetic field in the vicinity of a symmetrical dipole. We saw that the field intensity in the vicinity of the dipole is expressed by (2-25), (2-27) and (2-28). As follows from these expressions, in the equatorial plane of a symmetrical dipole, the com-

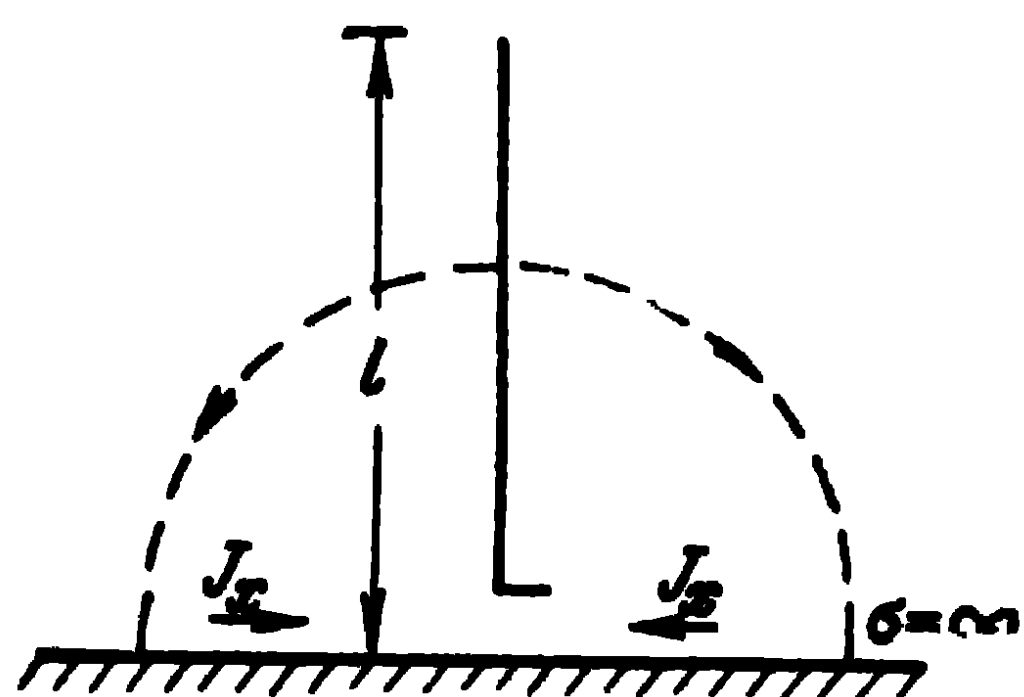


Fig. 5-5. An asymmetrical dipole.

ponent of the electric field intensity E_x normal to the dipole axis or, which is the same thing, tangential to the equatorial plane, equals zero. Consequently, the equatorial plane of a symmetrical dipole is an equipotential plane with a zero potential.

It is obvious that if we neglect the lower half of the dipole and align its equatorial plane with an ideally conducting plane surface of infinite extension, the electromagnetic field obtained in the upper half-space of the equatorial plane of the dipole is the same as for a symmetrical dipole (Fig. 5-5). On the surface of the conducting plane, the electric lines of force running normally to it will terminate on electric charges and there will arise surface currents caused by the change of the charges in time. The density of the surface charges and currents is determined by

the normal components of the electric field intensity E_z , and the magnetic field intensity H_ϕ from the expressions (2-25) and (2-27).

The density of the electric charges at the point of the plane is defined by the expression

$$q_x = \varepsilon_0 E_z = -i \frac{60 I_0}{\sin kl} \left\{ \frac{e^{-ik\sqrt{x^2+l^2}}}{\sqrt{x^2+l^2}} - \cos kl \frac{e^{-ikx}}{x} \right\}, \quad (5-9)$$

and the density of the electric surface current by the expression

$$J_x = H_\phi = i \frac{I_0}{2\pi x \sin kl} \left\{ e^{-ik\sqrt{x^2+l^2}} - \cos kl e^{-ikx} \right\}. \quad (5-10)$$

It follows from the above that the radiation of an asymmetrical dipole is determined by the currents flowing in the dipole itself and by the currents flowing on the surface of the conducting plane; furthermore, the radiation of the currents of the plane is equivalent to the radiation of the mirror image of the dipole relatively to this plane.

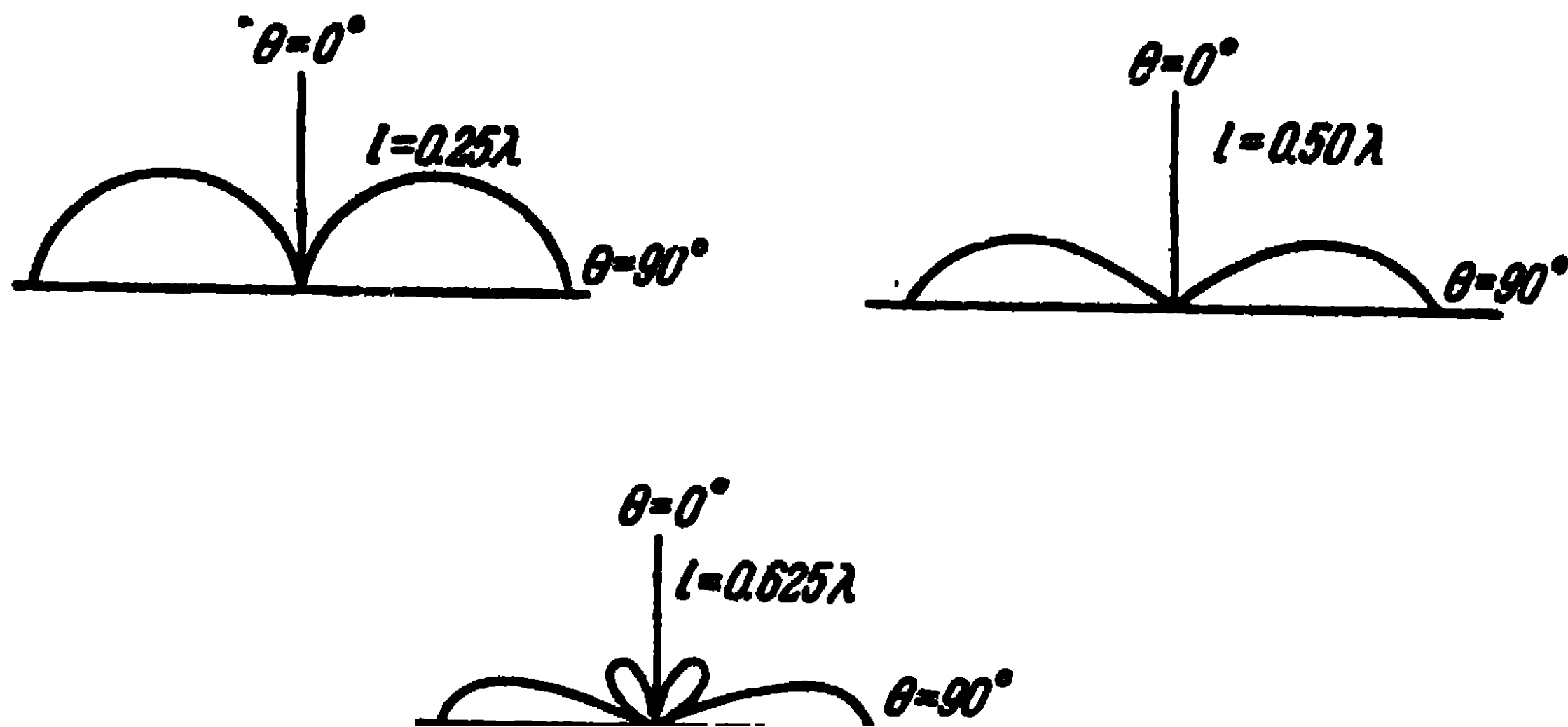


Fig. 5-6. Directional diagrams of an asymmetrical dipole in the vertical plane.

To excite in an asymmetrical dipole a current of the same amplitude as in a symmetrical dipole, it is, apparently, necessary to reduce by half the voltage fed to the dipole. Hence, the input resistance of an asymmetrical dipole is half that of the corresponding symmetrical dipole

$$Z_{\Sigma 0 \text{ asymm}} = \frac{Z_{\Sigma 0 \text{ symm}}}{2} \quad (5-11)$$

The same goes, of course, for the radiation resistance

$$R_{\Sigma \text{asymm}} = \frac{R_{\Sigma \text{symm}}}{2} . \quad (5-12)$$

In particular, the radiation resistance of a quarter-wave dipole ($l = \lambda/4$) is found to equal 36.6 ohms.

The directional diagrams of an asymmetrical dipole in the vertical plane are defined by the same expression (2-15) as for a symmetrical dipole.

Fig. 5-6 shows several directional diagrams of an asymmetrical dipole in the vertical plane in the case of ideally conducting earth.

5-3. The Influence of the Earth on the Radiation of Multiple Antennas

The method for estimating the influence of the earth on the radiation of symmetrical dipoles set forth above may be applied to any multiple antenna. In this case, the expression (5-5) remains unchanged, $F(\Lambda)$ designating the normalised directional characteristic of the antenna, taking

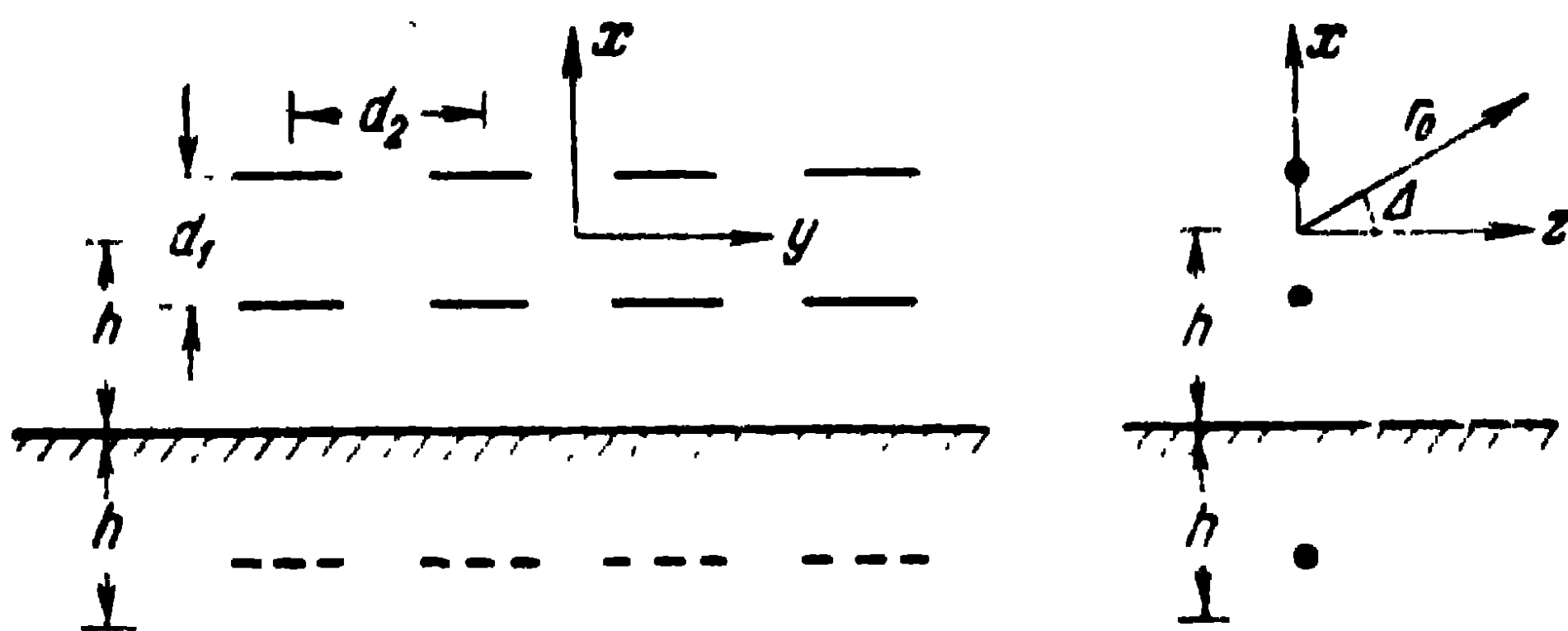


Fig. 5-7. Calculating the radiation of a co-phased array taking into account the influence of the earth.

no account of the influence of the earth and E_{max} , the field intensity of the antenna in the direction of the maximum radiation. Furthermore, the phase directional characteristic is determined relatively to the centre of the antenna and h designates the distance from the surface of the earth to the centre of the antenna.

Thus, for example, in the case of a co-phased plane array of half-wave horizontal dipoles situated at a height h above

the earth (Fig. 5-7), we have in the plane of the magnetic vector

$$E_{\max} = i \frac{60 I_a n m}{r_0} e^{-i k r_0};$$

$$F(\Delta) = \frac{1}{n} \frac{\sin \left(\frac{n k d_1}{2} \sin \Delta \right)}{\sin \left(\frac{k d_1}{2} \sin \Delta \right)},$$

where r_0 is the distance from the centre of the array to the point of observation of the field.

Substituting these expressions into (5-5), where h is determined from Fig. 5-7 and f_v in accordance with (5-6), we may construct the directional characteristic of the antenna in the vertical plane taking approximate account of the influence of the real earth. When calculating the radiation resistance of a co-phased array, one should take into account that the currents in the mirror image of horizontal dipoles have a negative sign relatively to the currents in the dipoles of the array, so that the signs of the values of the mutual resistances taken from A. Pistol-

kors's table should be reversed. For example, when $n=2$ and $m=2$, $d_2=\lambda/2$, $d_1=\lambda/2$, $h=\frac{3}{4}\lambda$ (Fig. 5-8), we have:

for the upper dipoles

$$R_1 = R_3 = R_{11} + R_{12} + R_{13} + R_{14} - R_{11'} - R_{12'} - R_{13'} - R_{14'} = 73.1 - 12.36 + 26.4 - 11.8 - 1.18 + 1.77 - 3.76 + 5.75 = 77.92 \text{ ohms};$$

for the lower dipoles

$$R_2 = R_4 = R_{21} + R_{22} + R_{23} + R_{24} - R_{21'} - R_{22'} - R_{23'} - R_{24'} = -12.36 + 73.1 - 11.8 + 26.4 + 1.77 - 4.08 + 5.75 - 8.83 = 67.95 \text{ ohms}.$$

The average magnitude of the radiation resistance of a dipole of the system will then be $R_{\Sigma a} = 72.93$ ohms and in accordance with (4-70), the directional gain is $D=6.58$.

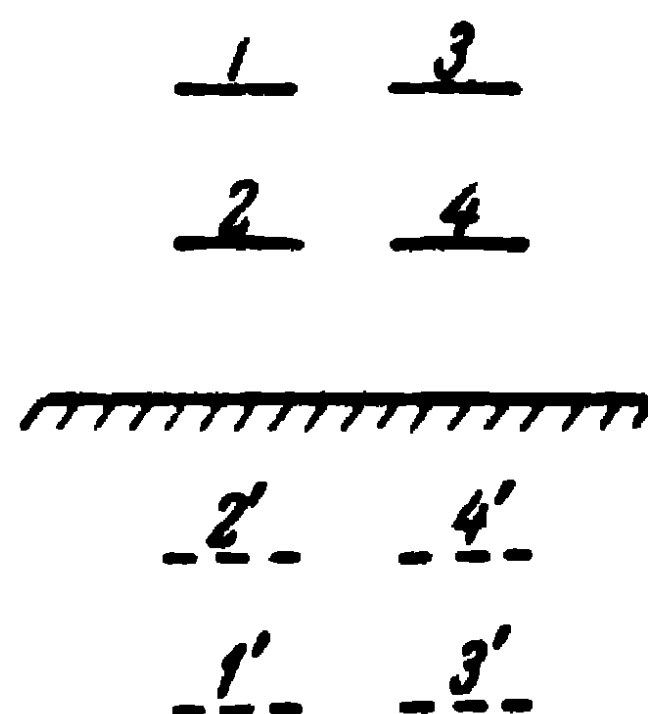


Fig. 5-8 Explaining the calculation of the resistance of a dipole array taking account of the influence of the earth.

5-4. The Influence of an Infinite Circular Cylinder on the Radiation of an Electric Dipole

The problem concerning the calculation of the influence of metal bodies of complex shape on the radiation of antennas situated in their vicinity has no exact solution. That is why the conditions of the problem have to be considerably idealised. Usually, the body is regarded as an ideal conductor and its surface as coinciding with the coordinate surface of the corresponding system of coordinates.

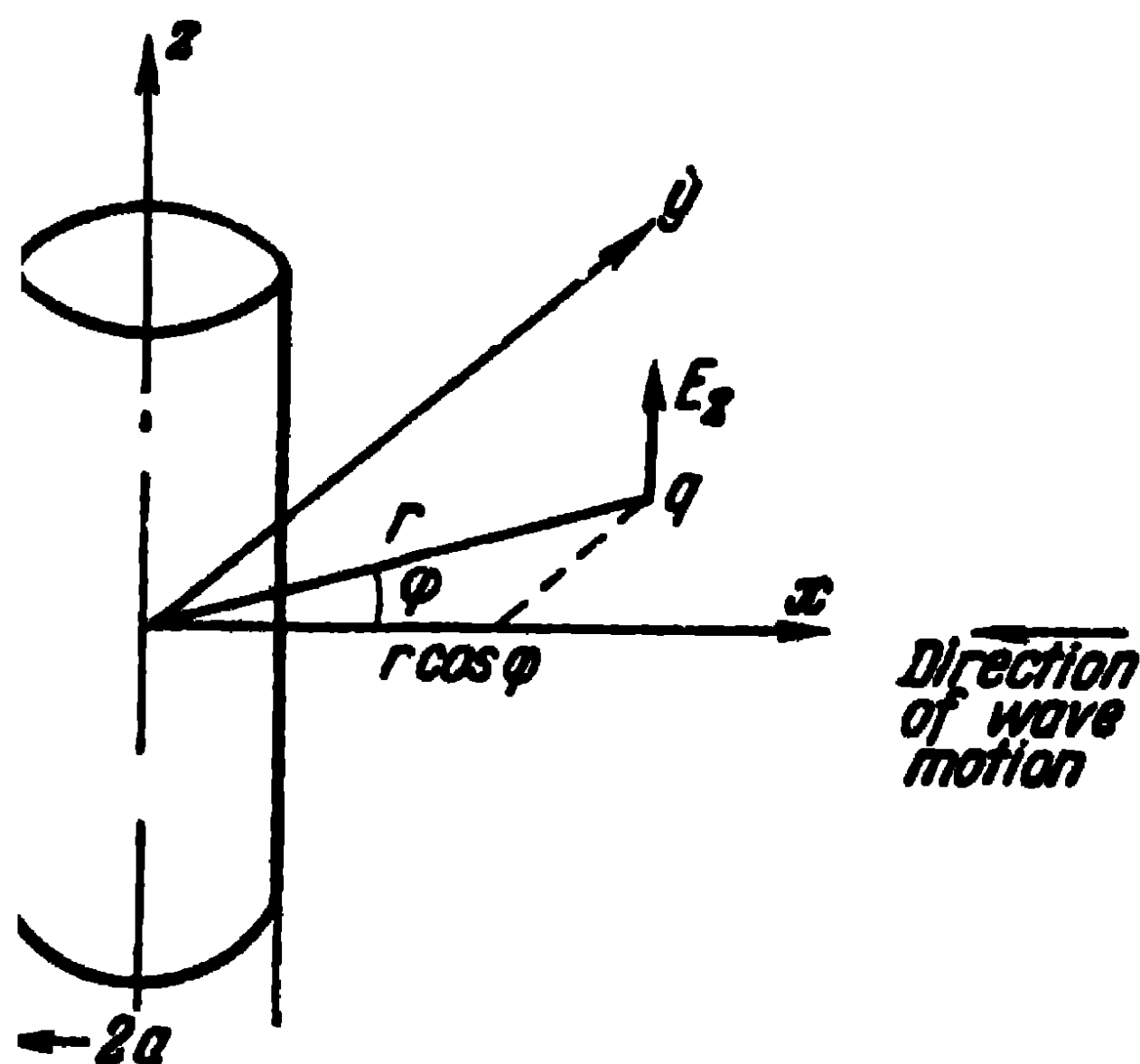


Fig. 5-9. Diffraction of a plane wave on a circular cylinder.

We shall examine here the radiation of an electric dipole situated near a circular, infinitely long and ideally conducting cylinder. We shall make use of the reciprocity principle. This example will serve to illustrate the main laws governing the influence of metal bodies on the radiation of antennas.

Let the cylinder be excited by a plane electromagnetic wave propagated in the direction of the x -axis from infinity to the origin of the coordinates (Fig. 5-9). Let the vector \mathbf{E} of the electromagnetic wave have only a z -th component. Then, assuming the magnitude of the field intensity in the plane $x=0$ to equal E_0 , we put down:

$$E'_z = E_0 e^{ikx} = E_0 e^{ikr \cos \varphi}, \quad (5-13)$$

where $k = \frac{2\pi}{\lambda}$.

Longitudinal electric currents are induced in the cylinder under the influence of the field of the electromagnetic wave acting upon it. These currents radiate a secondary field, i.e., set up waves reflected (diffracted) from the cylinder and moving away into infinity. The secondary field has also only the z -th component of the electric field intensity. This secondary field E''_z is such that the total electric field

on the surface of the cylinder equals zero:

$$E'_z + E''_z = 0 \text{ when } r = a. \quad (5-14)$$

In order to solve the problem, let us represent a plane electromagnetic wave in the form of the superposition of a spectrum of cylindrical waves, i.e., let us represent (5-13) in the form of the following expansion:

$$E'_z = E_0 e^{ikr \cos \varphi} = E_0 \sum_{n=0}^{\infty} \varepsilon_n i^n J_n(kr) \cos n\varphi, \quad (5-15)$$

where $\varepsilon_n = 1$, when $n = 0$ and $\varepsilon_n = 2$, when $n = 1, 2, 3 \dots$

It is easy to see that the expression (5-15) satisfies the wave equation $\Delta E + k^2 E = 0$, which, in the cylindrical system of coordinates, when $E = E_z$, will be written as:

$$\frac{1}{r} \frac{\partial}{\partial r} \left(r \frac{\partial E_z}{\partial r} \right) + \frac{1}{r^2} \frac{\partial^2 E_z}{\partial \varphi^2} + \frac{\partial^2 E_z}{\partial z^2} + k^2 E_z = 0. \quad (5-16)$$

Indeed, after substituting (5-15) into (5-16), we obtain the Bessel equation

$$\frac{1}{r} \frac{\partial}{\partial r} \left(r \frac{\partial J_n(kr)}{\partial r} \right) + \left(k^2 - \frac{n^2}{r^2} \right) J_n(kr) = 0. \quad (5-17)$$

Note that the other cylindrical functions likewise satisfy the equation (5-17), in particular the Neuman function and, consequently, the Hankel function

$$H_n^{(s)}(kr) = J_n(kr) - iN_n(kr),$$

which has the following asymptotic expression:

$$H_n^{(s)}(kr) \underset{kr \rightarrow \infty}{\approx} \sqrt{\frac{2}{\pi kr}} e^{-i \left(kr - n \frac{\pi}{2} - \frac{\pi}{4} \right)}, \quad (5-18)$$

i.e., this function represents a travelling wave moving away from the origin of the coordinates towards infinity.

For this reason, let us expand the secondary (reflected from the cylinder) field in a series of Hankel's functions

$$E''_z = E_0 \sum_{n=0}^{\infty} a_n \varepsilon_n i^n H_n^{(s)}(kr) \cos n\varphi, \quad (5-19)$$

where a_n are as yet unknown coefficients, which do not depend on the coordinates.

The expansion (5-19) is similar to the expansion (5-15); it satisfies the wave equation (5-16) and the principle of radiation at infinity.

To determine the coefficients of the expansion a_n , we add the expressions (5-15) and (5-19) and substitute (5-14) into the boundary conditions, thus obtaining:

$$a_n = - \frac{J_n(ka)}{H_n^{(2)}(ka)} \quad (5-20)$$

Thus, the total field is expressed as:

$$E_z = E_0 \sum_{n=0}^{\infty} e_n i^n \cos n\varphi \left[J_n(kr) - \frac{J_n(ka)}{H_n^{(2)}(ka)} H_n^{(2)}(kr) \right] \quad (5-21)$$

The expression (5-21) will be highly accurate if we regard the field set up by the electric dipole at the point $q(r, \varphi, 0)$

in the vicinity of the cylinder as parallel to the z -axis and situated at the distant point $(r', 0, 0)$ in the direction of the x -axis. In that case, in (5-21)

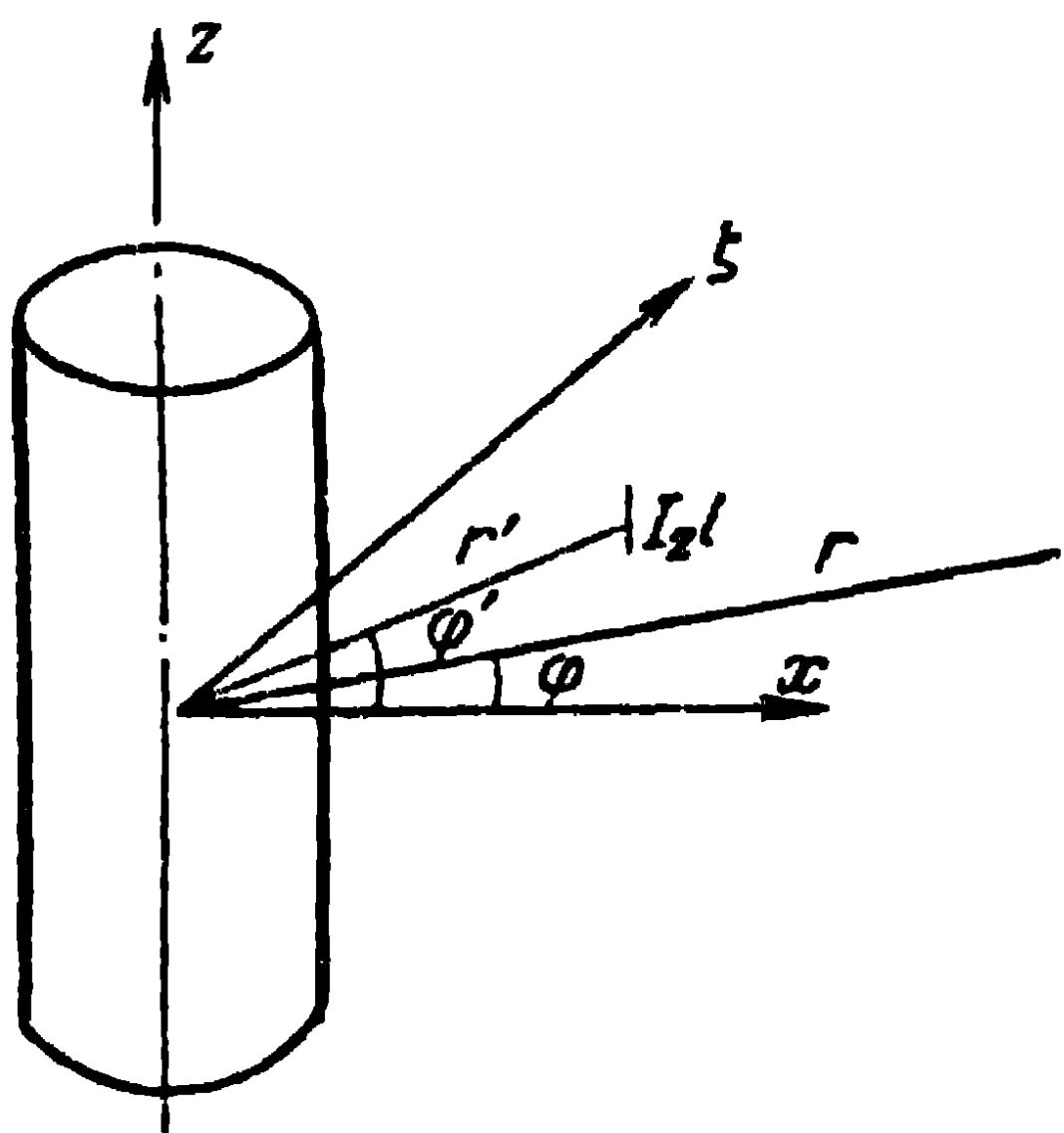


Fig. 5-10. Calculating the radiation of an electric dipole.

$$E_0 = - i \frac{I_2 l k^2}{4\pi\epsilon_0} \cdot \frac{e^{-ikr'}}{r'}.$$

Now, let us transfer the dipole which remains parallel to itself from the point p to the point q , maintaining its electric moment $I_2 l$ unchanged. Then, in accordance with the reciprocity theorem (formulated in the next chapter), the field

of that dipole at the point p is equal to the field which we had at the point q when the dipole was at the point p i.e., it is expressed by (5-21).

Thus, if we place an electric dipole at the point $(r', \varphi, 0)$ in the vicinity of the cylinder (Fig. 5-10), then the field set up by the dipole at a distant point $(r, \varphi, 0)$, is defined

by the expression

$$E_z = -i \frac{I_0 l k^2}{4\pi\omega\epsilon} e^{-ikr} \sum_{n=-\infty}^{\infty} \epsilon_n i^n \cos n(\varphi - \varphi') \times \\ \times \left[J_n(kr') - \frac{J_n(ka)}{H_n^{(2)}(ka)} H_n^{(2)}(kr') \right]. \quad (5-22)$$

It is clear that when the dipole is situated on the surface of the cylinder ($r' = a$), the field which it sets up equals zero everywhere. The expression (5-22) may be generalised for the case of the determination of the field of the dipole not

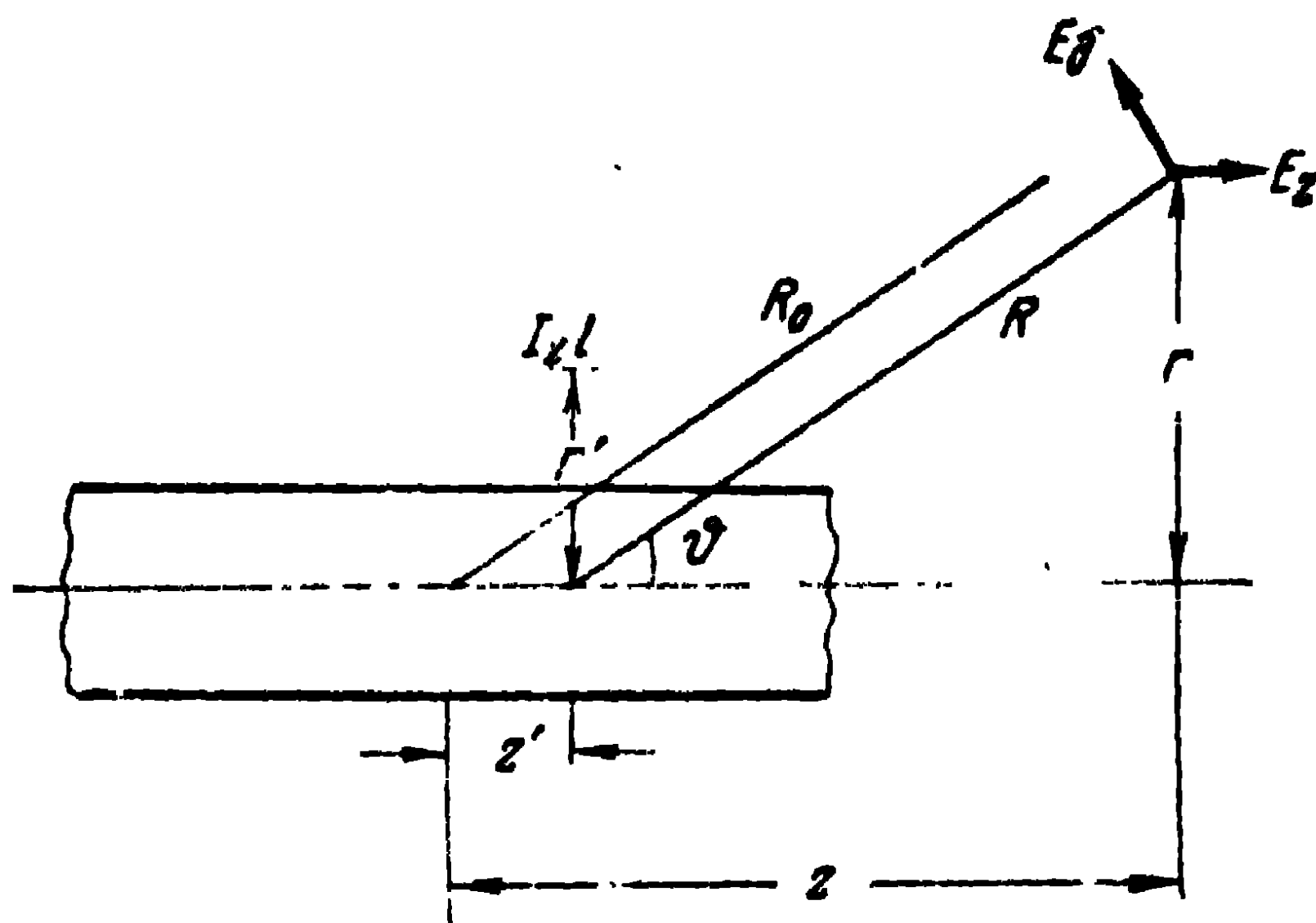


Fig. 5-11 Explaining the radiation of a longitudinal dipole in the meridional plane

only in the equatorial plane ($\theta = 90^\circ$), but also in any meridional plane, i.e., in the direction forming with the axis of the cylinder an angle θ lying in the interval $0 < \theta < 180^\circ$ (Fig. 5-11). Indeed, if a similar reasoning is adopted in the case of a plane wave arriving at the cylinder at an angle θ , then, for defining the field of the dipole in the radiation zone, we obtain:

$$E_z = -i \frac{I_0 l k^2 \sin^2 \theta}{4\pi\omega\epsilon} e^{-ikR} \sum_{n=-\infty}^{\infty} \epsilon_n i^n \cos n(\varphi - \varphi') \times \\ \times \left[J_n(kr' \sin \theta) - \frac{J_n(ka \sin \theta)}{H_n^{(2)}(ka \sin \theta)} H_n^{(2)}(kr' \sin \theta) \right], \quad (5-23)$$

where

$$R = \sqrt{r^2 + (z - z')^2}$$

Furthermore, in the spherical system of coordinates (R , ϑ , φ) the meridional component of the electric field intensity is defined from the expression

$$E_{\vartheta} = -\frac{E_z}{\sin \vartheta}, \quad (5-24)$$

whereas $E_{\varphi} = 0$ and $E_R = 0$.

The magnetic field intensity has only an azimuth component, which is defined from the expression

$$H_{\varphi} = \frac{\omega \epsilon}{k} E_{\vartheta}. \quad (5-25)$$

For a symmetrical dipole situated in the vicinity of a cylinder and lying in a longitudinal direction, the radiated field will be determined through the integration of (5-23) along the entire length of the dipole. Let the centre of the dipole coincide with the plane $z=0$. Then, assuming the distribution of the current in the dipole to be sinusoidal

$$I_z = I_0 \frac{\sin k(l - |z|)}{\sin kl}$$

and taking into account that $\frac{e^{-ikR}}{R} \approx \frac{e^{-ikR_0}}{R_0} e^{ikz' \cos \vartheta}$ (Fig. 5-11), the expression for the total field will be:

$$E_{\vartheta} = E \sum_{n=0}^{\infty} \epsilon_n i^n \cos n(\varphi - \varphi') \times \\ \times \left[J_n(kr' \sin \vartheta) - \frac{J_n(ka \sin \vartheta)}{H_n^{(2)}(ka \sin \vartheta)} H_n^{(2)}(kr' \sin \vartheta) \right], \quad (5-26)$$

where

$$E = i \frac{I_0 k}{2\pi \omega \epsilon \sin kl} \frac{\cos(kl \cos \vartheta) - \cos kl}{\sin \vartheta} \frac{e^{-ikR_0}}{R_0}, \\ R_0 = \sqrt{r^2 + z^2}.$$

Thus, the field of a symmetrical dipole is defined as the product of the field E of the dipole, situated in free space, by a factor which takes account of the existence of an infinite cylinder.

In the cross section of the cylinder ($\vartheta=90^\circ$), the directional characteristic of a longitudinal dipole does not depend on its length and is determined only by the radius

of the cylinder and the distance between the cylinder axis and the dipole. Fig. 5-12 shows several directional characteristics of a longitudinal dipole in the transverse plane as calculated by Carter [23]. All these characteristics concern a distance between the dipole and the cylinder axis equal to $r' = 0.24\lambda$; the variable parameter is the radius of the cylinder. We see that, when the radius of the cylinder is small and equals $a = 0.0016\lambda$, the directional characteristic differs insignificantly from a circle (Fig. 5-12, a). When the radius of the

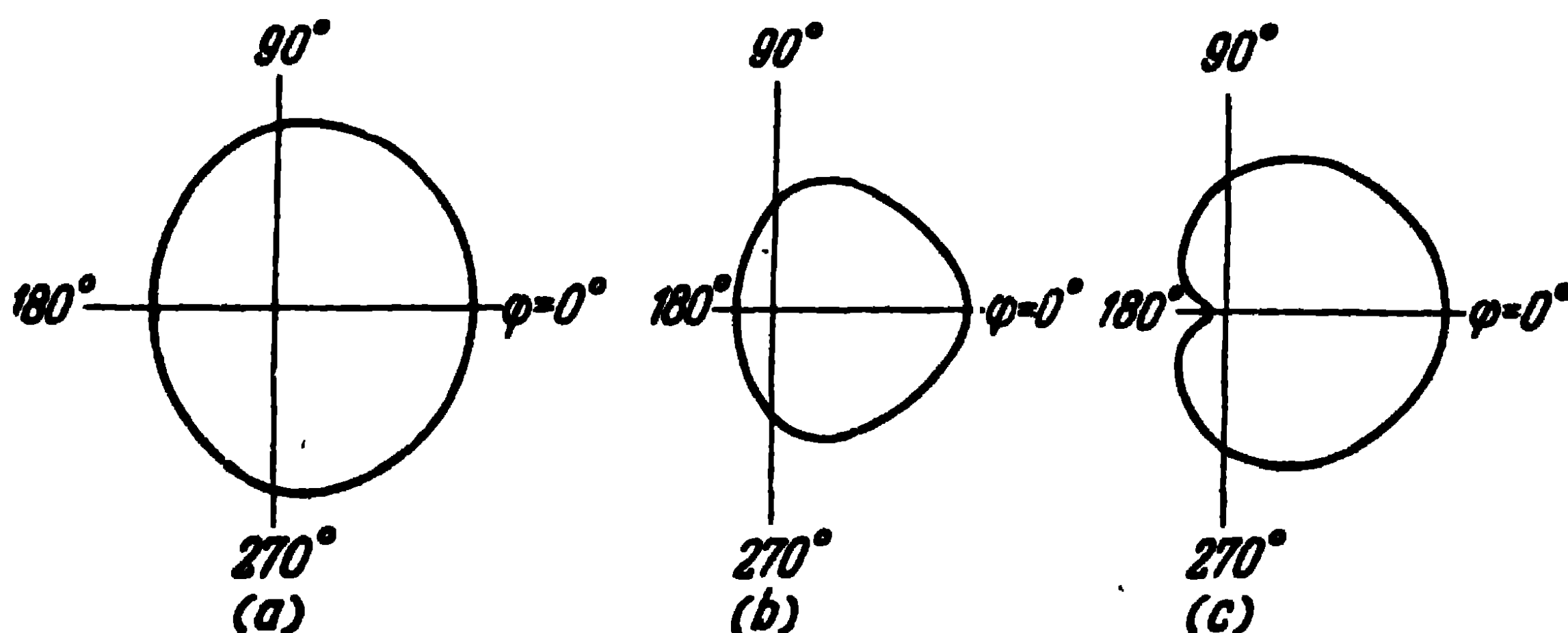


Fig. 5-12. Directional characteristics of a longitudinal dipole in the transverse plane:

$$a - r' = 0.24\lambda, \quad a = 0.0016\lambda; \quad b - r' = 0.24\lambda, \\ a = 0.08\lambda; \quad c - r' = 0.24\lambda; \quad a = 0.16\lambda.$$

cylinder becomes $a = 0.08\lambda$, there is a considerable decrease of the radiation in the blind region of the cylinder (Fig. 5-12, b). An additional increase of the radius of the cylinder leads to a further increase of its reflecting action and when the radius of the cylinder reaches $a = 0.16\lambda$ the characteristic becomes, in fact, unidirectional.

5-5. The Influence of an Infinite Circular Cylinder on the Radiation of a Longitudinal Slot

Let us examine the radiation of a longitudinal slot on an infinite ideally conducting circular cylinder excited from within the cylinder. To this end, we shall again make use of the diffraction of a plane electromagnetic wave on the cylinder, with the subsequent application of the reciprocity principle.

Let the plane electromagnetic wave be, just as before, propagated from infinity towards the x -axis (Fig. 5-9), but now let the magnetic field H'_z be longitudinal. Designating by H_0 the magnitude of the field intensity in the plane $x=0$, we may evidently write by analogy with the above:

$$H'_z = H_0 e^{-ikr \cos \varphi} = H_0 \sum_{n=0}^{\infty} \varepsilon_n i^n J_n(kr) \cos n\varphi. \quad (5-26)$$

Just as in the preceding case, we shall write for the reflected field:

$$H''_z = H_0 \sum_{n=0}^{\infty} b_n \varepsilon_n i^n H_n^{(2)}(kr) \cos n\varphi, \quad (5-27)$$

where b_n are unknown coefficients.

The electric field intensity in a cylindrical system of coordinates (r, φ, z) is determined from the expressions

$$E_r = \frac{1}{i\omega\varepsilon} \frac{1}{r} \frac{\partial H_z}{\partial \varphi}, \quad E_\varphi = -\frac{1}{i\omega\varepsilon} \frac{\partial H_z}{\partial r}, \quad E_z = 0. \quad (5-28)$$

Consequently, the boundary conditions on the surface of the cylinder are written as:

$$\frac{\partial}{\partial r} (H'_z + H''_z)_{r=a} = 0. \quad (5-29)$$

Substituting into (5-25) the expressions (5-26) and (5-27), we obtain for the coefficients b_n :

$$b_n = -\frac{J'_n(ka)}{H_n^{(2)'}(ka)}, \quad (5-30)$$

where the dashes in the cylindrical functions designate the derivative of these functions.

If we now take it that the plane electromagnetic wave is set up by the distant longitudinal magnetic dipole situated at the point $p(r', 0, 0)$, then

$$H_0 = -i \frac{I_z^M l k^2}{4\pi\omega\mu} \frac{e^{-ikr'}}{r'}$$

and the field set up by this dipole at the point $q(r, \varphi, 0)$ is:

$$H_z = -i \frac{I_z^M l k^2}{4\pi\omega\mu} \frac{e^{-ikr'}}{r'} \sum_{n=0}^{\infty} \varepsilon_n i^n \cos n\varphi \times \\ \times \left[J_n(kr) - \frac{J'_n(ka)}{H_n^{(2)'}(ka)} H_n^{(2)}(kr) \right]. \quad (5-31)$$

Making use of the reciprocity principle transfer the dipole from the point p to the point q . Then, the field of this dipole at the point p will equal the field at the point q when the dipole was at the point p , i.e., it is defined by (5-31).

Thus, if we place the magnetic dipole on the surface of the cylinder at the point $(a, \varphi', 0)$, the field set up by it at the distant point $(r, \varphi, 0)$ is defined by the expression

$$H_z = -i \frac{I_z^M l k^2}{4\pi\omega\mu} \frac{e^{-ikr}}{r} \sum_{n=-\infty}^{\infty} \varepsilon_n i^n \cos n(\varphi - \varphi') \times \\ \times \left[J_n(ka) - \frac{J'_n(ka)}{H_n^{(2)'}(ka)} H_n^{(2)}(ka) \right]. \quad (5-32)$$

Let us further note that

$$J_n(ka) H_n^{(2)'}(ka) - H_n^{(2)}(ka) J'_n(ka) = \frac{2}{\pi i k a}, \quad (5-33)$$

and generalise the expression (5-32) for the case when the direction from the antenna to the point of observation

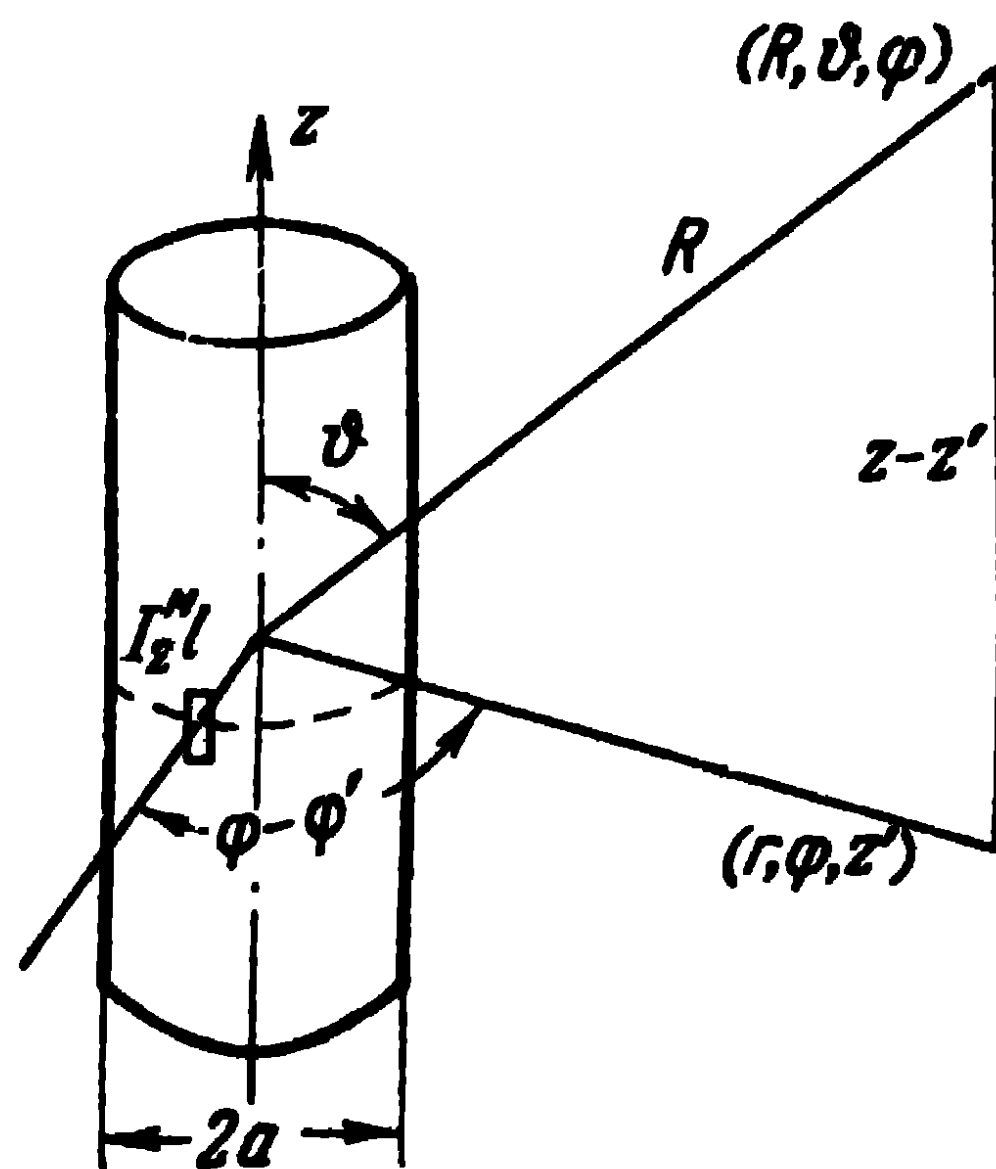


Fig. 5-13. Explaining the radiation of a longitudinal slot.

forms with the axis of the cylinder an angle ϑ (Fig. 5-13). We thus obtain:

$$H_z = - \frac{I_z^M l k \sin \vartheta}{2\pi^2 \omega \mu a} \frac{e^{-ikR}}{R} \sum_{n=-\infty}^{\infty} \varepsilon_n i^n \frac{\cos n(\varphi - \varphi')}{H_n^{(2)'}(ka \sin \vartheta)}, \quad (5-34)$$

where

$$R = \sqrt{r^2 + (z - z')^2}.$$

In spherical coordinates, the magnetic field intensity has only a meridional component defined from the expression

$$H_\theta = -\frac{H_z}{\sin \theta}, \quad (5-35)$$

and the electric field intensity, only an azimuth component

$$E_\varphi = -\frac{\omega \epsilon}{k} H_\theta. \quad (5-36)$$

A magnetic dipole situated on the surface of an ideally conducting cylinder forms a slot with a voltage $U_z = I_z^M$ between its edges.

Let the slot be narrow and have a length equal to half the wave. Then, the field of this slot at the distant point will be determined through the integration of the expression (5-34)

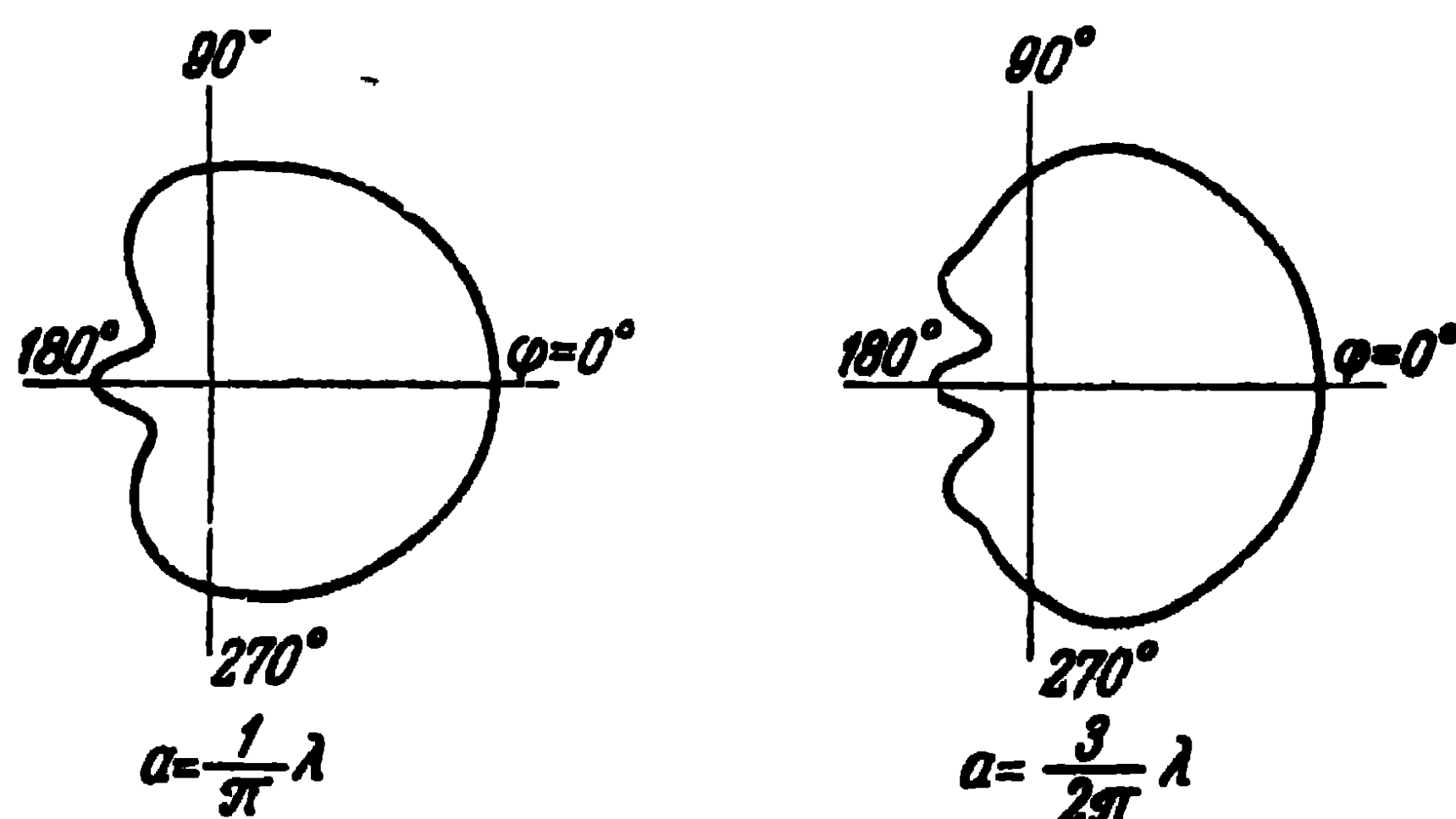


Fig. 5-14. Directional characteristics of a longitudinal slot in the transverse plane.

along the slot. Coinciding the centre of the slot with the plane $z=0$ and assuming the voltage in the slot to be distributed in accordance with the sine law $U_z = U_0 \cos kz$, we obtain:

$$H_\theta = H \frac{2}{\pi i k a \sin \theta} \sum_{n=0}^{\infty} \epsilon_n i^n \frac{\cos n(\varphi - \varphi')}{H_n^{(2)'}(ka \sin \theta)}, \quad (5-37)$$

where

$$H = i \frac{U_0 k}{2\pi\omega\mu} \frac{\cos\left(\frac{\pi}{2} \cos \vartheta\right)}{\sin \vartheta} \frac{e^{-ikR_0}}{R_0},$$

$$R_0 = \sqrt{r^2 + z^2}.$$

Fig. 5-14 shows the directional characteristics in the transverse plane, as calculated by A. A. Pistolokors [24] for cylinders with radius $a = \frac{1}{\pi} \lambda$ and $a = \frac{3}{2\pi} \lambda$. Fig. 5-15 shows the ratio of the field intensity in the blind side ($\varphi = \pi$) to the field intensity in the illuminated side ($\varphi = 0$) depending on the radius of the cylinder. The curve shows that for cylinders which are thin in relation to the wave-length, the directional diagram of the slot differs but little from a circular one. An increase of the radius of the cylinder leads to an increase of its screening effect.

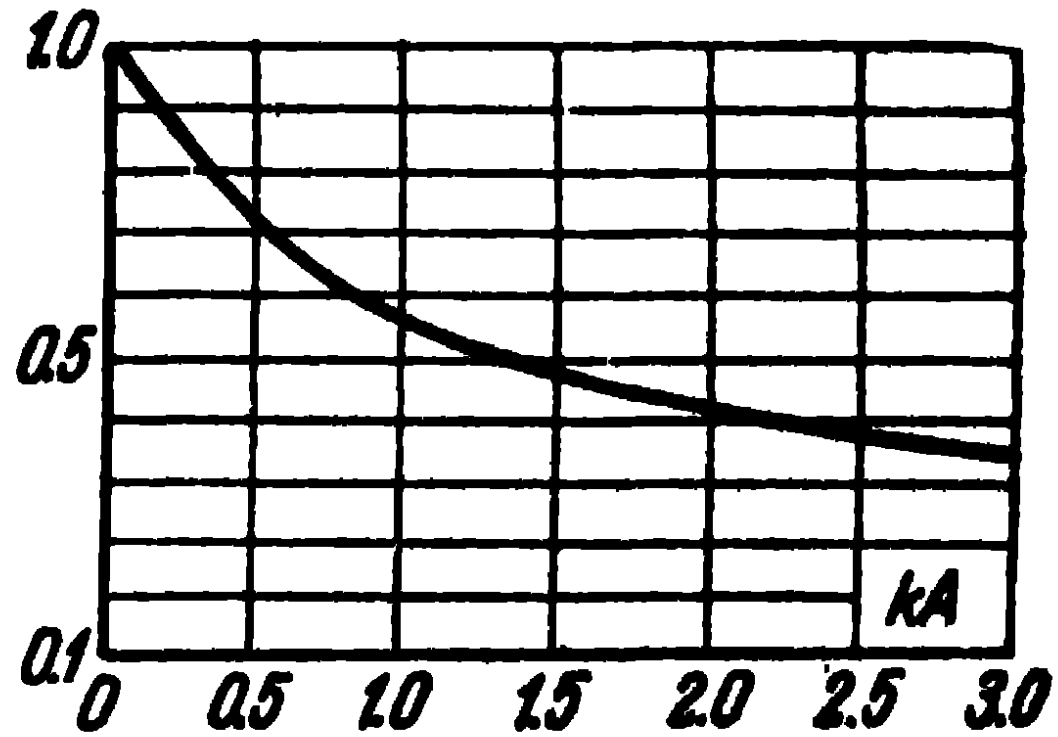


Fig. 5-15. Ratio of the field intensity in the blind side to that in the illuminated side.

Let us also determine the power radiated by the half-wave slot in the cylinder. Since the field in the radiation zone is defined by the two components E_φ and H_ϑ , then, in accordance with (1-10), the Poynting vector has only a radial component and, taking account of (5-36) is written as:

$$S_r = \frac{1}{240\pi} E_\varphi E_\varphi^*, \quad (5-38)$$

where

$$E_\varphi = - \frac{U_0 \cos\left(\frac{\pi}{2} \cos \vartheta\right)}{\pi^2 k a \sin^2 \vartheta} \frac{e^{-ikR_0}}{R_0} \sum_{n=0}^{\infty} \varepsilon_n i^n \frac{\cos n\varphi}{H_n^{(2)'}(ka \sin \vartheta)}. \quad (5-39)$$

It is supposed here that the azimuth coordinate of the slot $\varphi' = 0$. Substituting (5-39) into (5-38) and integrating over the surface of a sphere of radius R_0 , we obtain for the radiated power

$$P = \frac{1}{240\pi} \int_{\vartheta=0}^{\pi} \int_{\varphi=0}^{2\pi} \frac{U_0^2 \cos^2\left(\frac{\pi}{2} \cos \vartheta\right)}{\pi^4 k^2 a^2 \sin^4 \vartheta} \times$$

$$\times \sum_{n=0}^{\infty} \sum_{m=0}^{\infty} \frac{\varepsilon_n \varepsilon_m i^{n-m} \cos n\varphi \cos m\varphi R_0^2 \sin \vartheta}{[H_n^{(2)'}(ka \sin \vartheta)][H_m^{(2)'}(ka \sin \vartheta)]} d\vartheta d\varphi, \quad (5-40)$$

but

$$\int_{\varphi=0}^{2\pi} \cos n\varphi \cos m\varphi d\varphi = \begin{cases} 0 & \text{when } m \neq n \\ \frac{2\pi}{e_n} & \text{when } m = n \end{cases}$$

so that (5-40) will be written as:

$$P = \frac{U_0^2}{120\pi^2 k^2 a^2} \int_{\vartheta=0}^{\pi} \frac{\cos^2\left(\frac{\pi}{2} \cos \vartheta\right)}{\sin^2 \vartheta} \sum_{n=0}^{\infty} \frac{e_n}{|H_n^{(2)'}(ka \sin \vartheta)|^2} d\vartheta. \quad (5-41)$$

Now, if we relate the radiated power to the square of the voltage in the antinode of the slot, we obtain the expression for the external radiation conductivity of the slot in the cylinder

$$G = \frac{2P}{U_0^2}. \quad (5-42)$$

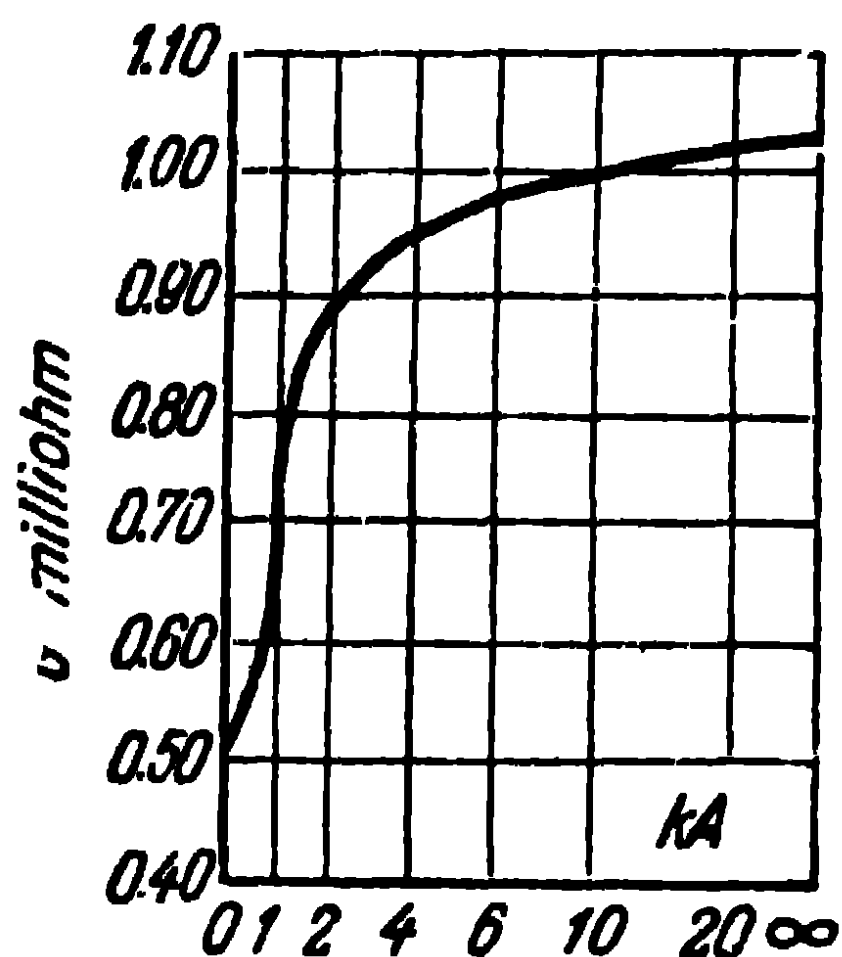


Fig. 5-16. Radiation conductivity of a narrow half-wave slot on a cylinder

Thus, the radiation conductivity of a narrow half-wave slot depends on the ratio of the radius of the cylinder to the wave-length. This dependence, calculated from (5-41) and (5-42) for the value of ka , which changes in the interval from 0 to ∞ , is represented in Fig. 5-16. We see that, for

infinitely thin cylinders, the calculated conductivity agrees with (2-54) and equals

$$G_{ka \rightarrow 0} = \frac{73.1}{(120\pi)^2} = 0.514 \text{ milliohm},$$

and, for infinitely thick cylinders, the conductivity agrees with (2-54a) and equals

$$G_{ka \rightarrow \infty} = \frac{2,73.1}{(120\pi)^2} = 1.028 \text{ milliohms}.$$

It can be seen from the curve that if the circumference of the cylinder exceeds 10 wave-lengths, the conductivity of a slot on a cylinder differs from the conductivity of a slot on an infinite plane screen by not more than 3 per cent.

CHAPTER SIX

Receiving Antenna Theory

6-1. A Symmetrical Dipole in the Field of a Plane Electromagnetic Wave

Let us examine a rectilinear electric dipole of length $2l$ and radius a . Assume that the radius of the dipole is very small in comparison with the wave-length.

Let this dipole lie in free space in the field of a plane electromagnetic wave propagated in a direction which forms with the z -axis of the dipole an angle θ (Fig. 6-1). Let the vector of the electric field intensity lie in a plane passing through the axis of the dipole. Since the vector \mathbf{E} forms a right angle with the direction of propagation of the wave, it has only the component E_θ in polar coordinates and its projection on the axis of the dipole is $E_z = -E_\theta \sin \theta$.

Designating by $E_{\theta 0}$ the field intensity in the centre of the dipole, the component along the axis of the dipole at the point with the z -coordinate is obtained from Fig. 6-1:

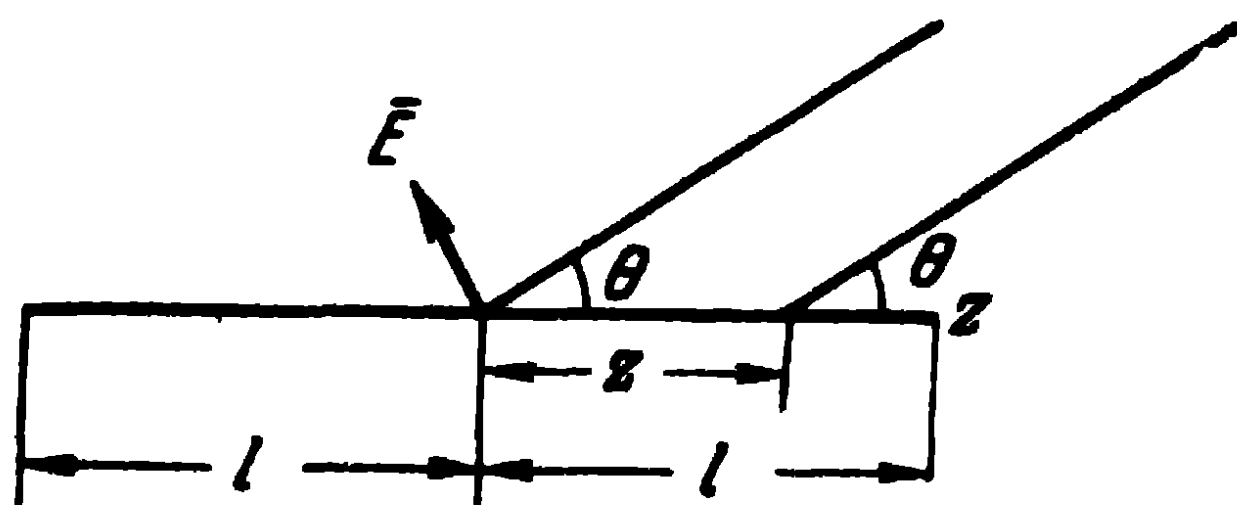


Fig. 6-1. Explaining the calculation of the emf induced in a dipole.

$$E_z = -E_{\theta 0} \sin \theta e^{ikz \cos \theta}. \quad (6-1)$$

The component of the electric field intensity along the dipole axis represents the emf per unit length of the dipole.

Thus, a plane electromagnetic wave induces in the dipole a distributed emf with a constant amplitude, i.e., independent of the z -coordinate, and with phase $kz \cos \theta$ changing in accordance with a linear law.

We shall now turn our attention to the load current connected in the centre of a receiving dipole. In accordance with the superposition principle and due to the simultaneous action of several emf's distributed randomly along the entire circuit, the current flowing at any point of the circuit consisting of active and reactive resistances of invariable magnitude equals the sum of the currents which would arise

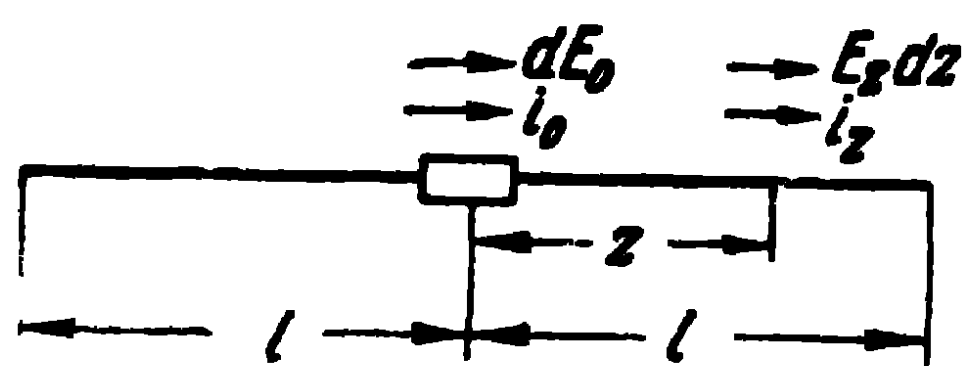


Fig. 6-2. Explaining the calculation of the current in the load of a dipole.

at that point in case each of the given emf's acted independently.

Let us suppose that an elementary emf $E_z dz$ exerts its effect at the point with the z -coordinate of the dipole and that at all the other points of the dipole, the emf's equal zero.

Under the influence of this emf, an elementary current i_0 arises in the centre of the dipole (in the load) (Fig. 6-2). The magnitude of this current will be defined in the following way: let us mentally switch off the emf $E_z dz$ and, instead, switch on in the centre of the dipole an emf $d\mathcal{E}_0$ of such a magnitude as to leave the value of the current i_0 unchanged. Current i_z arises at the point z of the dipole under the influence of the emf $d\mathcal{E}_0$.

Let us now make use of the reciprocity principle, well known in tetrapole theory, which states that if an emf of any kind, localised at any point of an electric circuit devoid of nonlinear resistances, gives rise to a current at any other point of this circuit, when transferred to the second point, the same emf gives rise at the first point to an electric current of the same strength as in the first case. The validity of this principle in antenna theory was proved by Sommerfeld and Sveshnikova [25]. According to this principle

$$\frac{d\mathcal{E}_0}{i_z} = \frac{E_z dz}{i_0} \quad (6-2)$$

or

$$d\mathcal{E}_0 = E_z f(z) dz. \quad (6-3)$$

Here $f(z) = \frac{i_z}{i_0}$ represents the function of the current dis-

tribution for an emf concentrated in the centre of the dipole. Note that this is not the function of the current distribution in a receiving dipole since it is the effect of the distributed emf.

The total current arising at the dipole centre is determined by the emf obtained through the integration of (6-3) along the entire length of the dipole

$$\mathcal{E}_0 = \int_{z=-l}^{+l} E_z f(z) dz. \quad (6-4)$$

Thus, in order to determine the electric current arising in the centre of the dipole under the influence of the emf distributed along it, we may replace the effect of this distributed emf by that of an equivalent emf concentrated in the centre of the dipole, i.e., at the same point of the dipole at which the current is determined. This emf is defined by (6-4).

Let Z_0 be the resistance of the receiver connected in the gap in the centre of the dipole. Determine current I_0 flowing through this resistance using the Thevenin's theorem which, in this case, states that if resistance Z_0 is connected to the two points of a gap in a dipole, current I_0 which will be set up in this resistance equals the ratio of the difference of potential between these points of the dipole, before connecting the resistance to the sum of this resistance Z_0 and resistance $Z_{\Sigma 0}$ measured between the points taken.

The difference of potential set up between the two points of a gap in a dipole is, evidently, equal to the equivalent emf determined above. Thus, the current in the resistance of the load is defined as

$$I_0 = \frac{\int_{z=-l}^{+l} E_z f(z) dz}{Z_0 + Z_{\Sigma 0}}. \quad (6-5)$$

The expression (6-5) shows that a receiving dipole may be regarded as a generator with an emf \mathcal{E}_0 and an internal resistance $Z_{\Sigma 0}$. The equivalent circuit of the dipole is shown in Fig. 6-3.

The resistance $Z_{\Sigma 0}$ is measured between the points of the gap in the wire and represents the input resistance of the dipole when dealing with a transmitting dipole.

Let us now calculate the current of the load of the dipole I_0 from (6-5). The function of the current distribution $f(z)$ is expressed as:

$$f(z) = \frac{\sin k(l-z)}{\sin kl} \quad \text{when } 0 < z < l,$$

$$f(z) = \frac{\sin k(l+z)}{\sin kl} \quad \text{when } 0 > z > -l. \quad (6-6)$$

Substituting into (6-4) the value $f(z)$ from (6-6) and the value E_z from (6-1) and performing the stated integration, we obtain:

$$I_0 = - \frac{E_0 \lambda}{\pi(Z_0 + Z_{\Sigma 0}) \sin kl} \frac{\cos(kl \cos \theta) - \cos kl}{\sin \theta}. \quad (6-7)$$

(6-7) expresses the relation of the load current in a receiving symmetrical dipole to the angle of arrival of the electromagnetic wave. This relation determines the directional characteristic of the receiving symmetrical dipole.

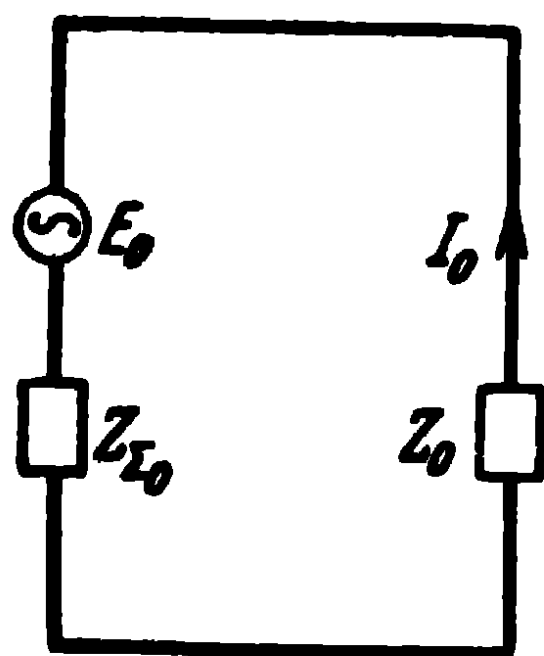


Fig. 6-3. Equivalent scheme of a receiving dipole.

We see that the relation between the current and the angle of arrival of the electromagnetic wave in a receiving symmetrical dipole is the same as the relation between the field intensity and the direction towards the point of observation in a transmitting symmetrical dipole.

Thus, the directional characteristics of a receiving symmetrical dipole coincide with those of a transmitting symmetrical dipole.

The magnitude of the current in the load for a prescribed electric length of the dipole and a prescribed angle of arrival of the electromagnetic wave is proportional to the product of the electric field intensity by the wave-length; furthermore, the maximum value of the current takes place when the dipole is tuned in resonance.

6-2. Power Dissipated in the Load of a Receiving Symmetrical Dipole

Let us determine the power dissipated in the load of a receiving symmetrical dipole. Note that $Z_{\Sigma 0} = R_{\Sigma 0} + iX_{\Sigma 0}$ and $Z_0 = R_0 + iX_0$. Then, the power dissipated in the load

evidently equals:

$$P_0 = \frac{I_0 I_0^* R_0}{2} = \frac{E_{0\eta} E_{0\eta}^* \lambda^2 R_0}{\pi_2 [(R_0 + R_{\Sigma 0})^2 + (X_0 + X_{\Sigma 0})^2]} \times \\ \times \frac{[\cos(kl \cos \theta) - \cos kl]^2}{\sin^2 kl \sin^2 \theta}. \quad (6-8)$$

The maximum power in the load is dissipated under the following conditions:

1) when the reactive part of the load resistance X_0 equals the reactive part of the dipole input resistance $X_{\Sigma 0}$ and is of opposite sign, i.e., when

$$X_0 = -X_{\Sigma 0};$$

2) when the active parts of the load and the input resistance equal:

$$R_0 = R_{\Sigma 0}.$$

Consequently, the maximum power dissipated in the load equals:

$$P_{0 \max} = \frac{E_{0\eta} E_{0\eta}^* \lambda^2}{4\pi^2 R_{\Sigma 0}} \frac{[\cos(kl \cos \theta) - \cos kl]^2}{\sin^2 kl \sin^2 \theta}. \quad (6-9)$$

For a wave arriving at the dipole at an angle $\theta = 90^\circ$, the maximum power will be

$$P_{0 \max} = \frac{E_{0\eta} E_{0\eta}^* \lambda^2}{4\pi^2 R_{\Sigma 0}} \frac{(1 - \cos kl)^2}{\sin^2 kl}. \quad (6-10)$$

Note that part of the power absorbed by the dipole from the passing electromagnetic wave is spent on the reverse radiation of the dipole. In the absence of an active resistance of the load ($R_0 = 0$), i.e., when the dipole is shortened or when a purely reactive resistance is connected to it ($X_0 \neq 0$), the whole of the power absorbed by the dipole is spent on reverse radiation.

As a result of the dipole reverse radiation, the field of the antenna currents (secondary field) is superimposed on the field of the passing plane electromagnetic wave. Due to interference between these fields, the distribution of the total field in the vicinity of the dipole presents a complicated picture. In particular, on the surface of the dipole (if it consists of an ideal conductor), the tangential component of the total electric field intensity and the normal component of the total magnetic field intensity equal zero.

6-3. Current Distribution in a Receiving Dipole

Note that the distribution of the electric current induced in a receiving dipole differs from the current distribution of the same dipole when it is used as a transmitter. This will become clear if we remember that the current distribution in a dipole depends on the distribution in it of the exciting emf.

Indeed, in the case of a receiving dipole, the exciting emf is distributed in accordance with the law expressed by (6-1), whereas in the case of a transmitting dipole, the exciting emf is concentrated; in particular, it is concentrated in the centre of the dipole.

Let us find the current distribution in a receiving dipole. To simplify the problem, we assume the dipole to be unloaded ($Z_0=0$) and infinitely thin. Turning to Fig. 6-1, let I_z^e be the current at the point z of the dipole and A_z^e , the vector potential set up by the current of the dipole on its surface. As we saw in Chapter Two, the vector potential on the surface of a dipole obeys the equation (2-6). In the case of an unloaded receiving dipole, this equation will be written as:

$$\frac{d^2 A_z^e}{dz^2} + k^2 A_z^e = -i\omega\epsilon E_z. \quad (6-11)$$

Substituting into the right-hand side of this equation the value E_z from (6-1) and making use of the approximate expression (2-8) which relates the current to the vector potential at the point z of the dipole, we obtain:

$$\frac{d^2 I_z^e}{dz^2} + k^2 I_z^e = \frac{i\omega\epsilon}{\Omega} E_{0\theta} \sin \theta e^{ikz \cos \theta}. \quad (6-12)$$

Let us limit ourselves to the case of a normal arrival of the electromagnetic wave on the wire ($\theta=90^\circ$). Then (6-12) will be written as:

$$\frac{d^2 I_z^e}{dz^2} + k^2 I_z^e = \frac{i\omega\epsilon}{\Omega} E_{0\theta}. \quad (6-13)$$

It is evident that, in this case, the current is an even function relatively to the origin of the coordinates and the boundary conditions for it are written as:

$$I_z^e = 0 \text{ when } z = \pm l \text{ and } \frac{dI_z^e}{dz} = 0 \text{ when } z = 0. \quad (6-14)$$

It may be shown that the solution of the equation (6-13) in the boundary conditions (6-14) is written as:

$$I_z^e = - \frac{i\omega\epsilon}{\Omega} E_0 \frac{1}{k^2 \cos kl} (\cos kz - \cos kl). \quad (6-15)$$

Observe that for a half-wave dipole, $kl=90^\circ$ and the current distribution is sinusoidal, i. e., it coincides with the current distribution in the case of a transmitting dipole. It may be said, as was pointed out in Chapter Two, that for a half-wave dipole, the current distribution does not depend on the distribution of the excited emf in the dipole. The same applies to dipoles excited on odd harmonics ($kl=n\frac{\pi}{2}$, where $n=3, 5, 7$).

For other lengths of the dipole, in accordance with (6-15) the current distribution differs from the sinusoidal one.

Since the question of the secondary radiation of antennas will no longer interest us, we shall not dwell any longer on the current distribution laws in a receiving dipole.

6-4. Application of the Principle of Reciprocity to the Study of the Properties of Receiving Antennas

Above we discussed the effect which a plane electromagnetic wave has on a receiving symmetrical dipole. To define the current in the antenna load, we made use of the reciprocity principle. It was found that, to define the current in the antenna load, the input resistance and the directional characteristic of the dipole when it is utilised as a vibrator should be known.

From a broader aspect, it appears that there is no necessity to work out a special theory for receiving antennas and that it is sufficient to make use of the transmitting properties of the antenna under investigation and apply the reciprocity principle. This is what M. S. Neuman did in 1935 [26].

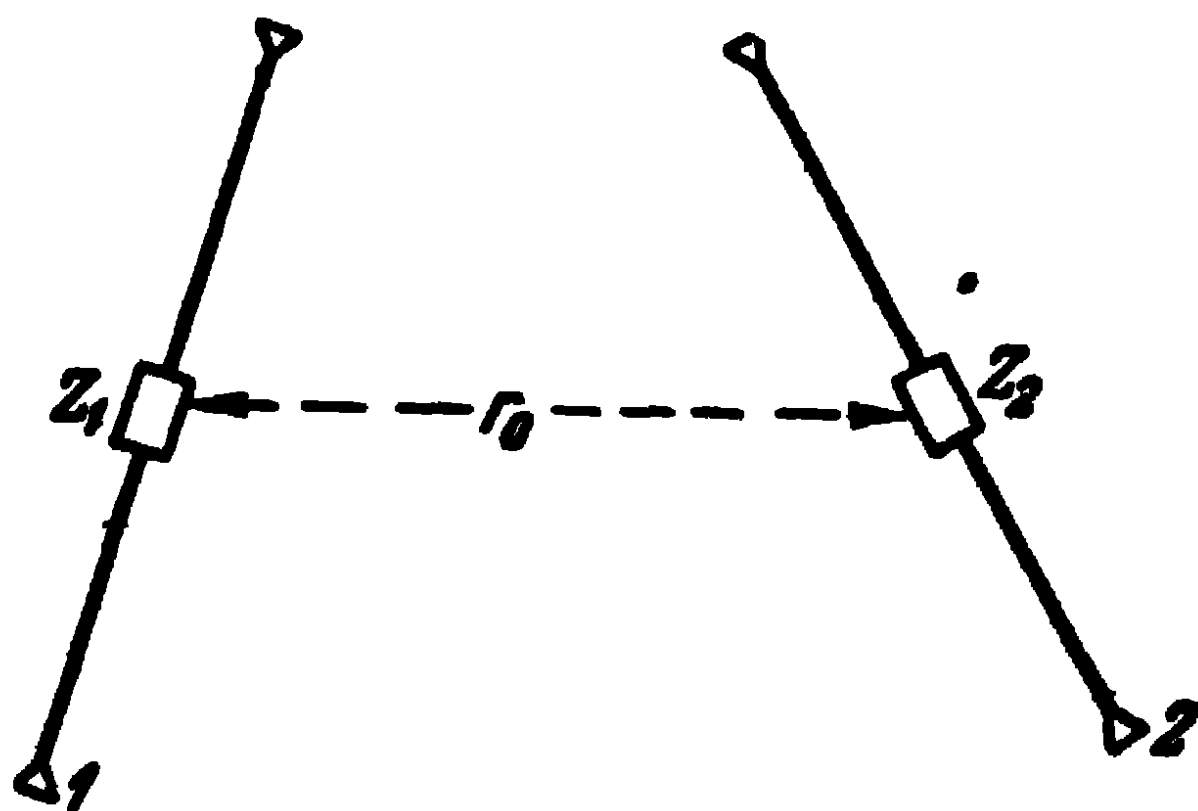


Fig. 6-4. Explaining the theory of receiving antennas.

Let us examine two arbitrary antennas 1 and 2, situated far apart. Let Z_1 be the resistance connected to the terminals of the first antenna and Z_2 , the resistance connected to the terminals of the second antenna (Fig. 6-4).

Let the antenna 1 be a transmitting antenna and the antenna 2 a receiving one and let \mathcal{E}_1 be the emf induced at the terminals of the antenna 1. Then, under the influence of this emf, a current will appear in the antenna 1 the magnitude of which at the terminals will be defined as

$$I_1 = \frac{\mathcal{E}_1}{Z_1 + Z_{in1}}, \quad (6-16)$$

where Z_{in1} is the input resistance of the antenna 1.

Under the influence of the current of the first antenna, a field intensity is set up in the vicinity of the second antenna, which, in accordance with (4-62), is expressed as

$$E_{21} = i \frac{30kh_1 I_1}{r_0} e^{-ikr_0} F_1(\theta, \varphi) e^{i\psi_1}, \quad (6-17)$$

and current I_{21} will be induced in the load of the second antenna.

Substituting into (6-17) the expression of the current from (6-16) and expressing \mathcal{E}_1 through the rest of the magnitudes:

$$\mathcal{E}_1 = \frac{E_{21} r_0 (Z_1 + Z_{in1})}{i 30kh_1 e^{-ikr_0} F_1(\theta, \varphi) e^{i\psi_1}}. \quad (6-18)$$

When the emf \mathcal{E}_1 in the antenna 1 and the emf \mathcal{E}_2 in the antenna 2 are switched off, the current arising at the terminals of the second antenna will be:

$$I_2 = \frac{\mathcal{E}_2}{Z_2 + Z_{in2}}, \quad (6-19)$$

where Z_{in2} is the input resistance of the second antenna.

The intensity of the field set up by the second antenna in the vicinity of the first one will, in accordance with (4-62) be expressed as:

$$E_{12} = i \frac{30kh_2 I_2}{r_0} e^{-ikr_0} F_2(\theta, \varphi) e^{i\psi_2}, \quad (6-20)$$

and current I_{12} will be induced in the load of the first antenna.

Substituting into (6-20) the expression for I_2 from (6-19) and defining \mathcal{E}_2 , we obtain:

$$\mathcal{E}_2 = \frac{E_{12} r_0 (Z_2 + Z_{in2})}{i30kh_2 e^{-ikr_0} F_2(\theta, \varphi) e^{i\psi_2}}. \quad (6-21)$$

According to the principle of reciprocity, the emf \mathcal{E}_1 switched on at the terminals of the antenna 1 is related to the current I_{21} induced under the effect of this emf at the terminals of the antenna 2, as the emf \mathcal{E}_2 switched on at the terminals of the antenna 2 is related to the current I_{12} induced under the effect of this emf at the terminals of the antenna 1:

$$\frac{\mathcal{E}_1}{I_{21}} = \frac{\mathcal{E}_2}{I_{12}}. \quad (6-22)$$

Substituting here the expressions \mathcal{E}_1 and \mathcal{E}_2 and transferring to the left-hand side of the equation thus obtained, the magnitudes relevant to the antenna 1 and to the right-hand side, the magnitudes relevant to the antenna 2 we obtain

$$\frac{I_{12} (Z_1 + Z_{in1})}{E_{12} k h_1 F_1(\theta, \varphi) e^{i\psi_1}} = \frac{I_{21} (Z_2 + Z_{in2})}{E_{21} k h_2 F_2(\theta, \varphi) e^{i\psi_2}}. \quad (6-23)$$

Assume that the parameters of the second antenna are changed without touching the first antenna. Since, when the parameters of the antenna are constant, the ratio of the current induced in the antenna to the field intensity of the electromagnetic wave acting on the antenna remains constant, the left-hand side of (6-23) will remain constant too no matter how we change the parameters of the second antenna. Consequently, the right-hand side of (6-23) will also remain constant.

Thus, we shall have the following relation for any receiving antenna:

$$\frac{I (Z_L + Z_{in})}{E h F(\theta, \varphi) e^{i\psi}} = N = \text{const}, \quad (6-24)$$

where E is the field intensity of the plane electromagnetic wave in the vicinity of the antenna;

I , the current in the antenna load;

Z_L , the load resistance;

Z_{in} , the antenna input resistance when dealing with a transmitting antenna;

h , the antenna effective length during transmission;

$F(\theta, \varphi)$ and ψ , the antenna amplitude and phase directional characteristics during transmission.

To determine the constant N use is made of the expression (6-7) obtained for a symmetrical dipole. Since, as we saw in Paragraph 4-9, for a symmetrical dipole

$$hF(\theta)e^{i\psi} = \frac{\lambda}{\pi} \frac{\cos(kl \cos \theta) - \cos kl}{\sin \theta \sin kl},$$

on comparing (6-24) with (6-7), we obtain:

$$N = -1.$$

Thus, the current induced in the load of any receiving antenna is expressed as:

$$I = - \frac{Eh}{Z_L + Z_{in}} F(\theta, \varphi) e^{i\psi}. \quad (6-25)$$

The expression (6-25) can also be represented in a different form. Indeed, by substituting (4-62) into (4-68) and taking into account that $P_{\Sigma} = \frac{1}{2} |I|^2 R_{\Sigma}$, we have:

$$D = \frac{30k^2 h^2 F^2(\theta, \varphi)}{R_{\Sigma}}. \quad (6-26)$$

Substituting the expressions (6-25) and (6-26), we obtain:

$$I = - \frac{\lambda E}{\pi (Z_L + Z_{in})} \sqrt{\frac{DR_{\Sigma}}{120}} e^{i\psi}. \quad (6-27)$$

The expression (6-27) (without the factor $e^{i\psi}$) was obtained by M. S. Neuman in the above-mentioned work. Subsequently, A. R. Volpert [27] introduced into this expression the factor $e^{i\psi}$, which takes into account the antenna phase characteristic.

The following conclusions can be drawn from the expressions (6-25) and (6-27):

1. The amplitude $F(\theta, \varphi)$ and phase $\psi(\theta, \varphi)$ directional characteristics of any receiving antenna, which give the dependence of the induced current on the angle of arrival of the electromagnetic wave are found to be the same as during transmission, provided the receiver and the transmitter are connected to the same points of the antenna.

2. Any receiving antenna can be regarded as an oscillator with an emf defined by the expression

$$\mathcal{E}_0 = -Eh F(0, \varphi) e^{i\psi} \quad (6-28)$$

or

$$\mathcal{E}_0 = -\frac{\lambda E}{\pi} \sqrt{\frac{DR_\Sigma}{120}} e^{i\psi}, \quad (6-29)$$

with an internal resistance $Z_{in} = R_{in} + iX_{in}$ and a load $Z_L = R_L + iX_L$.

3. The effective length of a receiving antenna, defined as the ratio of the magnitude of the induced emf to the magnitude of the field intensity when the electromagnetic wave comes from the principal direction,

$$h = \frac{|\mathcal{E}_0|}{|E|}, \quad (6-30)$$

is found to be the same in the case of both reception and transmission and is defined by the expression

$$h = \frac{\lambda}{\pi} \sqrt{\frac{D_0 R_\Sigma}{120}}, \quad (6-31)$$

where D_0 is the directive gain in the direction of the maximum radiation.

4. The maximum power dissipated in the load of any antenna takes place when $X_L + X_{in} = 0$ and $R_L = R_{in}$ and equals:

$$P_{\max} = \frac{\lambda E E^* D \eta}{\pi^2 960}, \quad (6-32)$$

where $\eta = \frac{R_{\Sigma 0}}{R_{in}}$ is the antenna efficiency ($R_{in} = R_{\Sigma 0} + R_{losses}$, R_{losses} , the resistance of the losses of the antenna).

The maximum power dissipated in the receiving antenna load is the greater, the more directive is the gain and the efficiency of the antenna.

5. The current arising in any receiving antenna gives rise to a reverse radiation of the antenna. Thus, part of the power absorbed by the antenna is spent in the receiver and part on reverse radiation.

6. The reciprocity principle leads to the reversibility of the antenna. Any transmitting antenna may be used as a receiving antenna and vice versa.

6-5. Effective Area of an Antenna

Let us dwell on one more concept of receiving antenna theory. It is sometimes useful to introduce the notion of the area of the front of an incoming electromagnetic wave,

from which the antenna absorbs energy. The power passing through the area s_{eff} perpendicular to the Poynting vector equals:

$$P = \frac{EE^*}{240\pi} s_{\text{eff}}. \quad (6-33)$$

On comparing (6-33) with (6-32), which represents the maximum power dissipated in the load of the receiving antenna, we obtain:

$$\frac{s_{\text{eff}}}{\lambda^2} = \frac{D\eta}{4\pi}, \quad (6-34)$$

i.e., the effective area of the wave front, expressed in fractions of the length of the wave from which the antenna absorbs energy, equals the product of the directive gain by the antenna efficiency, divided by 4π . This area is usually referred to as the effective area of the receiving antenna. Consequently, the larger the directive gain of the antenna, the larger the space from which the antenna derives energy.

Equation (6-34) coincides with (4-71) so that we may say that the effective area of an ideal plane antenna coincides with its geometrical area. For example, the effective area of a half-wave dipole equals (when $\eta=1$) $s_{\text{eff}}=0.522l^2$.

6-6. Mutual Resistance of Receiving and Transmitting Antennas

The expressions mentioned in Paragraph 6-4 enable us to write a fairly simple expression for the mutual resistance of receiving and transmitting antennas. Designating the transmitting antenna by the index 1 and the receiving antenna by the index 2 (Fig. 6-4), we shall, in accordance with (6-27), write for the receiving antenna current:

$$I_2 = - \frac{\lambda E_{21} \cos \gamma}{\pi (Z_{L2} + Z_{in2})} \sqrt{\frac{D_2 R_{\Sigma 2}}{120}} e^{i\psi_2}, \quad (6-35)$$

where we have introduced γ which is the difference between the polarisation angles of the field of receiving and transmitting antennas.

If we take into account (6-26), we shall, from (6-17) obtain for the field intensity of the transmitting antenna:

$$E_{21} = iI_1 \frac{e^{-ikr_0}}{r_0} \sqrt{30D_1 R_{\Sigma 1}} e^{i\psi_1}. \quad (6-36)$$

From the substitution of (6-36) into (6-35), we obtain:

$$\frac{I_2}{I_1} = -i \frac{\lambda \cos \gamma}{2\pi (Z_{L2} + Z_{in2})} \sqrt{D_1 D_2 R_{\Sigma 1} R_{\Sigma 2}} \frac{e^{-ikr_0}}{r_0} e^{i(\psi_1 + \psi_2)}. \quad (6-37)$$

Making use of the Kirchhoff's equation

$$I_2 (Z_{L2} + Z_{in2}) + I_1 Z_{12} = 0,$$

where Z_{12} is the mutual resistance of the antennas related to the currents at the feed points of the antenna, we obtain:

$$Z_{12} = i \frac{\lambda \cos \gamma}{2\pi} \sqrt{D_1 D_2 R_{\Sigma 1} R_{\Sigma 2}} \frac{e^{-ikr_0}}{r_0} e^{i(\psi_1 + \psi_2)}. \quad (6-38)$$

This simple expression enables us to determine the mutual resistance of two arbitrary antennas situated in relation to one another in the zone of radiation in accordance with their electric parameters. In practice, this expression may be used if the distance between the antennas satisfies the ratio

$$r_0 > \frac{2L^2}{\lambda}, \quad (6-39)$$

where L is the longest dimension of one of the antennas.

For example, for two half-wave parallel dipoles lying on one plane, the expression (6-38) becomes:

$$Z_{12} = i \frac{60\lambda}{\pi r_0} e^{-ikr_0} \quad (6-40)$$

and, as shown by direct calculations, it is in good accord with the data of V. V. Tatarinov's tables for distances exceeding one wave-length.

PART TWO

Transmission Lines of Radio Waves

CHAPTER SEVEN

Transmission Line Theory

7-1. General

Transmission lines of radio waves are devices for chaneling high-frequency energy from transmitters to antennas or from antennas to receivers. The transverse dimensions of the lines are small in comparison with the wave-length or are of the same order whereas their lengths are many times greater than that of the wave-lengths.

The first main requirement expected of devices of this kind is that, when transmitting energy from a transmitter to an antenna and from an antenna to a receiver, they should not radiate high-frequency energy and should not, therefore, distort the transmission or reception directional characteristics of antennas.

The second requirement is that they should transmit high-frequency energy with the maximum efficiency. Consequently, the losses on heating the line conductors and isolators should be kept down to a minimum.

The third requirement is that the high-frequency voltages arising in the lines should be as low as possible to avoid breakdowns in the line and thus, transmit the maximum of power.

The final main requirement is that the line should not allow any noticeable distortions of the signals transmitted along the channel.

In accordance with the above-listed requirements, different transmission lines are used for different wave ranges.

Fig. 7-1, *a* and *b* show a two-wire and a four-wire symmetrical lines (feeders) in which a transverse electromagnetic wave is excited, accompanied by forward and reverse currents, in the line. These lines are used on short and partly on ultrashort waves.

Coaxial cables and hard coaxial lines (Fig. 7-1, *c*), in which a transverse electromagnetic wave is excited, also accompanied by forward and reverse currents, are mainly used on metre and decimetre waves.

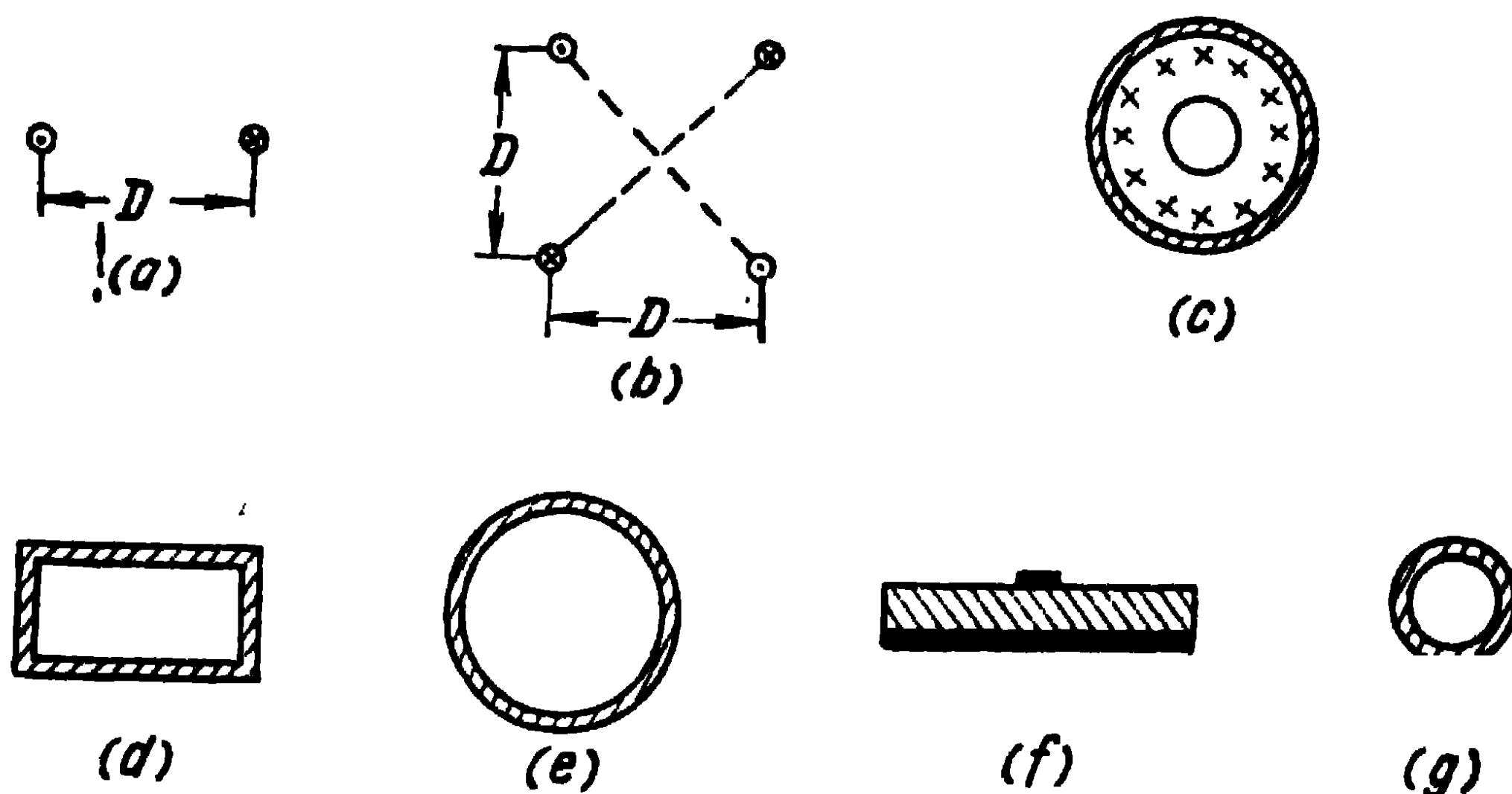


Fig. 7-1. Cross sections of transmission lines of radio waves.

Fig. 7-1, *d*, *e* shows a rectangular and a circular waveguides in which the lower types of transverse electric and partly transverse magnetic waves are used. As a rule, the waveguides are utilised on waves shorter than 10 cm.

Finally, on decimetre and centimetre waves, strip lines are used (Fig. 7-1, *d*, *e*) in which a wave of a mode close to the TEM mode is excited and single-wire lines with a thin layer of dielectric (Fig. 7-1, *g*) in which a so-called surface wave is excited. Other lines are also in use.

The present chapter deals with the theory of these lines. We presume that the reader is familiar with the theory of long lines and the propagation of the main modes in waveguides. These questions will therefore not be treated in any detail here and the line theory will be considered chiefly from the point of view of the excitation of radio waves. The lines in the present chapter will be assumed free from losses. The question regarding the evaluation of the energy losses in the lines will be dealt with in the subsequent chapters.

The present course being mainly concerned with ultrashort wave antennas, we shall begin our study of transmission lines with waveguides.

7-2. Rectangular Waveguide Theory

A rectangular waveguide, of which a longitudinal section is shown in Fig. 7-2, is usually excited by means of a probe introduced into the waveguide through an opening in its broad wall. The end of the waveguide close to the probe is shortened and the far end is connected to the antenna.

The direction of the electric current in the probe coincides with the x -axis of rectangular coordinates. This current

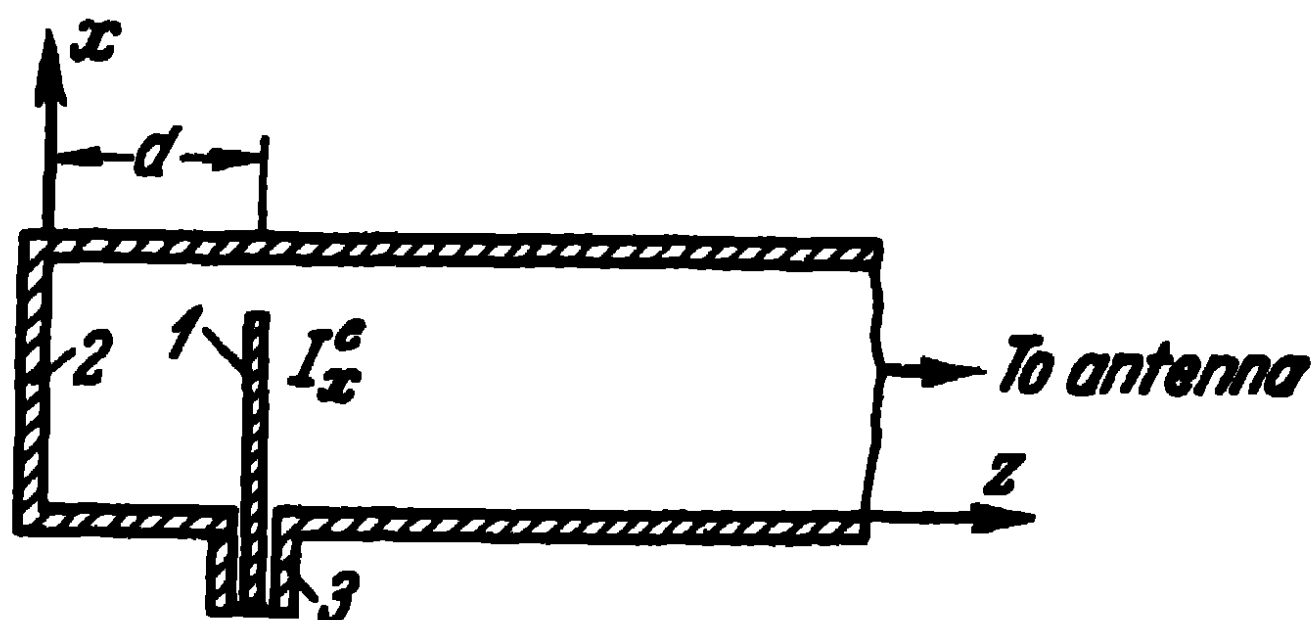


Fig. 7-2. Longitudinal section of a rectangular waveguide:

1—probe; 2—shortened wall; 3—coaxial line.

occupies inside the waveguide a certain limited volume with a certain density and, relatively to the currents induced on the walls of the waveguide, it is an external (exciting) current.

In accordance with the above, let us examine the problem of the excitation of the waveguide by an external electric current with a density J_x^e [28]. For simplicity, we shall assume the walls of the waveguide to be ideally conducting and its length infinitely great. Let a be the internal dimension of the narrow wall of the waveguide and b , that of the broad wall.

The electromagnetic field excited in the waveguide is described by the equations (I-4) and (I-5). Using the mirror method, it may be shown [29] that the direction of the vector potential of the excited field coincides with that of the current and has, therefore, only the x -th component $A^e = A_x^e$. Consequently, in rectangular coordinates,

the equations (1-4) and (1-5) will be written as:

$$\begin{aligned}
 E_x &= \frac{1}{i\omega\epsilon'} \left(k^2 A_x^e + \frac{\partial^2 A_x^e}{\partial x^2} \right); \\
 E_y &= \frac{1}{i\omega\epsilon'} \frac{\partial^2 A_x^e}{\partial y \partial x}, \quad E_z = \frac{1}{i\omega\epsilon'} \frac{\partial^2 A_x^e}{\partial z \partial x}; \\
 H_x &= 0, \quad H_y = \frac{\partial A_x^e}{\partial z}, \quad H_z = -\frac{\partial A_x^e}{\partial y}; \\
 \frac{\partial^2 A_x^e}{\partial x^2} + \frac{\partial^2 A_x^e}{\partial y^2} + \frac{\partial^2 A_x^e}{\partial z^2} + k^2 A_x^e &= -j_x^e.
 \end{aligned} \tag{7-1}$$

$$\tag{7-2}$$

Since the waveguide is an ideal conductor, the tangential components of the electric field intensity at the walls of the waveguide equal zero. In accordance with (7-1) this occurs under the condition

$$\left. \begin{aligned}
 A_x^e &= 0 \text{ when } y=0, y=b; \\
 \frac{\partial A_x^e}{\partial x} &= 0 \text{ when } x=0, x=a.
 \end{aligned} \right\} \tag{7-3}$$

Thus, the problem is reduced to the solution of the inhomogeneous waveguide equation (7-2) in the existence of the boundary conditions (7-3).

Equation (7-2) is with separable variables and we shall therefore seek its solution in the form of the product of three functions, each of which depends on one variable only,

$$A_x^e(x, y, z) = X(x) Y(y) Z(z). \tag{7-4}$$

The function $X(x)$ is prescribed in the interval $0 \leq x \leq a$. Let us represent this function in the form of a Fourier series expansion:

$$X(x) = \sum_{n=0}^{\infty} \left[a_n \cos\left(\frac{\pi n}{a} x\right) + b_n \sin\left(\frac{\pi n}{a} x\right) \right]$$

and, in order to satisfy the boundary condition (7-3), it is evidently necessary here to assume the coefficient at the sine to equal zero: $b_n = 0$.

The function $Y(y)$ is prescribed in the interval $0 \leq y \leq b$, so that we shall also represent this function in the form of

a Fourier series:

$$Y(y) = \sum_{m=0}^{\infty} \left[a_m \cos\left(\frac{\pi m}{b} y\right) + b_m \sin\left(\frac{\pi m}{b} y\right) \right],$$

and in order to satisfy the boundary condition (7-3), we must here assume that $a_m = 0$.

The function $Z(z)$ is prescribed in the infinite interval $-\infty < z < \infty$. We shall therefore represent it in the form of a Fourier integral expansion:

$$Z(z) = \int_{\kappa=-\infty}^{\infty} g(\kappa) e^{-i\kappa z} d\kappa.$$

Thus, the solution of the equation (7-2) which satisfies the boundary conditions (7-3) may be represented in the form of an expansion:

$$A_x^e(x, y, z) = \sum_{n=0}^{\infty} \sum_{m=1}^{\infty} \int_{\kappa=-\infty}^{\infty} a_{nm}(\kappa) \cos\left(\frac{\pi n}{a} x\right) \times \\ \times \sin\left(\frac{\pi m}{b} y\right) e^{-i\kappa z} d\kappa. \quad (7-5)$$

To determine the unknown coefficients $a_{nm}(\kappa)$ in (7-5), let us substitute it into (7-2); we shall then obtain:

$$\sum_{n=0}^{\infty} \sum_{m=1}^{\infty} \int_{\kappa=-\infty}^{\infty} \left[k^2 - \left(\frac{\pi n}{a}\right)^2 - \left(\frac{\pi m}{b}\right)^2 - \kappa^2 \right] \times \\ \times a_{nm}(\kappa) \cos\left(\frac{\pi n}{a} x\right) \sin\left(\frac{\pi m}{b} y\right) e^{-i\kappa z} d\kappa = -j_x^e(x, y, z). \quad (7-6)$$

Consequently, the distribution of the density of the exciting current is represented in the form of an expansion, using the same system of eigenfunctions of the given boundary problem as for the expansion of the vector potential.

Applying to (7-6) the reverse Fourier transformation, let us multiply the left- and right-hand sides of (7-6) by $\cos\left(\frac{\pi n'}{a} x\right) \sin\left(\frac{\pi m'}{b} y\right) e^{+i\kappa' z}$, where n' , m' , κ' are prescribed values of n , m and κ , and let us integrate the left- and right-hand sides of the expression thus obtained over the whole volume of the waveguide.

Let us, further, make use of the orthogonality conditions of the eigenfunctions of the discrete and continuous spectrums:

$$\begin{aligned} \frac{\varepsilon_n}{a} \int_{x=0}^a \cos\left(\frac{\pi n}{a} x\right) \cos\left(\frac{\pi n'}{a} x\right) dx &= \begin{cases} 0 & \text{when } n \neq n', \\ 1 & \text{when } n = n'; \end{cases} \\ \frac{2}{b} \int_{y=0}^b \sin\left(\frac{\pi m}{b} y\right) \sin\left(\frac{\pi m'}{b} y\right) dy &= \begin{cases} 0 & \text{when } m \neq m', \\ 1 & \text{when } m = m'; \end{cases} \\ \frac{1}{2\pi} \int_{z=-\infty}^{\infty} e^{-i(\kappa - \kappa') z} dz &= \delta(\kappa - \kappa'), \end{aligned} \quad (7-7)$$

where $\varepsilon_n = 1$ when $n = 0$, $\varepsilon_n = 2$ when $n = 1, 2, 3 \dots$

Here $\delta(\kappa - \kappa')$ is the delta-function, which equals zero everywhere except at the specific point $\kappa = \kappa'$, where it turns into infinity; moreover

$$\int_{\kappa=-\infty}^{\infty} \delta(\kappa - \kappa') d\kappa = 1.$$

As a result of this transformation, we obtain:

$$\begin{aligned} a_{nm}(\kappa) &= \frac{\varepsilon_n}{\pi ab} \int_V j_x(x', y', z') \cos\left(\frac{\pi n}{a} x'\right) \sin\left(\frac{\pi m}{b} y'\right) \times \\ &\times \frac{e^{i\kappa z'}}{\left[\kappa^2 + \left(\frac{\pi n}{a}\right)^2 + \left(\frac{\pi m}{b}\right)^2 - k^2\right]} dV, \end{aligned} \quad (7-8)$$

where the integral is taken over the volume which contains the external currents

Now, let us substitute (7-8) into (7-5) and calculate the integral

$$M = \int_{\kappa=-\infty}^{\infty} \frac{e^{-i\kappa(z-z')}}{\left[\kappa^2 + \left(\frac{\pi n}{a}\right)^2 + \left(\frac{\pi m}{b}\right)^2 - k^2\right]} d\kappa.$$

Applying to this integral the residual theory, we obtain for $(z - z') < 0$:

$$M = \pi \frac{e^{+\gamma(z-z')}}{\gamma} \quad (7-9)$$

and for $(z - z') > 0$:

$$M = \pi \frac{e^{-\gamma(z-z')}}{\gamma}, \quad (7-10)$$

where

$$\gamma = \sqrt{\left(\frac{\pi n}{a}\right)^2 + \left(\frac{\pi m}{b}\right)^2 - k^2} \quad (7-11)$$

is the propagation constant.

Thus, the final expression of the vector potential is

$$A_x^e(x, y, z) = \sum_{n=0}^{\infty} \sum_{m=1}^{\infty} \frac{e_n}{ab\gamma} \cos\left(\frac{\pi n}{a} x\right) \sin\left(\frac{\pi m}{b} y\right) \times \\ \times \int_s \cos\left(\frac{\pi n}{a} x'\right) \sin\left(\frac{\pi m}{b} y'\right) \left[e^{-\gamma z} \int_{z'=-\infty}^{z'=z} j_x^e(x', y', z') \times \right. \\ \left. \times e^{+\gamma z'} dz' + e^{+\gamma z} \int_{z'=z}^{z'=\infty} j_x^e(x', y', z') e^{-\gamma z'} dz' \right] ds, \quad (7-12)$$

where the index s of the sign of the integral indicates that the integration is performed over the cross section of the waveguide. The coordinates of the exciting current are shown in bold type.

The calculations we have given are useful because a whole series of conclusions of practical importance can be drawn from the expression (7-12). Together with (7-1), this expression provides a complete solution to the problem of the excitation of a rectangular waveguide by a transverse electric dipole lying in a direction parallel to the narrow wall of the waveguide.

Usually, in electromagnetic field theory courses, only the structure of the field in the waveguide is determined, no determination being given of the absolute magnitude of the field components. This is due to the fact that the exciting (external) currents are not introduced into Maxwell's equations and the wave equations derived from them. The solution of the problem regarding the excitation of a rectangular waveguide, i.e., the solution of the wave equation with the right-hand side (7-2) enables the field components in the waveguide to be determined also from the absolute magnitude. This, in turn, enables to solve a series of problems of practical importance, such as that of finding the radiation resistance of a dipole exciting a waveguide, which will be mentioned further.

Let us analyse the expressions obtained.

1. An electric antenna excites an infinitely large number of modes in a waveguide. To each pair of values of n and m there corresponds a definite mode which, in accordance with (7-11), has a definite propagation constant γ .

2. If the wave number k is a real quantity (as is usually assumed), the propagation constant γ may be real or imaginary, depending on the transverse dimensions a and b of the waveguide and the values of n and m . A real value of the quantity γ indicates that the wave process is non-existent and the field amplitude decreases as we move away from the dipole towards the axis of the waveguide in accordance with the exponential law. In that case, the wave is said to be damped (not propagated).

The imaginary value $\gamma = i\alpha$, where

$$\alpha = \sqrt{k^2 - \left(\frac{\pi n}{a}\right)^2 - \left(\frac{\pi m}{b}\right)^2},$$

indicates that a wave is propagated along the axis of the waveguide with a definite phase velocity. The field amplitude of this wave remains constant as we move away from the exciting dipole, since the walls of the waveguide are supposed to be ideal conductors.

3. The wave-length for which the propagation constant γ equals zero at the given values of n and m , is known as the critical wave-length.

The critical wave-length is expressed as

$$\lambda_{\text{crit } nm} = \frac{2\pi}{\sqrt{\left(\frac{\pi n}{a}\right)^2 + \left(\frac{\pi m}{b}\right)^2}}. \quad (7-13)$$

It can be seen from this expression that the higher the mode, i.e., the larger the values of n and m , the transverse dimensions a and b of the waveguide being prescribed, the smaller the critical wave-length.

4. When the wave-length of the oscillations becomes equal to the critical wave-length $\lambda_c = \lambda_{\text{crit } nm}$, the amplitude of the oscillations in the waveguide becomes infinite. In real conditions, the walls of the waveguide have a finite conductivity, so that although at the critical wave-length the amplitude does become large, it nevertheless remains finite.

5. To each propagated mode there correspond a definite phase velocity and a definite wave-length in the waveguide, which, in a boundless medium, are related to the phase

velocity v and the wave-length λ_0 as follows:

$$v_{ph} = \frac{v}{\sqrt{1 - \left(\frac{\lambda_0}{\lambda_{crit\ nm}}\right)^2}};$$

$$\lambda_w = \frac{\lambda_0}{\sqrt{1 - \left(\frac{\lambda_0}{\lambda_{crit\ nm}}\right)^2}}. \quad (7-14)$$

6. The propagated modes move away from the exciting sources towards infinity in the form of travelling waves. As can be seen from the expressions (7-12), within the volume of the exciting sources, there occurs a superposition of travelling waves moving towards one another in the direction of the axis of the waveguide.

When a rectangular waveguide is used as a transmission line of high-frequency energy from a transmitter to an antenna or from an antenna to a receiver, the dimensions of the waveguide are chosen in such a way as to allow the propagation of only the lowest modes, for which $n=0$ and $m=1$. We shall therefore dwell at length on this mode.

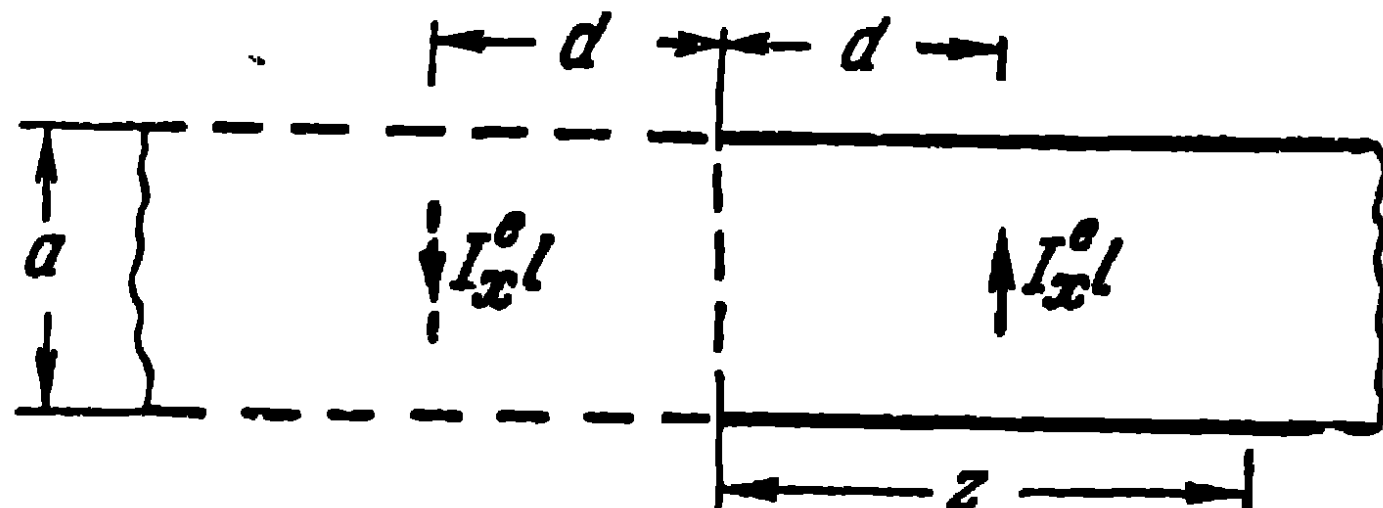


Fig. 7-3. Explaining the calculation of the field in a semi-infinite waveguide.

Let the exciting dipole be a linear dipole with a current moment $I_x^0 l$ and let the waveguide be semi-infinite, as shown in Fig. 7-2. Neglecting the higher modes ($n > 0$ and $m > 1$), for which the field amplitudes at a certain distance from the exciting dipole are small in comparison with the amplitude of the propagated mode, let us consider this dominant mode.

It may be shown that the field in a semi-infinite waveguide (Fig. 7-2) coincides with the field in an infinite waveguide (Fig. 7-3) in which the field of the mirror image of this dipole relatively to the end wall of the waveguide is added to the field of the dipole under investigation.

In the region $z > d$, in accordance with (7-12), we obtain for the dominant mode, excited by the antenna itself, and for the field excited by the mirror image of the dipole:

$$A_{x01}^e = -\frac{l_x^e l}{ab i \alpha_{01}} \sin\left(\frac{\pi}{b} y\right) \sin\left(\frac{\pi}{b} y'\right) e^{-i \alpha_{01} (z-d)}.$$

Thus, the total field in the region $z > d$ is:

$$A_{x01}^{e, \text{tot}} = \frac{2l_x^e l}{ab \alpha_{01}} \sin\left(\frac{\pi}{b} y\right) \sin\left(\frac{\pi}{b} y'\right) \sin(\alpha_{01} d) e^{-i \alpha_{01} z}. \quad (7-15)$$

Similarly, in the region $z < d$, we have for the total field:

$$A_{x01}^{e, \text{tot}} = \frac{2l_x^e l}{ab \alpha_{01}} \sin\left(\frac{\pi}{b} y\right) \sin\left(\frac{\pi}{b} y'\right) \sin(\alpha_{01} z) e^{-i \alpha_{01} d} \quad (7-16)$$

For this dominant mode, the expressions (7-1) are written as:

$$\begin{aligned} E_{x01} &= \frac{k^2}{i \omega \epsilon'} A_{x01}^e, \quad E_{y01} = 0, \quad E_{z01} = 0, \\ H_{x01} &= 0, \quad H_{y01} = \frac{\partial A_{x01}^e}{\partial z}, \quad H_{z01} = -\frac{\partial A_{x01}^e}{\partial y}. \end{aligned} \quad (7-17)$$

In the above-mentioned expressions

$$\alpha_{01} = \sqrt{k^2 - \left(\frac{\pi}{b}\right)^2}, \quad \lambda_{\text{crit } 01} = 2b, \quad \lambda_{\text{oper}} < 2b.$$

Thus, the lowest mode under consideration has only one transverse component of the electric field intensity. For this reason, the wave of this mode is referred to as the transverse electric TE_{01} wave and, since the magnetic field has a longitudinal component, it is also referred to as the magnetic H_{01} wave. The field of this wave does not depend on the coordinate x ($n=0$) and has one variation ($m=1$) in the direction of the y -axis.

In the $z > d$ region, the wave is a travelling wave and in the $z < d$ region, a standing one. Fig. 7-4 shows the distribution of the amplitude of the electric field intensity in the transverse and longitudinal planes of the waveguide.

The amplitude of the field in the waveguide depends on the location of the antenna. It is seen from (7-15) and (7-16) that if the dipole is placed near the lateral wall ($y' = 0, b$), the field of this dipole will equal zero everywhere. In just

the same way, the field in the $z > d$ region will equal zero if we assume $d = \frac{\lambda_w}{2}$. The field will be maximum for $y' = \frac{b}{2}$ and $d = \frac{\lambda_w}{4}$.

Having established the relation between the field intensity in a waveguide and the exciting current, it is relatively

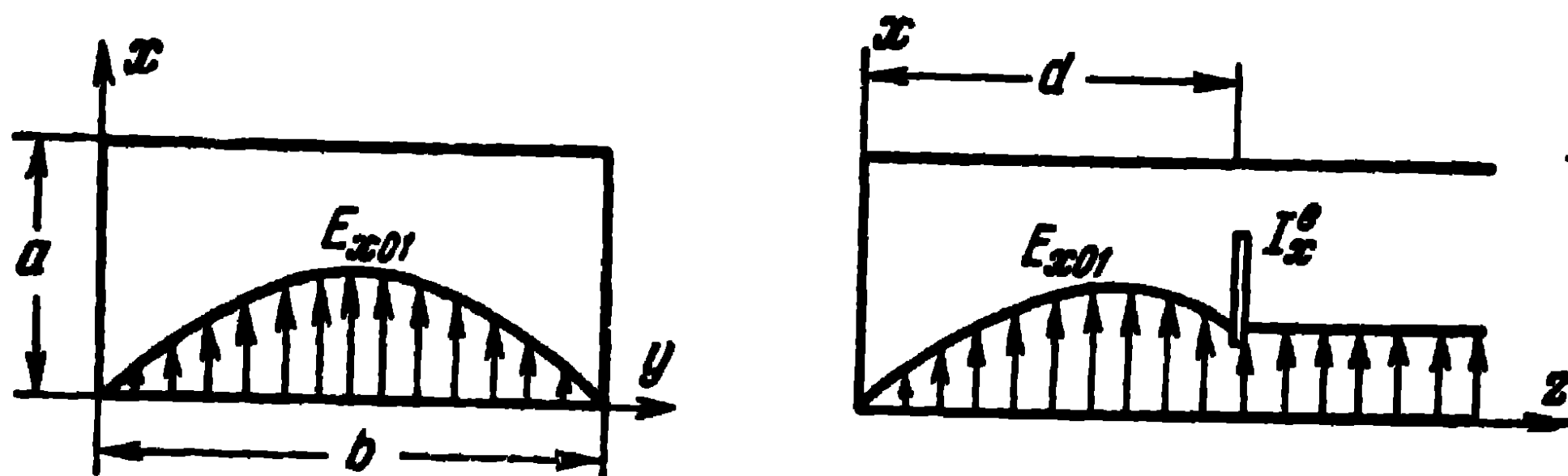


Fig. 7-4. Distribution of the electric field in a waveguide.

easy to calculate the power radiated by a dipole in a waveguide. Indeed, if we ensure the conditions for the propagation of only the H_{01} mode, the whole of the energy will be transferred along the waveguide only by that mode.

Applying the Poynting vector method and making use of the expression (1-10), we obtain:

$$P_{\Sigma} = \frac{1}{2} \int_{x=0}^a \int_{y=0}^b E_{x01} H_{y01}^* dx dy, \quad (7-18)$$

or, substituting here the expressions for the field intensity in accordance with (7-17) and (7-15), on integrating we obtain:

$$P_{\Sigma} = \frac{1}{2} I_x^{e0} R_{\Sigma d},$$

where $R_{\Sigma d}$ is the radiation resistance of the dipole in a semi-infinite waveguide, defined by the expression

$$R_{\Sigma d} = \frac{\sqrt{\frac{\mu}{\epsilon}}}{\sqrt{1 - \left(\frac{\lambda_0}{\lambda_{crit 01}}\right)^2}} \frac{2l^2}{ab} \sin^2\left(\frac{\pi}{b} y'\right) \sin^2(\alpha_{01} d). \quad (7-19)$$

By changing the quantities y' and d , one can regulate the radiation resistances of the dipole and, thus, match its coupling with the coaxial feed line.

Longitudinal or transverse slots of, as a rule, a length of half a wave, are often milled in the walls of rectangular waveguides and serve as energising and radiating devices. In this connection, let us investigate the question of the excitation of a waveguide by slots.

We know that slots can be regarded as magnetic dipoles. Let us therefore assume the distribution of the density of the external magnetic current to be prescribed in a certain volume of the waveguide [28]. Let this current have only the y -th component j_y^M . Then, the vector potential of this current will also have only the y -th component A_y^M . Hence, in that case, in rectangular coordinates, the field equations (1-4) and (1-5) will be written as:

$$\begin{aligned} E_x &= \frac{\partial A_y^M}{\partial z}; & E_y &= 0; & E_z &= -\frac{\partial A_y^M}{\partial x}; \\ H_x &= \frac{1}{i\omega\mu} \frac{\partial^2 A_y^M}{\partial x \partial y}; & H_y &= \frac{1}{i\omega\mu} \left[k^2 A_y^M + \frac{\partial^2 A_y^M}{\partial y^2} \right]; \\ H_z &= \frac{1}{i\omega\mu} \frac{\partial^2 A_y^M}{\partial z \partial y}; \end{aligned} \quad (7-20)$$

$$\frac{\partial^2 A_y^M}{\partial x^2} + \frac{\partial^2 A_y^M}{\partial y^2} + \frac{\partial^2 A_y^M}{\partial z^2} + k^2 A_y^M = -j_y^M. \quad (7-21)$$

The tangential components of the electric field intensity at the walls of the waveguide will equal zero under the conditions

$$\left. \begin{aligned} A_y^M &= 0 \text{ when } y=0, y=b, \\ \frac{\partial A_y^M}{\partial x} &= 0 \text{ when } x=0, x=a. \end{aligned} \right\} \quad (7-22)$$

The solution of the equation (7-21) in the boundary conditions (7-22) proceeds in just the same way in the case of the investigation of the excitation of the waveguide by an electric dipole and is written as follows:

$$\begin{aligned} A_y^M(x, y, z) &= \sum_{n=0}^{\infty} \sum_{m=1}^{\infty} \frac{e_n}{ab\gamma} \cos\left(\frac{\pi n}{a} x\right) \sin\left(\frac{\pi m}{b} y\right) \times \\ &\times \int_0^z \cos\left(\frac{\pi n}{a} x'\right) \sin\left(\frac{\pi m}{b} y'\right) \left[e^{-\gamma z'} \int_{z'=-\infty}^{z'} j_y^M(x', y', z') \times \right. \\ &\times e^{+\gamma z'} dz' + e^{+\gamma z} \int_{z'=z}^{\infty} j_y^M(x', y', z') e^{-\gamma z'} dz' \left. \right] ds. \end{aligned} \quad (7-23)$$

Of course, this expression coincides with (7-12) since the boundary conditions for the vector potentials are the same.

Now, let us use the solution thus obtained to define the radiation towards the inside of a waveguide of the narrow transverse slot of a length equal to half a wave shown in Fig. 7-5, *a*. Let a , y_0 , z_0 be the coordinates of the centre of the slot. Let U_0 be the voltage between the edges of the

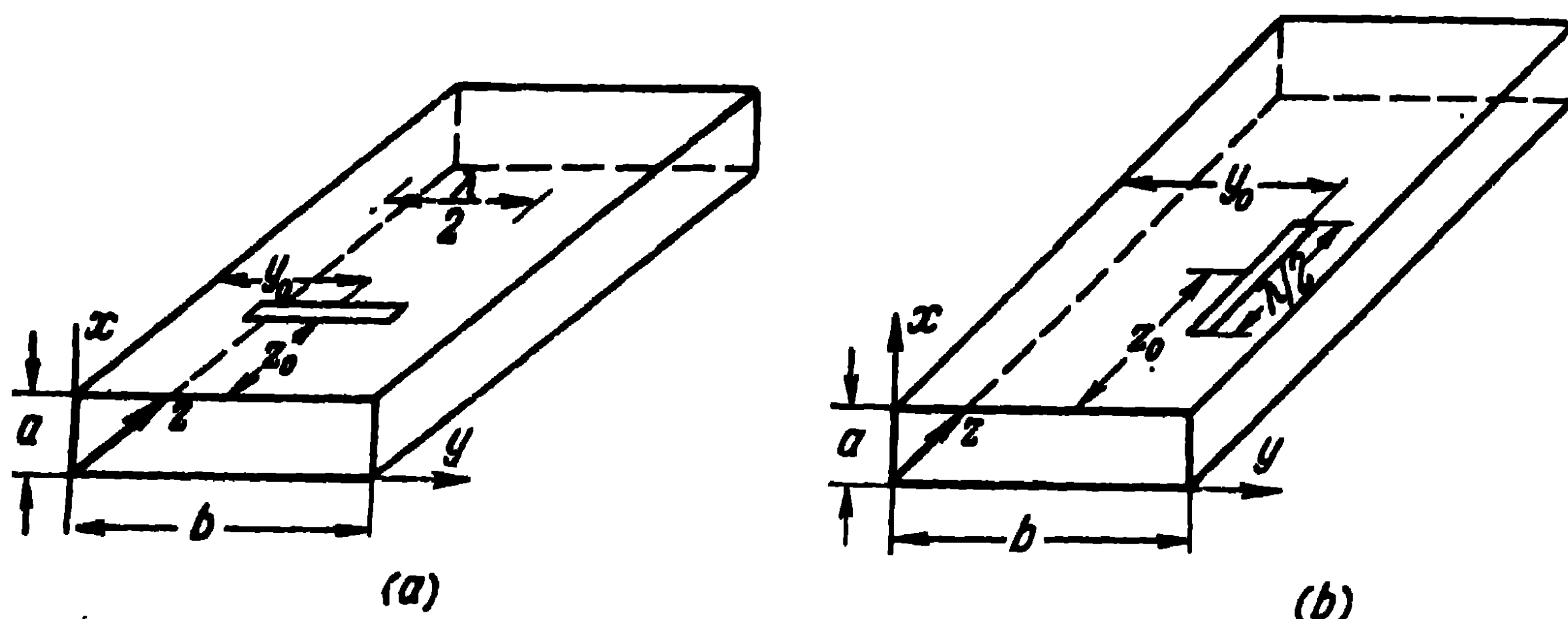


Fig 7-5 Excitation of a waveguide by a slot:
a—transverse slot; *b*—longitudinal slot

slot in the centre and let us assume the voltage distribution in the slot to be sinusoidal:

$$U_y = U_0 \cos k(y' - y_0). \quad (7-24)$$

Let us now identify the voltage in the slot with the linear magnetic current $I_y^M = U_y$ and let us write for the current density in (7-23):

$$j_y^M(x', y', z') = U_0 \cos k(y' - y_0) \delta(x' - a) \delta(z' - z_0), \quad (7-25)$$

where δ is the delta-function.

Substituting (7-25) into (7-23) and considering from now on only the lowest mode ($n=0$, $m=1$), we obtain:

$$A_{y01}^M = \frac{U_0}{abia_{01}} \sin\left(\frac{\pi}{b}y\right) e^{\pm ia_{01}(z-z_0)} \times \int_{y_0 - \lambda/4}^{y_0 + \lambda/4} \cos k(y' - y_0) \sin\left(\frac{\pi}{b}y'\right) dy', \quad (7-26)$$

where the negative sign (—) is taken for the $z > z_0$ region and the positive sign (+), for the $z < z_0$ region.

At the same time, it is assumed that the lowest mode is of the propagating kind ($\lambda_{\text{oper}} < 2b$).

Performing the integration indicated in (7-26), we obtain

$$A_{y01}^M = \frac{U_0 2k}{iab\alpha_{01}^3} \cos\left(\frac{\pi\lambda}{4b}\right) \sin\left(\frac{\pi}{b}y\right) \sin\left(\frac{\pi}{b}y_0\right) \times \\ \times e^{\pm i\alpha_{01}(z-z_0)}. \quad (7-27)$$

At the same time, in accordance with the equation (7-20), the components of the field intensity are:

$$E_{x01} = \mp \frac{U_0 2k}{ab\alpha_{01}^2} \cos\left(\frac{\pi\lambda}{4b}\right) \sin\left(\frac{\pi}{b}y\right) \times \\ \times \sin\left(\frac{\pi}{b}y_0\right) e^{\mp i\alpha_{01}(z-z_0)}; \\ H_{y01} = -\frac{1}{\omega\mu} \frac{U_0 2k}{ab\alpha_{01}} \cos\left(\frac{\pi\lambda}{4b}\right) \sin\left(\frac{\pi}{b}y\right) \times \\ \times \sin\left(\frac{\pi}{b}y_0\right) e^{\mp i\alpha_{01}(z-z_0)}; \\ H_{z01} = \mp \frac{1}{i\omega\mu} \frac{U_0 2k\pi}{ab^2\alpha_{01}^2} \cos\left(\frac{\pi\lambda}{4b}\right) \cos\left(\frac{\pi}{b}y\right) \times \\ \times \sin\left(\frac{\pi}{b}y_0\right) e^{\mp i\alpha_{01}(z-z_0)} \quad (7-28)$$

Thus, just as an electric dipole, a transverse slot generates an infinitely large number of modes in a waveguide. The lowest mode is the same as in the case of the electric dipole investigated above, i.e., the H_{01} mode.

Note that the expressions (7-28) apply to an infinite waveguide. To define the field in a semi-infinite waveguide, one must take account of the mirror image of the slot relatively to the end wall of the waveguide. This presents no difficulties and we shall therefore not dwell on it.

Let us now calculate the power radiated by a half-wave transverse slot in an infinite waveguide. Making use of (1-10) and taking the double value of the integral over the cross section of the waveguide when $z > z_0$ (the power radiated in the $z > z_0$ direction equals half the overall radiated power), we have:

$$P_\Sigma = \int_{x=0}^a \int_{y=0}^b E_{x01} H_{y01}^* dx dy. \quad (7-29)$$

Substituting here the expressions E_{x01} and H_{y01} from (7-28) when $z > z_0$, we obtain:

$$P_{\Sigma} = \frac{1}{2} U_0^2 G_{\Sigma\lambda/2},$$

where $G_{\Sigma\lambda/2}$ is the radiation conductivity of a transverse half-wave slot, defined by the expression

$$G_{\Sigma\lambda/2} = \frac{4k^2}{\omega\mu ab\alpha_{01}^3} \cos^2\left(\frac{\pi\lambda}{4b}\right) \sin^2\left(\frac{\pi}{b} y_0\right). \quad (7-30)$$

Let us now investigate the excitation of a waveguide by a half-wave slot milled in the broad wall of the waveguide (Fig. 7-5, *b*). Let us represent the slot as a longitudinal magnetic current of density j_z^M . The vector potential of such a current has only the longitudinal component A_z^M . Thus, in that case, the equations (I-4) and (I-5) are written as:

$$E_x = -\frac{\partial A_z^M}{\partial y}; \quad E_y = \frac{\partial A_z^M}{\partial x}; \quad E_z = 0;$$

$$H_x = \frac{1}{i\omega\mu} \frac{\partial^2 A_z^M}{\partial x \partial z}; \quad H_y = \frac{1}{i\omega\mu} \frac{\partial^2 A_z^M}{\partial y \partial z};$$

$$H_z = \frac{1}{i\omega\mu} \left[k^2 A_z^M + \frac{\partial^2 A_z^M}{\partial z^2} \right]; \quad (7-31)$$

$$\frac{\partial^2 A_z^M}{\partial x^2} + \frac{\partial^2 A_z^M}{\partial y^2} + \frac{\partial^2 A_z^M}{\partial z^2} + k^2 A_z^M = -j_z^M. \quad (7-32)$$

It is readily seen that the boundary conditions will be written as:

$$\left. \begin{aligned} \frac{\partial A_z^M}{\partial y} &= 0 \text{ when } y=0, y=b; \\ \frac{\partial A_z^M}{\partial x} &= 0 \text{ when } x=0, x=a. \end{aligned} \right\} \quad (7-33)$$

Solving the problem in the same way as above, the solution which satisfies the boundary conditions will be:

$$A_z^M(x, y, z) = \sum_{n=0}^{\infty} \sum_{m=0}^{\infty} \frac{\varepsilon_n \varepsilon_m}{2ab\gamma} \cos\left(\frac{\pi n}{a} x\right) \times \\ \cos\left(\frac{\pi m}{b} y\right) \int_s \cos\left(\frac{\pi n}{a} x'\right) \cos\left(\frac{\pi m}{b} y'\right) \left[e^{-\gamma z} \int_{z'=-\infty}^z j_z^M(x', y', z') e^{+\gamma z'} dz' + \right. \\ \left. + e^{+\gamma z} \int_{z'=z}^{\infty} j_z^M(x', y', z') e^{-\gamma z'} dz' \right] ds. \quad (7-34)$$

Let a, y_0, z_0 be the coordinates of the centre of the slot and U_0 , the voltage in the centre of the slot. Then, the space distribution of the current in (7-34) will be written as:

$$j_z^M(x', y', z') = U_0 \cos k(z' - z_0) \delta(x' - a) \delta(y' - y_0). \quad (7-35)$$

Substituting (7-35) into (7-34) and limiting ourself to the investigation of the lowest mode ($n=0, m=1$), we obtain for the $\left(z_0 - \frac{\lambda}{4}\right) < z < \left(z_0 + \frac{\lambda}{4}\right)$ region:

$$A_{z01}^M = \frac{U_0}{ab i \alpha_{01}} \cos\left(\frac{\pi}{b} y\right) \cos\left(\frac{\pi}{b} y_0\right) \times \\ \times \left[e^{-i\alpha_{01}z} \int_{z'=z_0-\lambda/4}^z \cos k(z' - z_0) e^{i\alpha_{01}z'} dz' + \right. \\ \left. + e^{i\alpha_{01}z} \int_{z'=z}^{z_0+\lambda/4} \cos k(z' - z_0) e^{-i\alpha_{01}z'} dz' \right]. \quad (7-36)$$

For the $z > (z_0 + \lambda/4)$ region, we have:

$$A_{z01}^M = \frac{U_0}{ab i \alpha_{01}} \cos\left(\frac{\pi}{b} y\right) \cos\left(\frac{\pi}{b} y_0\right) e^{-i\alpha_{01}z} \times \\ \times \int_{z'=z_0-\lambda/4}^{z_0+\lambda/4} \cos k(z' - z_0) e^{i\alpha_{01}z'} dz'. \quad (7-37)$$

A similar expression is obtained for the $z < \left(z_0 - \frac{\lambda}{4}\right)$ region. Performing in (7-37) the integration indicated there,

we obtain:

$$A_{z01}^M = \frac{2kbU_0}{a\pi^2\alpha_{01}} \cos\left(\frac{\pi}{b}y\right) \cos\left(\frac{\pi}{b}y_0\right) \cos\left(\alpha_{01}\frac{\lambda}{4}\right) \times \\ \times e^{-i\alpha_{01}(z-z_0)}. \quad (7-38)$$

Substituting (7-38) into (7-31), we obtain the following expressions for the field components for the region $z > (z_0 + \lambda/4)$:

$$E_{x01} = \frac{2kl_0}{a\pi\alpha_{01}} \sin\left(\frac{\pi}{b}y\right) \cos\left(\frac{\pi}{b}y_0\right) \cos\left(\alpha_{01}\frac{\lambda}{4}\right) e^{-i\alpha_{01}(z-z_0)}; \\ H_{y01} = \frac{1}{i\omega\mu} \frac{2kU_0}{a\pi} \sin\left(\frac{\pi}{b}y\right) \cos\left(\frac{\pi}{b}y_0\right) \cos\left(\alpha_{01}\frac{\lambda}{4}\right) e^{-i\alpha_{01}(z-z_0)}; \\ H_{z01} = -\frac{1}{i\omega\mu} \frac{2kU_0}{ab\alpha_{01}} \cos\left(\frac{\pi}{b}y\right) \cos\left(\frac{\pi}{b}y_0\right) \cos\left(\alpha_{01}\frac{\lambda}{4}\right) \times \\ \times e^{-i\alpha_{01}(z-z_0)}. \quad (7-39)$$

Thus, a longitudinal slot likewise excites an infinitely large number of modes and the lowest mode is the H_{01} mode.

Note that, when the longitudinal slot is situated in the middle of the broad wall of the waveguide ($y_0 = \frac{b}{2}$), all the components of the field of the H_{01} wave are found to equal zero everywhere. Slots of this kind are used in the installation of waveguide measuring lines.

Now, let us determine the power radiated by the slot towards the inside of the waveguide. Making use of (7-29) and substituting there (7-39), we obtain:

$$P_\Sigma = \frac{1}{2} U_0^2 G_{\Sigma\lambda/2},$$

where $G_{\Sigma\lambda/2}$ is the radiation conductivity of a longitudinal half-wave slot, which is defined by the expression

$$G_{\Sigma\lambda/2} = \frac{4k^2b}{\omega\mu a\pi^2\alpha_{01}} \cos^2\left(\frac{\pi}{b}y_0\right) \cos^2\left(\alpha_{01}\frac{\lambda}{4}\right). \quad (7-40)$$

It is seen from (7-40) that the internal radiation conductivity of the longitudinal slot equals zero when the slot is situated in the middle of the broad wall of the waveguide ($y_0 = \frac{b}{2}$) and reaches its maximum when the slot is situated at the edge of the broad wall of the waveguide ($y_0 = 0$ or $y_0 = b$).

The problem of the excitation of a waveguide by electric dipoles and slots in the walls of waveguides placed in an arbitrary way, can be solved in a manner analogous to the above. However, we shall limit ourself to the cases of the excitation of a rectangular waveguide mentioned above and pass on to the radiation of a circular waveguide.

7-3. Circular Waveguide Theory

Let us examine a circular waveguide of infinite length having ideally conducting walls (Fig. 7-6). Let this waveguide be excited by a longitudinal electric dipole [30]. Let a be the internal radius of the waveguide and let us introduce the cylindrical coordinates r, φ, z causing the waveguide axis to coincide with the z -axis of the coordinates.

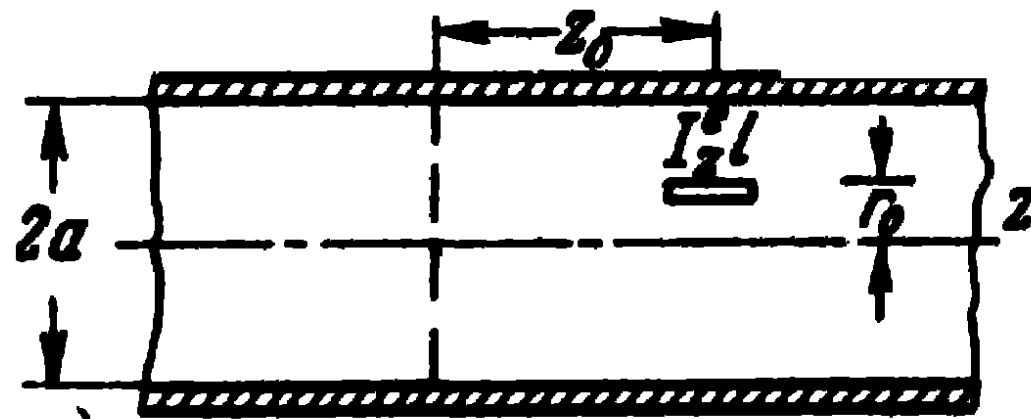


Fig. 7-6. Excitation of a circular tube by a longitudinal electric dipole.

Under the influence of the field of the dipole, electric currents are induced on the internal walls of the waveguide. These currents have only longitudinal components,

owing to the fact that the primary magnetic field, i.e., the magnetic field of the electric dipole has only transverse components and the corresponding secondary magnetic field, i.e., the magnetic field of the induced currents will also have only transverse components.

As a consequence, the vector potential of the electromagnetic field excited in the waveguide has only the $A^e = A_z^e$ longitudinal component and, in that case, the equations (1-4) and (1-5) will have the following expressions in cylindrical coordinates:

$$\left. \begin{aligned} E_r &= \frac{1}{i\omega\epsilon} \frac{\partial^2 A_z^e}{\partial z \partial r}, & E_\varphi &= \frac{1}{i\omega\epsilon} \frac{1}{r} \frac{\partial^2 A_z^e}{\partial \varphi \partial z}, \\ E_z &= \frac{1}{i\omega\epsilon} \left(k^2 A_z^e + \frac{\partial^2 A_z^e}{\partial z^2} \right), & H_r &= \frac{1}{r} \frac{\partial A_z^e}{\partial \varphi}, \\ H_\varphi &= -\frac{\partial A_z^e}{\partial r}, & H_z &= 0; \end{aligned} \right\} \quad (7-41)$$

$$\frac{1}{r} \frac{\partial}{\partial r} \left(r \frac{\partial A_z^e}{\partial r} \right) + \frac{1}{r^2} \frac{\partial^2 A_z^e}{\partial \varphi^2} + \frac{\partial^2 A_z^e}{\partial z^2} + k^2 A_z^e = -j_z^e. \quad (7-42)$$

As can be seen from the expressions (7-41), the boundary conditions relatively to the tangential components of the electric field intensity at the walls of the waveguide are satisfied if the vector potential obeys the condition

$$A_z^e = 0 \text{ when } r = a. \quad (7-43)$$

Thus, the given problem is reduced to the solution of the waveguide equation (7-42) in the existence of the boundary condition (7-43).

The equation (7-42) is of the separable variables kind and we shall, therefore, seek its solution as a product of three functions, each of which depends only on one independent variable

$$A_z^e(r, \varphi, z) = R(r) \Phi(\varphi) Z(z). \quad (7-44)$$

Let us imagine the function $R(r)$ to be dependent on the radial coordinates and prescribed in the interval $0 \leq r \leq a$ as an expansion in a series of cylindrical functions:

$$R(r) = \sum_{m=1}^{\infty} [a_m J_n(\kappa_m r) + b_m N_n(\kappa_m r)], \quad (7-45)$$

where n is an arbitrary index.

The Neuman function $N_n(\kappa_m r)$ tends towards infinity when $r \rightarrow 0$ and since the field in the waveguide must have a finite value on its axis, we assume that $b_m = 0$. It follows from the boundary condition (7-43) that, when $r = a$, the function $R(r)$ should equal zero. We shall satisfy this condition if we assume:

$$J_n(\kappa_m a) = 0. \quad (7-46)$$

Consequently, the quantities $\kappa_m a = r_{nm}$ should be the solutions of the equation (7-46). The index m is the numerator of the solution of this equation.

Let us represent the function $\Phi(\varphi)$ depending on the azimuth coordinates and prescribed in the interval $0 \leq \varphi \leq 2\pi$ in the form of a Fourier series expansion:

$$\Phi(\varphi) = \sum_{n=0}^{\infty} (a_n \cos n\varphi + b_n \sin n\varphi), \quad (7-47)$$

where n should be a whole number, since the excited field should be simple at all the points of the waveguide.

Let us represent the function $Z(z)$ depending on the longitudinal coordinate and prescribed in the infinite interval $-\infty < z < \infty$ in the form of a Fourier integral:

$$Z(z) = \int_{-\infty}^{\infty} g(\kappa) e^{-i\kappa z} d\kappa. \quad (7-48)$$

Thus, the solution of the equation (7-42) will be sought in the form of the following expansion, which satisfies the boundary conditions on the walls of the waveguide:

$$A_z^e(r, \varphi, z) = \sum_{n=0}^{\infty} \sum_{m=1}^{\infty} \int_{-\infty}^{\infty} [a_{nm}^e(\kappa) \cos n\varphi + b_{nm}^e(\kappa) \sin n\varphi] \times \\ \times J_n(\kappa_m r) e^{-i\kappa z} d\kappa. \quad (7-49)$$

Substituting (7-49) into the equation (7-42) and taking into account that the Bessel function satisfies the equation

$$\frac{1}{r} \frac{\partial}{\partial r} \left(r \frac{\partial J_n}{\partial r} \right) + \left(\kappa_m^2 - \frac{n^2}{r^2} \right) J_n = 0, \quad (7-50)$$

we obtain:

$$\sum_{n=0}^{\infty} \sum_{m=1}^{\infty} \int_{-\infty}^{\infty} (k^2 - \kappa^2 - \kappa_m^2) [a_{nm}^e(\kappa) \cos n\varphi + b_{nm}^e \sin n\varphi] \times \\ \times J_n(\kappa_m r) e^{-i\kappa z} d\kappa = -j_z^e. \quad (7-51)$$

We have thus represented the right-hand side of the equation (7-42), i.e., the distribution function of the exciting current in the form of an expansion in the same system of eigenfunctions of the given boundary problem as for the expansion of the vector potential.

To determine the coefficients of the expansion $a_{nm}^e(\kappa)$ and $b_{nm}^e(\kappa)$, let us apply to (7-51) the reverse Fourier transformation. To this end, we shall multiply the left- and right-hand sides of this expression by the complexly conjugate eigenfunctions, i.e., by $\begin{cases} \cos n'\varphi \\ \sin n'\varphi \end{cases} J_n'(\kappa_m' r) e^{+i\kappa' z}$, and shall integrate over the whole volume of the waveguide. Taking

into account that

$$\left. \begin{aligned} \int_{\varphi=0}^{2\pi} \cos n' \varphi \cos n \varphi d\varphi &= \begin{cases} 0 & \text{when } n \neq n', \\ \frac{2\pi}{\varepsilon_n} & \text{when } n = n'; \end{cases} \\ \int_{\varphi=0}^{2\pi} \sin n' \varphi \sin n \varphi d\varphi &= \begin{cases} 0 & \text{when } n \neq n', \\ \pi & \text{when } n = n'; \end{cases} \\ \int_{r=0}^a J_{n'}(\kappa_m r) J_{n'}(\kappa_m, r) r dr &= \begin{cases} 0 & \text{when } m \neq m', \\ \frac{a^2}{2} J_{n'}'^2(\kappa_m, a) & \text{when } m = m'; \end{cases} \\ \int_{z=-\infty}^{\infty} e^{-\iota z (\kappa - \kappa')} dz &= 2\pi \delta(\kappa - \kappa'), \end{aligned} \right\} (7-52)$$

we obtain:

$$\left. \begin{aligned} a_{nm}^e(\kappa) &= + \frac{\varepsilon_n}{2\pi^2 a^2} \int_V j_z^e(r', \varphi', z') \cos n\varphi' \times \\ &\quad \times \frac{J_n(\kappa_m r')}{J_n'^2(\kappa_m a)} \frac{e^{\iota \kappa z'}}{(\kappa^2 + \kappa_m^2 - k^2)} dV; \\ b_{nm}^e(\kappa) &= \frac{1}{\pi^2 a^2} \int_V j_z^e(r', \varphi', z') \sin n\varphi' \times \\ &\quad \times \frac{J_n(\kappa_m r')}{J_n'^2(\kappa_m a)} \frac{e^{\iota \kappa z'}}{(\kappa^2 + \kappa_m^2 - k^2)} dV, \end{aligned} \right\} (7-53)$$

where the integrals are taken over the volume which contains the exciting currents.

Now, let us substitute the expressions of the coefficients we have found (7-53) into the initial expression (7-49) and investigate the integral:

$$M = \int_{-\infty}^{\infty} \frac{e^{-\iota \kappa (z - z')}}{(\kappa^2 + \kappa_m^2 - k^2)} d\kappa,$$

which is calculated by means of the deductions theory and equals:

$$M = \pi \frac{e^{\pm \gamma (z - z')}}{\gamma}, \quad (7-54)$$

where

$$\gamma = \sqrt{\kappa_m^2 - k^2}. \quad (7-55)$$

Thus, the vector potential sought for is defined by the expression

$$A_z^e(r, \varphi, z) = \int_V dV \sum_{n=0}^{\infty} \sum_{m=1}^{\infty} \frac{e_n j_z^e}{2\pi a^2 \gamma} \cos n(\varphi - \varphi') \times \\ \times \frac{J_n(\kappa_m r) J_n(\kappa_m r')}{J_n'^2(\kappa_m a)} e^{\pm \gamma(z-z')}. \quad (7-56)$$

In (7-56) the positive sign (+) is taken for $(z - z') < 0$ and the negative sign (−) for $(z - z') > 0$.

The value of κ_m is determined from the expression

$$\kappa_m = \frac{r_{nm}}{a}, \quad (7-57)$$

where r_{nm} are the roots of the equation (7-46) equal, for a number of values of n and m , to:

$$r_{01} = 2.405, \quad r_{11} = 3.832, \quad r_{21} = 5.135, \quad r_{31} = 6.379,$$

$$r_{02} = 5.52, \quad r_{12} = 7.016, \quad r_{22} = 8.417, \quad r_{32} = 9.760.$$

The components of the electric and magnetic fields are determined from the substitution of (7-56) into (7-41).

The expression (7-56) shows that a longitudinal electric dipole excites in a waveguide an infinite number of modes. To each pair of values of n and m there correspond a definite mode and a definite propagation constant defined by (7-55). Depending on the frequency of the excited oscillations and the diameter of the waveguide, certain modes are propagated along the waveguide: for them, the propagation constant (when k is a real quantity) is an imaginary quantity; the other modes are damped (they are not propagated): for them, the propagation constant is a real quantity.

Under suitable conditions, the propagated modes are the lowest ones since they have the largest critical wave-length, which is determined through identifying (7-55) with zero. Since $k = \frac{2\pi}{\lambda}$, the expression obtained for the critical wave-length is:

$$\lambda_{\text{crit } nm} = \frac{2\pi a}{r_{nm}}. \quad (7-58)$$

In the case of the lowest mode ($n=0, m=1$), the critical wave-length equals $\lambda_{\text{crit } 01} = 2.62 a$. For the following mode ($n=1, m=1$), the critical wave-length equals $\lambda_{\text{crit } 11} = 1.64 a$. Consequently, if the wave-length of the oscillations, corresponding to the propagation in an unbounded

medium, satisfies the condition $1.64a < \lambda < 2.62a$, only one lowest mode with the indexes $n=0$, $m=1$ is propagated in the waveguide; all the other modes are damped; furthermore, the damping will be more pronounced for higher modes.

Note also that the waves excited by a longitudinal electric dipole in a circular waveguide are referred to as transverse magnetic waves TM_{nm} in accordance with the fact that $H_z=0$. They are also known as electric waves (E_{nm}) in accordance with the fact that $E_z \neq 0$.

The wave-length and phase velocity of a propagating mode in a waveguide are defined from the same expressions as for a rectangular waveguide, i.e., from the expressions (7-14).

Without dwelling on the higher modes, let us examine in greater detail the lowest mode E_{01} in the case of the excitation of a waveguide by a dipole, on condition that this mode is of the propagating kind. Let r_0 , z_0 be the coordinates of the dipole (Fig. 7-6). Then, in accordance with (7-56), the vector potential will be:

$$A_{z01} = \frac{I_z^e l}{2\pi a^2 i \alpha_{01}} \frac{J_0(\kappa_1 r) J_0(\kappa_1 r_0)}{J_0'^2(\kappa_1 a)} e^{\pm i \alpha_{01} (z - z_0)}, \quad (7-59)$$

where

$$\alpha_{01} = \sqrt{k^2 - \left(\frac{2.405}{a}\right)^2}.$$

The expressions for the field components (7-41) will be written as:

$$\left. \begin{aligned} E_r &= \pm \frac{1}{i\omega\epsilon} \frac{I_z^e l}{2\pi a^2} \frac{\kappa_1 J_0'(\kappa_1 r) J_0(\kappa_1 r_0)}{J_0'^2(\kappa_1 a)} e^{\pm i \alpha_{01} (z - z_0)}; \\ E_z &= \frac{\kappa_1^2}{i\omega\epsilon} \frac{I_z^e l}{2\pi a^2 i \alpha_{01}} \frac{\kappa_1 J_0'(\kappa_1 r) J_0(\kappa_1 r_0)}{J_0'^2(\kappa_1 a)} e^{\pm i \alpha_{01} (z - z_0)}; \\ H_\varphi &= - \frac{I_z^e l}{2\pi a^2 i \alpha_{01}} \frac{\kappa_1 J_0(\kappa_1 r) J_0(\kappa_1 r_0)}{J_0'^2(\kappa_1 a)} e^{\pm i \alpha_{01} (z - z_0)}. \end{aligned} \right\} \quad (7-60)$$

The rest of the components of the field intensity equal zero. The expressions (7-60) show that the wave of the E_{01} mode, excited by the dipole, moves away from it towards infinity to the right and left as travelling waves. At the same time, the radial component of the electric field intensity and the magnetic field intensity are in phase with one another and

the longitudinal component of the electric field intensity is in temporary quadrature with them.

Further, the magnetic lines of force of the field represent circles and lie in the transverse planes, the electric lines of force being confined to the walls and lying in the longitudinal planes of the waveguide.

The picture presented by the electric and magnetic lines of force in the longitudinal and transverse planes of the waveguide at a fixed moment of time are shown in Fig. 7-7.

Let us now compute the power conveyed by the E_{01} wave. In accordance with (I-10), the expression for the conveyed power is:

$$P_{\Sigma} = \int_{r=0}^a \int_{\varphi=0}^{2\pi} E_r H_{\varphi}^* r dr d\varphi.$$

Substituting here E_r and H_{φ} from (7-60) and performing the stated integration, we obtain:

$$P_{\Sigma} = \frac{|e^2| l^2}{4\pi a^4 \omega \epsilon a_{01}} \frac{J_0^2(\kappa_1 r_0)}{J_1^2(\kappa_1 a)} \quad (7-61)$$

If the E_{01} wave is the only propagating mode, the power defined by (7-61) related to the square of the effective

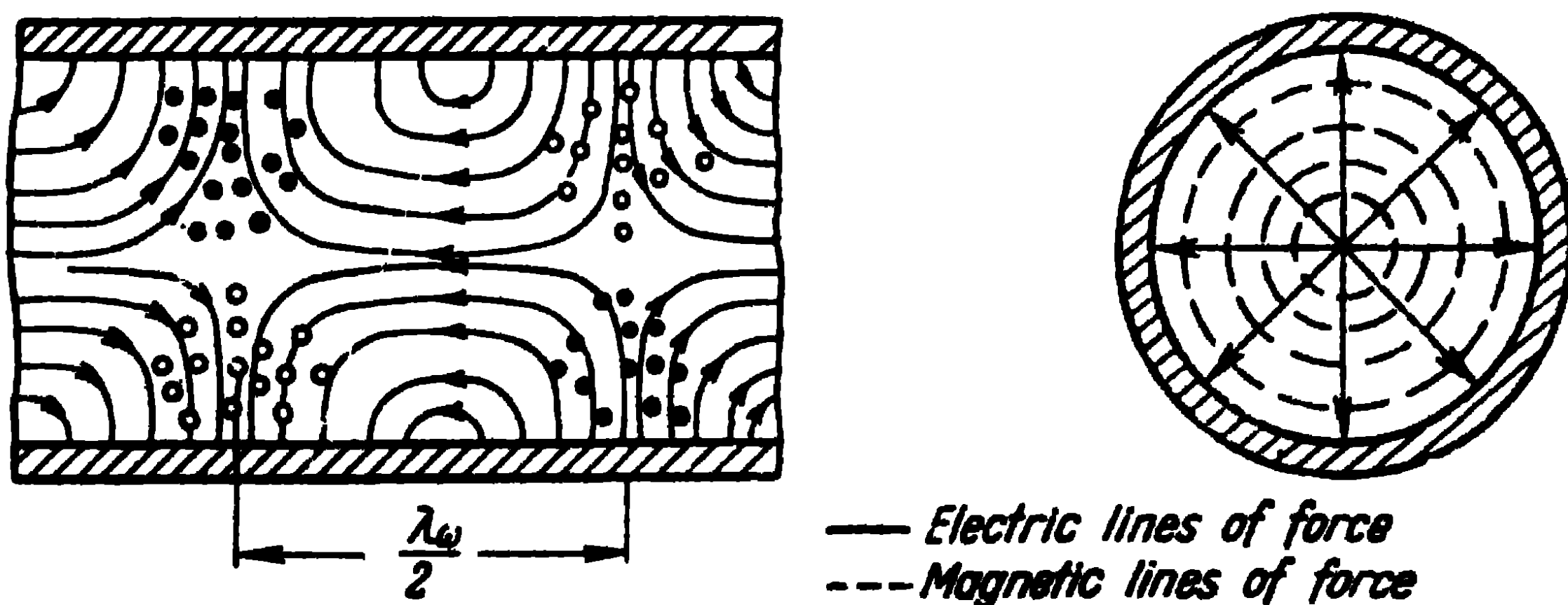


Fig. 7-7. The field in a circular waveguide for the E_{01} wave.

value of the current in the dipole represents the radiation resistance of the dipole in the waveguide. We shall have:

$$R_{\Sigma d} = \frac{1}{2\pi a^4 \omega \epsilon a_{01}} \frac{J_0^2(\kappa_1 r_0)}{J_1^2(\kappa_1 a)}. \quad (7-62)$$

It is clear that the radiation resistance equals zero when the dipole lies at the wall of the waveguide ($r_0 = a$) and reaches its maximum when it lies on the axis of the waveguide.

Now, let us pass on to the study of the excitation of a circular waveguide by a longitudinal slot cut in the wall of a waveguide. In this connection, let us investigate the excitation of a waveguide by a space distribution of a magnetic current having only a longitudinal component $j^M = j_z^M$. Similarly to the excitation of a waveguide by a longitudinal electric dipole, the field in the waveguide is, in the given case, defined by the vector potential, which has only a longitudinal component $A^M = A_z^M$.

The equations (I-4) and (I-5) will, in the given case, be written as:

$$\left. \begin{aligned} E_r &= -\frac{1}{r} \frac{\partial A_z^M}{\partial \varphi}, \quad E_\varphi = \frac{\partial A_z^M}{\partial r}, \quad E_z = 0, \\ H_r &= \frac{1}{i\omega\mu} \frac{\partial^2 A_z^M}{\partial r \partial z}, \quad H_\varphi = \frac{1}{i\omega\mu} \frac{1}{r} \frac{\partial^2 A_z^M}{\partial \varphi \partial z}, \\ H_z &= \frac{1}{i\omega\mu} \left(k^2 A_z^M + \frac{\partial^2 A_z^M}{\partial z^2} \right); \end{aligned} \right\} \quad (7-63)$$

$$\frac{1}{r} \frac{\partial}{\partial r} \left(r \frac{\partial A_z^M}{\partial r} \right) + \frac{1}{r^2} \frac{\partial^2 A_z^M}{\partial \varphi^2} + \frac{\partial^2 A_z^M}{\partial z^2} + k^2 A_z^M = -j_z^M. \quad (7-64)$$

As can be seen from the expressions (7-63), the boundary conditions are written as:

$$\frac{\partial A_z^M}{\partial r} = 0 \quad \text{when } r = a. \quad (7-65)$$

We shall write the solution of the equation (7-64) in the same form as (7-49):

$$\begin{aligned} A_z^M(r, \varphi, z) &= \sum_{n=0}^{\infty} \sum_{m=1}^{\infty} \int_{-\infty}^{\infty} [a_{nm}^M(\kappa) \cos n\varphi + b_{nm}^M(\kappa) \sin n\varphi] \times \\ &\quad \times J_n(\kappa_m r) e^{-i\kappa z} d\kappa. \end{aligned} \quad (7-66)$$

Furthermore, the boundary condition (7-65) will be satisfied if we assume that

$$J_n'(\kappa_m a) = 0. \quad (7-67)$$

Consequently, the quantities κ_m are defined by the expression

$$\kappa_m = \frac{r'_{nm}}{a}, \quad (7-68)$$

where r'_{nm} are the roots of the derivative of the Bessel function.

Substituting (7-66) into (7-64) and taking account of (7-50), we obtain:

$$\sum_{n=0}^{\infty} \sum_{m=1}^{\infty} \int_{-\infty}^{\infty} (k^2 - \kappa^2 - \kappa_m^2) [a_{nm}^M(\kappa) \cos n\varphi + b_{nm}^M(\kappa) \sin n\varphi] \times \\ \times J_n(\kappa_m r) e^{-i\kappa z} d\kappa = -j_z^M. \quad (7-69)$$

Applying to this expression the reverse Fourier transformation, just as we did it earlier, and taking account of the ratio (7-52), with the exception that in the present case

$$\int_{r=0}^a J_{n'}(\kappa_m r) J_{n'}(\kappa_{m'} r) r dr = \begin{cases} 0 & \text{when } m \neq m' \\ \frac{a^2}{2} \left(1 - \frac{n^2}{\kappa_m^2 a^2}\right) J_n^2(\kappa_m a) & \text{when } m = m', \end{cases} \quad (7-70)$$

we obtain for the coefficients of expansion, the expressions

$$a_{nm}^M(\kappa) = \frac{\varepsilon_n}{2\pi^2 a^2} \int_V j_z^M(r', \varphi', z') \cos n\varphi' \times \\ \times \frac{J_n(\kappa_m z')}{\left(1 - \frac{n^2}{\kappa_m^2 a^2}\right) J_n^2(\kappa_m a)} \frac{e^{i\kappa z'}}{(\kappa^2 + \kappa_m^2 - k^2)} dV; \\ b_{nm}^M(\kappa) = \frac{1}{\pi^2 a^2} \int_V j_z^M(r', \varphi', z') \sin n\varphi' \times \\ \times \frac{J_n(\kappa_m r')}{\left(1 - \frac{n^2}{\kappa_m^2 a^2}\right) J_n^2(\kappa_m a)} \frac{e^{i\kappa z}}{(\kappa^2 + \kappa_m^2 - k^2)} dV.$$

Further, taking into account (7-54), we obtain the required expansion of the vector potential of the longitudinal magnetic currents, satisfying the boundary conditions and the

principle of radiation at infinity, as:

$$A_z^M(r, \varphi, z) = \int_V dV \sum_{n=0}^{\infty} \sum_{m=1}^{\infty} \frac{e_n j_z^M}{2\pi a^2 \gamma} \times \\ \times \cos n(\varphi - \varphi') \frac{J_n(\kappa_m r) J_n(\kappa_m r')}{\left(1 - \frac{n^2}{\kappa_m^2 a^2}\right) J_n^2(\kappa_m a)} e^{\pm \gamma(z-z')}, \quad (7-71)$$

where the propagation constant γ is defined by (7-55) and the quantity κ_m by (7-68).

Let there be an elementary longitudinal slot in the wall of a waveguide. Regarding this slot as a magnetic dipole with a moment $I_z^M l$ lying at point a, φ_0, z_0 , we obtain:

$$A_z^M(r, \varphi, z) = \sum_{n=0}^{\infty} \sum_{m=1}^{\infty} \frac{e_n I_z^M l}{2\pi a^2 \gamma} \cos n(\varphi - \varphi_0) \times \\ \times \frac{J_n(\kappa_m r)}{\left(1 - \frac{n^2}{\kappa_m^2 a^2}\right) J_n(\kappa_m a)} e^{\pm \gamma(z-z_0)}. \quad (7-72)$$

Thus, here again, an infinite number of modes is excited. The waves are of the transverse electric kind, since $E_z = 0$ and are designated as TE_{nm} ; they are also known as magnetic waves, since $H_z \neq 0$ and are designated as H_{nm} .

The first few roots of the equation (7-67) equal

$$\begin{aligned} r'_{01} &= 3.38 & r'_{11} &= 1.84 & r'_{21} &= 3.05 \\ r'_{02} &= 7.02 & r'_{12} &= 5.83 & r'_{22} &= 6.71. \end{aligned}$$

The critical wave-length is defined from (7-58). For the H_{01} wave, it equals $\lambda_{crit 01} = 1.64$ and for the H_{11} wave, $\lambda_{crit 11} = 3.42$.

Thus, the lowest mode excited by a longitudinal slot is the H_{11} mode; it is the lowest relatively to all the modes of not only the transverse electric, but also the transverse magnetic waves.

Let the diameter of the waveguide be such that the H_{01} and H_{11} waves are of the propagating kind. Let us calculate the electromagnetic field components for these waves.

For the H_{01} wave, we have:

$$\left. \begin{aligned} E_{\varphi} &= \frac{I_z^M l}{2\pi a^2 i a_{01}} \frac{\kappa_1 J_0'(\kappa_1 r)}{J_0(\kappa_1 a)} e^{\pm i a_{01} (z - z_0)}; \\ H_r &= \pm \frac{1}{i\omega\mu} \frac{I_z^M l}{2\pi a^2} \frac{\kappa_1 J_0'(\kappa_1 r)}{J_0(\kappa_1 a)} e^{\pm i a_{01} (z - z_0)}; \\ H_z &= \frac{1}{i\omega\mu} \frac{I_z^M l}{2\pi a^2 i a_{01}} \frac{\kappa_1^2 J_0(\kappa_1 r)}{J_0(\kappa_1 a)} e^{\pm i a_{01} (z - z_0)}. \end{aligned} \right\} \quad (7-73)$$

As can be seen from the expressions (7-73), the H_{01} wave is characterised by the fact that the electric lines of force lying in the transverse plane are closed on themselves. The magnetic lines of force are entirely situated in the longitudinal plane. For this mode, the electric currents induced on the walls of the waveguide are transverse and, just as the field, do not depend on the azimuth. The picture presented by the electric and magnetic lines of force of this wave is shown in Fig. 7-8.

For the H_{11} wave, we have:

$$\begin{aligned} E_r &= \frac{I_z^M l}{\pi a^2 i a_{11}} \frac{\sin(\varphi - \varphi_0)}{r} \frac{J_1(\kappa_1 r)}{\left(1 - \frac{1}{\kappa_1^2 a^2}\right) J_1(\kappa_1 a)} e^{\pm i a_{11} (z - z_0)}; \\ E_{\varphi} &= \frac{I_z^M l}{\pi a^2 i a_{11}} \cos(\varphi - \varphi_0) \frac{\kappa_1 J_1'(\kappa_1 r)}{\left(1 - \frac{1}{\kappa_1^2 a^2}\right) J_1(\kappa_1 a)} e^{\pm i a_{11} (z - z_0)}; \\ H_r &= \pm \frac{1}{i\omega\mu} \frac{I_z^M l}{\pi a^2} \cos(\varphi - \varphi_0) \frac{\kappa_1 J_1'(\kappa_1 r)}{\left(1 - \frac{1}{\kappa_1^2 a^2}\right) J_1(\kappa_1 a)} e^{\pm i a_{11} (z - z_0)}; \\ H_{\varphi} &= \mp \frac{1}{i\omega\epsilon} \frac{I_z^M l}{\pi a^2} \frac{\sin(\varphi - \varphi_0)}{r} \frac{J_1(\kappa_1 r)}{\left(1 - \frac{1}{\kappa_1^2 a^2}\right) J_1(\kappa_1 a)} e^{\pm i a_{11} (z - z_0)}; \\ H_z &= \frac{1}{i\omega\epsilon} \frac{I_z^M l}{\pi a^2 i a_{11}} \cos(\varphi - \varphi_0) \times \\ &\quad \times \frac{\kappa_1^2 J_1(\kappa_1 r)}{\left(1 - \frac{1}{\kappa_1^2 a^2}\right) J_1(\kappa_1 a)} e^{\pm i a_{11} (z - z_0)}. \end{aligned} \quad (7-74)$$

The H_{11} wave has a more complex picture of the field. The electric currents corresponding to this wave, induced on the walls of the waveguide, have longitudinal as well as transverse components. The transverse components of the

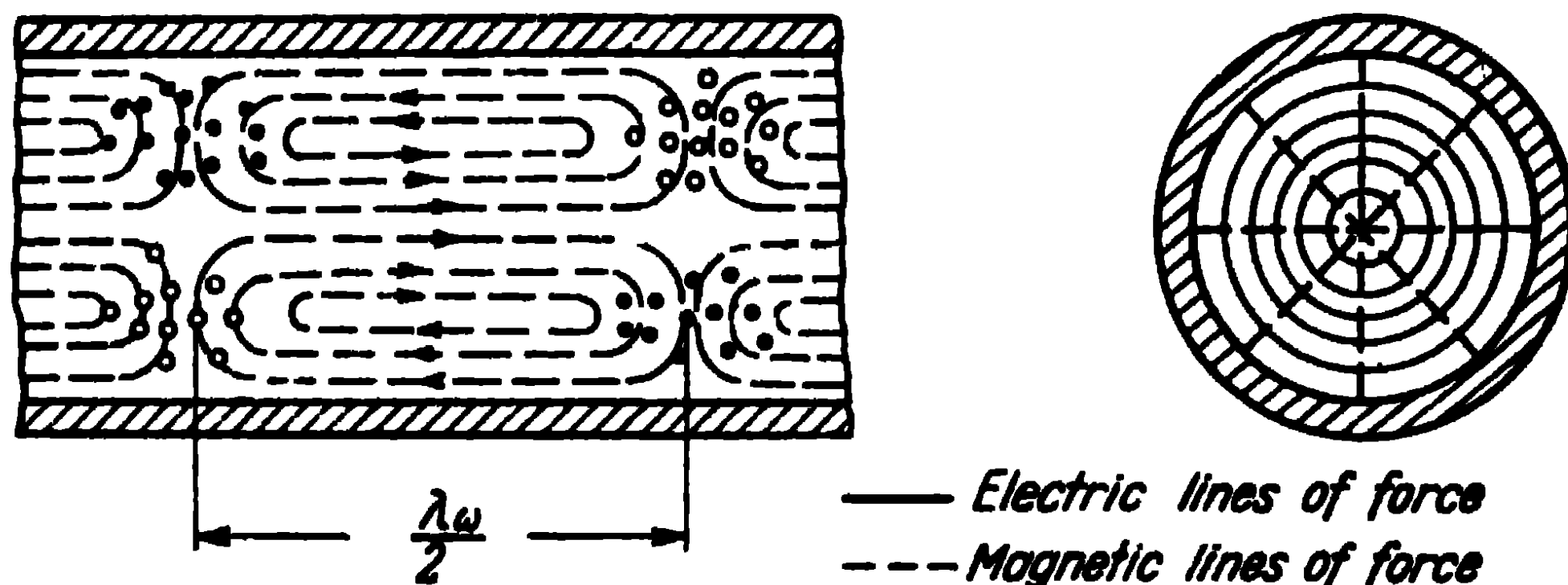


Fig. 7-8. Distribution of the field of the H_{01} wave in a circular waveguide.

currents are at a maximum in the plane of the exciting slot ($\varphi = \varphi_0$), and the longitudinal components are at a maximum in the plane perpendicular to the first one ($\varphi - \varphi_0 = 90^\circ$). The picture presented by the electric and magnetic lines of force of the H_{11} wave is shown in Fig. 7-9.

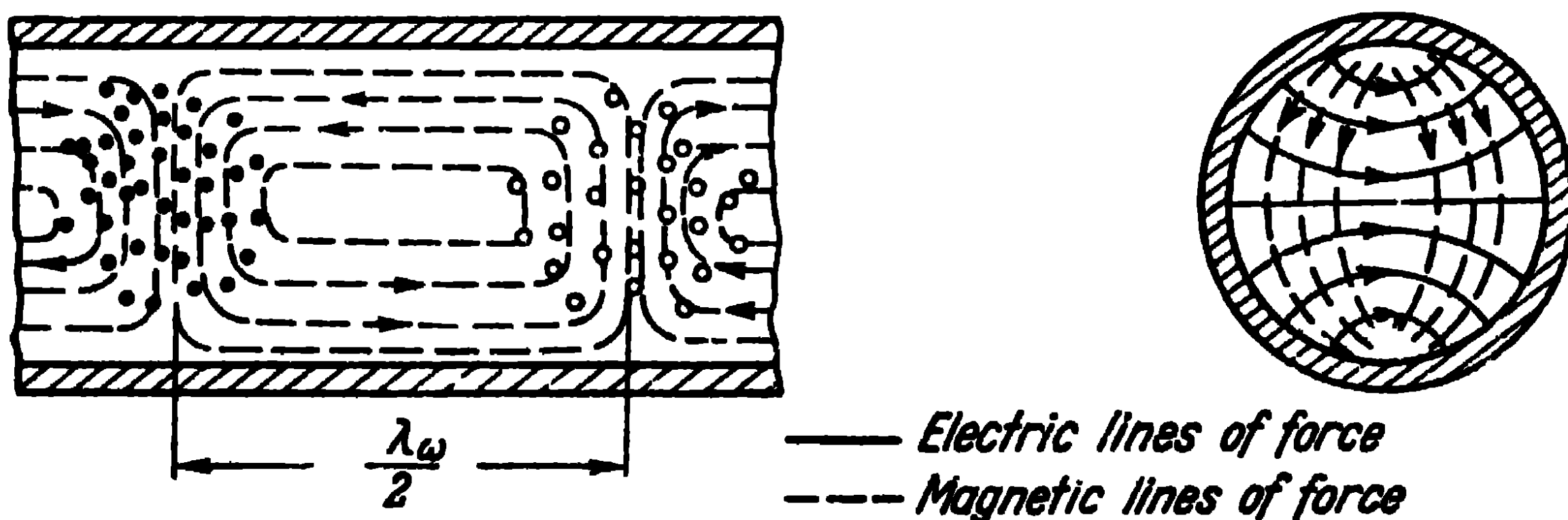


Fig. 7-9. Distribution of the field of the H_{11} wave in a circular waveguide.

We have investigated the excitation of a waveguide by a longitudinal electric dipole and a longitudinal slot. We could have, in the same way, examined the excitation of a waveguide by dipoles lying differently, for example, as is often met with, by an electric dipole lying in a radial direction.

However, the examples we have given are sufficient to illustrate the general picture of wave excitation and study the lowest modes, which are the ones applied in practice.

7-4. Brief Information Regarding Coaxial Lines

Similarly to rectangular and circular waveguides, coaxial lines may be excited by electric dipoles as well as by slots, arranged in various ways. The waves excited in the line are of various modes. However, the main difference between a coaxial line and a rectangular or circular waveguide consists in that a transverse electromagnetic wave (TEM) may be present in the coaxial line whereas no such wave can be present in hollow tubes.

In a transverse electromagnetic wave, the longitudinal components of the electric and magnetic fields equal zero and the phase velocity of the wave equals the velocity of light in the given medium. This type of oscillations has no critical wave-length and may be propagated no matter how small the transverse dimensions

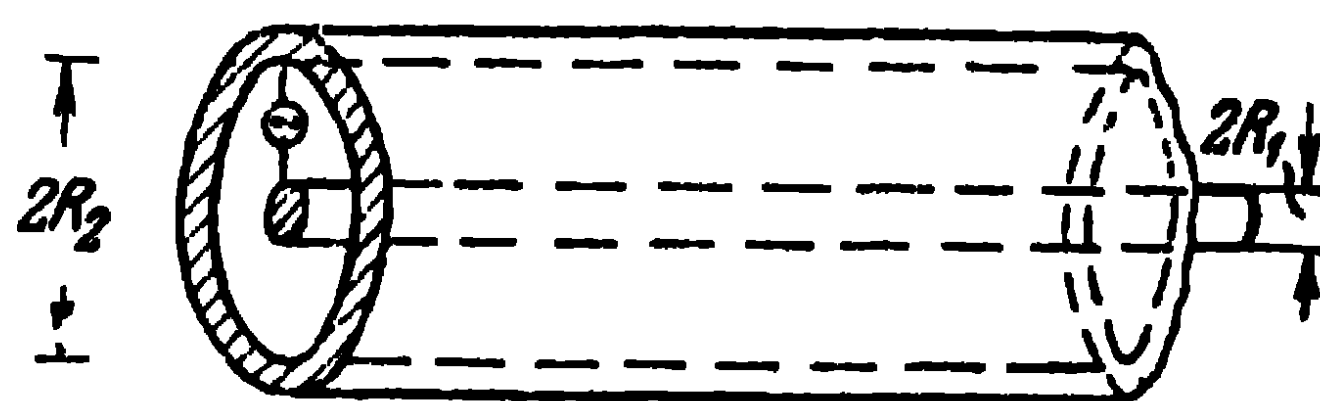
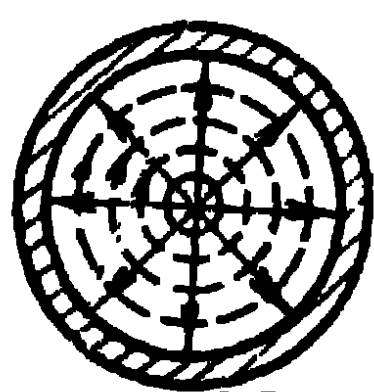


Fig. 7-10. Excitation of a coaxial line.

of the line. Usually, the TEM wave is excited in a coaxial line by a transverse electric dipole in accordance with the circuit shown in Fig. 7-10, i.e., simply by connecting the terminals of the emf generator to the internal and external conductors of the line. Of course, a dipole of this kind excites also higher modes, but the transverse dimensions chosen for the coaxial



——— *Electric lines of force*

- - - *Magnetic lines of force*

Fig. 7-11. The field in a coaxial line.

line are much smaller than the operating wave-length so that these higher modes are quickly damped and at a certain small distance from the point where the generator is connected, there remains only the TEM wave. The picture of the field of this wave is shown in Fig. 7-11.

The electric lines of force begin on the internal conductor and terminate on the external conductor and have only the radial components. The magnetic lines of force form circles surrounding the internal conductor and have only the azimuth components. The currents corresponding to this mode have only longitudinal components; furthermore, the current on the internal conductor equals that on the external conductor and is of opposite direction.

It is easy to show that the field of the transverse electromagnetic wave in an infinite coaxial line is described by the expressions

$$\begin{aligned} E_r &= \frac{C}{r} e^{-ikz}, \\ H_\varphi &= \frac{k}{\omega\mu} \frac{C}{r} e^{-ikz}, \end{aligned} \quad (7-75)$$

where the constant C depends on the power of the source.

Indeed, in cylindrical coordinates, when $E = E_r$ and $H = H_\varphi$, Maxwell's equations (I-1) will be written as:

$$\begin{aligned} -\frac{\partial H_\varphi}{\partial z} &= i\omega\epsilon E_r, \\ -\frac{\partial E_r}{\partial z} &= i\omega\mu H_\varphi, \end{aligned} \quad (7-76)$$

and the substitution of (7-75) into (7-76) shows immediately that the expressions (7-75) satisfy Maxwell's equations. These expressions also satisfy the boundary conditions on the walls of the line.

The ratio of the electric field intensity to the magnetic field intensity defines the wave impedance of the medium which fills the line,

$$\frac{E_r}{H_\varphi} = \frac{\omega\mu}{k} = \sqrt{\frac{\mu}{\epsilon}}. \quad (7-77)$$

The voltage in the z -section of the line will be defined from

$$U_z = \int_{r=R_1}^{R_2} E_r dr = C \ln \frac{R_2}{R_1} e^{-ikz}, \quad (7-78)$$

where R_1 is the radius of the internal conductor of the line;

R_2 , the internal radius of the external wire (tube) of the line.

The current on the internal conductor is defined from

$$I_z = 2\pi r H_\varphi = C 2\pi \frac{k}{\omega\mu} e^{-ikz}. \quad (7-79)$$

The wave impedance of the coaxial line will be defined as the ratio of the voltage to the current of the line and will equal:

$$W = \sqrt{\frac{\mu}{\epsilon}} \frac{1}{2\pi} \ln \frac{R_2}{R_1}. \quad (7-80)$$

If the transverse dimensions of the coaxial line are not small in comparison with the length of the excited wave, then, apart from the TEM wave, waves of the H_{nm} and E_{nm} modes can be propagated in the line and, in the first place, a transverse electric wave similar to the H_{01} wave in a rectangular waveguide. The critical wave-length of this mode is defined from the approximate expression

$$\lambda_{\text{crit}} \approx 2\pi \frac{R_1 + R_2}{2}, \quad (7-81)$$

i.e., it equals the length of the mean perimeter of the cross section of the coaxial line. And if the wave-length of the oscillations corresponding to the propagation in an unbounded space is smaller than $\pi (R_1 + R_2)$, then the wave of the mode under consideration will be propagated along the line and superposed on the main wave. Usually, a superposition of this kind is undesirable, so that the transverse dimensions of the line are chosen on the basis of the condition

$$\lambda_{\text{oper}} > \pi (R_1 + R_2) \quad (7-82)$$

The condition (7-82) limits the application of the coaxial line to the three-centimetre and shorter ranges of radio waves.

Coaxial cables also belong to the class of coaxial lines; they differ from rigid coaxial lines by their flexibility. The wave used in coaxial cables is the TEM wave, described by the expressions (7-75)-(7-80).

7-5. Single-Wire Line Theory

The utilisation of single-wire transmission lines with a surface wave is of recent date, although the possibility of the propagation of a symmetrical surface wave along a cylindrical conductor of finite conductivity was established by Sommerfeld as far back as 1899[31]. The reason is that the field of the wave investigated by Sommerfeld has a large extension in the space surrounding the conductor and requires therefore that a considerable part of the space surrounding the line should be free from obstacles. Furthermore, a very cumbersome exciting device is necessary to bring about an efficient excitation of the Sommerfeld wave. In 1950, Goubau [32] showed that if the surface of the wire was ribbed or covered with a layer of dielectric, then even in the case of a conductor of ideal conductivity, the field of

the surface wave would be excited and would, in the main, be concentrated in the vicinity of the wire; its extension in the transverse plane could be made insignificant and the exciting device of the acceptable dimensions.

A schematic illustration of a single-wire transmission line is shown in Fig. 7-12. It consists of a thin circular con-

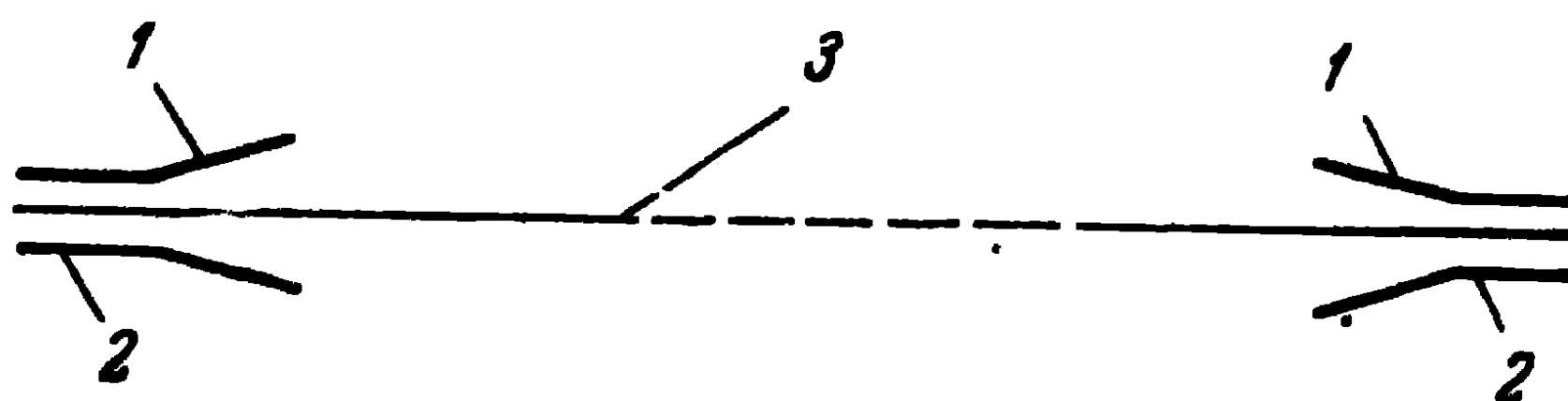


Fig. 7-12. Circuit of a single-wire transmission line:

1—horn; 2—coaxial line; 3—single-wire line

ductor covered with a layer of dielectric, and of coaxial lines at the transmitting and receiving ends with conical horn transitions. Owing to the presence of the dielectric layer on the internal conductor, the transverse electromagnetic wave (TEM) which is propagated in the coaxial line reaches the horn transition and is gradually transformed into a

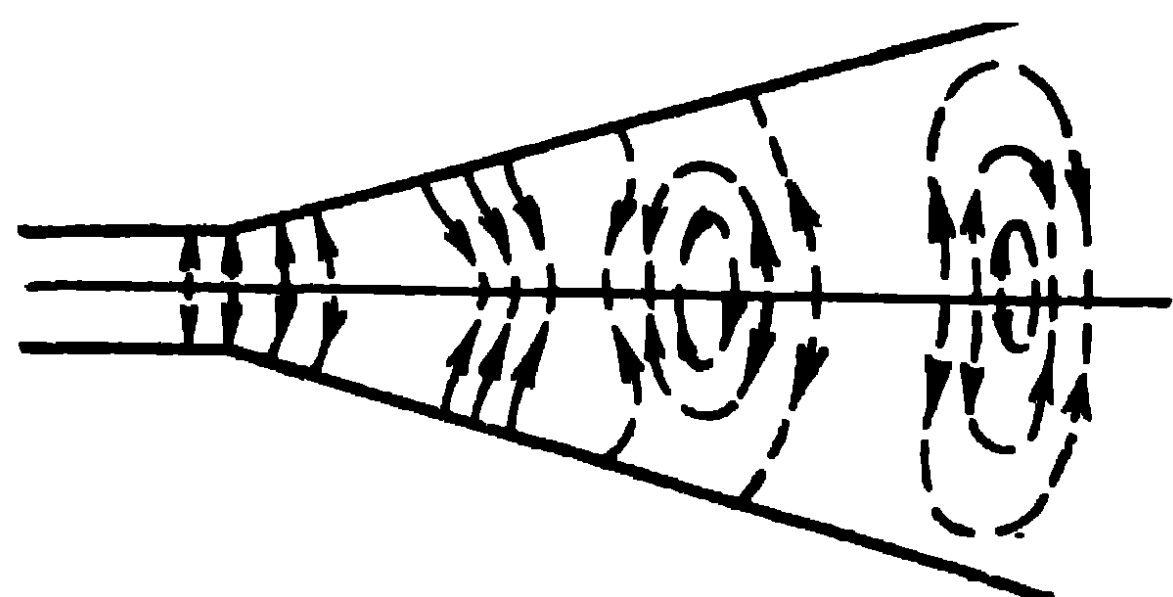


Fig. 7-13. Picture of the electric lines of force in a horn transition.

transverse magnetic wave, as shown in Fig. 7-13. On leaving the horn, the transverse magnetic wave of the surface mode E_0 is propagated along the single-wire line. On reaching the horn transition at the receiving end, this surface wave is gradually transformed in

the horn into a transverse electromagnetic wave which is further propagated in the coaxial line.

Let us investigate the theory of the single-wire line. The radius of the wire without a dielectric covering is a and, the radius of the wire with a dielectric covering a' .

The wave excited in the line has only a transverse component of the magnetic field intensity $H = H_\varphi$, so that in cylindrical coordinates, Maxwell's equations (I-1) will be written as:

$$-\frac{\partial H_\varphi}{\partial z} = i\omega\epsilon_0 E_r, \quad \frac{1}{r} \frac{\partial}{\partial r} (r H_\varphi) = i\omega\epsilon_0 E_z \quad (7-83)$$

for the first equation and

$$\frac{\partial E_r}{\partial z} - \frac{\partial E_z}{\partial r} = -i\omega\mu_0 H_\varphi \quad (7-84)$$

for the second one.

Substituting (7-83) into (7-84), we obtain for the magnetic field intensity, the following wave equation:

$$\frac{1}{r} \frac{\partial}{\partial r} \left(r \frac{\partial H_\varphi}{\partial r} \right) + \frac{\partial^2 H_\varphi}{\partial z^2} + k_0^2 H_\varphi - \frac{H_\varphi}{r^2} = 0, \quad (7-85)$$

where k_0 is the wave number (coefficient of phase) for free space.

It is readily seen by a direct substitution, that the solution of the equation (7-85) will be written as:

$$H_\varphi = A e^{-ihz} H_1^{(2)}(\gamma r), \quad (7-86)$$

where $H_1^{(2)}(\gamma r)$ is a Hankel function of the second order;

$\gamma = -i\sqrt{h^2 - k_0^2}$, the propagation constant in a radial direction;

h , the propagation constant in the direction of the z -axis.

Substituting (7-86) into (7-83) and taking into account that $\frac{1}{r} \frac{\partial}{\partial r} [r H_1^{(2)}(\gamma r)] = \gamma H_0^{(2)}(\gamma r)$, we obtain for the components of the electric field intensity, the following expressions:

$$\begin{aligned} E_r &= A \frac{h}{\omega \epsilon_0} e^{-ihz} H_1^{(2)}(\gamma r); \\ E_z &= A \frac{\gamma}{i\omega \epsilon_0} e^{-ihz} H_0^{(2)}(\gamma r). \end{aligned} \quad (7-87)$$

In order that the field expressed by (7-86) and (7-87) should be able to exist, the covering of the wire should possess a definite surface resistance, by which we understand the ratio of the tangential component of the electric field intensity to the tangential component of the magnetic field intensity on the surface of the layer. Let Z_s be this surface resistance. Then

$$Z_s = \frac{E_z}{H_\varphi} \text{ when } r = a'. \quad (7-88)$$

Substituting here (7-86) and (7-87), we obtain:

$$Z_s = \frac{\gamma}{i\omega\epsilon_0} \frac{H_0^{(2)}(\gamma a')}{H_1^{(2)}(\gamma a')}. \quad (7-89)$$

We are dealing with a radius of the wire and a thickness of the dielectric layer that are small in comparison with the wave-length and we shall therefore assume $|\gamma a'| \ll 1$. On that condition, the Hankel functions will approximately equal:

$$\begin{aligned} H_0^{(2)}(\gamma a') &\approx -\frac{2i}{\pi} \ln \left(0.89a' \sqrt{h^2 - k_0^2} \right); \\ H_1^{(2)}(\gamma a') &\approx -\frac{2}{\pi} \frac{1}{a' \sqrt{h^2 - k_0^2}}. \end{aligned} \quad (7-90)$$

Then, the equation (7-89) will be written as:

$$Z_s \approx \frac{(h^2 - k_0^2) a'}{i\omega\epsilon_0} \ln \left(0.89a' \sqrt{h^2 - k_0^2} \right). \quad (7-91)$$

In the case of a surface reactance of the covering of the wire, the equation (7-91) is satisfied on condition that this reactance is of an inductive nature and if $h > k_0$.

Note that the asymptotic expression of Hankel function is as follows:

$$H_1^{(2)}(\gamma r) \approx \sqrt{\frac{2}{\pi \gamma r}} e^{-i \left(\gamma r - \frac{3}{4}\pi \right)}$$

and since, when $h > k_0$, the propagation constant γ is a negative imaginary quantity, the field diminishes exponentially in a radial direction, and the larger the quantity γ , i.e., the more h differs from k_0 , the faster the field is damped when the point of observation moves away from the wire. Such a wave is called a surface wave and since the phase velocity v is smaller than that of light c , it is also called a slow wave.

Let us also define the relative power conveyed by a surface wave through a cylindrical surface of radius ρ , surrounding the wire. In accordance with (1-10), the power conveyed through a surface of radius $\infty > r > \rho$ will be defined from the expression:

$$P_0 = \frac{1}{2} \int_{r=\rho}^{\infty} E_r H_\phi^* 2\pi r dr. \quad (7-92)$$

The full power P , conveyed outside the wire, will be obtained if in the expression (7-92), the lower limit be extended as far as the surface of the wire $r=a'$. Then, the relative power with which we are concerned will be defined by the expression $(1-P_p/P)$. The substitution of the expressions E_r and H_φ from (7-86) and (7-87) into (7-92) leads to the

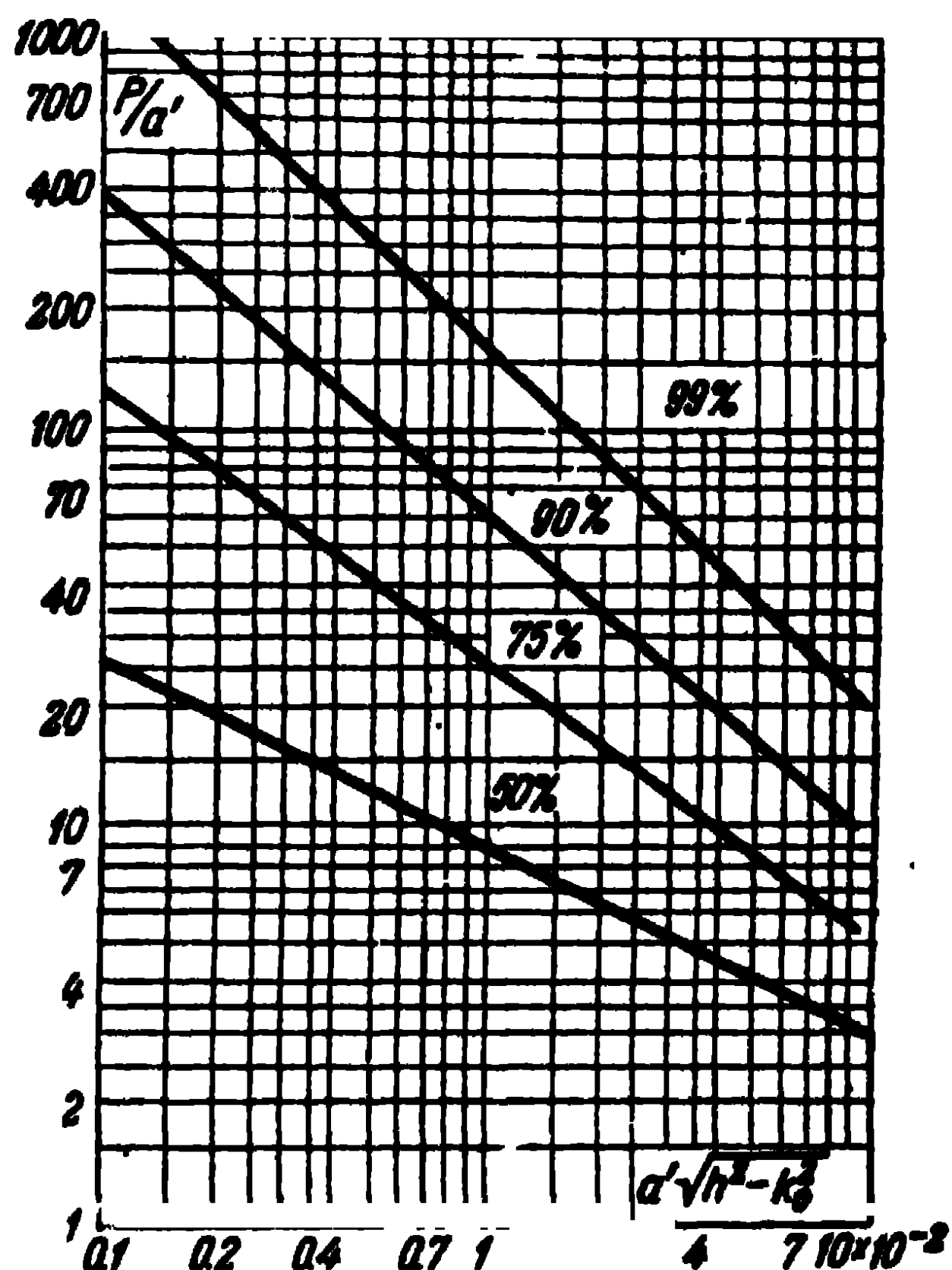


Fig. 7-14. Relative radii of a cylindrical surface inside which 50, 75, 90 and 99% of the power are propagated.

necessary calculation formula which we do not give here. The calculation based on this formula is represented in the form of graphs in Fig. 7-14, which shows the relative radii of the cylindrical surfaces ρ/a' inside which 50, 75, 90 and 99% of the total power conveyed by the surface wave is propagated, depending on the quantity $a'\sqrt{h^2-k_0^2}$.

We notice that an increase of $\sqrt{h^2-k_0^2}$, being prescribed, leads to the decrease of the radius of the cylindrical surface inside which a definite part of the power is conveyed. Let, for example,

$$a' = 1\text{cm}, \sqrt{h^2-k_0^2} = 2 \times 10^{-2}.$$

Then, 50% of the power is conveyed inside a cylinder of radius $\rho=6$ cm, 75% of the power is conveyed inside a cylinder of $\rho=16$ cm, 90% of the power is conveyed inside a cylinder of $\rho=33$ cm and 99% of the power is conveyed inside a cylinder of $\rho=86$ cm.

Apparently, the radius of the output opening of the conical transition of a line should correspond to the radius of a cylinder inside which the largest part of the power is being conveyed. In that case, when the TEM wave in a coaxial line is transformed into an E_0 wave in a homogeneous line, the largest part of the power will be contained in the surface wave and the smallest part, in the higher modes. The higher modes determine the radiation from the open end of a conical horn and lead to the decrease of the overall efficiency of the line.

Now, let us see how the surface resistance Z_s depends on the dielectric layer. The field in the layer obeys the equations (7-83)-(7-85) when ϵ_0 is replaced in them by ϵ and k_0 by k . In this case, the solution of the equation (7-85) is similar to the expression (7-86) except that instead of the second Hankel function, we must take in it the linear combination of the second and first Hankel functions. However, owing to the fact that the radius of the wire is small in comparison with the wave-length and the thickness of the layer is small in comparison with the radius of the wire, the magnetic field intensity inside the dielectric layer ($a' > r \geq a$) may be written in approximately the following form:

$$H_\varphi \simeq \frac{I_0}{2\pi r} e^{-ihz}, \quad (7-93)$$

where I_0 is the current in the wire at the cross section $z=0$.

This expression is accurate on the surface of the wire when $r=a$. When $r > a$, the error will not be large.

Substituting the expression (7-93) into the equation (7-83) and replacing ϵ_0 by ϵ , we obtain:

$$E_r \approx \frac{I_0}{2\pi r} \frac{h}{\omega\epsilon} e^{-ihz}. \quad (7-94)$$

Substituting further (7-93) and (7-94) into the equation (7-84), we have:

$$\frac{dE_z}{dr} = \frac{I_0}{2\pi r} \frac{h^2 - k^2}{i\omega\epsilon} e^{-ihz}. \quad (7-95)$$

Integrating this expression from a to r , we obtain:

$$E_z = \frac{I_0}{2\pi} \frac{h^2 - k^2}{i\omega\epsilon} \ln \frac{r}{a} e^{-ikz}. \quad (7-96)$$

It can be seen from (7-96) that, when $r=a$, $E_z=0$. Thus the expressions (7-93), (7-94) and (7-96) approximately satisfy Maxwell's equations and accurately satisfy the boundary conditions on the surface of the conductor.

Dividing E_z by H_φ and assuming that $r=a'$, we shall find the surface resistance of the dielectric layer

$$Z_s = \frac{h^2 - k^2}{i\omega\epsilon} a' \ln \frac{a'}{a}. \quad (7-97)$$

This resistance will have an inductive nature on condition that $h < k$. Thus, the surface wave is propagated with a phase velocity determined from the condition $k_0 < h < k$, i.e., the phase velocity of propagation lies within the interval

$$\frac{v_{r.w}}{\sqrt[4]{\epsilon/\epsilon_0}} < v < v_{r.w} \quad (7-98)$$

where $v_{r.w}$ is the velocity of propagation of radio waves in free space.

Regarding the expressions (7-91) and (7-97) as equal, we obtain:

$$\ln \frac{a'}{a} = \frac{\epsilon}{\epsilon_0} \frac{h^2 - k_0^2}{h^2 - k^2} \ln (0.89a' \sqrt{h^2 - k_0^2}). \quad (7-99)$$

Let us consider thin dielectric layers, for which $h^2 - k_0^2 \ll k_0^2$. Then, we may assume that $h^2 - k^2 \approx k_0^2 - k^2$ and write the expression (7-99) as:

$$\ln \frac{a'}{a} = \frac{\epsilon}{\epsilon - \epsilon_0} \left(\frac{\lambda_0}{a'} \right)^2 G \left(a' \sqrt{h^2 - k_0^2} \right), \quad (7-100)$$

where

$$\begin{aligned} G \left(a' \sqrt{h^2 - k_0^2} \right) &= \\ &= - \left(\frac{a' \sqrt{h^2 - k_0^2}}{2\pi} \right)^2 \ln (0.89a' \sqrt{h^2 - k_0^2}). \end{aligned} \quad (7-101)$$

The function G is represented in the form of a graph in Fig. 7-15.

Here is an example of calculation of a line. Let the radius of the line $a' = 1$ cm, the wave-length $\lambda_0 = 50$ cm and the radius of the cylindrical surface, inside which 90% of the

power is transmitted, $q=50$ cm. What will be the thickness of the dielectric layer if $\epsilon/\epsilon_0=4$?

From Fig. 7-14 we find that for the values q/a' , which correspond to 50 and 90% of the transmitted power, the quantity $a'\sqrt{h^2-k_0^2}$ equals 1.21×10^{-2} . The quantity G corresponding to this value is found from Fig. 7-15: it equals

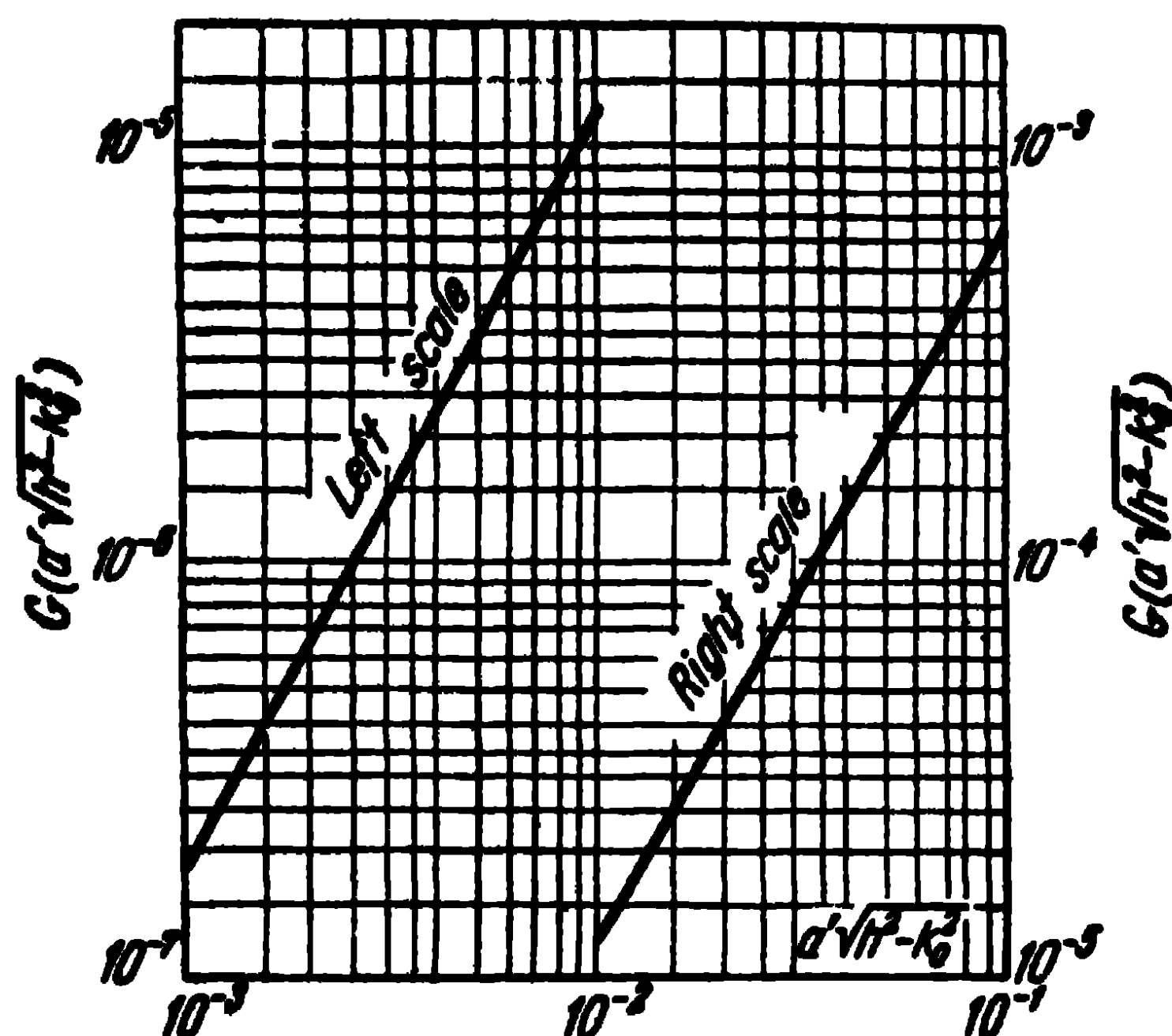


Fig. 7-15. Curves for determining the G function in the expression (7-100).

1.68×10^{-5} . Substituting this value G into (7-100), we find that the thickness of the dielectric layer should, in this case, equal 5.6×10^{-2} cm.

7-6. Other Transmission Lines

Apart from the transmission lines examined above, other lines have appeared in recent years.

Among them we have the so-called H -like waveguide of the open type with a surface electromagnetic wave [33]. The waveguide consists, as shown in Fig. 7-16, of the two parallel metal plates of width h , separated by a dielectric plate of thickness a . A surface electromagnetic wave, the energy of which is concentrated in the vicinity of the dielectric plate, may propagate along a waveguide of this kind. The amplitude of the field of this wave decreases

exponentially in the direction of the x -axis of the waveguide, and, in case the metal plates have a sufficient width h , almost all the energy conveyed by the electromagnetic wave is concentrated in the space between the plates and only an insignificant part of it is radiated through the open lateral walls of the waveguide.

The approximate theory of the H -like waveguide is relatively simple to build. Let the metal plates be ideal conductors and of infinite extension not only in the direction of the z -axis but also in the direction of the x ($h = \infty$)-axis. Let the parameters of the dielectric plate be ϵ , μ_0 , $\sigma = 0$ and the parameters of the surrounding medium, ϵ_0 , μ_0 , $\sigma = 0$. Assume that the vector potential of the electromagnetic wave has only the x -th component $A^e = A_x^e$.

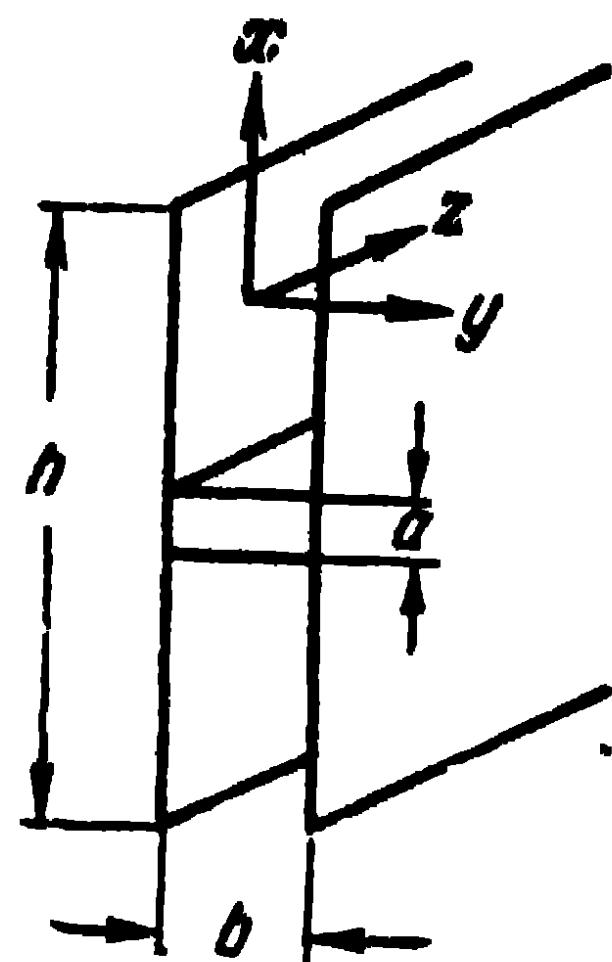


Fig. 7-16. H-shaped waveguide.

The vector potential inside the dielectric plate obeys the wave equation

$$\frac{\partial^2 A_x^e}{\partial x^2} + \frac{\partial^2 A_x^e}{\partial y^2} + \frac{\partial^2 A_x^e}{\partial z^2} + k^2 A_x^e = 0, \quad (7-102)$$

where

$$k = \omega \sqrt{\epsilon \mu_0},$$

and the components of the magnetic and electric field vectors are defined from the equations

$$\left. \begin{aligned} H_x &= 0, \quad H_y = \frac{\partial A_x^e}{\partial z}, \quad H_z = -\frac{\partial A_x^e}{\partial y}; \\ E_x &= \frac{1}{i\omega\epsilon} \left(k^2 A_x^e + \frac{\partial^2 A_x^e}{\partial x^2} \right), \quad E_y = \frac{1}{i\omega\epsilon} \frac{\partial^2 A_x^e}{\partial y \partial x}, \\ E_z &= \frac{1}{i\omega\epsilon} \frac{\partial^2 A_x^e}{\partial z \partial x}. \end{aligned} \right\} \quad (7-103)$$

The electromagnetic field outside the dielectric plate is defined from the same equations (7-102) and (7-103) by replacing k and ϵ by k_0 and ϵ_0 respectively.

The boundary conditions on the surface of the metal plates consist in that the tangential components of the electric field intensity equal zero, and on the surface of the

dielectric plates, in that the tangential components of the electric and magnetic fields intensities are continuous.

Thus, the boundary conditions relatively to the field vectors will be satisfied if the following conditions are imposed on the vector potential

$$\left. \begin{aligned} A_{x \text{ air}}^e &= A_{x \text{ die}}^e = 0 \text{ when } y = \pm \frac{b}{2}; \\ A_{x \text{ air}}^e &= A_{x \text{ die}}^e \text{ when } x = \pm \frac{a}{2}; \\ \frac{1}{\epsilon_0} \frac{\partial A_{x \text{ air}}^e}{\partial x} &= \frac{1}{\epsilon} \frac{\partial A_{x \text{ die}}^e}{\partial x} \text{ when } x = \pm \frac{a}{2}. \end{aligned} \right\} \quad (7-104)$$

We are interested in the lowest mode, propagated along the axis of the waveguide and decreasing exponentially outside the dielectric in the direction of the x -axis. Inside the dielectric, there will be a standing wave in the x -axis direction. In the y -axis direction, inside as well as outside the dielectric, there will also be a standing wave. Accordingly, the solution of the wave equation (7-102) will be written as:

$$\left. \begin{aligned} A_{x \text{ die}}^e &= A_0^e \cos k_x x \cos \frac{\pi}{b} y e^{-\alpha z}; \\ A_{x \text{ air}}^e &= A_0^e \frac{\cos k_x \frac{a}{2}}{e^{-\beta \frac{a}{2}}} e^{\mp \beta x} \cos \frac{\pi}{b} y e^{-\alpha z}. \end{aligned} \right\} \quad (7-105)$$

These solutions will satisfy the boundary conditions (7-104) if we impose on the wave number k_x and the attenuation constant β the condition

$$\beta = \frac{\epsilon_0}{\epsilon} k_x \tan k_x \frac{a}{2}. \quad (7-106)$$

On the other hand, from the substitution of (7-105) into (7-102), we obtain the equations

$$\left. \begin{aligned} k^2 - k_x^2 &= \alpha^2 + \left(\frac{\pi}{b} \right)^2; \\ k_0^2 + \beta^2 &= \alpha^2 + \left(\frac{\pi}{b} \right)^2. \end{aligned} \right\} \quad (7-107)$$

From the equations (7-106) and (7-107) we may determine the quantities α , β and k_x , depending on the transverse dimensions of the waveguide and the permittivity of the plate.

Fig. 7-17 shows the curves of the ratio of the wave-length in free space λ_0 to the wave-length λ_x and the curve of the attenuation of β in a transverse direction, as a function of the ratio $\frac{a}{\lambda_0}$ for $\epsilon/\epsilon_0=2.53$.

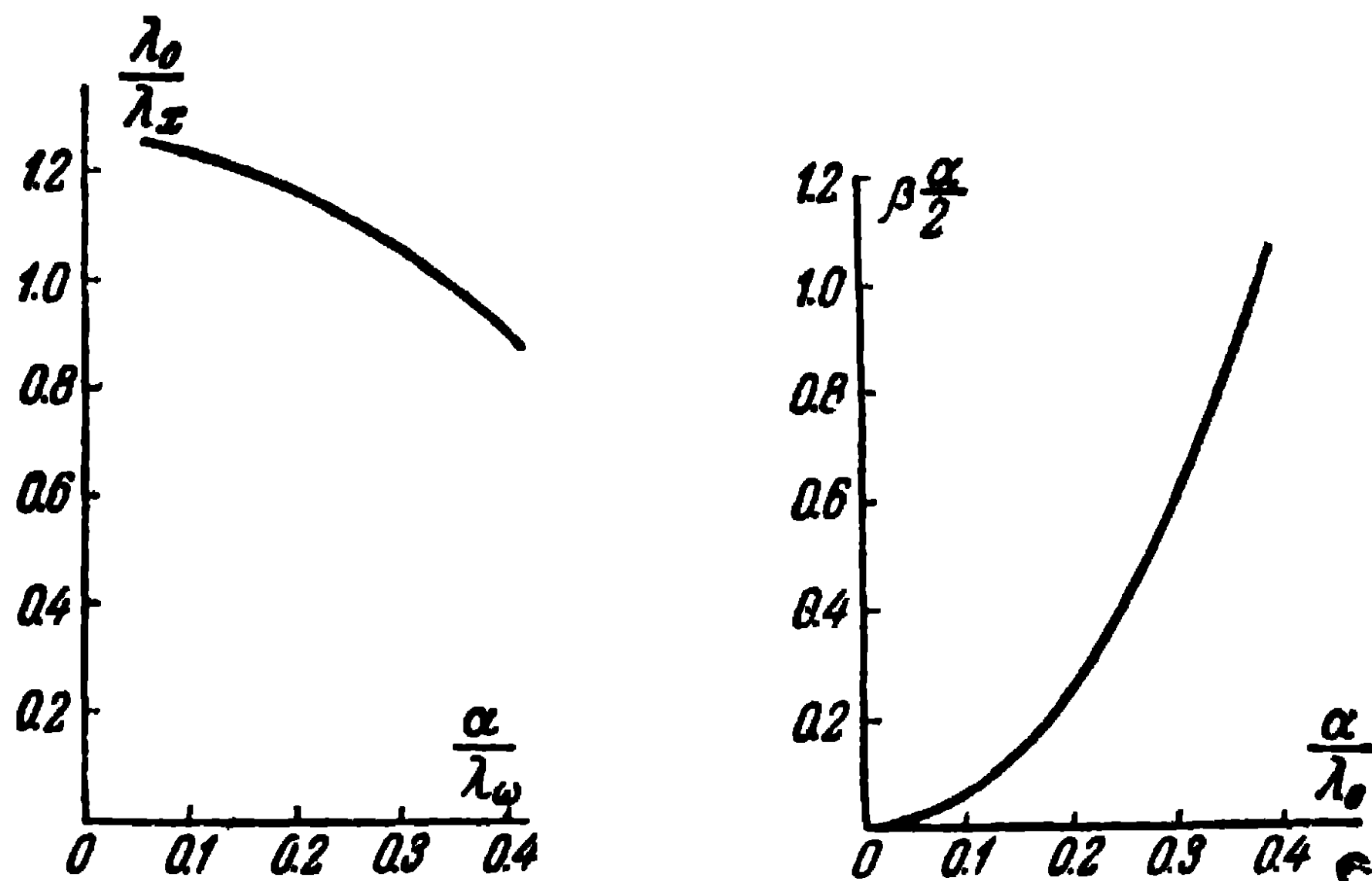


Fig. 7-17. The relative wave-length λ_x and attenuation β in an H-like waveguide.

Fig. 7-18 shows the relative wave-length in the waveguide λ_w depending on the transverse dimensions of the waveguide a and b . In the expressions cited, we have taken the following designations:

$$k_x = \frac{2\pi}{\lambda_x}, \quad k_0 = \frac{2\pi}{\lambda_0}, \quad \alpha = \frac{2\pi}{\lambda_w}.$$

Thus, in the system under consideration, there arises a surface wave, the phase velocity and wave-length of which may be determined from the curves in Fig. 7-18 and the decrease in a transverse direction, from the curve in Fig. 7-17. We see that at a certain, comparatively short distance from the dielectric plate, the field decreases to such an extent that one may considerably reduce the dimensions of the metal plates in the direction of the x -axis, without substantially changing the picture of the field in the waveguide and, consequently, without any substantial radiation of such a waveguide.

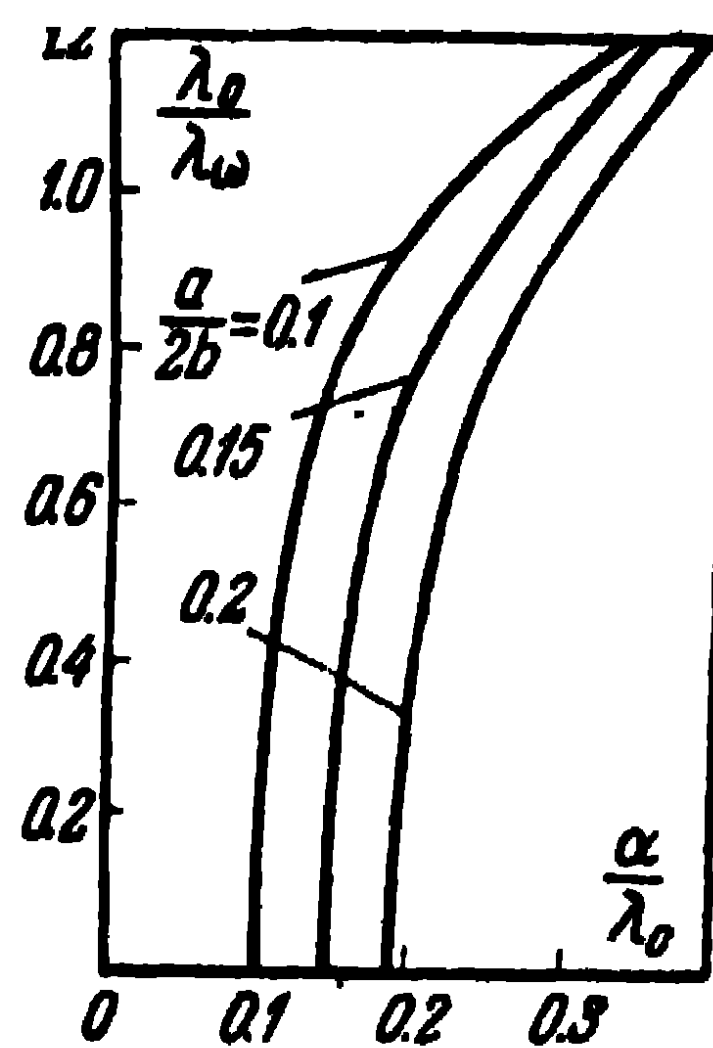


Fig. 7-18. Dependence of the wave-length in a waveguide on its transverse dimensions.

Fig. 7-19 shows the graphs of the dependence of the ratio of the power propagated along a waveguide in the vicinity of a dielectric plate within the limits of the width h to the full power propagated along a waveguide with infinite surfaces when $\epsilon/\epsilon_0=2.53$. From these curves, one may determine the transverse dimensions of the waveguide for a ratio of the powers $\frac{P_{\text{ext}}}{P_{\text{full}}}=0.001$; 0.01 and 0.1.

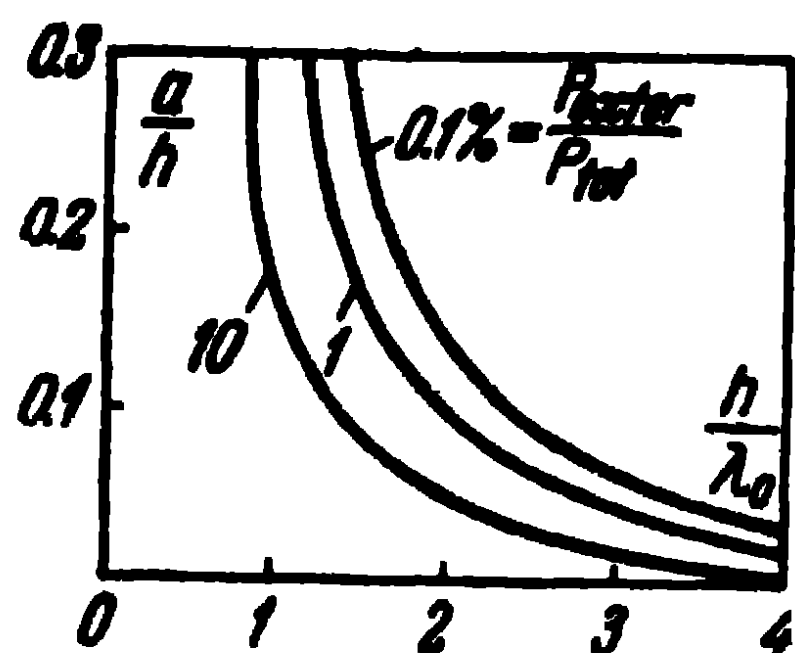


Fig. 7-19. Dependence of the transmitted power on the transverse dimensions of a waveguide.

Note that only transverse components of the electric currents arise on the metal plates, since $H_x=0$. This is quite a favourable circumstance since it enables to dispense with waveguide flanges when joining the separate sections of the waveguide.

Among the relatively new transmission lines used in the microwave range, we also find the strip waveguide, the cross section of which is shown in Fig. 7-20.

The line consists of a main plate, which plays the role of a screen, of a thin layer of dielectric and of a metal strip printed onto the dielectric. The dielectric is usually polystyrene and the strip is made from copper, silver or some other metal.

The dimension of the strip b and the thickness of the

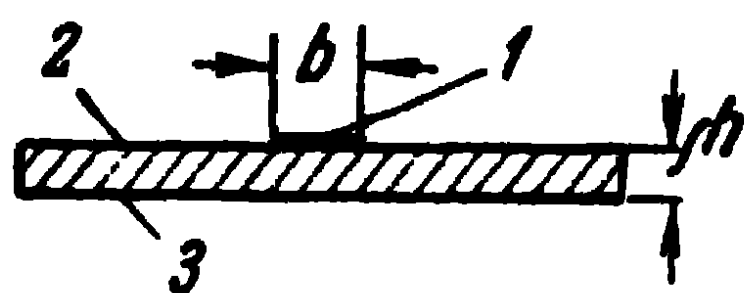


Fig. 7-20. Cross section of a strip line:
1—metal strip; 2—dielectric;
3—main plate

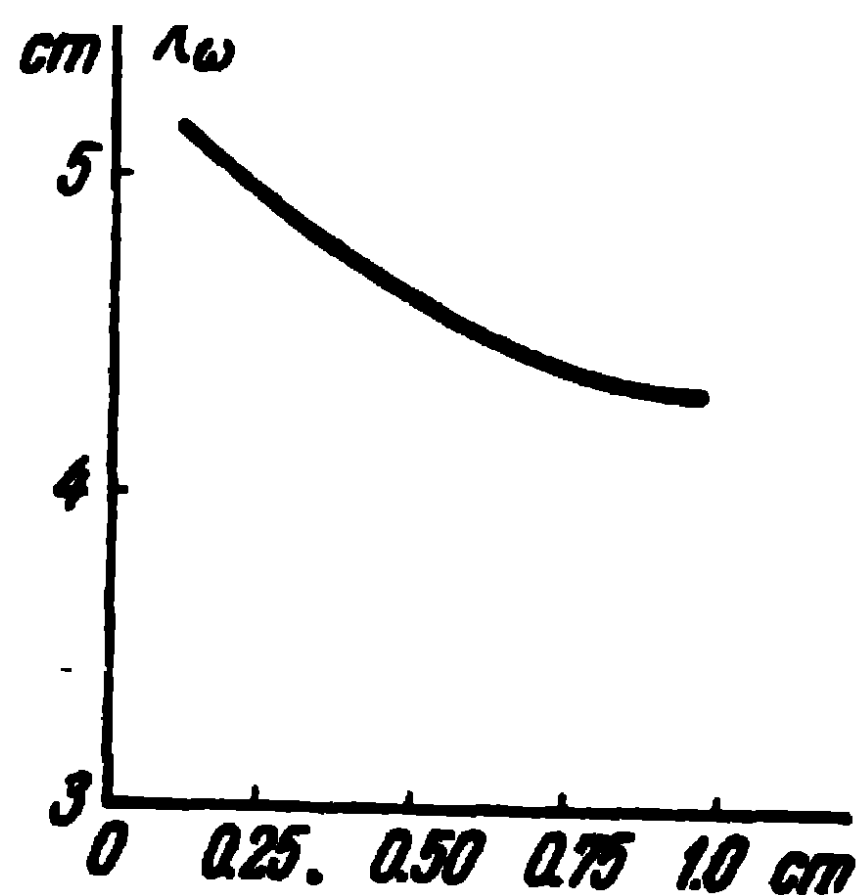


Fig. 7-21. Dependence of the wave-length on the width of the plate ($h=0.15$ cm; $f=4,700$ Mc/s; polystyrene dielectric).

dielectric h are chosen much smaller than the width of the main plate, so that the effect this plate has on the electromagnetic wave can be taken into account by constructing the mirror image of the strip relatively to the main

plate. Thus, one may approximately regard the line as a twin-plate symmetrical feeder along which a transverse electromagnetic wave is propagated.

The main part of the electromagnetic energy propagated along the line is concentrated in the dielectric between the strip and the main plate and this is all the more true as the dimension b of the strip is larger. That is why the wave

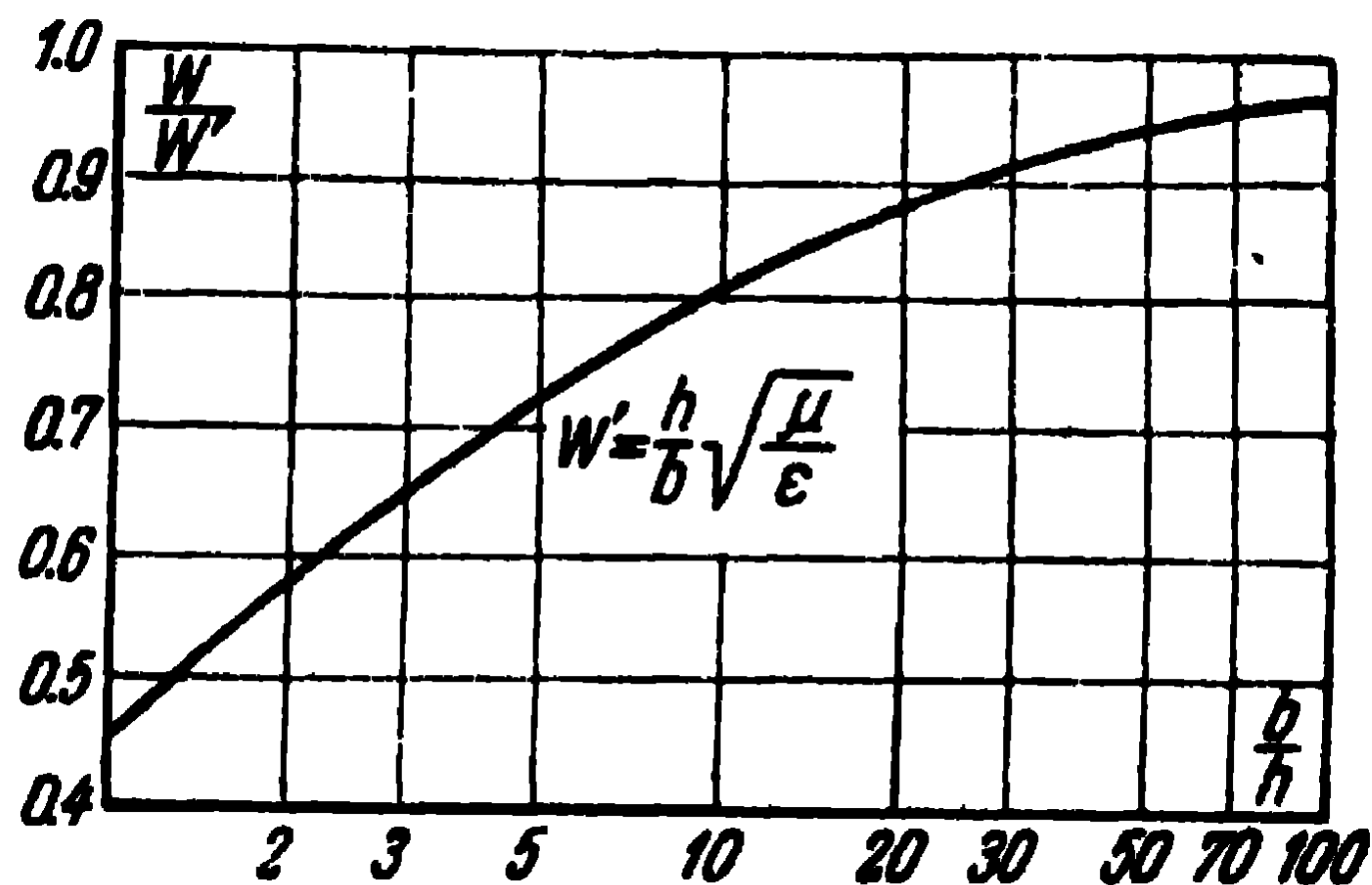


Fig. 7-22. Dependence of the wave impedance of a strip line on its transverse dimensions.

phase velocity in the line is close to that which we would have if the dielectric which surrounds the line were homogeneous. Fig. 7-21 shows the curve which characterises the wave-length in the line, depending on the width of the plate. We see that the wave-length in the line lies in the interval $\lambda_s < \lambda_w < \lambda_0$ where $\lambda_s = \frac{\lambda_0}{\sqrt{\epsilon/\epsilon_0}}$, λ_0 is the wave-length of the oscillations propagated in air.

The wave impedance of a strip line may be determined from the theoretical curve shown in Fig. 7-22 ($W' = \frac{h}{b} \sqrt{\frac{\mu}{\epsilon}}$ is the wave impedance without account of the edge effects in the strip line).

CHAPTER EIGHT

Methods for Matching the Line to the Load

8-1. Twin-Wire Line Equivalent to a Waveguide

In many respects, a waveguide with one unique propagating wave may be reduced to an equivalent twin-wire line. The question arises as to what we are to understand by the voltage, current and wave impedance in this twin-wire line.

To be explicit, let us investigate the H_{01} wave in a rectangular waveguide. As we know, the field of this wave in the waveguide is defined by the expressions (7-15)-(7-17). Passing from the waveguide with an H_{01} wave to an equivalent twin-wire line, the voltage in the latter may be understood to be the integral of the electric field intensity E_{x01} along the x -axis. In this case, we obtain:

$$U_{z>d} = \int_{x=0}^a E_{x01} dx = \frac{2I_x^e i a k^3}{i \omega \epsilon a b \alpha_{01}} \sin\left(\frac{\pi}{b} y\right) \sin\left(\frac{\pi}{b} y'\right) \times \\ \times \sin \alpha_{01} z e^{-i \alpha_{01} z}.$$

We see that the voltage between the walls of the waveguide depends on the transverse coordinate y and, by replacing the waveguide by an equivalent twin-wire line, the definition of the voltage of the latter is found to be non-unique.

The current in the equivalent twin-wire line should naturally be understood to be the longitudinal component of the total current flowing on one of the broad walls of the

waveguide. We obtain:

$$I_{z>d} = \int_{y=0}^b H_{y_{01}} dy = \frac{4I_x^e lb}{iab\pi} \sin\left(\frac{\pi}{b} y'\right) \sin \alpha_{01} e^{-i\alpha_{01} z}.$$

The voltage to current ratio will determine the wave impedance of the equivalent twin-wire line, which will be expressed as:

$$W = \frac{U}{I} = \frac{120\pi}{\sqrt{1 - (\lambda/2b)^2}} \frac{\pi a}{2b} \sin\left(\frac{\pi}{b} y\right), \quad (8-1)$$

where we assumed $\sqrt{\frac{\mu}{\epsilon}} = 120\pi$.

Thus, the wave impedance of the equivalent line is likewise non-unique. To be more certain, the voltage of the equivalent line may be understood as its maximum value in the waveguide. Then, the wave impedance is defined by the expression

$$W = \frac{120\pi}{\sqrt{1 - (\lambda/2b)^2}} \frac{\pi a}{2b}. \quad (8-2)$$

In a similar way, one may compare any mode in a rectangular, circular or other waveguide with the corresponding wave in an equivalent twin-wire line. In so doing, one has to ascribe to the equivalent twin-wire line the phase velocity characteristic of the mode under investigation in the waveguide. As we shall see below, the uncertainty in the choice of the wave impedance of the equivalent line may be removed by introducing the concept of the relative resistance of the line.

8-2. Transmission Lines of Finite Length

We have been considering lines of infinite length and assuming that they guide travelling waves. In practice, any line is finite and has some sort of a load at its end (antenna, receiver input, absorbing resistance, etc.).

In the general case, part of the energy is absorbed in the load and part is reflected from it. That is why there occurs in the line a superposition of the reflected wave on the incident one.

Making use of the concept of the equivalent twin-wire line, one may represent any sort of load as the complex

resistance Z_L , connected to the end of the line (8-1). Then, the voltage and current at the cross section z of the line may be represented by the expressions (we are dealing with lossless lines):

$$\begin{aligned} U_z &= U_{\text{inc}} e^{i\alpha z} + U_0 e^{-i\alpha z}, \\ I_z &= \frac{U_{\text{inc}}}{W} e^{i\alpha z} - \frac{U_0}{W} e^{-i\alpha z}, \end{aligned} \quad (8-3)$$

where U_{inc} is the complex amplitude of the voltage of the incident wave at the end of the line;

U_{refl} , the complex amplitude of the voltage of the reflected wave at the end of the line;

$\alpha = \frac{2\pi}{\lambda_w}$, the phase coefficient;

W , the wave impedance of the line.

One usually introduces the concept of the coefficient of reflection of the wave relative to the voltage, by which one understands the ratio of the voltage of the reflected wave to the voltage of the incident wave at the cross section z of the line:

$$\rho_z = \frac{U_0 e^{-i\alpha z}}{U_{\text{inc}} e^{i\alpha z}} = \rho_0 e^{-i2\alpha z}. \quad (8-4)$$

This expression shows that the coefficient modulus of reflection remains constant whereas its phase changes along the line in accordance with the linear law.

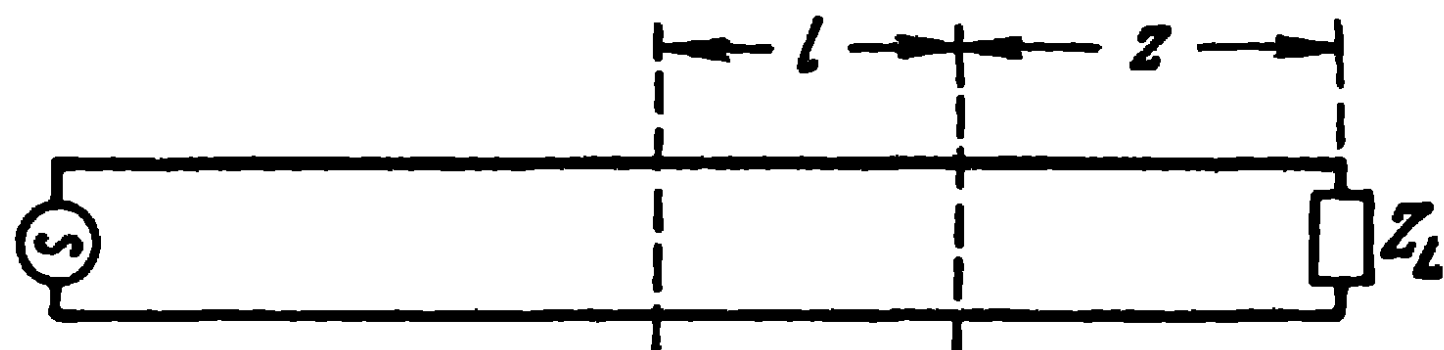


Fig. 8-1. Twin-wire line of finite length.

The ratio of the voltage to the current at the cross section of the line determines the equivalent resistance of the line, expressed as:

$$Z_z = W \frac{1 + \rho_z}{1 - \rho_z}. \quad (8-5)$$

Thus, the equivalent resistance of the line depends only on the wave impedance of the line and on the coefficient of reflection. From (8-5) we obtain the following useful expressions enabling us to determine the coefficient of

reflection from the wave impedance and equivalent resistance of the line or load resistance:

$$\rho_z = \frac{Z_z - W}{Z_z + W}, \quad \rho_L = \frac{Z_L - W}{Z_L + W}. \quad (8-6)$$

By analogy with (8-5), the equivalent resistance of the line at the cross section $l+z$ is defined by the expression

$$Z_{z+l} = W \frac{1 + \rho_{z+l}}{1 - \rho_{z+l}} = W \frac{1 + \rho_z e^{-i2\alpha l}}{1 - \rho_z e^{-i2\alpha l}}.$$

Substituting here the value ρ_z from (8-6), we have:

$$Z_{z+l} = W \frac{\frac{Z_z}{W} + i \tan \alpha l}{1 + i \frac{Z_z}{W} \tan \alpha l}. \quad (8-7)$$

This important expression relates the equivalent resistance at the cross section z of the line to the equivalent resistance at the cross section $z+l$. This expression leads to the following particular expressions:

a) when $\alpha l = 180^\circ$, $Z_{z+\lambda/2} = Z_z$, i.e., the equivalent resistances at cross sections of the line spaced half a wave apart are equal to one another;

b) when $\alpha l = 90^\circ$, $Z_{z+\lambda/4} \cdot Z_z = W^2$, i.e., the product of the equivalent resistances at cross sections of the line spaced a quarter of a wave-length apart is equal to the square of the wave impedance of the line;

c) when $Z_z = W$, $Z_{z+l} = W$, i.e., when the load of the line is equal to the wave impedance, the equivalent resistance of the line at any cross section equals the wave impedance,

d) when $Z_z = 0$, $Z_{z+l} = iW \tan \alpha l$, i.e., when the line is short-circuited, its equivalent resistance becomes reactive and changes along the line in accordance with the tangential law;

e) when $Z_z = \infty$, $Z_{z+l} = -iW \cot \alpha l$, i.e., in the case of an open-end line, its equivalent resistance likewise becomes reactive and changes along the line in accordance with the cotangential law.

Apart from the coefficient of reflection, the concept of the travelling-wave ratio is also introduced, under which the ratio of the voltage at the node to the voltage at the antinode of the line is understood

$$K = \frac{U_{\min}}{U_{\max}}. \quad (8-8)$$

The voltages at the node and antinode are defined by the expressions

$$U_{\min} = |U_a e^{iaz}| - |U_0 e^{-iaz}|;$$

$$U_{\max} = |U_a e^{iaz}| + |U_0 e^{-iaz}|,$$

and the travelling-wave ratio is therefore expressed through the coefficient of reflection by means of the expression

$$K = \frac{1 - |p_0|}{1 + |p_0|}, \quad (8-9)$$

where p_0 is defined from (8-6).

If the load resistance is purely active ($X_L = 0$), the expression (8-9) becomes:

$$K = \frac{1 - \left| \frac{R_L - W}{R_L + W} \right|}{1 + \left| \frac{R_L - W}{R_L + W} \right|},$$

and the travelling-wave ratio is then defined by the simple expressions

$$K = \frac{W}{R_L} \text{ when } R_L > W; \quad K = \frac{R_L}{W} \text{ when } R_L < W. \quad (8-10)$$

Owing to the fact that, in the first case, a voltage antinode is established at the end of the line, R_L represents the resistance of the line at the antinode R_a . In the second case, a voltage node is at the end of the line and, then, R_L represents the resistance at the node R_n .

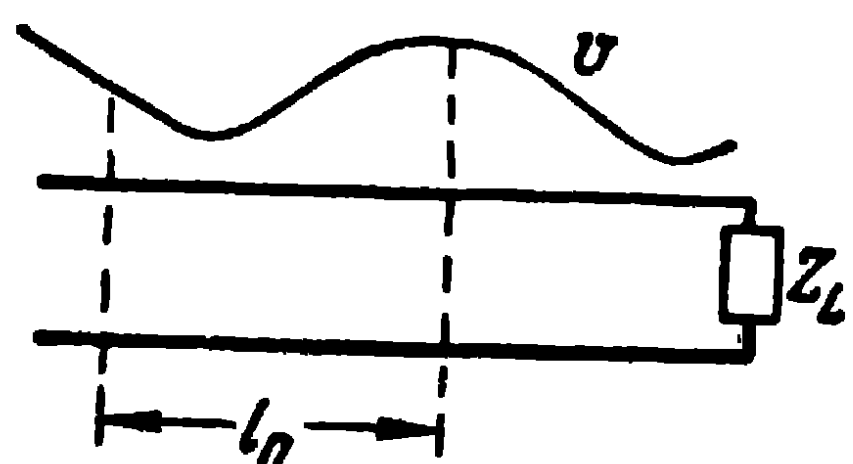


Fig. 8-2. Explaining the calculation of the line equivalent resistance.

The expression (8-8) is used to determine the travelling-wave ratio experimentally, when the voltage at the node and antinode of the line is measured with the

help of a measuring line. The expressions (8-9) and (8-10) are used when the load resistance is known.

Note that instead of the concept of the travelling-wave ratio, the concept of the standing-wave ratio is often used by which we understand a value which is the reverse of the travelling-wave ratio.

It is clear that when in (8-7), the cross section z coincides with the voltage antinode (Fig. 8-2), the resistance Z_z is

purely active. Then $K = \frac{W}{R_a}$ and (8-7) is written as:

$$Zl_a = W \frac{1 + iK \tan \alpha l_a}{K + i \tan \alpha l_a}, \quad (8-11)$$

where l_a is the distance between the voltage antinode towards the generator and the cross section in which the equivalent resistance is defined.

Note that the uncertainty in the expressions (8-5)-(8-11) with regard to the choice of a wave impedance for the twin-wire line equivalent to the waveguide may be removed if we make use of the concept of the relative equivalent resistance of the line $Z'_z = Z_z/W$. Then, the expressions (8-5), (8-7) and (8-11) become:

$$\left. \begin{aligned} Z'_z &= \frac{1 + \rho_z}{1 - \rho_z}; & Z'_{z+l} &= \frac{Z'_z + i \tan \alpha l}{1 + i Z'_z \tan \alpha l}; \\ Z'_{la} &= \frac{1 + iK \tan \alpha l_a}{K + i \tan \alpha l_a}. \end{aligned} \right\} \quad (8-12)$$

Consequently, in order to determine the relative equivalent resistances, the phase coefficient of the line, the travelling-wave ratio and the position of the voltage antinode (or node) on the line have to be known. The equations (8-12) are found to be valid for any transmission line with any mode.

When calculating the input resistance of a line, when re-evaluating the equivalent resistance from one cross section of the line to another, when defining the resistance of the load of the line at prescribed travelling-wave ratio and position of the voltage antinode (node) in the line, as well as in a number of other cases, it is quite convenient to make use of the so-called circular diagrams of impedances [34].

The use of these diagrams reduces the calculations to a minimum and saves much time, whilst the accuracy is quite satisfactory for engineering purposes.

8-3. Narrow-Band Matching of the Line to the Load

The transmission lines connecting a transmitter with an antenna or an antenna with a receiver are usually tuned on a travelling wave.

The travelling-wave type of operation makes it possible to decrease the relative power of the losses and, consequently, to raise the efficiency of the line. This type of operation reduces the voltages in the line, which eliminates the possibility of a breakdown at high transmitted powers. This type of operation is further characterised by the absence of oscillating power in the line, which leads to a widening of the pass-band of the line. Finally, the load on the generator remains constant regardless of the length of the line.

As a rule, the antenna input resistance differs from the wave impedance of the line, so that there is always an electromagnetic wave reflected from the load. To eliminate this reflected wave, some sort of reactive element absorbing

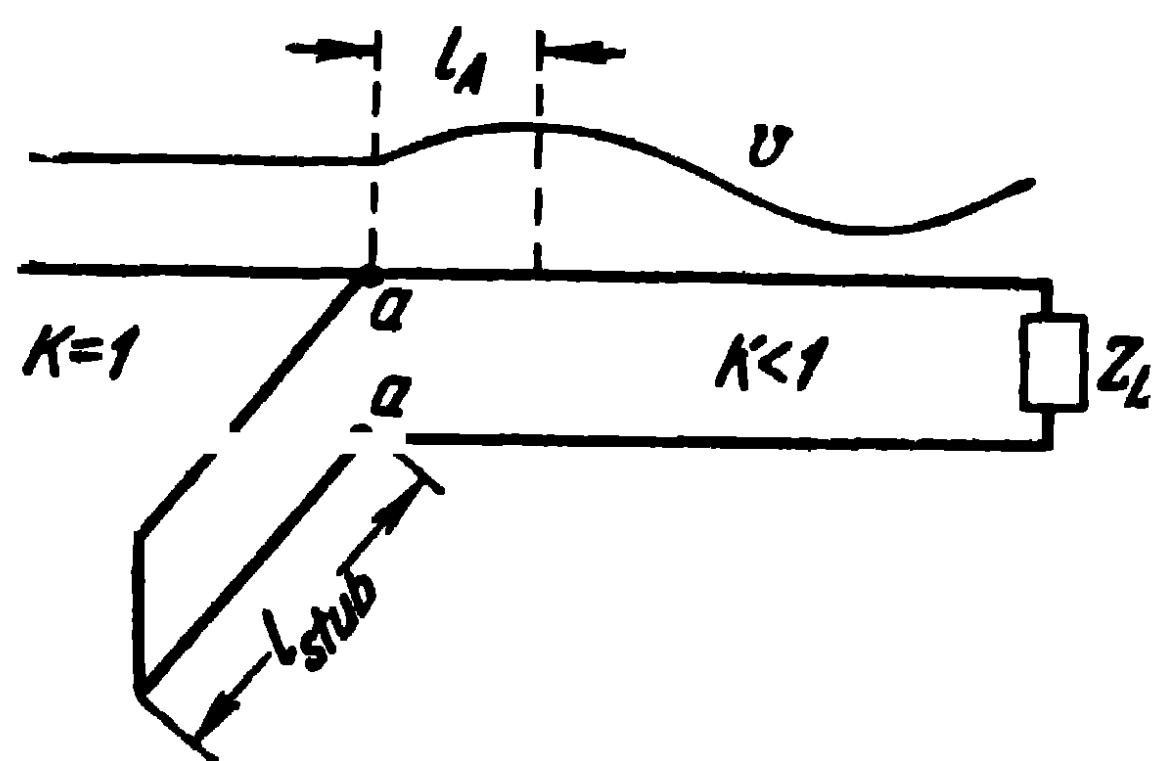


Fig. 8-3. Tuning the line on a travelling wave by means of an inductive stub.

no energy is introduced into the line. Then, in addition to the wave reflected from the antenna, there appears yet another wave, reflected from the reactive element. The proper choice of the size and position of the reactive element makes it possible to level these two waves in amplitude and make them to be opposed in phase. They will then cancel out and

there will only be the travelling wave propagated from the generator towards the load in the region between the connection point of the reactive element and the generator. In the region of the line between the load and the connection point of the reactive element, the type of operation of the line will remain the same all along its length.

V. Tatarinov has shown [2] that to tune the line on a travelling wave, a reactive shunt has to be inserted into it at the cross section where the active part of the equivalent conductivity of the line equals its wave conductivity. At the same time, the conductivity of the inserted shunt should equal the reactive part of the equivalent conductivity of the line at this section and be of opposite sign.

Let the reactive shunt be a close-ended twin-wire stub connected to the line in parallel (Fig. 8-3). Let the wave impedance of the stub equal the wave impedance of the line.

Its resistance will then be:

$$Z_{\text{stub}} = iW \tan \alpha l_{\text{stub}}. \quad (8-13)$$

This resistance is connected in parallel with the resistance of the line at the cross section aa defined by (8-11). Let the total conductivity at the cross section aa of the line equal its wave conductivity

$$\frac{1}{W} \frac{K + i \tan \alpha l_a}{1 + iK \tan \alpha l_a} + \frac{1}{iW \tan \alpha l_{\text{stub}}} = \frac{1}{W}.$$

The real and imaginary parts of the left-hand side being equal to the corresponding ones of the right-hand side, we obtain the following calculation formulas:

$$\cot \alpha l_a = \sqrt{K}, \quad \tan \alpha l_{\text{stub}} = \frac{\sqrt{K}}{1-K}. \quad (8-14)$$

Thus, to determine the length of the stub and the place of its connection into the line, the travelling-wave ratio and the position of the antinode in the line has to be known. These values are usually determined experimentally.

It should be noted that when $K \rightarrow 0$, the length of the stub $l_{\text{stub}} \rightarrow \lambda_w/4$ and $l_a \rightarrow \lambda_w/4$, i.e., the stub is very short and is connected close to the voltage node between this node and the generator. When $K \rightarrow 1$, the length of the stub $l_{\text{stub}} \rightarrow \lambda_w/4$ and $l_a \rightarrow \lambda_w/8$, i.e., in that limit case, the length of the stub is close to a quarter of a wave-length and it is connected close to the points situated at a distance $\lambda_w/8$ from the antinode, towards the generator. Thus, the inductive stub is always connected in the region situated at a distance of an eighth of a wave-length from the voltage node towards the load.

Note also that, apart from an inductive stub, a capacitive stub is also used although more seldom, it is connected into the line in the region comprised between the voltage antinode and the voltage node, towards the load, i.e., where the equivalent resistance of the line is of an inductive nature.

It is evident that, instead of one, two or three reactive elements, lying at a certain distance from one another can be inserted into the line. The proper selection of the impedances of these elements will make it possible to obtain a travelling-wave type of operation; furthermore, these reactive elements may be connected into the line not only in parallel but also in series.

The reactive elements may also consist of lumped inductances or capacitances or combinations of both, connected into the line in series as well as in parallel. Elements of this sort are utilised in the medium and long wave ranges and are investigated in Chapter Twelve.

In waveguides, reactive shunts are made in the shape of stubs and diaphragms; in a coaxial line, the reactive shunt is made in the shape of a segment of coaxial line. We shall dwell on this in greater detail in Chapter Nine. At this stage we shall only point out that the method for obtaining the

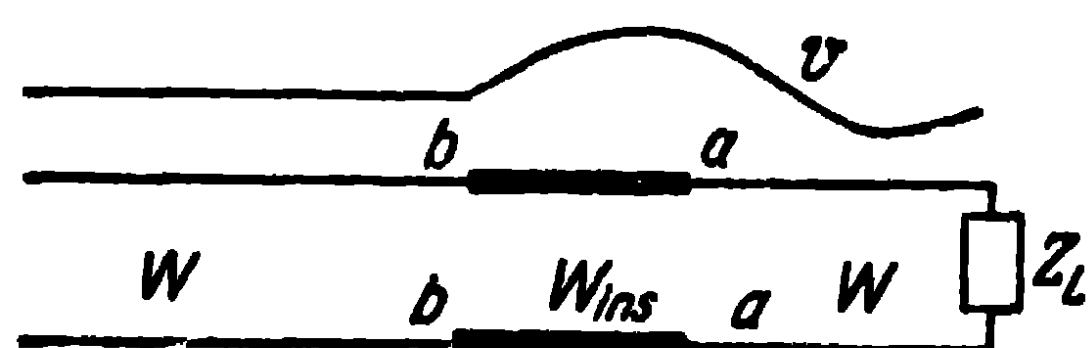


Fig. 8-4. Tuning a line on a travelling wave by means of a quarter-wave-length insert.

travelling-wave type of operation cited above remains valid for any transmission lines.

Note also that it is quite convenient to calculate the parameters of matching stubs by means of the diagram of impedances already mentioned.

Another method for tuning on a travelling wave consists in the insertion into the line of a segment of quarter-wave-length line with another wave impedance, as shown in Fig. 8-4. The quarter-wave-length line is inserted between the voltage node and antinode.

Let the wave impedance of the line which is being tuned equal W and the wave impedance of the quarter-wave-length insert equal W_{insert} . Then, if the insert is connected in the region comprised between the voltage antinode and the voltage node, towards the generator, the equivalent resistance of the line at the points aa will be:

$$R_{aa} = \frac{W}{K},$$

and the equivalent resistance at the points bb of the line will be:

$$R_{bb} = \frac{W_{\text{insert}}^2}{R_{aa}} = \frac{W_{\text{insert}}^2}{W} K.$$

And if the wave impedance of the insert is chosen so that the line equivalent resistance at the points bb be equal to the wave impedance of the principal line $R_{bb} = W$, a travelling wave in the line will thus be set up. Consequently,

the necessary wave impedance of the quarter-wave-length insert is defined from the expression

$$W_{\text{insert}} = W / \sqrt{K}. \quad (8-15)$$

When the quarter-wave-length insert is situated so that there is a voltage node at the points aa , the equivalent resistance of the line at these points equals:

$$R_{aa} = WK.$$

The equivalent resistance at the points bb will then be

$$R_{bb} = \frac{W_{\text{insert}}^2}{R_{aa}} = \frac{W_{\text{insert}}^2}{WK}.$$

Since the resistance is equal to the wave impedance of the principal line $R_{bb} = W$, the condition of the tuning of the line on the travelling wave is obtained here too

$$W_{\text{insert}} = W / \sqrt{K}. \quad (8-16)$$

In the first case, the necessary wave impedance of the quarter-wave-length insert is found to be larger than the wave impedance of the line; in the second case, it is smaller than the wave impedance of the line. The choice of this or that method of tuning is governed by considerations of assembly and of convenience of tuning.

Note that a purely travelling wave in the line occurs only in the region of the line comprised between the generator and the points bb of the insert. In the region of the line from the load to the points aa of the insert, the travelling-wave ratio will remain unchanged. In the region of the insert itself, the travelling-wave ratio will equal \sqrt{K} .

The two methods for tuning the line on a travelling wave cited above ensure the matching of the line to the load in a narrow pass-band, since the tuning of the line is effected on a fixed frequency. A change of frequency will lead to a change of the load resistance on the transmission line, a change of the magnitude of the travelling-wave ratio and of the position of the voltage node and antinode in the line. Consequently, the necessary impedances of the tuning elements and the points at which they are inserted into the line will also change.

The magnitude of detuning of the line in the event of a frequency change is all the larger the greater is the distance

in wave-lengths between the load resistances and the tuning element, because when the difference between these distances is very large, the magnitude of the displacement of the voltage node and antinode along the line is found to be relatively large.

Such a narrow-band matching (with a band of the order of 2%) is quite sufficient for many radio engineering devices. However, it is often necessary that the transmission line should be matched with the load in a wider frequency band (of the order of 5-10%). We shall deal with this point in the next paragraph of the present chapter.

8-4. Broad-Band Matching of the Line to the Load

As we saw above, to match the line to an arbitrary load by means of one reactive shunt or a quarter-wave insert is possible only on one fixed frequency. On that frequency, the travelling-wave ratio equals unity and when the frequency changes, it rapidly decreases.

From a strict theoretical standpoint [35], it is impossible to bring about a complete matching of an arbitrary resistance with the wave impedance of a transmission line, i.e., to tune the line on a purely travelling wave on all the frequencies within a certain frequency range. Complete matching can be obtained only on certain fixed frequencies within a prescribed range, for example on the medium frequency and the two extreme frequencies of a range. To this effect, one should make use of several tuning elements.

However, such a matching is not the optimum one from the point of view of the pass-band width. A broad-band matching is obtained if no such special conditions are imposed, provided we ensure that within the prescribed frequency band, the travelling-wave ratio does not fall below a definite value. Thus, in certain radio-engineering devices, the travelling-wave ratio in the transmission frequency band should not be lower than 0.6; in other cases it should not be lower than 0.95.

In order to get a better understanding of the idea of broad-band matching, use is made of the R_L - X_L diagram which shows how the load resistance of the line $R_L + iX_L$ changes when the oscillation frequency changes.

The characteristic aspect of the R_L - X_L diagram is shown in Fig. 8-5, where the values of R_L appear on the real axis

and the values of X_L on the imaginary axis. The values of the frequencies corresponding to the given values of the resistance $R_L + iX_L$ are marked by dots on the curve. On this diagram, the curves of the constant travelling-wave ratios form circles; their centres lie on the real axis and they intersect the real axis at the points WK and W/K .

If the curve of the load resistance intersects the circumference of the minimum permissible travelling-wave ratio

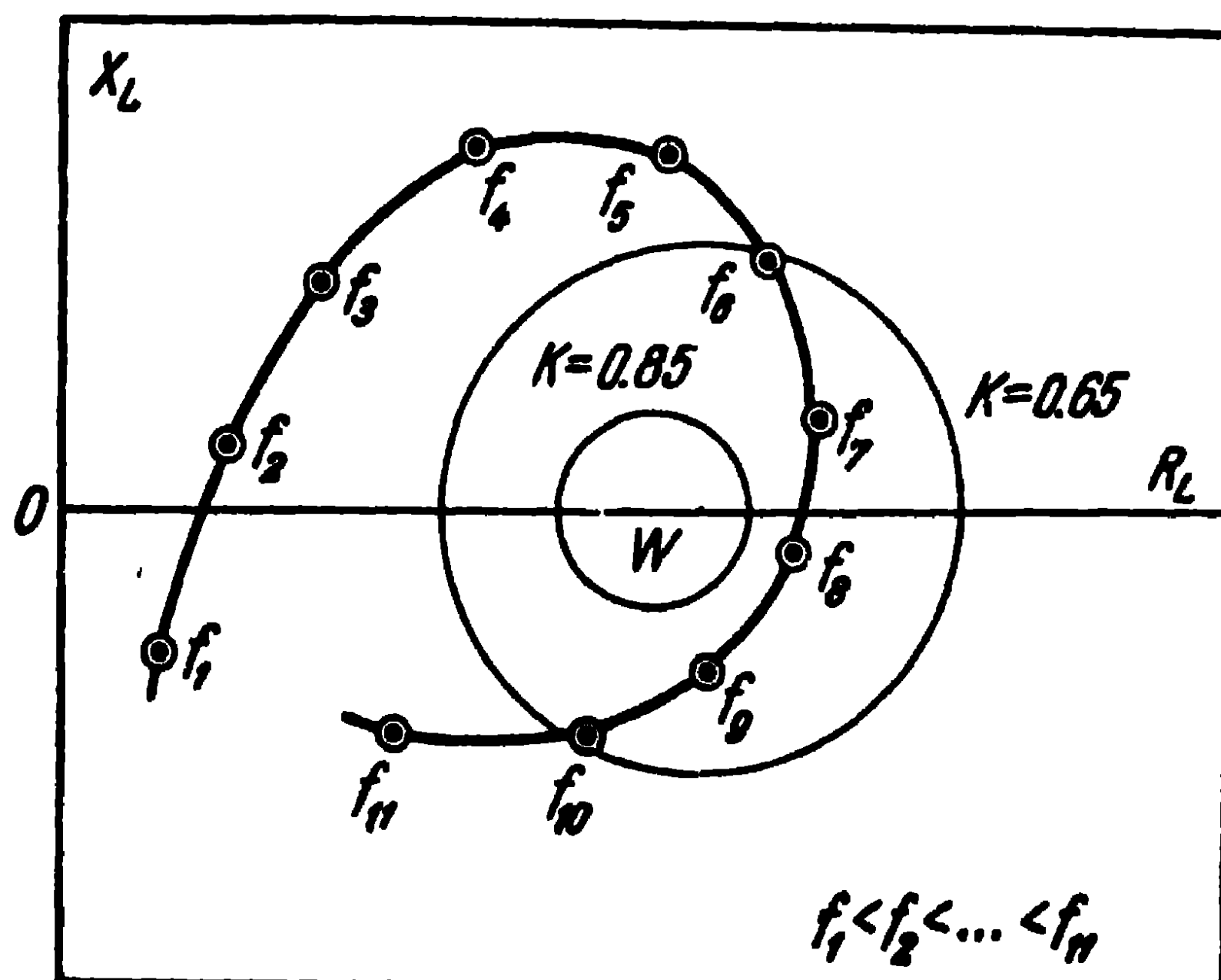


Fig. 8-5. R - X —diagram of the load resistance.

K_{perm} , the portion of the resistance curve which is inside this circle represents the matching band. Let, for example, the permissible travelling-wave ratio $K_{\text{perm}}=0.65$. Then, the frequencies on the curve of Fig. 8-5 lying between f_6 and f_{10} will, evidently, determine the matching band. If, on the other hand, we take $K_{\text{perm}}=0.85$, then, as can be seen from Fig. 8-5, the load resistance curve lies outside this circle and the necessary matching does not take place. Thus, the matching band is determined, on the one hand, by the dependence of the resistance $R_L + iX_L$ on the frequency and, on the other hand, by the circumference of the permissible travelling-wave ratio.

By inserting matching elements into the transmission line, one can distort the load resistance curve and transfer it on the R - X plane from one region to another. The problem of broad-band matching consists precisely in the

transfer of the most part of the resistance curve into the circle of the permissible travelling-wave ratio.

As shown in Fano's work mentioned earlier, there is a limit maximum frequency band, determined, for a prescribed change of the load resistance, by the circle of the permissible travelling-wave ratio attainable when there is an infinitely large number of matching elements. For a load which can be reduced to the series resonance circuit from R_L , L_L , C_L [36], this limit relative frequency band is defined as:

$$\left(\frac{\Delta f}{f_0}\right) Q = \frac{\pi}{\ln \frac{1+K_{\text{perm}}}{1-K_{\text{perm}}}}, \quad (8-17)$$

where f_0 is the resonance frequency of the series circuit of the substitution of the load;

Q , the quality of the circuit of the substitution of the load.

A satisfactory approximation to the relative matching band, defined by (8-17) is obtained by the use of one parallel reactive element connected at the points of the series resonance (i.e., in the voltage nodes) of the system that is being tuned. In many cases, the use of a large number of elements is not indicated, because of assembly complications and difficulties of tuning.

When a parallel matching element is being used, the load susceptance curve $G+iB$ is more convenient to be used than the resistance curve. Let the load susceptance on the plane $G-B$ (Fig. 8-6) be represented by the curve 1 and let the circumference of the minimum permissible travelling-wave ratio K_{perm} be given.

As shown by the broad-band matching theory, an approximation to the maximum frequency band, when one element of matching is used, is obtained when the curve 1 is rolled up into the loop 2 inside the circle of the permissible travelling-wave ratio, as shown in Fig. 8-6. The apex of the loop rests on the point $G_0 = \frac{1}{W_{\text{im}} K}$ and the intersecting ends of the loop, on the point $G_1 = \frac{K}{W_{\text{im}}}$ of the real axis. At the same time, W_{im} represents the wave impedance of the imaginary line chosen such as to cause the maximum value of the active admittance in the curve 1 to coincide with the maximum value of the active admittance in the loop 2.

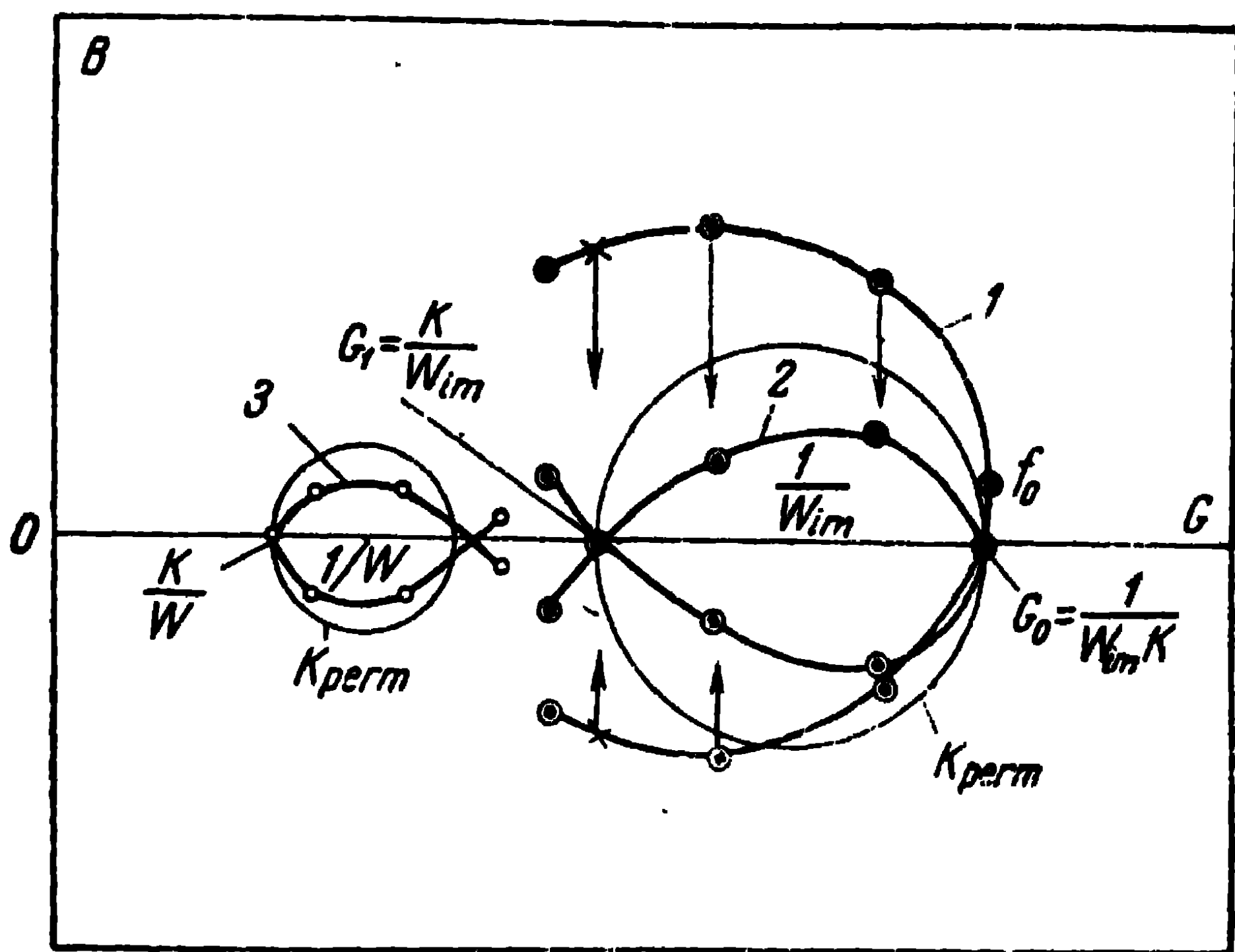


Fig. 8-6. G - B —diagram of the load admittance.

To determine the parameters of the matching element, let us plot the active and reactive admittances corresponding to the curve 1, against the frequency (Fig. 8-7). Let us mark out the points $G_1 = G_0 K^2$, corresponding to the frequencies f_1 and f_2 , on the curve of the active admittance. Evidently, the difference between these frequencies $\Delta f_c = f_2 - f_1$ will approximately define the matching band.

On the frequencies f_1 , f_0 and f_2 , the conductivity of the compensating device should have a magnitude equal to that of the susceptance of the matching device and be of opposite sign: $-B_1$, $-B_0$, $-B_2$. Let us draw through the point $-B_0$ a straight line approaching as close as possible to the points $-B_1$ and $-B_2$. It is readily seen that this straight line approximates the admittance curve of a parallel short-circuited stub, defined as:

$$B_{\text{stub}} = -\frac{1}{W_{\text{stub}}} \cot \frac{2\pi l_{\text{stub}}}{\lambda_{\text{stub}}}.$$

On the wave-length $\lambda_{0 \text{ stub}}$ corresponding to the frequency $f_{0 \text{ stub}}$, the admittance of the stub should equal zero. From here we define the length of the stub as:

$$l_{\text{stub}} = \frac{\lambda_{0 \text{ stub}}}{4} = \frac{v}{4f_0}, \quad (8-18)$$

where v is the phase velocity of the wave in the stub.

The inclination of the straight line of the admittance of the stub relative to the f -axis determines the magnitude of the wave impedance of the stub. If, for f_2 , the straight line passes through the point $-B_2$, the wave impedance of

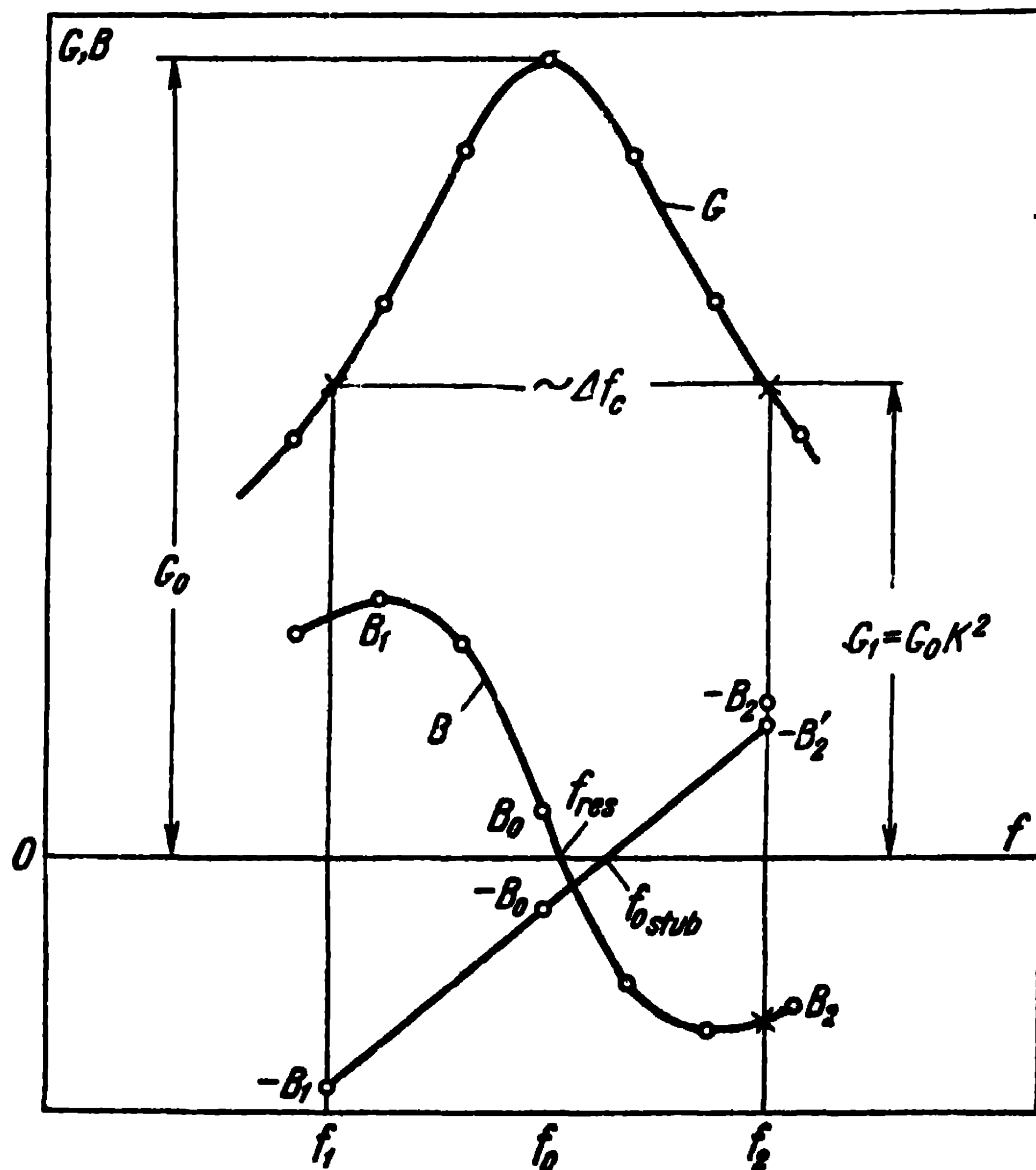


Fig. 8-7. Curves of the active admittance and susceptance of the load.

the stub will be defined as:

$$W_{\text{stub}} = -\frac{1}{B_n} \cot \frac{2\pi f_2}{v} l_{\text{stub}}. \quad (8-19)$$

In case a stub with a wave impedance, defined by (8-19), is difficult to realise because the magnitude of W_{stub} required is too small, one can use two short-circuited stubs of lengths l_1 and l_2 , connected in parallel to the same points of the matching device. The sum of the lengths of the stubs should

obey the condition

$$l_1 + l_2 = \frac{\lambda_{os \text{ tub}}}{2} = \frac{r}{2f_{os \text{ tub}}} \quad (8-20)$$

It will then be possible to define the relation between the lengths l_1 and l_2 from the expression

$$B_2 = -\frac{1}{W_{\text{stub}}} \left(\cot \frac{2\pi f_2}{v} l_1 + \cot \frac{2\pi f_2}{v} l_2 \right), \quad (8-21)$$

where f_2 and B_2 are the same values as in (8-19). The advantages of a stub of this kind consist in that we may vary at will the magnitude of the wave impedance of the stub W_{stub} .

After the wave impedance and the length of the compensating stub have been determined, one can specify the rolling up of the curve 1 into the loop 2 caused by the stub (Fig. 8-6).

Since the wave impedance of the real line W differs from that of the imaginary line W_{im} , we must also include into the line a quarter-wave insert with a wave impedance defined as

$$W_w = \sqrt{W W_{\text{im}}}. \quad (8-22)$$

Furthermore, the length of the insert should be taken equal to $\lambda_0/4$.

As can be seen in Fig. 8-6, a stub of this kind transfers the admittance loop 2 into the admittance loop 3 and, at the same time, somewhat narrows the matching band. This decrease may be determined when re-evaluating the curve 2 into the curve 3 with the help of the impedances diagram.

Two quarter-wave inserts or an exponential line can be used to transform the admittance loop 2 into the loop 3.

Note that a double quarter-wave transformer has a considerably broader band than one quarter-wave insert.

Since any mode in the waveguide may always be represented by an equivalent twin-wire line and the equivalent resistance of this line in the vicinity of the voltage node can

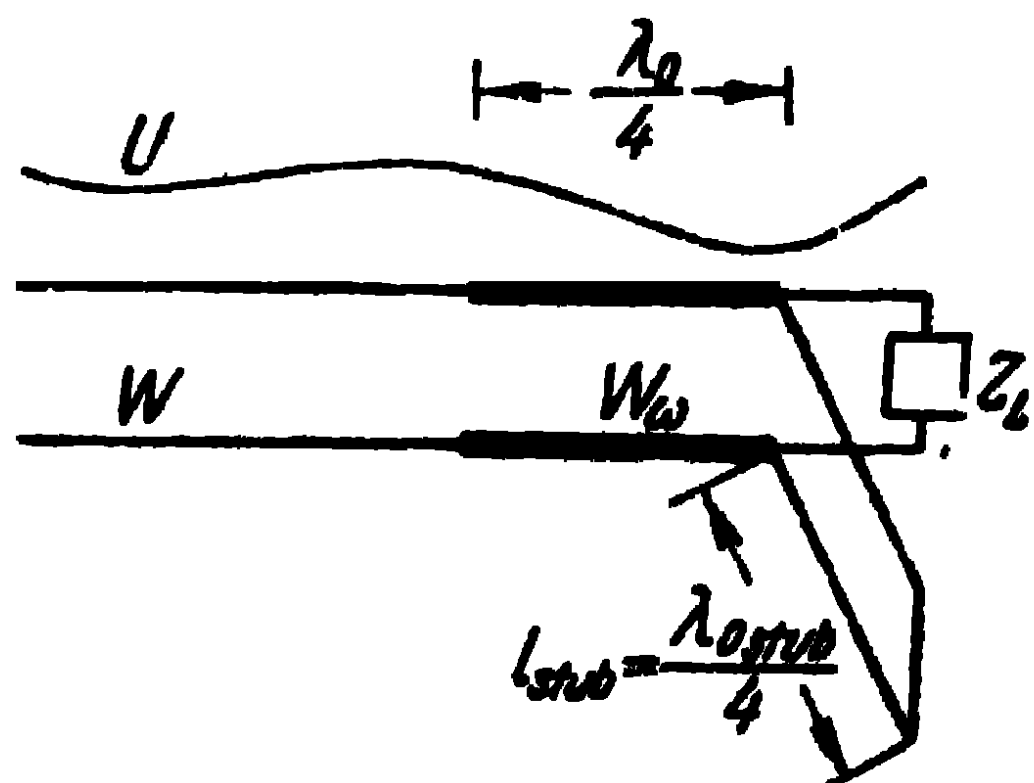


Fig. 8-8. Diagram of a broadband matching.

be represented as the resistance of the series resonance circuit, the broad-band matching method described above turns out to be applicable to any transmission line with an arbitrary load. The circuit of a matching device of this kind is shown in Fig. 8-8.

The broad-band matching can also be effected through the series insertion of a reactive stub in the vicinity of the voltage node. In this case, it is convenient to calculate the parameters of the matching device by means of the resistance diagram $R-X$.

Note in addition that the broad-band matching device should be placed as close as possible to the end of the line, i.e., in the first voltage node (or antinode) from the load, because at these places, the degree of change of the equivalent resistance of the line with the frequency is at a minimum and the matching will therefore have a broader band.

Finally, note that in the case of a broad-band matching, the dependency curve of the travelling-wave ratio on the frequency has two maximums whereas in the case of a narrow-band matching, this dependency curve, as was pointed out earlier, has one maximum.

8-5. Matching the Line to the Load in a Broad Frequency Range

We have investigated methods of narrow- and broad-band matching of a line to a load, which consist in the insertion into the line of reactive elements to compensate the reflections from the load. These methods are used when the load represents a narrow-band resonance system.

In some cases, the load resistance depends but little on the frequency. Thus, for example, the input resistance of a short-wave travelling-wave antenna in a broad frequency range remains almost constant. In cases of this kind, the matching of a constant resistance (or a resistance which changes only slightly with the frequency) to the wave impedance of the transmission line is obtained by means of so-called diverging lines. There are several types of diverging lines. We shall investigate the exponential line [37] represented in Fig. 8-9.

The equations for a long line are written as

$$\frac{dU}{dx} = -IZ, \quad \frac{dI}{dx} = -UY, \quad (8-23)$$

where Z_1 and Y_1 are the resistance and conductivity of the line per unit length.

Excluding the current from the first equation (8-23), we obtain the following equations for the voltage in the line:

$$\frac{d^2 U}{dx^2} - \frac{d \ln Z_1}{dx} \frac{dU}{dx} - Z_1 Y_1 U = 0. \quad (8-24)$$

Let the parameters of the line change along the length as

$$Z_1 = Z_0 e^{bx}, \quad Y_1 = Y_0 e^{-bx}, \quad (8-25)$$

where b is a certain positive quantity.

Let C_0 and L_0 be the linear capacity and inductance at the beginning of the line and let us assume that the line is free from losses. Then

$$Z_0 = i\omega L_0, \quad Y_0 = i\omega C_0,$$

and we obtain for the wave impedance of the exponential line the expression

$$W = \sqrt{\frac{Z_1}{Y_1}} = W_0 e^{bx}, \quad (8-26)$$

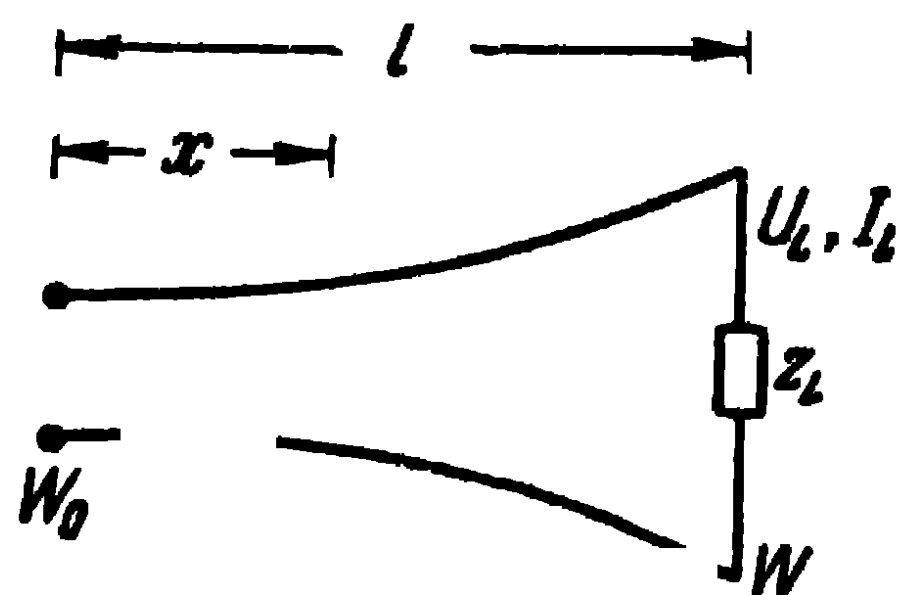


Fig. 8-9. Exponential line.

and for the wave number, the expression

$$k_0^2 = -Z_1 Y_1 = -Z_0 Y_0 = \omega^2 L_0 C_0.$$

At the same time, the differential equation for the voltage (8-24) will be written as

$$\frac{d^2 U}{dx^2} - b \frac{dU}{dx} + k_0^2 U = 0. \quad (8-27)$$

An immediate substitution will readily show that for a line of infinite length, the solution of the equation (8-27) is written as:

$$U = A e^{\left(\frac{b}{2} - i\alpha\right)x}, \quad (8-28)$$

where

$$\alpha = \sqrt{k_0^2 - \frac{b^2}{4}}. \quad (8-29)$$

We see that, as the wave moves, the amplitude of the voltage in the exponential line increases in accordance with the $e^{\frac{b}{2}x}$ exponential law. Further, from (8-29) we see that there

is a critical wave-length which equals:

$$\lambda_{\text{crit}} = \frac{4\pi}{b}. \quad (8-30)$$

For the oscillations to be propagated in the line, the condition $\lambda_0 < \frac{4\pi}{b}$ should be conformed with, i.e., the wave-length in free space should be smaller than critical wave-length.

The phase velocity of the wave is greater than that of light and is defined as:

$$v_{\text{ph}} = \frac{v_1}{\sqrt{1 - \left(\frac{b}{2k_0}\right)^2}}. \quad (8-31)$$

The wave of the current in the line is determined by substituting (8-28) into the first expression (8-23). Taking (8-25) into account, we obtain:

$$I = -\frac{1}{Z_0} \left(\frac{b}{2} - i\alpha \right) A e^{-\left(\frac{b}{2} + i\alpha\right)x}. \quad (8-32)$$

Thus, as the wave moves in the opposite direction to that of the voltage, the amplitude of the current decreases in accordance with the exponential law.

The equivalent resistance of the line in the x -section is defined by the ratio of (8-28) to (8-32)

$$Z_x = -\frac{Z_0 e^{bx}}{\left(\frac{b}{2} - i\alpha\right)} = \frac{W}{\frac{b}{2k_0} + \sqrt{1 - \left(\frac{b}{2k_0}\right)^2}} \quad (8-33)$$

and in accordance with the transformation of the current, the voltage is also transformed along the line in accordance with the exponential law. It is complex and for this reason, in order to eliminate the reflection in a line of finite length, the load resistance should contain a certain reactive component.

The quantity b is usually chosen so small that $\frac{b}{2k_0} \ll 1$. Then, in accordance with (8-33), the equivalent resistance of the line is close in magnitude to the wave impedance $Z_x \approx W$ and the line may serve as a transformer of active resistances.

Let the load resistance of the exponential line equal the wave impedance $Z_L = W$. Then, after substituting this

expression and (8-33) into (8-6), when $\frac{b}{2k_0} \ll 1$, we obtain approximately:

$$|p| = \left| \frac{Z - Z_L}{Z + Z_L} \right| \approx \frac{b}{4k_0}. \quad (8-34)$$

It follows from (8-34) that the reflection coefficient p will be all the smaller as the quantity b is smaller. This is attained by way of a continuous change of the distance between the wires of the line.

In accordance with (8-26), the length of the exponential line necessary to match the active load resistance $Z_L = W$ to the wave impedance of a homogeneous line W_0 is defined as:

$$l = \frac{l}{b} \ln \frac{W}{W_0}. \quad (8-35)$$

Thus, having prescribed the permissible magnitude of the reflection coefficient, we determine from (8-34) the magnitude b of the longest desirable wave. Then, by substituting the value b thus obtained into (8-35), we find the necessary length of the exponential line l .

Let, for example, $W = 600$ ohms, $W_0 = 300$ ohms, $p = 0.05$ and $\lambda = 50$ m. Then we shall obtain $b \approx 0.0252$ and $l \approx 27.5$ m. It is clear that the length of the exponential line should be of the order of half a wave-length on the longest desirable wave. On all shorter waves, the reflection coefficient will be smaller than $p = 0.05$.

Thus, the exponential line turns out to be a convenient device for matching active resistances in a broad frequency range.

CHAPTER NINE

Parameters and Elements of Transmission Lines

9-1. Two-Wire and Four-Wire Lines

We shall begin our study of transmission line devices by the simplest ones, viz., the aerial two-wire and four-wire lines, usually called feeders. They are open lines and, as indicated earlier, are used on short and partly on ultra-short (metre) waves, in the main for antennas utilised on major radio communication lines.

An aerial twin feeder (Fig. 7-1, *a*) is usually made of copper or bi-metal wires (3 to 6 mm in dia), spaced from 5 to 40 cm apart (D). The wave impedance of a feeder of this kind is calculated from the expression

$$W = 276 \log \left[\frac{D}{d} + \sqrt{\left(\frac{D}{d}\right)^2 + 1} \right], \quad (9-1)$$

which, when $D \gg d$ is reduced to the simpler expression

$$W = 276 \log \frac{2D}{d}. \quad (9-2)$$

On short waves, twin feeders are, as a rule, used with a wave impedance $W = 600$ ohms. The feeder is fixed on wooden supports 3 to 5 m high by means of ceramic insulators of the bar or stick type as shown in Fig. 9-1.

As a rule, aerial four-wire feeders are used for feeding antennas from a powerful transmitter. The wave impedance

of a feeder of this kind may be defined as:

$$W = 138 \log \left[\frac{2D_1}{d} \sqrt{1 + \frac{D_1^2}{D_2^2}} \right], \quad (9-3)$$

provided the wires lying in one vertical plane (Fig. 9-2) have a potential of one sign and the wires lying in another vertical plane have a potential of the other sign.

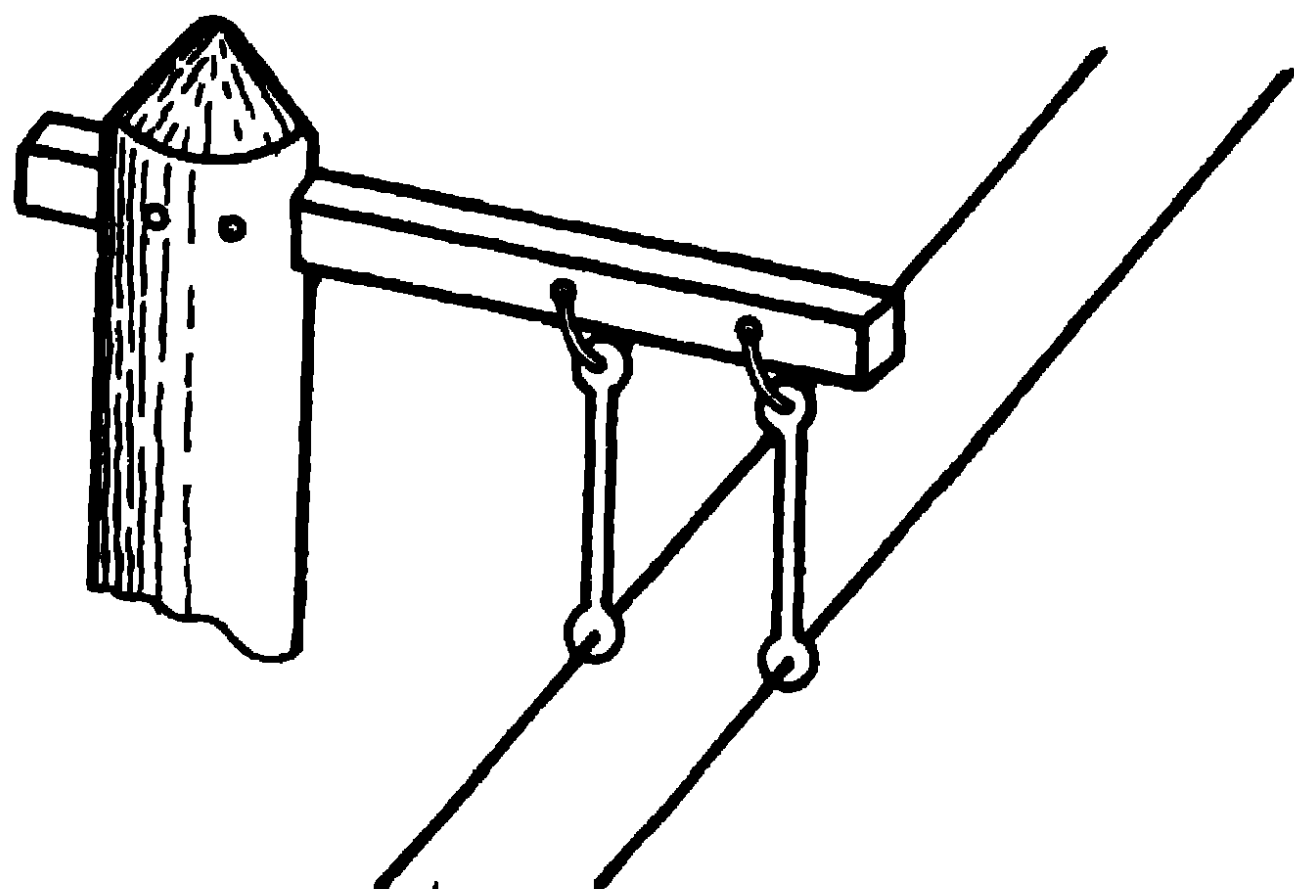


Fig. 9-1. Fixation of twin feeder.

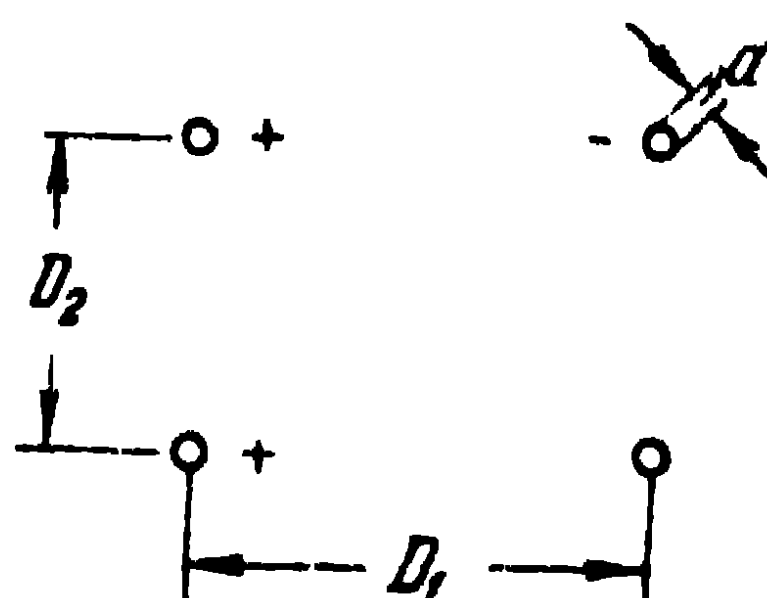


Fig. 9-2. Four-wire feeder.

In the case of a four-wire crossed feeder (wires lying crosswise have a potential of the same sign) the wave impedance is defined as

$$W = 138 \log \frac{2D_1}{d \sqrt{1 + \frac{D_1^2}{D_2^2}}}. \quad (9-4)$$

Usually, the four-wire crossed feeder utilised for transmitting antennas has a wave impedance $W \approx 300$ ohms. It is made of a 5 mm wires spaced 30 to 40 cm apart.

Four-wire crossed feeders used for receiving antennas of the professional type are made of 1.5 mm copper or bronze wires spaced at a distance $D_1 = D_2 = 3.3$ cm apart. The wave impedance of a feeder of this kind equals 200 ohms.

The feeders are tuned on a travelling wave by means of inductive stubs inserted in parallel.

All the lines investigated earlier were without losses. Under real conditions, part of the energy propagated along the line is lost on heating the wires and insulators. As a consequence, the field amplitude of the propagated wave is attenuated as the exponent $e^{-\beta z}$, where β is the attenuation constant.

We are now confronted with the problem of defining the attenuation constant of air feeders. Let P_0 be the power conveyed by the electromagnetic wave at a certain cross section of the line. Then, at the distance z from this section in the direction of propagation of the wave, the transmitted power will be:

$$P_z = P_0 e^{-2\beta z}$$

and the power of the losses per unit length of the feeder will be defined as:

$$\frac{dP_z}{dz} = -2\beta P_z.$$

The attenuation constant will therefore be defined as:

$$\beta = -\frac{1}{2P_z} \frac{dP_z}{dz}. \quad (9-5)$$

In real transmission lines, the energy losses are small, so that the expression (9-5) is used for the approximate calculation of the attenuation in all cases. This approximation consists in that when defining the conveyed power and the power of the losses, we shall assume that the field is unperturbed, i.e., that it does not differ from the field in lossless lines.

To begin with, let us find the attenuation of a twin air feeder. The energy losses on heating the insulators in an air feeder are small in comparison with the losses on heating the wires and will therefore be neglected. Let R_1 be the resistance of one of the wires of the feeder per 1 metre of length. Then, the power of the losses equals $\frac{dP_z}{dz} = -2I_z^2 R_1$, and the power conveyed along the feeder will be $P_z = I_z^2 W$. From this we obtain:

$$\beta = \frac{R_1}{W} \text{ [Np/m]}. \quad (9-6)$$

We know that the resistance of a copper wire to high-frequency currents is defined as:

$$R_1 = \frac{l}{r \sqrt{1.83\lambda}} \text{ [ohms/m]}, \quad (9-7)$$

where r is the radius of the wire in mm;
 λ , the wave-length in m.

If we again designate by R_1 the resistance of one wire per 1 m of length, the attenuation constant of a four-wire feeder (neglecting the losses in the insulators) is defined as:

$$\beta = \frac{R_1}{2W}. \quad (9-8)$$

Owing to the fact that the wave impedance of a four-wire feeder is about half that of the wave impedance of a twin feeder, the damping coefficient of these feeders is found to be of the same order.

As for the efficiency of the feeder, as was pointed out earlier, it is found to be at a maximum when the travelling-wave ratio equals unity. Indeed, in the case of a travelling wave, the power at the beginning of the feeder equals $P_1 = I_0^2 W$, and the power at the end of it equals $P_2 = I_0^2 e^{-2\beta l} W$ where I_0 is the magnitude of the current at the beginning of the feeder. Hence, for the travelling-wave type of operation, the efficiency of the feeder will be:

$$\eta = e^{-2\beta l}. \quad (9-9)$$

Now, let us suppose that the travelling-wave ratio in the feeder does not equal unity. Then, representing the type of operation in the line as the superposition of the reflected wave on the incident one, we shall write the power for the incident wave as $P_{1i} = I_0^2 W$ at the beginning of the line and as $P_{2i} = I_0^2 e^{-2\beta l} W$ at the end of the line; for the reflected wave, we shall write the power at the beginning of the line as $P_{1r} = I_0^2 e^{-2\beta l} W p^2$ and the power at the end of the line as $P_{2r} = I_0^2 e^{-4\beta l} W p^2$.

Hence, the expression for the efficiency will be:

$$\eta = e^{-2\beta l} \frac{1 - p^2}{1 - p^2 e^{-4\beta l}}, \quad (9-10)$$

where p is the reflection coefficient.

Fig. 9-3 illustrates the dependence of the feeder efficiency on the travelling-wave ratio when $\beta l = 0.06$. When the travelling-wave ratios are relatively high ($K > 0.3$), the efficiency depends but little on the magnitude of the travelling-wave ratio. At small values of the travelling-wave ratios ($K < 0.2$), this dependence becomes pronounced. the efficiency falls rapidly as the travelling-wave ratio decreases. The transmission line load should be such as to make

the travelling-wave ratio higher than 10% even prior to tuning the feeder. Otherwise, a large part of the energy might be wasted on heating the wires in the region of the feeder between the load and the tuning elements, where the reflection from the load is not compensated for.

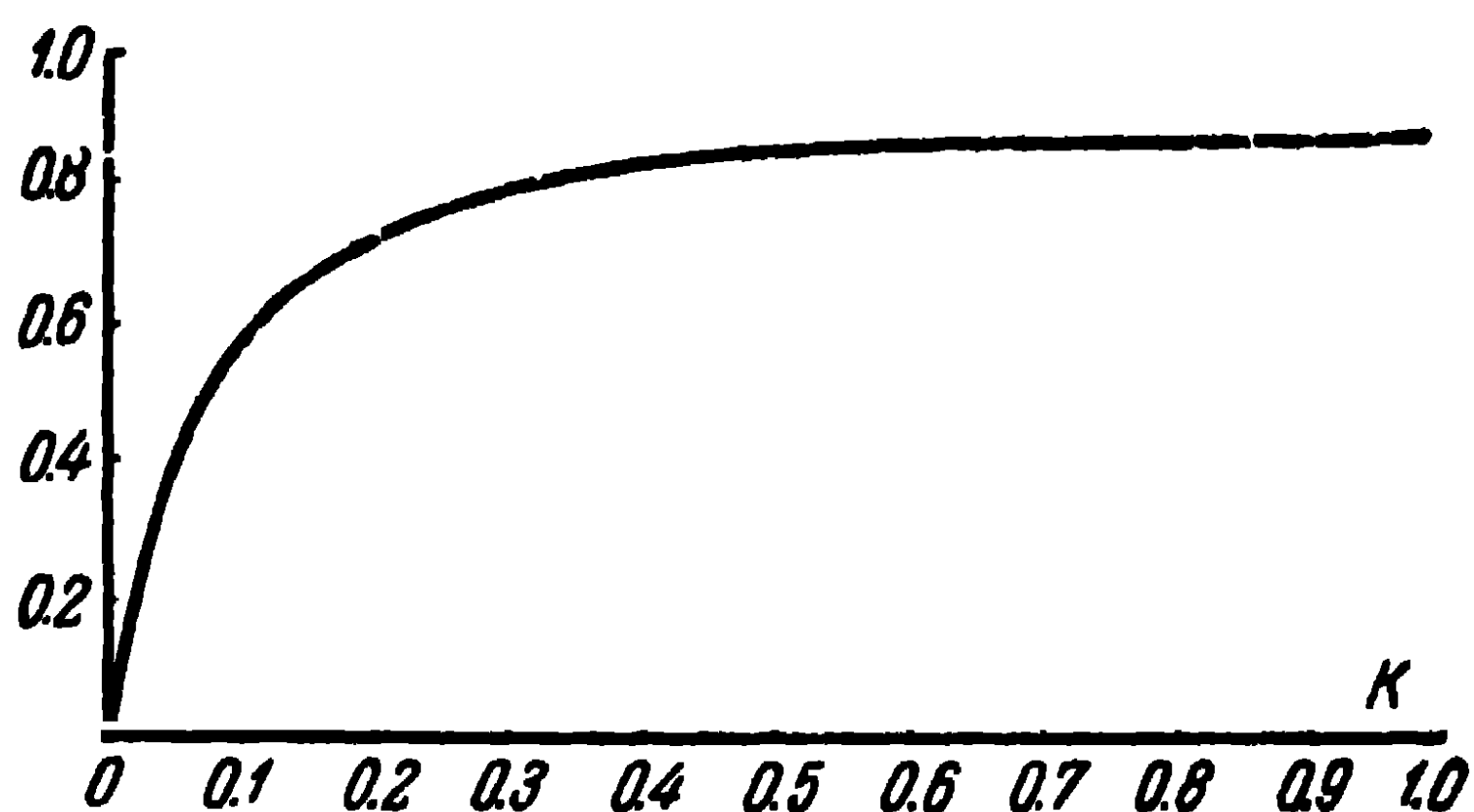


Fig. 9-3. Dependence of the efficiency on the value of the travelling-wave ratio.

Furthermore, at low travelling-wave ratios, there is an increase of the voltages in the line. The effective voltage in the antinode is defined as:

$$U_a = \sqrt{\frac{PW}{K}}, \quad (9-11)$$

and at low travelling-wave ratios, this voltage may exceed the permissible magnitude.

We know that the existence of high voltages in feeders of short-wave antennas may give rise to overvoltages, attended by the appearance of glow discharges. As was shown by M. S. Neuman [38], in the case of thin wires ($d \approx 2$ mm), the critical voltage in the short-wave range, i.e., the voltage for which we still have a glow discharge may be approximately defined as:

$$U_{crit} = \sqrt{19 + 0.029\lambda^2},$$

where λ is the wave-length, in m;

U_{crit} , kW.

For thicker wires, the critical voltage exceeds this value.

Energy losses in air feeders are also caused by radiation (the antenna effect of feeders). This radiation is all the greater as the distance between the wires is greater in comparison with the wave-length. The radiation of feeders,

at a prescribed spacing of the wires, also increases should there occur any dissymmetry in the feeder, leading to the appearance, apart from the usual antiphase wave, of an additional co-phasal wave (at every given moment, the currents in the wires are directed in the same direction). This dissymmetry arises because of the differences between the capacitances of the wires relatively to the surrounding objects and the earth, the differences between the lengths of the wires of the feeder and the differences between the loads on the wires at the end of the feeder, etc.

On short waves, the distance between the wires of the feeder is sufficiently small in comparison with the wavelength so that, provided the symmetry in the feeders is observed, the losses on radiation may be neglected. On ultrashort waves (metre and decimetre waves), the spacing between the wires is not so small in comparison with the wavelength. In this wave range, the electric dissymmetry of the wires exerts a greater influence, so that the radiation of the feeder increases considerably.

To reduce the radiation of feeders, as well as to make them stand weathering, twin feeders with a relatively small spacing between the wires are sometimes covered with a dielectric. In other cases, the twin feeders are screened (Fig. 9-4). Screened feeders are free from radiation and protected against weathering. However, due to the introduction of the screen and especially of the dielectric, there is an increase of the damping in feeders of this kind.

The wave impedance of a screened twin feeder with a solid dielectric filling may be defined as:

$$W = \frac{120}{\sqrt{\epsilon/\epsilon_0}} \ln \left[\frac{2a}{d} \left(\frac{D^2 - a^2}{D^2 + a^2} \right) \right].$$

The phase velocity is lower than the velocity of light in free space in lines of this kind and is defined as:

$$v_{ph} = \frac{v_1}{\sqrt{\epsilon/\epsilon_0}}.$$

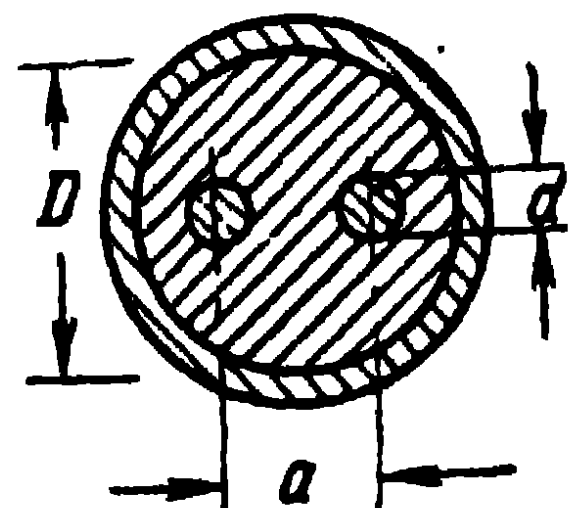


Fig. 9-4. Twin screened feeder.

9-2. Coaxial Lines

In the metre, decimetre and partly centimetre wave ranges, extensive use is made of coaxial lines, which take the form of rigid lines or of flexible coaxial cables. These lines are also utilised in the short- and medium-wave ranges.

Rigid coaxial lines are usually made of brass or copper tubes (often silver-plated) and the inner wire is fixed by means of either dielectric washers or metal insulators.

The washers are spaced sufficiently wide apart and are made of a dielectric with small losses. The only drawback

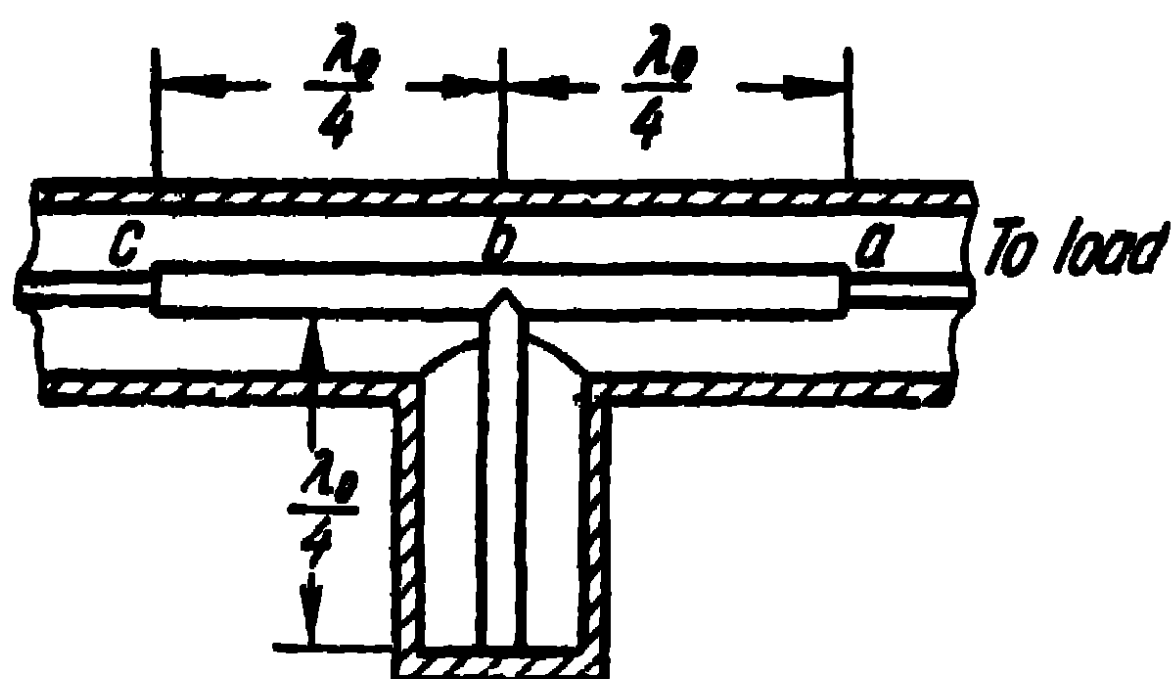


Fig. 9-5. Rigid coaxial line with metal insulators.

of such a line is that the conductivity of the washers depends on the moisture content of air, which may lead to extensive damping.

Lines with metal insulators (Fig. 9-5) are free from dielectric losses but are utilised in a comparatively narrow frequency band, due to the fact that metal insulators are

resonant. Lines of this kind are generally used in the centimetre wave range, where constructionally the line is compact.

To broaden the pass-band, the metal insulators are usually of the broad-band kind. This is achieved by the broad-band matching method described above. To begin with, an insert ab of length $\lambda_0/4$ (λ_0 is the mean wave-length of the range) is connected into the line to lower the wave impedance of the line and set up a voltage node at the point b of the line. Then, a stub (a metal insulator, in fact) of length $\lambda_0/4$ is connected to the point b of the line to compensate the reactance in the frequency band at that point of the line. Finally, yet another quarter-wave insert bc is connected into the line to transform the resistance compensated at the point b of the line into a resistance at the point c of the line close to the wave impedance of the line in the frequency band.

The attenuation in the coaxial line (neglecting the losses in the insulation) may be defined as:

$$\beta = \frac{R_1 + R_2}{2W}, \quad (9-12)$$

where R_1 is the resistance of the inner wire per unit length;
 R_2 , the resistance of the outer wire per unit length.

For copper wires, the resistances R_1 and R_2 may be calculated from the expression (9-7).

The wave impedance of a coaxial line is calculated from the expression

$$W = \frac{138}{\sqrt{\epsilon/\epsilon_0}} \log \frac{D}{d}, \quad (9-13)$$

where D is the diameter of the inner-surface of the outer conductor;

d , the diameter of the outer surface of the inner conductor.

The choice of the transverse dimensions of the coaxial line is based on two requirements: minimum attenuation and maximum admission of power by the line, on condition that higher modes are absent. For an air dielectric, the first requirement leads to a wave impedance of the line equal to 92.6 ohms and the second requirement, to a wave impedance equal to 44.5 ohms. Usually, the wave impedance of the coaxial lines equals 75 or 50 ohms. The effective value of the voltage set up in the coaxial line may be determined from (9-11). As for the breakdown voltage in the line, it may be defined as:

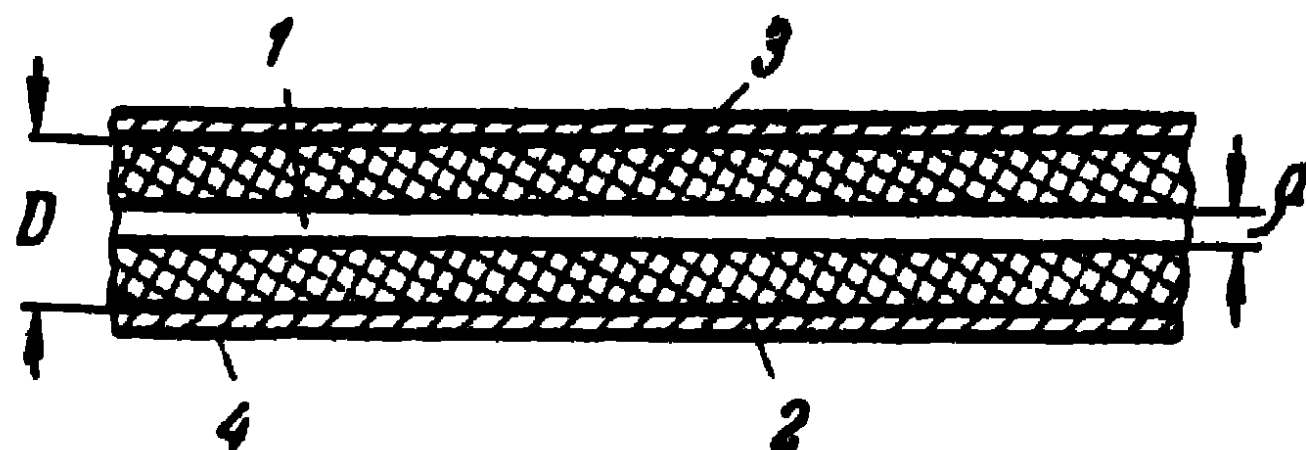


Fig. 9-6. Flexible coaxial cable:
 1—internal wire; 2—external wire; 3—polyethylene; 4—braiding.

$$U_{br} = \int_{d/2}^{D/2} E_{br} \frac{d}{2r} dr = E_{br} \frac{d}{2} \ln \frac{D}{d}, \quad (9-14)$$

where E_{br} is the electric field breakdown voltage of the inner conductor of the line.

For air, the amplitude of the breakdown voltage of the electric field is usually taken to be $E_{br, \max} = 30,000$ V/cm.

Flexible coaxial cables usually consist of a flexible inner conductor, an entire dielectric (of polyethylene), a metal braiding which plays the role of the outer conductor and of a protective cover (Fig. 9-6).

In a coaxial cable, losses in the insulator are added to those in the conductors; moreover, the former predominate and, on the whole, determine the attenuation. The attenuation in the cable increases rapidly as the frequency increases, so that flexible cables are used as transmission lines only on waves longer than 10 cm.

When high powers are being transmitted at high frequencies the dielectric gets very warm and there is a risk of breakdowns caused by overheating of the cable. That is why the operating voltage in coaxial cables seldom exceeds 3 to 5 kV.

The wave impedance of coaxial flexible cables may be determined from (9-13). For standard cables, it usually equals 50 or 75 ohms. The phase velocity of propagation of the wave in the cable is inferior to the velocity of light and is defined as:

$$v = \frac{v_1}{\sqrt{\epsilon/\epsilon_0}}.$$

Table 9-1 gives the data of a number of coaxial cables manufactured in this country.

Table 9-1

Type	Diameter		Per- mit- tivity ϵ/ϵ_0	Wave im- pedance W , ohms	Attenuation, db/m at frequency f . Mc/s					Oper- ating volt- age, kV
	D, mm	d, mm								
					10	100	300	1,000	3,000	
PK-3	9 0	1.37	2.27	75	0.017	0.070	0.13	0.26	0.52	5.5
PK-6	9.2	2.55	2 19	52	0.0165	0.052	0.12	0.27	0.59	4.5
PK-19	2.4	0.68	2.11	52	0.0565	0.20	0.32	0.60	1.1	1
PK-20	7.2	1.11	2.23	75	0.022	0.087	0.15	0.33	0.68	1

Rigid coaxial lines can be tuned on a travelling wave by means of either a quarter-wave insert or an inductive stub.

A convenient shape for the quarter-wave insert is that of a tube enclosing the inner conductor of the line. It is inconvenient to move the inductive stub along the line, so that one uses a two-stub transformer (see Fig. 9-7). By changing the length l_{stub1} of the first stub, one can change the position of the voltage node on the line and the length of the stub is chosen in such a way that at the connection points of the second stub, the active part of the line

equivalent conductivity should equal the reverse magnitude of the line wave impedance. Then, through the proper choice of the length $l_{\text{stub}2}$ of the second stub of the transformer, the reactive part of the conductivity of the line is compensated at these points and the line is thereby tuned on a travelling wave. The stubs are usually spaced $\frac{3}{8}\lambda$ apart. To tune the line on a travelling wave, one also occasionally uses a three-stub transformer.

When tuning a coaxial cable on a travelling wave, a single inductive stub can be used along with two-stub and three-stub transformers, which are connected to the line by means of special tees.

For matching two coaxial lines with different wave impedances or with the same wave impedances but different

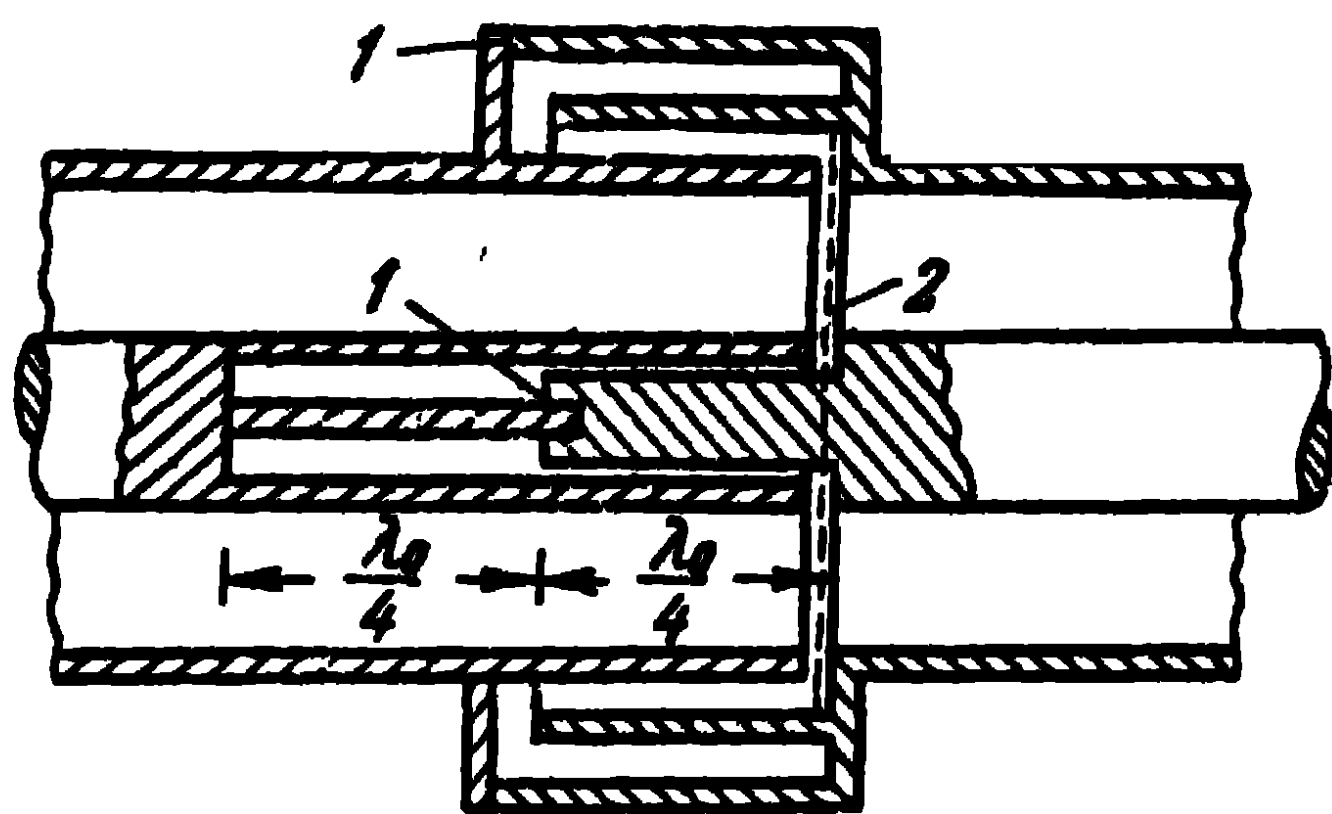


Fig. 9-9. Rotating joint of a coaxial line:
1—frictional contact; 2—section A.

cross sections, conical transitions are used, which imitate an exponential line. A conical transition of this kind is shown in Fig. 9-8. The length l of the conical transition is taken equal to several wave-lengths.

In the transmission lines of radar antennas, use is often

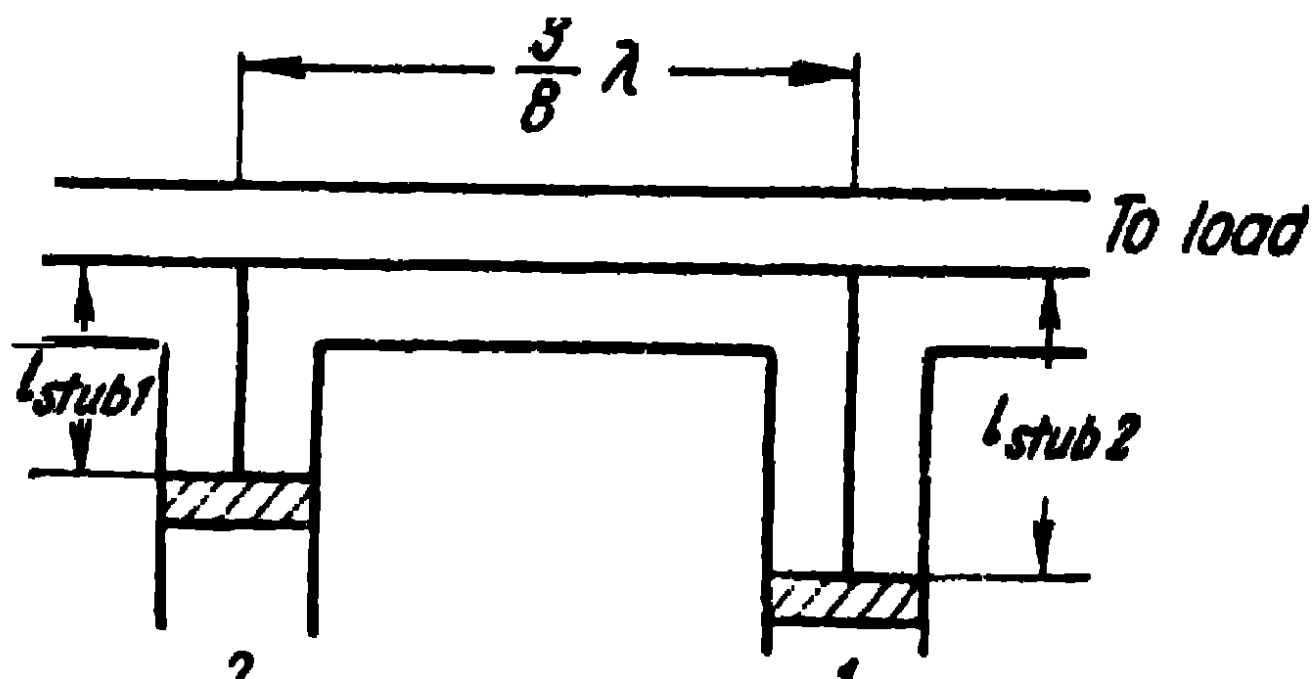


Fig. 9-7. Two-stub inductive transformer.

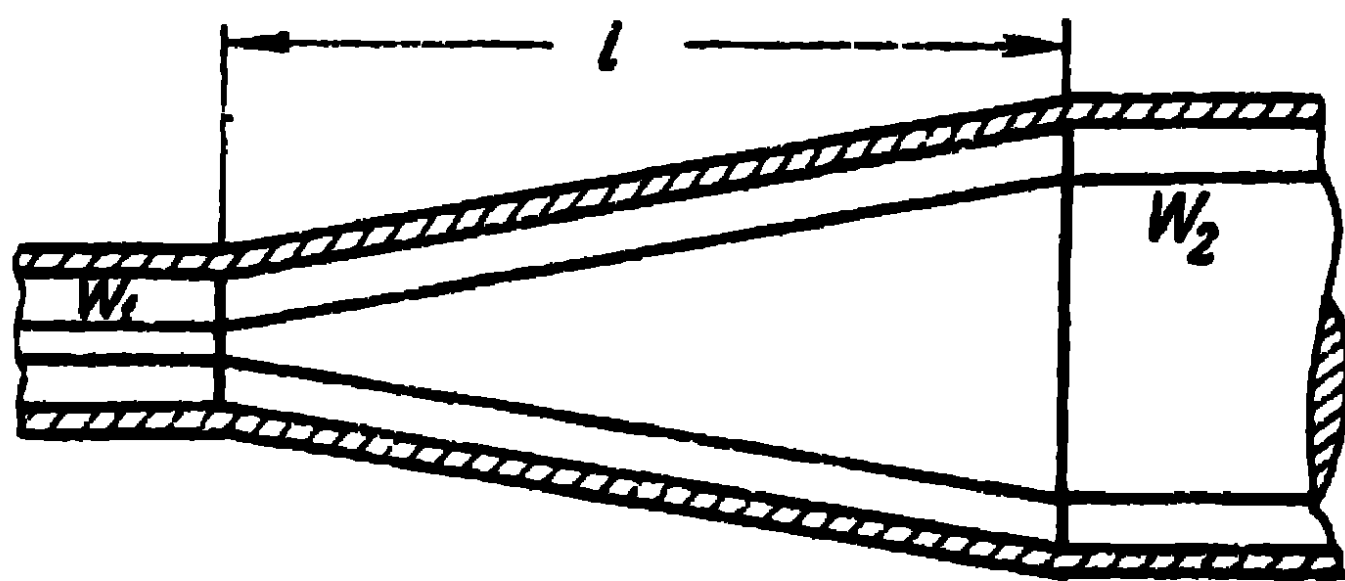


Fig. 9-8. Conical transition.

made of the rotation of one part of a coaxial line relatively to the other part. At the same time, a special choke is used in which the frictional contacts take place in the current

nodes; this reduces the energy losses in the transitions and ensures a continuous contact. A rotating device of this kind is shown in Fig. 9-9. As can be seen from this figure, close-ended half-wave lines are connected in series with the inner and outer conductors at the cross section A of the line; the half-wave lines enable to achieve a contactless short, at a high frequency, of the two lines rotating relatively to one another. The mechanical contact is effected in the current nodes of these half-wave lines.

9-3. Waveguide Lines

In the 10 cm and shorter wave range, waveguides and, in the first place, rectangular waveguides with an H_{01} mode are extensively used as transmission lines of the antenna systems. Circular waveguides are also occasionally used as waveguide channels in antenna installations.

Let us first dwell on the characteristics of the H_{01} mode in a rectangular waveguide. A fairly detailed analysis of the rectangular waveguide theory was given in Chapter Seven. Under real conditions, the energy lost on heating the walls of the waveguide has to be taken into consideration. As a consequence, the amplitude of the field of the wave decreases along the waveguide as the exponent and the attenuating constant can be determined from (9-5).

The problem of wave propagation in a waveguide with non-ideally conducting walls has no exact solution, therefore, usually the attenuating constant is determined approximately, on the basis of the unperturbed field.

As we know, this field is defined by the expressions

$$\left. \begin{aligned} E &= A_0 \frac{k^2}{i\omega\epsilon} \sin\left(\frac{\pi}{b} y\right) e^{-i\alpha_{01}z}; \\ H_{y_{01}} &= -A_0 i\alpha_{01} \sin\left(\frac{\pi}{b} y\right) e^{-i\alpha_{01}z}; \\ H_{z_{01}} &= -A_0 \frac{\pi}{b} \cos\left(\frac{\pi}{b} y\right) e^{-i\alpha_{01}z}, \end{aligned} \right\} \quad (9-15)$$

where A_0 is a constant quantity;

$$\alpha_{01} = k \sqrt{1 - (\lambda/\lambda_{crit\ 01})^2}.$$

The power conveyed along the waveguide will be determined from the substitution of the expressions (9-15) into

(7-18). We shall have:

$$P_z = A_0^2 \frac{k^2 a_0 b}{4\omega\epsilon}.$$

Owing to the fact that the waveguide conductivity is finite, the tangential component of the electric field intensity at the walls of the waveguide is not actually equal to zero. Since the conductivity of the walls is high and the skin effect very pronounced, this component of the field intensity can be obtained from the Leontovich boundary conditions

$$\frac{E_t}{H_t} = \sqrt{\frac{\mu}{\epsilon \left(1 - i \frac{\sigma}{\omega\epsilon}\right)}} \approx \sqrt{\frac{\omega\mu}{2\sigma}} (1 + i).$$

Substituting here, instead of H_t , the values of the unperturbed magnetic field from (9-15), we obtain the approximate expressions for the tangential components of the electric field intensity at the walls of the waveguide E_t .

Thus, the approximation consists in that the tangential component of the magnetic field intensity is taken unperturbed, i.e., determined from the expressions (9-15), the tangential component of the electric field intensity at the walls of the waveguide being determined approximately from the Leontovich boundary conditions.

The power absorbed by the walls of the waveguide can be calculated by the Poynting vector method. Thus, the power absorbed by the lateral walls per unit length of the waveguide will be

$$\left(-\frac{dP_z}{dz}\right)_{\text{lat}} = \sqrt{\frac{\omega\mu}{2\sigma}} \int_{x=0}^a H_{z\ 01} H_{z\ 01}^* \Big|_{y=0} dx = \sqrt{\frac{\omega\mu}{2\sigma}} \frac{a\pi^2}{b^2} A_0^2.$$

The power absorbed by the broad walls per unit length of the waveguide will be:

$$\begin{aligned} \left(-\frac{dP_z}{dz}\right)_{\text{broad}} &= \sqrt{\frac{\omega\mu}{2\sigma}} \int_{y=0}^b (H_{y\ 01} H_{y\ 01}^* + H_{z\ 01} H_{z\ 01}^*) \Big|_{x=0} dy = \\ &= \sqrt{\frac{\omega\mu}{2\sigma}} A_0^2 \frac{bk^2}{2}. \end{aligned}$$

Substituting the expressions obtained for the power conveyed along the waveguide and the power lost on heating the walls of the waveguide into (9-5), following a number

of transformations, we obtain:

$$\beta = \sqrt{\frac{\omega\epsilon}{2\sigma}} \frac{1}{a} \frac{\lambda_w}{\lambda} \left(1 + \frac{2a}{b} \frac{\lambda^2}{\lambda_{crit}^2} \right) [\text{Np/m}], \quad (9-16)$$

where all the dimensions are given in metres.

The expression just cited shows that the damping increases when the operating wave-length λ approaches the critical wave-length λ_{crit} . Then, the wave-length in the waveguide λ_w tends towards infinity and the attenuating constant β also tends towards infinity. In addition, the attenuating constant depends on the dimensions a and b . Thus, in the case of a constant value of the dimension b and a decrease of the dimension a , the attenuating constant increases. However, the dimensions of the waveguide cannot be chosen from the minimum attenuating condition due to the fact that to eliminate the higher modes in the waveguide, the dimension a should be smaller than $\lambda/2$ and the dimension b smaller than λ . When the ratio $a/b=0.5$, as generally adopted in practice, the attenuating constant in the centimetre wave range, in the case of copper waveguides, is higher than 0.005 db/m.

Usually, rectangular waveguides have an air insulation, so that the energy losses on heating the medium inside the waveguide can be neglected. In the case of a dielectric with losses, the propagation constant γ is defined as:

$$\begin{aligned} \gamma_{01} &= \sqrt{\left(\frac{\pi}{b}\right)^2 - \omega^2 \mu \epsilon \left(1 - i \frac{\sigma}{\omega \epsilon}\right)} = \\ &= ik \sqrt{\left(1 - \frac{\lambda_e^2}{\lambda_{crit 01}^2}\right) - i \frac{\sigma}{\omega \epsilon}} = \beta_s + i\alpha_s \end{aligned}$$

Hence, the attenuating constant will be approximately defined as:

$$\beta_s = \frac{k}{2} \frac{\tan \delta}{\sqrt{1 - \frac{\lambda_e^2}{\lambda_{crit 01}^2}}}, \quad (9-17)$$

where

$$k = \frac{2\pi}{\lambda_e}, \quad \tan \delta = \frac{\sigma}{\omega \epsilon}.$$

The general attenuating constant is determined by the sum of the expressions (9-16) and (9-17).

As for the maximum permissible power which a rectangular waveguide with an air filling can admit, it is defined as:

$$P_{\max} = 6.63 \times 10^{-4} E_{\text{perm}}^2 ab \frac{\lambda}{\lambda_w} K \text{ [W]}, \quad (9-18)$$

where E_{perm} is the maximum permissible field intensity, which is usually taken equal to 30 000 V/cm;

K , the travelling-wave ratio in the waveguide.

In the expressions (9-18), all the dimensions are given in metres. It can be seen from this expression that when the wave-length approaches its critical value, the permissible power in the waveguide goes down. The maximum power in the waveguide is obtained when $\frac{\lambda}{2b} \approx 0.5$. However, this ratio is critical with regard to the appearance of the H_{02} mode, so that one usually chooses $\frac{\lambda}{2b} \approx 0.7$.

Circular waveguides are utilised with the lowest modes: H_{11} , E_{01} and H_{01} . Of these, as was indicated above, the H_{11} mode has the highest critical wave-length ($\lambda_{\text{crit}} = 3.42 a$), so that, in that case, the transverse dimensions of the tube are the smallest. The E_{01} ($\lambda_{\text{crit}} = 2.62 a$) and H_{01} ($\lambda_{\text{crit}} = 1.64 a$) modes are excited in the case of tubes of larger dimensions and require therefore the use of filtering devices to eliminate the excitation of the lower modes.

As for the attenuation caused by the energy losses in the walls of the waveguides, in the case of the H_{11} and E_{01} modes, it increases with the frequency much in the same way as in a rectangular waveguide and in coaxial lines. The H_{01} mode is remarkable for the fact that the attenuating constant decreases when the frequency increases.

The attenuating constant can be calculated in the same way as for the H_{01} mode in a rectangular waveguide. Fig. 9-10 shows the curves of the attenuating constant plotted against the frequency, in a copper tube of radius $a = 5$ cm, for the three modes under consideration [39].

It can be seen that for the H_{01} mode, a very small attenuating constant can be obtained. However, the utilisation of this mode in practice is rather difficult because a special device is required to filter out the H_{11} and E_{01} modes, which are unavoidably excited when any inhomogeneities are introduced into the waveguide. One of the ways of obtaining a pure H_{01} mode is to utilise a circular waveguide made of copper rings insulated from one another.

Rings of this kind favour the excitation of transverse currents with which the H_{02} mode is associated and prevent the excitation of longitudinal currents with which the H_{11} and E_{01} modes are associated. Thus, in the millimetre wave range, a waveguide with an H_{01} mode can be utilised as the most efficient transmission line in antenna installations.

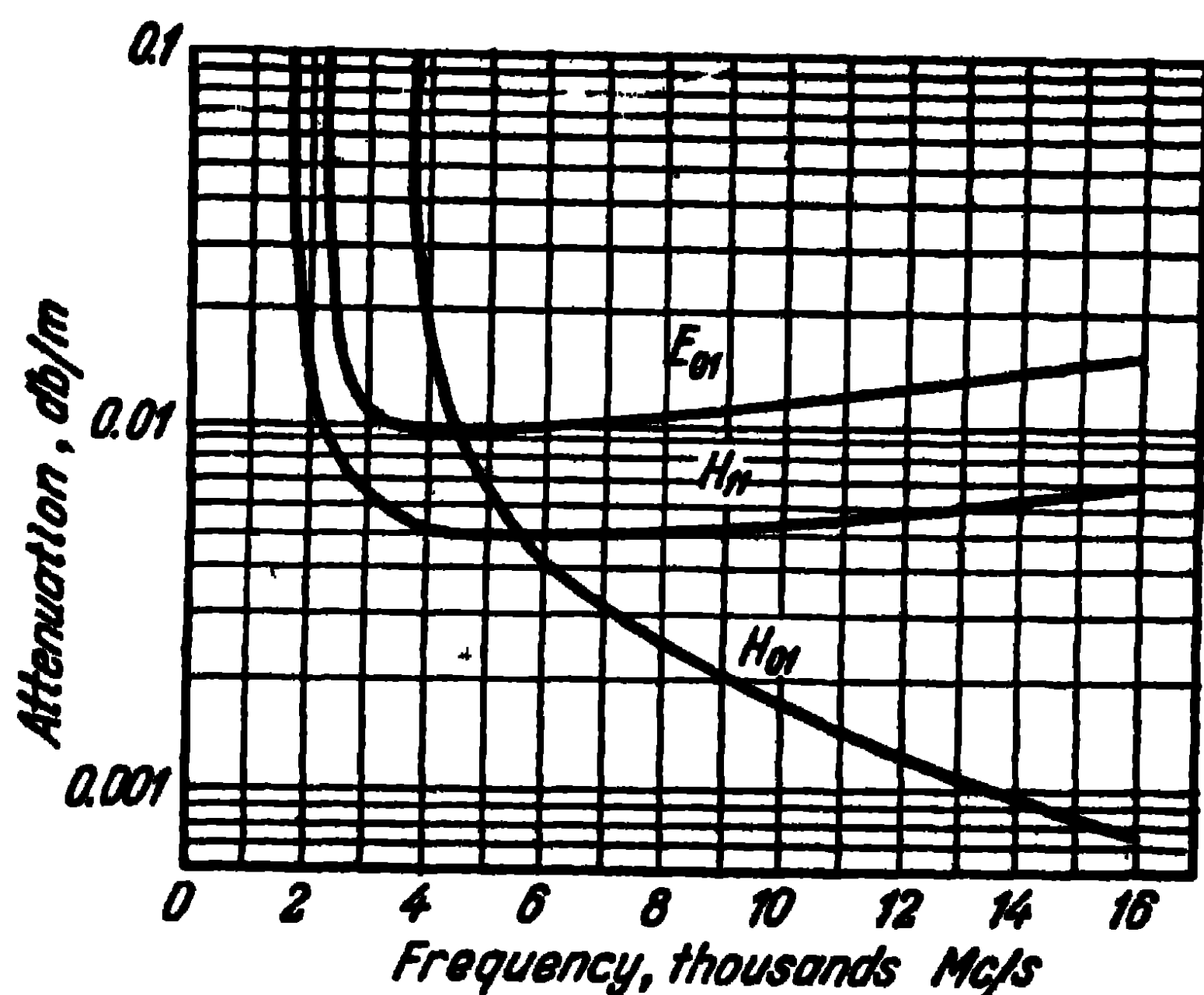


Fig. 9-10. Attenuation constant of the modes in a circular waveguide.

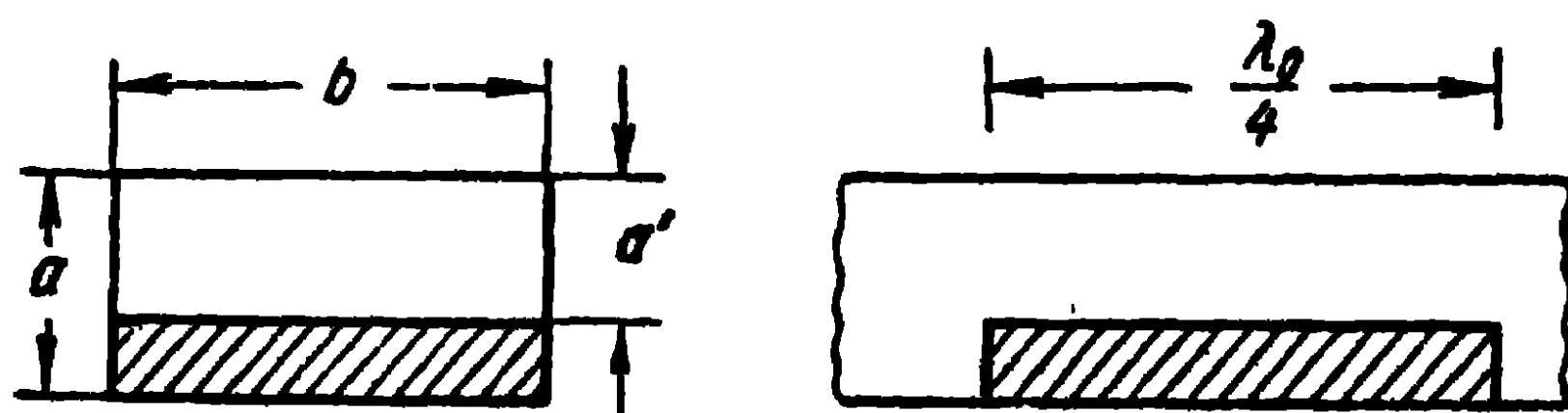


Fig. 9-11. Quarter-wave-length insert in a rectangular waveguide.

To tune waveguides on a travelling wave, quarter-wave-length inserts, reactive stubs, reactive diaphragms and waveguide stub transformers are utilised.

A quarter-wave-length insert in a rectangular waveguide with an H_{01} mode is shown in Fig. 9-11. It is connected between the node and the antinode of the electric field intensity (from the node towards the generator). The insert is a metal plate soldered to the broad wall of the waveguide. The insert reduces the narrow dimension of the cross section

of the waveguide, thereby reducing the wave impedance of the twin line equivalent to the waveguide. The required value of the insert wave impedance can be calculated with the help of (8-16) and since the wave impedance of the equivalent twin line is determined from (8-2), the transverse size of the insert will be defined as:

$$a' = a \sqrt{K}. \quad (9-19)$$

The reactive stub is inserted into the waveguide in a direction parallel to its narrow wall and, for a small length ($l < \lambda/4$), it acts as a capacitance connected in parallel to

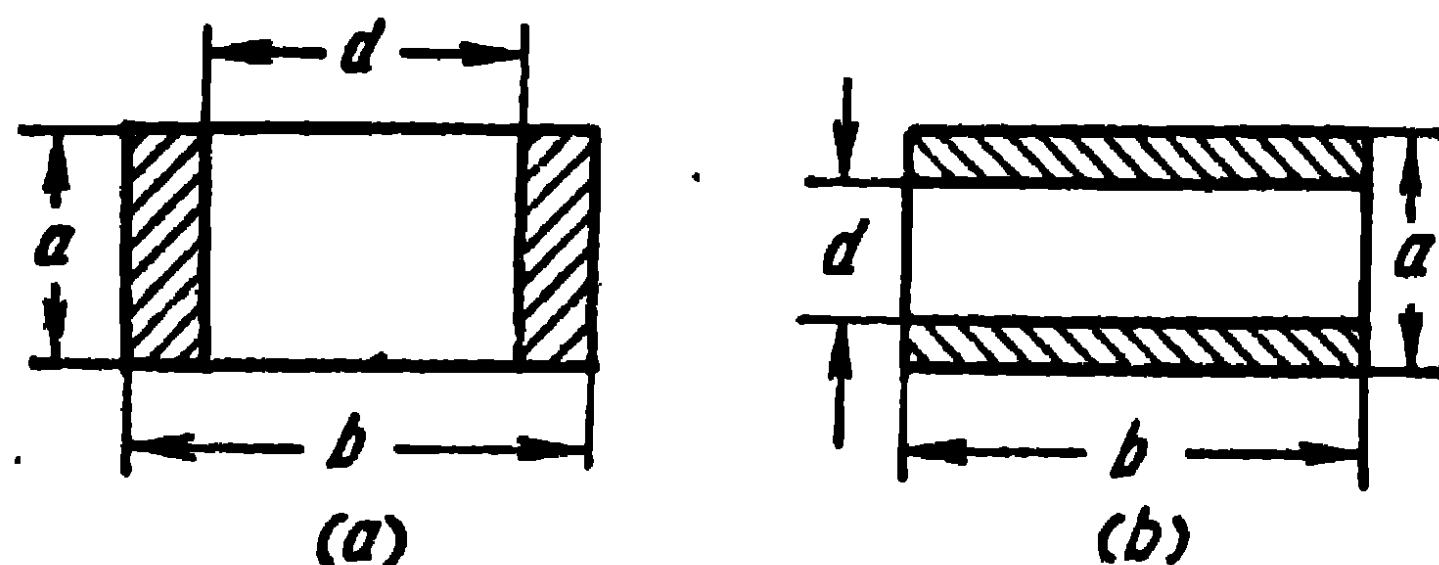


Fig. 9-12. Diaphragms:
a—inductive; b—capacitive.

the equivalent twin line. The stub is connected at a distance l from the antinode towards the load, calculated from (8-14). The calculation of the necessary length of the stub is fairly difficult, so that its length l is determined experimentally.

The waveguide is fairly often tuned by means of an inductive or a capacitive diaphragm (Fig. 9-12). The diaphragms are thin metal plates lying in the transverse plane of the waveguide. In the case of an inductive diaphragm, the dimension b of the waveguide decreases and the dimension a of the waveguide decreases in the case of a capacitive diaphragm. A decrease of the dimension b of the waveguide in a twin line is equivalent to the insertion of a shunting inductivity and a decrease of the dimension a of the waveguide is equivalent to the insertion of a shunting capacitance.

Let us investigate the theory of the inductive diaphragm. Let the diaphragm be connected at the section $z=0$ of an infinite waveguide and let a wave of the H_{01} mode come towards it from the left, in the direction of the rising values of z .

Under the influence of this wave, the diaphragm becomes excited and, as a result, a wave is formed after passing through the diaphragm and a wave of the same mode H_{01} is reflected from it. In addition, we get the excitation of higher modes. It is evident that the electric field set up at the opening of the diaphragm has a direction which coincides with the x -axis; furthermore, the amplitude of this field does not depend on the x -coordinate; in the direction of the y -axis, it changes in accordance with a definite law and on the metal part of the diaphragm, it equals zero.

The electromagnetic field excited by the diaphragm can be regarded as the field of the surface magnetic currents induced from the left and right on an entire, infinitely thin and ideally conducting metal plate which completely screens the waveguide. Thus, we assume that the wave which reaches the diaphragm is completely reflected from it and, in accordance with (7-15) and (7-17), the primary field in the region $z \leq 0$ is defined as:

$$\left. \begin{aligned} E_x &= \sin\left(\frac{\pi}{b} y\right) [e^{-i\alpha_{01}z} - e^{+i\alpha_{01}z}]; \\ H_y &= \frac{\alpha_{01}}{\omega\mu} \sin\left(\frac{\pi}{b} y\right) [e^{-i\alpha_{01}z} + e^{+i\alpha_{01}z}], \end{aligned} \right\} \quad (9-20)$$

where

$$\alpha_{01} = \sqrt{k^2 - \left(\frac{\pi}{b}\right)^2}.$$

In these expressions, the electric field amplitude of the incoming wave is assumed to be equal to unity; the longitudinal component of the magnetic field intensity will no longer be needed and is not given here.

A secondary field is superposed on the primary field in the region $z \leq 0$; it is set up by the surface magnetic current, which coincides in direction with the y -axis and is defined as

$$\mathbf{J}^M = [\mathbf{n}, \mathbf{E}] = [i_z, i_x] E_x(y) = i_y E_x(y),$$

where i_x, i_y, i_z are the unit vectors;

$E_x(y)$, the electric field intensity at the opening of the diaphragm.

This surface current density can be associated with the space current density in the region $z \leq 0$ by means of the delta-function

$$j_y^M = E_x(y) \delta(z-0). \quad (9-21)$$

And, consequently, the secondary field in the region $z \leq 0$ can be determined from the expressions (7-20) and (7-23). Substituting (9-21) into (7-23) and integrating over x and z , we obtain:

$$A_y^M(y, z) = \sum_{m=1}^{\infty} \frac{2}{b\gamma_{0m}} \sin\left(\frac{\pi m}{b} y\right) \times \\ \times e^{\gamma_{0m} z} \int E_x(y') \sin\left(\frac{\pi m}{b} y'\right) dy', \quad (9-22)$$

where $\gamma_{0m} = \sqrt{\left(\frac{\pi m}{b}\right)^2 - k^2}$ and the integration is performed within the limits of the opening of the diaphragm

$$\frac{b-d}{2} \leq y \leq \frac{b+d}{2}.$$

We have taken into consideration the fact that, due to the mirror image of the magnetic current in the metal partition of the waveguide (diaphragm), the field is doubled in comparison with the field of the same current in an infinite waveguide.

The surface magnetic current superimposed on the right side of the partition is defined as:

$$\mathbf{J}^M = [\mathbf{n}, \mathbf{E}] = [-i_z, i_x] E_x(y) = -i_y E_x(y)$$

and is associated with the space density of the magnetic current in the region $z \geq 0$ by the expression

$$j_y^M = -E_x(y) \delta(z-0). \quad (9-23)$$

Substituting (9-23) into (7-23), performing the integration over x and z and doubling the field on account of the mirror image of the current in the partition, we obtain for the region $z \geq 0$:

$$A_y^M(y, z) = - \sum_{m=1}^{\infty} \frac{2}{b\gamma_{0m}} \sin\left(\frac{\pi m}{b} y\right) \times \\ \times e^{-\gamma_{0m} z} \int E_x(y') \sin\left(\frac{\pi m}{b} y'\right) dy'. \quad (9-24)$$

The intensity of the secondary electric field is determined from the substitution of (9-22) and (9-24) into (7-20), as a result of which, for $z \leq 0$, we obtain:

$$E_x = \sum_{m=1}^{\infty} \frac{2}{b} \sin\left(\frac{\pi m}{b} y\right) e^{\gamma_{0m} z} \int E_x(y') \sin\left(\frac{\pi m}{b} y'\right) dy' \quad (9-25)$$

and for $z \geq 0$:

$$E_x'' = \sum_{m=1}^{\infty} \frac{2}{b} \sin\left(\frac{\pi m}{b} y\right) e^{-\gamma_{0m} z} \int E_x(y') \sin\left(\frac{\pi m}{b} y'\right) dy'.$$

The superposition of surface magnetic currents on the metal partition forms an opening and the continuity of the electric field in the diaphragm thus obtained is satisfied by the expressions (9-25) (when $z=0$, the primary field E_x' also equals zero).

The transverse component of the secondary magnetic field intensity is determined from the substitution of the expressions (9-22) and (9-24) into (7-20), as a result of which, for $z \leq 0$, we obtain:

$$\left. \begin{aligned} H_y'' &= \frac{1}{\omega \mu} \sum_{m=1}^{\infty} \frac{2i\gamma_{0m}}{b} \sin\left(\frac{\pi m}{b} y\right) \times \\ &\times e^{\gamma_{0m} z} \int E_x(y') \sin\left(\frac{\pi m}{b} y'\right) dy' \end{aligned} \right\} \text{and for } z \geq 0 \quad (9-26)$$

$$\left. \begin{aligned} H_y'' &= -\frac{1}{\omega \mu} \sum_{m=1}^{\infty} \frac{2i\gamma_{0m}}{b} \sin\left(\frac{\pi m}{b} y\right) \times \\ &\times e^{-\gamma_{0m} z} \int E_x(y') \sin\left(\frac{\pi m}{b} y'\right) dy'. \end{aligned} \right\}$$

For $z=0$, the transverse component of the intensity of the total magnetic field should be continuous within the limits of the opening:

$$H_y' + H_y''|_{z=-0} = H_y''|_{z=+0} \text{ at the opening.}$$

Substituting here the expressions (9-20) and (9-26), we obtain:

$$\begin{aligned} \sin\left(\frac{\pi}{b} y\right) &= \\ &= -\sum_{m=1}^{\infty} \frac{2i\gamma_{0m}}{b\alpha_{01}} \sin\left(\frac{\pi m}{b} y\right) \int E_x(y') \sin\left(\frac{\pi m}{b} y'\right) dy' \end{aligned} \quad (9-27)$$

at the opening.

Here, the unknown function $E_x(y')$ is the integrand, so that the equation (9-27) is the integral equation relatively to this unknown function.

The higher modes generated by the diaphragms are attenuated in its vicinity and at a certain, rather high, distance, there is only the propagated H_{01} wave. The total field of this wave in the region $z \leq 0$ is defined as:

$$E_x = E'_x + E''_x = \sin\left(\frac{\pi}{b} y\right) [e^{-i\alpha_{01}z} + p_0 e^{+i\alpha_{01}z}]; \quad (9-28)$$

$$H_y = H'_y + H''_y = \frac{\alpha_{01}}{\omega\mu} \sin\left(\frac{\pi}{b} y\right) [e^{-i\alpha_{01}z} - p_0 e^{+i\alpha_{01}z}],$$

where

$$p_0 = -1 + \frac{b}{2} \int E_x(y') \sin\left(\frac{\pi}{b} y'\right) dy' \quad (9-29)$$

is, evidently, the coefficient of reflection of the H_{01} wave coming from the diaphragm.

The relative conductivity of the waveguide for the H_{01} wave at the connection points of the diaphragm is determined by the ratio of the quantity $\frac{\omega\mu}{\alpha_{01}} H_y$ to the quantity E_x in the expressions (9-28) and is equal to the sum of the relative conductivity of the infinite waveguide, equal to unity, and the conductivity of the diaphragm iB' :

$$1 + iB' = \frac{1 - p_0}{1 + p_0}.$$

Hence, the conductivity of the diaphragm is defined as

$$iB' = -\frac{2p_0}{1 + p_0}. \quad (9-30)$$

Thus, having defined from the integral equation (9-27) the intensity of the electric field at the opening of the diaphragm $E_x(y')$, we can calculate from (9-29), the reflection coefficient p_0 and then, from (9-30) the conductivity of the diaphragm B' .

The solution of the integral equation (9-27) is difficult to obtain due to the fact that the functions $\sin\left(\frac{\pi m}{b} y\right)$ are not orthogonal within the limits of the opening of the diaphragm, i.e., on the section

$$\frac{b-d}{2} \leq y \leq \frac{b+d}{2}.$$

The solution of the integral equation relatively to $E_x(y)$ is given in L. Levine's book [40] to which the reader is

referred. The conductivity of the diaphragm in a quasi-static approximation is found to be defined as:

$$B' = -\frac{\lambda_w}{b} \cot^2 \left(\frac{\pi d}{2b} \right). \quad (9-31)$$

The quantity B' is negative, so that the diaphragm under investigation is inductive. If we take account of (8-13) and (8-14), we obtain for the calculation of the magnitude of the window d of the inductive diaphragm, the expression

$$\frac{1-K}{\sqrt{K}} = \frac{\lambda_w}{b} \cot^2 \left(\frac{\pi d}{2b} \right). \quad (9-32)$$

In a similar way, we can obtain the expression for the calculation of the capacitive diaphragm. The calculation of the window d of this diaphragm is done from the expression

$$\frac{1-K}{\sqrt{K}} = \frac{4a}{\lambda_w} \ln \csc \left(\frac{\pi d}{2a} \right), \quad (9-33)$$

where K is the travelling-wave ratio in the waveguide;
 λ_w , the wave-length in the waveguide.

These diaphragms are connected at a distance l_a from the antinode of the electric field intensity towards the generator in the case of an inductive diaphragm and towards the load in the case of a capacitive diaphragm, determined from (8-14).

The inductive diaphragm is preferable because it practically does not lower the power admitted by the waveguide, since the distance between the broad walls of the waveguide remains unchanged. In the capacitive diaphragm, the distance between the broad walls of the waveguide decreases and, consequently, so does the magnitude of the admitted power.

For the insertion into the waveguide of stub transformers, so-called tees are used, installed in the plane of the magnetic or electric vector of the field of the waveguide (Fig. 9-13).

In the case of an E -plane tee, a transverse slot is milled in the broad wall of the waveguide and the branched waveguide joined to the slot. Since the transverse slot is excited by the longitudinal component of the electric current, in a twin line equivalent to the waveguide, such a tee consists of a stub connected in series (Fig. 9-13, a). In the case of an H -plane tee, the slot is milled in the narrow wall of the waveguide and the branched waveguide joined to it. This slot is excited by the transverse components

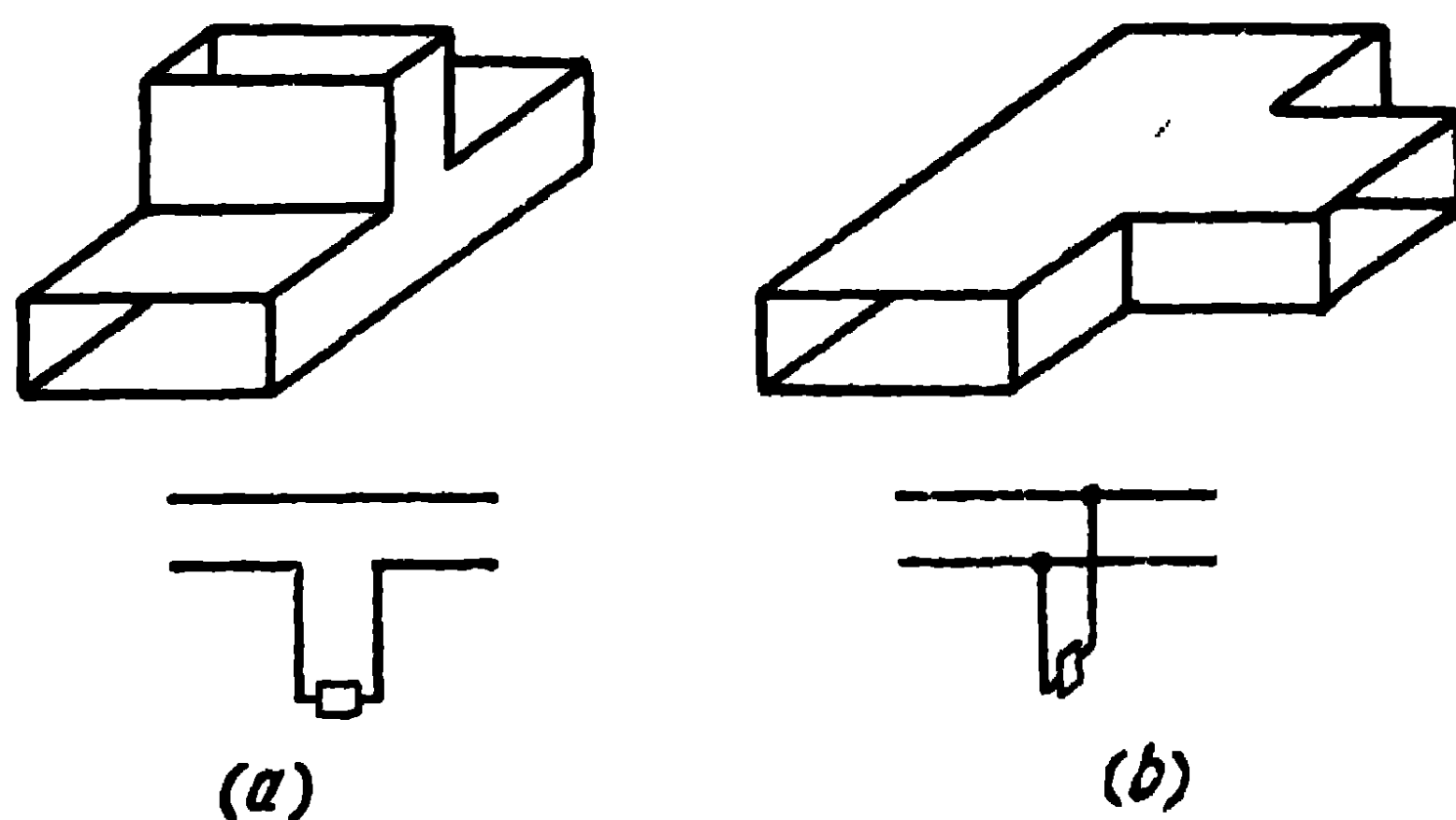


Fig. 9-13. Tees:
a—tee in the *E*-plane; *b*—tee in the *H*-plane.

of the current in the waveguide, so that in a twin line equivalent to the waveguide, such a tee consists of a stub connected in parallel (Fig. 9-13, *b*). A two-stub tuner consists of two *E*-plane tees shorted out at the end by means of short-circuiting plungers. The distance between the axes of the tees is made equal to an odd number of quarter-wave-lengths in the waveguide. Tees (stubs) of the proper length always make it possible to compensate the reflection from the load of the waveguide and obtain in it a travelling-wave type of operation (narrow-band matching).

The travelling-wave tuning elements described above concern a rectangular waveguide with an H_{01} wave. Similar tuning elements can also be utilised in a circular waveguide.

Now, let us discuss the other elements utilised in waveguide channels. On the whole, we shall have in mind elements utilised in a rectangular waveguide.

The waveguide channel must necessarily be assembled of separate sections and poor contacts at the junctions may cause considerable energy losses. Moreover, due to oxidation of the metal, the contact is not permanent. Considerable energy reflections may occur from the place of junction of two sections of the waveguide channel, thereby disturbing the matching of the waveguide to the load. To avoid these

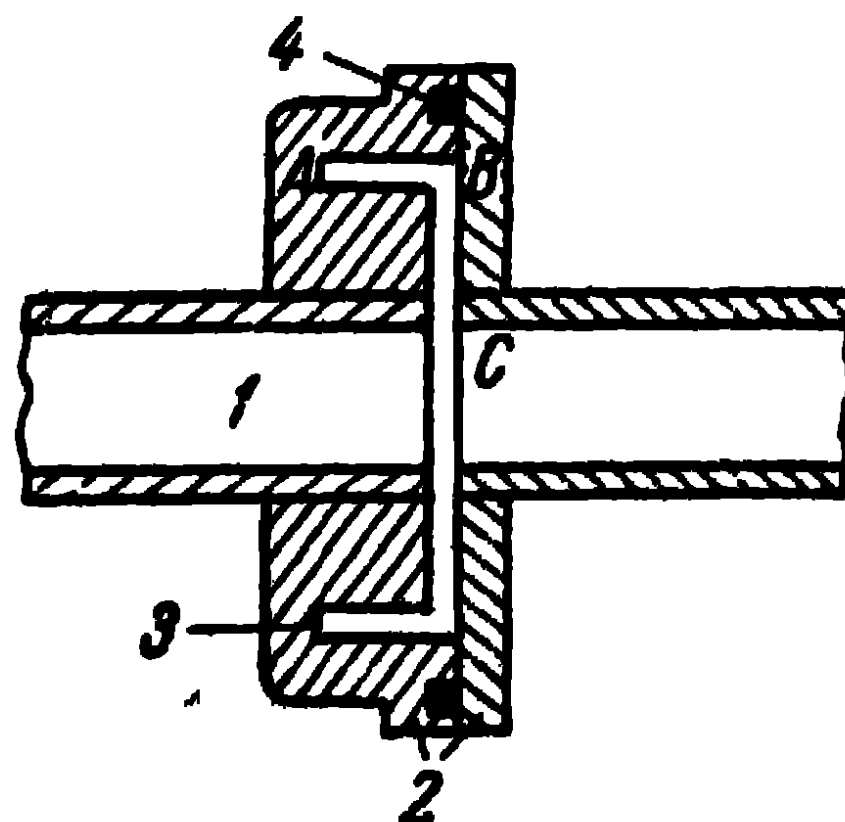


Fig. 9-14. Choke flange:
 1—waveguide; 2—flanges; 3—ring perforation; 4—ring washer ensuring hermetic sealing

undesirable occurrences, the waveguide sections are generally joined by means of choke flanges, as shown in Fig. 9-14. A coaxial perforation is made in the left flange of the junction; its length AB is equal to a quarter of a wave-length. In addition, the left flange has a circular groove forming together with the right flange a radial line BC of length also equal to a quarter of a wave-length. Thus, at the point C of the flange, two sections of the waveguide are electrically short-circuited. At the point B , where the flanges are in actual contact, there arises a current node. Owing to the fact that the resistance of this contact is connected in series to the input resistance of the coaxial quarter-wave-length line

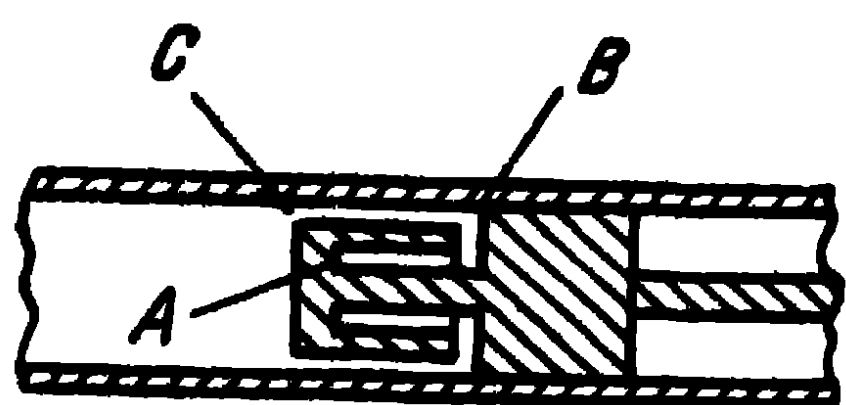


Fig. 9-15. Plunger with a throttle.

AB shorted out at the end, the magnitude of the resistance of this contact and its lack of permanency do not affect the operation of the wave in the waveguide. The energy lost on heating this contact is also small.

In the case of a circular waveguide with an E_{01} wave, transverse electromagnetic waves are set up in the coaxial line AB and radial line BC of the choke-flange junction, the lengths AB and BC of the groove being chosen appropriate to this mode. In the case of a rectangular waveguide, an H_{11} mode is set up in the coaxial line AB , the critical wave-length of which equals $\lambda_{crit H_{11}} = \pi d_{mean}$, where d_{mean} is the mean diameter of the coaxial line. An H_{11} mode is likewise set up in a radial line, with one variation on the periphery. Consequently, the lengths AB and BC of the grooves are chosen so as to suit the H_{11} modes in these lines.

In the case of the H_{01} mode in a circular waveguide, flanges can be dispensed with, since this mode is accompanied by transverse currents on the walls of the waveguide. The existence of a poor contact or even a clearance between two sections of the waveguide does not affect the propagation of the wave in the waveguide.

Special mobile plungers provided with the above-described throttle are utilised for producing a short-circuit in waveguides. Such a plunger is shown in Fig. 9-15. The length chosen for the groove AB is equal to a quarter of a wave-length and direct contact of the plunger with the waveguide takes place at the points B , where there occurs a current

node. The length of the groove BC is also equal to a quarter of a wave-length and, for this reason, a current antinode is produced at the points C and, consequently, an electric short-circuit of the waveguide.

Let us now pass on to the description of waveguide-to-coaxial-line and waveguide-to-waveguide transitions. Tran-

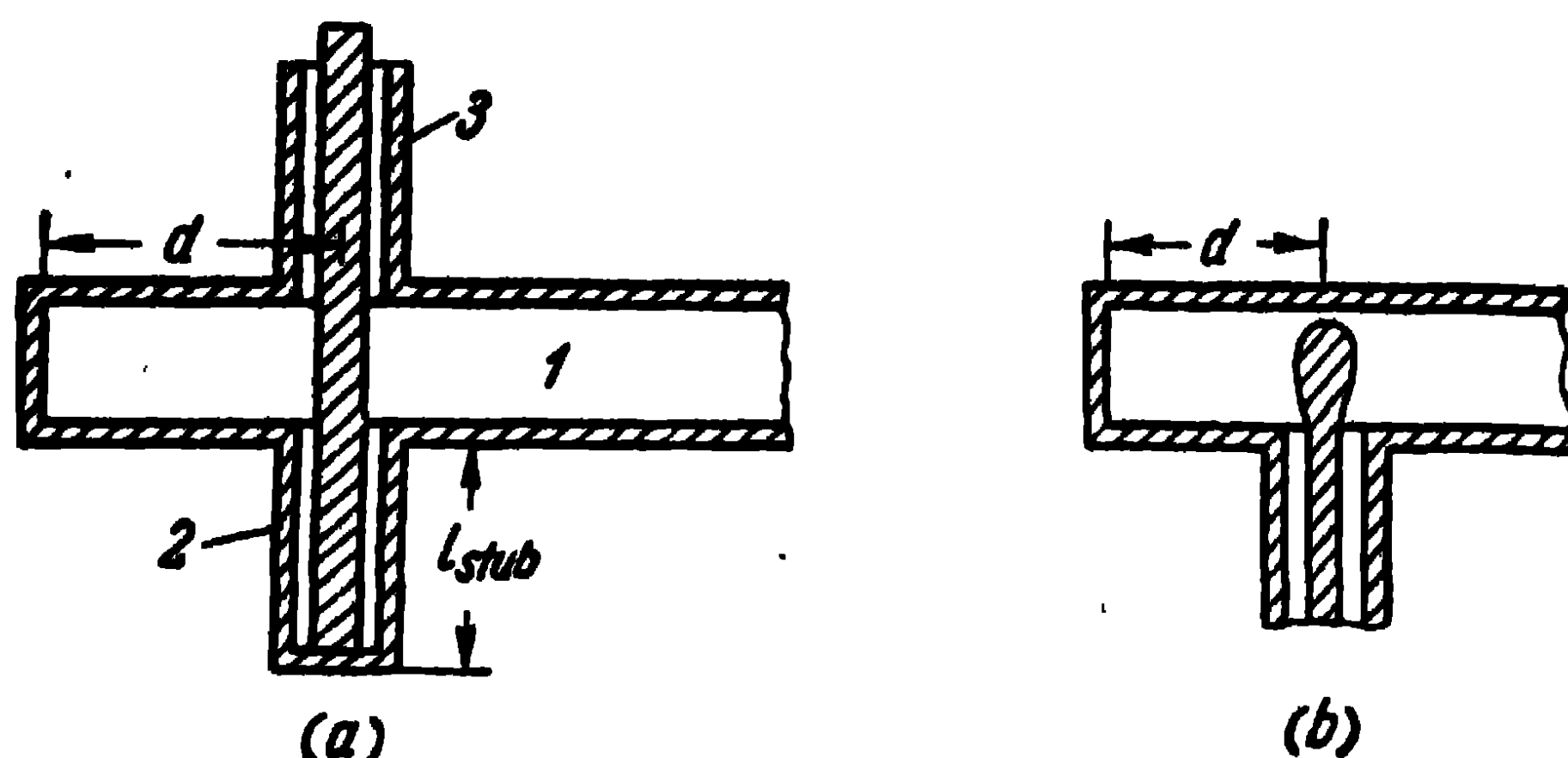


Fig. 9-16. Rectangular waveguide-to-coaxial-line transitions:
1—waveguide; 2—stub; 3—coaxial line.

sitions of this kind find frequent application in practice; the main considerations in their design are that they should be matched and should not narrow the pass-band and diminish the magnitude of the admitted power.

One type of rectangular waveguide-to-coaxial-line transition is illustrated in Fig. 9-16, *a*. In a transition of this kind, the proper choice of the length of the coaxial stub l_{stub} and of the length of the section of rectangular waveguide d makes it possible to obtain in the coaxial line, by means of which the energy is fed to the waveguide, a travelling-wave type of operation. Another type of waveguide-to-coaxial-line transition is illustrated in Fig. 9-16, *b*. In this transition the internal conductor of the coaxial line, introduced into the waveguide, thickens out, assuming a drop-like shape. A transition of this kind enables to widen the pass-band and increase the power passing through the transition.

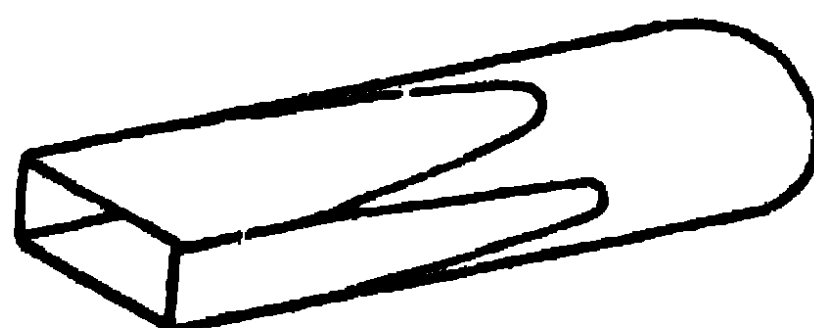


Fig. 9-17. Rectangular-to-circular waveguide transition.

Fig. 9-17 illustrates an H_{01} mode rectangular waveguide to H_{11} mode circular waveguide transition. The transition is accomplished by a gradual deformation of the cross section

of the tube into a circular cross section. If the length of this transition is of the order of one wave-length or more, in an equivalent twin line, it represents a dispersive line with gradually changing parameters. Such a transition is of the broad-band type.

H_{01} mode rectangular waveguide to E_{01} mode circular waveguide transitions are very frequently used. This is because the E_{01} mode is symmetrical relatively to the waveguide axis and is therefore convenient for use in rotary joints.

Fig. 9-18, *a* illustrates a transition of this kind, obtained by means of a stub placed on the axis of the circular wave-

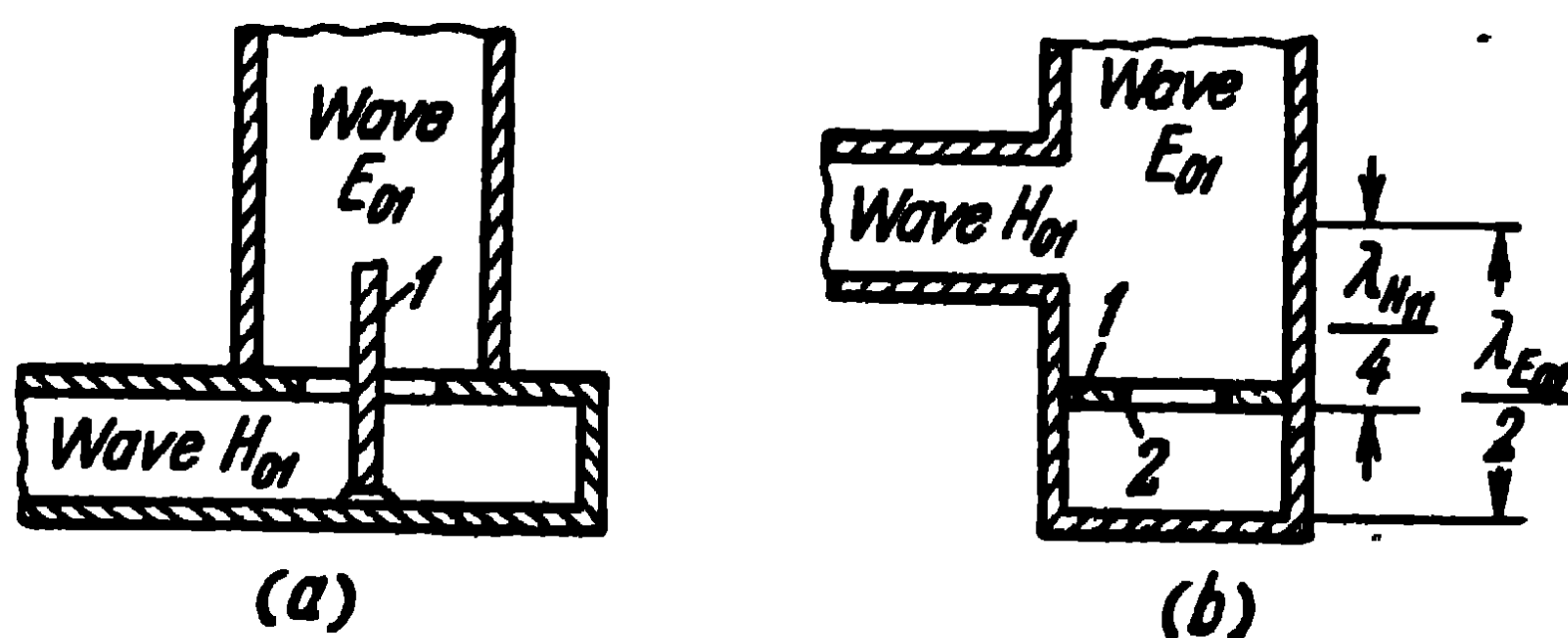


Fig. 9-18. Rectangular-to-circular waveguide transitions:

a—transition by means of a coaxial stub: 1—stub; *b*—transition with a resonance ring: 1—insulator; 2—metal ring.

guide and introduced into the rectangular waveguide through its broad wall. Although in a circular waveguide whose dimensions have been chosen so as to allow the propagation of an E_{01} mode, we may also get the propagation of an H_{11} mode, the latter is not excited because of the symmetrical position of the stub. Thus, in this device, we get the excitation of a pure E_{01} mode.

Another transition of this kind is illustrated in Fig. 9-18, *b*, in which the junction of the rectangular waveguide with the circular one is accomplished by means of a rectangular aperture in the lateral wall of the circular waveguide. In that case, the excitation is favoured of both the E_{01} and H_{11} modes in the circular waveguide. In order to eliminate the H_{11} mode, the short-circuited section of circular waveguide is given a length of half a wave-length of the E_{01} mode ($\lambda_{wE_{01}}/2$) and a metal resonance ring is placed in its transverse plane at a distance of a quarter of a wave-length of the H_{11} mode ($\lambda_{wH_{11}}/4$). This metal ring is excited by the H_{11} mode and

short-circuits it. At the same time, it allows the free passage of the E_{01} mode, since the electric lines of force of the E_{01} mode are directed perpendicularly to the ring. In a twin line equivalent to the waveguides, the short-circuited stub formed by a section of round waveguide is connected in series into the line and allows the free passage of the E_{01} mode, whilst preventing the excitation of the H_{11} mode. The metal ring is usually fixed on a dielectric support with small losses.

A rotary joint in a waveguide channel is formed by means of an inductive section in a circular waveguide. The latter

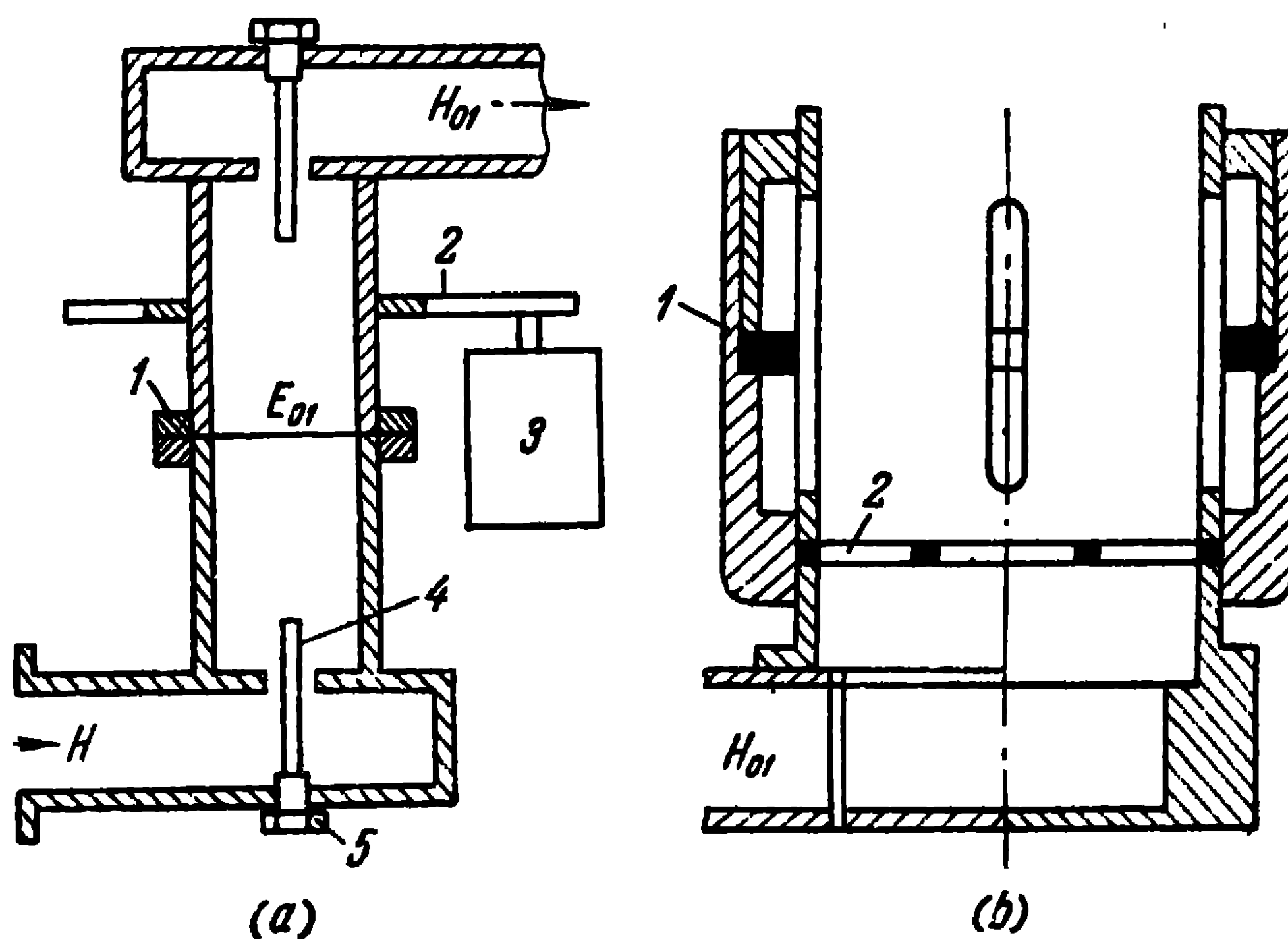


Fig. 9-19. Rotary joint:

a—transition with a coaxial stub: 1—Inductive section; 2—gears; 3—motor; 4—stub; 5—matching tuner;
b—transition with a resonance ring: 1—absorbing ring; 2—filtering metal ring

is similar to the inductive section shown in Fig. 9-9. In a rotary joint, rectangular-to-circular waveguide transitions are used along with circular-to-rectangular waveguide transitions similar to the ones described above. Fig. 9-19, *a* illustrates the arrangement of a rotary joint of this kind with an E_{01} wave in a circular waveguide in which the upper part rotates relatively to the lower one around the axis of the circular waveguide by means of gears. Fig. 9-19, *b* illustrates another rotary device in which a transition from a rectangular to a circular waveguide with a resonance ring is used. In this case, special absorbers are utilised to reinforce the

suppression of the H_{11} mode in the circular waveguide. Four longitudinal slots are cut in the circular waveguide disposed on the periphery at 90° angles to one another. The slots are excited by the H_{11} mode and oscillations of the H_{011} mode arise in the tuned coaxial resonator. The coaxial resonator is formed by the external surface of a circular waveguide and a metal tube enclosing the waveguide. An absorbing ring is placed in the antinode of the electric field intensity of the resonator and the H_{11} mode in the circular waveguide is thereby suppressed.

9-4. Switching Devices and Duplexers

Various switching devices are fairly often used in transmission lines. A brief description of some of them is given below.

The necessity may arise, for example, when two transmitters of different frequencies operate on the same antenna.

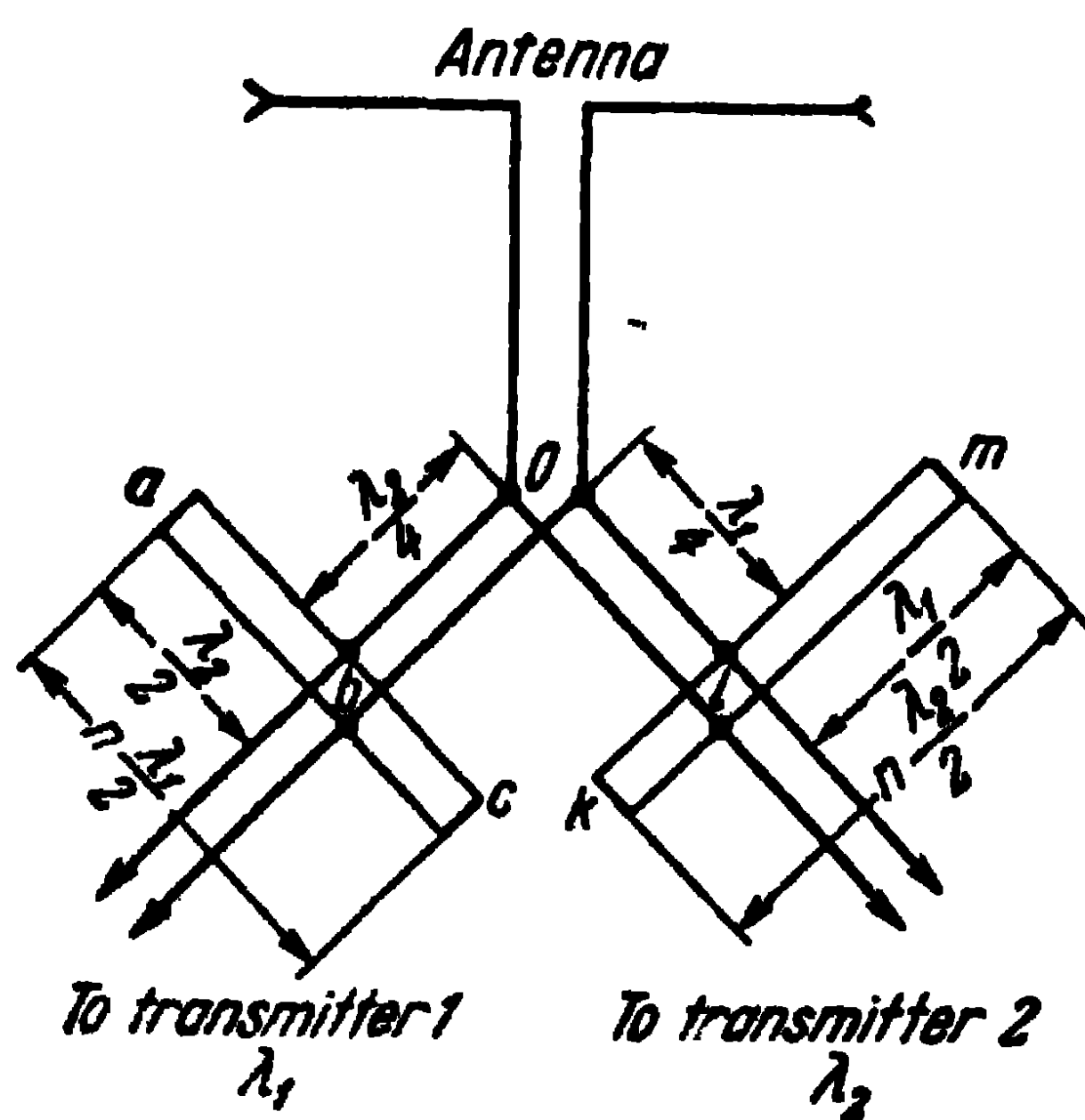


Fig. 9-20. Two transmitters employing one antenna.

Fig. 9-20 shows the circuit of a device of this kind in which two feeders, one from transmitter 1 and one from transmitter 2 are connected to the common feeder of an antenna at the point O . As suggested by S.I. Nadenenko, a combined stub is connected in parallel to each of the feeders at a distance of a quarter of a wave-length from this point. The combined stub consists of a short-circuited line of a length equal to an even number

of half-waves of one of the transmitters. The length of one of the arms of the stub between the connection points to the feeder and the short-circuit points is equal to half the wave-length of the other transmitter.

Thus, when the transmitter 1 operates on the λ_1 wave, the stub abc of length $n\lambda_1/2$ represents an infinitely large resistance and allows the free passage of the λ_1 wave, and the

stub klm , which lies at a distance $\lambda_1/4$ from the point O and one arm of which has a length equal to $\lambda_1/2$, short-circuits the feeder 2 at the point l and sets up an infinitely large resistance of the feeder 2 at the point O . When the transmitter 2 operates on the λ_2 wave, the stub klm of length $n\lambda_2/2$ represents an infinitely large resistance and allows the free passage of the λ_2 wave, and the stub abc , which lies at a distance $\lambda_2/4$ from the point O and one arm of which has a length equal to $\lambda_2/2$ short-circuits the feeder 1 at the point b and sets up on this wave an infinitely large resistance of the feeder 1 at the point O . Consequently, both transmitters operate on the same antenna, independently of one another.

If we take into account the finite resistance of the wires of the combined stub, we see that there is satisfactory degree of independence between the transmitters when the λ_1 and λ_2 wave-lengths are shifted off the frequency by 5 to 10%.

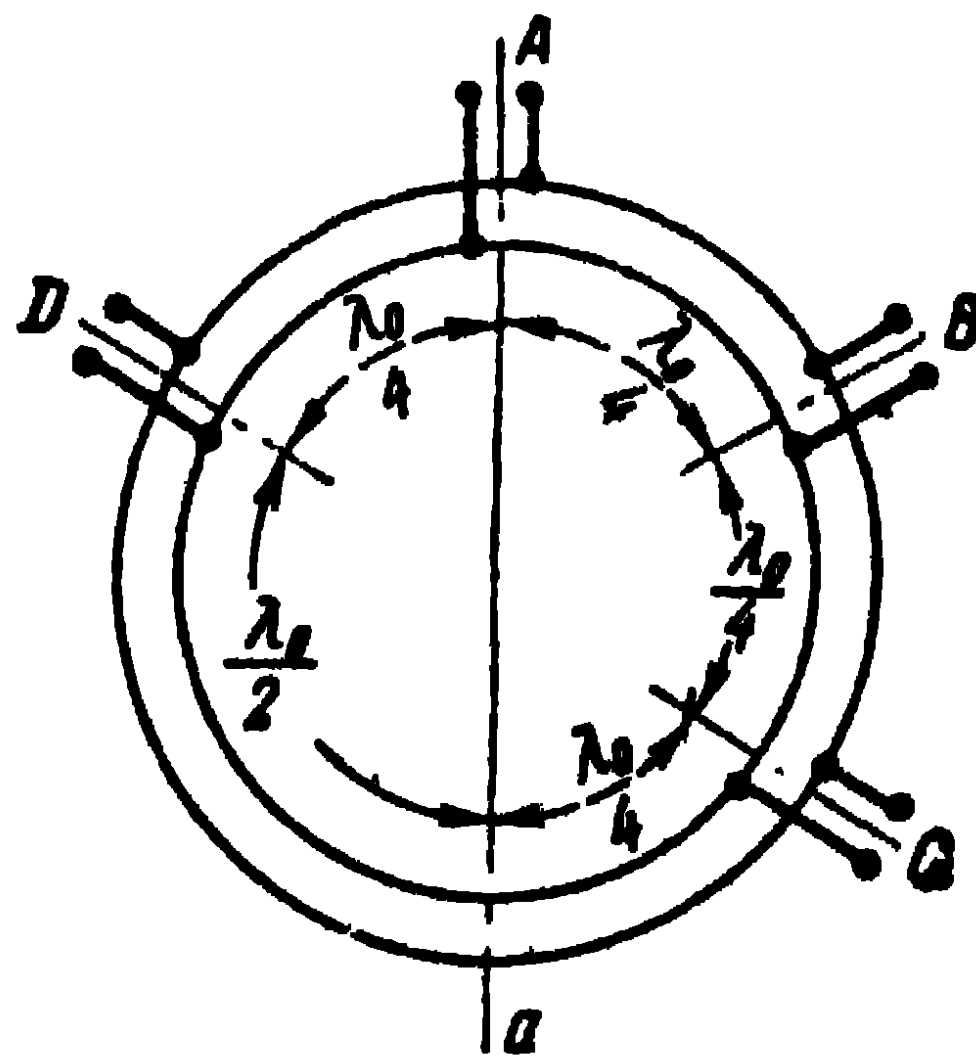


Fig. 9-21. Circuit of hybrid ring.

Another type of decoupling device is the hybrid ring, which consists of a twin feeder, a coaxial line or a waveguide (Fig. 9-21). The overall length of the ring is chosen equal to $1.5 \lambda_0$ and the distance between the terminals A and B , A and D , B and C are chosen equal to $\lambda_0/4$. If a generator is connected to the terminals A , a standing wave is set up in the annular line, provided all the other terminals are unloaded; furthermore, a voltage antinode is produced in the section a , a voltage node at the terminals C and once again a voltage antinode at the terminals B and D . Now, if loads are connected to the terminals B , D and C , no power whatsoever is delivered to the load C and, on condition that the loads are equal, the power is divided equally between the terminals B and D . Conversely, when the generator is connected to the terminals C , no power whatever is delivered to the load connected to the terminals A , but is divided between the loads at the terminals B and D . Similarly, the power fed to the terminals B is not delivered to the terminals D but divided between the loads at the terminals A and C .

It is readily seen that in the case of equal resistances of the loads connected to the terminals B, D ($Z_B = Z_D$), the input impedance at the terminals A , connected to the generator, is defined as:

$$Z_A = \frac{W_0^2}{2Z_B},$$

where W_0 is the wave impedance of the annular line.

Let W be the wave impedances of the matched lines connected to the terminals of the ring; the condition of full matching of the annular system is then reduced to the expression:

$$W_0 = W \sqrt{2}$$

Thus, on the principal frequency f_0 , the decoupling (ratio of the powers) between the terminals A and C equals infinity and the travelling-wave ratio in the feeder A equals unity. When the frequency is shifted off the principal frequency due to the fact that the hybrid ring is thrown out of balance, the decoupling and matching deteriorate. Calculations show that when the frequency is shifted off by 10% ($f = 0.9 f_0$), the decoupling is lowered down to 24.6 db. When $f = 0.9 f_0$ or $f = 1.1 f_0$, the travelling-wave ratio in the feeder is lowered down to $K = 0.88$, and when $f = 0.8 f_0$ or $f = 1.2 f_0$ it is lowered down to $K = 0.72$. When the junctions of the hybrid ring are not parallel, as shown in Fig. 9-21, but series junctions, the resistance loading the generator at the terminals A is defined on the principal frequency as:

$$Z_A = \frac{2W_0^2}{Z_B}$$

and the condition for the optimum matching of the annular system is defined as:

$$W_0 = \frac{W}{\sqrt{2}}.$$

The series junction in the hybrid ring occurs, for example, in the case of a rectangular waveguide, when E -plane tees are used.

The hybrid ring circuit can be used for the simultaneous operation of a transmitter and a receiver on a common antenna on the same frequency. In that case, the transmitter is connected to the terminals A , the receiver, to the termi-

nals *C* and the antenna, to the terminals *B*. A matched absorbing resistance is connected to the terminals *D*. Under these conditions, half the power of the transmitter is radiated and the other half is spent in the absorbing resistance. Likewise, only part of the power received by the antenna is spent in the receiver.

The decoupling device shown in Fig. 9-22 finds fairly frequent application in practice. This is the so-called magic tee in a rectangular waveguide with an H_{01} wave. As can be seen

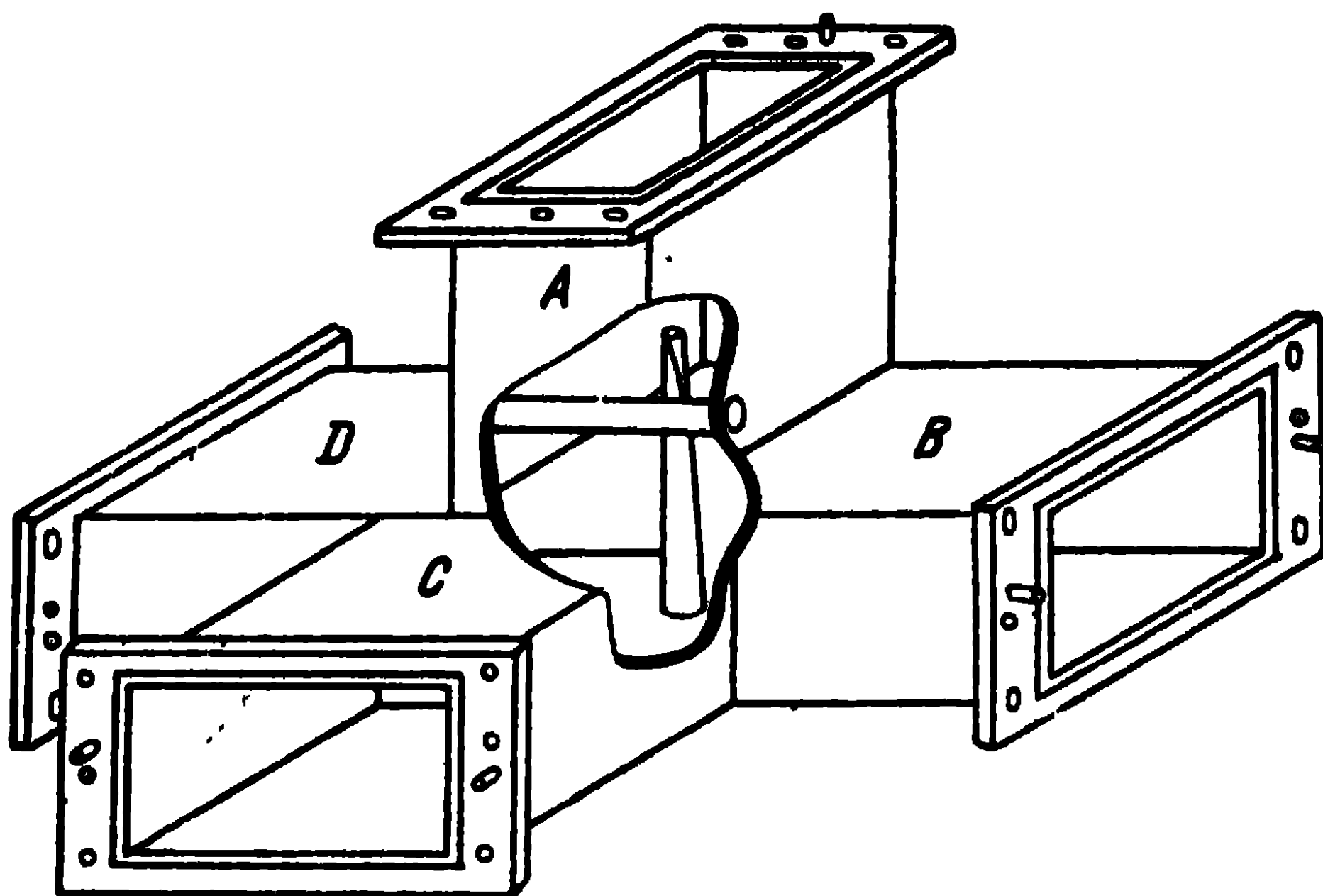


Fig. 9-22. Magic tee.

from the figure it is a combination of an *E*-plane tee and *H*-plane tee. The device operates in a way similar to the hybrid ring described above. When the power enters arm *A*, it is not delivered to arm *C* but divided equally between arms *B* and *D*. On the other hand, when the power enters arm *C*, it is not delivered to arm *A* but divided equally between arms *B* and *D*. Magic tees are matched by means of stubs, as shown in Fig. 9-22, the inductive stub being connected to arm *A* and the capacitive stub, to arm *C*. In the case of loads matched in this way, no reflections of the power take place when it enters any of the arms. Furthermore, when the power enters arm *B*, it is not delivered to arm *D* but divided equally between arms *A* and *C*. Similarly, when the power enters arm *D*, it is not delivered to arm *B* but divided equally between arms *A* and *C*.

The balanced bridge junction, shown in Fig. 9-23, *a*, finds application in the centimetre wave range. It consists of two sections of a rectangular waveguide joined along the narrow sides through rectangular windows of appropriate dimensions. In the case of matched loads, the high-frequency power entering arm *A* of the bridge is divided equally between arms *B* and *D*, none being delivered to arm *C*; furthermore, the field intensities in arms *B* and *D* have a 90° phase shift relatively to one another. In the absence of a window, the resultant field intensity in arm *B* has a 45° phase shift relatively to the

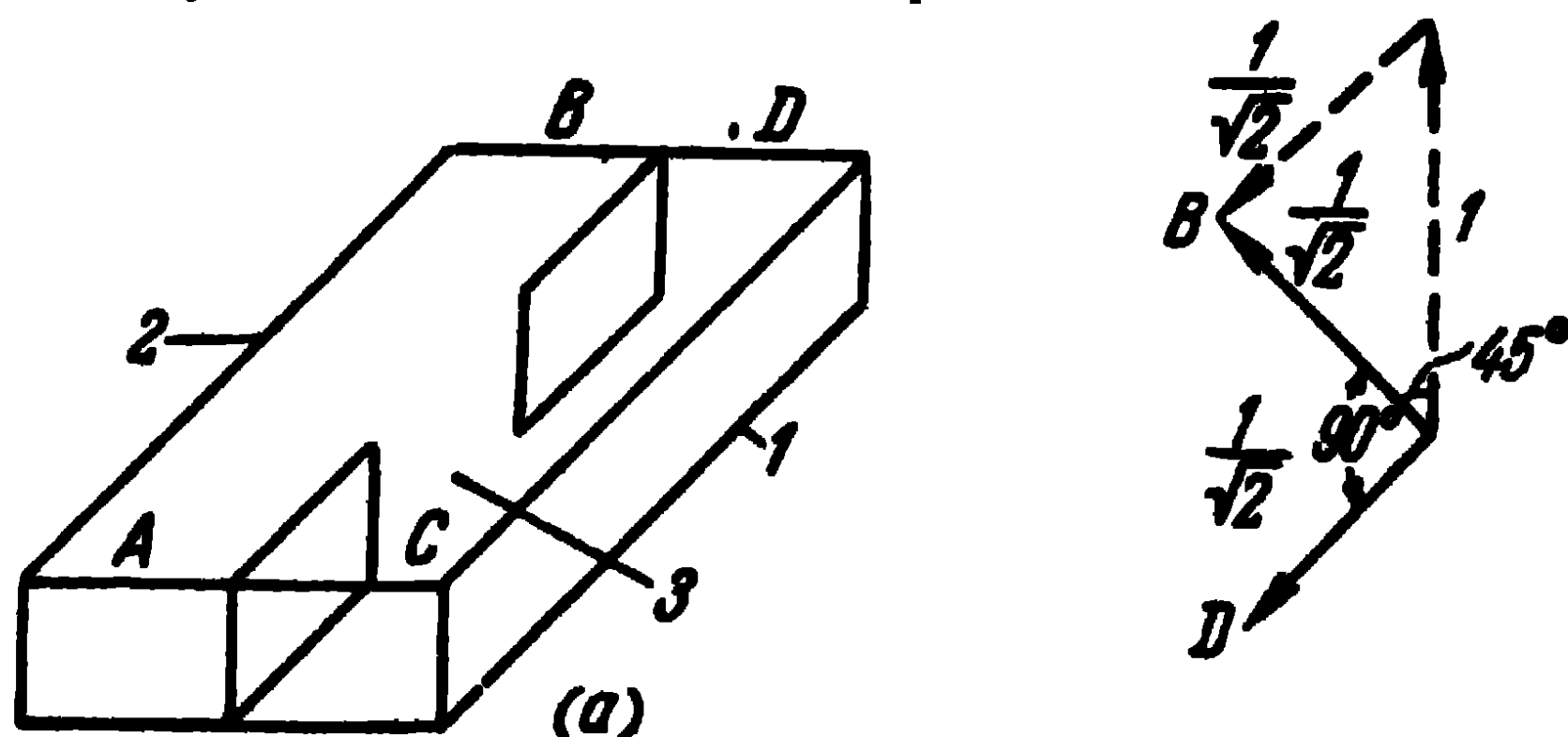


Fig. 9-23. Balanced bridge junction:
a—circuit of the junction: 1—principal waveguide;
 2—auxiliary waveguide; 3—coupling section; *b*—vector
 diagram of the field.

field intensity in that arm. This is shown in the vector diagram in Fig. 9-23, *b*.

From the physical standpoint, the wave incident from arm *A* excites the window in the common wall of the waveguide in such a way that the magnetic current of this window, which changes in accordance with the travelling-wave law, radiates co-phasal fields of equal amplitude in the direction of arms *B* and *D* and produces no radiation in the direction of arms *A* and *C*. The total field of the incident wave and of the wave excited by the window in arm *B* corresponds to the vector diagram in Fig. 9-23, *b*. These properties of a bridge connection are maintained in approximately 12% of the frequency band.

Now, let us give a brief explanation regarding antenna duplexers utilised in pulse radars, when transmitter and receiver are connected to the same antenna. During the transmission period (transmission of energy pulse), all of the power should reach the antenna, without branching off to the input of the receiver. During reception of the signal reflected from

the target, all of the received power should reach the input of the receiver, without branching off towards the transmitter. The alternating connection of the antenna to either transmitter or receiver is accomplished by means of a duplexer the speed of response of which should be 2 to 3 M/sec and the switching frequency, 50 to 3,000 times per second. Switchings of this kind are effected automatically, by means of spark gaps and resonance lines

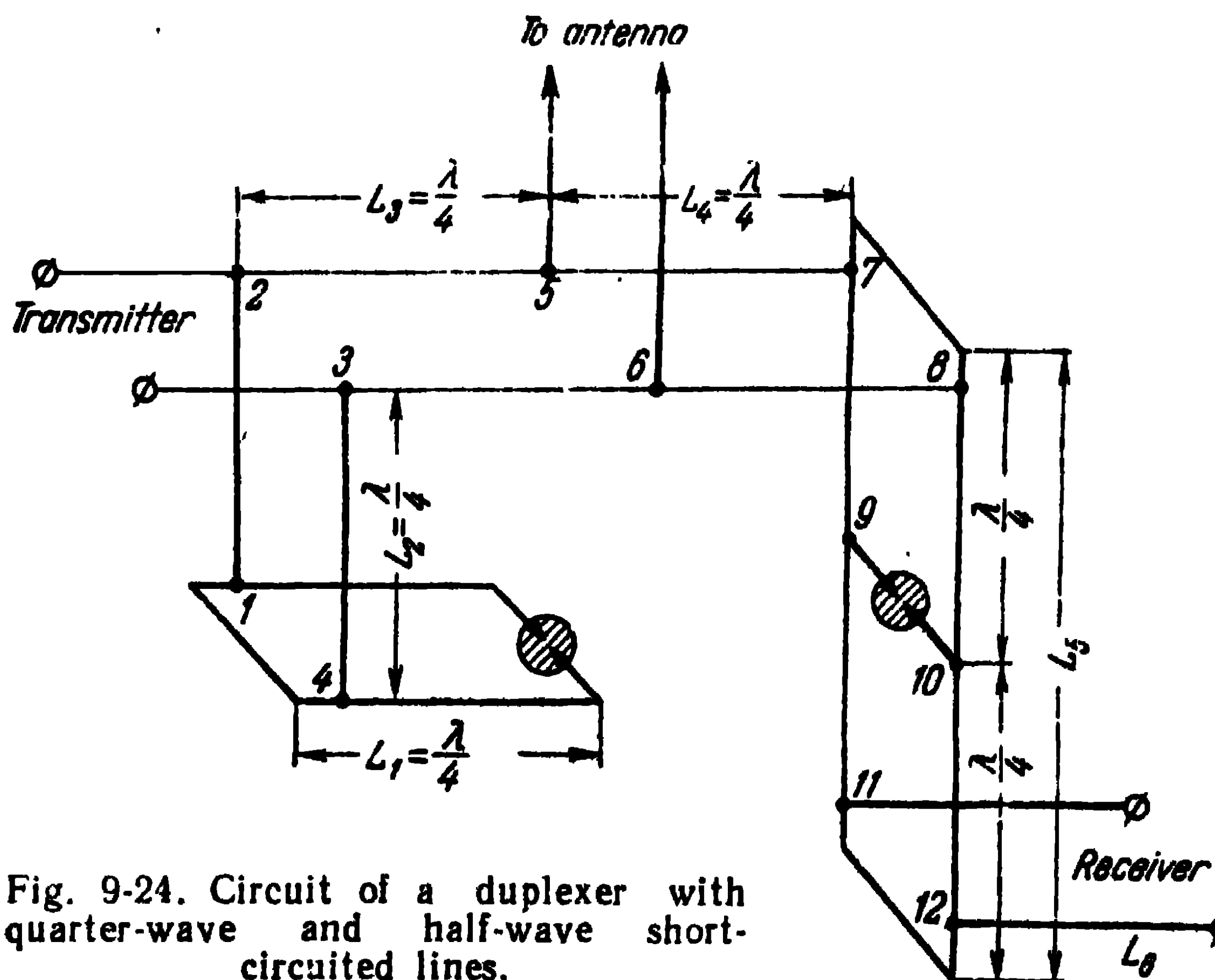


Fig. 9-24. Circuit of a duplexer with quarter-wave and half-wave short-circuited lines.

Fig. 9-24 shows the antenna duplexer circuit of the metre wave range employing twin or coaxial lines. Quarter-wave and half-wave resonance lines are used in this circuit, where they play the role of voltage set-up transformers. The resonance line L_1 is connected to the stub L_2 at the points 1, 4 near its short circuit, and the resonance line L_5 is connected to the lines L_4 and L_6 at the points 7, 8 and 11, 12, also near their short circuits.

During the transmission period, the spark gaps connected at the intensity antinodes of the resonance lines break down and short-circuit the resonance lines; the points 1, 4 and 7, 8 of the lines L_2 and L_4 are short-circuited and the resistances of these lines at the input at the points 2, 3 and 5, 6 are of

infinitely large magnitude. The energy pulse from the transmitter passes freely into the antenna without branching off towards the receiver input.

During reception, the spark gaps are deionised and the input resistance of the resonance line L_1 at the points 1, 4 becomes infinitely large while the input resistance of the stub L_2 at the points 2, 3 becomes infinitely small and the branch of the transmitter at the points 5, 6 is disconnected from the antenna. On the other hand, the input resistance of

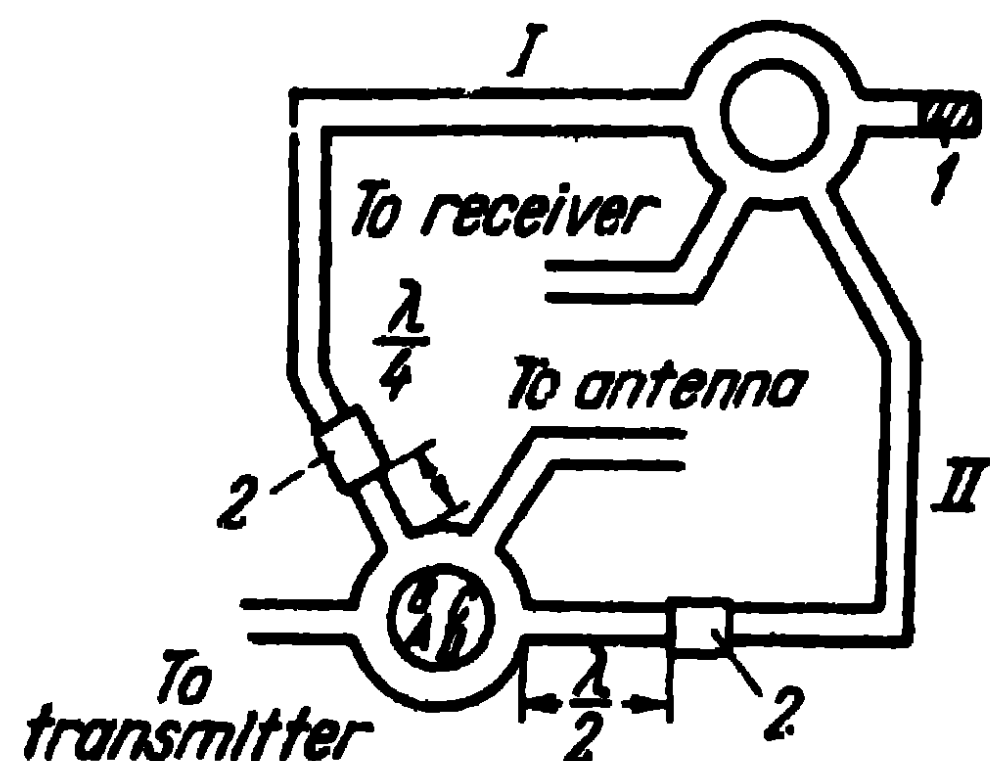


Fig. 9-25. Twin hybrid-ring duplexer:

1—load; 2—cavity resonator

the line L_6 at the points 11, 12 is transformed by the resonance line L_5 into the points 7, 8 without change and the line L_4 becomes loaded on a matched load. The signals picked up by the antenna pass freely to the input of the receiver.

Duplexers used in the centimetre wave range are similar to those with the above-described circuit, which makes use of waveguide lines and cavity resonators. There are other types

of transmit-receive duplexers. Fig. 9-25 shows a twin balance duplexer which makes use of two hybrid rings. The hybrid rings are coupled with the waveguides I and II, into which spark gap cavity resonators are inserted at a distance $\lambda/4$ in branch B and at a distance $\lambda/2$ in branch D.

During transmission, the resonators break down and branch B sets up an open circuit in the ring, while branch D sets up a short circuit. Since they are *E*-plane branches, the energy from the transmitter reaches the antenna via ADC, no energy whatever passing via ABC. During transmission, that part of the power which leaks through the spark cavity is directed towards the second hybrid ring along the connecting waveguides I and II and becomes absorbed in the load resistance without reaching the receiver. This constitutes the advantage of the circuit under consideration over the circuit of the duplexer represented in Fig. 9-24, where the power which leaks through the spark gap does reach the input of the receiver.

During reception, the power of the signals from the antenna branches off into branch C without reaching the output of the transmitter, passes through branches B and D along

the waveguides I and II to the second ring and is delivered in full to the receiver input. Since the path difference of the waves from the antenna to the load in the second ring along the waveguides I and II is equal to half a wave, no power is being dissipated in the load during reception.

The above-described balanced bridge junctions are also utilised in antenna duplexers in the centimetre wave range.

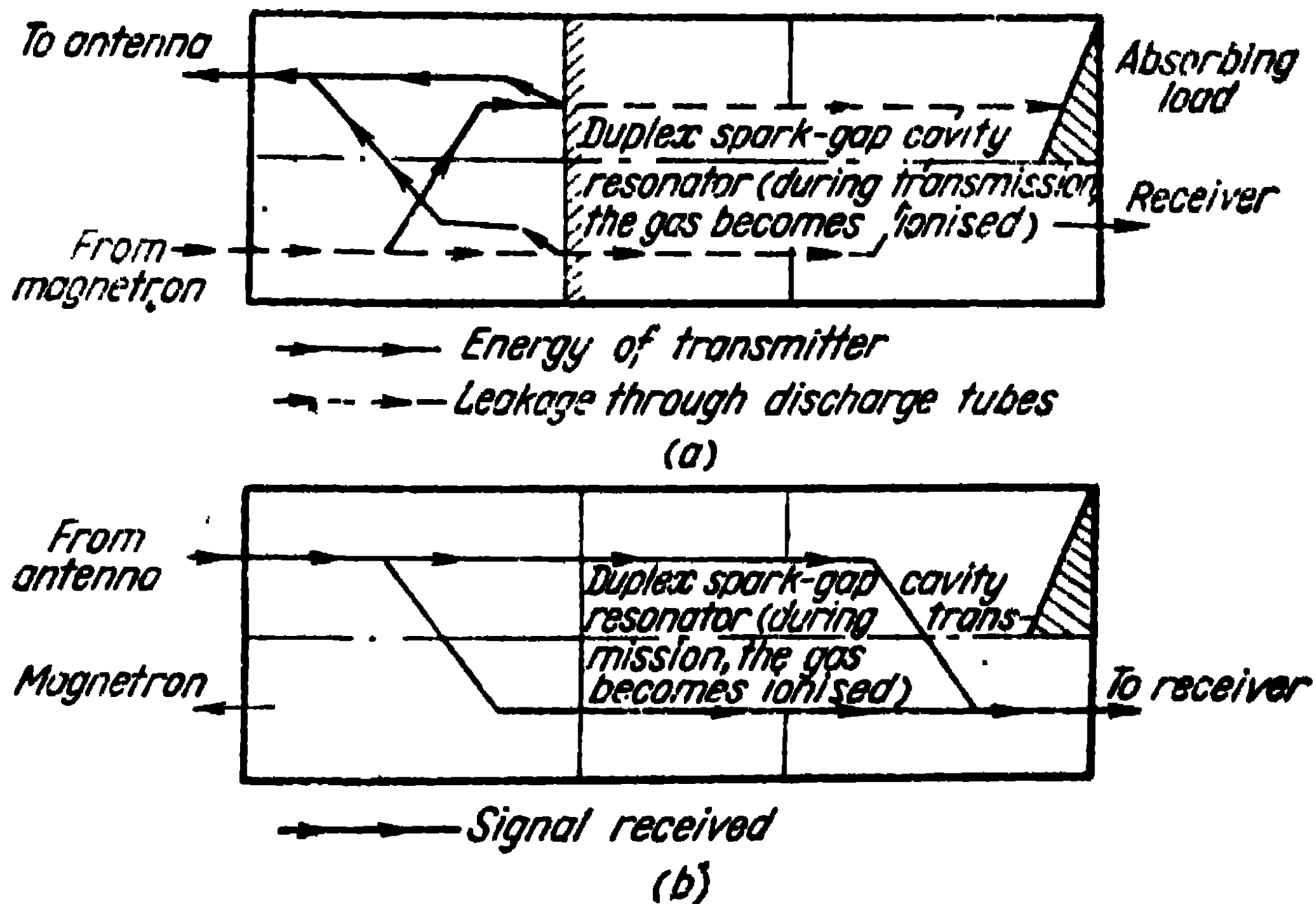


Fig. 9-26. Explaining the principle of the operation of a symmetrical duplexer with balanced bridge junctions:
a—during transmission; *b*—during reception.

Fig. 9-26 shows the circuit of such a duplexer consisting of two balanced bridges connected in series through duplex spark gap cavity resonators.

During transmission, the transmit-receive boxes (T-R boxes) break down and short-circuit the first bridge at the outputs *B* and *D*. As a result of the 90° phase shift of the voltages, the reflected signals cancel out in the transmitter arm and add up in the antenna arm. Thus, the power of the transmitter reaches the antenna. Here again, due to the 90° phase shift of the voltages, that part of the power which leaks through the T-R boxes is absorbed in the matched load and does not reach the input of the receiver.

During reception, the power from the antenna follows two paths and appears in full at the input of the receiver, no power reaching the output of the transmitter or the absorbing resistance.

9-5. Devices Employing Ferrites

Lately, extensive application has been made of ferrite waveguide devices. The ferrites, which are in a permanent magnetic field, enable to obtain waveguide systems that do not satisfy the reciprocity principle. The systems can be divided into three groups: gyrators, isolators and circulators.

The gyrator, the symbol of which is shown in Fig. 9-27, *a*, causes a 180° change of phase of the wave when the wave moves in the direction of the arrow and no change of phase

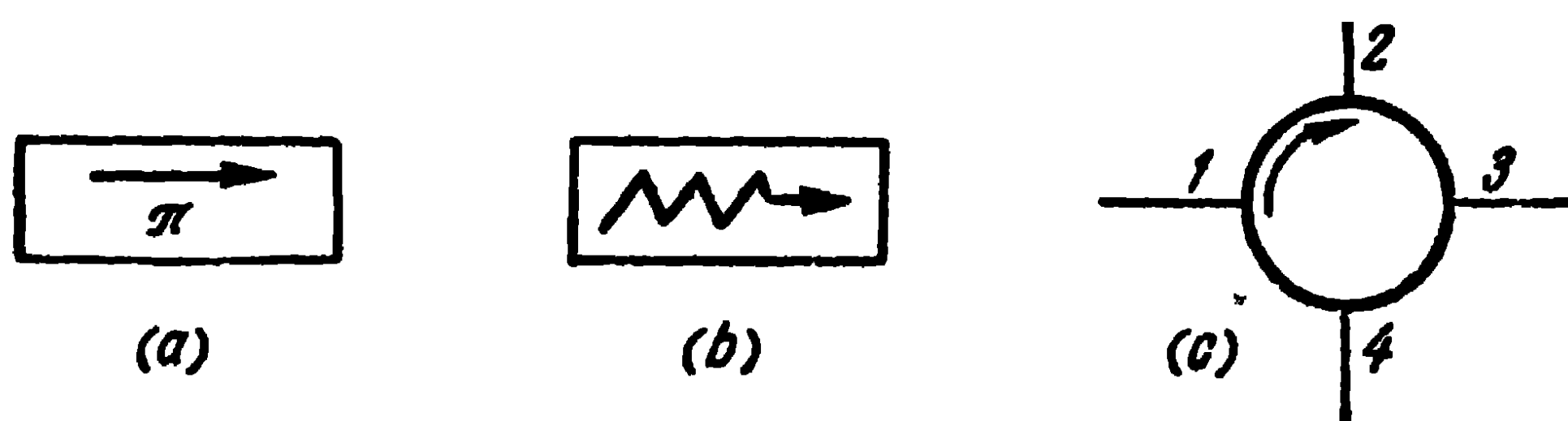


Fig. 9-27. Conventional signs of the waveguide ferrite devices.

when the wave moves in the reverse direction. Gyrators are used as components of more complex systems, in particular of circulators.

The isolator, the symbol of which is shown in Fig. 9-27, *b*, is a device for the admission almost without attenuation of the waves moving in one direction and the intense absorption of the waves moving in the opposite direction. Ferrite isolators are used for decoupling generators from loads and matching antennas to feeders. This is the most common device utilising ferrites.

A circulator is a device which, as a rule, has four inputs in which the energy is delivered as follows: signals fed to input 1 are delivered only to input 2, from input 2 the signals are delivered only to input 3, etc. In the conventional circuit of the circulator (Fig. 9-27, *c*), the arrow shows the direction of energy transmission. Circulators with a different number of inputs are also possible. The direction of energy delivery can be regulated by changing the direction of the permanent magnetic field, in which case the circulator operates as a non-contacting high-frequency commutator. In addition, circulators can be used for decoupling a receiver from a transmitter continuously employing only one antenna, and for other purposes.

Apart from the devices described above, ferrite phase switchers are also used, which utilise the property of ferrites to change the value of their permittivity under the influence of an external permanent magnetic field. Ferrite phase switchers can be of two types: those that satisfy the reciprocity principle and those that do not.

Here is a brief account of the physical and chemical properties of ferrites.

Ferrite is a very hard and brittle ceramic material usually of a dark colour. It does not readily yield to mechanical treatment and can only be polished.

By virtue of its electric and magnetic properties, ferrite is a unique material. On the one hand, it is a ferromagnetic, i.e., a material akin in properties to iron (the relative permeability of ferrites varies within a wide range depending on the wave range, the composition of the ferrite, the temperature, etc. It can be less than unity on centimetre waves and can reach as high as 2,000 at low frequencies). On the other hand, it is a dielectric of high specific resistance amounting to 10^6-10^8 ohms/cm. As a result, electromagnetic waves can be propagated in ferrites just as in ordinary dielectrics. Note that the relative dielectric constant of ferrite lies within $10-20$.

Ferrite is prepared from magnetite $\text{FeO} \cdot \text{Fe}_2\text{O}_3$. The bivalent iron in magnetite is replaced by some bivalent metal the dimensions of the ion of which are close to those of the ion of the bivalent iron. Suitable metals are Mn, Mg, Ni, Zn, Cu, Be, Li, Co, etc.

Combined ferrites, in particular lithium-zinc, manganese-zinc and nickel-zinc ferrites find wide application.

The production process of ferrite is approximately the same as that of ceramics. Powdered magnetite and oxides of the corresponding metals are very thoroughly mixed, finely ground and moulded after the addition of some binding material, such as paraffin. This is followed by preliminary kilning at a temperature of $300-400^\circ\text{C}$ during which the binder is burnt out. Then comes firing at a temperature of $1100-1400^\circ\text{C}$. The production process of ferrites is complicated by the fact that the properties of ferrites are influenced by a whole series of factors.

The gyromagnetic properties of ferrites require an explanation.

The motion of an electron around the nucleus of an atom gives rise to an orbital magnetic moment, due to the motion

of the electron in an orbit, and to a spin, due to the motion of the electron around its axis. A large amount of theoretical research and a series of classical experiments have shown that the dominant role in the nature of ferromagnetism is played by the spin and not the orbital moments, which can be neglected since they are always directed in a chaotic manner.

In most elements, the spins of all the electrons are mutually compensated. Ferromagnetics, which have no such compensation on one of the orbits, are an exception. It is these electrons with the non-compensating spins that are responsible for the phenomenon of ferromagnetism.

We know that all ferromagnetic materials consist of a large number of regions or domains of spontaneous magnetisation. Each domain contains quite a large number of atoms. Within the limits of a domain, the magnetic moments of the atoms are parallel to one another, so that, even in the absence of an external magnetic field, the domains are magnetised to saturation. When a ferromagnetic is introduced into a magnetic field, the separate domains become orientated in a direction close to that of the external field.

All these phenomena are very complex to analyse, but we can get a qualitative picture of the phenomena in a ferrite by considering the behaviour of one electron. This simplified theory was put forward by Polder [41]. Without dwelling on the mathematical calculations of this theory, we shall attempt to clarify its physical aspect.

As mentioned earlier, ferromagnetic phenomena are due to the possession by the electron of a spin, which may be roughly pictured as the rotation of the electron around its axis. As a result of this rotation, the electron has its own mechanical moment, like any rotating body, as well as its own magnetic moment, the appearance of which can be explained by regarding the rotating electron as an elementary winding with a current. Thus, the electron possesses on the one hand, the properties of a gyroscope and, on the other hand, those of an elementary magnet.

Let us imagine that the electron is located in a permanent magnetic field. Since the electron possesses the properties of an elementary magnet, it is subjected in the magnetic field to a pair of forces, which tend to turn the axis of the electron in such a way as to cause it to be parallel to the lines of force of the magnetic field (Fig. 9-28, *a*). However, due to the gyroscopic effect, instead of becoming orientated along

the lines of the field, the electron begins to wobble; moreover, the end of the magnetic moment vector of the electron describes a circumference (Fig. 9-28, *b*). The circular frequency of wobbling is proportional to the magnetic field applied: $\omega_0 = |\gamma| H$, where γ is a certain negative constant. Such a wobbling motion would continue indefinitely if it was not for the losses, due to which, the energy of the wobbling is rapidly damped and the electron axis becomes orientated in the direction of the lines of force of the magnetic field. The duration of the damping of the wobbling has been found from experiments to equal approximately 0.01 M/sec.

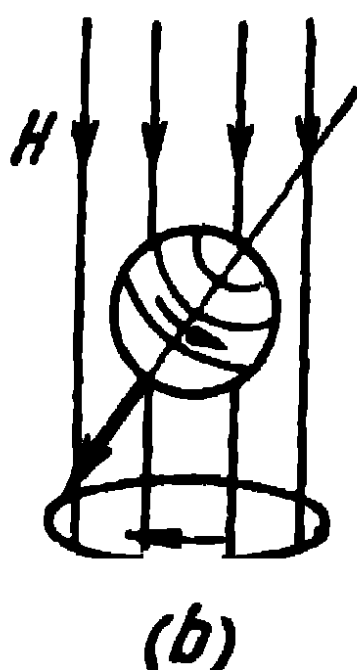
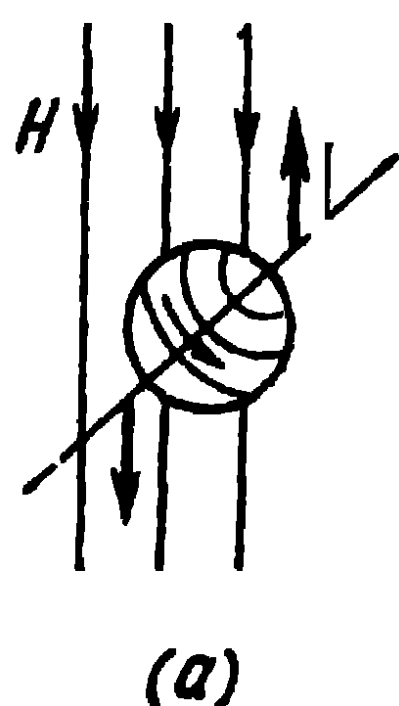


Fig. 9-28. The electron in the permanent magnetic field:

a—forces acting on the electron;
b—wobbling of the electron

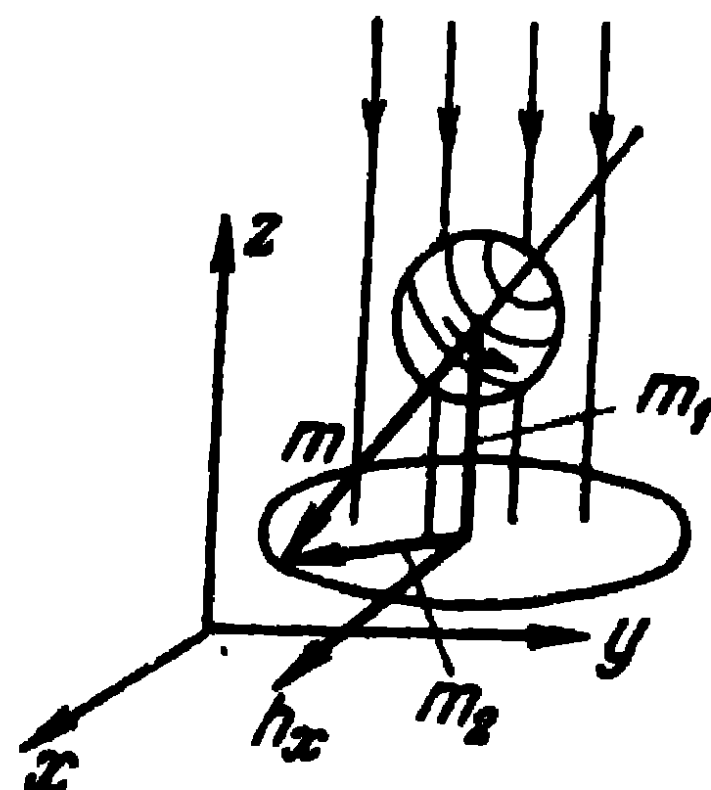


Fig. 9-29. Combined effect of the magnetising and high-frequency fields on the electron.

Now, in addition to the magnetising field, directed along the *z*-axis (Fig. 9-29) let the electron be subjected to the action of a high-frequency magnetic field *h* of frequency ω , directed along the *x*-axis. As a result of the action of the high-frequency field, the electron starts wobbling anew, but this time the wobbling is not damped and proceeds at the established pace with a frequency ω and not ω_0 . The phenomena described are close to those which take place in a resonant circuit: the wobbling occurring under the effect of the magnetising field resembles the natural oscillations of the circuit, the combined action of the magnetising field and the high-frequency field resembling the forced oscillations.

Thus, at the established pace of wobbling, the end of the vector of the magnetic moment *m* moves on a certain closed curve. Polder has shown that this curve is an ellipse lying in

a plane perpendicular to the direction of the magnetising field. Let us represent the vector of the magnetic moment \mathbf{m} as the sum of the constant vector \mathbf{m}_1 directed along the lines of the magnetising field plus the vector \mathbf{m}_2 rotating with a frequency ω and lying in the xy -plane (Fig. 9-29).

It is readily seen that when the amplitudes are not too high, the magnitude of the vector \mathbf{m}_2 is proportional to the magnitude of the vector \mathbf{h} . The rotating vector \mathbf{m}_2 can, in turn, be represented as the sum of two vectors oscillating with a frequency ω , having a 90° phase shift relatively to one another:

$$\mathbf{m}_2 = \kappa h_x \mathbf{i}_x + ikh_x \mathbf{i}_y, \quad (9-34)$$

where $\mathbf{i}_x, \mathbf{i}_y$ are unit vectors;

κ, k , constants, corresponding to the magnetic susceptibility in the case of an isotropic medium. They are defined by the expressions given below.

Thus, under the action of high-frequency oscillations, there arises in a magnetising ferrite medium, an internal high-frequency magnetic field, characterised by the magnetisation vector \mathbf{m}_2 . The magnetic induction vector of the high-frequency field \mathbf{b} is the sum of the vector $\mu_0 \mathbf{h}$ and the magnetisation vector \mathbf{m}_2 , i.e.,

$$\left. \begin{aligned} b_x &= (\mu_0 + \kappa) h_x; \\ b_y &= ikh_x. \end{aligned} \right\} \quad (9-35)$$

These expressions reveal the existence of a difference between a ferrite and an ordinary isotropic medium, in which the magnetic induction vector is parallel to the magnetic field intensity vector. This difference consists in that when a ferrite is subjected to a magnetic field with a unique component h_x , the vector \mathbf{b} has two components b_x and b_y . When the ferrite is subjected to a high-frequency field with a component h_y , the same reasoning yields:

$$\begin{aligned} b_x &= -ikh_y; \\ b_y &= (\mu_0 + \kappa) h_y. \end{aligned}$$

In the general case, when the electron is subjected to the effect of an arbitrarily orientated field \mathbf{h} , the relation

between the vectors \mathbf{b} and \mathbf{h} is as follows:

$$\left. \begin{aligned} b_x &= \mu h_x - ikh_y; \\ b_y &= ikh_x + \mu h_y; \\ b_z &= \mu_0 h_z. \end{aligned} \right\} \quad (9-36)$$

This same relation can be represented in an abbreviated form:

$$\mathbf{b} = \|\mu\| \mathbf{h},$$

where $\|\mu\|$ is the tensor of the permeability with the following coefficients:

$$\left\| \begin{array}{ccc} \mu & -ik & 0 \\ ik & \mu & 0 \\ 0 & 0 & \mu_0 \end{array} \right\|.$$

The quantities μ and k have been calculated by Polder. They are expressed as:

$$\left. \begin{aligned} \mu &= \mu_0 + \frac{|\gamma| M \omega_0}{\omega_0^2 - \omega^2}; \\ k &= -\frac{|\gamma| M \omega}{\omega_0^2 - \omega^2}, \end{aligned} \right\} \quad (9-37)$$

where M is the magnetisation of the ferrite (by the magnetising field).

The expressions (9-37) are valid for the electron. In the case of a ferrite, they give a good qualitative coincidence with experimental data.

The existence of a complex relation between the vectors \mathbf{b} and \mathbf{h} greatly complicates the solution of the field equations even in such a simple case as the propagation of a linearly-polarised wave in an infinite ferrite medium. The analysis is considerably simpler in the case of waves with a circular polarisation. This is not surprising, since the magnetisation vector in a ferrite is a rotating one.

Owing to the fact that the direction of wobbling of the electron depends only on the direction of the magnetic field lines, it is likewise convenient to relate the direction of rotation of the wave incident on the ferrite to the direction of the magnetic field lines and not to the direction of wave propagation, as is usually done. Let the wave, with vector \mathbf{h} rotating clockwise when looking towards the magnetic

field lines, be right-handed rotary. In the case of the left-handed rotary wave, the vector \mathbf{h} rotates anticlockwise.

Let the ferrite be subjected to a right-handed rotary wave. In the case of this wave, the relation for the components h_y and h_x is $h_y = -ih_x$, i.e., the component h_y has a 90° phase lag relatively to h_x . Let us calculate the components of the vector \mathbf{b} account taken of (9-36):

$$\begin{aligned} b_x &= (\mu - k) h_x; \\ b_y &= -i(\mu - k) h_x, \text{ or } b_y = -ib_x. \end{aligned}$$

Consequently, the vector \mathbf{b} is polarised exactly as the vector \mathbf{h} and the relation between these vectors will be the same as in an isotropic medium. The permeability, in the case of the right-handed rotary wave, is expressed as:

$$\mu_+ = \mu - k = \mu_0 + \frac{|\gamma| M}{\omega_0 - \omega}. \quad (9-38)$$

In the case of the left-handed rotary wave,

$$h_y = ih_x$$

and we get a similar picture, but the permeability is now expressed as:

$$\mu_- = \mu + k = \mu_0 + \frac{|\gamma| M}{\omega_0 + \omega}. \quad (9-39)$$

Thus, in the case of a rotary wave, the permeability is a scalar quantity but it is not the same for waves with a left-handed polarisation as for waves with a right-handed one. The relative permeability μ_r is plotted as a function of the magnitude of the magnetising field for waves with a left- and right-handed polarisation in Fig. 9-30.

It is seen from Fig. 9-30, *a* that at a definite value of the magnetising field, the quantity μ_+ undergoes a pronounced change. This value corresponds to the coincidence of the natural frequency of wobbling with the frequency of the forced oscillations ω . This phenomenon is known as ferroresonance. The same can be seen from the expressions, but the latter do not take account of losses whereas the graphs do.

The dotted curve in Fig. 9-30, *a*, characterises the losses in the ferrite and the solid curve, the quantity μ_+ . In the resonant region, the losses in the ferrite are very high. From

the physical standpoint, this is quite understandable, since, when the natural frequency of wobbling coincides with the frequency of the external field, the electron wobbles with the maximum possible amplitude and abstracts the maximum of energy from the field. Furthermore, a considerable part of this energy is spent on heating the ferrite. In the vicinity of the resonance, it is the permeability that undergoes the most pronounced change, since, as a result of the pronounced wobbling of the electron, the vector m_2 has its maximum value.

No such thing occurs in the case of a left-handed polarised wave (Fig. 9-30, *b*) due to the fact that, in the case of a right-handed polarised wave, the direction of rotation of the wave and of the vector m_2 coincide and the delivery of energy by the wave to the electron is continuous, whereas in the case of a left-handed polarised wave, the rotations are opposed and the electron receives energy at one part of the period and gives it up at the other part of the period.

Let us now return to the propagation in the ferrite of a linearly-polarised wave, which we shall represent in the form of a superposition of two waves of circular polarisation with opposed rotations.

Since the permeabilities of the left-handed and right-handed waves are different, so are the phase coefficients:

$$\alpha_+ = \omega \sqrt{\epsilon \mu_+}, \quad \alpha_- = \omega \sqrt{\epsilon \mu_-}.$$

As seen from Fig. 9-30, $\alpha_+ < \alpha_-$; consequently, these waves have different phase lag over one and the same distance. If, at a certain point, the vectors are directed as shown in Fig. 9-31, *a*, then, at a distance corresponding to a wavelength, the picture for a wave with a left-handed polarisation

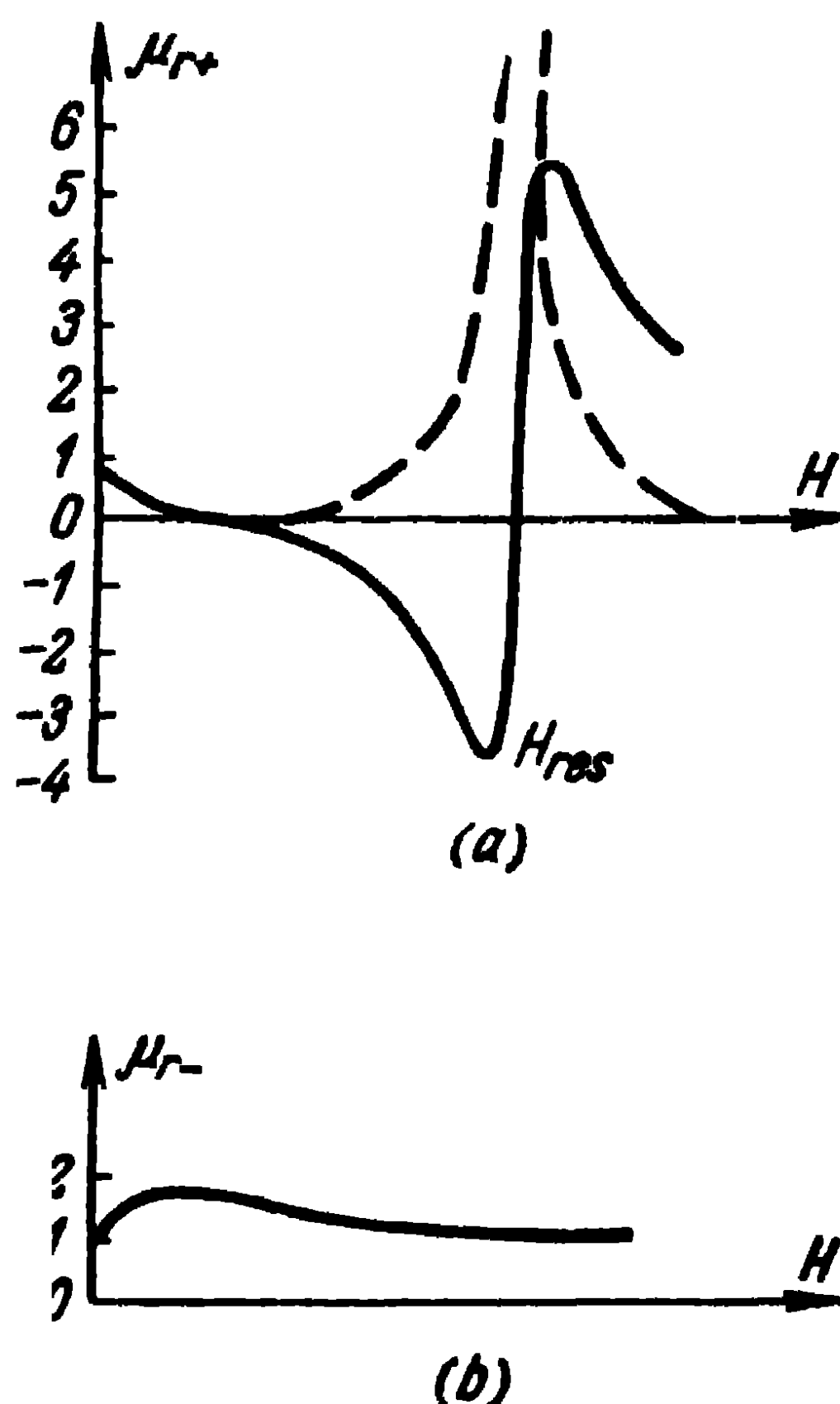


Fig. 9-30 The relative magnetic permeability μ_{r+} and μ_{r-} plotted as a function of the magnetising field.

is as represented in Fig. 9-31, *b*. The polarisation plane of the resultant vector will turn by an angle

$$\theta = \frac{1}{2} (\alpha_- - \alpha_+) l. \quad (9-40)$$

where l is the length of the wave path in the ferrite medium. It should be carefully noted that for an observer looking in the direction of the wave motion, the rotation of the polarisation plane occurs clockwise if the wave is propagated in the direction of the lines of force of the magnetising field, and anticlockwise, if the wave is propagated in the opposite direction to the lines of force of the magnetising field. In other words, the direction of rotation of the polarisation plane does

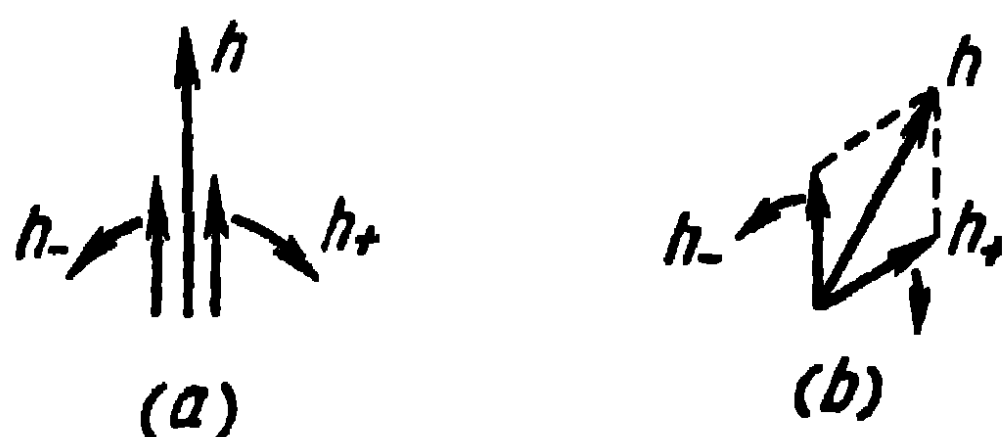


Fig. 9-31. Illustrating the Faraday effect:

a—representation of a linearly-polarised wave in the form of two waves with a rotary polarisation;
b—turn of the polarisation plane of the resultant vector of the magnetic field intensity.

not depend on the wave propagation direction if the observer looks all the time in the direction of the magnetising field (or against it).

The polarisation plane rotation effect is known as the Faraday effect; it is frequently made use of in various microwave ferrite devices.

All the above-given explanations concern the propagation of a plane linearly-polarised wave in an infinite ferrite medium. In devices used in practice, the ferrites are placed in waveguides. In particular, to utilise the Faraday effect, a ferrite rod is placed on the axis of a circular waveguide with an H_{11} wave. At the same time, the longitudinal magnetising field is set up by a solenoid whose axis coincides with that of the waveguide.

It is always desirable to get the maximum possible angle of rotation of the polarisation plane for minimum reflections from the ferrite rod, minimum losses, the smallest possible size and weight of the device. Let us consider the main points to be taken into consideration when choosing the size of the ferrite rod. The most important is the choice of the rod's diameter. When the diameter of the rod is small, only a very small part of the energy is propagated in the ferrite rod, so that the magnitude of the angle of rotation of the polarisation plane by a distance equal to the unit length of the rod θ_1 is small. Bigger diameter of the rod means an

increase of the amount of energy propagated in the ferrite and with it, of the angle θ_1 .

Due to the high permittivity constant of ferrite, even in the case of a relatively small diameter of the rod, almost all of the energy is propagated inside the ferrite and a further increase in diameter does not lead to an increase of angle θ_1 (Fig. 9-32). There is, therefore, no point in using ferrite rods of a large diameter.

Furthermore, bigger rod diameter means an increase of the losses and, due to the high permittivity of ferrite, an increase of the equivalent diameter of the waveguide and this favours the appearance of the higher modes. Thus, in practice, only the initial region of the curve is utilised (Fig. 9-32).

The influence of the length of the ferrite rod on the magnitude of the angle of rotation of the polarisation plane is seen from (9-40); it follows that the angle θ is directly proportional to the length of the ferrite. However, the length of the ferrite rod should not be too great since, at the same time, one has to increase also the length of the solenoid and the whole device becomes too bulky. Moreover, an excessive length of the ferrite leads to a narrowing of the bandwidth

due to the fact that the two sources of reflections, i.e., the ends of the ferrite rod, are spaced too far apart. To reduce the reflection from the ends of the ferrite rod, they are given a fairly elongated conical shape, but, even so, the reflection cannot be avoided altogether.

Let us now consider a number of devices based on the Faraday effect and, to begin with, the isolator, which is illustrated in Fig. 9-33, *a*. As was mentioned earlier, in an isolator, the attenuation is different for waves propagated in different directions. Let a wave be propagated from left to right. From the segment of rectangular waveguide 1, the wave is delivered to the continuous transition 2 from the rectangular to the circular waveguide. The wave propagated in the circular waveguide is an H_{11} wave. Owing to the ferrite rod 3,

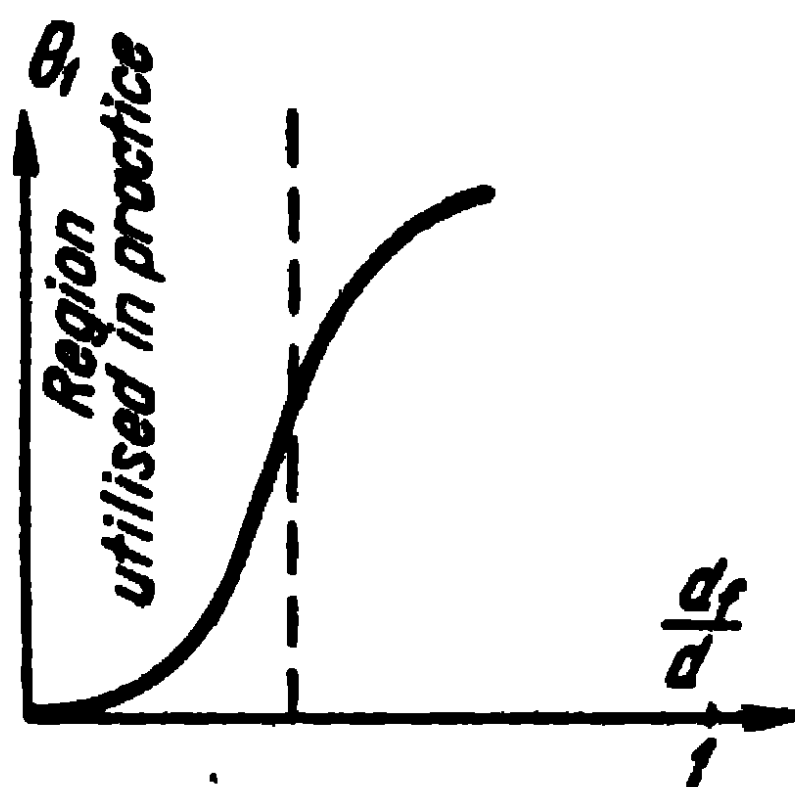


Fig. 9-32. Angle of rotation of the polarisation plane by a distance equal to a unit length of the ferrite rod plotted as a function of its diameter: d_f —diameter of the ferrite rod; d —diameter of the waveguide.

which is magnetised by the solenoid 4, the polarisation plane of the H_{11} wave rotates to the left by 45° (at the same time the wave moves against the direction of the lines of force of the magnetising field). The 45° turn is achieved through the appropriate choice of the diameter and length of the ferrite rod and the magnitude of the magnetising current. Subse-

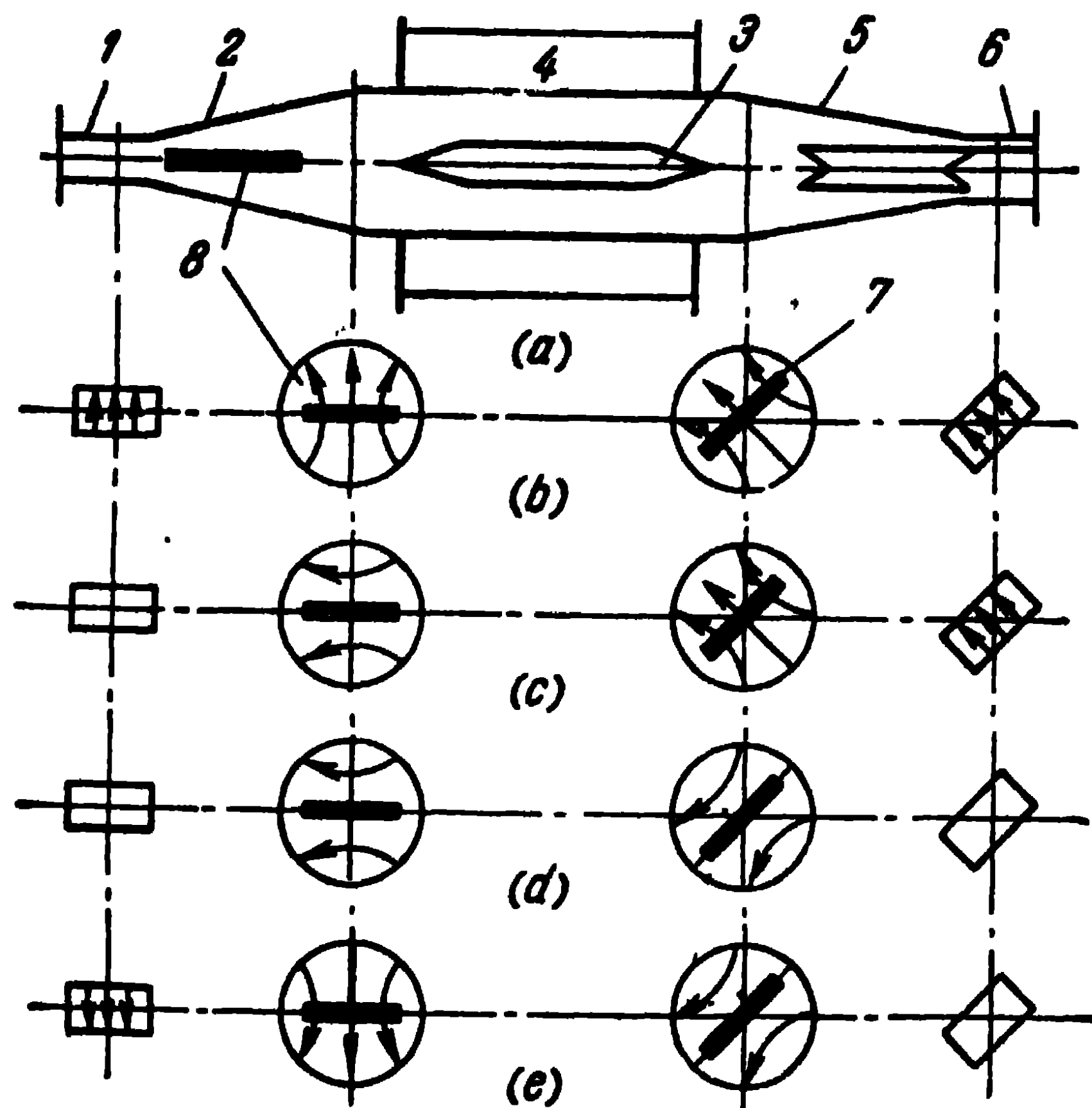


Fig. 9-33. Isolator adapted on a circular waveguide.

quently, the wave again reaches the continuous transition 5 from the circular to the rectangular waveguide. But the rectangular waveguide 6 is turned 45° to the left relatively to the waveguide 1 and, as a result, the wave passes freely through the isolator. The two absorbing plates 7 and 8 are perpendicular to vector E and have practically no influence on the propagation of the wave. The structure of the field in various regions of the isolator, when the wave is propagated from left to right, is shown in Fig. 9-33, *b*.

Now, let the wave be propagated from right to left (Fig. 9-33, *c*). The propagation takes place approximately as in the preceding case. However, owing to the fact that the angle of rotation of the polarisation plane does not depend on the

direction of wave propagation, the polarisation plane effects a further 45° turn to the left in addition to the rotation of the waveguide and the E vector is found to be parallel to the broad wall of waveguide I. This means that the wave cannot get into waveguide I. At the same time, as seen in Fig. 9-33, c, the E vector will be parallel to the absorbing plate 8 and the wave is intensely absorbed by this plate. If the wave has not been completely absorbed by plate 8, owing to the turn of the polarisation plane to the left, the wave reflected from the plate reaches plate 7, with the E vector parallel to that plate (Fig. 9-33, d) and is absorbed once again. Finally, that part of the energy which is not absorbed by plate 7 is delivered to the waveguide I (Fig. 9-33, e). Thus, in the device under consideration, the wave propagated from right to left will be considerably attenuated.

A circulator based on the same principle can also be constructed (Fig. 9-34, a); it differs from an isolator in having two additional outputs.

Let us investigate the way waves are propagated in a circulator when it is fed from different inputs. If the signal is delivered to input I, the picture of the fields in the various sections of the circulator is as shown in Fig. 9-34, b.

Here, as in the case of the isolator just examined, the wave passes freely to input II; the segments of waveguides III and IV are not excited. As can be seen from Fig. 9-34, b, from the point of view of the structure of the field of the circular waveguide, the inputs of these segments are analogous to longitudinal slots in the centre of the broad wall of a rectangular waveguide with an H_{01} wave, which, as we know, are not excited.

When the signal is fed to input II, we get the picture of the fields shown in Fig. 9-34, c, where the window coupling the segment of rectangular waveguide III with the circular waveguide is similar to a longitudinal slot cut in the centre of the narrow wall of a rectangular waveguide and is, therefore, quite intensely excited. Thus, the signal from input II reaches only input III. The processes which take place when the circulator is fed from input III (Fig. 9-34, d) and from input IV (Fig. 9-34, e) can be investigated in a similar way. As mentioned earlier, the circulator should deliver energy from input I only to input II, from input II only to input III and so on. The circulator described accomplishes such a delivery when all the inputs are well matched

to the circular waveguide. Inputs *I* and *II* are well matched by means of continuous transitions, but the same cannot be said of inputs *III* and *IV*. Thus, if a signal is fed to input *II*, the main part of the energy reaches input *III*, the energy reflected from input *III* reaches input *IV* and that which was

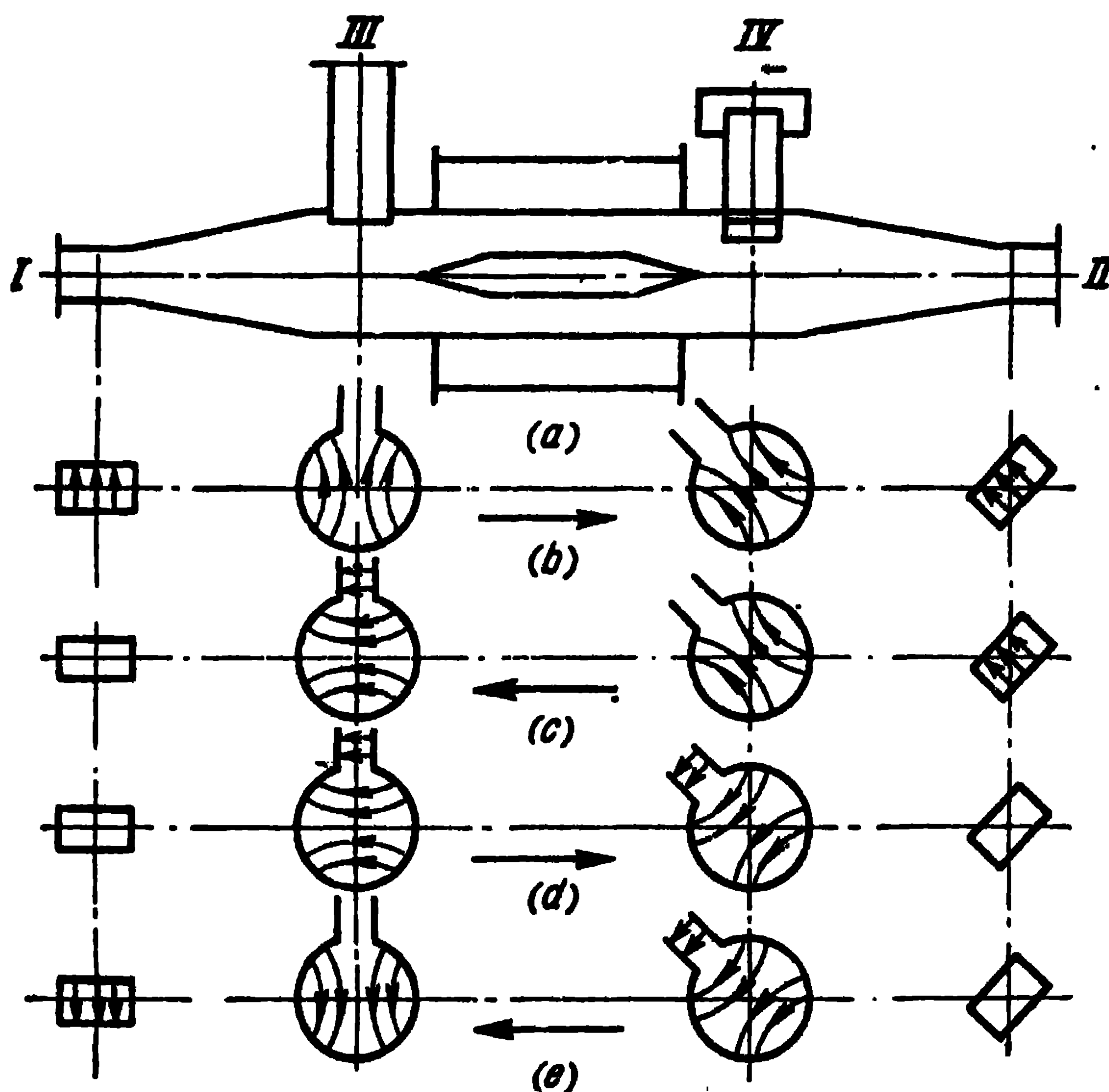


Fig. 9-34. Circulator adapted on a circular waveguide. The arrows show the direction of wave motion.

reflected from input *IV* reaches input *I*. This is the disadvantage of the circulator described.

The circulator shown in Fig. 9-34 can also serve as a non-contacting commutator. If we change the direction of the current in the solenoid, the rotation of the polarisation plane occurs in the other direction and the energy transfer takes place in a different order: from input *I* to input *IV*, from *IV* to *III*, from *III* to *II* and from *II* to *I*.

A ferrite rod placed in a circular waveguide may also be utilised as an electrically regulated phase inverter, in which

the Faraday effect is undesirable and measures should be taken to eliminate it.

One of such measures is the utilisation in the waveguide of a field with a rotating polarisation. A phase inverter of this kind is shown in Fig. 9-35. In outward appearance it also resembles the isolator described above. But contrary to the isolator, the phase inverter has two polarisers (1 and 2). Polariser 1 transforms the H_{11} wave with a linear polarisation into a wave with a rotary polarisation. The operating principle of a polariser is the following: a dielectric plate is

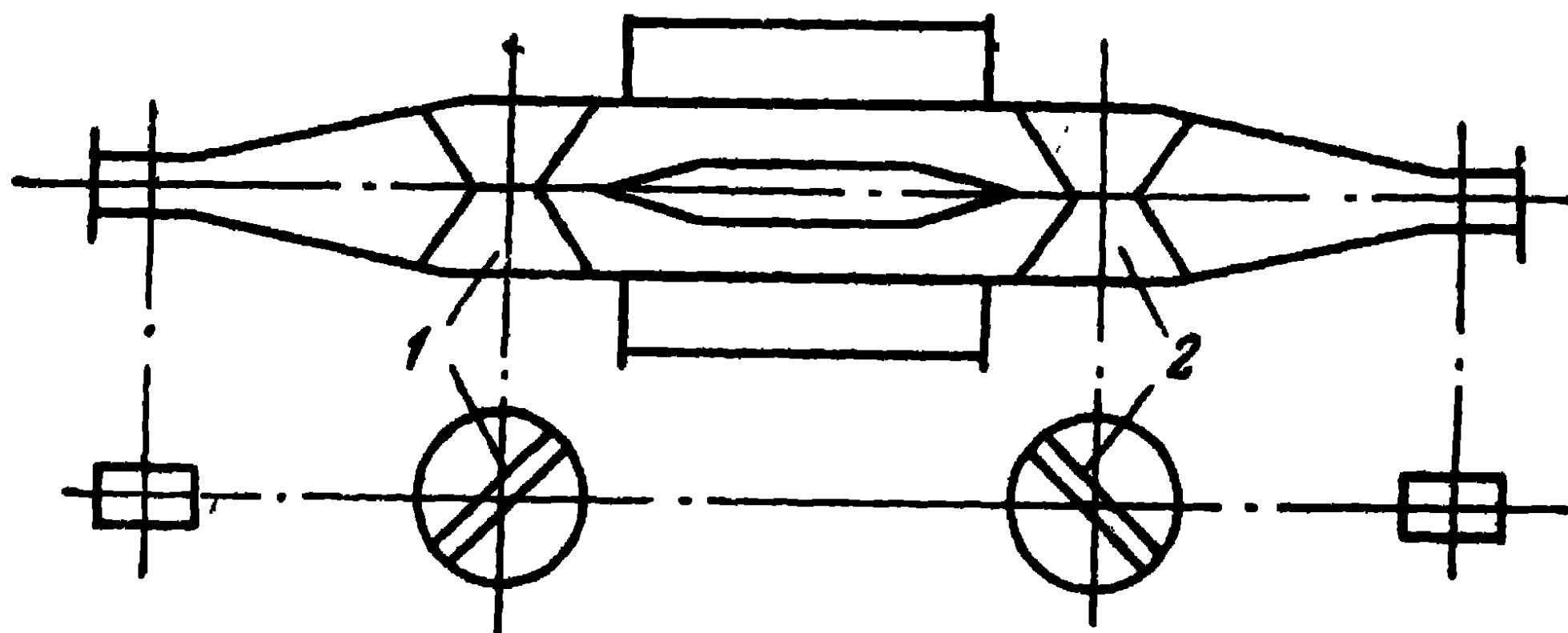


Fig. 9-35. Phase shifter.

placed in a circular waveguide at an angle of 45° relatively to the direction of the vector E of the H_{11} wave. The H_{11} wave in the waveguide can be regarded as the sum of two waves, the vector E of one of which is parallel to the dielectric plate and that of the other one, perpendicular to it. The wave, the vector E of which is parallel to the dielectric plate, is retarded by this plate to a greater extent than the second wave, so that a phase shift takes place between the two waves. The length of the plate can be chosen such as to obtain a phase shift of 90° . Then, after the plate, there will be waves polarised at a 90° angle to one another and having a 90° relative phase shift. Two such waves taken together produce a wave with a circular polarisation. The wave utilised in a phase shifter is usually a left-hand rotary wave, because, in this case, the losses in the ferrite are lower than in the case of a right-hand rotary wave.

The rotary wave passes through the section with the ferrite. A change in the magnetising field leads to a change of the magnetisation of the ferrite and, consequently, also of its permeability [expression (9-39)]. A change of permeability leads to a change of the phase velocity of propagation of the

wave in the section with the ferrite and, consequently, to a change of the phase of the oscillations at the output of the phase shifter. In depolariser 2, the rotating field is again transformed into a linearly-polarised one. The arrangement of depolariser 2 is similar to that of polariser 1.

The value of the maximum phase shift accomplished by such a phase shifter depends, on the whole, on its length, as well as on other factors. It lies within a range of several hundred degrees.

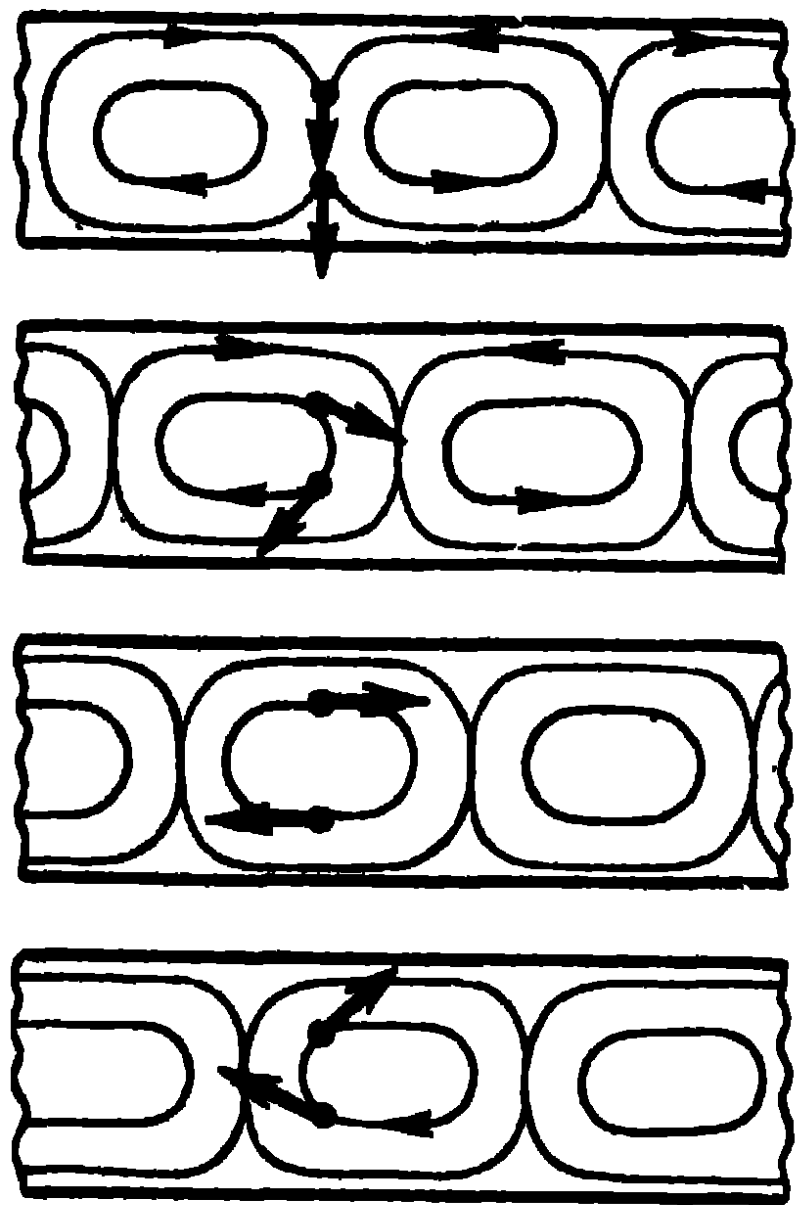


Fig. 9-36. Explaining the effect of the rotation of a magnetic field in a rectangular waveguide.

Devices with ferrites used in circular waveguides have a number of shortcomings, the need for a rectangular-to-circular waveguide transition, the presence of a long solenoid, the bulkiness of these devices among them. The devices have a number of other shortcomings, in particular the difficulty of obtaining small reflections from them in the frequency band.

The best results can be obtained in the case of devices in which the ferrite plate is placed in a rectangular waveguide. The operating principle of devices of this sort can be roughly explained as follows. Let us

consider the picture of the magnetic lines of force in a rectangular waveguide with an H_{01} wave. This picture is shown in Fig. 9-36 for four instants differing from one another by an eighth of a period.

As can be seen from these illustrations, at a certain distance from the middle of the waveguide, the magnetic field forms a rotating vector of constant magnitude. The direction of rotation of the h vector depends on the direction of wave propagation.

Let us place a ferrite plate in the waveguide, so that the region with the rotating magnetic field is situated in the ferrite (Fig. 9-37). The magnetising field should be made parallel to the narrow wall of the waveguide. The phenomena which occur in this case are similar to those considered earlier in the case of an unbounded ferrite medium and in a circular waveguide. Since the direction of rotation of the field

intensity vector depends on the direction of wave propagation, the permeability will not be the same for waves propagated in different directions; furthermore, it is determined in accordance with μ_+ and μ_- . The phase velocities of the waves moving from left to right and right to left are different too and, consequently, also the phase shifts. If the dimensions of the ferrite plate and magnetising field are chosen in such a way that the phase shifts in the forward and reverse directions differ by 180° , then such a plate in the rectangular waveguide acts as a gyrator.

A gyrator of the type described can be utilised as an element of more complex devices, such as circulators (Fig. 9-38). A circulator has two directed couplers 1 and 2 with a transitional attenuation of 3 db (an attenuation of this kind ensures the transmission of half the power into the second channel), a ferrite plate causing a $180^\circ + \psi$ phase shift in the forward direction (indicated by an arrow) and a phase shift equal to ψ in the reverse direction and, in the symmetrical channel, it has a dielectric plate causing a ψ phase shift in both directions.

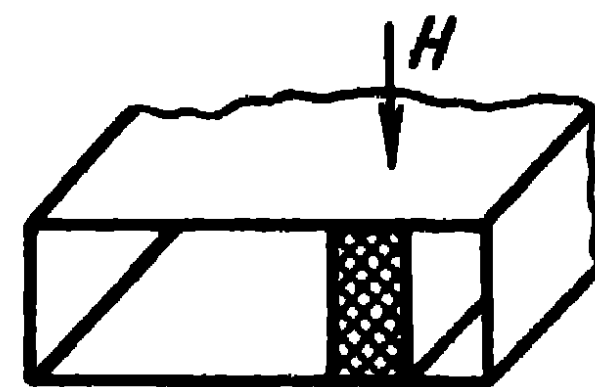


Fig. 9-37. Ferrite plate in a rectangular waveguide.

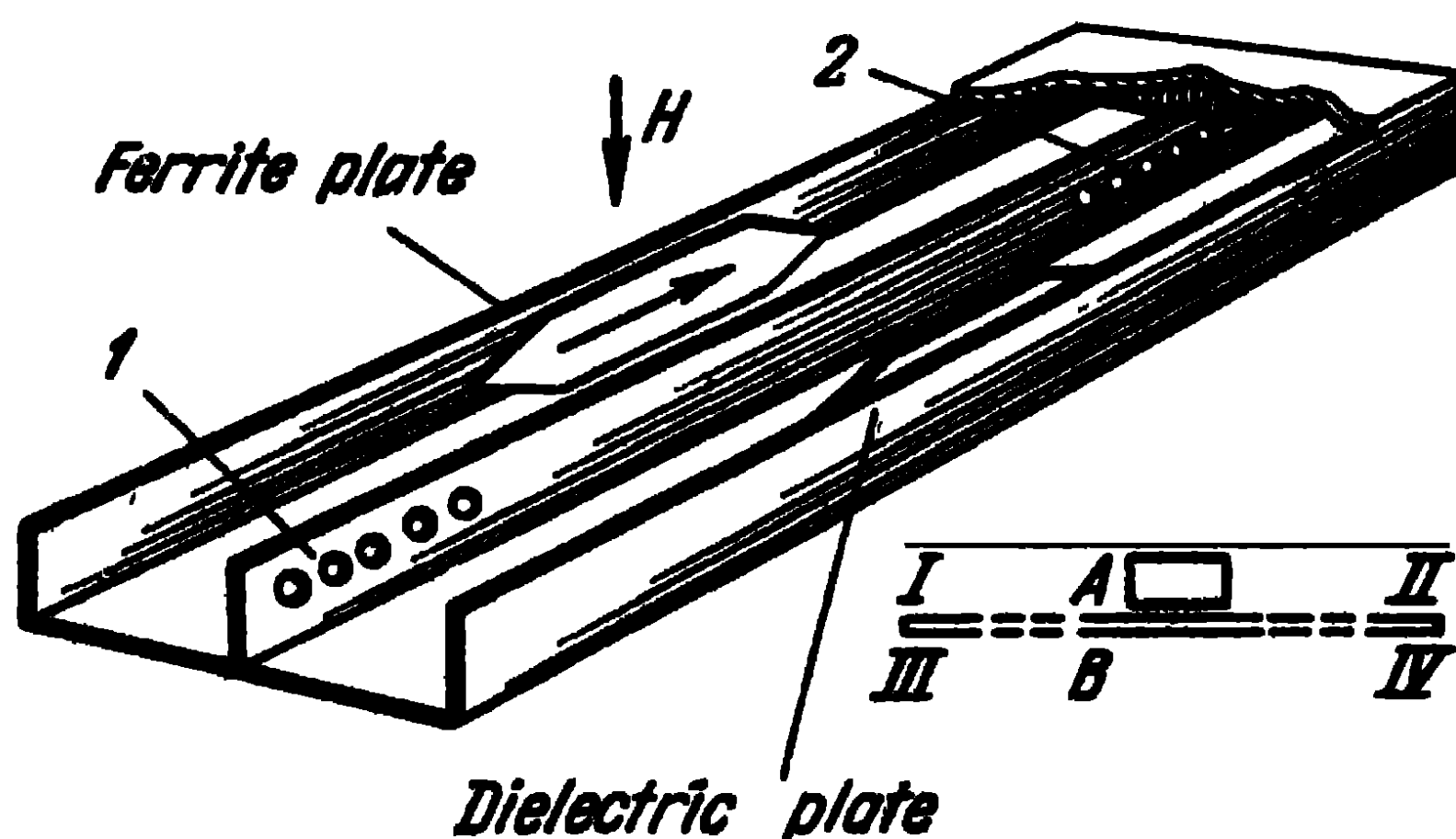


Fig. 9-38. Circulator adapted on a rectangular waveguide.

Let us investigate the behaviour of the circulator when it is fed at input I. The energy cannot reach input III, since both couplers 1 and 2 are directed and transmit energy into waveguide B in such a way that it moves in the same direction as in waveguide A. The energy can reach input II in two ways: directly through waveguide A or through coupler 1,

waveguide *B* and coupler 2. The wave propagated in the first way acquires a phase shift corresponding to the distance between input *I* and input *II* plus 180° plus ψ on account of the ferrite.

The wave which followed the second path acquires the same phase shift, it is obtained due to the fact that when the wave passes through the coupler with a transitional attenuation of 3 db, it acquires a 90° phase shift and when the wave passes through two couplers, the phase shift equals 180° plus a ψ phase shift on account of the dielectric plate.

The signal reaches input *III* likewise in two ways: through coupler 1 and waveguide *B* as well as through waveguide *A*

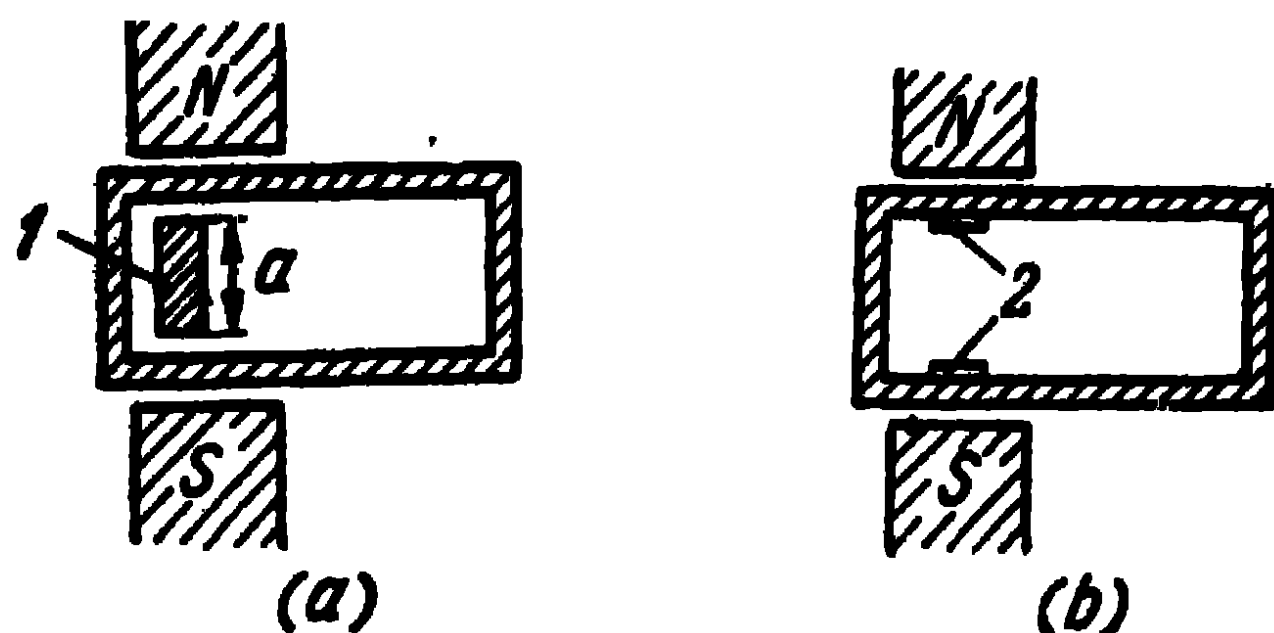


Fig. 9-39. Resonant isolators:

a—resonant isolator with one plate; 1—ferrite plate; *b*—resonant isolator with two plates; 2—ferrite plates.

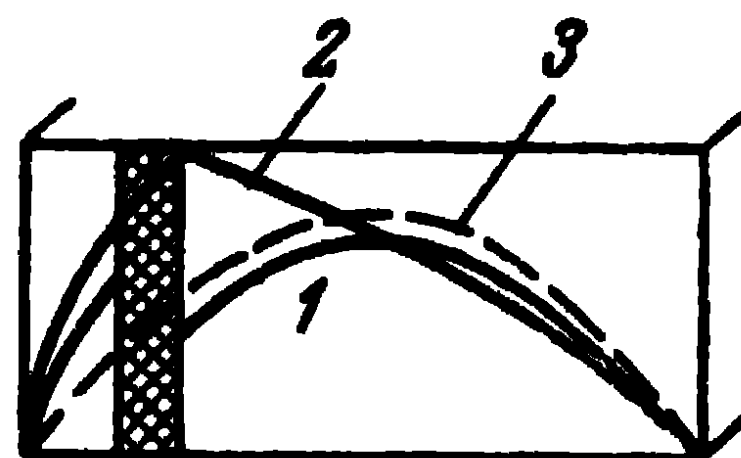


Fig. 9-40. Structure of the field in a waveguide with a ferrite:

1—forward wave; 2—reverse wave; 3—partially filled waveguide.

and coupler 2. Moreover, because of the ferrite, the phases of the waves propagated in these two ways differ by 180° and cancel out.

In a similar way, we can investigate the behaviour of the circulator when it is fed at the other inputs and ascertain that signals pass from input *II* to input *III*, from input *III* to input *IV* and from input *IV* to input *I*. The described circulator gives quite a high transitional attenuation between the inputs, which should not be coupled (e.g., *I* and *III*; *II* and *IV*, etc.). It amounts to approximately 30 db. It is impossible to obtain such a high transitional attenuation in a circular waveguide circulator.

With the help of a ferrite plate placed in a rectangular waveguide, one can obtain devices possessing the properties of isolators. In particular, resonance isolators have found fairly wide application. The magnitude of the magnetising field is chosen large enough to bring about a ferroresonance and, consequently, a high attenuation for the wave which

causes a right-hand rotation in the ferrite. There is no resonance for the wave moving in the opposite direction and it progresses without noticeable losses. The circuit of an isolator of this kind is shown in Fig. 9-39, *a*. In such an isolator, it is possible to obtain a ratio of the losses when the wave moves in the forward direction to the losses when the wave moves in the reverse direction of about 18 db. The best results are produced by the isolator illustrated in Fig. 9-39, *b*, in which the ratio of the forward losses to the reverse ones reach approximately 22 db. However, in the latter case, large fields have to be utilised and the system must be sufficiently long because the attenuation per unit length for the forward wave is lower here than in the isolator shown in Fig. 9-39, *a*.

Apart from resonant isolators, we should mention the application of isolators making use of the non-reciprocal distortion of the field in a waveguide with a ferrite plate. Fig. 9-40 shows the structure of the field for the forward and reverse waves obtained experimentally. It is seen that the reverse wave is concentrated in the vicinity of the ferrite plate. If the ferrite plate is coated with an absorbing film, the reverse wave is absorbed to a considerably greater extent than the forward one. This feature particularly is made use of in isolators. Isolators of this kind are more convenient than resonant isolators, because they require considerably smaller magnetising fields. The ratio of the losses for waves moving in different directions obtained in this case is of the order of 12-13 db.

It can be seen from the brief account given here that the technique of the application of ferrites in waveguides has reached a fairly good level of development. The same cannot be said of the utilisation of ferrites in coaxial lines. Placing a magnetised ferrite plate in a coaxial line does not lead to the appearance of irreversible properties. However, if a dielectric is placed near the plate (Fig. 9-41) and the configuration of the plate is matched to the dielectric, it is possible to obtain an isolator with a ratio of the losses of the order of 20 db in the 10 cm range and around 10 db in the 30 cm range. Apart from isolators, no other non-reciprocal devices are used in coaxial lines at the time of writing.

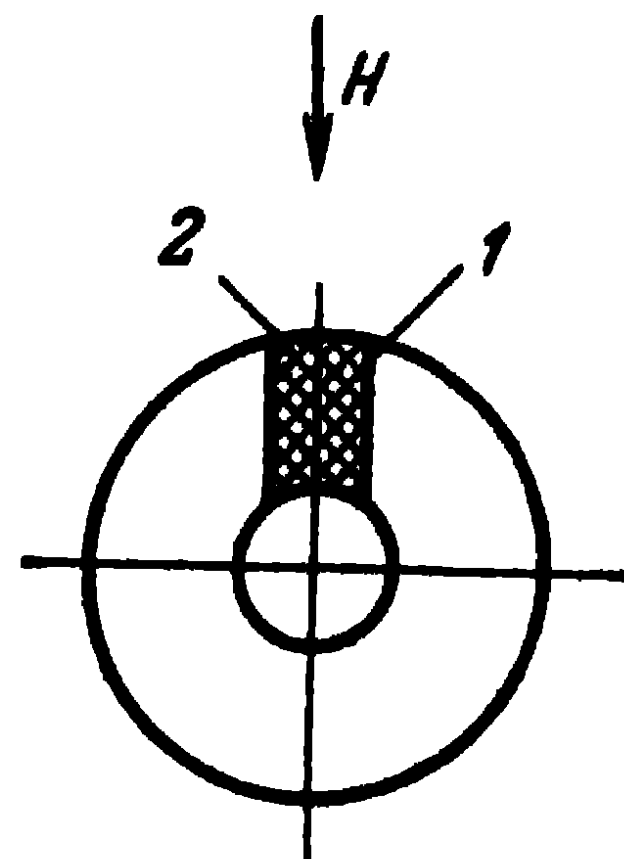


Fig. 9-41. Isolator in a coaxial line:
1—ferrite plate;
2—dielectric plate.

PART THREE

Types of Antenna Devices

CHAPTER TEN

Ultrashort-Wave Antennas

10-1. Antenna Types

The term ultrashort-wave antennas is generally applied to antennas used on waves shorter than 10 m. It covers antennas of the metre, decimetre, centimetre and millimetre wave ranges. Ultrashort-wave antennas are subdivided into several types: simple wire and slot antennas, multiple wire and slot antennas, horn-type antennas, lens antennas, reflector antennas, helical antennas, dielectric antennas and impedance antennas. These types are, in turn, subdivided into several varieties which will be dealt with below.

Ultrashort-wave antennas are used in radio communication and broadcasting, television, radar, radionavigation, radio-astronomy, radio control. They can be simple or multiple, of low directivity or highly directional. These antennas are utilised in ground and ship installations and on flying vehicles of various kinds.

Depending on their purpose, ultrashort-wave antennas are expected to satisfy the most varied requirements. The following requirements are common to all antenna types: maximum possible simplicity of construction and maintenance, high efficiency, relatively wide pass-band, high breakdown electric voltages and steady performance over a prolonged period.

We shall begin by an investigation of simple wire and slot antennas, before passing on to more complex ones.

10-2. Simple Antennas of the Wire Type

Simple antennas of the wire type are used as self-contained radiating and receiving devices and as components of many multiple antennas. They find frequent application

as feeds of multiple antennas, for example parabolic reflectors.

The simplest of antennas is the half-wave dipole fed by a twin feeder. When the twin line is connected to the dipole at its gap (Fig. 10-1, *a*), the travelling-wave ratio in the line is about 0.15 so that the line has to be tuned on a travelling wave. A suitable circuit is shown in Fig. 10-1, *b*. The proper choice of the dimensions L and l of the shunt ensures operation close to the travelling-wave type without supplementary

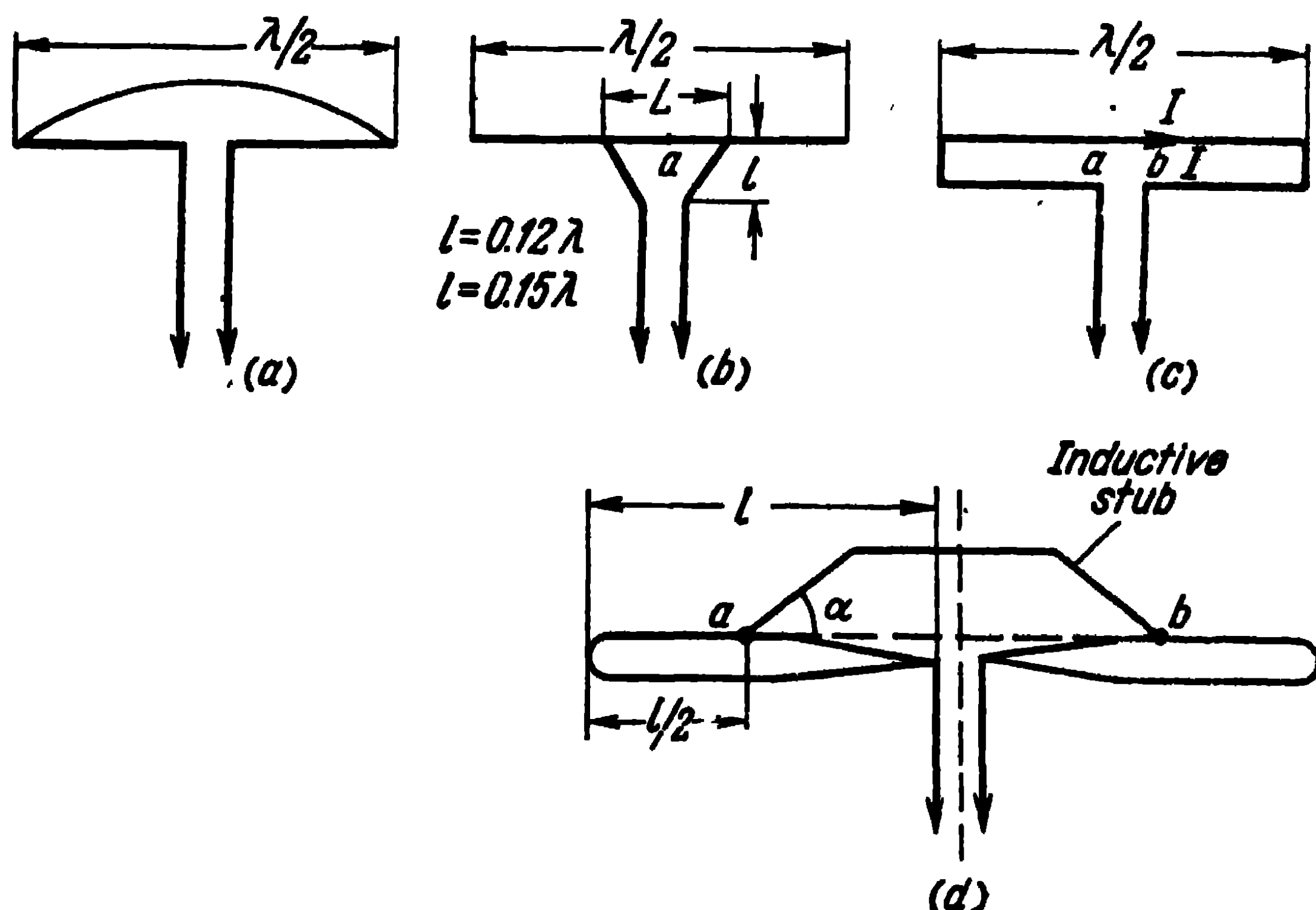


Fig. 10-1. Half-wave dipole fed by a twin feeder:
 - symmetrical half-wave dipole; *b*—dipole with shunt feed; *c*—loop-like
 Pistol Kors dipole; *d*—range shunt dipole.

tuning elements. An additional advantage of such a feed is that a voltage node is set up at the point *a* of the dipole securing the dipole to its support without insulators.

To increase its input resistance, the half-wave dipole can be given a loop-like shape (Pistol Kors's circuit). As shown in Fig. 10-1, *b*, two elements of the dipole are shorted out at the ends, a twin line being connected to the gap of one of them. The currents in these two elements are in co-phase and since the distance between them is small in comparison with the wave-length, the directional diagram of the loop dipole coincides with that of the usual half-wave dipole.

The input resistance of the loop dipole can be calculated from the power balance. Let the current in the antinode of each of the elements of the dipole equal I . The power radiated by the dipole will then equal:

$$P_{\Sigma} = (2I)^2 \times 73.1.$$

On the other hand, the radiated power equals:

$$P_{\Sigma} = I^2 R_{ab}.$$

Hence, the input resistance of a loop-like dipole is:

$$R_{ab} = 4 \times 73.1 = 292.4 \text{ ohms}$$

and the travelling-wave ratio in the feeder will be around 0.5, so that no additional adjustment of the feeder is necessary.

The loop-like dipole offers the additional advantage that it can be secured to its support without insulators, since a voltage node is set up in the centre of one of its elements. The loop-like dipole is generally used as a component of television receiving antennas and antennas of the wave channel type.

The dipoles considered above are not of the broadband type. The input resistance of any of these dipoles undergoes a sharp change in the event of a change of wave-length, giving rise to mismatch between dipole and feed line and a fall of the travelling-wave ratio in the feeder.

From this point of view, the so-called multiple-tuned shunt dipole proposed by G. Z. Eisenberg [16] is a considerable improvement. The circuit of this dipole is shown in Fig. 10-1, *d*. The action of an inductive stub (shunt) connected to the dipole at the points ab is similar to that of the reactive stub utilised in the case of broadband matching (see Paragraph 8-4) and which, within a certain wave range, backs off the input reactance of the dipole.

The proper choice of the points of connection of the stub, its geometrical dimensions, the angle α and the wave impedance of the feeder enables to obtain a satisfactory matching of the dipole to the feeder in about a quadruple wave range (from $\lambda \approx 6.5 l$ to $\lambda \approx 1.5 l$). Within that range, the travelling-wave ratio in the feeder does not fall below 0.3. Matching is likewise favoured by the fact that the dipole consists of broad plates (or of thick wires) which have a fairly low wave impedance.

The ordinary as well as loop-like half-wave dipole can also be fed by means of a flexible coaxial cable or a rigid coaxial line. In that case, the transition from the asymmetrical line, the coaxial cable being such an asymmetrical line, to the symmetrical dipole is effected by means of various balancers, the circuits of which are shown in Fig. 10-2 and 10-3.

Let us examine the U-elbow type balancer (Fig. 10-2, *a*).

If the coaxial cable is connected directly to the symmetrical dipole, i.e., if the internal conductor of the cable is connected to one of the arms of the dipole and its external conductor to the second arm of the dipole, the current flowing

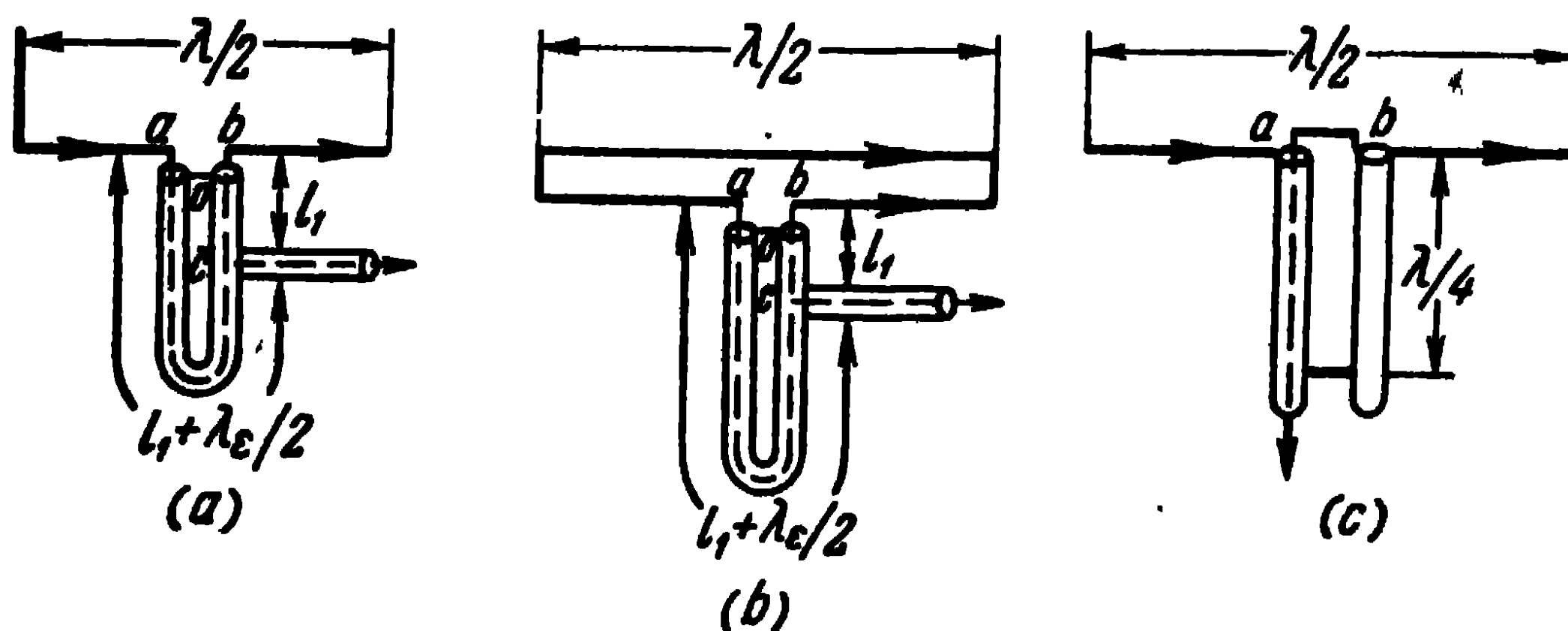


Fig. 10-2. Feeding a half-wave dipole by a coaxial cable:
a—feed of a symmetrical dipole using a U-elbow; *b*—feed of loop-like dipole using the U-elbow; *c*—feed by means of a metal insulator.

along the internal surface of the external conductor of the cable flows out of the cable, partly into the dipole and partly branching off towards the outer surface of the external conductor of the cable. As a result, the currents in the arms of the dipole are unequal. In addition, there arises a radiation of the cable, on account of the currents which branch off outside of it. This leads to a distortion of the directional diagram. The role of the balancing U-elbow is precisely to prevent branching of the currents. To this end, the difference between the lengths of the segments of cable in the U-elbow is taken equal to $\lambda_e/2$ and the external coatings of the segments of cable are shorted out at the ends. The length of the segment of cable l_1 in the balancer is chosen such as to enable the obtention of a travelling wave in the main coaxial cable.

In the circuit of Fig. 10-2, *a*, the input resistance of the antennas equals $R_{ab} = 73$ ohms, and the resistances loading

the segments of cable equal $R_{ao} = R_{bo} = 36.5$ ohms. If the wave impedance of the cable forming the U-elbow is given a value $W = 70$ ohms, and the length of the segment of cable l_1 is assumed equal to a quarter of a wave-length in the cable, the resistance at the points c loading the main cable will be:

$$R_c = \frac{W^2}{2R_{ao}} \approx 67 \text{ ohms}$$

and the travelling-wave ratio in the main feeder will be close to unity.

In the circuit of Fig. 10-2, *b*, the loop-like dipole has an input resistance $R_{ab} \approx 292.4$ ohms and the resistances loading the cable segments are equal to $R_{ao} = R_{bo} \approx 146.2$ ohms. If the length of the cable segment l_1 is taken equal to zero, the resistance loading the main cable is:

$$R_c = \frac{R_{ao}}{2} \approx 73.1 \text{ ohms}$$

and a travelling wave is set up again in the main cable.

Another balancer circuit is shown in Fig. 10-2, *b*. Here, two tubes with a short-circuiting bridge forming a quarter-wave metal insulator are joined to the symmetrical dipole. A coaxial cable is inserted through one of the tubes the external conductor of which is connected to the tube at point a and the internal conductor to the other tube at point b . This eliminates the excitation of the external surface of the cable and ensures that both halves of the dipole are symmetrically fed. The resistance loading the cable is equal to $R_{ab} = 73.1$ ohms, and if we take a coaxial cable with a wave impedance equal to 70 ohms, a travelling wave will be set up in it. Note that here, the metal insulator plays also the role of a stub, which backs off the reactive component of the input resistance of the dipole and widens the antenna pass-band.

In the centimetre wave range, the half-wave symmetrical dipole is fed by means of rigid coaxial lines. Here too, special balancers are used, which eliminate the excitation of the external surface of the coaxial line external conductor.

Fig. 10-3, *a* shows a feeding device of a half-wave dipole in which the coaxial line is enclosed within a quarter-wave-length tube short-connected with the coaxial line at one end. The new coaxial line thus formed, which is often referred to as a "quarter-wave" sleeve, represents a metal insulator,

which prevents the current from branching off to the external surface of the outer conductor of the coaxial line and ensures the symmetrical feeding of both halves of the dipole.

In another device (Fig. 10-3, *b*), the symmetrical dipole is excited by means of two longitudinal slots milled in the outer conductor of the coaxial line. As we know, a TEM wave is propagated in the coaxial line, accompanied by longitudinal currents. If longitudinal slots are milled in the coaxial line, they will not be excited. However, if, after that, at the place where the slots are situated, we connect the internal

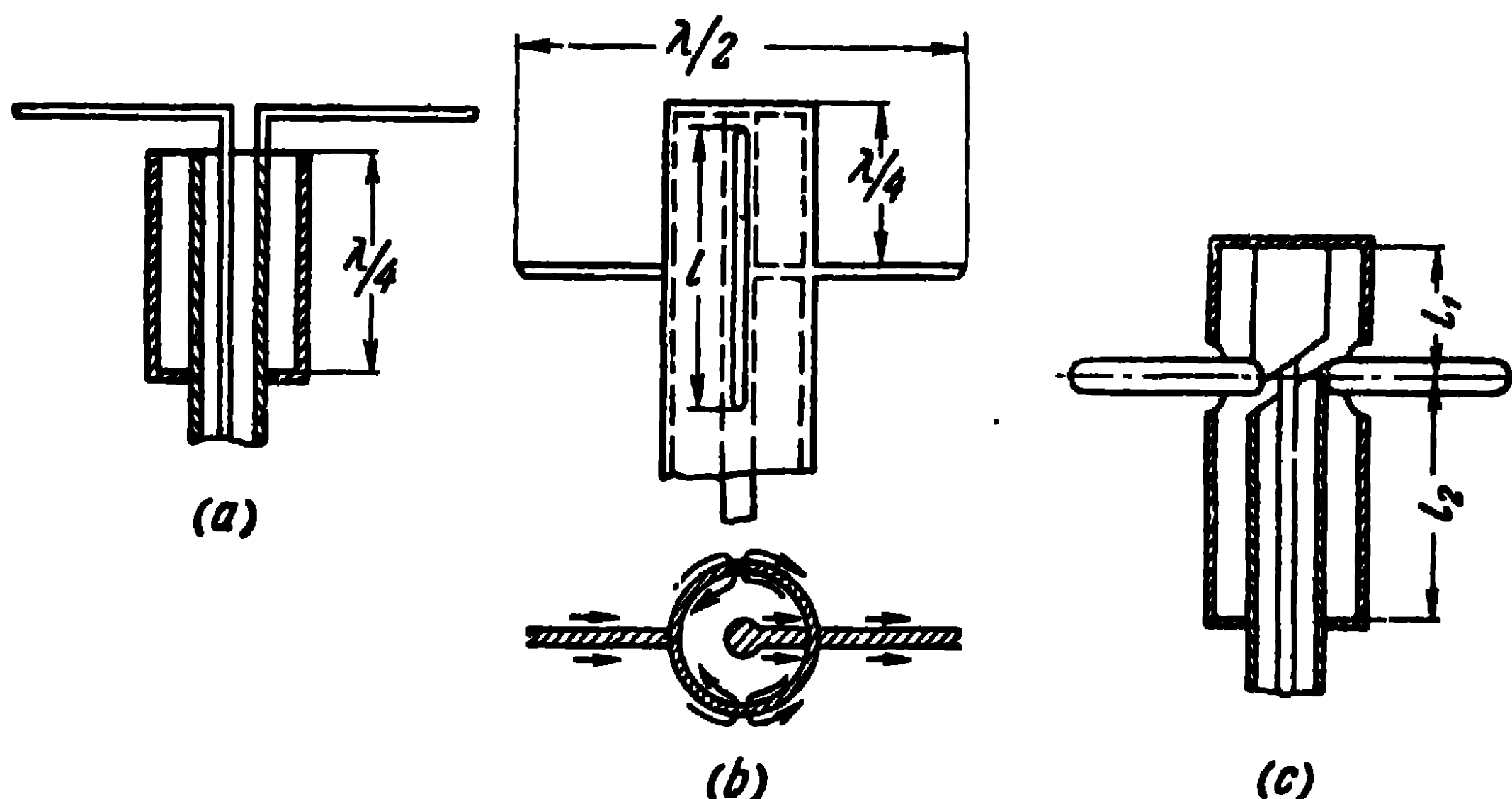


Fig. 10-3. Feeding a symmetrical dipole by a coaxial cable:
a—feeding by means of a quarter-wave sleeve; *b*—feeding by means of longitudinal slots; *c*—feeding by means of a double coaxial stub.

conductor to the external conductor by means of a crosspiece, i.e., if we short out the TEM wave, the current which flows along this crosspiece will generate higher-order modes and, in the first place an H_{11} wave in the coaxial line. Although this mode will not be propagated along the line ($\lambda_{\text{oper}} > \lambda_{\text{crit } H_{11}} = 2\pi R_{\text{mean}}$), it is accompanied by the local transverse components of the currents which intersect the slots in the external conductor and, thereby, excite the external space. Consequently, on the external surface of the outer conductor of the coaxial line, there arise transverse electric currents which excite the symmetrical dipole connected at that spot; this is seen from Fig. 10-3, *b*, which shows the cross section of the line at the place where the dipole is connected to it. The slots can be of any length, but the most intense excitation of the dipoles occurs when the slot length is resonant,

i.e., when $l \approx \lambda/2$. The coaxial line is shorted out at the end and the distance from the end of the line to the short-circuiting crosspiece is taken equal to approximately a quarter of a wave-length.

Feeding a symmetrical dipole by means of a broadband balancer is shown in Fig. 10-3, *b*. Here, the coaxial line is enclosed within a tube of length $l_1 + l_2$ shorted out at the ends; the tube has orifices for the passage of the arms of the half-wave dipole. One of the arms of the dipole is connected to the end of the outer conductor of the coaxial line and the other, to the internal conductor of the coaxial line, which, becoming thicker at the length l_2 is joined to the tube.

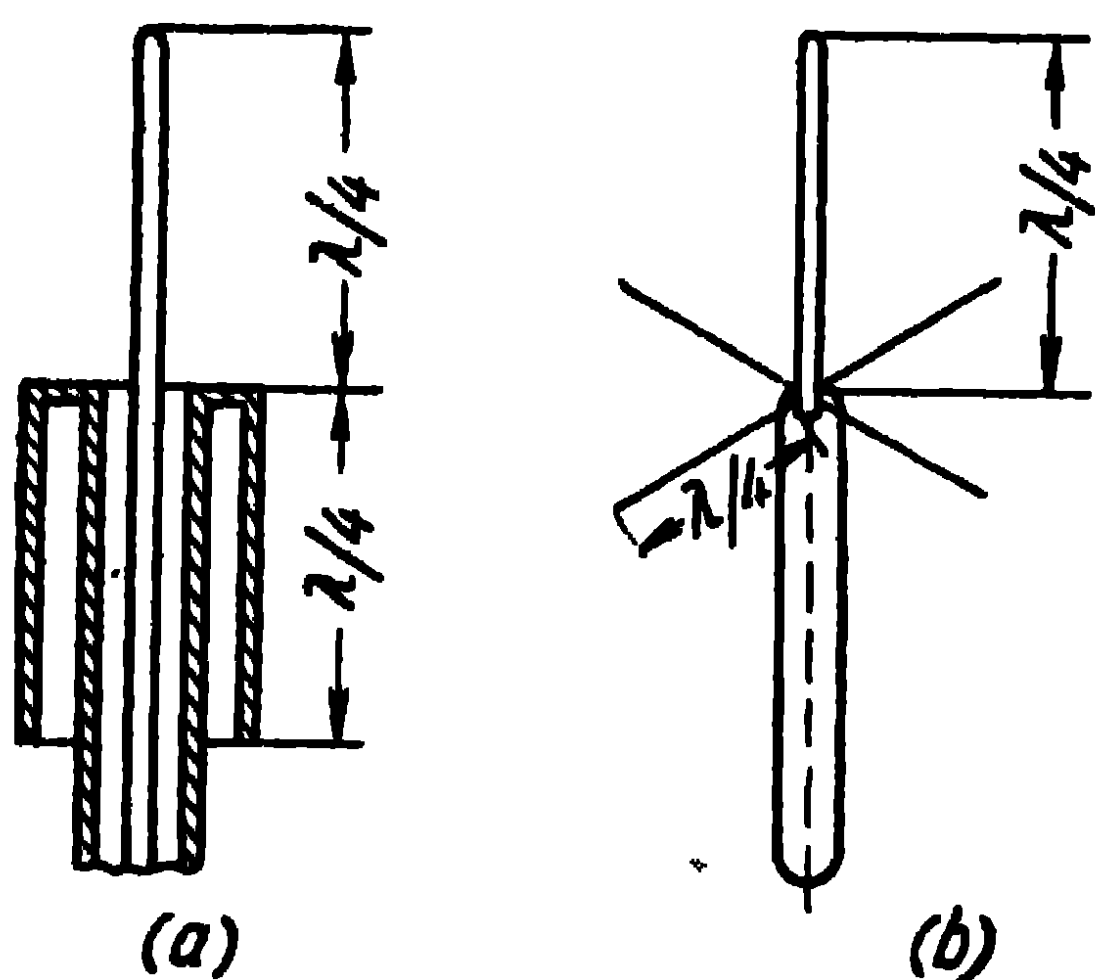


Fig. 10-4. Feeding a vertical dipole by a coaxial cable:

a—excitation by means of a quarter-wave-length sleeve; *b*—excitation by means of horizontal screening stubs.

The overall length of the balancing and compensating double coaxial stub is taken equal to half a wave-length and the ratio of the lengths of the stubs l_1 and l_2 is chosen so as to ensure the broadest possible pass-band.

A symmetrical (vertical) dipole may be formed by the continuation of the internal conductor of a coaxial line or cable and a quarter-wave-length sleeve, as shown in Fig. 10-4, *a*. In that case, the external surface of the quarter-wave-

length sleeve is excited and together with the quarter-wave-length projecting internal conductor it forms a half-wave dipole. In another case, instead of a quarter-wave-length sleeve, four horizontal wires of $\lambda/4$ length each are connected to the external conductor of a coaxial line (Fig. 10-4, *b*). The wires intercept the displacement currents branching off from the vertical dipole and thus screen the external surface of the coaxial line. In the horizontal wires, the currents flow towards one another and their radiation cancels out. In the main, the radiation is determined by the vertical quarter-wave stub. Of course, instead of wires, we can connect the disc to the external wire of the cable, but this will not lead to any significant change of the radiation and, at the same time, will complicate the construction of the antenna.

We have investigated a number of feed circuits of a simple dipole. There are many other feed circuits, but the ones mentioned above are the most frequently used in practice.

10-3. Simple Antennas of the Slot Type

In the first part of the book, we discussed the theory of slot antennas lying on infinite plane conductors. Making use of the duality principle and of the mirror method, we determined the directional diagrams of elementary slots. We established in the first approximation the voltage distribution law in a bilateral slot of finite length excited by a concentrated mmf. We also showed that in the case of resonant (half-wave) slots, this distribution did not depend on the distribution of the exciting mmf.

Thus, we defined the directional diagrams and radiation conductivities of the half-wave slot lying on an infinite plane screen, not only for a bilateral slot but also for a unilateral slot excited by means of a waveguide or a hollow resonator.

Knowing the voltage distribution in a resonant slot, we also defined by means of the eigenfunctions method the directional diagrams and the radiation conductivity of a half-wave longitudinal slot lying on an infinite circular cylinder.

In literature, one can also find the strict solution of the problem of the radiation of slots lying on bodies of regular shape, such as an infinite elliptical cylinder, a sphere, prolate or oblate spheroids.

We found, in particular, the strict solution of the problem of the radiation of a circular slot with a uniform voltage distribution lying on a prolate perfectly conducting spheroid.

In real conditions, surfaces on which slot antennas are located are finite and of irregular shape, so that no strict solutions of the problem can be obtained and we have to seek approximate solutions adequate for engineering purposes.

Usually, resonant half-wave slots are utilised, so that the voltage distribution in the slot is assumed sinusoidal. If, at the same time, we have in mind surfaces whose linear dimensions are of the order of one wave-length or more and whose curvature radii are of the same order, we can, as may be deduced from the theory of the half-wave slot lying on a circular cylinder, assume the radiation conductivity of the slot to be equal to the radiation conductivity of a slot

lying on an infinite plane screen, i.e., equal to $G_{\text{slot}} = 1,028$ milliohms.

Moreover, if we take into consideration the minimum dimensions of the resonator by means of which the half-wave slot is being excited, then one such resonator may be formed by a segment of short-circuited rectangular waveguide with an H_{01} mode of length equal to a quarter of a wave-length in the waveguide. Such a resonator plays the role of a metal insulator and its conductivity equals zero. Consequently, the

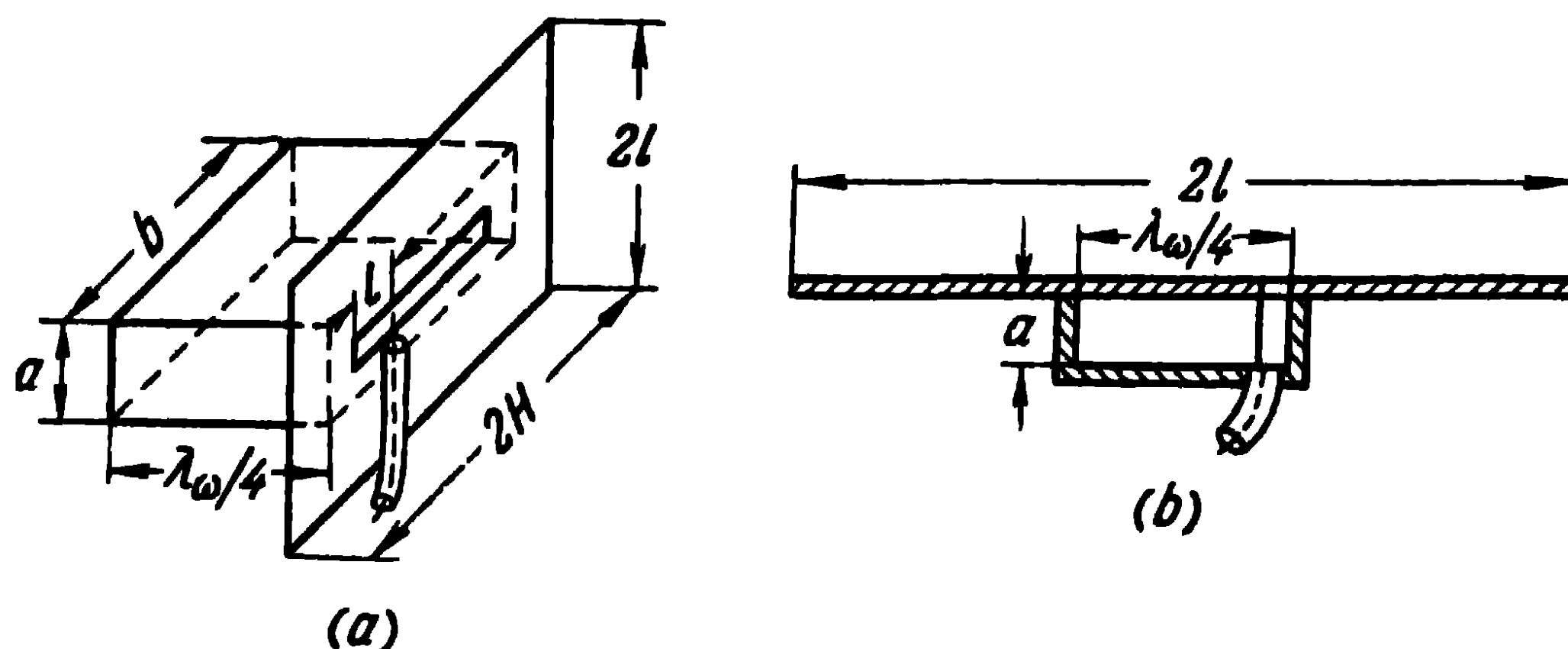


Fig. 10-5. Half-wave slot antenna with a quarter-wave resonator: *a*—first method of inserting the coaxial cable into the resonator; *b*—second method of inserting the coaxial cable into the resonator (longitudinal section).

input resistance of the half-wave slot antenna with a quarter-wave resonator will, in the voltage antinode (in the centre of the slot), equal $R_{\text{slot}} = \frac{1}{G_{\text{slot}}} = 970$ ohms.

In order to match the input resistance of the antenna to the wave impedance of the coaxial line which feeds the antenna, the line should be connected closer to the edge of the slot, at a distance l defined from the expression

$$\sin^2 kl = \frac{W}{R_{\text{slot}}},$$

where W is the wave impedance of the feed line;

$$k = \frac{2\pi}{\lambda};$$

l is the distance from the edge of the slot to the point of connection of the line.

Thus, we arrive at the circuit of the simple slot antenna shown in Fig. 10-5, *a*.

Designing considerations make it convenient to abut the resonator with one broad side against the screen and to

insert the feed line into the resonator through its other broad side. The longitudinal section of such a device is shown in Fig. 10-5, *b*.

As regards the directional diagrams, they differ, of course, from those that are obtained when the slot is situated in an infinite screen. It can be asserted that, owing to the fact that the radiation along the slot is zero, the amount

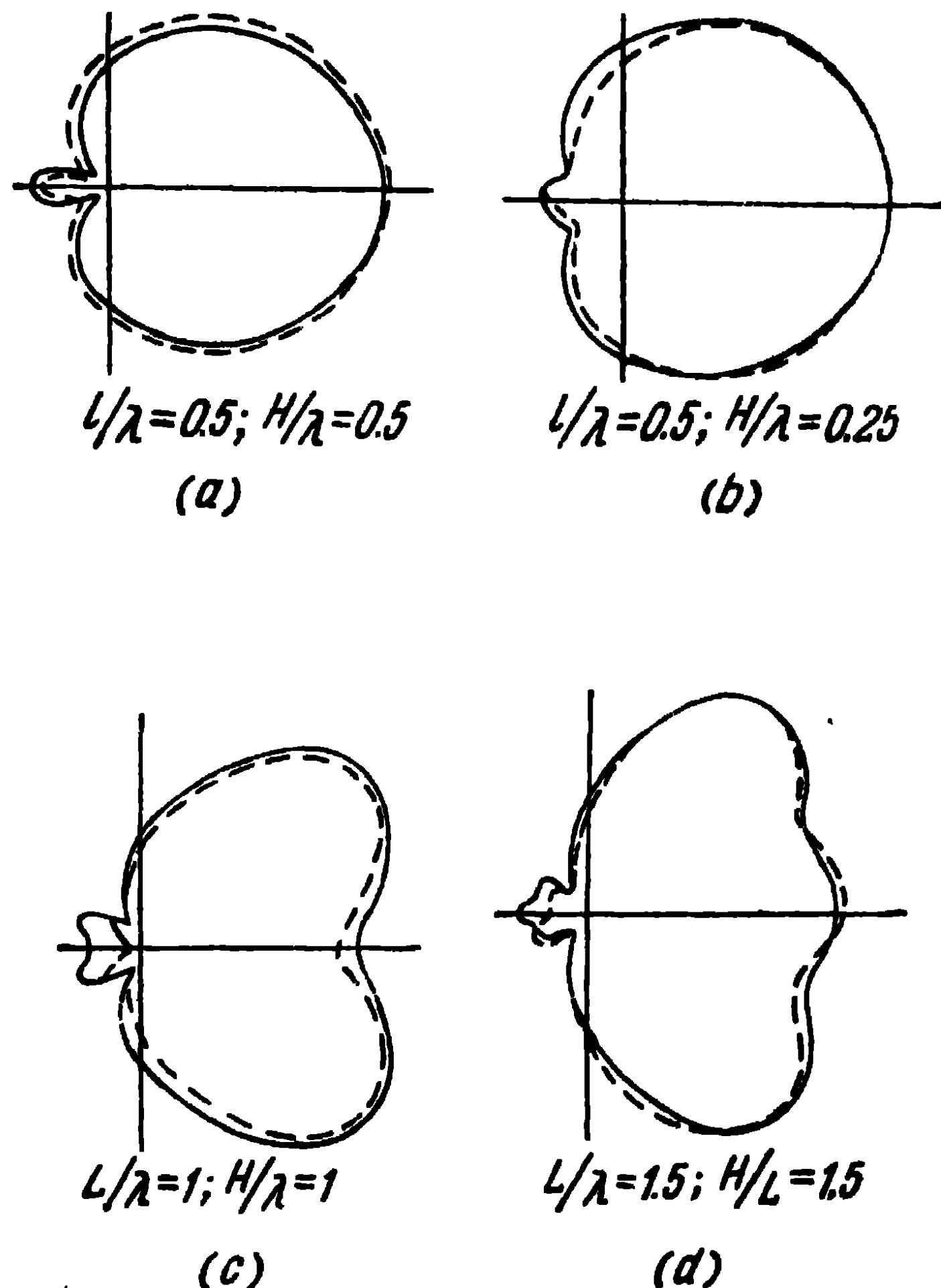


Fig. 10-6. Directional diagram of a slot antenna in the **E** vector plane.

of diffraction in the plane of the slot (in the plane of the magnetic vector) is only slight and the directional diagram depends but to an insignificant extent on the dimensions of the screen. In the front half-space, it approximately coincides with the directional diagram of a slot milled in an infinite screen; in the rear half-space, there is a small lobe. In a plane perpendicular to the slot (in the plane of the electric vector), the directional diagram depends to a considerable extent on the dimension of the screen $2L$ and depends only slightly on the dimension of the screen $2H$. In that plane, the wave

diffraction effect at the edge of the screen is pronounced. In that plane, the slot radiation is superimposed by the radiation which appears when the waves are reflected from the edge of the screen, i.e., due to the diffraction of the radio wave which leads, on the one hand, to the radiation of energy towards the shadow side of the screen and to the distortion of the directional diagram on the irradiated side of the screen,

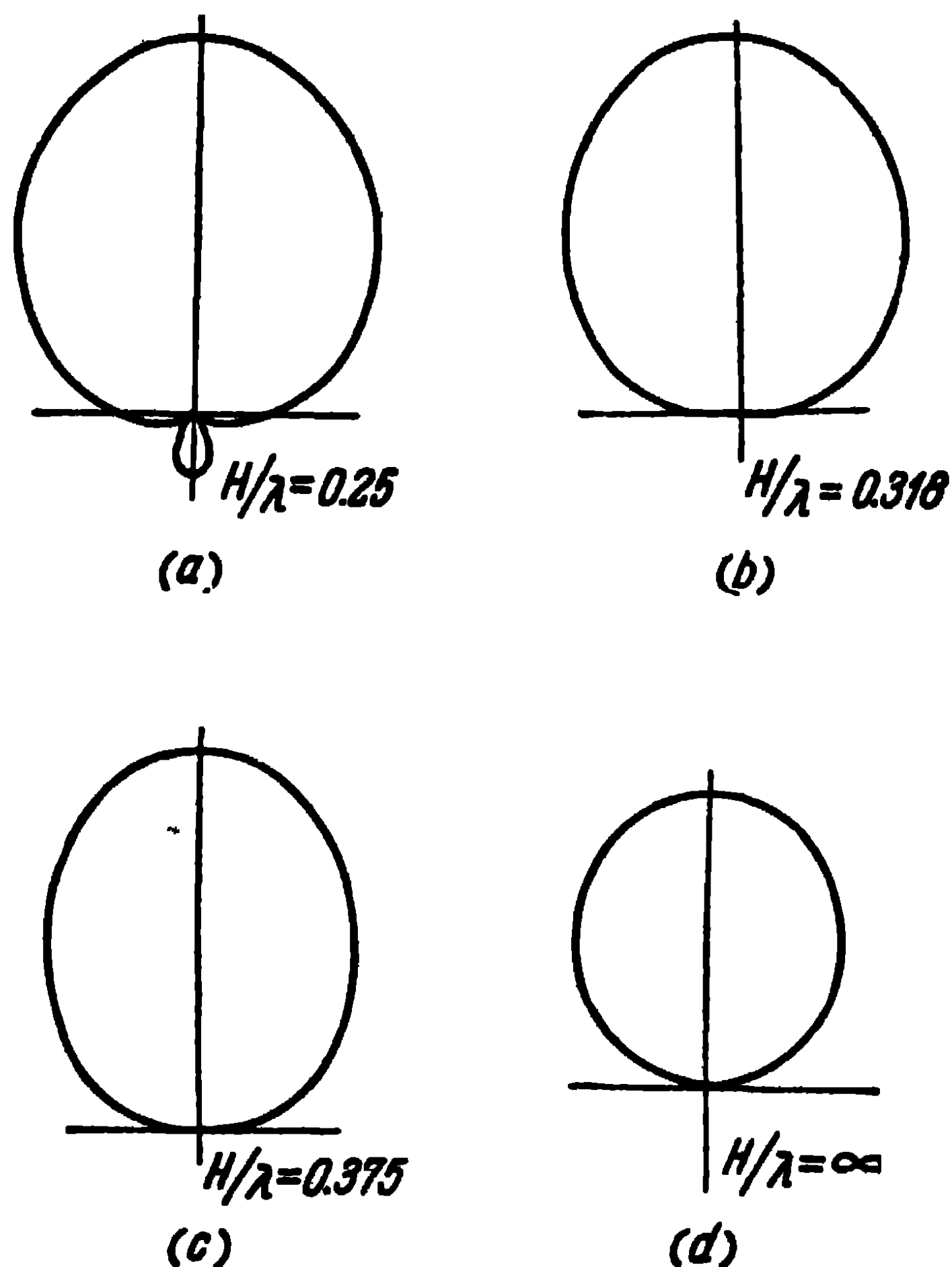


Fig. 10-7. Directional diagram of a slot antenna in the H vector plane.

on the other. Due to the interference of the waves radiated directly by the slot and, as a result of diffraction at the edges of the screen, there appear radiation minimums and maximums, whose number is all the greater as the dimension $2L$ of the screen is larger in comparison with the wave-length.

Experimental directional diagrams of a slot antenna in the electric vector plane depending on the dimensions of the screen are shown in dotted-line curves in Fig. 10-6. As can be seen, these curves do confirm what has been said above. The theoretical curves obtained by means of an approximate

theory are shown in the same figure. These curves have been calculated from the distribution of the surface electric current on the irradiated side of the screen, this distribution being assumed to coincide with the distribution of the surface electric current in an infinite screen [42].

Fig. 10-7 shows the theoretical directional diagrams in the magnetic vector plane, calculated on the assumption that the dimension $2H$ is finite and the dimension $2L$ infinite. In that case, the screen represents an infinite strip which is a degenerated infinite elliptical cylinder. The theoretical calculations were based on the eigenfunctions method [43].

A half-wave slot antenna with a resonator in the form of a quarter-wave metal insulator, can be placed on a segment of a circular cylinder as shown in Fig. 10-8. A cylinder of this kind may be afforded by, for example, the structure of a tower or the fuselage of an aircraft. The theory of this antenna has, on the whole, been expounded in Chapter Five and its directional diagrams and input conductivity related to the voltage in the antinode shown in Figs. 5-14 and 5-16.

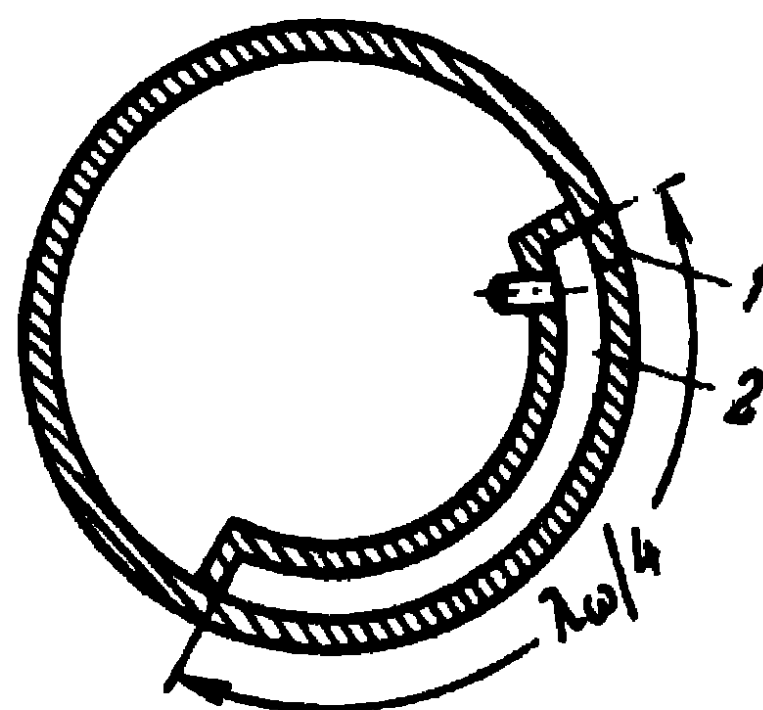


Fig. 10-8. Cross section of a circular cylinder with a quarter-wave resonator and longitudinal slot:

1—slot; 2—resonator.

In practice, not only unilateral but also bilateral slots lying on planes of limited dimensions are utilised. Thus, in Fig. 10-5, a bilateral slot antenna is obtained when the resonator is removed. The directional diagrams are now bilateral and approximately the same as in Figs. 10-6 and 10-7 for the illuminated region of the screen.

As regards the input resistance of a bilateral slot antenna, in the case of a sufficiently large screen in comparison with the wave-length, it can be defined from the expressions (2-54b) and (2-55b). For a resonant half-wave slot, it equals $R_{in} = 485$ ohms.

Fig. 10-9 shows the experimental curves of the input resistance in the vicinity of the resonance of a bilateral slot antenna with a sufficiently large screen. The length of the slot $l = 70$ cm, and the width of the slot, equal to 2, 4, 6 and 8 cm. The measurements were taken in the 170-240 Mc/s frequency range. It is seen from the curves that the resonant

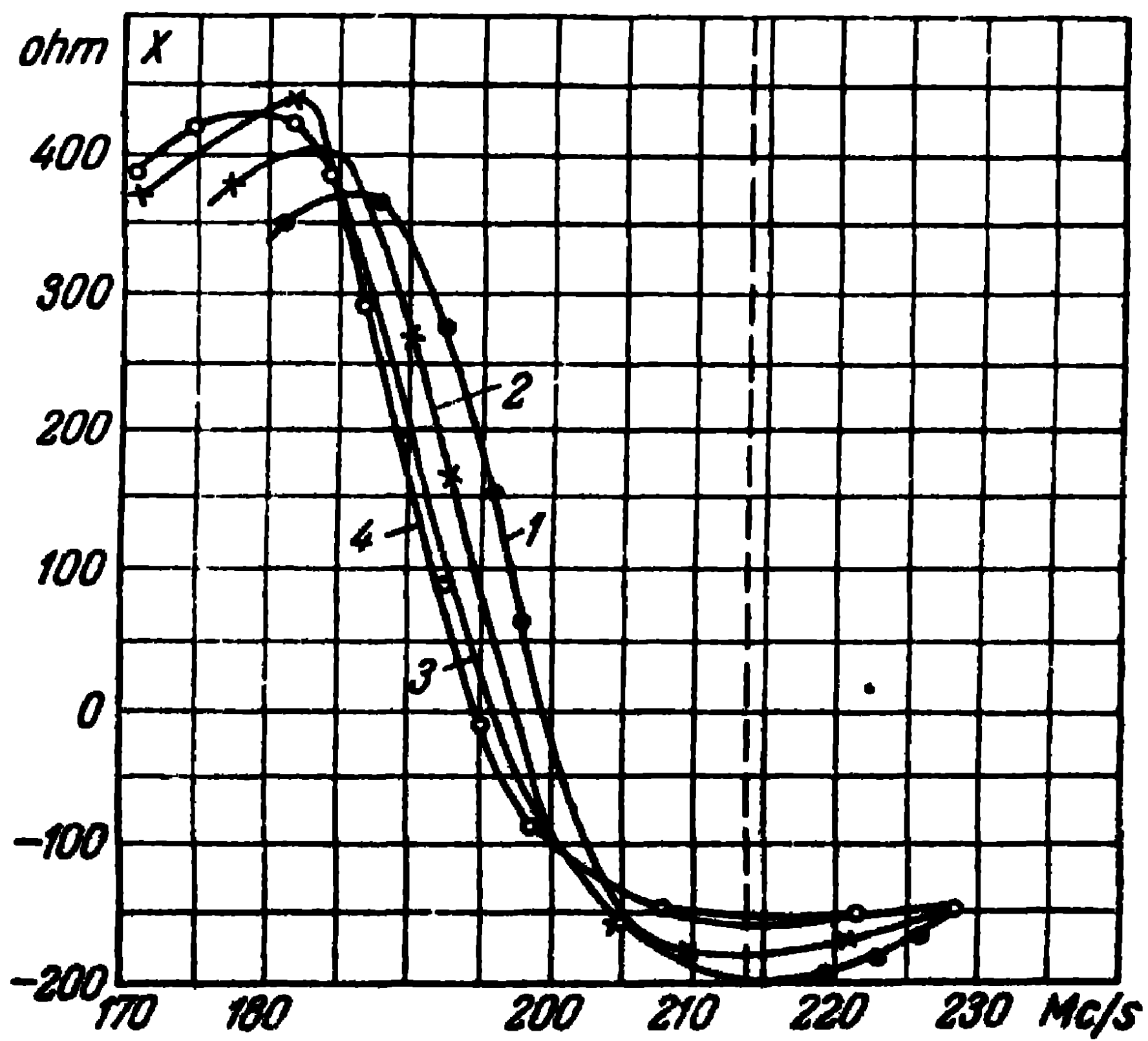
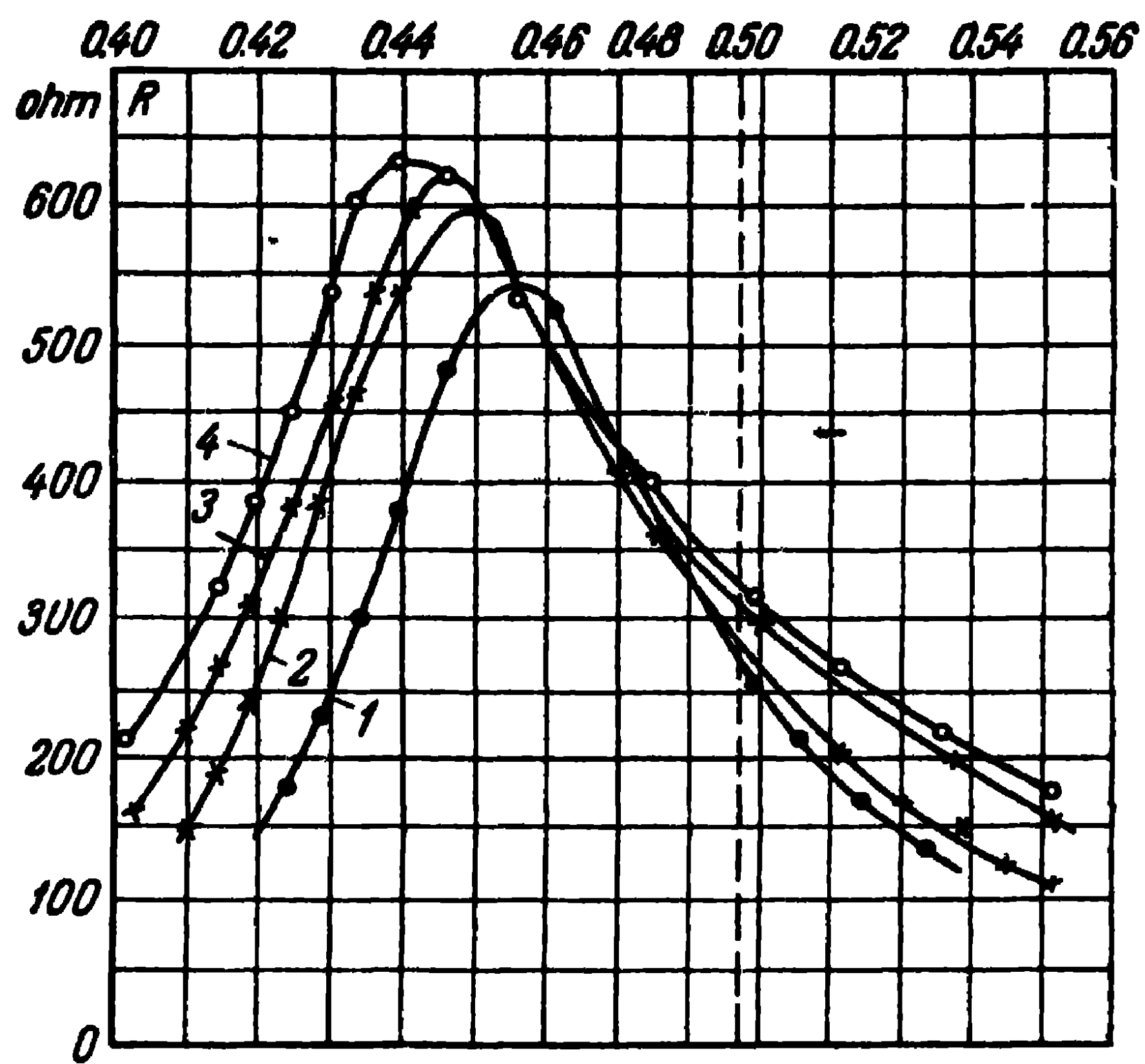


Fig. 10-9. Experimental curves of the input resistance of a bilateral slot antenna. Width of slot: 1-2 cm, 2-4 cm, 3-6 cm, 4-8 cm.

length of the slot is somewhat less than half a wave-length and decreases as the width of the slot increases.

The plane short-circuited dipole shown in Fig. 10-10 can also be regarded as a slot antenna; it is utilised as a component of turnstile antennas of transmitting television stations [44].

This dipole represents essentially one half of a bilateral slot antenna. It is evident that, in the case of sufficiently large linear dimensions of the screen relatively to the wave-length, the input resistances of such a dipole are approximately twice as large as those shown in Fig. 10-9. When

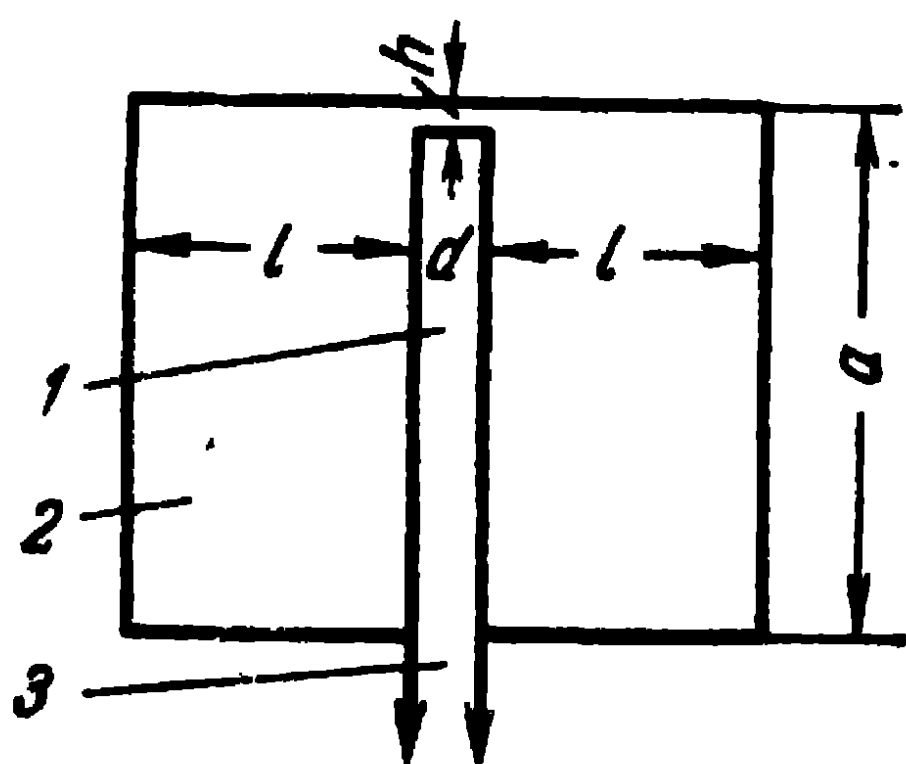


Fig. 10-10. Plane short-circuited dipole:

1—slot; 2—metal plane; 3—feeder.

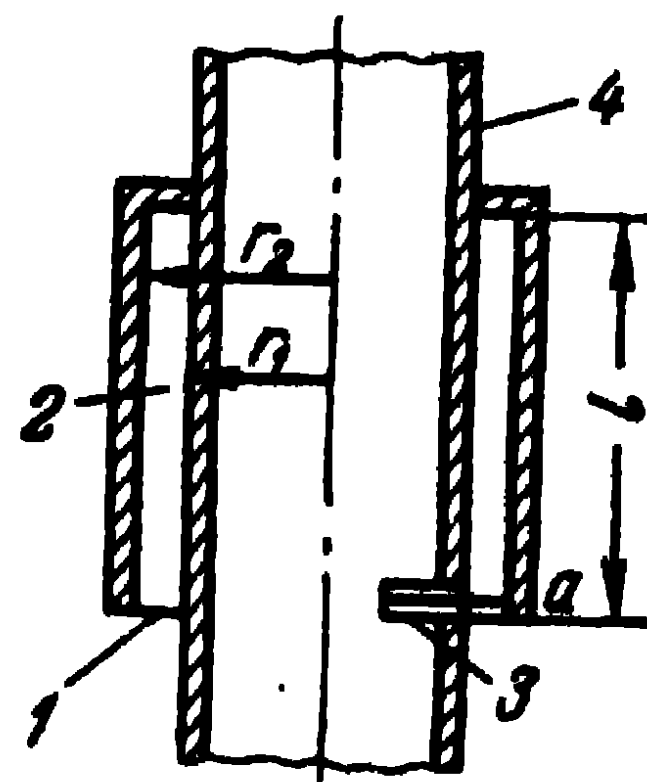


Fig. 10-11. Ring slot antenna:

1—slot; 2—coaxial resonator; 3—cable; 4—cylinder.

the screen decreases, the volume and character of the input resistance of the antenna change. B. V. Braude has shown that the antenna with the widest pass-band is obtained when the ratio of the dimensions of the screen a and l is equal to $a/l=1.5$. For these dimensions and for $d/\lambda=0.09$, $h=2$ cm within the range $0.25 < \frac{a}{\lambda} < 0.4$, the antenna input resistance changes insignificantly and the antenna pass-band is quite wide in that region.

Ring slot antennas arranged on a circular cylinder find an application as non-directive antennas (Fig. 10-11). Here, the circular slot is executed by means of a resonator in the shape of a quarter-wave metal sleeve, similar to the one shown in Fig. 10-4, a . The resonator is fed by means of a cable at the point a .

When the average length of the periphery of the resonator $\pi(r_1+r_2)$ is less than the operating wave-length, a TEM

mode is excited in it. The voltage in the slot is distributed uniformly and we get an antenna similar to a symmetrical wire dipole, whose radiation depends on the length of the exciting cylinder.

If the average radius of the resonator is greater than the wave-length, i.e., $\pi(r_1 + r_2) > \lambda$, then, apart from the TEM mode, an H_{11} mode is excited in the resonator the critical wave-length of which is equal to the average periphery of the resonator. If, at the same time, the length l of the resonator is taken equal to $\frac{\lambda}{2}$, there is no excitation of the TEM mode, while the excitation does take place in the case of the H_{11} mode whose wave-length is defined by the expression $\lambda_w = \frac{\lambda}{\sqrt{1 - \left(\frac{\lambda}{\lambda_{crit}}\right)^2}}$. The voltage in the slot will be found

to be distributed in accordance with the cosine law, transverse components of electric currents will arise on the excited body

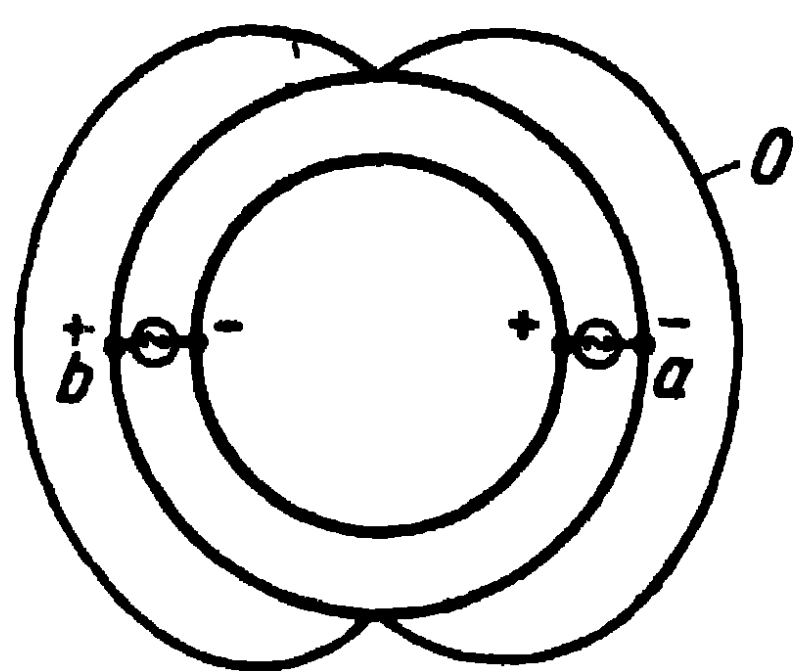


Fig. 10-12. Excitation of an antenna by a wave H_{11} in a ring slot.

and the radiation of the antenna will be substantially modified. Due to the transverse current components, there will occur a radiation along the axis of the cylinder. As shown by theoretical analysis and practice, such an antenna radiates uniformly in all directions. Moreover, the directional diagrams depend but little on the length of the excited cylinder.

Fig. 10-12 represents the feed circuit of an antenna at two diametrically opposed points of the resonator. The voltage at point a differs in phase from the voltage at point b by 180° , so that, for any length of the resonator l , the voltage in the slot will be distributed in accordance with the cosine law, as shown in the figure. Here, the length of the resonator is taken equal to $\lambda_w/4$.

10-4. Construction of Simple Wideband Antennas

In the two preceding paragraphs we gave an account of various simple wire and slot antennas. The present paragraph deals with a number of questions regarding the construction

of wideband as well as multiple-tuned antennas of a simple type.

The magnitude of the frequency band in which each antenna can be utilised is one of its important parameters; it is determined by the degree of permanency of such characteristics as the travelling-wave ratio in the feeder and the directional diagrams in the major planes of the antenna.

Depending on the relative operating frequency band, all modern antennas can be roughly divided into the following groups: a) narrowband antennas with a relative bandwidth of less than 10%; b) wideband antennas with a relative bandwidth of from 10 to 50%; multiple-tuned antennas, for which the ratio of the upper and lower limits of the operating band exceeds 1.5 : 1.0.

The problem most frequently met with in practice is that of designing wideband and multiple-tuned dipole antennas. The operating band of these antennas is limited mainly by the frequency dependence of their input resistance. That is why we shall, to begin with, dwell on the problem of designing wideband antennas by matching them to the feeder. There are two possible ways of increasing the matching band of antennas: designing a wideband antenna with a barely changing input resistance close to the wave impedance of the feeder, or the application of wideband matching methods to existing antennas. It follows from the theory of the wideband matching of a line to a load dealt with in Paragraph 8-4, that such a matching cannot in itself solve the problem of designing wideband antennas and represents but a certain correction of the behaviour of the antenna input resistance, possible in a limited frequency band. Hence, wideband matching plays an auxiliary role, the main task in solving the problem of designing wideband antennas being the design of radiators with a barely changing input resistance in the frequency band.

Let us elucidate the reasons of the frequency dependence of the antenna input resistance. Assume the antenna in the form of some transition device accomplishing the transformation of the coupled electromagnetic waves of the feeder into freely propagated space waves. It is evident that if this transition device constitutes a sufficiently continuous and electrically extended transition between the segments in which there are only coupled and space waves, then the reflections which arise upon the transformation of the modes are not high and can

partly cancel out, on account of the phase difference between them. The total reflection in the feeder which supplies such an antenna is small and is not critical relatively to the oscillation frequency and the length of the transition device. The input resistance of such an antenna depends but very little on the frequency, whereas the existence in the antenna of segments with an abrupt change of dimensions gives rise to pronounced reflections. If there are several sources of such pronounced reflections and the distance between them is commensurable with the wave-length, then even an insig-

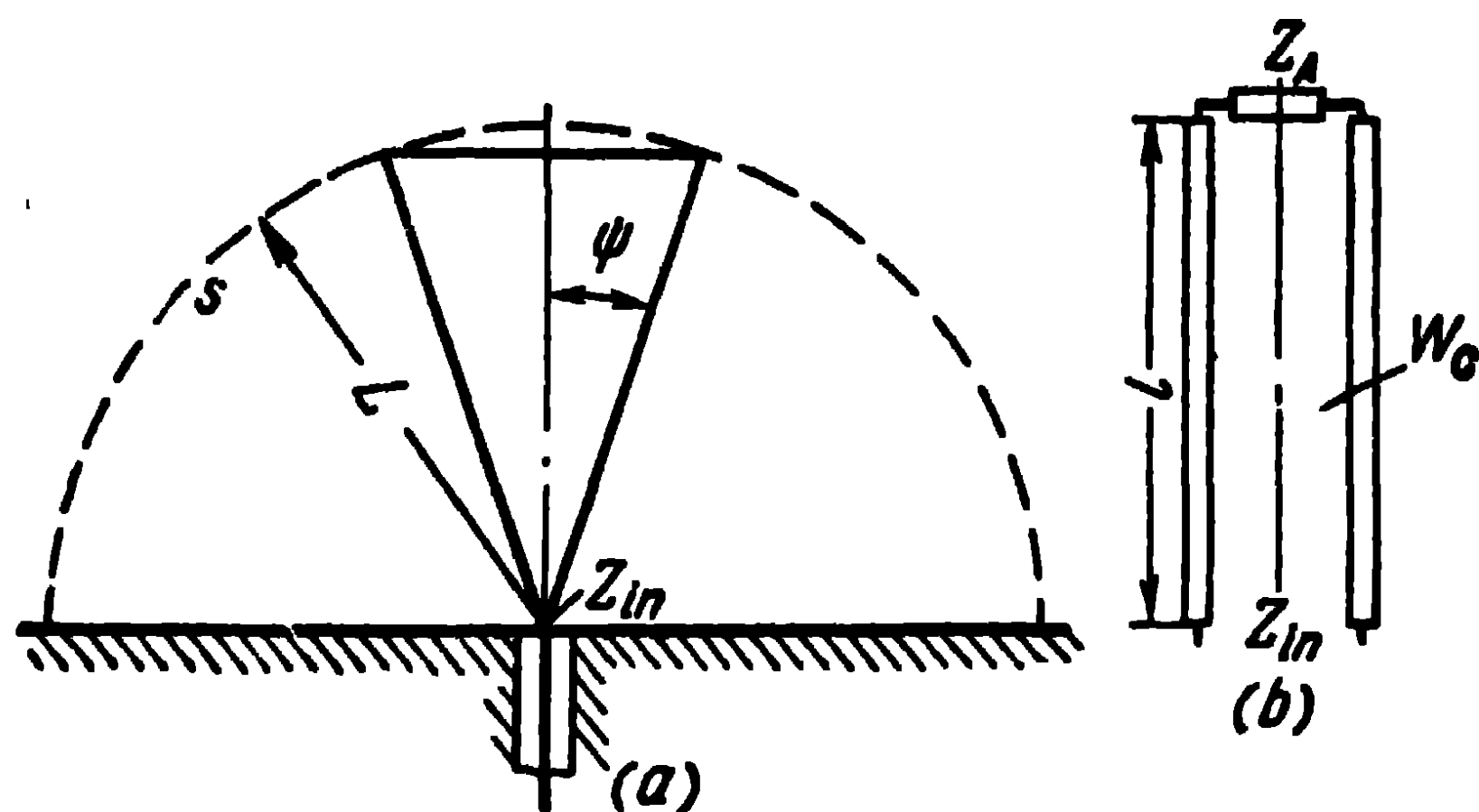


Fig. 10-13. Asymmetrical conical dipole:
a—circuit of dipole; b—equivalent circuit.

nificant change of frequency will lead to a considerable mutual phase difference between the individual reflected waves and a pronounced frequency dependence of the input resistance. Let us illustrate this on the example of the asymmetrical conical dipole shown in Fig. 10-13, a.

As we know, a cone of infinite extension over a metal surface constitutes a homogeneous transmission line with TEM mode and wave impedance $W_c = 138 \log \cot \psi/2$ [45]. In the case of an infinitely long dipole, its input resistance is not frequency dependent and equals the wave impedance. In the case of a conical dipole of finite length, there appears in it a reflected TEM wave; moreover, one can consider the source of the reflections to be the surface s , on which part of the incident TEM wave is transformed into a sum of azimuth-symmetrical TM waves formed on the outside as well as inside space. In accordance with the above, the equivalent circuit of the dipole can be represented, as shown in Fig. 10-13, b, as a segment of homogeneous line with a wave impedance W_c and length L , loaded with a certain complex

resistance Z_A which itself depends on L and the wave impedance W_c . Thus, the total reflection in the feeder is due to the presence of two partial reflections: from the surface s (end of the dipole) and from the apex of the cone (when $W_c \neq W_1$).

In the case of an asymmetrical dipole of different form, e.g., cylindrical, the equivalent circuit will comprise a segment of, in this case, inhomogeneous transmission line with variable wave impedances for the TEM waves along its

length; distributed reflections from each segment will be added to the reflections from the end and beginning of this segment.

The most significant reflection from the end of the dipole can be checked either by compensating it through another reflection or by reducing it directly through the appropriate choice of the form of the dipole. The idea regarding the compensation of the end reflection can be illustrated by means of the example of the asymmetrical sleeve-stub dipole with a raised feed point shown in Fig. 10-14.

In a dipole of this kind, the current wave reflected from the upper end is compensated at the feed point by another current wave of opposite phase arising from the reflection off the metal plane at the low end of the dipole. In other words, the capacitive reactance of the upper half of the dipole is compensated by the inductive resistance of the lower half of the dipole, connected in series with it. A satisfactory compensation can be obtained only through the correct choice of the geometrical dimensions and in a limited frequency band, not exceeding 10-15%.

To continue, returning to the conical dipole in Fig. 10-13 and considering that its length L is not inferior to 0.2-0.25 of the wave-length, let us investigate the influence of the angle at the apex of the cone ψ on the total reflection coefficient in the feeder. As the angle ψ increases from zero, to begin with, there is a decrease of the reflection coefficient from the base of the dipole due to the rapid fall of the wave

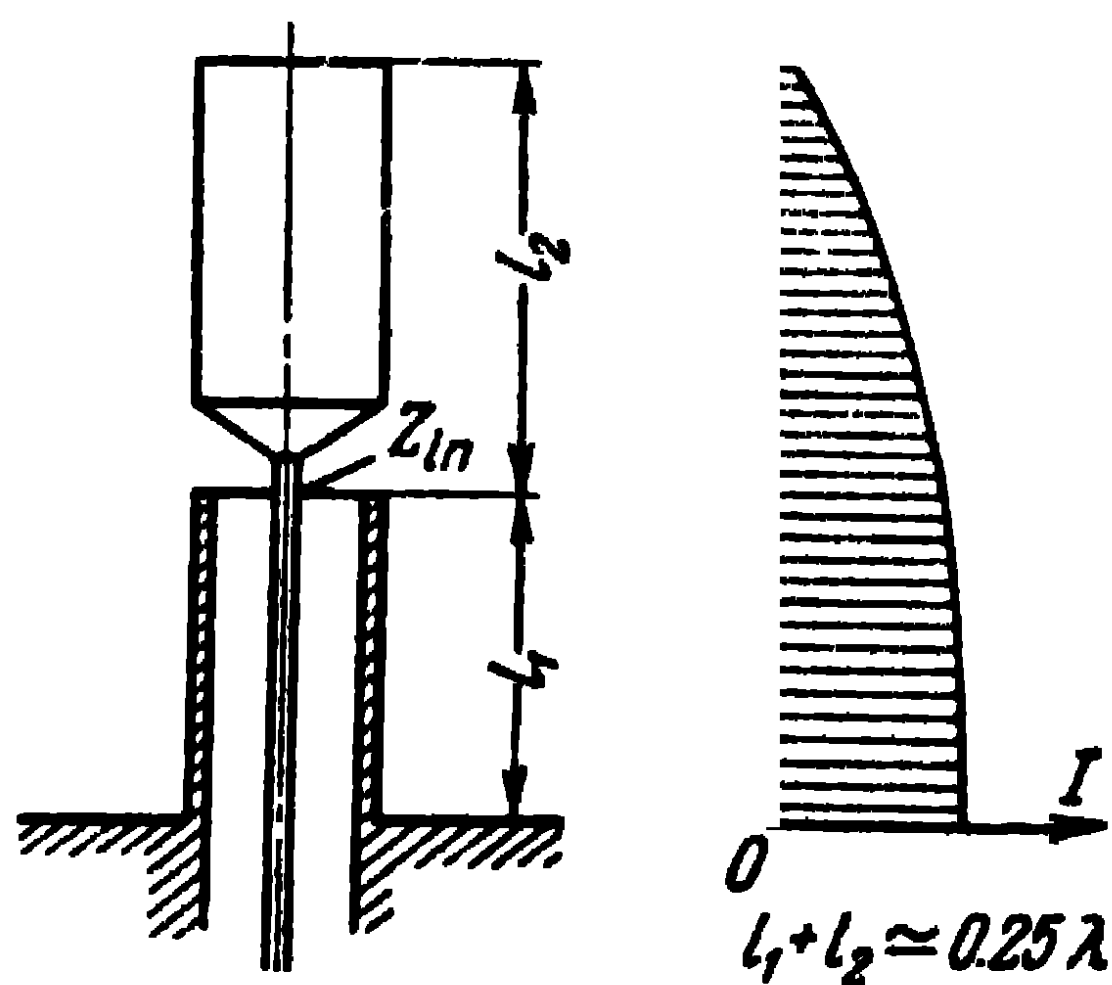


Fig. 10-14. Asymmetrical sleeve-stub dipole and its current distribution.

impedance and its approximation to the quantity Z_A . As for the quantity Z_A , it remains almost constant owing to the fact that the main role in the radiation is played by the equatorial regions of the sphere s (it is through them that the largest part of the radiated power comes out into the surrounding space). In a certain region of the mean values of the angle ψ , the coefficient of reflection from the end of the dipole falls down to its smallest value; moreover, the wave

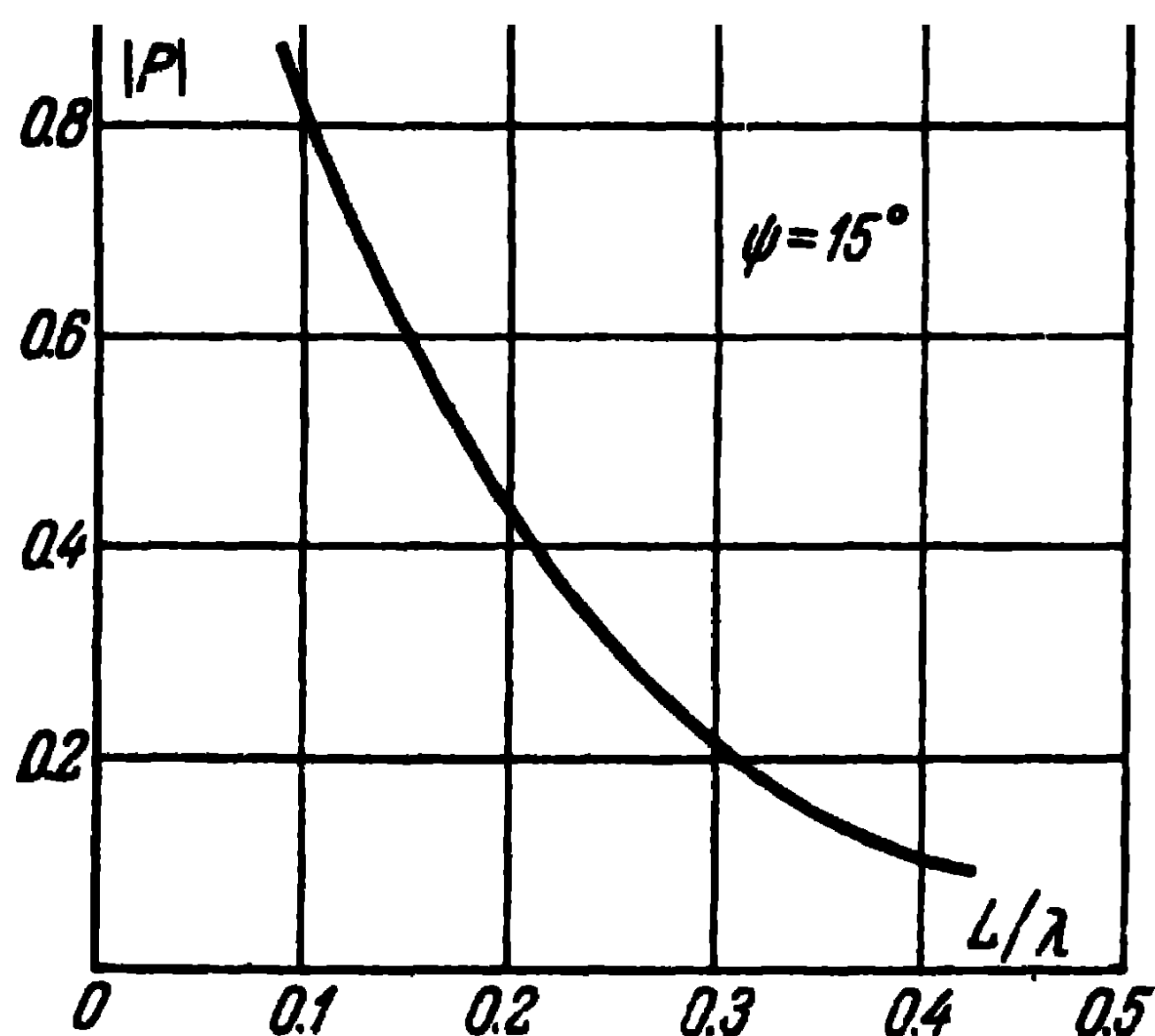


Fig. 10-15. Coefficient of reflection in a conical dipole with an angle $\psi = 15^\circ$ plotted as a function of the ratio $\frac{L}{\lambda}$.

impedance of the cone approaches the wave impedances of the lines generally used (50-75 ohms). A further increase of the angle ψ leads to the increase of the coefficient of reflection from the end, due to the fact that the radiation occurs through a narrowing ring-like slot and the resistance Z_A acquires a large reactive part. Thus, there is a certain average optimum magnitude of the wave impedance of the dipole for which the reflection from the base and that from the apex of the dipole are at a minimum.

Let us now examine the dependence of the coefficient of reflection at the base of the dipole on the frequency or, which is absolutely the same, on the length of the dipole. The typical curve of the modulus of the coefficient of reflection $|p|$ plotted as a function of the ratio of the dipole length to the wave-length L/λ obtained experimentally [46] is shown in Fig. 10-15. It follows from this graph that $|p|$ becomes

sufficiently small when the length of the dipole exceeds $0.2-0.3\lambda$. Such a dependence of the modulus of the coefficient of reflection is explained by the fact that as L/λ increases, the ratio of the transverse components of the **E** and **H** vectors in the space TM waves tends towards the value of the wave impedance of the TEM waves in air equal to $\sqrt{\mu_0/\epsilon_0} = 120 \pi$ ohms. It should be noted that in thin (for example $\psi < 3^\circ$) or too

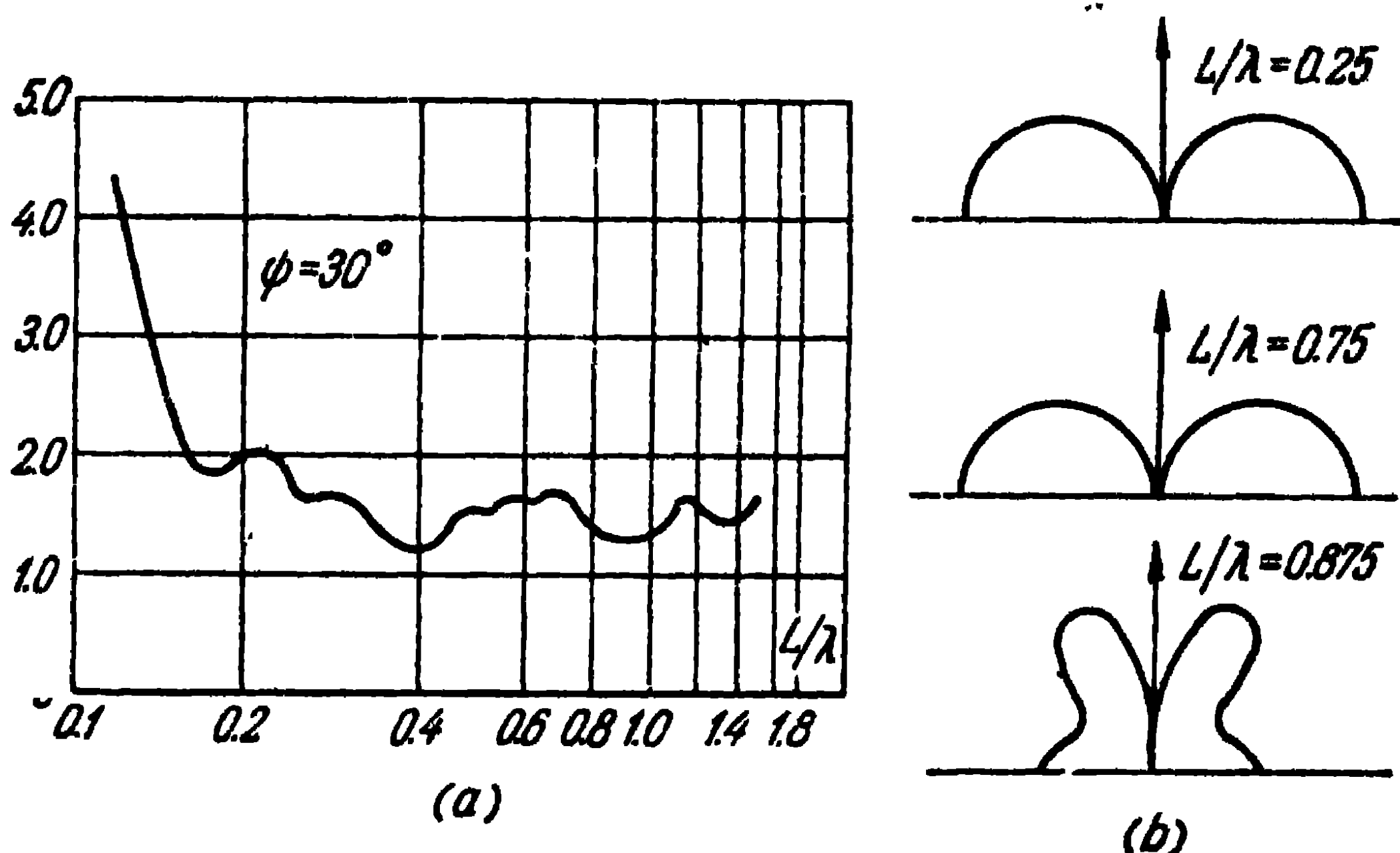


Fig. 10-16. Standing wave ratio and directional diagrams of a conical dipole ($\psi = 30^\circ$):

a—experimental curve of the SWC plotted as a function of the ratio $\frac{L}{\lambda}$, *b*—experimental directional diagrams

thick (for example $\psi > 80^\circ$) conical dipoles, there occurs a pronounced reflection from the end even for significant lengths of the arms, due to the sharp difference between the wave impedance of the dipole and the equivalent loading resistance Z_A . Thus, a conical dipole with an optimum wave impedance may be regarded as a multiple-tuned radiator from the point of view of the input resistance on condition that $L > 0.2 \lambda_{\max}$, where λ_{\max} is the maximum wave-length of the operating range of the antenna. Fig. 10-16, *a* shows the experimental characteristic of the standing wave ratio in a coaxial feeder with a wave impedance $W_1 = 50$ ohms for one of the designs of the conical dipole. It can be seen from the figure that such an antenna is satisfactorily matched in a sevenfold frequency range. However, the directional diagrams of this conical dipole change substantially already when

$L > 0.75\lambda$ (Fig. 10-16, *b*), which is due to the change of the electrical dimension of the dipole when the frequency changes.

Another example of an antenna with wideband properties with respect to the input resistance is the disc-conical radiator shown in Fig. 10-17, *a*, which consists of a cone and a disc

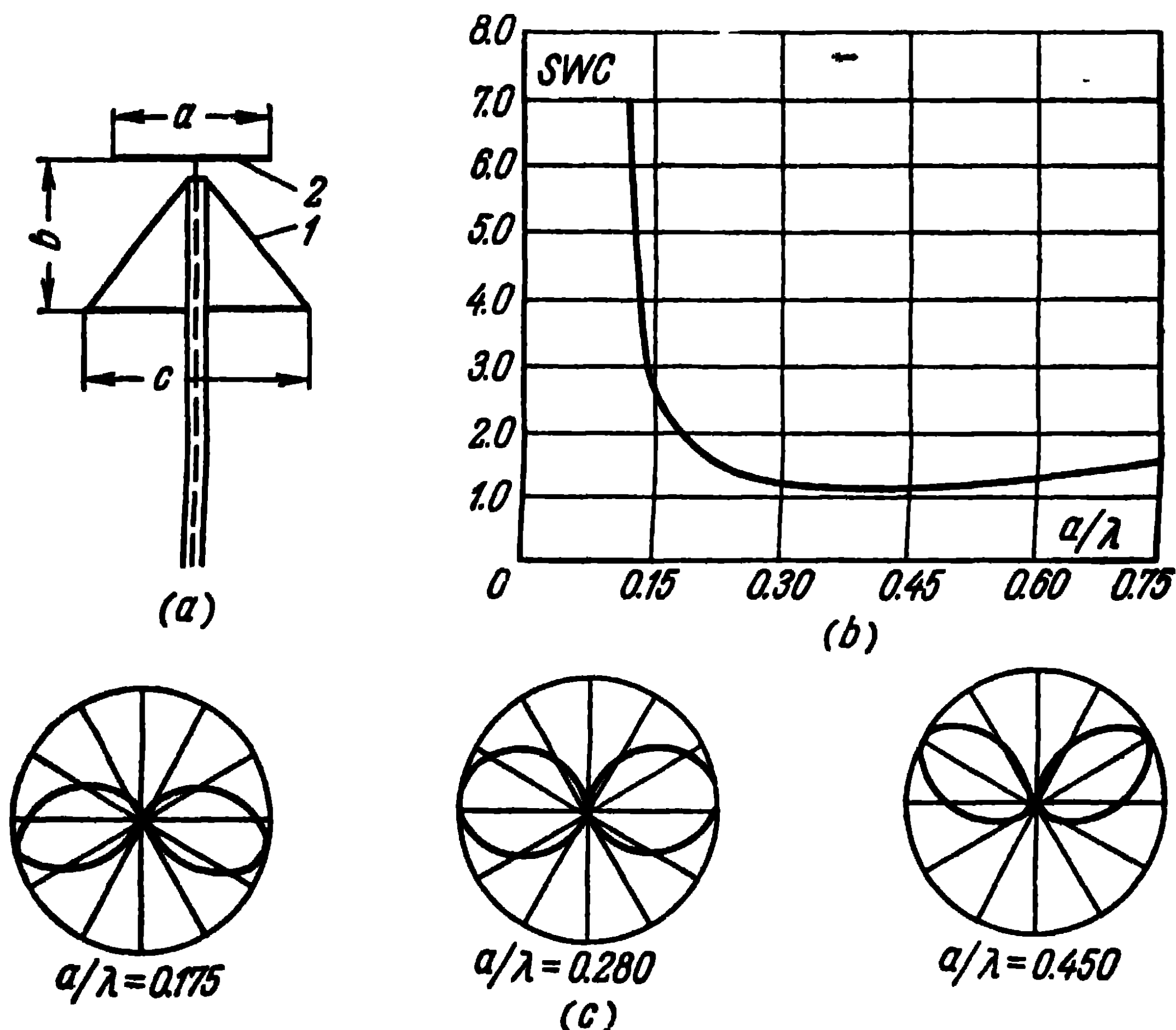


Fig. 10-17. Disc-conical radiator:

a—circuit of radiator: 1—cone; 2—disc; *b*—experimental curve of the SWC plotted as a function of the ratio a/λ ; *c*—experimental directional diagrams.

between which an exciting voltage is applied with a coaxial feeder. The cone is connected to the outer coating of the feeder, the disc, to the inner conductor. For a wave impedance of the feeder of 50 to 75 ohms, the disc-conical radiator is matched up to $K=0.6$ at all frequencies exceeding a certain limit frequency determined by its geometrical dimensions [46]. Figs. 10-17, *b* and 10-17, *c* show the characteristics obtained experimentally of the matching of a disc-conical antenna with dimensions $a/\lambda_{\max}=0.175$, $b/\lambda_{\max}=0.25$, $c/\lambda_{\max}=0.275$ to a coaxial feeder whose wave impedance equals 50 ohms, as well as the directional diagrams on a number of frequencies.

A study of these figures reveals that the operating range of this antenna is also limited by the frequency dependence of the directional diagrams.

Analysing all that has been said regarding antennas of wideband properties with respect to the input resistance, the following conclusions can be drawn: 1) such antennas can only be constructed with dimensions comparable to the maximum length of the operating range wave; 2) their directional diagrams have a pronounced frequency dependence due to the fact that frequency changes lead to changes of the electric lengths of the radiator elements.

Owing to the fact that dipole antennas of low directivity with good matching characteristics and constant directional diagrams in a wide frequency range are required for many practical radio-engineering purposes, we shall investigate a number of fundamental considerations which can serve as a basis for designing such antennas.

A starting point can be afforded by the electric modeling principle, which establishes the identity of the input resistance and directional diagrams of two separate antennas in two different frequencies if the shape of the antennas is the same and the dimensions change proportionately to the ratio of the frequencies. In the case of antennas of infinite extension, whose shape is defined only by the angular dimensions (e.g., for conical dipoles), a change of scale proportional to the change of frequency does not lead to changes in the antenna. That is why antennas which are defined only by angular dimensions have the parameters of frequency-independent antennas. The construction of finite antennas defined by angular dimensions is impossible. However, one may attempt to find such forms of infinite structures as are defined only by angular dimensions, the behaviour of the end part of which will, above a certain limit frequency, tend asymptotically towards the behaviour of the corresponding infinite structure from the point of view of the constancy of the input resistance as well as from the point of view of the constancy of the directional diagrams.

With regard to plane antennas, the class of curves outlining infinite structures defined only by angular dimensions can be found in the following way [47]. Let us introduce the polar coordinates r , φ and cause the curve $r(\varphi)$ which limits the form of the plane antenna to pass into itself in the event of changes of scale along r and to differ from

the original curve only by a turn of a certain angle relatively to the axis of the coordinates. Mathematically, this can be written as follows:

$$Kr(\varphi) = r(\varphi + \gamma),$$

where K is the coefficient of change of scale; γ , the angle of rotation of the whole original curve, corresponding to such a change of scale. It is obvious that the angle γ should depend on K , but neither K nor γ should depend on r and φ . This condition leads to the following relations:

$$r(\varphi) \frac{dK}{d\gamma} = \frac{\partial r(\varphi + \gamma)}{\partial r}; \quad (10-1)$$

$$K \frac{dr(\varphi)}{d\varphi} = \frac{\partial r(\varphi + \gamma)}{\partial \varphi}, \quad (10-2)$$

moreover, the following equality should also be satisfied:

$$\frac{\partial r(\varphi + \gamma)}{\partial \gamma} = \frac{\partial r(\varphi + \gamma)}{\partial(\varphi + \gamma)} = \frac{\partial r(\varphi + \gamma)}{\partial \varphi}. \quad (10-3)$$

Taking account of (10-3), we shall obtain from (10-1) and (10-2) the following differential equation for the function $r(\varphi)$:

$$r(\varphi) \frac{dK}{d\gamma} = K \frac{dr(\varphi)}{d\varphi} \quad \text{or} \quad \frac{dr}{d\varphi} = ar \quad (10-4)$$

where $a = \frac{1}{K} \frac{dK}{d\gamma}$ is a certain new constant. The solution of the equation (10-4) is represented by a logarithmic (equiangular) helix

$$r(\varphi) = Ae^{a(\varphi + \varphi_0)}.$$

In this expression, A and φ_0 represent certain constant quantities defining the scale in the r -direction and the original angle of rotation of the winding. The parameter a is equal to the cotangent of the angle θ between the radius r and the tangent to the curve.

Thus, we may conclude that the shape of plane infinite frequency-independent antennas should be limited by logarithmic helixes having the same magnitude of the parameter a . The latter is indispensable to avoid the overlapping of separate parts of the antenna at the origin of the coordinates where the excitation should take place. An example of such a structure is shown in Fig. 10-18.

A similar analysis for finding out the class of frequency-independent infinite structures can be performed in a three-dimensional space in the spherical coordinates r , θ , φ taking into consideration the condition

$$Kf(\theta, \varphi) = f(\theta', \varphi'), \quad (10-5)$$

where $f(\theta, \varphi)$ is the original shape of the antenna; $f(\theta', \varphi')$ corresponds to a rotation of the antenna in space, equivalent to a change of the dimensions by K times. It is

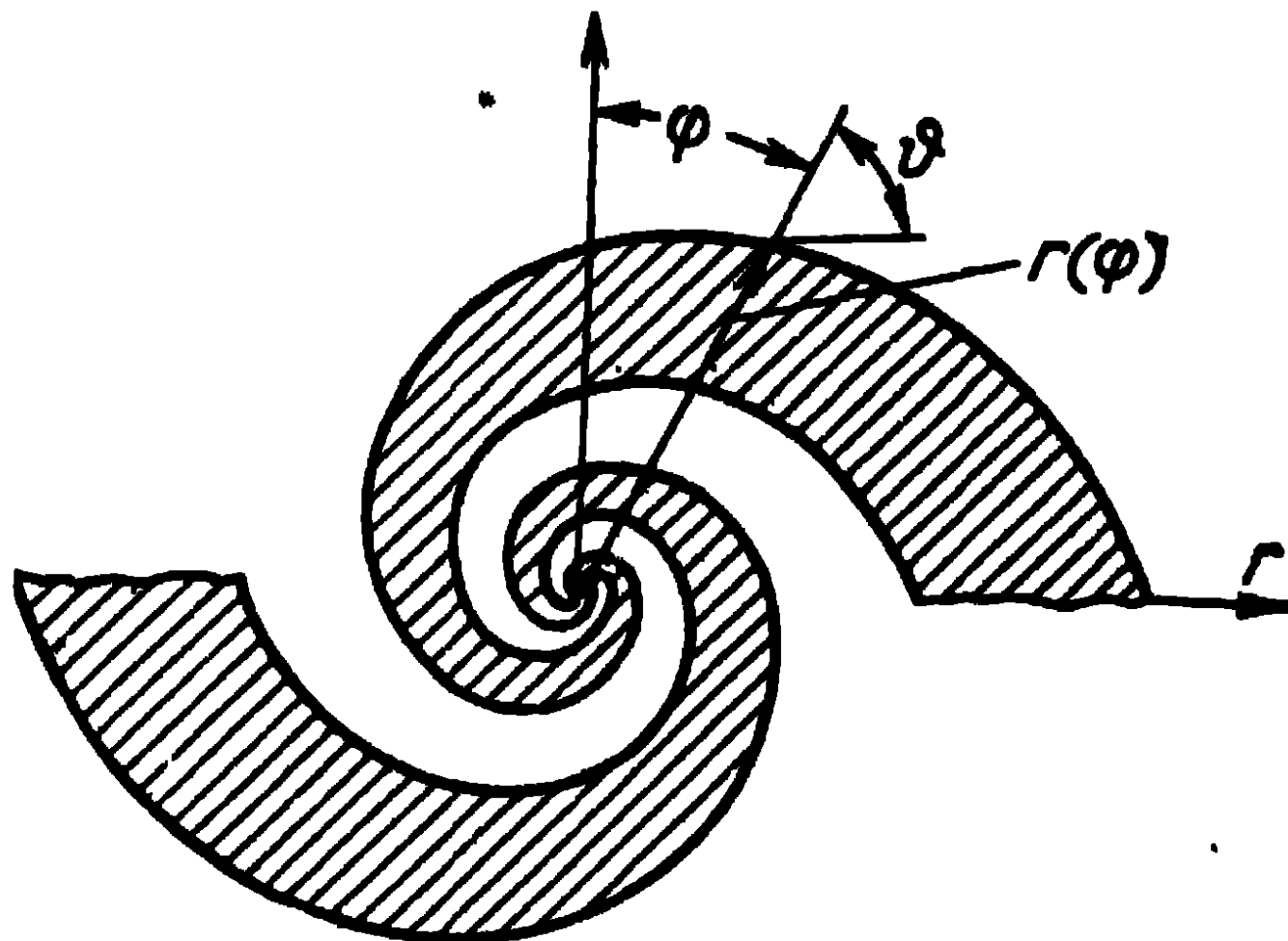


Fig. 10-18. Infinite structure defined by angular dimensions.

readily seen that the condition (10-5) is satisfied by a solution in the following form:

$$r = e^{u(\varphi + \varphi_0)} F(\theta),$$

where $F(\theta)$ represents any function, and the direction of the change of scale should coincide with the axis of the spherical coordinates.

Of great importance for the proper understanding of the operation of an antenna formed by the finite part of the structure shown in Fig. 10-18 is the following experimentally discovered fact: the intensity of the current in the arm of the antenna, when it is excited in the centre by an emf generator, sharply decreases (100 times and more) after it has passed that turn of the structure whose periphery is approximately equal to the wave-length. It is precisely due to this peculiar automatic "cut-off" of the current at the spot, defined by the frequency of the exciting generator, that the electric dimension of the radiating part of the antenna is maintained constant

on different frequencies. As a result, such an antenna of finite dimensions can have an almost constant input resistance and the same directional diagram in a twentyfold and even larger frequency range. The lower limit of the operating range is defined from the condition of the equality of the wave-length to the periphery of the last turn of the antenna. The upper limit of the operating range is determined by the commensurability with the wave-length of the central region of excitation of the antenna where the geometry of the helical lines is disturbed due to the existence of a connection with the feed line. It is also important to observe the following conditions with regard to plane antennas defined by angular dimensions: the form of the metal part of the antenna should coincide with that of its slot (additional) part.

It is clear that a plane antenna defined by the angular dimensions can be simultaneously regarded as an electric as well as a magnetic (i.e., "slot") antenna. Let Z_1 be the input resistance of the plane antenna and note that in accordance with the duality principle, an interchange of the metal and "slot" parts of the antenna leads to a change of its input resistance, which becomes equal to Z_2 , this being expressed as (see Paragraph 2-9):

$$Z_2 = \frac{(60\pi)^2}{Z_1}.$$

On condition that the forms of the electric and magnetic parts of the antenna coincide, we get the equality $Z_1 = Z_2$ and the input resistance of such an antenna is equal to $Z_1 = Z_2 = Z_{in} = 60\pi$ ohms on any frequency. In antennas of finite dimensions, this condition regarding the coincidence of forms is, in a sense, equivalent to the concept of the optimum wave impedance of the transmission line formed by the arms of a plane antenna and constitutes an additional guarantee that the latter is multiple-tuned. An example of the fulfilment of this condition is shown in Fig. 10-19.

Fig. 10-20 shows the experimentally investigated construction of a multiple-tuned plane antenna [48], whose arms are bounded by four logarithmic helixes defined by the equations:

$$r_1 = Ae^{a\varphi}, \quad r_2 = Mr_1, \quad r_3 = Ae^{a(\varphi-\pi)}, \quad r_4 = Mr_3.$$

This antenna, which is cut out of a metal sheet of large dimensions, is fed by means of a flexible coaxial cable placed

along one of the arms of the antenna. When the number of windings equals 1.5, the directional diagram of the antenna consists of two wide lobes whose maximums are perpendicular to the plane of the antenna. The radiated field in the main directions has, in the operating frequency range 20 : 1, an elliptical polarisation with a coefficient of ellipticity exceeding 1 : 2.

Owing to the fact that for an antenna of this kind, a change of frequency is equivalent to its rotation in space relatively

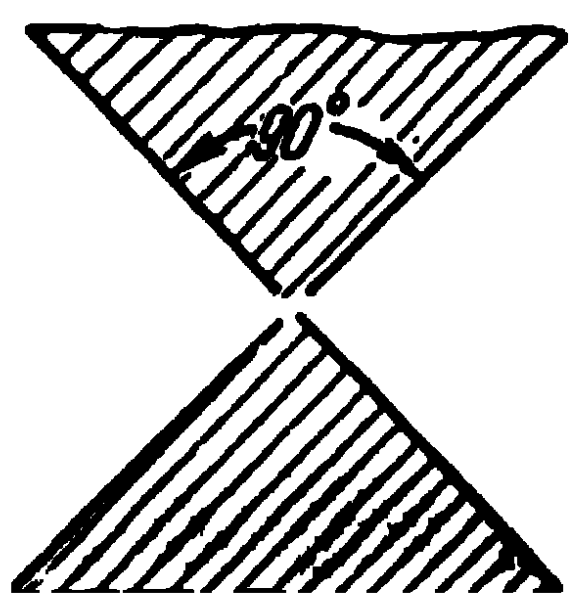


Fig. 10-19. Plane antenna of infinite dimensions.

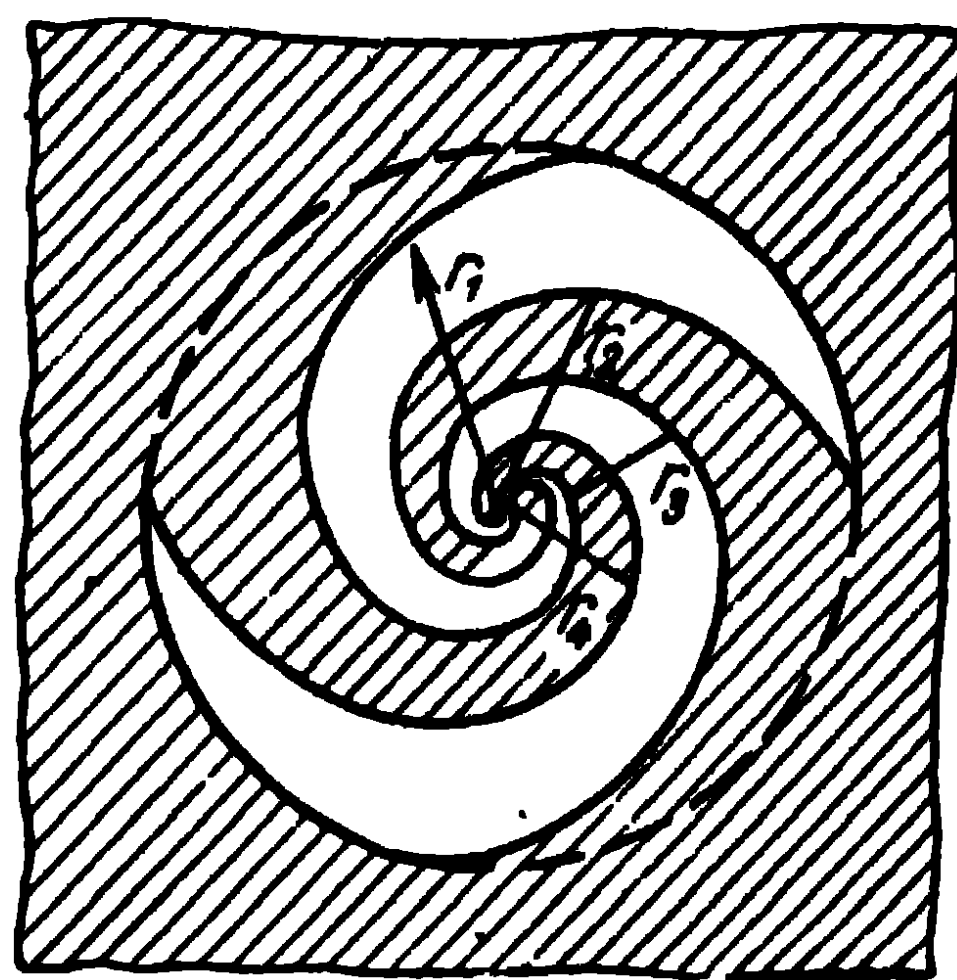


Fig. 10-20. Equiangular helical antenna in a metal sheet of large dimensions.

to the axis perpendicular to the plane of the sheet, the width of the lobes at half-power oscillates periodically from 40 to 50° in the whole of the operating range. The travelling-wave ratio in the feeder with a wave impedance $W_f = 50$ ohms constitutes no less than 50% on all the frequencies of the operating range. A change of the parameters a and M has no significant influence on the multiple-tuning properties of the antenna and leads mainly to a change of the average magnitude of its input resistance. However, the best results are obtained when $a = 0.30$ and $M = 0.62$.

The idea of an automatic cut-off of the radiating current at the spot determined by the frequency of the generator has also been put to use in plane antennas with a "logarithmic periodicity" of the parameters as a function of the frequency [49-50]. The form of such an antenna is shown in Fig. 10-21. The antenna arms consist of peculiar plane structures with alternating depressions and projections. The geometry of the structures is characterised by relative period $\tau = \frac{R_n + 1}{R_n}$,

coefficient of form $\sigma = \frac{r_n}{R_n}$ and angles α and β . In the

structures generally used, the condition $\sigma = \sqrt{\tau}$ is fulfilled. At the origin of the coordinates, the arms of the antenna are divided by a gap to which the exciting voltage is applied. As a feeder, one can utilise a twin-wire symmetrical line, as well as a coaxial cable. In the latter case, as shown in

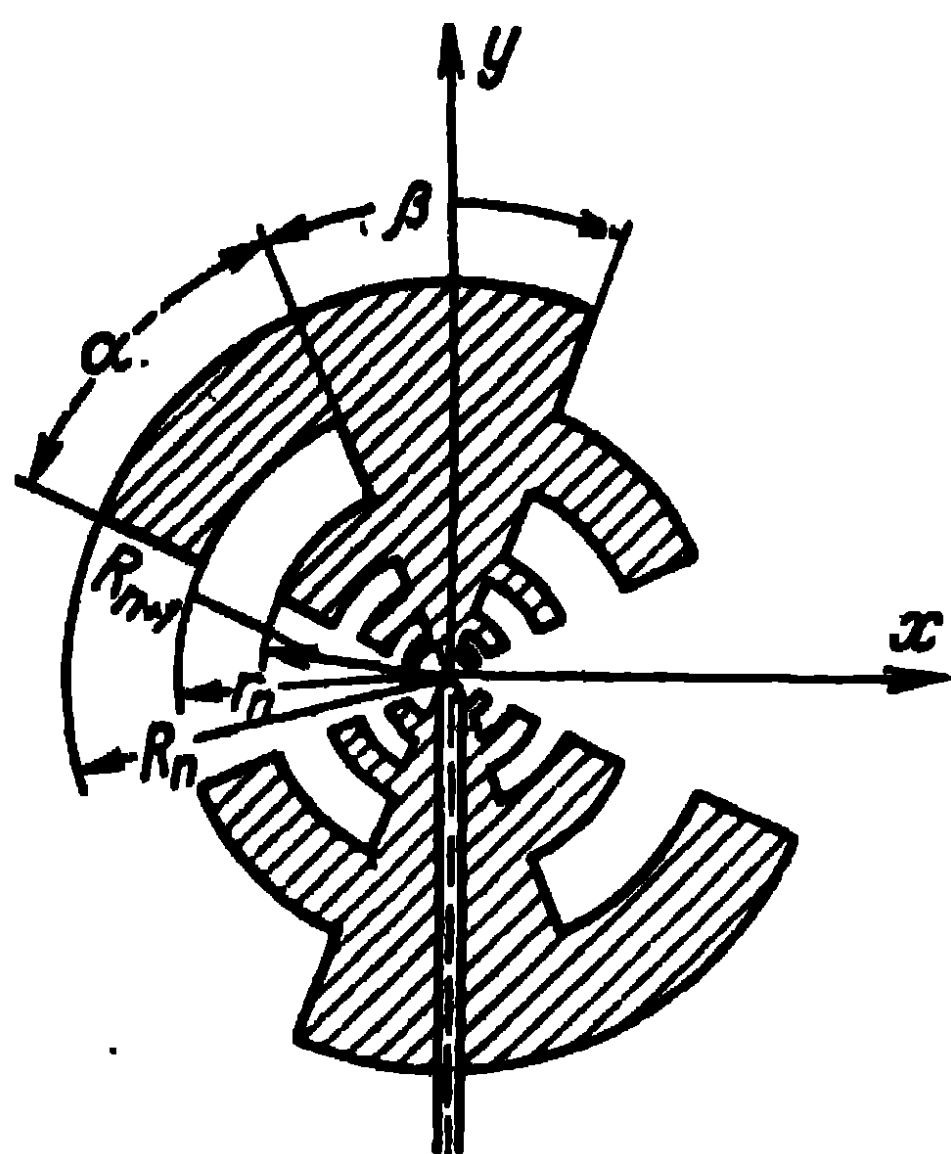


Fig. 10-21. Plane antenna with logarithmic periodicity of parameters as a function of the frequency of the oscillations.

the antenna and is electrically connected with it along its entire length. The inner conductor of the coaxial cable is connected to the beginning of the other arm of the antenna.

It has been experimentally established that the magnitude of the current in the arms of such an antenna increases away from the centre, reaching its maximum at the place where the resonant projections and depressions of approximately quarter-wave-length are located. Beyond these points of resonant inhomogeneities, the magnitude of the current sharply falls by 100 and more times. A decrease of frequency of the radiated

oscillations leads to the successive appearance of the resonances of the inhomogeneities that are more distant from the centre. It is readily seen that the ratio of the two frequencies $f_1 < f_2$ for which the resonances of the neighbouring inhomogeneities occur constitutes exactly the quantity $\tau = f_1/f_2$. Accordingly, the directional diagrams and the antenna input resistance are found to be the periodical function of the logarithm of the oscillation frequency. The change of the antenna characteristics within the limits of one period is not large granted the appropriate choice of the parameters of the structure. The exact repetition of these changes from period to period ensures the satisfactory behaviour of the antenna characteristics within a considerable frequency range. The limits of the operating range are determined by the resonant frequencies of the extreme inhomogeneities (i.e., those that are closest to

and farthest from the centre of the antenna). A magnitude of the operating range of 10 : 1 and more can easily be achieved.

The low dependence of the antenna input resistance on the frequency within the limits of one period can be explained as follows. The resonant projections and depressions on the antenna arms are in fact the electric and magnetic dipoles, the coefficients of the reflection from which are approximately equal in magnitude and opposite in phase. As a result, the reflected waves cancel out at the feed point. The same phenomenon was observed during the investigation of a sleeve-stub dipole (Fig. 10-14) with a raised feed point.

The average value of the antenna input resistance with a logarithmic periodicity of the parameters represented in Fig. 10-21 usually exceeds 100 ohms and depends on the choice of the angles α and β . In the event of the equality $\alpha = \beta = 45^\circ$, the form of the metal part of the antenna coincides with that of its slot part and, in accordance with the expression $Z_1 \cdot Z_2 = (60\pi)^2$, its input resistance should amount to 188 ohms. Measurements made with an experimental model of such an antenna gives a somewhat smaller value (~ 150 ohms). A further decrease of the average value of the input resistance, desirable from the point of view of a better matching of the antenna to the coaxial cables generally used, can be obtained by decreasing the angle β , but this leads to a greater unevenness of the antenna input resistance within the limits of one period.

The directional diagrams of the antenna represent two wide lobes orientated perpendicularly to the plane of the arms. The radiation in the antenna plane is low for all directions. A characteristic feature is that, in the maximum radiation direction, the vector \mathbf{E} is polarised in a direction parallel to the x -axis, the radiation with a polarisation parallel to the y -axis being small. The width of the lobes of the directional diagram depends to a great extent on the relative period of the structure τ . For example, when the parameter τ changes from 0.81 to 0.25 in an antenna in which angles $\alpha = \beta = 45^\circ$, the width of the lobes at half-power from 73° to 38° gradually decreases. When the arms of the antenna shown in Fig. 10-21 are rotated about the x -axis by an angle less than 180° , a unidirectional radiation can be obtained in the direction of the acuteness thus formed. At the present time antennas with a logarithmic periodicity of the parameters are being subjected to intensive

research and improvements. However, they are already used quite extensively as individual antennas, multiple-tuned feeds of parabolic and lens antennas, antennas for radio communications on short waves, etc. [51 and 52].

10-5. Multi-Unit Antennas

In the preceding two paragraphs, we investigated simple antennas of the wire and slot types. We shall now investigate multi-unit antennas of the highly directional as well as non-directional types.

To begin with, let us examine a co-phased antenna consisting of an array of half-wave wire dipoles. The theory of

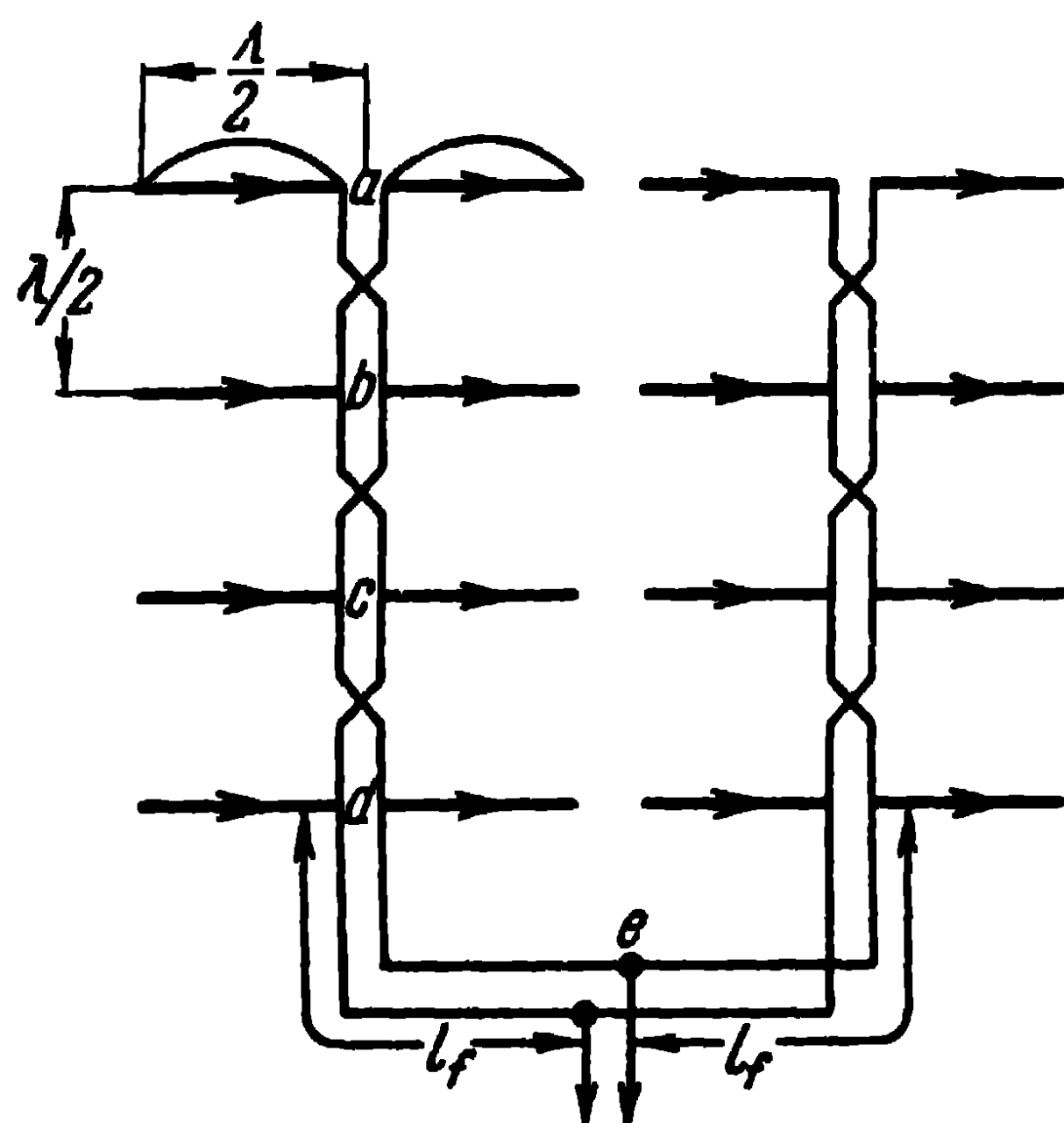


Fig. 10-22. Co-phased antenna.

the co-phased array of dipoles was investigated in Chapter Four. Here we shall investigate the feed circuit of such an antenna, its construction and application.

Fig. 10-22 shows the most commonly used circuit of co-phased feed of an array of dipoles. The half-wave dipoles are arranged in one vertical plane with their centres spaced half a wavelength apart and are connected in pairs to a twin vertical feeder, forming a so-called section. For the

dipoles to be fed in co-phase, the wires of the feeder should intersect between the stages. The two segments shown in Fig. 10-22 are connected by the feeder in parallel. The arrows show the direction of the currents in the dipoles at a fixed instant. The dipoles are taken somewhat shorter than half a wave-length, so that they should be tuned in resonance.

The input resistance of each pair of dipoles can be defined by the approximate expression (2-50):

$$R_a = \frac{W^2}{R_{\Sigma \text{ mean}}} \quad (2-50)$$

where W_w is the wave impedance of each pair of dipoles, which can be defined by (2-43),

$R_{\Sigma \text{ mean}}$, the radiation resistance of each dipole, defined by (4-18) and averaged for all the dipoles of the antenna so as to simplify the calculations.

Because each pair of dipoles is connected to the feeder at a distance of half a wave-length from one another and the length of the feeder l_f , which connects the segments, is usually taken a multiple of half a wave-length, the antenna input resistance is expressed as:

$$R_e = \frac{W_w^2}{2n R_{\Sigma \text{ mean}}},$$

where n is the number of stages in the antenna.

The wave impedance W_w is usually of the order of a few hundreds of ohms and the radiation resistance $R_{\Sigma \text{ mean}}$ of the order of 70 to 80 ohms. Hence, the antenna input resistance R_e , loading the antenna feeder is close to the wave impedance of the feeder and the type of operation obtained in the latter is close to the travelling-wave type, without the use of any tuning elements.

The antenna radiates the maximum of energy in a direction perpendicular to its plane. The directional diagrams of the antenna can be calculated from (4-8) and (4-9).

In order to get rid of reverse radiation and raise the directive gain, a reflector is generally used, placed at a distance of approximately a quarter of a wave-length from the antenna. It can be a tunable system, i.e., exactly like the antenna system shown in Fig. 10-22. In that case, it is made passive and tuned by means of a short-circuited stub connected to the points e of the reflector. In the metre wave range, e.g., for radar purposes, it is convenient to use a reflector consisting of a wire-net, the dimensions of which are not inferior to those of the active antenna system. Such a reflector is aperiodical and requires no tuning. In the decimetre wave range, the reflector can be in the form of a rigid metal plane. This reflector is convenient from the constructional point of view because the active antenna system can be fastened to it.

Fig. 10-23 represents the photograph of a decimetre wave antenna with a solid reflector. The antenna is mounted in an aluminium box, the back wall of which plays the role of

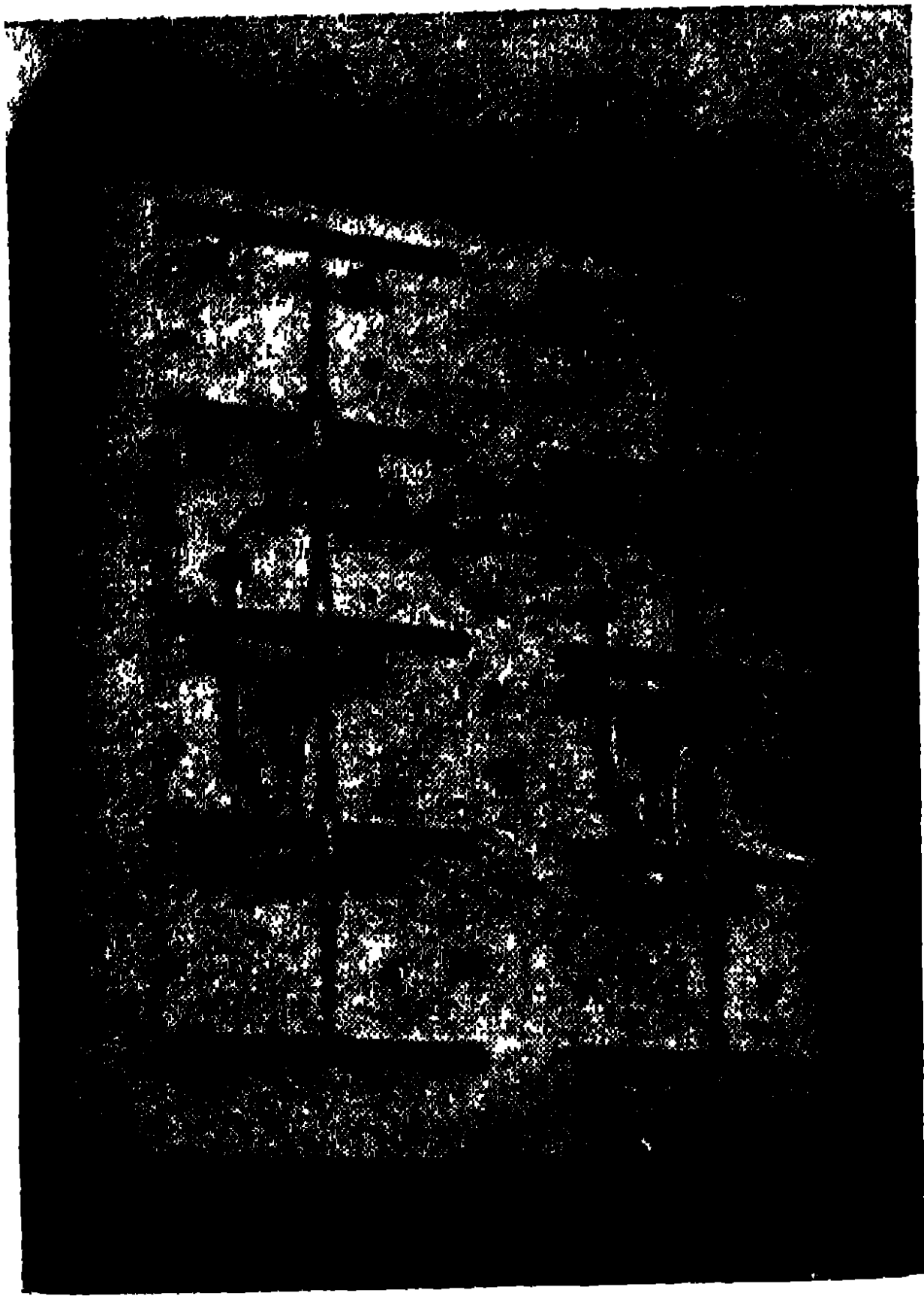


Fig. 10-23. A photograph of the co-phased decimetre wave antenna.

the reflector, the active antenna system being fixed to it by means of quarter-wave metal insulators. The insulators are rods connected to the dipoles at the voltage nodes. In order to widen the antenna pass-band, the dipoles are made with a low wave impedance in the shape of laths 17-17.5 cm long and 5-6 cm wide. The antenna has five stages and two sections. The sections are formed by means of a twin feeder and connected with one another by a single wire tubular line placed above the screen (the second wire of the line is its mirror

image in the screen). The transition from the single to the twin feeder is effected by means of a single-wire U-elbow, connected to the sections in their middle. The single-wire line is fed by a coaxial cable the coating of which is connected to the screen. The type of operation established in the cable is close to the travelling-wave type in the whole band of the operating frequencies ($K > 0.7$). The coaxial cable has a wave impedance of 70 ohms and its attenuation equals 1.9 db per 1 km on the 50 cm wave. The antenna is placed on special supports and is protected from weathering by a thin radiotransparent lid.

Among the non-directional multi-unit antennas, mention should be made of the turnstile antenna utilised in telecasting stations. Television antennas must satisfy specific requirements.

First of all, the antennas should radiate uniformly in all directions in the horizontal plane since television transmitters are usually situated in the centre of the region which they serve. In the vertical plane, the directivity should be sufficiently large in order that the radiation

should be concentrated in the horizontal plane. Moreover, the antenna should radiate electromagnetic energy with a horizontal E -field polarisation, due to the fact that the sources of interference on ultrashort waves are industrial installations of all kinds which radiate an electromagnetic field mainly with a vertical polarisation.

An important requirement is that concerning the pass-band of the antenna system. The antenna together with the feeder should possess a sufficiently wide pass-band in order to avoid distortions of the transmitted image. Furthermore, the antenna-feeder system should be free from feeder echo, which gives rise to a ghost image. The echo will be insignificant if the wave reflection from the antenna is negligibly small in the entire pass-band.

The antenna should also be reliable from the mechanical point of view because it has to be placed on very high supports where it is exposed to high winds and quite often to icing. It should also be lightning-proof, this being achieved through the direct grounding of the antenna elements.

In order to obtain a radiation with a horizontal polarisation, uniform in all directions in a horizontal plane, use is made of the cross-shaped elements described in Paragraph 1-7, which radiates a rotating field. Such elements, which, in the simplest case, consist of half-wave dipoles, are placed horizontally in several stages spaced $\lambda/2$ apart and fed in co-phase (Fig. 10-24). In the case of an even number of elements, the radiation in the direction of the axis of the system (up and down) is zero and the maximum of radiation occurs in the horizontal plane. The dipoles situated in one vertical plane are fed by one feeder and those situated in the other vertical plane are fed by another feeder. The feeders are tuned on a travelling wave and connected in parallel; moreover, one feeder is a quarter of a wave-length longer than the other, thus ensuring a 90° phase shift of the currents in the dipoles of the cross. The antenna circuit, usually called a turnstile antenna, is shown in Fig. 10-25.

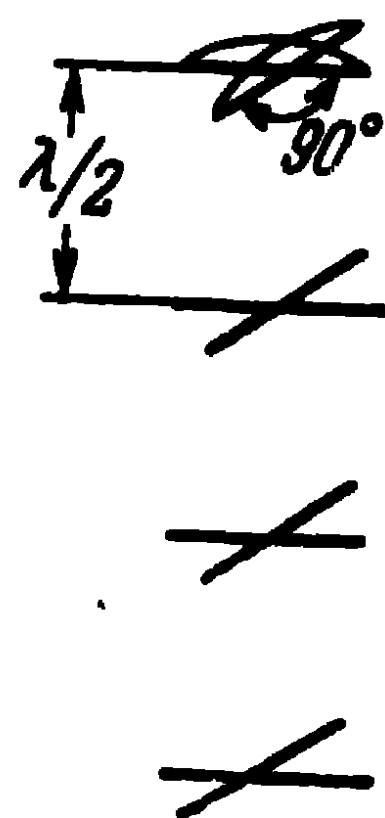


Fig. 10-24. Arrangement of cross-shaped elements in television antenna.

In order to reduce the reflection from the antenna in the transmission band to a negligibly low level, the dipoles should have a wide pass-band, i.e., their input resistance in the frequency band should change but insignificantly.

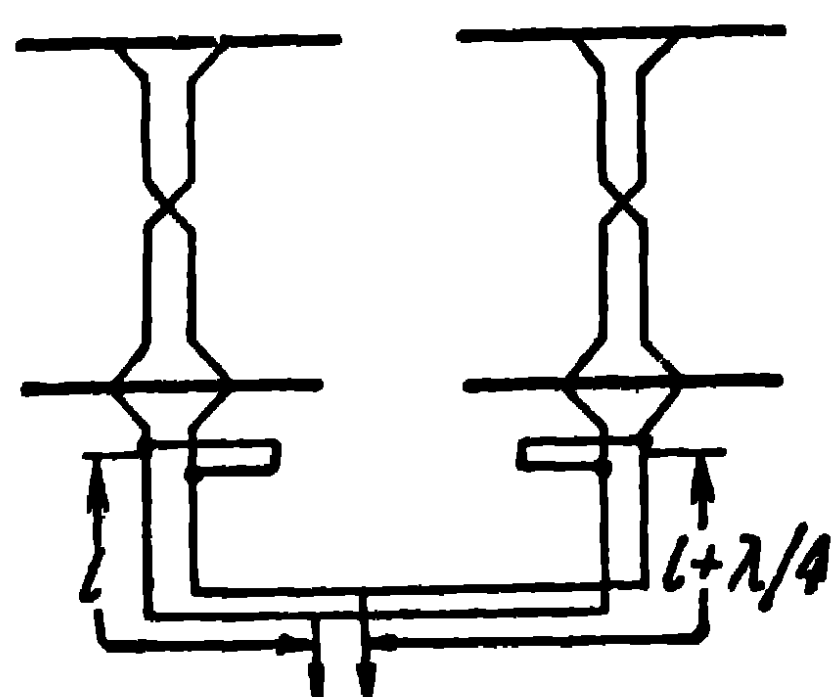


Fig. 10-25. Feed circuit of turnstile antenna.

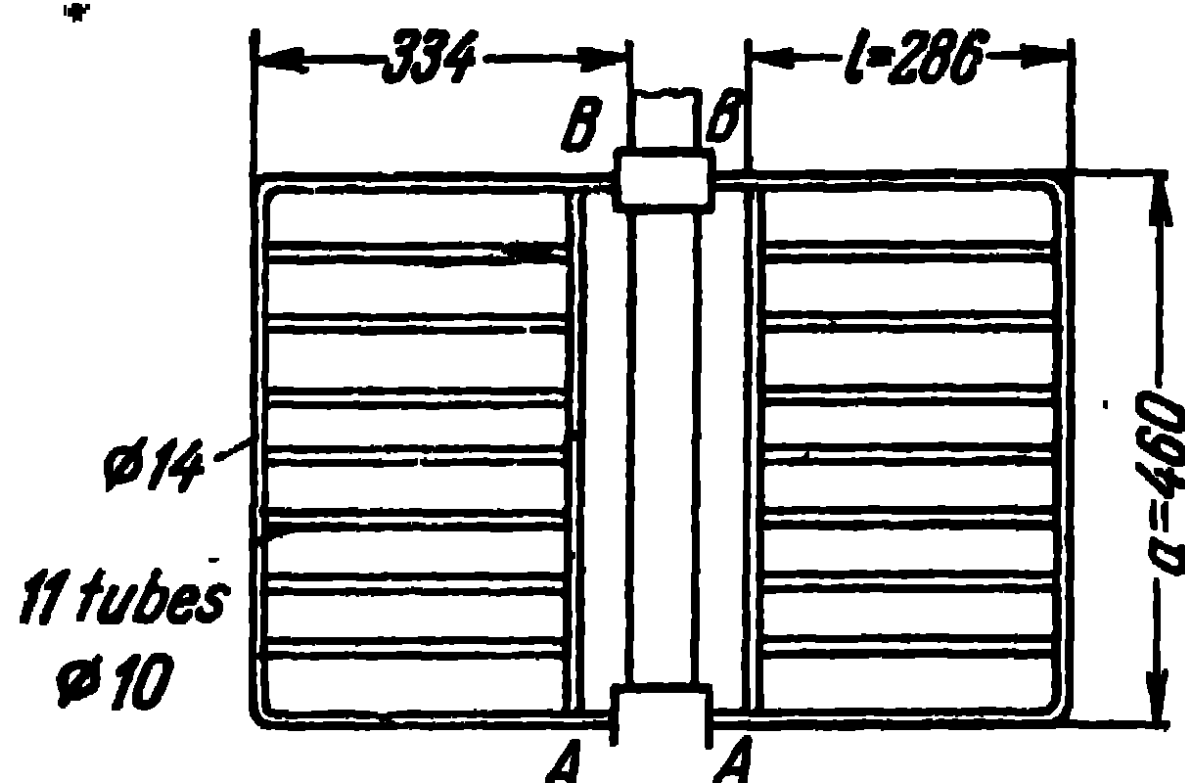


Fig. 10-26. Plane Braude antenna.

The plane dipole described in Paragraph 10-3 is of this type. In order to reduce the resistance to wind and strengthen the dipole, it is made of several tubes. A dipole of this kind is shown in Fig. 10-26. The antenna system consists of 11 tubes 10 mm in diameter; its dimensions for

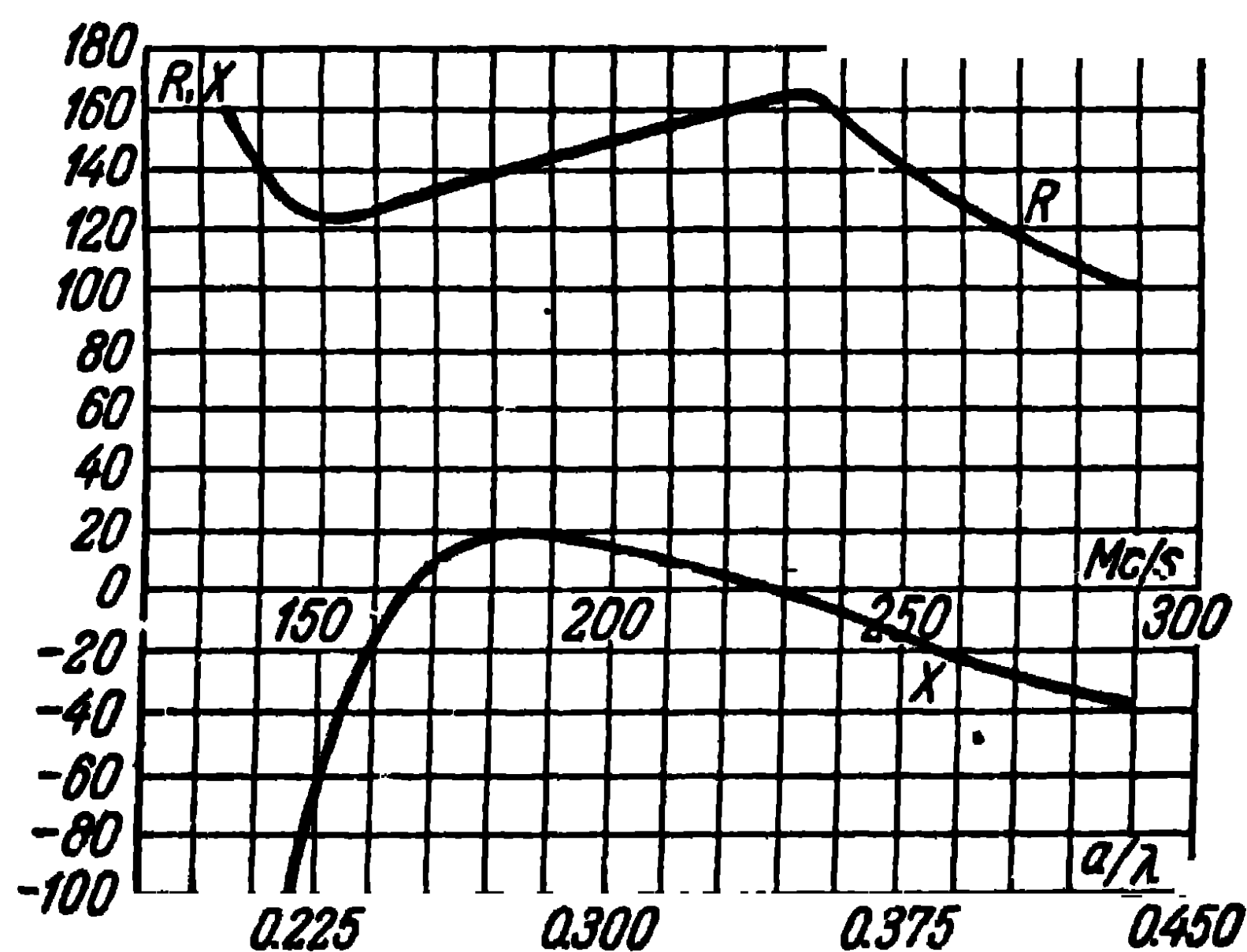


Fig. 10-27. Input resistance of a plane antenna.

operating in a 155 to 180 Mc/s frequency band are: $a=460$ mm and $l=286$ mm. The dipole is short-circuited to the support at the points BB and insulated from it at the points AA .

Fig. 10-27 shows the experimental curves of the antenna input resistance. It is seen that, in the 155-180 Mc/s frequency

band, it is almost constant and equal to 140 ohms. Hence, it is found convenient to feed this antenna by means of a coaxial cable with a wave resistance of the order of 70 ohms. Two such antennas arranged crosswise and fed with a 90° phase displacement form a turnstile element. The antenna is light, so that it can be of the stacked type. In the case of three turnstile elements spaced $\lambda/2$ apart, the directive gain of the antenna equals 3.2.

A plane antenna of this kind has been devised by the American firm RCA [53]. An element of this antenna is shown in Fig. 10-28. It is short-circuited to the pole at the points BB as well as AA and fed in the middle at the points CC . Its input resistance in a wide frequency band is of the order of 150 ohms.

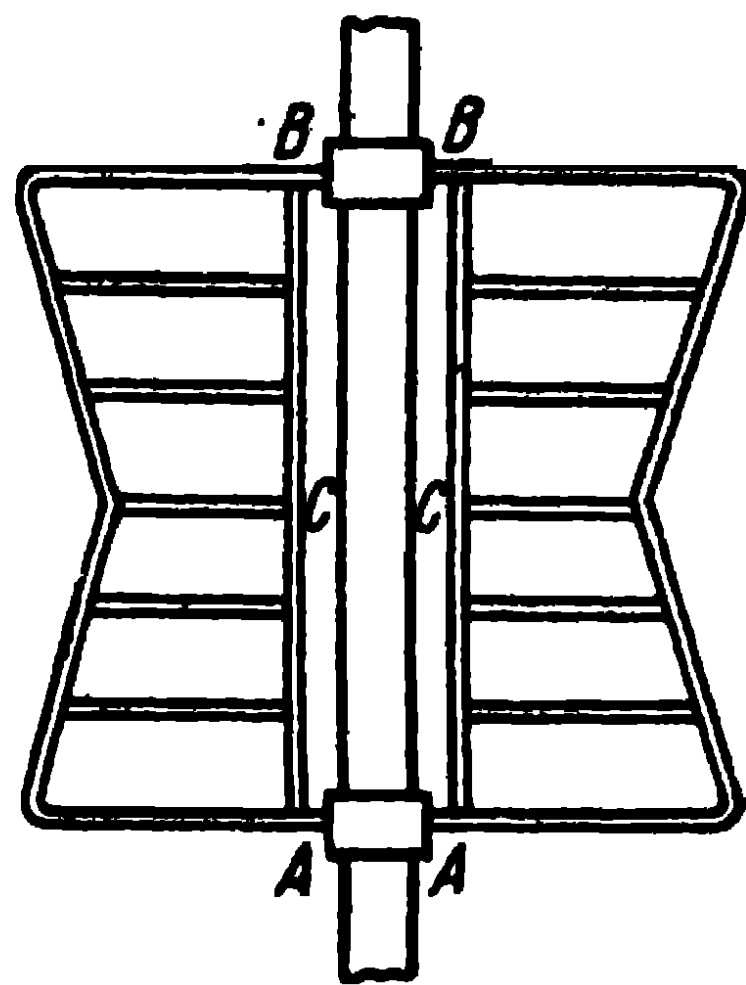


Fig. 10-28. RCA plane television antenna.

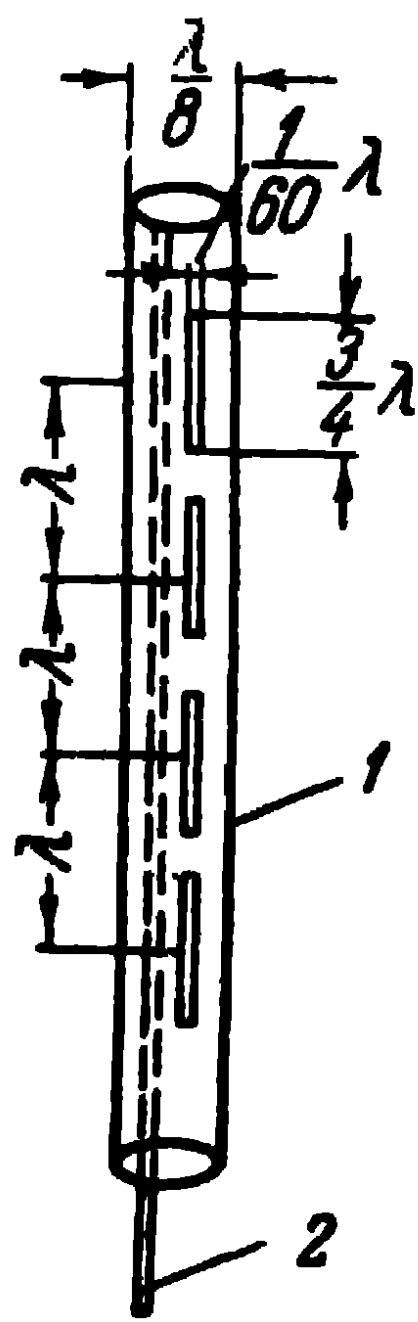


Fig. 10-29.
Cylindrical
slot antenna:
1—slot; 2—cable

Now, let us examine the multislot antenna disposed on a circular vertical tube and shown in Fig. 10-29. It consists of four longitudinal slots milled in a tube $\lambda/8$ in diameter spaced at a distance λ apart. The slots are $3/4\lambda$ long each and are fed by a coaxial cable.

In this case, the length of the slot, equal to $3/4\lambda$, is found to be resonant due to the fact that the slot is shunted by the inner cavity of the tube, which, owing to the relatively small diameter of the tube with respect to the wave-length, represents an inductive resistance. In order that the resultant input resistance of the slot should be purely active, the natural (external) resistance of the slot should be of a capacitive nature. This, as we know, occurs for a length of the slot higher than $\lambda/2$. The increase of the resonant length of the slot can also be explained in a somewhat

different way. Let there be a twin line in free space. Then, its wave has a phase velocity equal to that of light. If this line is shunted with inductances, the phase velocity

of the wave in the line increases, and all the more so as the shunting inductances are smaller. An increase of the number of shunts eventually leads to the formation of a tube with a longitudinal slot.

The antenna radiates a horizontal polarised field and its directional diagram in the horizontal plane has a low directivity (Fig. 5-15). In the vertical plane, the antenna is highly directive. Such an antenna is useful for broadcasting on ultrashort waves.

10-6. Slot Waveguide Antennas

In the centimetre wave range, wide use is made of slot waveguide antennas. They are mainly utilised in radar systems. The slots are usually cut in the broad wall of a rectangular waveguide and an H_{01} mode used for their excitation. The slots are made resonant, i.e., of a length equal to approximately half a wave-length and disposed in such a way that their excitation should be in co-phase. In this way, they form a co-phased array and radiate maximum energy in a direction perpendicular to the plane of the waveguide.

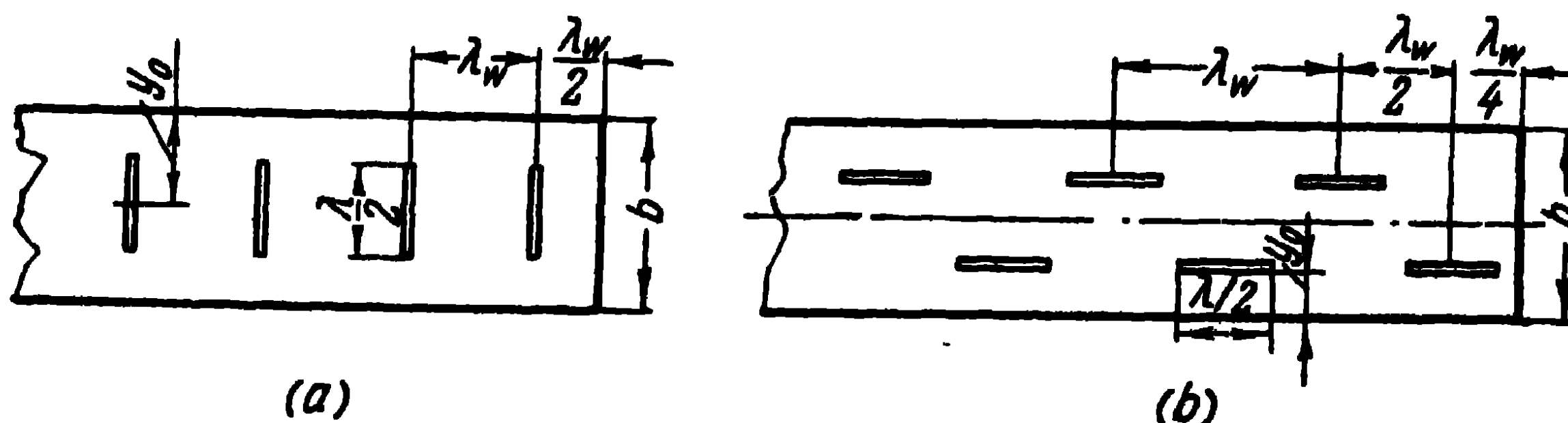


Fig. 10-30. Resonant slot waveguide antenna:
a—antenna with transverse slots; *b*—antenna with longitudinal slots.

Fig. 10-30, *a* represents a slot waveguide antenna consisting of transverse slots in a waveguide spaced one wave-length apart. Fig. 10-30, *b* represents a slot waveguide antenna consisting of longitudinal slots arranged in staggered rows on both sides of the waveguide axis and spaced half a wave-length apart in the waveguide. The end of the waveguide is short-circuited by a plunger, the last transverse

and longitudinal slots lying at distances of $\lambda_w/2$ and $\lambda_w/4$ respectively from the plunger.

Due to the presence of the short-circuiting plungers, the waveguide has a standing wave type of operation and the antennas are therefore known as resonant slot antennas.

Let us dwell in greater detail on the question of the excitation of the slots. As we know from expressions (7-16) and (7-17), in the absence of slots, the field of the H_{01} wave in a waveguide short-circuited at one end is expressed as:

$$\left. \begin{aligned} E_{x_{01}} &= C \frac{k^2}{i\omega\epsilon} \sin\left(\frac{\pi}{b} y\right) \sin(\alpha_{01} z); \\ H_{y_{01}} &= C \alpha_{01} \sin\left(\frac{\pi}{b} y\right) \cos(\alpha_{01} z); \\ H_{z_{01}} &= -C \frac{\pi}{b} \cos\left(\frac{\pi}{b} y\right) \sin(\alpha_{01} z), \end{aligned} \right\} \quad (10-6)$$

where C is a constant quantity, independent of the coordinates

$$\alpha_{01} = k \sqrt{1 - (\lambda/2b)^2}.$$

It is seen from the expressions (10-6) that the transverse slots are situated at the points $z_0 = \frac{1}{2} \lambda_w, 1 \frac{1}{2} \lambda_w, 2 \frac{1}{2} \lambda_w, \dots$, i.e., in the antinodes of the transverse component of the magnetic field intensity, the longitudinal slots being disposed at the points $z_0 = \frac{1}{4} \lambda_w, 1 \frac{1}{4} \lambda_w, 2 \frac{1}{4} \lambda_w, \dots$ when $y < \frac{b}{2}$ and at the points $z_0 = \frac{3}{4} \lambda_w, 1 \frac{3}{4} \lambda_w, 2 \frac{3}{4} \lambda_w, \dots$ when $y > \frac{b}{2}$, i.e., at the antinodes of the longitudinal component of the magnetic field intensity. At the points indicated, the fields are of equal magnitude and phase, so that the slots are excited in co-phase and with equal amplitudes.

The intensity of excitation of the slots depends on their location relatively to the waveguide axis. Thus, if the longitudinal slots are disposed in the middle of the broad wall of the waveguide ($y_0 = \frac{b}{2}$), $H_{z_{01}} = 0$ and the slots are not excited. The maximum excitation of the longitudinal slots occurs when $y_0 = 0$ and $y_0 = b$, in particular when they

are situated on the lateral walls of the waveguide, and the maximum excitation of the transverse slots occurs when $y_0 = \frac{b}{2}$. In other words, the most intense excitation of the slots occurs at those points of the waveguide at which the components of the surface electric currents, which intersect the slots, have their maximum value.

Let us now turn our attention to the fact that the slots in the waveguide can be regarded as receiving elements. They receive energy propagated along the waveguide of the H_{01} wave. Part of the received energy is radiated by them into the surrounding space and the other part (in the absence of losses) is radiated into the inner space.

Considering a slot waveguide antenna from this point of view, let us, for simplicity, imagine an infinitely long waveguide with one single half-wave transverse or longitudinal slot. Let this slot be excited by an H_{01} wave propagated in the z -direction. The electromagnetic field of the wave is written as:

$$\left. \begin{aligned} E_{x01}^{inc} &= B \sin \left(\frac{\pi}{b} y \right) e^{-i\alpha_{01}z}; \\ H_{y01}^{inc} &= B \frac{\alpha_{01}}{\omega\mu} \sin \left(\frac{\pi}{b} y \right) e^{-i\alpha_{01}z}; \\ H_{z01}^{inc} &= B \frac{\pi/b}{i\omega\mu} \cos \left(\frac{\pi}{b} y \right) e^{-i\alpha_{01}z}. \end{aligned} \right\} \quad (10-7)$$

Regarding the slot as a magnetic receiving dipole, we can find the magnitude of the magnetic current induced in it, in a way similar to that which was adopted when investigating the receiving electric dipole in Chapter Six. i.e., from the expression

$$I^M = \frac{M}{G_{\Sigma} + G}, \quad (10-8)$$

where M is the equivalent mmf induced in the slot;

G_{Σ} , the external conductivity of the slot radiation;

G , the internal conductivity of the slot radiation.

For a transverse slot (Fig. 10-31), the mmf is expressed as:

$$M = \int_{y=y_0-\lambda/4}^{y=y_0+\lambda/4} H_{y01}^{inc} \cos k(y_0 - y) dy.$$

Substituting here the expression $H_{y_{01}}$ from (10-7), performing the integration and substituting into (10-8), we obtain the expression of the voltage (of the magnetic current) applied in the centre of the slot in the following form:

$$I_{y_0}^M = \frac{1}{G_\Sigma + G} \frac{2k}{\omega \mu \alpha_{01}} B \cos\left(\frac{\pi}{b} \frac{\lambda}{4}\right) \sin\left(\frac{\pi}{b} y_0\right) e^{-i\alpha_{01} z_0}. \quad (10-9)$$

The reverse radiation of the slot into the waveguide (field reflected from the slot) can be defined from (7-28). The electric field in the region $z < z_0$ is expressed as:

$$E_{x_{01}}^0 = \frac{2k I_{y_0}^M}{ab \alpha_{01}^2} \cos\left(\frac{\pi}{b} \frac{\lambda}{4}\right) \sin\left(\frac{\pi}{b} y_0\right) \sin\left(\frac{\pi}{b} y\right) e^{+i\alpha_{01} (z - z_0)}.$$

Substituting here the expression $I_{y_0}^M$ from (10-9) and dividing by the expression $E_{x_{01}}^{\text{inc}}$ for the incident field, we obtain the expression for the reflection coefficient of the wave from the slot:

$$\rho = \frac{E_{x_{01}}^0}{E_{x_{01}}^{\text{inc}}} = \frac{1}{G_\Sigma + G} \frac{4k^2}{\omega \mu ab \alpha_{01}^3} \cos^2\left(\frac{\pi}{b} \frac{\lambda}{4}\right) \times \\ \times \sin^2\left(\frac{\pi}{b} y_0\right) e^{+i\alpha_{01} 2(z - z_0)}.$$

If we assume here that $z = z_0$ and take into account that the internal radiation conductivity of the half-wave transverse slot is expressed as (see Paragraph 7-2):

$$G = \frac{4k^2}{\omega \mu ab \alpha_{01}^3} \cos^2\left(\frac{\pi}{b} \frac{\lambda}{4}\right) \sin^2\left(\frac{\pi}{b} y_0\right), \quad (7-30)$$

the expression for the reflection coefficient will be:

$$\rho_0 = \frac{G}{G_\Sigma + G}. \quad (10-10)$$

If we now reduce H_{01} waveguide to the equivalent twin line and take account of the fact that the transverse resonant slot in this line will be represented by a series resistance, the coefficient of the reflection of the wave from this resistance will be expressed as:

$$\rho_0 = \frac{r'}{2 + r'}, \quad (10-11)$$

where r' is the relative (normalised) resistance

$$\left(r' = \frac{r}{W}\right).$$

From a comparison of (10-10) with (10-11), we obtain for the relative resistance the expression

$$r' = \frac{2G}{G_{\Sigma}}. \quad (10-12)$$

The external conductivity of the slot radiation in the waveguide G_{Σ} can be approximately defined from the expression $G = \frac{2R_{\Sigma}}{W^2}$ where $R_{\Sigma} = 73.1$ ohms and $W = 377$ ohms. Substituting this expression as well as the expression G

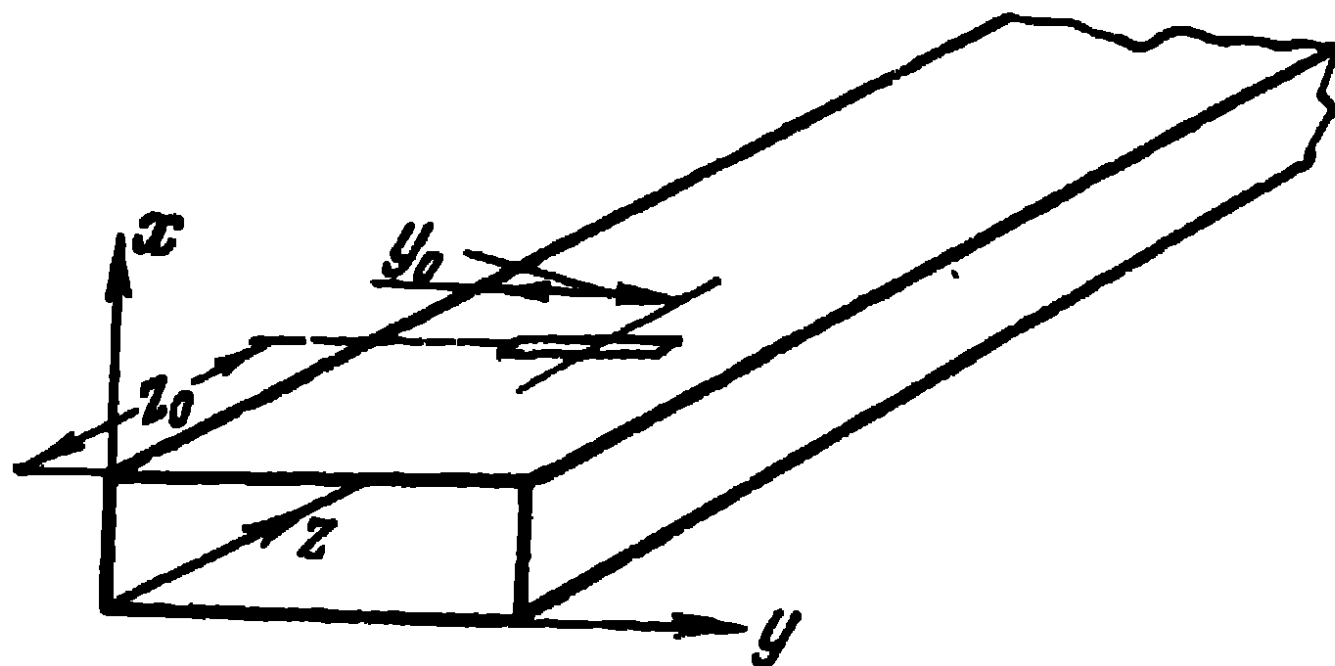


Fig. 10-31. Calculation of the reaction of the transverse slot.

from (7-30) into (10-12), we obtain the well-known expression [54]

$$r' = 0,523 \left(\frac{\lambda_w}{\lambda}\right)^3 \frac{\lambda^2}{ab} \cos^2\left(\frac{\pi\lambda}{4b}\right) \sin^2\left(\frac{\pi}{b} y_0\right). \quad (10-13)$$

Thus, the slot antenna represented in Fig. 10-30, *a*, can be reduced to an equivalent loaded twin line (Fig. 10-32). In order that a travelling-wave type of operation should be established in that line (at its input), it is evidently necessary that the condition $r'n = 1$, where n is the number of slots in the antenna, should be fulfilled.

For a longitudinal slot in an infinite waveguide (Fig. 10-33), the mmf is expressed as:

$$M = \int_{z = z_0 - \frac{\lambda}{4}}^{z = z_0 + \frac{\lambda}{4}} H_{z01}^{inc} \cos k(z - z_0) dz.$$

Substituting here the expression $H_{z_{01}}^{inc}$ from (10-7), integrating and substituting the expression thus obtained into (10-8), we obtain:

$$I_{z_0}^M = \frac{1}{G_\Sigma + G} \frac{2k \frac{b}{\pi}}{i\omega\mu} B \cos\left(\alpha_{01} \frac{\lambda}{4}\right) \cos\left(\frac{\pi}{b} y_0\right) e^{-i\alpha_{01} z_0}. \quad (10-14)$$

In accordance with the expressions (7-39), the reverse radiation of the slot into the waveguide (reflected field) is:

$$E_{x_{01}}^0 = \frac{2k I_{z_0}^M}{a\pi i \alpha_{01}} \cos\left(\alpha_{01} \frac{\lambda}{4}\right) \cos\left(\frac{\pi}{b} y_0\right) \sin\left(\frac{\pi}{b} y\right) e^{-i\alpha_{01} (z_0 - z)}.$$

Substituting here (10-14) and dividing by the field of the incident wave $E_{x_{01}}^{inc}$, we obtain for the coefficient of

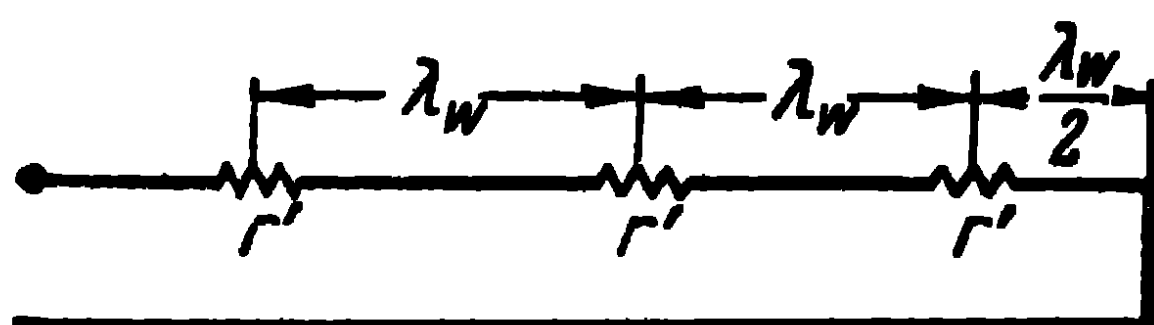


Fig. 10-32. Equivalent loaded line.

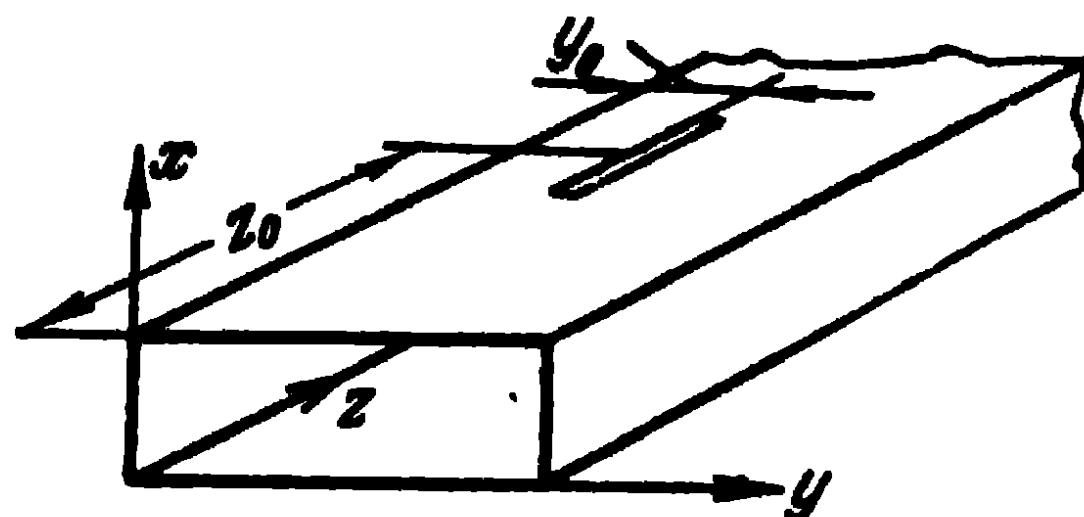


Fig. 10-33. To the calculation of the reaction of a longitudinal slot.

reflection the expression

$$\rho = - \frac{1}{G_\Sigma + G} \frac{4k^2 b}{a\pi^2 \omega \mu \alpha_{01}} \cos^2\left(\alpha_{01} \frac{\lambda}{4}\right) \times \\ \times \cos^2\left(\frac{\pi}{b} y_0\right) e^{+i\alpha_{01} z (z - z_0)}. \quad (10-15)$$

Assuming here that $z = z_0$ and taking into account that the internal conductivity of a longitudinal half-wave slot in an infinite waveguide is expressed as (see Paragraph 7-2):

$$G = \frac{4k^2 b}{a\pi^2 \omega \mu \alpha_{01}} \cos^2\left(\alpha_{01} \frac{\lambda}{4}\right) \cos^2\left(\frac{\pi}{b} y_0\right) \quad (7-40)$$

we obtain:

$$\rho_0 = - \frac{G}{G_\Sigma + G}. \quad (10-16)$$

If we now reduce the waveguide to the equivalent twin line and take into account that the longitudinal slots in that line will be represented by shunting resistances, the

coefficient of reflection in the line will be expressed as:

$$\rho_0 = -\frac{g'}{2+g'}, \quad (10-17)$$

where g' is the relative conductivity ($g' = gW$). From a comparison of (10-16) with (10-17), we obtain:

$$g' = \frac{2G}{G_\Sigma}. \quad (10-18)$$

The radiation conductivity of the slot G_Σ can be approximately expressed as $G_\Sigma = \frac{2R_\Sigma}{W^2}$. Substituting this value, as well as the value G from (7-40), into (10-18), we obtain:

$$g' = 2.09 \frac{b}{a} \frac{\lambda_w}{\lambda} \cos^2 \left(\alpha_0, \frac{\lambda}{4} \right) \cos^2 \left(\frac{\pi}{b} y_0 \right). \quad (10-19)$$

Thus, the slot antenna represented in Fig. 10-30, *b*, can be reduced to the equivalent loaded twin line (Fig. 10-34). In order that a travelling-wave type of operation should be established in that line (at its input), the condition $g'n=1$, where n is the number of slots in the antenna, should evidently be satisfied.

Let us now calculate the directional diagrams of resonant slot waveguide antennas. The problem of the calculation of the directional diagrams of such a system has not been solved. However, for engineering purposes, one can make use of the duality principle. In particular, this concerns the longitudinal plane of the antenna, in which the dimensions of the antenna are large in comparison with the wavelength and the approximate expressions for this plane are well in agreement with experiments. The antenna directional diagram consisting of transverse slots can, in the longitudinal plane, be calculated from the expression (4-8) concerning a co-phased array of electric dipoles,

$$F(\alpha) = \frac{1}{n} \frac{\sin \left(\frac{nk d_1}{2} \sin \alpha \right)}{\sin \left(\frac{k d_1}{2} \sin \alpha \right)}, \quad (4-8)$$

where, in this case, $d_1 = \lambda_w$.

Of course, this expression characterises the radiation of the antenna in the half-space containing the slots and does not define the radiation in the shadow region.

To calculate the directional diagram in the longitudinal plane of the antenna consisting of longitudinal slots, the expression (4-9) is used

$$F(\beta) = \frac{1}{m} \frac{\cos\left(\frac{\pi}{2} \sin \beta\right)}{\cos \beta} \frac{\sin\left(\frac{mkd_2}{2} \sin \beta\right)}{\sin\left(\frac{kd_2}{2} \sin \beta\right)}, \quad (4-9)$$

where, in this case, $d_2 = \lambda_w/2$.

This expression is likewise not valid for the field in the shadow region of the antenna.

Note that the level of the side lobes in the case of an antenna with transverse slots is considerably larger than in the case of an antenna with longitudinal slots. This is due to the large distance (equal to λ_w) between the transverse slots.

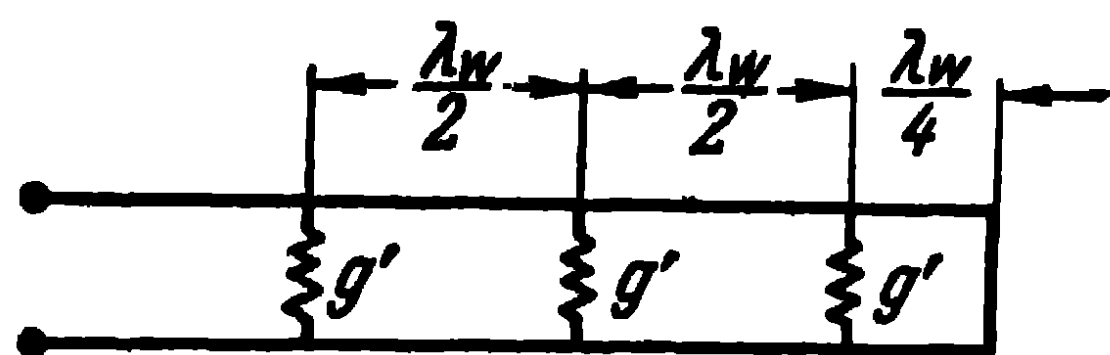


Fig. 10-34. Equivalent loaded line.

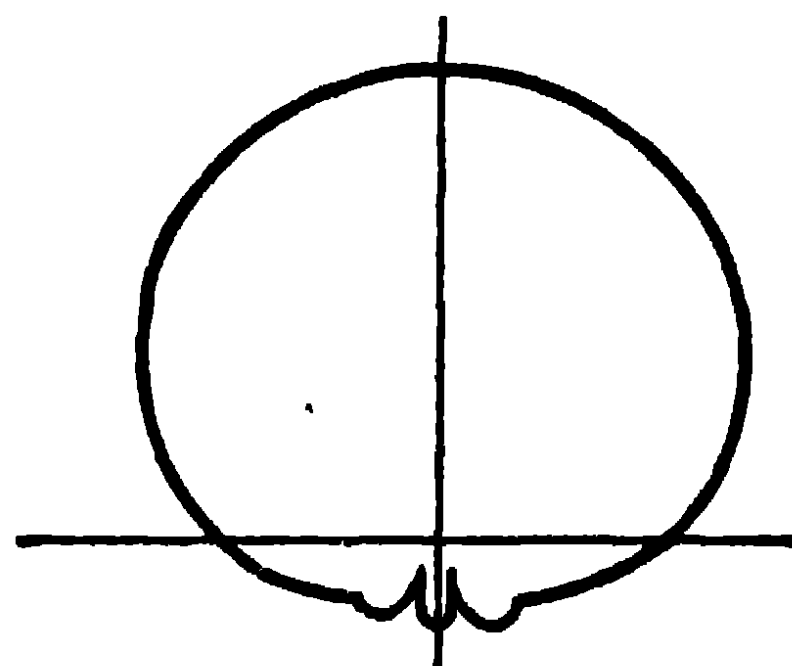


Fig. 10-35. Directional diagram of slot antenna in transverse plane.

As regards the directional diagrams in the antenna transverse plane, in the case of an antenna with transverse slots, the expressions obtained in accordance with the duality principle produce results which are still satisfactory. But the results are unsatisfactory when the duality principle is used for antennas with longitudinal slots. The diagrams calculated from the expressions obtained for elliptical cylinders agree more satisfactorily. Thus, Fig. 10-35 gives the directional diagram of the antenna shown in Fig. 10-30, *b*, in the transverse plane. In this calculation, the rectangular waveguide with the dimensions $b=47.8$ mm and $a=16$ mm was replaced by an elliptical cylinder of eccentricity $e=0.9$ [55].

Apart from resonant antennas, non-resonant slot waveguide antennas are also used; they differ from the former in that the waveguide is loaded at its end on an absorbing resistance

in such a way that a travelling wave is set up when there are no slots in the waveguide. The slots can be spaced at a distance $d = \lambda_w/2$ apart in the case of longitudinal slots and $d = \lambda_w$ in the case of transverse ones, whereupon they are excited in phase with the same amplitudes. The directional diagrams are then calculated by means of the expressions mentioned above, in particular the expressions (4-8) and (4-9).

Usually, the slots are spaced at distances which differ somewhat from $\lambda_w/2$ and λ_w . They are then excited with a

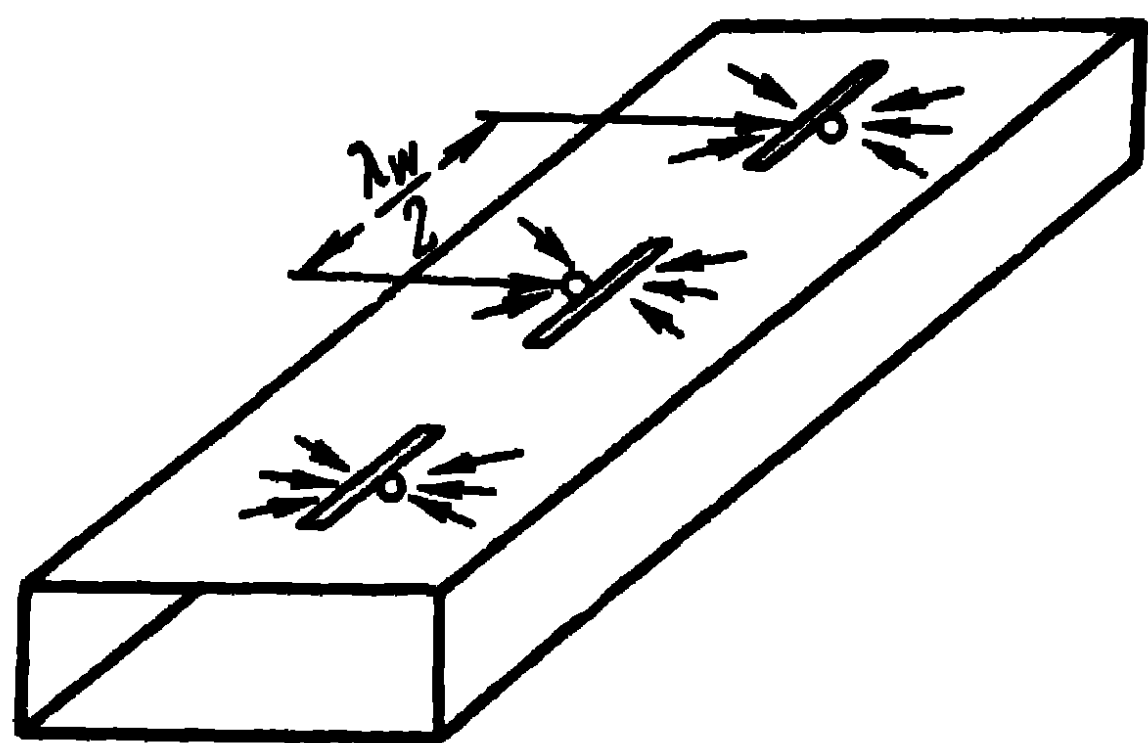


Fig. 10-36. Excitation of slots by reactive stubs.

certain phase shift and the maximum radiation is inclined at a certain angle to the axis of the waveguide in the direction of propagation of the wave. Moreover, the angle of inclination of the maximum radiation can be controlled by changing the frequency of the oscillations or of the critical wave-length in the wave-

guide. The necessary distribution of the amplitude and phase of the field in the slots can be specially chosen, for example, through an appropriate displacement of the slots away from the middle line of the broad wall of the waveguide.

Slot waveguide antennas can also be obtained by disposing the slots on the narrow wall of the waveguide. Of course, transverse slots on the narrow wall of the waveguide will not radiate, since they are situated along the lines of electric current.

Fig. 10-36 represents a slot waveguide antenna in which the slots are disposed in the middle of the broad wall of the waveguide and excited by means of reactive stubs. The stubs are inserted into the waveguide on both sides of the slots and arranged along the lines of the electric field of the H_{01} wave. The electric current excited by the H_{01} wave in these stubs spreads along the wall of the waveguide, crosses the slots and thereby excites them. The neighbouring stubs are excited by the H_{01} wave in antiphase and since they are situated on both sides of the slots, the latter are all excited in phase. The advantage of the excitation by

means of reactive stubs consists in the fact that the intensity of excitation of the individual slots can be regulated by changing the depth of insertion of the stubs.

10-7. Director Antennas

Director antennas or antennas of the waveguide channel type, often called after the name of their inventor Yagi [56], consist of wire half-wave dipoles arranged in parallel in one plane (Fig. 10-37). One of them is an active dipole and the rest are passive; one of the passive dipoles, situated behind the active one, plays the role of a reflector and the other dipoles, situated in front of the active dipole, play the role of directors.

We know from the theory of coupled dipoles that for a passive dipole to act as a reflector, its reactive resistance

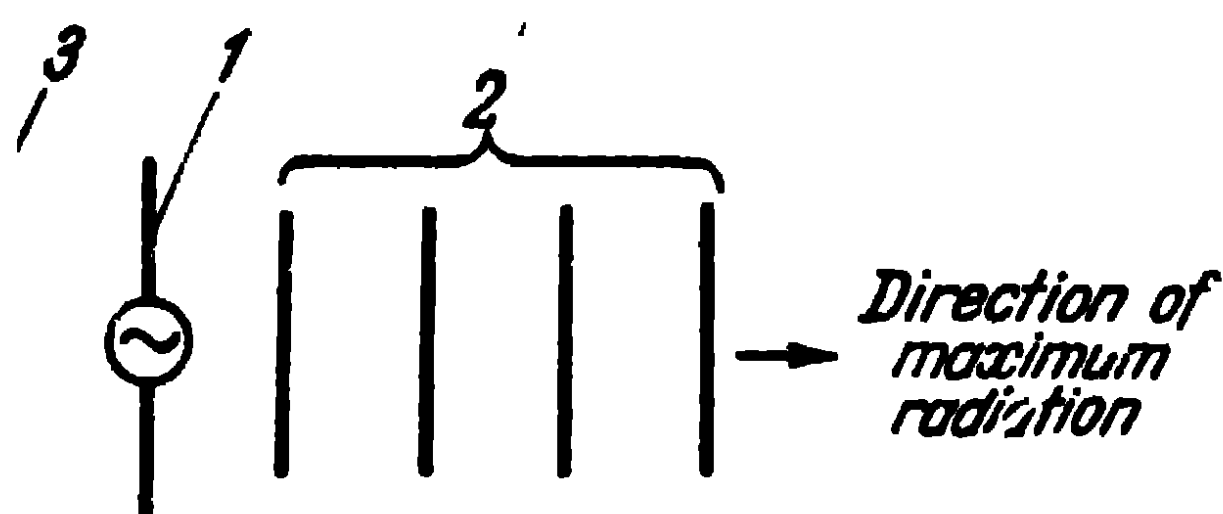


Fig. 10-37. Director antenna:
1—active dipole; 2—directors; 3—reflector.

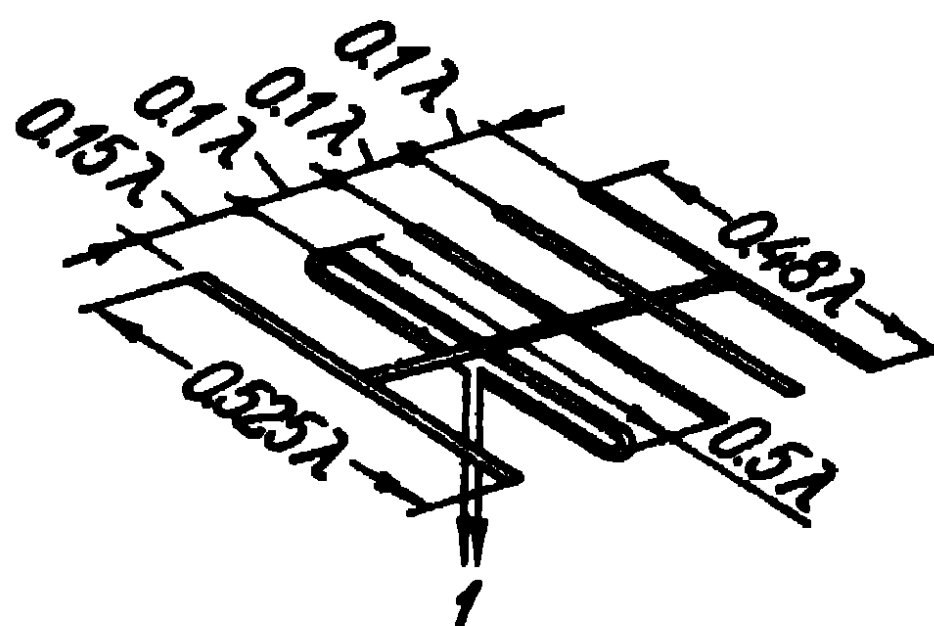


Fig. 10-38. Design of director antenna:
1—feeder.

should be inductive. That is why the length of the reflector is taken somewhat greater than $\lambda/2$. A passive dipole becomes a director when its resistance is capacitive. Hence, the length of the director is taken somewhat smaller than $\lambda/2$. Only one dipole is utilised as a reflector because the subsequent reflectors would be only weakly excited and would not exert any noticeable influence on the radiation of the antenna. As for the number of directors, it can be large, because the radiation of the antenna is directed towards the directors and, consequently, they are fairly intensively excited in series, forming a waveguide channel. The number of directors varies from 2 to 10 and more.

Director antennas are utilised on metre and decimetre waves; the dipoles are rigid and fastened in their middle to a metal rod (Fig. 10-38). This rod does not become excited due to the fact that the electric field of the antenna

intersects it at right angles. The active dipole is usually made in the shape of a loop-like dipole and fastened to the rod in the middle of its uncut part, so that the antenna is mounted without insulators, and is quite compact and rigid.

The distance between the active dipole and the reflector is from 0.15 to 0.25λ , while between the active dipole and the first director as well as between the neighbouring directors, it is from 0.10 to 0.35λ . In order to obtain the maximum radiation in the main direction, the distances between the directors as well as their length are specially chosen on the prescribed frequency of excitation so as to get definite ratios between the currents in the dipoles. It is evident that the magnitudes of the currents should be approximately equal and close to the magnitude of the current in the active dipole. As for the phases of the currents, they should lag behind by a definite magnitude from dipole to dipole towards the end of the antenna. Under this condition, the fields of the individual dipoles reinforce one another in the main direction whereas in the other directions the radiations cancel out. As a rule, the radiation maximum of the antenna towards the directors coincides with the radiation minimum towards the reflector. In this way, the antenna sets up a unidirectional radiation.

The input impedance of a director antenna is quite sensitive to frequency changes of the oscillations, so that it has a narrow bandwidth (the width of the pass-band of the antenna amounts to a few per cent). In the case of a large number of directors, the tuning-up process, which consists in the proper choice of the lengths of the directors and their spacing, is most tedious because a change of length or position of one of the dipoles leads to a change of the amplitudes and phases of the currents in all the dipoles. For this reason and also because the inten-

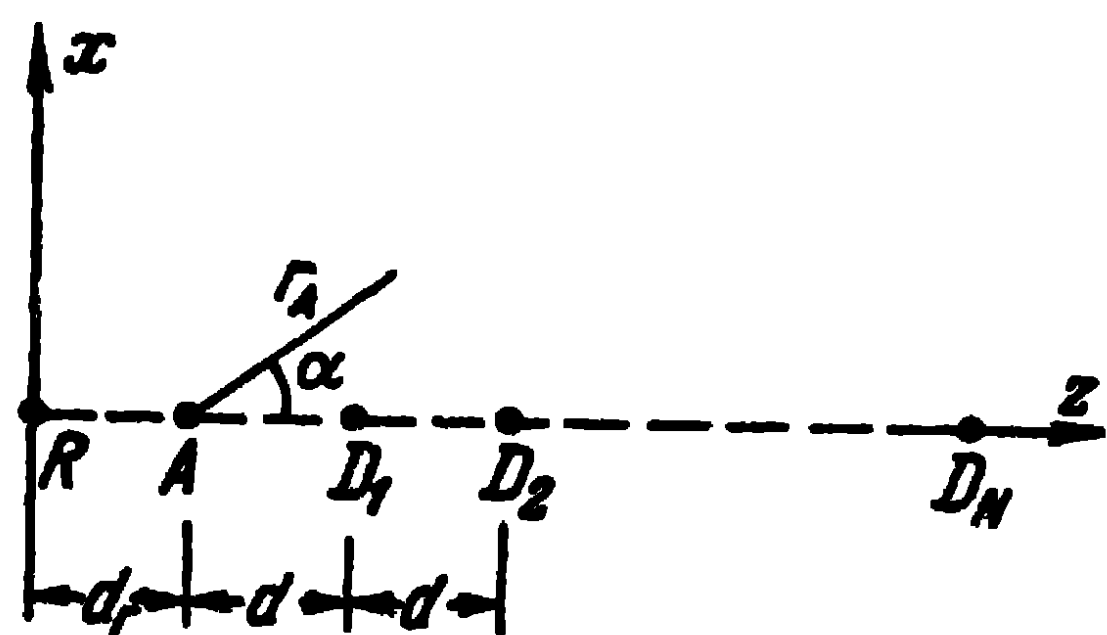


Fig. 10-39. Calculating the radiation of a director antenna.

sity of excitation of the directors towards the end of the antenna somewhat decreases, the number of directors usually taken is small and the width of the directional diagrams of director antennas adopted in practice is never less than 15-20% at half-power.

If the ratio of the amplitudes and phases of the currents in the dipoles is known, the directional diagrams can be calculated from the expressions of the antenna array (see Chapter Four). For the equatorial plane of the dipoles (Fig. 10-39), the antenna field intensity in the radiation zone can be calculated from the expression

$$E_{xz} = E_A \left[\frac{I_R}{I_A} e^{+ikd \cos \alpha} + 1 + \frac{I_{D1}}{I_A} e^{-ikd \cos \alpha} + \right. \\ \left. + \frac{I_{D2}}{I_A} e^{-i2kd \cos \alpha} + \dots + \frac{I_{DN}}{I_A} e^{-iNkd \cos \alpha} \right], \quad (10-20)$$

where

I_R , I_A , I_{Dm} are the complex amplitudes of the currents in the reflector, the actively fed dipole and the m -th director respectively;

$E_A = i \frac{60 I_A}{r_A} e^{-ikr_A}$ is the field of the active dipole in the zone of radiation;

α is the angle between the direction towards the point of observation and the antenna axis. The expression (10-20) is based on the assumption that the distances between neighbouring directors as well as between the first director and the actively fed dipole are the same.

For the meridional plane of the dipoles, the field is calculated from the expression (10-20) multiplied by the ratio

$$\frac{\cos \left(\frac{\pi}{2} \sin \alpha \right)}{\cos \alpha}.$$

To calculate the complex current amplitudes excited in the dipoles, use can be made of the coupled dipoles theory (see Chapter Three). For the director antenna, the Kirchhoff's equations are written as follows:

$$\left. \begin{aligned} 0 &= I_R Z_{RR} + I_A Z_{AR} + I_{D_1} Z_{D_1 R} + \dots + I_{DN} Z_{DNR}; \\ U_A &= I_R Z_{RA} + I_A Z_{AA} + I_{D_1} Z_{D_1 A} + \dots + I_{DN} Z_{DNA}; \\ 0 &= I_R Z_{RD_1} + I_A Z_{AD_1} + I_{D_1} Z_{D_1 D_1} + \dots + \\ &\quad + I_{DN} Z_{DN D_1}; \\ . &. \\ 0 &= I_R Z_{R DN} + I_A Z_{A DN} + I_{D_1} Z_{D_1 DN} + \dots + \\ &\quad + I_{DN} Z_{DN DN}. \end{aligned} \right\} \quad (10-21)$$

The difficulty in calculating the complex current amplitudes consists, in the first place, in that the mutual resistances of dipoles of arbitrary length are not tabulated and their calculation is complicated because one has to know the $\frac{N(N+1)}{2}$ of these values. Another difficulty in calculating the currents is due to complexity of computing the determinants of the equations (10-21). This explains why the calculations effected so far have not gone beyond antennas with a number of directors not exceeding four.

Once the currents in the antenna dipoles have been calculated, the determination of the input resistance of the actively fed dipole from the following expression presents no difficulty:

$$Z_A = \frac{I_R}{I_A} Z_{RA} + Z_{AA} + \frac{I_{D1}}{I_A} Z_{D1A} + \dots + \frac{I_{DN}}{I_A} Z_{DNA}. \quad (10-22)$$

After that, the directive gain of the antenna can be defined from the expression (4-68).

The above-mentioned method was applied to the calculation of a director antenna consisting of one active dipole and from one to four directors [57]. The distances between the dipoles were assumed to be the same and the mutual resistances were taken from the tables for half-wave dipoles. The directional diagrams, input resistances of the active dipole and the amplification coefficients of the antennas were calculated. We quote the calculation data regarding an antenna with four directors, for three different spacings between them: $d=0.1\lambda$, $d=0.2\lambda$ and $d=0.3\lambda$. The data were obtained as a function of the magnitude of the natural reactance of the directors. The natural reactance of the actively fed dipole was taken equal to zero.

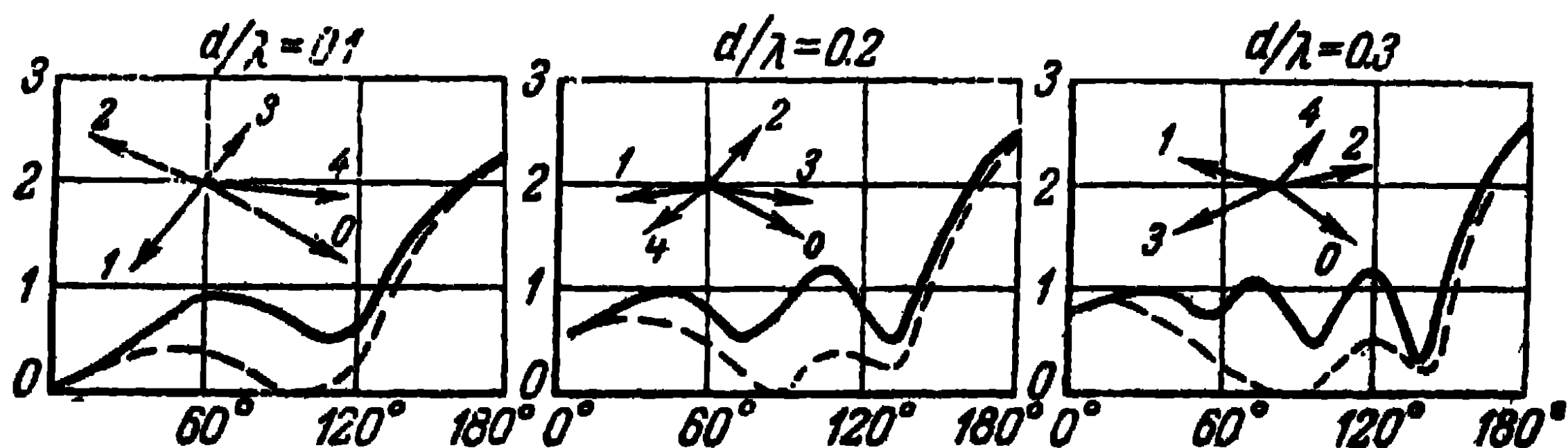


Fig. 10-40. Directional diagrams of a director antenna.

Fig. 10-40 represents the directional diagrams of the antenna in a plane perpendicular to the dipoles (solid lines) and in the plane of the antenna (broken lines) in the case of a reactance of the directors $X = -40$ ohms. It can be seen that an increase of the length of the antenna leads to a decrease of the width of the major lobe of the directional diagram. Shown above the curves are the vector diagrams of the currents in the dipoles, figure 0 designating the current in the active dipole and figures 1, 2, 3 and 4, the currents in the directors in the order of their position, starting from the active dipole.

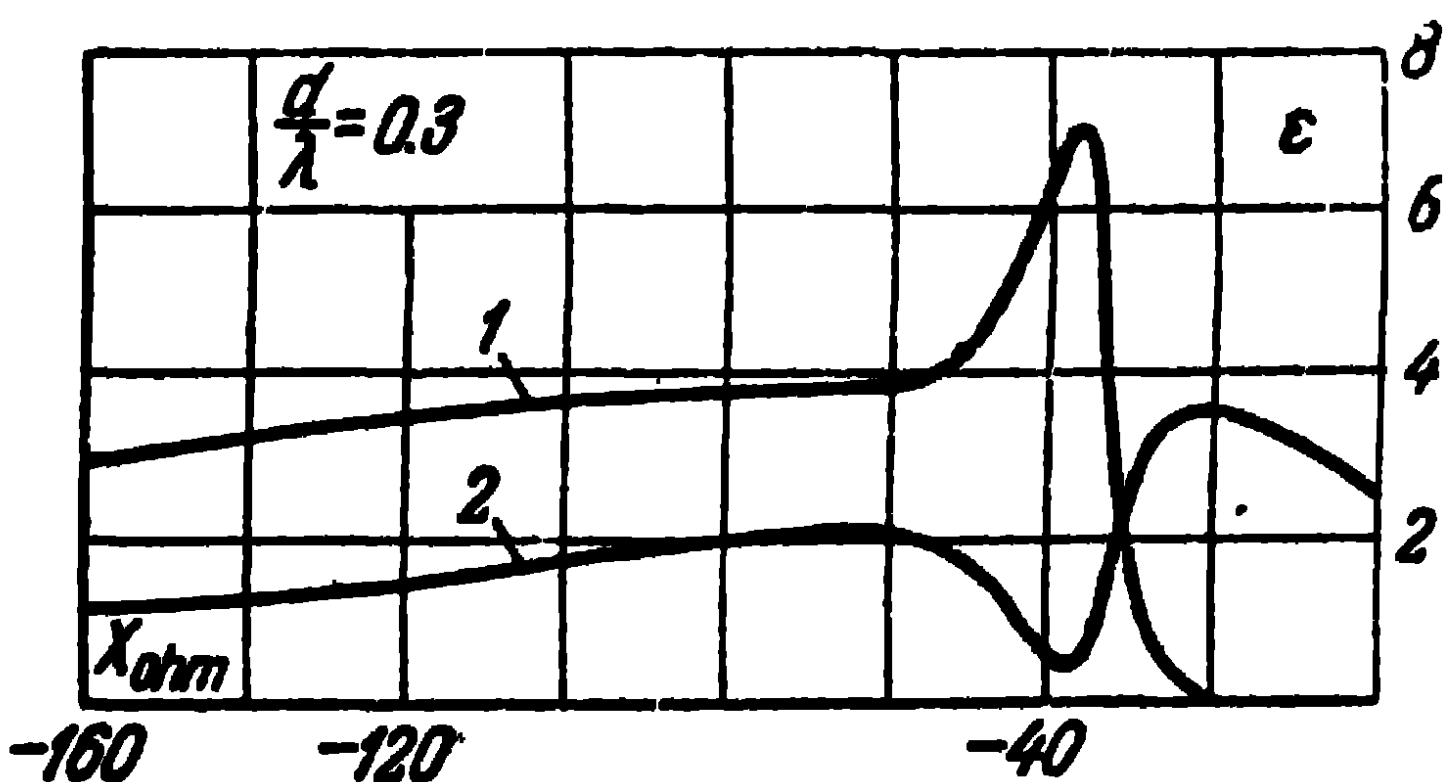
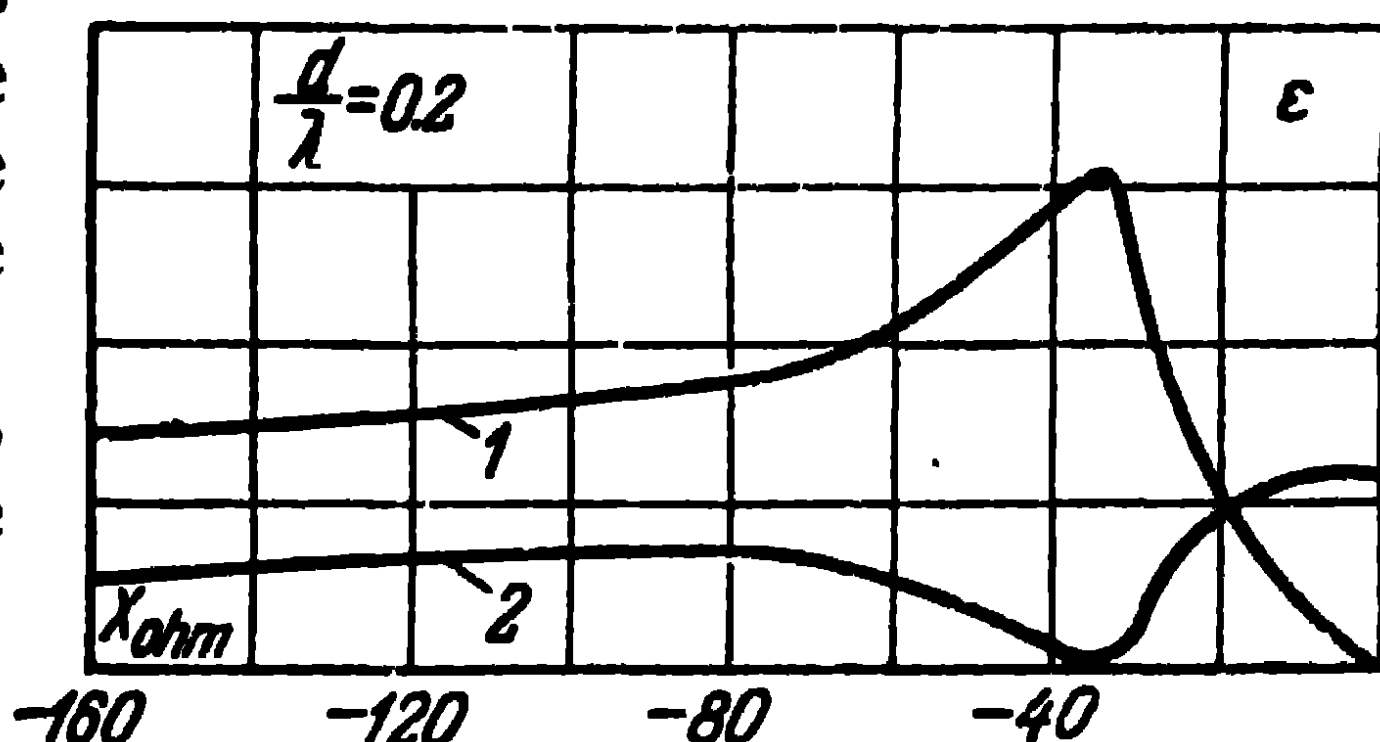
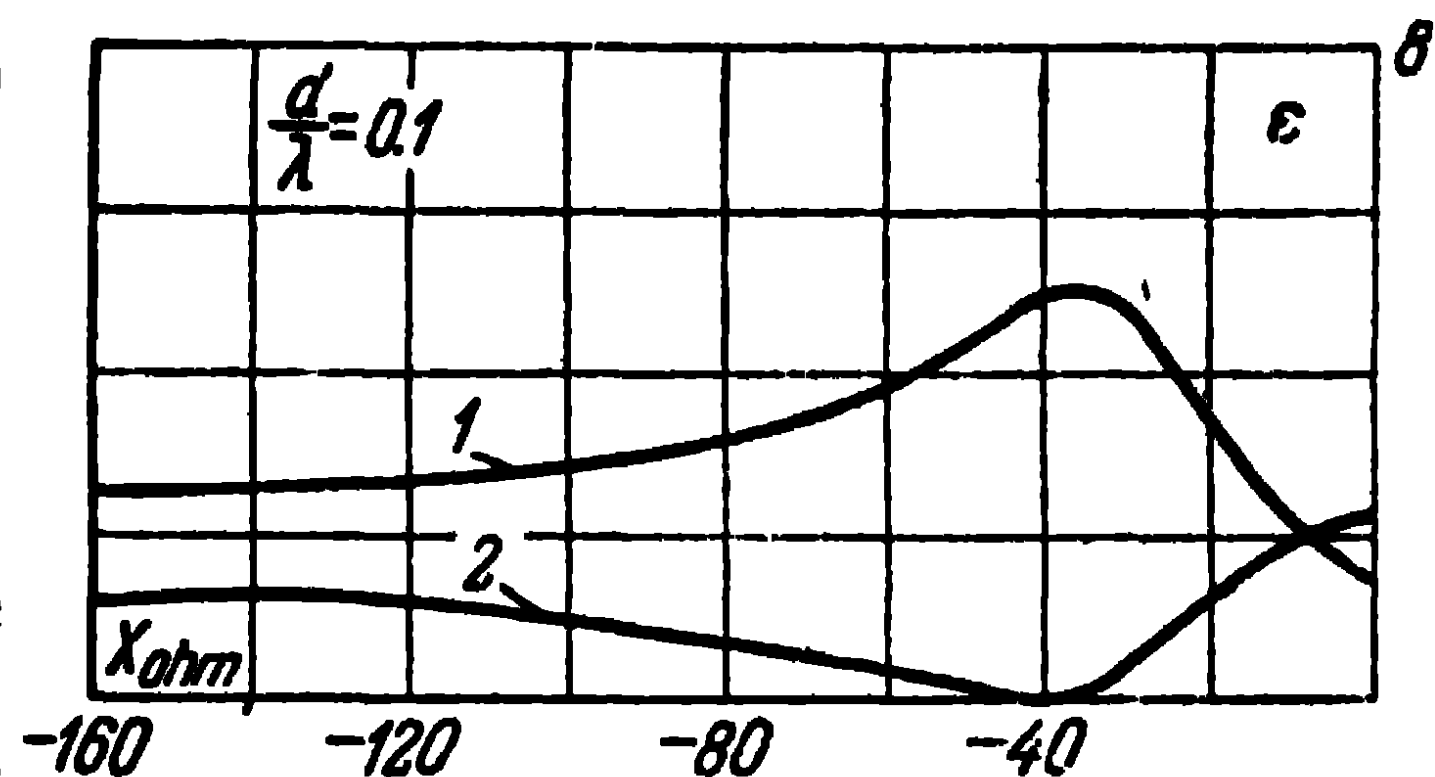


Fig. 10-41 represents the amplification coefficients of the antenna ($\epsilon = \frac{D}{1.54}$)

plotted as a function of the magnitude of the reactance of the directors. The curves indicate the magnitudes of the amplification coefficients in the direction of the directors (forward) and in the reverse direction (back). It is seen that the maximum of the antenna radiation ($\epsilon = 5 - 7$) occurs in the vicinity of the reactance of the directors which is approximately 40 ohms; moreover, the forward radiation maximum corresponds to the backward radiation minimum.

Fig. 10-41. Antenna amplification coefficients curves:
1—forward; 2—back

Fig. 10-42 represents the curves of the active part of the input resistance of an actively fed dipole. On comparing these curves with those in Fig. 10-41, it is seen that when the antenna is tuned on maximum radiation forward, the input resistance of the actively fed dipole decreases and has

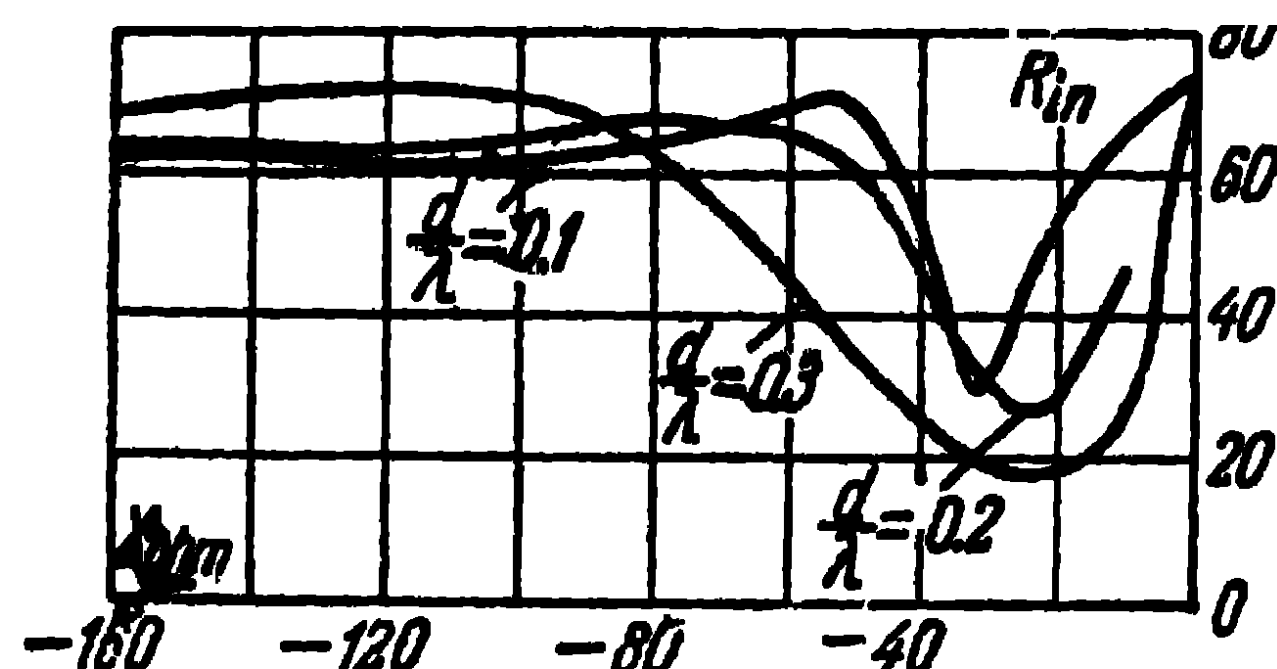


Fig. 10-42. Curves of the active part of the input resistance of an active dipole.

a value of $R_{in} = 20 - 30$ ohms instead of 73 ohms for one single dipole.

There are other methods for computing director antennas, such as the approximate method based on reducing the system of equations (10-21) to a difference equation with linear coefficients [58].

We quote the experimental data of a director antenna consisting of a series of directors spaced 0.34λ apart and of the same length. Table 10-1 gives the width of the directional diagram at the 0.25 power level and the power gain of the antenna. Table 10-2 gives the lengths of the directors corresponding to different number of them, for which the level of the first minor lobe is of the order of 30% of that of the directional diagram major lobe.

It is seen from tables 10-1 and 10-2 that, as the number of directors increases, the directional diagrams become narrower, and the power gain increases. The necessary length of the directors decreases as their number goes up.

Table 10-1

Number of directors	Width of directional diagram in degrees	Power gain
30	22	—
20	26	21
13	31	15
9	37	13
4	46	8

Table 10-2

Number of directors	Length of director in wave-lengths
42	0.385
30	0.40
20	0.407
13	0.414
10	0.42
7	0.423
5	0.434

It should be pointed out that a director antenna can be regarded as an axial radiation antenna of retarded phase velocity. Indeed, dipoles shorter than half a wave-length can be regarded as elements with capacitive resistances connected to the transmission line in a way similar to that in which capacitive resistances are connected in parallel to a twin line. The phase velocity of the wave in such a system is less than that of light. The actively fed dipole can be regarded as an element which excites a retarded wave in such a line.

Thus, we can apply to the director antenna the axial radiation antenna of retarded phase velocity theory and use the corresponding expressions to calculate its parameters. Thus, the width of the directional diagram of the antenna can be evaluated from the expressions (4-26) and (4-27) and the directive gain, from (4-72).

10-8. Helical Antennas

Helical antennas, which radiate a field of circular polarisation in the direction of their axis, find extensive application in the centimetre and decimetre wave range, more seldom in the metre wave range.

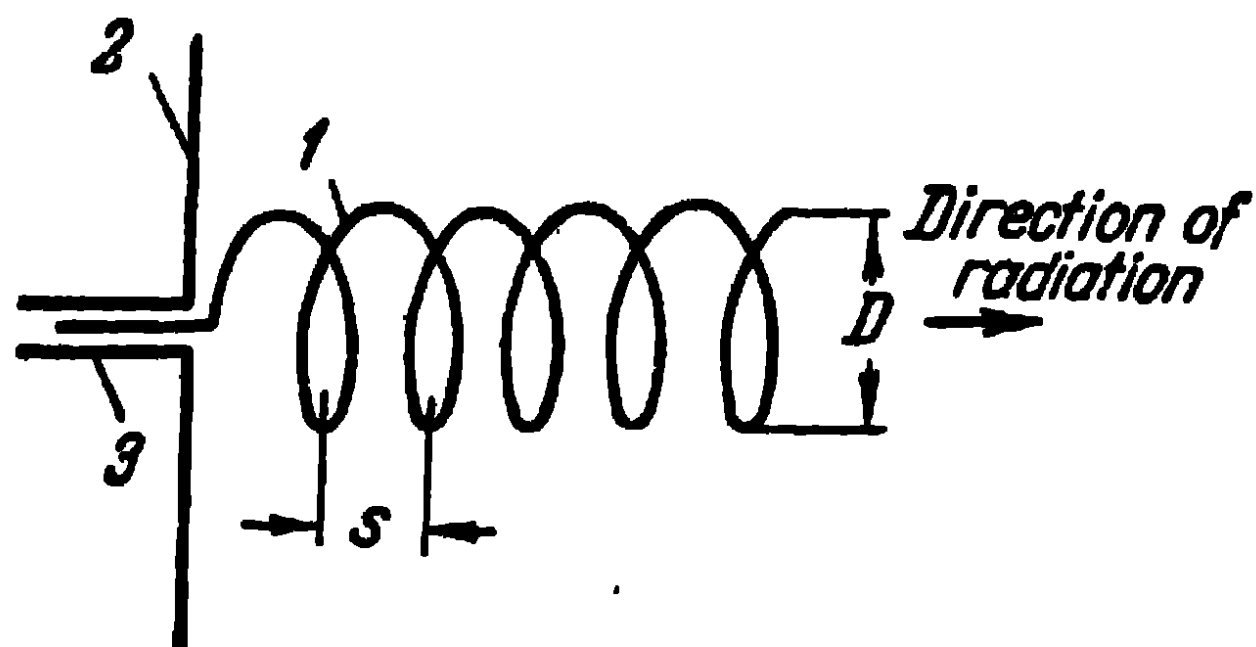


Fig. 10-43. Helical antenna:
1—helix; 2—disc; 3—coaxial line.

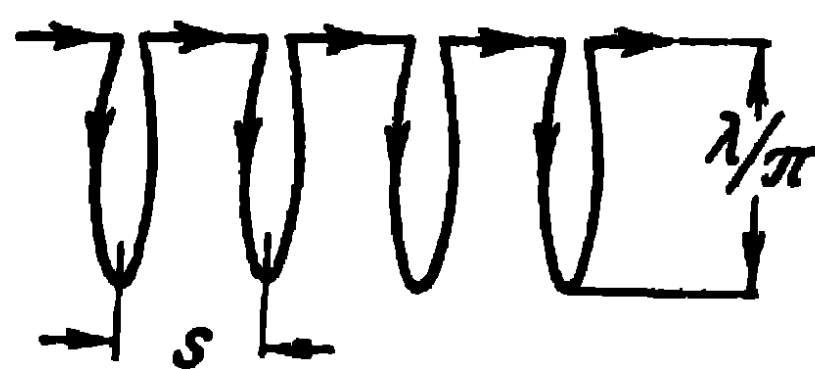


Fig. 10-44. Equivalent circuit of the helix.

The antenna consists of a wire helix several wave-lengths long and of winding diameter of the order of a third of a wave-length (Fig. 10-43). One end of the helix remains free and the other is connected to the inner wire of a coaxial line. The external conductor of the feed coaxial line is connected to a metal disc with an aperture for the inner conductor of the line. The disc plays the role of a counterbalance and prevents the penetration of electric currents to the outer surface of the external conductor of the coaxial line.

A travelling wave of electric current arises in the helix and the antenna radiates maximum energy along its axis in the direction of motion of the current wave. In order to get a clearer understanding of the operating principle of a helical antenna, let us represent it in the form of plane circular loops of diameter $D = \lambda/\pi$, spaced at a distance S apart on the axis and series fed by a single-wire feeder (Fig. 10-44). Let us investigate the radiation of one of the windings and assume the current in the winding to be distributed as $I_0 e^{-ikl}$, where I_0 is the magnitude of the current at the beginning of the winding; $k = \frac{2\pi}{\lambda}$; l is the length along the winding.

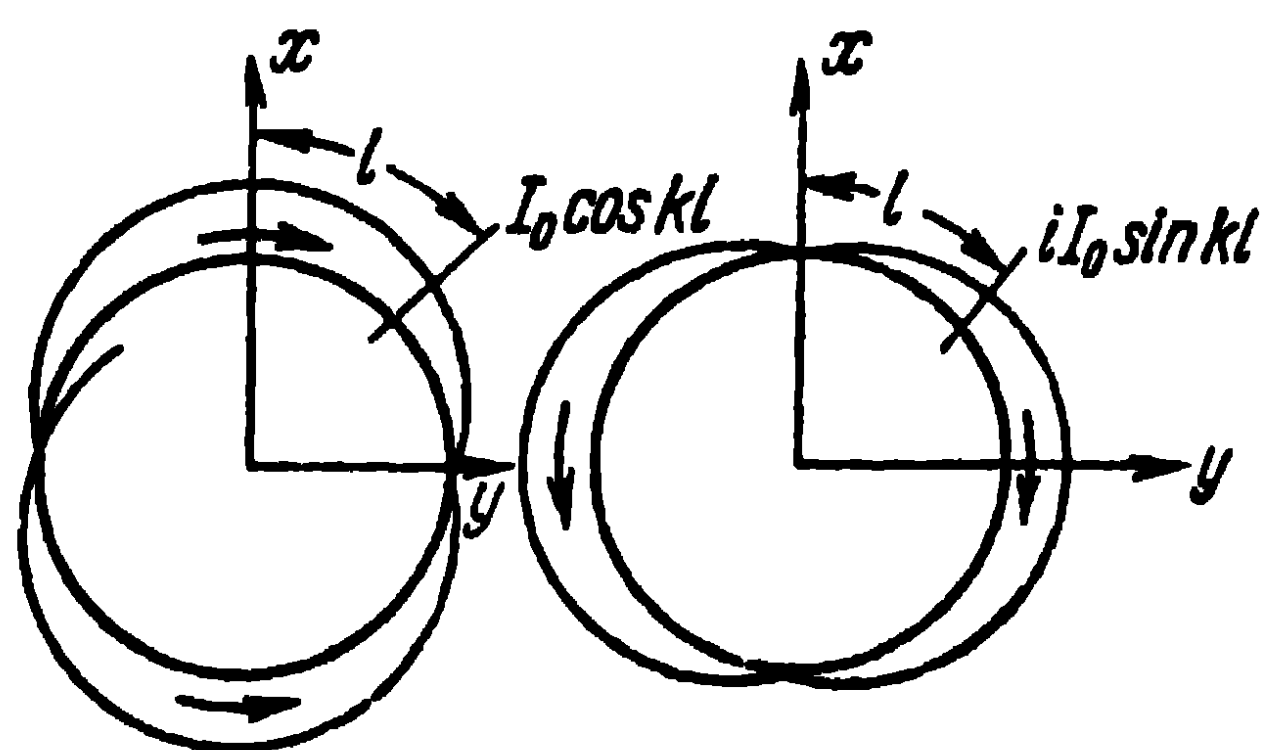


Fig. 10-45. Current distribution helix winding.

This expression can be written as $I_0 \cos kl - i I_0 \sin kl$ and thus represent the current as the superposition of two standing waves with a 90° phase shift, the amplitude

of one of which changes along the winding in accordance with the cosine law and the other, with the sine law (Fig. 10-45). We obtain four bent half-wave dipoles oscillating in phase pair by pair: one pair of dipoles is orientated in the direction of the y -axis and radiates maximum energy in the direction of the z -axis with the vector of the electric field intensity coinciding with the y -axis; the other pair of dipoles is orientated in the direction of the x -axis and radiates maximum energy also in the direction of the z -axis, but this time, the vector of the electric field intensity coincides with the x -axis. Since the pairs of dipoles oscillate with a 90° phase shift, the field radiated in the z -axis direction has a circular polarisation. At a certain angle to the z -axis the polarisation of the field is elliptical and in the xy -plane, it is linear.

Note that, as a result of the co-phased oscillation of the dipoles and mutual coupling, the radiation resistance in each pair is rather high. The input resistance of each winding is close to its wave impedance and if, in addition, account is taken of the fact that neighbouring windings in the helix oscillate almost in phase due to the small value

of S/λ , it will become clear that a travelling-wave type of operation is set up in the helix. The phase velocity of the wave in the antenna (in a single-wire feeder Fig. 10-44) is somewhat inferior to the velocity of light, and we get an antenna with a retarded phase velocity radiating along its axis. From this point of view, a helical antenna is akin to a director antenna.

If the diameter of the helical antenna is small in comparison with the wave-length ($D \ll \lambda/\pi$), the currents at diametrically opposed points of a winding are opposed in direction and the radiation resistance of the winding is very small (loop effect). As a result, a standing wave type of operation is established in the antenna, the radiation along the axis of the helix being zero and the radiation maximum of each winding and of the whole antenna occurring in the transverse plane of the antenna.

When the diameter of the antenna is large ($D \gg \lambda/\pi$), the currents at diametrically opposed points of a winding and in neighbouring windings are again out of phase and, owing to mutual influence, the radiation resistance of the winding decreases, the travelling-wave type of operation is upset and the radiation from individual elements in the direction of the axis of the winding cancels out; the radiation maximum of the antenna is at a certain angle to the antenna axis.

The picture of the radiated field corresponding to the three types of antennas described above is shown in Fig. 10-46.

The qualitative picture of the electric current distribution in a helical antenna is confirmed by theoretical research on wave distribution along an infinite helix conducted by S. Kogan [59 and 60]. In accordance with his investigations, in the general case, we get the excitation in an infinite helix of a superposition of three travelling waves of current of different phase velocities; the first type of current wave of increased phase velocity predominates in

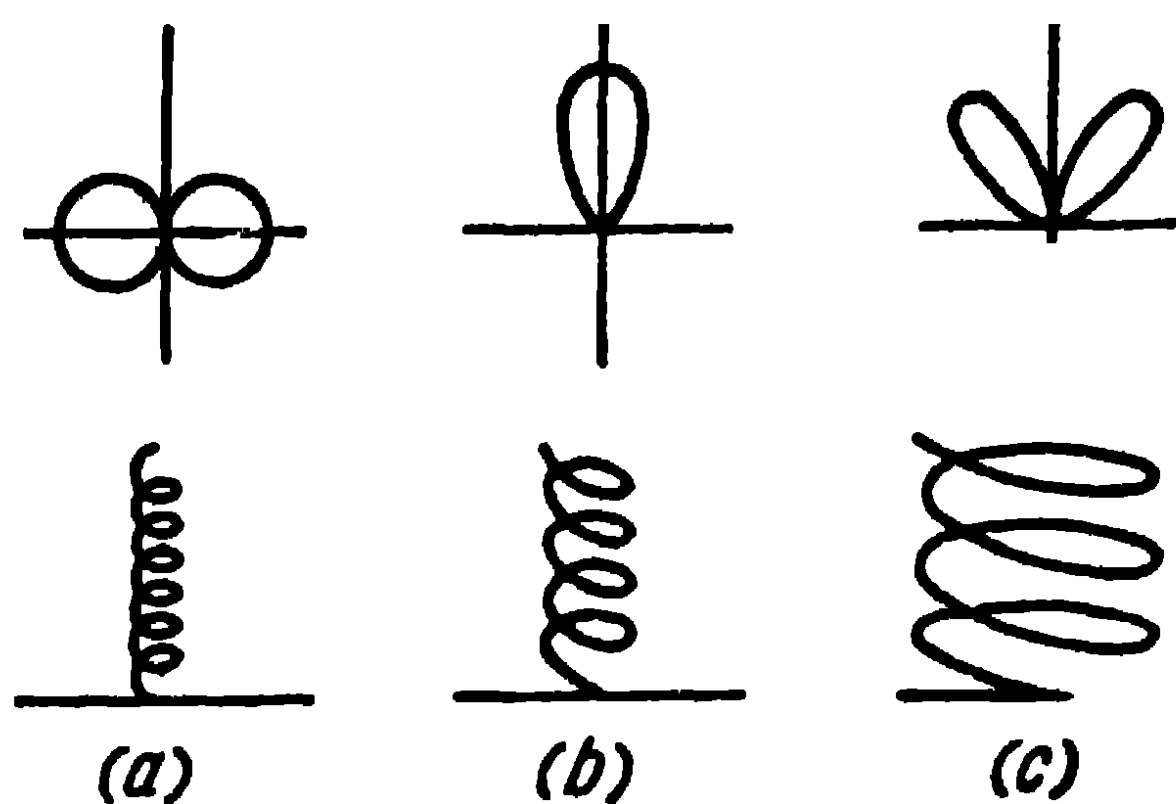


Fig. 10-46. Three types of helical antenna:

a—non-directional radiation; *b*—axial radiation; *c*—conical radiation.

a helix of small diameter ($kD \ll 1$), and the third type of current wave of slow phase velocity predominates in a helix whose diameter approaches one-third of a wavelength; moreover, for frequencies higher than the critical one, which is approximately expressed as:

$$\frac{\omega_{\text{crit}}}{v_1} \approx \frac{\cos \alpha}{(1 + \sin \alpha) \frac{D}{2}},$$

there remains only the third type of current wave, corresponding to the axial radiation type of operation.

Fig. 10-47 shows the experimental curves of the current amplitude distribution in the wire of an antenna with the

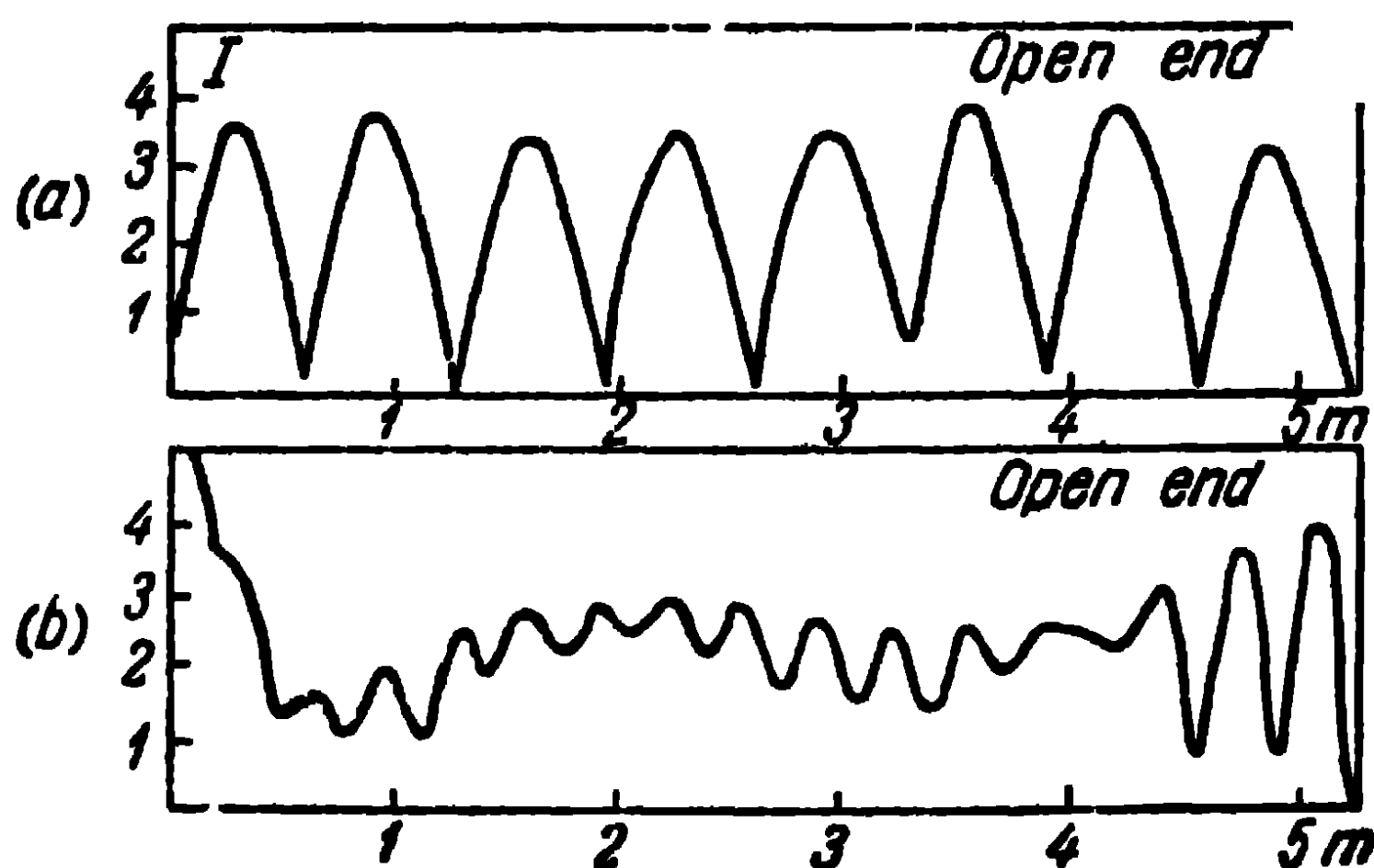


Fig. 10-47. Current distribution in a helix:
a—non-directional radiation; b—axial radiation.

following parameters: number of windings $n=7$; angle of inclination of the windings $\alpha=12^\circ$; antenna diameter $D=22.5$ cm; winding pitch of the helix $S=15$ cm [61]. The upper curve corresponds to the current distribution on a frequency $f=250$ Mc/s ($D \approx 0.187 \lambda$), and the lower curve, on a frequency $f=450$ Mc/s ($D \approx 0.338 \lambda$). It is seen that in the first case, there is considerable reflection from the end of the helix and a standing wave is set up in the antenna. In the second case, the reflection from the end of the antenna occurs too but the amplitude of the travelling wave in the middle region of the helix is more or less constant. Fig. 10-48 represents the schematic picture of the current distribution in the antenna in the axial radiation type of operation. It can be said that the reflected wave 4 is superposed on the incident wave 2; moreover, higher

modes arise at the end and beginning of the antenna to which the attenuated currents 3 and 1 correspond. The current amplitude of the reflected wave 4 constitutes about 20% of the current amplitude of the incident wave 2 and in the first approximation, when investigating the antenna radiation, the currents 1, 3 and 4 can be neglected.

As regards the phase velocity, measurements show that in an axial radiation helical antenna the deceleration coefficient of the phase velocity of the current wave in the wire $\xi =$

$= \frac{v_1}{v}$ is found to be frequency de-

pendent. Thus, for a helical antenna of

seven windings with an angle of inclination $\alpha = 12^\circ$, a diameter $D = 23$ cm and relative length of winding $L/\lambda = 0.72 \div 1.2$, the deceleration coefficient changes from a value $\xi = 1.67$ on the frequency $f = 300$ Mc/s to a value $\xi = 1.1$ on a frequency $f = 500$ Mc/s.

If the deceleration of the phase velocity and the fact that a helix winding has a certain winding pitch are taken into account the following condition should be observed to obtain a circularly polarised field in the direction of the helix axis:

$$k\xi L - kS = 2\pi$$

or

$$L = \frac{S + \lambda}{\xi} \quad (10-23)$$

However, if we regard a helical antenna as a slow phase velocity antenna then, as we know, to obtain the maximum directive gain, the phase shift of the field radiated by the first and last elements of the antenna should equal π . Hence, instead of the condition (10-23), we obtain:

$$k\xi L - kS = 2\pi + \frac{\pi}{n}$$

or

$$L = \frac{S + \lambda + \frac{\lambda}{2n}}{\xi} \quad (10-24)$$

Thus, if the condition observed in the direction of the principal radiation is (10-23), we obtain a circular

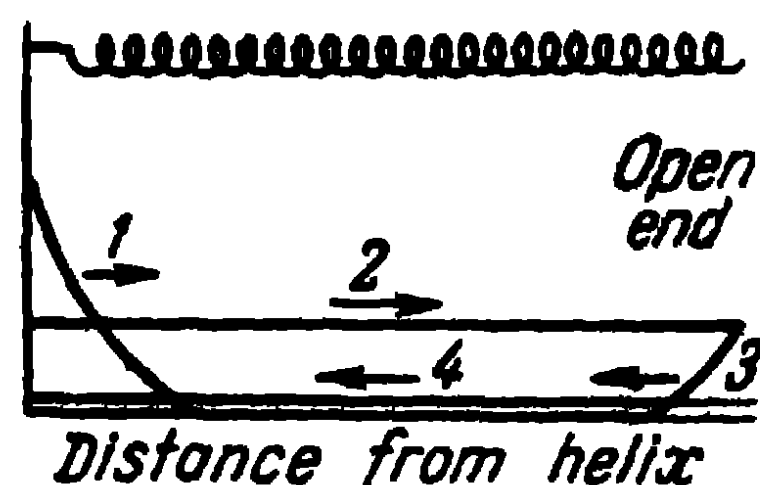


Fig. 10-48. Schematic picture of the current distribution.

polarisation; no such polarisation is obtained if it is (10-24) but the directive gain is then at its highest.

Empirical expressions based on experimental data have been obtained for a helical antenna with an angle of inclination $\alpha = 12^\circ \div 16^\circ$ for a number of windings larger than three. The expressions are given below.

The width of the directional diagram at half-power is

$$2\beta_{1/2} = \frac{52}{\frac{L}{\lambda} \sqrt{\frac{nS}{\lambda}}} [\text{degrees}]. \quad (10-25)$$

The width of the directional diagram at the radiation zero is:

$$2\beta_0 = \frac{115}{\frac{L}{\lambda} \sqrt{\frac{nS}{\lambda}}} [\text{degrees}]. \quad (10-26)$$

The directive gain is

$$D = 15 \left(\frac{L}{\lambda} \right)^2 n \frac{S}{\lambda}. \quad (10-27)$$

The antenna input resistance is

$$R_{in} \approx 140 \frac{L}{\lambda} [\text{ohms}]. \quad (10-28)$$

Due to the fact that the deceleration coefficient of the phase velocity of the wave ξ increases to some extent as the wave-length increases, the relations (10-23) and (10-24) are but little affected by changes of wave-length and the antenna maintains its directive properties in a wide wave range. This wave range lies between approximately $0.7 \lambda_0$ and $1.2 \lambda_0$, where λ_0 is the wave-length for which the optimum dimensions of the antenna have been chosen.

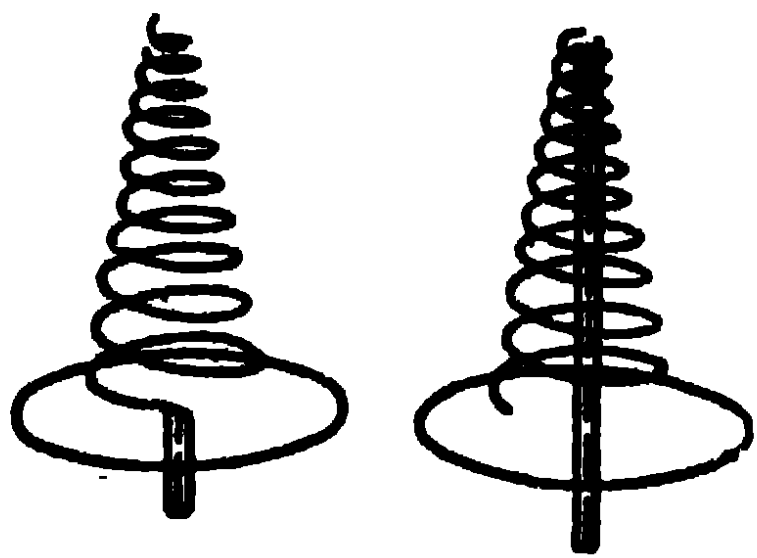


Fig. 10-49. Conical helical antennas.

Apart from the cylindrical helical antennas described above, conical helical antennas also find application. Examples of two helical antennas facing a screen with their broad part are shown in Fig. 10-49. In one case, the helix is fed at the base, in the other, the helix is fed from the apex. Measurements effected on conical helices with the following parameters: $n=10$, $\alpha=6^\circ$, $D_0=20$ cm, $D_{max}=60$ cm show

that the axial radiation of antennas fed from underneath is maintained in approximately a twofold wave range and that of antennas fed from above, in approximately a three-fold wave range.

10-9. Dielectric Rod Antennas

Dielectric rod antennas employed in the centimetre wave range represent dielectric rods of circular or rectangular cross section, several wave-lengths long, excited by a segment of circular or rectangular metal waveguide (Fig. 10-50). In the case of a circular cross section, the excitation of the rod is caused by an H_{11} wave in a circular waveguide, and in the case of a rectangular cross section, the excitation of the rod is caused by an H_{01} wave in a rectangular waveguide.

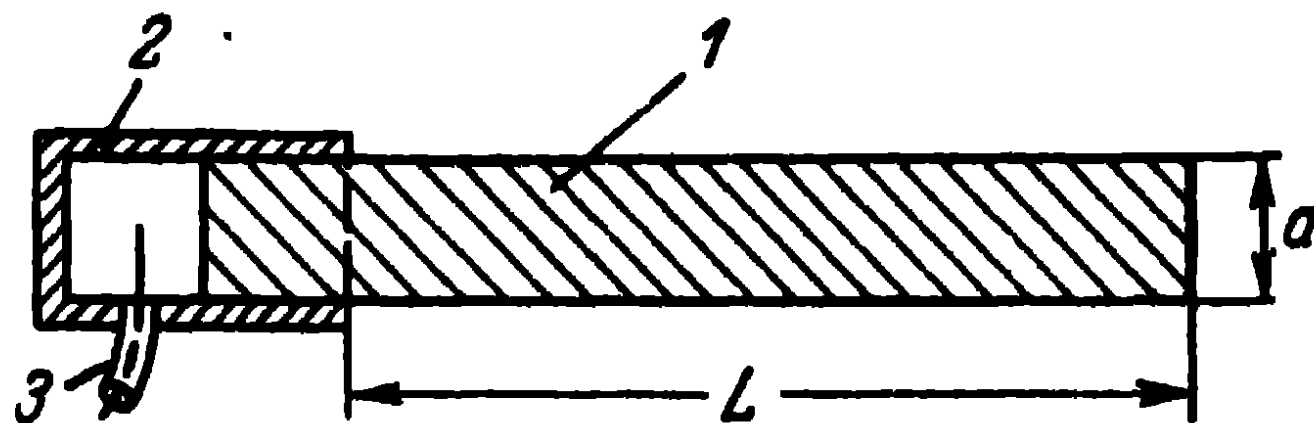


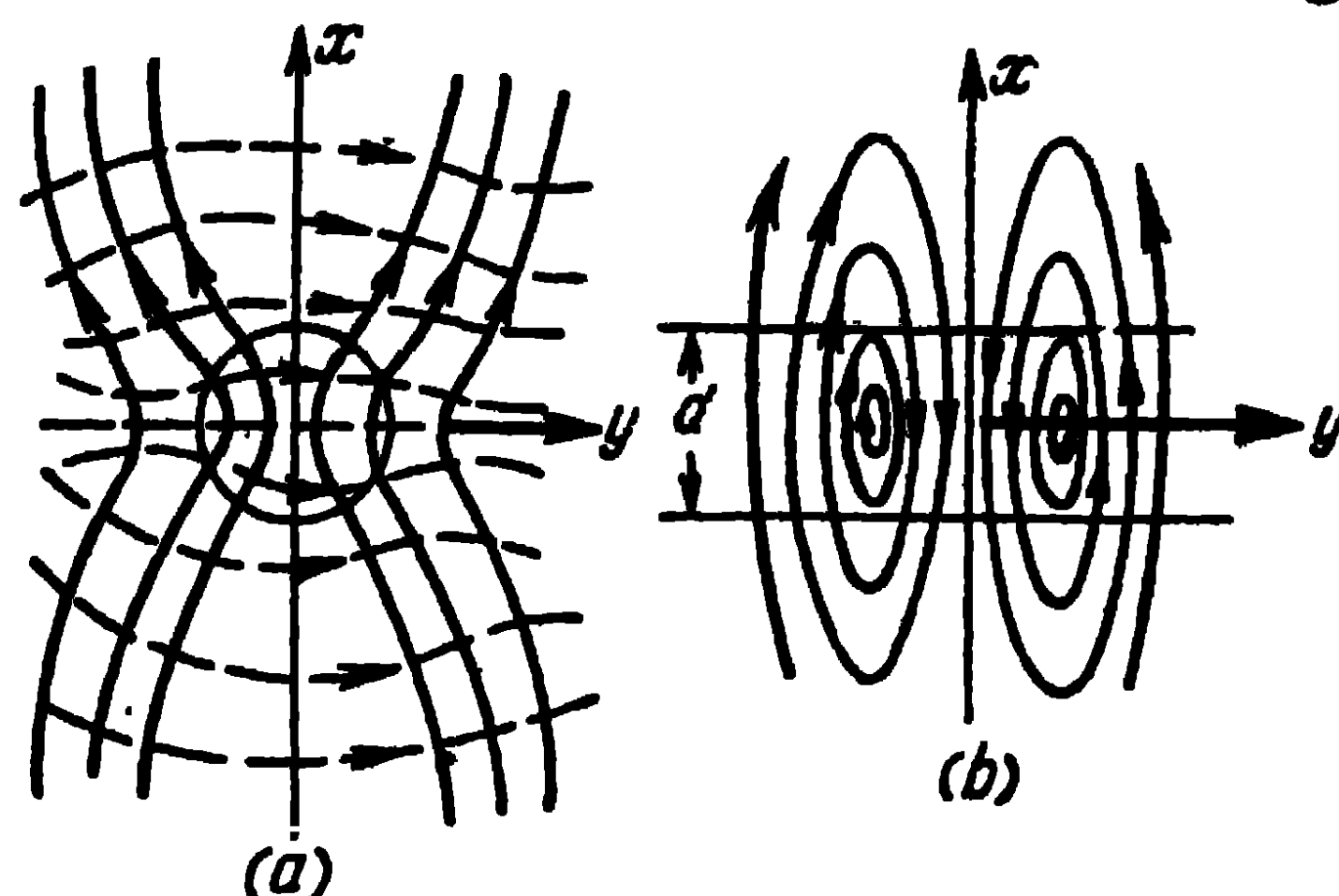
Fig. 10-50. Dielectric rod antenna:
1—dielectric rod; 2—metal waveguide;
3—coaxial line

The wave excited in the dielectric rod, which is the prolongation of the metal waveguide, is an electromagnetic wave, akin to the H_{11} and H_{01} waves in metal waveguides. This electromagnetic wave is propagated along the rod with a phase velocity inferior to the velocity of light in free space. It has the structure of the field shown in Fig. 10-51, from which one can see that the predominant direction of the electric field in the rod coincides with the x -axis. The components of the electric field intensity in the rod, coinciding with the y - and z -axes, have an insignificant value; furthermore, they are of opposite directions in different parts of the cross section. Hence, polarisation currents $j = \omega(\epsilon - \epsilon_0)E$ are excited in the rod which, on the whole, are transverse and coincide with the x -axis of the rod.

Thus, a dielectric rod antenna can be regarded as a continuous system of transverse radiators disposed in the direction of the z -axis of the rod. The distribution of the amplitudes of the polarisation currents in the direction of the system axis can be considered as constant and the distribution of the phases of the polarisation currents as changing linearly. Hence, a dielectric rod antenna can be reduced to a travelling-wave antenna with a slow phase velocity. As

we know, an antenna of this kind radiates energy along its axis in the direction of motion of the wave in the antenna.

The phase velocity of the wave in the rod is defined by the ratio of the amount of electromagnetic energy conveyed



(a)
— Electric field
--- Magnetic field

Fig. 10-51. Field structure in a dielectric waveguide:

a—in cross section; *b*—in longitudinal section.

by the wave inside the rod to the total amount of electromagnetic energy conveyed by the wave along the rod. If the rod is thin relatively to the wave-length, most of the energy is conveyed by the wave into the space surrounding the rod, the phase velocity is mainly determined by the sur-

rounding medium and becomes close to the velocity of light. If the rod is thick relatively to the wave-length, most of the energy moves inside the rod, the phase velocity is mainly determined by the internal medium and becomes close to the velocity of light in the given medium. Thus,

the phase velocity of the wave lies in the interval $v_1 > v > \frac{v_1}{\sqrt{\epsilon/\epsilon_0}}$, where ϵ/ϵ_0 is the relative permittivity of the rod.

The above-cited arguments with regard to the structure and phase velocity of the electromagnetic wave in a dielectric rod are based on the theory of waves in an infinite circular dielectric cylinder. In accordance with this theory, an infinitely large number of modes, symmetrical as well as asymmetrical, can be present in a cylinder of this kind. The wave we have described is an asymmetrical wave of mixed mode (superimposition of electric and magnetic waves) the field of which is determined by all six components of the *E* and *H* vectors. The peculiarity of this type of oscillations lies in the fact that a critical wave-length is equal to infinity, i.e., a wave of this mode can theoretically be propagated in a rod of any thinness. The phase velocity of this wave along the rod is represented by the curves shown in Fig. 10-52 as a function of the ratio of the

rod diameter to the wave-length at various dielectric permittivities of the rod.

It can be seen from the curves that in the case of thin rods ($d/\lambda \ll 1$), the wave phase velocity in the rod is close to that of light, and when the diameter of the rod approaches half a wave-length, it begins to fall rapidly. This diameter ($d/\lambda \approx 0.5$) is precisely chosen as the operating diameter for the rod dielectric antennas.

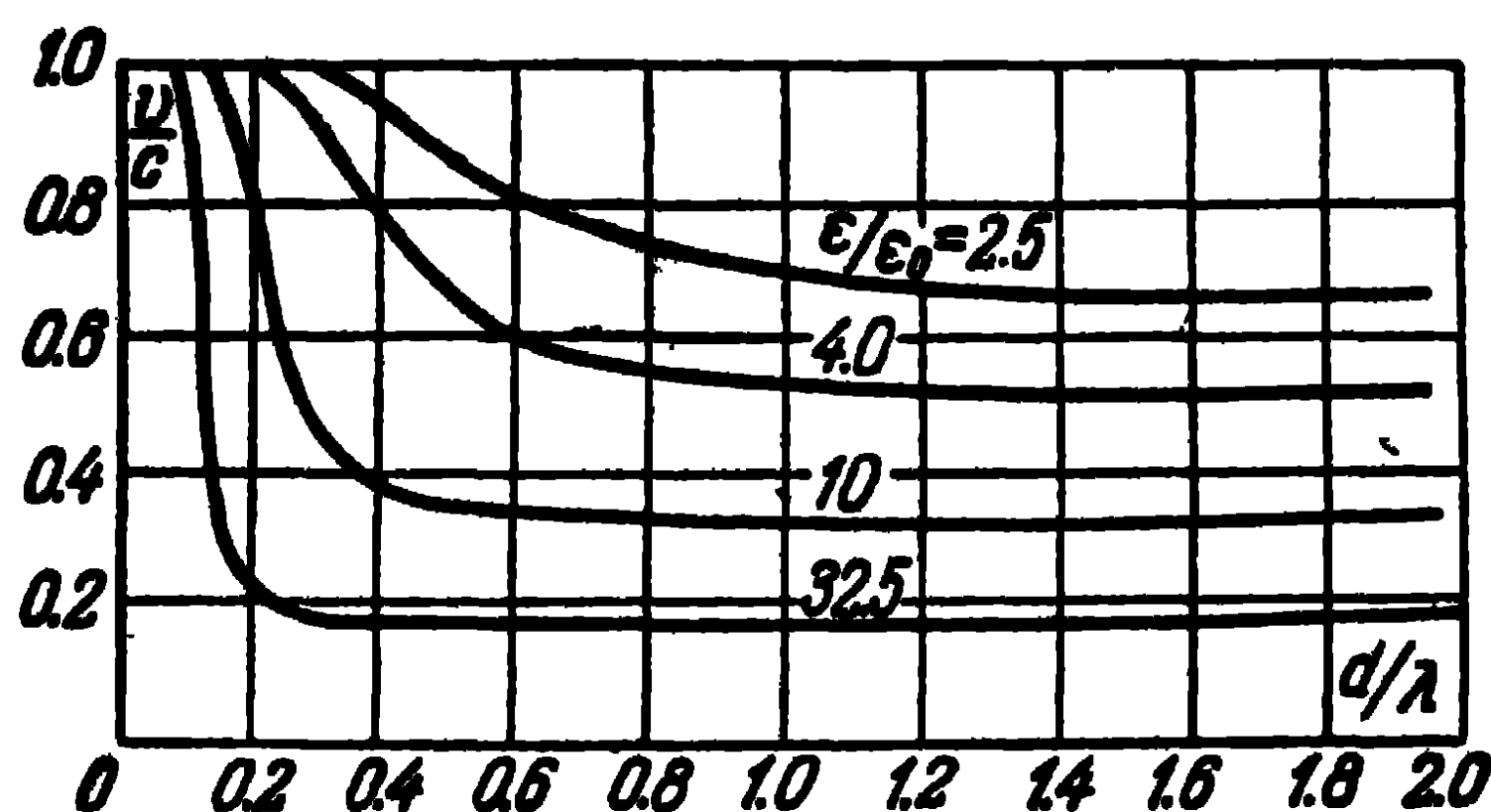


Fig. 10-52. Relative phase velocity in an infinite dielectric cylinder.

The approximate calculation of the directional diagram of the antenna can be approximately calculated with the help of the expression (4-22) which we shall write as:

$$f(\alpha) = \frac{\sin \left[\frac{\pi L}{\lambda} \left(\frac{v_{r.w}}{v} - \cos \alpha \right) \right]}{\frac{\pi L}{\lambda} \left(\frac{v_{r.w}}{v} - \cos \alpha \right)}, \quad (10-29)$$

where α is the angle between the antenna axis and the direction towards the point of observation;
 L/λ , the length of the antenna in wave-lengths;
 $v/v_{r.w}$, the relative phase velocity of the wave in the antenna.

The expression (10-29) concerns a travelling-wave antenna with point sources and does not take into account the radiation directivity of the element of the rod length. Indeed, as can be seen from the picture of the electric field in the rod (Fig. 10-51), the polarisation currents in the rod have transverse (in the direction of the x - and y -axes) as well as longitudinal components and the superimposition of the fields set up by these current components forms

a rather complex radiation characteristic of the element of the rod length, in particular in the transverse section. However, the combination factor of the antenna (10-29) "cuts out" from this complex radiation comprised within relatively narrow angles α (up to 20-30°). But the radiation within these angles is on the whole defined by the components of the polarisation currents, parallel to the x -axis, and for the element of the rod length, it has a low directivity in the planes of the \mathbf{H} as well as \mathbf{E} vectors. Hence, the expression (10-29) must fairly accurately define the major lobe of the direction diagram and is not valid for the minor lobes.

Another reason why the expression (10-29) is only approximate is that it takes no account of the radiation set up by the polarisation current wave, reflected from the rod end. However, the wave phase velocity in the antenna is close to that of light ($d/\lambda \leq 0.5$) and the coefficient of reflection of the current wave from the end of the rod is not high (of the order of 0.15). Hence the radiation of the reflected wave, directed in the opposite side, can be neglected.

Since it is a travelling-wave antenna of slow phase velocity, the dielectric rod antenna has an optimum length which is expressed as:

$$\frac{L}{\lambda} = \frac{1}{2 \left(\frac{v_1}{v} - 1 \right)}. \quad (4-25)$$

At the same time the width of the antenna directional diagram can be evaluated from the expressions (4-26) and (4-27) and the directive gain can be expressed as:

$$D = 7.2 \frac{L}{\lambda}. \quad (4-75)$$

Fig. 10-53 shows the experimental directional diagrams of a polyrod antenna of uniform rectangular section with approximate dimensions $\lambda/2 \times \lambda/3$ for three different lengths: $L/\lambda = 3; 6; 9$. The same figure gives the measured values of the directive gain in decibels. An examination of the curves reveals that the dielectric antennas have large minor lobes. Note, in addition, the absence of radiation zeros between the lobes.

This can be explained by the attenuation of the wave during its propagation in the dielectric rod, due to the

energy lost on heating the dielectric. As regards the width of the major lobe and the directive gain, they are in fair agreement with the expressions given above (to within 20%).

The radiation of dielectric rod antennas can be regarded from a point of view somewhat different from that mentioned above when we were considering the radiation of polarization currents excited in the dielectric rod. Indeed, when the electromagnetic energy conveyed by a wave in a metal waveguide reaches its extremity, it is partly radiated

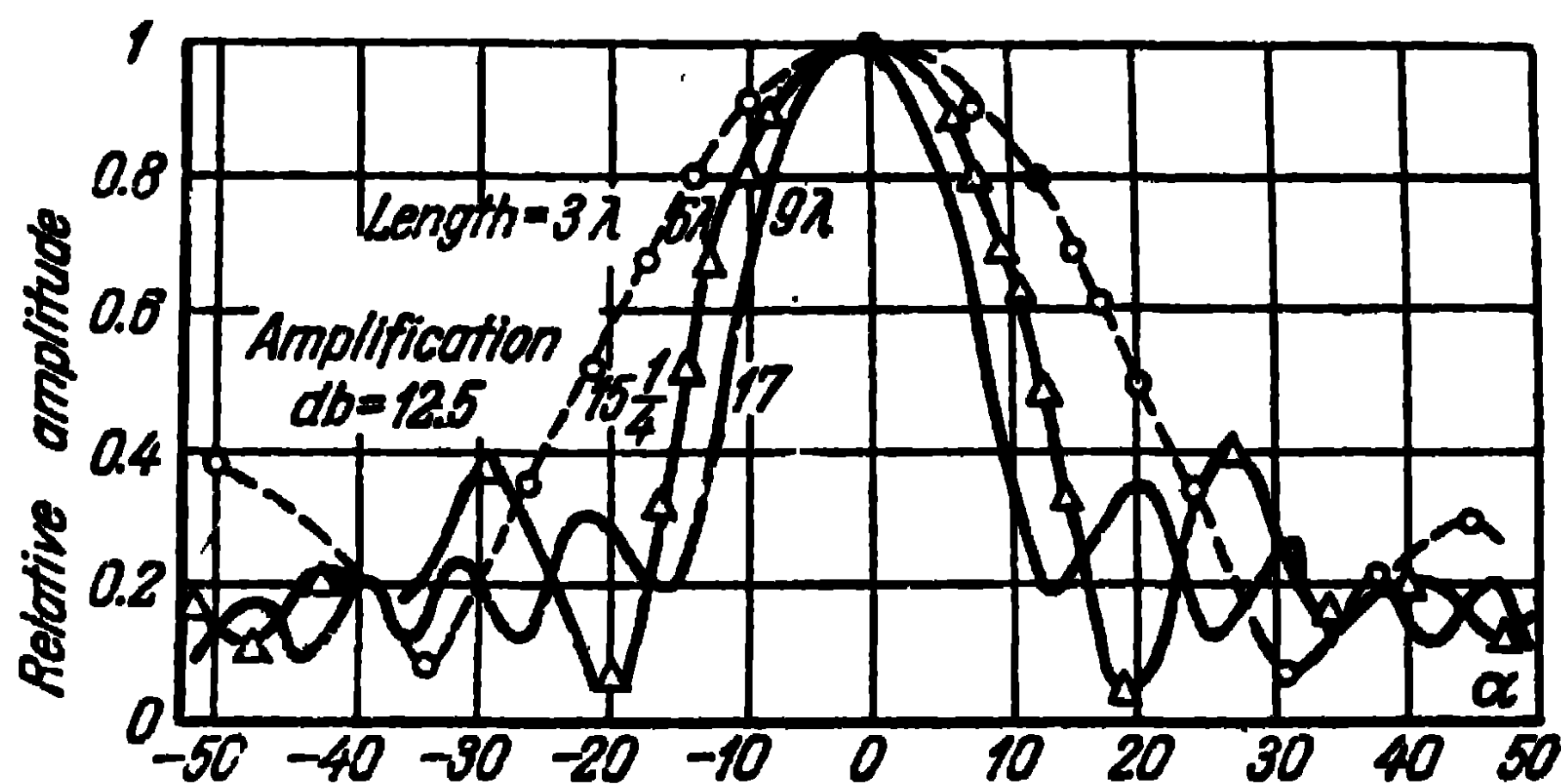


Fig. 10-53. Experimental directional diagrams.

directly into the surrounding space and partly passes into energy of a retarded (surface) wave in the dielectric rod. The latter part of the energy is conveyed by the retarded wave to the extremity of the rod where it is radiated, due to a gap in the continuity of the medium.

Thus, the directional diagram of a dielectric rod antenna of uniform cross section can be said to be formed by the radiation of energy in two sections: in the section of the transition from the metal waveguide to the dielectric waveguide (rod) and at the end of the dielectric waveguide. Since the field amplitude of the retarded wave diminishes exponentially away from the rod in a radial direction, the field amplitude distribution of the radiating surface at the end of the rod is pointed towards the axis, the radiation from the end of the rod being highly directional and without lobes [62]. On the other hand, the radiation at the junction of the metal and dielectric waveguides originates (in the main) from an area equal to that of the waveguide cross section and has a low directivity. Interfering

with one another, the two radiations form a directional diagram of the antenna depending on the length of the rod as well as on its diameter.

If the diameter of the rod is large in comparison with the wave-length, the larger part of the energy passes into energy of a slow wave and the smaller part is radiated directly at the junction of the waveguides. But due to the great deceleration of the wave, the amplitude of the field decreases more sharply as we move away from the rod and the radiating area at the end of the rod diminishes, that

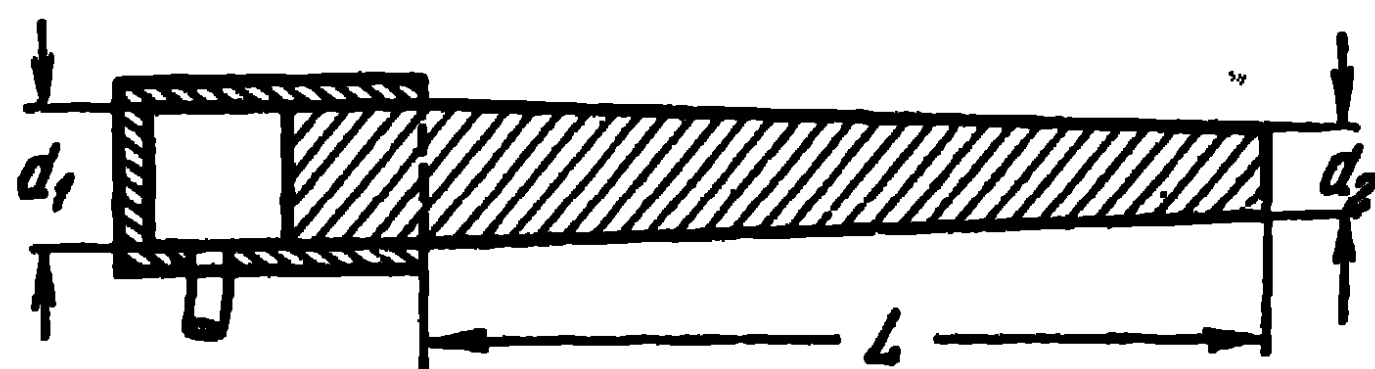


Fig. 10-54. Conical dielectric antenna.

leads to the widening of the major lobe of the resulting directional diagram and at the same time to the relative decrease of the size of the minor lobes.

If the diameter of the rod is small in comparison with the wave-length, the larger part of the energy is radiated directly at the junction of the two waveguides and the smaller part passes into energy of a slow wave and is radiated at the end of the dielectric rod. However, since the phase velocity of the wave in the rod approaches that of light, the decrease of field amplitude away from the rod becomes low, the radiating area at the end of the rod increases, which leads to a more directional radiation from the end of the waveguide. As a result, the width of the major lobe of the directional diagram narrows down, but the relative magnitude of the minor lobes increases.

Thus, it is desirable that the diameter of the rod at the junction of the two waveguides should be large relatively to the wave-length in order that the phase velocity of the wave should be small and the larger part of the delivered energy should pass into energy of a slow wave in the rod. At the same time the diameter of the rod at its end should be small in comparison with the wave-length, in order that the phase velocity of the wave should approach the velocity of light and the radiating area at the end of the rod should increase.

This leads us to the idea of a dielectric antenna with a variable (by jumps or continuous) cross section. Fig. 10-54 shows the structure of a conical rod antenna of circular

section. It is readily seen that the conical part of the antenna can span either the whole length of the antenna or only part of it, the other part remaining uniform.

Fig. 10-55 shows a dielectric rod antenna [63] of rectangular cross section linearly tapering along a little over half the length of the rod (the length of the rod being 6λ). At the beginning, the rod has a square section of side $\lambda/2$ and at the end, a rectangular section of sides $\lambda/2$ and $\lambda/4$. The same figure shows the curve of the wave phase velocity measured at various sections of the rod as well as the experimental directional diagram. We see that the phase

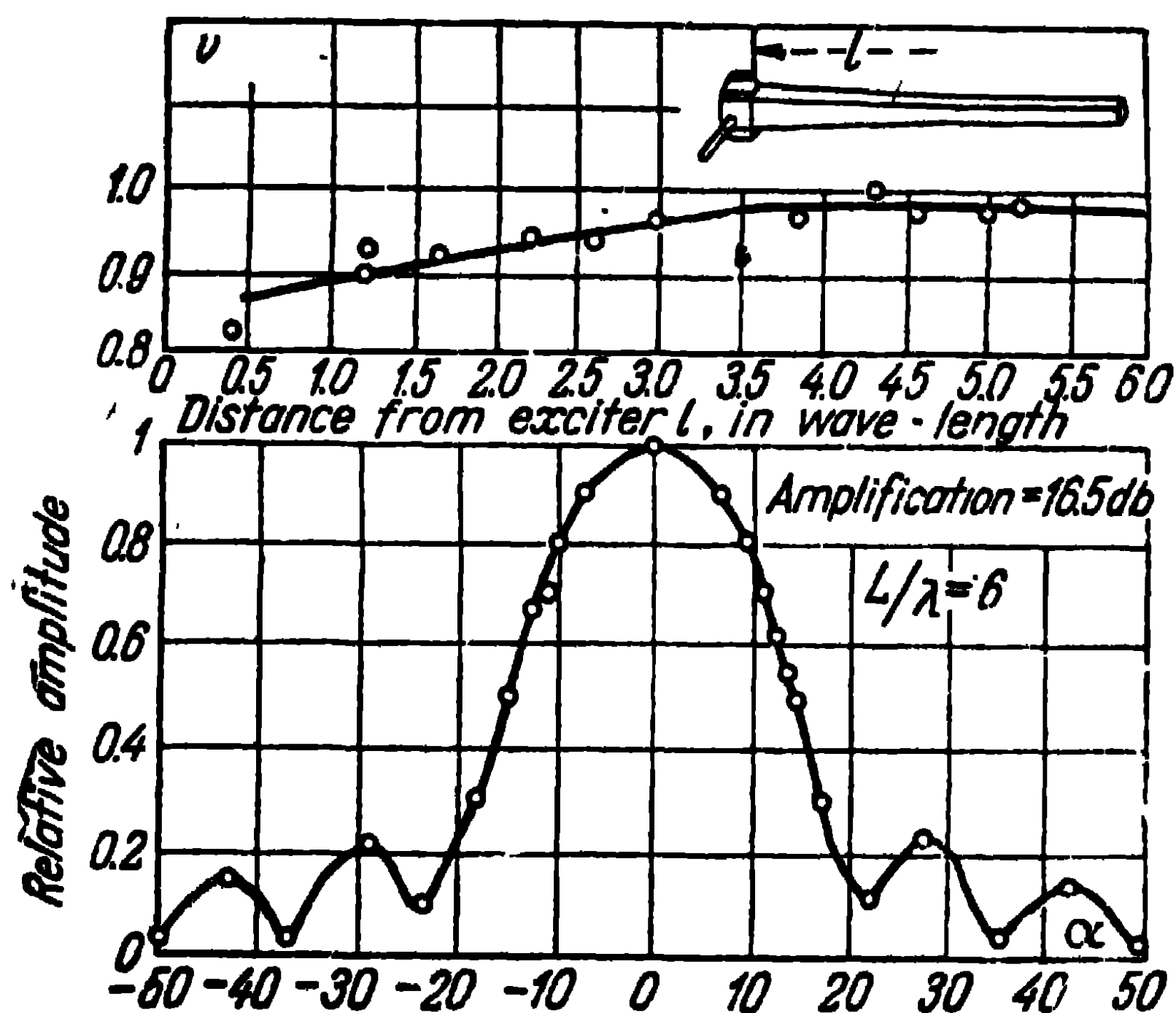


Fig. 10-55. Directional diagram of a tapering antenna of rectangular section.

velocity in the tapering part of the rod changes from section to section in accordance with the linear law, remaining constant in the uniform portion of the rod. The minor lobes are insignificant as compared with those in Fig. 10-53.

A conical antenna of circular cross section the tapering part of which extends approximately as far as the middle of the length of the rod has nearly the same directional diagram; the overall length of the rod equals 6λ . The diameter of the rod decreases from $d_1 = 0.5\lambda$ to $d_2 = 0.3\lambda$.

A few more points should be mentioned regarding the properties of dielectric rod antennas. To begin with, it should be pointed out that several dielectric antennas can

be connected in parallel, thus forming a co-phased array giving a high-directional radiation. Owing to the fact that surface waves are propagated along the rods and the field of the waves diminishes exponentially as we move away from the rods in radial directions, the interaction between the rods in the array is insignificant. They operate almost independently one from the other and the directive gain in the main direction is proportional to the number of elements in the system, i.e., to the number of rods. Secondly, since rod dielectric antennas have no resonant elements, they themselves have a wide pass-band. The width of the pass-band of a dielectric antenna is conditioned by the resonant properties of the exciting element (of the dipole in a metal waveguide). Thirdly, the dielectric from which the antenna is made should have low losses, otherwise the efficiency of the antenna will be poor and, in addition, the exciting dipole in a metal waveguide should be arranged, as shown in Figs. 10-50 and 10-54, outside the dielectric. This leads to an increase of the efficiency of the antenna, due to the fact that the higher modes generated by the dipole are attenuated in the vicinity of the dipole and do not penetrate into the dielectric medium.

10-10. Horn Antennas

Horn antennas, and in particular antennas formed by the open end of a rectangular or circular waveguide find application in the centimetre wave range. Antennas of this type are utilised independently or as radiators in more complex antennas, such as lens antennas and parabolic antennas.

Let us first of all consider the radiation from the open end of a rectangular waveguide, excited by an H_{01} wave. Let a segment of rectangular waveguide be shorted out at one end and open at the other and let it be excited by an elementary dipole (Fig. 10-56). On reaching the open end of the waveguide, the electromagnetic energy conveyed by the H_{01} wave is partly reflected and partly passes into space and is radiated in all directions. The radiation from the open end of the waveguide can be calculated by means of the equivalency theorem (principle). Enclosing the waveguide with a surface s adjoining its outer surface, one can neglect the radiation of the currents flowing on the shadow sides of the waveguide in view of their low intensity

and take account only of the radiation of the equivalent currents on the illuminated portion of the surface s , i.e., at the open end of the waveguide.

The equivalent currents on the surface s can be calculated from the expressions:

$$\mathbf{J}^e = [\mathbf{H}, \mathbf{n}], \quad \mathbf{J}^M = [\mathbf{n}, \mathbf{E}],$$

where \mathbf{n} is the perpendicular to the surface s , external relatively to the point of observation.

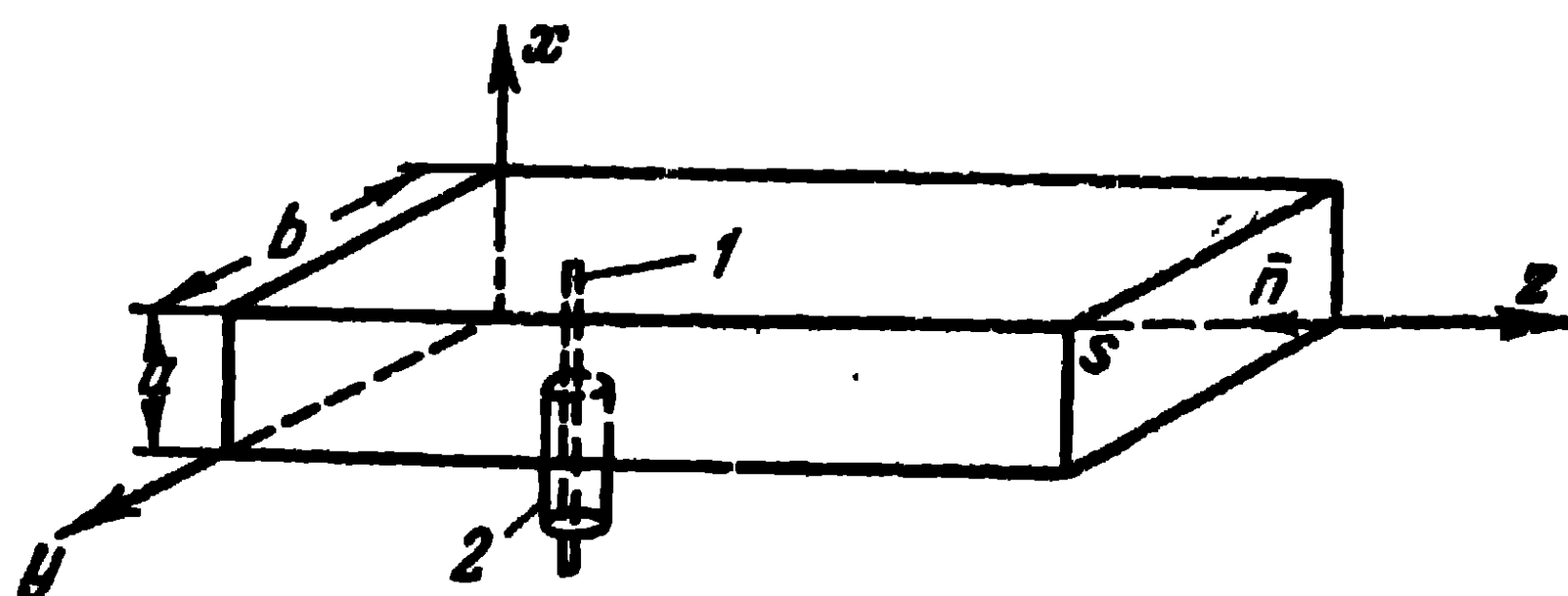


Fig. 10-56. Radiation from the end of a rectangular waveguide:

1—antenna; 2—coaxial cable

To simplify the problem, the field at the output aperture of the waveguide is assumed unexcited and expressed as:

$$\begin{aligned} E_{x01} &= B \frac{k^2}{i\omega\epsilon} \sin\left(\frac{\pi}{b} y\right) e^{-i\alpha_{01}z}; \\ H_{y01} &= -B i\alpha_{01} \sin\left(\frac{\pi}{b} y\right) e^{-i\alpha_{01}z}; \\ H_{z01} &= -B \frac{\pi}{b} \cos\left(\frac{\pi}{b} y\right) e^{-i\alpha_{01}z}. \end{aligned}$$

Then the equivalent surface currents are expressed as:

$$J_x^e = -H_{y01}, \quad J_y^M = -E_{x01}$$

and their ratio equals:

$$\frac{J_y^M}{J_x^e} = \frac{120\pi}{\sqrt{1 - (\lambda/2b)^2}}.$$

Taking this into consideration and integrating the radiated field over the open end of the waveguide as was done in

Paragraph 4-7, we obtain the expression of the radiated field in the plane of the electric vector

$$E_{(x, z)} = -A_1 \frac{60R^2 a b^2}{\pi^2 r_0} [1 + \sqrt{1 - (\lambda/2b)^2} \cos \alpha] \times \\ \times \frac{\sin \left(\frac{ka}{2} \sin \alpha \right)}{\frac{ka}{2} \sin \alpha} e^{-ikr_0} \quad (10-30)$$

and in the plane of the magnetic vector

$$E_{(y, z)} = -A_2 \frac{60a}{r_0} [\sqrt{1 - (\lambda/2b)^2} + \cos \beta] \times \\ \times \frac{\cos \left(\frac{kb}{2} \sin \beta \right)}{(\lambda/2b)^2 - \sin^2 \beta} e^{-ikr_0}. \quad (10-31)$$

In these expressions, r_0 is the distance from the centre of the aperture to the point of observation of the field; α and β are the angles between the direction r_0 and the z -axis in the xz - and yz -planes respectively.

The width of the directional diagram at half-power in the electric plane is defined by the same expression as for an ideal plane antenna, i.e.,

$$2\alpha_{1/2} = 51^\circ \frac{\lambda}{a}. \quad (4-45)$$

Thus, for standard waveguides, we have a) $\lambda_{\text{oper}} \approx 3.4$ cm, $a = 1.28$ cm, $b = 2.86$ cm and $2\alpha_{1/2} = 136^\circ$; b) $\lambda_{\text{oper}} = 10.5$ cm, $a = 3.4$ cm, $b = 7.2$ cm and $2\alpha_{1/2} = 157^\circ$.

The width of the directional diagram at the radiation zeros in the electric plane is expressed as:

$$\sin \alpha_0 = \frac{\lambda}{a}. \quad (4-42)$$

However, for standard waveguides $\frac{\lambda}{a} > 1$, therefore the directional diagram in the plane of the electric vector has no zeros.

In the plane of the magnetic vector, the width of the directional diagram at half-power is expressed as:

$$2\beta_{1/2} = 67^\circ \frac{\lambda}{b}, \quad (4-52)$$

and the width of the directional diagram at the radiation zeros as:

$$\sin \beta_0 = 1.5 \frac{\lambda}{b},$$

derived from (4-51).

For standard waveguides $\lambda/b > 1$, hence the directional diagrams in that plane likewise have no zeros.

As seen from (10-30) and (10-31), when the operating wave-length approaches the critical one ($\lambda \rightarrow 2b$), the radiation in the opposite

direction ($\alpha = \beta = 180^\circ$) increases due to the fact that when $\lambda \rightarrow 2b$, the ratio J_y^M/J_x^e tends towards infinity, i.e., in that case, we get a predominance of the electric field at the open end and, for small a/λ , the directional diagram in the E-vector plane becomes non-directional.

As regards the H-vector, in that case the directional diagram acquires the shape of a "figure of eight":

The expressions (10-30) and (10-31) are approximate since they do not take account of the distortion of the field during reflection of the electric waves at the open end of the waveguide and their branching off to the outer surface of the waveguide.

However, in practice these expressions are found to give sufficiently accurate results.

Fig. 10-57 gives the power directional diagrams in the E- and H-planes. The solid curves are the calculated ones

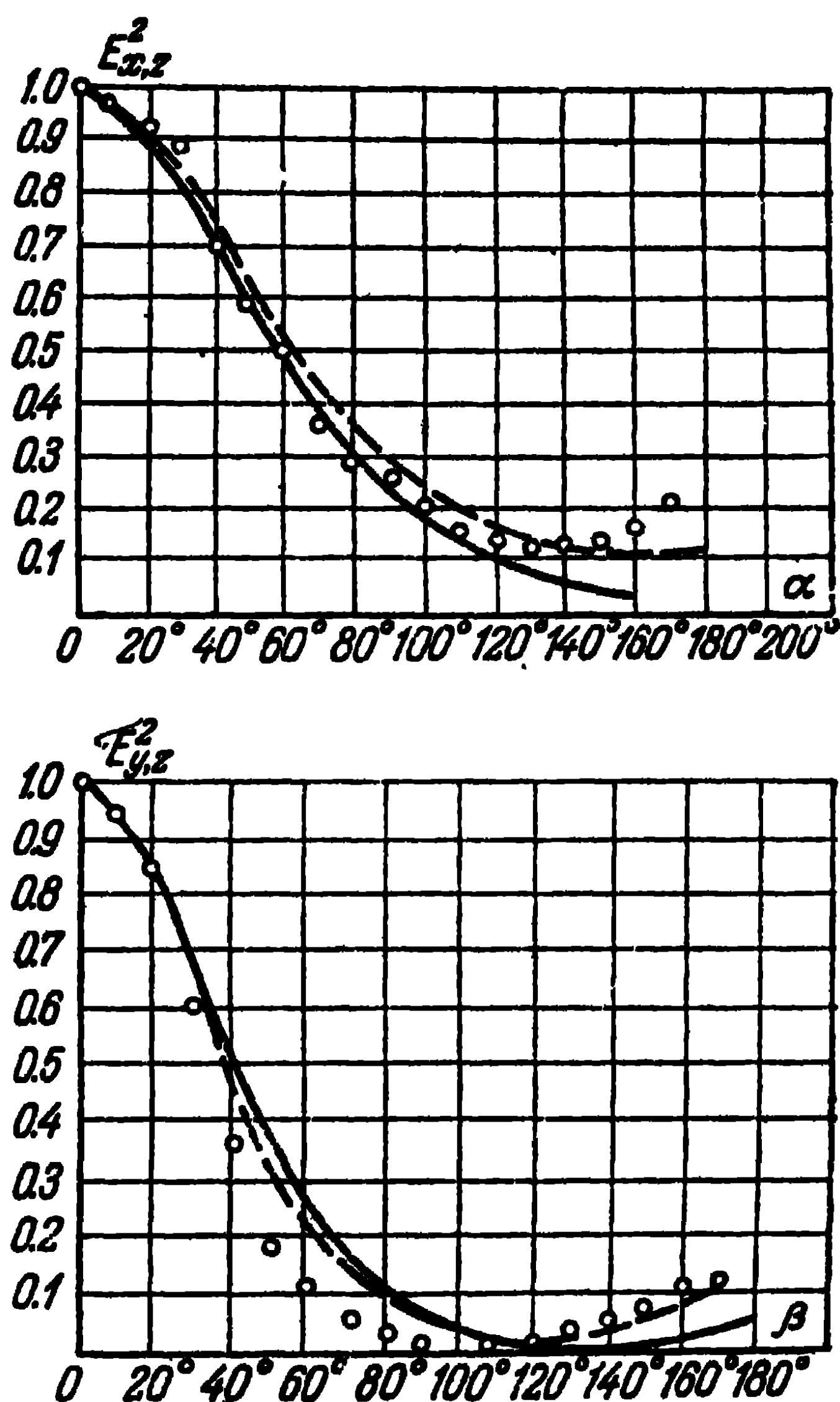


Fig. 10-57. Directional diagrams of rectangular waveguide:

$$\lambda = 3.2 \text{ cm}; \quad \frac{a}{\lambda} = 0.32; \quad \frac{b}{\lambda} = 0.71.$$

and the small circles correspond to the measured values. The broken line curves have been constructed with an account of the reflection from the open end of the waveguide.

The directive gain of the open end of a rectangular waveguide can be calculated from the expression

$$D \approx \frac{8}{\pi} \frac{[1 + \sqrt{1 - (\lambda/2b)^2}]^2}{\sqrt{1 - (\lambda/2b)^2}} \frac{ab}{\lambda^2}. \quad (10-32)$$

As a radiator, the open end of a waveguide has a fairly wide pass-band. The pass-band is, on the whole, determined by the device which excites the waveguide, i.e., the radiator connected to the coaxial cable. In order to widen the pass-band, this radiator usually is made thick and has a special shape, as shown in Chapter Nine (Fig. 9-16, *b*).

To decrease the reactive part of the input resistance of the radiator, its length is taken close to $\lambda/4$.

The active part of the radiator input resistance is adjusted by changing d (the distance from the radiator to the short-circuiting plunger) or the appropriate choice of the distance between the radiator y_0 and the lateral wall of the waveguide. Indeed, if a travelling wave is set up from the radiator towards the open end of the waveguide, the active part of the radiator input resistance can be determined from the expression

$$R_{in} = \frac{\sqrt{\mu/\epsilon}}{\sqrt{1 - (\lambda/2b)^2}} \frac{2l^2}{ab} \sin^2 \left(\frac{2\pi}{\lambda_w} d \right) \sin^2 \left(\frac{\pi}{b} y_0 \right),$$

where l is the effective length of the dipole. Thus, the equality between the radiator input resistance and the wave impedance of the feed coaxial cable, i.e., complete matching, can be achieved by the proper choice of d and y_0 .

Another circuit of the exciting radiator is shown in Fig. 10-58, where use is made of a transverse stub, which makes the radiator rigid, electrically more reliable, and widens its pass-band. Other circuits for connecting coaxial cables to waveguides are also applied.

To lower the reflection from the open end of the waveguide and increase the directivity, horn radiators are employed. Thus, Fig. 10-59 shows a so-called sectoral horn flared in the H -plane, in which the dimension b gradually increases.

The wave arising in a sectoral horn is similar to the wave in a rectangular waveguide and the picture of its

field is shown in Fig. 10-60. A sectoral horn differs from a waveguide in that the wave front in it forms a cylindrical surface, the phase velocity of the wave is a variable quantity which is a function of the ratio b/λ and the field at a great

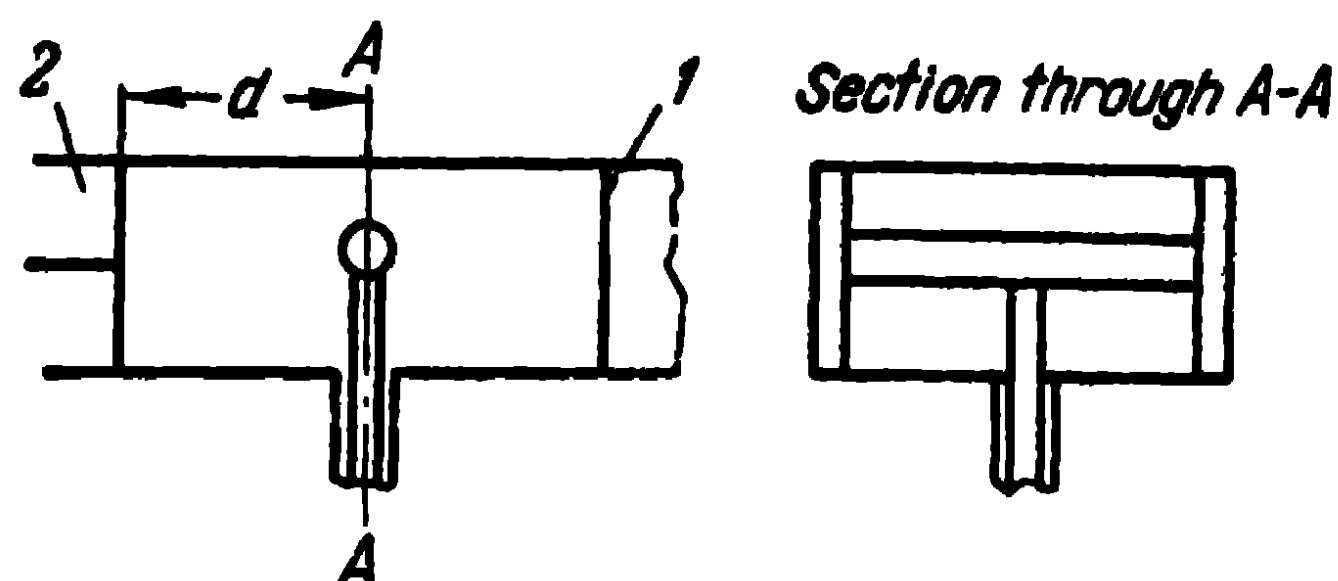


Fig. 10-58. Circuit of excitation by means of a transverse stub:

1—matching diaphragm; 2—plunger.

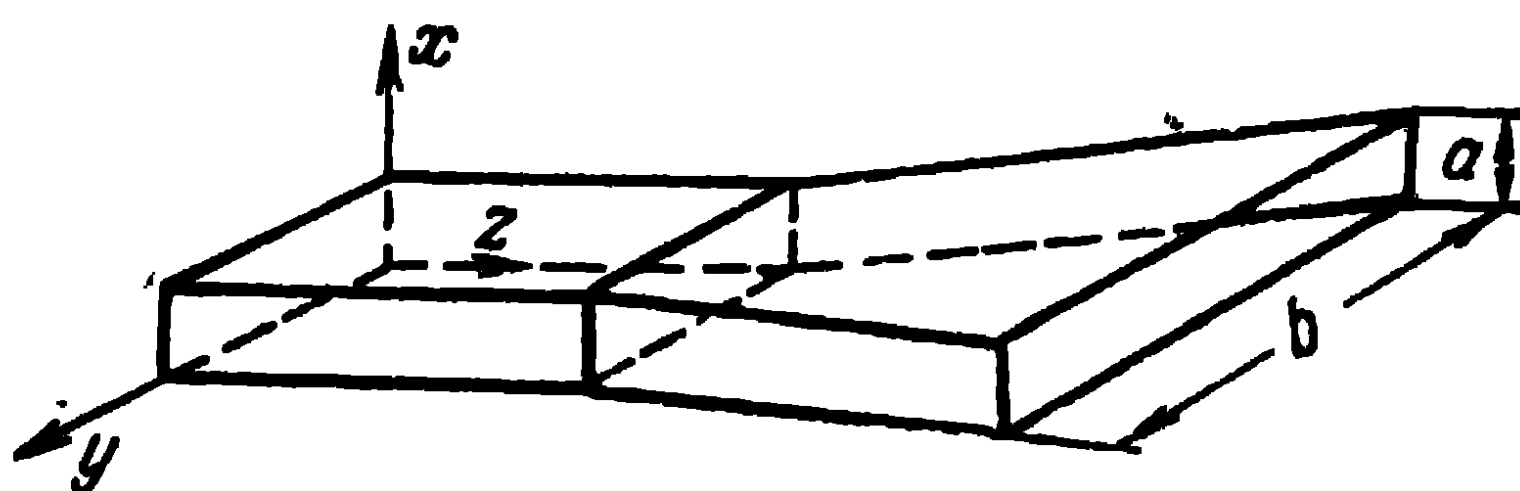


Fig. 10-59. Sectoral horn, widening in the H -plane.

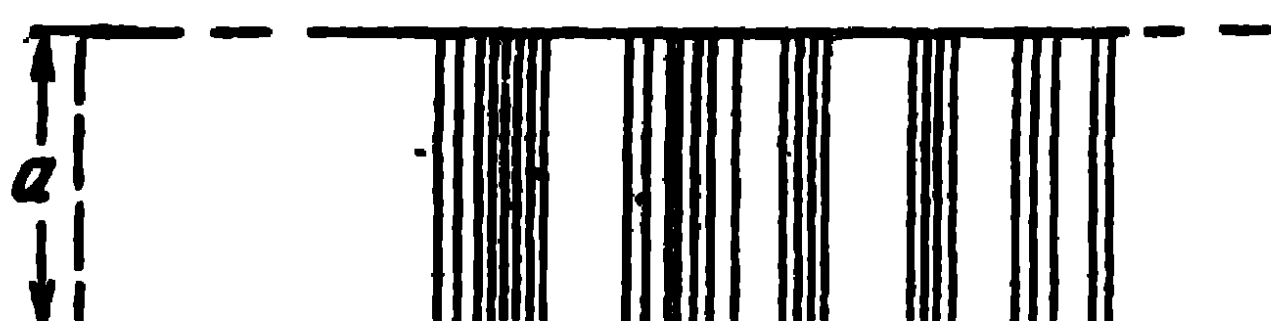
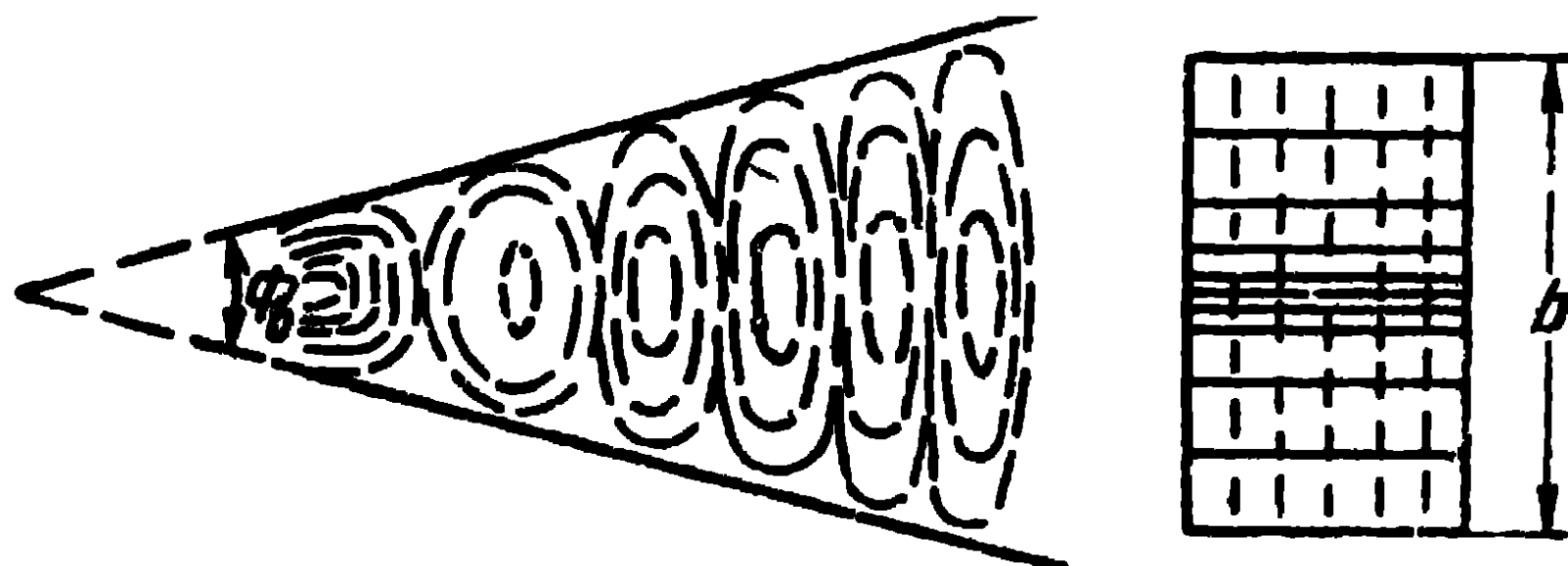


Fig. 10-60. The field in a sectoral horn.

distance from the throat of the horn assumes the character of a purely transverse wave. The wave phase velocity is approximately expressed as $v = \frac{v_1}{\sqrt{1 - (\lambda/2b)^2}}$ and in the vicinity of the horn opening, it approaches the velocity of light, which leads to a decrease of the reflection of the wave from the radiating surface of the horn.

If the flare angle of the horn Φ_0 is small, the wave front at the opening is approximately plane and the radiation characteristic in the yz -plane can be calculated by means of the expressions (10-31) as well as (4-52) and (4-50). Thus, the major lobe of the directional diagram narrows down by about as many times as the dimension b of the horn opening increases relatively to the dimension b of the opening of a rectangular waveguide.

However if the flare angle of the horn Φ_0 is large, the wave front at its opening differs considerably from a plane

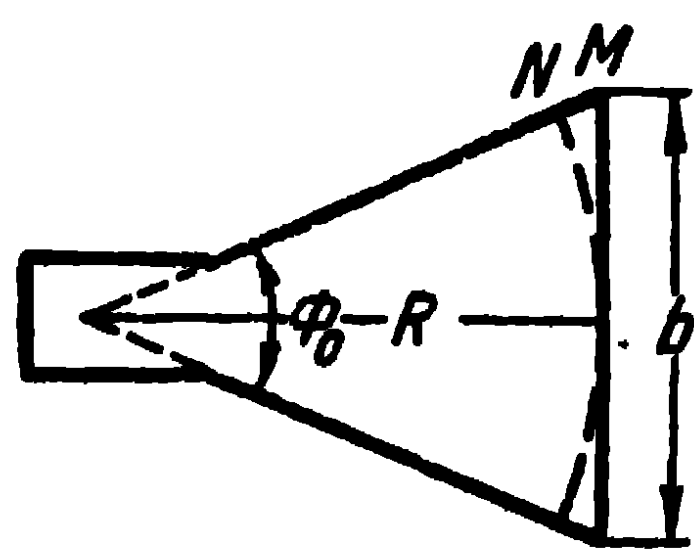


Fig. 10-61. Determining the distortion of the field phase at the horn opening.

one and the radiation instead of being concentrated in a narrow beam will, on the contrary, be dissipated in all directions (the directional diagram of the horn will be wide).

The difference of phase of the field in the middle and at the edge of the opening can be determined from the approximate expression obtained from the geometrical dimensions in Fig. 10-61

$$\psi = \frac{2\pi}{\lambda} MN \approx \frac{\pi b^2}{4\lambda R} = \frac{\pi}{2} \frac{b}{\lambda} \tan \frac{\Phi_0}{2}, \quad (10-33)$$

where R is the length of the horn.

Thus, the field phase at the horn opening changes in accordance with the square law. As revealed by detailed calculations, maximum radiation in the principal direction, at a prescribed length of the horn, occurs when the difference of the field phase $\psi = 135^\circ$. This is due to the fact that an increase of the flare angle of aperture Φ_0 leads, on the one hand, to an increase of the relative dimension of the horn b/λ and a narrowing of the directional diagram, and, on the other hand, to an increase of the difference of the field phase ψ and a widening of the directional diagram. As a result of the action of these opposed factors, the directive gain is found to be at a maximum precisely when the angle of the difference of phase $\psi = 135^\circ$. The horn corresponding to the condition $\psi = 135^\circ$ is referred to as optimum horn.

The directional diagram of an optimum horn and of horns in which $\psi < 135^\circ$, can be calculated from the expressions (10-30) and (10-31).

Apart from sectoral horns flared in the H -vector plane, sectoral horns flared in the E -vector plane are also employed (Fig. 10-62). In that case, the width of the directional diagram in the H -plane is the same as at the open end of a waveguide; and in the E -plane, the width of the directional diagram decreases as the dimension a of the horn increases, provided the flare angle Φ_e is taken small enough. In that case, the difference of phase of the field corresponding to the optimum is $\psi=90^\circ$ and the directional diagram in the plane electric vector can be calculated from (10-30).

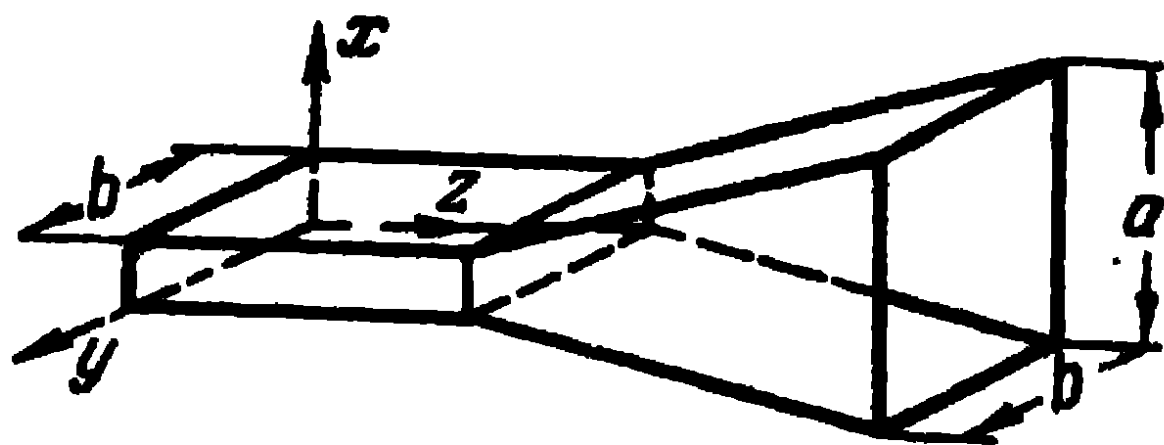


Fig. 10-62. Sectoral horn flared in the E -plane.

Pyramidal horns of rectangular cross section (Fig. 10-63) are widely used. These horns enable to narrow down the directional diagrams in the H -plane as well as in the E -plane.

In a pyramidal horn we get the formation of a spherical wave, the phase velocity of the wave is variable and as it moves towards the open end of the horn, the wave front

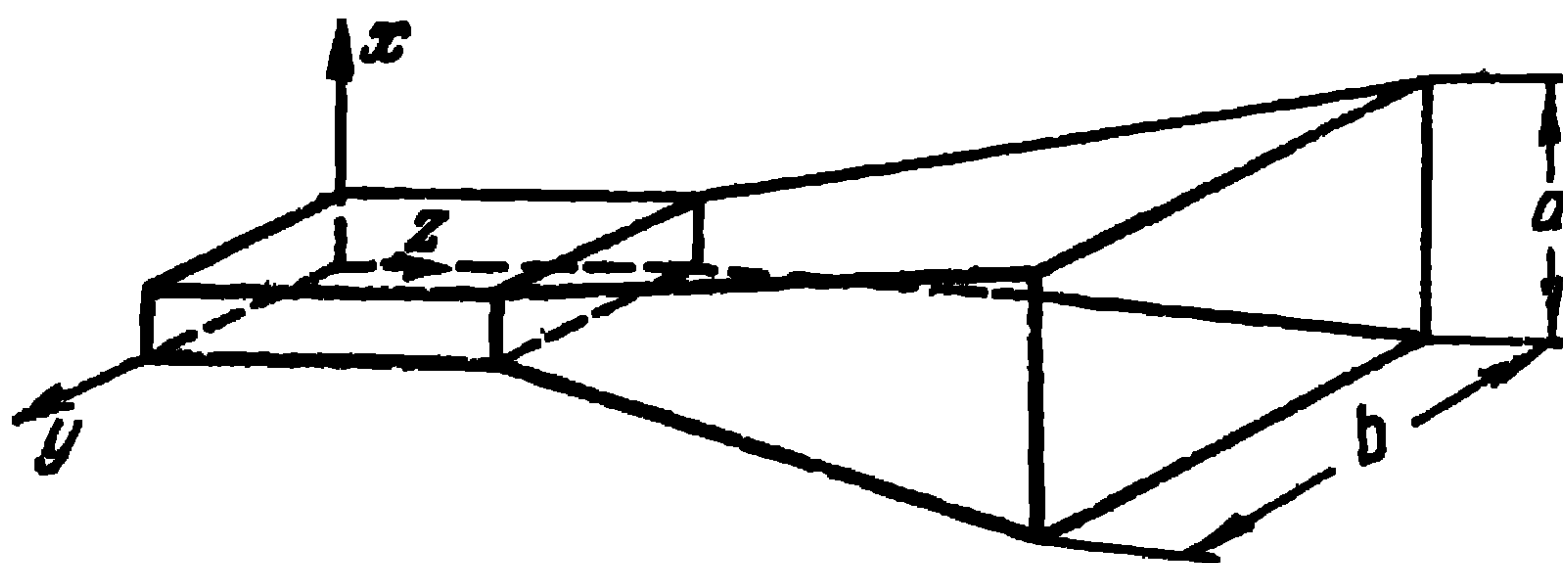


Fig. 10-63. Pyramidal horn.

turns into a plane one with a phase velocity approaching that of light. As a result, the reflection of the wave from the opening of the horn is insignificant: the horn matches the waveguide to open space.

The phase distortions of the field at the opening of a pyramidal horn can be determined from the expression (10-33) in the H -plane and from an analogous expression (replacing b by a) in the E -plane. If the distortion of the field phase at the opening is insignificant (ψ small), the directional diagrams of the horn differ but little from the directional diagrams of the co-phased plane and can be calculated from (10-30) and (10-31).

However, small phase distortions necessitate the use of long horns. To reduce the length of the horn, the distortion tolerated for the field phase amounts to $\psi=135^\circ$ in the H -plane and $\psi=90^\circ$ in the E -plane. As indicated above, a horn of this kind is referred to as an optimum horn and a sufficiently accurate definition of its directional diagram is given by the expressions (10-30) and (10-31).

As regards the directive gain of sectoral and pyramidal optimum horns, it can be approximately calculated from (10-32) which, due to the fact that $\lambda/2b \ll 1$, can be written as:

$$D = \frac{4\pi ab}{\lambda^2} k_1, \quad (10-34)$$

where $k_1=0.81$.

The coefficient $k_1=0.81$ applies to a co-phased surface. If we take into account that the field phase at the horn opening is not constant but changes in accordance with the square law, it will be found that this coefficient k_1 equals 0.64.

Fig. 10-64 shows the directional diagram of a pyramidal horn with dimensions $a/\lambda=9.4$, $b/\lambda=11.6$ and $R/\lambda=41$.

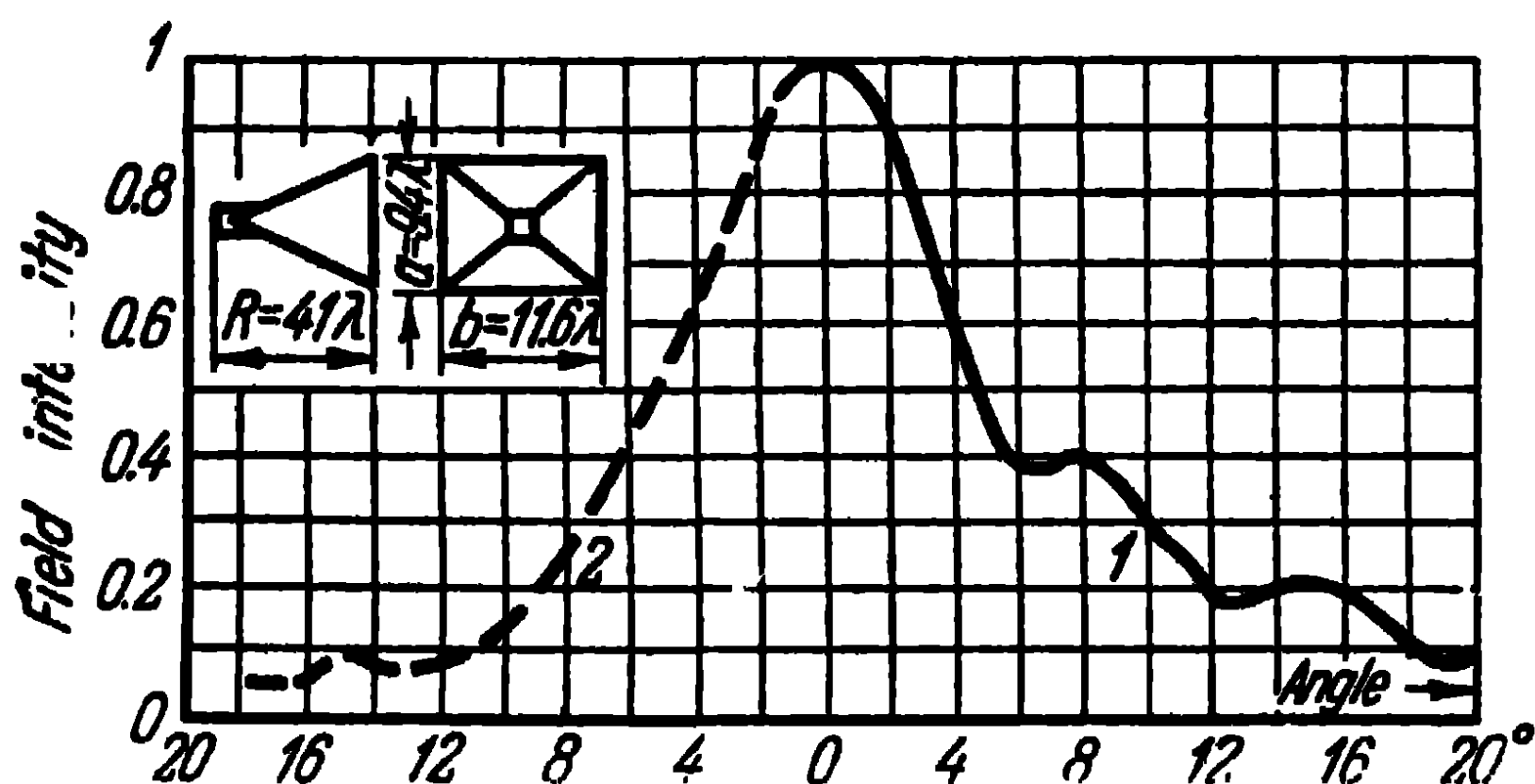


Fig. 10-64. Directional diagram of a pyramidal horn:
1—in the E -plane; 2—in the H -plane.

The directive gain of this horn is of the order of $D \approx 900$ (28 db). The directional diagram in the H -plane is characterised by relatively small side lobes, which is due to the co-sinusoidal distribution of the field amplitude in the H -plane of the horn.

Apart from horns of a rectangular cross section, horns of a circular cross section, i. e., conical horns, also find application. Horns of this kind are formed by flaring the open end of a circular waveguide excited by an H_{11} wave. The

radiation of a conical horn is similar to that of a pyramidal one and it likewise has optimum dimensions, which can be regarded as intermediate between those of optimum E -plane and H -plane sectoral horns. The same directive gain corresponds approximately to the same dimensions of optimum pyramidal and conical horns.

10-11. Slow Phase Velocity Impedance Antennas

Apart from director, helical and polyrod antennas, which belong to the class of slow phase velocity axial radiation antennas, slow phase velocity impedance antennas (antennas of surface waves) have also found application in recent years in the centimetre wave range. An antenna of this kind is shown in Fig. 10-65.

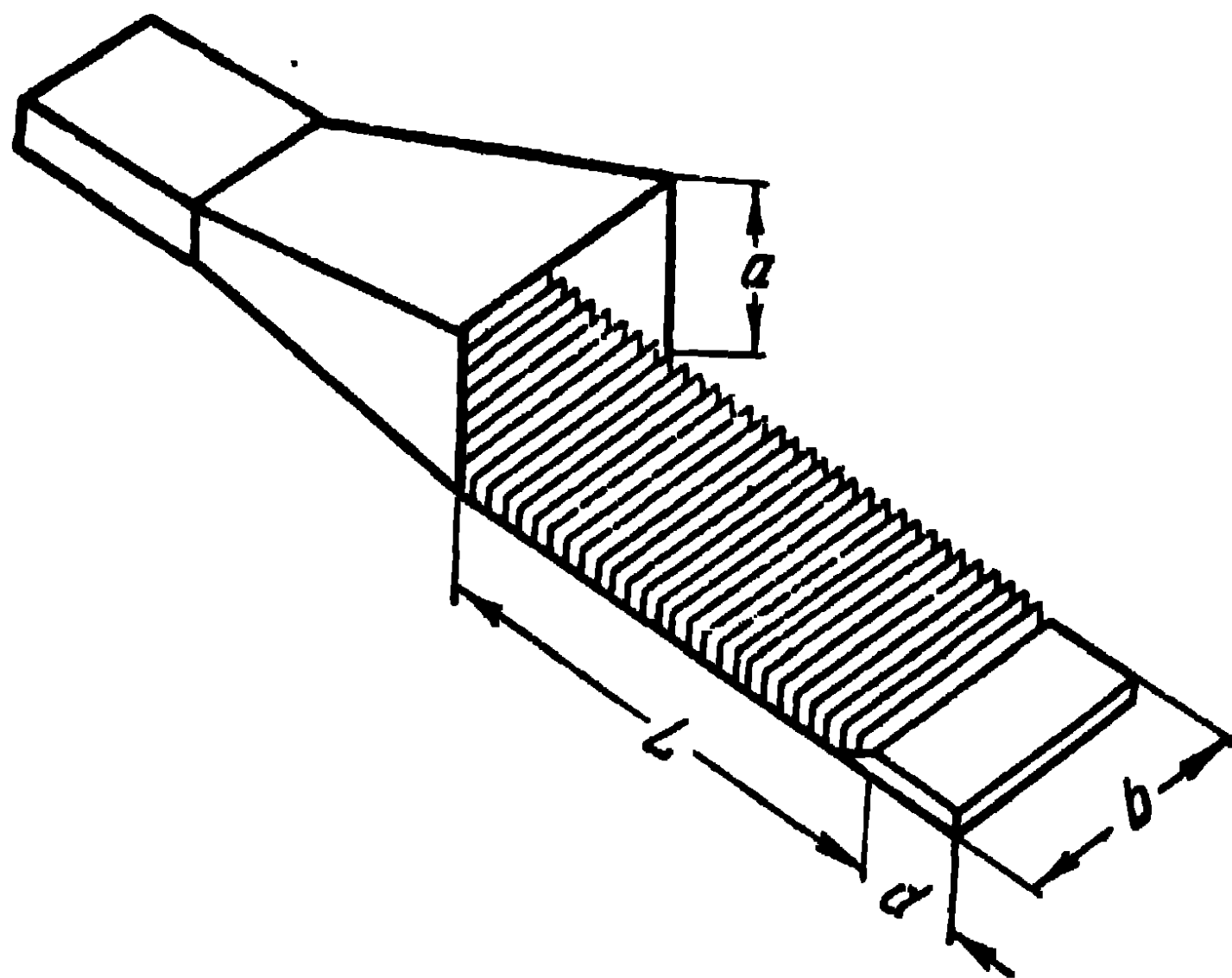


Fig. 10-65. Impedance antenna.

The antenna consists of a ridged surface of length L and width b , excited by a pyramidal horn. The surface wave excited by the horn is propagated along the impedance structure without change of the field amplitude (taking no account of energy losses in the structure). On reaching the end of the structure, the energy conveyed by the slow wave is radiated. Moreover, part of the energy is radiated on leaving the horn. The proper choice of the length L of the impedance structure, depth of the grooves l formed by the ridges of the structure and dimension a of the opening of the horn produces a rather intensive radiation in the direction coinciding with the direction of motion of the wave in the antenna. As shown by theory and experimental investigations impedance antennas radiate in a way similar to polyrod antennas, so that the corresponding expressions of travelling-wave antennas may be applied to them.

Let us investigate the formation of the surface wave. Let the magnetic intensity of the surface wave be expressed as:

$$H_y = H_0 e^{-px - ihz}, \quad (10-35)$$

i. e., assume that the H vector coincides in direction with the y -axis and does not depend on that coordinate. The dependence of the field on the x -coordinate is supposed to be exponential (p is a real positive quantity). The field is assumed to depend on the z -coordinate in accordance with the travelling-wave law (h is a real positive quantity). Since the magnetic intensity must satisfy the wave equation $\frac{\partial^2 H_y}{\partial x^2} + \frac{\partial^2 H_y}{\partial z^2} + k_0^2 H_y = 0$, we get the following relation between p and h :

$$p = \sqrt{h^2 - k_0^2}. \quad (10-36)$$

Since p is a real quantity, $h > k_0$, and the phase velocity of the wave $v = \frac{\omega}{h}$ is lower than the velocity of light

$$v_1 = \frac{\omega}{k_0}.$$

The electric field intensity is defined from the equation $\text{rot } \mathbf{H} = i\omega\epsilon_0 \mathbf{E}$ and has only two components

$$\left. \begin{aligned} E_x &= \frac{h}{\omega\epsilon_0} H_0 e^{-px - ihz}, \\ E_z &= -\frac{p}{i\omega\epsilon_0} H_0 e^{-px - ihz}. \end{aligned} \right\} \quad (10-37)$$

The transverse component of the electric field intensity E_x is in phase with the magnetic intensity H_y and the energy flow density in the direction of the z -axis $S_z = \frac{1}{2} E_x H_y^*$ is a real quantity. The longitudinal component of the electric field E_z has a phase displacement of 90° relatively to the magnetic field intensity H_y , and the energy flow density in the direction of the x -axis $S_x = -\frac{1}{2} E_z H_y^*$ is an imaginary quantity.

For the slow wave mentioned above to be maintained, the surface impedance of the structure should be defined by the quantity

$$Z = \frac{E_z}{H_y} = -\frac{p}{i\omega\epsilon_0}, \quad (10-38)$$

and since ρ is a real and positive quantity, it must be purely reactive and of an inductive nature.

A surface impedance of this kind can be obtained by means of an infinite ridged structure (Fig. 10-66). Indeed, the intensity of the magnetic field arising inside the ridged structure (in the grooves) has the same component as in surrounding space, viz.,

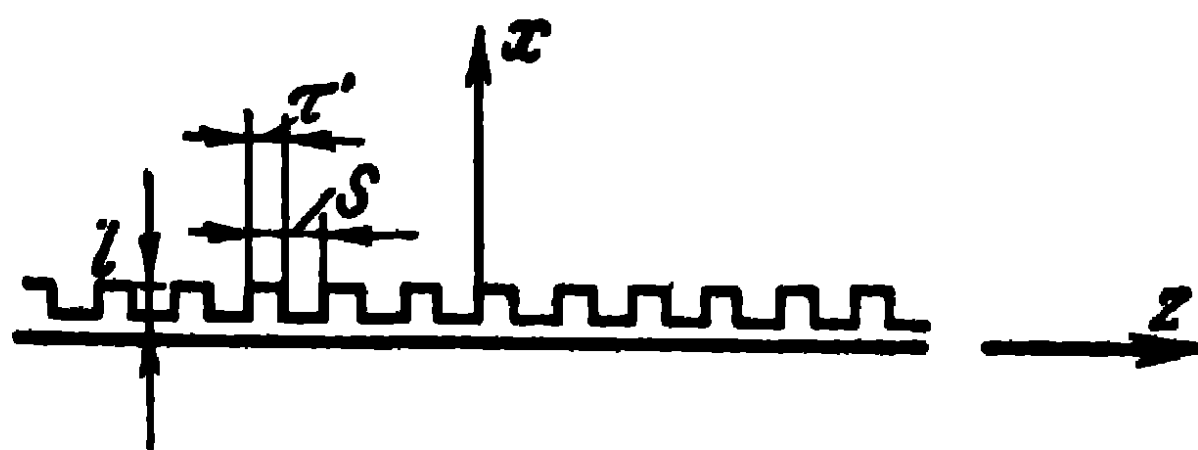


Fig. 10-66. Ridged surface.

$H_{\text{ridge}} = H_{\nu}^{\text{ridge}}$. Assume further that the field inside each cell of the ridged structure does not depend on the z -coordinate. This approximation occurs on condition that

$$h(s + \tau) \ll 1,$$

where s is the width of the groove;
 τ , the width of the rib.

Then the wave equation for the magnetic field intensity will be

$$\frac{\partial^2 H_{\nu}^{\text{ridge}}}{\partial x^2} + k_0^2 H_{\nu}^{\text{ridge}} = 0$$

and its solution will be written as:

$$H_{\nu}^{\text{ridge}} = H_0^{\text{ridge}} \cos k_0 x. \quad (10-39)$$

Hence the components of the electric field intensity will be

$$E_x^{\text{ridge}} = E_{\nu}^{\text{ridge}} = 0$$

and

$$E_z^{\text{ridge}} = -\frac{k_0}{i\omega\epsilon_0} H_0^{\text{ridge}} \sin k_0 x. \quad (10-40)$$

The expressions (10-39) and (10-40) represent a TEM wave in the grooves and satisfy the boundary conditions on the surface of the grooves.

The surface impedance averaged over the period of the ridged structure will be:

$$Z^{\text{ridge}} = \frac{s}{\tau + s} \frac{E_z^{\text{ridge}}}{H_{\nu}^{\text{ridge}}} = -\frac{s}{\tau + s} \frac{k_0}{i\omega\epsilon_0} \tan k_0 l. \quad (10-41)$$

Identifying (10-38) with (10-41), we obtain:

$$\rho = \frac{s}{\tau + s} k_0 \tan k_0 l. \quad (10-42)$$

It follows that in order to maintain a surface wave, the depth of the grooves should be less than a quarter of a wavelength ($k_0 l < 90^\circ$). When $s \rightarrow 0$ or $k_0 l \rightarrow 0$, $p \rightarrow 0$, the phase velocity of the wave approaches that of light and the attenuation of the field intensity in the direction of the x -axis decreases.

Let us now investigate the radiation of the ridged antenna. The directional diagram in the yz -plane is determined by the dimension of the antenna and can be calculated from the corresponding expression for the radiation of a pyramidal horn. In the present case we are interested in the directional diagram of the ridged structure in the xz -plane. Several methods are available for calculating the radiation but the most convenient is to use the equivalent surface currents principle [64]. Turning to Fig. 10-67 and

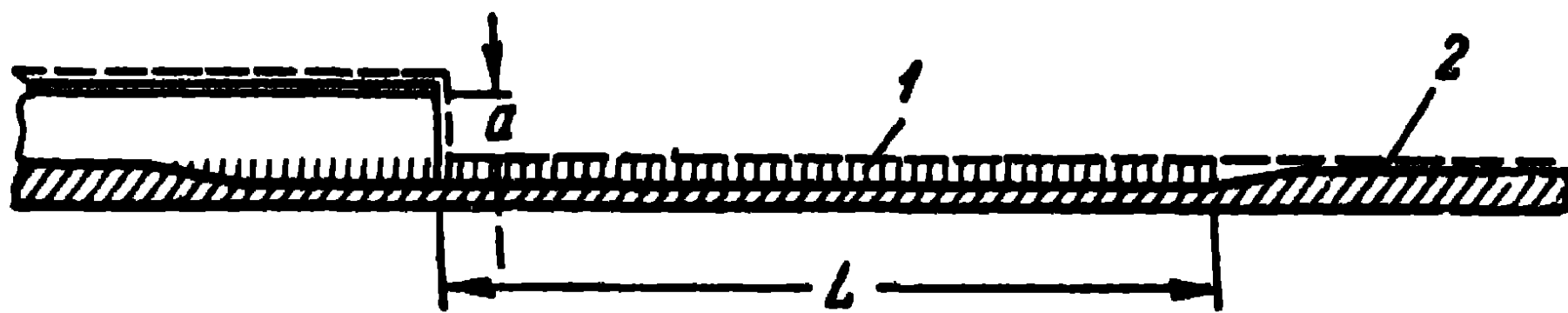


Fig. 10-67. Diagram of the antenna longitudinal section:
1—ridges; 2—conducting surface.

assuming, for simplicity, that the surface behind the ridged structure is an ideal conductor of an infinite length, we can integrate the radiation of the electric and magnetic equivalent surface currents over the contour outlining of the antenna (broken line in Fig. 10-67). At the same time we can, as is usually done, neglect the integration over the external surface of the horn and limit ourselves to the integration over the open end of the waveguide and over the surface $x=l$. However, due to the mirror image of the electric and magnetic surface currents distributed over the surface $x=l$, the radiation of the electric currents is cancelled and that of the magnetic currents is doubled. Thus, the radiated field will be defined by the double value of the magnetic surface currents distributed over the surface of the ridged structure and the radiation of the electric and magnetic surface currents distributed over the open end of the waveguide and over its mirror image relatively to the $x=l$ plane.

In case of adequate matching of the ridged structure to the horn, the larger part of the energy delivered to the

open end of the waveguide (horn) passes into energy of the surface wave and the smaller part is radiated directly. Hence, the radiation is, on the whole, determined by the surface magnetic currents J_y^M of the ridged structure and the directional diagram is expressed as:

$$f(\alpha) = \frac{\sin \frac{\pi L}{\lambda} \left(\frac{v_1}{v} - \cos \alpha \right)}{\frac{\pi L}{\lambda} \left(\frac{v_1}{v} - \cos \alpha \right)} \quad (10-29)$$

moreover, the maximum directivity of the radiation occurs for the condition

$$\frac{L}{\lambda} = \frac{1}{2 \left(\frac{v_1}{v} - 1 \right)} \quad (4-56)$$

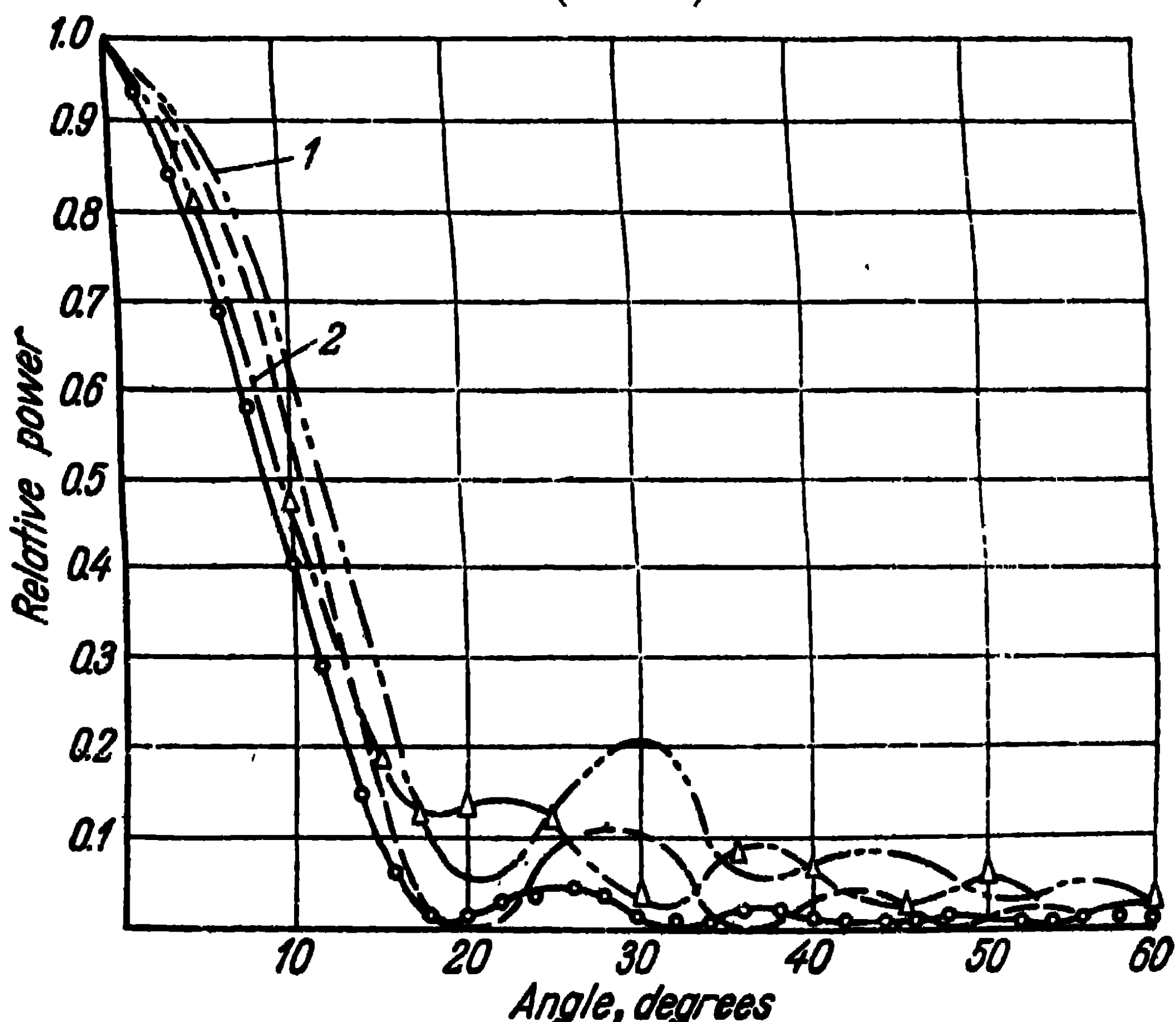


Fig. 10-68. Directional diagrams of impedance antenna:
1—exciter and surface are in phase; 2—exciter and surface are in antiphase.

Fig. 10-68 shows the theoretical and experimental directional diagrams of an antenna of length $L=7.33 \lambda$, in which the condition of the optimum (4-25) is observed. The solid curve is the experimental one and the broken curve, the calculated one, no account being taken of the radiation

from the open end of the waveguide. The same figure shows two calculated curves, plotted with account of the radiation of the open end of the waveguide, for various phase relations of the field of the surface wave at the beginning of the impedance structure and of the field at the waveguide aperture. It is seen that the theoretical and experimental directional diagrams coincide fairly well and that it is possible to obtain a matching of the horn to the impedance structure for which the direct radiation of the horn affects only on the side lobes, the major lobe changing but little.

Note that, in reality, the surface behind the ridged structure (Fig. 10-65) has finite dimensions (b and d) so that the mirror method used above is not valid. When calculating the radiation of the antenna, the radiation of the magnetic as well as electric surface currents have to be integrated over the impedance structure. At the same time, neglecting the reflection of the surface wave from the end of the impedance structure, which is particularly justified in case the depth of the grooves towards the end of the antenna gradually decreases down to zero (Fig. 10-67), one can regard the surface currents distribution to be the same as in the case of an infinite plane. Then the directional diagram, with account of the radiation of the open end of the waveguide and when $d=0$, is expressed as:

$$f(\alpha) = \sqrt{\left(\frac{v_1}{v}\right)^2 - \cos^2 \alpha} \frac{\sin \left[\frac{\pi L}{\lambda} \left(\frac{v_1}{v} - \cos \alpha \right) \right]}{\frac{\pi L}{\lambda} \left(\frac{v_1}{v} - \cos \alpha \right)}, \quad (10-43)$$

$$(0 < \alpha < \pi).$$

Here, in contradistinction to the expression (10-29), the first factor appeared as a result of the superimposition on the radiation of the magnetic current J_y^M of the radiation of the electric current J_z^e ; these currents are distributed in the antenna in accordance with the expressions (10-35) and (10-37) and the laws

$$J_y^M = \frac{p}{i\omega\epsilon_0} H_0 e^{-pl - ihz}$$

and

$$J_z^e = H_0 e^{-pl - ihz}.$$

It is seen from (10-43) that when the ratio $\frac{v_1}{v}$ is close to unity, the radiation in the direction of the antenna

axis ($\alpha=0$) is close to zero and the maximum radiation of the antenna is directed at a certain angle to the plane.

Fig. 10-69 shows the experimental directional diagrams of an impedance antenna of length $L=7.33 \lambda$. The solid

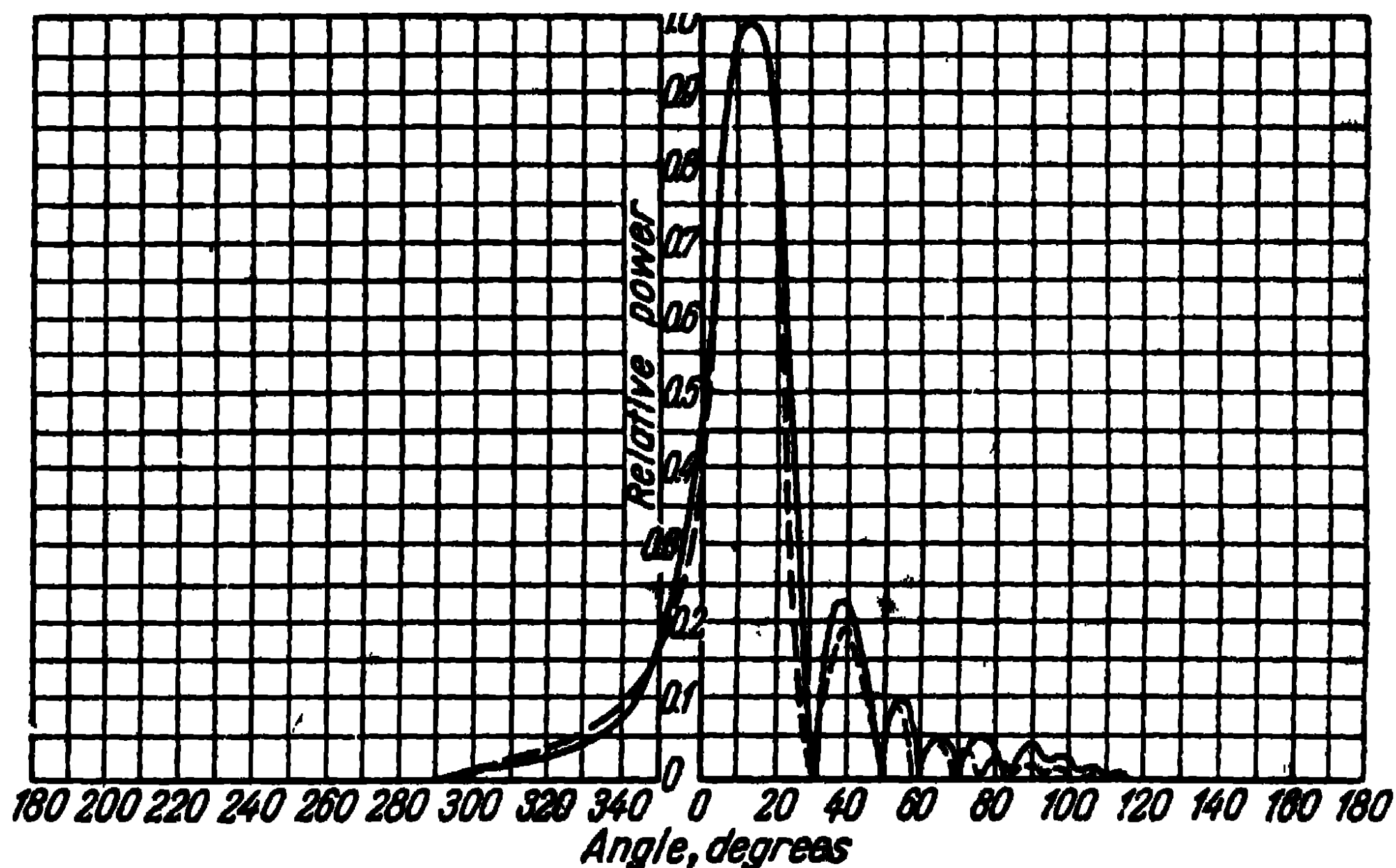


Fig. 10-69. Directional diagrams of an impedance antenna with a finite plane.

curve applies to an antenna in which the ratio of the width of the ridges to the width of the grooves τ/s equals 3, and the dotted curve applies to an antenna in which this ratio equals $1/3$. In both cases, the dimension d of the antenna is taken equal to $\lambda/2$. It can be seen from this figure that the radiation maximum is approximately at an angle $\alpha=15^\circ$ to the plane, the radiation in the direction of the plane constitutes approximately 20% of the power relatively to the radiation in the main direction

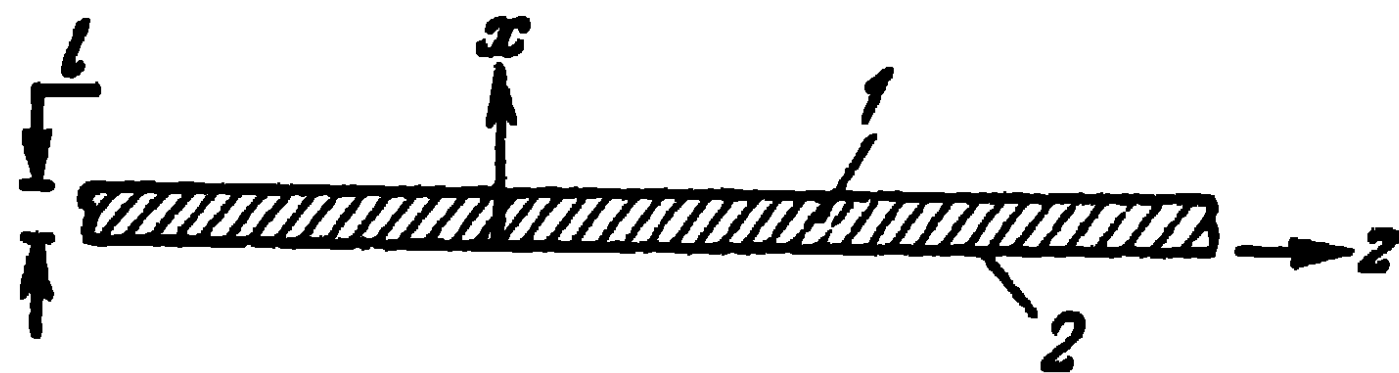


Fig. 10-70. Layer of dielectric (1) on a metal plane (2).

and the radiation in the shadow region ($180^\circ < \alpha < 360^\circ$), which is not taken into account in (10-43), is found to be insignificant.

Note that the impedance structure of the antenna represented in Fig. 10-65 can be formed not of a metal ridged structure but of a dielectric layer (Fig. 10-70). In that

case, the electromagnetic field in the dielectric, for the surface wave described by (10-35) and (10-37), is represented by the following expressions:

$$\begin{aligned} H_y^d &= H_0^d \cos gxe^{-ihz}; \\ E_x^d &= \frac{h}{\omega\epsilon_1} H_0^d \cos gxe^{-ihz}; \\ E_z^d &= -\frac{g}{i\omega\epsilon_1} H_0^d \sin gxe^{-ihz}, \end{aligned} \quad (10-44)$$

where $g = \sqrt{k_1^2 - h^2}$;
 $k_1 = k_0 \sqrt{\epsilon_1/\epsilon_0}$;
 ϵ_1/ϵ_0 is the relative permittivity of the dielectric layer.

It is readily seen that the expressions (10-44) satisfy Maxwell's equations and the boundary conditions on the metal plane coated with a dielectric layer.

From the expression (10-44) one defines the surface impedance of the dielectric layer

$$Z^d = \frac{E_z^d}{H_y^d} = -\frac{g}{i\omega\epsilon_1} \tan gl. \quad (10-45)$$

Identifying (10-38) with (10-45), we obtain the condition for which the surface wave will be maintained:

$$\frac{\epsilon_1}{\epsilon_0} p \cos gl = g \sin gl. \quad (10-46)$$

It is readily seen that the equation (10-46) is observed when $k_0 < h < k_1$ and $gl < 90^\circ$. This equation serves to define the magnitude of the propagation constant h and, consequently, of the phase velocity v .

In the existence of suitable matching at the horn output, a sufficiently accurate definition of the directional diagrams of an impedance antenna with a dielectric layer is given by the expressions (10-29) and (10-43). Experience shows that impedance antennas with a dielectric layer have higher losses than ridged antennas. The efficiency of these antennas is adequate only on decimetre waves.

10-12. Lens Antennas

Lens antennas of various designs find fairly frequent application in the centimetre wave range. In these antennas use is made of the optical properties of electromagnetic

waves, since the dimensions and curvature radii of the surface of the antennas greatly exceed the wave-length of the excited oscillations. The purpose of lens antennas is the formation of highly directive radiation diagrams and the transformation of a cylindrical or spherical wave front into a plane one.

Fig. 10-71 represents a dielectric lens on which a spherical wave of length λ_0 is incident from a source F . Due to the convex form of the irradiated surface of the lens, the

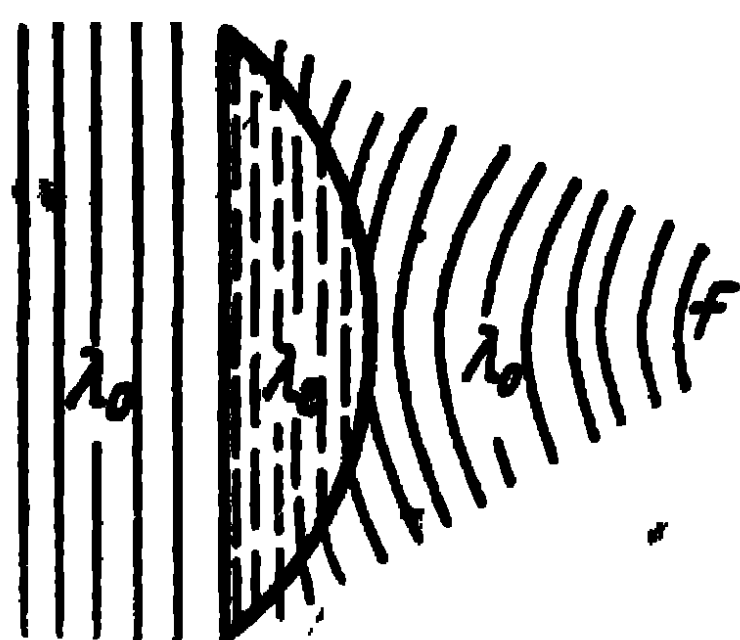


Fig. 10-71. Dielectric lens.

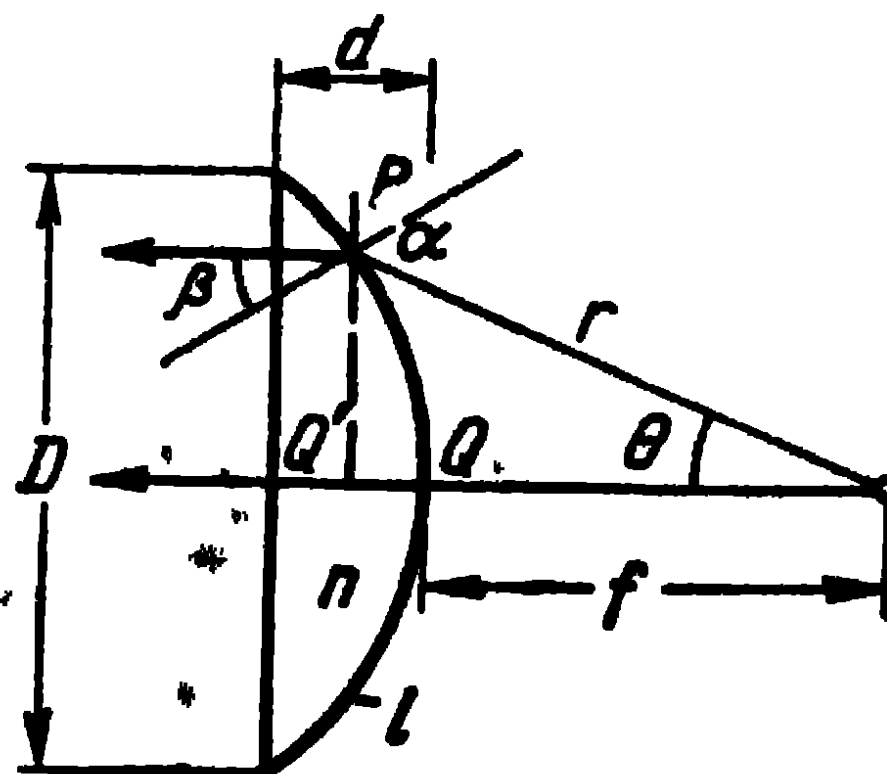


Fig. 10-72. Explaining the calculation of the lens profile:
l—hyperbolic shape of surface.

spherical wave front is transformed into it into a plane one with a wave-length $\lambda_e = \frac{\lambda_0}{\sqrt{\epsilon/\epsilon_0}}$. The output surface of the lens is flat, so that, on leaving the lens, the wave front remains flat. Because the dimensions of the output surface of the lens are large in comparison with the wave-length, its radiation is highly directional.

Let us now turn to Fig. 10-72 and define the lens profile. Let a ray fall from point F on point P on the lens surface and let α be the angle of incidence of the ray and β , the angle of refraction. We have:

$$\sin \alpha = n \sin \beta,$$

where $n = \sqrt{\epsilon/\epsilon_0}$ is the coefficient of refraction.

The equation of the lens profile will be determined from the condition that the length of the optical path (electric length) from the equal phase surface undergoing transformation to the transformed one should be constant in any direction, i.e., $FP = FQ + nQQ'$. Hence we obtain:

$$r = f + n(r \cos \theta - f)$$

or

$$r = \frac{(n-1)f}{n \cos \theta - 1}, \quad (10-47)$$

where f is the focal distance, i.e., the distance from the focus F to the apex of the lens Q ;

θ , the angle between the axis of the lens and the ray;

r , the distance between the focus and the reference point of the lens.

The equation (10-47) is that of an hyperbola. Thus, the convex surface of the lens has an hyperbolic shape.

The thickness of the lens d is determined along the optical path and is related as follows to the diameter of the lens D :

$$d = \frac{1}{n} \left(\frac{D}{2 \sin \theta_{\max}} - f \right). \quad (10-48)$$

The expressions (10-47) and (10-48) enable to calculate the profile and dimensions of the lens.

Since the output surface of the lens is a co-phased surface, it can be regarded as an ideal plane antenna. In the case

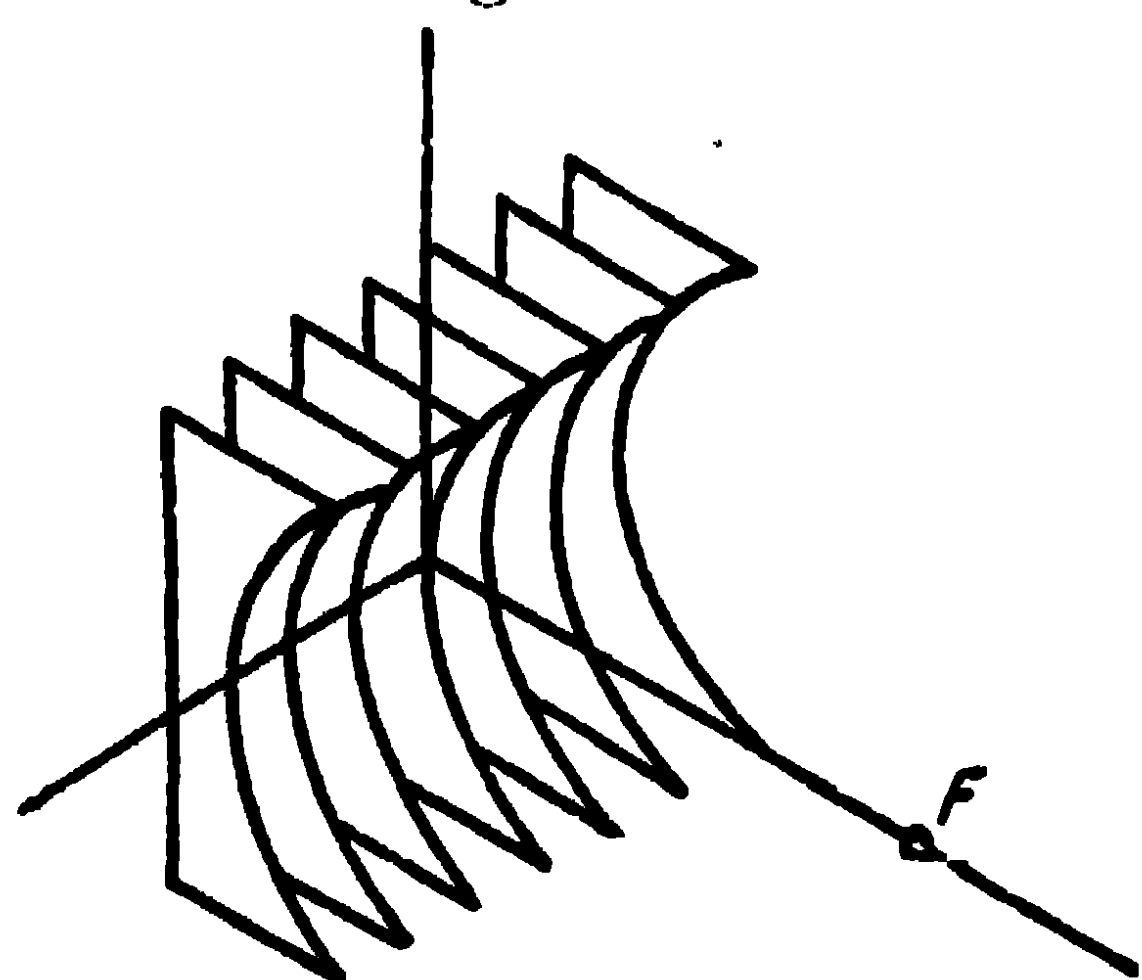


Fig. 10-73. Metal-plate lens.

of a point source (Hertz dipole), placed in the focus of the lens F , the lens should be circular and its output surface will have a circular form. In the case of a linear source, placed on the focal line F , the lens should be cylindrical and its output surface will have a rectangular form.

Dielectric lenses have a wide pass-band, due to the

fact that the coefficient of refraction n is frequency independent in a wide frequency range, including even the highest ones. However, they are relatively seldom used on account of their weight, considerable energy losses and relatively high cost.

High phase velocity metal-plate lenses find application in antenna technique. Lenses of this kind consist of parallel metal plates spaced at a distance b apart and forming a concave surface (Fig. 10-73). The electric field vector E

excited by a source situated at the focus of the lens, should be parallel to the plates. Then, the space between two neighbouring plates represents a waveguide in which we get the excitation of an H_{01} mode with a phase velocity $v = \frac{v_1}{\sqrt{1 - (\lambda/2b)^2}}$. Thus, the medium formed has a coefficient of refraction lower than unity,

$$n = \frac{v_1}{v} = \sqrt{1 - (\lambda/2b)^2} < 1. \quad (10-49)$$

It is clear that the distance between the plates b should be taken larger than half a wave-length but smaller than a wave-length, i.e., $\frac{\lambda}{2} < b < \lambda$, in order that only one mode, viz., H_{01} , should be propagated between the plates. Consequently, the coefficient of refraction of a lens of high phase velocity lies within the interval $0 < n < \sqrt{0.75}$.

The equation of the lens profile will be defined from Fig. 10-74. The ray incident from focus F on point P of the input surface of the lens is refracted in accordance with the law of geometrical optics $\sin \alpha = n \sin \beta$. The optical length of the path FQ should be equal to the optical length of the path FP' , i.e., $FQ = FP + nPP'$.

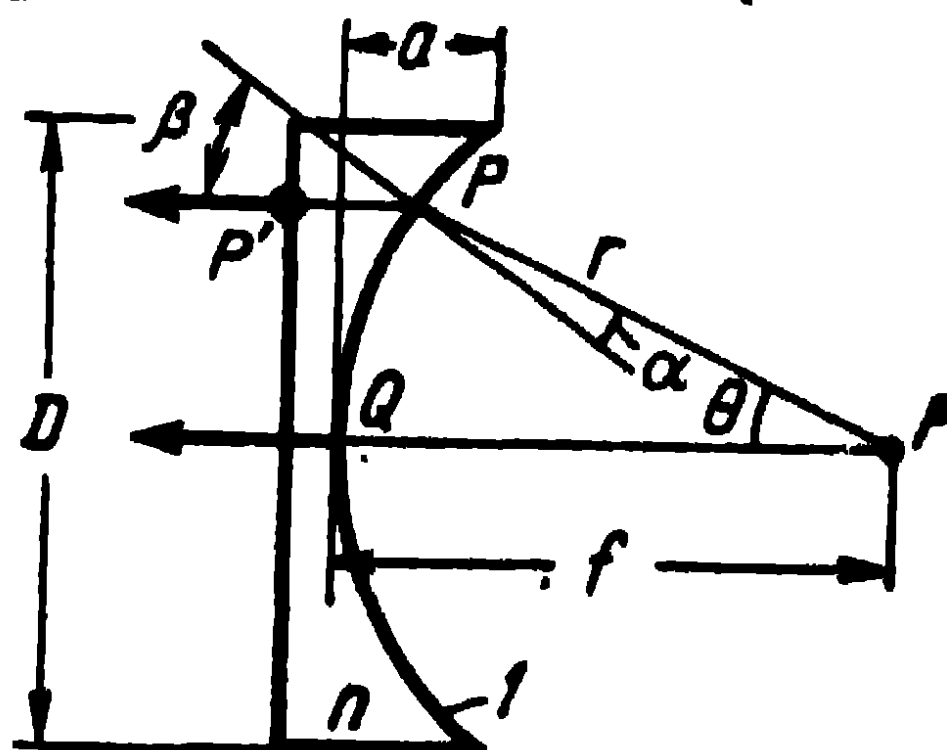


Fig. 10-74. Explaining the calculation of the lens profile: 1—elliptical form of surface.

Whence we obtain the equation of the lens profile

$$f = r + n(f - r \cos \theta)$$

or

$$r = \frac{(1-n)f}{1-n \cos \theta} \quad (10-50)$$

which is the equation of an ellipse.

The thickness of the lens d is related to its diameter as follows:

$$d = \frac{1}{n} \left(f - \frac{D}{2 \sin \theta_{\max}} \right). \quad (10-51)$$

A lens consisting of identical plates of elliptical profile focusses electromagnetic energy in the electric vector plane.

If the lens consists of rectangular plates of different thickness (d), which also form an elliptical profile, it focusses electromagnetic energy in the magnetic vector plane. In order that the energy should be focussed both in the electric and magnetic vector planes, the lens should consist of plates of elliptical profile of different thicknesses.

Thus, a high phase velocity metal-plate lens transforms a spherical wave front (in the case of a point radiator) or a cylindrical wave front (in the case of a linear radiator) into a plane front and enables to obtain a co-phasal surface at the output of the lens. The construction of these lenses is very simple. The use of a metal-plate lens in combination with a horn, for example, considerably reduces its length. Thus, in order to obtain an opening size $b = 40 \lambda$ in an optimum horn, the latter should be given a length $R \approx 800 \lambda$, whereas the use of a lens at the opening of the horn enables to reduce the length of the horn down to the size of the opening, i.e., $R \approx 40 \lambda$.

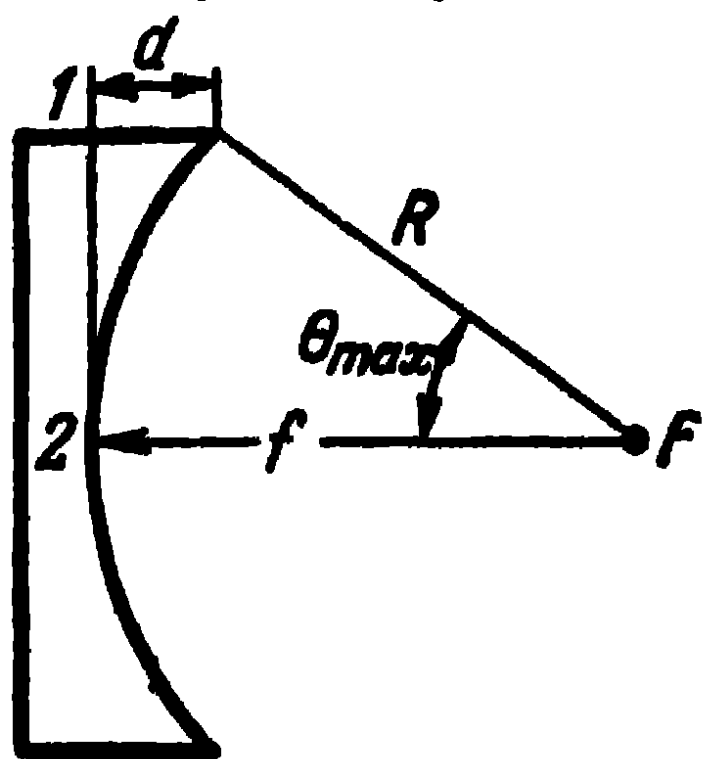


Fig. 10-75. Explaining the calculation of the distortion of the field phase in a lens.

considerably reduces its length. Thus, in order to obtain an opening size $b = 40 \lambda$ in an optimum horn, the latter should be given a length $R \approx 800 \lambda$, whereas the use of a lens at the opening of the horn enables to reduce the length of the horn down to the size of the opening, i.e., $R \approx 40 \lambda$.

Metal-plate lenses have a relatively narrow pass-band, due to the fact that the coefficient of refraction, as can be seen from the expression (10-49), is a function of the frequency. Let us calculate the distortion of the field phase at the opening of the lens in case of a change of frequency and estimate the pass-band of the antenna. Let ψ_1 be the field phase at point 1 of the lens and ψ_2 , that at point 2 (Fig. 10-75). Then, the difference of phase of the field at these two points will be:

$$\psi = \psi_2 - \psi_1 = kf - k(R + nd).$$

Let n_0 be the coefficient of refraction for the wave-length λ_0 in the middle of the pass-band. On that wave-length, the difference of phase ψ will be zero. On the wave-length $\lambda_0 + \Delta\lambda$, the coefficient of refraction will be:

$$n = n_0 + \left. \frac{\partial n}{\partial \lambda} \right|_{n=n_0} \Delta\lambda$$

and the difference of phase will be expressed as:

$$\psi \approx -k_0 d \left. \frac{\partial n}{\partial \lambda} \right|_{n=n_0} \Delta\lambda.$$

But since

$$\left. \frac{\partial n}{\partial \lambda} \right|_{n=n_0} = \frac{-\frac{\lambda_0}{(2b)^2}}{\sqrt{1-(\lambda_0/2b)^2}} = \frac{-\frac{\lambda_0}{(2b)^2}}{n_0} = -\frac{1-n_0^2}{n_0 \lambda_0},$$

the difference of phase of the field will be written as:

$$\psi \approx 2\pi \frac{1-n_0^2}{n_0} \frac{\Delta f}{f_0} \frac{d}{\lambda_0}. \quad (10-52)$$

The permissible value of distortion of the phase is taken equal to $\psi = \frac{\pi}{2}$. In order to avoid considerable reflections when the wave is incident from the radiator on the lens, as well as to avoid the use of a lens of excessive thickness the coefficient of refraction is usually taken equal to $n_0 = 0.5$. Then, the antenna pass-band equals:

$$\frac{2\Delta f}{f_0} = 33 \frac{\lambda_0}{d} [\%]. \quad (10-53)$$

As can be seen from this expression, the antenna pass-band is inversely proportional to the thickness of the lens d , and if $d \gg \lambda_0$, the pass-band is very narrow.

In order to reduce the thickness of the lens d and widen its pass-band, as well as make it easier to manufacture, the lens is usually zoned (Fig. 10-76). The irradiated part of the lens is stepped, and the steps are taken of a depth (t) such that the rays refracted in neighbouring zones of the lens arrive at the output of the lens with a phase shift equal to 2π .

Each of the zones of the lens has its focal distance and the equation of the profile of the m -th zone will be:

$$r_m = \frac{(1-n) f_m}{1-n \cos \theta}, \quad (10-54)$$

where $f_m = f + (m-1)t$, $m = 1, 2, 3, \dots$

The size t is precisely chosen so that on the calculated wave-length λ_0 , the field at the output of the lens should be co-phased:

$$k_0 t - k_0 n t = 2\pi,$$

from which we derive:

$$t = \frac{\lambda_0}{1-n}. \quad (10-55)$$

As a consequence of the zoning, there are non-irradiated areas at the lens input, which cause shadow regions at its output (Fig. 10-76). These shadow regions somewhat lower the directive gain of the antenna. The lowering of the directive gain is evidently due to the dispersion of part of the energy on the steps.

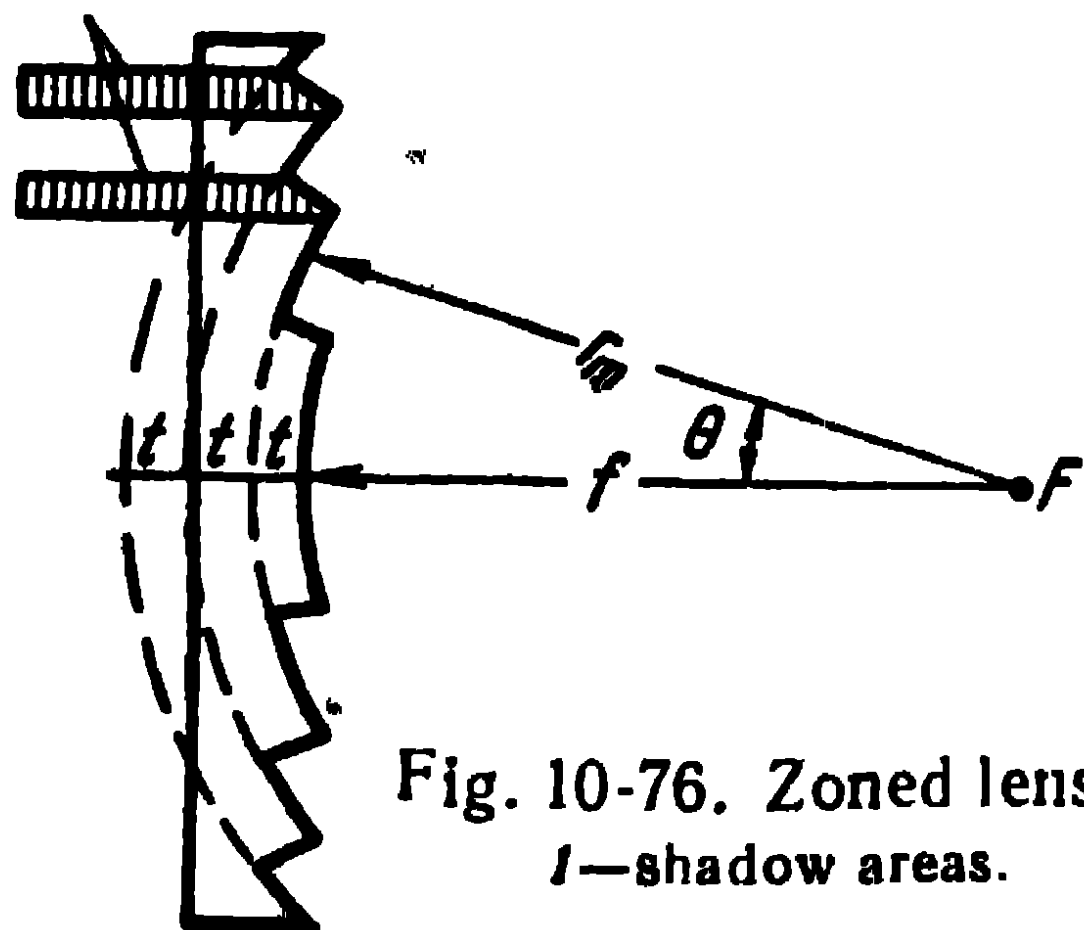


Fig. 10-76. Zoned lens:
1—shadow areas.

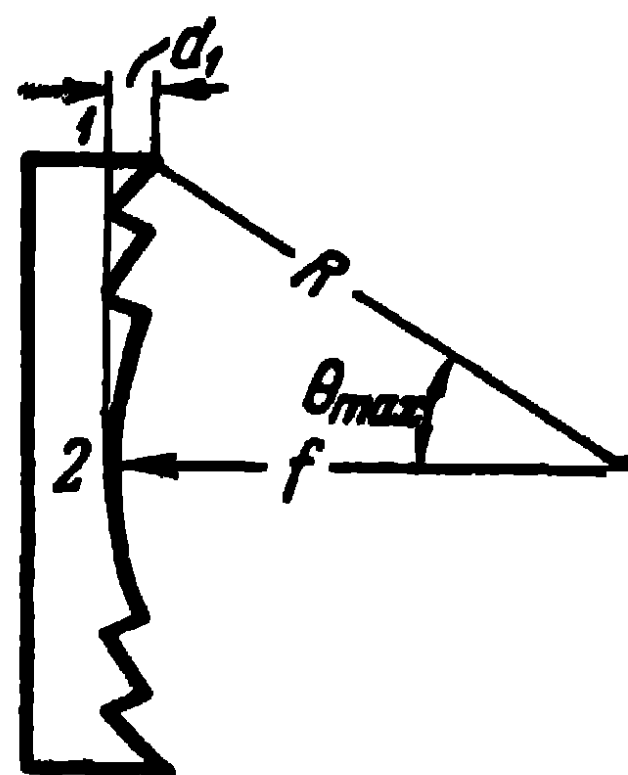


Fig. 10-77. Explaining
the calculation of the
frequency band.

Let us examine the width of the pass-band of a zoned lens. The field phase at point 1 of the lens (Fig. 10-77) equals $\psi_1 = k(R + nd_1)$, and that at point 2 equals $\psi_2 = kf$. On the calculated wave-length λ_0 , the phase difference will be:

$$\psi = kf - k_0(R + n_0 d_1) = -k_0(M - 1)\lambda_0,$$

where M is the number of zones of the lens.

On the wave-length $\lambda_0 + \Delta\lambda$, the phase difference will be:

$$\begin{aligned} \psi &= (k_0 + \Delta k)f - (k_0 + \Delta k)[R + (n_0 + \Delta n)d_1] = \\ &= -(k_0 + \Delta k)(M - 1)\lambda_0 - (k_0 + \Delta k)\Delta n d_1 = \\ &= -2\pi(M - 1) - (M - 1)\lambda_0 \Delta k - k_0 d_1 \Delta n. \end{aligned}$$

Discarding $2\pi(M - 1)$ and taking into account that

$$\Delta n = \left. \frac{\partial n}{\partial \lambda} \right|_{n=n_0} \Delta \lambda = -\frac{1 - n_0^2}{n_0 \lambda_0} \Delta \lambda$$

and

$$\Delta k = \left. \frac{\partial k}{\partial \lambda} \right|_{\lambda=\lambda_0} \Delta \lambda = -k_0 \frac{\Delta \lambda}{\lambda_0},$$

we obtain for the phase difference

$$\psi' \approx 2\pi(M - 1) \frac{\Delta f}{f_0} + 2\pi \frac{1 - n_0^2}{n_0} \frac{\Delta f}{f_0} \frac{d_1}{\lambda_0}. \quad (10-56)$$

If we assume that $\psi' = \frac{\pi}{2}$ and $n_0 = 0.5$, the expression for the pass-band will be:

$$\frac{2\Delta f}{f_0} = \frac{50}{(M-1) + 1.5 \frac{d_1}{\lambda_0}} [\%]. \quad (10-57a)$$

A comparison of (10-57a) with (10-53) shows that a zoned lens has a wider pass-band than an unzoned one. Indeed, the relation of the quantity d_1 in (10-57a) to the quantity d in (10-53) is $d_1 = d - (M-1)t$ and the expression (10-57a), account taken that $t = 2\lambda_0$, becomes:

$$\frac{2\Delta f}{f_0} = \frac{50}{1.5 \frac{d}{\lambda_0} - 2(M-1)} [\%]. \quad (10-57b)$$

Thus, at a prescribed value of d , an increase of M leads to an increase of the pass-band.

As regards the distribution of the field amplitudes at the output opening of a metal-plate lens of high phase velocity, in the case of a uniform irradiation of the lens, the field amplitude increases towards the edges of the lens due to the fact that when the angle θ increases, the value of the surface at the lens output, corresponding to the same increment of the angle θ , decreases, which can be seen from Fig. 10-78. The distribution of the field amplitudes at the lens output when it is illuminated by a spherical wave (spherical lens) is expressed as

$$E \equiv \sqrt{\frac{(1 - n \cos \theta)^2}{f^2 (1 - n)^2 (\cos \theta - n)}} F(\theta),$$

where $F(\theta)$ is a factor which takes into account the directivity of the radiator.

For a cylindrical wave front (cylindrical lens), the distribution of the amplitudes at the output of the lens is expressed as:

$$E \equiv \sqrt{\frac{(1 - n \cos \theta)^2}{f(1 - n)(\cos \theta - n)}} F(\theta).$$

The proper choice of the directional characteristic of the radiator $F(\theta)$ enables to obtain the desired distribution of the

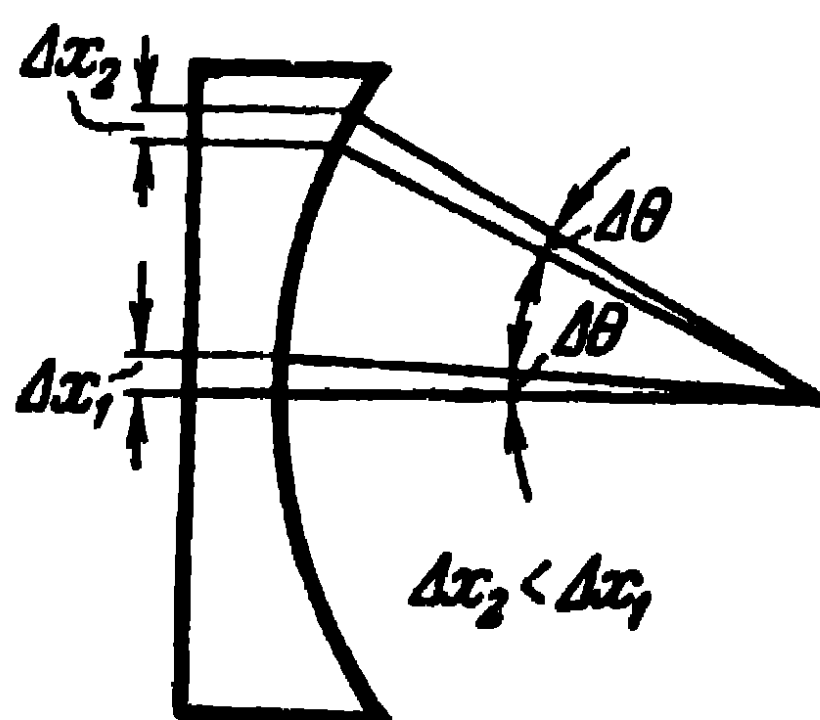


Fig. 10-78. Explaining the calculation of the field amplitude in the lens.

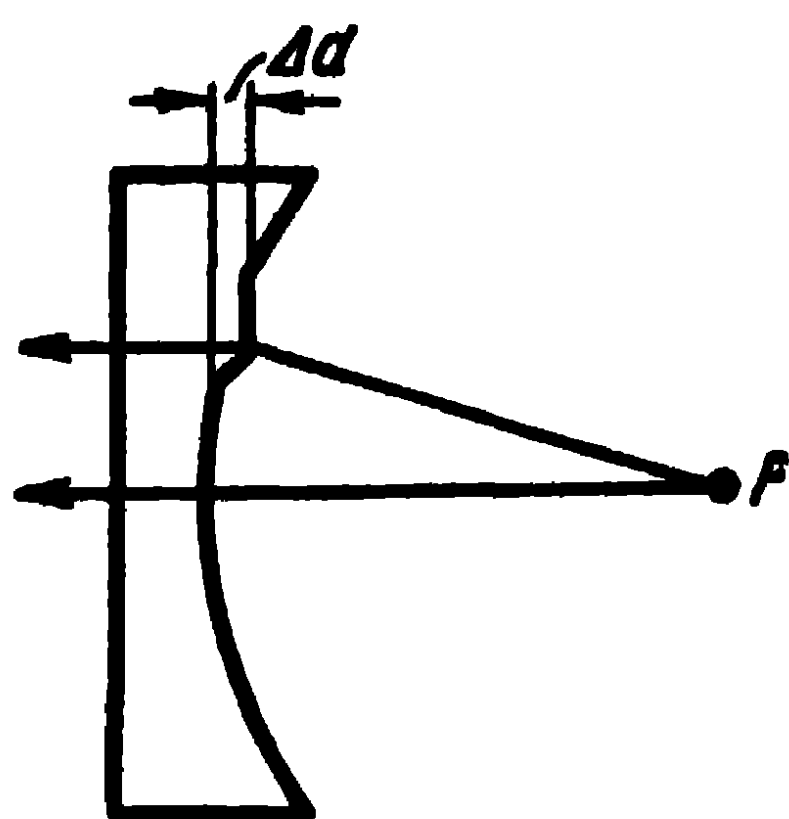
field amplitudes at the lens output. Moreover, the directional diagrams can be calculated from the corresponding expressions of the co-phased plane antennas. The directive gain of a lens antenna, in particular a horn lens, can be expressed as:

$$D = \frac{4\pi s}{\lambda^2} k_1,$$

where s is the area of the output surface of the lens;

k_1 , the coefficient taking account of the distribution law of the field amplitudes at the output of the lens which is usually equal to 0.5-0.7.

Let us now examine the requirements concerning the accuracy with which metal-plate lenses should be made.



The accuracy is determined by the permissible phase distortions which occur when the dimensions of the lenses do not correspond to the calculated ones. Let Δd represent the inaccuracy to size of the thickness of the lens (Fig. 10-79). Then the phase distortion will be:

$$\psi_1 = k_0 \Delta d (1 - n_0),$$

Fig. 10-79. Explaining the calculation of the accuracy to size of the lens.

and if we take the permissible phase distortion to be $\psi_1 = \frac{\pi}{8}$, the permissible inaccuracy to size of the thickness of the lens will be expressed as:

$$\Delta d = \frac{\lambda_0}{16(1 - n_0)}. \quad (10-58)$$

It follows that the closer is n_0 to unity, the higher the inaccuracy to size of the lens that can be tolerated.

Let now Δb represent the inaccuracy to size of the distance between the plates within the limits of a certain thickness d' of the lens. Then, the phase distortion will be:

$$\psi_2 = k_0 d' \frac{\partial n_0}{\partial b} \Delta b.$$

But $\frac{\partial n_0}{\partial b} = \frac{1 - n_0^2}{bn_0}$, and if we assume that $\psi_2 = \frac{\pi}{8}$, the permissible inaccuracy to size of the distance between the plates will be:

$$\Delta b = \frac{\lambda_0 b}{16 d'} \frac{n_0}{1 - n_0^2}. \quad (10-59)$$

Apart from metal-plate lenses, use is also made in antenna technique of artificial dielectric lenses of slow phase velocity. These lenses consist of metal balls, circular discs, plates of rectangular or other form, as well as metal tapes. In fact they are artificial dielectric lenses. Fig. 10-80 represents a lens of this kind, consisting of metal balls of a diameter small in comparison with the wave-length, spaced apart at distances small in comparison with the wave-length. The profile of this lens has an hyperbolic form and is described by the equation (10-47).

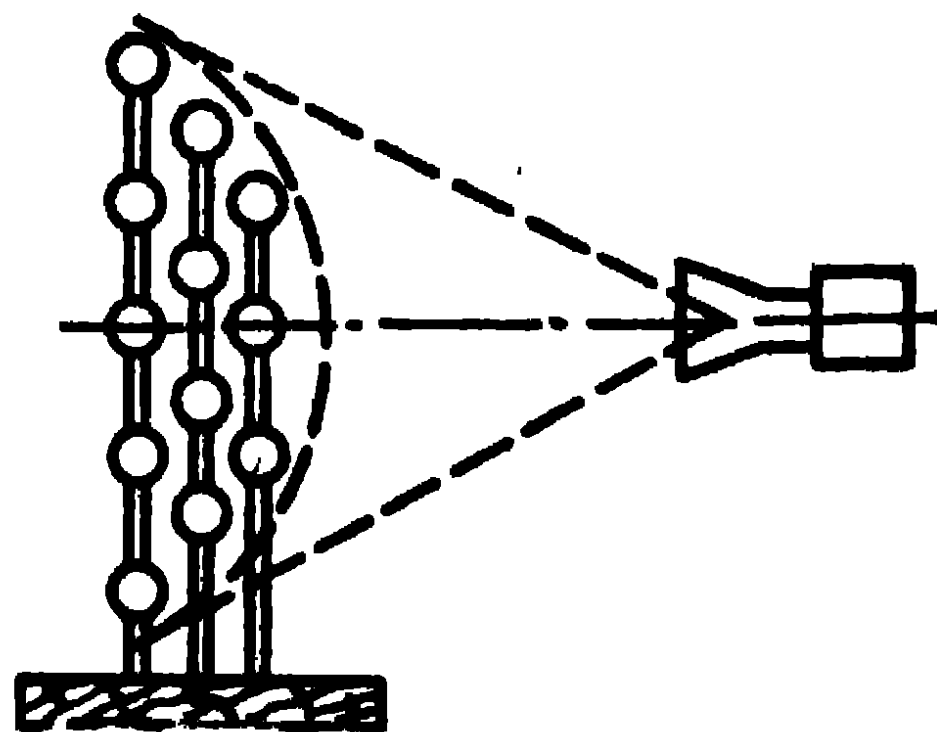


Fig. 10-80. Lens antenna consisting of metal balls.

Let us briefly investigate the artificial dielectric theory. Let small metal particles be suspended in a certain volume. Under the influence of the field of the electromagnetic wave incident on the medium thus formed, the electric charges of the particles are displaced and form electric dipoles, the moment of each of which will be designated by p_e . If there are N such dipoles in a unit of volume, the polarisation of the medium will be $P = Np_e$. The electric induction will then be expressed as:

$$D = \epsilon_0 E + P.$$

On the other hand, if ϵ is the effective permittivity of the medium,

$$D = \epsilon E$$

whence we obtain:

$$\epsilon = \epsilon_0 + \frac{Np_e}{E},$$

and if we take into account that the moment of the dipole is proportional to the acting electric field $p_e = \alpha_e E$ where α_e is the electric polarisability or susceptiveness of the dipole, the expression for the effective relative permittivity will be:

$$\frac{\epsilon}{\epsilon_0} = 1 + \frac{N\alpha_e}{\epsilon_0}. \quad (10-60)$$

Assume that the particles are ideally conducting balls. Let the electric field acting on a ball be E_e ; its meridional component will then equal $E_0 = E_e \sin \theta$. The field

excited by one ball (the influence of the neighbouring ones is not taken into account) will be:

$$E_{\theta}'' = \frac{\rho_e \sin \theta}{4\pi\epsilon_0 r^3}.$$

From the boundary conditions on the ball surface $E_{\theta}' + E_{\theta}'' = 0$, we obtain:

$$\rho_e = 4\pi\epsilon_0 a^3 E_z, \quad -$$

where a is the ball radius.

Hence, the electric susceptiveness of the dipole is:

$$\alpha_e = 4\pi\epsilon_0 a^3. \quad (10-61)$$

Substituting this expression into (10-60), we obtain:

$$\frac{\epsilon}{\epsilon_0} = 1 + N4\pi a^3.$$

At the same time, the coefficient of refraction of the medium will be:

$$n = \sqrt{\frac{\epsilon}{\epsilon_0}} = \sqrt{1 + 4\pi N a^3}. \quad (10-62)$$

The expression for the electric susceptiveness and effective coefficients of refraction of the media formed of metal particles of a different shape is:

a) for an ellipsoid of major axis $2a$ and minor axis $2b$

$$\alpha_e = 4\pi\epsilon_0 ab^2, \quad n = \sqrt{1 + 4\pi N ab^2}; \quad (10-63)$$

b) for a thin circular disc of radius a , the electric vector being parallel to the plane of the disc,

$$\alpha_e = \frac{16}{3} \epsilon_0 a^3, \quad n = \sqrt{1 + \frac{16}{3} N a^3}; \quad (10-64)$$

c) for a thin rectangular tape of width a and relatively large length b ($b \gg \lambda$), the electric vector being parallel to the narrow side,

$$\alpha_e = \frac{\pi}{4} \epsilon_0 a^3, \quad n = \sqrt{1 + \frac{\pi}{4} N a^3}; \quad (10-65)$$

here α_e is the polarisability of one unit length of tape; N , the number of tapes per unit surface of longitudinal section of the medium.

On defining the coefficient of refraction of the artificial dielectric, we proceeded from the existence of the electric dipole moment of the particle.

However, the excited metal particle possesses also a magnetic dipole moment. Indeed, the electromagnetic wave incident on the metal particle excites a higher current on the irradiated side of the particle than on its shadow side. The electric current induced in the particle can be represented, as shown in Fig. 10-81, as the superposition of the dipole current (solid curves) and loop current (dotted curves).

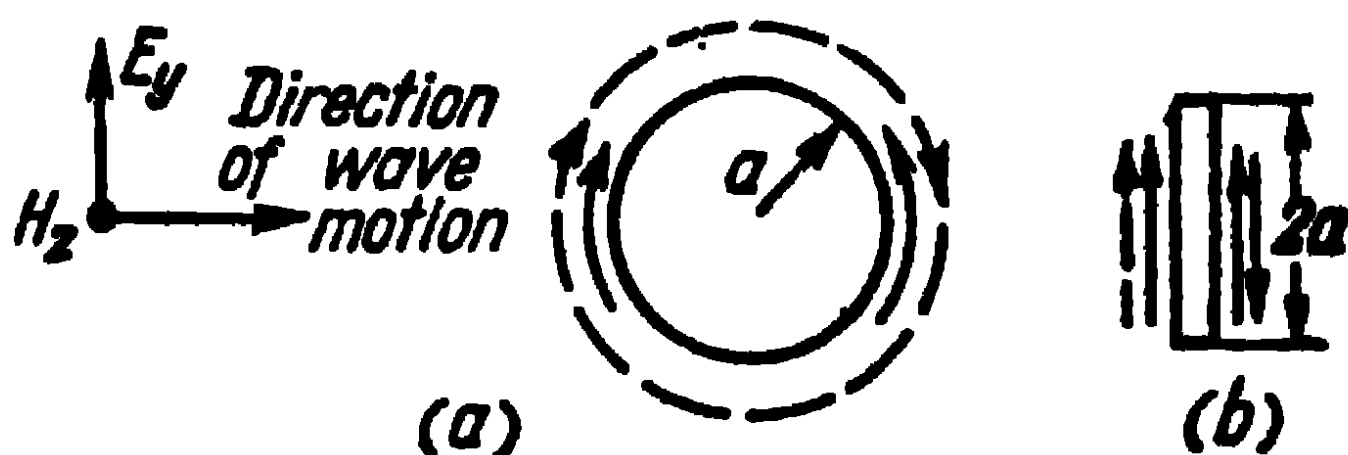


Fig. 10-81. Influence of an electromagnetic wave on metal particles:
a—ball; b—disc.

An elementary electric loop can be regarded as a magnetic dipole whose axis is perpendicular to the plane of the loop.

If p_m is the magnetic moment of the dipole (of the electric loop) and N , the number of magnetic dipoles in a unit volume, the magnetic induction will be:

$$B = \mu_0 H + p_m N.$$

Since the magnetic moment of the particle is proportional to the intensity of the acting magnetic field $p_m = \alpha_m H$, where α_m is the magnetic susceptiveness of the particle, the following expression will be obtained for the effective relative permittivity of the medium

$$\frac{\mu}{\mu_0} = 1 + \frac{N\alpha_m}{\mu_0}. \quad (10-66)$$

Let us examine the magnetic field of the loop electric current induced on the ball (Fig. 10-81). Let H_z be the magnetic field intensity of the electromagnetic wave incident on the ball. The incident wave component of the magnetic field intensity radial to the ball will be:

$$H_r' = H_z \cos \theta.$$

The radial component of the intensity of the magnetic field set up by one magnetic dipole (no account taken of the influence of the neighbouring ones) is expressed as:

$$H_r'' = \frac{p_m \cos \theta}{2\pi\mu_0 r^3}.$$

From the boundary condition on the surface of an ideally conducting ball $H_r' + H_r'' = 0$, we obtain

$$p_m = -H_z 2\pi\mu_0 a^3.$$

Since $p_m = \alpha_m H_z$, we shall have for the magnetic susceptibility of the particle:

$$\alpha_m = -2\pi\mu_0 a^3.$$

Substituting this expression into (10-66), we find:

$$\frac{\mu}{\mu_0} = 1 - N 2\pi a^3. \quad (10-67)$$

Thus, the effective permittivity of the medium decreases and the coefficient of refraction of the medium, instead of being defined by (10-62), is defined as:

$$n = \sqrt{\frac{e\mu}{e_0\mu_0}} = \sqrt{(1 + 4\pi N a^3)(1 - 2\pi N a^3)}. \quad (10-68)$$

In the case of, for example, a disc lying relatively to the incoming wave as shown in Fig. 10-81, *b*, the loop effect occurs too, but the area of the loop is small, so that the magnetic moment is insignificant [see (1-16)]. In that case the expression (10-64) is sufficient. If, on the other hand, the discs should be placed in the plane of the incoming wave, the loop effect of the induced current cannot be neglected and, as a result of the decrease of the permittivity of the medium, the coefficient of refraction will go down. The same reasoning goes for particles of a different shape.

Thus, to avoid lowering the coefficient of refraction of the medium (at a prescribed number of particles in a unit volume), the particles should be disposed in such a way that their minimum dimension should coincide with the direction of the wave progress in the medium.

Fig. 10-82 represents sketches of metal-dielectric lenses consisting of discs and tapes.

Note that to reduce their weight and dimensions, artificial dielectric lenses, just like metal-plate ones, are zoned (Fig. 10-83). The equation of the profile of each zone of the lens is expressed as:

$$r_m = \frac{(n-1) f_m}{n \cos \theta - 1}. \quad (10-69)$$

where

$$f_m = f + (m-1)t, \quad m=1, 2, 3, \dots$$

The dimension t of the lens is defined as:

$$t = \frac{\lambda_0}{n-1}. \quad (10-70)$$

In the operating wave range, the unzoned artificial dielectric lens constitutes an aperiodic system. Due to the fact that the equality (10-70) is upset, zoned lenses are frequency dependent. The phase shift of the field at the output of the

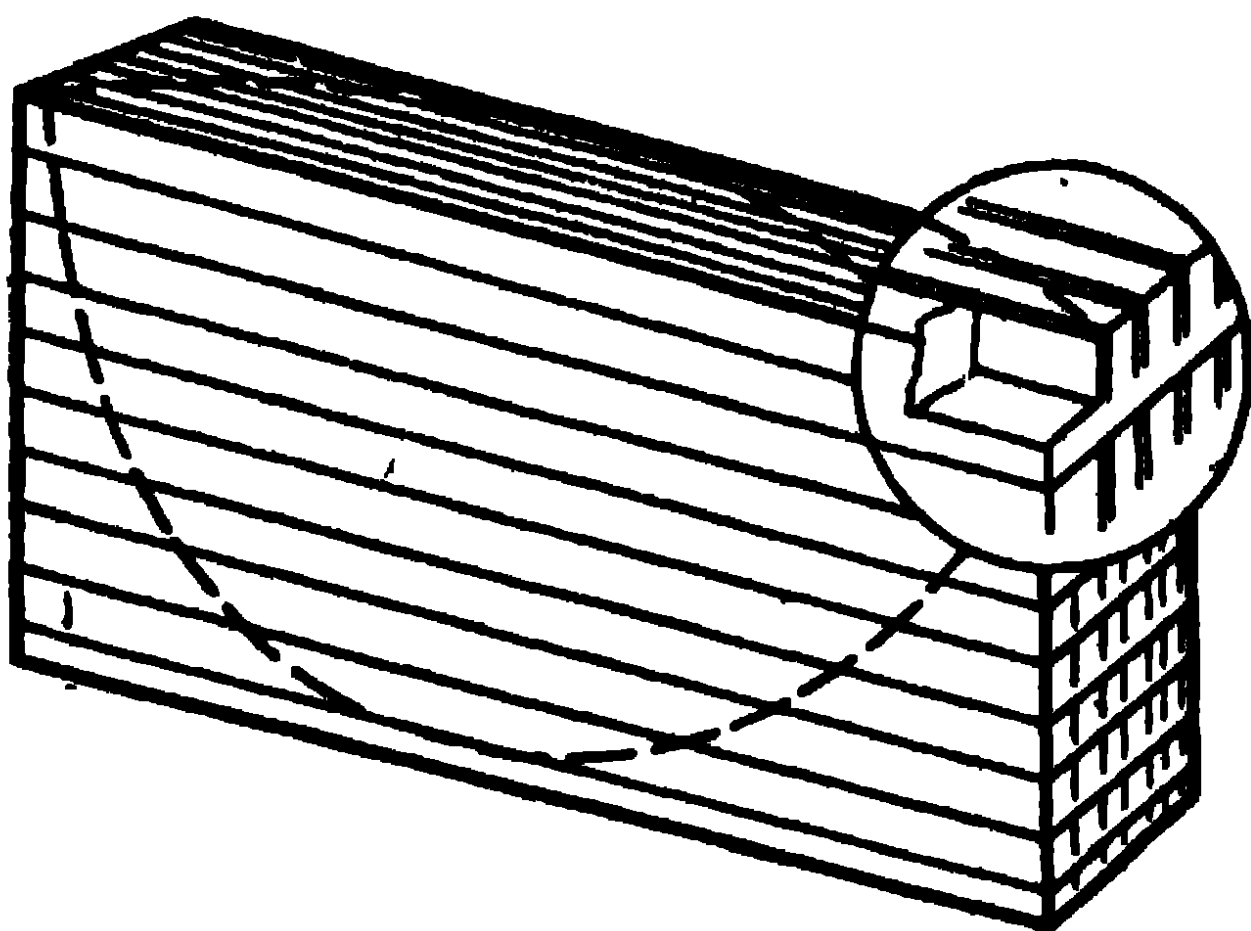


Fig. 10-82. Metal-dielectric lenses consisting of discs and tapes.

lens between the first (central) and last zones is expressed as:

$$\psi = k(M-1)t - kn(M-1)t = -k(M-1)\lambda_0.$$

On the calculated wave-length λ_0 , this phase shift equals $-2\pi(M-1)$, i.e., the fields are in phase. On the wave-length $\lambda = \lambda_0 + \Delta\lambda$, we have $k = k_0 + \Delta k = k_0 - k_0 \frac{\Delta\lambda}{\lambda_0}$ and the phase shift equals:

$$\psi = 2\pi(M-1)\frac{\Delta\lambda}{\lambda_0} - 2\pi(M-1).$$

Discarding $2\pi(M-1)$, we obtain the distortion of the phase at the output of the lens

$$\psi' = 2\pi(M-1)\frac{\Delta\lambda}{\lambda_0}.$$

If we regard $\psi' = \frac{\pi}{2}$ as the permissible phase distortion,

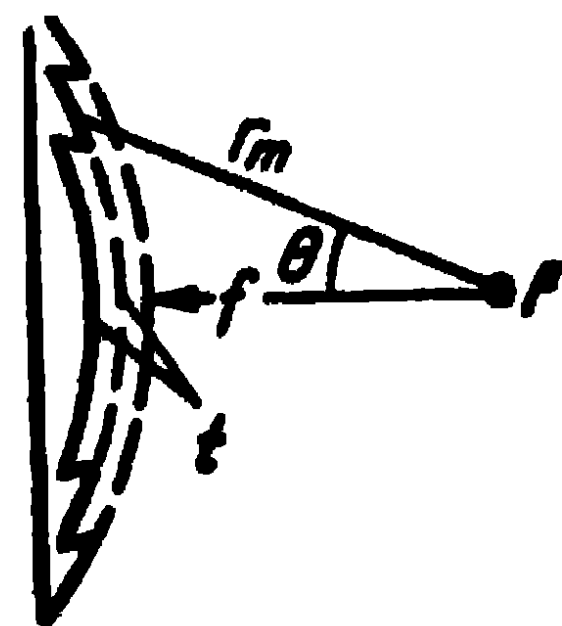


Fig. 10-83. Zoned artificial dielectric lens.

it will be found that the pass-band of the artificial dielectric lens is expressed as:

$$\frac{2\Delta f}{f_0} = \frac{50}{M-1} [\%]. \quad (10-71)$$

The accuracy to size of artificial dielectric lenses is defined by the same expressions as for metal-plate ones.

The observations made earlier regarding the formation of shadow regions in zoned metal-plate lenses fully apply also to artificial dielectric ones.

Note further that part of the energy radiated by the source F and incident on the lens is reflected from it. That part of the energy which is reflected from the illuminated (input) surface of the lens is, on the whole, dissipated and distorts the directional diagram of the antenna, whereas that part of the energy which is reflected from the shadow (output) surface is, on the whole, focussed in the radiator and leads to a change of the coefficient of reflection in the line feeding the radiator. The coefficient of reflection from the output surface of the lens is expressed as:

$$p = \frac{n-1}{n+1}.$$

This same quantity also approximately defines the coefficient of reflection in the line feeding the radiator. If we regard $p=0.3$ as permissible, it will be found that the coefficient of refraction of the lens should equal $n=1.86$ ($n=0.54$ for a metal-plate lens). To reduce the coefficient of reflection, it would be desirable to take n close to unity, but this would necessitate a lens of greater thickness. For this reason, other means are used to reduce the reaction of the lens on the radiator. Thus, Fig. 10-84, *a* represents a lens of slow phase velocity one part of the surface of which is displaced by a quarter of a wave-length relatively to the other part. As a consequence, the waves reflected from neighbouring elements of the lens reach the radiator with a 180° phase shift and, therefore, cancel out. One can also make use of the inclination of the output surface of the lens, as shown schematically in Fig. 10-84, *b*, which prevents the rays reflected by the lens from being focussed. Use is also made of quarter-wave surface layers of dielectric, the coefficient of refraction of which is taken equal to the square root of the coefficient of refraction of the lens. Sometimes

the layer is of the same material as the lens but has quarter-wave depressions, and that leads to a lowering of the effective value of the coefficient of refraction. The quarter-wave layers

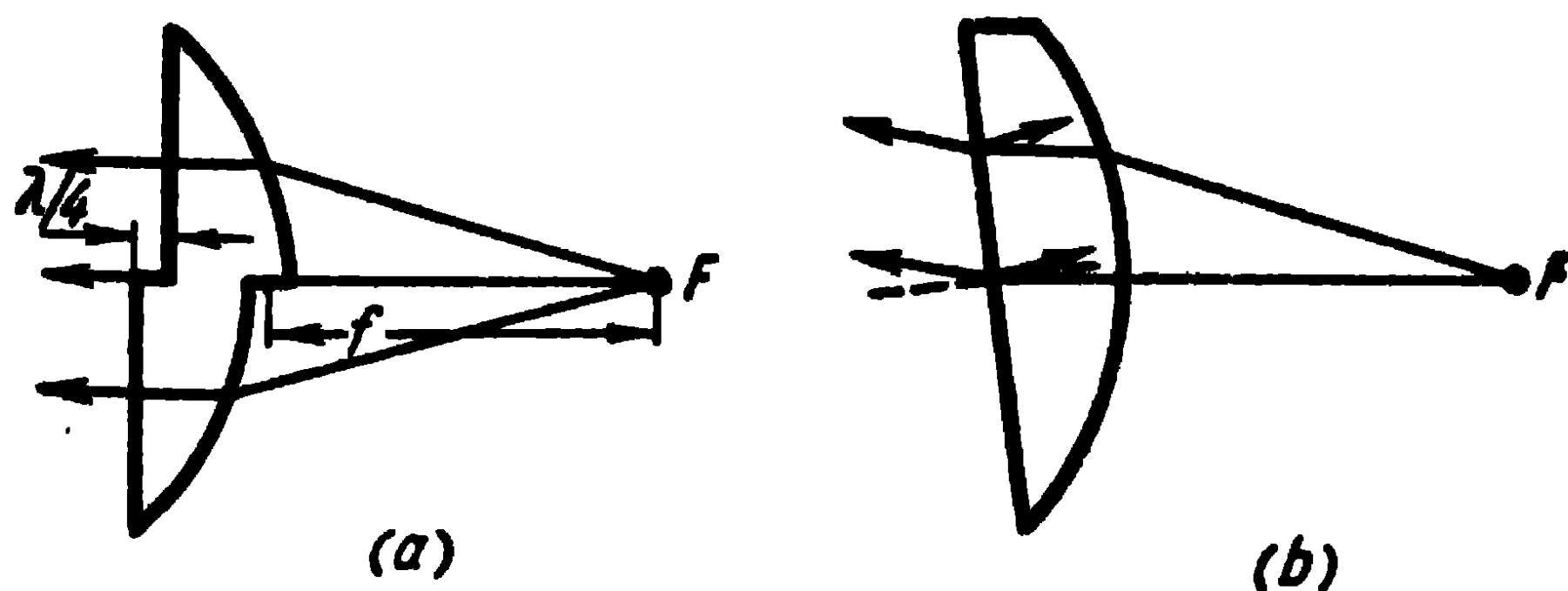


Fig. 10-84. Methods for reducing the effect of the lens on the radiator:

a—displacement of one part of the surface relatively to the other; *b*—inclination of the lens output surface.

on the input and output surface of the lens lead to a considerable decrease (theoretically down to zero) of the coefficient of reflection of the wave from the lens.

Let us now consider the accuracy of coincidence of the radiator with the focus of the lens. There can be two kinds

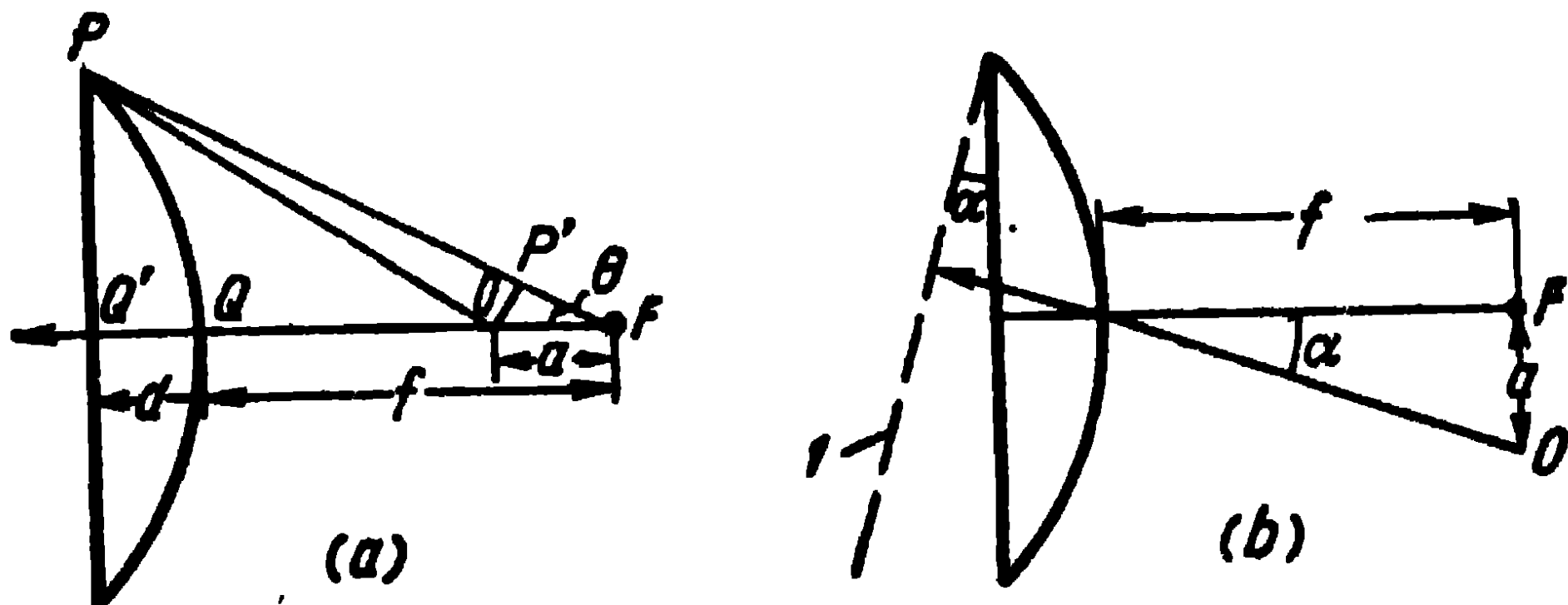


Fig. 10-85. Removal of the radiator out of the focus of the lens:

a—displacement of the radiator in the direction of the lens axis; *b*—displacement of the radiator in a direction perpendicular to the axis; *l*—wave front.

of displacement of the radiator: *a*) in the direction of the axis of the lens and *b*) in a direction perpendicular to the axis. In the first case, when the radiator is removed from the focus to the point *O* (Fig. 10-85, *a*), the difference of phase of the field at points *P* and *Q'* at the output of the lens will be:

$$\psi = k [OP - (OQ + nQQ')],$$

and since

$$\begin{aligned} OP &\approx FP - FP' = f + nd - a \cos \theta; \\ OQ &= f - a; \\ QQ' &= d, \end{aligned}$$

we get

$$\psi = ka(1 - \cos \theta).$$

If we regard $\psi = \frac{\pi}{8}$, as the permissible phase distortion, the permissible displacement of the radiator along the axis of the lens equals:

$$a = \frac{\lambda}{16(1 - \cos \theta)}. \quad (10-72)$$

The angle θ_{\max} is usually of the order of 30° , so that displacing the radiator along the axis by rather large distances causes an insignificant distortion of the directional diagram.

It should be noted that when the radiator is displaced in a longitudinal direction, the phase distortions, as can be seen from the expression obtained, are of a symmetrical nature relatively to the axis of the lens and are a parabolic function of the distance from the axis of the lens (for small angles $\theta \psi \approx ka \frac{\theta^2}{2}$). A phase distortion of this sort does not change the maximum radiation direction of the lens antenna but does change the form of the directional diagram (widens it).

A slight displacement of the radiator out of the focus in a direction perpendicular to the lens axis (Fig. 10-85, *b*) leads, on the whole, to a linear distortion of the field phase at the output of the lens, i.e., to a rotation of the wave front. This, in turn, rotates the directional diagram by an angle α , approximately equal to the angle by which the radiator is removed out of the focus ($\sin \alpha \approx \frac{a}{f}$) without distorting the diagram. Large displacement angles of the radiator give rise, apart from a linear distortion, to a noticeable cubic distortion of the phase, leading to a distortion of the form of the directional diagram, the relative increase of the side lobes on one side of the major lobe and their relative decrease on the other side.

The displacement of the radiator out of the focus in a direction perpendicular to the axis is made use of in radar

for scanning directional diagrams in the horizontal or vertical planes or for conical scanning. However, due to distortion of the directional diagram, it can be done only within the limits of a double or triple width of the major lobe of the directional diagram.

There are methods for scanning the directional diagrams of lens antennas in a very wide range of angles. Let us describe one of such rather widespread lenses, named after Luneberg, its inventor. The lens is a sphere (Fig. 10-86) with

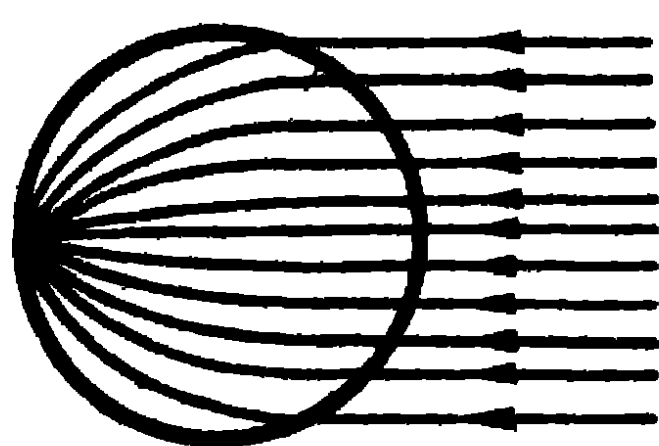


Fig. 10-86. Trajectory of the rays in a Luneberg lens.

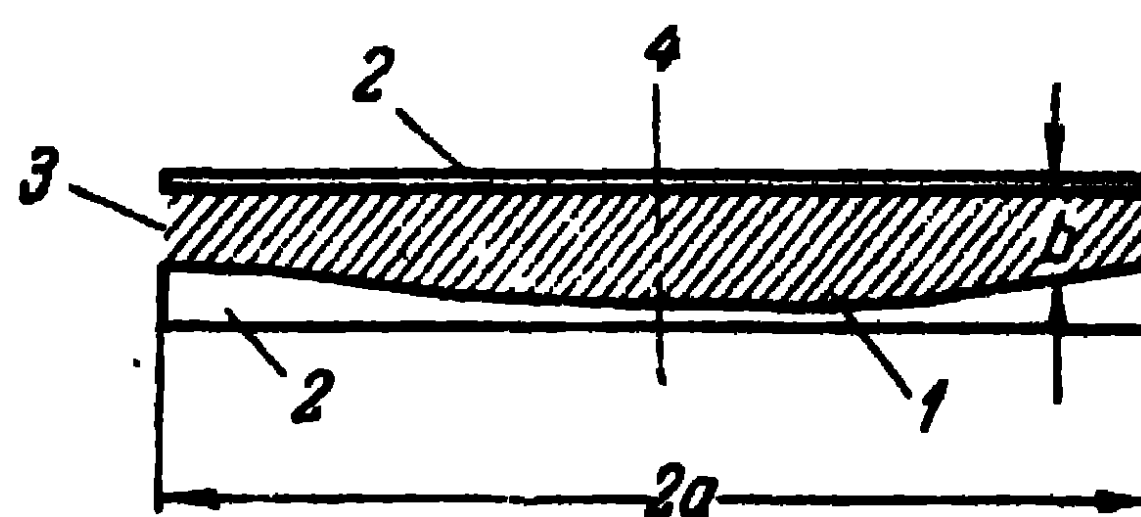


Fig. 10-87. Longitudinal section of a Luneberg lens:

1—dielectric; 2—metal plates; 3—area of radiation; 4—axis of symmetry.

an inhomogeneous dielectric, the refractive index of which changes according to the law

$$n = \sqrt{2 - \left(\frac{r}{a}\right)^2}, \quad (10-73)$$

where a is the radius of the sphere;

r , the distance from the centre of the sphere.

A lens of this kind focusses a parallel beam incident on it at a point of the surface of the sphere. If, in accordance with the law (10-73), the lens has the shape of a cylinder, it will focus a parallel beam in a line lying on the forming element of the cylinder. In practice, the lens can be made of two circular metal plates, one plane and the other curved, the space in between being filled with a homogeneous dielectric medium (Fig. 10-87). If the vector of the electric field intensity is parallel to the plates, the coefficient of refraction is expressed as:

$$n = \sqrt{\frac{\epsilon}{\epsilon_0} - \left(\frac{\lambda_0}{2b}\right)^2}. \quad (10-74)$$

Identifying (10-73) with (10-74), we obtain for the variable distance b between the plates, the expression

$$b = \frac{\lambda_0}{2 \sqrt{\frac{\epsilon}{\epsilon_0} - 2 + \left(\frac{r}{a}\right)^2}}, \quad (10-75)$$

where a is the radius of the plates;
 ϵ/ϵ_0 , the relative permittivity of the medium;
 λ_0 , the wave-length in vacuum.

To irradiate the lens shown in Fig. 10-87, use is made of the open end of a rectangular waveguide, the broad walls of which narrow down to a dimension equal to the distance between the plates at the input of the lens.

10-13. Parabolic Antennas

Parabolic antennas find very wide application in many fields of radio engineering, especially in radar. They are utilised in the centimetre, decimetre and, sometimes, metre wave range.

Parabolic antennas are given the shape of a paraboloid, a parabolic cylinder or a parabolic cylinder bounded by

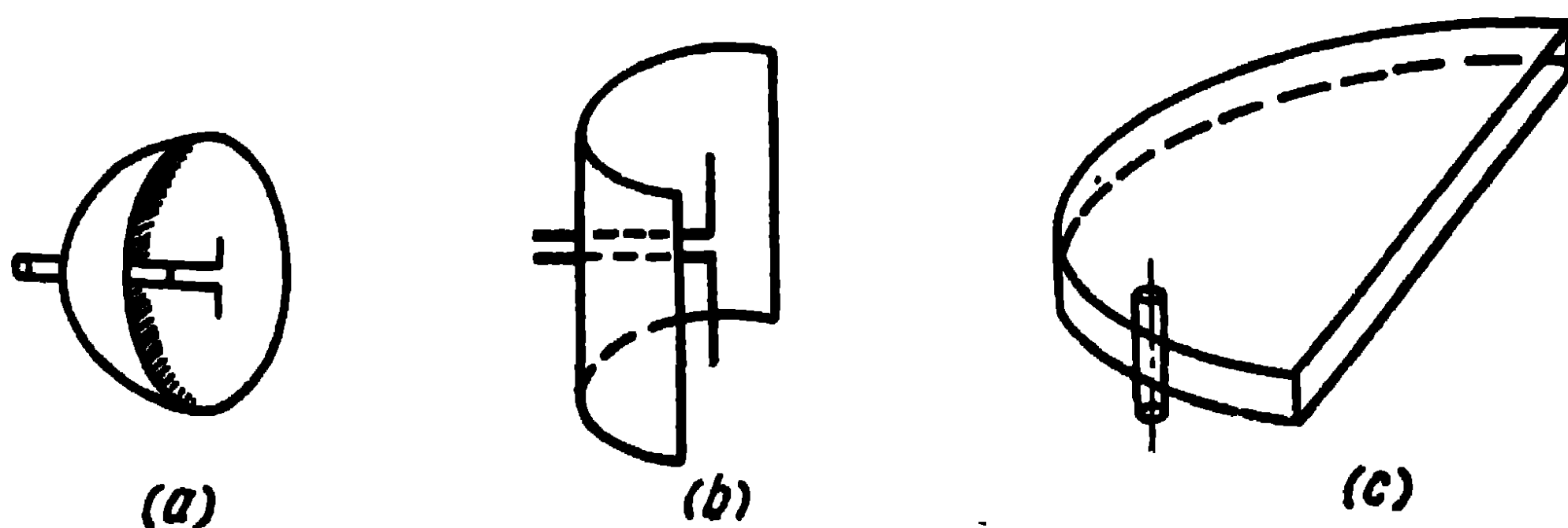


Fig. 10-88. Types of parabolic antennas:
 a —paraboloid; b —parabolic cylinder; c —parabolic cylinder bounded by parallel planes.

parallel conducting walls (Fig. 10-88). The paraboloid is excited by a dipole antenna placed in the focus and transforms the spherical wave front into a plane one. The parabolic cylinder is excited by a linear antenna lying on the focal line and transforms the cylindrical wave front into a plane one.

In these antennas, just as in lenses, use is made of the optical properties of radio waves. The geometrical properties

of the parabola are such that the rays directed from the focus and reflected from the parabola become parallel to the axis of the parabola, and the length of the path from the focus to the parabola and then to the line parallel to the x -axis passing through the edges of the parabola is the same for any angle θ (Fig. 10-89). In this way, a co-phasal surface is formed at the opening of the parabolic antenna and its radiation is highly directional.

In Cartesian coordinates, the parabolic surface is defined by the equation (the origin of the coordinates coincides with the apex of the paraboloid)

$$x^2 + y^2 = 4fz,$$

and in spherical ones, by the equation (the origin of the coordinates coincides with the focus of the paraboloid)

$$\rho = \frac{2f}{1 + \cos \theta}.$$

Parabolic antennas can be of the short-focus or long-focus kind. In a short-focus antenna, the focus is inside the antenna ($f < \frac{R}{2}$), in a long-focus one, the focus is outside the antenna

($f > \frac{R}{2}$). The limit value is the case $f = \frac{R}{2}$, when the focus coincides with the opening of the antenna.

To calculate the radiation of parabolic antennas, use is made of the equivalent surface electric and magnetic current method. Two methods of integration can be used: 1) over the surface which passes over the shadow side of the paraboloid and over its opening, and 2) over the surface which passes over the shadow and illuminated sides of the paraboloid. To simplify the problem, in both cases, the radiation of the electric surface currents distributed over the shadow side of the paraboloid is neglected and only the radiation of the surface currents distributed over the irradiated part of surface is taken into account.

In the first case, the irradiated part of the surface is plane, the equivalent electric and magnetic surface currents are regarded as co-phasal and the distribution of their amplitudes assumed proportional to the quantity

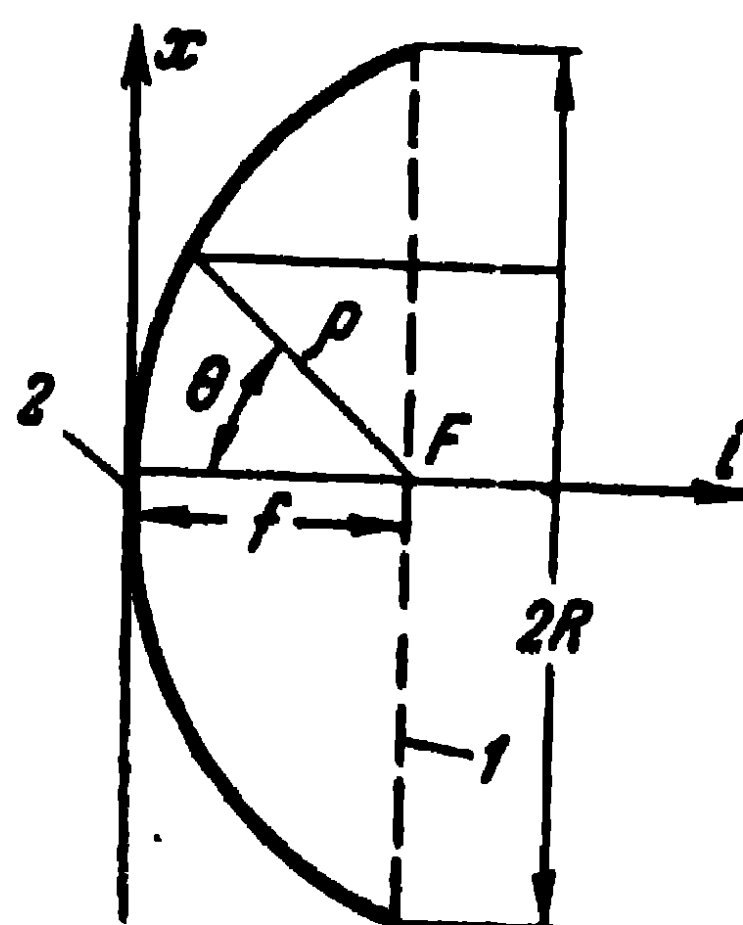


Fig. 10-89. Profile of a parabolic antenna: 1—opening; 2—apex of the parabola.

$\frac{1}{\rho}F(\theta)$, where ρ is the distance from the focus to the paraboloid and $F(\theta)$, the amplitude directional characteristic of the radiator. Thus, in this case, the calculation of the radiation of a parabolic antenna is reduced to the calculation of the radiation of a co-phasal circular surface with a corresponding distribution of the amplitudes of the equivalent surface currents.

In the second case, the irradiated part of the surface coincides with the surface of the paraboloid, so that the equivalent surface magnetic currents on this surface equal zero and the surface electric currents are real currents induced on the irradiated side of the paraboloid. The electric surface current is approximately defined as double the value of the component (tangential to the surface) of the magnetic field intensity of the incident wave from the radiator. In this case, the distribution of the amplitudes and phases of the induced currents is a more complex function of the coordinates than in the first case and, in addition, the direction of the currents changes from point to point on the surface of the paraboloid. Consequently, in the second case, the calculation of the radiation of a parabolic antenna is effected by integrating the radiation of the electric currents induced on the paraboloid.

Both methods of calculating the radiation of a parabolic antenna are approximate, since the distribution of the surface currents is determined approximately. However, the first method is less accurate since, because of the finite dimensions of the paraboloid, the rays reflected from the reflector and progressing towards the opening are not exactly parallel and this is not taken into account in the calculation. On the other hand, the first method is less cumbersome than the second one.

Let us examine the picture of the distribution of the currents induced by the radiator on the irradiated side of the paraboloid. Assume the radiator to be an elementary electric dipole directed along the x -axis with a plane counter-reflector in the shape of a disc. If the counter-reflector is approximately replaced by the mirror image of the dipole, the phase centre of the radiator can be regarded as coinciding with the centre of the counter-reflector, so that this point should be caused to coincide with the focus of the paraboloid (Fig. 10-90). Then, the magnetic field intensity of the

radiator on the paraboloid surface in spherical coordinates will be expressed as:

$$H_{\varphi}(\theta, \varphi) = F(\theta, \varphi) \frac{e^{-ik\rho}}{\rho}.$$

In rectangular coordinates, the magnetic field intensity has two components: H_y and H_z . The vector of the surface electric current density is defined as $\mathbf{J}^e = [\mathbf{H}, \mathbf{n}]$ where \mathbf{n} , is the vector equal to unity and perpendicular to the surface of the paraboloid. Since \mathbf{n} has all three components,

there are all three components

of the electric current: J_x^e ,

J_y^e and J_z^e . Accordingly, the

picture of the electric field

distribution projected on the

xy -plane looks as is shown in

Fig. 10-91. In the case of the

long-focus system, the electric

current components J_x^e have

the same direction in all four

quadrants, and the direction

of the current components J_y^e

changes from quadrant to quadrant.

In the case of the

short-focus system, current nodes

are present in the

paraboloid, situated at the points of intersection of the axis

of the electric dipole of the radiator with the surface of

the paraboloid; and the picture of the current distribution

on the xy -plane differs (on part of the surface) from that

in the case of the long-focus paraboloid. Now, in certain parts

of the reflector, the electric current component parallel to

the x -axis is of opposite direction relatively to the same

component in the main part of the reflector.

The radiation characteristic of a parabolic antenna is

defined in this way, in the two principal planes: xz and yz ,

by the current components J_x^e , with the radiation of the

current components J_y^e being cancelled out in these planes.

The polarisation of the radiated field is linear. In the other

planes passing through the z -axis, radiation occurs too,

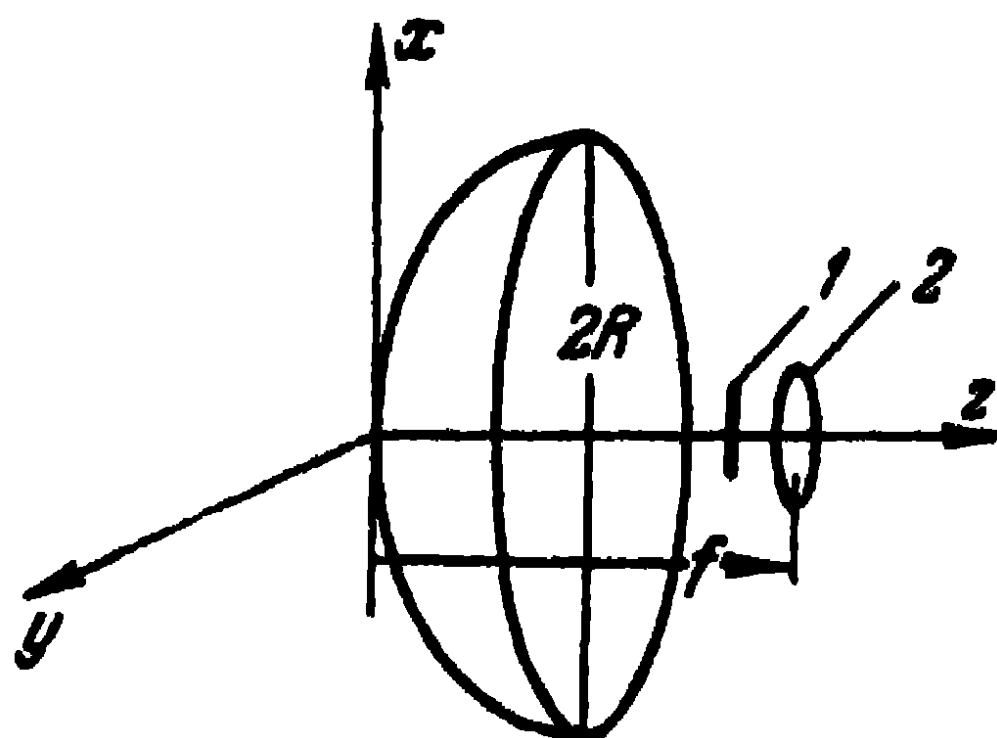


Fig. 10-90. Parabolic reflector:
1—electric dipole; 2—metal disc.

planes passing through the z -axis, radiation occurs too, defined by the current components J_y^e and, as a consequence, there appears a transverse (relatively to the principal one) polarisation of the radiated field. The total field is elliptically polarised. The transverse polarisation, called cross

polarisation, is parasitic and its presence decreases the antenna directive gain.

The level of cross polarisation is determined by the curvature of the paraboloid surface: the smaller the radius of the curvature of the reflector, at a prescribed diameter $2R$, i.e., the less long-focussed the reflector, the higher

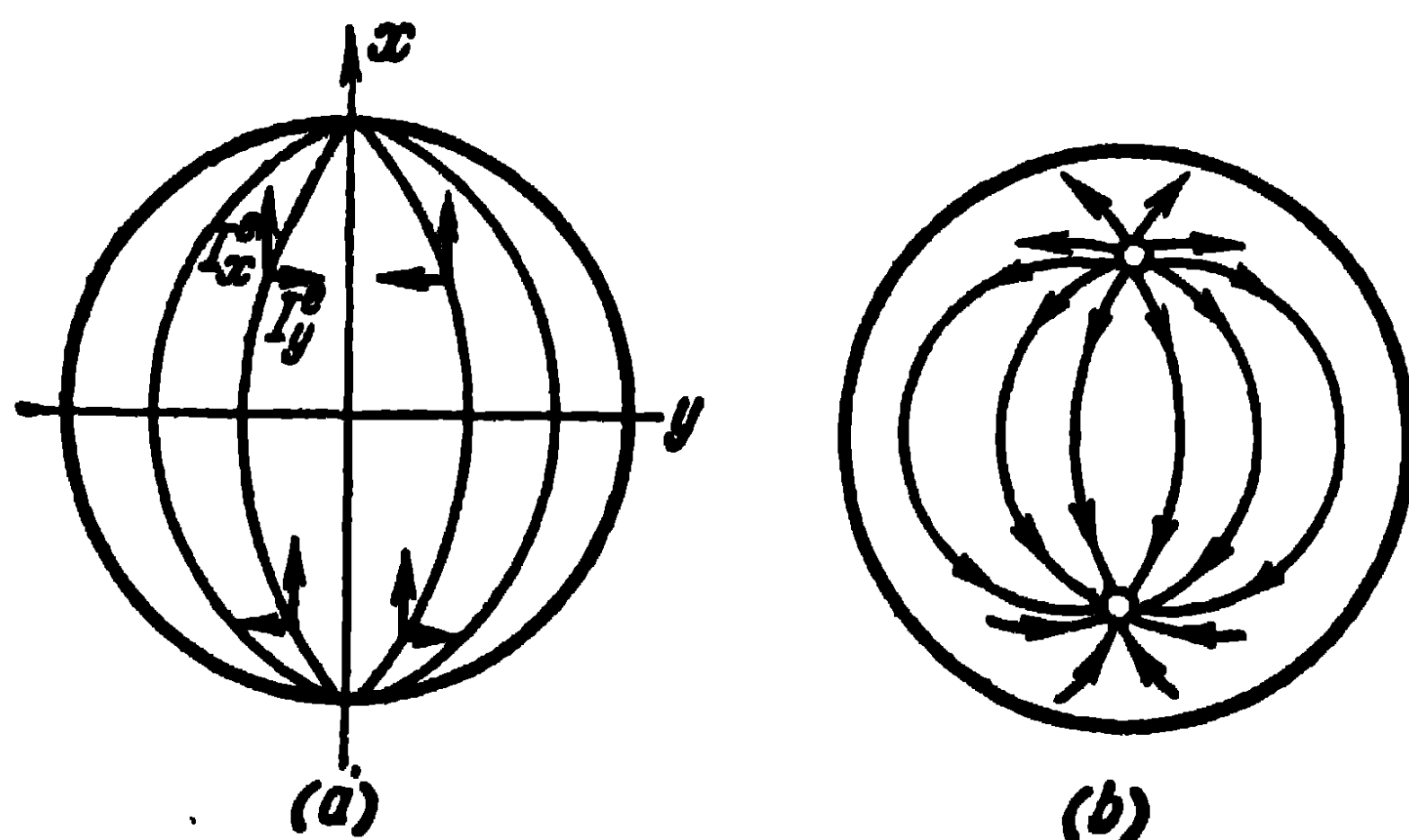


Fig. 10-91. Distribution of the electric current in a paraboloid:

a —long-focus reflector; b —short-focus reflector.

the level of the current components J_y^e relatively to the components J_x^e , the larger the field with a parasitic polarisation.

In the short-focus paraboloid, due to the appearance of current nodes (in the case of a dipole radiator), apart from an increased cross polarisation, the additional undesirable radiation of the zones of the reflector appears, in which the current components parallel to the x -axis are of the opposite direction. These zones of the paraboloid reduce the radiation in the main direction and increase the side lobes of the directional diagram.

The directional characteristics of a parabolic antenna irradiated by a dipole with a counter-reflector calculated from the current distribution in the reflector, is defined as:

$$f(\theta) = 1.48 \frac{aJ_1(a)J_0(b) - bJ_0(a)J_1(b)}{a^2 - b^2} + \frac{0.52J_1(b)}{b} + 0.5 \frac{bJ_2(1.5a)J_1(b) - 1.5aJ_2(b)J_1(1.5a)}{(1.5a)^2 - b^2}, \quad (10-76)$$

where

$$a = 3.5 \frac{R}{2f}, \quad b = kR \sin \theta,$$

R is the radius of the paraboloid opening;

θ , the angle with the paraboloid axis;

$J_n(x)$, a Bessel function of the n -th order.

This expression defines the directional diagram of the antenna in the xz -plane (E -plane). To define the directional diagram in the yz -plane (H -plane) the $(+)$ sign in front of the last item of this expression should be replaced by the $(-)$ sign.

In the limit case of a long-focus reflector, when $\frac{R}{f} \rightarrow 0$, the expression (10-76) takes the following form:

$$f(\theta) = 2 \frac{J_1(b)}{b}. \quad (10-77)$$

The expression (10-77) corresponds to a uniform distribution of the field amplitude at the paraboloid opening.

Indeed, for small values of the argument $bJ_1(b) \approx \approx 0.5 \sin b$ and the expression (10-77) becomes $f(\theta) = \frac{\sin b}{b}$, which corresponds to the radiation characteristic of an ideal plane antenna.

Fig. 10-92 represents the directional diagram of a paraboloid, calculated from (10-76) for various values of R/f . It is seen from this figure that when the ratio R/f decreases, the major lobe of the directional diagram narrows down, whereas the side lobes increase, this being connected with the increase of the uniformity of distribution of the field amplitude at the opening of the antenna.

It should be noted that the cited directional diagrams are characteristic also in the case of a radiator of another type.

Indeed, in the case of any radiator of sufficiently small dimensions, the phase centre of which coincides with the paraboloid focus, the field at the opening of the paraboloid

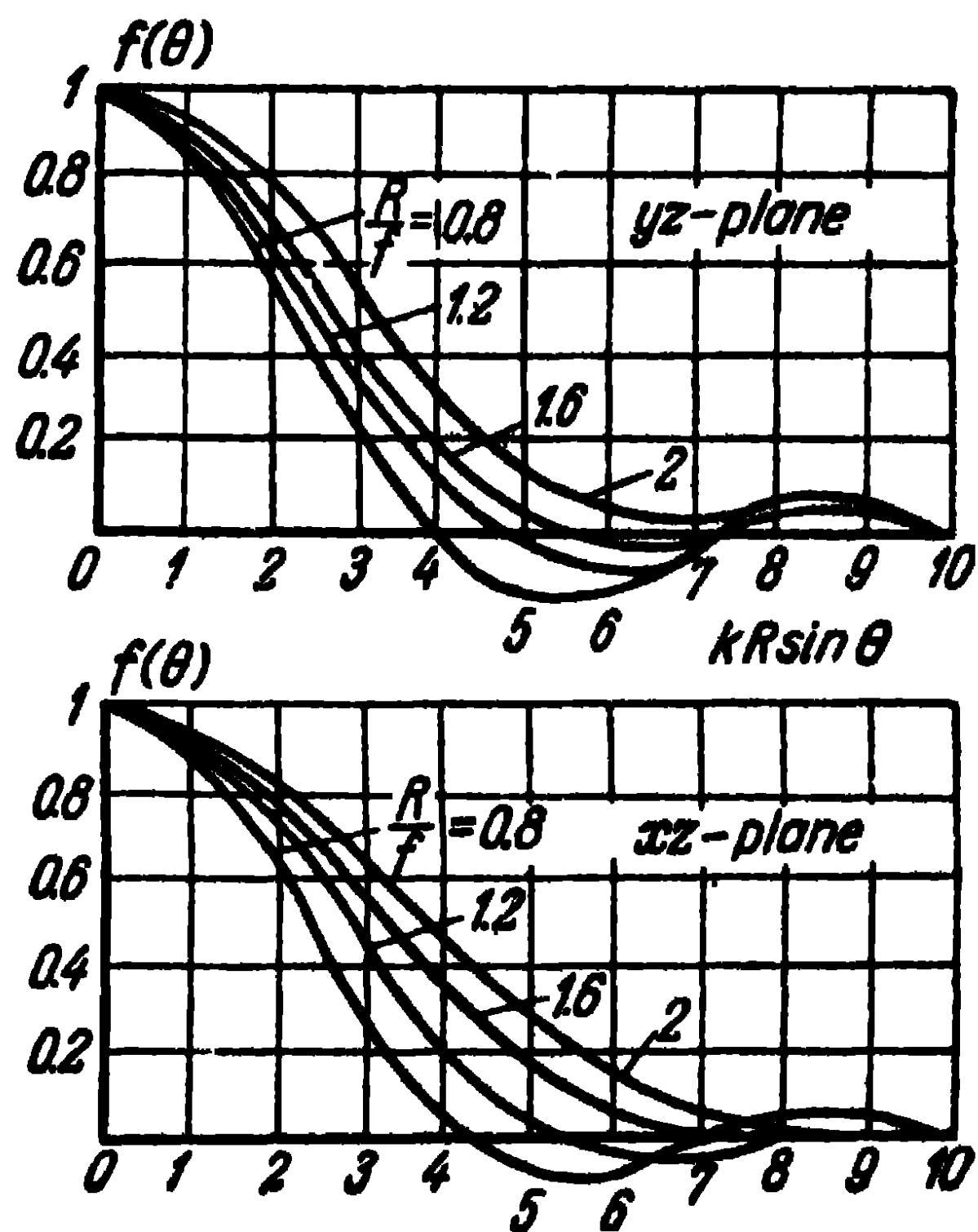


Fig. 10-92. Directional diagrams of a parabolic antenna.

will be co-phasal, and if the directional diagram of the radiator under consideration is identical to the directional diagram of a dipole radiator with a counter-reflector, the directional diagrams of the paraboloid will likewise be identical.

The directive gain of a parabolic antenna can be expressed as:

$$D = \frac{4\pi s}{\lambda^2} k_1, \quad s = \pi R^2,$$

where k_1 is the utilisation factor of the surface of the reflector. It depends on the law governing the distribution of the field amplitudes at the opening of the paraboloid. For a radiator consisting of an elementary dipole with a counter-reflector, the quantity k_1 can be expressed as:

$$k_1 = 5.15 \left[0.423 J_1 \left(3.5 \frac{R}{2f} \right) + 0.26 \frac{R}{2f} \right]^2.$$

This quantity is represented graphically in Fig. 10-93. It is seen from the graph that the utilisation factor of the

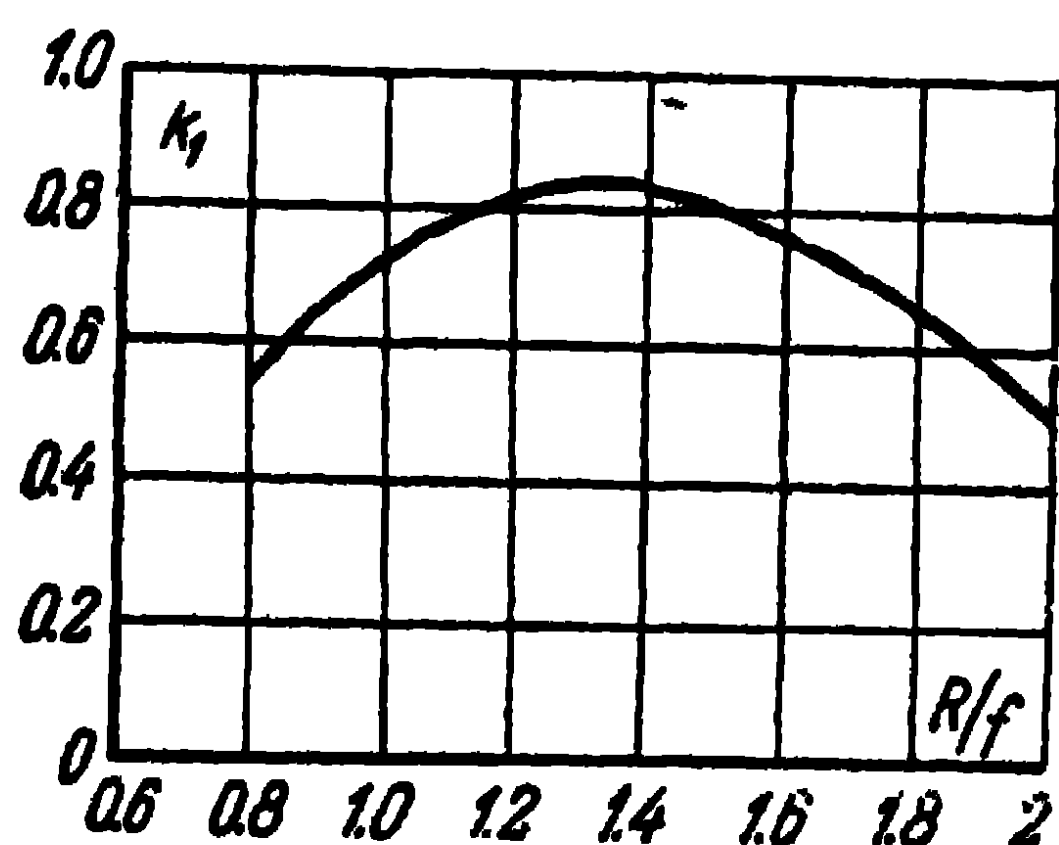


Fig. 10-93. Curve of utilisation factor of reflector surface.

reflector has an optimum value, which occurs when $R/f=1.3$ and equals $k_1=0.83$. This optimum occurs as a result of the action of two opposed factors. In the case of small values of R/f , the reflector is irradiated uniformly which leads to a narrowing of the major lobe of the directional diagram, but, at the same time, a considerable part of the energy

emitted by the radiator does not reach the reflector (flowing over its edge), which leads to a lowering of the directive gain. On the other hand, in the case of large values of R/f , almost all the energy of the radiator reaches the reflector but, at the same time, the edges of the reflector are only very slightly irradiated, which leads to a widening of the directional diagram and, once again, to a lowering of the directive gain. In the case of an optimum value of the ratio R/f , the field intensity at the edge of the opening of

the reflector constitutes approximately $1/2$ of the field intensity in the centre of the opening.

The above-mentioned optimum relatively to k_1 occurs for any radiator, but if the directional diagram of the radiator under consideration is sharper than in the case of a dipole radiator, the optimum value of k_1 occurs when the ratio R/f is smaller than 1.3. Conversely, for a wider directional diagram of the radiator, this optimum occurs for a ratio R/f larger than 1.3.

Let us now define the width of the directional diagram of the paraboloid corresponding to the maximum directive gain of the antenna (when $R/f=1.3$). It follows from the graphs in Fig. 10-92 that the width of the directional diagram at half-power in the E-vector plane can be defined as:

$$2\theta_{1/2} \approx 75^\circ \frac{\lambda}{2R},$$

and in the H-vector plane, as:

$$2\theta_{1/2} \approx 70^\circ \frac{\lambda}{2R}.$$

If a lower level of the side lobes is required than in the case when $R/f=1.3$, one has to be content, at a prescribed diameter of the opening, with a wider directional diagram and smaller directive gain of the antenna, choosing the ratio R/f equal, for example, to two.

Note that the value of the side lobes in real conditions is larger than can be defined from the graphs in Fig. 10-92, because the above-cited expression (10-76) takes no account of a series of factors: a) the branching off of the electric currents to the shadow surface of the reflector; b) the effect of cross polarisation; c) the overflow of part of the energy of the radiator over the edges of the reflector; d) the shadows set up by the radiator itself which is located on the path of the rays reflected from the reflector.

Various devices can be used as radiators of parabolic antennas. The choice of the type of radiator often depends on whether a coaxial line or a waveguide is used as a feed line for the radiator. Thus, when an electric dipole with a counter-reflector is fed by a coaxial line, use can be made of the dipole feed circuit shown in Figs. 10-3, *b* or 10-3, *c*. In that case, the dipole is placed at a distance of approximately $\lambda/4$ from the counter-reflector and the diameter of the counter-

reflector is taken equal to approximately 0.8λ . In another case, a horn is utilised as the radiator, fed by a rectangular waveguide. In that case, in order to prevent the horn from shadowing the radiation of the reflector, as well as to reduce the effect the reflector has on the horn, frequent use is made of a displaced horn shown in Fig. 10-94. Fig.

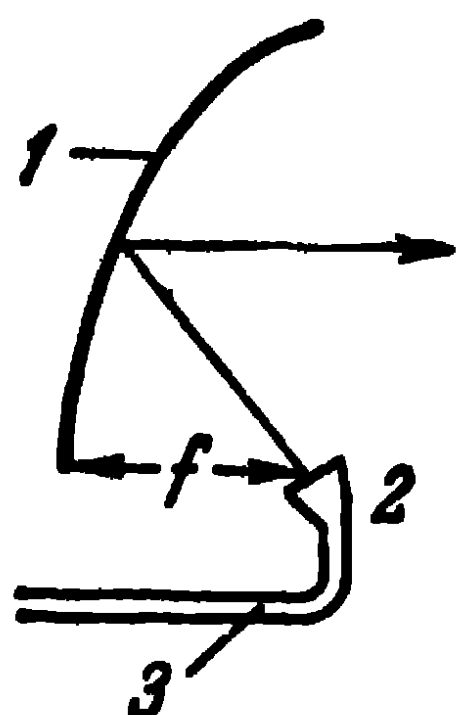


Fig. 10-94. Horn radiator:

1—reflector; 2—horn; 3—waveguide.

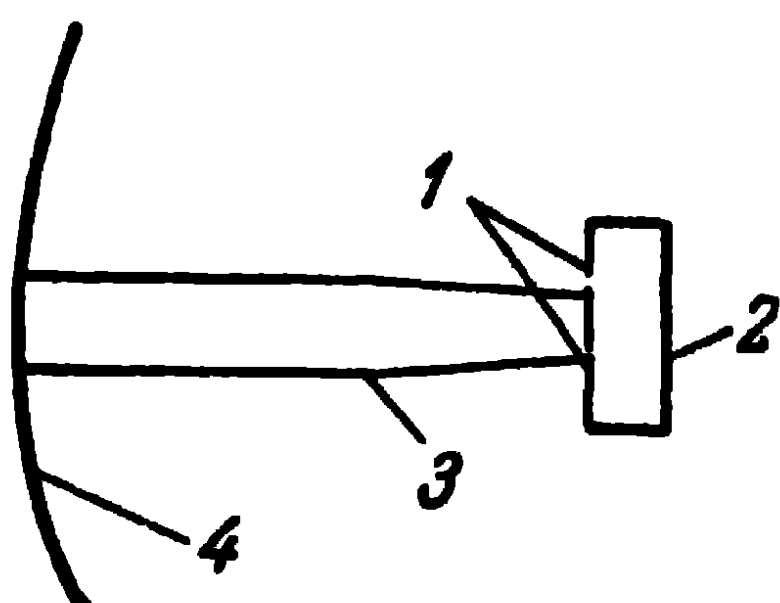


Fig. 10-95. Slot radiator:

1—slots; 2—resonator; 3—waveguide; 4—reflector.

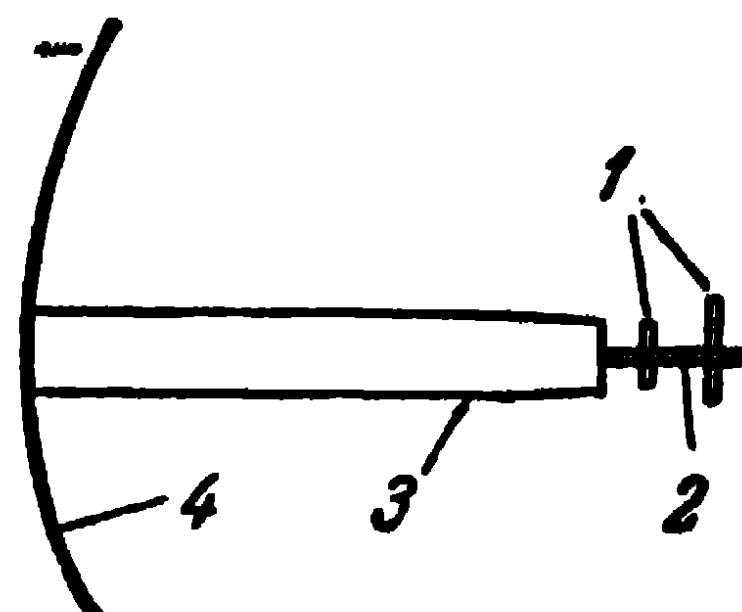


Fig. 10-96. Dipole radiator:

1—dipoles; 2—metal plate; 3—waveguide; 4—reflector.

10-95 represents a twin-slot radiator in which slots of half-wave-length are located on a rectangular resonator fed by a narrowing rectangular waveguide. The distances between the slots of the radiator are chosen such as to obtain the desirable directional diagram. Fig. 10-96 represents a dipole radiator with a dipole reflector fed by a rectangular waveguide. Both dipoles are secured on a metal plate and excited by the open end of the waveguide. Their lengths are chosen such that the energy maximum should be radiated by them towards the parabolic reflector. Fig. 10-97 shows a dipole radiator with a plane counter-reflector fed by a coaxial line. The segment of coaxial line $\lambda/4$ long between the dipole and the counter-reflector plays the role of a metal insulator.

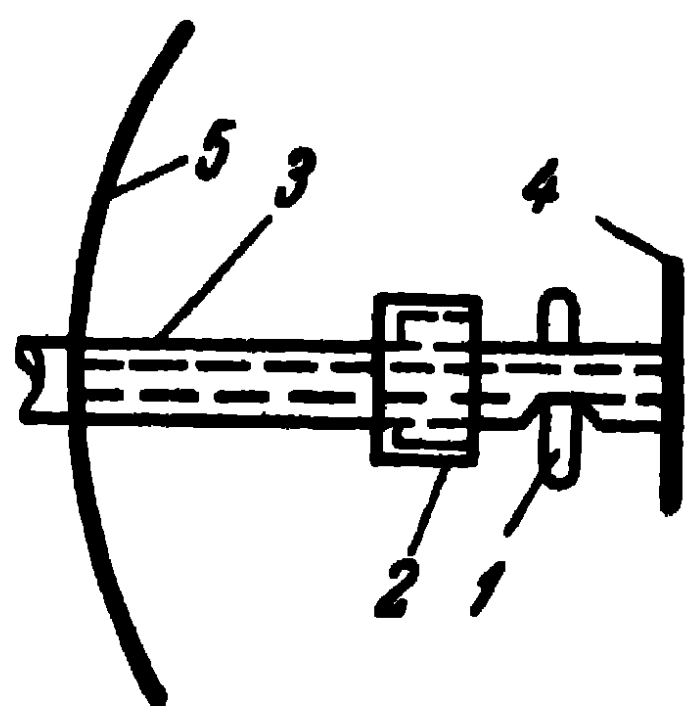


Fig. 10-97. Dipole radiator with a plane counter-reflector:

1—dipole; 2—quarter-wave sleeve; 3—coaxial line; 4—counter-reflector; 5—reflector.

The purpose of the metal sleeve in the dipole radiator in Fig. 10-97 is to prevent the electric currents from branching off to the outer surface of the coaxial line. However, the currents on the coaxial line cannot be eliminated altogether and, in the region between the metal sleeve and the counter-

reflector, they are of considerable magnitude. The radiation of these parasitic currents B is superimposed on that of the dipole currents A (Fig. 10-98) and this causes the wave front to rotate by a certain angle (dotted line) at the opening of the paraboloid. As a consequence, the direction of the radiation maximum of the antenna is deviated by a certain angle from its axis. When the radiator rotates around its axis, the directional diagram of the antenna describes a cone, the minimum of radiation occurring along the antenna axis. This rotation is made use of in radar for target location, in which case, the distortion of the phase wave front at the opening of a parabolic reflector turns out to be a desirable factor.

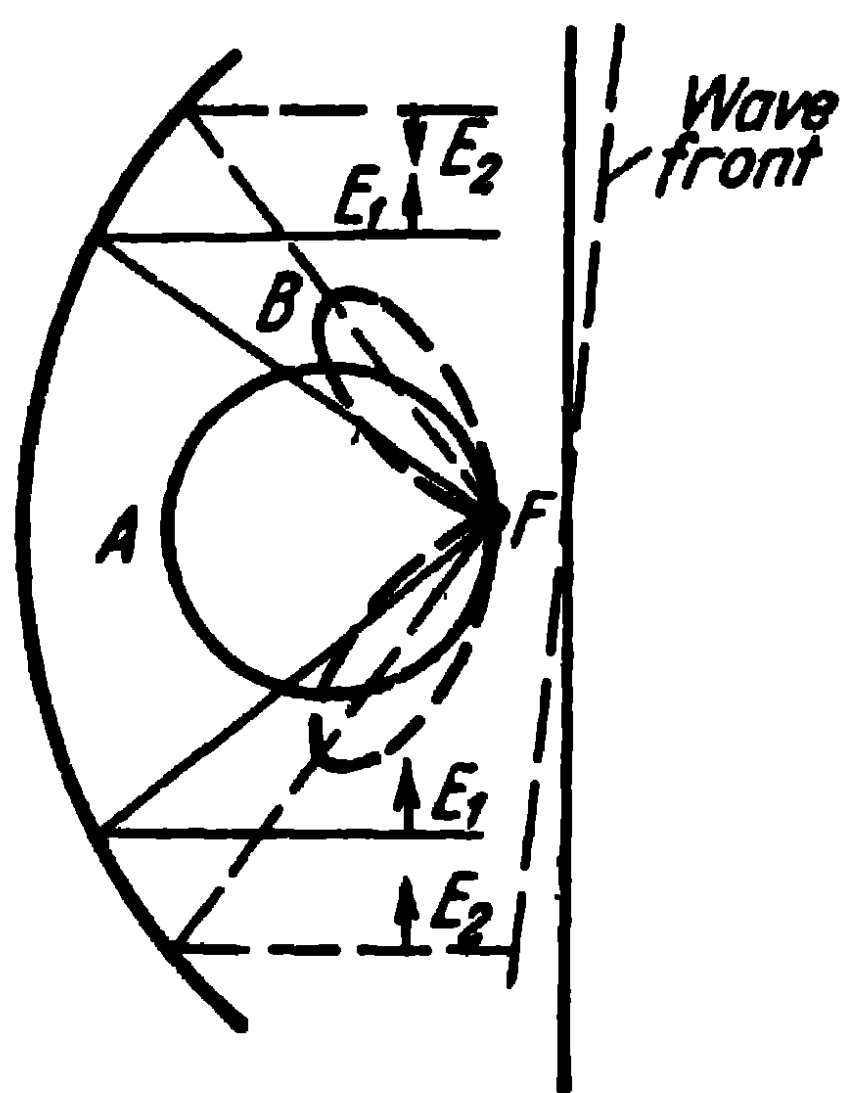


Fig. 10-98. Distortion of the antenna radiation phase front.

For rotation or scanning purposes of the directional dia-

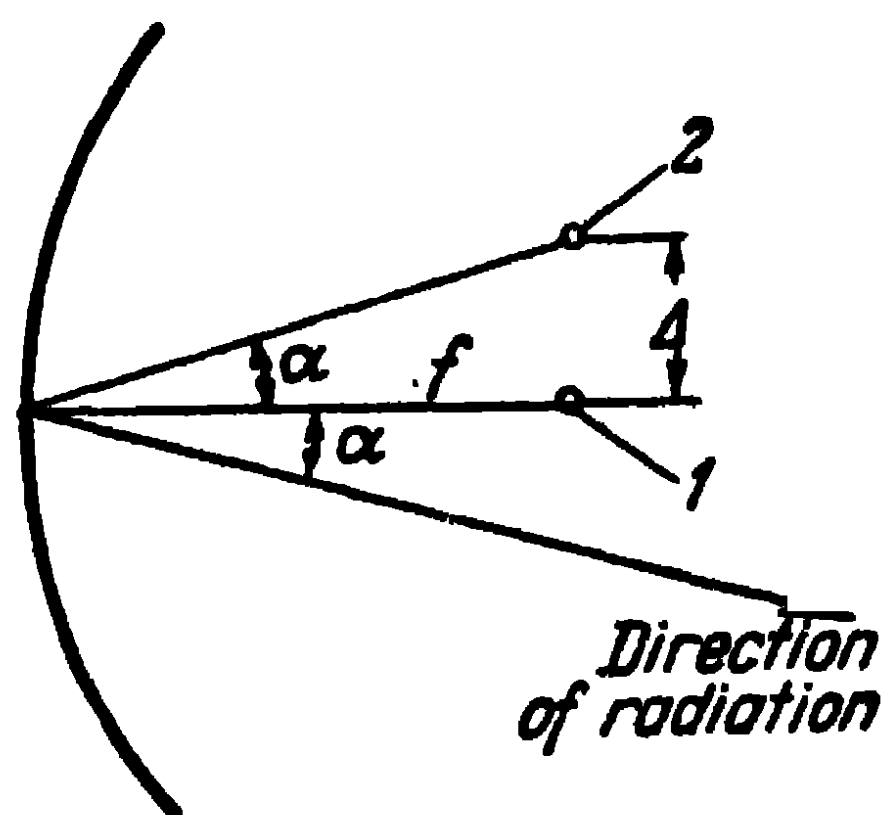


Fig. 10-99. Displacement of radiator out of focus:
1—focus; 2—radiator.

gram, the phase centre of the radiator is often intentionally removed at a certain distance Δ from the focus as shown in Fig. 10-99. At the same time, the rays reflected from the reflector are deviated to the opposite side from the antenna axis and form with the antenna axis an angle α , approximately defined by the expression $\tan \alpha = \frac{\Delta}{f}$. Consequently, the wave front and the maximum radiation direction of the antenna rotate by an angle α . Apart from rotating, the wave front becomes also distorted, which leads to a widening of the directional diagram and an increase (from the inner side) of the side lobes. However, when the displacement Δ is small, the distortions are insignificant, so that, in practice, such displacements of the radiator are used for scanning the

directional diagrams within the limits of its double or triple width.

Let us now consider the reaction of the reflector on the radiator. As was mentioned earlier, part of the energy reflected from the reflector returns to the radiator, since it is on the path of the rays reflected from the reflector. If the radiator was matched to the feed line in the absence of a reflector, the introduction of a reflector leads to the appearance in the feed line of a reflected wave with a reflection coefficient which can be evaluated from the expression

$$|p| = \sqrt{\frac{P_1}{P_0}},$$

where P_1 is the power reflected from the reflector and received by the radiator;

P_0 , the power radiated by the radiator.

If we designate by E_1 the electric field intensity of the wave reflected from the reflector and incident on the radiator, then in accordance with Paragraph 6-4, the power received by the radiator is:

$$P_1 = \frac{\lambda^2 E_1^2}{\pi^2} \frac{D\eta}{960}, \quad (6-32)$$

where D is the radiator directive gain;

η , the radiator efficiency.

The field intensity of the reflected wave of the radiator E_1 can be regarded as approximately equal to the field intensity of the wave radiated by the radiator at the apex of the paraboloid E_0 , which is expressed as:

$$E_0 = \frac{\sqrt{60 P_0 D \eta}}{f}.$$

Substituting this expression into (6-32), we obtain for the reflection coefficient

$$|p| = \frac{\lambda D \eta}{4\pi f}.$$

To eliminate the effect of the reflector in the line it can be tuned up by introducing into it a complementary reflection cancelling the reflection caused by the effect of the reflector. However, this can only be done on one fixed frequency. When the frequency of the oscillations changes, the phase of the coefficient of the reflection caused by the reflector under-

goes a sharp change, due to the fact that the ratio of the focal distance to the wave-length f/λ is much higher than unity. This leads to a narrowing of the radiator pass-band. Consequently, special measures have to be adopted in order to decrease the magnitude of the coefficient of reflection from the reflector, i.e., to decrease the reaction of the reflector on the radiator.

One of the ways of decreasing the effect of the reflector on the radiator is to remove the radiator from the antenna field (see Fig. 10-94). Another way is to set up a supplementary reflection of the energy from the reflector, which

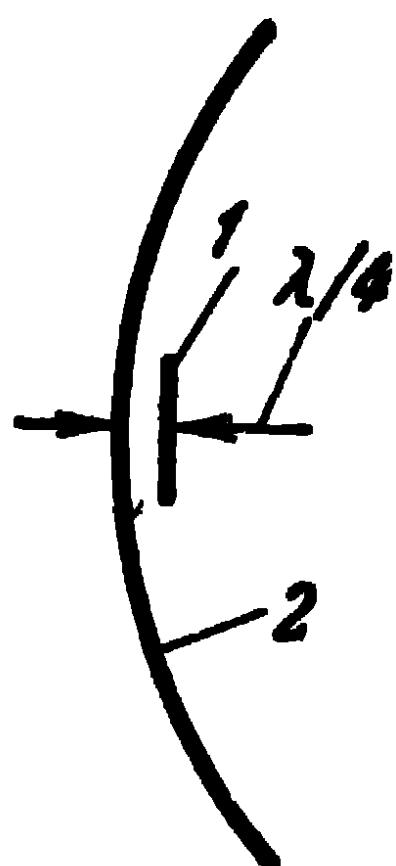


Fig. 10-100. Installation of a supplementary disc reflector:
1—disc; 2—reflector.

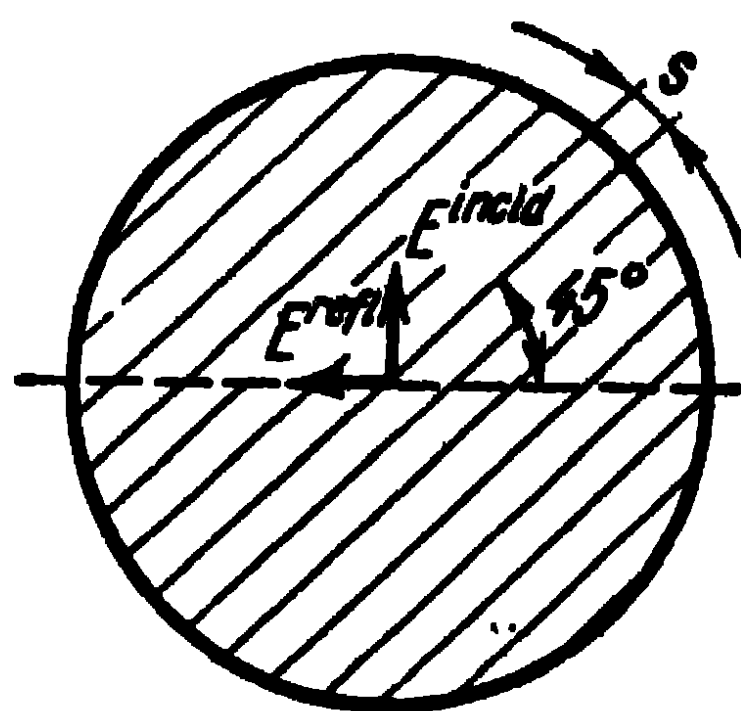


Fig. 10-101. Quarter-wave lattice on a reflector.

leads to a decrease of the magnitude of the field of the radiator reflected wave (Fig. 10-100).

To this end, a metal disc is placed at a distance of approximately a quarter of a wave-length from the apex of the reflector. The electric current induced in the disc sets up in the radiator a supplementary field opposed in phase to the main field reflected from the reflector. The proper choice of the diameter of the disc considerably reduces the radiator total field, thereby substantially eliminating the effect the reflector has on the radiator.

This effect can also be eliminated by installing a quarter-wave lattice on the reflector (Fig. 10-101). The lattice consists of parallel metal plates $\lambda/4$ wide placed on the irradiated side of the paraboloid at a distance s apart, small in comparison with the wave-length. The plates form

an angle of 45° together with the vector E^{inc} of the field incident from the radiator. The field reflected from the reflector rotates the plane of the polarisation by 90° relatively to the incident field, so that the reflected field does not affect the radiator.

As regards the accuracy to size of the parabolic reflector, it can be determined from Fig. 10-102. Suppose dimension

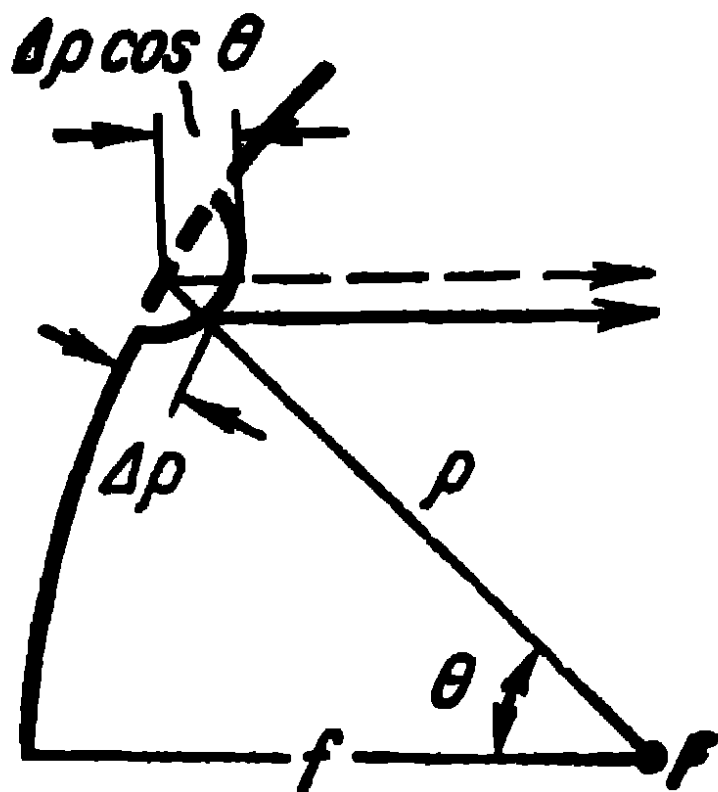


Fig. 10-102. Calculating the accuracy of design of the reflector.

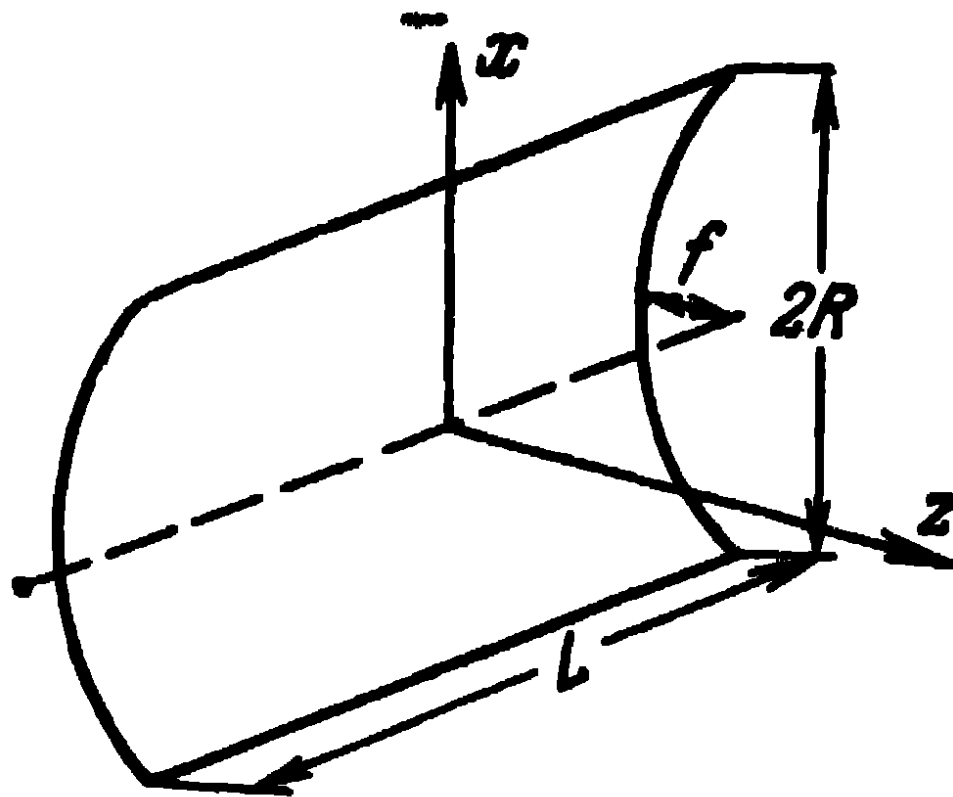


Fig. 10-103. Reflector in the shape of a parabolic cylinder.

$\Delta \rho$ is projected on the surface of the reflector; the distortion of the field phase at the opening of the reflector is then:

$$\psi_1 = k \Delta \rho (1 + \cos \theta),$$

and if we regard $\psi_1 = \frac{\pi}{8}$, as the permissible field phase distortion, the permissible inaccuracy of execution of the reflector is expressed as:

$$\Delta \rho = \frac{\lambda}{16 (1 + \cos \theta)}.$$

It can be seen from this expression that the accuracy to size of the reflector in the central part should be greater than at the edges of the reflector. Furthermore, the edges of the reflector are less intensely excited, which reduces the effect the inaccuracy to size of the edges of the reflector has on the antenna directional diagram.

Let us now pass on to the investigation of parabolic cylinders. Reflectors in the shape of parabolic cylinders find particularly frequent application when the object is to obtain directional diagrams of different width in mutually

perpendicular planes. The radiator of the parabolic cylinder (Fig. 10-103) placed on the focal line is a co-phasal linear antenna of length L . It can consist of, for example, half-wave dipole shown in Fig. 10-103. The radiator sets up a cylindrical wave front and because the reflector profile in the xz -plane has a parabolic form, a plane wave front is set up at the antenna opening. At the same time, the distribution of the field amplitudes in the y -axis direction at the opening is uniform, and, in the x -axis direction, it depends on the directional diagram of the radiator in the xz -plane. In this way, the directional diagram of the parabolic cylinder in the yz -plane is determined by the dimension L and, in the xz -plane, by the dimension $2R$. The directional diagrams can be given different forms in two mutually perpendicular planes by the proper choice of L and R . The dimension $2R$ should be chosen such that the reflector should capture the main part of the energy radiated by the radiator.

Linear radiators can be of the most varied forms, such as waveguide slot antennas, sectoral horns, arrays of half-wave dipoles excited by a rectangular waveguide, etc.

The linear radiator often consists of a parabolic cylinder bounded by parallel planes (segment-parabolic antenna) and, in turn, excited by the open end of a rectangular waveguide (Fig. 10-104).

The distance between the plates (Δ) of a segment-parabolic antenna is chosen such as to preclude the propagation of higher-order modes. As a rule, the E-vector of the excited field is chosen perpendicular to the parallel planes of the radiator. The dimension Δ should then be smaller than $\lambda/2$. In that case, the velocity of propagation of the wave (of TEM mode) between the planes equals that of light. Sometimes, the E-vector is chosen parallel to the planes of the radiator, in which case, the dimension Δ is defined from the condition $\Delta < \lambda < 2\Delta$ and an H_{01} mode is propagated in the inter-plane space. In the latter case, the accuracy to size of the distance Δ should be greater than in the first case.

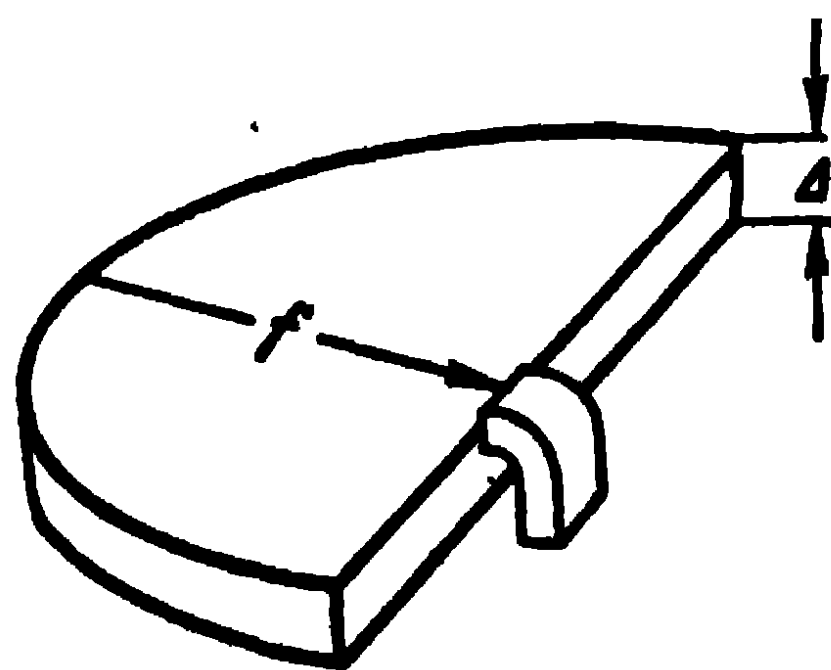


Fig. 10-104. Segment-parabolic antenna.

10-14. Other Reflector Antennas

The present paragraph will be devoted to a brief description of a number of other reflector antennas. For further details, the reader is referred to the special literature.

To begin with, let us describe the reflector antenna shown in Fig. 10-105. The antenna consists of a cylindrical reflector of special form 1, forming a directional diagram in the vertical plane, and of a linear radiator 2 in the shape of a

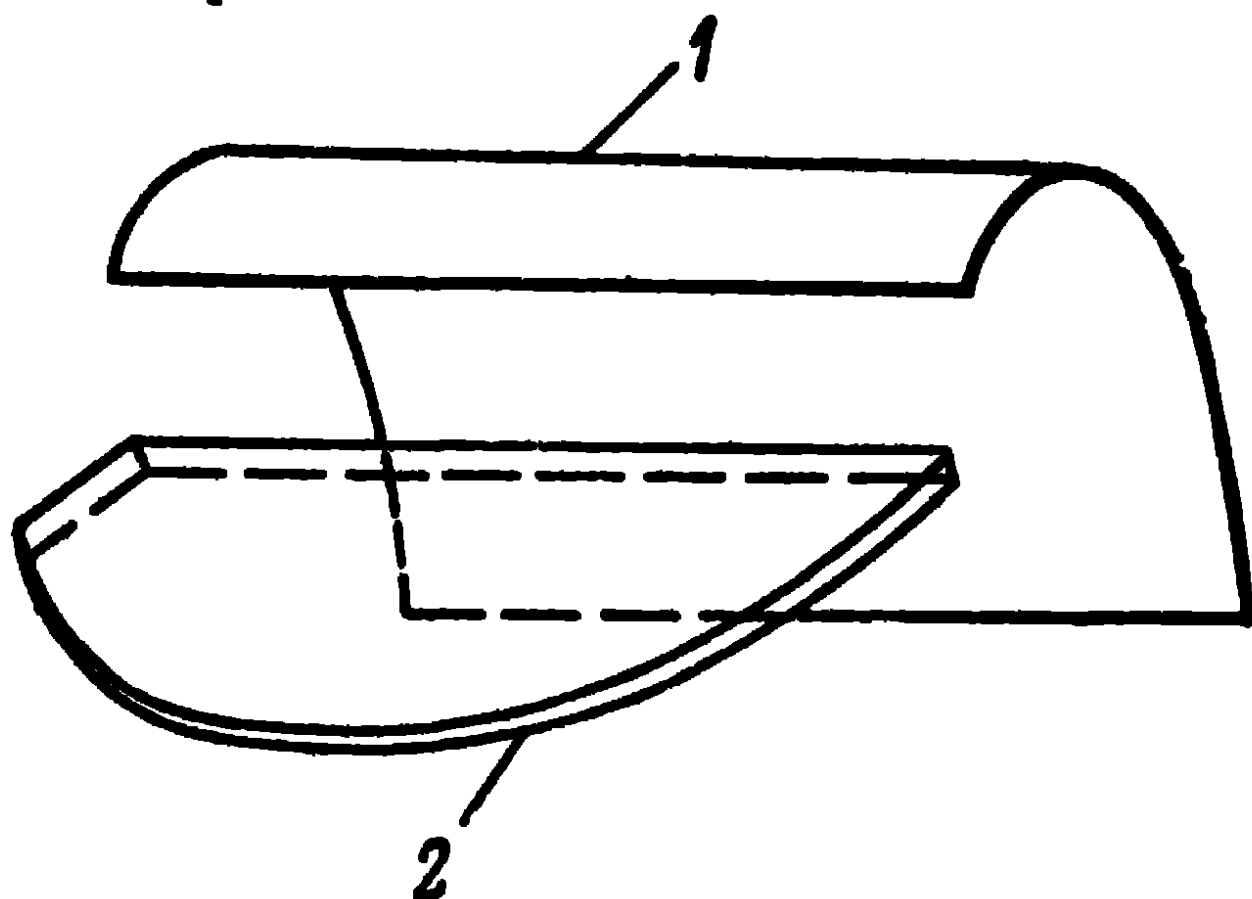


Fig. 10-105. Cylindrical reflector of special form.

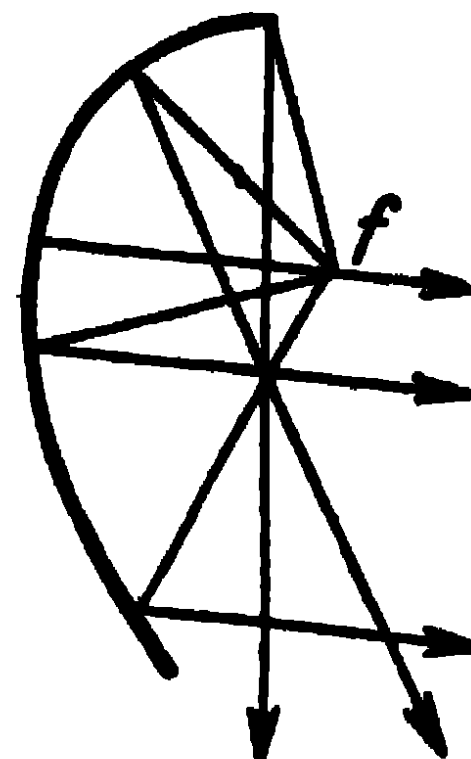


Fig. 10-106. Reflector cross section.

parabolic cylinder with bounding planes, forming a directional diagram in the horizontal plane.

As shown in Fig. 10-106, the lower part of the reflector is of a nearly parabolic shape and sets up a parallel beam of reflected rays, whereas the upper part has a nearly spherical shape and sets up dispersive reflected rays. The directional

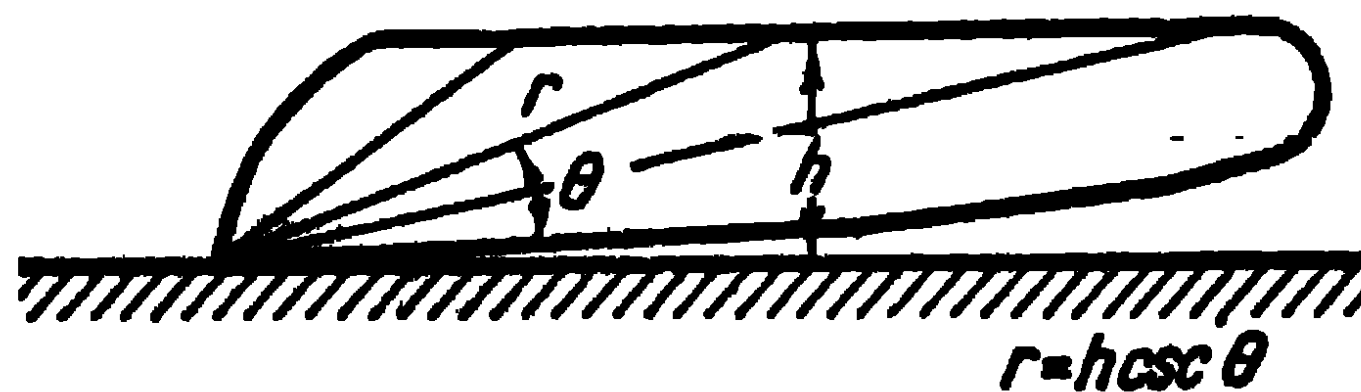


Fig. 10-107. Directional diagram of a ground radar.

diagram of the antenna in the vertical plane is approximately expressed as $f(\theta) = \csc \theta$ and has the form of a vertical fan.

Antennas of this kind, used, in particular, in ground

radars ensuring radiation of in-coming or out-going aircraft with equal intensity (Fig. 10-107).

Spherical reflectors find application in radar technique. When the radiator is situated at the point $f = \frac{R}{2}$, the spherical reflector operates just as a parabolic reflector.

Indeed, from a comparison of the equation of the curve of the circumference (Fig. 10-108)

$$x^2 + (R - z)^2 = R^2$$

or

$$x^2 = 2Rz \left(1 - \frac{z}{2R} \right)$$

with the equation of a parabola ($x^2 = 4fz$), it is seen that part of the circumference in the vicinity of the apex ($\frac{z}{2R} \ll 1$) can be regarded as part of a parabola with a focus lying at the point $f = R/2$. Consequently, a spherical reflector irradiated by a point source enables to transform a spherical wave in a nearly plane one and, thereby, ensure the formation of narrow directional diagrams. At the same time, by displacing the radiator along a circumference of radius $R/2$, such a reflector enables to scan the directional diagram of the antenna within the limits of a very narrow angle.

The property of spherical reflectors is utilised for obtaining a highly directional radiation, the directional diagram of which has a 360° scanning angle. We have in mind the helical-spherical antenna [66], which consists of a closed sphere (Fig. 10-109), made of current-conducting strips lying close to one another at an angle of 45° to the meridians of the sphere. The radiator situated inside the sphere sets up

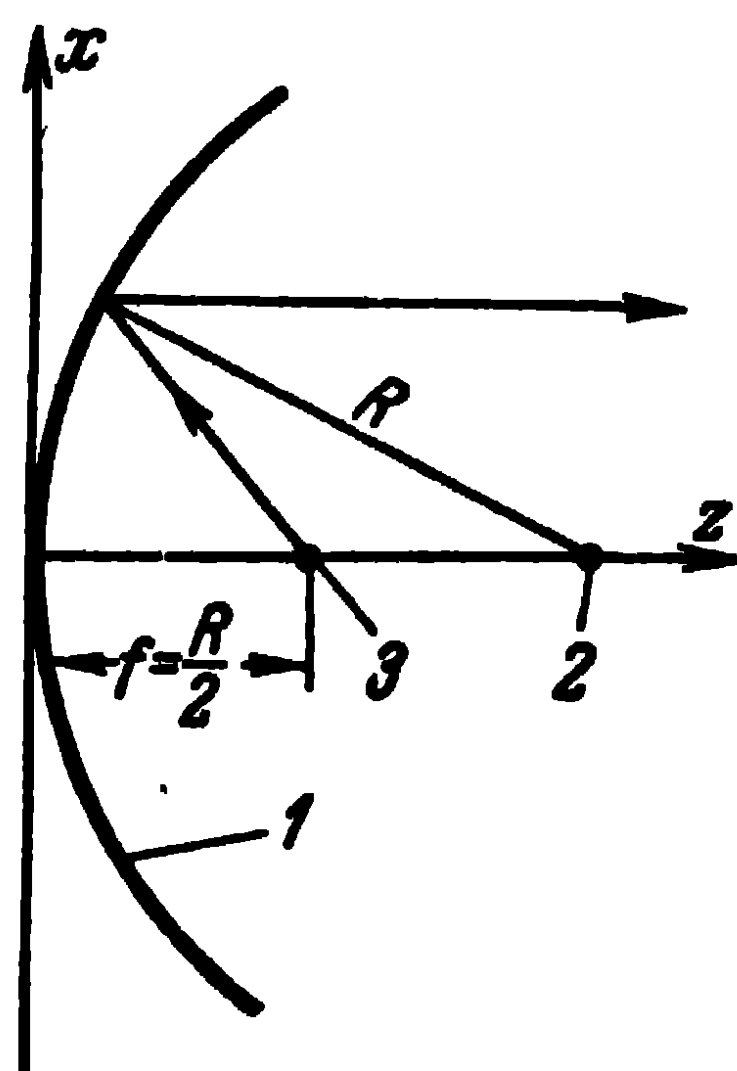


Fig. 10-108. Spherical reflector:

1—circumference; 2—centre of the circumference; 3—focus of the parabola.

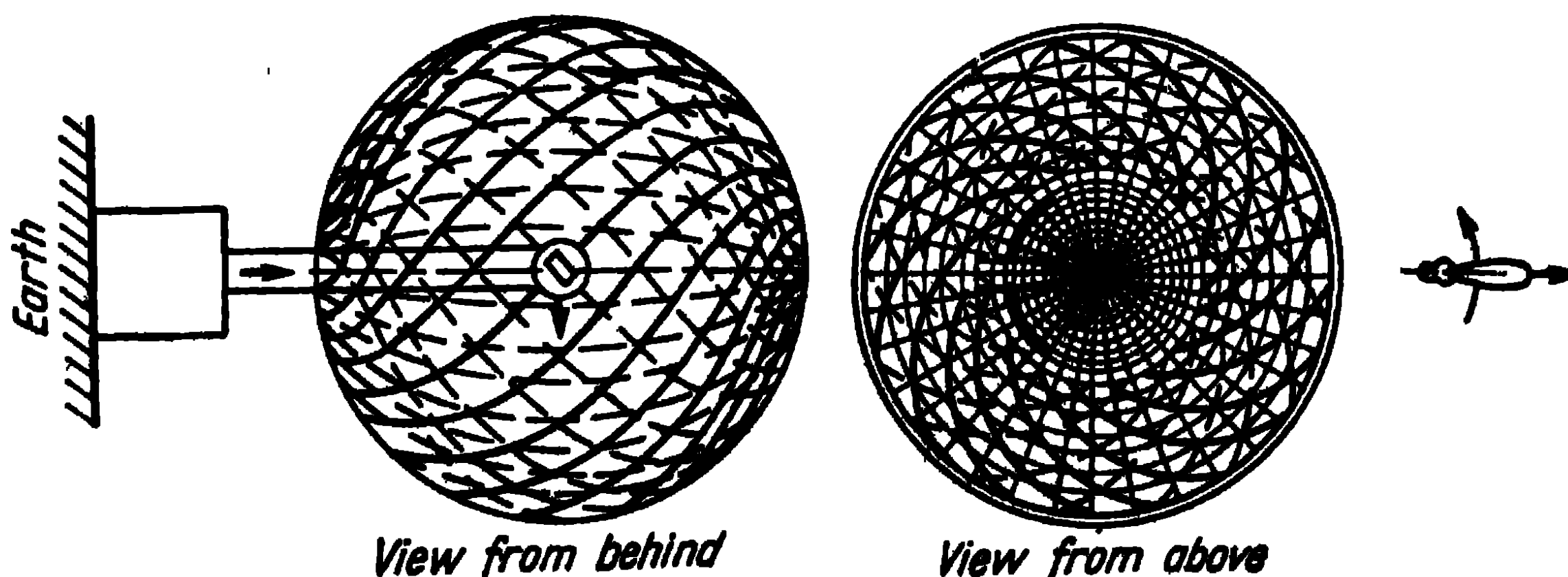


Fig. 10-109. Helical-spherical antenna.

in the wave incident upon the reflector an electric field intensity vector parallel to the current-conducting strips of the reflector. The part of the surface of the sphere thus irradiated entirely reflects the incident wave towards the radiator, forming a parallel beam which, on the diametrically opposed parts of the reflector, meets the current-conducting strips orientated towards the electric field vector at an angle of 90° and pass freely through the reflector. The radiator, which lies half-way between the centre of the sphere and its surface, rotates in the horizontal plane, this leading to the rotation of the directional diagram in that plane. When it is displaced along the circumference in the vertical plane the directional diagram can scan in the vertical plane within a certain angle.



Fig. 10-110. Horn-parabolic antenna:

1—horn; 2—parabolic surface; 3—opening

The spherical shape of the reflector is very convenient for making large collapsible air reflectors enabling the rapid unfolding and folding of the antenna. The antenna consists of a canvas envelope carrying current-conducting strips. The advantage of such an antenna consists in that the canvas envelope reproduces a spherical surface with the utmost ease and accuracy.

Horn-parabolic antennas find application in radio-relay lines (Fig. 10-110); they are a successful combination of a pyramidal horn with part of a parabolic surface. The focus of the parabolic surface coincides with the phase centre of the horn and the electromagnetic waves incident from the horn upon the parabolic reflector are reflected towards the opening without returning to the horn.

Horn-parabolic antennas are characterised by a small level of the side lobes and reverse radiation and are, therefore, suitable for radio-relay lines in which receiving antennas are combined with transmitting ones. Thus, horn-parabolic antennas operating on a certain radio-relay line [67] and standing side by side, have a transient attenuation of the order of 90 db.

The flare angles of the horns are taken equal to $30-40^\circ$,

and continuous transitions of the hyperbolic type of a length of the order of $(10 \div 15) \lambda$ are inserted between the inputs of the horns and the feed waveguides. This lowers the coefficient of reflection from the horn in the waveguide down to 1-2%.

Plane reflectors find application in radio-relay lines; they are placed on top of a mast at an angle of 45° to the horizon and rotate by an angle of 90° a beam set up by a highly directional antenna at the foot of the mast (Fig. 10-111). The advantage of devices of this kind consists in that long feed lines are no longer needed when the antennas are placed on top of a mast. As, shown by theoretical calculations [68], the efficiency factor of plane reflectors can be higher than unity. In this case, the efficiency factor is the ratio of the power P_1 received by the receiver when using a plane reflector (Fig. 10-112) to the power P_2 received by the receiver

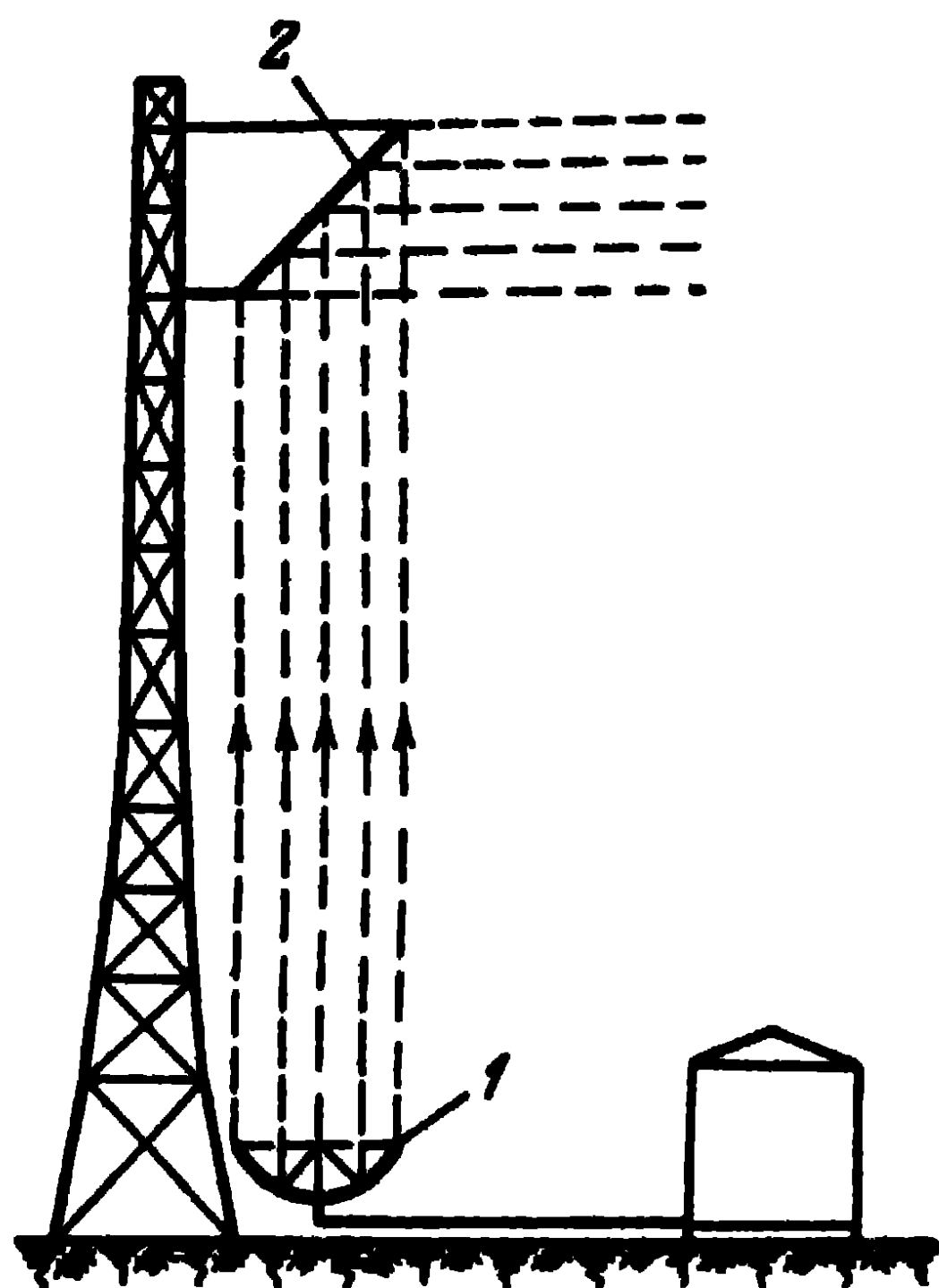


Fig. 10-111. Antenna system of radio-relay line:
1—antenna; 2—plane reflector.

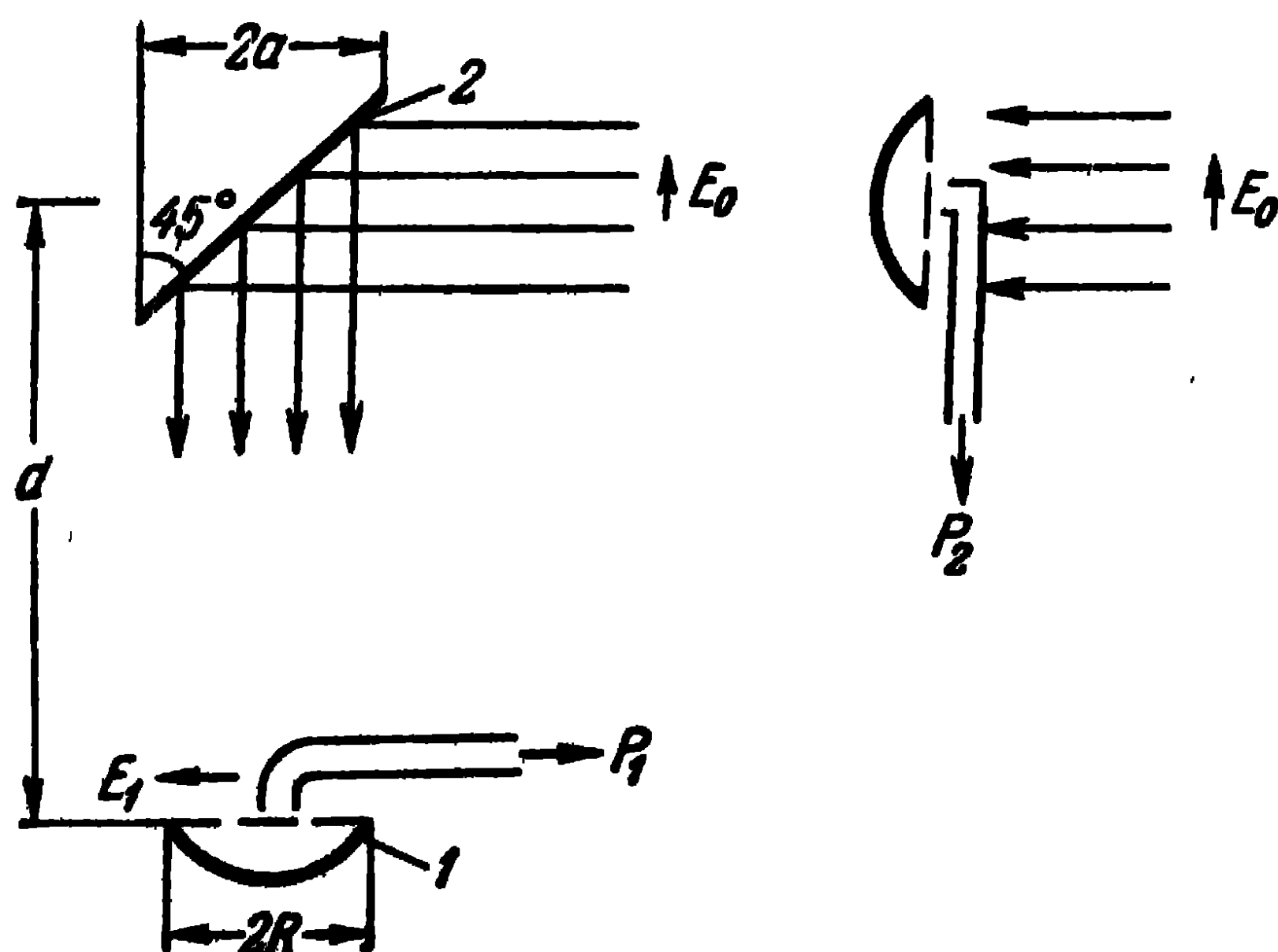


Fig. 10-112. Determining the efficiency of a plane reflector:
1—antenna; 2—reflector.

when no reflector is present and the antenna is located at the place where the plane reflector was situated. The calculated curves are given in Fig. 10-113, where the quantity $k_2 = 10 \log \frac{P_1}{P_2}$ is plotted on the Y-axis and the quantity $\frac{\lambda d}{4a^2}$ on the X-axis; the curves are given for a series of values of R/a .

The curves represented in Fig. 10-113 apply to the case when the distance between the reflector and the antenna d is large in comparison with the output opening of the antenna R and the reflector a ($\frac{R+a}{d} \leq 0.176$). The calculation has been effected for the case when the field distribution at the

output opening of the antenna during transmission is defined by the function

$$h(\xi) = 1 - 0.684 \frac{\xi^2}{l^2}$$

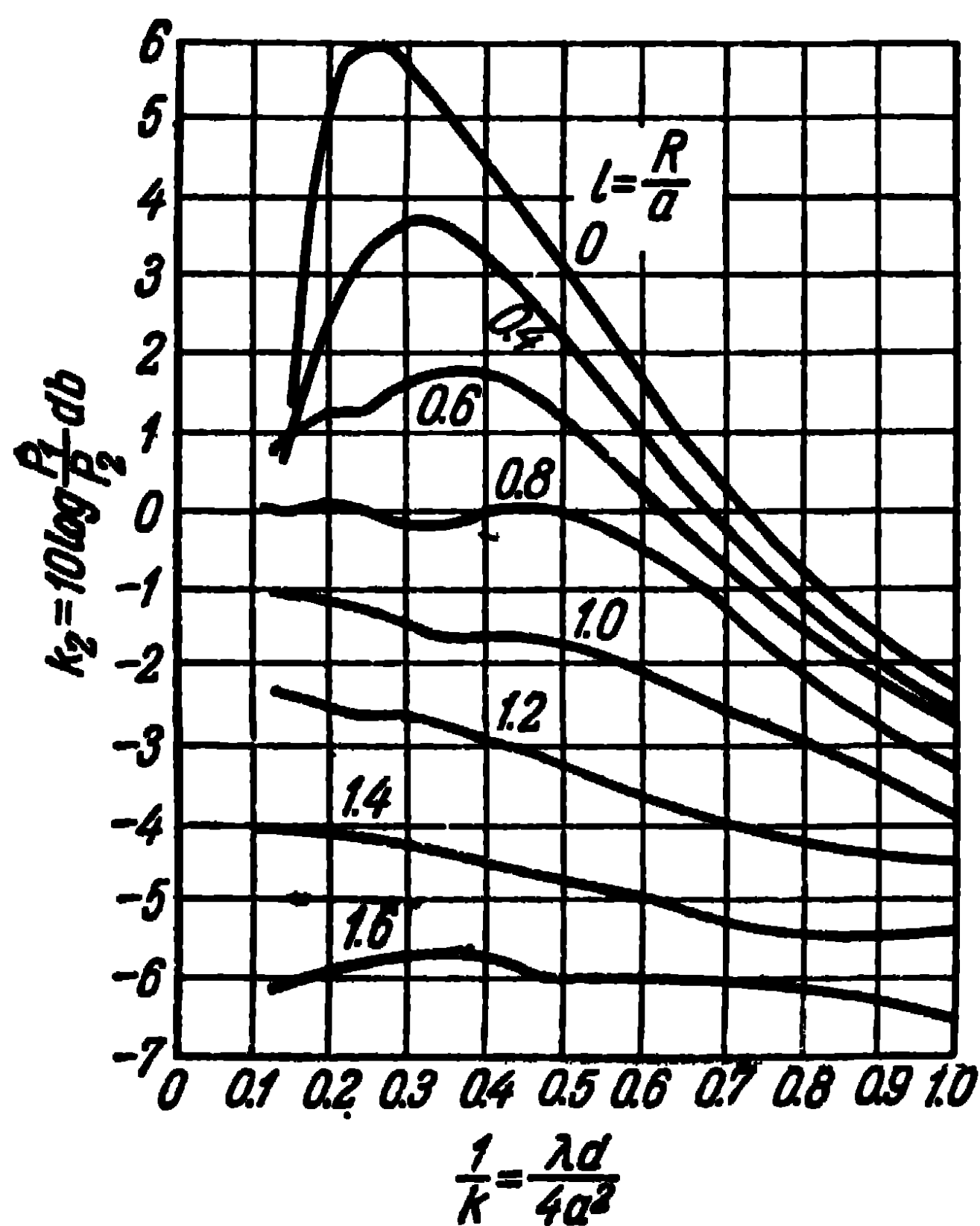


Fig. 10-113. Efficiency of a plane reflector.

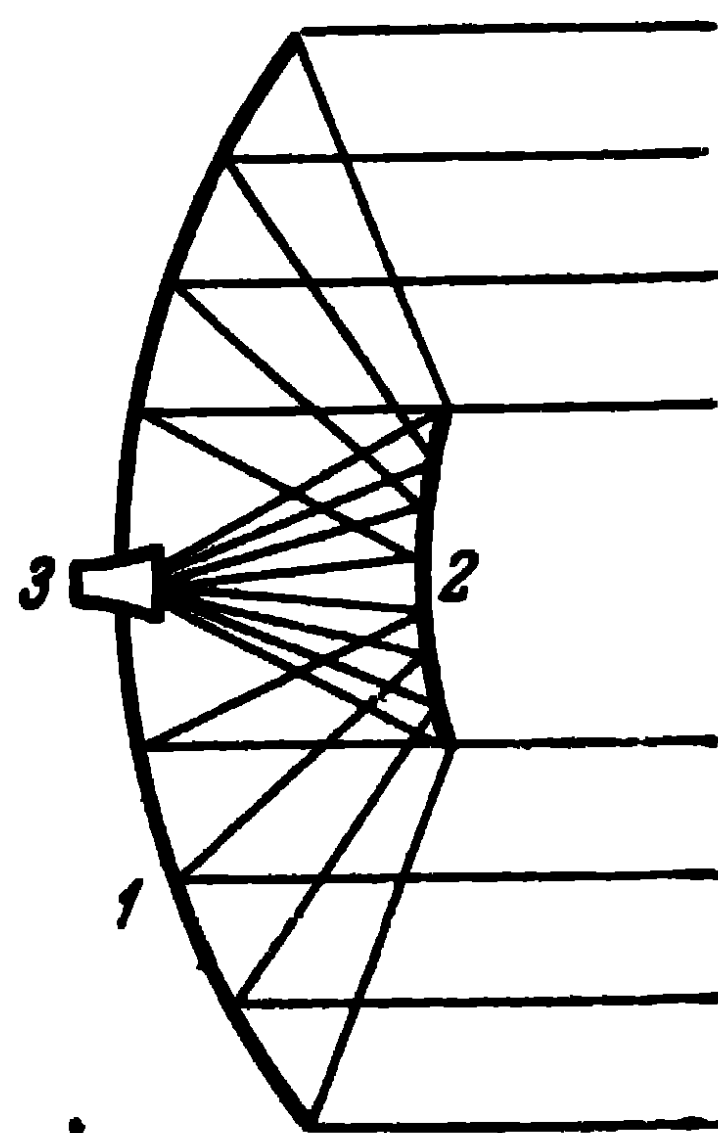


Fig. 10-114. Double-mirror antenna.

where $l = R/a$ and $\xi = r/a$ (r being the radial distance from the centre of the output opening of the antenna).

It can be seen from the curves that the plane reflector is capable of amplifying the received power up to 4 times.

Apart from the antennas described above, double-mirror antennas find application in radar. Their main advantage is

the possibility of reducing the size of antenna systems. An antenna of this kind is shown in Fig. 10-114. The antenna consists of a parabolic reflector 1, an hyperbolic reflector 2 and a radiator 3. The radiator is placed near the apex of the parabolic reflector; the waves from the reflector are incident upon the hyperbolic reflector and are reflected towards the parabolic reflector which forms a plane wave. The hyperbolic reflector gives rise to a certain shadowing of the reflected rays, but its dimensions are taken much smaller than those of the parabolic reflector, so that the shadowing is insignificant.

CHAPTER ELEVEN

Short-Wave Antennas

11-1. Classification of Antennas

The term short-wave antennas applies to antennas used in the 10 to 100 m wave range and, in particular, from 15 to 60 m. They are used in telegraph and telephone communications, phototelegraph and long-distance broadcasting. The antennas are also used for special purposes in local communications.

Short-wave antennas must satisfy a number of specific requirements arising from the conditions of propagation of radio waves. Indeed, three or four waves are necessary, as a rule, to ensure round-the-clock radio communications: one for day-time, one for night-time and one or two for the intermediate periods. The wave-lengths are shortened in summer and lengthened in winter as required. Furthermore, all operating waves are shortened during the years of maximum solar activity and lengthened during those of minimum solar activity. This requires the use of antennas of the multiple-tuned type.

Furthermore, long-distance communications on short waves rely on space (ionospheric) waves which, in their path, are being reflected one or more times from the ionospheric layers of the atmosphere and reach the reception point at a different angles to the horizon; since ionospheric conditions change in time, so do the angles of incidence of the waves. Accordingly, the width of the antenna directional diagram in the vertical plane must satisfy the following requirement: it should not be too narrow, otherwise the signal will fluctuate and eventually fade out.

On being reflected from the upper layers of the ionosphere, radio waves are deviated from their regular path (deviation of the ray) by up to several degrees, so that the antenna directional diagram in the horizontal plane should not be too narrow either.

Experimental data show that, as a rule, the optimum width of the directional diagram amounts to several tens of degrees in the vertical plane, and 10 to 15° in the horizontal plane.

Due to the existence of a round-the-world echo the radiation diagrams should be unidirectional and, owing to interference caused by thunderstorms, it is desirable to use antennas, the directional diagrams of which have small side lobes. As regards the plane of polarisation of the electromagnetic field, it undergoes a rotation during its reflection from the ionosphere, so that, in practice, antennas with a horizontal as well as vertical polarisation are used. However, transmitting antennas with vertical dipoles produce a strong radiation along the earth, giving rise to considerable losses in the earth. Hence, horizontal antennas are usually preferred.

Horizontal antennas are also preferred for reception because various noises have, on the whole, a vertical field polarisation.

The antennas used on short waves are of the simple as well as multiple types. The antennas are further subdivided into tuned antennas, destined to operate on one fixed frequency, and multiple-tuned ones, destined to operate in a twofold or threefold wave range.

Simple antennas comprise symmetrical horizontal dipoles, multiple-tuned dipoles, corner dipoles, etc. Multiple antennas comprise co-phased horizontal antennas, travelling-wave antennas and rhombic antennas.

To begin with, we shall discuss simple antennas of the tuned type.

11-2. Simple Dipoles of the Tuned Type

First we shall deal with the symmetrical horizontal dipole shown in Fig. 11-1. The dipole is made of a copper or bimetal wire 3 to 5 mm in diameter and is secured on two supporting masts. It can be of any length within the limits

of $0.25 \leq \frac{l}{\lambda} \leq 0.64$, which ensures a constant direction to the maximum radiation in the horizontal plane, forming with the axis of the dipole a 90° angle. The dipole is installed at a height H of the order of $\frac{\lambda}{2} \div \lambda$, in which case, the maximum radiation direction in the vertical plane forms with the horizon an angle of $30-15^\circ$.

The dipole is fed by a twin feeder with a wave impedance W of the order of 600 ohms, which is tuned on a travelling wave by means of, as a rule, an inductive stub.

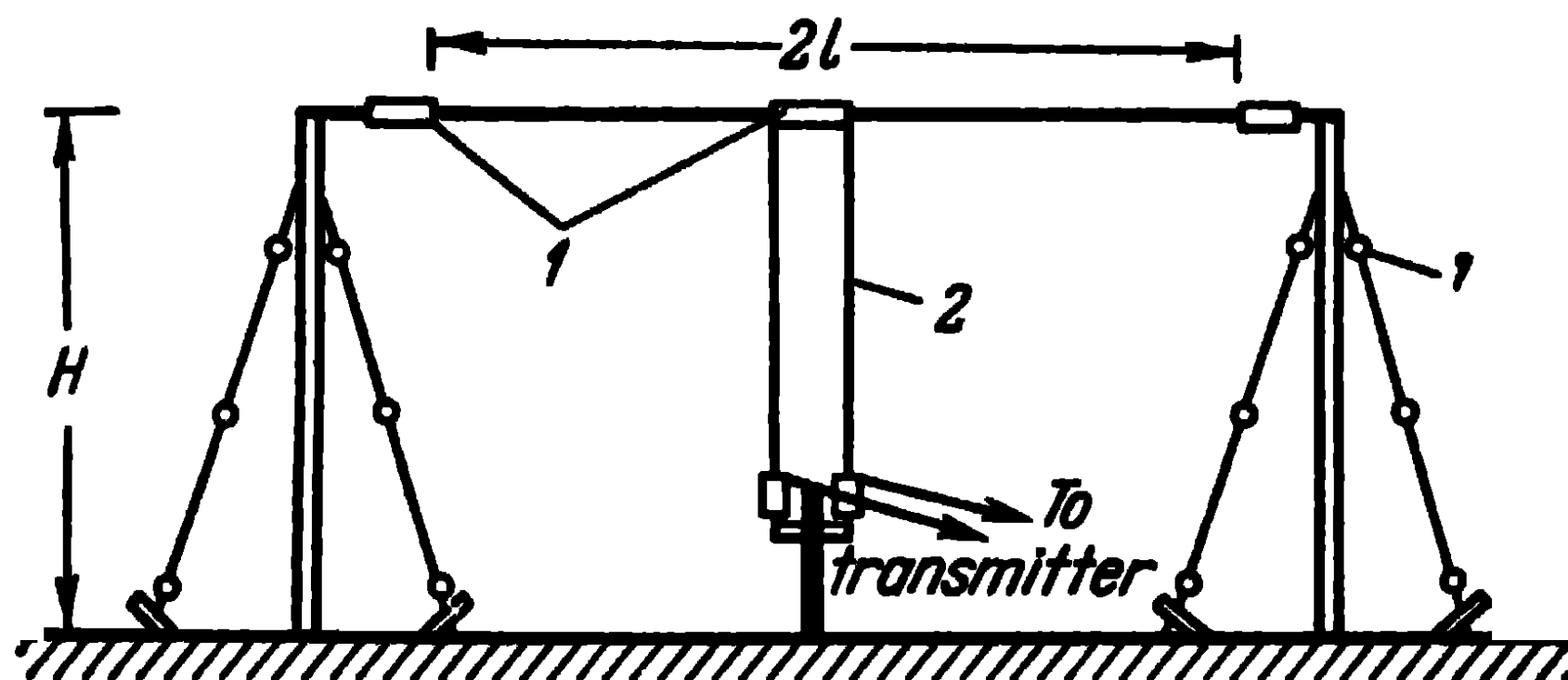


Fig. 11-1. Symmetrical horizon dipole:
1—insulator; 2—feeder.

To avoid the distortion of the directional diagram, insulators are inserted in the guys of the masts, forming segments of less than quarter-wave-length, so that the electric currents induced in the guys have a small magnitude and their radiation is insignificant.

The length of the dipole is often taken so that $\frac{l}{\lambda} = 0.25$ (half-wave dipole) and, at the same time, the dipole is shunt-fed, as was shown in Fig. 10-1, b.

Simple short-wave antennas of the tuned type are sometimes made loop-like, in accordance with the circuit shown in Fig. 10-1, c. In that case, a travelling-wave ratio equal to 0.5 is set up in the twin feeder with a wave impedance $W = 600$ ohms.

11-3. Simple Dipoles of the Multiple-Tuned Type

As indicated above, the operating waves of radio communications have to be frequently changed. This has led to the use of multiple-tuned antennas. The multiple-tuned dipole suggested by S. I. Nadenenko is of this kind (Fig. 11-2).

The dipole is secured to two masts, just as a simple symmetrical dipole and is made of thin wires of diameter $2r=3$ to 5 mm and number $n=8$ to 12, forming a cylinder of a diameter of the order of 1 m. It is destined for operation in a wave range satisfying the condition $0.25 \leq \frac{l}{\lambda} \leq 0.64$ and is fed by a four-wire feeder with a wave impedance of the order of $W=300$ ohms.

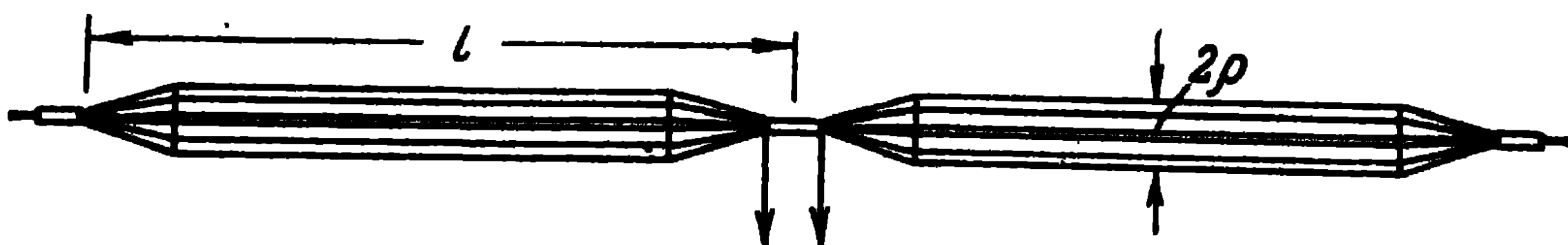


Fig. 11-2. Multiple-tuned Nadenenko dipole.

The wave impedance of the dipole can be expressed as:

$$W = 120 \left(\ln \frac{2l}{Q_{\text{equiv}}} - 1 \right), \quad (11-1)$$

where Q_{equiv} is the equivalent radius of the dipole related to the radius of the cylinder q formed by the wires as follows:

$$Q_{\text{equiv}} = q \sqrt[n]{\frac{nr}{q}}.$$

The wave impedance of the dipole is of the order of 300 ohms and the input resistance curves of the dipole are considerably smoothed out (Figs. 2-13 and 2-14). The travelling-wave ratio in the feeder in the operating wave range lies within the interval $K \approx 0.25 \div 0.70$, which enables to operate without specially tuning the feeder on a travelling wave and, consequently, to pass rapidly from one operating wave to another.

The power gain of a multiple-tuned dipole (with the influence of the earth taken into account) is found to equal $\epsilon=4.24$ when $\frac{l}{\lambda}=0.25$ and $\epsilon=6.9$ when $\frac{l}{\lambda}=0.5$.

The multiple-tuned dipole can also consist of a biconical antenna (Fig. 11-3). When $q \approx 1$ m, a dipole of this kind becomes multiple-tuned on short waves. Its wave impedance is defined as:

$$W = 120 \ln \left(\cot \frac{\psi}{2} \right) \quad (11-2)$$

or, for small values of the angle ψ , approximately by the expression $W = 120 \ln \left(\frac{2}{\psi} \right) = 120 \ln \frac{l}{\rho}$. In this dipole, the gradual decrease of the diameter of the dipole towards the feed points serves to match the input resistance of the antenna to the wave impedance of the feeder.

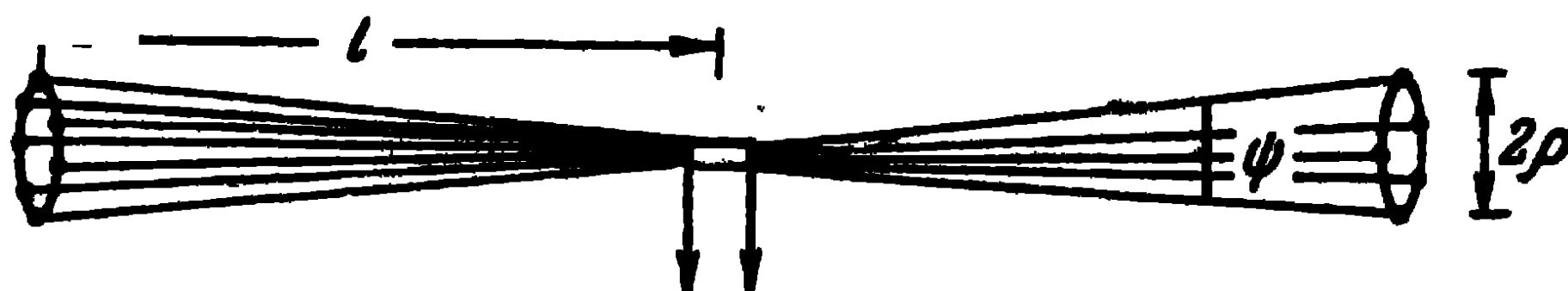


Fig. 11-3. Biconical dipole.

11-4. Corner Antenna

Just like the dipoles discussed above, the corner antenna is symmetrical (Fig. 11-4). It was designed by A. A. Pistol-kors with the object of obtaining a multidirectional radiation in the horizontal plane. The antenna consists of mutually perpendicular wires and is horizontal to the earth.

The directional diagrams of the corner antenna in the horizontal plane can be expressed as:

$$f(\varphi) = \left[\frac{\cos(kl \cos \varphi) - \cos kl}{\sin \varphi} - \frac{\cos(kl \sin \varphi) - \cos kl}{\cos \varphi} \right] + \\ + i \left[\frac{\sin(kl \cos \varphi) - \cos \varphi \sin kl}{\sin \varphi} - \frac{\sin(kl \sin \varphi) - \sin \varphi \sin kl}{\cos \varphi} \right]. \quad (11-3)$$

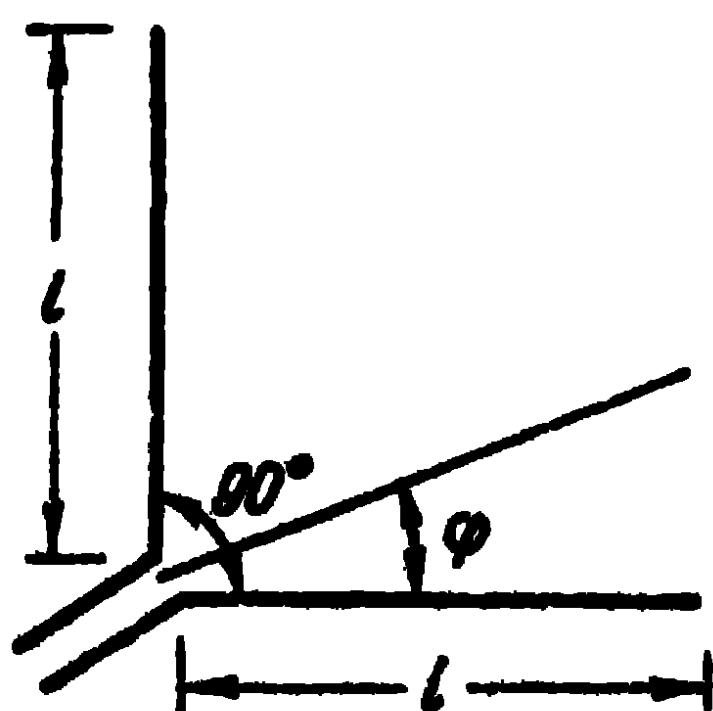


Fig. 11-4. The Pistol-kors corner antenna.

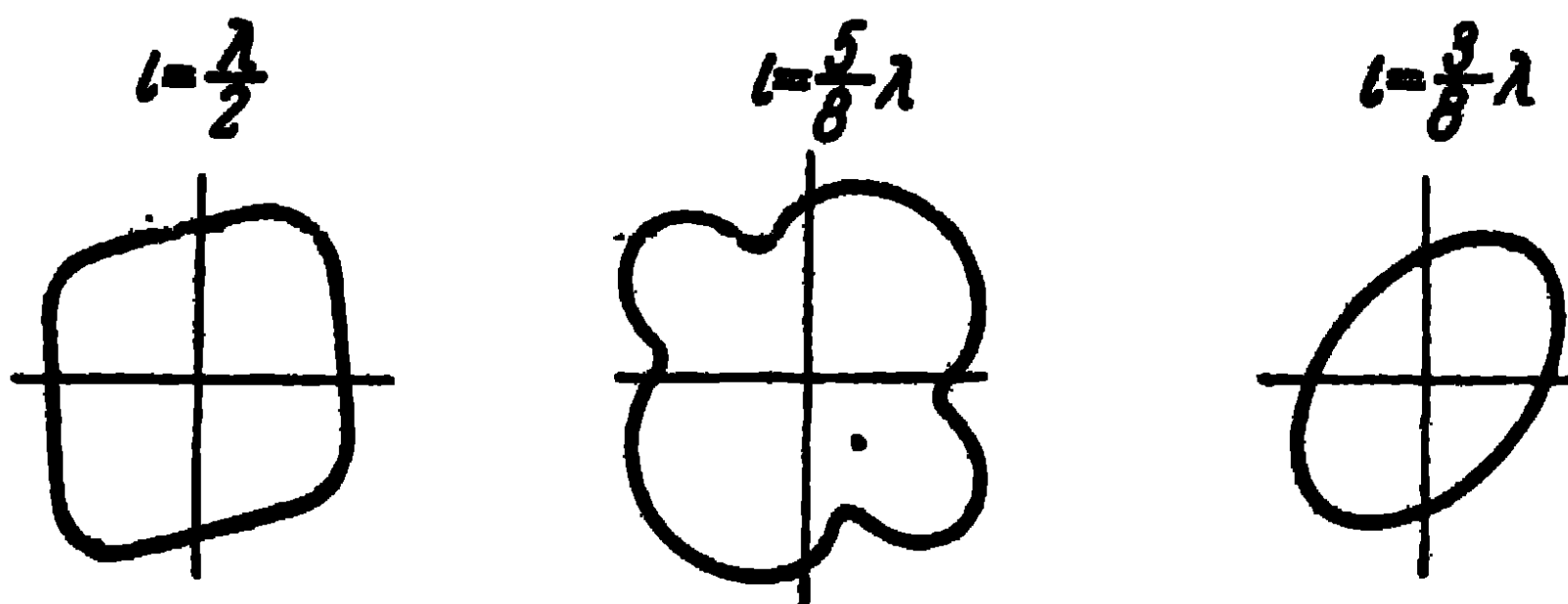


Fig. 11-5. Directional diagrams of a corner antenna.

They are shown in Fig. 11-5 and, in the wave range of $\frac{l}{\lambda} = 0.5 \div 0.64$, are close to non-directional ones.

Corner antennas are sometimes made of thick cylinders of the Nadenenko dipole type and, in this way, ensure the operation in the wave range, without retuning of the feeders.

The angle α of corner antennas can even be less than 90° , in which case the directional diagrams of the antenna differ from the ones shown in Fig. 11-5. Corner antennas of this kind with an angle $\alpha = 70^\circ$ were used for radio communications on the first artificial satellite of the earth. As we know, for operating on the waves $\lambda = 15\text{m}$ and $\lambda = 7.5\text{m}$, the lengths of the dipoles were $l = 2.9\text{m}$ and $l = 2.4\text{m}$.

11-5. Multiple Short-Wave Antennas of the Tuned Type

The main circuits of antennas of the tuned type consist of a number of half-wave dipoles forming a co-phasal array. The distances between the dipoles in the antenna array are usually chosen equal to half a wave-length. Fig. 10-22 shows the circuit of the most commonly used co-phasal antenna utilised in the short-wave range. Fig. 11-6 shows the way the co-phasal antenna is secured on metal supporting masts.

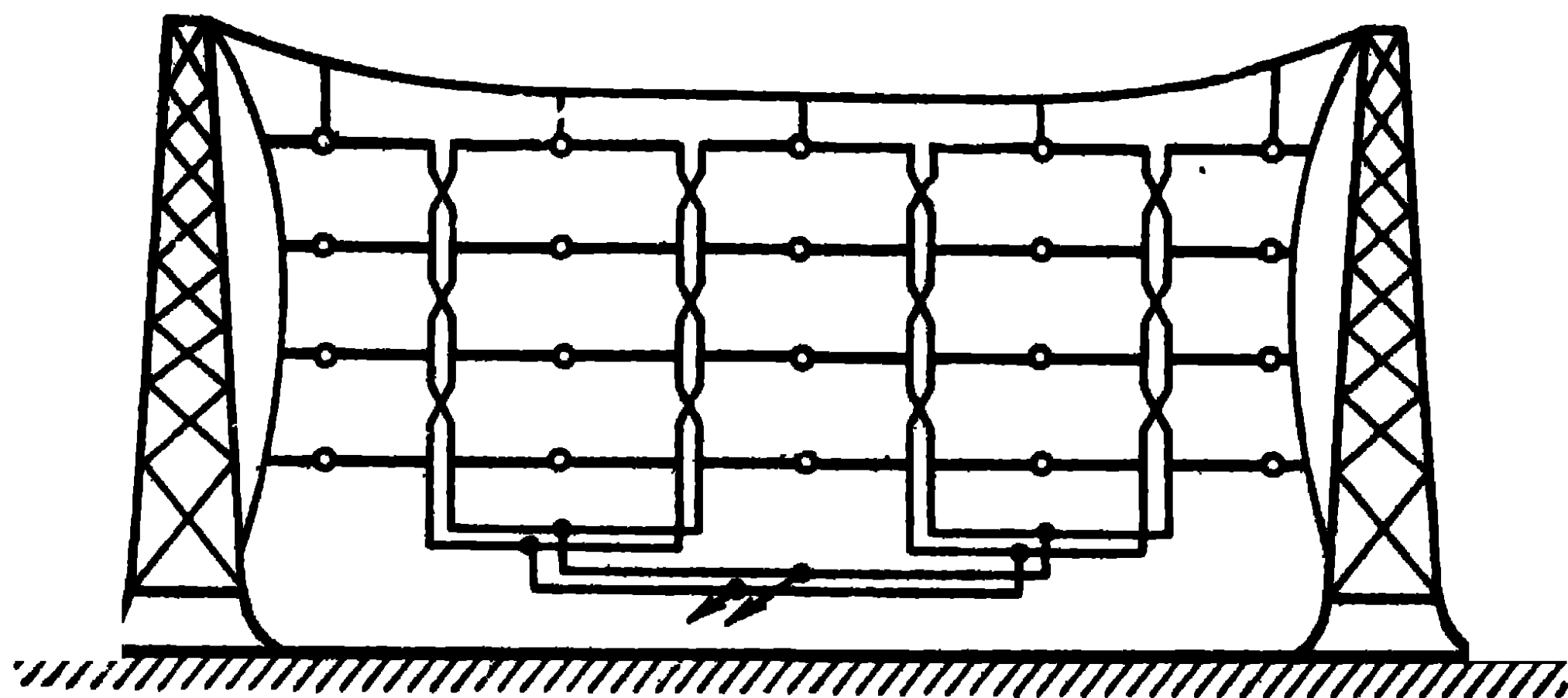


Fig. 11-6. Fastening of co-phasal antenna.

Co-phasal horizontal antennas are generally used with a reflector which presents exactly the same aspect as the antenna proper. The reflector lies at a distance $d = (0.22 \div 0.25) \lambda$ from the antenna. In most cases, a passive reflector is used, in which a twin line (stub) approximately half a wave-length long, which serves for tuning up the reflector, is connected to the points c of the distributing feeders (Fig. 11-7, *a*). In an active reflector, the points c of the distributive feeder (Fig. 11-7, *b*) are connected to the feeder of the antenna by means of phasing circuits. The phasing circuits are chosen such that the current in the reflector should be equal to the current in the antenna and precede it in phase by 90° .

The antenna directional diagrams in the horizontal plane depend on the number of dipoles in one tier of the antenna system (m) and on the type of tuning of the reflector. They can be calculated from the expression

$$E_h = \frac{60nI_p}{r_0} \frac{\cos\left(\frac{\pi}{2}\cos\theta\right)}{\sin\theta} \frac{\sin\left(m\frac{\pi}{2}\cos\theta\right)}{\sin\left(\frac{\pi}{2}\cos\theta\right)} \times \sqrt{1 + m_1^2 + 2m_1 \cos\left(\psi - \frac{2\pi d}{\lambda} \sin\theta\right)}, \quad (11-4)$$

where d is the distance between the antenna and the reflector;

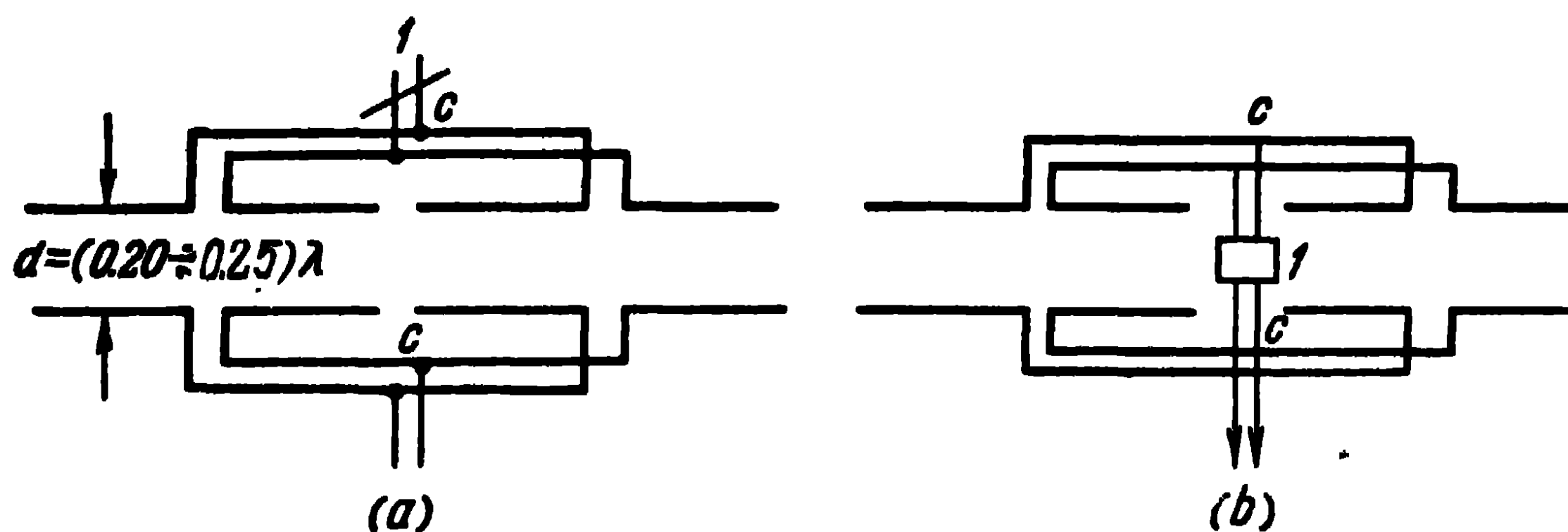


Fig. 11-7. Antenna circuit with a reflector:

a—passive reflector: *1*—tuning stub. *b*—active reflector: *1*—phasing circuit.

m_1 , the ratio of the current amplitude in the reflector to the current amplitude in the antenna;
 ψ , the angle by which the current in the reflector precedes the current in the antenna

For an active reflector $m_1=1$, $\psi=90^\circ$ and $d=\frac{\lambda}{4}$, the directional diagram obtained is unidirectional with a zero of radiation when $\theta=270^\circ$ and with radiation maximum when $\theta=90^\circ$. In the case of a passive reflector, it is impossible to obtain simultaneously $m_1=1$ and $\theta=90^\circ$, hence the radiation in the direction $\theta=270^\circ$ cannot be cancelled completely.

The directional diagrams of a co-phasal antenna in the vertical plane depend on the number of tiers in the antenna (n) and on the height at which it is fastened above the surface of the earth. As a rule, the first tier of the antenna is at a height $h=\frac{\lambda}{4} + \frac{\lambda}{2}$; there is no point in having it lower because, in that case, due to the influence of the finite

conductivity of the earth, the antenna may radiate in the direction of the axis of the dipoles. If the earth is regarded as an ideal conductor, which is the case in engineering practice, the directional diagram in the vertical plane is expressed as:

$$E_v = \frac{120mI_p}{r_0} \frac{\sin\left(n\frac{\pi}{2}\sin\Delta\right)}{\sin\left(\frac{\pi}{2}\sin\Delta\right)} \sin\left(\frac{2\pi h_{\text{mean}}}{\lambda}\sin\Delta\right) \times \\ \times \sqrt{1 + m_1^2 + 2m_1 \cos\left(\psi - \frac{2\pi d}{\lambda}\cos\Delta\right)}, \quad (11-5)$$

where h_{mean} is the distance between the surface of the earth and the centre of the antenna system;

Δ , the angle between the horizon and the direction to the point of observation of the field.

It is evident that along the earth surface ($\Delta=0^\circ$) we get radiation zero, since the currents of the mirror image of the antenna are of opposite direction relatively to the antenna currents.

The antenna directive and power gain can be calculated from the expressions

$$D = \frac{E^2 r_0^2}{30 I_0^2 R_\Sigma}, \quad \epsilon = \frac{D\eta}{1.64}.$$

Here, the radiation resistance R_Σ can be calculated from the expressions of Chapter Three, taking account of the influence of the earth. The antenna directive gain η is usually taken equal to unity, since the antenna radiation resistance is much larger than the resistance of the losses in the antenna.

Table 11-1 gives the values of the parameters of the antennas utilised in practice ($\text{CH}\frac{n}{m}\text{R}$ designates a co-phasal horizontal antenna with a reflector of n tier and m dipoles in a tier).

Apart from co-phasal horizontal antennas for operating on one fixed wave, co-phasal horizontal antennas can be used for operating on two fixed waves. The antenna circuit of this kind is shown in Fig. 11-8. Since the distance from the transmitter to any of the dipoles is the same, the dipoles are found to be co-phasal when operating on any wavelength. Consequently, the radiation maximum maintains its

Table 11-1

Antenna	Height above the earth h_{mean}	Directive gain D	Power gain s	Angle of maximum radiation, Δ_0 , in degrees	Width of directional dia- gram in horizontal plane at half-intensity, in degrees	Width of diagram in vertical plane at half- intensity, in degrees
CH $\frac{2}{2}$ R	0.75λ	35.3	21.5	17	65	26
CH $\frac{2}{16}$ R	0.75λ	230-280	140-170	17	9	26
CH $\frac{4}{4}$ R	1.75λ	167.5	102	8	35	9.5
CH $\frac{6}{16}$ R	1.75λ	740-820	450-500	7	9	10

direction and the antenna is utilised as a multiple-tuned antenna when the condition $0.25 \leq \frac{l}{\lambda} \leq 0.64$ is observed. In

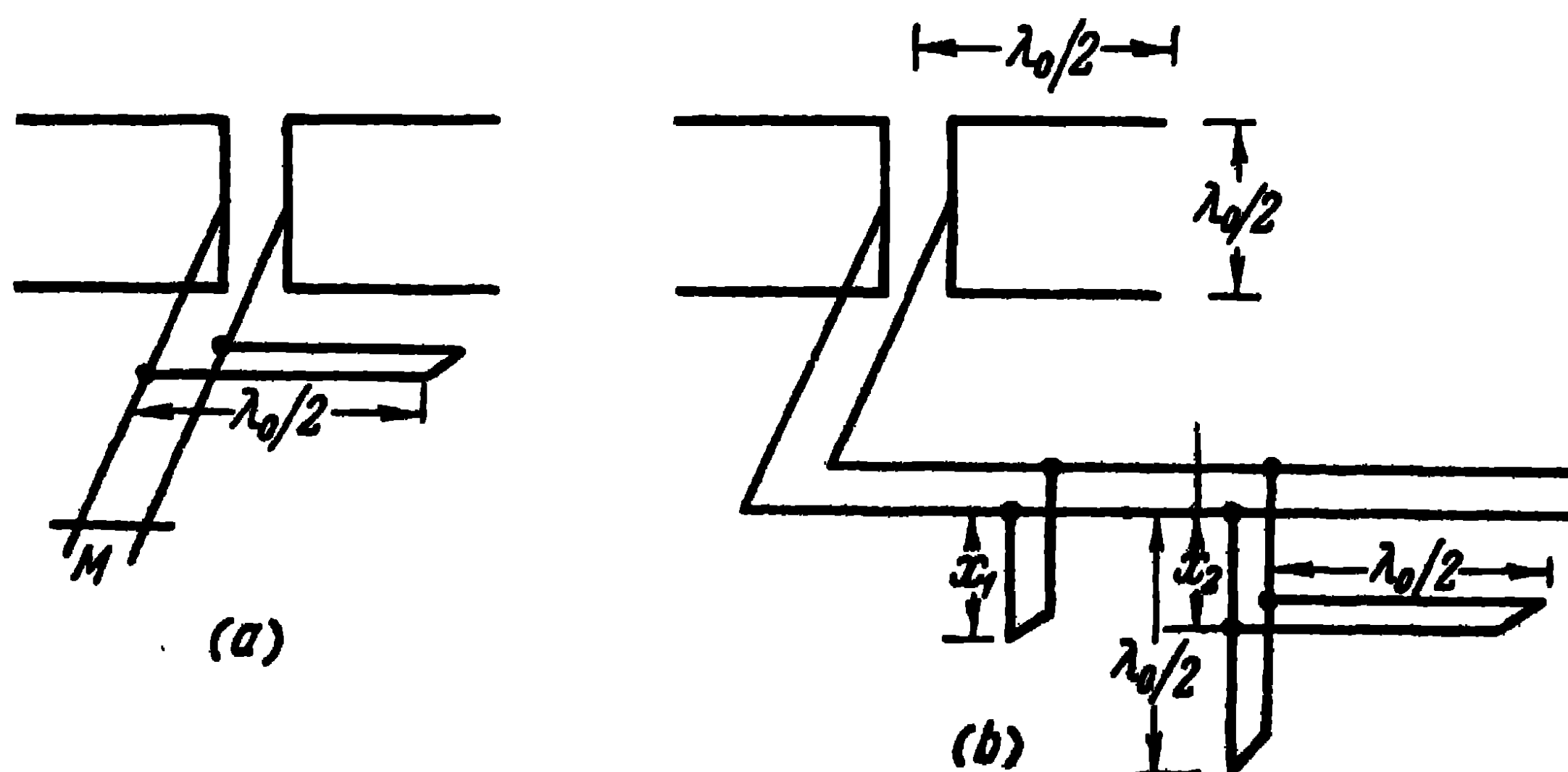


Fig. 11-8. Tuning circuit of antenna on multiple waves:
a—reflector tuning circuit; b—antenna tuning circuit.

practice, it is found convenient to tune the antenna on two multiple waves λ_0 and $2\lambda_0$. At the same time, the dimensions of the antenna are chosen such that $d = 0.25\lambda_0$ and $2l = \lambda_0$.

The electric parameters of the antenna on multiple waves are given in Table 11-2 and the circuits of the simultaneous tuning of the reflector and feeder on two waves, in Fig. 11-8.

The reflector is tuned on the wave $2\lambda_0$ by displacing the short-circuiting bridge M along the tuning stub and, on the wave λ_0 , by displacing the other stub, which, on the wave λ_0 gives a short-circuit and on the wave $2\lambda_0$, an infinitely large resistance (Fig. 11-8, *a*)

The feeder is tuned on a travelling wave, first on the wave $2\lambda_0$, and, after the tuning stub of length x_1 has been secured, the feeder is tuned on a travelling wave on the wave λ_0 . At the same time, instead of an inductive stub of length x_2 , a combined stub is used, as shown in Fig. 11-8, *b*.

In this way, tuning is automatic both on the λ_0 and $2\lambda_0$ waves of reflector as well as feeder, no additional tuning being necessary when passing from one operating wave to another.

Table 11-2

Antenna	Operating wave-length	Height above the earth h_{mean}	Power gain	Angle of maximum radiation Δ_0 . in degrees	Width of directional diagram in horizontal plane at half-intensity. in degrees	Width of directional diagram in vertical plane at half-intensity. in degrees
$\text{MCH } \frac{2}{2} R$	$\frac{\lambda_0}{2\lambda_0}$	$0.75\lambda_0$	$\frac{21.5}{8.25}$	$\frac{17}{38}$	$\frac{65}{84}$	$\frac{24}{60}$
$\text{MCH } \frac{2}{4} R$	$\frac{\lambda_0}{2\lambda_0}$	$0.75\lambda_0$	$\frac{36.5}{8.8}$	$\frac{17}{40}$	$\frac{35}{60}$	$\frac{24}{85}$
$\text{MCH } \frac{2}{8} R$	$\frac{\lambda_0}{2\lambda_0}$	$0.75\lambda_0$	$\frac{70.7}{13.3}$	$\frac{17}{40}$	$\frac{18}{32}$	$\frac{22}{75}$

11-6. Multiple Short-Wave Antennas

Type of the Multiple-Tuned

As was indicated before, the multiple co-phasal antennas discussed earlier are antennas of the tuned type, because they enable to operate either on one fixed wave or on two fixed waves (antenna on multiple waves).

In the case of an antenna of the first kind, when operating on waves differing from the nominal one (λ_0), the equality of the current amplitudes and phases at various tiers of the antenna is upset, which leads to a distortion of the directional diagram in the vertical plane. The directional properties undergo an insignificant deterioration only in a narrow range (of the order of a few per cent) in the vicinity of the nominal (rated) wave; moreover, the larger the number of tiers, the more narrow this range.

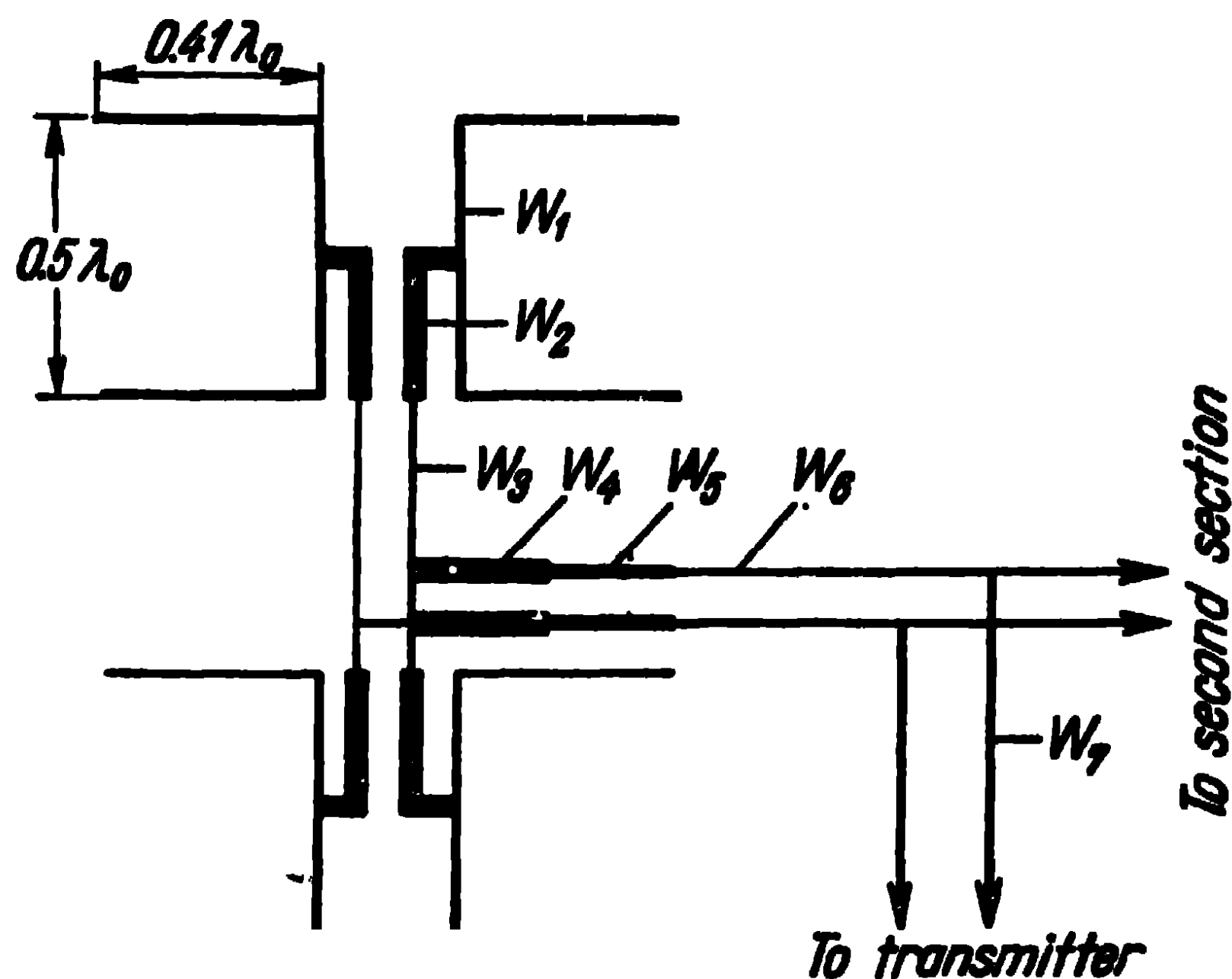


Fig. 11-9. Section of co-phasal multiple-tuned antenna.

In the case of an antenna on multiple waves, the antenna is matched to the feeder line and the reflector tuned automatically only on two fixed waves.

Recently, a complex horizontal co-phasal four-tier antenna has been designed, which can operate in a continuous wave range with a ratio of 1 : 2.5 [69]. The circuit of one section of an antenna of this kind is shown in Fig. 11-9. As can be seen from the figure, the antenna is fed in exactly the same way as in the case of an antenna on multiple waves and, as a consequence, the phase of excitation of the dipoles is not frequency dependent. The distance between the stages is taken equal to $0.5\lambda_0$.

To obtain a sufficiently high travelling-wave ratio in the feeder, quarter-wave step-up transformers are used, thereby ensuring satisfactory matching of the antenna to the feeder in a wide wave range: the travelling-wave ratio does

not fall below 0.5 in the range $(0.9 \div 1.7)\lambda_0$ and below 0.3 in the range $(0.7 \div 1.9)\lambda_0$.

The use of quarter-wave set-up transformers enables also to utilise feed lines of relatively high wave impedances. In the absence of set-up transformers, one would have to use feed lines of low wave impedances, which complicates the manufacture of vertical feeders.

The inter-tier connections are accomplished by means of a feeder line with a wave impedance $W_1 = 550$ ohms. The first two-stage quarter-wave transformer consists of two feeder segments of length $0.25\lambda_0$ each with a wave impedance $W_2 = 396$ ohms and $W_3 = 550$ ohms. The second two-stage transformer consists of two quarter-wave feeder segments with a wave impedance $W_4 = 366$ ohms and $W_5 = 480$ ohms. The antenna pass-band can be improved by using dipoles of low wave impedance. A dipole of this kind consists either of three wires 4 to 6 mm in diameter, lying at the apices of an equilateral triangle of side $0.035\lambda_0$ or of four wires lying at the apices of a quadrangle.

The antenna can be of two kinds: with a tunable or an aperiodical reflector. In the first case, the reflector system is entirely analogous to the antenna system and situated at a distance $d = 0.264\lambda_0$ from it.

In the second case, the reflector, consisting of a grid of horizontal wires (copper or bimetel) 6.6 mm in diameter spaced $0.073\lambda_0$ apart, is at a distance $d = 0.23\lambda_0$ from the antenna. The height of the grid is approximately equal to $2\lambda_0$ and its width $L = L_0 + 0.18\lambda_0$, where L_0 is the width of the antenna system.

The antenna consists of two identical sections connected by a distributive feeder ($W_6 = 550$ ohms). The main feeder ($W_7 = 275$ ohms) is connected to the inter-section distributive feeder in its centre. Displacing the connection points of the main feeder towards one or the other section leads to the rotation of the directional diagram of the antenna by a certain angle (8 to 20°).

11-7. Rhombic Antenna

Rhombic antennas have been in use as receiving short-wave antennas since the end of the twenties. As transmitting antennas, they have been used since the middle of the thirties.

The antenna consists of four wires of length l each and has the form of a rhombus. An absorbing resistance R_a , equal to the wave impedance of the antenna, is connected to one of the acute angles of the rhombus, the feeder being connected to the other one. Thus, a travelling wave is formed in the antenna and travels towards the absorbing resistance.

In a wire with a travelling-current wave, the radiation maximum forms with the axis of the wire an angle smaller than 90° (Figs. 4-10 and 4-11), furthermore the angle of

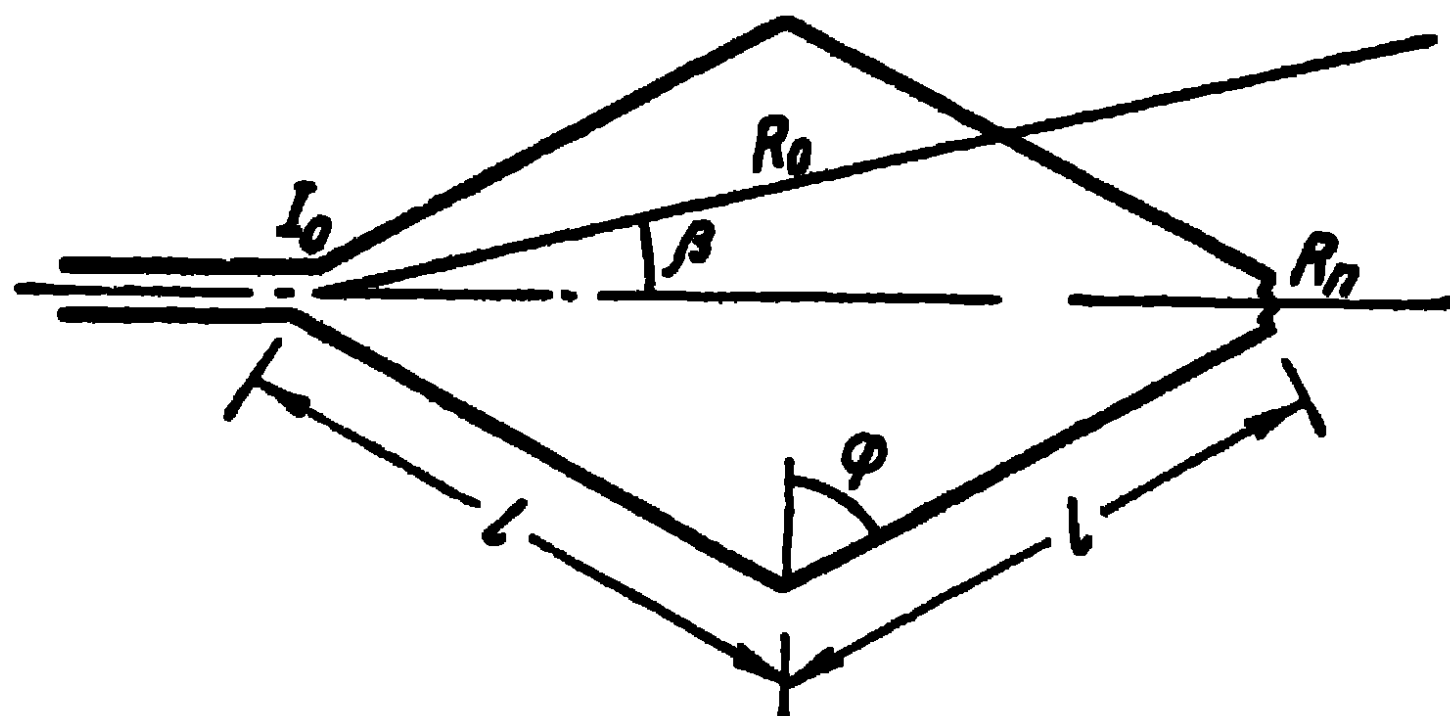


Fig. 11-10. Circuit of rhombic antenna.

maximum radiation is a function of the ratio of the length of the wire to the wave-length $\frac{l}{\lambda}$. By disposing the wires at a certain angle to one another, the maximum total radiation can be coincided with the bisectrix of this angle; furthermore, this maximum radiation is found to be directed towards the absorbing resistance.

The antenna lies horizontally above the earth and its directional diagram in the horizontal plane is expressed as

$$E_h = \frac{240I_0}{r_0} \frac{\cos \varphi}{1 - \sin \varphi} \sin \left[\frac{kl}{2} (1 - \sin (\varphi - \beta)) \right] \times \\ \times \sin \left[\frac{kl}{2} (1 - \sin (\varphi + \beta)) \right], \quad (11-6)$$

where I_0 is the current at the beginning of the antenna;
 β , the angle between the antenna axis and the direction towards the point of observation;
 l , the length of the side of the rhomb;
 φ , half the obtuse angle of the rhomb.

The directional diagrams calculated from this expression are shown in Fig. 11-11 for $l=2\lambda$, $\varphi=65^\circ$ and for $l=4\lambda$

and $\varphi=65^\circ$. The directional diagrams are characterised by the possession of relatively large side lobes.

The directional diagram in the vertical plane, with the influence of the earth taken into account (assumed to be ideally conducting) is expressed as:

$$E_v = \frac{480I_0}{r_0} \frac{\cos \varphi}{1 - \cos \Delta \sin \varphi} \sin^2 \times \\ \times \left[\frac{kl}{2} (1 - \cos \Delta \sin \varphi) \right] \sin(kh \sin \Delta), \quad (11-7)$$

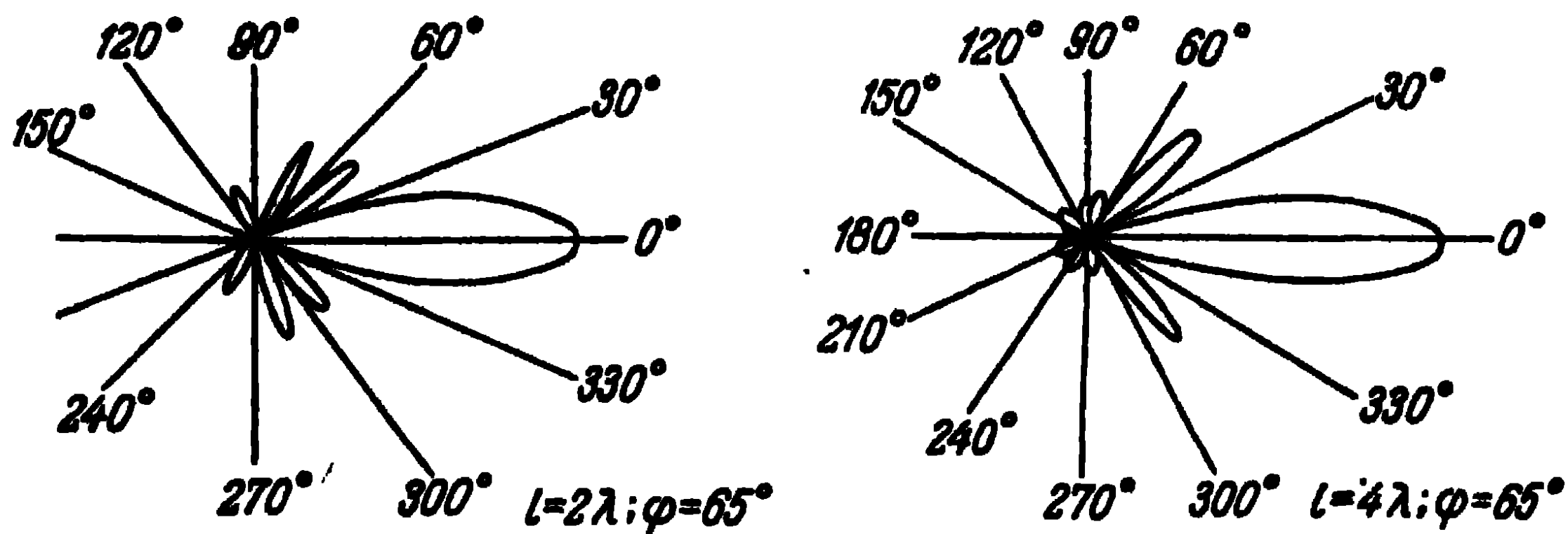


Fig. 11-11. Directional diagrams of a rhombic antenna in the horizontal plane.

where Δ is the angle between the horizon and the direction towards the point of observation;

h , the height of the antenna above the earth.

Fig. 11-12 shows the directional diagrams of a rhombic antenna for $l=2\lambda$, $h=0.5\lambda$, $\varphi=65^\circ$ and $l=4\lambda$, $h=\lambda$, $\varphi=65^\circ$.

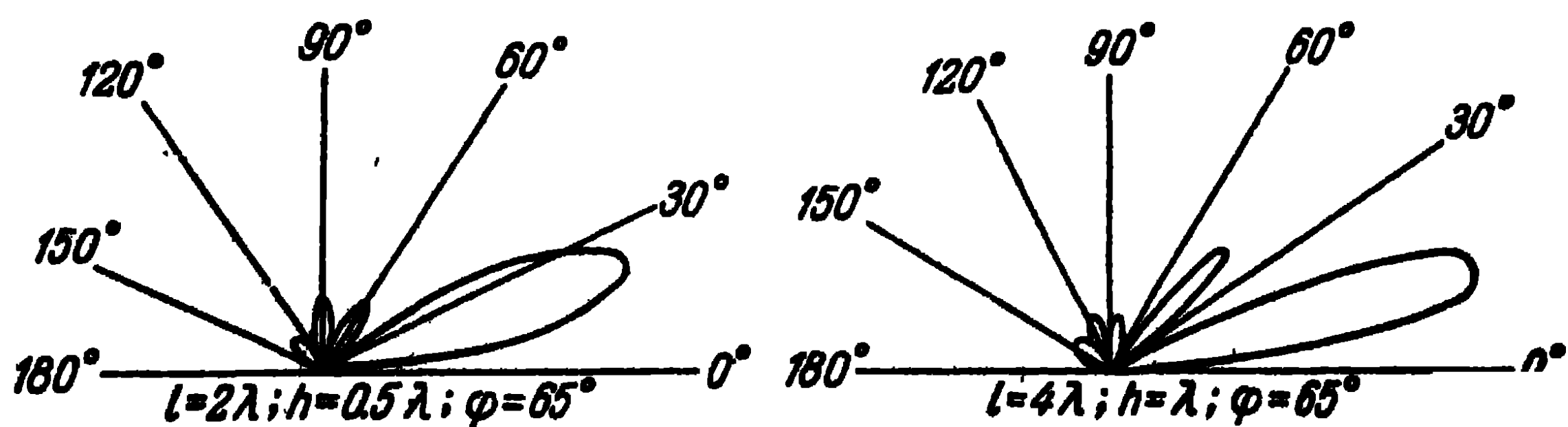


Fig. 11-12. Directional diagrams of a rhombic antenna in vertical plane.

$\varphi=65^\circ$, calculated from this expression. We see that the radiation along the earth is zero and the angle of elevation of the radial maximum is a function of the ratio h/λ . In that plane, as can be seen from the diagrams, relatively large side lobes occur.

It can be seen from the directional diagram in the vertical and horizontal planes that the direction of the maximum radiation and the unidirectivity are maintained in a wide wave range.

The radiation resistance of a rhombic antenna was calculated by the induced emf method, no account being taken of the attenuation of the current in the wires, by Li-Chan [70]. It was found to equal $R_{\Sigma} = 780$ ohms for $l = 4\lambda$ and $h = \lambda$.

An approximate calculation (no account taken of the reciprocal influence of the wires and the influence of the earth) of the radiation resistance of a rhombic antenna can be obtained from the expression

$$R_{\Sigma} \simeq 240 \left[C - 1 + \ln 2kl - \text{Ci } 2kl + \frac{\sin 2kl}{2kl} \right], \quad (11-8)$$

where $C = 0.5772...$

The calculation obtained by this expression yields the value of 800 to 500 ohms for the radiation resistance in the wave range $(0.8 \div 2.5)\lambda_0$, where $\lambda_0 = \frac{l}{4}$.

Part of the energy fed to the rhombic antenna is lost in the absorbing resistance. Hence, the antenna efficiency is less than unity. If we take into consideration the fact that the current amplitude changes along the wire as a result of the exponential radiation $I_x = I_0 e^{-\beta x}$, the antenna efficiency can be determined from the balance of the powers. Indeed, the power fed to the antenna is:

$$P_{\text{in}} = \frac{I_0^2}{2} W.$$

At the same time, it is assumed that the antenna input resistance equals its wave impedance. The power radiated by the antenna equals

$$P_{\Sigma} = \frac{I_0^2}{2} e^{-2\beta l} R_{\Sigma}$$

and the power lost in the absorbing resistance is:

$$P_{\text{losses}} = \frac{I_0^2}{2} e^{-4\beta l} W,$$

at the same time, the absorbing resistance is taken to be equal to the wave impedance of the antenna. Substituting

the cited expressions into the condition $P_{in} = P_{\Sigma} + P_{losses}$, we obtain:

$$\frac{R_{\Sigma}}{W} = 2 \operatorname{sh} 2\beta l.$$

In the case of small attenuations, we get approximately $\operatorname{sh} 2\beta l \approx 2\beta l$, the attenuation constant being then expressed as:

$$\beta = \frac{R_{\Sigma}}{4lW}. \quad (11-9)$$

The efficiency factor of the rhombic antenna is expressed as:

$$\eta = \frac{P_{\Sigma}}{P_{in}} = \frac{R_{\Sigma}}{W} e^{-2\beta l} = 1 - e^{-4\beta l}. \quad (11-10)$$

Experimental data give the following values for the efficiency factor of a rhombic antenna: on the long wave of the operating range, $\eta = 0.5$ and on the short wave of the range, $\eta = 0.75$. Thus, from 25 to 50% of the power is spent on heating the absorbing resistance. If the absorbing resistance is removed ($R_a = 0$ or $R_a = \infty$), the efficiency factor becomes close to unity. But then, a reflected wave is set up in the antenna, which gives rise to a radiation in the opposite direction, thereby lowering the directivity of the antenna. The antenna input resistance will then be frequency dependent.

The antenna directive gain can be expressed as:

$$D = \frac{E_v^2 r_0^2}{30 I_0^2 R_{\Sigma 0}}$$

and if we take into account that $R_{\Sigma 0} = R_{\Sigma} e^{-2\beta l} = W (1 - e^{-4\beta l})$, on substituting (11-7) into this expression, we obtain the following calculating expression for the directive gain:

$$D = 7,680 \frac{e^{-2\beta l}}{W (1 - e^{-4\beta l})} \frac{\cos^2 \varphi}{(1 - \cos \Delta \sin \varphi)^2} \times \\ \times \sin^4 \left[\frac{kl}{2} (1 - \cos \Delta \sin \varphi) \right] \sin^2 (kh \sin \Delta). \quad (11-11)$$

Now, let us examine the question of the choice of the main dimensions of a rhombic antenna. The antenna will have its maximum radiation in a given direction when the separate factors in (11-11) assume their maximum value. The factor $\sin^2 (kh \sin \Delta)$ will have its maximum value for

$kh \sin \Delta_0 = \frac{\pi}{2}$, from which we derive the optimum height of the antenna above the earth

$$h = \frac{\lambda_0}{4 \sin \Delta_0}, \quad (11-12)$$

where λ_0 is the calculated (main) wave-length; the angle Δ_0 should be defined from the condition of the propagation of radio waves. The factor $\frac{\cos^2 \varphi}{(1 - \cos \Delta_0 \sin \varphi)^2}$ is at a maximum for the condition

$$\sin \varphi = \sin \Delta_0. \quad (11-13)$$

From this we derive the value of half the obtuse angle of the rhombus. And finally, the maximum of the factor

$$\sin^4 \left[\frac{kl}{2} (1 - \cos \Delta_0 \sin \varphi) \right]$$

occurs on the condition

$$\frac{kl}{2} (1 - \cos \Delta_0 \sin \varphi) = \frac{\pi}{2}.$$

From this we derive the length of the side of the rhomb

$$l = \frac{\lambda_0}{2 (1 - \cos \Delta_0 \sin \varphi)}. \quad (11-14)$$

λ_0 is generally referred to as the optimum wave-length of the antenna. Calculations show that when $\Delta_0 = 15^\circ$, we get the following data for the antenna: $h = \lambda_0$, $\varphi = 75^\circ$ and $l = 7.5$. However, in practice, the following dimensions are taken for the antenna: $h = \lambda_0$, $\varphi = 65^\circ$ and $l = 4\lambda_0$. In that case, the power gain is down only by 15% and, at the same time, the size of the antenna is considerably reduced.

Above, the wave impedance of the antenna W was assumed to be a constant quantity. However, it increases as we move towards the obtuse angle, since the distance between the wires of the rhombus increases. To maintain a constant wave impedance of the antenna along its length, the rhombus is usually formed of two wires diverging towards the obtuse angle, as shown in Fig. 11-13. The wave impedance of the antenna is then expressed as:

$$W = 276 \log \frac{2s}{\sqrt{dH}}, \quad (11-15)$$

where s is the distance between the diverging sides of the rhombus in any section;

H , the distance between the wires forming a side of the rhombus;

d , the diameter of the wires.

In practice, the value H of the obtuse angle of the rhombus is taken of the order of 2 m. Then, as shown by experience, the travelling-wave ratio in the feeder is found to be close to unity in the operating wave range.

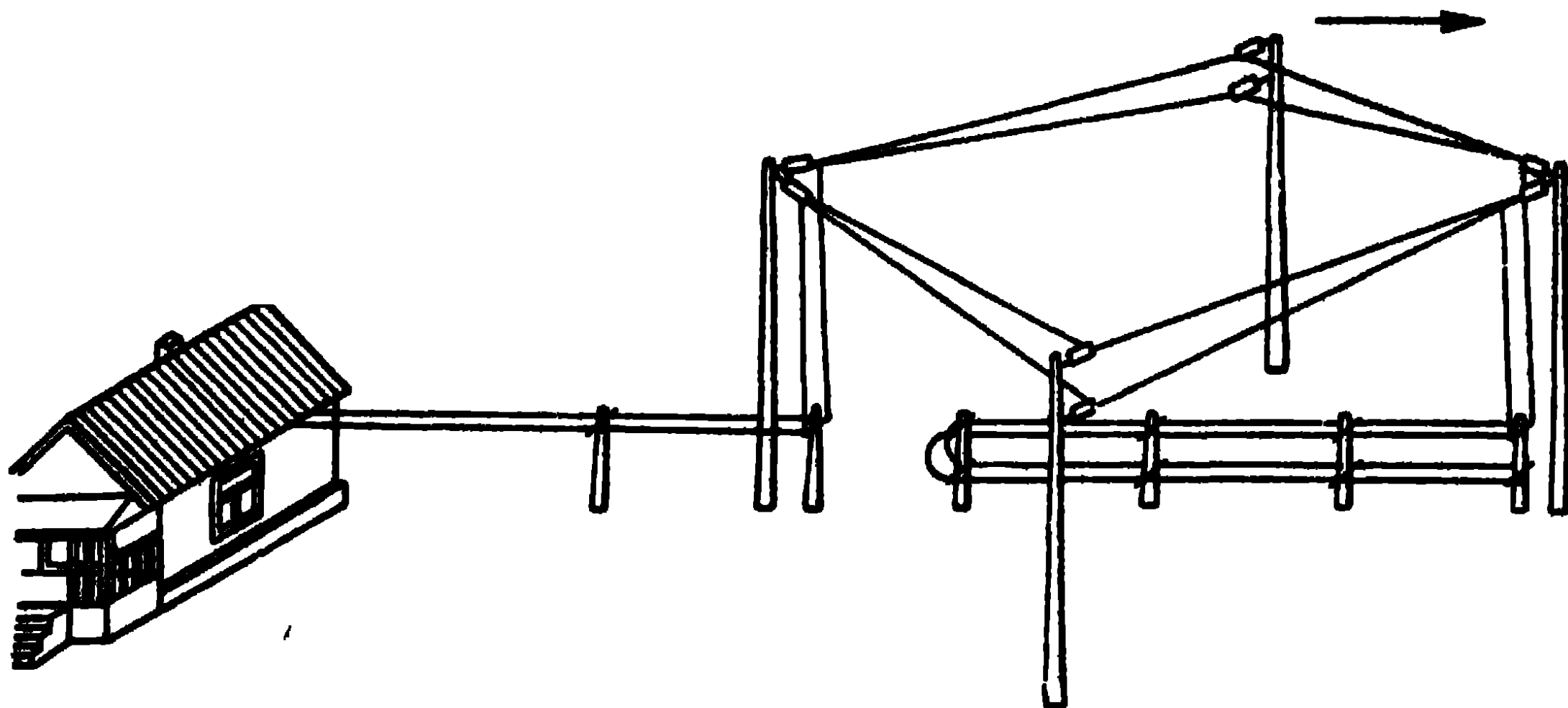


Fig. 11-13. General view of a rhombic antenna.

In the case of transmitting antennas, the absorbing resistance is a twin-wire iron line, because a rather high power has to be dissipated in that resistance.

The length of the iron line is chosen so that the intensity of the reflected wave at its input should be much lower than the intensity of the incident wave. If we designate by p the ratio of these intensities, the length of the line will be defined as:

$$p = e^{-2\beta l},$$

where the attenuation constant in the iron line is expressed as:

$$\beta = \frac{R_1}{W_1}, \quad R_1 = \frac{5.5 \times 10^8}{r} \sqrt{\frac{\mu_r \rho}{\lambda}} \text{ [ohms/m]},$$

where r is the radius of the wire, in mm;

μ_r , the relative permittivity (for short waves $\mu_r \approx 80$);

ρ , the resistivity, in ohms·m;

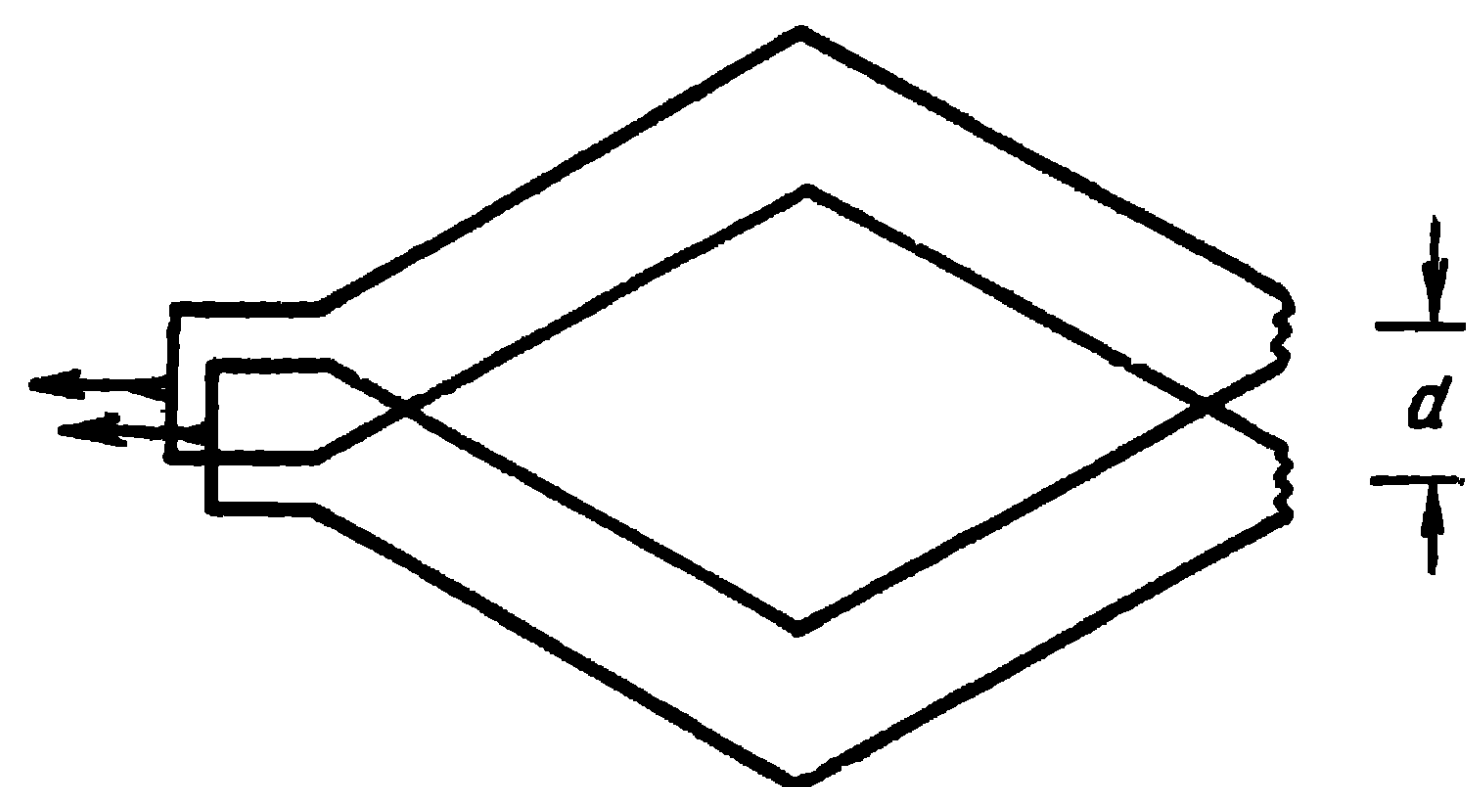
λ , the wave-length, in m;

W_1 , the wave impedance of the iron line.

If $W = 700$ ohms, $r = 1$ mm, $p = 0.1$, the necessary length of the iron line for the wave range $\lambda = 15 \div 45$ m is $l = 350$ m.

The absorbing line is usually placed on wooden posts under the antenna, as shown in Fig. 11-13.

In practice, to increase the directivity, the rhombic antennas are connected in parallel. Fig. 11-14 shows a



so-called duplex rhombic antenna designed by G. Z. -Eisenberg. The distance between the diagonals of the rhombus is taken equal to $d=0.8 \lambda_0$. In that case, the antenna directional

horizontal plane narrow down and the relative magnitude of the side lobes decreases. This is defined by the factor

$$2 \cos \left(\frac{kd}{2} \sin \beta \right),$$

which should be introduced into the expression (11-6).

Calculations and experiments show that the coefficient of amplification of a double rhombus is about twice that of a single rhombus.

Table 11-3

Antenna	Operating wave-length λ	Height of antenna above earth h	Directive gain D	Power gain e	Angle of elevation of major lobe Δ_0 , in degrees	Width of directional diagram in horizontal plane $2\beta_{1/4}$, in degrees	Width of directional diagram in vertical plane $2\Delta_{1/4}$, in degrees	Efficiency factor η
Single rhombus $l=4\lambda_0$, $\varphi=65^\circ$	$0.8\lambda_0$	λ_0	108	50	9.6	16	13.6	0.75
	λ_0		104	48	13	20	17	0.75
	$2\lambda_0$		38	15	28	31	32	0.65
Double rhombus $l=4\lambda_0$, $\varphi=65^\circ$	$0.7\lambda_0$	λ_0	218	100	9.6	14	13.6	0.75
	λ_0		208	95	13	18	17	0.75
	$2\lambda_0$		55	25	28	29	32	0.75

Table 11-3 gives the values of the electric parameters of a single and double rhombic antennas.

In table 11-3, $2\beta_{1/4}$ and $2\Delta_{1/4}$ represent the width of the directional diagram at a quarter of the radiated power.

11-8. Travelling-Wave Antenna

The rhombic antenna described in the preceding paragraph is used both as a transmitting and a receiving short-wave antenna.

The short-wave travelling-wave antenna discussed below is used only as a receiving antenna. It consists of an array of symmetrical dipoles connected through capacitances of

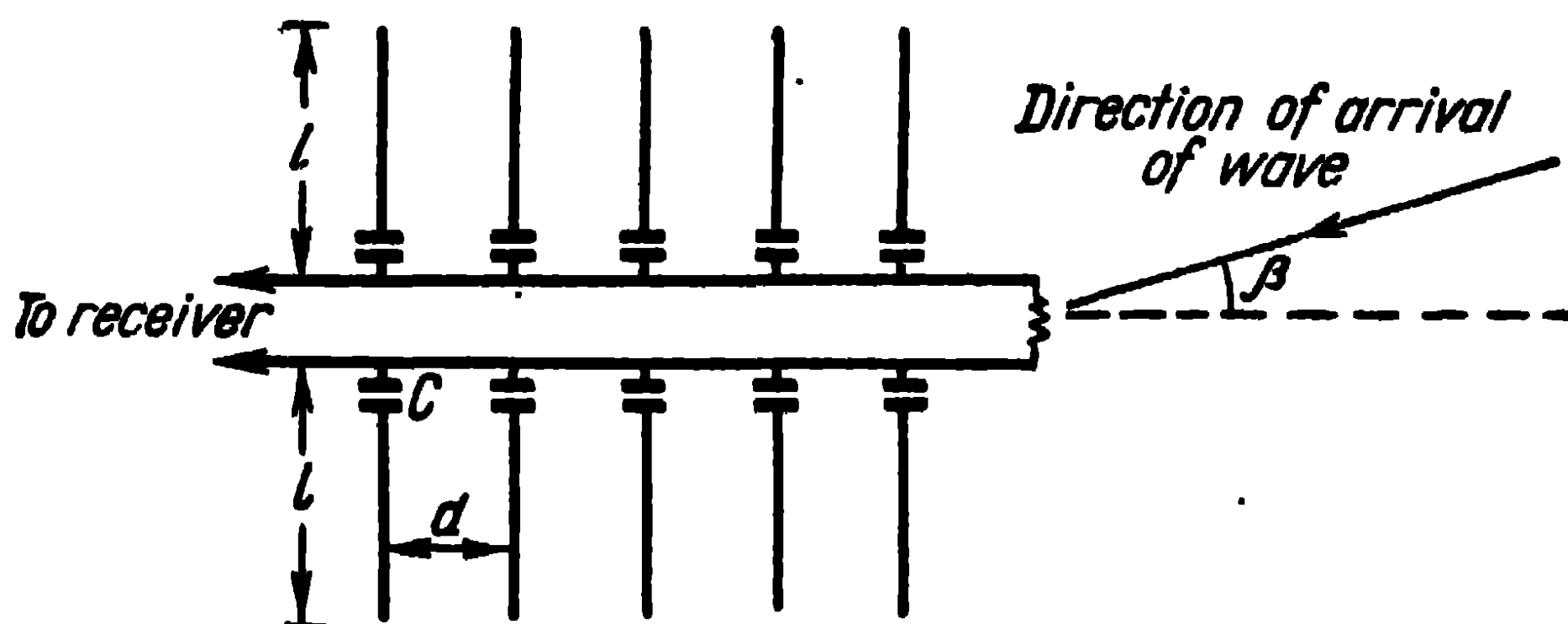


Fig. 11-15. Circuit of a travelling-wave antenna.

small value to a twin-wire gathering line (Fig. 11-15). The length of each half of a symmetrical dipole l is taken less than a quarter of a wave-length. The distance between neighbouring dipoles is taken of the order of one-tenth of a wave-length. At one end, the twin-wire line is loaded with an absorbing resistance equal to its wave impedance. At the other end, the line is connected to the receiver input, the resistance of which is also taken equal to the wave impedance of the line. Due to the presence of capacitors (uncoupling elements), the input resistance of the dipoles increase and they shunt the gathering line but insignificantly.

The electromagnetic wave in the field of which the antenna lies induces in the symmetrical dipoles emf's equal in amplitude but with a phase shift between neighbouring dipoles equal to angle $kd \cos \beta$, where β is the angle between the direction of incidence of the wave and the antenna axis. Current waves arise in the twin-wire line due to the action of these elementary emf's, which are propagated from each dipole to both ends of the twin-wire line. Since at both ends,

the line is loaded on resistances equal to its wave impedance and the input resistances of the dipoles are considerably higher than the wave impedance of the line, these current waves are hardly at all reflected along their path of propagation and are fully absorbed by the end resistances. The influence of the dipoles, the input resistance of which is of a capacitive nature and which are close to one another relatively to the wave-length manifests itself in a decrease of the phase velocity of propagation of the current waves along the line.

If we assume that the velocity of propagation of the current waves along the line equals the velocity of light, the elementary current waves at the receiver input when the electromagnetic wave comes from the absorbing resistance ($\beta=0$) should reinforce one another, being added up arithmetically. At the same time, the value of the total field at the receiver input will be proportional to the number of dipoles N . It might seem that the antenna could be taken as long as desired and the longer, the better. However, due to the influence of the dipoles, the phase velocity of the current waves along the line is always less than the velocity of electromagnetic waves in space, so that the elementary current waves from each of the dipoles at the receiver input differ in phase by a certain small angle and are added up geometrically. At preset phase velocity and wave-length, the elementary current waves from the first and last dipoles at a certain, definite (optimum) length of the antenna, are in antiphase. The total current at the receiver input is then at a maximum and any further increase or decrease of the length of the antenna causes the current to fall. In practice, the optimum length of the antenna is found to equal approximately three to five wave-lengths. In just the same way, at prescribed wave-length and length of antenna, there is an optimum phase velocity for which the currents at the receiver input from the first and last dipoles are in antiphase.

When the electromagnetic wave is propagated from other directions, in particular from that end of the line to which the receiver is connected, the elementary current waves at the receiver input are also added up geometrically but with a large phase shift. Hence, they will cancel instead of intensifying one another and the total current will, generally speaking, be all the closer to zero as the direction of reception is closer to the antenna axis from its receiving

end. As a result, the directional diagram of the antenna has the form shown in Fig. 11-16, *a*.

Travelling-wave antennas are multiple-tuned and retain a directional diagram of approximately the same shape as that shown in Fig. 11-16, in a 2÷2.5-fold wave range. With respect to long waves, this range has the limitation that the antenna loses its directivity and receives less power because the input resistance of the dipoles becomes very large. With respect to short waves, this range has the limitation that the dipoles reach resonance, as a result of which, the phase velocity of the wave is considerably lowered and the reception from the main direction decreases.

As can be seen from the diagrams in Fig. 11-16, the antenna has a considerable directive gain. However, due to the

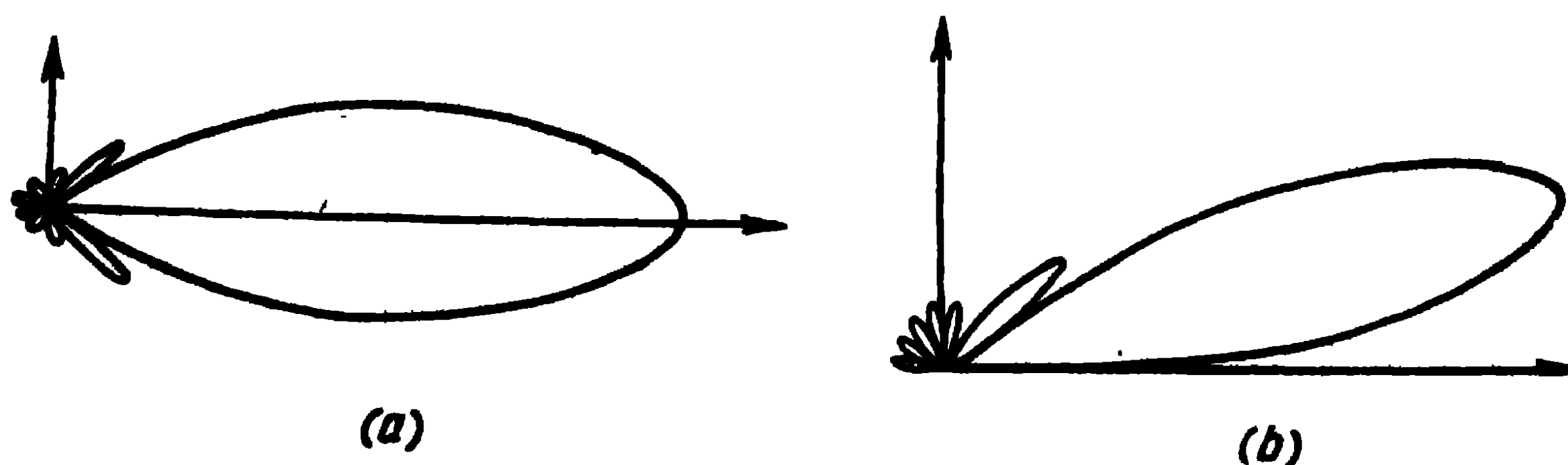


Fig. 11-16. Directional diagram of a travelling-wave antenna:
a—horizontal plane; *b*—vertical plane.

presence of an absorbing resistance and the weak coupling of the dipoles with the line, the antenna efficiency is low and the directive gain is found to be of the order of unity. For this reason, travelling-wave antennas are only used for reception. The relatively small size of the side lobes of the directional diagram makes the antenna quite suitable for short-wave reception, especially when the ratio of the power of the signal to that of the interference is more important than the absolute power of the signal.

The antenna is usually secured in a horizontal position on approximately 17m high supports (so as to lower the cost of production) and consists of two separate arrays: one for night-time and for day-time duty. The night-time array consists of one array of dipoles and that of day-time—of two single arrays of dipoles connected in parallel. As indicated earlier, in the day-time system, the dipoles are coupled with the line through capacitances and, in the night-time array,

the coupling is conductive. The antenna has the following characteristics:

a) *Day-time array*

Length of array $L=87.5$ m.
 Length of dipoles $l=3.9$ m.
 Distance between dipoles $d=2.5$ m.
 Number of dipoles $N=36$.
 Capacitance of coupling capacitors $C=5.5-8$ pf.
 Operating wave range $\lambda=15 \div 35$ m.

b) *Night-time array*

Length of array $L=87.5$ m.
 Length of dipoles $l=8$ m.
 Distance between dipoles $d=2.5$ m.
 Operating wave range $\lambda=35 \div 60$ m.

Let us now investigate the mathematical side of the problem. Let the antenna have N dipoles. Let β be the angle between the antenna axis and the direction of incidence of the electromagnetic wave in the antenna plane (Fig. 11-15). Taking the phase of the field intensity in the vicinity of dipole number 0 (near the receiver) as equal to zero, the expression for the emf induced by the electromagnetic wave in the n -th dipole will be:

$$E_n = \frac{E_0 \lambda}{\pi \sin kl} \frac{\cos(kl \sin \beta) - \cos kl}{\cos \beta} e^{lnkd \cos \beta}. \quad (11-16)$$

The current at the receiver input caused by the emf equals:

$$I_n = \frac{E_0 \lambda}{(W_A + 2Z_A) \pi \sin kl} \frac{\cos(kl \sin \beta) - \cos kl}{\cos \beta} \times \\ \times e^{lnkd \cos \beta - ln \xi kd}, \quad (11-17)$$

where Z_A is the input resistance of each of the dipoles, with the resistance of the coupling capacitors taken into account;

W_A , the wave impedance of the line, with the influence of the dipoles taken into account;

$\xi = \frac{v_1}{v}$, the ratio of the velocity of propagation of the wave in space to the phase velocity of the wave propagation in the line.

The total current in the receiver from all the dipoles equals:

$$I'_{\text{rec}} = \frac{E_0 \lambda}{\left(Z_A + \frac{W_A}{2}\right) 2\pi \sin kl} \frac{\cos(kl \sin \beta) - \cos kl}{\cos \beta} \times \\ \times \frac{\sin \left[\frac{N kd}{2} (\cos \beta - \xi) \right]}{\sin \left[\frac{kd}{2} (\cos \beta - \xi) \right]}. \quad (11-18)$$

(11-18) expresses the current in the load depending on the incidence angle of the wave β and defines the antenna directional diagram in the horizontal plane (in the plane of the antenna).

When two parallel systems are connected to a common matched load, as in the day-time antenna, the expression (11-18) should be multiplied by the quantity

$$2 \cos \left(\frac{kD}{2} \sin \beta \right),$$

where D is the distance between the axes of the arrays.

Note that in (11-18), Z_A is expressed as:

$$Z_A = R_{\Sigma 0} - iW_w \cot kl - i \frac{1}{\omega C_{sd}}, \quad (11-19)$$

where $R_{\Sigma 0}$ is the radiation resistance of a symmetrical dipole related to the point of its connection to the line;

W_w , the wave impedance of the dipoles;

C_{sd} , the capacitance of two series connected condensers in each symmetrical dipole.

The expression defining the directional diagram in the vertical plane passing through the antenna axis is:

$$I'_{\text{rec}} = \frac{E_0 \lambda (1 - \cos kl)}{\left(Z_A + \frac{W_A}{2}\right) \pi \sin kl} \frac{\sin \left[\frac{N kd}{2} (\cos \Delta - \xi) \right]}{\sin \left[\frac{kd}{2} (\cos \Delta - \xi) \right]} \times \\ \times \sin(kh \sin \Delta), \quad (11-20)$$

where h is the height of the antenna above the earth;

Δ , the angle of elevation of the ray above the horizon.

Fig. 11-16, *b* shows the directional diagram of the antenna in the vertical plane on the wave $\lambda = 15$ cm.

Let us now define the conditions of maximum reception of the travelling-wave antenna. When the radio waves come from the main direction ($\beta=0$), in accordance with (11-18), the current in the receiver becomes equal to zero on condition that:

$$\frac{Nkd}{2}(1-\xi)=-\pi,$$

whence we see that if the phase velocity of the wave in the antenna satisfies the condition $\xi-1=\frac{\lambda}{Nd}$, there is no reception from the main direction. The maximum of reception from the main direction will occur on condition that:

$$\frac{Nkd}{2}(1-\xi)=-\frac{\pi}{2},$$

from which we get the condition of optimum reception:

$$\xi-1=\frac{\lambda}{2Nd}\approx\frac{\lambda}{2L}, \quad (11-21)$$

where L is the length of the antenna.

If, for example, $L=5\lambda$ (which is what we get in practice for the short waves of the operating range), then $\xi-1=0.1$ and $v=0.9v_1$. The length of the dipoles and the value of the capacitance of the coupling capacitors should be chosen such that the velocity of the wave propagation should not be less than that value.

When the length of the dipoles is $l<\frac{\lambda}{4}$ (which is what we get in practice), the reactive part of the input resistance of the dipoles is of a capacitive nature and equals:

$$\frac{1}{\omega C_d}=W_d \cot kl,$$

where C_d is the equivalent capacitance of the dipoles.

The maximum shunting effect of the dipoles occurs on a wave for which $l=\frac{\lambda}{4}$. That is why it is advisable to define the necessary capacitance of the coupling capacitors for precisely that case.

The velocity of propagation of the electromagnetic wave in a twin line is expressed as:

$$\frac{1}{v_1}=\sqrt{L_1 C_1},$$

where L_1 is the distributed inductance, in hy/m ;
 C_1 , the distributed capacitance, in f/m .

If the wave-length is resonant for the dipoles, the velocity of propagation of the wave in the line is expressed as:

$$\frac{1}{v} = \sqrt{L_1 \left(C_1 + \frac{C_c}{d} \right)},$$

where C_c is the coupling capacitance, in f;
 d , the distance between two neighbouring dipoles, in m.

The ratio of these velocities is:

$$\xi = \frac{v_1}{v} = \sqrt{\frac{C_1 + \frac{C_c}{d}}{C_1}}. \quad (11-22)$$

For a twin line

$$C_1 = \frac{10^9}{36 \ln \frac{D}{r}} [\text{pf/m}], \quad (11-23)$$

where D is the distance between the wires;
 r , the radius of the wires.

The necessary capacitance of the coupling capacitors can be defined from (11-22) and (11-23). Assuming, for example, that $D=90$ mm, $r=1.5$ mm, $\xi=1.1$, we get $C_c \approx 3.6$ pf and, consequently, each of the two series connected capacitors should have a capacitance of the order of 7.2 pf.

In the case of the above-mentioned dimensions of the line ($D=90$ mm and $r=1.5$ mm), the wave impedance of the line equals 500 ohms. Since the coupling capacitors increase the distributed capacitance between the wires, the wave impedance of the line decreases. It depends on the wave-length and, in the case of the above-cited example, it equals approximately 400 ohms.

Consequently, the absorbing resistance should be 400 ohms. In the case of two arrays connected in parallel, the receiver input resistance should be 200 ohms. If the antenna is connected to the receiver through a feeder, the wave impedance of the latter should be 200 ohms, which is the case in practice.

The line of the night-time antenna array is usually of four wires, with a wave impedance of approximately 200 ohms. A plane view of the antenna is shown in Fig. 11-17.

The electric parameters of the antenna array are given in Table 11-4.

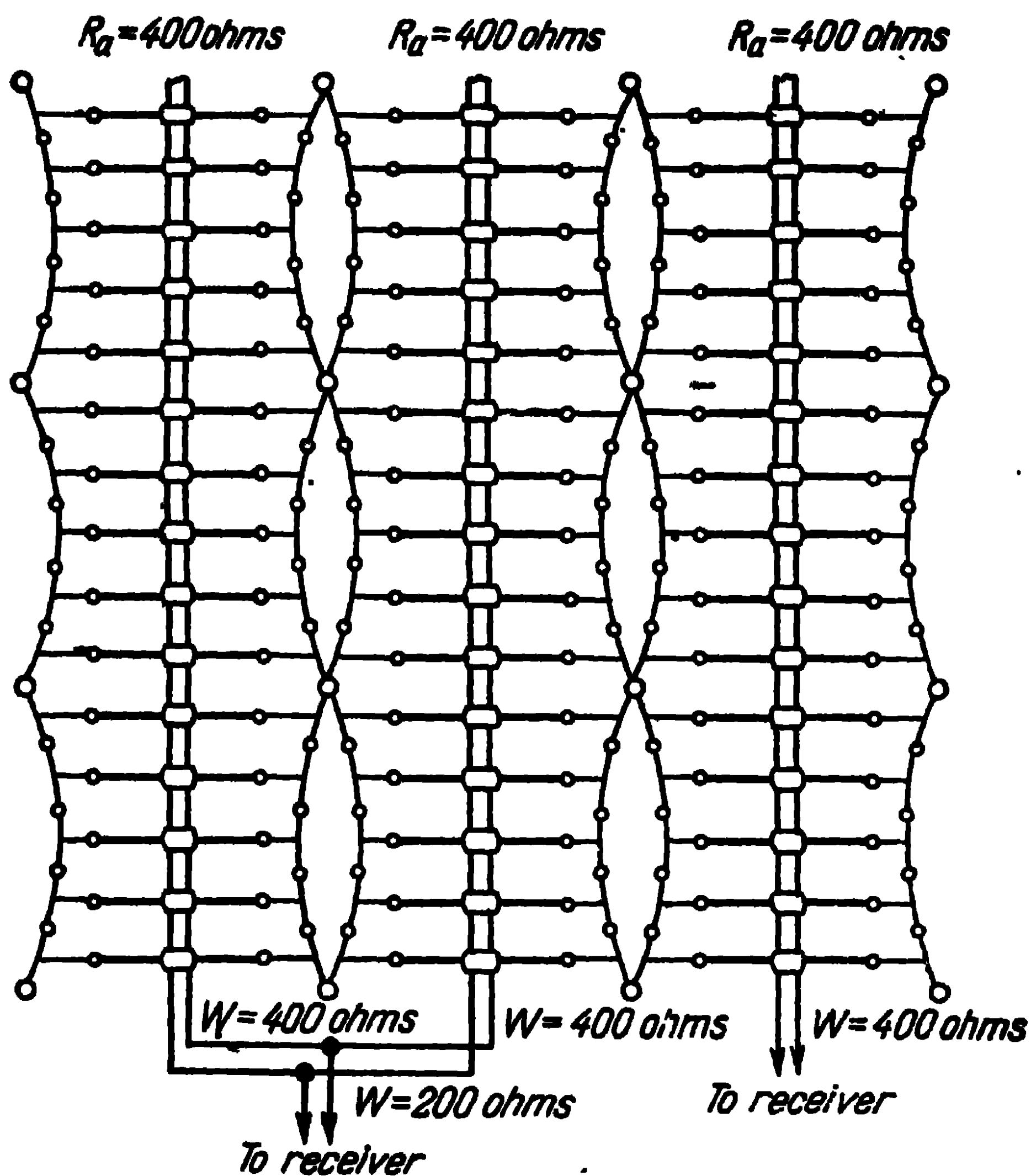


Fig. 11-17. Travelling-wave antenna.

As follows from the travelling-wave antenna theory investigated in Paragraph 4-5, the phase velocity of waves in antennas of this kind should be inferior to the velocity of radio waves in free space.

Table 11-4

Wave-length λ	Height of antenna above the earth h	Directive gain D	Coefficient of amplification e	Angle of elevation of principal ray Δ_0 , in degrees	Width of directional diagram in horizontal plane $2\beta_{1/2}$, in degrees	Width of directional diagram in vertical plane, $2\Delta_{1/2}$, in degrees	Efficiency factor
λ_0	$0.7\lambda_0$	80	2.75	15	24	18	0.0565
$2\lambda_0$	$0.7\lambda_0$	20	0.28	25	40	32	0.023

However, in the case of the short-wave travelling-wave antenna investigated above, the use of capacitors as coupling elements for dipoles with a distributive line is not indispensable. These elements can consist of, for example, active resistances. The use of inductive coupling elements is inadvisable because, in that case, the phase velocity in the line throughout the operating wave range exceeds the velocity of radio waves in free space, as a result the directive properties of the antenna are considerably impaired.

The use of active resistances as coupling elements enables to obtain a considerable improvement of the antenna parameters in comparison with those of antennas which have capacitors as coupling elements [71].

This can be explained as follows. The directive gain of a travelling-wave antenna (as of any other antenna) decreases as the wave-length increases. Hence, it may be particularly desirable to increase the directive gain in the long-wave margin of the range. Here, the input resistance of the dipoles (without coupling element) is of a capacitive nature and of a magnitude which enables to obtain in the line a regimen close to optimum type of operation (the phase shift between the currents of the first and last dipoles amounts to 180-230°). However, when a capacitive coupling element is being used, the equivalent capacitance of the dipole turns out to be quite small and the magnitude of the phase velocity in the line exceeds the optimum value, which results in a deterioration of the directive properties. In the case of an active coupling resistance, the dipole input resistance ensures by itself a velocity close to the optimum in the long-wave margin of the range.

Since the capacitive coupling impedance increases linearly with an increase of the wave, this causes a decrease of the antenna efficiency approximately proportional to the square of the wave-length. The antenna power gain decreases correspondingly. If the resistance of the coupling element was not frequency dependent, the decrease of power gain would be proportional to the ratio $\frac{L^2}{\lambda^2}$ (here, L is the length of the antenna). Thus, in the case of a travelling-wave antenna with coupling capacitors, an increase in wave-length causes a decrease of the power gain approximately proportional to the fourth power of the wave-length. But in the case of an active coupling resistance, the fall of the power gain

is considerably slower. Calculations as well as experiments show that the efficiency of the antenna with resistances (double-array system) lies between 20 and 60%, whereas the efficiency of an antenna with capacitors is 0.5 to 20%. In both antennas, the efficiency decreases as the wave-length increases. It has been established that the optimum magnitude of the active coupling resistances (for antennas consisting of two arrays) is 180-200 ohms.

Antennas of this kind have recently found application at radio centres of the Soviet Union.

11-9. Diversity Radio Reception

On short waves, as a rule, several beams arrive at various angles to the horizon. Due to the instability of the ionised layers of the atmosphere, the difference of path of the beams changes in time causing weakening or fading out of the signals and, in telegraphy, to the disappearance of isolated letters or even whole words.

The routine way of checking fading is through diversity reception. It has been experimentally established that fading is not identical in two even relatively close spots. At any given instant, antennas situated at these spots give rise to signals of different magnitude; moreover, full fading out of the signals does not occur simultaneously for different antennas.

To eliminate fading, two or three receiving antennas are installed on the premises of the radio centre, approximately 300 m apart.

It has been shown by experiments that the best results in this respect are obtained when the antennas are situated along the line of arrival of the wave. This is due to the fact that a displacement towards the arrival of the rays leads to a more pronounced interference of the rays falling at different angles to the horizon.

In telegraphy, three separate receivers are used, one for each antenna, and the signals are aggregated following rectification at the receiver's outputs.

Three receivers are likewise used in telephony, but the signal delivered to the telephone comes from that receiver which picks up the clearest signals at the given moment, the other receivers being switched out. The object is to avoid noises from the receivers which, at the given moment, deliver weak signals.

CHAPTER TWELVE

Medium- and Long-Wave Antennas

12-1. Classification of Antennas

Taking into consideration the conditions of propagation of medium and long waves, i.e., waves of from 100 m upwards, the antennas used on these waves must have a vertical polarisation of the electromagnetic field. In most cases, the directional diagrams in the horizontal plane should represent circumferences; directional antennas can also be used for broadcasting, chiefly in a preset direction, or for radio communications between two points, or to eliminate interference. On long waves, the maximum radiation of antennas should be directed along the surface of the earth. From the point of view of their directional properties, long-wave antennas are relatively simple.

Long-wave antennas comprise antennas of the wire type (T-antennas, L-antennas, umbrella antennas, etc.) and of the tower or mast type (antennas on insulators, shunt-fed antennas, mast antennas of upper feed, etc.). For reception, antennas of the frame type (simple or screened) are used, as well as antennas of the goniometrical type.

Let us begin with an investigation of T- and L-antennas.

12-2. T- and L-antennas

T- and L-antennas find wide application in broadcasting and radio communications, on medium and long waves. The general view of these antennas is shown in Fig. 12-1. As a rule, they are secured on two 100 to 250 m high masts spaced 100 to 250 m apart and represent a plane net of horizontal

and vertical wires. The antenna array has two to sixteen wires spaced 1 to 1.5 m apart. The copper wires are usually 5 to 8 mm in diameter. The supporting masts are secured by

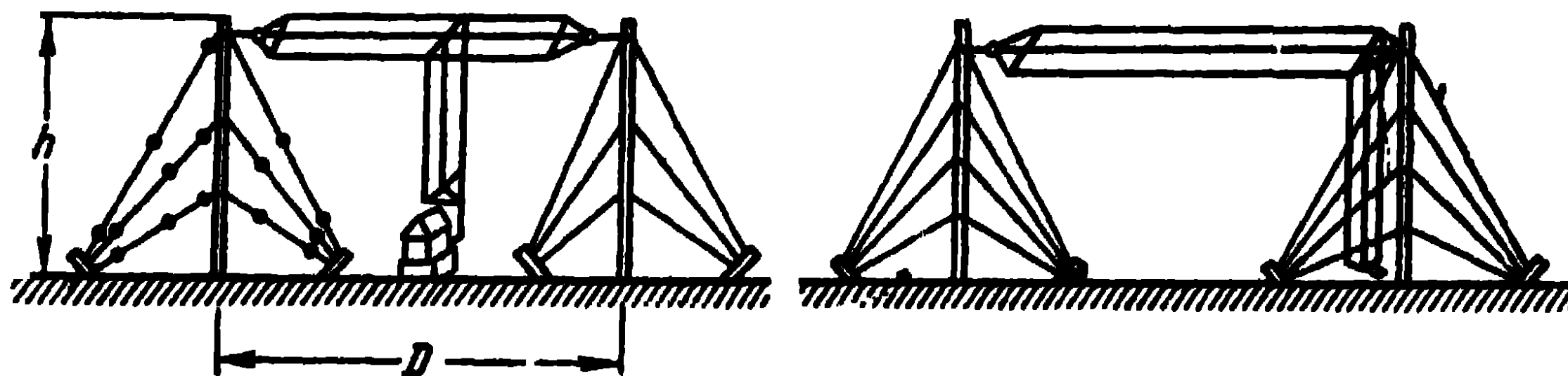


Fig. 12-1. General view of T- and L-antennas.

means of several tiers of guys into which insulators are inserted to eliminate the influence of the guys on the antenna radiation. The antenna downleads directly connect the radio transmitter; hence there is no need for the feed lines.

The electric current distribution along the antenna is shown in Fig. 12-2. Since the geometrical dimensions of the

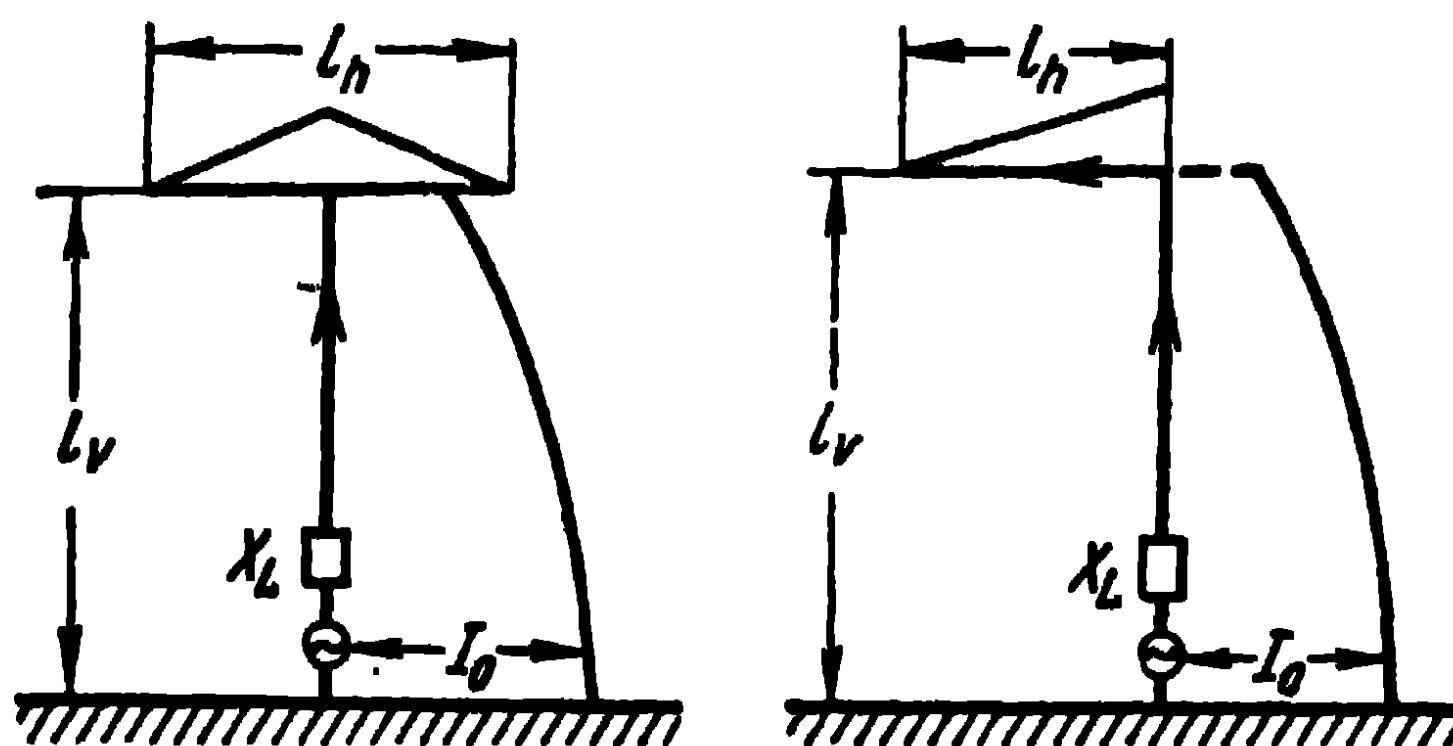


Fig. 12-2. Current distribution in the antenna.

antenna are small as compared with the operating wavelength, the influence of the earth adds to the radiation of the vertical part of the antenna and weakens the radiation of the horizontal part. The horizontal part of the antenna is destined to increase the capacitance of the antenna and ensure a more uniform current distribution along its vertical part.

The coupling of the transmitter with the antenna downlead can be inductive, conductive or capacitive. Apart from a coupling circuit, a circuit for tuning the antenna in resonance is also inserted into the antenna; the circuit acts as an inductance coil in case of lengthening and as a condenser in case of shortening. Examples of the antenna coupling and tuning are shown in Fig. 12-3.

The antennas are fastened to masts (of wood or metal) by means of insulators and are fixed in position by means of cables through pulleys secured to the top of the supporting masts.

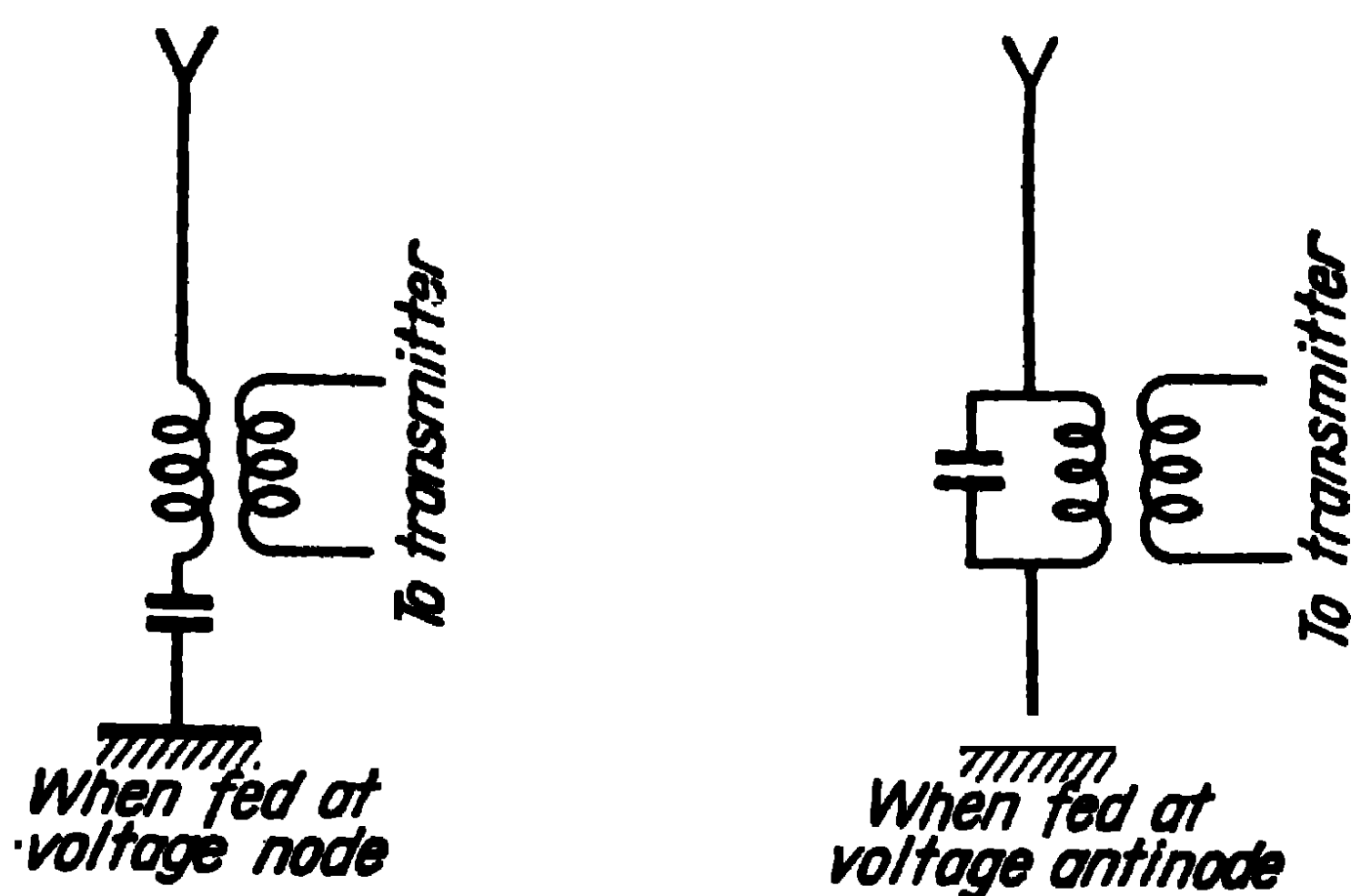


Fig. 12-3. Coupling of antenna with transmitter.

To reduce losses into the earth, the lower end of the antenna downlead is connected to the earthing through tuning and coupling circuits.

T- and L-antennas find frequent application among radio hours. Small in size they are often installed on the roofs of houses.

To simplify calculations of T- and L-antennas, in particular the calculation of the current and voltage distribution

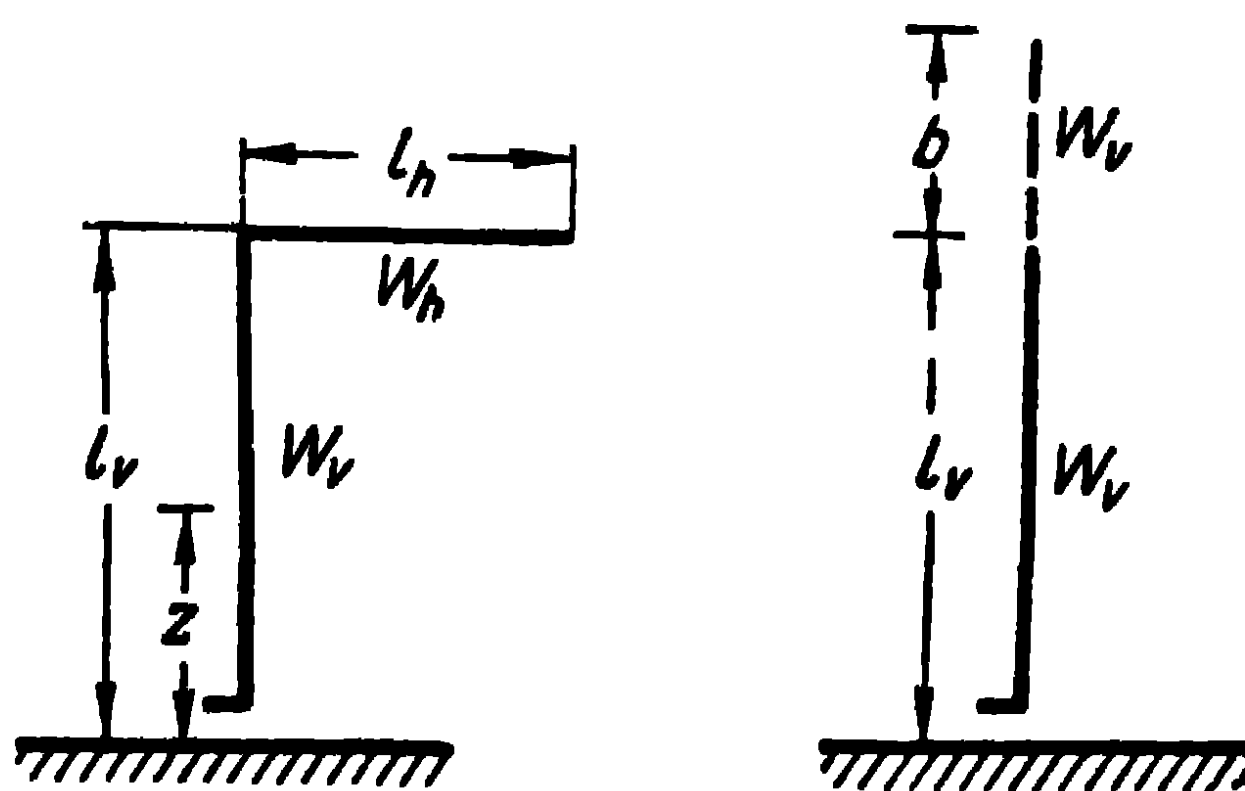


Fig. 12-4. Calculating the equivalent length of the antenna.

along the antenna, the horizontal part of the antenna is replaced by an equivalent length b of the same wave impedance as the vertical part (Fig. 12-4). The current and voltage distribution in the antenna is expressed as:

$$\left. \begin{aligned} I_z &= I_0 \frac{\sin k(l_v + b - z)}{\sin k(l_v + b)}; \\ U_z &= U_0 \frac{\cos k(l_v + b - z)}{\cos k(l_v + b)}, \end{aligned} \right\} \quad (12-1)$$

where I_0 and U_0 are the current and voltage at the base of the antenna;

b , the equivalent length of the horizontal part of the antenna;

l_v , the length of the vertical part (downlead) of the antenna.

The equivalent length b is chosen such that the current and voltage distribution in the vertical part should remain the same as in the antenna with a horizontal part. It also means that the input resistance of the horizontal part of the antenna is equal to the input resistance of a vertical segment of equivalent length.

From (12-1) one can define the current and voltage at the upper end of the vertical part of the antenna:

$$\left. \begin{aligned} I_{lv} &= I_0 \frac{\sin kb}{\sin k(l_v + b)}; \\ U_{lv} &= U_0 \frac{\cos kb}{\cos k(l_v + b)}. \end{aligned} \right\} \quad (12-2)$$

Along the horizontal part of an L-antenna, the current and voltage are distributed as

$$\begin{aligned} I_x &= I_{lv} \frac{\sin k(l_h - x)}{\sin kl_h}; \\ U_x &= U_{lv} \frac{\cos k(l_h - x)}{\cos kl_h}. \end{aligned}$$

Along the horizontal part of a T-antenna, the current and voltage are distributed as

$$\begin{aligned} I_x &= \frac{I_{lv}}{2} \frac{\sin k\left(\frac{l_h}{2} - x\right)}{\sin \frac{kl_h}{2}}; \\ U_x &= U_{lv} \frac{\cos k\left(\frac{l_h}{2} - x\right)}{\cos \frac{kl_h}{2}}, \end{aligned}$$

where l_h is the length of the horizontal part of the antenna;
 x , the distance along the horizontal part, measured from the connection point of the vertical part of the antenna

Knowing the current and voltage at the base of the antenna, as well as the equivalent length of the horizontal

part, one can calculate the current and voltage at any point of the antenna.

Let us define the equivalent length of the horizontal part of the antenna. For an L-antenna, the resistance of the horizontal part at the point where the vertical part is connected to it, equals:

$$X_h = -iW_h \cot kl_h,$$

where W_h is the wave impedance of the horizontal part of the antenna.

Let us replace the horizontal part of the antenna by an equivalent wire of length b with a wave impedance equal to the wave impedance W_v of the vertical part of the antenna, so that its input resistance should remain the same as before

$$X_h = -iW_v \cot kb.$$

This leads us to the equivalent length of the horizontal part of the L-antenna

$$\cot kb = \frac{W_h}{W_v} \cot kl_h. \quad (12-3)$$

For a T-antenna, the resistance of each arm of the horizontal part equals $-iW_h \cot \frac{kl_h}{2}$. The resistance of the horizontal part loading the vertical part of the antenna equals:

$$X_h = -i \frac{W_h}{2} \cot \frac{kl_h}{2}.$$

The equivalent length of the horizontal part of a T-antenna is then expressed as:

$$\cot kb = \frac{W_h}{2W_v} \cot \frac{kl_h}{2}. \quad (12-4)$$

The above expressions enable the easy calculation of the reactive part of the input resistance of the antenna. T- and L-antennas are usually applied on long waves, for which the length of the antenna is small relatively to the operating wave-length. That is why the reactive part of the input resistance of the antenna can be calculated by means of the expression valid in the case of a sinusoidal distribution,

$$X_v = -iW_v \cot k(l_v + b). \quad (12-5)$$

To make the calculation and definition of the character of the reactive part of the antenna input resistance easier the

concept of the natural wave-length of the antenna is usually introduced, by which one understands the longest wave for which the antenna is tuned in resonance without the introduction into the antenna of a tuning resistance. The natural wave-length λ_0 is defined from the condition

$$k_0(l_v + b) = \frac{\pi}{2},$$

where $k_0 = \frac{2\pi}{\lambda_0}$, and b is a function of the wave-length.

For an unloaded antenna, the natural wave-length equals

$$\lambda_0 = 4l_v.$$

Due to the fact that $k_0 l_v = \frac{\pi}{2} - k_0 b$, we obtain the following ratios for the definition of the natural wave-length from the expressions (12-3) and (12-4)

$$\left. \begin{aligned} \tan k_0 l_v &= \frac{W_h}{W_v} \cot k_0 l_h; \\ \tan k_0 l_v &= \frac{W_h}{2W_v} \cot \frac{k_0 l_h}{2}. \end{aligned} \right\} \quad (12-6)$$

The equations (12-6) are transcendental and are solved graphically.

Consequently, in the general case, the natural wave-length does not equal the quadruple value of the wave-length and depends on the ratio of the wave impedance of the vertical and horizontal parts of the antenna.

Let us now deal with antenna tuning. On operating waves differing from the natural wave-length, the antenna has to be tuned in resonance by inserting a reactive resistance at its base. Furthermore, we should have the ratio

$$X_v + X_t = 0,$$

where X_t is the antenna tuning resistance.

There are two possible cases. Let $\lambda_{\text{oper}} > \lambda_0$; then, in accordance with (12-5), the antenna represents a capacitive resistance. In that case, to be tuned in resonance, the antenna has to be lengthened, i.e., an inductance lengthening coil inserted at its base, the resistance of which should equal

$$\omega L_{\text{length}} = W_v \cot k(l_v + b). \quad (12-7)$$

Now let $\lambda_{\text{oper}} < \lambda_0$. In that case, the electric length of the antenna will be greater than 90° . The antenna represents

an inductive resistance and the insertion of a shortening capacitance is necessary to tune it in resonance

$$\frac{1}{\omega C_{\text{shrtn}}} = -W_v \cot k(l_v + b). \quad (12-8)$$

The expressions (12-7) and (12-8) are utilised to define the tuning elements of the antenna.

Let us pass on to the determination of the radiation resistance of T- and L-antennas. In the case of antennas that are short in comparison with the wave-length, in the present case, of antennas operating on waves larger than the natural wave-length, they can be regarded as dipoles and the radiation resistance calculated from the expression

$$R_{\Sigma 0} = 160\pi^2 \left(\frac{h_{\text{eff}}}{\lambda_{\text{oper}}} \right)^2, \quad (12-9)$$

where h_{eff} represents the effective height of the antenna, which is calculated from an equivalent surface of current in the antenna and expressed as:

$$h_{\text{eff}} = \frac{1}{k} \frac{\cos kb - \cos k(l_v + b)}{\sin k(l_v + b)}. \quad (12-10)$$

In practice, the calculations based on the expressions (12-9) and (12-10) are found to be sufficiently accurate.

As regards the calculation of the directional diagram of T- and L-antennas, the radiation of the horizontal part in comparison with the radiation of the vertical part is usually neglected. The radiation of the antennas in the horizontal plane is then uniform and, in the vertical plane, the directional diagrams are the same as for dipole antennas.

When operating on waves shorter than the natural wave-length, a more accurate expression is to be preferred, viz.,

$$E = \frac{60I_0}{r_0 \sin k(l_v + b)} \times \frac{\cos kb \cos(kl_v \cos \theta) - \cos \theta \sin kb \sin(kl_v \cos \theta) - \cos k(l_v + b)}{\sin \theta}, \quad (12-11)$$

where θ is the angle between the antenna axis and the direction towards the point of observation.

Note that the full power fed to the antenna can be characterised by the expression

$$P_A = \frac{I_0^2}{2} (R_{\Sigma 0} + R_{\text{losses}}),$$

where R_{losses} is the resistance of the losses.

In that case, the efficiency of the antenna can be expressed as:

$$\eta = \frac{R_{\Sigma 0}}{R_{\Sigma 0} + R_{\text{losses}}}$$

The resistance of the losses is mainly determined by the power lost on heating the earth. The expression generally used for calculating the losses in the earth on long waves is M Shuleikin's empirical expression

$$R_{\text{losses}} = A \frac{\lambda_{\text{oper}}}{\lambda_0} \quad (12-12)$$

The coefficient A is defined by the electric parameters (ϵ , σ) of the soil and the earthing system of the antenna. It changes within rather large limits: from 0.5 to 7. When the earthing is properly done, the quantity A does not exceed 2.5 ohms (for $\lambda_{\text{oper}} = \lambda_0$).

Thus, the expression for the full active resistance of the antenna is

$$R_{\text{in}} = 160\pi^2 \left(\frac{h_{\text{eff}}}{\lambda_{\text{oper}}} \right)^2 + A \frac{\lambda_{\text{oper}}}{\lambda_0} \quad (12-13)$$

At a certain wave-length, R_{in} is at a minimum. When measuring the minimum input resistance of the given antenna and calculating the radiation resistance, the quantity A can be defined from (12-13), after which, the resistance of the losses can be determined from (12-12).

The earthing system often consists of a wire net buried at a small depth. The wires capture the displacement currents branching off from the antenna and terminating on the earth and, thereby, result in a decrease of the losses in the earth (Fig. 12-5). The larger the number of wires of the earthing system and the greater their length, the smaller the part of the current branching off from the antenna and flowing directly through the earth, the smaller the energy losses in the earth and the higher the efficiency.

The power fed to the antenna being prescribed, the current at the base of the antenna equals:

$$I_0 = \sqrt{\frac{2P_A}{R_{\Sigma 0} + R_{\text{losses}}}}.$$

The voltage at the base of the antenna is expressed as:

$$U_0 = I_0 \sqrt{(R_{\Sigma 0} + R_{\text{losses}})^2 + X_{\text{in}}^2}.$$

The voltages and current at the upper ends of the antenna can be defined from (12-2).

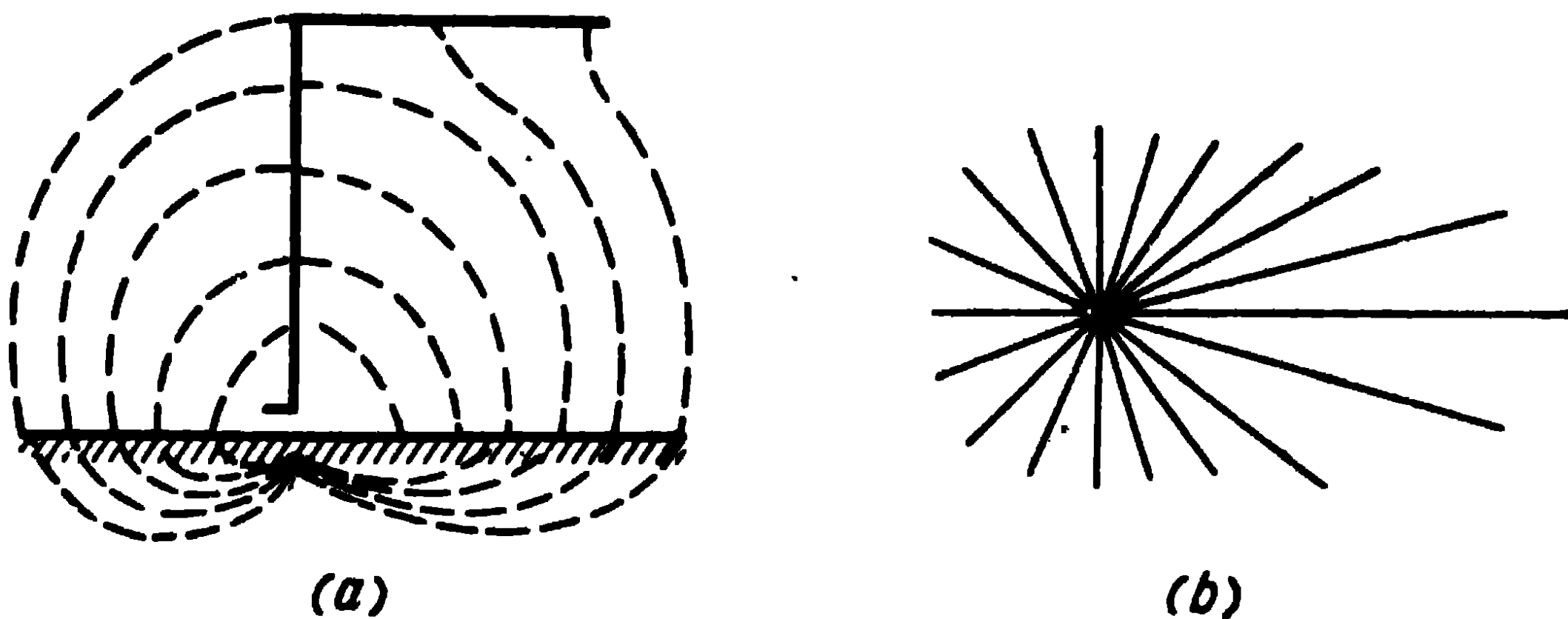


Fig. 12-5. Earthing system of an L-antenna:
a—central earthing; b—radial earthing

The wave impedance of the vertical and horizontal parts of the antenna of the above expressions can be defined through the static capacitance of the antenna by means of the expression

$$W = \frac{30}{C[\text{cm/cm}]}.$$

The distributed capacitance C , measured in centimetres per centimetre of length of the vertical or horizontal part, are usually calculated by the approximate Howe method, according to which, the static charge is assumed to be distributed uniformly over the surface of the wire. It is then found possible to calculate the potential in the conductor, the potential which changes along the conductor. Taking the mean value of the potential all along the length of the conductor and dividing by it the full charge of the wire, the capacitance of the wire and then, the capacitance per unit length of the wire can be defined. To calculate the capacitances of T- or L-antennas, the potentials induced on each conductor by the other conductors of the net and its mirror image in the earth have to be taken into account.

Let us now consider the pass-band of the antennas. Due to the fact that the geometrical dimensions of T- and L-antennas are small in comparison with the wave-length, these antennas are highly directional. The problem of the transmission of telephone or telegraph signals without distortion is therefore an important one and the antenna pass-band has to be defined in order to evaluate its possibilities in this respect.

When the operating waves are considerably larger than the natural wave-length ($\lambda_{\text{oper}} \gg \lambda_0$), the expression (12-5) which defines the reactive part of the antenna input resistance can be expressed approximately as follows:

$$X_{\text{in}} \approx -i \frac{W_v}{k(l_v + b)} = -i \frac{1}{\omega C_A}, \quad (12-14)$$

where C_A is the total capacitance of the antenna array, in farads.

This expression indicates that when the antenna is lengthened, the reactive energy accumulated in the antenna is mainly concentrated in the electric field. Then, the quality of the antenna circuit, for the tuning of which a lengthening coil L_{length} is inserted, can be approximately defined as the ratio of the expression (12-14) to the active resistance of the antenna, under resonant condition

$$\left(\omega_r L_{\text{length}} \approx \frac{1}{\omega_r C_A} \right) : Q = \frac{W_v}{R_{\text{in}} k_r (l_v + b)}. \quad (12-15)$$

Hence, in the case of lengthening, the pass-band of T- or L-antennas is expressed as:

$$\frac{2F}{f_r} = \frac{R_{\text{in}}}{W_v} k_r (l_v + b). \quad (12-16)$$

Thus, the pass-band of the antenna will be all the larger as the electric length of the antenna and the radiation resistance are larger and the antenna wave impedance is smaller. When the antenna is shortened, the expressions (12-15) and (12-16) are no longer valid. In that case, the tuning of the antenna is obtained through the insertion into it of a shortening capacitor C_{shortn} , and the coupling with the generator, through the insertion of an inductance coil L . Thus, the reactive part of the general input impedance of

the antenna, i.e., of the impedance of an array with tuning elements, is expressed as:

$$X_{in} = i\omega L + \frac{1}{i\omega C_{shrtn}} - iW_v \cot k(l_v + b).$$

On the resonant frequency, this impedance equals zero:

$$X_{in}(\omega_r) = i\omega_r L + \frac{1}{i\omega_r C_{shrtn}} - iW_v \cot k_r(l_v + b) = 0. \quad (12-17)$$

On frequencies close to the resonant one, it can be approximately represented by two terms of a Taylor series:

$$X_{in}(\omega) \approx X_{in}(\omega_r) + \Delta\omega X'_{in}(\omega_r), \quad (12-18)$$

where $\Delta\omega$ is the increment of angular frequency.

Taking (12-17) into account and performing the differentiation indicated in (12-18), we obtain:

$$\begin{aligned} X_{in}(\omega) &\approx \Delta\omega \left| \frac{dX_{in}(\omega)}{d\omega} \right|_{\omega=\omega_r} = \\ &= i\Delta\omega \left[L + \frac{1}{\omega_r^2 C_{shrtn}} + \frac{W_v}{C} \frac{l_v + b}{\sin^2 k_r(l_v + b)} \right]. \end{aligned}$$

But according to (12-17)

$$\frac{1}{\omega_r^2 C_{shrtn}} = L - \frac{W_v}{\omega_r} \cot k_r(l_v + b).$$

So that we obtain

$$X_{in}(\omega) \approx i2\Delta\omega \times \left[L + \frac{W_v}{4\omega_r} \frac{2k_r(l_v + b) - \sin 2k_r(l_v + b)}{\sin^2 k_r(l_v + b)} \right].$$

Designating the second item of this expression by L_e , sometimes called the antenna effective inductance, the antenna input impedance on frequencies close to the resonant one, is written as:

$$Z_{in} \approx R_{in} + i2\Delta\omega(L + L_e). \quad (12-19)$$

Thus, the reactive part of the antenna input impedance is proportional to the frequency increment. The active part of the input resistance can be regarded as constant within the pass-band. We know that the antenna pass-band is the band on the limit frequencies of which the current in the antenna decreases by $\sqrt{2}$ in comparison with the current at resonance. It can be shown that the frequency increment ($\Delta\omega$) for which such a decrease of current occurs, is defined by assuming that in the expression (12-19), the active

and reactive parts of the input resistance are equal. The pass-band can then be found from the equality $R_{in} = 2\Delta\omega_{max}(L + L_e)$ which yields the expression

$$\frac{2\Delta\omega_{max}}{\omega_r} = \frac{R_{in}}{\omega_r(L + L_e)}. \quad (12-20)$$

This is the expression generally used for calculating shortened antennas. However, the pass-band is often simply defined from the curves of the antenna input impedance plotted as a function of the frequency.

12-3. U-Antennas and Antennas with Multiple Downleads

Apart from the T- and L-antennas described above, U-antennas and antennas with multiple downleads are also used in the long-wave range.

The circuit of a U-antenna is shown in Fig. 12-6. The energy from the transmitter is fed to one of the downleads, a reactance being connected to the second downlead in order to obtain a co-phasal distribution of the current in the downleads of the antenna shown in Fig. 12-6.

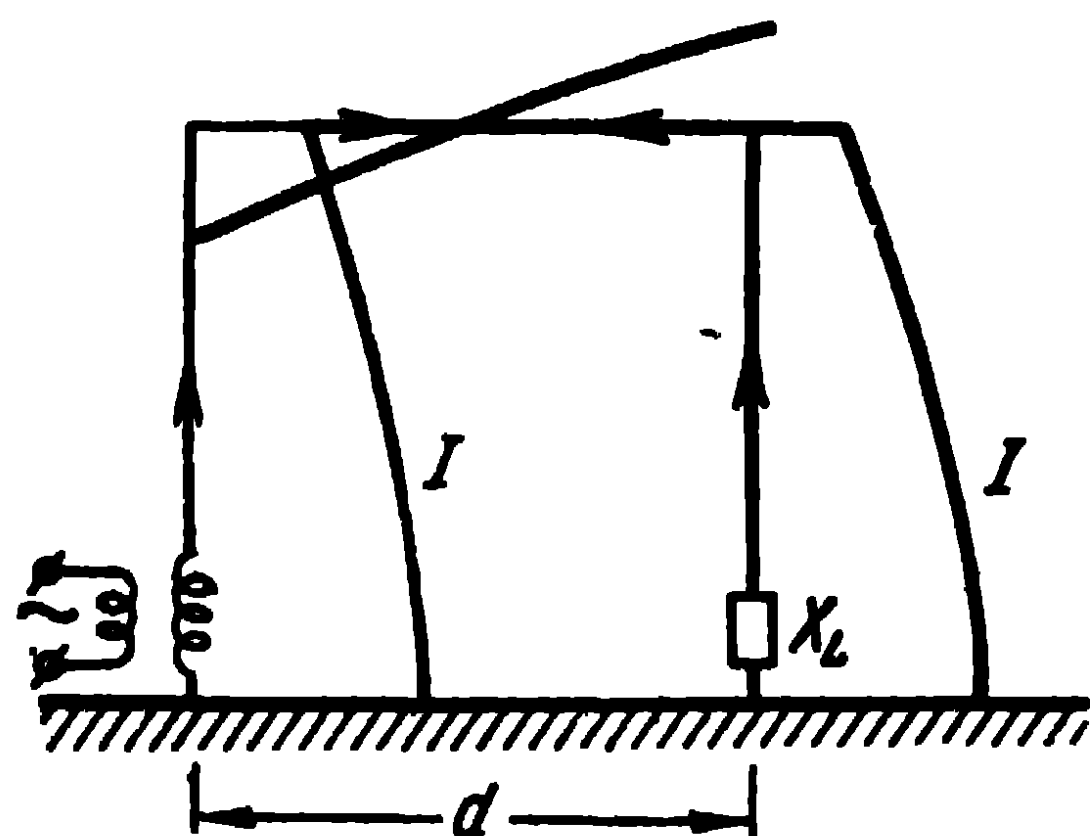


Fig. 12-6. U-antenna.

A U-antenna in actual fact is two L-antennas, so both are calculated by the same methods. However, due to the reciprocal influence of the downleads, the radiation resistance of the antenna downlead increases. It can be expressed as:

$$R_{\Sigma} = R_{\Sigma 0} + R_{\Sigma 1},$$

where $R_{\Sigma 1}$ is the induced resistance, defined from the expression

$$R_{\Sigma 1} = \frac{3}{2} R_{\Sigma 0} \left[\frac{\cos kd}{k^2 d^3} - \frac{(1 - k^2 d^2) \sin kd}{k^2 d^3} \right], \quad (12-21)$$

where $R_{\Sigma 0}$ is the radiation resistance defined from the expression (12-9);

d , the distance between the downleads of the antenna.

The expression (12-21) is obtained by the induced emf method. The field of one of the downleads in the vicinity

of the other one is defined by replacing the downleads by dipoles of corresponding effective heights.

As a result of the increase of the radiation resistance of the antenna in comparison with an L-antenna, its efficiency and pass-band are higher. In addition, we get a certain directivity in the horizontal plane, expressed as:

$$E = 2E_{01} \cos \left(\frac{kd}{2} \cos \varphi \right),$$

where E_{01} is the field intensity set up by one downlead; φ , the angle between the plane of the antenna and the direction towards the reference point.

An antenna with multiple downleads, proposed by Alexandersen is shown in Fig. 12-7.

The energy from the transmitter is fed to the middle downlead of the antenna. Reactances are connected to two other downleads, their magnitudes being chosen in such a way as to obtain a co-phasal oscillation of the currents in all the downleads. The current distribution in the tuned antenna is shown in Fig. 12-7. The antenna can be regarded as consisting of three T-antennas, so that its calculation is reduced to the calculation of a T-antenna. The only difference is the calculation of the radiation resistance of the downlead, which can be defined from the expression

$$R_{\Sigma} = R_{\Sigma 0} + 2R_{\Sigma 1},$$

where $R_{\Sigma 1}$ is the radiation resistance induced by the neighbouring downlead, defined from the expression (12-21).

To calculate the resistance induced in the extreme downleads, d in the expression (12-21) should be replaced by $2d$. The radiation impedance of the antenna related to the current in the downlead to which the energy is fed, is the sum of all the natural and induced resistances, because the currents in all the downleads are co-phasal. This concerns also U-antennas.

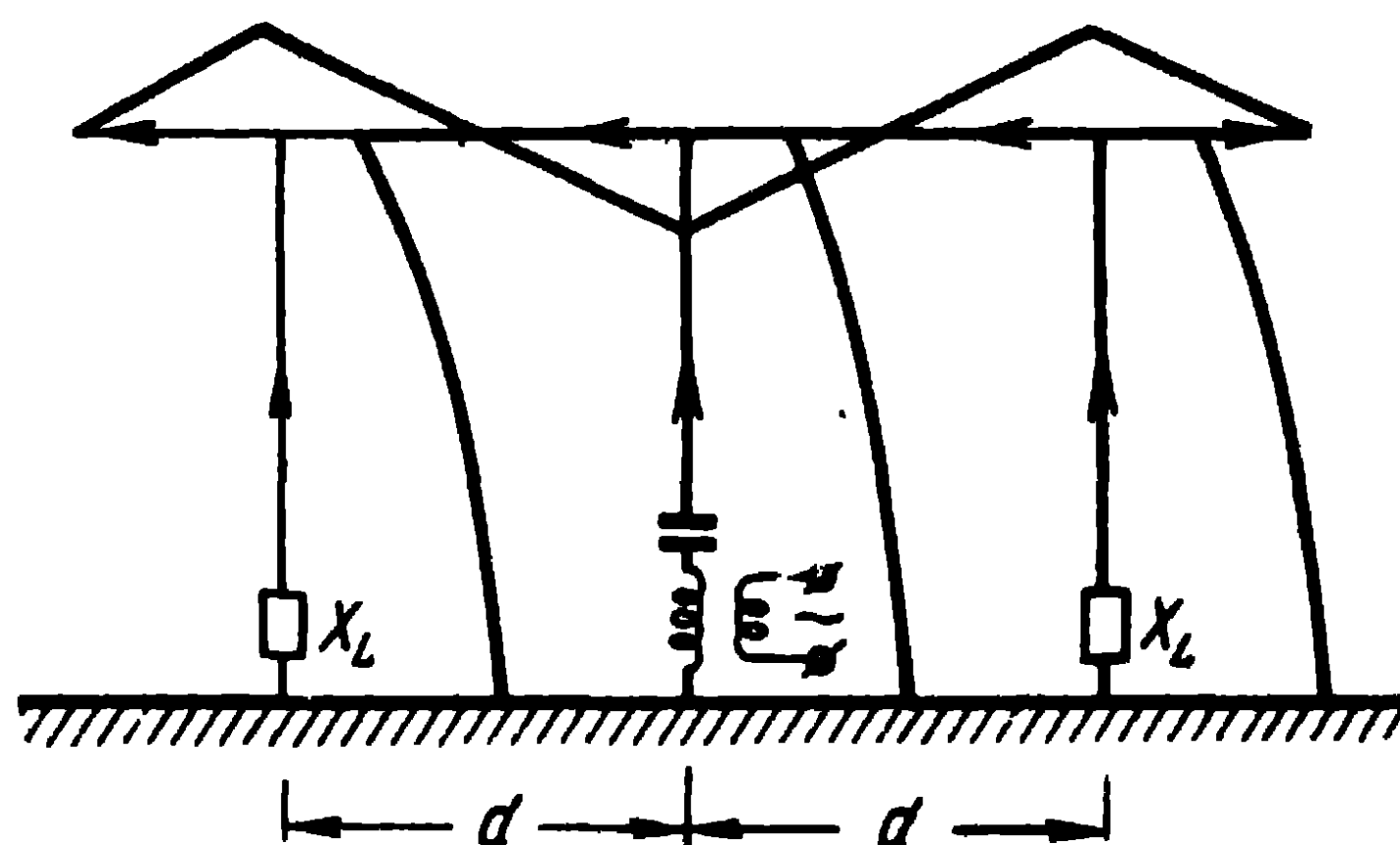


Fig. 12-7. Antenna with multiple downleads.

The directional diagram in the horizontal plane of an antenna with two downleads is expressed as:

$$E = E_{01} [1 + 2 \cos (kd \cos \varphi)].$$

Just as in the case of U-antennas, the efficiency and pass-band of the antenna are higher than in the case of a T-antenna.

The antenna is coupled directly to the transmitter by introducing one of the downleads into the transmitter building, but the antenna can also be fed by means of a feeder.

12-4. Mast Antennas

The disadvantages of T- and L-antennas and other antennas of this type are: a) the need for two or more masts and b) the distortion of the directional diagrams caused by the influence of the supporting cables.

Consequently, mast antennas are used on medium waves (especially in the 300 to 800 m range). Fig. 12-8 shows three

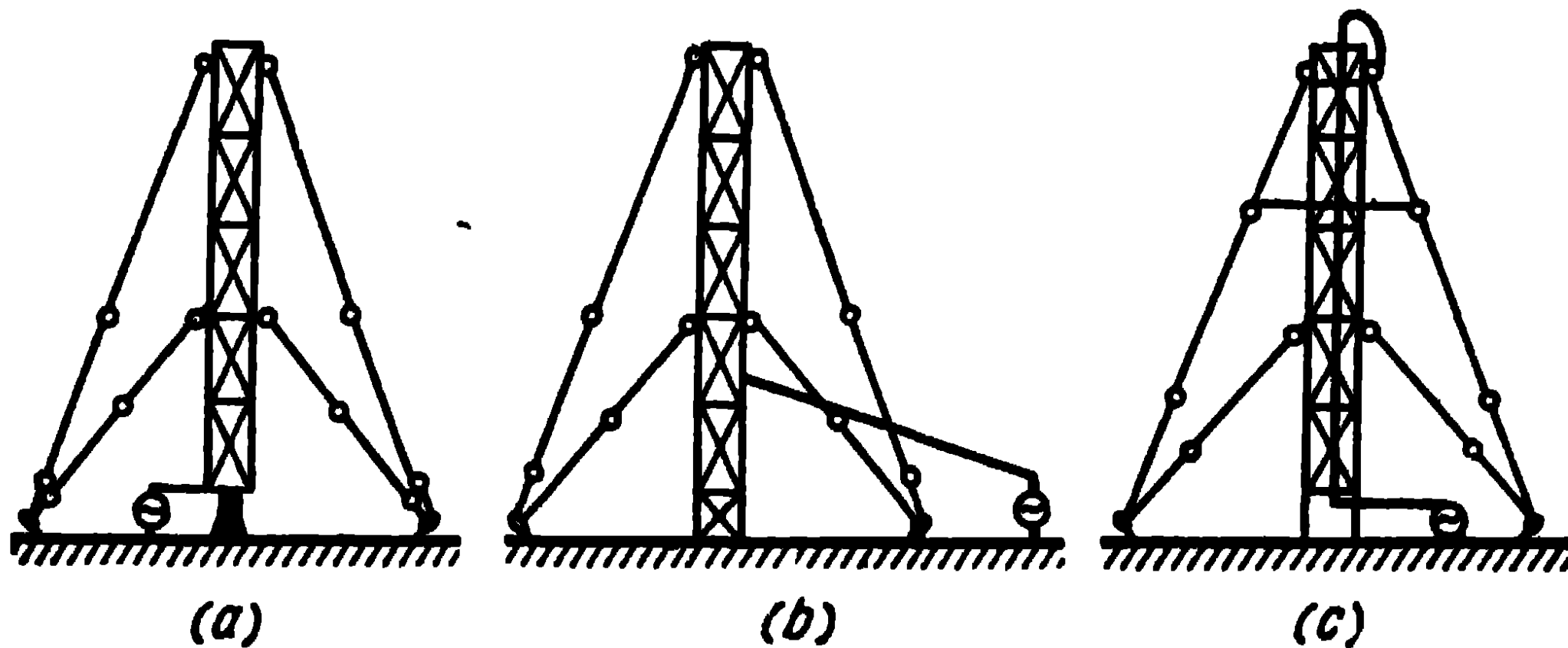


Fig. 12-8. Mast antennas:

a—mast on an insulator; *b*—shunt-fed mast; *c*—mast fed from the top.

methods of excitation of the masts: at the base of the mast, which requires a supporting insulator, by means of a shunt, and by feeding the antenna from the top.

From the electrical point of view, a mast antenna on an insulator (Fig. 12-8, *a*) represents a base-fed vertical rod. It is calculated like an asymmetrical dipole without a load at the upper end. The current and voltage distribution in the antenna are calculated from the expressions

$$I_z = I_0 \frac{\sin k(l-z)}{\sin kl}, \quad U_z = U_0 \frac{\cos k(l-z)}{\cos kl},$$

where l is the length of the dipole (Fig. 12-9).

The current and voltage at the antenna base are defined from the expressions

$$I_0 = \sqrt{\frac{2P_A}{R_{\Sigma 0} + R_{\text{losses}}}}, \quad U_0 = I_0 \sqrt{(R_{\Sigma 0} + R_{\text{losses}})^2 + X_{\text{in}}^2}.$$

The input resistance of the antenna placed on an insulator can be calculated from the expressions

$$R_{\text{in}} = W_A \frac{\text{sh } 2\beta l - \frac{\beta l}{kl} \sin 2kl}{\text{ch } 2\beta l - \cos 2kl};$$

$$X_{\text{in}} = -W_A \frac{\sin 2kl + \frac{\beta l}{kl} \text{sh } 2\beta l}{\text{ch } 2\beta l - \cos 2kl}.$$

In these expressions, the attenuation is defined from the expressions

$$\beta l = \frac{R_1 l}{W_A}, \quad R_1 l = \frac{R_{\Sigma a}}{1 - \frac{\sin 2kl}{2kl}}$$

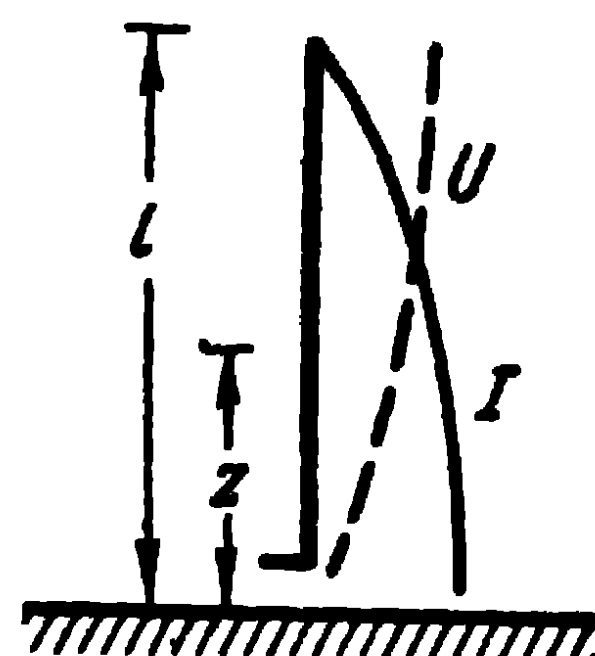


Fig. 12-9. Current and voltage distribution in an asymmetrical dipole.

and the wave impedance of the antenna, from the expression

$$W_A = 60 \left(\ln \frac{2l}{r} - 1 \right),$$

where r is the mean radius of the mast cross section.

For antennas that are short relatively to the wave-length ($\frac{l}{\lambda} < 0.2$), simpler expressions can be used:

$$R_{\text{in}} = \frac{R_{\Sigma a}}{\sin^2 kl}, \quad X_{\text{in}} = -W_A \cot kl.$$

The values of the radiation resistances of mast antennas are given in Table 12-1.

Table 12-1

l/λ	0.125	0.150	0.20	0.25	0.30	0.35	0.40	0.45	0.50	0.55	0.60	0.65	0.675
$R_{\Sigma a}$ ohms	3.2	6.5	18	36.5	60	84	100	106	99.5	83	63.5	46.5	42

For short antennas, the radiation resistance related to the current at the base can be calculated from the expressions (12-9) and (12-10) for $b = 0$.

Table 12-2

Symbols	Parameters	Mast $W_A = 200$ ohms		Fine wire $W_A = 500$ ohms	
kl	Electric length of antenna	180°	45°	180°	45°
$R_{\Sigma a}$	Radiation resistances	99.5 ohms	3.2 ohms	99.5 ohms	3.2 ohms
βl	Attenuation	0.497	0.044	0.199	0.0176
R_{in}	Input resistance	435 ohms	6.5 ohms	2,045 ohms	6.5 ohms
X_{in}	Input reactance	0	200 ohms	0	500 ohms
$\sqrt{R_{in}^2 + X_{in}^2}$	Input impedance	435 ohms	200 ohms	2,045 ohms	500 ohms
I_0	Current at base	15.2 A	124 A	7 A	124 A
U_0	Voltage at base	6,600 V	24,800 V	14,300 V	62,000 V
U_a	Voltage at the antenna end	5,850 V	35,000 V	14,000 V	88,000 V

The earthing system of mast antennas usually consists of 60 to 120 radial earthed wires 0.3λ long. In the case of an adequate earthing system, the resistance of the losses of mast antennas of this kind related to the current antinode usually amounts to approximately 5 to 10 ohms and the antenna efficiency is about 80 to 90%. From the electrical point of view, mast antennas have a definite advantage over thin dipoles. Let us investigate the type of operation of two antennas: a mast antenna ($W_A = 200$ ohms) and a wire antenna ($W_A = 500$ ohms) without a load at the upper end, operating in a range from $\frac{l}{\lambda} = 0.125$ to $\frac{l}{\lambda} = 0.5$. Let the power fed to the antenna equal 100 kW and the efficiency, for simplicity, equal 100%.

The calculated data are given in Table 12-2.

It can be seen from Table 12-2 that the voltage of mast antennas at the lower as well as the upper ends is considerably low than that of wire antennas. This simplifies the operating conditions of the insulators and enables to accommodate a larger power into mast antennas than into wire antennas for the same breakdown voltages.

Due to the difficulty of installing and maintaining masts placed on insulators, shunt-fed earthed mast antennas are preferred (see Fig. 12-8, *b*). The feed line is usually connected to the mast at a height equal to $\frac{1}{8}$ to $\frac{1}{10}$ of the height of the mast. The lower and upper parts of the antenna are connected in parallel relatively to the feed line and, if the antenna is short in comparison with the wave-length, the lower part of the antenna represents an inductance and the current on it has a cosinal distribution with the antinode at the earthed end, whereas the upper part represents a capacitance and the current on it has a sinal distribution (Fig. 12-10). At the connection point of the feeder, the antenna current has a finite discontinuity and the directions of the current in the upper and lower parts of the antenna coincide. The equivalent circuit of the antenna is shown in the same Fig. 12-10.

Fig. 12-8, *c* represents the mast antenna designed by G. Eisenberg. The circuit of this antenna showing the direction of the conduction and displacement currents is given in Fig. 12-11, *a*. The antenna is fed at its upper end by means of a coaxial line (formed by a vertical wire inside the body of the mast).

The antenna equivalent circuit is shown in Fig. 12-11. *b*. Since the antenna is fed from the top, a current antinode is always formed at the earthed end of the mast antenna.

The advantages of such a mast antenna consist 1) in a more uniform distribution of its current as compared with a mast antenna on an insulator, the current distribution being all the more uniform as the electric length of the antenna is

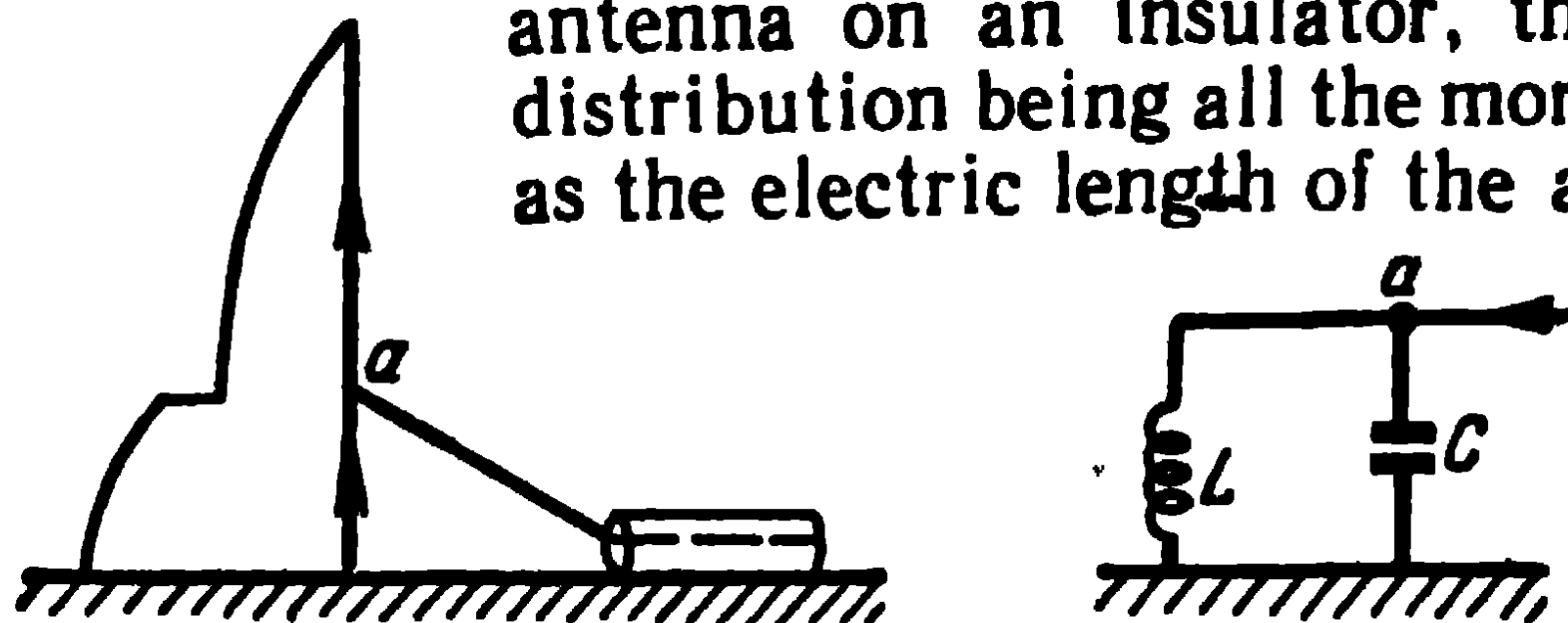


Fig. 12-10. Current distribution in a shunt-fed antenna and its equivalent circuit.

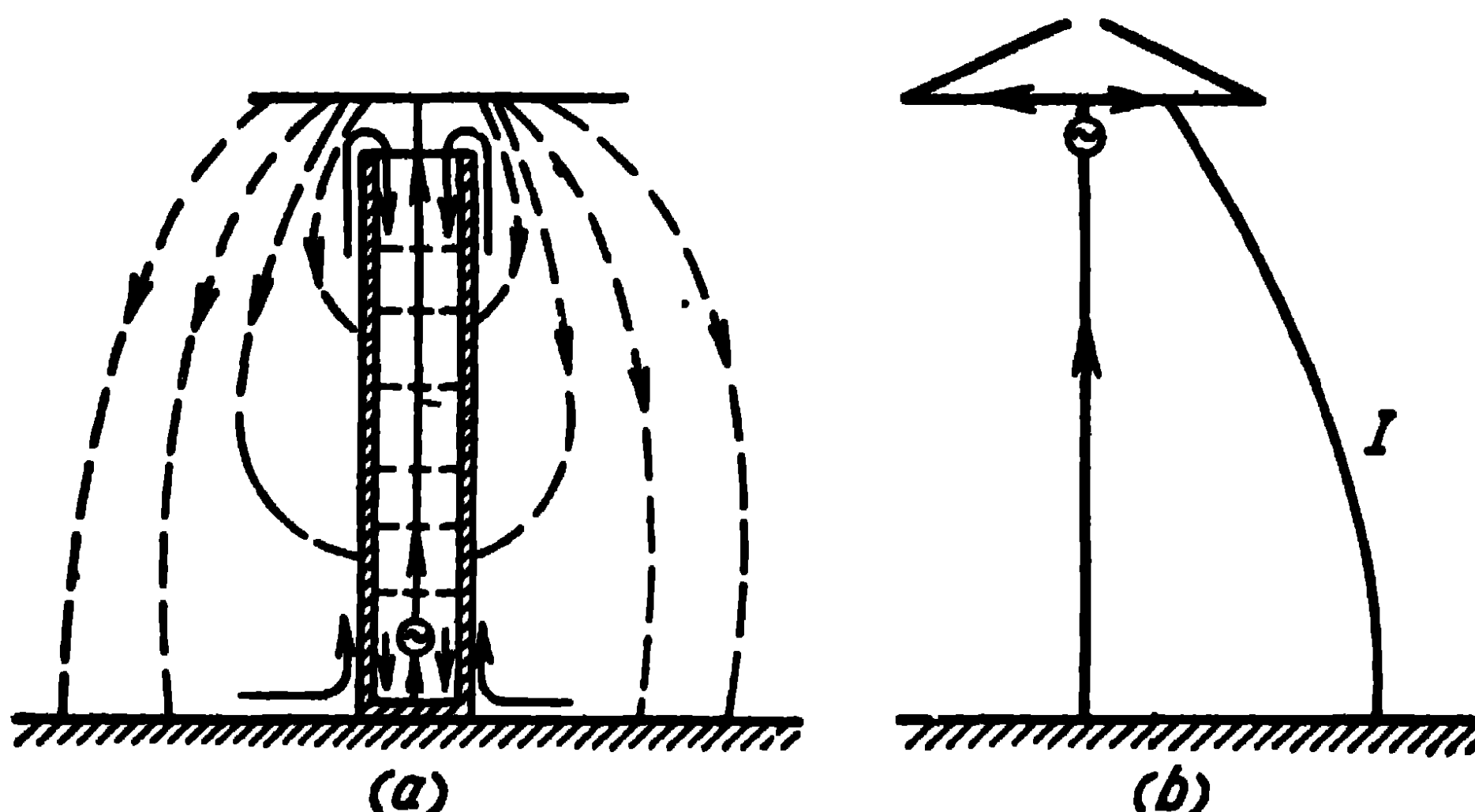


Fig. 12-11. Mast antenna fed from the top:
a—antenna circuit, b equivalent circuit

shorter, and 2) in the absence of a supporting insulator. Consequently, mast antennas fed from the top have a higher radiation resistance and, as shown by calculations and experiments, a higher efficiency.

Part of the upper row of guys is utilised as a capacitive load at the upper end of the mast, as shown in Fig. 12-8, *c*. The feed wire runs inside the mast in a special container or without it and is fixed by means of supporting or stick insulators.

Now let us consider the utilisation of mast antennas as anti-fading broadcasting antennas. At night, medium waves,

especially in the 200 to 600 m range, are propagated in two ways: along the surface of the earth, as in day-time, and by being reflected from the upper, ionised layers of the atmosphere. Being superposed on one another, the surface wave and the wave reflected from the ionosphere interfere and cause a distortion and deterioration of the signals.

There are three zones of audibility in the night-time. In the first zone, which is in the vicinity of the transmitter, the field intensity of the reflected wave is much smaller than the field intensity of the surface wave. In the second zone, which is at a somewhat greater distance (80 to 160 km), the signal of the surface wave gradually weakens and the signal of the reflected wave grows more powerful, the two signals having the same value at a certain distance. In the third zone, which is still further out, the signal of the reflected wave grows still more powerful and remains constant up to rather large distances; as for the signal of the surface wave, it is so weak that the interference between these two signals is practically non-existent.

To move away the second zone, known as the zone of near fading, the use of so-called anti-fading antennas is necessary. Consequently the zone of reliable reception can be widened only through the use of antennas of an appropriate design. The directional diagram of the antenna should be such that the maximum energy be radiated along the surface of the earth and no radiation occur at high angles (45 to 55°) to the horizon. It is not found possible, in practice, to get rid of the reflected wave, but one can appreciably weaken it and amplify the surface wave.

The maximum value of the field of the surface wave is obtained when the antenna has a height $l=0.64\lambda$ ($kl=230^\circ$). However, at that height, there occurs a considerable radiation at high angles to the horizon and, as a result, the reflected wave has a considerable field at angles of 45 to 55°. An antenna of length $l=0.53\lambda$ ($kl=190^\circ$) gives a considerably smaller field intensity at these angles, although, in that case, the field intensity of the ground (surface) wave decreases by approximately 10%.

Thus, the best anti-fading antenna has a height $l=0.53\lambda$. The desirable directional diagram can also be obtained in the case of antennas with a load at the top. In that case, the optimum results are obtained when the equivalent length of the antenna equals approximately 190° . This is

particularly valuable in the case of anti-fading antennas operating on long waves. Moreover, the desirable directional diagrams can be obtained with sectionalised antennas, i.e., antennas into which inductance coils are inserted (at points higher than the middle). The equivalent length of such antennas should also be approximately 190° .

It should be pointed out that antennas of a high wave impedance have satisfactory directional diagrams because, in that case, the current in the node is close to zero and the directional diagram at the desirable angles to the horizon (45° to 55°) has deep minimums.

The current distribution in anti-fading antennas has the aspect shown in Fig. 12-12. In all the three above-examined cases (antennas without a load at the top, with a load at the top, and sectionalised antennas) the current node occurs at the lower end of the antenna. Such a current distribution corresponds to a small radiation of the antenna in a 45 to 55° direction of the angles and, in the second zone, raises the ratio of the strength of the signal of the surface wave to that of the signal of the reflected wave.

Fig. 12-13 shows the curves of the field intensity of the surface and reflected waves depending on the distance on a wave $\lambda = 300$ m, set up by a short mast antenna and a mast antenna of length $l = 0.53\lambda$. It can be seen that the use of an anti-fading antenna moves away the zone of 100% fading by approximately two times.

Because they cannot be installed at a distance smaller than the height of the mast from the radio station building, mast antennas are fed by means of a coaxial cable. Moreover, an antenna hut is erected in the vicinity of the mast; it houses the circuits for tuning the antenna in resonance and coupling it with the cable. The coupling of the antenna with the cable is chosen in such a way that a travelling wave should be set up in the latter.

The tuning circuits of mast antennas and their coupling with the cable are shown in Fig. 12-14. It represents the circuits with an inductive, a conductive and a capacitive coupling. Let us investigate in detail the circuit with a capacitive coupling. The antenna should be tuned in resonance so that the condition

$$X_{in} + X_t + X_c = 0$$

should be observed.

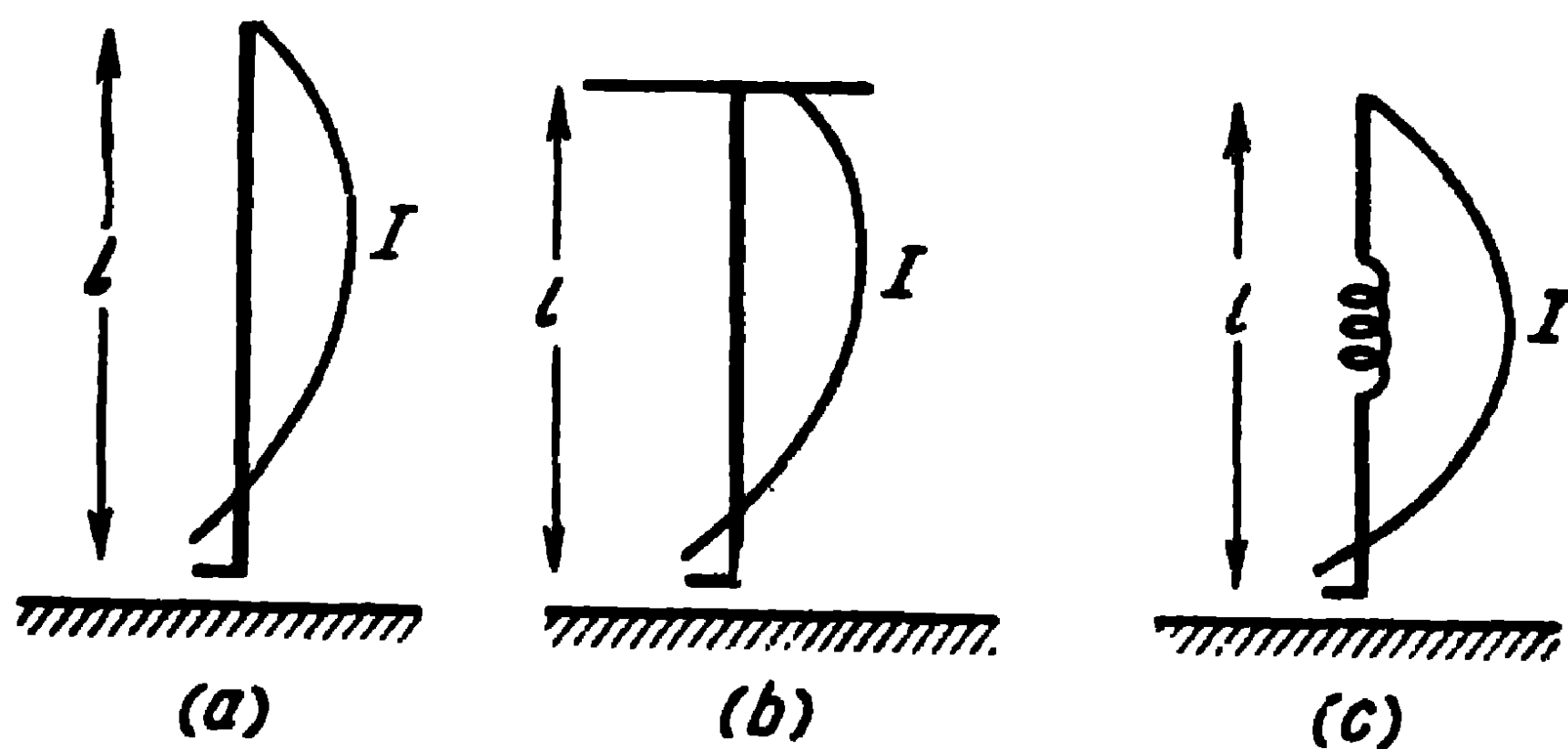


Fig. 12-12. Current distribution in anti-fading antennas:

$$a - kl = 190^\circ; \quad b - k(l+b) = 190^\circ; \quad c - kl_e = 190^\circ$$

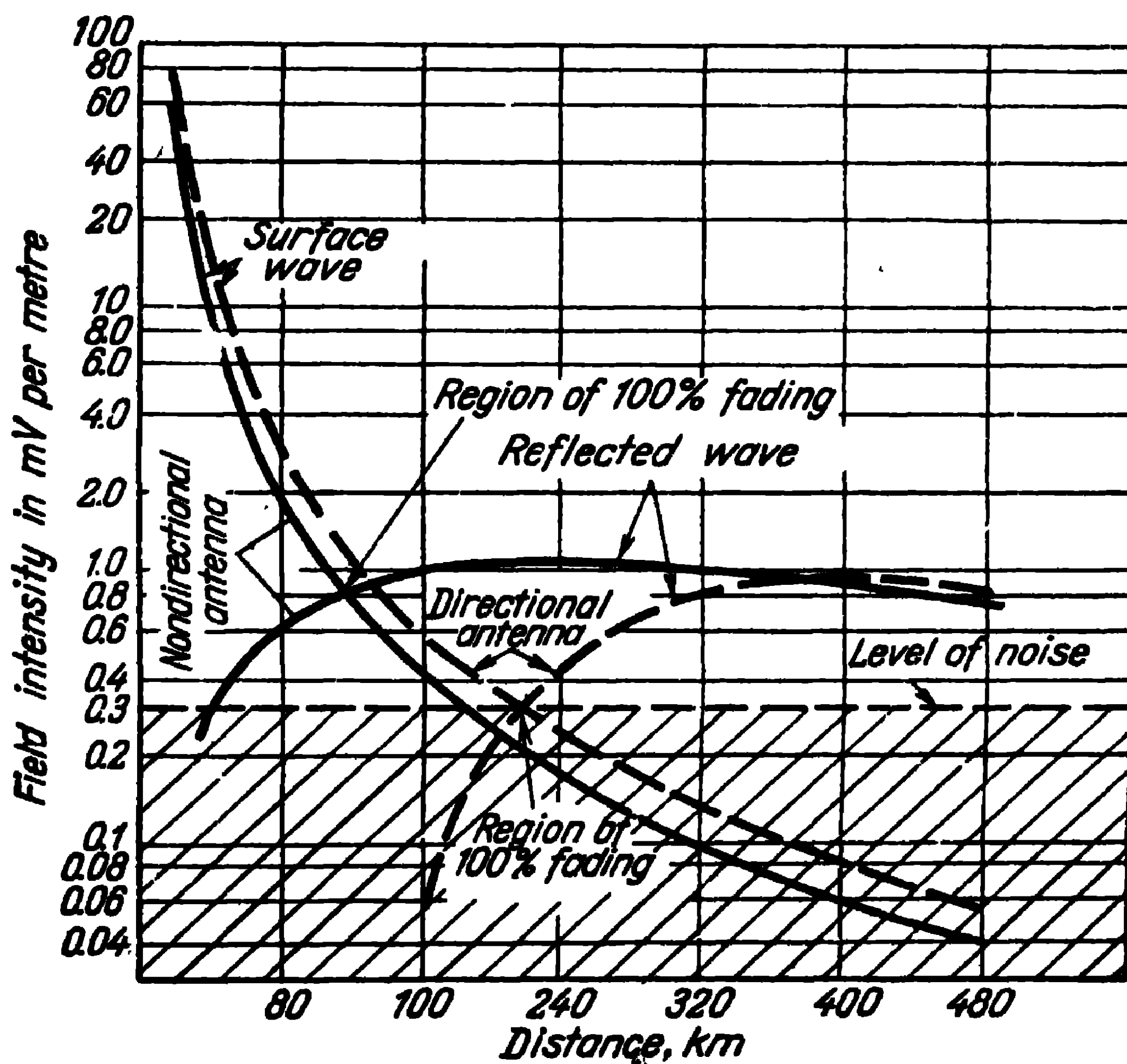


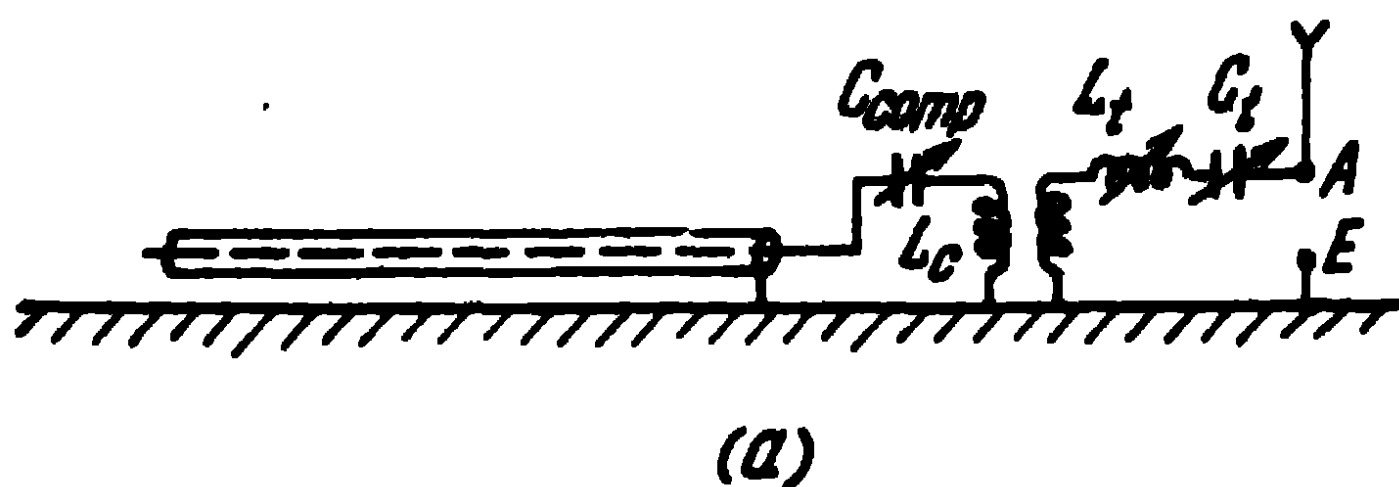
Fig. 12-13. Intensity of the field set up by an anti-fading antenna. The power of the transmitter is 50 kW, the conductivity of the soil $\sigma = 5 \cdot 10^{-3}$ ohms/m, directional antenna $l = 0.53\lambda$ (the mast is earthed); non-directional antenna: short earthed mast.

Under this condition, the resistance inserted into the circuit of the feeder equals:

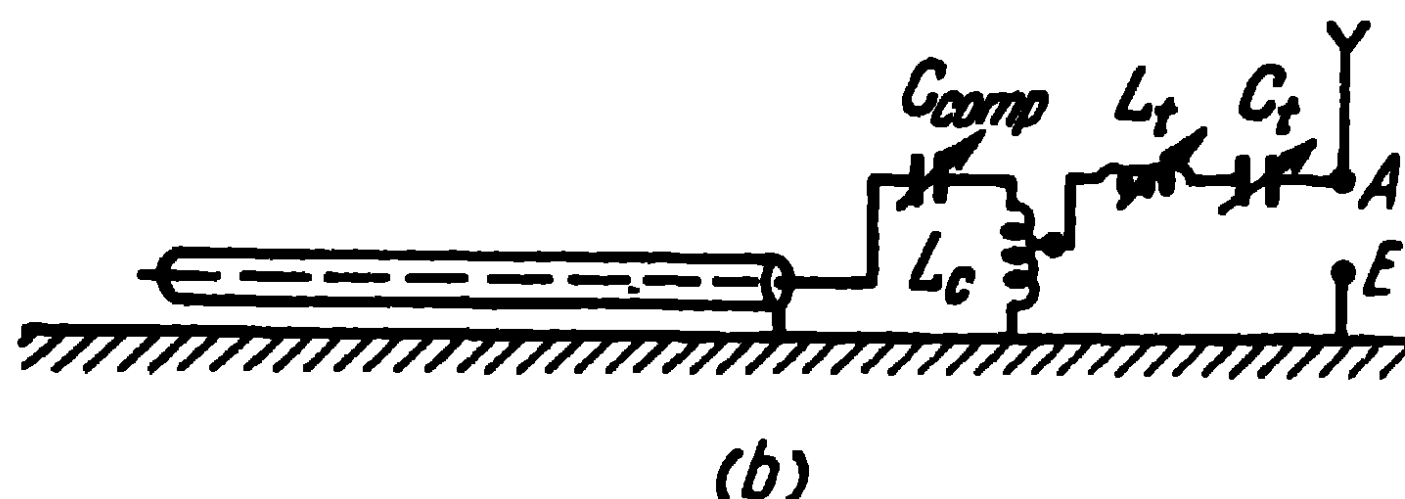
$$R_{\text{ins}} = \frac{X_c^2}{R_{\text{in}}}.$$

The feeder is then loaded on that resistance plus the resistance of the coupling capacitor. To back off the latter, an

inductive resistance is inserted in parallel into the feeder; it is defined from the condition

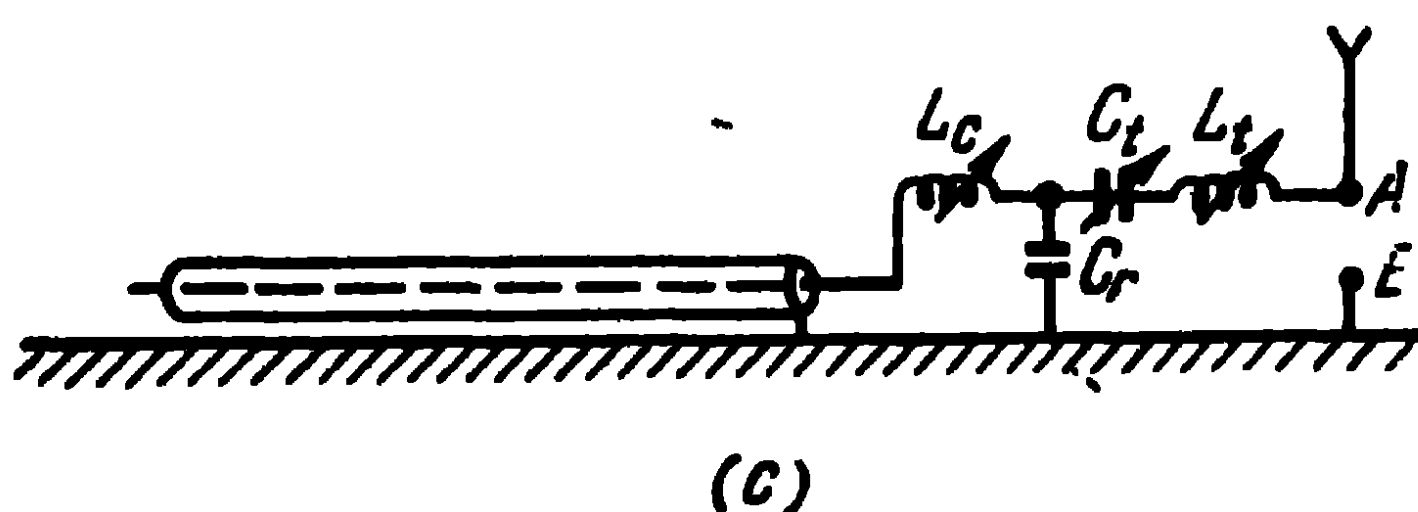


$$X_{\text{comp}} + X_c = 0.$$



To obtain a travelling wave in the feeder, one has to satisfy the condition

$$R_{\text{ins}} = W_f.$$



The resistance of the coupling capacitor is defined from the above-cited expressions

$$X_c = \sqrt{W_f R_c} \quad (12-22)$$

Fig. 12-14. Tuning circuits of mast antennas:

a—circuit with an inductive coupling; b—circuit with a conductive coupling; c—circuit with a capacitive coupling

as well as the tuning resistance of the antenna X_t and the compensation resistance X_{comp} .

In the case of a transmitter of low power, the feeder is not tuned on a travelling wave. In that case, the antenna is connected to the feeder directly, without transition devices and the tuning of the antenna-feeder system is effected in the building of the transmitter.

12-5. Slot Antennas on Low Supports

Mast antennas and tower antennas, which are widely used in the medium-wave range, have a height of the order of 100 to 250 m. However, the use of high masts and towers is

undesirable for a number of reasons. The main ones are: the high cost of the antennas and the considerable technical difficulties attending their design (for example, the problems concerning the insulation of the base and guys of the mast are quite complicated).

The replacement of high mast antennas (of the order of $0.16 \div 0.2\lambda$, not lower) by low ones, results in a lowering of the antenna efficiency, due to an increase of the losses into

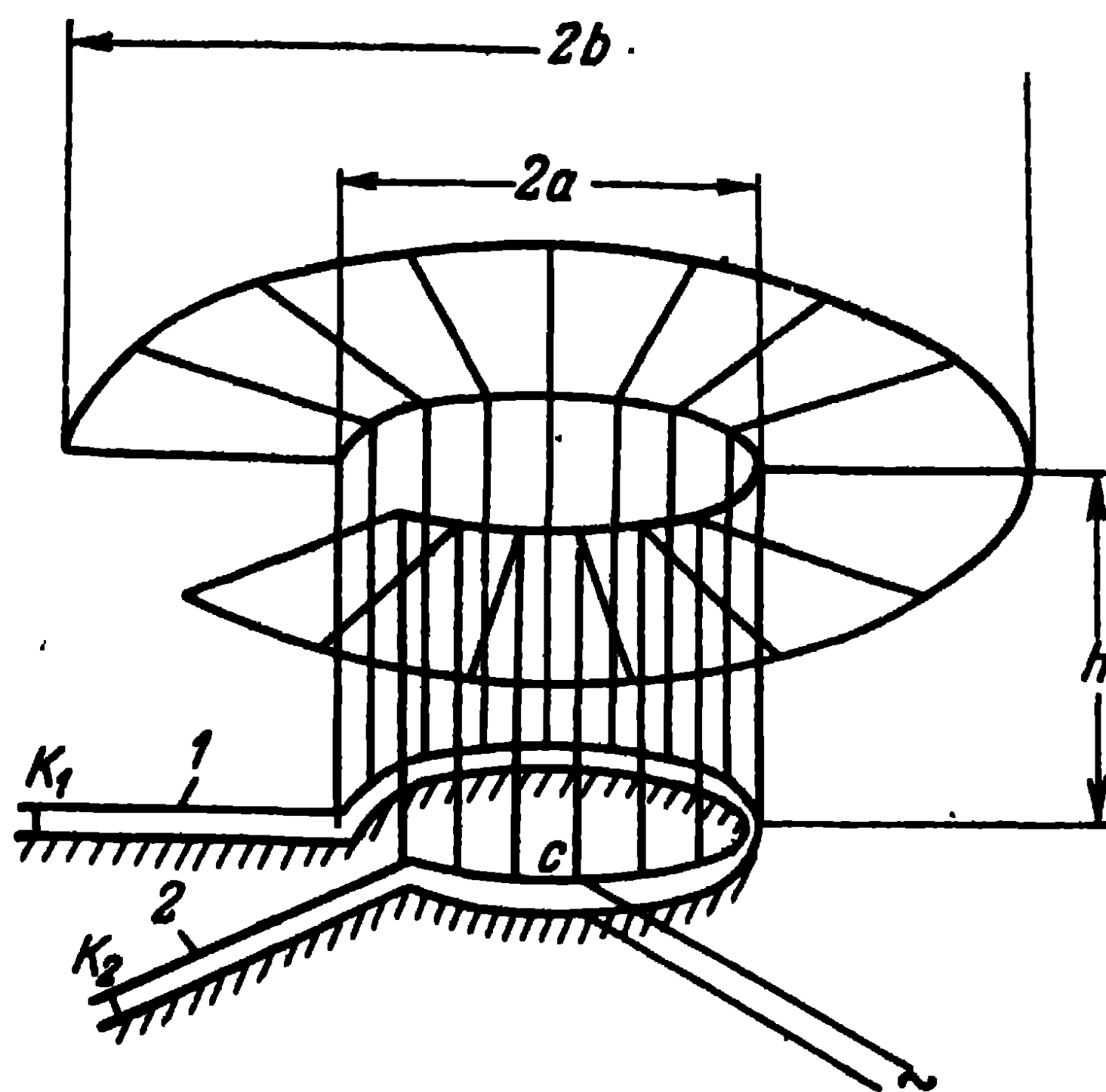


Fig. 12-15. Slot antenna on low supports.

the earth caused by high current densities occurring in the vicinity of the antenna base.

In this connection, a medium-wave antenna on low supports of adequate efficiency has been devised in the Soviet Union [74].

The principle of the antenna is similar to that of the cylindrical dipole excited by a transverse slot used on centimetre and decimetre waves. However, the dipole has been considerably modified in order to make it suitable for operation on medium waves.

The antenna consists of a cylindrical wire net fed by a ring wire feeder (distributive feeder) (Fig. 12-15). Vertical wires forming a cylinder are connected to one of the wires of the ring feeder, the other wire being earthed. If we supplement this device by its mirror image, the distributive feeder becomes a ring slot exciting a cylindrical dipole.

As in the case of a usual wire antenna, the vertical part of the dipole is supplemented by a horizontal part consisting of a number of radial wires of radius b . This widens the pass-band of the antenna and, by reducing the current density in the earth in the vicinity of the dipole, reduces the losses.

The feeder from the transmitter is connected to the points cd of the distributive (ring) feeder, which are chosen so as to ensure matching of the antenna to the feeder. To tune the antenna in resonance, i.e., in order that the reactive component of the input resistance should be zero at the point cd , the short-circuited stubs 1 and 2 are used, the length of which is regulated by means of the short circuiters K_1 and K_2 .

Such a construction enables to decrease the density of the currents arising in the earth close to the antenna, because, instead of gathering at one point at the base of the antenna as in the case of ordinary antennas, the currents flow over the whole periphery of the slot. Owing to the decrease of the current density in the earth, the antenna efficiency for quite a small height of the vertical part and simple earthing (120 radial wires) is of the same order as that of high mast antennas. The efficiency is further improved through the use of tuning elements, of segments of long lines instead of the lumped inductances and capacitances generally used.

The antenna, which is destined for operation on 200 to 600 m, has the following geometrical dimensions:

- height of the vertical part $h=22$ m;
- radius of the cylinder $a=24$ m;
- radius of the horizontal part $b=67.5$ m;
- length of the tuning stubs $l=30$ m.

12-6. Wave Antennas .

The wave antenna designed by Beveridge is utilised for the reception of signals from long-wave radio stations. It consists of a wire half a wave to several wave-lengths long, directed towards the transmitter and suspended at a height of up to 8 m above the earth. The end of the wire towards the transmitter is earthed through a resistance equal to the wave impedance of the antenna. The other end of the wire is connected to the receiver, the wave impedance of which is also equal to the wave impedance of the antenna (Fig. 12-16).

The antenna responds to the horizontal component of the intensity of the electric field caused by the finite conductivity of the soil. As shown in Fig. 12-16, the front of the wave propagated along the surface of the earth is inclined towards the direction of motion of the wave. When the wave comes from the direction of the absorbing resistance to the receiver, the horizontal component of the electric field intensity vector is directed along the axis of the wire. When the wave comes from other directions, it is the projection of the horizontal component of the electric field intensity vector that acts along the axis of the wire. The projection is equal to the product of the horizontal component of the

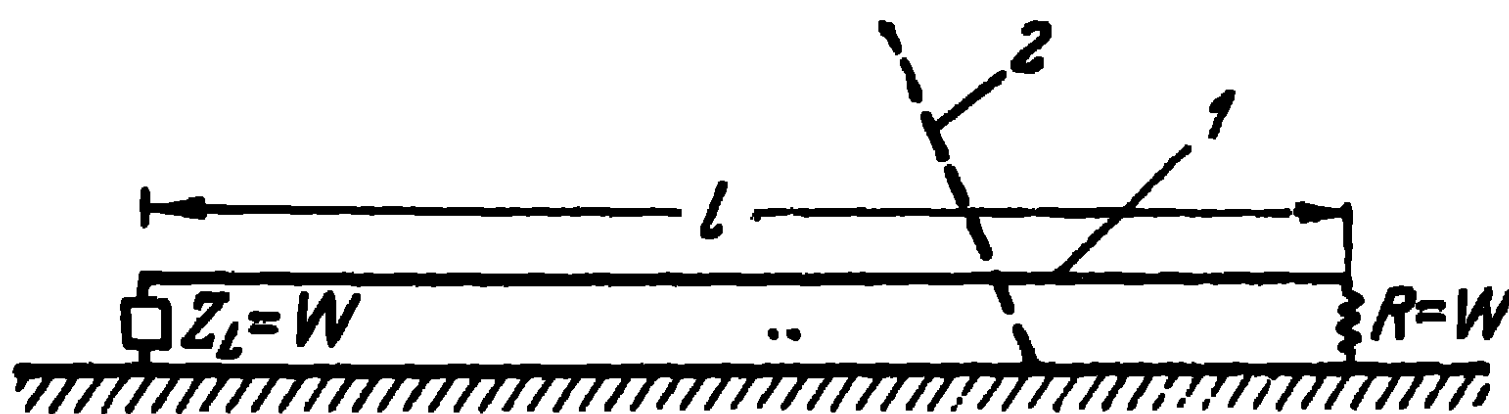


Fig. 12-16. Wave antenna:
1—antenna; 2—wave front.

electric field intensity vector by the cosine of the angle between the antenna and the direction towards the transmitter.

As in the case of short-wave travelling-wave antennas, the current in the receiver is at its maximum when the direction of motion of the wave coincides with the direction from the absorbing resistance to the receiver along the wire axis. If the phase velocity of propagation of the current wave along the wire were equal to the velocity of the incident electromagnetic wave, the current would be all the higher as the wire is longer. However, due to the fact that the reverse conductor for the current is the earth, the conductivity and permittivity of which differ from those of air, the phase velocity of propagation of the current wave along the wire is inferior to the velocity of propagation of the incident electromagnetic wave. For this reason, the current maximum in the receiver occurs at a certain definite ratio of l/λ .

When the wave comes from the direction opposed to that of maximum response, the current maximum occurs in the absorbing resistance, the current in the receiver itself being at a minimum or even zero. This is due to the fact that the

elementary current waves, excited in the wire as a result of the action of the elementary emf's induced by the wave in the various regions of the wire, will cancel instead of reinforcing one another.

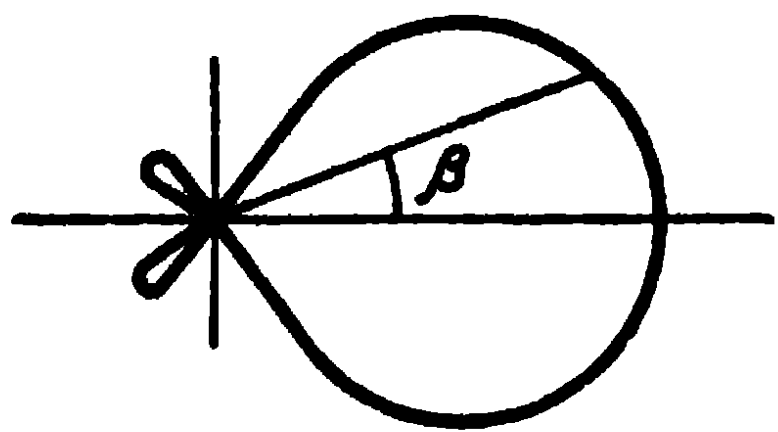


Fig. 12-17. Directional diagram of wave antenna.

Thus, the directional diagram of the antenna has the aspect shown in Fig. 12-17.

It is clear that the directional diagram of a wave antenna is characterised by the factor

$$F(\theta) = \frac{\cos \theta}{\xi - \cos \theta} \sin \left[\frac{kl}{2} (\xi - \cos \beta) \right],$$

where β is the angle between the axis of the wire and the direction of arrival of the wave;

l , the length of the antenna;

$\xi = \frac{v_1}{v}$, the ratio of the velocity of propagation of the electromagnetic wave to the velocity of propagation of the current wave.

The Beveridge antenna is made use of as a reception antenna to eliminate atmospheric interference on long waves, as well as interference from stations of neighbouring frequencies. As a rule, the antenna is not utilised for transmission on account of its low efficiency.

To explain the existence of important losses in the antenna as well as to illustrate the directivity of the antenna from

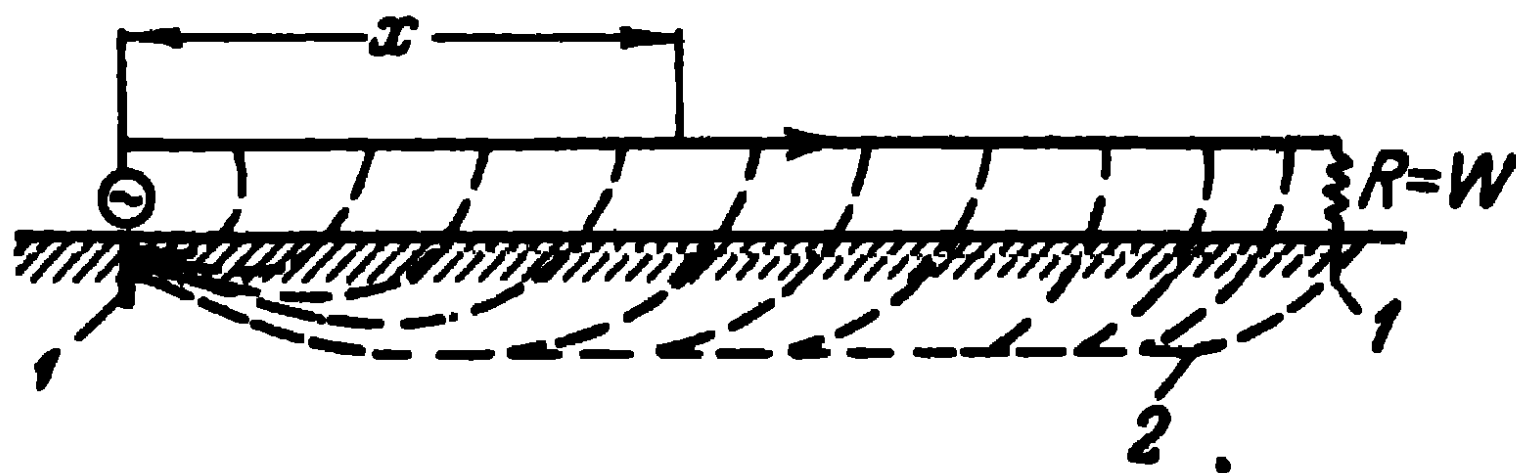


Fig. 12-18. Wave antenna used for transmission:

1—earthing; 2—currents in the earth

the point of view of transmission, let us examine the circuit of Fig. 12-18, similar to Fig. 12-16 but with a transmitter instead of a receiver. Due to the fact that the wire is loaded on a resistance equal to its wave impedance, there arises in it a current wave travelling towards the load. The displacement currents branching off from each element of the wire are transformed in the earth into conduction currents and

polarisation currents. Due to the finite conductivity of the earth, the currents penetrate down to a certain depth and have vertical as well as horizontal components. The horizontal component of the current in the earth, which is equal to the current in the antenna, gives no radiation of electromagnetic energy, because its radiation is cancelled by the radiation of the current antenna. The radiation component is the vertical component of the current in the earth. In the direction along the antenna axis, this current has approximately the same density, but its phase changes from point to point as $e^{-\xi kx}$, where $\xi = \frac{v_1}{v}$, kx is the distance in degrees from the transmitter to the point under consideration on the wire. It is clear that the maximum of radiation of this current is in

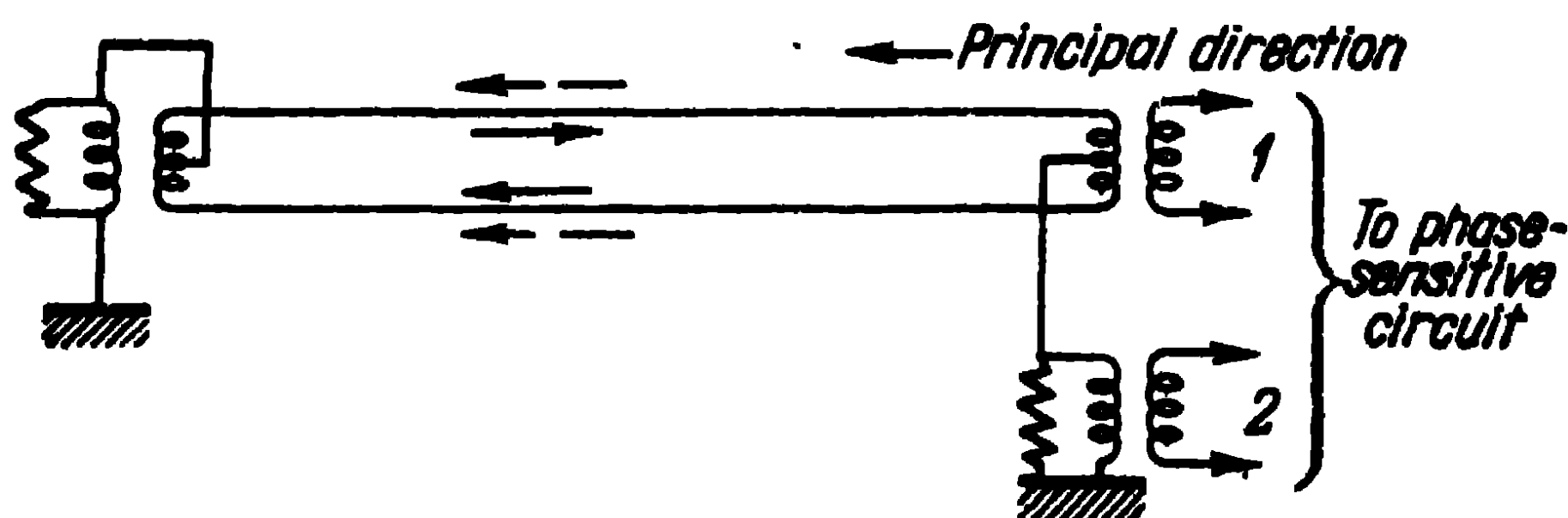


Fig. 12-19. Circuit of wave antenna with variable direction of zero reception.

the direction of the absorbing resistance along the antenna axis and the directional diagram has the shape already shown in Fig. 12-17.

As a result of the radiation as well as losses in the earth, the current wave is attenuated in the course of its travel to the far end of the antenna. Elementary calculations would show that the radiation resistance of the antenna forms an insignificant quantity of the overall resistance of the losses in the antenna, so that the efficiency of the antenna is low. The antenna is therefore not used for transmission.

In practice, it is found necessary to regulate the direction of the zero of reception, so that use is often made of the wave antenna circuit shown in Fig. 12-19. The antenna represents a horizontal twin line. The electromagnetic waves arriving from the main direction induce in both wires electric currents (dotted arrows) of equal magnitude, which escape into the earth through the primary of the transformer at the far end. Furthermore, these currents induce in the secondary of the transformer an emf under the influence of which,

antiphase currents (solid lines) arise in the wires. The emf induced by these currents in the winding 1 is fed to the phasing circuit. The wave of the current (co-phasal) moving towards the receiver is led into the earth and induces in the winding 2 an emf which is likewise fed to the phasing circuit. This emf has a phase shift relatively to the emf in the winding 1 and differs from it in amplitude.

Thus, by regulating the ratio of these two emf's in the phasing circuit, one can obtain a zero of the signal at the input of the receiver for a wave arriving from any undesirable direction and, in so doing, get rid of the interference.

12-7. Frame Antennas

A frame antenna in its simplest form is shown in Fig. 12-20. The frame constitutes a directive system with two zero reception directions. The dimensions of the frame relatively

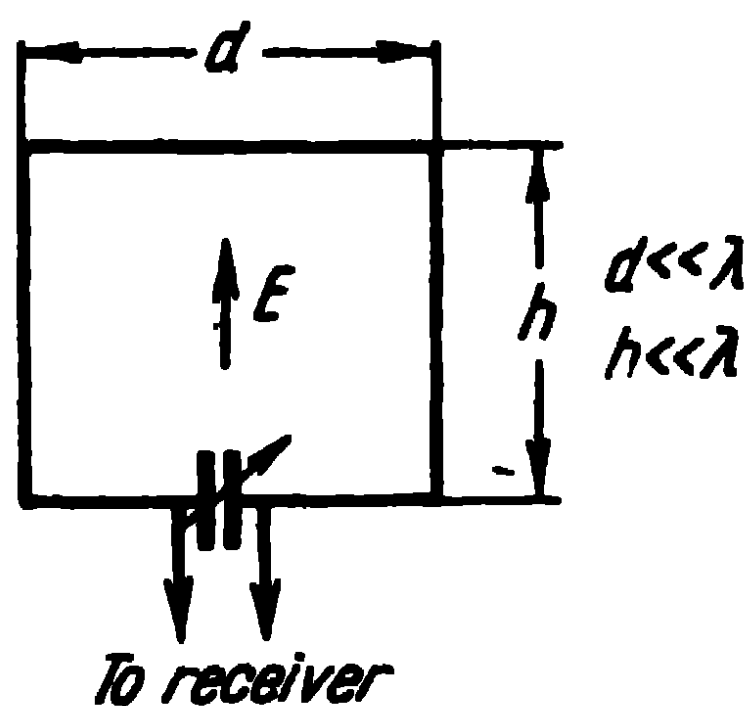


Fig. 12-20. Frame antenna.

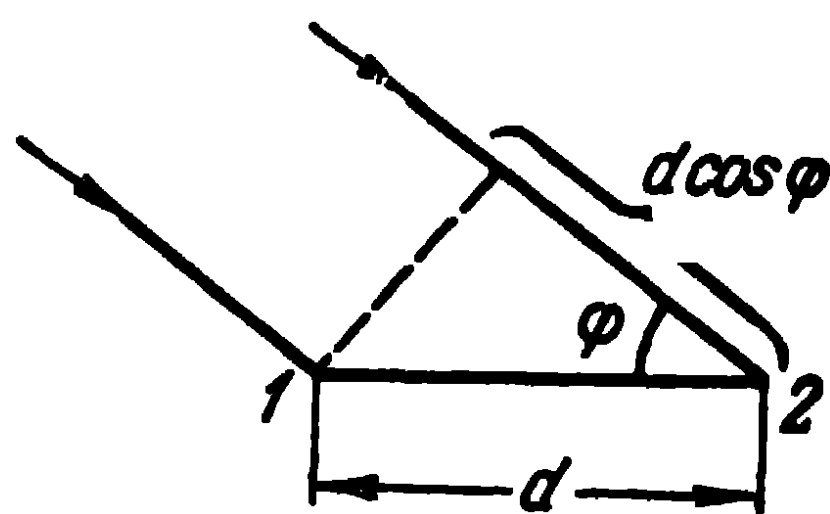


Fig. 12-21. Calculating the directional diagram of a frame antenna.

to the wave-length are usually small and it can be regarded as a magnetic dipole.

Let us consider the frame as a vertical reception system. Let the vector of the electric field intensity of the wave be parallel to the sides h of the frame and let the direction of the electromagnetic wave form with the plane of the frame an angle φ (Fig. 12-21). Let E be the electric field intensity in the centre of the frame. Then, an emf

$$\mathcal{E}_1 = E h e^{i \frac{kd}{2} \cos \varphi}$$

will be induced in the vertical side of the frame 1, and an emf

$$\mathcal{E}_2 = E h e^{-i \frac{kd}{2} \cos \varphi}$$

will be induced in the vertical side of the frame 2. The emf's act in opposite directions, so that the total emf giving rise to the current in the frame and determining the difference of potential at the capacitor (and input of the receiver), equals:

$$\mathcal{E}_1 = \mathcal{E}_2 - \mathcal{E}_3 = i2Eh \sin\left(\frac{kd}{2} \cos \varphi\right). \quad (12-23)$$

If, as is usually the case, the dimensions of the frame are small in comparison with the wave-length, we can approximately write:

$$\mathcal{E}_1 = iEh kd \cos \varphi. \quad (12-24)$$

The expression (12-24) shows 1) that the directional diagram of the frame is the same as that of a dipole ("figure of eight") and 2) that the emf induced in the frame has a phase shift of 90° relatively to the intensity of the field of the wave.

The effective height of the frame is understood to mean the ratio of the induced emf to the field intensity when the energy is received from a direction lying in the plane of the frame ($\varphi=0$),

$$h_{\text{eff}} = hkd.$$

If the frame consists of n windings connected in series, the emf induced in the frame increases by n times, so that the effective height of such a frame is:

$$h_{\text{eff}} = \frac{2\pi ns}{\lambda}, \quad (12-25)$$

where $s=hd$ is the area of the frame.

The radiation resistance of the frame, which is small in comparison with the wave-length and distant from the earth, can be calculated from the expression $R_{\Sigma} = 80\pi^2 \times \left(\frac{h_{\text{eff}}}{\lambda}\right)^2$, which, taking account of (12-25), leads to the expression

$$R_{\Sigma} = 31,200 \left(\frac{ns}{\lambda^2}\right)^2, \quad (12-26)$$

which, when $n = 1$, coincides with the expression (1-19). To take an example, let us suppose that $\lambda = 1,000$ m, $n = 10$, $s = 4$ m². R_{Σ} will then be found to equal $5 \cdot 10^{-5}$ ohms. Thus, the radiation resistance of a frame antenna on long waves is very small and it is difficult to cause the resistance

of the losses of the frame to be equally small. Hence, the efficiency of a frame antenna is very low and it is not utilised for transmission on long waves in the version described above, being only used for reception.

Note that the obtention of a directional diagram of the frame antenna in the shape of a pure "figure of eight" described by the expression (12-24) requires a strict electrical symmetry of the frame system. This means, in particular, that the input of the receiver should also be symmetrical, otherwise the frame will receive also a single-wire system:

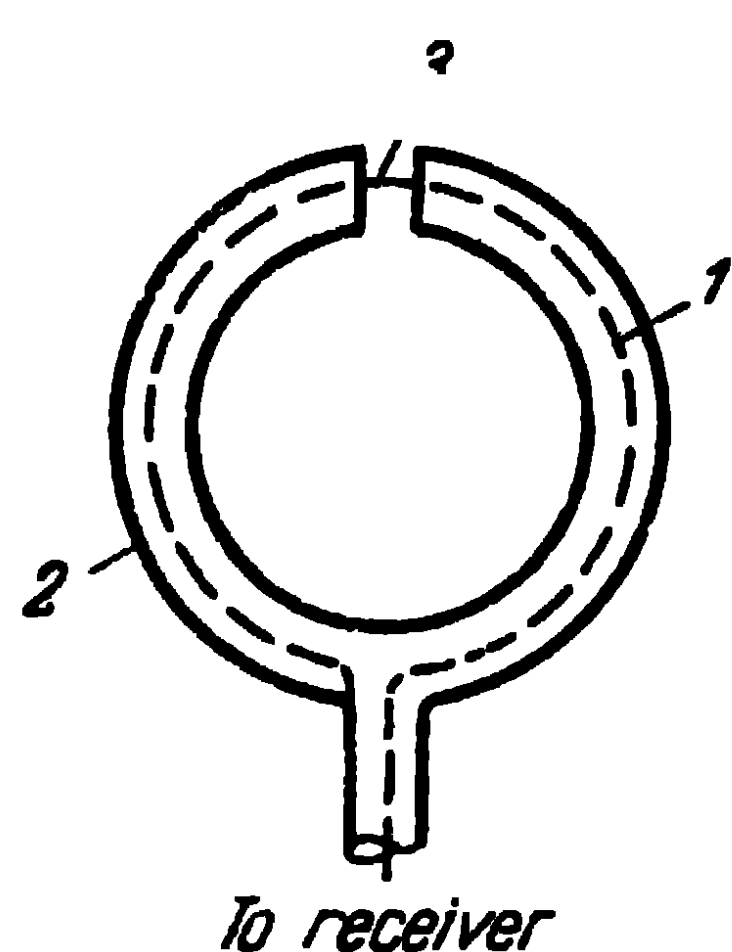


Fig. 12-22. Screened frame:

1—frame; 2—screen; 3—gap

the directional diagram of a vertical dipole (circumference) will be superimposed on the directional diagram of the frame and the resulting directional diagram of the frame antenna will be distorted. This undesirable effect of the frame is referred to as the antenna effect.

Frame antennas are made use of in measuring apparatus (comparators), as reception antennas of long-wave stations with the object of eliminating interference stations and directive noise, in radiogoniometrical installations determining the direction of the radio station received, etc.

The frame is generally mounted on a wooden or other non-metal framework and placed in a vertical position so as to be able to rotate it around the vertical axis. Frames of this kind are often enclosed within a circular screen with a gap at the top (Fig. 12 22). At the same time, the receiver is enclosed in the same screen as the frame, so that an antenna of this kind is, in essence, symmetrical, with good receiving qualities. Indeed, an electromagnetic wave coming towards the frame axis induces on the screen currents, which are so distributed that no difference of potential is set up at the gap of the screen and the inner region of the screen, i.e., the frame is not excited. When the electromagnetic wave comes from other directions, a difference of potential is set up at the gap of the screen and the frame is excited. The antenna effect of the frame is thus eliminated and the directional diagram suffers no distortion (there are directions of zero reception).

12-8. Radiogoniometers

A radiogoniometer represents two stationary external frames (Fig. 12-23) situated at an angle of 90° to one another. The frames are usually triangular and are secured on one mast, approximately 70 m high. The frames are connected to the receiver by means of two twin lines. Each line is connected to one of the two coils of the goniometer (to the stator). These coils are disposed at an angle of 90° to one another and coupled with a third mobile coil called the searcher. From the searcher, the voltage induced by the stationary frames is fed to the input of the receiver.

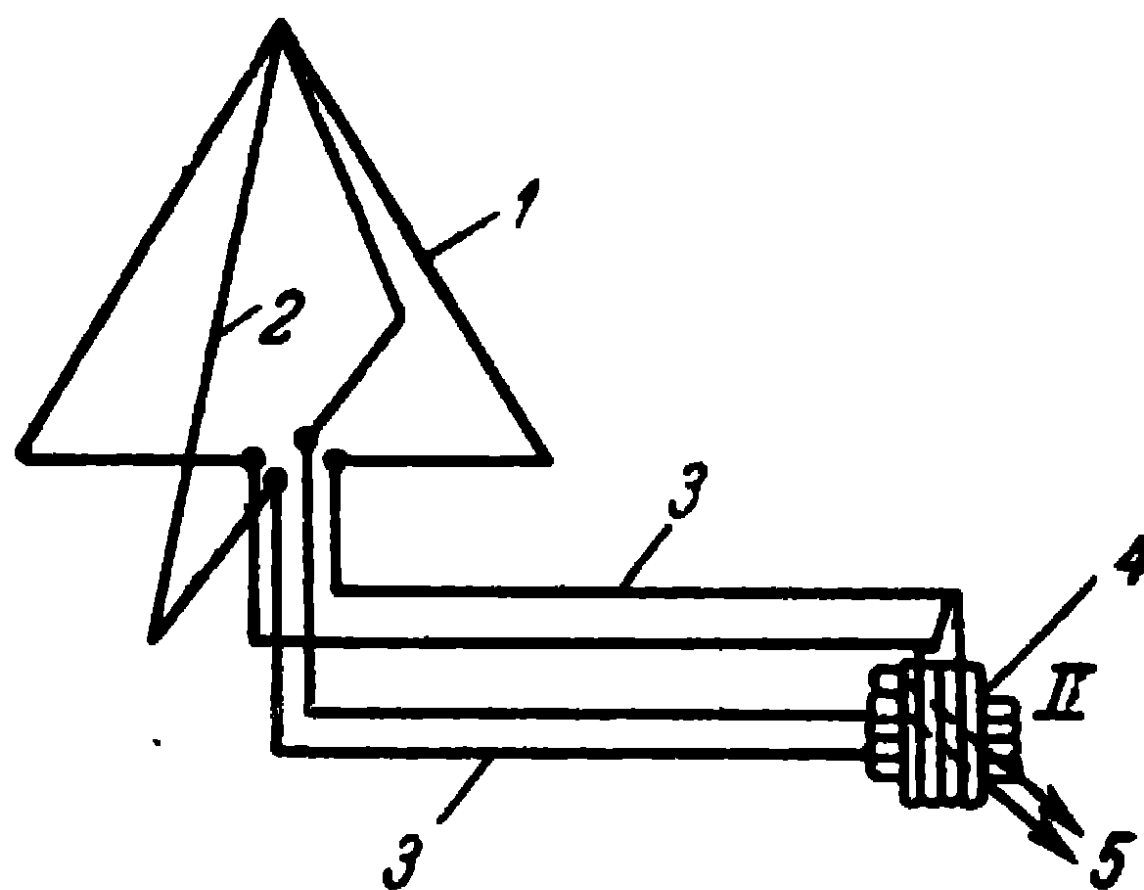


Fig. 12-23. Radiogoniometer:
1, 2 — frames; 3 — feeder; 4 — goniometer;
5 — searcher

Let the direction of arrival of the wave which is being received form with the frame 1 an angle φ (Fig. 12-24) and let the current induced in the stator I equal I_0 when the angle $\varphi = 0$. Then, when the wave arrives from any other direction, the current induced in the stator I will equal:

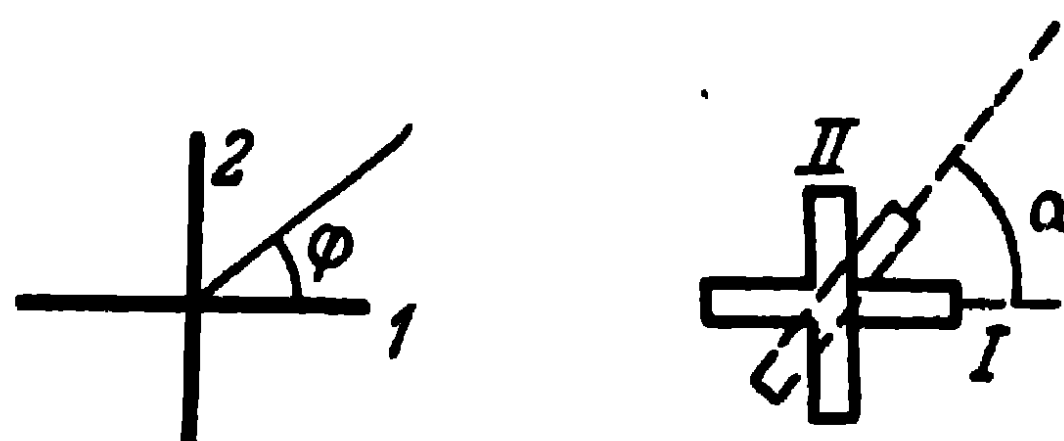


Fig. 12-24. Explaining the emf induced in the radiogoniometer.

$$I_1 = I_0 \cos \varphi,$$

and in the stator II,

$$I_2 = I_0 \sin \varphi.$$

Let the mutual induction between the stator and the rotor equal M when their coupling is at its maximum. Then, if the angle between them equals α , the emf induced in the searcher by the stator I will be:

$$\mathcal{E}_1 = I_0 \omega M \cos \varphi \cos \alpha,$$

and the emf induced by the second stator in the searcher will be:

$$\mathcal{E}_2 = I_0 \omega M \sin \varphi \sin \alpha.$$

The total emf will equal:

$$\mathcal{E} = I_0 \omega M \cos(\varphi - \alpha). \quad (12-27)$$

It is seen from (12-27) that when α is constant and φ is variable, the maximum of reception will occur for $\varphi = \alpha$. In this way, the directional diagram of an antenna of this kind does not differ from that of an ordinary frame antenna but the maximum reception direction is determined by the position of the searcher. The rotation of the coil of the searcher at the output of the receiver gives rise to the same effect as in the case of a rotating frame antenna.

If to the frame system described above, we add a vertical antenna, we can obtain a device which gives a unidirectional (cardioid) reception (Fig. 12-25).

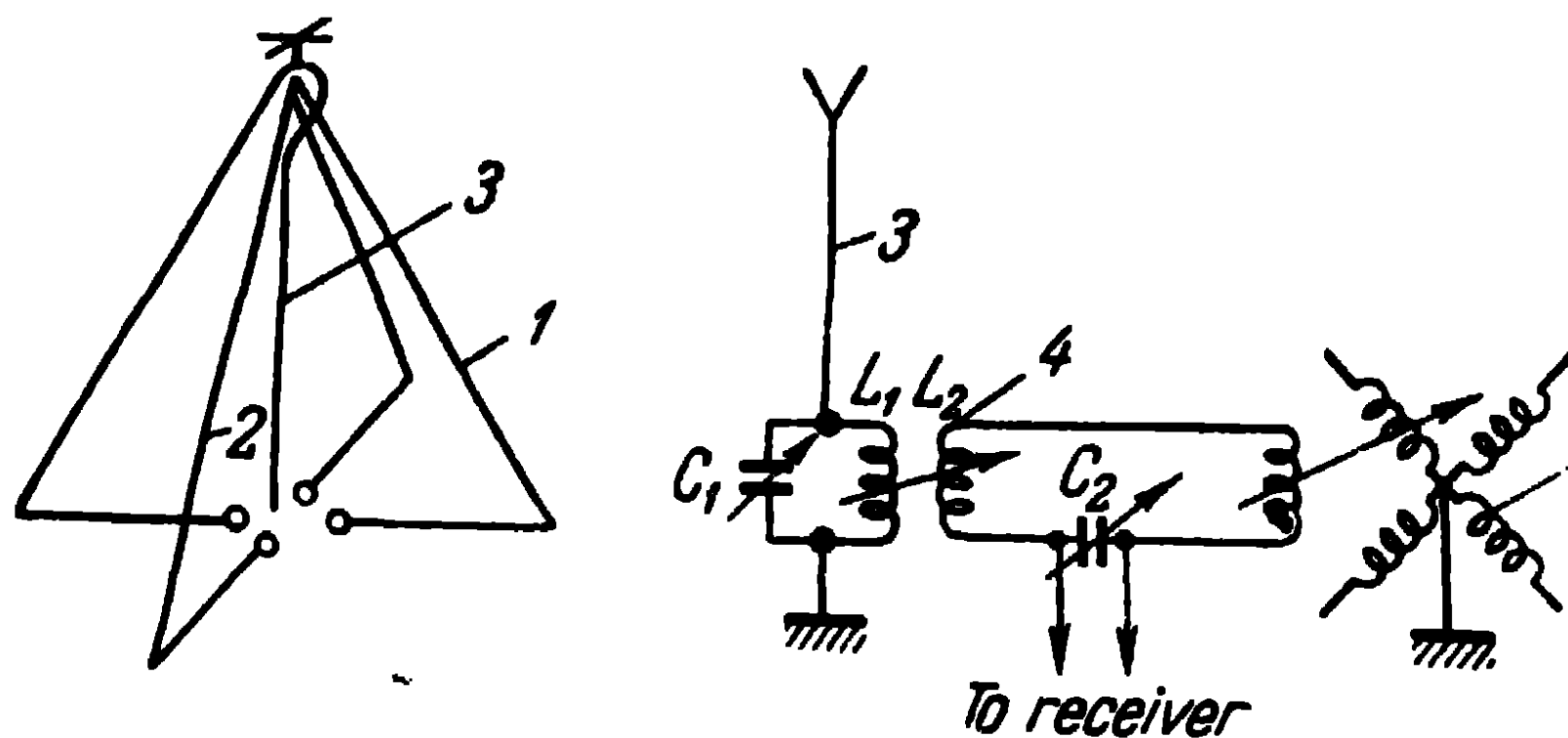


Fig. 12-25. Circuit of cardioid reception:
1, 2—frames; 3—vertical antenna; 4—adding circuit; 5—goniometer.

From the antenna and goniometer, the voltage is fed to the adding circuit. By regulating the ratios of the emf's introduced into the adding circuit by the antenna and the goniometer, one can obtain a total emf, which will change as:

$$\mathcal{E} = I_0 \omega M [1 + \cos(\varphi - \alpha)]. \quad (12-28)$$

The phasing of the emf is effected by the capacitor C_1 and the control of the amplitude, by changing the coupling between the coils L_1 and L_2 . The capacitor C_2 serves for tuning the adding circuit in resonance.

The directional diagram of the antenna system, expressed by (12-28) has the shape of a cardioid. A diagram of this kind presents considerable advantages over the directional diagram of a frame. It enables to define a unique direction towards the radio station which is being received, as well as to eliminate interference coming from a direction lying within

an angle of 90 to 270°, without any substantial weakening of the signal received.

Note that it is impossible to obtain a totally zero signal either in a frame system (goniometer) or in a system giving a cardioid reception. The ratio of the maximum to the minimum reception, known as the anti-interference factor, does not, as a rule, exceed a few tens. This is due to the fact that, even in the event of full symmetry of the system, it can only be tuned on one frequency, say the carrier frequency. On the side frequencies of the signal received, the system is found to be somewhat out of phase, so that no zero of reception can be obtained.

Furthermore, in the medium wave range, at night, apart from the ground ray, a sky ray also reaches the point of reception. It is not found possible to cancel the action of these two rays in the frequency band and the anti-interference factor of the antenna is thereby lowered.

Appendix I

Table of Values R_{12}

$\begin{array}{c} d \\ h \end{array}$	0.0	0.5	1.0	1.5	2.0	2.5	3.0	3.5
0.0	+73.29	-12.36	+4.08	-1.77	+1.18	-0.75	+0.42	-0.33
0.5	+26.40	-11.80	+8.83	-5.75	+3.76	-2.79	+1.86	-1.54
1.0	-4.065	-0.78	+3.56	-6.26	+6.05	-5.67	+4.51	-3.94
1.5	+1.78	+0.80	-2.92	+1.96	+0.16	-2.40	+3.24	-3.76
2.0	-0.96	-1.00	+1.13	+0.56	-2.55	+2.74	-2.07	+0.74
2.5	+0.58	+0.45	-0.42	-0.96	+1.59	-0.28	-1.59	+2.66
3.0	-0.43	-0.30	+0.13	+0.85	-0.45	-0.10	+1.74	-1.03

$\begin{array}{c} d \\ h \end{array}$	4.0	4.5	5.0	5.5	6.0	6.5	7.0	7.5
0.0	+0.21	-0.18	+0.15	-0.12	+0.12	-0.10	+0.06	-0.03
0.5	+1.08	-0.85	+0.69	-0.57	+0.51	-0.45	+0.36	-0.30
1.0	+3.08	-2.50	+2.10	-1.80	+1.56	-1.18	+1.14	-1.00
1.5	+3.68	-3.40	+3.14	-2.90	+2.61	-2.31	+2.06	-1.86
2.0	+0.51	-1.30	+1.82	-2.24	+2.28	-2.29	+2.26	-2.14
2.5	-2.49	+2.00	-1.35	+0.49	-0.06	-0.45	+0.85	-1.03
3.0	-0.09	+1.12	-1.87	+1.77	-2.02	+1.71	-1.32	+0.66

Appendix II

Table of Resistances

$$h = 0$$

d	R_{12}	Δ	X_{12}	Δ	d	R_{12}	Δ	X_{12}	Δ
0.00	+73.1		+42.5		0.10	+67.3		+7.5	
		0.2		7.4			2.4		6.1
0.02	+72.9		+35.1		0.12	+64.9		+1.4	
		0.6		7.3			2.9		5.8
0.04	+72.3		+27.8		0.14	+62.0		-4.4	
		1.3		7.0			3.2		5.4
0.06	+71.0		+20.8		0.16	+58.8		-9.8	
		1.6		6.8			3.6		4.9
0.08	+69.4		+14.0		0.18	+55.2		-14.7	
		2.1		6.5			3.8		4.5
		3.8		4.5			1.0		1.8
0.20	+51.4		-19.2		1.12	+13.4		+9.5	
		4.0		4.0			0.8		1.9
0.22	+47.4		-23.2		1.14	+14.2		+7.6	
		4.3		3.6			0.6		1.8
0.24	+43.1		-26.8		1.16	+14.18		+5.8	
		4.6		3.0			0.4		1.9
0.26	+38.5		-29.8		1.18	+15.2		+3.9	
		4.5		2.6			0.0		2.0
0.28	+34.0		-32.4		1.20	+15.2		+1.9	
		4.7		2.0			0.0		1.8
0.30	+29.3		-34.4		1.22	+15.2		+0.1	
		4.7		1.6			0.3		1.9
0.32	+24.6		-36.0		1.24	+14.9		-1.8	

Continued

d	R_{12}	Δ	X_{12}	Δ	d	R_{12}	Δ	X_{12}	Δ
0.34	+20.0	4.6	-37.1	1.1	1.26	+14.3	0.3	-3.5	1.7
0.36	+15.2	4.8	-37.7	0.6	1.28	+13.5	0.8	-5.1	1.6
0.38	+10.6	4.6	-37.8	0.1	1.30	+12.6	0.9	-6.7	1.6
0.40	+6.2	4.4	-37.5	0.3	1.32	+11.5	1.1	-8.1	1.4
0.42	+2.0	4.2	-36.7	0.8	1.34	+10.3	1.2	-9.3	1.2
0.44	-2.0	4.0	-35.6	1.1	1.36	+8.9	1.4	-10.4	1.1
0.46	-5.8	3.8	-33.9	1.7	1.38	+7.5	1.4	-11.2	0.8
0.48	-9.4	3.6	-32.1	1.8	1.40	+6.0	1.5	-11.9	0.7
0.50	-12.5	3.1	-29.9	2.2	1.42	+4.4	1.6	-12.4	0.5
0.52	-15.4	2.9	-27.5	2.4	1.44	+2.8	1.6	-12.6	0.2
0.54	-17.9	2.5	-24.9	2.6	1.46	+1.2	1.6	-12.7	0.1
0.56	-20.1	2.2	-22.0	2.9	1.48	-0.4	1.6	-12.6	0.1
0.58	-21.9	1.8	-19.0	3.0	1.50	-1.8	1.4	-12.3	0.3
0.60	-23.3	1.4	-15.9	3.1	1.52	-3.4	1.6	-11.8	0.5
0.62	-24.4	1.1	-12.7	3.2	1.54	-4.8	1.4	-11.2	0.6
0.64	-25.0	0.6	-9.5	3.2	1.56	-6.0	1.2	-10.4	0.8
0.66	-25.3	0.3	-6.4	3.1	1.58	-7.1	1.1	-9.5	0.9
0.68	-25.3	0.0	-3.3	3.1	1.60	-8.1	1.0	-8.4	1.1
		0.4		3.1			0.9		1.2

Continued

d	R_{12}	Δ	X_{12}	Δ	d	R_{12}	Δ	X_{12}	Δ
0.70	-24.9		-0.2		1.62	-9.0		-7.2	
		0.7		2.8			0.8		1.3
0.72	-24.2		+2.6		1.64	-9.8		-5.9	
		1.1		2.7			0.5		1.2
0.74	-23.1		+5.3		1.66	-10.3		-4.7	
		1.3		2.6			0.4		1.4
0.76	-21.8		+7.9		1.68	-10.7		-3.3	
		1.5		2.3			0.2		1.3
0.78	-20.3		+10.2		1.70	-10.9		-2.0	
		1.8		2.0			0.0		1.4
0.80	-18.5		+12.2		1.72	-10.9		-0.6	
		1.9		1.8			0.2		1.4
0.82	-16.6		+14.0		1.74	-10.7		+0.8	
		2.1		1.6			0.2		1.2
0.84	-14.5		+15.6		1.76	-10.5		+2.0	
		2.3		1.3			0.5		1.3
0.86	-12.2		+16.9		1.78	-10.0		+3.3	
		2.4		1.0			0.6		1.1
0.88	-9.8		+17.9		1.80	-9.4		+4.4	
		2.3		0.6			0.7		1.1
0.90	-7.5		+18.5		1.82	-8.7		+5.5	
		2.4		0.5			0.8		1.0
0.92	-5.1		+19.0		1.84	-7.9		+6.5	
		2.4		0.1			0.9		0.9
0.94	-2.7		+19.1		1.86	-7.0		+7.4	
		2.2		0.2			1.1		0.6
0.96	-0.5		+18.9		1.88	-5.9		+8.0	
		2.3		0.4			1.1		0.7
0.98	+1.8		+18.5		1.90	-4.8		+8.7	
		2.2		0.8			1.2		0.4
1.00	+4.0		+17.7		1.92	-3.6		+9.1	
		2.0		0.9			1.2		0.3
1.02	+6.0		+16.8		1.94	-2.5		+9.4	
		1.8		1.1			1.2		0.1
1.04	+7.8		+15.7		1.96	-1.3		+9.5	
		1.7		1.2			1.2		0.0
1.06	+9.5		+14.5		1.98	-0.1		+9.5	
		1.5		1.6			1.2		0.1

Continued

d	R_{12}	Δ	X_{12}	Δ	d	R_{12}	Δ	X_{12}	Δ
1.08	+11.0		+12.9		2.00	+1.1		+9.4	
		1.4		1.6			0.7		0.5
1.10	+12.4		+11.3						
		1.0		1.8					
2.00	+1.1		+9.4		2.90	-3.4		+5.6	
		1.1		0.3			0.7		0.3
2.02	+2.2		+9.1		2.92	-2.7		+5.9	
		1.1		0.5			0.8		0.3
2.04	+3.3		+8.6		2.94	-1.9		+6.2	
		1.0		0.6			0.8		0.1
2.06	+4.3		+8.0		2.96	-1.1		+6.3	
		0.9		0.6			0.8		0.1
2.08	+5.2		+7.4		2.98	-0.3		+6.4	
		0.9		0.7			0.8		0.1
2.10	+6.1		+6.7		3.00	+0.5		+6.3	
		0.7		0.9			0.8		0.1
2.12	+6.8		+5.8		3.02	+1.3		+6.2	
		0.6		1.0			0.7		0.3
2.14	+7.4		+4.8		3.04	+2.0		+5.9	
		0.5		0.9			0.7		0.3
2.16	+7.9		+3.9		3.06	+2.7		+5.6	
		0.3		1.0			0.7		0.4
2.18	+8.2		+2.9		3.08	+3.4		+5.2	
		0.2		1.1			0.6		0.5
2.20	+8.4		+1.8		3.10	+4.0		+4.7	
		0.1		1.1			0.5		0.6
2.22	+8.5		+0.7		3.12	+4.5		+4.1	
		0.1		1.0			0.4		0.6
2.24	+8.4		-0.3		3.14	+4.9		+3.5	
		0.1		1.1			0.4		0.7
2.26	+8.3		-1.4		3.16	+5.3		+2.8	
		0.3		0.9			0.3		0.6
2.28	+8.0		-2.3		3.18	+5.6		+2.2	
		0.4		1.0			0.1		0.8
2.30	+7.6		-3.3		3.20	+5.7		+1.4	
		0.6		0.9			0.2		0.7
2.32	+7.0		-4.2		3.22	+5.9		+0.7	
		0.7		0.8			0.0		0.8

Continued

d	R_{12}	Δ	X_{12}	Δ	d	R_{12}	Δ	X_{12}	Δ
2.34	+6.3		-5.0		3.24	+5.9		-0.1	
		0.7		0.7			0.1		0.7
2.36	+5.6		-5.7		3.26	+5.8		-0.8	
		0.7		0.6			0.2		0.7
2.38	+4.9		-6.3		3.28	+5.6		-1.5	
		0.9		0.5			0.3		0.6
2.40	+4.0		-6.8		3.30	+5.3		-2.1	
		0.9		0.4			0.3		0.7
2.42	+3.1		-7.2		3.32	+5.0		-2.8	
		0.9		0.2			0.5		0.6
2.44	+2.2		-7.4		3.34	+4.5		-3.4	
		1.0		0.2			0.4		0.5
2.46	+1.2		-7.6		3.36	+4.1		-3.9	
		1.0		0.0			0.5		0.5
2.48	+0.2		-7.6		3.38	+3.6		-4.4	
		0.9		0.1			0.7		0.3
2.50	-0.7		-7.5		3.40	+2.9		-4.7	
		0.9		0.2			0.6		0.3
2.52	-1.6		-7.3		3.42	+2.3		-5.0	
		0.9		0.2			0.6		0.3
2.54	-2.5		-7.1		3.44	+1.7		-5.3	
		0.8		0.5			0.7		0.1
2.56	-3.3		-6.6		3.46	+1.0		-5.4	
		0.8		0.5			0.7		0.1
2.58	-4.1		-6.1		3.48	+0.3		-5.5	
		0.7		0.6			0.7		0.1
2.60	-4.8		-5.5		3.50	-0.4		-5.4	
		0.6		0.7			0.7		0.1
2.62	-5.4		-4.8		3.52	-1.1		-5.3	
		0.5		0.7			0.6		0.2
2.64	-5.9		-4.1		3.54	-1.7		-5.1	

Continued

d	R_{12}	Δ	X_{12}	Δ	d	R_{12}	Δ	X_{12}	Δ
2.66	-6.3	0.4	-3.3	0.8	3.56	-2.3	0.6	-4.8	0.3
2.68	-6.7	0.4	-2.5	0.8	3.58	-2.9	0.6	-4.5	0.3
2.70	-6.9	0.2	-1.6	0.9	3.60	-3.4	0.5	-4.1	0.4
2.72	-6.9	0.0	-0.7	0.9	3.62	-3.8	0.4	-3.6	0.5
2.74	-6.9	0.0	+0.1	0.8	3.64	-4.2	0.4	-3.1	0.5
2.76	-6.5	0.1	+1.0	0.9	3.66	-4.6	0.4	-2.5	0.6
2.78	-6.5	0.3	+1.9	0.9	3.68	-4.8	0.2	-1.9	0.6
2.80	-6.3	0.2	+2.6	0.7	3.70	-5.0	0.2	-1.3	0.6
2.82	-5.8	0.5	+3.3	0.7	3.72	-5.1	0.1	-0.7	0.6
2.84	-5.3	0.5	+4.0	0.7	3.74	-5.1	0.0	0.0	0.7
2.86	-4.8	0.5	+4.6	0.6	3.76	-5.0	0.1	+0.6	0.6
2.88	-4.1	0.7	+5.1	0.5	3.78	-4.9	0.1	+1.2	0.6
3.80	-4.7	0.7	+1.8	0.5	3.92	-2.1	0.2	+4.4	0.3
3.82	-4.4	0.2	+2.3	0.6	3.94	-1.5	0.5	+4.6	0.2
		0.3		0.5			0.6		

Continued

d	R_{12}	Δ	X_{12}	Δ	d	R_{12}	Δ	X_{12}	Δ
3.84	-4.1	0.3	+2.9	0.6	3.96	-1.0	0.5	+4.7	0.1
3.86	-3.6	0.5	+3.3	0.4	3.98	-0.4	0.6	+4.8	0.1
3.88	-3.2	0.4	+3.8	0.5	4.00	+0.2	0.6	+4.7	0.1
3.90	-2.6	0.6	+4.1	0.3					
		0.5							

$h=0.5$

d	R_{12}	Δ	X_{12}	Δ	d	R_{12}	Δ	X_{12}	Δ
0.00	+26.4		+20.2		0.60	-14.1		+0.4	1.7
0.02	+26.3	0.1	+16.4	3.8	0.62	-13.9	0.2	+2.1	1.7
0.04	+25.9	0.4	+12.9	3.5	0.64	-13.5	0.4	+3.7	1.6
0.06	+25.4	0.5	+9.4	3.5	0.66	-13.0	0.5	+5.2	1.5
0.08	+24.6	0.8	+6.2	3.2	0.68	-12.2	0.8	+6.7	1.5
0.10	+23.5	1.1	+3.1	3.1	0.70	-11.3	0.9	+8.1	1.4
0.12	+22.3	1.2	+0.2	2.9	0.72	-10.3	1.0	+9.3	1.2
0.14	+20.9	1.4	-2.4	2.6	0.74	-9.1	1.2	+10.4	1.1
0.16	+19.3	1.6	-4.8	2.4	0.76	-7.7	1.4	+11.3	0.9
0.18	+17.6	1.7	-7.0	2.2	0.78	-6.4	1.3	+12.0	0.7
0.20	+15.7	1.9	-8.9	1.9	0.80	-4.9	1.5	+12.6	0.6
0.22	+13.8	1.9	-10.6	1.7	0.82	-3.3	1.6	+13.0	0.4
		2.1		1.3			1.4		0.3

Continued

σ	R_{12}	Λ	X_{12}	Δ	d	R_{12}	Δ	X_{12}	Δ
0.24	+11.7		-11.9		0.84	-1.9		+13.3	
		2.1		1.1			1.6		0.0
0.26	+9.6		-13.0		0.86	-0.3		+13.3	
		2.2		0.9			1.6		0.1
0.28	+7.4		-13.9		0.88	+1.3		+13.2	
		2.2		0.6			1.5		0.4
0.30	+5.2		-14.5		0.90	+2.8		+12.8	
		2.1		0.3			1.4		0.4
0.32	+3.1		-14.8		0.92	+4.2		+12.4	
		2.0		0.2			1.4		0.7
0.34	+1.1		-15.0		0.94	+5.6		+11.7	
		2.1		0.3			1.2		0.8
0.36	-1.0		-14.7		0.96	+6.8		+10.9	
		2.0		0.4			1.2		0.9
0.38	-3.0		-14.3		0.98	+8.0		+10.0	
		1.9		0.6			1.0		1.0
0.40	-4.9		-13.7		1.00	+9.0		+8.9	
		1.7		0.8			0.9		1.2
0.42	-6.6		-12.9		1.02	+9.9		+7.7	
		1.6		1.1			0.8		1.2
0.44	-8.2		-11.8		1.04	+10.7		+6.5	
		1.4		1.2			0.6		1.4
0.46	-9.6		-10.6		1.06	+11.3		+5.1	
		1.2		1.3			0.4		1.3
0.48	-10.8		-9.3		1.08	+11.7		+3.8	
		1.1		1.4			0.3		1.4
0.50	-11.9		-7.9		1.10	+12.0		+2.4	
		0.8		1.6			0.1		1.5
0.52	-12.7		-6.3		1.12	+12.1		+0.9	
		0.7		1.6			0.1		1.4
0.54	-13.4		-4.7		1.14	+12.0		-0.5	
		0.4		1.7			0.2		1.4
0.56	-13.8		-3.0		1.16	+11.8		-1.9	
		0.3		1.7			0.4		1.3
0.58	-14.1		-1.3		1.18	+11.4		-3.2	
		0.0		1.7			0.6		1.3
		0.6		1.3			0.3		0.9
1.20	+10.8		-4.5		2.12	+7.5		+2.9	

Continued

d	R_{12}	Δ	X_{12}	Δ	d	R_{12}	Δ	X_{12}	Δ
1.22	+10.1	0.7	-5.7	1.2	2.14	+7.8	0.3	+1.9	1.0
1.24	+9.3	0.8	-6.9	1.2	2.16	+7.9	0.1	+1.0	0.9
1.26	+8.4	0.9	-7.8	0.9	2.18	+7.9	0.0	+0.0	1.0
1.28	+7.4	1.0	-8.6	0.8	2.20	+7.8	0.1	-1.0	1.0
1.30	+6.3	1.1	-9.3	0.7	2.22	+7.5	0.3	-1.9	0.9
1.32	+5.1	1.2	-9.9	0.6	2.24	+7.2	0.3	-2.7	0.8
1.34	+3.8	1.3	-10.4	0.5	2.26	+6.8	0.4	-3.6	0.9
1.36	+2.5	1.3	-10.7	0.3	2.28	+6.2	0.6	-4.3	0.7
1.38	+1.2	1.3	-10.8	0.1	2.30	+5.6	0.6	-5.1	0.8
1.40	-0.1	1.3	-10.8	0.0	2.32	+4.9	0.7	-5.7	0.6
1.42	-1.3	1.2	-10.6	0.2	2.34	+4.1	0.8	-6.2	0.5
1.44	-2.6	1.3	-10.3	0.3	2.36	+3.3	0.8	-6.6	0.4
1.46	-3.7	1.1	-9.8	0.5	2.38	+2.5	0.8	-6.9	0.3
1.48	-4.8	1.1	-9.2	0.6	2.40	+1.6	0.9	-7.1	0.2
1.50	-5.8	1.0	-8.5	0.7	2.42	+0.7	0.9	-7.2	0.1
1.52	-6.8	1.0	-7.7	0.8	2.44	-0.2	0.9	-7.2	0.0
1.54	-7.6	0.8	-6.8	0.9	2.46	-1.0	0.8	-7.1	0.1
1.56	-8.3	0.7	-5.8	1.0	2.48	-1.9	0.9	-6.8	0.3
1.58	-8.8	0.5	-4.7	1.1	2.50	-2.7	0.8	-6.5	0.3

Continued

d	R_{12}	Δ	X_{12}	Δ	d	R_{12}	Δ	X_{12}	Δ
1.60	-9.2	0.4	-3.6	1.1	2.52	-3.4	0.7	-6.1	0.4
		0.3		1.2			0.7		0.5
1.62	-9.5		-2.4		2.54	-4.1		-5.6	
		0.2		1.1			0.6		0.6
1.64	-9.7		-1.3		2.56	-4.7		-5.0	
		0.0		1.2			0.6		0.6
1.66	-9.7		-0.1		2.58	-5.3		-4.4	
		0.2		1.1			0.4		0.7
1.68	-9.5		+1.0		2.60	-5.7		-3.7	
		0.2		1.2			0.4		0.8
1.70	-9.3		+2.2		2.62	-6.1		-2.9	
		0.4		1.0			0.3		0.8
1.72	-8.9		+3.2		2.64	-6.4		-2.1	
		0.6		1.1			0.1		0.8
1.74	-8.3		+4.3		2.66	-6.5		-1.3	
		0.6		0.9			0.1		0.8
1.76	-7.7		+5.2		2.68	-6.6		-0.5	
		0.7		0.8			0.0		0.8
1.78	-7.0		+6.0		2.70	-6.6		+0.3	
		0.9		0.7			0.2		0.8
1.80	-6.1		+6.7		2.72	-6.4		+1.1	
		0.9		0.7			0.2		0.8
1.82	-5.2		+7.4		2.74	-6.2		+1.9	
		0.9		0.5			0.3		0.7
1.84	-4.3		+7.9		2.76	-5.9		+2.6	
		1.0		0.4			0.4		0.7
1.86	-3.3		+8.3		2.78	-5.5		+3.3	
		1.1		0.2			0.5		0.6
1.88	-2.2		+8.5		2.80	-5.0		+3.9	
		1.0		0.2			0.5		0.6
1.90	-1.2		+8.7		2.82	-4.5		+4.5	
		1.1		0.0			0.6		0.5
1.92	-0.1		+8.7		2.84	-3.9		+5.0	
		1.0		0.1			0.7		0.4
1.94	+0.9		+8.6		2.86	-3.2		+5.4	
		1.1		0.3			0.7		0.3
1.96	+2.0		+8.3		2.88	-2.6		+5.7	

Continued

d	R_{12}	Δ	X_{12}	Δ	d	R_{12}	Δ	X_{12}	Δ
1.98	+3.0	1.0	+8.0	0.3	2.90	-1.8	0.7	+5.9	0.2
2.00	+3.9	0.9	+7.5	0.5	2.92	-1.0	0.8	+6.1	0.2
2.02	+4.7	0.8	+6.9	0.6	2.94	-0.3	0.7	+6.1	0.0
2.04	+5.5	0.8	+6.2	0.7	2.96	+0.5	0.8	+6.1	0.0
2.06	+6.1	0.6	+5.5	0.7	2.98	+1.3	0.8	+6.1	0.2
2.08	+6.7	0.6	+5.5	0.8	3.00	+1.9	0.6	+5.9	0.2
2.10	+7.2	0.5	+4.7	0.9	3.02	+2.6	0.7	+5.7	0.3
3.04	+3.2	0.3	+3.8	0.9	3.04	+2.6	0.6	+5.4	0.4
3.06	+3.8	0.6	+5.0	0.4	3.06	+2.6	0.5	+5.4	0.3
3.08	+4.4	0.6	+4.5	0.5	3.08	-2.6	0.6	-4.5	0.4
3.10	+4.7	0.6	+3.9	0.6	3.10	-3.2	0.4	-4.1	0.4
3.12	+5.1	0.3	+3.4	0.5	3.12	-3.6	0.4	-3.7	0.4
3.14	+5.4	0.4	+2.8	0.6	3.14	-4.0	0.4	-3.2	0.5
3.16	+5.6	0.3	+2.1	0.7	3.16	-4.3	0.3	-3.2	0.6
3.18	+5.7	0.2	+1.4	0.7	3.18	-4.3	0.3	-2.6	0.5
3.20	+5.6	0.1	+0.8	0.6	3.20	-4.6	0.2	-2.1	0.6
3.22	+5.6	0.1	0.0	0.8	3.22	-4.8	0.2	-1.5	0.6
3.24	+5.5	0.0	-0.7	0.7	3.24	-4.8	0.1	-0.9	0.6
3.26	+5.2	0.1	-1.3	0.6	3.26	-4.9	0.0	-0.2	0.7
3.28	+4.9	0.3	-2.0	0.7	3.28	-4.9	0.0	+0.4	0.6
3.30	+4.5	0.3	-2.6	0.6	3.30	-4.8	0.1	+1.0	0.6
3.32	+4.1	0.4	-3.2	0.6	3.32	-4.6	0.2	+1.6	0.5
3.34	+3.5	0.4	-3.7	0.5	3.34	-4.4	0.2	+2.1	0.5
		0.6	-4.1	0.4	3.36	-4.1	0.3	+2.6	0.5
		0.5		0.4	3.38	-3.7	0.4	+3.1	0.5
					3.40	-3.3	0.4	+3.5	0.4
					3.42		0.5		0.4

Continued

<i>d</i>	<i>R</i> ₁₂	Δ	<i>X</i> ₁₂	Δ	<i>d</i>	<i>R</i> ₁₂	Δ	<i>X</i> ₁₂	Δ
3.36	+3.0	0.6	−4.5	0.3	3.86	−2.8	0.5	+3.9	0.3
3.38	+2.4	0.6	−4.8	0.3	3.88	−2.3	0.6	+4.2	0.2
3.40	+1.8	0.7	−5.1	0.1	3.90	−1.7	0.5	+4.4	0.2
3.42	+1.1	0.6	−5.2	0.1	3.92	−1.2	0.6	+4.6	0.0
3.44	+0.5	0.7	−5.3	0.0	3.94	−0.6	0.6	+4.6	0.1
3.46	−0.2	0.6	−5.3	0.1	3.96	0.0	0.6	+4.7	0.1
3.48	−0.8	0.7	−5.2	0.2	3.98	+0.6	0.5	+4.6	0.1
3.50	−1.5	0.6	−5.0	0.2	4.00	+1.1		+4.5	
3.52	−2.1	0.5	−4.8	0.3					

h = 1.0

<i>d</i>	<i>R</i> ₁₂	Δ	<i>X</i> ₁₂	Δ	<i>d</i>	<i>R</i> ₁₂	Δ	<i>X</i> ₁₂	Δ
0.00	−4.1	0.0	−0.7	0.0	0.20	−4.0	0.0	+0.5	0.2
0.02	−4.1	0.0	−0.7	0.0	0.22	−3.9	0.1	+0.7	0.2
0.04	−4.1	0.0	−0.7	0.1	0.24	−3.8	0.1	+0.9	0.2
0.06	−4.1	0.0	−0.6	0.1	0.26	−3.8	0.0	+1.2	0.3
0.08	−4.1	0.0	−0.5	0.1	0.28	−3.6	0.2	+1.5	0.3
0.10	−4.1	0.0	−0.4	0.1	0.30	−3.5	0.1	+1.8	0.3
0.12	−4.1	0.0	−0.3	0.1	0.32	−3.3	0.2	+2.0	0.2
0.14	−4.1	0.0	−0.1	0.2	0.34	−3.1	0.2	+2.3	0.3
0.16	−4.1	0.1	+0.1	0.2	0.36	−2.9	0.2	+2.6	0.3
0.18	−4.0		+0.3		0.38	−2.7	0.2	+2.8	0.2

Continued

d	R_{12}	Δ	X_{12}	Δ	d	R_{12}	Δ	X_{12}	Δ
		0 0		0.2			0.3		0.3
		0.3		0.3			0.5		0.6
0.40	-2.4	0.2	+3.1	0.2	1.32	-5.0	0.4	-3.9	0.5
0.42	-2.2	0.3	+3.3	0.3	1.34	-5.4	0.4	-3.4	0.5
0.44	-1.9	0.3	+3.6	0.2	1.36	-5.8	0.3	-2.9	0.7
0.46	-1.6	0.3	+3.8	0.2	1.38	-6.1	0.2	-2.2	0.6
0.48	-1.3	0.5	+4.0	0.1	1.40	-6.3	0.1	-1.6	0.7
0.50	-0.8	0.5	+4.1	0.1	1.42	-6.4	0.1	-0.9	0.7
0.52	-0.3	0.4	+4.2	0.0	1.44	-6.5	0.0	-0.2	0.7
0.54	+0.1	0.5	+4.2	0.0	1.46	-6.5	0.1	+0.5	0.7
0.56	+0.6	0.4	+4.2	0.1	1.48	-6.4	0.2	+1.2	0.7
0.58	+1.0	0.5	+4.3	0.1	1.50	-6.2	0.2	+1.9	0.6
0.60	+1.5	0.4	+4.2	0.1	1.52	-6.0	0.3	+2.5	0.7
0.62	+1.9	0.5	+4.1	0.2	1.54	-5.7	0.4	+3.2	0.6
0.64	+2.4	0.4	+3.9	0.2	1.56	-5.3	0.5	+3.8	0.5
0.66	+2.8	0.4	+3.7	0.2	1.58	-4.8	0.5	+4.3	0.5
0.68	+3.2	0.4	+3.5	0.3	1.60	-4.3	0.5	+4.8	0.5
0.70	+3.6	0.4	+3.2	0.4	1.62	-3.8	0.6	+5.3	0.4
0.72	+4.0	0.3	+2.8	0.3	1.64	-3.2	0.7	+5.7	0.3
0.74	+4.3	0.3	+2.5	0.4	1.66	-2.5	0.6	+6.0	0.2

Continued

d	R_{12}	Δ	X_{12}	Δ	d	R_{12}	Δ	X_{12}	Δ
0.76	+4.6	0.3	+2.1	0.5	1.68	-1.9	0.7	+6.2	0.2
0.78	+4.9	0.2	+1.6	0.5	1.70	-1.2	0.7	+6.4	0.1
0.80	+5.1	0.1	+1.1	0.5	1.72	-5.0	0.8	+6.5	0.0
0.82	+5.2	0.1	+0.6	0.5	1.74	+0.3	0.7	+6.5	0.1
0.84	+5.3	0.1	+0.1	0.6	1.76	+1.0	0.7	+6.4	0.2
0.86	+5.4	0.0	-0.5	0.5	1.78	+1.7	0.7	+6.2	0.2
0.88	+5.4	0.1	-1.0	0.6	1.80	+2.4	0.6	+6.0	0.3
0.90	+5.3	0.1	-1.6	0.5	1.82	+3.0	0.6	+5.7	0.4
0.92	+5.2	0.2	-2.1	0.6	1.84	+3.6	0.6	+5.3	0.5
0.94	+5.0	0.3	-2.7	0.5	1.86	+4.2	0.5	+4.8	0.5
0.96	+4.7	0.3	-3.2	0.5	1.88	+4.7	0.4	+4.3	0.5
0.98	+4.4	0.3	-3.7	0.5	1.90	+5.1	0.4	+3.8	0.6
1.00	+4.1	0.4	-4.2	0.4	1.92	+5.5	0.3	+3.2	0.7
1.02	+3.7	0.5	-4.6	0.4	1.94	+5.8	0.2	+2.5	0.7
1.04	+3.2	0.5	-5.0	0.4	1.96	+6.0	0.2	+1.8	0.7
1.06	+2.7	0.6	-5.4	0.3	1.98	+6.2	0.1	+1.1	0.7
1.08	+2.1	0.6	-5.7	0.2	2.00	+6.3	0.0	+0.4	0.7
1.10	+1.5	0.6	-5.9	0.2	2.02	+6.3	0.2	-0.3	0.7
1.12	+0.9	0.6	-6.1	0.0	2.04	+6.1	0.1	-1.0	0.7

Continued

d	R_{12}	Δ	X_{12}	Δ	d	R_{12}	Δ	X_{12}	Δ
1.14	+0.3	0.7	-6.1	0.1	2.06	+6.1	0.3	-1.7	0.6
1.16	-0.4	0.6	-6.2	0.1	2.08	+5.7	0.3	-2.3	0.7
1.18	-1.0	0.6	-6.1	0.1	2.10	+5.4	0.4	-3.0	0.6
1.20	-1.6	0.7	-6.0	0.2	2.12	+5.0	0.4	-3.6	0.5
1.22	-2.3	0.6	-5.8	0.1	2.14	+4.6	0.6	-4.1	0.5
1.24	-2.9	0.6	-5.7	0.4	2.16	+4.0	0.5	-4.6	0.4
1.26	-3.5	0.6	-5.3	0.4	2.18	+3.5	0.6	-5.0	0.3
1.28	-4.1	0.4	-4.9	0.4	2.20	+2.9	0.7	-5.3	0.3
1.30	-4.5	0.5	-4.5	0.6	2.22	+2.2	0.6	-5.6	0.2
		0.6		0.2			0.1		0.5
2.24	+1.6	0.7	-5.8	0.1	3.12	+5.0	0.2	-1.0	0.6
2.26	+0.9	0.7	-5.9	0.1	3.14	+4.8	0.3	-1.7	0.6
2.28	+0.2	0.7	-6.0	0.1	3.16	+4.5	0.3	-2.2	0.5
2.30	-0.5	0.7	-5.9	0.1	3.18	+4.2	0.4	-2.7	0.5
2.32	-1.2	0.7	-5.8	0.2	3.20	+3.8	0.4	-3.2	0.4
2.34	-1.9	0.6	-5.6	0.2	3.22	+3.4	0.5	-3.6	0.4
2.36	-2.5	0.6	-5.4	0.4	3.24	+2.9	0.5	-4.0	0.3
2.38	-3.1	0.5	-5.0	0.4	3.26	+2.4	0.5	-4.5	0.2
2.40	-3.6	0.5	-4.6	0.5	3.28	+1.9	0.5	-4.5	0.2

Continued

d	R_{12}	Δ	X_{12}	Δ	d	R_{12}	Δ	X_{12}	Δ
2.42	-4.1	0.4	-4.1	0.5	3.30	+1.4	0.6	-4.7	0.1
2.44	-4.5	0.4	-3.6	0.5	3.32	+0.8	0.6	-4.8	0.0
2.46	-4.9	0.3	-3.1	0.7	3.34	+0.2	0.6	-4.8	0.0
2.48	-5.2	0.2	-2.4	0.6	3.36	-0.4	0.5	-4.8	0.1
2.50	-5.4	0.2	-1.8	0.6	3.38	-0.9	0.6	-4.7	0.2
2.52	-5.6	0.1	-1.2	0.7	3.40	-1.5	0.5	-4.5	0.2
2.54	-5.7	0.0	-0.5	0.7	3.42	-2.0	0.5	-4.3	0.3
2.56	-5.7	0.1	+0.2	0.6	3.44	-2.5	0.5	-4.0	0.4
2.58	-5.6	0.2	+0.8	0.7	3.46	-3.0	0.4	-3.6	0.3
2.60	-5.4	0.2	+1.5	0.6	3.48	-3.4	0.3	-3.3	0.5
2.62	-5.2	0.3	+2.1	0.6	3.50	-3.7	0.3	-2.8	0.5
2.64	-4.9	0.4	+2.7	0.5	3.52	-4.0	0.3	-2.3	0.5
2.66	-4.5	0.5	+3.2	0.5	3.54	-4.3	0.1	-1.8	0.5
2.70	-3.6	0.5	+4.2	0.3	3.56	-4.4	0.1	-1.3	0.6
2.72	-3.1	0.6	+4.5	0.4	3.58	-4.5	0.1	-0.7	0.5
2.74	-2.5	0.6	+4.9	0.2	3.60	-4.6	0.1	-0.2	0.6
2.76	-1.9	0.6	+5.1	0.2	3.62	-4.5	0.0	0.4	0.5
2.78	-1.3	0.6	+5.3	0.1	3.64	-4.5	0.2	0.9	0.5

Continued

d	R_{12}	Δ	X_{12}	Δ	d	R_{12}	Δ	X_{12}	Δ
2.80	-0.7		+5.4		3.66	-4.3		1.4	
		0.7		0.0			0.3		0.5
2.82	0.0		+5.4		3.70	-3.8		2.4	
		0.6		0.1			0.3		0.4
2.84	+0.6		+5.3		3.72	-3.5		2.8	
		0.6		0.1			0.4		0.4
2.86	+1.2		+5.2		3.74	-3.1		3.2	
		0.6		0.2			0.4		0.4
2.88	+1.8		+5.0		3.76	-2.7		3.6	
		0.6		0.3			0.5		0.3
2.90	+2.4		+4.7		3.78	-2.2		3.9	
		0.5		0.3			0.5		0.2
2.92	+2.9		+4.4		3.80	-1.7		4.1	
		0.5		0.4			0.5		0.1
2.94	+3.4		+4.0		3.82	-1.2		4.2	
		0.4		0.4			0.6		0.1
2.96	+3.8		+3.6		3.84	-0.7		4.3	
		0.4		0.5			0.6		0.0
2.98	+4.2		+3.1		3.86	-0.1		4.3	
		0.3		0.6			0.5		0.0
3.00	+4.5		+2.5		3.88	+0.4		4.3	
		0.3		0.5			0.5		0.1
3.02	+4.8		+2.0		3.90	+0.9		4.2	
		0.2		0.7			0.5		0.1
3.04	+5.0		+1.3		3.92	+1.4		4.1	
		0.1		0.5			0.5		0.2
3.06	+5.1		+0.8		3.94	+1.9		3.9	
		0.1		0.7			0.4		0.3
3.08	+5.2		+0.1		3.96	+2.3		3.6	
		0.1		0.6			0.4		0.3
3.10	+5.1		-0.5		3.98	+2.7		3.3	
		0.1		0.5			0.4		0.4
		0.1			4.00	+3.1		+2.9	

Continued

 $h=1.5$

d	R_{12}	Δ	X_{12}	Δ	d	R_{12}	Δ	X_{12}	Δ
0.0	+1.7	0.0	+0.2	0.1	2.1	-1.9	1.8	-3.8	0.4
0.1	+1.7	0.0	+0.1	0.2	2.2	-3.6	1.7	-2.4	1.4
0.2	+1.7	0.1	-0.1	0.4	2.3	-4.3	0.7	-0.2	2.2
0.3	+1.6	0.2	-0.5	0.4	2.4	-3.8	0.5	+2.0	2.2
0.4	+1.4	0.3	-0.9	0.5	2.5	-2.2	1.6	+3.7	1.7
0.5	+1.1	0.6	-1.4	0.4	2.6	0.0	2.2	+4.3	0.6
0.6	+0.5	0.9	-1.8	0.2	2.7	+2.3	2.3	+3.6	0.7
0.7	-0.4	0.9	-2.0	0.1	2.8	+3.8	1.5	+1.9	1.7
0.8	-1.3	0.8	-1.9	0.6	2.9	+4.1	0.3	+1.9	2.3
0.9	-2.1	0.6	-1.3	0.1	3.0	+3.3	0.8	-0.4	2.2
1.0	-2.7	0.1	-0.3	1.3	3.1	+1.4	1.9	-2.6	1.3
1.1	-2.8	0.6	+1.0	1.2	3.2	-0.9	2.3	-3.9	0.1
1.2	-2.2	1.1	+2.2	1.0	3.3	-2.9	2.3	-4.0	1.2
1.3	-1.1	1.5	+3.2	0.3	3.4	-3.9	1.0	-2.8	2.0
1.4	+0.4	1.7	+3.5	0.4	3.5	-3.7	0.2	-0.8	2.3
1.5	+2.1	1.3	+3.1	1.3	3.6	-2.2	1.5	+1.5	1.7
1.6	+3.4	0.6	+1.8	1.8	3.7	-0.1	2.1	+3.2	0.7
1.7	+4.0		0.0		3.8	+2.0	2.1	+3.9	0.7
								+3.2	

Continue

d	R_{12}	Δ	X_{12}	Δ	d	R_{12}	Δ	X_{12}	Δ
1.8	+3.6	0.4	-1.9	1.9	3.9	+3.4	1.4	+1.5	1.7
1.9	+2.2	1.4	-3.5	1.6	4.0	+3.6	0.2	-0.6	2.1
2.0	-0.1	2.3	-4.2	0.7					

$h=2.0$

d	R_{12}	Δ	X_{12}	Δ	d	R_{12}	Δ	X_{12}	Δ
0.0	-1.0	0.0	-0.1	0.0	1.5	+0.6	0.7	-2.1	0.5
0.1	-1.0	0.1	-0.1	0.1	1.6	-0.4	1.0	-2.3	0.2
0.2	-0.9	0.0	0.0	0.2	1.7	-1.4	1.0	-2.0	0.3
0.3	-0.9	0.0	+0.2	0.2	1.8	-2.2	0.8	-1.3	0.7
0.4	-0.9	0.2	+0.4	0.2	1.9	-2.6	0.4	-0.3	1.0
0.5	-0.7	0.2	+0.6	0.2	2.0	-2.5	0.1	+1.0	1.3
0.6	-0.5	0.3	+0.8	0.2	2.1	-1.9	0.6	+2.1	1.1
0.7	-0.2	0.4	+1.0	0.2	2.2	-0.8	1.1	+2.8	0.7
0.8	+0.2	0.5	+1.2	0.1	2.3	+0.6	1.4	+2.9	0.1
0.9	+0.7	0.4	+1.1	0.2	2.4	+2.0	1.4	+2.3	0.6
1.0	+1.1	0.4	+0.9	0.4	2.5	+2.9	0.9	+1.1	1.2
1.1	+1.5	0.2	+0.5	0.7	2.6	+3.1	0.2	-0.4	1.5

Continued

d	k_{12}	Δ	X_{12}	Δ	d	R_{12}	Δ	X_{12}	Δ
1.2	+1.7	0.0	-0.2	0.7	2.7	+2.5	1.2	-1.9	1.0
1.3	+1.7	0.4	-0.9	0.7	2.8	+1.3	1.7	-2.9	0.3
1.4	+1.3	0.7	-1.6	0.5	2.9	-0.4	1.5	-3.2	0.6
		1.5		0.6			1.5		0.8
3.0	-1.9	1.1	-2.6	1.3	3.6	+2.1	1.0	+2.3	1.4
3.1	-3.0	0.2	-1.3	1.8	3.7	+3.1	0.0	+0.9	1.8
3.2	-3.2	0.7	+0.5	1.5	3.8	+3.1	1.0	-0.9	1.5
3.3	-2.5	1.4	+2.0	1.0	3.9	+2.1	1.6	-2.4	0.7
3.4	-1.1	1.7	+3.0	0.1	4.0	+0.5		-3.1	
3.5	+0.6	1.5	+3.1	0.8					

$h=2.5$

d	R_{12}	Δ	X_{12}	Δ	d	R_{12}	Δ	X_{12}	Δ
0.0	+0.6	0.0	+0.1	0.1	2.1	+1.9	0.3	+0.1	0.7
0.1	+0.6	0.0	0.0	0.0	2.2	+1.8	0.1	-0.7	0.8
0.2	+0.6	0.0	0.0	0.1	2.3	+1.4	0.4	-1.5	0.8
0.3	+0.6	0.1	-0.1	0.1	2.4	+0.7	0.7	-2.0	0.5
0.4	+0.5	0.0	-0.2	0.1	2.5	-0.3	1.0	-2.1	0.1
		0.0					0.9		0.2

Continued

d	R_{12}	Δ	X_{12}	Δ	d	R_{12}	Δ	λ_{12}	Δ
0.5	+0.5	0.1	-0.3	0.2	2.6	-1.2	0.8	-1.9	0.7
0.6	+0.4	0.1	-0.5	0.1	2.7	-2.0	0.3	-1.2	1.0
0.7	+0.3	0.2	-0.6	0.1	2.8	-2.3	0.1	-0.2	1.2
0.8	+0.1	0.2	-0.7	0.1	2.9	-2.2	0.8	+1.0	0.9
0.9	-0.1	0.3	-0.8	0.1	3.0	-1.4	1.0	+1.9	0.5
1.0	-0.4	0.3	-0.7	0.1	3.1	-0.4	1.2	+2.4	0.0
1.1	-0.7	0.3	-0.6	0.2	3.2	+0.8	1.1	+2.4	0.8
1.2	-1.0	0.1	-0.4	0.4	3.3	+1.9	0.5	+1.6	1.0
1.3	-1.1	0.0	0.0	0.4	3.4	+2.4	0.0	+0.6	1.3
1.4	-1.1	0.1	+0.4	0.5	3.5	+2.4	0.7	-0.7	1.3
1.5	-1.0	0.3	+0.9	0.3	3.6	+1.7	1.1	-1.8	0.7
1.6	-0.7	0.5	+1.2	0.3	3.7	+0.6	1.3	-2.5	0.0
1.7	-0.2	0.6	+1.5	0.2	3.8	-0.7	1.2	-2.5	0.7
1.8	+0.4	0.7	+1.7	0.4	3.9	-1.9	0.6	-1.8	1.2
1.9	+1.1	0.5	+1.3	0.5	4.0	-2.5		-0.6	
2.0	+1.6		+0.8						

Continued

$h=3.0$

d	R_{12}	Δ	X_{12}	Δ	d	R_{12}	Δ	X_{12}	Δ
0.0	-0.5	0.0	0.0	0.0	0.3	-0.5	0.0	+0.1	0.1
0.1	-0.5	0.0	0.0	0.0	0.4	-0.5	0.0	+0.1	0.0
0.2	-0.5	0.0	0.0	0.0	0.5	-0.4	0.1	+0.2	0.1
		0.0		0.1			0.1		0.1
		0.1		0.1			0.1		0.6
0.6	-0.3	0.1	+0.3	0.1	2.4	-1.4	0.4	+0.6	0.6
0.7	-0.2	0.1	+0.4	0.1	2.5	-1.0	0.4	+1.2	0.3
0.8	-0.1	0.2	+0.5	0.0	2.6	-0.5	0.7	+1.5	0.1
0.9	+0.1	0.1	+0.5	0.1	2.7	+0.2	0.7	+1.6	0.2
1.0	+0.2	0.1	+0.6	0.1	2.8	+0.9	0.6	+1.4	0.4
1.1	+0.3	0.2	+0.5	0.1	2.9	+1.5	0.3	+1.0	0.8
1.2	+0.5	0.2	+0.4	0.1	3.0	+1.8	0.1	+0.2	0.8
1.3	+0.7	0.1	+0.3	0.2	3.1	+1.7	0.4	-0.6	0.7
1.4	+0.8	0.1	+0.1	0.3	3.2	+1.3	0.7	-1.0	0.5
1.5	+0.9	0.1	-0.2	0.3	3.3	+0.6	0.9	-1.8	0.1
1.6	+0.8	0.2	-0.5	0.3	3.4	-0.3	0.9	-1.9	0.3
1.7	+0.6	0.3	-0.8	0.2	3.5	-1.2	0.6	-1.6	0.7
1.8	+0.3	0.4	-1.0	0.1	3.6	-1.8	0.2	-0.9	1.0
1.9	-0.1	0.4	-1.1	0.0	3.7	-2.0	0.3	+0.1	1.0

Continued

d	R_{12}	Δ	X_{12}	Δ	d	R_{12}	Δ	X_{12}	Δ
2.0	-0.5	0.4	-1.1	0.2	3.8	-1.7	0.6	+1.1	0.7
2.1	-0.9	0.4	-0.9	0.4	3.9	-1.1	1.0	+1.8	0.3
2.2	-1.3	0.2	-0.5	0.5	4.0	-0.1		+2.1	
2.3	-1.5	0.1	0.0	0.6					

$h=3.5$

d	R_{12}	Δ	X_{12}	Δ	d	R_{12}	Δ	X_{12}	Δ
0.0	+0.3	0.0	0.0	0.0	2.1	+0.3	0.4	+0.9	0.0
0.1	+0.3	0.0	0.0	0.0	2.2	+0.6	0.3	+0.8	0.1
0.2	+0.3	0.0	0.0	0.1	2.3	+0.8	0.2	+0.6	0.2
0.3	+0.3	0.0	-0.1	0.0	2.4	+1.0	0.2	+0.3	0.3
0.4	+0.3	0.0	-0.1	0.0	2.5	+1.1	0.1	-0.2	0.5
0.5	+0.3	0.0	-0.1	0.1	2.6	+1.0	0.1	-0.6	0.4
0.6	+0.3	0.1	-0.2	0.1	2.7	+0.7	0.3	-1.0	0.4
0.7	+0.2	0.1	-0.3	0.1	2.8	+0.3	0.4	-1.3	0.3
0.8	+0.1	0.0	-0.3	0.0	2.9	-0.2	0.5	-1.2	0.1
0.9	+0.1	0.1	-0.4	0.1	3.0	-0.7	0.5	-1.2	0.0
1.0	0.0		-0.4	0.0	3.1	-1.2	0.5	-1.2	0.4

Continued

d	R_{12}	Δ	X_{12}	Δ	d	R_{12}	Δ	X_{12}	Δ
1.1	-0.1	0.1	-0.4	0.0	3.2	-1.4	0.2	-0.2	0.6
1.2	-0.3	0.2	-0.4	0.0	3.3	-1.4	0.0	+0.5	0.7
1.3	-0.4	0.1	-0.3	0.1	3.4	-1.1	0.3	+1.0	0.5
1.4	-0.5	0.1	-0.2	0.1	3.5	-0.6	0.5	+1.4	0.4
1.5	-0.6	0.1	-0.1	0.1	3.6	+0.1	0.7	+1.6	0.2
1.6	-0.6	0.0	+0.1	0.2	3.7	+0.8	0.7	+1.4	0.2
1.7	-0.6	0.0	+0.3	0.2	3.8	+1.3	0.5	+0.9	0.5
1.8	-0.5	0.1	+0.5	0.2	3.9	+1.6	0.3	+0.2	0.7
1.9	-0.3	0.2	+0.7	0.2	4.0	+1.6	0.0	-0.6	0.8
2.0	-0.1	0.2	+0.9	0.2					

